UCLA
UCLA Electronic Theses and Dissertations

Title
Ozonolysis and Dealkenylation

Permalink
https://escholarship.org/uc/item/36q672b3

ISBN
9798184190280

Author
Dworkin, Jeremy

Publication Date
2026-07-24

Peer reviewed|Thesis/dissertation

eScholarship.org Powered by the California Digital Library
University of California

UNIVERSITY OF CALIFORNIA

Los Angeles

Ozonolysis and Dealkenylation

A dissertation submitted in partial satisfaction of the

requirements for the degree Doctor of Philosophy in Chemistry

by

Jeremy Herman Dworkin

2026

© Copyright by

Jeremy Herman Dworkin

2026

ABSTRACT OF THE DISSERTATION

Ozonolysis and Dealkenylation

by

Jeremy Herman Dworkin

Doctor of Philosophy in Chemistry

University of California, Los Angeles, 2026

Professor Ohyun Kwon, Chair

About 2.7% of the 187 years spent researching ozone are encapsulated in this dissertation. The main goal of the research conducted was to improve dealkenylation, an emerging organic chemistry method for synthesis through $C(sp^3)$–$C(sp^2)$ bond scission. The first generation of dealkenylation required the use of ozone to generate a high-energy peroxide intermediate which enabled radical cascades to break bonds and create new, valuable products. A second generation was developed through this work to bypass the ozone requirement and thereby diversify the chemical space available to dealkenylation. Not only did this second generation solve issues regarding incompatibilities of alkenes with ozone, but also it broadened the products available after radical functionalization. Further research into the ozonolysis reaction led to the development of a predictive tool to quantify the dealkenylation peroxide intermediate and provide a more complete understanding of the overall transformation.

Additionally, two new transformations involving ozone were uncovered. The first applies dealkenylation to cycloalkanones to access their 1-carbon deleted analoges. Samarium iodide was the key to both initiate the radical cascade and to reform the ring after carbon excision. The second is the ozonolysis of a C–C σ-bond. The bridging C–C σ-bond of a bicyclo[1.1.0]butane and a bicyclo[2.1.0]pentane was activated to enable radical addition of ozone. Computational studies predicted two mechanistic pathways, of which the major supports the formation of a 1,2,3-trioxane, which has never been realized in a flask.

Chapters one, two, and four originate from review articles that provide background on the field of peroxide chemistry (chapter one), and present day dealkenylation (chapter two and chapter four). Chapters two and four are each included with permission from the first authors. Chapter three introduces the second generation of ozone-free dealkenylation. Chapter five offers solutions to enable ozonation of some compound classes previously thought to be incompatible. Chapter six discusses the experimental work completed to generate the dataset for the machine learning model to quantify ozonolysis products. Chapter seven provides a proof of concept for the dealkenylative ring contraction strategy. Finally, chapter eight reveals the first ozonolysis of C–C σ-bonds.

Overall, this research advances the dealkenylation methodology, expanding into ozone-free techniques, predictive tools, and new atom-editing strategies. This work culminates with the discovery of C–C σ-bond ozonolysis.

The dissertation of Ozonolysis and Dealkenylation is approved.

K. N. Houk

Abigail G. Doyle

Keriann M. Backus

Ohyun Kwon, Committee Chair

University of California, Los Angeles

2026

DEDICATION

“I will suffer through the bad for the heights of the good”

– Pat Tillman

To my family, I am both lucky and grateful for your everlasting support

CONTENTS

ABSTRACT OF THE DISSERTATION ii

DEDICATION v

LIST OF FIGURES xiii

LIST OF TABLES xviii

ACKNOWLEDGEMENTS xxi

VITA xxxi

CHAPTER ONE *When All C–C Breaks LO–Ose* 1

1.1 Abstract 2

1.2 Significance of Organic Peroxides 2

1.3 Historical Background 3

1.4 Synthesis of Organic Peroxides 6

1.5 C–C Scission 12

1.5.1 Mechanism 12

1.5.2 Hydrogenation 19

1.5.3 Nitrogenation 21

1.5.4 Cyanation 23

1.5.5 Halogenation 25

1.5.6 Chalcogenation 26

1.5.7 Olefination 29

1.5.8 Arylation 32

1.5.9 Alkynylation and Allylation 34

1.5.10 Borylation and Silylation 36

1.6 Safety 37
1.7 Future Directions 41
1.8 Outstanding Questions 43
1.9 References 44
CHAPTER TWO *Dealkenylative Functionalizations: Conversion of Alkene C(sp^3)–C(sp^2) Bonds into C(sp^3)–X Bonds via Redox-Based Radical Processes* 60
2.1 Abstract 61
2.2 Introduction 62
2.3 Mechanism 63
2.4 History 65
2.5 Motivation to Pursue Dealkenylation 80
2.6 Dealkenylation in the Present 81
2.7 Conclusion 92
2.8 References 97
CHAPTER THREE *Hydrodealkenylative C(sp^3)–C(sp^2) Bond Fragmentation Using Isayama–Mukaiyama Peroxidation* 112
3.1 Abstract 113
3.2 Introduction 114
3.3 Results and Discussion 117
3.3.1 Electron-Rich Aromatics 121
3.3.2 Unproductive Substitution Patterns 124
3.3.3 Sterically Hindered Alkenes 126
3.3.4 Internal Nucleophiles 129

3.3.5 Internal Electrophiles 131
3.3.6 Allylic Alcohols and Ethers 134
3.3.7 Other Alkene Substrates 136
3.4 Mechanistic Discussion 141
3.5 Conclusions 146
3.6 Supporting Information and Experimental Section 147
3.6.1. Materials and Methods 147
3.6.2 Safety 148
3.6.3 Preparation of Starting Materials 150
3.6.4 Ozonolysis 164
3.6.5 Ozonolysis-Incompatible Alkene Examples 168
3.6.6 Reaction Optimization 176
3.6.7 Experimental Procedures 195
3.6.8. Characterization Data 197
5.6.9 Differential Scanning Calorimetry (DSC) 314
3.6.10 Copies of NMR Spectra 315
3.6.11. X-Ray Diffraction 450
3.7 References 462
CHAPTER FOUR *Synthesis through C(sp^3)–C(sp^2) Bond Scission in Alkenes and Ketones* 487
4.1 Conspectus 488
4.2 Initial Discoveries 490
4.3 Historical Background 493

4.4 Hydrodealkenylation 496
4.5 Thiodealkenylation 498
4.7 Oxodealkenylation 501
4.8 Mechanistic Discussion 503
4.9 Dealkenylative Alkynylation with Catalytic Iron(II) and Vitamin C 505
4.10 Halodealkenylation 507
4.11 Aminodealkenylation 509
4.12 IMP–Hydrodeakenylation 513
4.13 Deacylative Homolysis of Ketone C(sp^3)–C(sp^2) Bonds 517
4.14 Conclusions and Outlook 521
4.15 References 522
CHAPTER FIVE *Ozonolysis of Alkenes Containing Amines, Allylic Alcohols, and Electron-Rich Arenes for Dealkenylation* 533
5.1 Abstract 534
5.2 Introduction 535
5.3 Alkenes with Amines 538
5.4 Allylic Alcohols 541
5.5 Alkenes with Electron-Rich Aromatics 543
5.6 Insoluble Alkenes 547
5.7 Conclusion 549
5.8 Supporting Information and Experimental Details 550
5.8.1 Materials and Methods 550
5.8.2 Safety 551

5.8.3 Preparation of Alkene Starting Materials 552
5.8.4 Ozone Generator Calibration 571
5.8.5 Experimental Procedures 579
5.8.6 Mechanism of Hydrodealkenylation 586
5.8.7 Isayama–Mukaiyama Peroxidation Hydrodealkenylation 587
5.8.8 Failed Substrates 588
5.8.9 Characterization Data 590
5.8.10 Copies of NMR Spectra 622
5.9 References 648
CHAPTER SIX *An Ab Initio Machine Learned Model to Predict Molozonide retro-(3+2) Cycloaddition Selectivity for Dealkenylation* 659
6.1 Abstract 660
6.2 Introduction 661
6.3 Regiochemical Considerations 662
6.4 Computational Design 665
6.5 Experimental Results 667
6.6 Results and Discussion 682
6.7 Conclusions 685
6.8 Supporting Information and Experimental Section 686
6.8.1 Materials and Methods 686
6.8.2 Safety 689
6.8.3 Preparation of Starting Materials 690
6.8.4 Direct Quantitative NMR (qNMR) Measurement of Alkene Ozonolysis 729

6.8.5 Computational Section 948
6.8.6 Data Analysis 949
6.8.7 Copies of NMR Spectra 950
6.9 References 1033
CHAPTER SEVEN *Extraction of Cycloalkanone α-C(sp^3) atoms with ozone and Samarium* 1039
7.1 Abstract 1040
7.2 Proposal and Background 1041
7.3 Enol Ether Synthesis 1050
7.4 Ozonolysis Optimization 1051
7.5 Hydrodealkenylation with Samarium(II) 1053
7.6 Cycloalkanone α-C(sp^3) Extraction Efforts 1057
7.7 Iododealkenylation 1061
7.8 Conclusion and Future Directions 1063
7.9 Supporting Information and Experimental Details 1065
7.9.1 Materials and Methods 1065
7.9.2 Safety 1068
7.9.3 Preparation of Starting Materials 1069
7.10 References 1154
CHAPTER EIGHT *Ozonolysis of a C–C σ-Bond* 1163
8.1 Abstract 1164
8.2 Introduction 1165
8.3 Experimental Results 1168

8.4 Computational Results 1171
8.5 Conclusion 1176
8.6 Supporting Information and Experimental Details 1177
8.6.1 Materials and Methods 1177
8.6.2 Safety 1180
8.6.3 Substrate Preparation 1181
8.6.4 Ozonolysis Products 1203
8.6.5 Kinetic Competition Experiments 1209
8.6.6 Ozonolysis of *tert*-Butyl 3-phenylbicyclo[1.1.0]butane-1-carboxylate in MeOD-*d4* 1225
8.6.7 Attempts to Capture a 1,2,3-Trioxane 1234
8.6.8 Computational Section 1242
Computational Energies calculated by Alexander J. Maertens 1242
8.6.9 Copies of NMR Spectra 1243
8.7 References 1259
CHAPTER NINE Closing Remarks 1265

LIST OF FIGURES

Figure 1.1 Peroxide Chemistry Milestones 4
Figure 1.2 Organic Peroxide Syntheses 8
Figure 1.3 Mechanistic Overview 13
Figure 1.4 Alkylation 16
Figure 1.5 Hydrogenation 20
Figure 1.6 Nitrogenation 22
Figure 1.7 Cyanation and Halogenation 24
Figure 1.8 Chalcogenation 27
Figure 1.9 Olefination 30
Figure 1.10 Arylation 33
Figure 1.11 Alkynylation, Allylation, Borylation, and Silylation 35
Figure 1.12 Safety 38
Figure 2.1 Mechanism for Ozone-Mediated Peroxidation and Iron(II) Reduction of Feedstock Olefins 64
Figure 2.2. Initial Studies on Iron(II) Reduction of Hydrogen Peroxide 66
Figure 2.3 Early Reports of β-Scission and Characterization of Products When Reacting Tertiary Peroxides (Part 1) 67
Figure 2.4 Early Reports of β-Scission and Characterization of Products When Reacting Tertiary Peroxides (Part 2) 69
Figure 2.5 Early Reports of Reducing Tertiary Hydroperoxides with Iron(II) and Coper(I) with Intentional Radical Functionalization (Part 1) 71
Figure 2.6 Early Reports of Reducing Tertiary Hydroperoxides with Iron(II) and Coper(I) with Intentional Radical Functionalization (Part 2) 73
Figure 2.7 Early Methods of Peroxide Synthesis 74
Figure 2.8 Various Methods of Peroxide Synthesis that Employ Pericyclic Reactions or Metal Salts 76
Figure 2.9 Combinations of Ozone Mediated Addition of Alkenes and Subsequent Degradation 78
Figure 2.10. Motivation to Pursue Dealkenylation 80
Figure 2.11 Hydrodealkenylation 82
Figure 2.12. Dealkenylative Thiylation 84
Figure 2.13 Oxodealkenylation 85
Figure 2.14 Dealkenylative Alkenylation 87
Figure 2.15 Dealkenylative Alkynylation 90
Figure 2.16 Dealkenylation Substrates (Part 1) 93
Figure 2.17 Dealkenylation Substrates (Part 2) 94

Figure 2.18 Dealkenylation Substrates (Part 3) 95
Figure 2.19 Dealkenylation Substrates (Part 4) 96
Figure 3.1 Strategy and Design 115
Figure 3.2 Electron Rich Aromatics 123
Figure 3.3 Unproductive Alkene Substitution Patterns 125
Figure 3.4 Sterically Hindered Alkenes 128
Figure 3.5 Internal Nucleophiles 130
Figure 3.6 Internal Electrophiles 133
Figure 3.7 Allylic Alcohols and Ethers 135
Figure 3.8 Ozonolysis– vs IMP–Hydrodealkenylation 137
Figure 3.9 Alkenes, IMP, and Hydrodealkenylation 140
Figure 3.10 β-Scission Kinetics 142
Figure 3.11 Mechanism 145
Figure 3.12 TLC Analysis 167
Figure 3.13 Electron-Rich Aromatics 168
Figure 3.14 Electron-Rich Aromatics 169
Figure 3.15 Sterically Hindered 170
Figure 3.16 Sterically Hindered 171
Figure 3.17 Internal Nucleophiles 172
Figure 3.18 Internal Electrophiles 173
Figure 3.19 Allylic Alcohols and Ethers 174
Figure 3.20 Allylic Alcohols and Ethers 175
Figure 3.21 Failed IMP Substrates 185
Figure 3.22 Failed Reductive Hydrogenation Substrates 194
Figure 3.23 X-Ray Structure of $Co(modp)_2(EtOH)_2$ 450
Figure 4.1 From Synthetic Needs to the Discovery of New Methodology 491
Figure 4.2 Historical Milestones Leading to Peroxide-Based Deconstructive Synthetic Strategies 494
Figure 4.3 Hydrodealkenylation 497
Figure 4.4 Thiodealkenylation 498
Figure 4.5 Dealkenylative Alkenylation 500
Figure 4.6 Oxodealkenylation 501
Figure 4.7 Kinetic Analysis 504
Figure 4.8 Dealkenylative Alkynylation 506
Figure 4.9 Halodealkenylation 508
Figure 4.10 Aminodealkenylation and Primary Amine Synthesis 510

Figure 4.11 Mechanism for Hydroperoxide–Amine C(sp^3)–N Cross-Coupling 512
Figure 4.12 Ozone-Incompatible Alkene Classes 513
Figure 4.13 IMP–Hydrodealkenylation 515
Figure 4.14 Silylperoxide Radical Hydrogenation Mechanism 516
Figure 4.15 Hydrodeacylation of Cycloalkanones 518
Figure 4.16 Selected Applications of Homolytic Deacylation in the Total Synthesis of NPs 520
Figure 5.1 Hydrodealkenylation Mechanism 536
Figure 5.2 Ozone Incompatible Functionalities 537
Figure 5.3 Hydrodealkenylation of Amino-Alkenes 540
Figure 5.4 Formal Syntheses of (±)-Pinidinone, GB17, and GnRH Agonist from *N*-Boc Norpseudopelletierine 540
Figure 5.5 Hydrodealkenylation of Allylic Alcohols 542
Figure 5.6 Dealkenylation of Alkenes with ERAs 546
Figure 5.7 Hydrodealkenylation of Insolubles 548
Figure 5.8 Plot of Iodometric Titration of Ozone 574
Figure 5.9 Plot of qNMR Spectroscopic Titration of Ozone 576
Figure 5.10 Hydrodealkenylation Mechanism 586
Figure 5.11 IMP–Hydrodealkenylation of Steviol Methyl Ester 587
Figure 5.12 TLC (50% v/v EtOAc/hexanes + UV/vanillin stain) of the ozonolysis of eugenol (13) in methanol (0.1 M) at –78 ºC with lanes spotted every 30 seconds. 589
Figure 5.13 Failed Substrates 589
Figure 6.1 Abstract 660
Figure 6.2 Mechanism of Criegee Ozonolysis in Methanol 662
Figure 6.3 Scope and Qualitative Regiochemical Considerations 664
Figure 6.4 Computational Pipeline 665
Figure 6.5 Experimental Pipeline 668
Figure 6.6 *retro*-(3+2) Cycloaddition Selectivity for ‘Intuitive’ Alkenes 672
Figure 6.7 *retro*-(3+2) Cycloaddition Selectivity for ‘Ambiguous’ Alkenes 677
Figure 6.8 *retro*-(3+2) Cycloaddition Selectivity for Polarized, Electron-Rich Enol Derivatives 679
Figure 6.9 *retro*-(3+2) Cycloaddition Selectivity for Polarized, Electron-Deficient α,β-Unsaturated Carbonyl Derivatives 681
Figure 6.10 Model Performance per Category 682
Figure 6.11 ML Model Accuracy vs Frequency 684
Figure 6.12 ML Model Error vs Frequency 684
Figure 6.13 Sample Preparation 729

Figure 6.14 Felkin–Ahn Analysis for 32a$_S$ 847
Figure 6.15 1D Gradient Selective TOCSY (800 MHz, 10:1 $CDCl_3$:CD_3OD) signal for the peroxide β-CH of (32a$_S$)..... 847
Figure 6.16 Felkin–Ahn Analysis for 32a$_R$ 849
Figure 6.17 1D Gradient Selective TOCSY (800 MHz, 10:1 $CDCl_3$:CD_3OD) signal for the peroxide β-CH of Compound (B$_R$)..... 849
Figure 6.18 Felkin–Ahn Analysis for 32b$_S$ 851
Figure 6.19 1D Gradient Selective TOCSY (800 MHz, 10:1 $CDCl_3$:CD_3OD) signal for the peroxide β-CH of Compound (32b$_S$) 851
Figure 6.20 Felkin–Ahn Analysis for 32b$_R$ 853
Figure 6.21 1D Gradient Selective TOCSY (800 MHz, 10:1 $CDCl_3$:CD_3OD) signal for the peroxide β-CH of Compound (32b$_R$) 853
Figure 6.22 Felkin-Ahn Analysis of 33a$_S$ 857
Figure 6.23 1D Selective Gradient TOCSY (800 MHz, 10:1 $CDCl_3$:CD_3OD) signal for the peroxide β-CH of Compound (33a$_S$) 858
Figure 6.24 Felkin–Ahn Analysis of 33a$_R$..... 859
Figure 6.25 1D Gradient Selective TOCSY (800 MHz, 10:1 $CDCl_3$:CD_3OD) signal for the peroxide β-CH of Compound (33a$_R$) 860
Figure 6.26 Felkin–Ahn Analysis of 33b$_S$..... 861
Figure 6.27 1D Selective Gradient COSY (800 MHz, 10:1 $CDCl_3$:CD_3OD) signal for the peroxide β-CH of Compound (33b$_S$) 862
Figure 6.28 Felkin–Ahn Analysis of 33b$_R$..... 863
Figure 6.29 1D Gradient Selective TOCSY (800 MHz, 10:1 $CDCl_3$:CD_3OD) signal for the peroxide β-CH of Compound (33b$_R$) 864
Figure 6.30 Felkin–Ahn Analysis for 40a 891
Figure 6.31 Felkin–Ahn analysis of 41a..... 896
Figure 6.32 Felkin–Ahn analysis of 42a..... 900
Figure 6.33 Felkin–Ahn Analysis of 43a 906
Figure 6.34 Felkin–Ahn Analysis of 45a 915
Figure 6.35 Felkin–Ahn Analysis of 48 925
Figure 7.1 Initial Plan 1043
Figure 7.2 Backup Plan 1046
Figure 7.3 Alternative Plans..... 1049
Figure 7.4 Ketals and Enol Ethers 1050
Figure 7.5 Ozonolysis of Enol Ether Optimization 1052
Figure 7.6 SmI_2 Hydrodealkenylation: Solvent Screen 1053
Figure 7.7 Proposed TS‡ for SmI_2 reduction of peroxides with a proton source..... 1054

Figure 7.8 SmI_2 Hydrodealkenylation: Equivalent Screen 1054
Figure 7.9 Colors of SmI_2 (s) in MeOH 1055
Figure 7.10 4-Phenylcyclohexanone Potential Reaction Products 1058
Figure 7.11 Iododealkenylation: Iodide Source 1061
Figure 7.12 Iododealkenylation: TMSI Quantities 1062
Figure 7.13 Iododealkenylation: Ligand Screen 1062
Figure 7.14 SmI_2 Titration 1071
Figure 7.15 HTE Results: MeOH vs Dimer 1099
Figure 7.16 HTE Results: MeOH vs Hydro 1100
Figure 7.17 HTE Results: MeOH vs PDT 1100
Figure 7.18 HTE Results: MeOH vs Ketoester 1101
Figure 7.19 HTE Results: MeOH vs Other Products 1101
Figure 7.20 HTE Results MeOH vs Reaction 1102
Figure 7.21 4-Phenylcyclohexanone α-C(sp^3) Analyte GCMS Traces 1116
Figure 7.22 Calibraiton Curve for 2c 1118
Figure 7.23 Calibration Curve for 2d 1118
Figure 7.24 Calibration Curve for 2e 1119
Figure 7.25 Calibration Curve for 2f 1119
Figure 7.26 Calibration Curve for 2g 1120
Figure 7.27 Calibration Curve for 2h 1120
Figure 8.1 Introduction to Ozone 1167
Figure 8.2 Experimental Results 1170
Figure 8.3 Computational Mechanistic Investigations 1175
Figure 8.4 Potential Energy Surface for Ozonolysis of BCB σ-Bond 1242
Figure 8.5 Potential Energy Surface for BCB Second Ozone Addition 1242

LIST OF TABLES

Table 3.1 Optimization of Radical Hydrogenation 119
Table 3.2 Co(II) Catalyst Survey 176
Table 3.3 Optimization of Catalyst Loading 177
Table 3.4 Optimization of Reductant, Solvent, and Concentration 179
Table 3.5 Optimization of IMP with Trimethylsilane 181
Table 3.6 Optimization of Ferrous Reductive Hydrogenation 187
Table 3.7 Optimization of Reductive Hydrogenation 191
Table 3.8 Crystal Data and Structure Refinement for C1 452
Table 3.9 Atomic Coordinates and U_{eq} [Å^2] for C1 453
Table 3.10 Anisotropic Displacement Parameters [Å2] for C1. The anisotropic displacement factor exponent takes the form: $-2\pi^2[\, h^2(a^*)^2U_{11} + k^2(b^*)^2U_{22} + \ldots + 2hka^*b^*U_{12}\,]$ 455
Table 3.11 Torsion Angles for C1 456
Table 3.12 Bond Lengths for C1 457
Table 3.13 Bond Ancles for C1 459
Table 5.1 Optimization of Hydrodealkenylation for Amino-Alkenes 539
Table 5.2 Experimental Values for Iodometric Titration of Ozone 573
Table 5.3 Experimental Values for qNMR Spectroscopic Titration of Ozone 577
Table 6.1 1-hexene (1) ozonolysis qNMR Data 736
Table 6.2 1-decene (2) ozonolysis 740
Table 6.3 vinylcyclohexane (3) ozonolysis 744
Table 6.4 3,3-dimethyl-1-butene (4) ozonolysis qNMR Data 748
Table 6.5 4-bromobutene (5) ozonolysis qNMR Data 752
Table 6.6 6-bromohexene (6) ozonolysis qNMR Data 756
Table 6.7 2-methyl-1-butene (7) ozonolysis qNMR Data 759
Table 6.8 methylenecycloheptane (8) ozonolysis qNMR Data 762
Table 6.9 methylenecycloheptane (9) ozonolysis qNMR Data 765
Table 6.10 α-methyl styrene (10) ozonolysis qNMR Data 767
Table 6.11 (prop-1-en-2-yl-3,3,3-d_3)benzene (11) ozonolysis qNMR Data 770
Table 6.12 (3,3,3-trifluoroprop-1-en-2-yl)benzene (12) 774
Table 6.13 (1-cyclopentylvinyl)benzene (13) qNMR Data 777
Table 6.14 (1-cyclobutylvinyl)benzene (14) qNMR Data 780
Table 6.15 2-methylallyl 4-(trifluoromethyl)benzoate (15) qNMR Data 783
Table 6.16 2-methylallyl 4-bromobenzoate (16) qNMR Data 786

Table 6.17 2-methylallyl (*S*)-2-(4-isobutylphenyl)propanoate (17) qNMR Data 789
Table 6.18 3-methylbut-3-en-1-yl (*S*)-2-(4-isobutylphenyl)propanoate (18) qNMR Data 793
Table 6.19 2-methyl-2-butene (19) qNMR Data 796
Table 6.20 (–)-β-citronellol (20) qNMR Data 799
Table 6.21 (–)-α-cedrene (21) qNMR Data 802
Table 6.22 (1*S*,2*S*,9*R*,*E*)-6,10,10-trimethylbicyclo[7.2.0]undec-5-en-2-yl benzoate (22) qNMR Data 806
Table 6.23 1-methylcyclododecene (23) qNMR Data 810
Table 6.24 (+)-phtyol (24) qNMR Data 813
Table 6.25 (*E*)-2,2-dimethylhex-3-ene (25) qNMR Data 819
Table 6.26 (*trans*)-pent-2-en-1-ol (26) qNMR Data 823
Table 6.27 *trans*-anethole (27) qNMR Data 828
Table 6.28 capsaicin (28) qNMR Data 831
Table 6.29 (22*R*,23*R*)-5α-hydroxy-22,23-stigmasten-3,6-dione (29) qNMR Data 836
Table 6.30 1,2-dihydronapthalene (30) qNMR Data 839
Table 6.31 3-methylcyclohexene (31) qNMR Data 843
Table 6.32 (+)-*trans*-p-menth-2-ene (32) qNMR Data 854
Table 6.33 (–)-*cis*-p-menth-2-ene (33) qNMR Data 865
Table 6.34 oleic acid (34) qNMR Data 869
Table 6.35 ricinoleic acid (35) qNMR Data 874
Table 6.36 3-methyl-2-phenylbut-2-ene (36) qNMR Data 877
Table 6.37 propan-2-ylidenecyclohexane (37) qNMR Data 880
Table 6.38 1-methyl-2-(propan-2-ylidene)cyclohexane (38) qNMR Data 883
Table 6.39 (2-(propan-2-ylidene)cyclohexyl)benzene (39) qNMR Data 886
Table 6.40 4-methoxy-1,2,3,6-tetrahydro-1,1'-biphenyl (40) qNMR Data 891
Table 6.41 trimethyl(2-((1,2,3,6-tetrahydro-[1,1'-biphenyl]-4-yl)oxy)ethoxy)silane (41) qNMR Data 896
Table 6.42 1,2,3,6-tetrahydro-[1,1'-biphenyl]-4-yl acetate (42) qNMR Data 901
Table 6.43 diethyl (1,2,3,6-tetrahydro-[1,1'-biphenyl]-4-yl) phosphate (43) qNMR Data 906
Table 6.44 4,4-difluorocyclohex-1-en-1-yl diethyl phosphate (44) qNMR Data 909
Table 6.45 2-(4-methoxycyclohex-3-en-1-yl)isoindoline-1,3-dione (45) qNMR Data 915
Table 6.46 3,4-dihydrofuran (46) qNMR Data 918
Table 6.47 3,4-dihydro-2*H*-pyran (47) qNMR Data 921
Table 6.48 *tert*-butyl(((1S*,3aR*,6aR*)-4-methoxy-1,2,3,3a,6,6a-hexahydropentalen-1-yl)oxy)dimethylsilane (48) qNMR Data 925

Table 6.49 (+)-bis(trimethylsilyl)hydromutilin enol diethylphosphate (49) qNMR Data 929
Table 6.50 methyl styryl ketone (50) qNMR Data 934
Table 6.51 cinnamic acid (51) qNMR Data 937
Table 6.52 methyl cinnamate (52) qNMR Data 941
Table 6.53 cinnamonitrile (53) qNMR Data 944
Table 6.54 cyclohexenone (54) qNMR Data 947
Table 7.1 Ring Contraction Optimization 1060
Table 7.2 Enol Ether Hydrodealkenylation Optimization 1091
Table 7.3 Hydrodealkenylation with SmI_2 Solvent Screen 1094
Table 7.4 Hydrodealkenylation with SmI_2 Equivalents Screen 1096
Table 7.5 Hydrodealkenylation with SmI_2 Temperature Screen 1097
Table 7.6 Ring Contraction Reaction Screening 1121
Table 7.7 Iododealkenylation: Iodide Source 1124
Table 7.8 Iododealkenylation: TMSI Quantities 1126
Table 7.9 Iododealkenylation: Ligand Screen 1128
Table 8.1 qNMR data from partial competitive Criegee ozonolysis of BCB 1 and *t*BuA. 1212
Table 8.2 qNMR data from partial competitive Criegee ozonolysis of BCP 2 and *t*BuA 1215
Table 8.3 qNMR data from partial competitive Criegee ozonolysis of BCB 1 and AMS 1218
Table 8.4 qNMR data from partial competitive Criegee ozonolysis of BCP 2 and AMS 1221
Table 8.5 qNMR data from Criegee ozonolysis of BCB 1 1228

ACKNOWLEDGEMENTS

To Professor Ohyun Kwon, thank you for your mentorship. When I first came to UCLA as a graduate student I had almost no research experience, yet you saw something in me. You decided to take a chance and give me the opportunity to grow as a scientist, a learner, and a leader. I appreciate your patience as I struggled with my projects and how you always pushed me to succeed. Supporting you as your teaching assistant for Chem 244A will forever be one of my favorite parts of my graduate experience. I think you are a brilliant chemist, and I am honored to have studied under you.

To my committee members, Processor Ken Houk, Professor Abby Doyle, and Professor Keri Backus, thank you for being a source of wisdom and guidance. Ken, I am inspired by your work and impact in the computational chemistry field. I truly enjoyed your class, and I appreciate the time you spent answering my abstract questions posed to satisfy my own curiosities. I feel privileged to be able to collaborate on a project with you. Abby, it has been an honor to have you supporting me. I look up to you as a mentor because of your kindness. Keri, you gave me my start here at UCLA. You have made a huge impact on how I conduct research and set up experiments because your lab reinforced the value of organization and communication. You have also fostered an amazing community of graduate students in your lab, many of whom have become some of my best friends here at school. I have always been interested in biology, and although I chose to dive into organic chemistry, I am very grateful to have spent time with you learning how to conduct molecular biology research.

To my parents, Jim and Patty, I love you and your unconditional support for me. You have taught me many things as I grew up, but the two that most impacted my

graduate studies are to have integrity and to always try my best. One of the things I learned during my time at UCLA, related to the value of integrity, is how to hold myself accountable. The unstructured schedule of a student can be challenging but sticking to who I am and how I show up for others got me through it. Throughout my life you have always taught me to try my best, with no expectation of what you think my best could be. In reflection, I think this lack of an expectation was extremely important because I was able to focus within and work towards how I great I wanted to be and not work towards a goal of idea someone else set for me. Feeling free to set my own goals, work towards them, and hold myself accountable through it all is the best gift you could have provided.

To my brothers, Zachary, Matthew, and Evan thank you for your unintentional competition. Without realizing it, I have been inspired by your successes. Being “stuck” in school has forced me to watch you all progress in your careers. Although I do feel a bit jealous, knowing you all are working just as hard to succeed has felt oddly reassuring. I know I chose a much different path than all of you and I am grateful for your support.

To my partner, Lydia, thank you for supporting with me and staying with me for the entirety of my graduate studies. We made it through long distance for a few years to eventually being in the same city. You have made me into a real, well-rounded adult because you have helped me to get in touch with my feelings, to learn how to communicate not only my science but also with others, and to be a good partner. Growing with you has kept me grounded. You have always been a source of light and hope for me. Your love has helped me stay focused and to get through graduate school in one piece. I am excited for our next chapter together. I love that you are pursuing your dreams and I cannot wait to see you achieve them.

To my extended family, thank you for staying curious about my life. I know a lot of what I do is difficult to explain but I love that you have continued to ask me about it regardless. Grammy, thank you for always sending my mail for holidays and making sure I take time off to recharge. Knowing that you are thinking about me means a lot to me. To the Stephenson family, you all have provided me with a second home. From the family dinners Sunday nights at Berkeley to the wild nights in southern California, I have loved hanging out with you. I feel grateful that you include me in your activities. To the Williams family, thank you for your support throughout graduate school and in life. I love how adventurous you all are, and I am always amazed to hear about the cool trips and places you have visited. You inspire me to be more worldly. To JJ, thank you for believing in me. You removed a lot of the fear I had at the beginning of graduate school because of your kindness and love. To Sophie and Sacha, thank you for keeping me fed and entertained. I feel very lucky to have been able to visit you at UCSB during my first year of school. I remember feeling extremely stressed but you provided an essential escape and a safe space. Looking back, I wish I could have “stopped to smell the roses” just a little bit more with you. Some of my favorite memories from school are those I spent hanging out with you both.

To my friends, Matt, Brian, and Jake, thank you for all of our crazy adventures. The super bowl rotisserie chicken, pickle night, and all of our insane costumes were unbelievably fun and incredibly wild. When I think back on my twenties it will be mostly about the memories of our shenanigans. Matt, you have given me so much more than your friendship. You have always supported me, checked in on me, and been there for me when I needed someone. Brian, my surfing buddy, thank you for always taking me to

Costco and for listening to my problems out on the water. You always were on the lookout for me and I appreciate your support. Jake, you are an amazing and hilarious human. I know I can always count on you. I appreciate you for coaching me through some of hardest times.

To KC, my lab partner from Berkeley. It has been a pleasure to keep in touch with you over the years since graduation. I always loved to hear about all the things going on in your life and about everyone else from Berkeley living in the Bay Area. I have missed seeing everyone and I am grateful to have been able to feel like I have been there with you all despite living in a different city. Go Bears!

To my cohort at UCLA. We did it. You all have been an awesome group of scientists, and I am excited to see what we all do as we embark on the next step of our lives. The time has gone by so quickly, but it still feels like yesterday when we were sitting in class together or hanging out at the beach on a weekend. It was a pleasure getting to know all of you and I hope we can stay in touch throughout our lives.

To my lab mates, thank you for teaching me, supporting me, listening to me, and working with me to do great work. You are all extremely capable scientists, and I am proud of the community we have created during my time at UCLA. I love that we have been able to do things together to strengthen our teamwork, such as going to work out classes or setting up group activities together. I am very grateful for all of the insights you have each provided into my own work. A lot of what I have been able to do would not have been possible without your reassurance and support. Tom, you were one of the major reasons I joined the group. Your humor and charisma are inspiring. Tony, you have always been a constant source of wisdom. Thank you for your integrity and attention to

detail. Brady, we did it. Liz and Betsy, thank you for helping me to plan lab events. I love that we were able to foster a community and help everyone to be more friendly with one another. Cameron and Jason, you are two of the brightest people that I know. I love your obscure chemistry knowledge. Clifford, you are one of the hardest workers I have ever met and your efficiency is inspiring. Jett (and Jacob), your pursuit of total synthesis is impressive, and I wish you luck in finishing the molecule. Jasmin, your passion and energy are motivating and refreshing. You bring a smile to those around you, and it has been a pleasure helping you get set up in the lab. Ethan, I think you are extremely talented. You are both observant and critical which contribute massively to your successes. I know you will achieve great things. I am also grateful for your companionship these last couple of years, especially at BHIP/BSTRONG. Michelle, I am so proud of you and what you have accomplished. Serving as your mentor has been more rewarding than just completing projects with you. Your friendship has meant the world to me, and I feel extremely lucky to have had you working with me. Go Bears! Jeff, you have what it takes to be a phenomenal chemist. I am grateful for the work you have done with me and I wish I could have had more time to teach you how to do research.

To the Backus lab, Nik, Ashley, Andrew (and Rachel), Flow, Eli, Adi, Nithesh, Miranda, Alex, Lisa, Heta, and Halime thank you for being so inviting and caring. Each of you have positively impacted my time here at UCLA in your own way, but collectively you all have been a community for me. Nik, you were the first student I got in touch with, and you showed me how things work. You have been a source of advice whenever I needed it. Ashely, you were my first mentor here and I appreciate your patience, mentorship, and friendship. A lot of the success I had during my rotation was because of your coaching.

Thank you for giving me my start. Andrew, spending time hanging out with you has been very rewarding. You are very caring and empathetic. I value our chats and I am grateful for the trips to San Diego and back. Thank you for choosing me to take care of Lila while you were away. Flow, physical fitness is something I value and I am so happy we were able to connect as gym buddies. I also admire your organization and the balance you have in your life. Eli, Adi, and Nithesh, thank you for bringing me out to hang with the bros. I think you all are awesome and I am grateful that you included me in your activities.

To Dr. Michal Šimek, you showed me what it takes to be a chemist and a good person. Watching you succeed and learning from you during such a pivotal time of my studies was one of the luckiest and best things to happen for me. A lot of the success I have had in graduate school has come from your guidance. You showed me how to conduct proper, efficient research while simultaneously setting aside time for others and myself. You are a well-rounded individual, and you have proven to me that it is possible to achieve your dreams. I am happy to have been able to share surfing with you. You have truly impacted me in such a positive way, and I cannot thank you enough.

To Dr. T.J. O'Connor, thank you for teaching me about industry and for your advice into my research. Your work ethic is inspiring. Emulating your efficiency and approach to research have helped me to succeed and I feel lucky that you chose UCLA for your postdoctoral studies.

To Professor Evan Miller and Dr. Monica Gonzalez, thank you for giving me the opportunity to do undergraduate research with you. Monica, you showed me how to set up my first reaction, and I am grateful that you chose me to work with you.

To Dr. Pete Marsden, you are one of the reasons why I chose to pursue chemistry. My first taste of the subject was your Chem 1A class at UC Berkeley. I can still remember countless office hours sessions with you asking obscure questions just because I was curious about the subject. You cultivated my passion and provided me the resources to grow. You are an excellent instructor, and I am constantly reminded of the basics I learned in your classes.

To UCLA Hillel and my Jewish friends, thank you for creating a community where I could explore my Judaism as a young adult. My time here at UCLA would not have been as much fun without all of the amazing events I attended. To the staff, thank you for always being there for me, for putting a smile on my face, and filling my stomach multiple days a week for five years. I feel blessed.

Chapter One of this dissertation is an adaptation of the material as it appears in Dworkin, J. H.; Dehnert, B. W.; Kwon, O. When All C–C Breaks LO–Ose. *Trends Chem.* **2023**, *5*, 174–200. The additional authors listed in this publication are Brady W. Dehnert and Ohyun Kwon. Ohyun Kwon directed and supervised the research.

Chapter Two of this dissertation is an adaptation of the material as it appears in Dehnert, B. W.; Dworkin, J. H.; Kwon, O. *Dealkenylative Functionalizations: Conversion of Alkene C(sp^3)–C(sp^2) Bonds into C(sp^3)–X Bonds via Redox-Based Radical Processes Synthesis* **2024**, 56, 71–86. The additional authors listed in this publication are Brady W. Dehnert, first author, and Ohyun Kwon. Ohyun Kwon directed and supervised the research.

Chapter Three of this dissertation is an adaptation of the material as it appears in Dworkin, J. H.; Chen, Z. M.; Cheasty, K. C. C.; Rubio, A. V.; Kwon, O. Hydrodealkenylative C(sp^3)–C(sp^2) Bond Fragmentation Using Isayama–Mukaiyama Peroxidation**.** *J. Am. Chem. Soc.* **2025**, *147*, 13531–13544. The additional authors listed in this publication are Zhuoxi (Michelle) Chen, Kathleen C. Cheasty, Aris V. Rubio, and Ohyun Kwon. Ohyun Kwon directed and supervised the research.

Chapter Four of this dissertation is an adaptation of the material as it appears in Šimek, M.; Dworkin, J. H.; Kwon, O. Synthesis through C(sp^3)–C(sp^2) Bond Scission in Alkenes and Ketones. *Acc. Chem. Res.* **2025**, *58*, 1547–1561. The additional authors listed in this publication are Michal Šimek, first author, and Ohyun Kwon. Ohyun Kwon directed and supervised the research.

Chapter Five of this dissertation is an adaptation of the material as it appears in Dworkin, J. H.; Chen, Z. M.; Prout, E. S.; Kwon, O. *Ozonolysis of Alkenes Containing*

Amines, Allylic Alcohols, and Electron-Rich Arenes for Dealkenylation. Org. Lett. **2025**, *27*, 7833–7839**.** The additional authors listed in this publication are Zhuoxi (Michelle) Chen, Ethan S. Prout, and Ohyun Kwon. Ohyun Kwon directed and supervised the research.

Chapter Six contains unpublished results to be submitted in collaboration with the Xin Hong group as Dworkin, J. H.; Li, J.-Q.; Foker, E. A.; Dehnert, B. W.; Prout, E. S.; Silva, T. G.; Tuermer-Lee, J. X.; Leung, C. B.; Chen, Z. M.; Yu Liao, L. Wang, J. M. Hong, X.; Kwon, O. An *Ab Initio* Machine Learned Model to Predict Molozonide *Retro*-(3+2) Cycloaddition Selectivity for Dealkenylation. The dissertation author was the primary researcher and co-first author of this manuscript. The additional authors listed are Jia-Qi Li (Hong Group), Elizabeth A. Foker (Kwon Group), Brady W. Dehnert (Kwon Group), Ethan S. Prout (Kwon Group), Thais G. Silva (Kwon Group), Jason X. Tuermer-Lee (Kwon Group), Clifford B. Leung, (Kwon Group), Zhuoxi (Michelle) Chen (Kwon Group), Lorena Yu Liao (Kwon Group), Jeffery M. Wang (Kwon Group), Xin Hong, and Ohyun Kwon. Xin Hong supervised the research by Jia-Qi Li. Ohyun Kwon directed and supervised the research by the dissertation author. The dissertation author was the primary investigator and co-first author of this manuscript.

Chapter Seven contains unpublished results which comprise of a proof-of-concept for the project goal but require further experimentation. The current contributors to the project are Dworkin, J. H.; Chen, Z. M.; Prout, E. S.; Bioteau, J. A.; Wang, J. M.; Kwon, O. The dissertation author was the primary investigator of this manuscript and invented the original idea for this work.

Chapter Eight contains unpublished results to be submitted in collaboration with the Ken Houk group as Dworkin, J. H.; Maertens, A. J.; Houk, K. N.; Kwon, O. Ozonolysis of C–C σ-Bonds. The additional authors listed are Alexander J. Maertens (Houk Group), K. N. Houk, and Ohyun Kwon. K. N. Houk supervised the research by Alexander J. Maertens. Ohyun Kwon supervised the research by the dissertation author. The dissertation author was the primary investigator and author of this manuscript.

Financial support was provided by the University of California, Los Angeles, NIH grants R01GM071779 and R01GM141327, NIH Office of Research Infrastructure Program grants S10OD028644, S10OD025073, and 1S10OD016387-01, NSF grant CHE-1048804, DE program of the Department of Energy grant DE-FC03-02ER63421. Funds from the Mighael E. Jung Excellence in Teaching Award, John Stauffer Award Excellence in Second Year Academics and Research, Majeti-Alaparti Excellence in Research Award, Christopher S. Foote Graduate Fellowship in Organic Chemistry, Saul Winstein Fellowship, and the Doctoral Student Travel Grant were also applied towards the financial support of the dissertation author.

VITA

EDUCATION

2021–2026 Doctor of Philosophy in Chemistry, University of California Los Angeles (expected)
2021–2023 Master of Science in Chemistry, University of California Los Angeles
2017–2021 Bachelor of Science in Chemical Biology, University of California Berkeley

PUBLICATIONS

1. Dworkin, J. H.; Chen, Z. M.; Kwon, O. Ozonolysis of alkenes containing amines, allylic alcohols, and electron-rich arenes for dealkenylation. *Org. Lett.* **2025**, *27*, 7833–7839.
2. Šimek, M.; Dworkin, J. H.; Kwon, O. Synthesis through C(sp^3)–C(sp^2) bond scission in alkenes and ketones. *Acc. Chem. Res.* **2025**, *58*, 1547–1561.
3. Dworkin, J. H.; Chen, Z. M.; Cheasty, K. C.; Rubio, A. V.; Kwon, O. Hydrodealkenylative C(sp^3)–C(sp^2) bond fragmentation using Isayama–Mukaiyama peroxidation. *J. Am. Chem. Soc.* **2025**, *147*, 13531–13544.
4. Dehnert, B. W.; Dworkin, J. H.; Kwon, O. Dealkenylative Functionalization: Conversion of alkene C(sp^3)–C(sp^2) bonds to C(sp^3)–X bonds using redox-based radical processes. *Synthesis* **2024**, *45*, 71–86.
5. Dworkin, J. H.; Dehnert, B. W.; Kwon, O. When all C–C breaks LO–Ose. *Trends Chem.* **2023**, *5*, 174–200.

RESEARCH TRAINING

2021–2026 Graduate Research Fellow, University of California Los Angeles

Advisor: Professor Ohyun Kwon

Synthetic organic chemistry research in ozonolysis and dealkenylation

2021 Postbaccalaureate Researcher, University of California Los Angeles

Advisor: Professor Keriann Backus

Investigated mRNA–protein interactions with quantitative proteomics

2020–2021 Undergraduate Researcher, University of California Berkeley

Advisor: Associate Professor Evan W. Miller

Synthesis and imaging of near infrared phosphine oxide rhodamine voltage sensitive fluorophores

HONORS AND AWARDS

2026 Saul Winstein Fellowship

2026 Christopher S. Foote Graduate Fellowship in Organic Chemistry

2025 Majeti-Alaparti Excellence in Research Award

2024 John Stauffer Award, Excellence in Second Year Academics and Research

2023 Michael E. Jung Excellence in Teaching Award

2021 High Honors in Chemical Biology

2019 Most Spirited Bear of the Year

2017 Dean’s List

CHAPTER ONE

When All C–C Breaks LO–Ose

Adapted from Dworkin, J. H.; Dehnert, B. W.; Kwon, O.
Trends Chem. **2023**, *5*, 174–200.

1.1 Abstract

Organic peroxides are becoming popular intermediates for novel transformations in chemistry. The weak O–O bond is readily reduced by transition metals, including iron and copper, to initiate a radical cascade process that breaks C–C bonds. Great potential exists for the rapid generation of complexity, originating from the ability to couple the resulting free radicals with a wide range of partners. First, this review article discusses the history and synthesis of organic peroxides to provide the context necessary to understand this methodology. Then, it highlights 91 examples of recent applications of the radical functionalization of C–C bonds accessed through the transition metal–mediated reduction of organic peroxides. Finally, we provide some comments about safety when working with organic peroxides.

1.2 Significance of Organic Peroxides

Deconstructive and editing techniques are becoming increasingly popular in organic synthesis, supplementing the constructive processes used traditionally. Among these techniques, C–H functionalization has become an attractive tool for late-stage diversification, converting C–H bonds into C–R bonds. In contrast, C–C activation has received much less attention, perhaps because it is counterintuitive to cleave a C–C bond when synthesizing organic molecules [1]. Nevertheless, C–C bond breaking can be a non-obvious strategy for realizing novel transformations unavailable to traditional constructive processes.

Organic peroxides are powerful precursors for C–C activation. They are readily available high-energy species primed for C–C bond cleavage through O–O scission. The weakness of the O–O bond (ca. 45 kcal/mol, 298 K) provides an opportunity for alkoxy

radical formation through homolysis or reduction [2]. Transition metals are excellent mediators of peroxide reduction, producing alkoxy radicals for subsequent C–C scission. This review article showcases methods developed recently for transition metal–mediated reduction of organic peroxides leading to the breaking and functionalization of C–C bonds. To begin, a brief historical background of radical–peroxide chemistry is provided. The syntheses of organic peroxide are then summarized, followed by contemporary examples of C–C activation. To end, safety concerns relating to peroxides are addressed and future perspectives are put forth.

1.3 Historical Background

The foundation for radicals, peroxides, and their relationship with C–C scission originated with the discovery of synthetic organic peroxides, the preparation of organic radicals, elucidation of the decomposition products of organic peroxides, and the gradual discovery of metal–peroxide redox chemistry. Synthetic organic peroxides emerged in the 1850s, as did the discovery of radicals. The first synthesis of an organic peroxide occured through the acylation of sodium peroxide with benzoyl chloride, reported in 1858 by Brodie (Figure 1.1) [3]. Chemists of the 1850s were also publishing articles related to a new idea: radicals [4,5]. These two concepts—radicals and peroxides—were combined and published a decade later by Brodie [6–8]. Thereafter, in 1900, Gomberg serendipitously prepared triphenylmethyl radical—the first isolation and characterization of a free radical [9]. Formal studies of the generation and reactions of free radicals had begun.

The late 19th century was also pivotal for the chemistry of metals and peroxides. In 1868, Parnell reported the reduction of hydrogen peroxide mediated by ferrous sulfate

[10]. Fenton would clarify this observation in 1894 by chemically altering tartaric acid through the actions of hydrogen peroxide and ferrous salt [11]. Then, in 1932, Häber and Weiss formalized the mechanism of ferrous salt oxidation and peroxide reduction [12]. With the discovery of organic radicals and the redox relationship between metals and peroxides established, it became possible to use metal salts as mediators for the formation of radicals from peroxides.

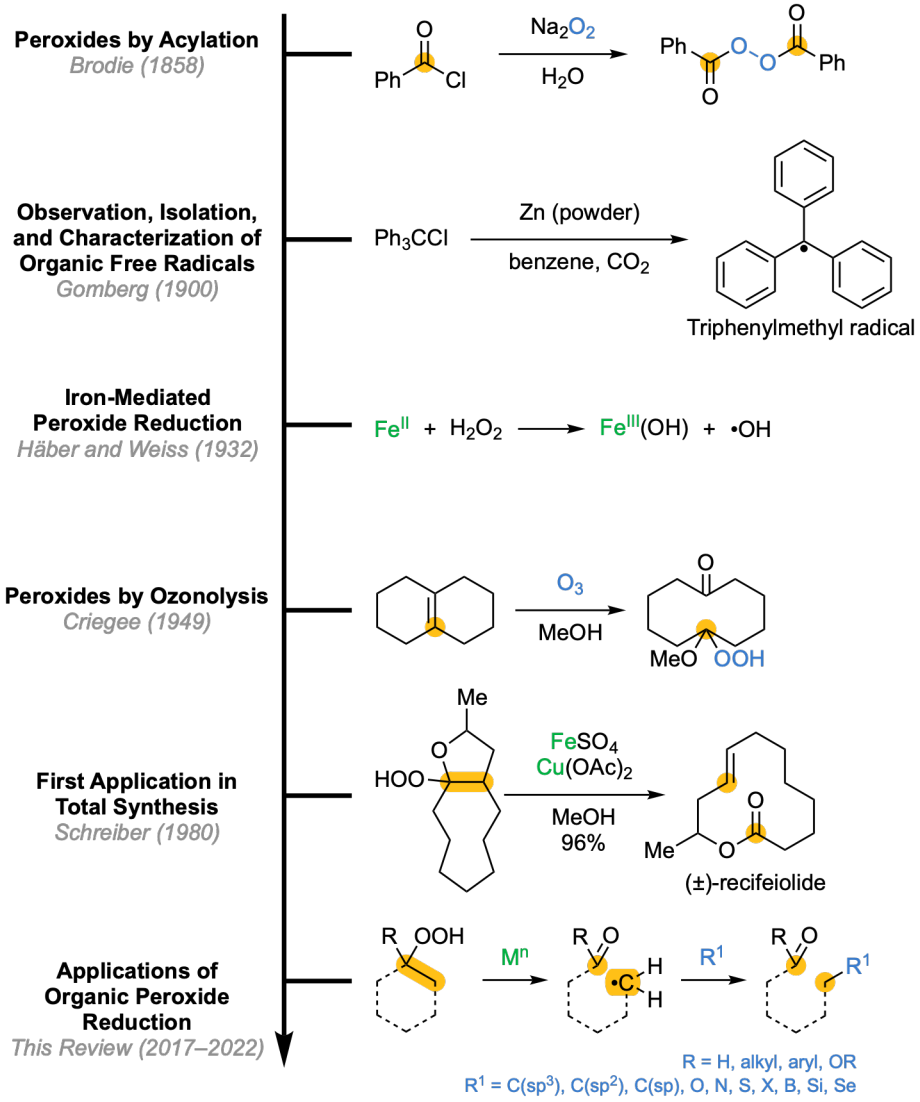


Figure 1.1 Peroxide Chemistry Milestones

Between the 1930s and 1960s, there was an explosion of research relating to the chemistry of organic peroxides. Initial studies involved the thermal decomposition of peroxides. Seminal papers by Gelissen and Hermans described the role of the thermal decomposition of benzoyl peroxide in the formation of polyphenyl derivatives, work that clarified ideas put forth by Lippmann in 1886 [13–16]. The thermal decomposition of peroxides grew beyond acyl peroxides, with Milas' 1930s series, "Studies in Organic Peroxides," covering both thermal decomposition and peroxide synthesis [17]. From these initially studied decomposition processes, ideas emerged for a fragmentation mechanism originating from peroxides. Research by Criegee on the ozonation of alkenes to generate peroxide intermediates supplemented these investigations [18–22]. Notably, in 1946, George and Walsh explicitly reported the concept of β-scission as the mechanism of fragmentation of reduced organic peroxides, thereby formalizing the involvement of radicals in this field of chemistry [23]. In the 1950s, the groups of Raley––Rust–Vaughn, Hawkins, Kharash, and Milas pioneered the use of Fenton's reagent and the Häber–Weiss method for peroxide decomposition, with their results reported in the published series "Decompositions of Di-*t*-Alkyl Peroxides," "Reactions of Organic Peroxides," "The Chemistry of Hydroperoxides," and "Organic Peroxides," respectively [17,24–26]. With the availability of metal salts to mediate peroxide fragmentation, it became unnecessary to heat peroxides to extreme temperatures to initiate their decomposition. From those reports, the predictability of these radical processes was established, and methods to control the decomposition were explored [27–29]. The effects of various metals and solvents were also tested. Together, these discoveries laid the groundwork for the application of radicals in organic synthesis [30–33].

With the accumulated knowledge of the mechanism and fission products of peroxides, the focus of peroxide chemistry shifted toward its applications [34]. Successful efforts to trap the radical intermediates generated at the various stages of the decomposition cascade opened up new areas of research [35]. Publications from Kharasch, Kochi, and Minisci began to emerge, demonstrating the use of ferrous and cuprous salts for the reduction, fragmentation, and subsequent functionalization of organic peroxides [36]. In 1980, the utility of this methodology was realized—and popularized—by Schreiber through the total synthesis of (±)-recifeiolide. In the present day, such studies have been reclaimed, and expanded upon, to provide access to a variety of transformations designed to meet synthetic demands.

1.4 Synthesis of Organic Peroxides

Many standard organic precursors, including alcohols, carbonyls, epoxides, alkyl halides, and olefins, can be transformed into organic peroxides. The first synthetic organic peroxides to be generated were peresters. First reported by Brodie in 1858, the acylation of sodium peroxide with benzoyl chloride in water is the oldest known synthesis of an organic peroxide (Figure 1.2A) [3]. Since then, peresters have interested chemists for their unique stability and ease of synthesis. In the late 1940s, Milas employed aqueous potassium hydroxide and a variety of acid chlorides at 10 to 20 °C to synthesize *tert*-butyl peresters from *tert*-butyl hydroperoxide [37]. A new electrophile, the anhydride, was adopted in the early 1950s by Davies, Foster, and White for the synthesis of peresters. In particular, the reaction of phthalic anhydride and *tert*-butyl hydroperoxide in pyridine at room temperature yielded the mono-perester [38]. In 1963, peresters were first synthesized from carboxylic acids. Hecht and Rüchardt used *N*,*N*-carbonyl-di-imidazole

to activate benzoic acid for the acylation of *tert*-butyl hydroperoxide [39]. More recently, Baj and Chrobok reported the alkylation of alkyl and aryl peracids, using an alkyl sulfonate or oxonium with tetrabutylammonium hydrogensulfate, to generate peresters [40]. These highlighted examples represent only a sampling of the methods available for perester synthesis; for more information, see three reviews articles on peresters that have been published recently [41–43].

In the simplest case, autoxidation involves the insertion of O_2 into a C–H bond to yield an organic hydroperoxide (Figure 1.2B). This technique is limited to weak C–H bonds and is not widely applicable, but it can be useful in certain situations. The earliest examples of intentional autoxidation were reported simultaneously by Bach (in France) and Engler and Wild (in Germany) in 1897; they mixed carbon monoxide with oxygen over water to form percarbonic acid [44,45]. Since then, many reports of autoxidation have appeared. In 1931, Milas published a review of autoxidation, discussing its criteria, classes, and methods of study [46]. Although dated as a practical process, an understanding of autoxidation is important for peroxide synthesis and general safety. Common solvents, such as tetrahydrofuran, can autoxidize into explosive peroxides, as reported by Robertson in 1948 [47]. If the conditions allow, autoxidation can be used as a clean method to add peroxides to organic molecules.

Peroxides are readily synthesized through condensation chemistry from ketones and aldehydes (Figure 1.2C). They can form hemi-peracetals and hemi-perketals, or condense water to form perhydroxyhydrates. One of the first reports of this condensation chemistry was by Wolffenstein in 1895: the synthesis of triacetonetriperoxide (TATP) from acetone and hydrogen peroxide at room temperature [48]. Just last year, in 2021,

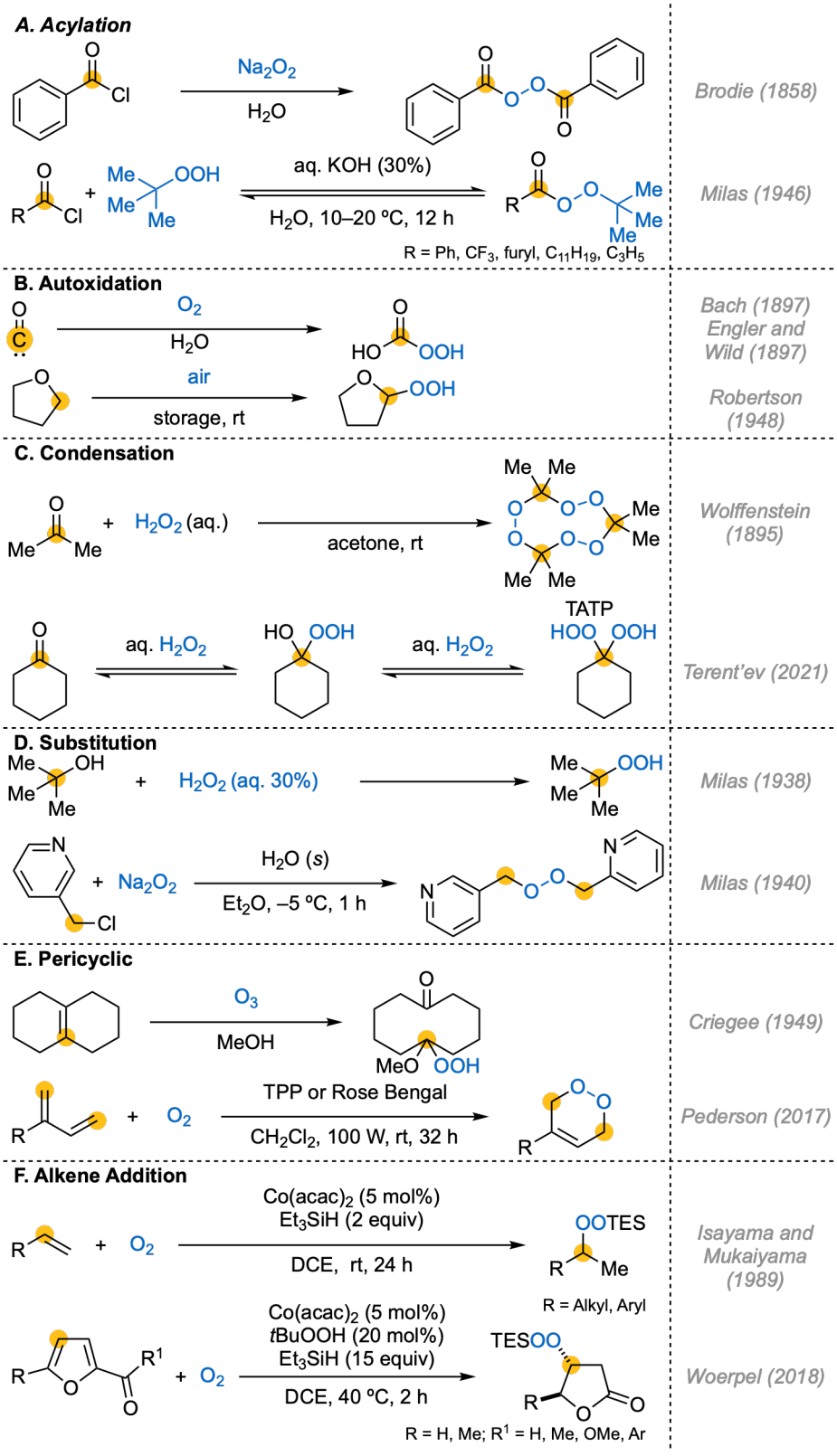


Figure 1.2 Organic Peroxide Syntheses

Terent'ev demonstrated a reaction similar to Wolffenstein's, using cyclohexanone to form the hemi-perketal and perhydrate [49]. In the same year, Terent'ev also reported the use of dicarbonyl species and ammonium acetate to form endoperoxides, demonstrating the compatibility of imines with the peroxide condensation methodology [50].

Classical nucleophilic substitution methods are applicable to organic peroxide synthesis (Figure 1.2D). Hydroperoxides, with increased nucleophilicity, may undergo substitution reactions directly through S_N1 and S_N2 mechanisms [51]. The conditions for the S_N1 process are rather harsh and have inherent limitations. For example, primary and secondary alcohols are not very reactive in S_N1 substitution [38]. Tertiary alcohols can be treated with aqueous hydrogen peroxide to form tertiary hydroperoxides, as exemplified by *tert*-butanol yielding *tert*-butyl hydroperoxide, as reported by Milas in 1938 [52]. The use of an acid catalyst with hydrogen peroxide and *tert*-butanol was demonstrated by Davies and White in 1952 to yield the *tert*-butyl hydroperoxide [53]. A similar process has been used recently by Maruoka to generate tertiary hydroperoxides [54]. For S_N2 reactivity, anionic hydrogen peroxide is typically required. Anionic peroxides are not ideal nucleophiles for S_N2 reactions with alkyl halides because peroxides can inhibit the reaction and promote side reactions [55]. Nevertheless, such reactions are still possible. In 1940, Milas reacted sodium peroxide and nicotinyl chloride in water and diethyl ether to synthesize nicotinyl peroxide [56]. Despite the inherent limitations of substitution reactions, modern techniques allow such routes to organic peroxides that could not be achieved before. In 2013, Dussault reported the alkylation and subsequent hydrolysis of gem-dihydroperoxides with silver oxide, then treatment with refluxing sulfuric acid in methanol, to yield primary hydroperoxides [57]. Peroxides can also readily substitute

other types of electrophiles. For example, epoxides can be opened by hydrogen peroxide to form trans-1,2-hydroxy hydroperoxides, as reported in 2021 by Darcel [58]. New methods using an S_H2 mechanism to form organic peroxides are being developed. Zhong published a technique in 2019 for replacing benzyl halides with hydroperoxides [59]. Using an indium mesh in air, a single electron reduction event forms a benzylic radical for capture by molecular oxygen to install the peroxide. Overall, substitution methods are viable synthetic options for generating organic peroxides.

Pericyclic reactions can quickly generate complexity and are applicable to peroxide synthesis (Figure 1.2E). The oldest pericyclic reaction involving peroxide formation is ozonolysis. In the 1830s, Schönbein first speculated that ozone could react with olefins to generate organic peroxides [60]. One of the most important discoveries thereafter was made by Criegee, who, in 1949, found that a (3+2) dipolar cycloaddition and retro-(3+2) cycloaddition of ozone and 9,10-octalin in methanol formed an α-methoxy hydroperoxide [20,21]. In 1955, the capabilities of ozone and olefins for peroxide generation were expanded upon by Milas, such that Criegee intermediates have since been applied widely in synthesis—with subsequent oxidations or reductions used to formally break the σ- and π-bonds of the original olefin and convert it into a di-carbonyl [61]. Cycloadditions with singlet oxygen have been used to form endoperoxides. One example, from Pearson in 2017, involves triplet oxygen being sensitized *in situ* to singlet oxygen, mediated by a porphyrin (or Rose Bengal) and light (100 W), for stereoselective cycloaddition with a diene [62,63]. The ene reaction adds molecular oxygen alpha to an olefin, thereby allowing peroxide insertion adjacent to olefins. In 2003, Foote and Houk published a Rose Bengal–sensitized ene reaction for the generation of an allylic hydroperoxide [64]. These

sensitized pericyclic reactions do not typically require harsh conditions, making them ideal for peroxide installation. Organic peroxides have also been used in click reactions to add further complexity [65]. With their ability to generate complexity rapidly and their general compatibility with other functional groups, pericyclic reactions are excellent tools for organic peroxide synthesis.

Olefins are not only useful in pericyclic peroxide-forming reactions (Figure 1.2F). A simpler transformation is the Markovnikov addition of a peroxide across an olefin in the presence of an acid, but this method suffers from limitations similar to those of S_N1 reactions. Nevertheless, it is still possible to achieve the Markovnikov addition of a hydrogen atom and a peroxide unit across an alkene. In 1989, Isayama and Mukaiyama reported the application of a cobalt(II) catalyst and triethylsilane under an oxygen atmosphere to achieve the novel hydrosilylperoxidation of an olefin [66]. In 2016, Shenvi published a review article on this transformation, which has been applied successfully in recent years. In 2018, Woerpel used the conditions of Isayama–Mukaiyama hydrosilylperoxidation to functionalize furans with silylperoxides [67]. Consistent with a finding from Isayama and Mukaiyama, *tert*-butyl hydroperoxide was added to decrease the induction period for the reaction. Woerpel also demonstrated the applicability of this chemistry with enones as substrates (in 2019) and for the direct hydroperoxidation of olefins (in 2021) [68–70. Other additions across olefins are also possible. The Li group developed a trifluoromethythiylation–peroxidation of alkenes and allenes in 2020 by using a cupric catalyst and potassium persulfate to add *tert*-butyl hydroperoxide and trifluoromethylthianate to an olefin [71]. Li also demonstrated the germylperoxidation of alkenes in 2022, using germyl hydride and a cuprous catalyst [72]. Furthermore, in 2020,

Wu used sodium molybdate–glycine as a catalyst for hydrogen peroxide to transform allylic alcohols into *cis*-2,3-diol-*trans*-hydroperoxides in one pot [73].

1.5 C–C Scission

Organic peroxides are highly energetic species that are primed for chemical reactions. As opposed to thermal or photolytic processes, catalytic quantities of transition metals, including iron and copper, can offer semi-controlled single-electron pathways through which the energy of peroxides can be harnessed for useful chemical transformations. Because of the redox capabilities of metals, these reactions do not need to be performed stoichiometrically, but rather catalytically, with two benefits. First, the side reactions of the free radicals are limited, because the quantity of radicals generated is restricted by the concentration of the reduced metal ions. Second, lower quantities of total metal are required, thereby decreasing both the expense and environmental impact. This section focuses on reports from the last five years regarding metal–mediated reduction of organic peroxides to achieve C–C activation for alkylation [C–C(sp^3)], hydrogenation (C–H), amination (C–N), amidation (C–NHCO), azidation (C–N_3), cyanation (C–C≡N), halogenation (C–X), chalcogenation (C–O/C=O, C–S, or C–Se), olefination (C–C=C), arylation (C–Ar), alkynylation (C–C≡C), allylation (C–C–C=C), borylation (C–B), and silylation (C–Si). With such a large variety of transformations available, this methodology is compatible with most synthetic needs.

1.5.1 Mechanism

In general, methodologies involving the reduction of organic peroxides follow the generalized steps in Figure 1.3A. First, in step A, single-electron transfer (SET) from the

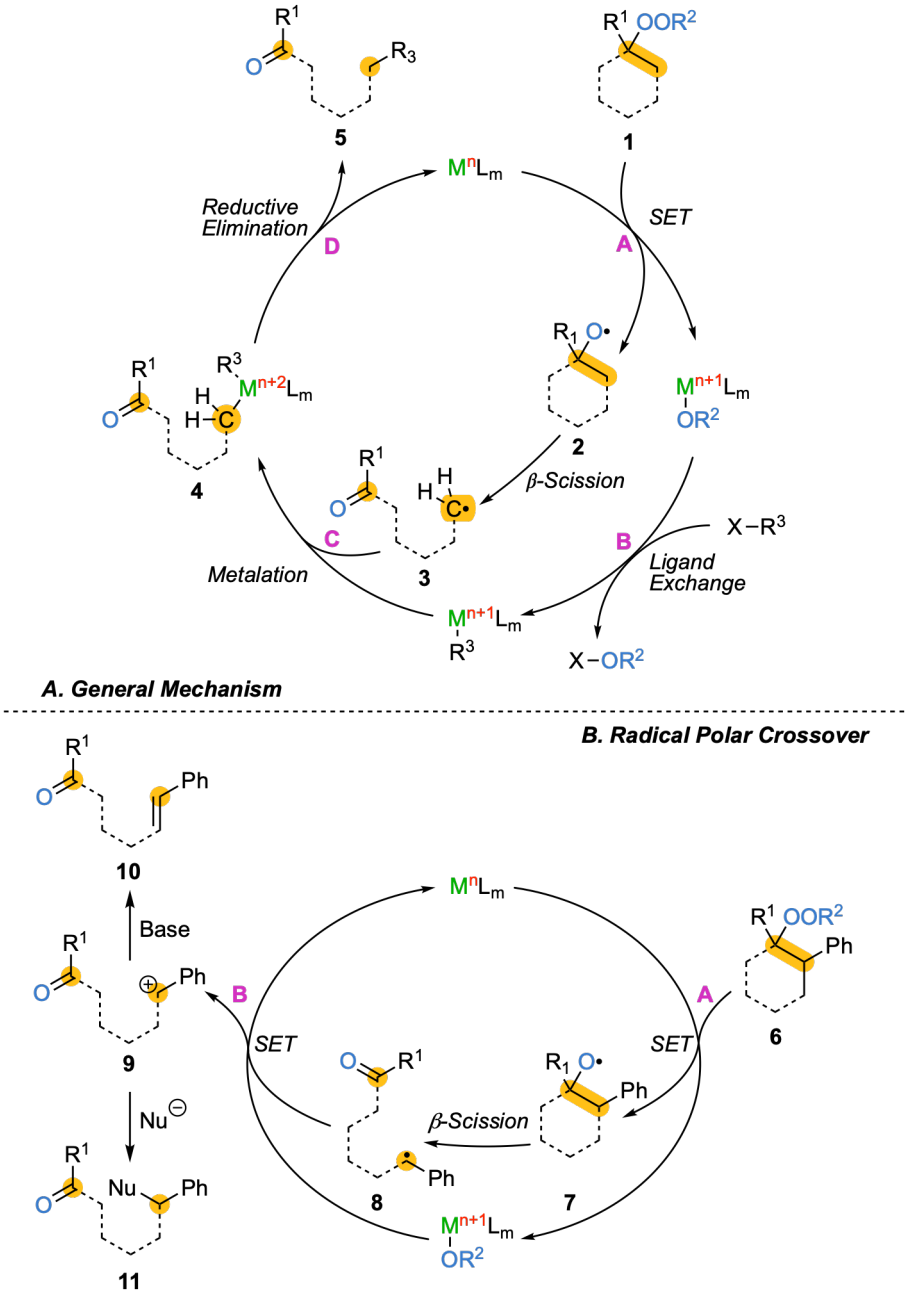


Figure 1.3 Mechanistic Overview

metal to the peroxide **1** mediates the formation of the alkoxy radical **2**. Subsequent β-scission, or decarboxylation with acyl peroxides, of the alkoxy radical **2** leads to the carbonyl–alkyl radical **3**. The regioselectivity of the C–C cleavage is dependent on the stability of the resulting radical [74]. The alkoxide formed during this step coordinates to the oxidized metal ion. Next, in step B, a ligand exchange swaps the alkoxide for the

coupling partner R^3. Subsequently, in step C, the metal coordinates with the alkyl radical **3** to form the metal–alkyl complex **4**. Finally, in step D, reductive elimination releases the product **5** and restarts the catalytic cycle. Some coupling partners do not participate in the ligand exchange step, but can couple directly to the alkyl radical. In these examples, the metal acts simply as a reducing agent, and is used in a stoichiometric quantity.

While most of the methodologies covered in this review article follow the general mechanism, some substrates are known to participate in a radical–polar crossover mechanism shown in Figure 1.3B. In step A of this mechanism, SET from the metal reduces the peroxide **6** to an alkoxy radical **7**. After β-scission, or decarboxylation with acyl peroxides, the benzylic radical intermediate **8** remains. The catalyst is regenerated in step B when the higher oxidation metal formed during step A oxidizes the benzyl radical intermediate **8** to the benzyl carbocation **9**, crossing over from a radical to a polar species. The fate of carbocation intermediate **9** depends on the presence of a base or a nucleophile. With base, styrenyl product **10** is generated in an E1-type fashion**.** However, in the presence of a nucleophile, the benzylic carbocation **9** is trapped to form adduct **11**. Of note, it is possible that the radical intermediate **8** performs radical couplings, such as addition to alkenes, before oxidation in step B.

1.5.2 Alkylation

Reactions that break and build C–C σ-bonds in one pot are powerful. As early as 1950, Hawkins first noted that alkyl radicals from peroxide degradation could be trapped by carbon species to form new C–C bonds [75]. Upon addition of ferrous sulfate to a methylcycloalkyl hydroperoxide, with no designated radical trap, two separate alkyl radical species dimerized to form a new C–C bond (Figure 1.4). Many years later, several

papers appeared concerning radical alkylation from peroxides. In 2018, Bao and Li reported the use of light to activate a ruthenium complex to an excited state for the reduction of copper(II) to copper(I) [76]. This cuprous species mediates SET to the diacyl peroxide to form an alkyl radical after rapid decarboxylation. The alkyl radical undergoes carbonation with the olefin to form a benzyl radical. By radical–polar crossover this radical is then oxidized by ruthenium(III) to form a benzyl cation, which is trapped by nucleophilic fluoride to yield the product. In 2018, Du reported that iron(II) mediates a similar SET process with a perester, providing an alkyl radical post-decarboxylation [77]. After carbonation into a cinnamimide, the benzyl radical is trapped through cyclization to form a dihydroquinolinone radical species. With an oxidation from iron(III) and base in radical–polar crossover fashion, a neutral dihydroquinoline remains. Also in 2018, Sodeoka reported using copper with bis(chlorodifluoroacetyl) peroxides to form allyl chlorodifluoromethyl groups and β-chlorodifluoromethyl aziridines [78]. The proposed mechanism involves a reduction event followed by decarboxylation to yield a chlorodifluoromethyl radical which adds into an alkene. Subsequent oxidation of the resulting radical returns the copper(I) catalyst and generates a carbocation. Basic conditions promote the formation of allyl chlorodifluoromethyl groups upon elimination. Alternatively, aziridines may be formed through addition of a neighboring amine to the carbocation, exemplifying the great synthetic utility of this process.

In 2018, the Zhu group reported five different types of radical methylation. The first was termed alkoxy methylation [79]. A copper(I) species reduces dicumyl peroxide, producing methyl radicals. This radical adds into a styrene derivative to form a benzyl

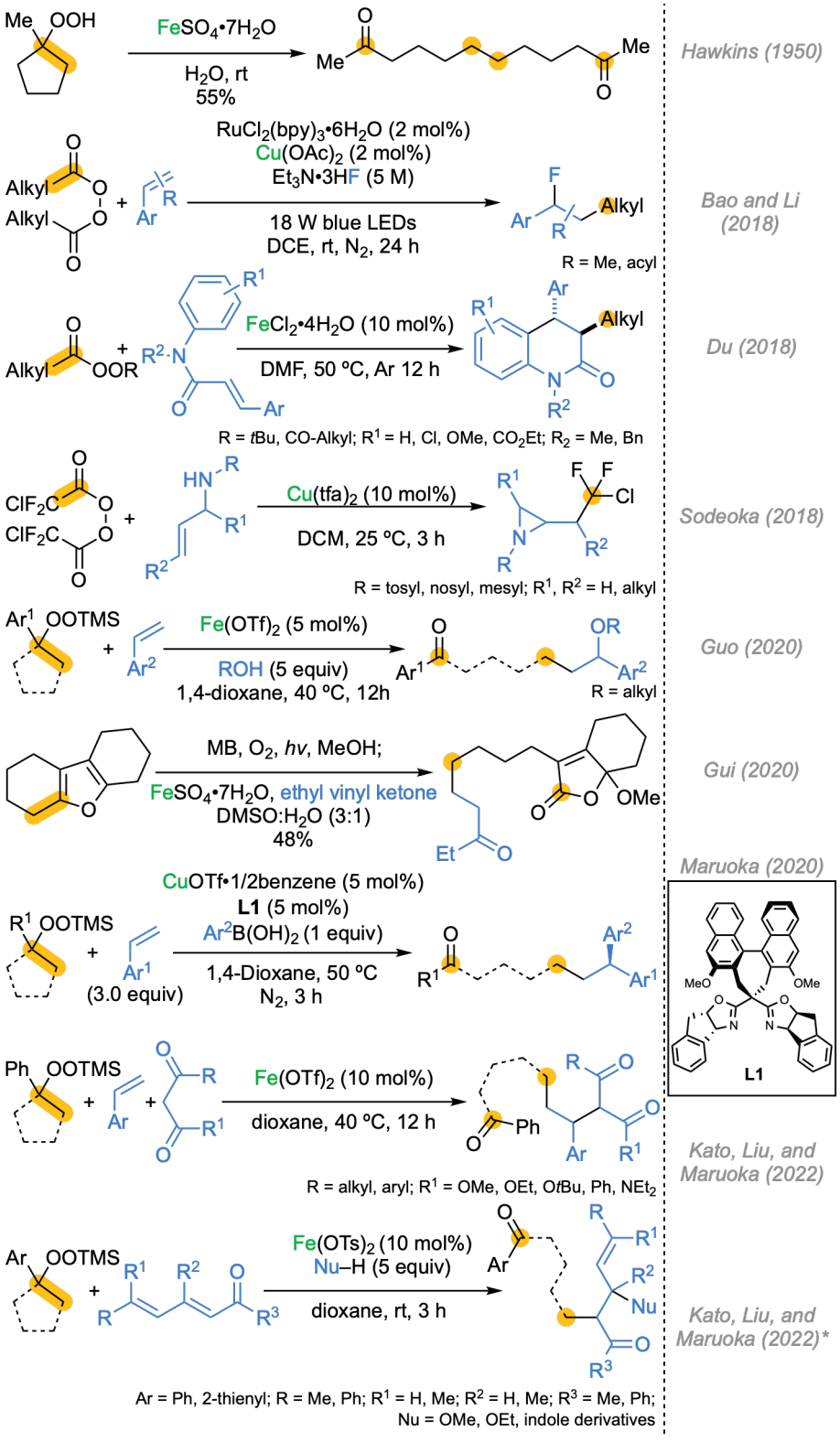


Figure 1.4 Alkylation

*only the major β-product is shown, the δ-adduct is minor

radical. The resulting copper(II) species oxidizes the benzyl radical to a benzyl carbocation through a radical–polar crossover, which is then trapped by a nucleophilic alcohol. The second method uses the same strategy, except that the resulting benzyl carbocation is trapped by lithium azide, achieving azido-methylation. The final three methods are intramolecular ring closing strategies for forming cycloethers, lactones, and cycloamines, where the benzyl carbocation is trapped by alkoxides, carboxylates, and sulfonamides, respectively.

The Bao group, in 2020, reported the use of catalytic iron(II) to methylate 1,1-disubstituted alkenes [80]. The methyl radical, which arises from lauroyl peroxide through β-scission, adds into the terminal side of a 1,1-disubstituted alkene that contains an aryl group and an electron-withdrawing group. Coupling of the resulting benzyl radical to form the azido product is mediated by an iron(III) azido species that was generated *in situ* through a ligand exchange. In the same year, the Bao group also reported the alkylarylation of styrenes [81]. In these cases, catalytic amounts of a cuprous species are used to reduce the diacyl peroxide to an alkyl radical through β-scission. Similarly, the radical adds into the alkene to form the benzyl radical. Meanwhile, the copper(II) species undergoes ligand exchange with the arylboronic acids and, through the effects of copper(III) and reductive elimination, gives the geminal-diaryl product. Also in 2020, the Guo group reported the iron(II) triflate–mediated opening of cyclopentyl silylperoxides to alkyl radicals. The radicals are, again, trapped by various styrene derivatives for alkylation [82]. In this case, the benzyl radical is oxidized to a benzyl carbocation and trapped by an alkoxy group. Finally, the Gui group demonstrated that radical alkylation could be achieved through intermolecular reductive radical addition when using iron(II) sulfate

heptahydrate [83]. For their reaction, singlet oxygen generated from photosensitization with methylene blue (MB) engages in a (4+2) cycloaddition with a furan to form an endoperoxide. In the presence of methanol, a simple substitution yields the hydroperoxide which serves as the reactive species for reduction. The Gui group uses these oxidation conditions for a few other types of reductive functionalizations.

From 2020 to 2022, the Maruoka group released several papers concerning radical alkylation. Their first publication was related to the report from Bao in 2020 regarding the alkyl radical from β-scission being trapped by a styrene, with ligand exchange between the copper(II) species and arylboronic acid resulting in radical alkylation and copper-mediated coupling [84]. The difference was that the Maruoka group used cycloalkyl silylperoxides, rather than diacyl peroxides, with their method being the first instance of a catalyst-controlled enantioselective radical addition. Two other papers from the Maruoka group featured cycloalkyl silylperoxides. One report, from Kato and Maruoka in 2021, described the use of perfluoroalkyltrimethylsilanes and silyl enol ethers (both cyclic and acyclic) as radical traps [85]. Interestingly, the reactions that used the silyl enol ethers as radical traps required the presence of potassium fluoride and [18]crown-6 to avoid significant side reactions. Also in 2021, the Maruoka group reported twice that methylene activated by two electron-withdrawing groups could be used to trap alkyl radicals when using a copper(I) catalyst [86,87].

To complete the cases from 2021, the Sodeoka group provided two reports demonstrating perfluoroalkylation. The first is an example of mono-perfluoroalkylation of an alkene with a copper(I) salt to form an allylic perfluoroalkyl group [88]. The perfluoroalkyl radical originates from a perfluoroalkyl anhydride that is transformed into

an organic peroxide using urea and hydrogen peroxide. Their subsequent example is similar in that it also uses a perfluoroalkyl anhydride with urea and hydrogen peroxide to form the organic peroxide and employs a copper(I) salt to catalyze radical formation. The difference lies not only in the addition of a 2,2-bipyridine (bpy) ligand to promote bis-perfluroalkylation, instead of mono-perfluoroalkylation, of alkenes and alkynes but also in a transition from catalytic to stoichiometric copper loading [89]. Moving into 2022, the Maruoka group reported the use of alkyl radicals that were trapped by styrenes [90]. Upon regeneration of iron(II) from radical–polar crossover by promoting the benzyl radical to a benzyl carbocation, the reaction was completed with trapping from anionic β-keto carbonyl derivatives. Finally, Maruoka's most recent report demonstrated that the alkyl radical from a cycloalkyl silylperoxide and an iron(II) catalyst could be trapped by a dienone [91]. Because nucleophiles could be trapped on the allylic carbocations, it is proposed that the alkyl radical is oxidized to a carbocation in a radical–polar crossover fashion.

1.5.2 Hydrogenation

Replacement of a C–C bond with a C–H bond is a common functionalization option. The first reports of radical hydrogenation through peroxide degradation were provided by Kharasch and Hawkins, both in 1950. Kharasch reported that the reduction of cumyl hydroperoxide by iron(II) releases a methyl radical, which could be trapped by a hydrogen atom from dextrose to form methane gas (Figure 1.5) [92]. Hawkins discovered another hydrogenation product when conducting experiments concerning the dimerization mentioned in the "Alkylation" section [93]. When reducing cyclopentyl methyl

hydroperoxide with ferrous salt, one of the products purified through distillation was 2-hexanone. These examples of hydrogenation were not intended products.

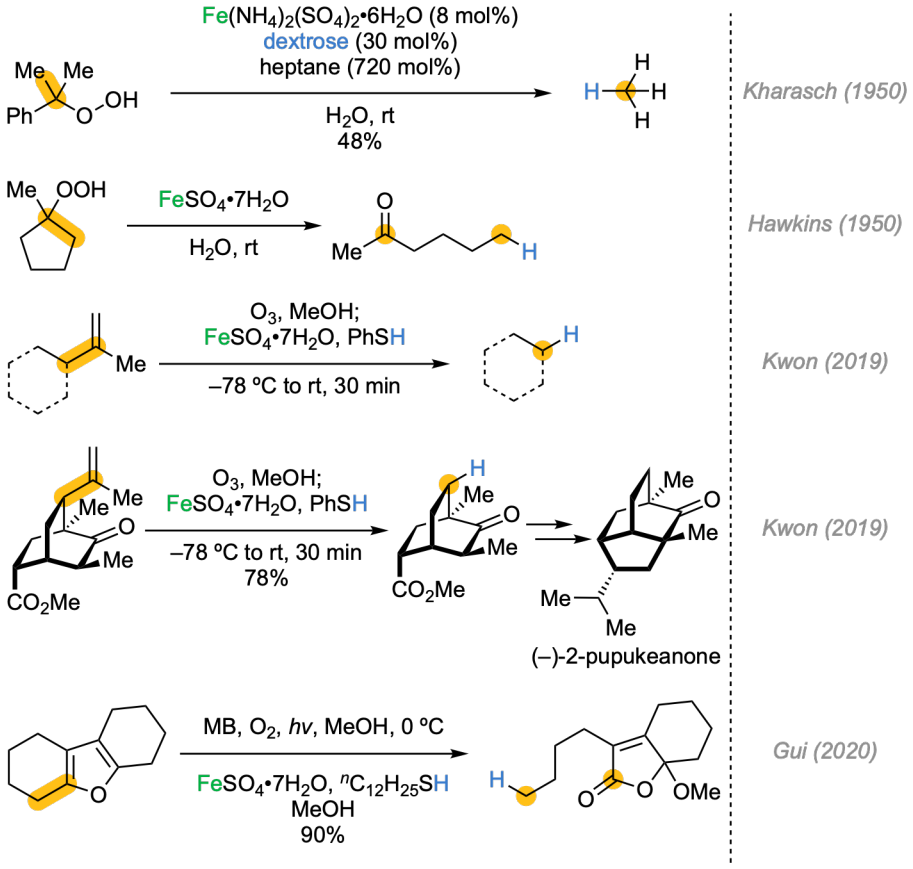


Figure 1.5 Hydrogenation

Almost 70 years later, deliberate hydrogenation was achieved by the Kwon group. In 2019, they realized that the Criegee intermediate from ozonolysis could be trapped with methanol and used as the peroxide for hydrogenation in an iron(II)-mediated process. By bubbling ozone into a methanol solution containing a terpenoid at –78 °C, the Criegee hydroperoxide forms; with immediate addition of an iron(II) salt, alkyl radicals form and are trapped by hydrogen atom donors. The first in this series of reports described hydrogenation, where benzenethiol was selected as the hydrogen atom donor. The power of this type of process is highlighted by the synthesis of (–)-2-pupukeanone, where a dealkenylated [2.2.2]-bicyclic ketoester was achieved in one step, in contrast to the six

steps required previously [94]. Finally, Gui demonstrated that hydrogenation was possible in butenolide formation when using iron(II) sulfate heptahydrate and a mercaptan as the hydrogen donor [83].

1.5.3 Nitrogenation

Methods for direct coupling to nitrogen atoms are essential for chemical synthesis, particularly because nitrogen is one of the six most common elements for life on Earth, and because over 75% of medicines today feature nitrogen atoms. One of the first uses of nitrogen as a radicophile for radical peroxide degradation was reported by Minisci in 1958 (Figure 1.6A). When a cyclohexyl hydroxyhydroperoxide was reacted with ferrous sulfate, the alkyl radical from β-scission was trapped by nitric oxide, forming an alkyl nitric oxide intermediate. With water as a solvent and an excess of nitric oxide, the alkyl nitric oxide group was converted to an aldoxime in 18% yield [95]. Amination was reinvestigated by the Maruoka group in 2019, using cycloalkyl silylperoxides, a catalytic amount of a cuprous iodide/phenanthroline complex as a reducing agent, and aniline derivatives as radical traps [96]. This approach was explored in 2020 by Gui, with furan oxidation used to form a hydroperoxide for fragmentation with iron sulfate heptahydrate and trapping with di-*tert*-butyl azodicarboxylate (DBAD) to generate the new C–N bond [83]. The most recent example was reported by the Li group in 2021, where diacyl peroxides and a cuprous/phenanthroline catalyst produced alkyl radicals through decarboxylation for trapping by various arylamine derivatives [97].

Another class of C–N bond formation is amidation (Figure 1.6B). Two examples have been reported by the Maruoka group, each using a cuprous iodide–mediated process to

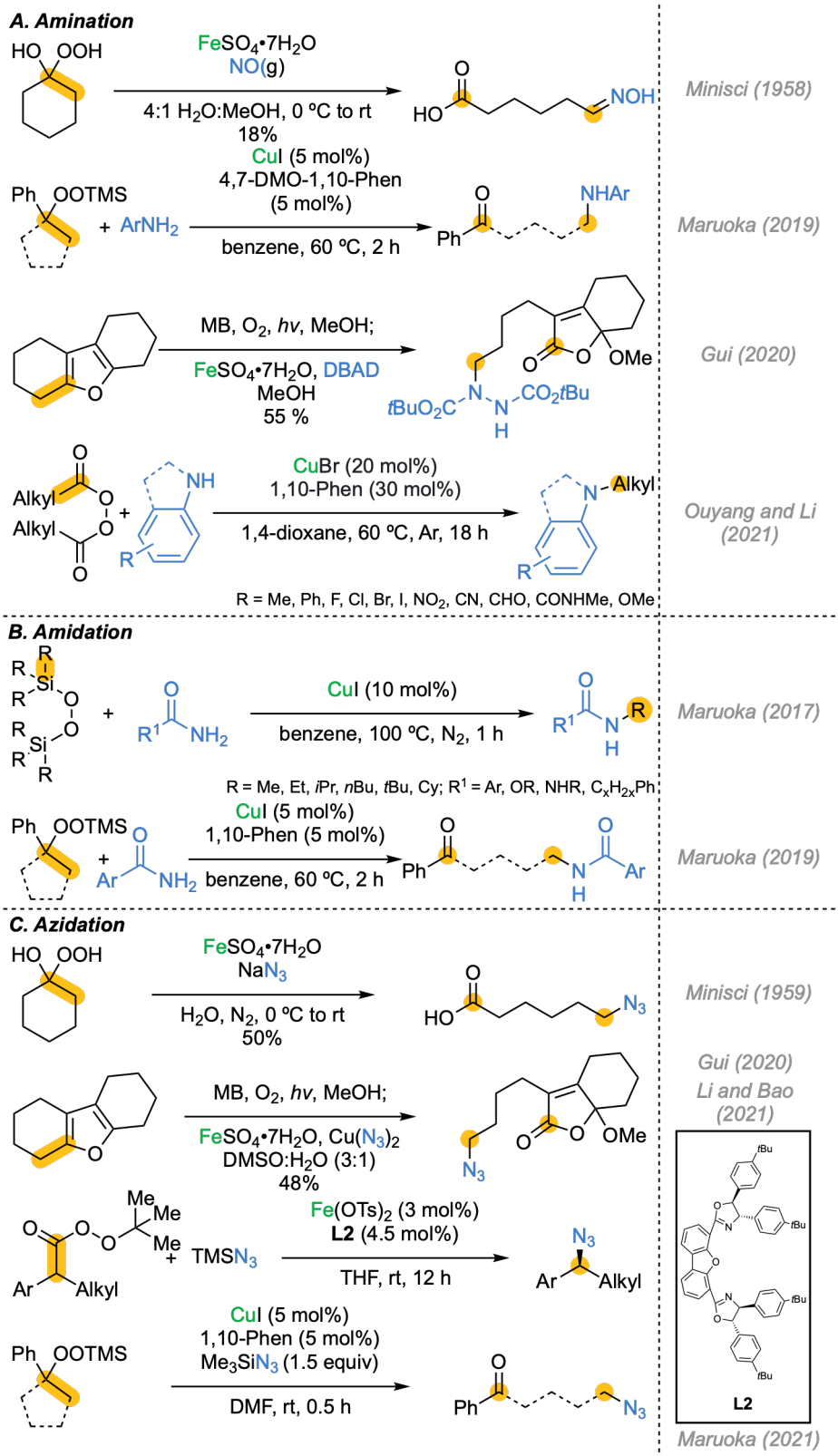


Figure 1.6 Nitrogenation

quench alkyl radicals from both cyclic and acyclic alkyl silylperoxides with primary arylamides. In their reports from 2017 and 2019, they provided many examples of amidation by varying the silylperoxide and the amide [96,98]. These experiments demonstrated the versatility of radical amidation to provide diverse products.

The final class of nitrogenation is azidation (Figure 1.6C). The first example was reported by Minisci in 1959, where cyclic hydroxyhydroperoxides were used with ferrous or cuprous salts and sodium azide to achieve radical azidation [99]. Azidation reappeared when the Gui group, in 2020, trapped their alkyl radical with copper(II) azide [83]. In 2021, Li and Bao demonstrated an enantioselective decarboxylative azidation involving a chiral ligand, ferrous triflate, and trimethylsilylazide [100]. Remarkably, this reaction achieved enantiomeric excesses of up to 92%. Azidation was further studied by the Maruoka group in 2021; like Minisci, they used cyclic silylperoxides. Through the standard cuprous/phenanthroline mechanism, the azidation from trimethylsilyl azide was successful in trapping the alkyl radical [85]. Their next two papers on this subject, from 2021 and 2022, also concerned azidation, but the starting material was a cyclic hydroperoxide that was transformed into an alkyl silylperoxide *in situ* from the trimethylsilylazide, which doubled as the azide source [54, 101].

1.5.4 Cyanation

Minisci, in 1959, was the first to add nitriles to the alkyl radicals formed through transition metal–mediated reduction of hydroperoxides (Figure 1.7A). Here, cuprous cyanate and potassium cyanate were used to achieve this transformation [99]. This approach remained dormant for over six decades, until Gui and Kato, Liu, and Maruoka reported their studies of cyanation in 2020 and 2021, respectively. Displaying versatility

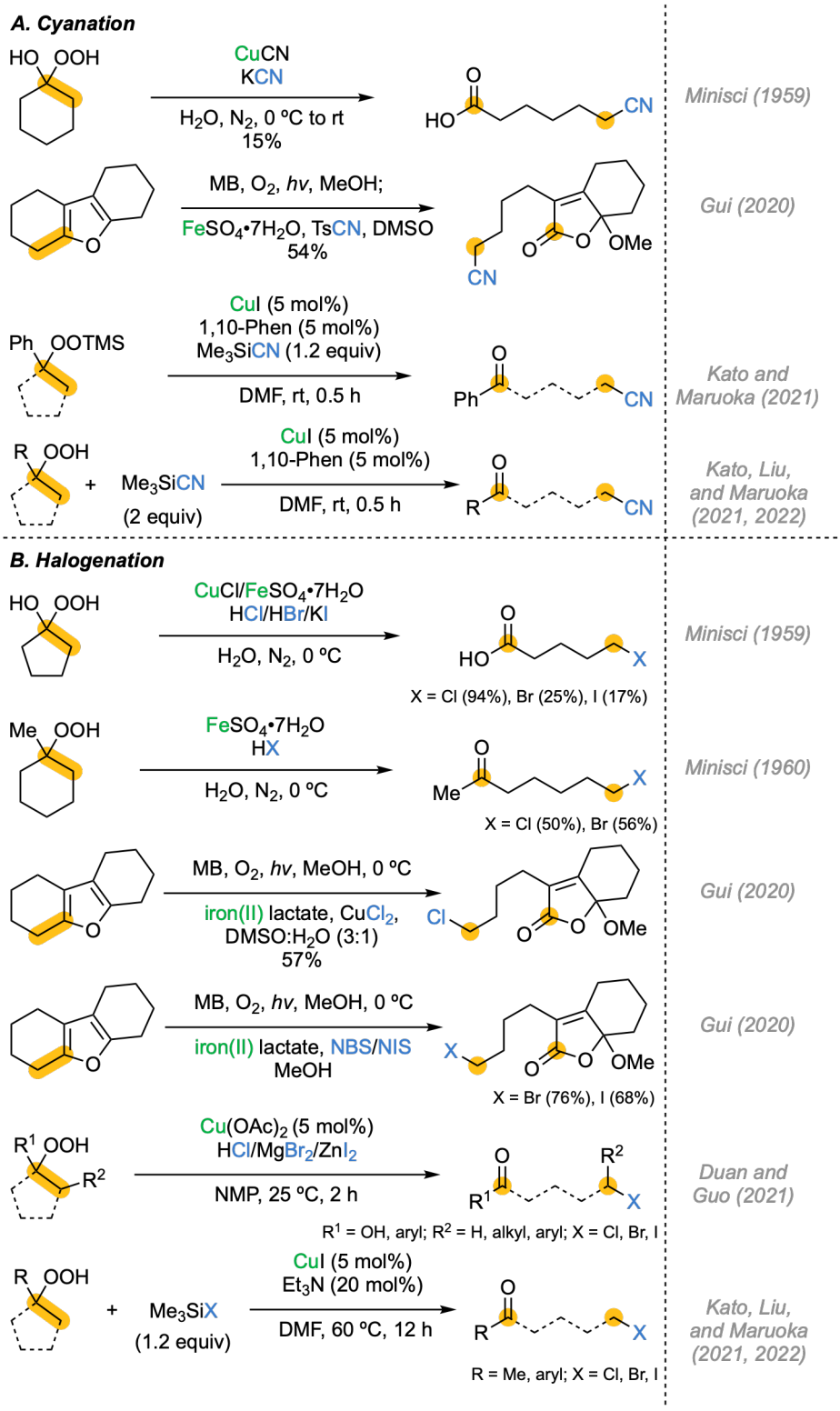


Figure 1.7 Cyanation and Halogenation

for butenolide formation, the resulting alkyl radical was trapped using tosyl cyanide [83]. Again, copper was the metal of choice, with the nitrile originating from trimethylsilyl cyanide [85]. Another two papers from the Maruoka group, one in 2021 and the other in 2022, employed the same reagents, but with an alkyl hydroperoxide to generate the reactive intermediate *in situ* [54, 101]. The further application of these products, after introduction of cyanate or thiocyanate groups, is promising.

1.5.5 Halogenation

Organic chlorides, bromides, and iodides participate in a variety of chemical reactions: they are good leaving groups, they can be converted into nucleophiles through metal–halogen exchange, and they are common precursors of alkyl radicals. In addition, their installation is relevant for certain medicinal purposes. In turn, the alkyl radicals generated from β-scission of alkoxy radicals are readily functionalized into alkyl halides. Seminal work in this area was published in 1959 and 1960 by Minisci, who used halohydric acids as halogen pools and ferrous or cuprous salts to reduce cycloalkyl peroxides (Figure 1.7B) [102–104]. More recently, acids, inorganic salts, and organic halogens have been demonstrated as halogen donors, providing reactivity equivalent to that obtained through reduction of peroxides. In 2020, the Gui group demonstrated chlorination, bromination, and iodination by trapping the radicals with copper(II) chloride, *N*-bromosuccinimide, and *N*-iodosuccinimide, respectively [83]. In 2021, Guo reported the use of hydrochloric acid, magnesium bromide, and zinc iodide as halogen sources [105]. In the same year, and in 2022, Maruoka employed triethylamine with trimethylsilyl chloride, bromide, and iodide as halogen sources to obtain the desired products from alkyl hydroperoxides [54, 101]. These newer methods avoid the use of strong acids and are more compatible with labile

functional groups. Halogenation in this manner offers a pathway to simultaneously install a leaving group while breaking C–C bonds.

1.5.6 Chalcogenation

Chalcogenation is one of the more conceptually straightforward types of reactivity stemming from peroxide fragmentation. Two of the most well-established radical trapping reagents are diphenyl disulfide and 2,2,6,6-tetramethypiperid-1-yloxy (TEMPO), both of which readily trap alkyl radicals arising from C–C scission, forming C–S and C–O bonds, respectively. The first example of a carbon–chalcogen bond formed through radical peroxide degradation was published by Minisci in 1959 (Figure 1.8A) [106]. Here, ferrous and cuprous salts were used to promote the formation of alkyl radicals, with a thiocyanate group as the radical trap. In 2019, Kwon reported that this reactivity resulted from ferrous sulfate heptahydrate–mediated reduction of α-methoxyhydroperoxides generated by ozonolysis and trapping with diphenyl disulfide [107]. In 2020, the Gui group demonstrated fluoromethylthiylation, thiylation, and thiocyanation when using various sulfur-containing radical traps [83]. Using diphenyl disulfide, in 2021 Guo reported that ferric triflate could reduce tertiary hydroperoxides, achieving a similar result with ring-opening capabilities [108].

For C–O bond formation, the most common radicophile is TEMPO, which has been used widely as an experimental tool to prove the presence of radicals. The first instance of an alkyl radical originating from a peroxide being trapped with oxygen-containing species aside from TEMPO, was achieved by the Maruoka group in 2019 (Figure 1.8B). Here, the reactivity was very similar to that in the amidation described previously by the Maruoka group, except that they used free carboxylic acids as nucleophiles, rather than

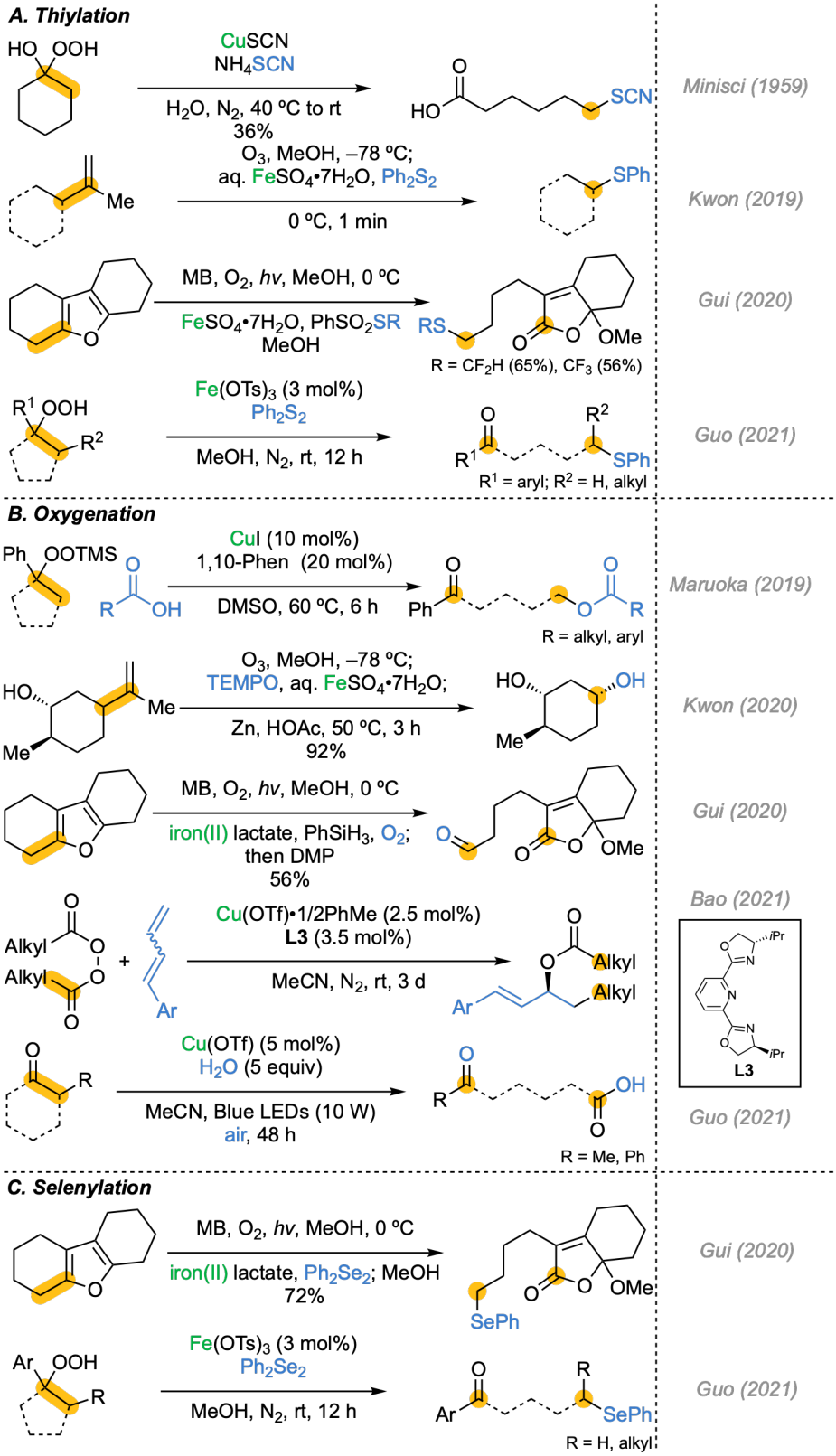


Figure 1.8 Chalcogenation

primary amides [96]. The intentional use of TEMPO for C–O and C=O bond formation was reported by the Kwon group in 2020 [109]. Hydroperoxides formed through ozonolysis in methanol, followed by reduction with ferrous sulfate heptahydrate in the presence of TEMPO, created the C–O bonds. Then, under reductive conditions (using zinc dust and acetic acid) or oxidative conditions [with magnesium bis(monoperoxyphthalate) (MMPP)], the 1-hydroxy-2,2,6,6-tetramethylpiperidine (TEMPOH) unit was removed, leaving behind a hydroxyl or carbonyl group, respectively. The Gui group, in 2020, applied oxygenation in a unique way: oxygenating cycloalkyl-fused furans [84]. Selective oxygenation of the furan system with singlet oxygen, followed by immediate addition of iron(II), led to formation of a butenolide and an alkyl radical, with concomitant oxidation of the ferrous salt. This radical was then trapped by oxygen to give a mixture of an alcohol and an aldehyde. Oxidizing or reducing agents could be used to prepare either the carbonyl or the alcohol selectively [83]. The following year, Bao demonstrated radical carboesterification of dienes. The alkyl radicals are formed by decarboxylative β-scission upon reduction of a diacyl peroxide by copper(I). With a chiral ligand, the carboxylate generated is coupled to the allyl radical intermediate to form the product. Two different chiral ligands were reported to provide each enantiomer with enantiomeric excesses of up to 94% [110]. Also in 2021, Maruoka published two reports on O-alkylation. In the first, appearing in July, various silylperoxyacetals were reduced by the iron(II) species formed *in situ* from the oxidation of TEMPO by iron(III) triflate. The resulting alkyl radical was trapped by an additional equivalent of TEMPO [111]. In the second, published in November, a pyridinyl-imidazole–based ligand was used with a cuprous species to reduce an alkyl silylperoxide that was trapped with phenol derivatives

[112]. To complete this overview of oxygenation processes, in June of 2021 Guo demonstrated that cycloalkanones could be cleaved to yield various keto acids. It was proposed that copper(II) triflate enolizes the ketone, with blue light excitation promoting the formation of a peroxide intermediate. Although the authors suggested two likely mechanistic pathways, the absolute mechanism remains elusive. Overall, reduction of the O–O bond results in two carbonyl species [113].

Incorporation of selenyl groups into organic molecules can occur through radical processes (Figure 1.8C). In 2020, Gui reported the trapping of an alkyl radical with diphenyl diselenide during butenolide formation [83]. A year later, Guo published the selenylation of alkyl radicals generated through the reduction of tertiary hydroperoxides [108]. In this process, ferric tosylate was used as the catalyst, with diphenyl diselenide as the selenyl source. Instead of the transmetalation step observed for some other modes of reactivity, the alkyl radical could add directly to the Se–Se bond to form a selenyl radical. The selenyl radical could release an electron to the ferric species and form a Se–O bond, thereby restarting the catalytic cycle.

1.5.7 Olefination

Olefins are multipurpose functional groups. They build rigidity through their defined geometry, and they are used extensively in organic synthesis because of their compatibility with a vast number of chemical reactions. Pertinent to this review article, excised alkyl radicals have been demonstrated to undergo copper(II)- and iron(III)-mediated oxidation processes, yielding olefins.

The oxidation of alkyl radicals to alkenes is well established. In 1961, De La Mare, Kochi, and Rust outlined the basis of this transformation (Figure 1.9) [114]. Initially,

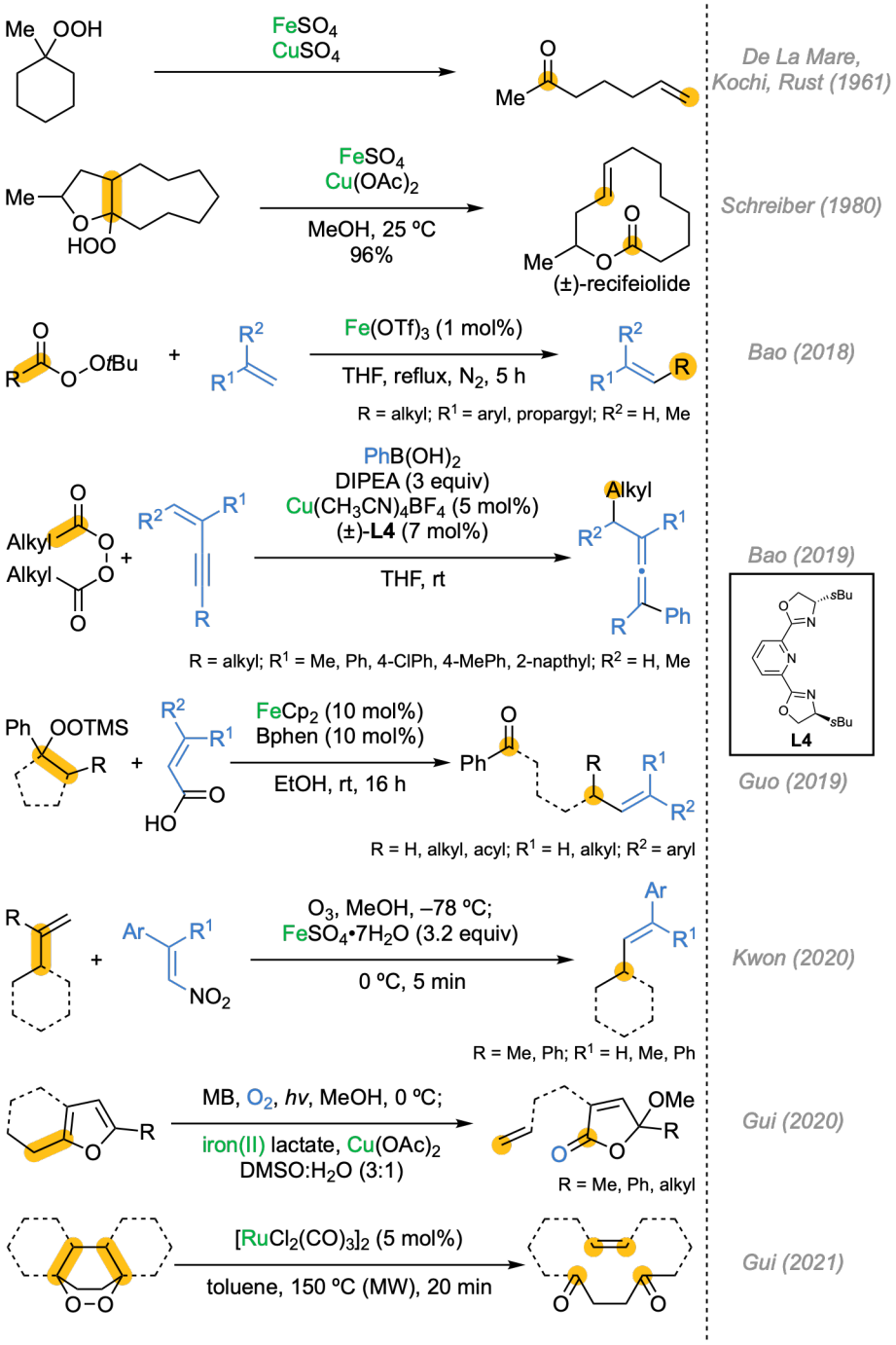


Figure 1.9 Olefination

ferrous salts were used to reduce the peroxide, generating an alkoxy radical for β-scission. The alkyl radical resulting from β-scission was oxidized by a cupric salt in solution, generating an olefin. The application of this reaction to the total synthesis of the natural product (±)-recifeiolide was realized by Schreiber in 1980 [115].

Since the 1980s, radical olefination from peroxides has been employed only sporadically, but it was picked up again by the Bao group in 2018 [116]. This time, the olefin served as the radicophile. The alkyl radicals formed from decarboxylation of a *tert*-butyl perester were added into an olefin with the aid of an iron(III) catalyst. Via radical–polar crossover, the resulting radical species was oxidized to a carbocation where a base promoted the elimination to yield the olefin product. The Bao group also applied the same methodology for use with tertiary propargyl alcohols, with the novelty stemming from a tandem SET/Lewis acid cycle [117]. The Lewis acid cycle helped eliminate the original alcohol *in situ*, forming terminal 1,3-enynes, to which the alkyl radical added. Both of these reports utilized radical–polar crossover and base to form the resulting olefin. Direct use of the 1,3-eneyne was demonstrated by Bao in 2019 [118]. Through a similar mechanism, this ligand-mediated copper(I)-catalyzed process first forms a propargyl radical with a stable allenyl radical resonance form, followed by trapping of the alkyl radical with an arylboronic acid to form an allene product. In another report in the same year, the group published a similar reaction in which the radical was trapped by a trimethyl cyanide [119].

Radical olefination has also been pursued by the Guo and Kwon groups with the use of peroxides and iron(II) catalysts. In 2019, the Guo group used cycloalkylsilyl peroxides and β-scission to form alkyl radicals [120], which then added into the olefinic units of cinnamic acids. Oxidation of these species enabled a decarboxylation pathway to form the stable olefin products. In 2020, that group also reported the olefination of alkyl radicals with styrene derivatives [82]. Here, the ferric species in solution could oxidize the persistent benzylic radical to form the olefin and restart the catalytic cycle. The Kwon group used a dealkenylative approach for alkenylation. The alkyl radical generated was

added to a β-nitrostyrene, with subsequent β-elimination of the nitro group forming the olefinated product [121]. In the Gui publication mentioned previously, the largest portion of the substrate scope involved olefination [83]. Using copper(II) acetate and no designated radical trap, the resulting radical was transformed into a monosubstituted alkene. Finally, the Gui group also reported ruthenium(II)-catalyzed endoperoxide fragmentation. From bicyclic endoperoxides, the ruthenium catalyst mediated the O–O bond cleavage to facilitate the formation of two ketones and an olefin. The power of this method was exemplified with a phenanthrene system where the three fused rings were converted into one macrocycle—another demonstration of how peroxides can be used in unique ways [122].

1.5.8 Arylation

Arylation of alkyl radicals resembles cross-coupling reactions in both the outcome and relevance (Figure 1.10). In a traditional sense, cross-couplings involve an aryl component and an organometallic nucleophile. Here, the metal salt serves as a reductant by donating an electron to the peroxide, initiating a cascade to yield an alkyl radical that can be coupled to various aryl sources. In 1970, Minisci demonstrated that an alkyl radical, formed through reduction of an α-methoxy hydroperoxide, could be trapped by pyridine [123]. Recently, the Minisci reaction has been expanded by Bao to include reactions of organic peroxide precursors with arenes. Catalytic iron(III) has been employed to promote radical decarboxylation in the presence of an electron-deficient arene, resulting in a delocalized radical intermediate that is oxidized, in a radical–polar

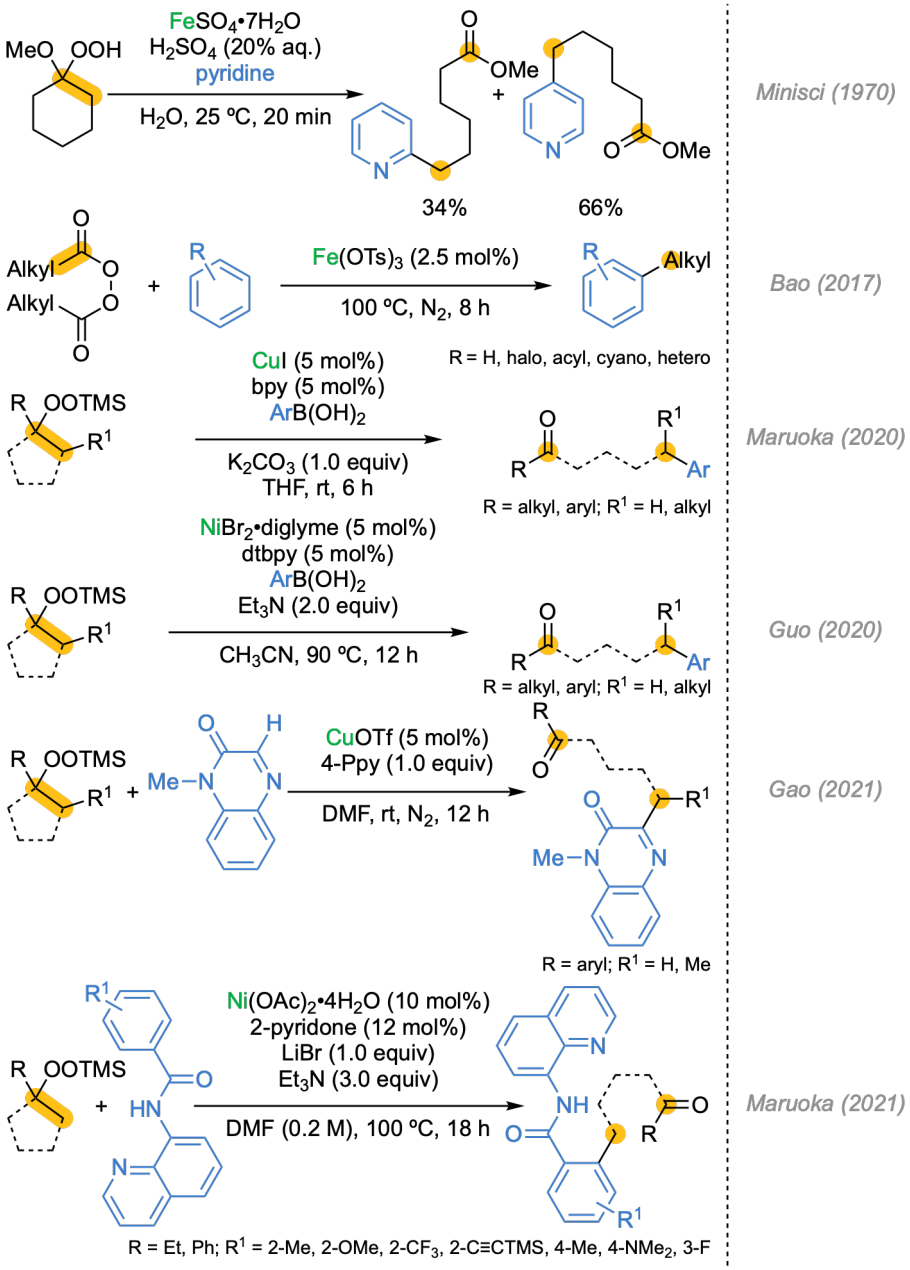


Figure 1.10 Arylation

crossover manner, to a delocalized carbocation to restore aromaticity, with concomitant reduction of the metal to turn over the catalyst [124]. In January of 2020, Maruoka reported using copper(I) iodide and a bipyridine ligand with potassium bicarbonate to reduce tertiary silylperoxides and provoke the coupling of arylboronic acids with the alkyl

radical [125]. In April that same year, Guo demonstrated a similar reaction using a bis(diglyme)nickel bromide with di-*tert*-butyl dipyridine (dtbpy) and triethylamine [126]. Both the Maruoka and Guo reactions required the use of a base, as in a typical Suzuki–Miyaura coupling. In 2021, Gao introduced this mode of C–C activation to the quinoxaline system, using cuprous triflate 4-pyrrolidinopyridine (4-Ppy) as a ligand, expanding upon the known methodologies [127]. By means of radical–polar crossover, the group proposes an aminyl radical that is oxidized to an amino cation. Deprotonation causes elimination that forms the imine. The most recent arylation reported from the Maruoka group employed a nickel(II) catalyst to reduce cyclic silylperoxides. The resulting alkyl radical was then trapped by benzamide derivatives in the ortho-position relative to the amide [128].

1.5.9 Alkynylation and Allylation

Alkynylation and allylation of radicals stemming from the reduction of peroxides are more recent discoveries. Alkynes are desirable because of their functional versatility, rigidity, and prevalence in natural products. There have been only three examples of such alkynylations to date (Figure 1.11A). In 2018, Maruoka reported a catalytic cuprous iodide–mediated reduction of tertiary silylperoxides performed in the presence of terminal alkynes or alkylnylsulfones to achieve the desired coupling [129]. An amine base was required to obtain sufficient reactivity, suggesting some similarity to Sonogashira coupling. The versatility of the installed alkyne functionality was demonstrated through syntheses of tetrahydropyrans and enones. Two years later, the Gui group reported alkynylation using an activated allylphenylsulfone to trap the alkyl radical [83]. In 2022,

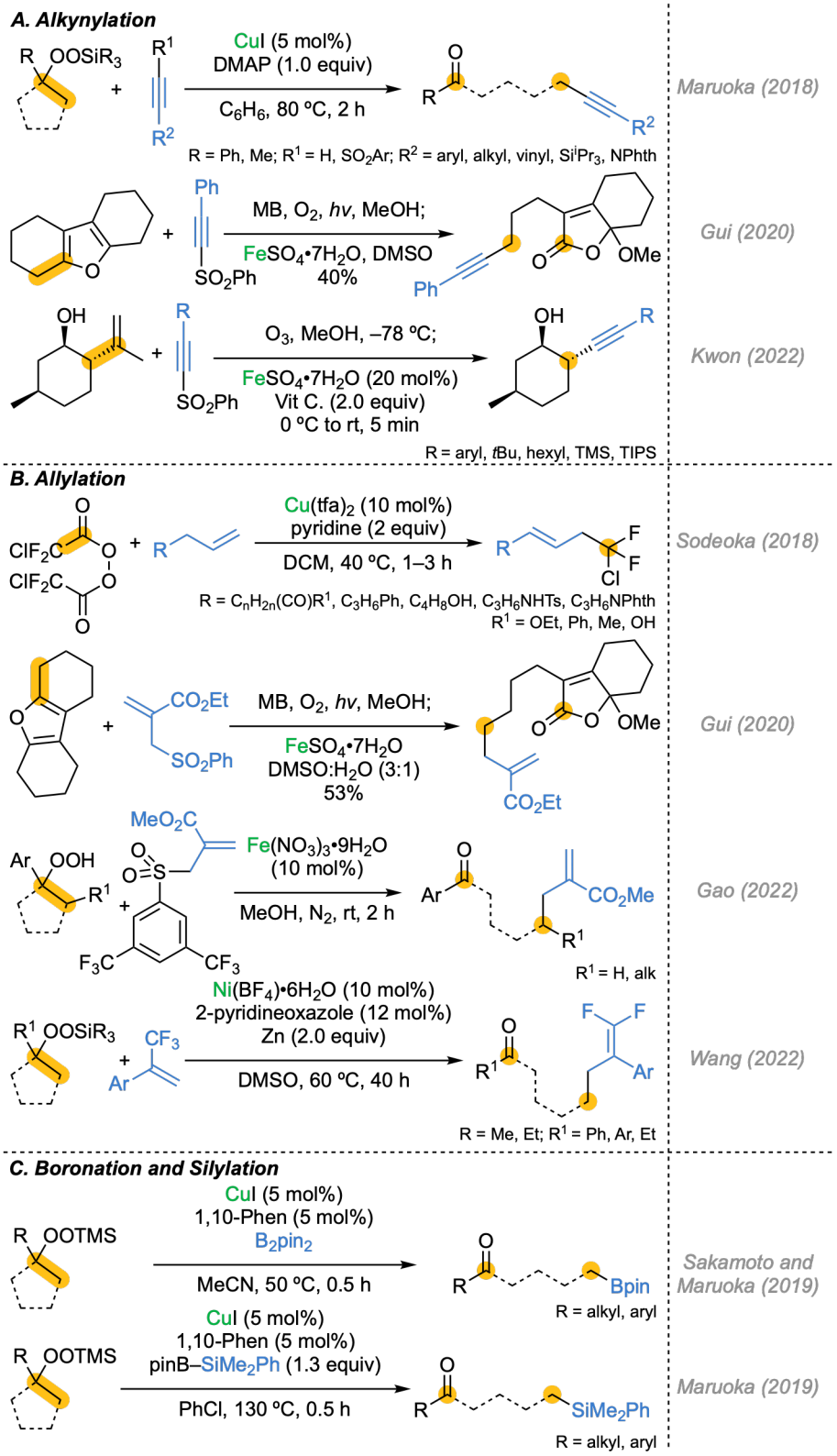


Figure 1.11 Alkynylation, Allylation, Borylation, and Silylation

Kwon published a study of the reduction of the Criegee ozonolysis product in methanol, mediated by iron(II) in the presence of various alkynylsulfones, thereby trapping the alkyl radical while releasing a benzene sulfonyl radical and producing an alkynylated product [130].

For allylation, in 2018 the Sodeoka group reported using copper(II) to reduce bis(chlorodifluoroacetyl) peroxide (Figure 1.11B) [78]. After subsequent decarboxylation, the alkyl radical added into a terminal alkene. Basic conditions allowed the formation of an allyl chlorodifluoromethane. Further adding to the butenolide functionalization, the Gui group used an α-sulfonylmethyl acrylate to achieve allylation [83]. In 2022, Gao reported radical allylation of an alkyl radical originating from a tertiary hydroperoxide [131]. The group used catalytic ferric nitrate nonahydrate and an α-sulfonylmethyl acrylate for their allylation. Most recently, the Wang group described a nickel(I)-mediated reduction of a silylperoxide. They trapped the radical with an α-trifluoromethyl styrene. Through a defluorinative mechanism, allylation was achieved to give a tetrasubstituted alkene [132]. With only a few examples of allylation and alkynylation, this area is open for further exploration.

1.5.10 Borylation and Silylation

Access to boryl- and silyl- compounds with distal keto groups remains problematic. Boron is an interesting coupling partner because of the versatility of C–B bonds. Silanes have been studied less, but the ability to install silyl groups could be useful for niche applications. In 2019, two papers relating to borylation were published, by Maruoka and Guo. Sakamoto and Maruoka were the first to describe borylation through the use of bis(pinacolato)diborane (Figure 1.11C) [133]. Here, cuprous iodide reduced tertiary

silylperoxides to form alkoxy radicals and a cupric species. The cupric species transmetalated with bis(pinacolato)diboron to form a cupric–boron bond and a borate ester. The alkyl radical then added into the copper, forming a species that could reductively eliminate to form a new C–B bond. In the same report, an experiment was performed by the Maruoka group involving a (dimethylphenylsilyl)boronic pinacol ester for transmetalation to form a silyl–cupric species, which went on to forge a C–Si bond [134]. Guo published a boronation similar to that of Maruoka, but using acetone instead of acetonitrile as the solvent, with 4-dimethylaminopyridine (DMAP) as a base/ligand to forge the C–B bond [134].

1.6 Safety

A common concern with peroxide chemistry is related to the explosivity of peroxides. It might be easier to simply eschew any reactions involving organic peroxides, to reduce the risk of accidents in laboratory settings, but organic peroxides are not necessarily as hazardous as they seem to be. Almost all of the publications cited in this review article describe the use of organic peroxides, so it is imperative that potential safety hazards be addressed.

One method to minimize risk is to conduct risk assessment calculations of molecules before working with them. Historically, simple oxygen balance (O.B.) calculations have been used to estimate the potential explosive nature of compounds [135]. To calculate this number, the counts of carbon, hydrogen, and oxygen atoms are considered with respect to the overall molecular weight of a molecule to produce the O.B. (Figure 1.12A). Essentially, lower values correspond to more hazardous compounds. For example, acetyl peroxide has an O.B. of –95, corresponding to “high risk.” Unfortunately, this approach is

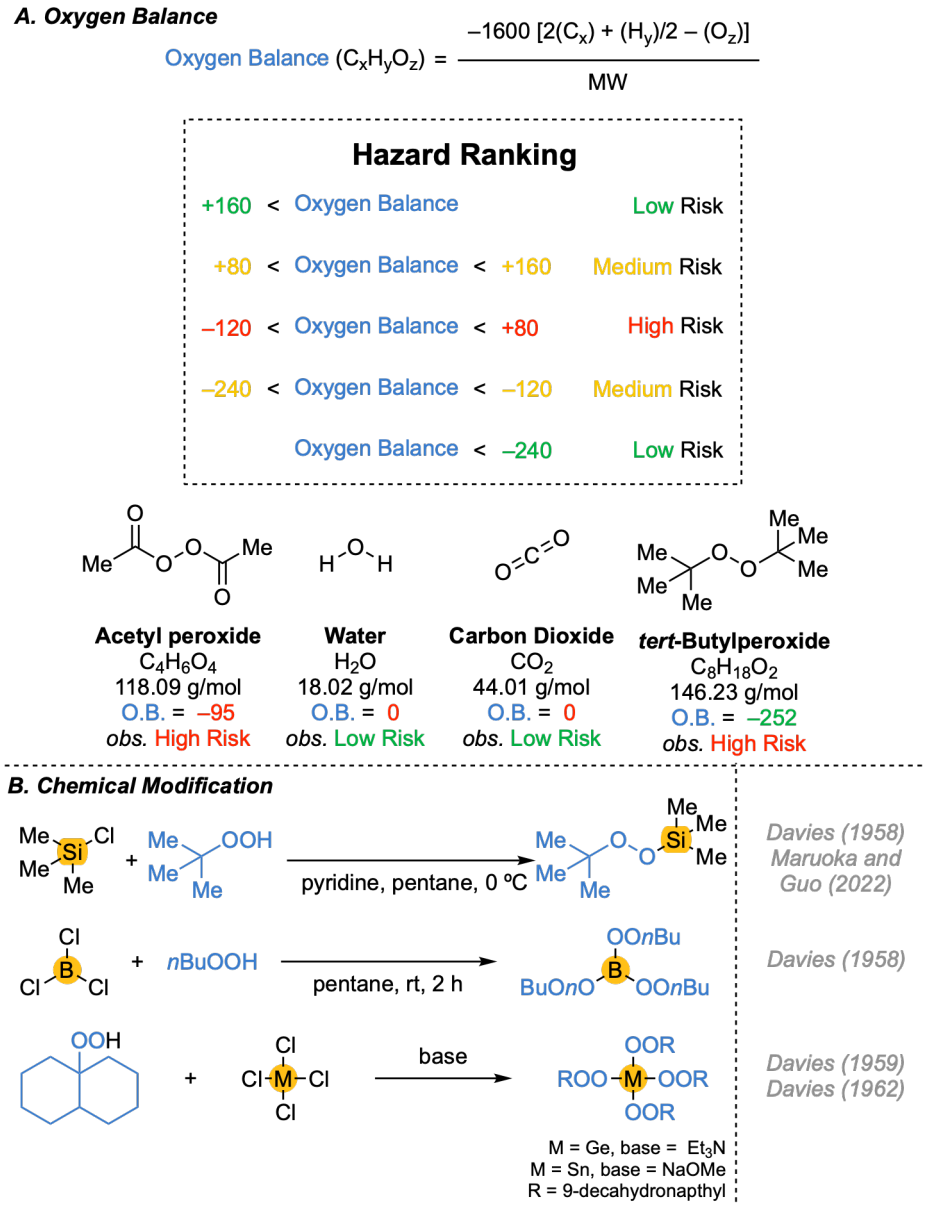


Figure 1.12 Safety

flawed because some compounds, including water and carbon dioxide, have an O.B. of zero, but no associated explosive hazards. Additionally, *tert*-butylperoxide has an O.B. of –252, corresponding to “low risk,” but has an observed hazard rank of “high risk” [136]. Nevertheless, O.B. calculations are useful as a baseline estimate for the risk assessment of organic peroxides, but the resulting value should be interpreted with caution.

There are several chemical modifications that can improve the stability of organic peroxides, facilitate extractions and purifications, and minimize hazards. Many of the reactions described in this review article employ silylperoxides, which behave almost identically to hydroperoxides, but have much larger absolute values of O.B. Chemically transforming hydroperoxides into silylperoxides is a straightforward and simple process that has been performed since 1958. Davies was the first to report the synthesis of a silylperoxide from an organic hydroperoxide, using trimethylsilyl chloride and *tert*-butyl hydroperoxide in pyridine and pentane at 0 °C (Figure 1.12B) [137]. Even today, this technique is used, for example in the studies of Maruoka and Guo [90, 125]. Silylperoxides have multiple advantages over hydroperoxides. The alkyl substituents on the silicon atom can improve the solubility in organic solvents and the overall stability, potentially yielding bench- and column-stable organic peroxides. Davies also published the functionalization of hydroperoxides with boron (1958), germanium (1959), and tin (1962), using the chlorinated species of these metals to functionalize organic hydroperoxides, although some or all of these modified molecules are potentially explosive [138–140].

More recently, chemists have turned toward calculations to identify the hazards of peroxides. The computer program “Chemical Thermodynamic and Energy Release” (CHETAH) can perform calculations to estimate the explosive risk associated with a compound, by comparing various parameters to a library of known explosive compounds [141]. The CHETAH-calculated energy and detonation values for the known explosives triacetonetriperoxide (TATP) and hexamethylene triperoxide diamine are comparable to their known empirical risks [142]. Density functional theory (DFT), complete basis set

(CBS) theory, and Gaussian software have also been applied to calculate the bond dissociation energies of various organic peroxides. It has been demonstrated that intramolecular hydrogen bonding in *gem*-1,2-hydroperoxide and acyl-hydroperoxides helps to stabilize their O–O bonds and lower the risk of accidental cleavage [2, 143]. With the development of these computer programs, conducting quick calculations before running an experiment in a laboratory setting can help chemists to minimize accidents. While this review article is focused on organic peroxides, these types of calculations have broader use with other types of reactions.

Safety is an important factor to consider when creating new methodologies or planning organic syntheses. Organic peroxides, to the uneducated chemist, may present a safety hazard, but with a few quick and easy calculations, and/or chemical modifications, laboratory accidents can hopefully be avoided.

1.7 Future Directions

The take-home message from this review article is that organic peroxides are relatively overlooked molecular motifs that provide the opportunity for facile C–C activation. Traditionally, peroxides have been viewed as explosive, corrosive, and hazardous, but with proper precautions they can be synthetically useful, allowing access otherwise difficult-to-prepare complex molecules. When applied to radical chemistry, the issue of undesirable and uncontrolled side reactivity is a legitimate concern. Nevertheless, the moderately high-yielding reactions appearing in this review article prove that it can mostly be avoided. Presumably, the use of catalytic quantities of metals to mediate this reactivity limits the generation of free radical species to a level dependent on the concentration of the oxidizable metal present in solution. Thus, the concentration of radicals available at any time is restricted. Overall, organic peroxides provide an accessible handle for selective C–C activation through a metal–mediated radical cascade, where a variety of functional groups that can be coupled for any synthetic need.

There are three foreseeable areas for future improvement (see outstanding questions). First, developing simpler methods for the tolerable integration of peroxides to make this methodology applicable to a wider range of molecules. Second, asymmetric cyclic peroxides and methods to couple radicals enantioselectively have yet to be investigated. Most of the recent examples provided in this review article involve tertiary peroxides, demonstrating one of the current limitations. Although there are methods available to form secondary peroxides, they require more thorough investigation. Finally, the products isolated after C–C activation have immense potential for further

derivatization and application in complex syntheses. The future of C–C activation chemistry, as it relates to peroxide precursors, is here for those ready to seize it.

1.8 Outstanding Questions

There are many different radical trapping methods presented in this review article. Does a universal leaving group, such as boron, sulfur, or nitrogen, exist to enable the addition of any desired coupling partner?

Does the reactivity of primary and secondary organic peroxides differ from that of tertiary organic peroxides? What factors, such as solvent, temperature, ligands, or additives, may influence the C–C scission process for secondary organic peroxides to produce a desired outcome? How do each of these factors affect the mechanism? What is the exact mechanism for these processes? How can computational chemistry help provide insight on the mechanism of this methodology?

How large of a role does the redox potential of the chosen metal play a role in the reduction of organic peroxides. What is the corresponding redox potential of organic peroxides such as hydroperoxides, silylperoxides, and boroperoxides? Is it possible to predict the best reducing metal based on these conditions? What other metals may be applicable for this chemistry?

How will this methodology be utilized in synthetic organic chemistry or total synthesis? When will the stereotype of wild, uncontrollable radical chemistry be eliminated for synthetic chemists to embrace the power of this methodology?

How can the safety techniques for working with organic peroxides be streamlined to minimize risk? Will existing computational programs become free-of-charge and publicly available to quickly ascertain the risk of a particular substance? How can these methods be improved to provide reliable data?

1.9 References

[1] Dong, G. *C–C Bond Activation*; Springer-Verlag, 2014.

[2] Bach, R. D.; Schlegel, H. B. Bond dissociation energies of peroxides revisited. *J. Phys. Chem. A* **2020**, *124*, 4742–4751.

[3] Brodie, B. C. Ueber die bildung der hyperoxyde organischer saureradicale. *Justus Liebigs Ann. Chem.* **1858**, *108*, 79–83.

[4] Graham, T. On the action of solar light upon iodide of ethyl. *J. Chem. Soc.* **1851**, *3*, 321–347.

[5] Kolbe, H. On the chemical constitution and nature of organic radicals. *Q. J. Chem. Soc.* **1851**, *3*, 389–405.

[6] Brodie, B. C. On the peroxides of radicals of the organic acids. *J. Chem. Soc.* **1864**, *17*, 206–281.

[7] Brodie, B. C. The organic peroxides theoretically considered. *J. Chem. Soc.* **1864**, *17*, 281–294.

[8] Brodie, B. C. On the oxidation and disoxidation effected by the alkaline peroxides. *J. Chem. Soc.* **16**, 316–342.

[9] Gomberg, M. An instance of trivalent carbon: triphenylmethyl. *J. Am. Chem. Soc.* **1900**, *22*, 757–771.

[10] Parnell, J. On the reducing action of peroxide of hydrogen and carbolic acid. *J. Chem. Soc.* **1868**, *21*, 356–357.

[11] Fenton, H. J. H. Oxidation of tartaric acid in the presence of iron. *J. Chem. Soc. Trans.* **1894**, *65*, 899–910.

[12] Haber, F.; Weiss, J. Über die katalyse des hydroperoxydes. *Die Naturwissenschaften* **1932**, *20*, 949–950.

[13] Gellissen, H.; Hermans, P. H. Über neue synthesen mittels organischer peroxyde, mitteilung I: die einwirkung des dibenzoylperoxyds und einiger seiner derivate auf siedendes benzol. *Ber. Dtsch. Chem. Ges.* **1925**, *58*, 285–294.

[14] Gellissen, H.; Hermans, P. H. Über neue synthesen mittels organischer peroxyde, II. Die einwirkung des dibenzoylperoxyds auf toluol. *Ber. Dtsch. Chem. Ges.* **1925**, *58*, 476–479.

[15] Gellissen, H.; Hermans, P. H. Über neue synthesen mittels organischer peroxyde, V. Die einwirkung von dibenzoylperoxyd auf äthen. *Ber. Dtsch. Chem. Ges.* **1925**, *58*, 764–765.

[16] Lippmann, E. V. Über wasserstoffentziehung mittelst benzoyl-superoxyd. *Monatsh. Chem.* **1886**, *7*, 521–528.

[17] Milas, N. A.; Harris, S. A. Studies in organic peroxides: I. Peroxides in the camphoric acid series. *J. Am. Chem. Soc.* **1933**, *55*, 349–352.

[18] Criegee, R. The rearrangement of decalin peroxide esters as a result of cationic oxygen. *Justus Liebigs Ann. Chem.* **1948**, *560*, 127–135.

[19] Criegee, R.; Dietrich, H. Preparation and esterification of tertiary hydroperoxides. *Justus Liebigs Ann. Chem.* **1948**, *560*, 135–141.

[20] Criegee, R.; Schnorrenberg, W. A methyl lactolide via methyl ether rearrangement. *Justus Liebigs Ann. Chem.* **1948**, *560*, 141–148.

[21] Criegee, R.; Wenner, G. The ozonation of 9,10-octaline. *Justus Liebigs Ann. Chem.* **1949**, *564*, 9–15.

[22] Criegee, R. About the course of ozone fission. *Justus Liebigs Ann. Chem.* **1953**, *583*, 1–36.

[23] George, P.; Walsh, A. D. A note on the decomposition of tertiary alkyl peroxides. *Trans. Faraday Soc.* **1946**, *42Trace*, 94–97.

[24] Raley, J. H.; Rust, F. F.; Vaughan, W. E. Decompositions of di-t-alkyl peroxides. I. Kinetics. *J. Am. Chem. Soc.* **1948**, *70*, 88–94.

[25] Hawkins, E. G. E. The reactions of organic peroxides. Part I. 2-Phenyl-2-butyl hydroperoxide. *J. Chem. Soc.* **1949**, 2076–2077.

[26] Kharasch, M. S.; Fono, A.; Nudenberg, W. The chemistry of hydroperoxides I. The acid catalyzed decomposition of alpha,alpha-dimethylbenzyl (alpha-cumyl) hydroperoxide. *J. Org. Chem.* **1950**, *15*, 748–752.

[27] Youngman, E. A.; Rust, F. F.; Coppinger, G. M.; Vaughan, W. E. The autoxidation of nonvicinal glycols. Ester formation via cyclic ethers and their peroxides. *J. Org. Chem.* **1963**, *28*, 144–148.

[28] Kochi, J. K. Chemistry of alkoxy radicals. Cleavage reactions. *J. Am. Chem. Soc.* **1962**, *84*, 1193–1197.

[29] De La Mare, H. E.; Rust, F. F. Intramolecular radical reactions. Decomposition of pure bis-(2-methyl-2-hexyl) peroxide in the liquid phase. *J. Am. Chem. Soc.* **1959**, *81*, 2691–2694.

[30] Kharasch, M. S.; Fono, A. Metal salt-induced homolytic reactions. I. A new method of introducing peroxy groups into organic molecules. *J. Org. Chem.* **1959**, *24*, 72–78.

[31] Kharasch, M. S.; Fono, A. New metal salt-induced homolytic reactions. II. Modification of free radical reactions by copper salts. *J. Org. Chem.* **1959**, *24*, 606–614.

[32] De La Mare, H. E.; Kochi, J. K.; Rust, F. F. The oxidation and reduction of free radicals by metal salts. *J. Am. Chem. Soc.* **1963**, *85*, 1437–1449.

[33) Bacha, J. D.; Kochi, J. K. Polar solvent effects in the cleavage of alkoxy radicals. *J. Org. Chem.* **1965**, *30*, 3272–3278.

[34] Kochi, J. K.; Mains, H. E. Studies on the mechanism of the reaction of peroxides and alkenes with copper salts. *J. Org. Chem.* **1965**, *30*, 1862–1872.

[35] Kumamoto, J.; De La Mare, H. E.; Rust, F. F. The use of cupric and ferric chlorides in the trapping of radical intermediates and the synthesis of alkyl chlorides. *J. Am. Chem. Soc.* **1960**, *82*, 1935–1939.

[36] Minisci, F. Peroxides and diazonium salts. *Gazz. Chim. Ital.* **1959**, *89*, 626–637.

[37] Milas, N. A.; Surgenor, D. M. Studies in organic peroxides. XI. t-Butyl peresters. *J. Am. Chem. Soc.* **1946**, *68*, 642–643.

[38] Davies, A. G.; Foster, R. V.; White, A. M. Organic peroxides. Part I. The preparation of alkyl hydroperoxides from hydrogen peroxide. *J. Chem. Soc.* **1953**, 1541–1547.

[39] Hecht, R.; Rüchardt, C. Darstellung von percarbonsäure-tert-butylestern über carbonsäure-imidazolide. *Chem. Ber.* **1963**, *96*, 1281–1284.

[40] Baj, S.; Chrobok, J. Alkylation of peroxyacids: a new method of peroxyester synthesis. *J. Chem. Soc., Perkin Trans. 1* **2000**, 2575–2578.

[41] Lockart, M.; Dussault, P. H. The chemistry of peresters. *Eur. J. Org. Chem.* **2020**, *2021*, 4914–4940.

[42] Kawamura, S.; Coppinger, G. M.; Sodeoka, M. Recent advances in reactions using diacyl peroxides as sources of O- and C-functional groups. *Org. Biomol. Chem.* **2021**, *19*, 2096–2109.

[43] Liu, H.; Kato, K.; Maruoka, K. Diacyl peroxides—practical reagents as aryl and alkyl radical sources. *Chem. Commun.* **2021**, *57*, 6707–6724.

[44] Engler, C.; Wild, W. Ueber die sogenannte activierung des sauerstoffs und über superoxydbildung. *Ber. Dtsch. Chem. Ges.* **1897**, *30*, 1669–1681.

[45] Bach, A. Du rôle des peroxydes dans les phénomènes d'oxydation lente. *C. R. Hebd. Séances Acad. Sci.* **1897**, *124*, 951–964.

[46] Milas, N. A. Auto-oxidation. *Chem. Rev.* **1932**, *10*, 295–364.

[47] Robertson, A. Tetrahydrofuran hydroperoxide. *Nature* **1948**, *162*, 153.

[48] Wolffenstein, R. Über die einwirkung von wasserstoffsuperoxyd auf aceton und mesityloxyd. *Ber. Dtsch. Chem. Ges.* **1895**, *28*, 2265–2269.

[49] Bilyukov, O. V.; Yaremenko, I. A.; Terent'ev, A. O. Synthesis of acyclic geminal bis-peroxides. *Russ. J. Org. Chem.* **2021**, *57*, 854–878.

[50] Yaremenko, I. A.; Radulov, P. S.; Terent'ev, A. O. Marriage of peroxides and nitrogen heterocycles: selective three-component assembly, peroxide-preserving

rearrangement, and stereoelectronic source of unusual stability of bridged ozonides. *J. Am. Chem. Soc.* **2021**, *143*, 6634–6648.

[51] Edwards, J. O.; Pearson, R. G. The factors determining nucleophilic reactivities. *J. Am. Chem. Soc.* **1962**, *84*, 16–24.

[52] Milas, N. A.; Harris, S. A. Studies in organic peroxides. V. t-Butyl hydroperoxide. *J. Am. Chem. Soc.* **1938**, *60*, 2434–2436.

[53] Davies, A. G.; White, A. M. Preparation of alkyl hydroperoxides. *Nature* **1952**, *170*, 668.

[54] Xu, W.; Ouyang, Y.; Maruoka, K. In-situ-generation of alkylsilyl peroxides from the alkyl hydroperoxides and their subsequent copper-catalyzed functionalization with organosilicon compounds. *Tetrahedron Lett.* **2021**, *75*, 153144.

[55] Pearson, R. G.; Edgington, D. N. Nucleophilic reactivity of the hydrogen peroxide anion; distinction between SN2 and SN1CB mechanisms. *J. Am. Chem. Soc.* **1962**, *84*, 4607–4608.

[56] Milas, N. A.; Panagiotakos, P. C. Studies in organic peroxides. VIII. Dinicotinyl peroxide. *J. Am. Chem. Soc.* **1940**, *62*, 1878.

[57] Kyasa, S.; Dussault, P. H.; Silver, O. Synthesis of alkyl hydroperoxides via alkylation of gem-dihydroperoxides. *J. Org. Chem.* **2013**, *78*, 3452–3456.

[58] Bordier, C.; Darcel, C.; Thomas, J. B. Past and current routes to beta-hydroxy hydroperoxides: a functional group with high potential in organic synthesis. *Tetrahedron* **2021**, *97*, 132370.

[59] Hou, Y.; Zhong, W.; Zhang, X. Indium-mediated synthesis of benzylic hydroperoxides. *Org. Lett.* **2019**, *21*, 4428–4432.

[60] Rubin, M. B. The history of ozone. The Schönbein period, 1839-1868. *Bull. Hist. Chem.* **2001**, *26*, 40–55.

[61] Milas, N. A.; Davis, P.; Nolan, J. T. Organic Peroxides. XX. Peroxides from the ozonation of olefins in the presence of carbonium ions. *J. Am. Chem. Soc.* **1955**, *77Trace*, 2536–2541.

[62] Domeyer, S.; Pederson, E.; Lind, J. Exploiting endoperoxides as a new entry for the synthesis of branched azasugars. *Beilstein J. Org. Chem.* **2017**, *13*, 644–647.

[63] Xu, Z.; Foote, C. S.; Houk, K. N. Probing the peroxycarbenium (3+2) cycloaddition reactions with 1,2-disubstituted ethylenes: results and insights. *Chem. Eur. J.* **2017**, *23*, 2031–2034.

[64] Singleton, D. A.; Foote, C. S.; Houk, K. N. Mechanism of ene reactions of singlet oxygen. A two-step no-intermediate mechanism. *J. Am. Chem. Soc.* **2003**, *125*, 1319–1328.

[65] Horn, A.; Dussault, P. H. A click-based modular approach to introduction of peroxides onto molecules and nanostructures. *RSC Adv.* **2020**, *10*, 44406–44429.

[66] Isayama, S.; Mukaiyama, T. Novel method for the preparation of triethylsilyl peroxides from olefins by the reaction with molecular oxygen and triethylsilane catalyzed by bis(1,3-diketonato)cobalt(II). *Chem. Lett.* **1889**, *18*, 573–576.

[67] Oswald, J. P.; Woerpel, K. A. Cobalt-catalyzed oxygenation and dearomatization of furans. *J. Org. Chem.* **2018**, *83*, 9067–9075.

[68] Zuckerman, D. S.; Woerpel, K. A. Diastereoselective peroxidation of derivatives of Baylis-Hillman adducts. *Tetrahedron* **2019**, *75*, 4118–4129.

[69] Oswald, J. P.; Woerpel, K. A. Cobalt-catalyzed intramolecular silylperoxidation of unsaturated diisopropylsilyl ethers. *J. Org. Chem.* **2019**, *84*, 7564–7574.

[70] Peralta-Neel, Z.; Woerpel, K. A. Hydroperoxidations of alkenes using cobalt picolinate catalysts. *Org. Lett.* **2021**, *23*, 5002–5006.

[71] Chen, Y.; Li, P.; Wang, X. Copper-catalyzed trifluoromethylthiolation: peroxidation of alkenes and allenes. *Org. Chem. Front.* **2020**, *7*, 1837–1844.

[72] Luo, Y.; Li, M.; Wu, X. Copper-catalyzed three-component germylperoxidation of alkenes. *Org. Lett.* **2022**, *24*, 2425–2430.

[73] Wang, X.; Glycine, N.; Molybdate, S. Regio- and stereoselective addition of HO/OOH to allylic alcohols. *J. Org. Chem.* **2020**, *85*, 10007–10021.

[74] Buback, M.; Kling, M.; Schmatz, S. Decomposition of tertiary alkoxy radicals. *Z. Phys. Chem.* **2005**, *219*, 1205–1222.

[75] Hawkins, E. G. E.; Young, D. P. Reactions of organic peroxides. Part V. Reaction of ferrous sulphate with methylcyclopentyl and methylcyclohexyl hydroperoxides. *J. Chem. Soc.* **1950**, 2804–2808.

[76) Deng, W.; Bao, X.; Li, Y. Merging visible-light photocatalysis and transition-metal catalysis in three-component alkyl-fluorination of olefins with a fluoride ion. *Org. Lett.* **2018**, *20*, 4245–4249.

[77] Cui, Z.; Du, D. FeCl2-catalyzed decarboxylative radical alkylation/cyclization of cinnamamides: access to dihydroquinolinone and pyrrolo[1,2-a]indole analogues. *J. Org. Chem.* **2018**, *83*, 6149–6159.

[78] Kawamura, S.; Sodeoka, M.; Tagami, T. Reactivity and properties of bis(chlorodifluoroacetyl) peroxide generated in situ from chlorodifluoroacetic anhydride for chlorodifluoromethylation reactions. *Chem. Commun.* **2018**, *54*, 11276–11279.

[79] Bao, X.; Li, P.; Zhu, Y. Method for alkylation-alkoxylation of olefin compound. *Nat. Commun.* **2018**, *9*, 3725.

[80] Wu, R.; Bao, X.; Li, Y. Iron-catalyzed alkylazidation of 1,1-disubstituted alkenes with diacylperoxides and TMSN3. *Org. Lett.* **2020**, *22*, 3196–3199.

[81] Zhu, X.; Bao, X.; Li, Y. Cu-catalyzed alkylarylation of vinylarenes with masked alkyl electrophiles. *Org. Lett.* **2020**, *22*, 620–625.

[82] Guo, M.; Duan, Y.; Suo, L. Iron-catalyzed ketoalkylation and ketoalkylation-etherification of styrenes initiated by selective C-C bond cleavage. *Org. Chem. Front.* **2020**, *7*, 2414–2418.

[83] Ban, J.; Gui, J.; Methylene, B. Modular synthesis of functionalized butenolides by oxidative furan fragmentation. *Eur. J. Org. Chem.* **2020**, *2020*, 339–347.

[84] Sakurai, S.; Maruoka, K.; Kato, K. Cu-catalyzed enantioselective alkylarylation of vinylarenes enabled by chiral binaphthyl-BOX hybrid ligands. *J. Am. Chem. Soc.* **2020**, *142*, 19017–19022.

[85] Xu, W.; Liu, H.; Maruoka, K. The formation of C-C or C-N bonds via the copper-catalyzed coupling of alkylsilyl peroxides and organosilicon compounds: a route to perfluoroalkylation. *Org. Lett.* **2021**, *23*, 1809–1813.

[86] Lyu, J.; Zhou, C.; Maruoka, K. The copper-catalyzed selective monoalkylation of active methylene compounds with alkylsilylperoxides. *Org. Biomol. Chem.* **2021**, *19*, 2658–2662.

[87] Zhou, C.; Lyu, J.; Maruoka, K. Highly selective monoalkylation of active methylene and related derivatives using alkylsilyl peroxides by a catalytic CuI-DMAP system. *Asian J. Org. Chem.* **2021**, *10*, 2625–2631.

[88] Aoki, Y.; Kawamura, S.; Sodeoka, M. Cu-catalyzed allylic perfluoroalkylation of alkenes using perfluorocarboxylic anhydrides: preparation of N-(5,5,6,6,6-pentafluoro-2-hexen-1-yl)phthalimide. *Org. Synth.* **2021**, *98*, 84–96.

[89] Tagami, T.; Kawamura, S.; Sodeoka, M. 1,2-Bis-perfluoroalkylations of alkenes and alkynes with perfluorocarboxylic anhydrides via the formation of perfluoroalkylcopper intermediates. *Org. Biomol. Chem.* **2021**, *19*, 9148–9153.

[90] Xu, W.; Kato, K.; Maruoka, K. Fe-catalyzed dicarbofunctionalization of vinylarenes with alkylsilyl peroxides and beta-keto carbonyl substrates. *Org. Lett.* **2022**, *24*, 2641–2645.

[91] Liu, H.; Kato, K.; Maruoka, K. Fe-catalyzed three-component coupling reaction of alpha,beta-unsaturated carbonyl compounds and conjugate dienes with alkylsilyl peroxides and nucleophiles. *J. Org. Chem.* **2022**, *87*, 8824–8834.

[92] Kharasch, M. S.; Wald, M.; Nudenberg, W. The chemistry of hydroperoxides. III. The free-radical decomposition of hydroperoxides. *J. Org. Chem.* **1950**, *15*, 753–762.

[93] Hawkins, E. G. E. Reactions of organic peroxides. Part III. Reactions of methylcyclopentyl and methylcyclohexyl hydroperoxides. *J. Chem. Soc.* **1950**, 2801–2804.

[94] Smalligo, A. J.; Dworkin, J. H.; Kwon, O. Hydrodealkenylative $C(sp^3)$-$C(sp^2)$ bond fragmentation. *Science* **2019**, *364*, 681–685.

[95] Crucioli, G. P.; Minisci, F. Radical reactions of nitric oxide. Nitrated acids from nitric oxide and peroxide. *Gazz. Chim. Ital.* **1888**, 261–270.

[96) Sakurai, S.; Sakamoto, R.; Maruoka, K. Generation of alkyl radicals from alkylsilyl peroxides and their applications to C-N or C-O bond formations. *Tetrahedron* **2019**, *75*, 172–179.

[97] Tang, Z.; Ouyang, Y.; Li, P. Decarboxylative C(sp3)-N cross-coupling of diacyl peroxides with nitrogen nucleophiles. *Org. Lett.* **2021**, *23*, 1000–1004.

[98] Sakamoto, R.; Sakurai, S.; Maruoka, K. Alkylsilyl peroxides as alkylating agents in the copper-catalyzed selective mono-N-alkylation of primary amides and azylamines. *Chem. Eur. J.* **2017**, *23*, 9030–9033.

[99] Minisci, F.; Portolani, A. Peroxides and diazonium salts. III. Azides and nitriles of 1-hydroxyhydroperoxides. *Gazz. Chim. Ital.* **1959**, *89*, 1941–1949.

[100] Wang, K.; Li, P.; Bao, X. Iron-catalyzed asymmetric decarboxylative azidation. *Org. Lett.* **2021**, *23*, 8847–8851.

[101] Zhong, W.; Xu, W.; Maruoka, K. A new approach for the copper-catalyzed functionalization of alkylhydroperoxides with organosilicon compounds via in-situ-generated alkylsilyl peroxides. *Tetrahedron* **2022**, *112*, 132627.

[102] Minisci, F. Peroxides and diazonium salts. V. Halo derivatives of caproic acid. *Gazz. Chim. Ital.* **1959**, *89*, 1910–1921.

[103] Minisci, F.; Portolani, A. Peroxides and diazonium salts. II. Halogen derivatives of 1-hydroxyhydroperoxides. *Gazz. Chim. Ital.* **1959**, *89*, 1922–1940.

[104] Minisci, F.; Belvedere, G. Peroxides and diazonium salts. VI. Halogenated ketones and esters from alicyclic hydroperoxides. *Gazz. Chim. Ital.* **1960**, *90*, 1299–1308.

[105] Liu, S.; Duan, Y.; Guo, M. Copper-catalyzed radical ring-opening halogenation with HX. *Chem. Commun.* **2021**, *57*, 8652–8655.

[106] Minisci, F. Peroxides and diazonium salts. IV. Thiocyanate and dithio derivatives of 1-hydroxyhydroperoxides. *Gazz. Chim. Ital.* **1959**, *89Trace*, 2428–2437.

[107] Smaligo, A. J.; Kwon, O. Dealkenylative thiylation of $C(sp^3)$-$C(sp^2)$ bonds. *Org. Lett.* **2019**, *21*, 8592–8597.

[108] Sun, Q.; Guo, M.; Duan, Y. Iron-catalyzed thiolation and selenylation of cycloalkyl hydroperoxides via C-C bond cleavage. *J. Org. Chem.* **2021**, *86*, 11987–11997.

[109] Smaligo, A. J.; Dehnert, B. W.; Kwon, O. Oxodealkenylative cleavage of alkene C(sp3)-C(sp2) bonds: a practical method for introducing carbonyls into chiral pool materials. *Angew. Chem. Int. Ed.* **2020**, *59*, 1211–1215.

[110] Zhu, X.; Li, P.; Bao, X. Asymmetric radical carboesterification of dienes. *Nat. Commun.* **2021**, *12*, 6670.

[111] Matsumoto, A.; Sakurai, S.; Maruoka, K. Synthesis of functionalized aliphatic esters via the generation of alkyl radicals from silylperoxyacetals. *Chem. Asian J.* **2021**, *16*, 2431–2434.

[112] Sakurai, S.; Matsumoto, A.; Maruoka, K. Cu-catalyzed *O*-alkylation of phenol derivatives with alkylsilyl peroxides. *Chem. Commun.* **2021**, *57*, 81–84.

[113] Xin, H.; Duan, Y.; Guo, M. Visible light-driven, copper-catalyzed aerobic oxidative cleavage of cycloalkanones. *J. Org. Chem.* **2021**, *86*, 8263–8273.

[114] De La Mare, H. E.; Kochi, J. K.; Rust, F. F. The oxidation of free radicals by metal ions. *J. Am. Chem. Soc.* **1961**, *83*, 2015–2016.

[115) Schreiber, S. Fragmentation reactions of alpha-alkoxy hydroperoxides and application to the synthesis of the macrolide (+/-)-recifeiolide. *J. Am. Chem. Soc.* **1980**, *102*, 6165–6166.

[116] Ge, L.; Bao, X. Iron-catalyzed vinylic C-H alkylation with alkyl peroxides. *Chem. Asian J.* **2018**, *13*, 2522–2528.

[117] Ye, C.; Li, P.; Bao, X. Iron-catalyzed dehydrative alkylation of propargyl alcohols with alkyl peroxides to form substituted 1,3-enynes. *Org. Lett.* **2018**, *20*, 3202–3205.

[118] Ye, C.; Zhang, X.; Bao, X. Copper-catalyzed 1,4-alkylarylation of 1,3-enynes with masked alkyl electrophiles. *Chem. Sci.* **2019**, *10*, 3632–3636.

[119] Zhu, X.; Zhang, X.; Bao, X. Copper-catalyzed radical 1,4-difunctionalization of 1,3-enynes with alkyl diacyl peroxides and N-fluorobenzenesulfonimide. *J. Am. Chem. Soc.* **1919**, *141*, 548–559.

[120] Guo, P.; Duan, Y.; Guo, M. Iron-catalyzed decarboxylative olefination of unstrained carbon-carbon bonds relying on alkoxyl radical induced cascade. *Org. Lett.* **2019**, *21*, 7104–7108.

[121] Swain, M.; Sadykov, G.; Wang, R.; Kwon, O. Dealkenylative alkenylation: formal sigma-bond metathesis of olefins. *Angew. Chem. Int. Ed.* **2020**, *59*, 17565–17571.

[122] Ning, Y.; Gui, J.; Terent'ev, A. O. Biogenesis-guided synthesis and structural revision of surocladione enabled by ruthenium-catalyzed endoperoxide fragmentation. *Angew. Chem. Int. Ed.* **2021**, *60*, 11222–11226.

[123] Minisci, F. Nucleophilic character of alkyl radicals - I. Selective alkylation of pyridine, quinoline, and acridine by hydroperoxides and oxaziridines. *Tetrahedron* **1970**, *26*, 4083–4091.

[124] Yu, F.; Zhang, X.; Bao, X. Iron(III)-catalyzed ortho-preferred radical nucleophilic alkylation of electron-deficient arenes. *Org. Lett.* **2017**, *19*, 6538–6541.

[125] Sakurai, S.; Kato, K.; Maruoka, K. Cu-catalyzed generation of alkyl radicals from alkylsilyl peroxides and subsequent C(sp^3)-C(sp^2) cross-coupling with arylboronic acids. *J. Org. Chem.* **2020**, *85*, 3973–3980.

[126] Chen, L.; dtbpy, D.; Guo, M. Nickel-catalyzed Suzuki coupling of cycloalkyl silyl peroxides with boronic acids. *J. Org. Chem.* **2020**, *85*, 7515–7525.

[127] Chen, H.; Gao, L.; Ppy, P. Copper-catalyzed redox-neutral ketoalkylation of C(sp^2)-H bonds via C-C bond cleavage. *Org. Chem. Front.* **2021**, *8*, 5866–5871.

[128] Tsuzuki, S.; Kato, K.; Maruoka, K. Ni-catalyzed C(sp^2)-H alkylation of N-quinolylbenzamides using alkylsilyl peroxides as structurally diverse alkyl sources. *Chem. Commun.* **2021**, *57*, 7942–7945.

[129] Sakamoto, R.; Sakurai, S.; Maruoka, K. Copper-catalyzed C(sp^3)-C(sp) coupling of terminal alkynes with alkylsilyl peroxides via a radical mechanism. *Org. Lett.* **2018**, *20*, 1400–1403.

[130] Xuan, M.; Vitamin, C.; Kwon, O. Dealkenylative alkynylation using catalytic Fe and vitamin C. *J. Am. Chem. Soc.* **2022**, *144*, 14828–14837.

[131] Wang, M.; Gao, L.; Nonahydrate, F. Iron-catalyzed ring-opening allylation of cycloalkyl hydroperoxides with allylic sulfones. *Asian J. Org. Chem.* **2022**, *11*, e202200031.

[132] Dong, H.; Wang, M.; Wang, X. Nickel-catalyzed allylic defluorinative cross-electrophile coupling with cycloalkyl silyl peroxides as the alkyl source. *J. Org. Chem.* **2022**, *87*, 892–903.

[133] Sekamoto, T.; Sakamoto, R.; Maruoka, K. Synthesis of functionalized organoboron and silicon compounds by copper-catalyzed coupling of alkylsilyl peroxides and diboron / silylborane reagents. *Org. Lett.* **2019**, *21*, 2477–2481.

[134] Yang, J.; Sakamoto, R.; Maruoka, K. Copper-catalyzed borylation of cycloalkyl silyl peroxides via radical C-C bond cleavage. *Org. Chem. Front.* **2019**, *6*, 2792–2795.

[135] Meyer, R.; Köhler, J.; Homburg, A. *Explosives*, 7th ed.; John Wiley and Sons, 2015.

[136] Shanley, E. S.; Melhem, G. A. The oxygen balance criterion for thermal hazards assessment. *Process Saf. Prog.* **1995**, *14*, 29–31.

[137] Buncel, E.; Davies, A. G. Peroxides of elements other than carbon. Part I. The preparation and reactions of peroxysilanes. *J. Chem. Soc.* **1958**, 1550–1556.

[138] Davies, A. G.; Moodie, R. B. Peroxides of elements other than carbon. Part III. The formation of boron peroxides by nucleophilic substitution. *J. Chem. Soc.* **1958**, 2372–2377.

[139] Davies, A. G.; Hall, C. D. Peroxides of elements other than carbon. Part VI. Peroxides of germanium. *J. Chem. Soc.* **1959**, 3835–3838.

[140] Alleston, D. L.; Davies, A. G. Peroxides of elements other than carbon. Part VIII. Organoperoxides of tin. *J. Chem. Soc.* **1962**, 2465–2471.

[141] Maienschein, J. L. Estimating Equivalency of Explosives Through a Thermochemical Approach; U.S. D.O.E., Lawrence Livermore National Laboratory, 2002.

[142] Price, M. A.; Gheee, A. H. Modeling for detonation and energy release from peroxides and non-ideal improvised explosives. *Cent. Eur. J. Energ. Mater.* **2009**, *6*, 239–254.

[143] Gamage, N. H.; Dominici, N.; Homburg, A. Less sensitive oxygen-rich peroxides containing geminal hydroperoxy groups. *Chem. Commun.* **2015**, *51*, 13298–13300.

CHAPTER TWO

Dealkenylative Functionalizations: Conversion of Alkene $C(sp^3)$–$C(sp^2)$ Bonds into $C(sp^3)$–X Bonds via Redox-Based Radical Processes

Adapted from Dehnert, B. W.; Dworkin, J. H.; Kwon, O.

Synthesis **2024**, 56, 71–86

2.1 Abstract

This review highlights the history and recent advances in dealkenylative functionalization. Through this deconstructive strategy, radical functionalizations occur under mild, robust conditions. The reactions described proceed with high efficiency, good stereoselectivity, tolerate many functional groups, and are completed within a matter of minutes. By cleaving the $C(sp^3)$–$C(sp^2)$ bond of terpenes and terpenoid-derived precursors, rapid diversification of natural products is possible.

2.2 Introduction

Within the broad scope of natural products, alkenes are abundant functional groups that are seemingly quintessential to organic chemistry [1]. Recent analysis based on a dataset of 13 million structures has estimated that 39.85% of natural products contain olefinic units, and that they are the second most encountered functionality [1]. Their wide availability and synthetic versatility have guided many prominent chemists to seek synthetic transformations for building, cleaving, and functionalizing olefins.

Over the years, numerous reactions have been devised to cleave the $C(sp^2)$–$C(sp^2)$ π-bonds of alkenes, including traditional ozonolysis or oxidative cleavage using osmium tetroxide and sodium periodate or potassium permanganate. Relatively recently, transition-metal-catalyzed alkene cleavage reactions (e.g., olefin metathesis) have become popular synthetic strategies.

There have been, however, few literature precedents of $C(sp^3)$–$C(sp^2)$ σ-bond fissions of alkenes [2–7] , despite the abundance of olefinic units in natural products and commodity/feedstock chemicals. Gratifyingly, methods have been developed recently to strategically cleave alkenyl $C(sp^3)$–$C(sp^2)$ σ-bonds to expand the existing potential of olefinic compounds. Indeed, several examples of fragmenting these 'inert' bonds and installing useful synthetic motifs in their wake—including $C(sp^3)$–H [8,9], $C(sp^3)$–S [10], $C(sp^3)$–O [11], $C(sp^3)$=O [11], $C(sp^3)$–$C(sp^2)$ [12], and $C(sp^3)$–C(sp) [13] functionalities—have been explored since 2018.

While there are plenty of methods to cleave C–C bonds through radical, heterolytic, or transition-metal-mediated means [14] , the functionalizations that we present herein stem from iron(II)-mediated single-electron reductions of the α-alkoxyhydroperoxides that

originate from alcohol-intercepted ozonolysis of alkenes, thereby producing fleeting alkyl radicals that are trapped by radical acceptors. The utility of ozone-mediated oxidation and iron(II)-mediated fragmentation–radical functionalization arises from their ease of operation and applications to natural products synthesis.

These dump-and-stir, open-to-the-air reactions are usually complete within minutes, enabling quick and robust functionalization. Using terpenes and terpenoids from Nature's chiral pool allows the rapid derivatization of feedstock olefins into enantiopure terpene derivatives that are relevant synthetically. For example, many natural products [3,9,12,15,16] and chiral phosphine catalysts [8] have been synthesized efficiently and selectively using this approach. Overall, dealkenylative functionalization is a powerful method that allows synthetic chemists to take advantage of ubiquitous alkenes and provides access to unprecedented building blocks from Nature.

2.3 Mechanism

Criegee ozonolysis and metal-mediated peroxide cleavage form the basis for dealkenylative functionalization (Figure 2.1). In this one-pot process, a solution of an alkene substrate in methanol is cooled to –78 °C and bubbled with ozone. In a matter of minutes, the alkene is transformed into an α-methoxyhydroperoxide. First, a (3+2) cycloaddition forms a molozonide that rapidly engages in a *retro*-(3+2) cycloaddition to form a carbonyl oxide—the so-called 'Criegee intermediate'.

The methanol charge-ablates to form a neutral α-methoxyhydroperoxide. After the excess ozone is removed through an argon sparge, the radical acceptor, reductant (if applicable), and iron(II) sulfate heptahydrate are added directly into the reaction mixture. While the mixture is warmed to room temperature, iron(II) sulfate heptahydrate dissolves

completely, enabling a single-electron transfer (SET) event to reduce the hydroperoxide. This process forms an alkoxy radical, a hydroxide anion, and iron(III).

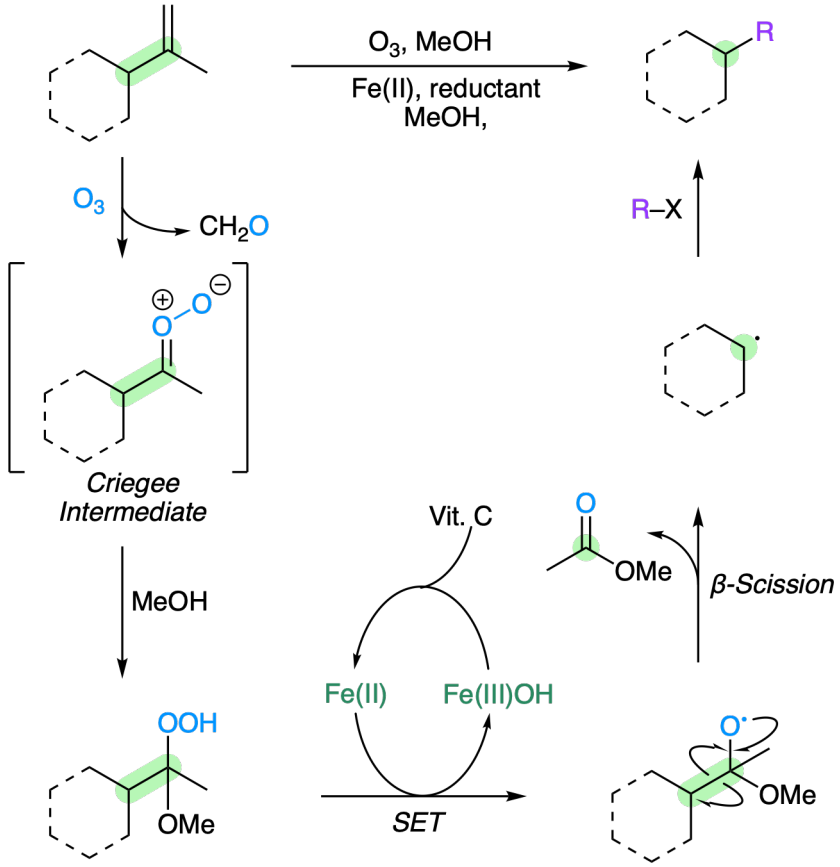


Figure 2.1 Mechanism for Ozone-Mediated Peroxidation and Iron(II) Reduction of Feedstock Olefins

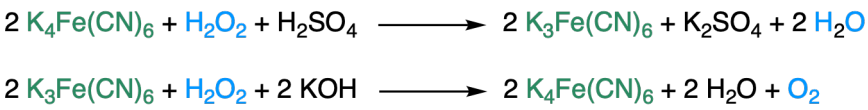
Rapid β-scission of the alkoxy radical generates an alkyl radical, expelling a methyl ester. Radical addition into a radical trap terminates the reaction cascade to yield the dealkenylated product. To make this method catalytic, a benign stoichiometric reductant can be used to turn over the iron(III) back to iron(II), which restarts the cycle. A variety of radical traps have been used to ensure hydrodealkenylation [C(sp^3)–H], dealkenylative thiylation [C(sp^3)–SPh], dealkenylative aminoxylation [C(sp^3)–OR], oxodealkenylation [C=O], dealkenylative alkenylation [C(sp^3)–C(sp^2)], and dealkenylative alkynylation [C(sp^3)–C(sp)].

2.4 History

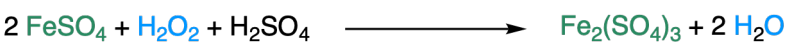
Dealkenylative functionalization combines three ideas into one powerful methodology. First, ozone-mediated oxidation of an olefin generates a peroxide. Second, SET from an iron(II) salt to the peroxide initiates a radical cascade. Third, the resulting alkoxy radical undergoes β-scission to give an alkyl radical species that is immediately coupled with a desired functional group to yield the final product. Precedents for each of these processes have been developed over the course of the last century, with the discovery of various methods to synthesize peroxides, the elucidation of SET from metals to peroxides to form radicals, and a survey of the potential transformations available from these radicals.

Since their discovery, peroxides have served as attractive synthetic intermediates because of their unique interactions with metal salts (Figure 2.2). In 1862, Brodie provided preliminary results regarding the reactions of hydrogen peroxide with various metals [17,18]. In particular, he observed ferrocyanide oxidation mediated by hydrogen peroxide under acidic conditions and reduction under basic conditions, marking one of the first observations of the redox relationship between peroxide and iron. A few years later, Parnell published his findings on the reducibility of hydrogen peroxide with iron(II) sulfate, directly resulting in an iron(III) species [19]. Subsequently, in 1894, Fenton demonstrated the catalytic capability of iron(II) sulfate through the oxidation of tartaric acid with hydrogen peroxide [20]. The connection between ferrous species and peroxides was clarified in 1932 with contributions from Häber and Weiss. They proposed a mechanism

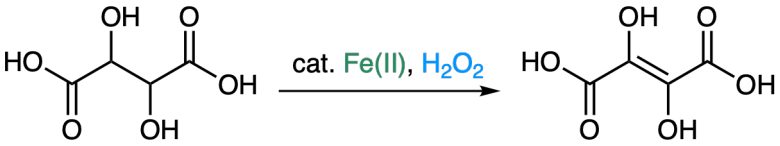
Brodie, 1862



Parnell, 1868



Fenton, 1894



Häber–Weiss, 1932

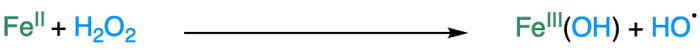


Figure 2.2. Initial Studies on Iron(II) Reduction of Hydrogen Peroxide

in which hydrogen peroxide, in the presence of iron(II), would be reduced to a hydroxide ion and a hydroxyl radical [21]. Thereafter, iron(II) salts and other low-valent transition metals were studied extensively in the context of organic peroxide fission.

With the mechanism of peroxide decomposition mediated by metal salts revealed, prominent peroxide chemists from the 1940s and early 1950s began further investigations into alkyl hydroperoxide reduction (Figure 2.3). These chemists were primarily interested in the methods and mechanism of peroxide decomposition, with β-scission surfacing as the main mechanistic idea. George and Walsh, in their critical review from 1946, explicitly introduced the concept of β-scission for carbonyl bond (C=O) formation and concomitant scission of the weakest σ-bond [22]. They made this claim based on their unpublished

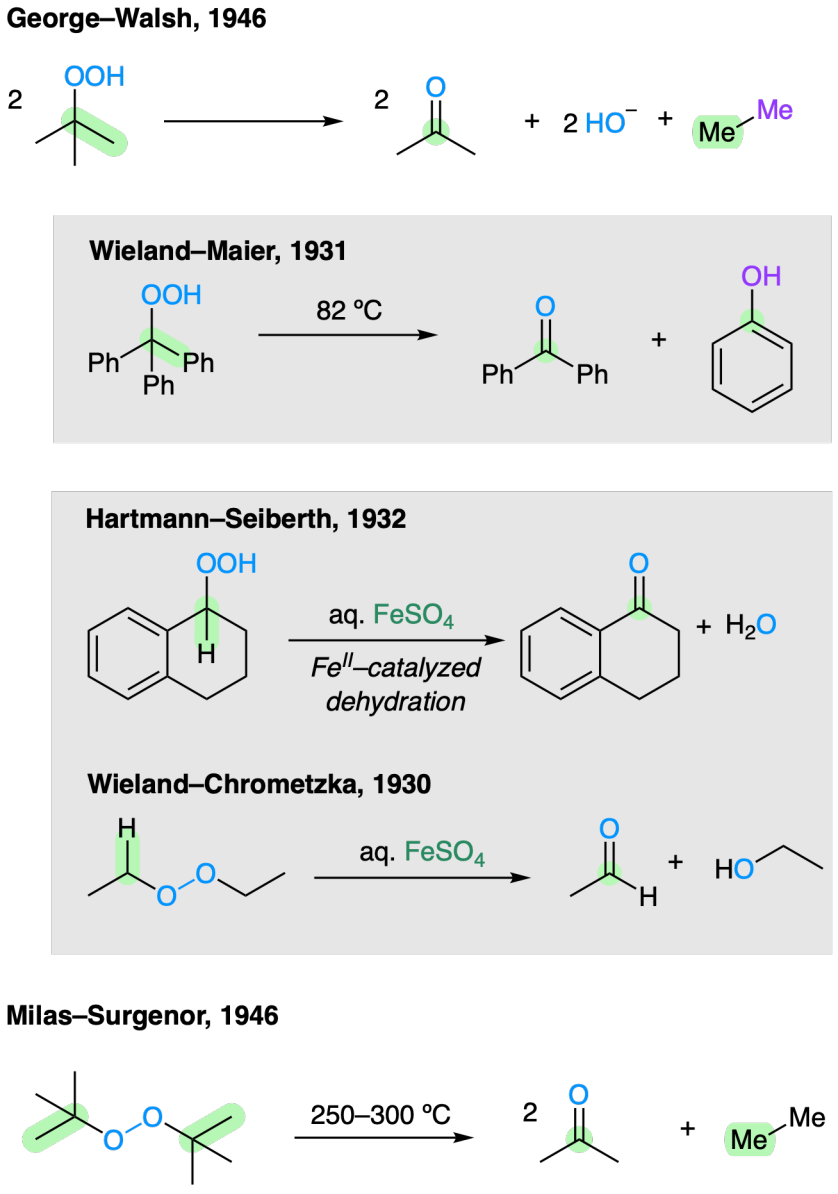


Figure 2.3 Early Reports of β-Scission and Characterization of Products When Reacting Tertiary Peroxides (Part 1)

work into the degradation of *tert*-butyl hydroperoxide. The β-scission of alkyl hydroperoxides was, however, observed earlier, in 1931, by Wieland and Maier with the formation of acetophenone and phenol from the pyrolysis of trityl hydroperoxide [23]. Acyl peroxides, on the other hand, have been known to undergo β-scission through a decarboxylative degradation pathway, but they are not applicable intermediates for dealkenylative functionalization, so we have excluded them from the scope of this review

[24,25]. Furthermore, secondary hydroperoxides tend to lead to dehydration reactions, often predominantly over scission, as observed by Hartmann and Seiberth in 1932 with the reduction of tetralin hydroperoxide to tetralone mediated by ferrous sulfate [26]. Similar reactivity was shown by Wieland and Chrometzka when they used iron(II) to reduce diethyl peroxide to acetaldehyde and ethanol [27]. Thus, only alkyl hydroperoxide scissions that result in $C(sp^3)$–$C(sp^3)$ bond cleavage are considered within the scope of this review.

The idea of alkyl hydroperoxide β-scission-guided explorations of the decomposition process climaxed separately in series of papers released by Milas, Raley-Rust-Vaughan, Hawkins, Kharasch, Kochi, and Youngman-Rust-Coppinger-De La Mare (Figure 2.4). We have selected a few examples from each of these series as markers of the progress of this field and how they relate to dealkenylative functionalization. In 1946, Milas focused mainly on the synthesis of peroxides and the thermal decomposition of hydroperoxides [28,29]. After thermolytic cleavage of di-tert-butyl peroxide, analysis of the decomposition products revealed the production of acetone and ethane gas. Milas also suggested that the decomposition of hydroperoxides leads to 'formation of intermediate free radicals'—an important observation for future work. In 1948, Raley, Rust, and Vaughan examined the rates of di-tert-amyl peroxide decomposition and concluded that 'alkoxy and methyl radicals' were produced [30]. Then, in 1949, Hawkins demonstrated the reduction of 2-phenyl-2-butyl hydroperoxide with ferrous salt, but failed to mention a radical pathway [31]. A year later, however, Hawkins realized that radical intermediates were formed in a

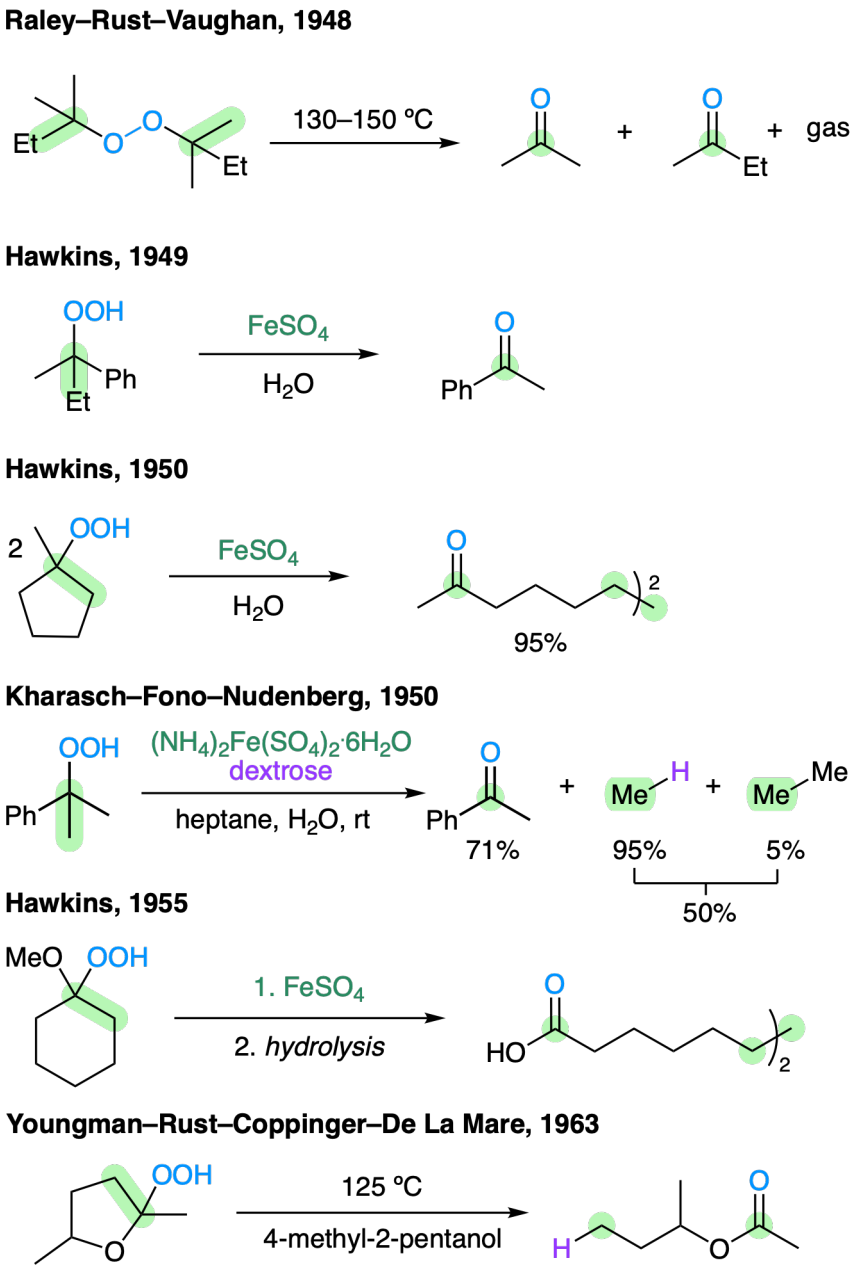


Figure 2.4 Early Reports of β-Scission and Characterization of Products When Reacting Tertiary Peroxides (Part 2)

ferrous sulfate promoted dimerization from methylcyclopentyl hydroperoxide [32]. Kharasch also explored decomposition products during this time [24g,33,34]. In one of his reports, he used ferrous ammonium sulfate to reduce α-cumyl hydroperoxide and emphasized the ratio of decomposition products and the effects of additives [35].

Kharasch observed the formation of acetophenone in 71% yield, resulting from β-scission, and collected 50% of the expected mixed gas containing 5% ethane and 95% methane originating from the β-scission. The ethane gas arose through dimerization of two methyl radicals, and the methane gas from a methyl radical abstracting a hydrogen atom from dextrose, the hydrogen atom donor. In 1955, the first report emerged of the reduction of an α-alkoxyhydroperoxide to produce an alkyl radical that was trapped immediately. Hawkins used iron(II) sulfate to reduce methoxycyclohexyl hydroperoxide to induce a ring-opening cascade terminating in a dimethyl ester dimer, which yielded a diacid after immediate hydrolysis [36]. Finally, Youngman and co-workers identified a ring-opening product from the thermal fragmentation of 2,5-dimethyltetrahydrofuran-2-hydroperoxide, adding another example of an alkoxy hydroperoxide degradation that is relevant to dealkenylative functionalization [37]. The 1940s through 1960s was a tremendous era for peroxide decomposition chemistry, in which the patterns for β-scission were realized, the scission rates were first measured, and α-alkoxyhydroperoxides—the main intermediates in dealkenylative functionalization—were first used in this context.

The ability to reliably generate alkyl radicals from alkyl peroxides led chemists toward research into functionalization methods (Figure 2.5). Minisci, Kumamato-De La Mare-Rust, De La Mare-Kochi-Rust, and Kochi-Mains published several reports of the reduction of peroxides to alkoxy radicals and attempts to functionalize alkyl radicals. Until this point, most researchers had focused on identifying the degradation products from the thermolysis and iron(II)-mediated reduction of peroxides. Minisci, on the other hand, had

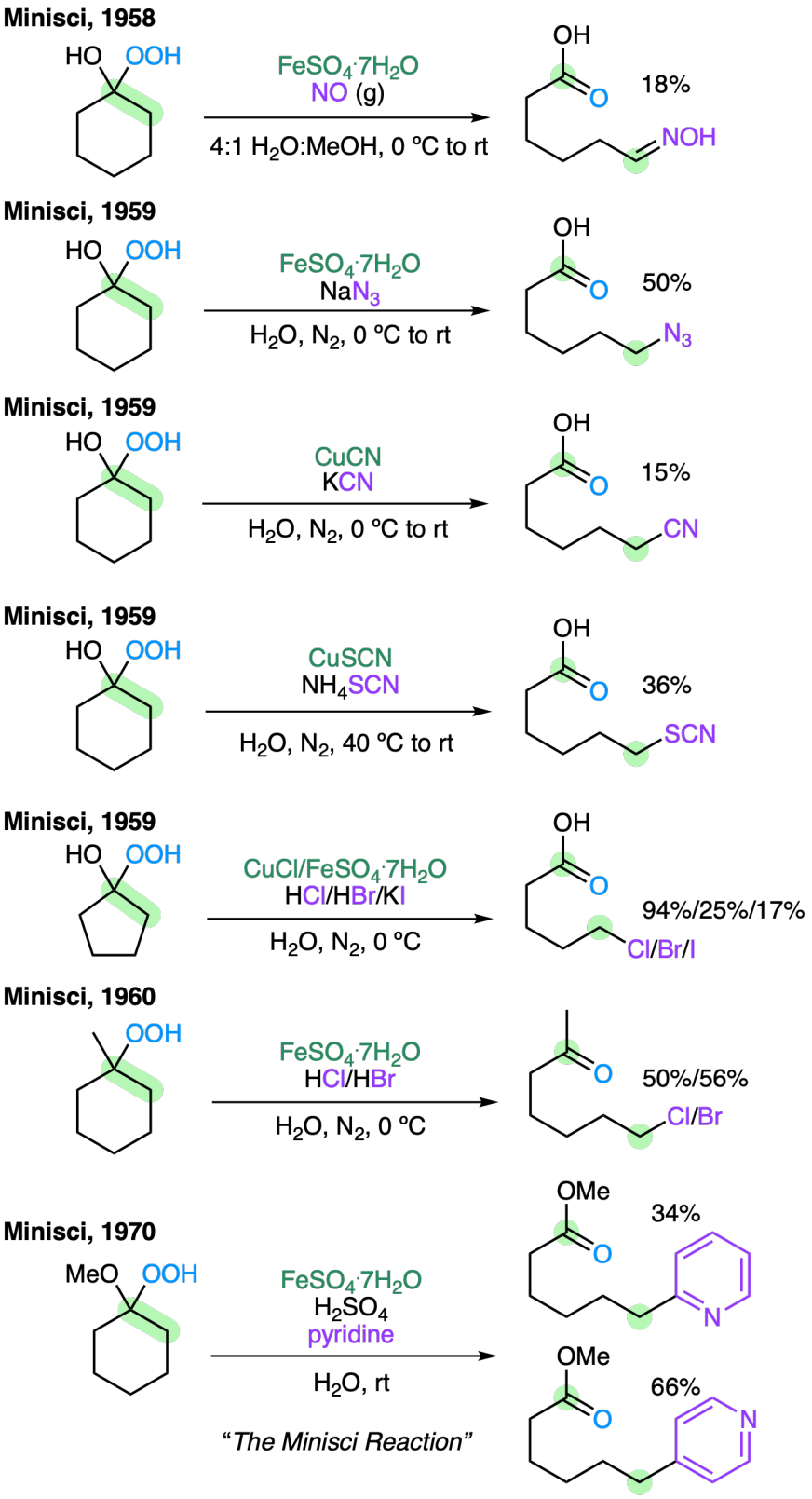


Figure 2.5 Early Reports of Reducing Tertiary Hydroperoxides with Iron(II) and Coper(I) with Intentional Radical Functionalization (Part 1)

an eye for the synthetic opportunities available for alkyl radicals. From 1958 to 1970, Minisci reported several instances of alternative radical functionalizations, achieving nitrosation [38], azidation [39], cyanation [39], isothiocyanation [40], halogenation [41–43], and arylation [44]. From various tertiary hydroperoxides and alkoxy hydroperoxides, Minisci used ferrous or cuprous salts to initiate the radical cascades. He coupled the alkyl radicals with nitric oxide, sodium azide, potassium cyanide, ammonium thiocyanate, hydrohalic acids or potassium iodide, and pyridine to realize these novel transformations. The last transformation, using pyridine as the radical trap, constitutes the venerable 'Minisci reaction'. In 1960, Kumamoto, Rust, and De La Mare demonstrated a chlorination through the reduction of 2-tetrahydropyranyl hydroperoxide with iron(II) chloride or a combination of iron(II) sulfate and copper(II) chloride (Figure 2.6) [45]. In 1961, just one year later, De La Mare, Kochi, and Rust found that, after ring opening of the reduction product from methylcyclohexyl hydroperoxide, the primary alkyl radical was oxidized by cupric sulfate to yield an olefin after copper(II)-promoted β-hydride elimination [46]. In 1963, this same trio proved that the same ferrous/cupric conditions were suitable for the reduction of hydroxycyclohexyl hydroperoxide to yield 5-hexenoic acid [47]. In 1965, Kochi and Mains moved from iron(II) to a copper(I) catalyst to initiate tertiary hydroperoxide fragmentation, detecting acetone and ethylene gas as products [48]. In the period from 1955 to 1970, the synthetic potential of peroxide degradation gained the momentum that led to today's applications of alkyl peroxide reduction [49].

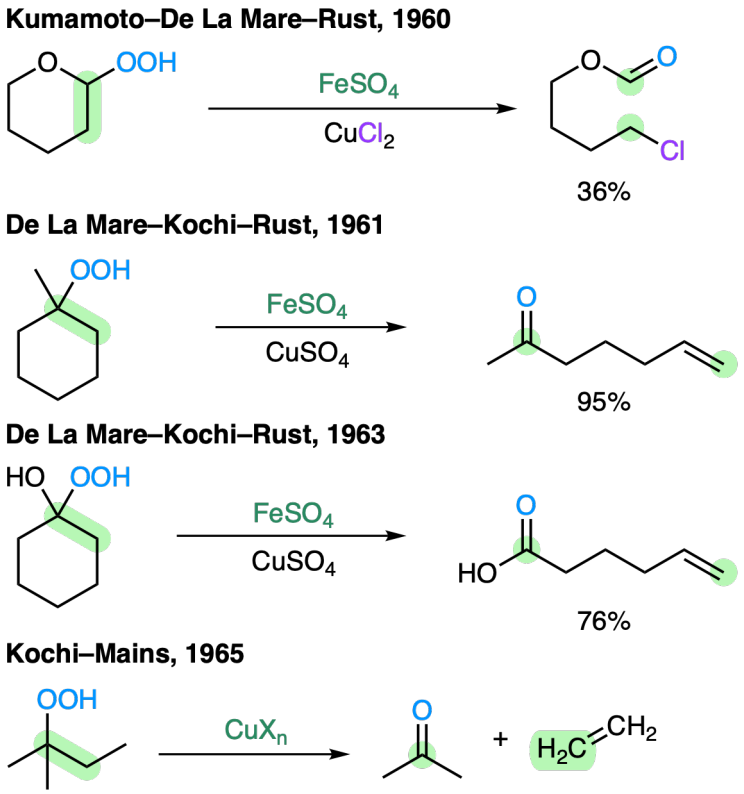


Figure 2.6 Early Reports of Reducing Tertiary Hydroperoxides with Iron(II) and Coper(I) with Intentional Radical Functionalization (Part 2)

Dealkenylative functionalization is powerful because it both installs the peroxide and reduces it within a streamlined process. Early studies of peroxide degradation were limited by the few synthetic options available for preparing alkyl peroxides, requiring isolation of the peroxide prior to decomposition. Acylation, autoxidation, condensation, and substitution dominated the early techniques for peroxide synthesis (Figure 2.7). In 1858, Brodie generated the first synthetic perester from benzoyl chloride and sodium peroxide [50]. In the 1940s, Milas expanded the scope of acylation by using tert-butyl hydroperoxide and a variety of acid chlorides [51]. Another simple method for peroxide formation is condensation, with the first instance reported in 1895 by Wolffenstein, who

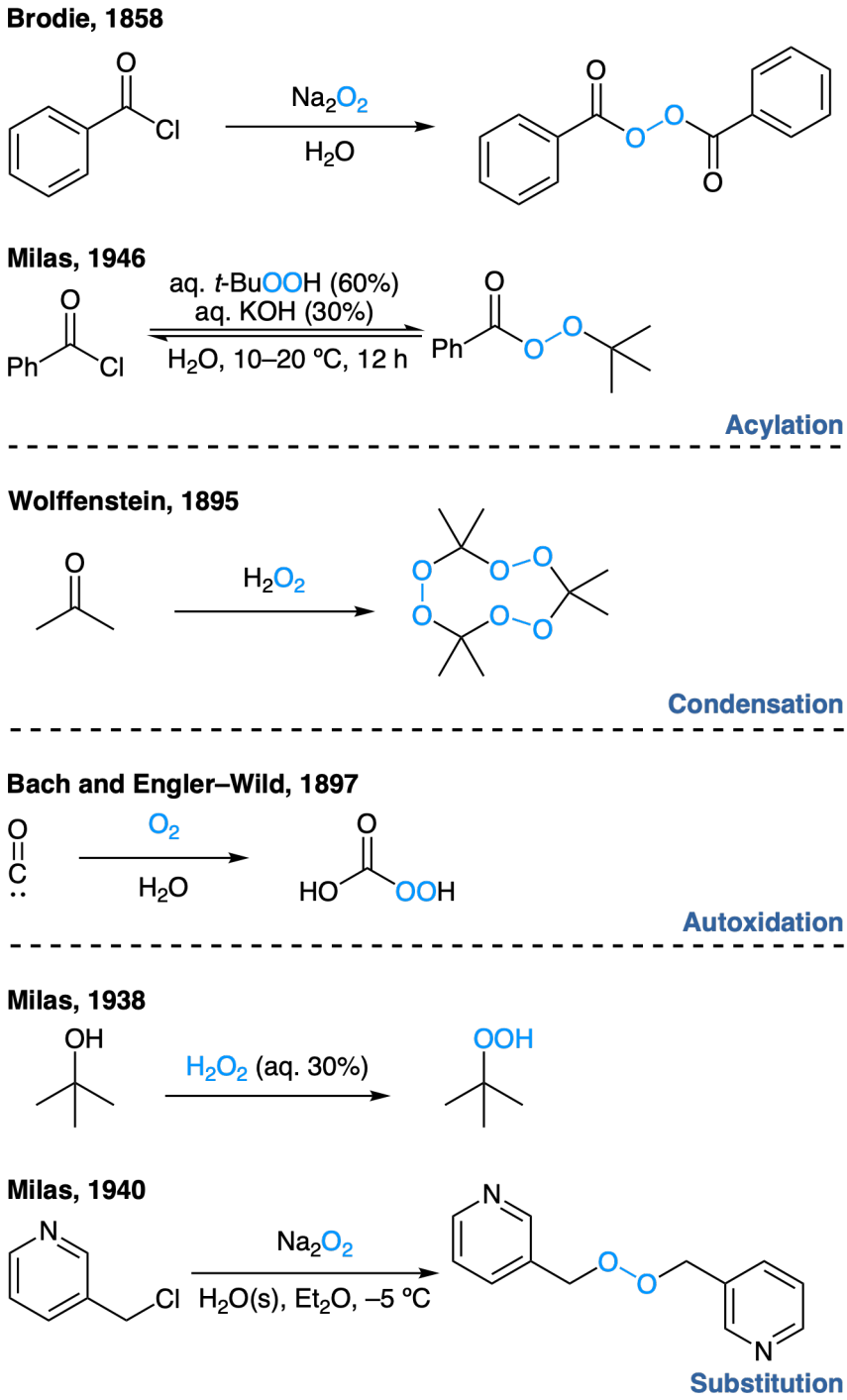


Figure 2.7 Early Methods of Peroxide Synthesis

stirred three equivalents of acetone with hydrogen peroxide and formed the explosive triacetonetriperoxide [52]. Autoxidation was also common in this era. Two separate groups conducted the first intentional autoxidations in 1897. Both Bach and Engler-Wild

combined carbon monoxide and oxygen over water to form percarbonic acid [53,54]. Alternatively, peroxides may be formed through substitution. In 1938, Milas demonstrated S_N1 chemistry with tertiary alcohols and hydrogen peroxide [55]; in 1940, he described S_N2 chemistry with a primary alkyl halide and sodium peroxide [56]. Variations of these four methods have been expanded upon over time, but none of them is capable of introducing a peroxide from an alkene.

Following the discovery of the Diels-Alder cycloaddition, alkenes became a target for peroxide synthesis using pericyclic chemistry or metal-mediated methods (Figure 2.8). Oxygen and ozone were quickly identified as renewable and compatible pericyclic partners for alkene peroxidation. In 1928, Windaus and Brunken formed a six-membered endoperoxide through (4+2) photochemical cycloaddition of singlet oxygen with ergosterol [57]. Almost 40 years later, Bartlett and Schapp conducted the first (2+2) photochemical cycloaddition to form a four-membered endoperoxide. They irradiated a solution of diethoxyethylene and oxygen with a porphyrin photosensitizer to form the cycloadduct [58]. Singlet oxygen was also used in the 1953 Schenck-ene reaction to install an allylic hydroperoxide [59]. Criegee explored the interaction between ozone, discovered by Schönbein in 1838 [60], and alkenes. In the late 1940s, Criegee identified peroxide intermediates formed through a (3+2) dipolar cycloaddition and *retro*-(3+2) cycloaddition [61–63]. He discovered that the ozonation of 1,2,3,4,5,6,7,8-octahydronaphthalene in methanol led to a stable α-methoxyhydroperoxide, a reactive intermediate that would later be exploited for dealkenylative functionalization [64]. These three species—singlet oxygen, ozone, and triplet oxygen—are ideal reagents for subsequent reduction of the peroxide intermediate because they may not require isolation

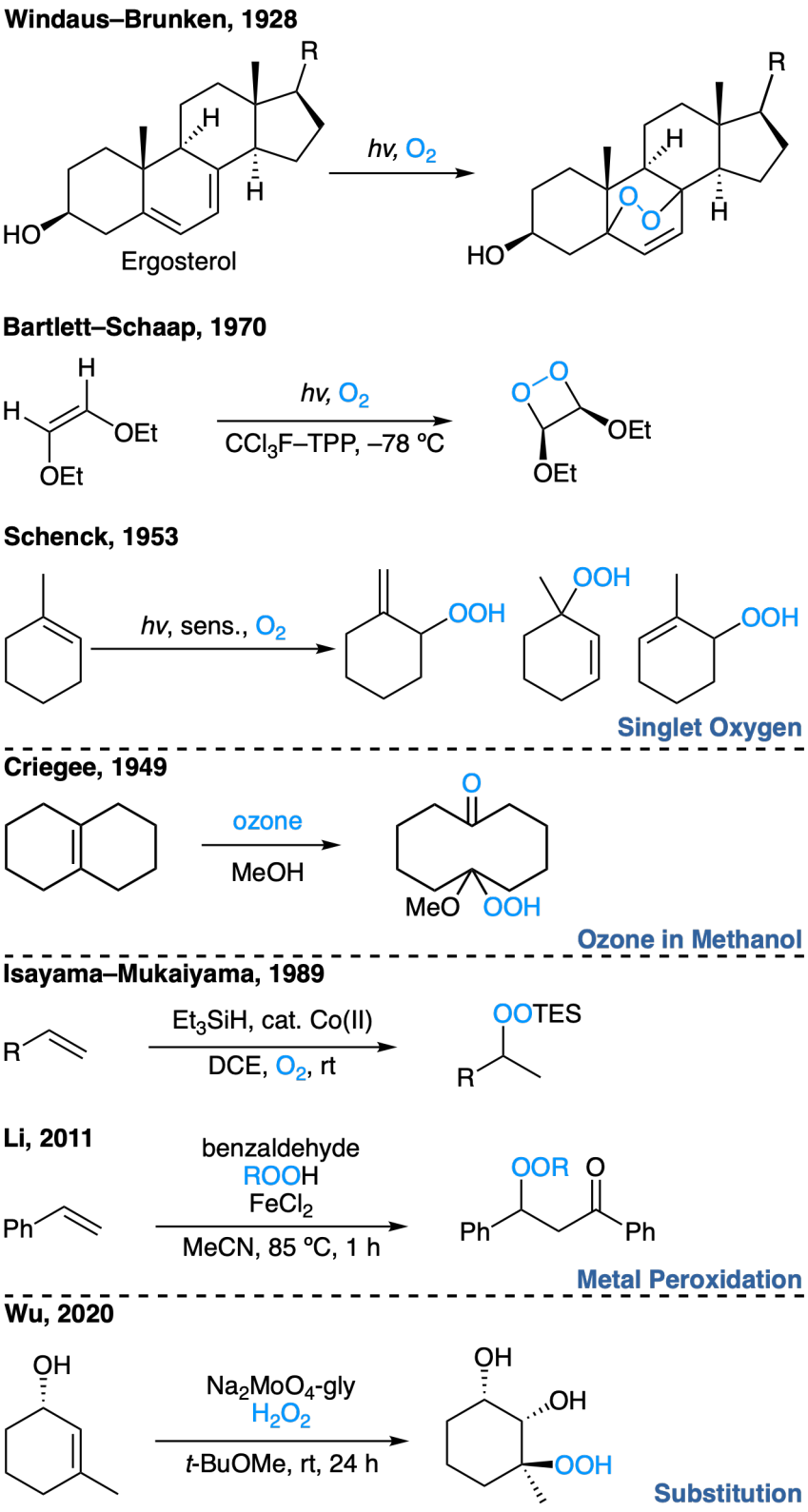


Figure 2.8 Various Methods of Peroxide Synthesis that Employ Pericyclic Reactions or Metal Salts

of the alkyl peroxide product, with excess ozone and oxygen being removable without a trace. In 1989, Isayama and Mukaiyama developed a method using triplet oxygen to install an alkyl peroxide [65]. With catalytic cobalt(II) and an alkylsilane, they added triplet oxygen regioselectively to an alkene via radical intermediates, marking the first example of a metal-catalyzed peroxidation. In more recent metal-mediated peroxidations, Li spearheaded the subfield of metal-mediated difunctionalization of alkenes. In a 2011 example, Li's group used iron(II) chloride, *tert*-butyl hydroperoxide, and aldehyde derivatives to difunctionalize styrenes with peroxide and β-peroxy ketones [66]. While Li pioneered the field, other groups difunctionalized alkenes with peroxides and a plethora of other functionalities by applying metal salts of manganese, iron, copper, silver, cobalt, and rhodium [67]. Finally, a very recent method for peroxidation, from 2020, involved molybdenum(VI)-catalyzed epoxidation of allylic alcohols in a Henbest manner and in situ attack of peroxide to open the epoxide [68]. This stereoselective method of peroxidation used known stereoselective epoxidation methods. Whether it involves oxygen/ozone or a metal-mediated process, the peroxidation of alkenes is a relevant topic for peroxide chemists because it is critical for dealkenylative functionalization.

Toward the end of the 1950s, all of the pieces necessary for dealkenylative functionalization were available, and chemists began using them in tandem (Figure 2.9). In 1957, Bailey and Bath published an early example of ozone-mediated peroxide degradation. By treating dibenzoylpropene with ozone, they induced a hydroperoxide, which degraded under thermolytic conditions [69]. Despite the lack of an initiator, a radical process was postulated, due to the formation of benzil, an unexpected side product. The next example of peroxide installation by ozone and subsequent radical peroxide

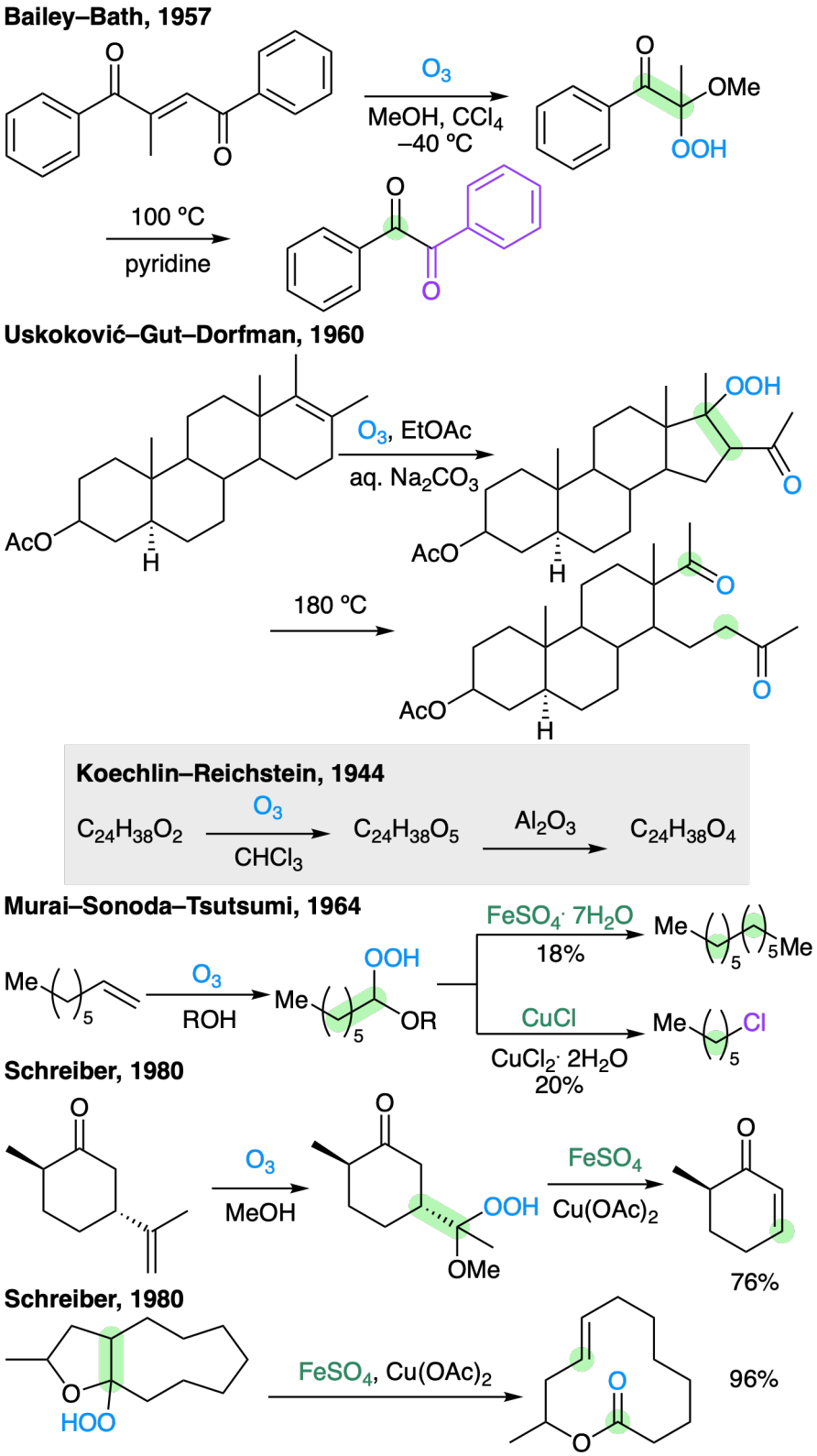


Figure 2.9 Combinations of Ozone Mediated Addition of Alkenes and Subsequent Degradation

degradation appeared in 1960, reported by Uskoković-Gut-Dorfman [70]. They thermolyzed a hydroperoxide at 180 ºC to initiate the radical cascade and noted that the elemental analysis and melting point of their decomposition product were similar to those reported by Koechlin and Reichstein in 1944 [71]. Although they had not mentioned the word 'hydroperoxide,' Koechlin and Reichstein reported the aluminum oxide assisted degradation of $C_{24}H_{38}O_5$ to $C_{24}H_{38}O_4$, without reporting any structures for this reaction. This paper provides possibly the first instance of radical peroxide degradation from an ozone-generated peroxide. In 1964, Murai, Sonada, and Tsutsumi finally combined ozonolysis and transition-metal-mediated peroxide reduction for chemical synthesis [2]. The Criegee intermediate from the ozonolysis of 1-octene was trapped with ethanol, forming an α-ethoxyhydroperoxide. Using either iron(II) sulfate or CuCl-$CuCl_2$ the dimerized or chlorinated products from the reduction of this hydroperoxide were identified as *n*-dodecane and *n*-hexyl chloride. Schreiber employed a similar method in 1980. He used ozone to install a hydroperoxide and then iron(II) sulfate and copper(II) acetate to form a dealkenylated enone product from (–)-dihydrocarvone, a terpenoid [3]. The same article contained the first example of metal-mediated reduction of a hydroperoxide in the total synthesis of a natural product, (±)-recifeiolide [3]. Since then, the conditions popularized by Schreiber were applied in several total syntheses, but only oxidative termination had ever been achieved [72]. Dealkenylative functionalization, initiated in 2018, revamped this historic method, improving upon precedent to make it a more relevant tool for the synthetic organic chemist.

2.5 Motivation to Pursue Dealkenylation

In 2014, the Kwon group designed *trans*-4-hydroxy-L-proline-derived [2.2.1] bicyclic phosphines (HypPhos) for catalysis of enantioselective allene-imine [3+2] annulations to obtain chiral pyrroline products (Figure 2.10) [73]. While both the endo- and exo-HypPhos catalysts performed excellently, achieving up to 99% yield and greater than 99% enantiomeric excess (ee), only one antipode of HypPhos was readily available. To address this limitation, they selected carvone to build the [2.2.1] phosphine because it is a chiral terpenoid available commercially in both enantiomeric forms.

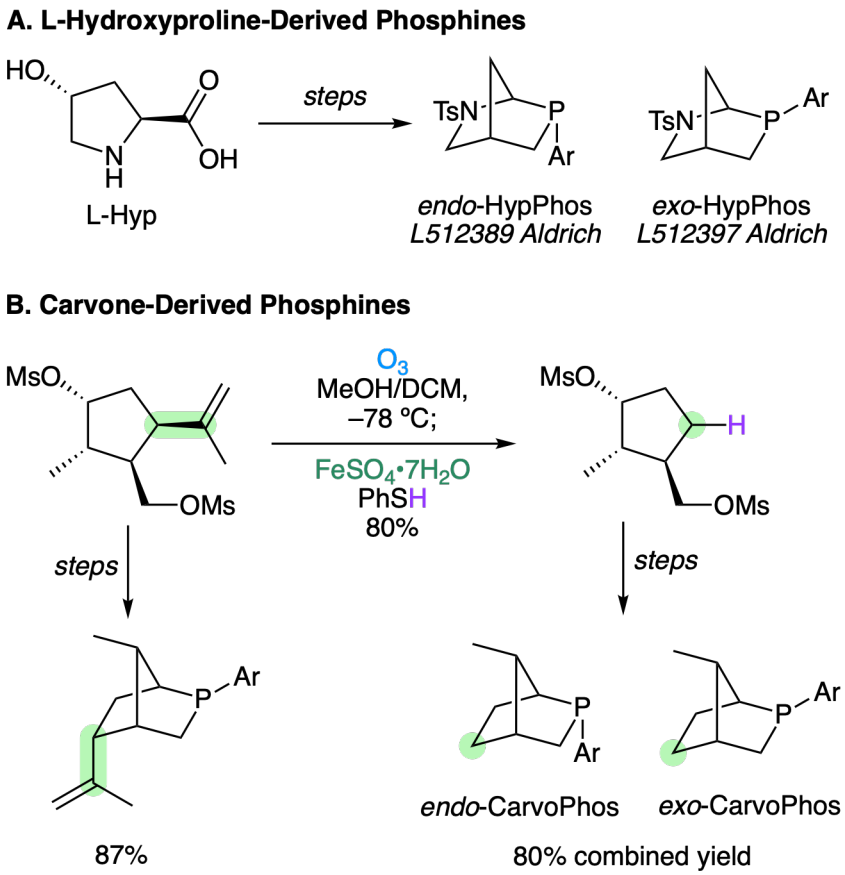


Figure 2.10. Motivation to Pursue Dealkenylation

In 2018, the group set out to make (–)-carvone-derived [2.2.1] bicyclic phosphines (CarvoPhos). From a common dimesylate intermediate, they synthesized several [2.2.1] bridged bicyclic phosphines, but isolated only *exo*-CarvoPhos derivatives. The performance of these catalysts was mediocre, achieving ee values in the range of 35-98%. Working under the assumption that steric crowding of the endo-face of the catalyst by the isopropenyl group precluded the formation of *endo*-CarvoPhos, they considered the hydrodealkenylative removal of the isopropenyl group.

Employing iron(II) sulfate heptahydrate and benzenethiol, a hydrogen atom donor (HAD), provided access to the hydrodealkenylated product from the α-methoxyhydroperoxide intermediate. Lacking the isopropenyl group, both exo- and endo-CarvoPhos performed similarly to the previously reported HypPhos catalyst, achieving yields ranging from 88 to 99% and ee values from 84 to 99%. With successful hydrodealkenylation of the isopropenyl group from the dimesylate, the Kwon group launched an investigation into the extent and applications of this methodology.

2.6 Dealkenylation in the Present

Building on their success in using hydrodealkenylation in the synthesis of CarvoPhos, the Kwon group pursued peroxide reduction with a HAD as a powerful synthetic tool for cleaving the C(sp^3)–C(sp^2) bonds of alkenes and installing C(sp^3)–H bonds in terpene derivatives (Figure 2.11). The group coined the term 'hydrodealkenylation' to describe this transformation. Using iron(II) sulfate heptahydrate and benzenethiol as the HAD, bicyclic and monocyclic terpenes bearing an isopropenyl group underwent clean removal of this substituent with installation of a hydrogen atom. Isopropenyl-containing substrates that fared well in this transformation, with yields from 62 to 94%, included nootkatone, (–)-

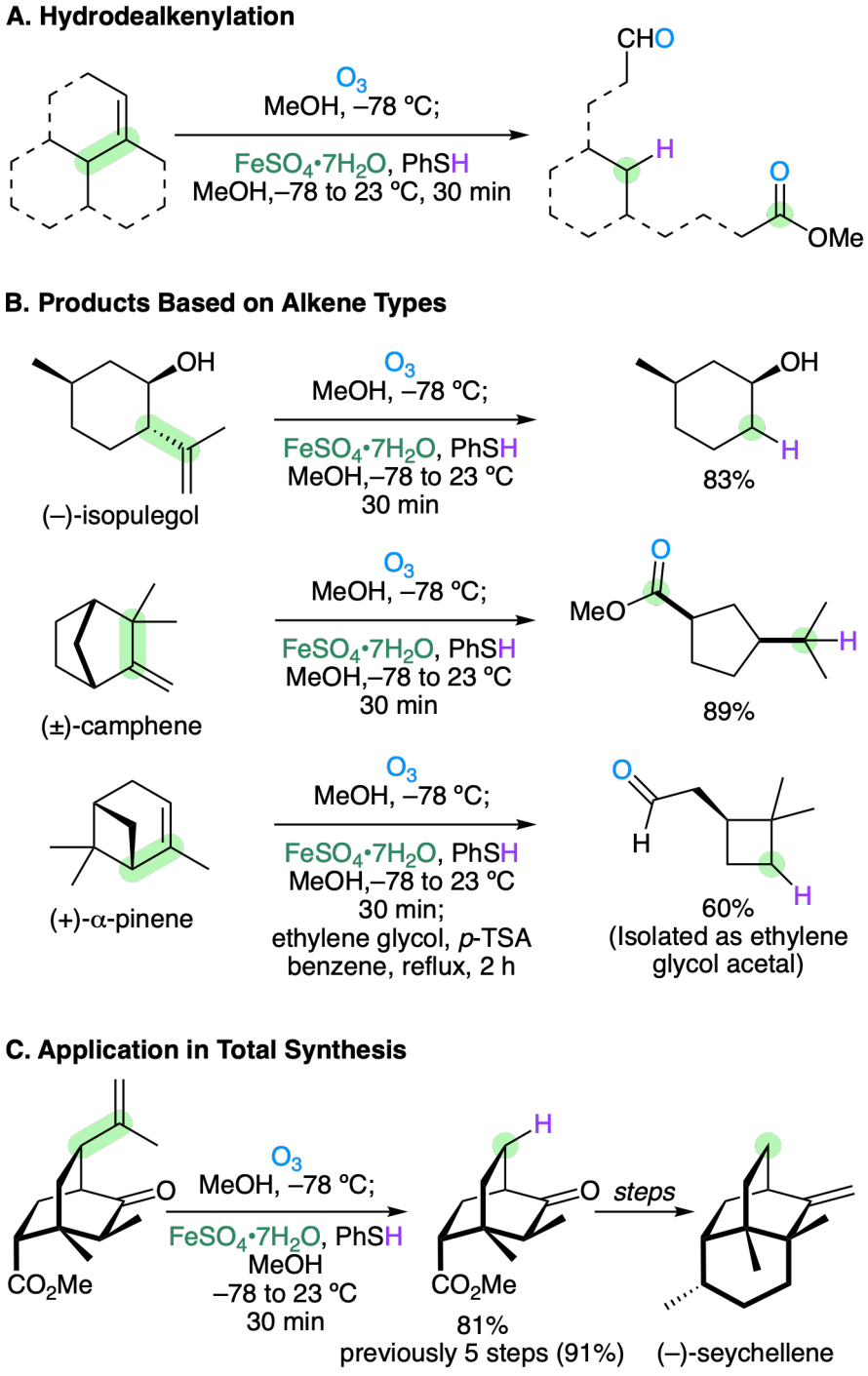


Figure 2.11 Hydrodealkenylation

isopulegol, (–)-cis-limonene oxide, Wieland-Meischer ketone precursors, betulin, and betulinic acid. Even when reacting (–)-isopulegol on a scale of 100 mmol, a high isolated yield of 89% was achieved.

Cyclic substrates bearing exomethylene units underwent radical ring-opening processes to form esters tethered to the alkyl chain in yields of 26-89%. Methylenecyclohexanes [e.g., (±)-camphene and (–)-β-pinene] smoothly underwent the ring-opening transformation. Cycloalkenes [e.g., methylcyclohexene, (+)-α-pinene, (–)-nopol and (–)-α-cedrene] efficiently produced aldehyde products in yields of 60-88%. Because some of the substrates were fairly low in weight, instant acetal protection of the aldehydes was performed.

Hydrodealkenylation was exemplified as a powerful synthetic strategy for organic chemistry by application in the formal syntheses of five natural products: (–)-pupukeanone [74], (–)-seychellene [75], (–)-7-epibakkenolide [76], periconianone A [72f], and a chiral steroid [77], with their known synthetic routes shortened by five, four, three, two, and two steps, respectively. On ChemRxiv in late 2022, the Newhouse group demonstrated the first use of hydrodealkenylation in a total synthesis in their construction of (carvone-derived) (+)-shearilicine [15]. The group used the method to cleave an isopropenyl group from a tricycle. In 2023, the natural product vilmoraconitine was also synthesized using hydrodealkenylation to open a bicycloalkene moiety and access an aldehyde [16]. The benefits of this reaction are self-evident in terms of both strategic and sustainability standpoints.

After the success of hydrodealkenylation, it became apparent that conditions for the addition of other radical coupling partners needed to be explored. A few months after their

publication of hydrodealkenylation, the Kwon group released dealkenylative thiylation (Figure 2.12) [10]. In this method, after cleavage of the C(sp^3)–C(sp^2) bond, a C(sp^3)–S bond is formed through radical trapping using a diaryl disulfide. From an optimization study with a bicyclic hydroxyketone bearing an isopropenyl group, diphenyl disulfide and other diaryl disulfides proved to be the best thiylating reagents. Moving away from hydrogen atom donors caused the rate of radical addition to decrease; therefore, the number of equivalents of disulfide was doubled (3.0 equivalents instead of 1.5) to compensate.

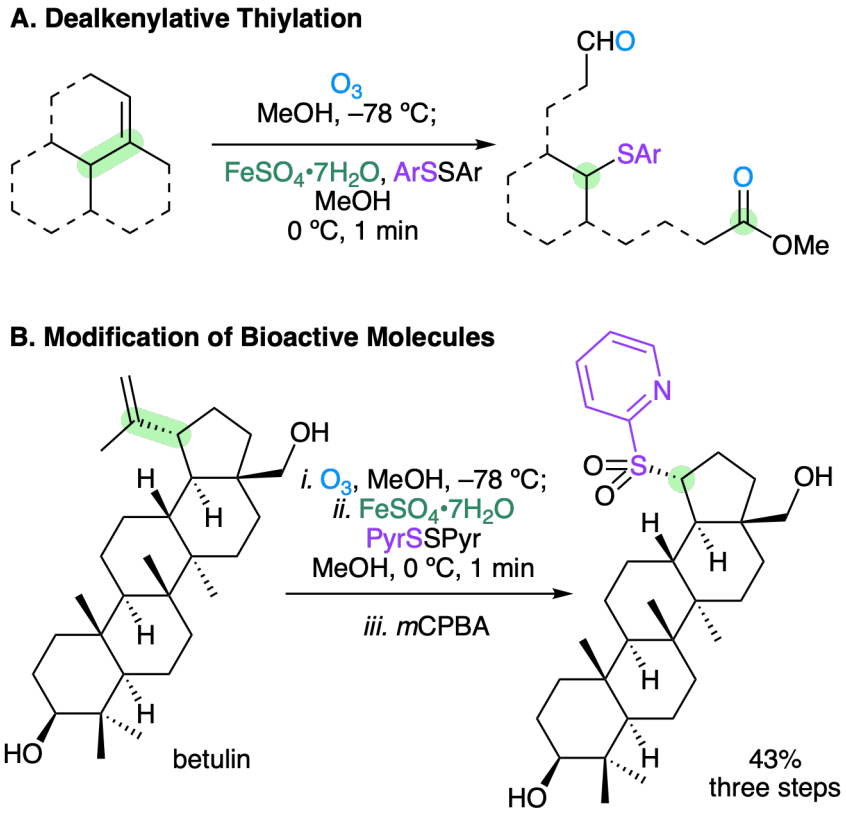


Figure 2.12. Dealkenylative Thiylation

With optimized conditions in hand, many of the terpene substrates that had not been employed in hydrodealkenylation—including (±)-sabinene, (+)-2-carene, α-terpineol, and

norbornylene—were used to demonstrate the pertinence of the thiylation process. The yields of isopropenyl cleavage products ranged from 58 to 80%, exo-methylenecycloalkane cleavage products from 35 to 80%, and cycloalkene cleavage products from 5 to 75%. Several synthetic transformations applicable to thiylated products were explored, including oxidation, alkylation, elimination, 'cross-coupling,' and lactonization. In the provided example, betulin was subjected to dealkenylative thiylation, with the resulting thioether then oxidized to the sulfone derivative for use in cross-coupling reactions (Figure 2.13A) [78].

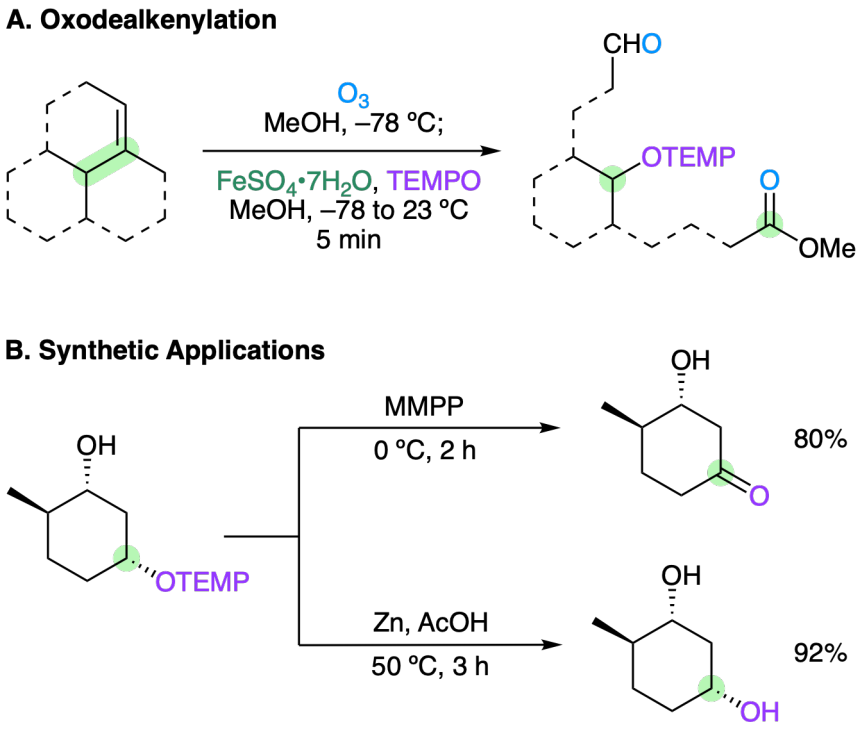


Figure 2.13 Oxodealkenylation

After dealkenylative thiylation, the next logical step was to use (2,2,6,6-tetramethylpiperidin-1-yl)oxyl (TEMPO), a well-known persistent radical reagent, to achieve aminoxylation (Figure 2.13B). The reaction conditions for dealkenylative

aminoxylation were similar to those for hydrodealkenylation. First, ozonolysis of the alkene in methanol yielded a hydroperoxide, which was subjected to reduction mediated by iron(II) sulfate, leading to an alkyl radical that was terminated by TEMPO to form a C(sp^3)–O bond. The rate constant for alkyl radical coupling with TEMPO (>7.6 × 10^8 M^{-1} s^{-1}) [79] was larger, by a few orders of magnitude, than that for thiylation with diaryl disulfides (ca. 6 × 10^5 M^{-1} s^{-1}) [80] and similar to that for hydrogen atom transfer with benzenethiol (1.3 × 10^8 M^{-1} s^{-1}) [81]. Therefore, only 1.5 equivalents of TEMPO were required.

The TEMPO adduct was further oxidized to achieve Cope elimination, furnishing the oxodealkenylation product. Optimization revealed that 2.5 equivalents of magnesium monoperoxyphthalate hexahydrate (MMPP) was the best oxidant, providing access to the desired ketone in one pot. Isopropenyl cleavage resulted in yields of 50–95%. For non-isopropenyl-containing substrates, there were two reported instances of keto-ester formation (58% and 87%), one instance of aldehyde-methyl ester formation (82%), and keto-aldehyde formation (67%) with two regioisomers. The Kwon group focused mainly on oxidation of the TEMPO adduct, but reduction is also possible. For example, zinc-mediated reduction of the TEMPO adduct from (–)-dihydrocarveol, in the presence of acetic acid, produced the alcohol rather than the ketone.

The next approach that the Kwon group took was cleaving the C(sp^3)–C(sp^2) bonds to form new C(sp^3)–C(sp^2) bonds. The first example of this type of C–C bond formation was dealkenylative alkenylation (Figure 2.14A) [12]. Alkene formation is important in organic synthesis because olefins are among the most versatile synthetic intermediates [1]. Early olefinations from alkyl radicals relied on β-hydride elimination using a copper(II)

species, as demonstrated by De La Mare–Kochi–Rust [46,47]. The Kwon group considered β-nitroolefins such that the resulting radicals could undergo radical elimination of the nitro group to form alkenes instead.

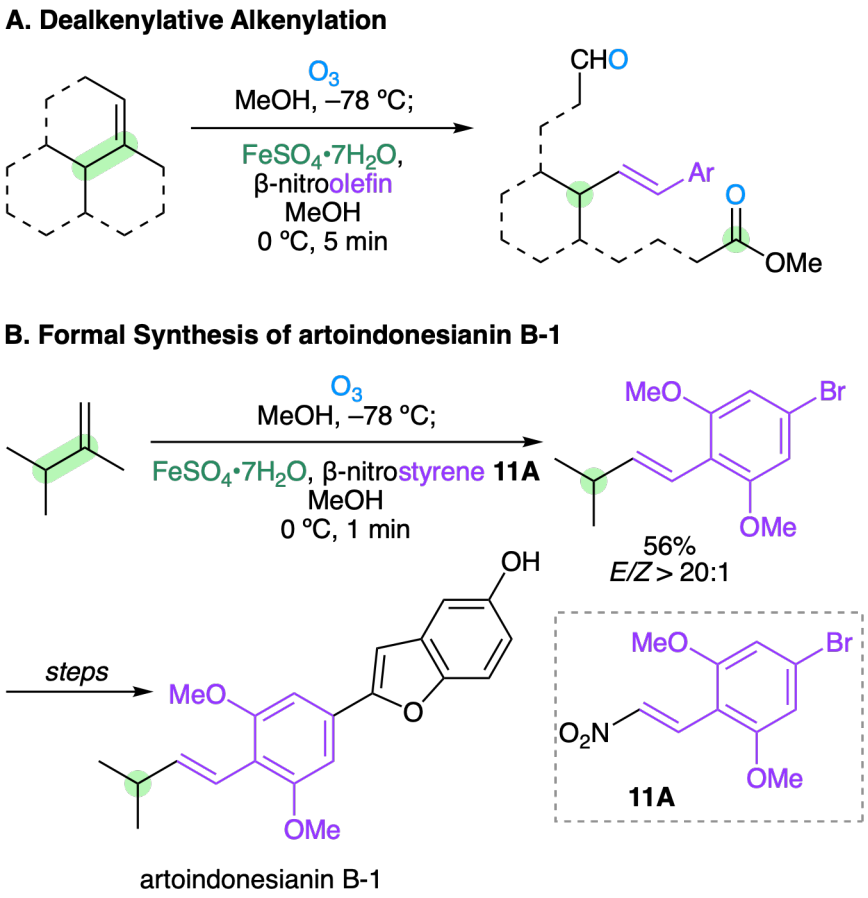


Figure 2.14 Dealkenylative Alkenylation

Monoterpenoids [e.g., (–)-isopulegol, cis-(–)-limonene oxide, trans-(+)-dihydrocarvone], a diterpenoid [(+)-nootkatone], and a triterpenoid (betulin) all underwent dealkenylative styrylation. After successes with other monoterpenoid derivatives with yields of 30–76%, the Kwon group explored altering the nitroolefin by adding substituents to various positions of styrene and keeping the alkene consistent. This approach fared

well, with product yields ranging from 42 to 78%. The product yield decreased dramatically when the nitroolefin did not contain a β-aryl group and/or if there was a substituent on the α-carbon atom of the nitroolefin, due to steric repulsion.

Furthering the scope of the reaction, esters and aldehydes were obtained from exo-methylenecycloalkanes (21–67%) and cycloalkenes (41–60%). In terms of geometric isomers, exclusive formation of the more stable *E*-alkenylated product was typical; in the absence of exclusive formation, the *E*-isomer outcompeted the formation of the *Z*-isomer by an order of magnitude. Because alkenes were obtained as products, subsequent hydrogenation, ozonolysis, and ring-forming reactions confirmed that the alkenylated products had utility for further transformations. Finally, the Kwon group completed formal syntheses of artoindonesianin B-1 (Figure 2.14B) [82] and the synthesis of the drug (*E*)-metanicotine [83].

One final takeaway from that report was that the rate of radical addition for alkenylation ($<7.6 \times 10^5$ M^{-1} s^{-1}) [84] was, like that for thiylation, lower by orders of magnitude relative to the rates of hydrogen atom abstraction and aminoxylation. Optimization of the alkenylation process revealed that switching the alkene (peroxide after exposure to ozone) from the limiting reagent to an excess and increasing the number of equivalents of iron(II) sulfate heptahydrate to 3.2 led to the highest product yields. For hydrogenation and aminoxylation, the radical addition rates were sufficiently speedy to outcompete undesired side reactions. With thiylation and alkenylation, however, increasing the number of equivalents of a reagent was necessary to thwart side reactions.

The most recent pertinent report from the Kwon group describes dealkenylative alkynylation mediated by catalytic iron(II), with vitamin C added to regenerate the iron(II)

catalyst (Figure 2.15A) [13]. Again, Criegee ozonolysis and iron(II)-mediated reduction of peroxides allowed the addition of alkynes to terpenes, transformations that had not been accomplished previously through dealkenylative routes. Similar to alkenylation, addition into the alkyne produced a vinyl radical that underwent β-elimination of an arylsulfonyl unit, rather than a nitro group. In that report, the Kwon group found that the lower rate of radical addition affected the yield of the dealkenylated product, leading them to use catalytic, rather than stoichiometric, iron(II). A greater concentration of the alkyl radical in the reaction pot led to greater formation of undesired side products.

As stated earlier, adding a greater number of equivalents of diphenyl disulfide sufficed for thiylation, and increasing the number of equivalents of iron(II) and using the alkene in excess sufficed for alkenylation. The consequence of increasing the number of equivalents of a reagent or using the alkene in excess is an increase in the general cost of a reaction—not ideal from the standpoint of atom economy. Because of the relatively low rate of radical addition into the ethynylsulfone ($<1.8 \times 10^5$ M^{-1} s^{-1}) [84], the solution for alkynylation was to decrease the concentration of the alkyl radical by decreasing the amount of iron(II) catalyst in the reaction pot at any single point in time. Optimization revealed that L-ascorbic acid (vitamin C) was a cheap and robust reductant for regenerating iron(II).

Using various terpenes, terpenoids, and their derivatives, isopropenyl cleavage was successful in installing substituted alkynes. Employing substrates similar to those in the previous reports, yields of 41–86% were achieved. With exomethylene-substituted cycloalkanes, the yields of ring-opened products were 45–67%. With yields from 32 to 45%, cycloalkenes were successfully opened to form alkynylated aldehydes. Widening

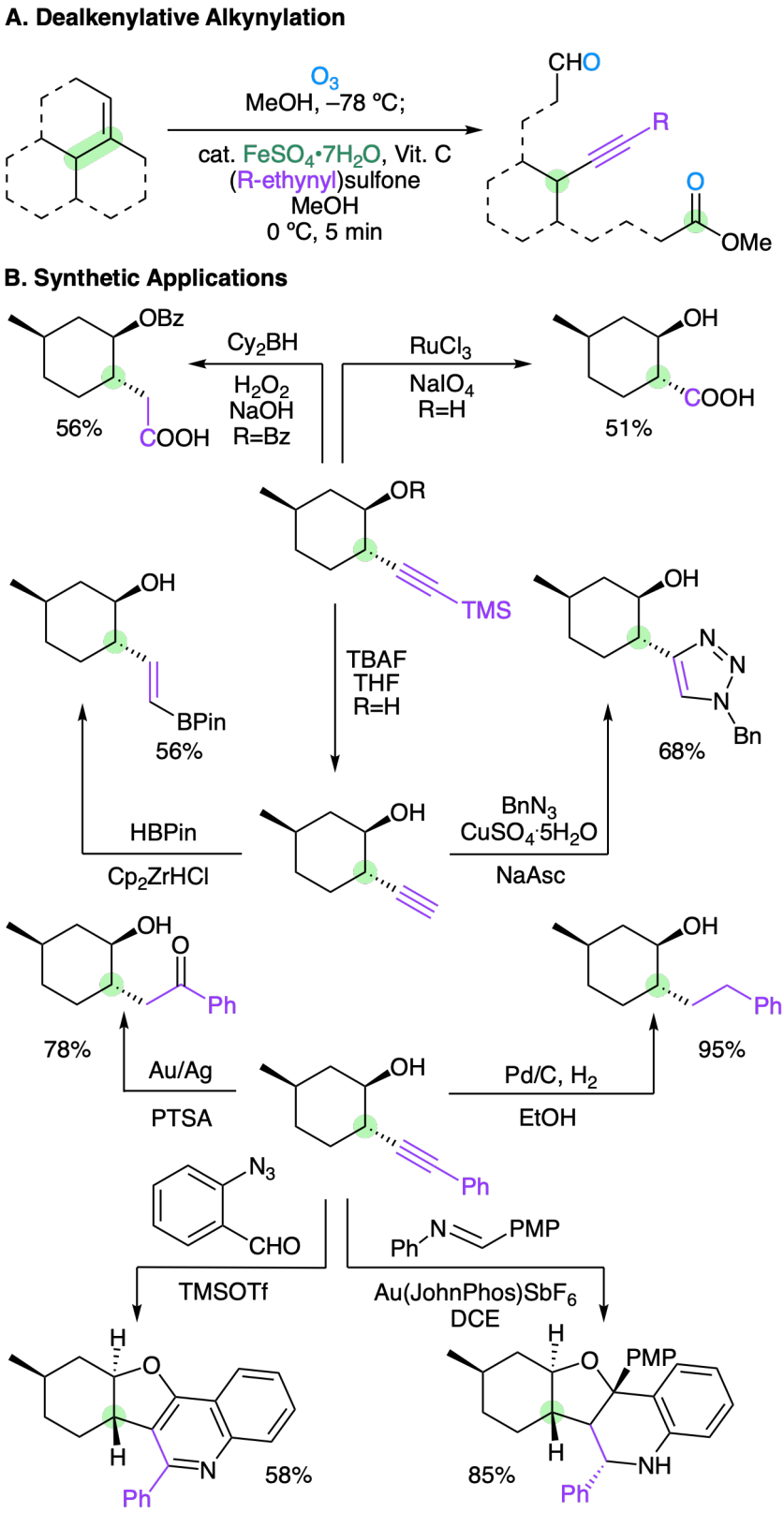


Figure 2.15 Dealkenylative Alkynylation

the substrate scope, modifying the arylethynyl sulfones with electron-withdrawing and electron-donating substituents proved to be successful, with the alkynylated products obtained in yields from 42 to 83%. In contrast to alkenylation, the alkynylations were successful when the aryl group was replaced by an alkyl or silyl substituent, with yields ranging from 41 to 55%.

Because alkynes are synthetically amenable to various transformations, the Kwon group performed many relevant reactions with the alkynylated products (Figure 2.15B). Using a trimethylsilyl (TMS)-substituted alkyne, some of these synthetic transformations included hydroboration/oxidation to form a carboxylic acid and Ru/periodate-mediated formation of a chiral carboxylic acid. Upon deprotection of the TMS-substituted alkyne using tetra-n-butylammonium fluoride (TBAF), the terminal alkyne was hydroborated to produce a vinylboronate ester, while a copper-catalyzed Huisgen (3+2) cycloaddition allowed the synthesis of 1,2,3-triazoles. For phenyl-substituted alkynes, hydrogenation formed an aliphatic chain in quantitative yield. A silver/gold-mediated hydration to give a phenone proved to be possible. Formation of a hexahydrobenzofuran-fused quinoline, using o-azidobenzaldehyde and trimethylsilyl triflate, succeeded with moderate yield. Furthermore, through a gold-catalyzed hydroalkoxylation/Povarov cascade, a tetrahydroquinoline was successfully synthesized from an alkynol.

2.7 Conclusion

Dealkenylative functionalization elegantly addresses a historically underutilized chemical operation: fission of alkenyl $C(sp^3)$–$C(sp^2)$ σ-bonds. This one-pot, dump-and-stir, open-to-the-air reaction is powerful because it pairs a two-electron pericyclic process with the one-electron chemistry of iron(II) to yield a method that is simultaneously quick and robust, operationally efficient, and step-economical.

The abundance of alkene archetypes (Figures 16–19) of terpenes and terpenoids elevates the technique because these molecules serve as multipurpose model substrates while also providing platforms for method development and opportunities for rapid derivatization into new feedstock chiral building blocks. Manifested into six modes—hydro, thiyl, oxo, hydroxy, alkenyl, and alkynyl—dealkenylative functionalization captures nearly all desirable outcomes, although there are examples of radical trapping still to be tested. As modern single-electron chemistry becomes more popular, dealkenylative strategies will likely serve as promising tools for applications in organic synthesis.

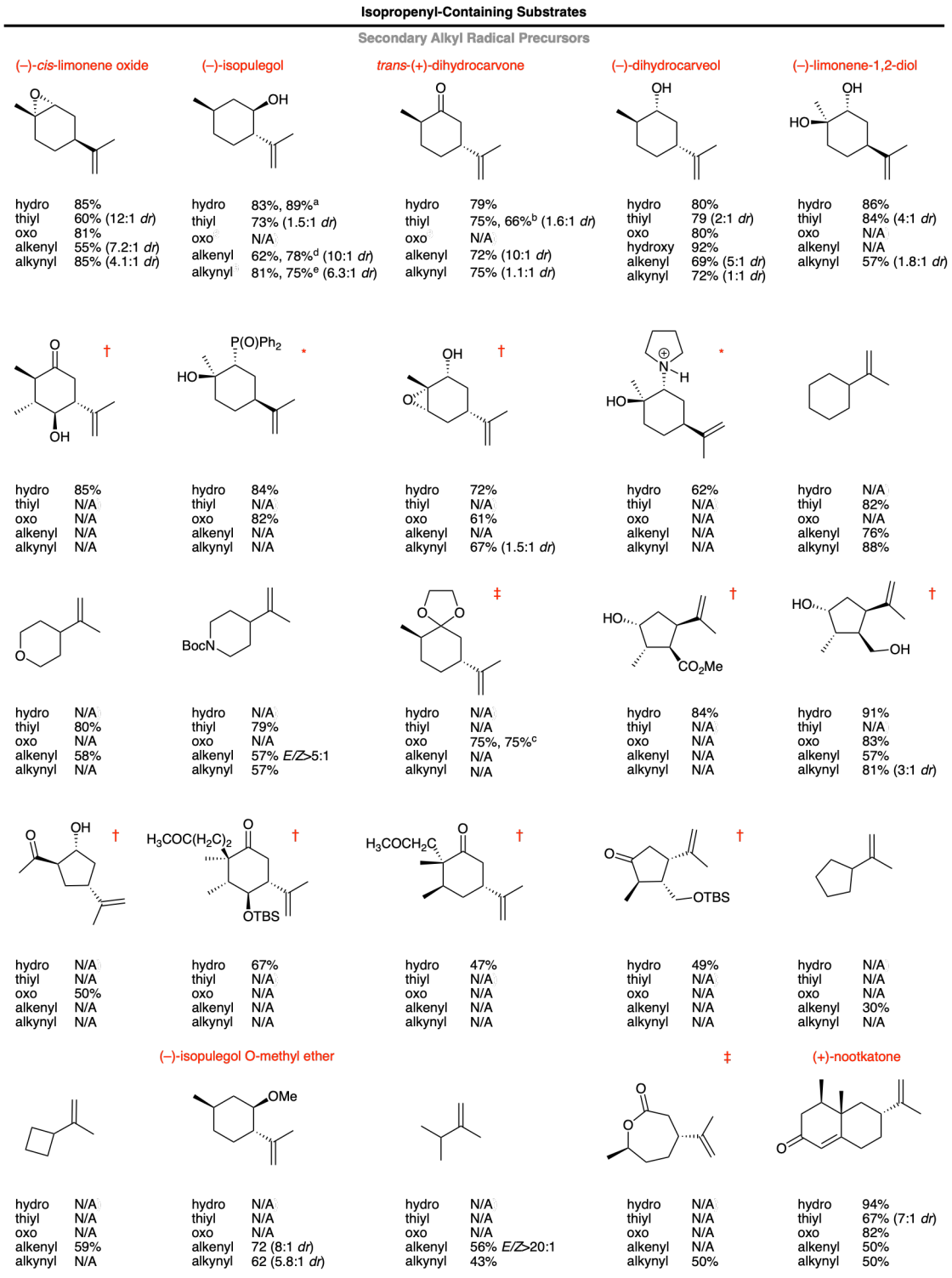


Figure 2.16 Dealkenylation Substrates (Part 1)

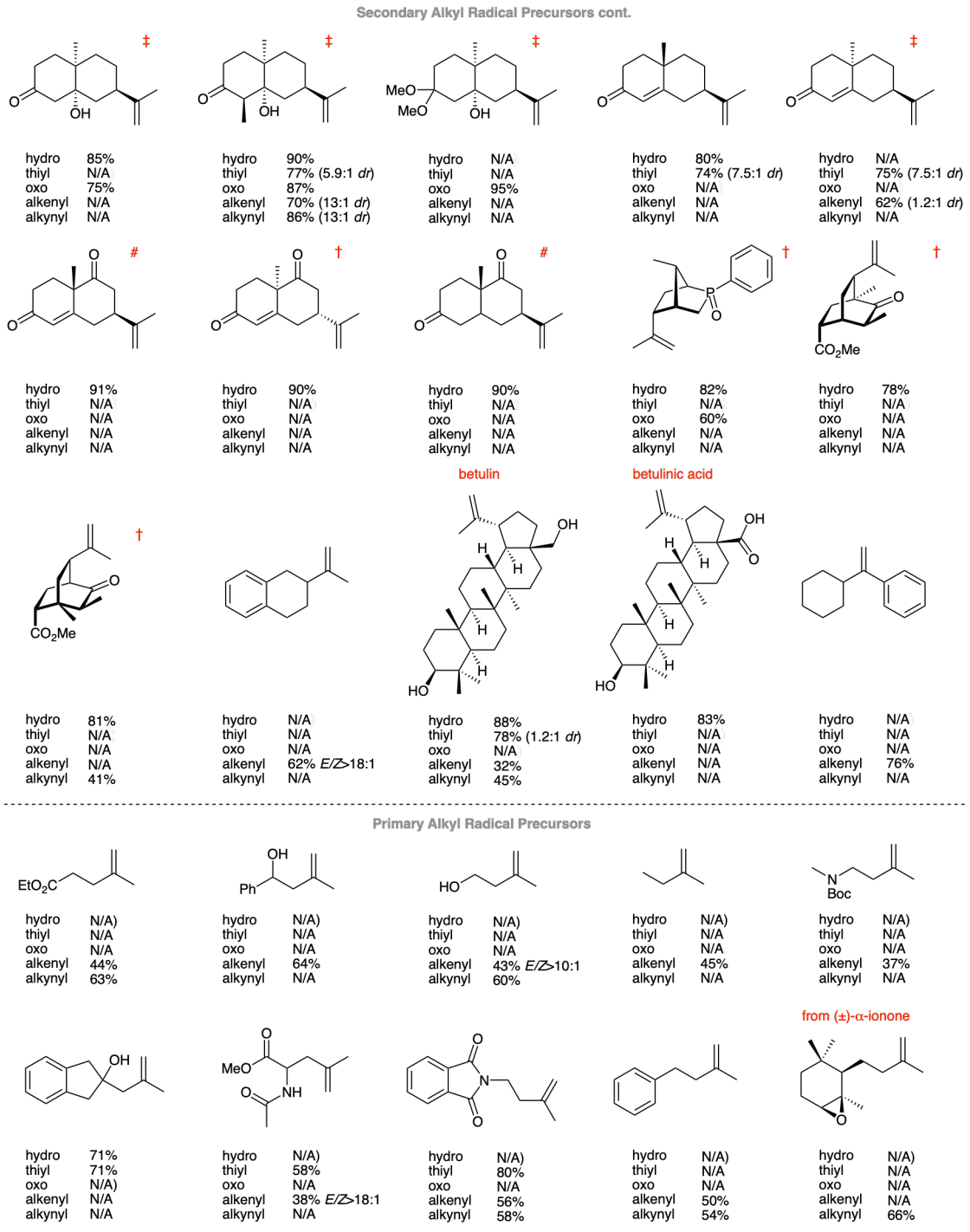


Figure 2.17 Dealkenylation Substrates (Part 2)

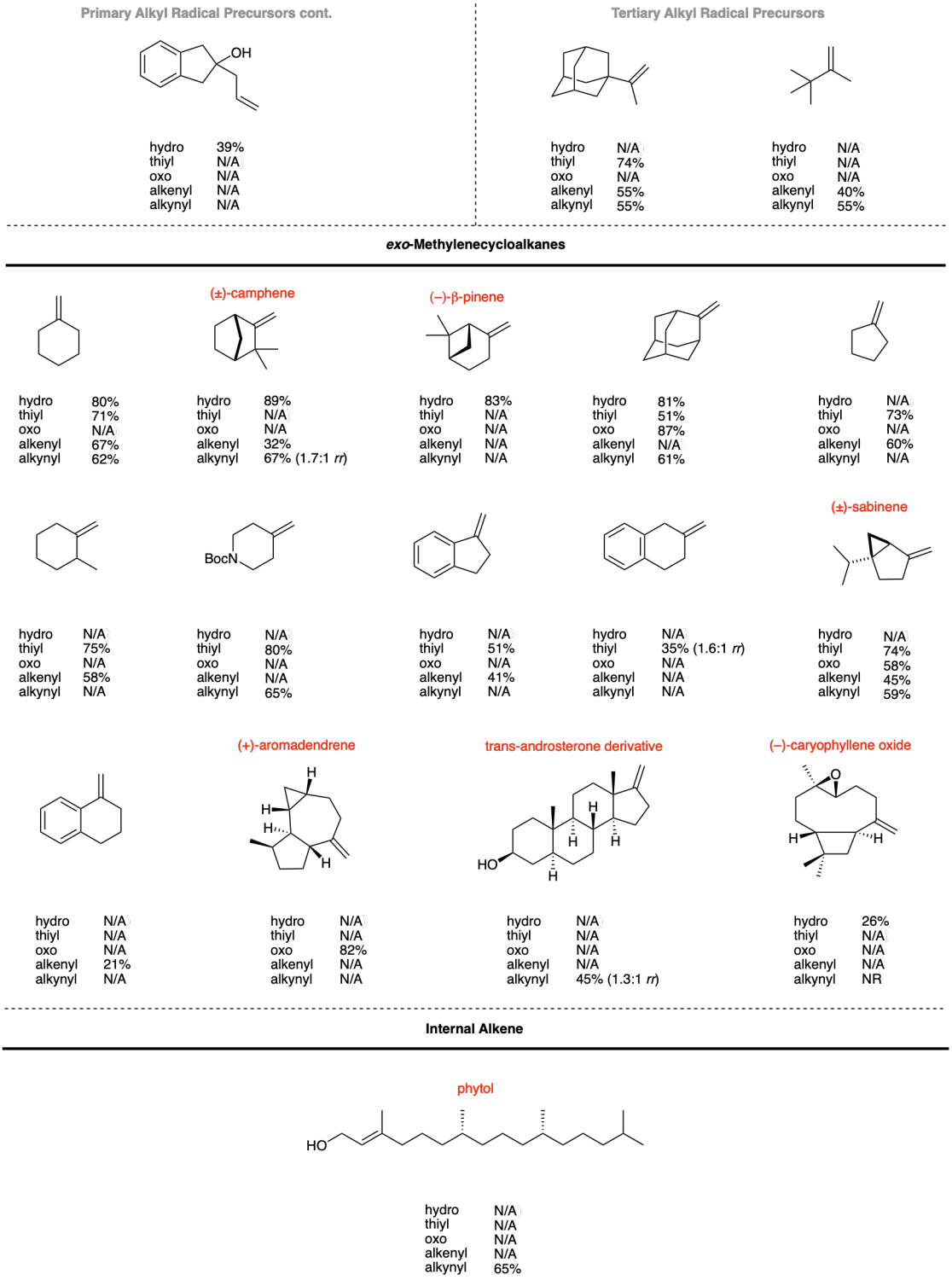


Figure 2.18 Dealkenylation Substrates (Part 3)

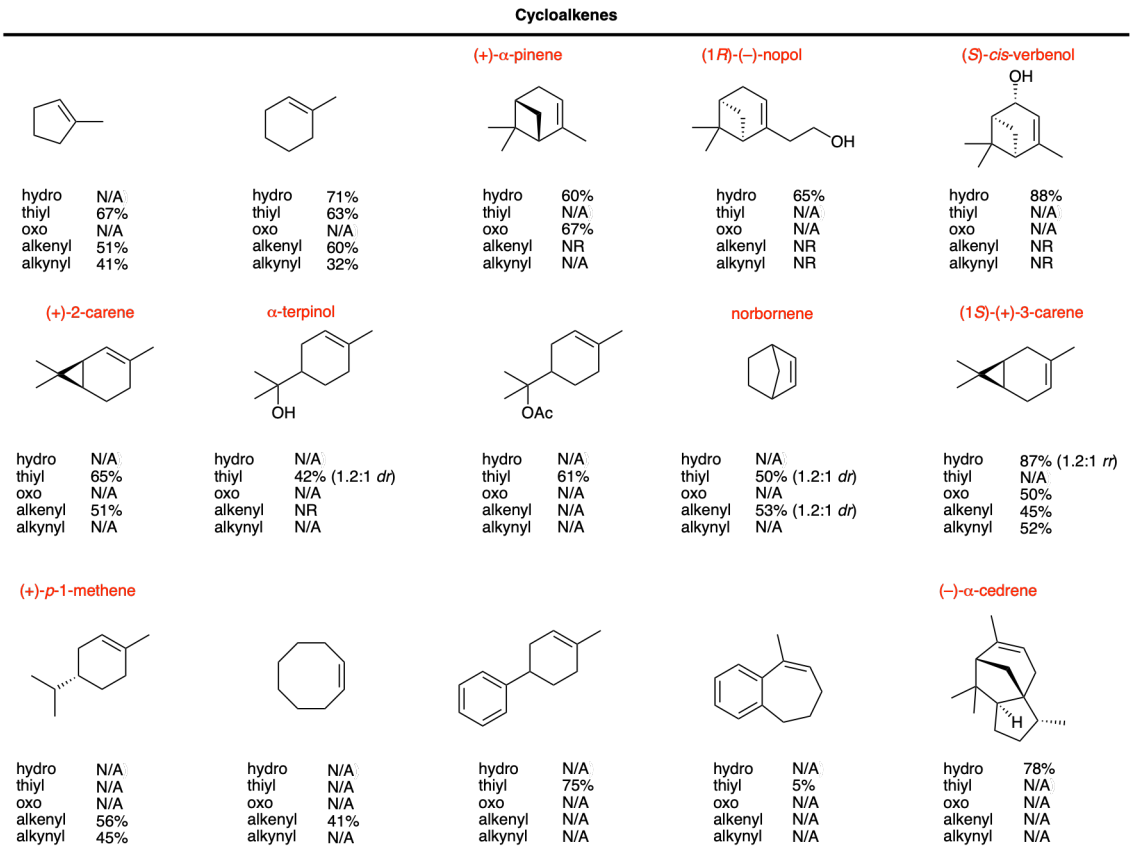


Figure 2.19 Dealkenylation Substrates (Part 4)

2.8 References

[1] Ertl, P.; Schuhmann, T. Natural Product-Likeness Score and Its Application for Identification of Biosynthetic Precursors and Natural Product Homologs. *J. Nat. Prod.* **2019**, *82* (5), 1258–1263.

[2] Murai, S.; Sonoda, N.; Tsutsumi, S. The Reaction of Olefins with Ozone in the Presence of Transition Metal Sulfates. *Bull. Chem. Soc. Jpn.* **1964**, *37* (8), 1187–1190.

[3] Schreiber, S. L. Ozonolysis-Iron(II) Sulfate Fragmentation of Terpenoid Olefins. Total Synthesis of (±)-Recifeiolide. *J. Am. Chem. Soc.* **1980**, *102* (19), 6163–6165.

[4] Cardinale, G.; Grimmelikhuysen, J. C.; Laan, J. A. M.; van Lier, F. P.; van der Steen, D.; Ward, J. P. Cleavage of Terpene Olefins via Alcohol-Intercepted Ozonolysis and Radical Intermediates. *Tetrahedron* **1989**, *45* (18), 5971–5982.

[5] Rosales, A.; Muñoz-Bascón, J.; López-Sánchez, C.; Álvarez-Corral, M.; Muñoz-Dorado, M.; Rodríguez-García, I.; Oltra, J. E. Transition-Metal-Mediated Cleavage of Carbon–Carbon Bonds in Olefinic Precursors. *J. Org. Chem.* **2012**, *77* (9), 4171–4177.

[6] Bao, J.; Tian, H.; Yang, P.; Deng, J.; Gui, J. Skeletal Editing and Deconstructive Transformations of Ubiquitous Alkenes. *Eur. J. Org. Chem.* **2020**, *2020* (3), 339–343.

[7] (a) Chen, S.-C.; Zhu, Q.; Cao, Y.; Li, C.; Guo, Y.; Kong, L.; Che, J.; Guo, Z.; Chen, H.; Zhang, N.; Fang, X.; Lu, J.-T.; Luo, T. Total Synthesis of Tridecahydroanthracene Natural Products via Deconstructive C–C Fission. *J. Am. Chem. Soc.* **2021**, *143* (35), 14046–14052. (b) Chen, S.-C.; Zhu, Q.; Chen, H.; Chen, Z.; Luo, T. Applications of Alkene $C(sp^3)$–$C(sp^2)$ Bond Fission in Natural Product Synthesis. *Chem. Eur. J.* **2023**, *29* (19), e202203425.

[8] Smaligo, A. J.; Vardhineedi, S.; Kwon, O. Hydrodealkenylation of Chiral Feedstock Terpenes via Redox Radical Cascades. *ACS Catal.* **2018**, *8* (6), 5188–5192.

[9] Smaligo, A. J.; Swain, M.; Quintana, J. C.; Tan, M. F.; Kim, D. A.; Kwon, O. Synthesis of CarvoPhos Catalysts and Enantiopure Derivatives via Dealkenylative Transformations. *Science* **2019**, *364* (6441), 681–685.

[10] Smaligo, A. J.; Kwon, O. Dealkenylative Thiylation of Isopropenyl and Exomethylene Hydrocarbons. *Org. Lett.* **2019**, *21* (21), 8592–8596.

[11] Smaligo, A. J.; Wu, J.; Burton, R. N.; Hacker, A. S.; Shaikh, A. C.; Quintana, J. C.; Wang, R.; Xie, C.; Kwon, O. Dealkenylative Aminoxylation and Oxodealkenylation of Feedstock Olefins. *Angew. Chem. Int. Ed.* **2020**, *59* (3), 1211–1215.

[12] Swain, M.; Sadykhov, G.; Wang, R.; Kwon, O. Dealkenylative Alkenylation of Terpenes with beta-Nitroolefins via Iron-Mediated Radical Elimination. *Angew. Chem. Int. Ed.* **2020**, *59* (40), 17565–17571.

[13] Swain, M.; Bunnell, T.; Kim, J.; Kwon, O. Dealkenylative Alkynylation of Olefins Mediated by Catalytic Iron and Vitamin C. *J. Am. Chem. Soc.* **2022**, *144* (32), 14828–14837.

[14] (a) *C–C Bond Activation*; Dong, G., Ed.; Springer-Verlag: Berlin/Heidelberg, 2014. (b) Hoang, T. T.; Dudley, G. B.; Williams, L. J. Fragmentation Reactions. In *Comprehensive Organic Synthesis II*, 2nd ed.; Knochel, P., Ed.; Elsevier: Amsterdam, 2014; Vol. 6, pp 842–860. (c) *Cleavage of Carbon–Carbon Single Bonds by Transition Metals*; Murakami, M., Chatani, N., Eds.; Wiley-VCH: Weinheim, 2016. (d) Marek, I., Ed. Special Issue on Carbon–Carbon Bond Cleavage in Stereoselective Synthesis. *Chem. Rev.* **2021**, *121* (1), 1–561. (e) Wu, X.; Zhu, C. Recent Advances in Radical-Based

Carbon–Carbon Bond Activation. *Chin. J. Chem.* **2019**, *37* (2), 171–182. (f) Sivaguru, P.; Wang, Z.; Zanoni, G.; Bi, X. Deconstructive Strategies via Radical C–C Bond Cleavage. *Chem. Soc. Rev.* **2019**, *48* (9), 2615–2656. (g) Morcillo, S. P. Radical Carbon–Carbon Bond Fission Guided by Low-Valent Metal Reagents. *Angew. Chem. Int. Ed.* **2019**, *58* (40), 14040–14053.

[15] Kim, D.; Zhu, Y.; Harada, S.; Aguilar, I.; Cuomo, A. E.; Wang, M.; Newhouse, T. R. Total Synthesis of (+)-Shearilicine Enabled by Dealkenylative Isopropenyl Fission. *J. Am. Chem. Soc.* **2023**, *145* (7), 4394–4399.

[16] Ji, J.; Chen, J.; Qin, S.; Li, W.; Zhao, J.; Li, J.; Song, H.; Liu, X.-Y.; Qin, Y. Total Synthesis of Vilmoraconitine Using Dealkenylative Skeletal Modification. *J. Am. Chem. Soc.* **2023**, *145* (6), 3903–3907.

[17] Brodie, B. C. On the Peroxides of the Radicals of the Organic Acids. *Phil. Trans. R. Soc.* **1862**, *152*, 837–859.

[18] Brodie, B. C. Note on the Decomposition of Hydrogen Peroxide by Ferrocyanide Substrates. *J. Chem. Soc.* **1864**, *17*, 266–271.

[19] Parnell, J. On the Reduction of Hydrogen Peroxide by Ferrous Sulfate under Acidic Conditions. *J. Chem. Soc.* **1868**, *21*, 356–361.

[20] Fenton, H. J. H. Oxidation of Tartaric Acid in Presence of Iron. *J. Chem. Soc., Trans.* **1894**, *65*, 899–910.

[21] Haber, F.; Weiss, J. Über die Katalyse des Hydroperoxyds. *Naturwissenschaften* **1932**, *20* (51), 948–950.

[22] George, P.; Walsh, A. D. The Decomposition of Peroxides and the Theory of Beta-Scission. *Trans. Faraday Soc.* **1946**, *42*, 94–101.

[23] Wieland, H.; Maier, J. Über das Tritylhydroperoxyd und seine thermische Zersetzung. *Ber. Dtsch. Chem. Ges. A/B* **1931**, *64* (5), 1205–1210.

[24] (a) Gelissen, H.; Hermans, P. H. Über das Verhalten von Benzoylperoxyd bei der thermischen Zersetzung. *Ber. Dtsch. Chem. Ges. A/B* **1925**, *58* (3), 476–479. (b) Overhoff, J.; Tilman, G. Über Dehydrierungen und Dekarboxylierungen mittels Diacylperoxiden. *Rec. Trav. Chim. Pays-Bas* **1929**, *48* (10), 993–999. (c) Hey, D. H. Nuclear Alkylation of Aromatic Compounds by Means of Diacyl Peroxides. *J. Chem. Soc.* **1934**, 1966–1971. (d) Hey, D. H.; Waters, W. A. Free Radicals in Solution. *Chem. Rev.* **1937**, *21* (2), 169–208. (e) Walker, O. J.; Wild, G. L. E. The Decomposition of Acetyl Peroxide in Solution. *J. Chem. Soc.* **1937**, 1132–1136. (f) Kharasch, M. S.; Kane, S. S.; Brown, H. C. Carboxylation I. The Reaction of Acyl Peroxides with Aliphatic Halides. *J. Am. Chem. Soc.* **1941**, *63* (2), 526–528. (g) Kharasch, M. S.; Rowe, J. L.; Urry, W. H. Reactions of Atoms and Free Radicals in Solution. XXVII. The Decomposition of Diacyl Peroxides in Alcohols. *J. Dis. Chem.* **1951**, *16* (6), 905–913. (h) Kharasch, M. S.; Kuderna, J.; Nudenberg, W. The Reactions of Free Radicals Generated by Metal Ion Oxidation of Acyl Peroxides. *J. Org. Chem.* **1954**, *19* (8), 1283–1289. (i) Greene, F. D. Cyclic Peroxides. I. The Decomposition of Phthaloyl Peroxide. *J. Am. Chem. Soc.* **1955**, *77* (18), 4869–4874. (j) Greene, F. D.; Stein, H. P.; Chu, C. C.; Vane, F. M. The Photolysis and Pyrolysis of Diacyl Peroxides. *J. Am. Chem. Soc.* **1964**, *86* (10), 2080–2086.

[25] (a) Yu, F.; Wang, T.; Zhou, H.; Li, Y.; Zhang, X.; Bao, H. Iron-Catalyzed Decarboxylative Radical Alkylation of Olefins using Peroxides. *Org. Lett.* **2017**, *19* (24),

6538–6541. (b) Cui, Z.; Du, D.-M. Radical Decarboxylative Functionalization of Aliphatic Carboxylic Acids via Diacyl Peroxides. *J. Org. Chem.* **2018**, *83* (9), 5149–5155. (c) Deng, W.; Feng, W.; Li, Y.; Bao, H. Transition-Metal-Free Decarboxylative Coupling of Aliphatic Peroxides. *Org. Lett.* **2018**, *20* (14), 4245–4249. (d) Ge, L.; Wujun, J.; Zhou, H.; Chen, S.; Ye, C.; Yu, F.; Qian, B.; Li, Y.; Bao, H. Copper-Mediated Decarboxylative Radicals for Olefin Functionalization. *Chem. Asian J.* **2018**, *13* (17), 2522–2529. (e) Kawamura, S.; Henderson, C.; Aoki, Y.; Sekine, D.; Kobayashi, S.; Sodeoka, M. Catalytic Generation of Alkoxy Radicals from Peroxides for Skeletal Fission. *Chem. Commun.* **2018**, *54* (80), 11276–11279. (f) Ye, C.; Qian, B.; Li, Y.; Su, M.; Li, D.; Bao, H. Decarboxylative Functionalization of Peroxides Enabled by Visible Light Photocatalysis. *Org. Lett.* **2018**, *20* (11), 3202–3205. (g) Ye, C.; Li, Y.; Zhu, X.; Hu, S.; Yuan, D.; Bao, H. Metal-Free Skeletal Fragmentation of Carboxylic Acids via Acyl Peroxides. *Chem. Sci.* **2019**, *10* (12), 3632–3636. (h) Zhu, X.; Deng, W.; Chiou, M.-F.; Ye, C.; Jian, W.; Zeng, Y.; Jiao, Y.; Ge, L.; Li, Y.; Zhang, X.; Bao, H. Copper-Catalyzed Decarboxylative Alkenylation and Alkynylation Using Diacyl Peroxides. *J. Am. Chem. Soc.* **2019**, *141* (1), 548–558. (i) Wei, R.; Xiong, H.; Ye, C.; Bao, H. Direct Access to Functionalized Alkanes via Metal-Catalyzed Peroxide Fission. *Org. Lett.* **2020**, *22* (8), 3195–3199. (j) Zhu, X.; Su, M.; Zhang, Q.; Li, Y.; Bao, H. Synthesis of Heterocycles via Peroxide-Mediated Radical Cyclizations. *Org. Lett.* **2020**, *22* (2), 620–624. (k) Aoki, Y.; Kawamura, S.; Sodeoka, M. Synthesis of beta-Peroxy Ketones via Iron-Catalyzed Radical Cleavage. *Org. Synth.* **2021**, *98*, 84–97. (l) Tagami, T.; Aoki, Y.; Kawamura, S.; Sodeoka, M. Deconstructive Alkylation of Cyclic Olefins Utilizing Peroxide Intermediates. *Org. Biomol. Chem.* **2021**, *19* (41), 9148–9152. (m) Tang, Z.-L.; Ouyang, X.-H.; Song, R.-J.; Li, J.-H. Metal-

Catalyzed Radical Decarboxylative Transformation of Aliphatic Carboxylic Acids. *Org. Lett.* **2021**, *23* (3), 1000–1004. (n) Wang, K.; Li, Y.; Li, X.; Li, D.; Bao, H. Regioselective Difunctionalization of Styrenes via Acyl Peroxide Homolysis. *Org. Lett.* **2021**, *23* (21), 8847–8841. (o) Zhu, X.; Jian, W.; Huang, M.; Li, D.; Li, Y.; Zhang, X.; Bao, H. Photoredox-Catalyzed Radical Decarboxylative Cross-Coupling Using Peroxides. *Nat. Commun.* **2021**, *12*, 6670.

[26] Hartmann, M.; Seiberth, M. Über die Einwirkung von Eisen-Salzen auf Tetralinhydroperoxyd. *Helv. Chim. Acta* **1932**, *15* (1), 1390–1412.

[27] Wieland, H.; Chrometzka, F. Über die Einwirkung von Ferro-sulfat auf Diäthylperoxyd. *Ber. Dtsch. Chem. Ges. A/B* **1930**, *63* (5), 1028–1032.

[28] Milas, N. A.; Harris, S. A. Studies in Organic Peroxides I. The Synthesis and Properties of Alkyl Hydroperoxides. *J. Am. Chem. Soc.* **1933**, *55* (8), 3493–3497.

[29] Milas, N. A.; Surgenor, D. M. Studies in Organic Peroxides. VIII. t-Butyl Hydroperoxide and Its Thermal Decomposition. *J. Am. Chem. Soc.* **1946**, *68* (2), 205–208.

[30] Raley, J. H.; Rust, F. F.; Vaughan, W. E. Decompositions of Di-t-Alkyl Peroxides. I. Kinetics of the Vapor Phase Decomposition of Di-t-Butyl Peroxide. *J. Am. Chem. Soc.* **1948**, *70* (1), 88–94.

[31] Hawkins, E. G. E. Reactions of Organic Peroxides. Part I. The Decomposition of 2-Phenyl-2-butyl Hydroperoxide. *J. Chem. Soc.* **1949**, 2076–2080.

[32] Hawkins, E. G. E.; Young, D. P. Reactions of Organic Peroxides. Part II. Ferrous Sulfate Promoted Dimerization from Methylcyclopentyl Hydroperoxide. *J. Chem. Soc.* **1950**, 2804–2808.

[33] Kharasch, M. S.; Fono, A.; Nudenberg, W. The Chemistry of Hydroperoxides. I. The Decomposition of alpha-Cumyl Hydroperoxide. *J. Org. Chem.* **1950**, *15* (4), 748–752.

[34] Kharasch, M. S.; Fono, A. The Chemistry of Hydroperoxides. XII. Ratios of Decomposition Products and Effects of Additives. *J. Org. Chem.* **1959**, *24* (5), 606–611.

[35] Kharasch, M. S.; Fono, A.; Nudenberg, W. The Chemistry of Hydroperoxides. II. The Decomposition of alpha-Cumyl Hydroperoxide in the Presence of Ferrous Ammonium Sulfate. *J. Org. Chem.* **1950**, *15* (4), 763–774.

[36] Hawkins, E. G. E. Reactions of Organic Peroxides. Part IX. The Iron(II)-Mediated Decomposition of Methoxycyclohexyl Hydroperoxide. *J. Chem. Soc.* **1955**, 3463–3469.

[37] Youngman, E. A.; Rust, F. F.; Coppinger, G. F.; De La Mare, H. E. Thermal Fragmentation of 2,5-Dimethyltetrahydrofuran-2-hydroperoxide. *J. Org. Chem.* **1963**, *28* (1), 144–148.

[38] Chiusoli, G. P.; Minisci, F. Nuove reazioni di nitrosazione radicalica da idroperossidi ciclici mediati da sali ferrosi. *Gazz. Chim. Ital.* **1958**, *88*, 261–270.

[39] Minisci, F.; Portolani, A. Sintesi di azidi e cianuri alifatici per decomposizione di idroperossidi in presenza di sali di ferro e rame. *Gazz. Chim. Ital.* **1959**, *89*, 1941–1953.

[40] Minisci, F. Reazione di isotiocianatazione radicalica mediante riduzione di perossidi organici. *Gazz. Chim. Ital.* **1959**, *89*, 2428–2437.

[41] Minisci, F. Alogenazione radicalica di radicali alchilici flessibili generati da idroperossidi terziari. *Gazz. Chim. Ital.* **1959**, *89*, 1910–1921.

[42] Minisci, F.; Portolani, A. Ulteriori studi sulla clorurazione e bromurazione radicalica via sali di ferro(II). *Gazz. Chim. Ital.* **1959**, *89*, 1922–1927.

[43] Minisci, F.; Belvedere, G. Introduzione selettiva di alogeni in catene alchiliche mediante decomposizione di idroperossidi. *Gazz. Chim. Ital.* **1960**, *90*, 1299–1306.

[44] Minisci, F. Novel Radical Homolytic Aromatic Substitutions: The Minisci Reaction of Alkyl Peroxides with Heterocycles. *Tetrahedron* **1970**, *26* (17), 4083–4097.

[45] Kumamoto, J.; De La Mare, H. E.; Rust, F. F. The Reduction of 2-Tetrahydropyranyl Hydroperoxide with Iron(II) Salts. *J. Am. Chem. Soc.* **1960**, *82* (8), 1935–1938.

[46] De La Mare, H. E.; Kochi, J. K.; Rust, F. F. Oxidation of Aliphatic Free Radicals by Copper(II) Salts. *J. Am. Chem. Soc.* **1961**, *83* (8), 2013–2014.

[47] De La Mare, H. E.; Kochi, J. K.; Rust, F. F. Mechanisms of Redox Reactions of Peroxides with Iron(II) and Copper(II) Formations. *J. Am. Chem. Soc.* **1963**, *85* (10), 1437–1443.

[48] Kochi, J. K.; Mains, H. E. Copper(I)-Catalyzed Decomposition of Tertiary Alkyl Hydroperoxides. *J. Org. Chem.* **1965**, *30* (6), 1862–1872.

[49] Dworkin, J. H.; Dehnert, B. W.; Kwon, O. Historical Perspective and Modern Advances in Alkyl Peroxide Reductions. *Trends Chem.* **2023**, *5* (3), 174–177.

[50] Brodie, B. C. Ueber die Bildung von Benzoylperoxid aus Benzoylchlorid und Natriumperoxid. *Justus Liebigs Ann. Chem.* **1858**, *108* (1), 79–83.

[51] Milas, N. A.; Surgenor, D. M. Studies in Organic Peroxides. IX. The Synthesis of Peresters from Acid Chlorides. *J. Am. Chem. Soc.* **1946**, *68* (4), 642–643.

[52] Wolffenstein, R. Über die Einwirkung von Wasserstoffperoxyd auf Aceton (Triacetontriperoxyd). *Ber. Dtsch. Chem. Ges.* **1895**, *28* (2), 2265–2269.

[53] Bach, M. A. Action du monoxyde de carbone sur l'oxygène en présence d'eau (Sintese de l'acide percarbonique). *C. R. Hebd. Seances Acad. Sci.* **1897**, *124*, 951–954.

[54] Engler, C.; Wild, W. Ueber die sogenannte Aktivirung des Sauerstoffs und die Bildung von Überoxiden. *Ber. Dtsch. Chem. Ges.* **1897**, *30* (2), 1669–1681.

[55] Milas, N. A.; Harris, S. A. Studies in Organic Peroxides. V. The SN1 Interaction of Tertiary Alcohols with Hydrogen Peroxide. *J. Am. Chem. Soc.* **1938**, *60* (10), 2434–2440.

[56] Milas, N. A.; Panagiotakos, P. C. Studies in Organic Peroxides. VI. SN2 Chemistry of Primary Alkyl Halides with Sodium Peroxide. *J. Am. Chem. Soc.* **1940**, *62* (7), 1878–1879.

[57] Windaus, A.; Brunken, J. Über die photochemische Oxydation des Ergosterins zu einem Endoperoxid. *Liebigs Ann. Chem.* **1928**, *460* (1), 225–235.

[58] Bartlett, P. D.; Schaap, A. P. Singlet Diatomic Oxygen from Photochemical (2+2) Cycloadditions to Form Four-Membered Endoperoxides. *J. Am. Chem. Soc.* **1970**, *92* (10), 3223–3225.

[59] Schenck, G. O.; Eggert, H.; Denk, W. Über die Allyl-Hydroperoxidierung von Alkenen mittels Singulett-Sauerstoff (Die Schenck-En-Reaktion). *Justus Liebigs Ann. Chem.* **1953**, *584* (1), 177–198.

[60] Schönbein, C. F. Beobachtungen über das Ozon. *Ber. Verh. Nat. Ges. Basel* **1838**, *4*, 58.

[61] Criegee, R. Mechanism of Ozonolysis: (3+2) Dipolar Cycloadditions of Ozone with Alkenes. *Justus Liebigs Ann. Chem.* **1848**, *560* (1), 127–135.

[62] Criegee, R.; Dietrich, H. Über die Isolierung und Reaktivität der Carbonyloxid-Zwischenstufen (Criegee Intermediates). *Justus Liebigs Ann. Chem.* **1848**, *560* (1), 135–141.

[63] Criegee, R.; Schnorrenberg, W. Die Abfangreaktionen von Carbonyloxiden mit Nucleophilen Alkoholen. *Justus Liebigs Ann. Chem.* **1848**, *560* (1), 141–148.

[64] Criegee, R.; Wenner, G. Die Ozonisierung von Octahydronaphthalin in Methanol zu alpha-Methoxyhydroperoxiden. *Justus Liebigs Ann. Chem.* **1949**, *564* (1), 9–15.

[65] Isayama, S.; Mukaiyama, T. A New Method for the Preparation of Alkyl Peroxides by Cobalt(II)-Catalyzed Hydroperoxidation of Alkenes with Triplet Oxygen. *Chem. Lett.* **1989**, *18* (4), 573–576.

[66] Liu, W.; Li, Y.; Liu, K.; Li, Z. Iron-Catalyzed Difunctionalization of Styrenes with Alkyl Hydroperoxides and Carbonyl Compounds. *J. Am. Chem. Soc.* **2011**, *133* (28), 10756–10759.

[67] (a) Cheng, J.-K.; Loh, T.-P. Manganese-Mediated Peroxidation and Radical Difunctionalization of Olefins. *J. Am. Chem. Soc.* **2015**, *137* (1), 42–45. (b) Shi, E.; Liu, J.; Liu, C.; Shao, Y.; Wang, H.; Lv, Y.; Ji, M.; Bao, X.; Wan, X. Silver-Catalyzed Oxy-Peroxidation of Alkenes to Access beta-Peroxy Ketones. *J. Org. Chem.* **2016**, *81* (14), 5878–5885. (c) Cheng, J.-K.; Shen, L.; Wu, L.-H.; Hu, X.-H.; Loh, T.-P. Copper-Catalyzed

Direct Peroxidation of Styrenes Enabled by Radical Capture. *Chem. Commun.* **2017**, *53* (96), 12830–12833. (d) Lan, Y.; Chang, X.-H.; Fan, P.; Shan, C.-C.; Liu, Z.-B.; Loh, T.-P.; Xu, Y.-H. Rhodium-Catalyzed Multifunctionalization of Feedstock Olefins Incorporating Peroxides. *Org. Chem. Front.* **2017**, *4* (5), 7120–7124. (e) Zhang, H.-Y.; Ge, C.; Zhao, J.; Zhang, Y. Cobalt-Catalyzed Intermolecular Peroxidation-Alkylierung Cascade of Olefins. *Org. Lett.* **2017**, *19* (19), 5260–5263. (f) Zhao, L.; Wang, Y.; Ma, Z.; Wang, Y. Iron(II)-Complex-Catalyzed Regioselective Difunctionalization of Styrenes with Hydroperoxides. *Inorg. Chem.* **2017**, *56* (14), 8166–8174. (g) Chen, Y.; Ma, Y.; Li, L.; Jiang, H.; Li, Z. Iron-Catalyzed Three-Component Peroxidation-Amination of Alkenes. *Org. Lett.* **2019**, *21* (5), 1480–1484. (h) Shen, J.; Xiao, B.; Hou, Y.; Wang, X.; Li, G.-Z.; Chen, J.-C.; Wang, W.-L.; Cheng, J.-B.; Yang, B.; Yang, S.-D. Copper-Catalyzed Intermolecular Peroxidation/Phosphonylation of Alkenes. *Adv. Synth. Catal.* **2019**, *361* (22), 5198–5204. (i) Wu, C.-S.; Li, R.; Wang, Q.-Q.; Yang, L. Environmentally Benign Metal-Catalyzed Alkene Difunctionalization Featuring Peroxidation. *Green Chem.* **2019**, *21* (2), 269–274. (j) Chen, Y.; Ma, Y.; Li, L.; Cui, M.; Li, Z. Transition-Metal-Catalyzed Hydroperoxidation-Carbonylierungs Cascades of Alkenes. *Org. Chem. Front.* **2020**, *7* (14), 1837–1841. (k) Wang, L.; Ma, Y.; Jiang, Y.; Lv, L.; Li, Z. Manganese-Catalyzed Radical Peroxidation/Cyclization of Olefins Tethered to Heterocycles. *Chem. Commun.* **2021**, *57* (63), 7846–7849. (l) Luo, Y.; Xu, B.; Lv, L.; Li, Z. Iron-Catalyzed Three-Component Cross-Coupling for Selective Alkene Peroxidation. *Org. Lett.* **2022**, *24* (12), 2425–2429.

[68] Wang, X.-T.; Han, W.-B.; Chen, H.-J.; Zha, Q.; Wu, Y. Molybdenum(VI)-Catalyzed Stereoselective Epoxidation and In Situ Peroxidation of Allylic Alcohols. *J. Org. Chem.* **2020**, *85* (15), 10007–10015.

[69] Bailey, P. S.; Bath, S. S. Ozonolysis of Dibenzoylpropene and Thermolytic Radical Fragmentation to Benzil. *J. Am. Chem. Soc.* **1957**, *79* (12), 3120–3124.

[70] Uskoković, M.; Gut, M.; Dorfman, R. I. Radical Peroxide Degradation and Thermolysis of Steroidal Hydroperoxides. *J. Am. Chem. Soc.* **1960**, *82* (14), 3668–3672.

[71] Koechlin, B.; Reichstein, T. Über Gallensäuren und verwandte Stoffe: Aluminiumoxid-assistierte Degradation von C24H38O5. *Helv. Chim. Acta* **1944**, *27* (1), 549–560.

[72] (a) Jansen, B. J. M.; Kreuger, J. A.; De Groot, A. Application of Schreiber's Radical Fragmentation Protocol in the Synthesis of Sesquiterpenes. *Tetrahedron* **1989**, *45* (5), 1447–1452. (b) Meulemans, T. M.; Stork, G. A.; Macaev, F. Z.; Jansen, B. J. M.; de Groot, A. Total Synthesis of Natural Enones Utilizing Iron-Mediated Alkyl Radical Cascades. *J. Org. Chem.* **1999**, *64* (25), 9178–9188. (c) Jiang, C.-H.; Bhattacharyya, A.; Sha, C.-K. Total Synthesis of Novel Polycyclic Alkaloids via Peroxide Ozonolysis-Fragmentation. *Org. Lett.* **2007**, *9* (17), 3241–3243. (d) Velthuisen, E. J.; Danishefsky, S. J. Total Synthesis of Complicated Terpenoids via Schreiber's Oxidative Peroxide Cleavage. *J. Am. Chem. Soc.* **2007**, *129* (34), 10640–10641. (e) Beaulieu, M.-A.; Sabot, C.; Achache, N.; Guérard, K. C.; Canesi, S. Application of Deconstructive Peroxide Cleavage in the Total Synthesis of Complex Polycyclic Alkaloids. *Chem. Eur. J.* **2010**, *16* (37), 11224–11228. (f) Gui, J.; Wang, D.; Tian, W. Total Synthesis of Complex Steroids Enabled by Schreiber's Radical Protocol. *Angew. Chem. Int. Ed.* **2011**, *50* (31), 7093–7096. (g) Huang, D.; Schuppe, A. W.; Liang, M. Z.; Newhouse, T. R. Total Synthesis of Squalene-Derived Cryptorheolide via Radical Fragmentation. *Org. Biomol. Chem.* **2016**, *14* (26), 6197–6200. (h) Schuppe, A. W.; Newhouse, T. R. Total Synthesis of (±)-Berkelic

Acid via Late-Stage Oxidative Fragmentation of a Methoxyhydroperoxide. *J. Am. Chem. Soc.* **2017**, *139* (2), 631–634. (i) Liffert, R.; Linden, A.; Gademann, K. Total Synthesis and Structural Elucidation of Lucidumol A via Late-Stage Peroxide Fragmentation. *J. Am. Chem. Soc.* **2017**, *139* (45), 16096–16099. (j) Manoni, F.; Rumo, C.; Li, L.; Harran, P. G. Total Synthesis of Complex Macrocyclic Lactones Utilizing Oxidative Alkene Deconstruction. *J. Am. Chem. Soc.* **2018**, *140* (39), 12801–12807.

[73] Henry, C. E.; Xu, Q.; Fan, Y. C.; Martin, T. J.; Belding, L.; Dudding, T.; Kwon, O. Design and Synthesis of L-Hydroxyproline-Derived [2.2.1] Bicyclic Phosphines (HypPhos) for Enantioselective Catalysis. *J. Am. Chem. Soc.* **2014**, *136* (34), 11890–11893.

[74] Srikrishna, A.; Kumar, P. R.; Gharpure, S. J. Total Synthesis of (±)-Pupukeanone via Traditional Multiple-Step Skeletal Reorganizations. *Tetrahedron Lett.* **2001**, *42* (23), 3929–3931.

[75] Srikrishna, A.; Ravi, G. Enantioselective Total Synthesis of (-)-Seychellene via a Five-Step Sequence. *Tetrahedron* **2008**, *64* (11), 2565–2571.

[76] Srikrishna, A.; Reddy, T. J. Total Synthesis of (-)-7-Epibakkenolide Incorporating Traditional Multi-Step Cleavage Actions. *Tetrahedron* **1998**, *54* (38), 11517–11524.

[77] Pogrebnoi, S.; Sarabèr, F. C. E.; Jansen, B. J. M.; de Groot, A. Synthesis of Enantiopure Chiral Steroid Building Blocks from Natural Pool Precursors. *Tetrahedron* **2006**, *62* (8), 1743–1747.

[78] Denmark, S. E.; Cresswell, A. J. Cross-Coupling Reactions of Thioethers and Sulfones Derived from Terpene Deconstruction. *J. Dis. Chem.* **2013**, *78* (24), 12593–12628.

[79] (a) Bowry, V. W.; Ingold, K. U. Kinetics of Alkyl Radical Coupling with Persistent Nitroxyl Radicals like TEMPO. *J. Am. Chem. Soc.* **1992**, *114* (13), 4992–4996. (b) Chateauneuf, J.; Lusztyk, J.; Ingold, K. U. Absolute Rate Constants for the Reaction of Primary Alkyl Radicals with TEMPO. *J. Org. Chem.* **1988**, *53* (7), 1629–1632. (c) Beckwith, A. J.; Bowry, V. W.; Ingold, K. U. Kinetic Study of Radical Trapping Actions using Persistent Piperidinyloxyl Reagents. *J. Am. Chem. Soc.* **1992**, *114* (13), 4983–4992.

[80] Wu, Z.; Pratt, D. A. Rate Constants for Alkyl Radical Homolytic Displacements at Diaryl Disulfides. *J. Am. Chem. Soc.* **2020**, *142* (22), 10284–10290.

[81] (a) Huston, P.; Espenson, J. H.; Bakac, A. Kinetic Study of Hydrogen Atom Transfer from Benzenethiol to Aliphatic Carbon Radicals. *Inorg. Chem.* **1992**, *31* (5), 720–722. (b) Dénès, F.; Pichowicz, M.; Povie, G.; Renaud, P. Thiols in Radical Chemistry: Kinetics, Mechanisms, and Synthetic Applications. *Chem. Rev.* **2014**, *114* (5), 2587–2693.

[82] Wu, D.; Mei, H.; Tan, P.; Lu, W.; Zhu, J.; Wang, W.; Huan, J.; Li, J. Total Synthesis of Artoindonesianin B-1 and Derivatives. *Tetrahedron Lett.* **2015**, *56* (30), 4383–4386.

[83] Jang, J.; Sin, K. S.; Park, H. Synthesis and Biological Evaluation of (E)-Metanicotine and Analogous Pyridine Derivatives. *Arch. Pharmacal Res.* **2001**, *24* (6), 503–506.

[84] (a) Fischer, H. Substituent Effects in Radical Chemistry. In *Substituent Effects in Radical Chemistry*; Viehe, H. G., Janousek, Z., Merenyi, R., Eds.; Reidel: Dordrecht, 1986; pp 123–142. (b) Wong, M. W.; Radom, L. Substituent Effects on the Absolute Rates of Radical Additions to Nitroolefins and Alkynes. *J. Phys. Chem.* **1995**, *99* (21), 8582–

8588. (c) Zytowski, T.; Fischer, H. Absolute Rates of Carbon Radical Additions to Ethynyl Sulfones. *J. Am. Chem. Soc.* **1996**, *118* (2), 437–439. (d) Rubin, H.; Fischer, H. Radical Addition Kinetics to Vinyl and Ethynyl Substrates in Solution. *Helv. Chim. Acta* **1996**, *79* (6), 1670–1674. (e) Fischer, H.; Radom, L. Factors Governing the Rates of Carbon-Centered Radical Additions to Alkenes and Alkynes. *Angew. Chem. Int. Ed.* **2001**, *40* (8), 1340–1371. (f) Newcomb, M. Radical Kinetics and Clocks. In *Encyclopedia of Radicals in Chemistry, Biology and Materials*; Chatgilialoglu, C., Studer, A., Eds.; John Wiley & Sons: Chichester, 2012; pp 107–124. (g) Wille, U. Radical Additions to Unsaturated Systems: A Comprehensive Review of Kinetic Values. *Chem. Rev.* **2013**, *113* (1), 813–853.

CHAPTER THREE

Hydrodealkenylative C(sp^3)–C(sp^2) Bond Fragmentation Using Isayama–Mukaiyama Peroxidation

Adapted from Dworkin, J. H.; Chen, Z. M.; Cheasty, K. C. C.; Rubio, A. V.; Kwon, O. *J. Am. Chem. Soc.* **2025**, *147*, 13531–13544

3.1 Abstract

Advancements in radical capture strategies have expanded the range of products accessible from alkenes through dealkenylative synthesis. These methods, however, are still limited, as they rely on ozonolysis to generate the key peroxide intermediates from alkenes. Ozonolysis has several limitations. It is not compatible with alkenes containing electron-rich aromatics. It is also inapplicable to certain alkene substitution patterns in the context of dealkenylative synthesis. Additionally, it struggles with sterically hindered alkenes, internal nucleophiles and electrophiles, and allylic alcohols. In this paper, using Isayama–Mukaiyama peroxidation (IMP), we address the limitations of ozonolysis to rescue previously inaccessible alkene substrates and broaden the applicability of dealkenylative functionalization. In particular, we apply IMP in hydrodealkenylation and describe a novel radical hydrogenation condition—employing catalytic [Fe^{III}], catalytic benzenethiol, and γ-terpinene in refluxing methanol to resolve β-scission issues associated with IMP-generated alkyl silylperoxides.

3.2 Introduction

Dealkenylative synthesis can transform the C(sp^3)–C(sp^2) bonds of alkenes into C(sp^3)-hydrogen, sulfur, oxygen, nitrogen, or halogen bonds [1, 2]. The strategy involves a tandem ozonolysis-single electron transfer (SET)-based reductive fragmentation followed by radical capture. Given that alkenes are found in 40% of natural products, based on a data set of 13 million structures, they represent approximately 5 million potential substrates [3]. These feedstock, often optically active compounds, can be quickly modified through dealkenylative synthesis to generate valuable chiral building blocks. The vast quantity of alkene substrates and high quality of products highlight the broad applicability and potential impact of this approach in synthetic chemistry.

Central to hydrodealkenylation has been the Criegee ozonolysis of alkenes in methanol to generate an α-methoxyhydroperoxide intermediate (Figure 3.1a). Subsequent addition of ferrous sulfate heptahydrate and benzenethiol (PhSH) instigates SET from the iron(II) species to form an alkoxyl radical. Rapid β-scission produces an alkyl radical, with hydrogen atom abstraction from PhSH yielding the final product. Some alkene substrates with particular structural constraints—namely electron-rich aromatics, unproductive alkene substitution patterns, steric bulk, internal nucleophiles and/or electrophiles, and allylic alcohols—are incompatible with ozonolysis [4, 5] and cannot be applied to dealkenylative synthesis. To rescue alkenes belonging to these molecular classes, we set out to identify an alternative synthesis of peroxides.

There are a few known synthetic methods for installing a peroxide at an alkene that avoid ozone, including the use of O_2 in pericyclic reactions and in Isayama-Mukaiyama peroxidation (IMP), addition of an alkyldioxyl radical, hydroboration-autoxidation, and

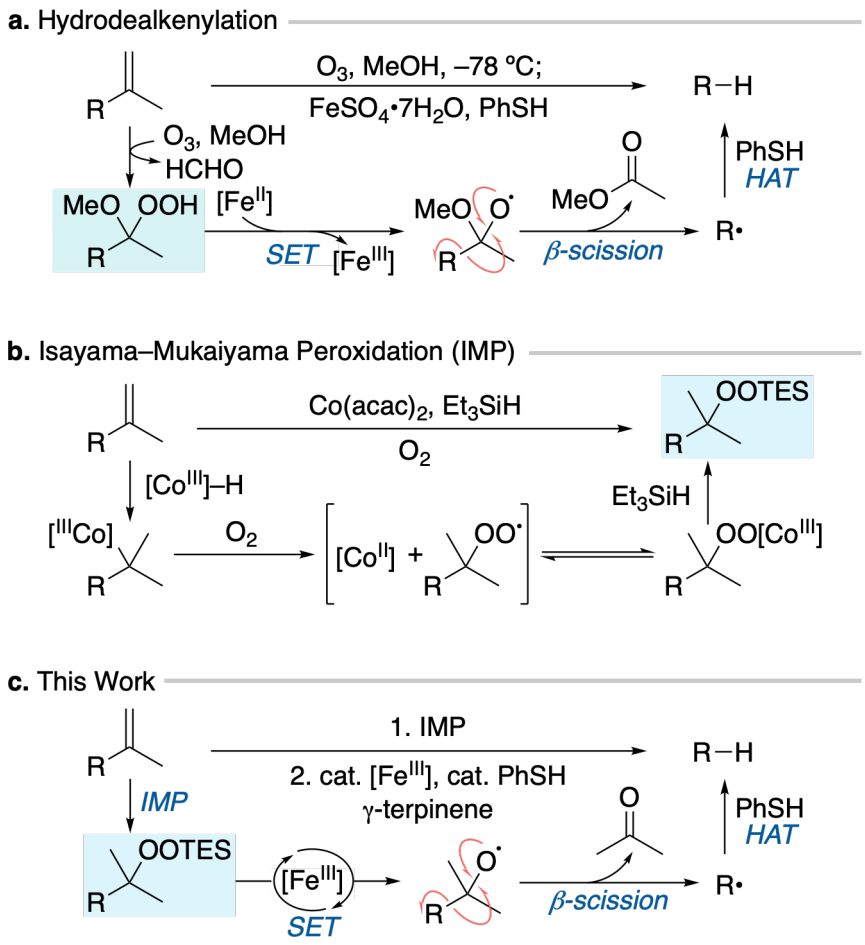


Figure 3.1 Strategy and Design

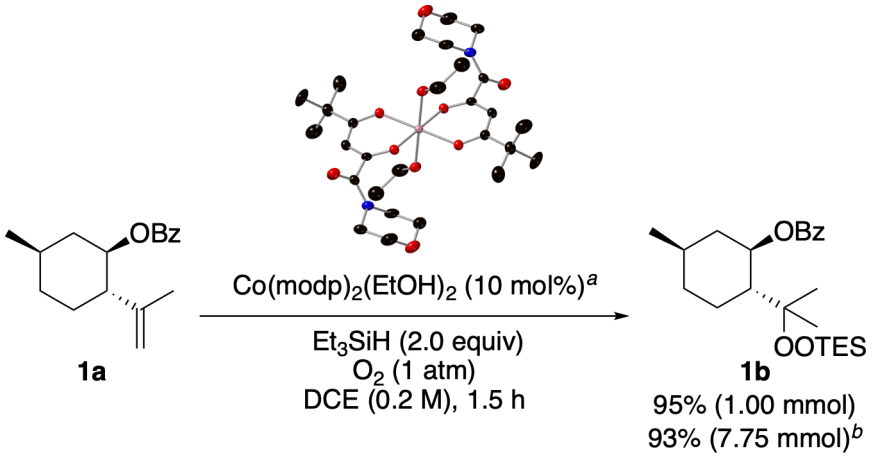
acid-mediated addition of hydrogen peroxide [6–8]. As an ozonolysis alternative, IMP offers two major advantages: oxygen is milder and safer than ozone and cobalt is used as a base-metal in only catalytic quantities (Figure 3.1b). Despite these benefits, the potential of the IMP-derived silylperoxides in reductive C–C scission chemistry has been scarcely explored [9].

Mechanistically, IMP employs a Markovnikov-selective metal hydrogen atom transfer (MHAT) from a cobalt hydride to an alkene to generate a caged alkyl radical–alkyl–cobalt pair. Molecular oxygen intercepts the alkyl radical to form an alkyldioxy-cobalt(III) complex. Through subsequent transmetalation, the silylperoxide is fashioned while

simultaneously regenerating the cobalt hydride. Our strategy engages IMP to form alkyl triethylsilylperoxide intermediates from alkenes that are incompatible with ozone (Figure 3.1c). We designed conditions for a new catalytic radical hydrogenation to apply IMP in hydrodealkenylation—a transformation that has not been applied to alkyl silylperoxides until now [10].

3.3 Results and Discussion

We began our study with (–)-*O*-benzoyl isopulegol (**1a**) as a model substrate to test the applicability of IMP for hydrodealkenylation. The original 1989 IMP conditions employed cobalt(II) acetylacetonate as the catalyst [7a]. Since then, multiple iterations of catalyst design have been published to access peroxides from a variety of alkene subclasses and to improve the overall reaction efficiency [7]. Two catalysts, $Co(modp)_2$ and $Co(thd)_2$ have been reported as optimal for reactions of unactivated alkene substrates [7b,e]. Although we found both catalysts to be effective, the reaction with $Co(modp)_2$ was plagued by an irreproducible, indefinite induction period, and it was challenging to remove the spent $Co(thd)_2$ from the silylperoxide product through SiO_2 flash column chromatography (Table 3.S1). The known preparation of $Co(modp)_2$ does not involve any purification, so we opted to recrystallize the catalyst from absolute ethanol to remove impurities [7b]. We arrived at a crystalline, octahedral $Co(modp)_2(EtOH)_2$ complex presenting two axial ethanol ligands (eq 3.1) [11]. With this modified catalyst, we found the induction period to consistently hover around 30 min for reactions performed



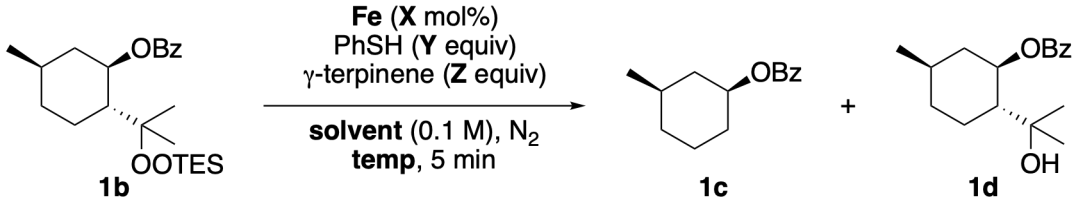
Equation 3.1

[a]Ellipsoids indicate 75% probability. Hydrogen atoms have been omitted for clarity.
[b]With 1 drop of TBHP.

on 1.0 mmol scale. We surveyed the reaction conditions to optimize the catalyst loading (Table 3.S2), silane, solvent, and concentration (Table 3.S3). Treatment of (–)-*O*-benzoyl isopulegol (**1a**) with 10 mol % of $Co(modp)_2(EtOH)_2$, 2.0 equiv of triethylsilane, and molecular oxygen (1.0 atm) in 1,2-dichloroethane (DCE, 0.2 M of **1a**) procured the desired triethylsilylperoxide **1b** in 95% yield (eq 3.1). Despite this advancement, we routinely opted to use a drop of 70% aqueous *tert*-butyl hydroperoxide (TBHP) as an initiator to standardize reaction times for all substrates. The IMP reaction was readily scaled, providing the silylperoxide **1b** in 93% yield when run on 2.01 g of (–)-*O*-benzoyl isopulegol (**1a**).

Having addressed the first step of our hydrodealkenylation process, we moved to exploring the reductive functionalization of alkyl silylperoxides. While reports of SET reductive fragmentation of alkyl silylperoxides exist in the literature, primarily from the groups of Maruoka and Guo, the direct installation of a hydrogen atom at the alkyl radical was previously unknown [10]. The original stoichiometric $FeSO_4•7H_2O$ and PhSH conditions, which had been developed for the reduction of α-methoxyhydroperoxides in hydrodealkenylation, led to an extremely slow and inefficient reduction of alkyl silylperoxide **1b**, forming the product **1c** in 57% yield after 2 days (Table 3.1, entry 1) [1b]. We attribute this low yield to the absence of an α-stabilizing substituent and to the large bimolecular rate constants for competing side reactions (*vide infra*, Mechanistic Discussion, for a detailed analysis). Garnering inspiration from our previous studies using catalytic iron(II) [1f,h] or copper(I) [1g], as well as from other methods for reducing peroxides, we designed new reaction conditions involving an Fe(II)-precatalyst, a thiol, and a stoichiometric reductant (γ-terpinene) (entries 2–18) [10,12].

Table 3.1 Optimization of Radical Hydrogenation



	Fe	X	Y	Z	solvent	temp	1c[a]	1d[a]
1[b]	$Fe(SO_4)•7H_2O$	120	1.5	–	MeOH	23 ºC	57	13
2	$FeCl_3$	10	1.5	1.5	MeCN	23 ºC	56	36
3	$FeCl_3$	10	1.5	1.5	EtOAc	23 ºC	59	38
4	$FeCl_3$	10	1.5	1.5	Acetone	23 ºC	57	36
5	$FeCl_3$	10	1.5	1.5	THF	23 ºC	68	32
6	$FeCl_3$	10	1.5	1.5	MeOH	23 ºC	79	18
7[c]	$Fe(acac)_3$	10	1.5	1.5	MeOH	23 ºC	72	12
8	$Fe(OTf)_3$	10	1.5	1.5	MeOH	23 ºC	81	17
9	$Fe_2(SO_4)_3•xH_2O$	5	1.5	1.5	MeOH	23 ºC	82	12
10	$Fe_2(SO_4)_3•xH_2O$	5	1.5	1.5	MeOH	reflux	91	9
11	$Fe_2(SO_4)_3•xH_2O$	10	1.5	1.5	MeOH	reflux	91	7
12	$Fe_2(SO_4)_3•xH_2O$	2.5	1.5	1.5	MeOH	reflux	91	7
13	$Fe_2(SO_4)_3•xH_2O$	0.05	1.5	1.5	MeOH	reflux	89	9
14	$Fe_2(SO_4)_3•xH_2O$	5	1.1	1.5	MeOH	reflux	92	5
15	$Fe_2(SO_4)_3•xH_2O$	5	0.1	1.5	MeOH	reflux	95	5
16	none	–	1.1	1.5	MeOH	reflux	–	–
17	$Fe_2(SO_4)_3•xH_2O$	5	–	3.0	MeOH	reflux	86	5
18	$Fe_2(SO_4)_3•xH_2O$	5	2.2	–	MeOH	reflux	88	5

[a]NMR Yield determined with 1-chloro-2,4-dinitrobenzene as internal standard

[b]48 h reaction time, [c]1 h reaction time

Guided by previously reported silylperoxide reductions using [Fe^{III}], we began our screen with catalytic $FeCl_3$ [10]. We identified methanol as the best solvent, achieving 79% (by NMR spectroscopy) of the desired product **1c** and 18% of the alcohol side-product **1d** (Table 3.1, entries 2–6). In surveying Fe^{III} salts, a relatively weakly coordinating sulfate counterion performed the best, generating significantly less of the alcohol 1d (entries 6–9). Heating under reflux dramatically favored **1c** over **1d** (entry 10).

There was little effect across the varied Fe^{III} quantities (entries 10–13). We found the ratio of **1c** to **1d** slightly improved when using only a catalytic quantity of the thiol (entries 10, 14, and 15). Consequently, 5 mol % $Fe_2(SO_4)_3 \bullet xH_2O$, 10 mol % PhSH, and 1.5 equiv of γ-terpinene in refluxing methanol became the standard conditions for the second step of our IMP-based hydrodealkenylation (entry 15). Control experiments demonstrated that an iron(III) salt was necessary for the reaction to occur, and the use of a mixture of thiol and γ-terpinene provided the best results (entries 15–18).

3.3.1 Electron-Rich Aromatics

With optimum conditions in hand for both steps of our IMP-based hydrodealkenylation, we turned to addressing the limitations of ozonolysis. The first class of ozone-incompatible alkenes that we addressed, electron-rich aromatics, are rapidly oxidized by ozone, but are more tolerant toward IMP [13]. For example, treatment of the pentoxifylline-derived alkene **3a** with the standard hydrodealkenylation conditions provided **3x** in 42% yield, via epoxidation, *N*-oxide formation, and rearrangement of the dihydropurine-2,6-dione heterocycle during ozonolysis (Figure 3.2a) [14]. In contrast, the alkene **3a** underwent IMP and subsequent radical hydrogenation in isolated yields of 94 and 64%, respectively (Figure 3.2b). We needed a slightly elevated reflux temperature to boost the efficiency of the second step, achieved by swapping methanol for a mixture of *n*-propanol and water (4:1). Rotenone (**4a**), also a member of the allylic alcohol/ether class, was a good substrate for IMP, achieving 80% yield of the silylperoxide. The hydrodealkenylation product **4c** was formed near-quantitatively (98%) after reduction. The Wittig olefination product **5a** from nabumetone formed the corresponding silylperoxide in 98% yield. A higher reflux temperature was, again, necessary for the second step, resulting in 13% of **5c**. IMP of phenol-containing eugenol was unsuccessful. We suspected that the acidic phenol unit removed the modp ligand from the Co complex through protonation and halted the reaction. Acetyleugenol (**6a**), however, performed well (87%) in IMP. Further investigation into phenolic substrates revealed that the acetate protecting group was also necessary for 2-allylphenol (**7a**, 90%) during IMP. With our radical hydrogenation conditions, a hydrogen atom was installed at the benzylic positions

of both **6c** and **7c**, a feat not demonstrated previously for the original hydrodealkenylation [1b].

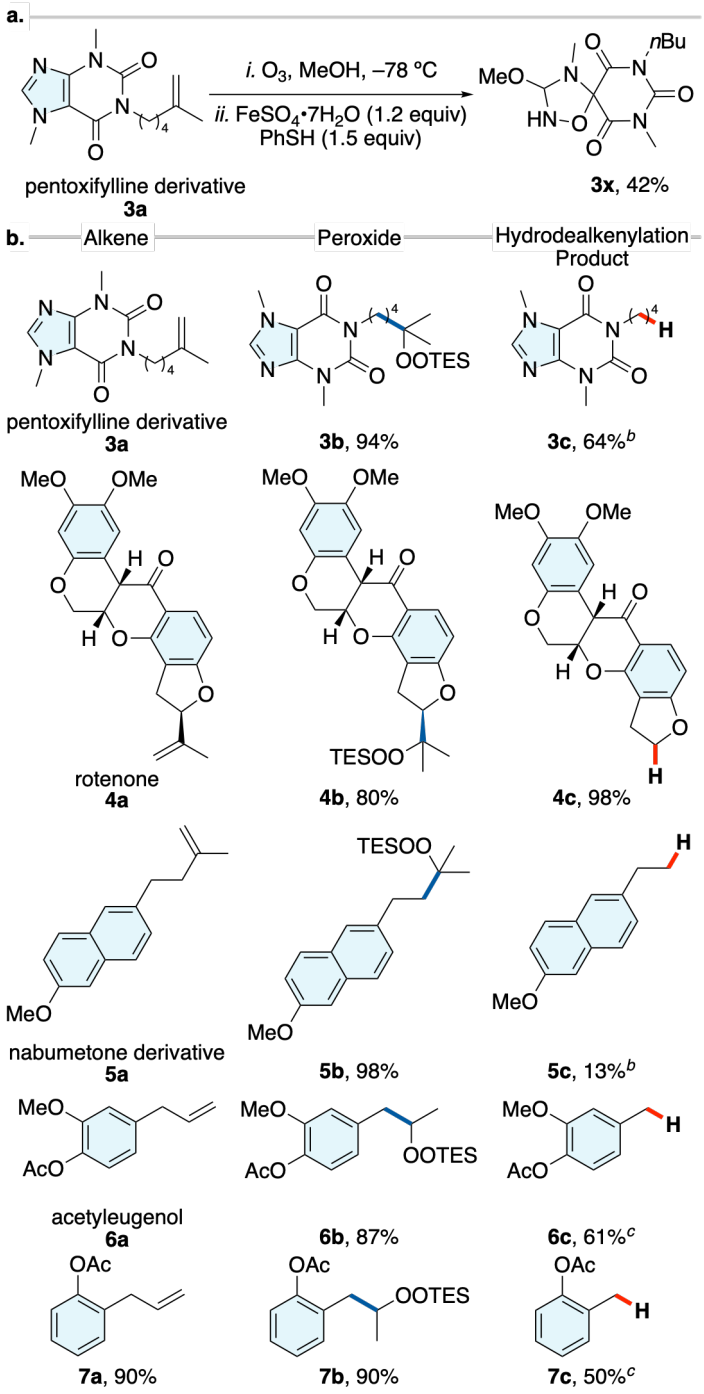


Figure 3.2 Electron Rich Aromatics

(a) Ozone-induced oxidative degradation of the 3,7-dihydropurine-2,6-dione heterocycle. (b) IMP conditions from Eq. 3.1, with a drop of TBHP, and radical hydrogenation conditions from Table 3.1, entry 15 were used to convert the starting alkene into the product. Electron-rich aromatic rings are highlighted in glacial blue. [a]4:1 *n*PrOH/H_2O was used instead of MeOH in the radical hydrogenation. [b]NMR spectral yield determined with 2,4-dinitro-1-chlorobenzene as internal standard, for volatile compounds.

3.3.2 Unproductive Substitution Patterns

Figure 3.3 presents our results from studying the second ozone-incompatible class: alkenes with unproductive substitution patterns. For the trisubstituted alkene (–)-citronellol (**8a**), the Criegee intermediate forms at the more-substituted carbon atom, excising the chiral functionality as the aldehyde **8x**, thereby barring useful radical functionalization (Figure 3.3a) [15]. IMP, on the other hand, does not suffer from this limitation because the C=C π-bond is simply transformed while all other functionalities remain intact. In this category, (–)-citronellol (**8a**) and (–)-*O*-benzoylcitronellol (**9a**) were transformed into their corresponding silylperoxides with yields of 97 and 89%, respectively (Figure 3.3b). We did not observe any useful conversion of the peroxide **9b** in the radical hydrogenation in refluxing methanol. A reaction temperature of 140 °C in DMSO helped to promote β-scission with γ-terpinene omitted and PhSH (2.2 equiv) used exclusively. With these changes, we isolated the product **9c** in 40% yield. (+)-Methyl citronellate (**10a**) delivered the silylperoxide and hydrodealkenylation product with yields of 94 and 67% (GCMS), respectively. When employed in an ozonolysis-based hydrodealkenylation, compound **11a**, the styrene derived from benzosuberone, would result in the extrusion of a methyl radical during β-scission. With IMP, however, we obtained the peroxide with 95% efficiency, and the acetophenone **11c** in 75% yield.

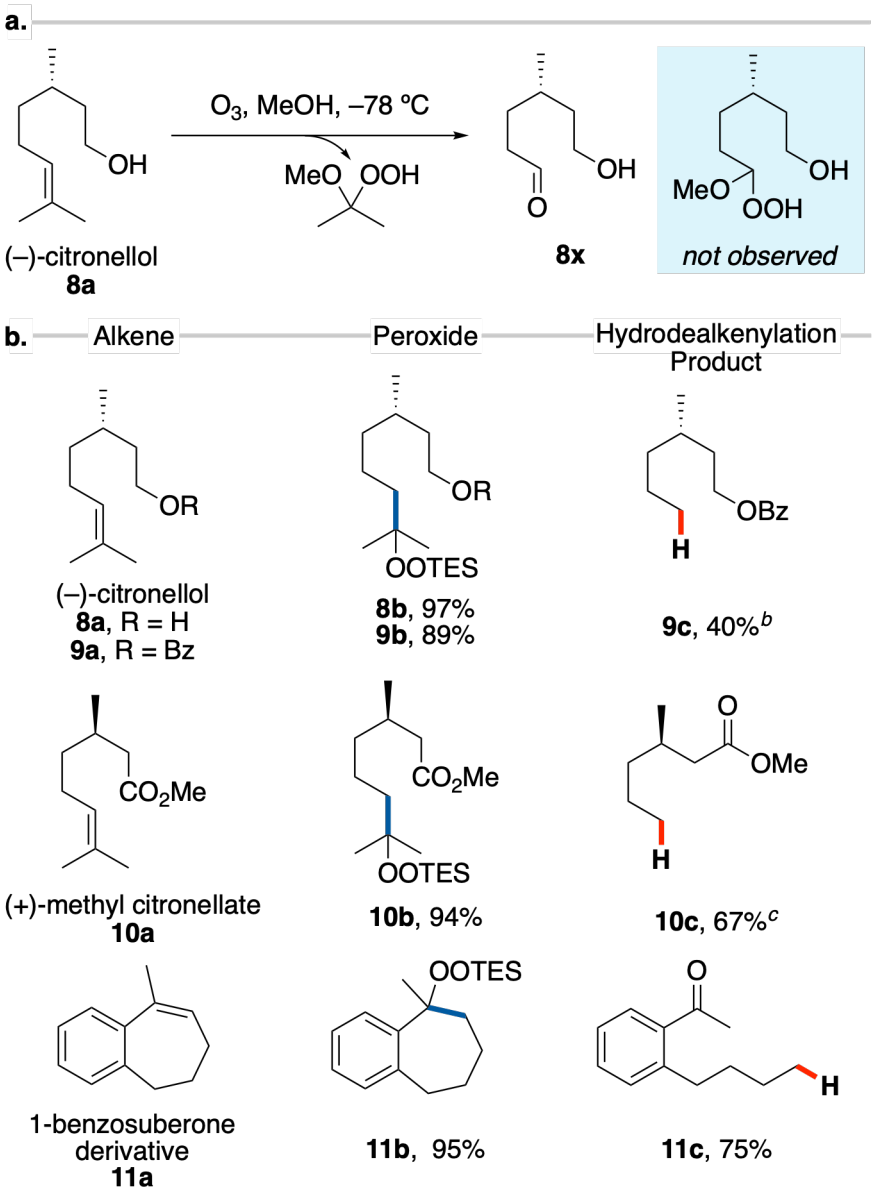


Figure 3.3 Unproductive Alkene Substitution Patterns

(a) Criegee ozonolysis outcome of (–)-citronellol. (b) IMP conditions from Eq. 3.1, with a drop of TBHP, and radical hydrogenation conditions from Table 3.1, entry 15 were used to convert the starting alkene into the product. [a]$Fe_2(SO_4)_3$•xH_2O (5 mol%), PhSH (2.2 equiv), DMSO, 140 °C. [b]GCMS yield

3.3.3 Sterically Hindered Alkenes

The third ozone-incompatible class, sterically hindered alkenes, are challenging to react in both ozonolysis and IMP. Ozonolysis of sterically confined alkenes, a class most famously represented by (+)-longifolene (**12a**), can provide anomalous products. During ozonation of **12a**, molecular oxygen is extruded as the epoxide **12x** forms (Figure 3.4a) [16]. Treatment of **12a** with the standard IMP conditions provided a complex mixture of oxidized products, a phenomenon for which we concluded that the alkyldioxy–cobalt(III) intermediate is too sterically hindered to effectively interact with triethylsilane. We revisited our model substrate *O*-benzoyl isopulegol (**1a**) and attempted to address this issue by substituting Et_3SiH with Me_3SiH (bp 6.7 °C) and conducting the reaction at temperatures from –78 to –20 °C [17]. We also exchanged DCE (mp –35.7 °C) for DCM (mp –95.1 °C) [18]. With these new conditions, the addition of stoichiometric TBHP was required to consume the alkene. With 2.0 equiv of both Me_3SiH and TBHP, we isolated 93% of the hydroperoxide **1b'** (see Table 3.S4 for more details). A control experiment using 2.0 equiv of both Et_3SiH and TBHP generated the hydroperoxide **1b'** in 92% along with 8% of the triethylsilylperoxide **1b**. This unexpected result led us to hypothesize that IMP with superstoichiometric TBHP deviated from the standard IMP mechanism at the step of transmetalation/σ-bond metathesis. TBHP may have intercepted the alkylperoxy–cobalt(III) intermediate to furnish the alkyl hydroperoxide [7g]. The cobalt–hydride unit was then regenerated from the formed tBuOO–[Co] after transmetalation with silane. GCMS-revealed *tert*-butyl trimethylsilylperoxide was evident, thus supporting this hypothesis. For sterically hindered alkenes, this alternative mechanism enabled the synthesis of hydroperoxides where the transmetalation step was too slow.

Encouraged by this result, we returned to (+)-longifolene (**12a**) and formed the hydroperoxide **12b'** in 83% yield with an *exo*/*endo* ratio of 3.0:1.0 when using 1.5 equiv of TBHP and 2.0 equiv of Et_3SiH. Treatment of **12b'** with the conditions listed in Table 3.1, entry 18 provided a 1.0:1.0 mixture of the ketones **12c** in 86% yield (Figure 3.4b). Ozonation of cholesterol (**13**) is known to provide small quantities (14.5%) of C5,C6-epoxides in polar media [19]. With IMP of cholesterol (**13**), we observed steric inhibition of transmetalation, similar to that of (+)-longifolene (**12a**), where the alkyldioxy–cobalt(III) intermediate was blocked by the cholestane A/B rings. The reaction proceeded slowly, with some alkene left unconsumed after 2 days. A portion of cholesterol (**13**) had also crystallized out of the solution during the course of the reaction. Protection of the C3 hydroxyl unit with a triethylsilyl group provided compound **13a**, which enabled dissolution and progress of the reaction. The standard IMP conditions, however, provided a complex mixture of remote oxidation products (eq 3.1) [20]. With 2.0 equiv each of TBHP and Me3SiH we obtained 83% of the hydroperoxide **13b'**; with Et_3SiH (2.0 equiv) and TBHP (1.5 equiv), only 57% (Figure 3.4c). All attempts at reduction of the peroxide **13b'** failed to provide ketone products. The particularly reversible β-scission of the 9-decalinoxyl radical, studied by Beckwith in 1983, explains the issues related to radical hydrogenation in the cholesterol system [21]. Despite initial obstacles for sterically hindered alkene substrates, we discovered that the addition of superstoichiometric TBHP in IMP promoted the formation of alkyl hydroperoxides.

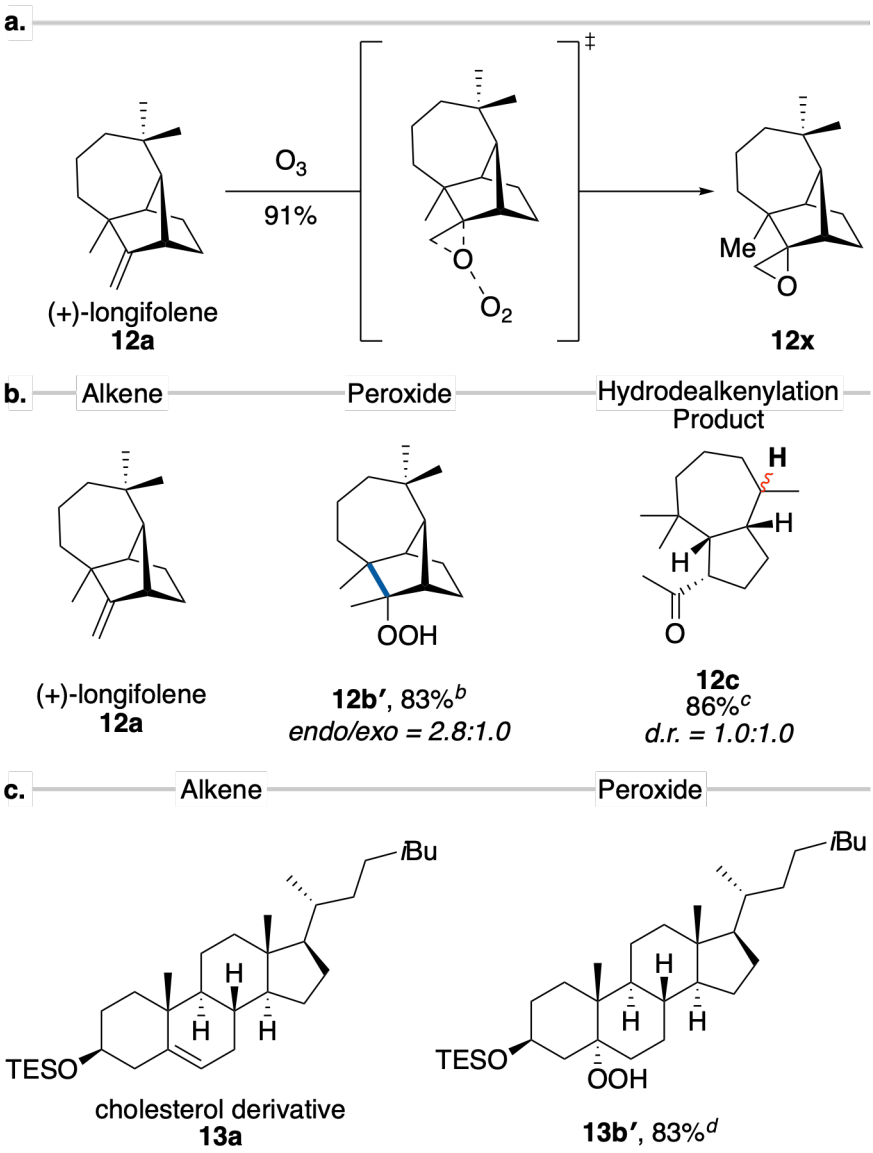


Figure 3.4 Sterically Hindered Alkenes

(a) Ozonolysis of (+)-longifolene. (b) Products after IMP and radical hydrogenation of (+)-longifolene. [a]$Co(modp)_2(EtOH)_2$ (10 mol%), Et_3SiH (2.0 equiv), 70% aqueous TBHP (1.5 equiv), O_2 (1 atm), DCE (0.2 M), 23 ºC, 5 min. [b]Table 3.1, entry 18. (c) IMP of *O*-triethylsilyl cholesterol. [c]$Co(modp)_2(EtOH)_2$ (10 mol%), Me_3SiH (2.0 equiv), 70% aqueous TBHP (2.0 equiv), O_2 (1 atm), DCM (0.1 M), from –78 to –20 ºC, 4 h.

3.3.4 Internal Nucleophiles

The fourth class of troublesome alkenes, those possessing internal nucleophiles, highlights issues related to the ambiphilic Criegee intermediate formed during ozonolysis. In most cases, methanol intermolecularly intercepts the carbonyl oxide to yield the α-methoxyhydroperoxide, but internal nucleophiles can outcompete it [22]. Cholesterol (**13**) also belongs to this category because after *retro*-(3+2)-cycloaddition of the molozonide, the aldehyde unit adds to the carbonyl oxide [22b] before methanol can intercept. Ozonolysis of acetyl-protected cholesterol (**13w**) in 1:1 methanol/dichloromethane is known to form **13x** in 56% yield (Figure 3.5a) [22b]. Triethylsilyl-protected cholesterol **13a** was discussed earlier, however, because it required stoichiometric TBHP during IMP (Figure 3.4). Substrates with a hydroxyl group positioned 5 or 6 atoms away from the anticipated carbonyl oxide of ozonolysis, namely (±)-carvomenthenol (**14a**), (±)-α-terpineol (**15a**), and (±)-*trans*-sobrerol (**17a**), provided their silylperoxides in yields of 91% (*trans*/*cis* = 1.4:1.0), 88% (*cis*/*trans* = 1.1:1.0), and 67% (*trans*/*cis* = 6.0:1.0), respectively (Figure 3.5b). The yield from *trans*-sobrerol (**17a**) was relatively low because of the presence of the allylic alcohol moiety [4,23]. We rationalize the observed diastereoselectivities for the silylperoxide products arising from tertiary cyclohexyl radicals by considering the Cieplak effect [1h,24]. Reduction of the silylperoxide from (±)-carvomenthenol (**14a**) and (±)-α-terpineol (**15a**) resulted in an equilibrating mixture of hydroxyketones and lactols. We observed a 2.0:1.0 mixture of the lactols **14c** (46%, *cis*/*trans* = 1.2:1.0) and the γ-hydroxyketone **14c'** (23%). We avoided a similar mixture for α-terpineol (**15a**) by instead using α-terpinyl acetate (**16a**), which provided an 85% yield of the silylperoxide **16b** (*cis*/*trans* = 1.3:1.0) which resulted exclusively in the formation of

the ketone **16c** (65%) after reduction. The acetal **17c** formed as a 1.9:1.0 mixture of *trans*/*cis* isomers in 64% yield after treatment of **17b** with the reduction conditions.

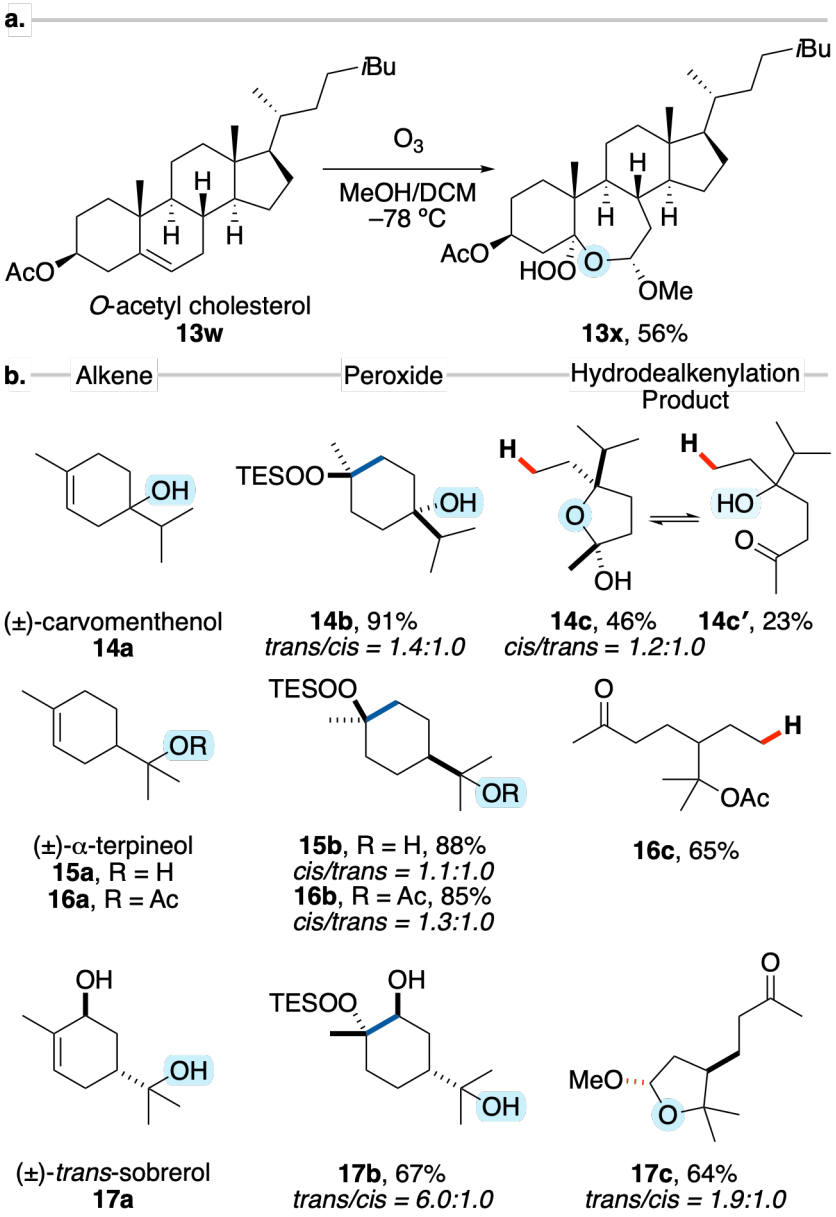


Figure 3.5 Internal Nucleophiles

(a) Ozonolysis of *O*-acetyl cholesterol. (b) IMP conditions from Eq. 3.1, with one drop of TBHP, and radical hydrogenation conditions from Table 3.1, entry 15 were used to convert the starting alkene into the product. Locations of internal nucleophile positions are highlighted in glacial blue.

3.3.5 Internal Electrophiles

Alkenes with internal electrophiles make up the fifth class of ozonolysis-incompatible substrates. Both the Criegee intermediate and the α-methoxyhydroperoxide may act as nucleophiles to create additional compounds. For instance, during the ozonolysis of (–)-*trans*-isopulegone (**18a**), the ketone acted as an electrophile, resulting in a 59% yield of the endoperoxide **18x** (Figure 3.6a). The reduction of **18x** posed challenges, however, due to the regioselectivity of alkoxyl radical formation after SET (Figure 3.6b). This issue was not unique to **18x** and could be extended to other compounds featuring a similarly substituted peroxide. In contrast, IMP produced the triethylsilylperoxide **18b** in 36% yield along with an additional 31% of the hemialkyldioxyketal **18b'** (Figure 3.6c) [25]. After radical hydrogenation of **18b**, we observed both **18c** and **18c'**, indicating that **18b'**/**18b''** must have formed as an intermediate (Figure 3.6b). When using only PhSH (2.2 equiv) and γ-terpinene was omitted (as in Table 3.1, entry 18), the yield of **18c** increased by 12%. Interestingly, the formation of **18b'**/**18b''** mirrors the structural features of **18x**, suggesting a similar mechanism of electrophilic activation by the β-ketone. Notably, however, **18b'**/**18b''** lack the methoxy group that complicates the SET reduction of **18x**. The observed regioselectivity in the reduction of **18b'** may be explained by a Curtin–Hammett relationship between the regioisomeric alkoxyl radicals and ferric alkoxides. The faster rate of β-scission for the α-hydroxy-alkoxyl radical, compared with that of the tertiary alkoxyl radical, led to the observed products. The reduction of **18x** would not benefit from such a scenario because the α-hydroxy- and α-methoxy-alkoxyl radicals would have similar rates of β-scission. In addition, an electron withdrawing effect imparted by the ferric alkoxide on the β-scission transition state led to a 2.6:1.0 ratio in the isolated yields of

18c (from a primary alkyl radical) and **18c** (from a secondary alkyl radical). The product **18c'** was formed through radical–polar crossover enabled by the nearby ferric alkoxide and the addition of methanol. The carbonyl groups of carbic anhydride (**19a**) are known to react as electrophiles during ozonolysis [26]. Nevertheless, IMP furnished the silylperoxide **19b** in 56% yield, with exclusively the *exo*-configuration. Reduction of this secondary silylperoxide resulted in the acetal **19c** in 39% yield.

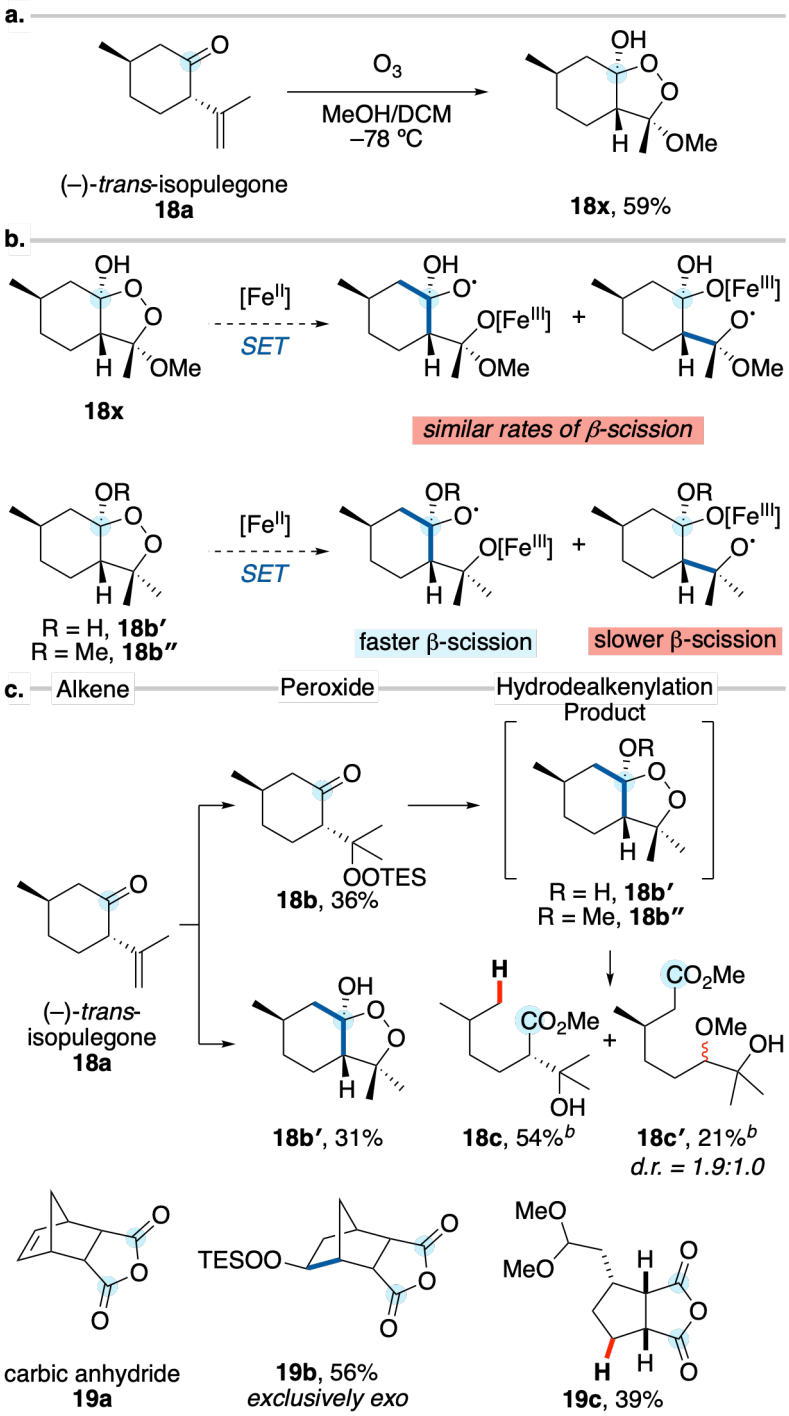


Figure 3.6 Internal Electrophiles

(a) Ozonolysis of (–)-*trans*-isopulegone. (b) IMP conditions from Eq. 3.1, with one drop of TBHP, and radical hydrogenation conditions from Table 3.1, entry 15 were used to convert the starting alkene into the peroxide and product, respectively. Isolated yields are provided. Locations of internal nucleophile positions are highlighted in glacial blue. [a]Table 3.1, entry 18.

3.3.6 Allylic Alcohols and Ethers

The sixth ozone-incompatible class of alkenes comprises allylic alcohols and ethers. Criegee ozonolysis products from allylic alcohols, α-alkoxy-β-hydroxyperoxides, can undergo Grob fragmentation [4]. Treatment of steviol methyl ester (**20a**) with ozone has been reported to form the secosteroid **20x** in 46% yield (Figure 3.7a) [4b]. Steviol methyl ester (**20a**) was challenging for IMP, but we were able to isolate 35% of the triethylsilylperoxide **20b** [8c]. Subjection of **20b** to the radical hydrogenation condition provided diketone **20c** in 78% yield. Product **20c** may have arisen from either a SET–β-scission–[Fe^{III}]–oxidation pathway or from Grob fragmentation [23]. As we discussed above, the allylic ether **4a** did not pose a significant problem for IMP or radical hydrogenation (Table 3.1). However, peroxide **17b** from (±)-*trans*-sobrerol (**17a**) behaved in a similar fashion as **20b** during radical hydrogenation and provided **17c** from either oxidation or from Grob fragmentation (Figure 3.7b).

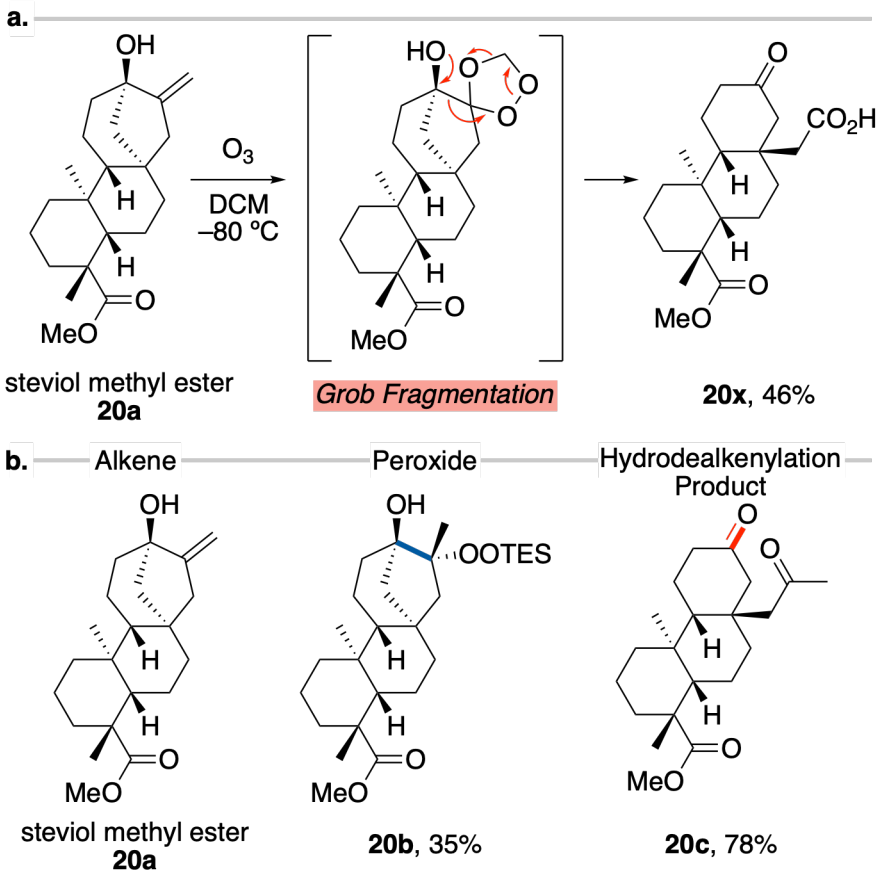


Figure 3.7 Allylic Alcohols and Ethers

(a) Ozonolysis of steviol methyl ester. (b) IMP conditions from Eq. 1, with one drop of TBHP, and radical hydrogenation conditions from Table 1, entry 15 were used to convert the starting alkene into the product.

3.3.7 Other Alkene Substrates

Having rescued ozonolysis-incompatible alkenes for hydrodealkenylation, we turned to evaluating other alkene substrates for IMP–hydrodealkenylation. The IMP–hydrodealkenylation products from cycloalkenes or methylidenecycloalkanes are different from those of ozonolysis-hydrodealkenylation. For example, Criegee ozonolysis of α-(+)-pinene (**21a**) in methanol generates the α-methoxyhydroperoxide **21b'**, which, after SET, β-scission, and HAT, yields the aldehyde **21c'** (Figure 3.8a) [1b]. In contrast, with IMP-hydrodealkenylation, the triethylsilylperoxide **21b** formed and was subsequently converted into the ketone **21c**. An ester or ketone hydrodealkenylation product can be chosen from methylidenecycloalkanes by using either ozonolysis or IMP to access the peroxide intermediate (Figure 3.8b). Ozonolysis of (±)-camphene (**22a**) in methanol provided the α-methoxyhydroperoxide **22b'**, with the ester **22c'** as the hydrodealkenylation product [1b], whereas IMP generated the silylperoxide **22b** and gives the ketone **22c** as the hydrodealkenylation product. This fundamental difference can be leveraged to create diverse hydrodealkenylation products from cycloalkenes and methylidene cycloalkanes that are ozonolysis-compatible.

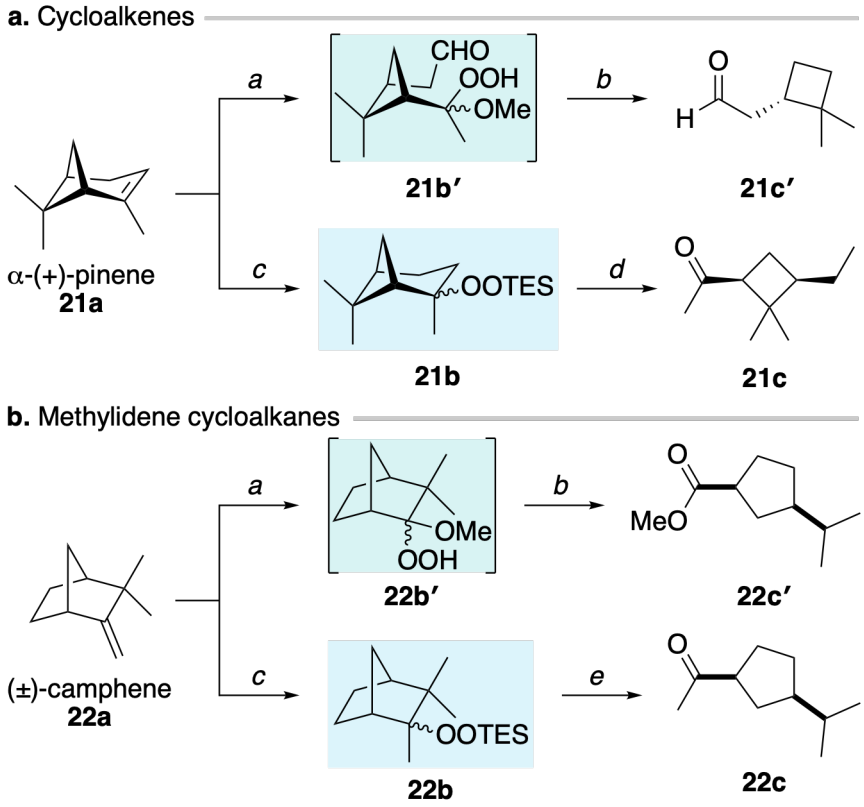


Figure 3.8 Ozonolysis– vs IMP–Hydrodealkenylation

[a] O_3, MeOH, –78 ºC. [b] $FeSO_4$•$7H_2O$ (1.2 equiv), PhSH (1.5 equiv). [c] $Co(modp)_2(EtOH)_2$ (10 mol%), Et_3SiH (2.0 equiv), O_2 (1 atm), DCE, 23 ºC. [d] $Fe_2(SO_4)_3$•xH_2O (5 mol%), PhSH (10 mol%), γ-terpinene (1.5 equiv), MeOH, reflux. [e] $Fe_2(SO_4)_3$•xH_2O (5 mol%), PhSH (1.5 equiv), MeOH, reflux.

(–)-Isopulegol (**2a**), similar to the model substrate **1a**, provided the silylperoxide **2b** in 83% yield and the hydrodealkenylation product **2c** in 76% yield (Figure 3.9). The cycloalkenes and methylidene cycloalkanes **21a**–**38a** procured the desired triethylsilylperoxides **21b**–**38b** in yields of 65–99%. Some ketone products were volatile, so we report their crude NMR spectral yields in Table 8. For characterization, we added *p*-toluenesulfonylhydrazide (3.0 equiv) to the crude reaction mixtures and isolated the corresponding *p*-tosylhydrazones (see Chapter 3 Supporting Information for isolated yields of the hydrazones). Increasing the steric bulk around the alkene, in general,

resulted in lower yields of the silylperoxides during IMP. For example, compounds **23a**, **24a**, and **25a**, differing in the number of α-methyl substituents, yielded the corresponding silylperoxides in yields of 99, 94 (*cis*/*trans* = 1.7:1.0) and 80%, respectively. Despite the steric factors impacting IMP, all three of these compounds performed well during reduction. The products from the more stable secondary and tertiary radicals, **24c** and **25c**, respectively, resulted in a higher yield than that of the primary radical to form **23c**, reflecting the fact that the rate of β-scission impacted the reaction efficiency. We observed a similar steric effect for IMP of 1-methylcyclohexene (**26a**) and 1,3-dimethyl-2-methylenecyclohexane (**27a**) (93% versus 73%). The yields for **26c** and **27c** (79% versus 86%) differed because of the stability of the corresponding alkyl radicals. The alkenes **28a** and **29a** formed the peroxides in yields of 97 (*cis*/*trans* = 1.4:1.0) and 95% (*cis*/*trans* = 1.1:1.0), respectively. The subsequent ketones **28c** and **29c** were fashioned in good yields (89 and 61%, respectively). The alkene **30a** suffered from a slight steric effect of the two β-quaternary centers during IMP (82%). Reduction of the resulting peroxide **30b** provided only 10% of the ketone **30c**. We speculate that the low yield was due to the Thorpe–Ingold effect favoring of the alkoxyl radical within the β-scission equilibrium [27].

Although (+)-2-carene (**31a**) and (+)-3-carene (**32a**) both generated the same silylperoxide **31b**, the allylic cyclopropane in (+)-2-carene (**31a**) contributed to the diminished yield of **31b** (89%) versus the homoallylic cyclopropane in (+)-3-carene (99%), both with a *cis*/*trans* ratio of 1.1:1.0. The boat conformation of the cyclohexyl radical formed from carene favored an equatorial approach of molecular oxygen, as opposed to the usual axial approach [1h,24,28]. Reduction of the carene silylperoxide created an α-cyclopropyl radical upon β-scission; it underwent ring opening to generate **31c** in 80%

yield. Compound **33a**, generated from Wittig olefination of norcamphor, provided the silylperoxide **33b** in 99% yield (*exo*/*endo* = 3.3:1.0). We found, however, that the α,α-dimethyl substituents of (±)-camphene (**22a**) tempered the efficiency of IMP (74%, exclusively *exo*-configuration). Reduction of the peroxide **33b** produced the ketone **33c** in 80% yield, formed via the cyclopentyl radical. We used the conditions from Table 3.1, entry 18 for reduction of the peroxide **22b**, because of the occurrence of radical–polar–crossover oxidation of the tertiary radical under the standard reduction conditions, and obtained an 88% yield of the ketone **22c**. The reaction of the methylidene unit of β-pinene (**34a**) was more efficient (99%) than that of the methylcyclohexene unit of α-pinene (**21a**) (89%) for IMP because of a difference in the kinetic profiles for *gem*-1,2-disubstituted alkenes and trisubstituted alkenes [6d]. Both **21b** and **34b** were formed with a 2.0:1.0 *exo*/*endo* ratio. The hydroxyl groups of (–)-myrtenol (**35**) and (–)-nopol (**36**) required acetylation for IMP [4,23]. After acetylation, we isolated the peroxide **35b** in 94% yield (*exo*/*endo* = 2.3:1.0) and peroxide **36b** in 84% yield (*exo*/*endo* = 4.0:1.0). We isolated the silylperoxide **37b** from (S)-*cis*-verbenol (**37a**) in 92% yield as a 3.0:1.0 mixture of *exo*/*endo* isomers. The pinane-2-triethylsilylperoxides **21b**, **35b**, **36b**, and **37b** were converted into their alkylcyclobutanes, with only their products from primary radicals being isolated (68, 58, 82, and 29%, respectively). Norbornene (**38a**) resulted in 65% (*exo*/*endo* = 2.6:1.0) of the secondary peroxide **38b** after IMP. The lower IMP yield was presumably due to the formation of a ketone through a known degradation pathway. Radical hydrogenation of **38b** afforded the expected aldehyde product, which was converted to the corresponding dimethyl acetal **38c** in 59% yield during the reaction in methanol.

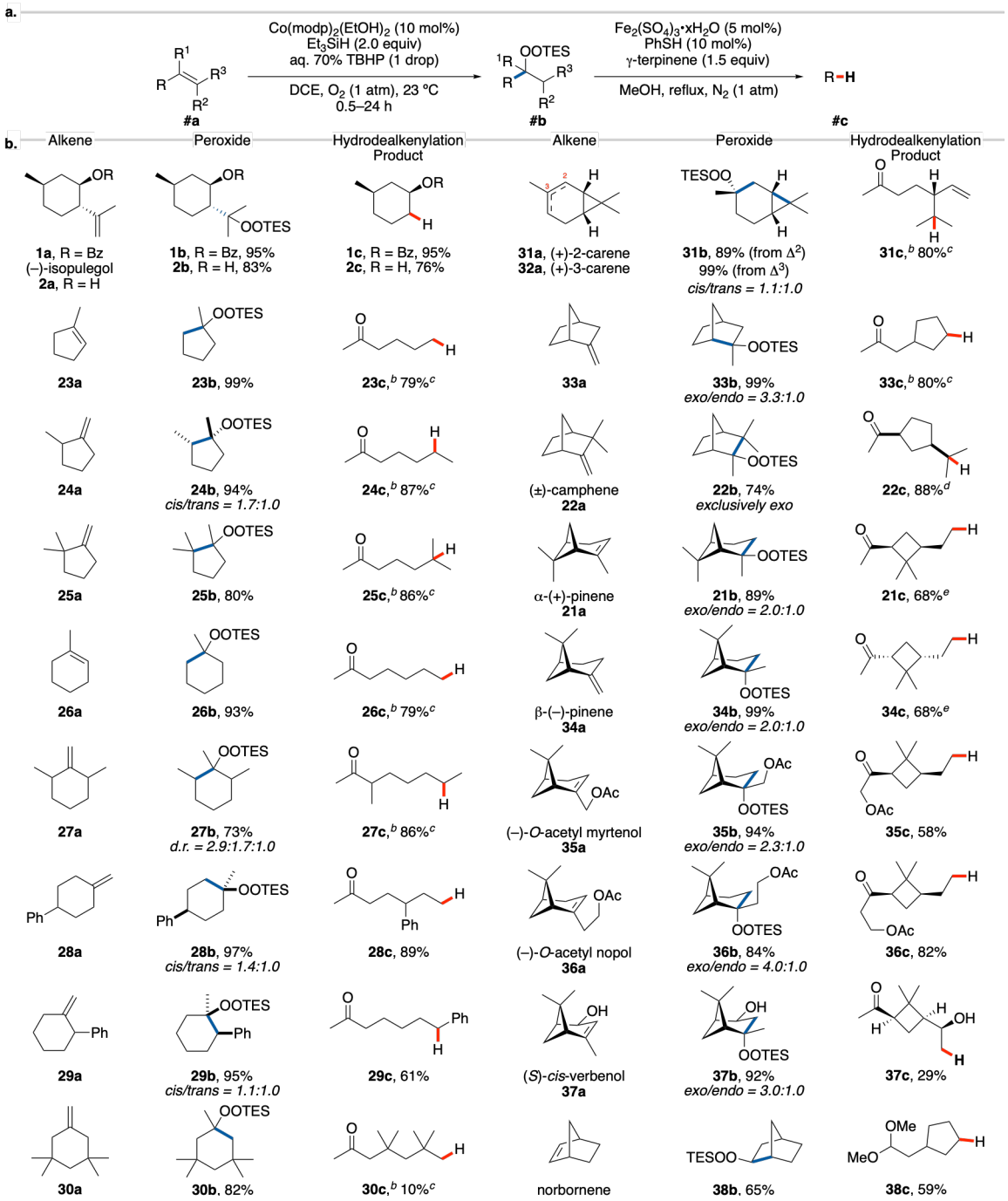


Figure 3.9 Alkenes, IMP, and Hydrodealkenylation

(a) Reaction conditions. (b) Isolated yields are provided, unless otherwise noted. [a]Because of the volatility of the ketone, the corresponding *p*-toluenesulfonylhydrazone derivative was isolated for characterization. [b]NMR spectral yield determined with 2,4-dinitro-1-chlorobenzene as internal standard. [c]Hydrodealkenylation was run under the conditions in Table 3.1, entry 18. [d]Isolated yield of the corresponding *p*-toluenesulfonylhydrazone derivative. Overlapping signals in crude NMR spectrum prevented accurate determination of NMR spectral yield.

3.4 Mechanistic Discussion

Naturally occurring alkenes, such as the examples we highlighted in our IMP-based hydrodealkenylation, produced silylperoxides that are α-substituted with alkyl groups or hydrogen atoms. Compared with the often-studied α-methoxyhydroperoxide and α-phenylsilylperoxide, both of which bear an α-stabilizing substituent, the alkoxyl radicals formed from alkyl silylperoxides via SET from iron(II) face a few challenges related to their β-scission [10,29,30]. First, the rate constants of β-scission (k_2) of the alkoxyl radicals bearing α-methoxy, α-phenyl, and α-methyl groups, with all other substituents equal, are 6.21×10^8, 7.4×10^5 and 6.40×10^3 s^{-1} respectively (Figure 3.10a) [31–34]. The β-scission rate constants (k_2) further diminish upon proceeding from the *tert*-butyloxyl (6.40×10^3 s^{-1}) to the *iso*-propoxyl (8.43×10^2 s^{-1}) to the ethoxyl radical (1.63 s^{-1}). The observed difference in rate constants can be partially attributed to a lack of orbital stabilization for the developing C=O π-bond. As the sp^3 hybridized α-carbon atom of the alkoxyl radical converts to the sp^2 hybridized carbonyl carbon atom, its substituents must migrate approximately 10.5° to reach the 120° necessary for a planar center, thereby developing steric and torsional strain (Figure 3.10b). The lone pair of electrons of the α-methoxy group and the π-electrons of the phenyl ring can mix with the forming C=O π-bond and compensate for the strain penalties (Figure 3.10c). The relative fragmentation rate constants display a positive correlation between faster β-scission and a stronger α-stabilizing substituent along with greater radical stability. The formation of primary, secondary, and tertiary alkyl radicals from *tert*-alkylalkoxyl radicals occur with rate constants (k_2) of 7.70×10^6, 1.44×10^9 and 8.31×10^{10} s^{-1} respectively, where only α-stabilization by hyperconjugation exists to improve β-scission [34–39]. Considering both

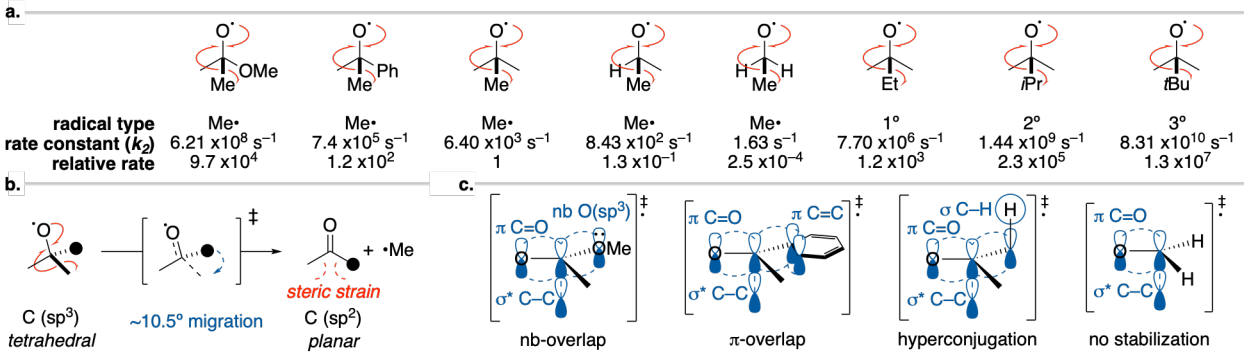


Figure 3.10 β-Scission Kinetics

(a) Comparison of rate constants for β-scission. (b) Steric strain during β-scission. (c) Orbital stabilization during β-scission

α-substituent stabilization and radical stability, it is, therefore, inherently more difficult to induce fragmentation in the alkoxyl radical resulting from reduction of the IMP products of unactivated alkenes, particularly when the ensuing alkyl radical is a primary one.

A second challenge involves the reversibility of β-scission for cycloalkyloxyl radicals. Beckwith and Hay measured the rate constants for radical ring opening/closing from cyclopentyloxyl and cyclohexyloxyl radicals [40]. For cyclopentyloxyl radicals, the rate constant for β-scission at 80 °C was 4.7×10^8 s^{-1} and for cyclization it was 8.7×10^5 s$^{-1,}$ while for cyclohexyloxyl radicals the rates were 1.1×10^7 and 1.0×10^6 s^{-1}, respectively, attributable to the +6.5 kcal mol–1 ring strain of the cyclopentane ring. Not only are cyclopentane rings more susceptible to β-scission than cyclohexanes but also a larger kinetic window (10^3 s^{-1}) exists for bimolecular functionalization of the opened alkyl radical before recyclization. Despite the unimolecular nature of β-scission, the Walling–Padwa and Beckwith–Hay studies identified that an increase in reaction temperature skews the reaction toward fragmentation [40]. A higher reaction temperature exploits the difference in entropy for the open chain versus the closed ring conformations (see **II** and **III** in Figure

3.11a). Indeed, we observed this beneficial effect during optimization (Table 3.1, entries 9 and 10). We further manipulated the solvent mixtures to increase the reaction temperature beyond the boiling point of methanol for some unactivated primary alkyl radical substrates.

A third challenge relates to the bimolecular rate constants involved in our proposed mechanism (Figure 3.10a). Three major steps are required to form the desired product: SET, β-scission, and hydrogen atom transfer (HAT). First, iron(II) must commit one electron to reduce the alkyl silylperoxide **I**, forming an alkoxyl radical **II** and a siloxide anion [12]. The rate constant k_1 for this transformation is 1.2×10^7 M^{-1} s^{-1} (at 298 K) [41]. The alkoxyl radical II may then undergo unimolecular β-scission with a rate constant (k_2) between 10^3 and 10^{10} s^{-1} (see Figure 3.10a for rate constants) to form an alkyl radical **III** [32–39]. Finally, the alkyl radical III is intercepted through HAT by an HAD to provide the hydrodealkenylation product **IV**. PhSH transfers a hydrogen atom with a rate constant (k_3) of 3.54×10^8 M^{-1} s^{-1} (at 310 K) [12,42]. γ-Terpinene is expected to undergo HATs with rate constants of 1.3×10^5, 5.8×10^4, 9.4×10^3, and $< 10^2$ M^{-1} s^{-1}, for primary, secondary, tertiary, and allylic/benzylic radicals, respectively (rates based on 1,4-cyclohexadiene at 300 K) [43].

If there is an excess of iron(II) or PhSH, then prevention of the three potential off-cycle pathways to form the alcohol **V** becomes a major challenge. The alkyl silylperoxide **I** may be reduced by PhSH in a slow two-electron process. PhSH-mediated reduction of an alkylperoxide at 298 K is accelerated by a metal catalyst, a base, or an acid, all of which were present in our reaction mixtures [12,44]. Alternatively, excess PhSH coordinated to iron expedites HAT to the alkoxyl radical **II**, quenching it before β-scission and directly

furnishing the alcohol **V** [45]. HATs in this manner occur with rate constants (k_5) of 6.28×10^8 M^{-1} s^{-1} from PhSH (at 310 K) and 1.1×10^8 M^{-1} s^{-1} from γ-terpinene (to hydroxyl radical in the gas phase at 298 K) [42,43]. With stoichiometric iron(II), the alkoxyl radical **II** may also be over-reduced ($k_6 > 1.2 \times 10^6$ M^{-1} s^{-1} at 303 K) [46]. To suppress these three bimolecular pathways, we adopted a condition with catalytic [Fe^{III}]–PhSH. We also employed γ-terpinene as a stoichiometric reductant, which we hypothesized would primarily interact with radicals outside the ligand sphere of iron.

Under our reaction conditions (catalytic [Fe^{III}], catalytic PhSH, and stoichiometric γ-terpinene), we propose two pathways for the formation and regeneration of the [Fe^{II}] species for SET. Although low yielding, oxidation of γ-terpinene by [Fe^{III}] would form 1/2 *p*-cymene, [Fe^{II}] and a proton (Figure 3.11b) [47]. Alternatively, a catalytic cycle involving PhSH and γ-terpinene can be envisioned (Figure 3.11c). Dissolution of iron(III) sulfate hydrate, abbreviated as [Fe^{III}]–(H_2O) **VI**, in methanol would create [Fe^{III}]–(MeOH) **VII**. Substitution of MeOH with PhSH forms [Fe^{III}]–(PhSH) **VIII** [48]. Subsequent deprotonation provides [Fe^{III}]–SPh **IX**, which is known to disproportionate into [Fe^{II}] and a phenylthiyl radical [45,49]. The formed [Fe^{II}] can then undergo SET with the alkyl silylperoxide **I** to result in the alkoxyl radical **II** and [Fe^{III}]–OTES **X**. The conversion of **X** to **IX** can occur in two ways. In one scenario, **X** undergoes protonation and ligand exchange with the solvent, methanol, to form **VII** [50]. In the other, direct substitution of PhSH leads to **IX** and triethylsilanol. The phenylthiyl radical can react with 1/2 γ-terpinene to regenerate PhSH along with 1/2 *p*-cymene.

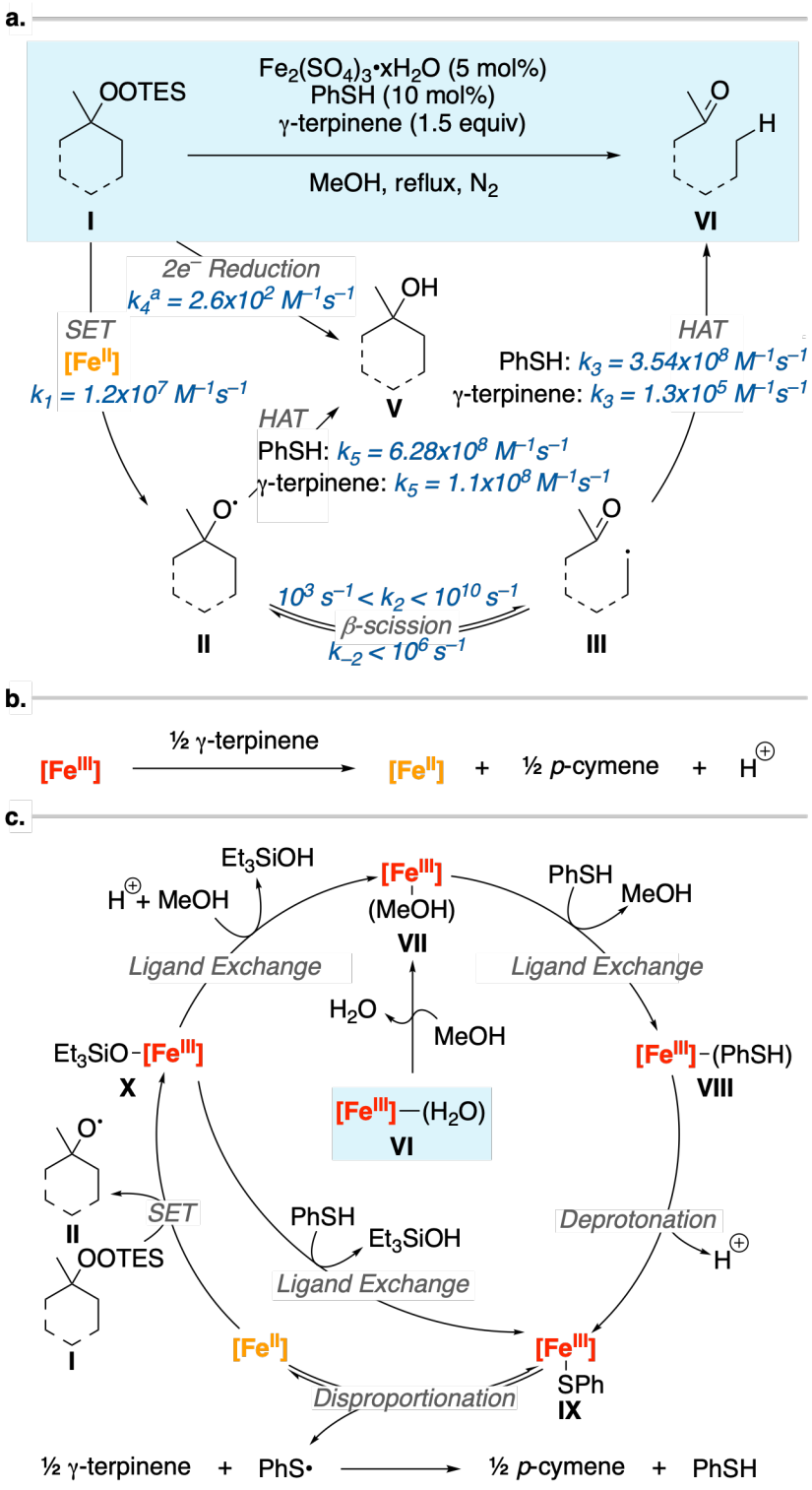


Figure 3.11 Mechanism

(a) Mechanism of IMP–hydrodealkenylation. (b) Formation of [Fe^{II}] with γ-terpinene. (c) Formation of [Fe^{II}] with PhSH and γ-terpinene. [a]Rate of H_2O_2 reduction by dimethylsulfide at 298 K [44].

3.5 Conclusions

We have developed an alternative hydrodealkenylation strategy based on the IMP reaction and [Fe^{III}]–PhSH catalysis. Our approach salvages ozonolysis-incompatible alkene substrates—featuring electron-rich aromatics, unproductive substitution patterns, steric hindrance, internal nucleophiles or electrophiles, and allylic alcohols by employing IMP with our modified catalyst, $Co(modp)_2(EtOH)_2$ to synthesize peroxides. We subjected the IMP alkylperoxides to new conditions for radical hydrogenation, using catalytic loadings of both ferric sulfate hydrate and benzenethiol and a stoichiometric reductant (γ-terpinene) at elevated temperatures, thereby accelerating β-scission and suppressing over-reduction. We further diversified the hydrodealkenylation products by creating ketones from cycloalkenes and methylidenecycloalkanes, instead of the aldehydes and esters that have previously been prepared through the ozonolysis-based method. We anticipate IMP-hydrodealkenylation may serve as a selective and mild synthetic method for direct functionalization of a wider range of renewable, enantiopure, feedstock alkenes.

3.6 Supporting Information and Experimental Section

3.6.1. Materials and Methods

Unless otherwise stated, all reactions were conducted in oven-dried glassware (which had been washed sequentially with 12M HCl then Alconox) fitted with rubber septa and stirred with Teflon-coated magnetic stirrer bars. For dry or air-free reactions, standard Schlenk techniques were used to transfer liquid reagents and solvents. Methanol (MeOH) was distilled over magnesium under an argon atmosphere. Dichloromethane (DCM), acetonitrile (MeCN) and triethylamine (Et_3N) were distilled over calcium hydride under an argon atmosphere. Tetrahydrofuran (THF), benzene, toluene, and diethyl ether were distilled over sodium/benzophenone ketyl under an argon atmosphere. All other solvents and reagents were used as received from commercial sources, unless otherwise noted. Reaction temperatures above room temperature (23 ºC) and below 80 ºC refer to water bath temperatures, unless otherwise stated. Reaction temperatures above 80 ºC refer to silicone oil bath temperatures. Thin layer chromatography (TLC) was performed using SiliCycle silica gel 60 F-254 precoated plates (0.25 mm) and visualized under UV irradiation and with a silica-iodine (SiO_2–I_2), cerium ammonium molybdate (CAM) stain, potassium permanganate ($KMnO_4$) stain, or vanillin stain. SiliCycle Silica-P silica gel (particle size: 40–63 μm) was used for flash column chromatography (FCC). ^1H, ^{13}C and 2D NMR spectra were recorded using Bruker 800 Avance, NEO-600, AV-500, AV-400 or AV-300 MHz spectrometers, with ^{13}C NMR spectroscopic operating frequencies of 151 MHz, 126 MHz, 101 MHz, or 75 MHz, respectively. Chemical shifts (δ) are reported in parts per million (ppm) relative to the (residual protonated) signal of the solvent $CDCl_3$ (choloroform-d, δ = 7.26 for ^1H NMR; δ = 77.2 for ^{13}C NMR) or C_6D_6 (benzene-d6, δ =

7.16 for ^{1}H NMR; δ = 128.1 for ^{13}C NMR). Data for ^{1}H NMR spectra are reported as follows: chemical shift, multiplicity, coupling constants (Hz), and number of hydrogen atoms. Data for ^{13}C NMR spectra are reported in terms of chemical shift. The following abbreviations are used to describe the multiplicities: s = singlet; d = doublet; t = triplet; q = quartet; m = multiplet; br = broad. Melting points are uncorrected and were recorded using an Electrothermal® capillary melting point apparatus. IR spectra were recorded using a Jasco FTIR-4100 spectrometer with an ATR attachment. High-resolution mass spectrometry (HRMS) was performed using a Thermo Fisher Scientific Exactive Plus spectrometer equipped with an IonSense ID-CUBE DART source or an Agilent 6545 Q-TOF LC/MS with 1260 Infinity LC. Low-resolution mass spectrometry was performed with an Agilent 7250 Q-TOF GC/MS with low energy EI or an Agilent Intuvo 9000 GC with a 5977B GC/MSD. Elemental analysis (EA) was performed in triplicate using an Exter Analytical Inc. CE-440 Elemental Analyzer. Specific rotation was recorded using an Autopol IV polarimeter and a 50 mm cell, at concentrations of 0.1 g/100 mL. Differential scanning calorimetry (DSC) was measured using a Perkin Elmer DSC 8000. Data for X-ray diffraction (XRD) were collected from a shock-cooled single crystal at 100(2) K on a Bruker D8 three-axis goniometer three-circle diffractometer with a sealed X-ray tube using a Bruker Apex-II CCD detector. The diffractometer was equipped with an Oxford Cryostream 700 low temperature device and used MoK_{α} radiation (λ = 0.71073 Å).

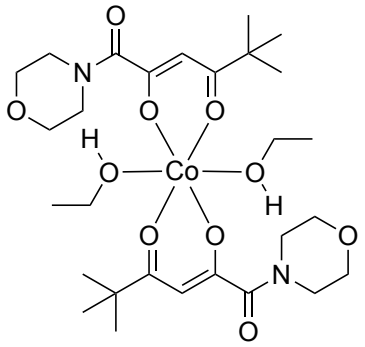
3.6.2 Safety

Caution: Organic peroxides are typically high-risk shock-sensitive compounds that are prone to explosions. Although we have not encountered any peroxide-related safety issues in our lab, the peroxides generated in this method should be handled only by

properly trained individuals and the isolated compounds stored at cryogenic temperatures. The use of a blast-shield is also recommended, especially for reactions performed on larger scales.

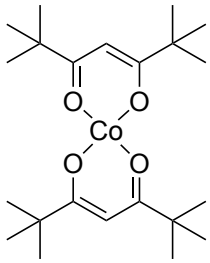
3.6.3 Preparation of Starting Materials

3.6.3.1 Co(II) Catalysts



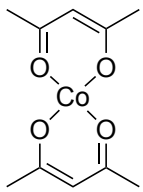
C1

$Co(modp)_2(EtOH)_2$ **C1** was prepared by following a literature procedure [51]. The complex was recrystallized from absolute ethanol to afford red/orange crystals. For characterization, see Sections 3.6.9 and Section 3.6.11.



C2

$Co(thd)_2$ **C2** was prepared by following a literature procedure [52]. The complex was purified through vacuum sublimation at 1 mbar and 135 ºC (bath temperature) to afford purple crystals.

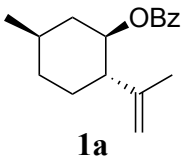


C3

$Co(acac)_2$ **C3** was purchased from a commercial source and used as received.

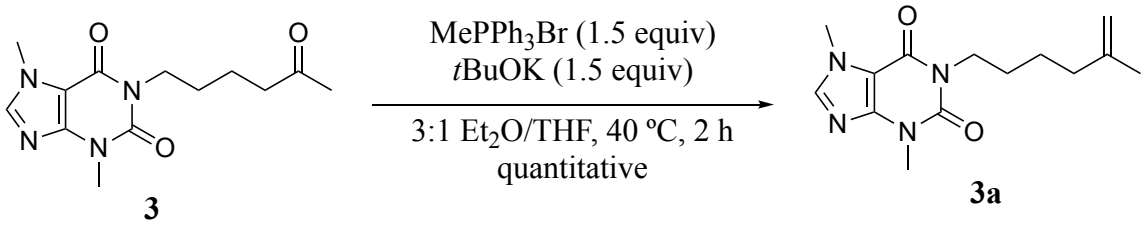
3.6.3.2 Alkenes

Pentoxifylline (**3**), rotenone (**4a**), nabumetone (**5**), acetyleugenol (**6a**), 2-allylphenol (**7**), (–)-citronellol (**8a**), (+)-citronellic acid (**10**), 1-benzosuberone (**11**), (+)-longifolene (**12a**), cholesterol (**13**), (±)- carvomenthenol (**14a**), (±)-a-terpineol (**15a**), (±)-a-terpinyl acetate (**16a**), carbic anhydride (**19a**), stevioside (**20**), (–)-a-pinene (**21a**), (±)-camphene (**22a**), 1-methylcyclopentene (**23a**), 2-methylcyclopentanone (**24**), 2,2-dimethylcyclopentanone (**25**), 1-methylcyclohexene (**26a**), 2,6- dimethylcyclohexanone (**27**), 4-phenylcyclohexanone (**28**), 2-phenylcyclohexanone (**29**), 3,3,5,5-tetramethylcyclohexanone (**30**), (+)-2-carene (**3qa**), (+)-3-carene (**3wa**), norcamphor (**3e**), (+)-b-pinene (**3ra**), (–)-myrtenol (**3t**), (–)-nopol (**3y**), *cis*-(*S*)-verbenol (**37a**), norbornylene (**38**), cinchonidine (**F1a**), tropinone (**F2**), eugenol (**6**), andrographolide (**F3a**), (–)-citronellal (**F4a**), (±)-sabinene (**F5a**), vitamin K1 (**F6a**), geraniol (**F8**), 1-Boc-4-methylenepiperidine (**F9a**), and *N*-Boc-norpseudopelletierine (**F10**) were purchased from commercial sources and used as received. (–)-Isopulegol (**2a**) was purchased from a commercial source and distilled under reduced pressure prior to use. *trans*-Sobrerol (**17a**) was purchased from a commercial source and recrystallized from DCM prior to use. Picrotoxinin (**F7a**) was purified through FCC (SiO_2) from commercially available picrotoxin (**F7**), which existed as a 1:1 mixture of picrotoxinin (**F7a**) and picrotin (**F7a'**).



1a

(–)-*O*-Benzoyl isopulegol (**1a**) was prepared from (–)-isopulegol (**2a**) according to a literature procedure [53]. This compound was purified through distillation (boiling point: 161 ºC, 6 mmHg), providing a 90% yield.



3 **3a**

Compound **3a** was prepared from pentoxifylline (**3**).

Procedure: To a flame-dried 2-neck flask with a Teflon-coated magnetic stirrer bar and a water condenser, added $MePPh_3Br$ (7.50 mmol, 2.68 g, 1.5 equiv) and *t*BuOK (7.50 mmol, 842 mg, 1.5 equiv). The system was evacuated and backfilled three times with argon, then Et_2O (30 mL) was added. This mixture was stirred for 30 min at room temperature until a homogeneous canary yellow color was observed. Pentoxifylline (**3**, 5.00 mmol, 1.40 g, 1.0 equiv) was added to a separate flame-dried round bottom flask then evacuated and backfilled 3x with argon. Dry THF (5 mL) was added to dissolve and the solution was transferred dropwise via cannula. Additional THF (5 mL) was used to rinse the second flask. After complete addition, the reaction was heated at 40 ºC and stirred for 2 h (complete conversion monitored by TLC). The reaction mixture was cooled, and the reaction was quenched with water. Filtration (washing with Et_2O), concentration

of the filtrate, and purification through FCC (*i*PrOH) afforded 3,7-dimethyl-1-(5-methylhex-5-en-1-yl)-3,7-dihydro-1*H*-purine-2,6-dione (**3a**) in quantitative yield.

Yield: quantitative

Physical State: clear liquid

Purification: SiO_2 (*i*PrOH)

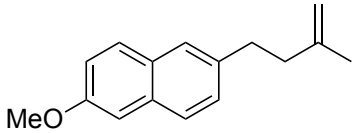
R_f = 0.53 (5% *v/v* MeOH/EtOAc + UV)

IR (ATR, neat) $\tilde{\nu}_{max}$: 3075, 3007, 2967, 2931, 2849, 1648, 1635, 1606, 1505, 1485, 1452, 1393, 1372, 1263, 1229, 1196, 1173, 1162, 1117, 1029, 963, 926, 888, 849, 816, 660, 650, 639, 622, 606 cm^{-1}

HRMS–ESI (*m/z*): $[M + H]^+$ calc'd for $C_{14}H_{21}N_4O_2$, 277.1659, found 277.1658

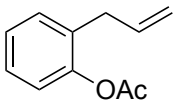
^{1}H NMR (400 MHz, $CDCl_3$) δ 7.49 (s, 1H), 4.78–4.59 (m, 2H), 4.05–3.95 (m, 3H), 3.98 (s, 3H), 3.56 (d, *J* = 1.3 Hz, 3H), 2.05 (t, *J* = 7.6 Hz, 2H), 1.74–1.70 (m, 3H), 1.69–1.59 (m, 2H), 1.56–1.44 (m, 2H)

^{13}C NMR (101 MHz, $CDCl_3$): δ 155.3, 151.5, 148.8, 145.7, 141.3, 110.0, 107.7, 41.3, 37.5, 33.6, 29.7, 27.7, 25.0, 22.3



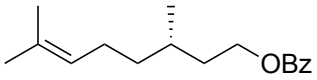
5a

Compound **5a** was prepared from nabumetone (**5**) according to a literature procedure [54].



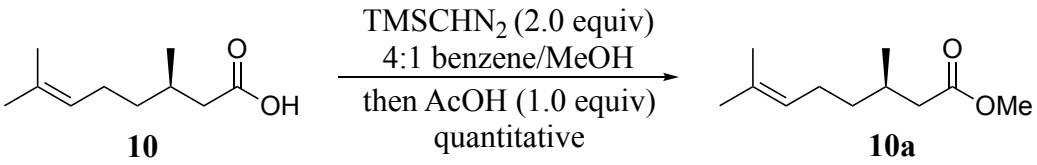
7a

Compound **7a** was synthesized from 2-allylphenol (**7**) according to a literature procedure [55].



9a

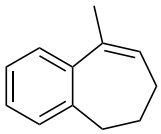
(–)-*O*-Benzoyl citronellol (**9a**) was prepared from (–)-citronellol (**8a**) according to a literature procedure [56].



10 **10a**

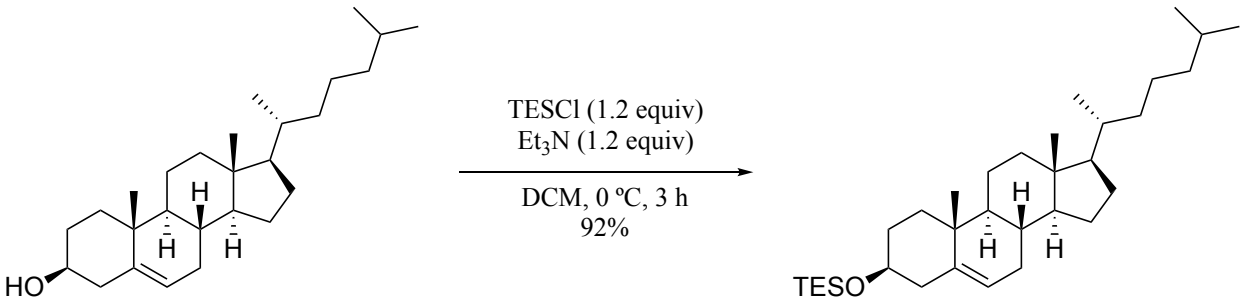
(+)-Methyl citronellate (**10a**) was prepared from (+)-citronellic acid (**10**).

Procedure: (+)-Citronellic acid (**10**, 910 mg, 5.24 mmol, 1.0 equiv) was dissolved in dry benzene (4 mL) and dry MeOH (1 mL) in a flask with and a Teflon-coated magnetic stirrer bar. $TMSCHN_2$ (1.20 g, 10.5 mmol, 2.0 equiv) was added dropwise as a 2 M solution in diethyl ether. The reaction mixture became yellow, and gas evolved as bubbles. After the bubbling ceased and the reaction was complete by TLC, glacial acetic acid (300 µL, 5.24 mmol, 1.0 equiv) was added causing the reaction mixture to decolorize. The mixture was concentrated through rotatory evaporation at 0 ºC and then the residue was distilled (bp: 78 ºC, 3 mmHg, and (+)-methyl citronellate (**10a**) was recovered in quantitative yield. Characterization data matched the literature values [57].



11a

Compound **11a** was prepared in two steps from 1-benzosuberone (**11**) according to literature procedure [58].

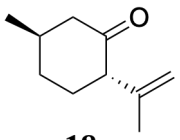


13 **13a**

Compound **13a** was prepared from cholesterol (**13**).

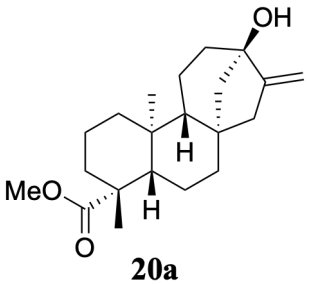
Procedure: A flame-dried round bottom flask equipped with a Teflon-coated magnetic stirrer bar, was charged with cholesterol (**13**, 3.00 g, 7.76 mmol, 1.00 equiv) and then evacuated and backfilled three times with argon. The solids were dissolved in in dry dichloromethane (30 mL) and then the flask was cooled to 0 ºC with an ice-water bath. Triethylamine (1.30 mL, 9.31 mmol, 1.20 equiv) was added, followed by the dropwise addition of chlorotriethylsilane (1.56 mL, 9.31 mmol, 1.20 equiv). The mixture was stirred at 0 ºC for 3 h then diluted with hexanes (50 mL) and transferred to a separatory funnel. The reaction was quenched with 1:3 sat. aq. $NaHCO_3/H_2O$. The aqueous phase was extracted three times with hexanes (3 x 15 mL) then the combined organics were washed with brine, dried (sodium sulfate), filtered through cotton, and concentrated. The crude

material (white solid, 3.59 g, 92% yield) was used without further purification. Characterization data matched literature values [59].



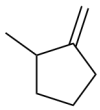
18a

(–)-*trans*-Isopulegone (**18a**) was prepared from (–)-isopulegol (**1b**) according to a literature procedure [60].



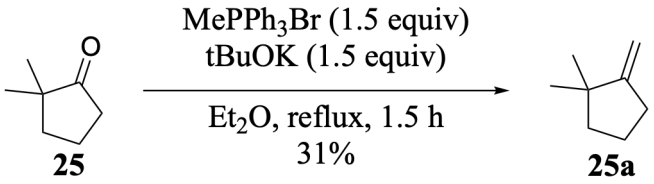
20a

Steviol methyl ester (**20a**) was prepared in two steps from stevioside (**20**). Stevioside (**20**) was oxidized and saponified according to a literature procedure to provide steviol after recrystallization from methanol [61]. Steviol was esterified by treatment with $TMSCHN_2$ (2.0 equiv) according to a literature procedure [62].



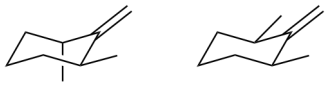
24a

Compound **24a** was prepared from 2-methylcyclopentanone (**24**) according to a literature procedure [63].



Compound **25** was prepared from 2,2-dimethylcyclopentanone (**25a**).

Procedure: $MePPh_3Br$ (5.39 g, 15.0 mmol, 1.5 equiv) and *t*BuOK (1.68 g, 15.0 mmol, 1.5 equiv) were placed in a flame-dried two-neck round-bottom flask equipped with a magnetic stirrer bar and a water condenser. The system was evacuated and backfilled three times with argon, then dry Et_2O (20 mL) was added. The mixture was stirred for 30 min at room temperature until a homogeneous canary yellow color was observed. The ketone (**25**, 1.12 g, 10.0 mmol, 1.0 equiv) was added to a separate flame-dried round bottom flask which was then purged with argon. Dry Et_2O (5 mL) was added, and the solution was transferred dropwise to the first flask via cannula. Additional Et_2O (2 x 2.5 mL) was used to rinse the second flask. After complete addition, the reaction mixture was stirred under reflux until complete conversion had occurred (TLC, 3 h). The reaction mixture was cooled and quenched with acetone. The precipitate was filtered off and washed with pentane. The filtrate was concentrated through rotatory evaporation at 0 ºC and purified through FCC (pentane) to give *exo*-methylidine-2,2-dimethylcyclopentane (**25a**) in 31% yield. Characterization data matched literature values [64].



***trans*-27a** ***cis*-27a**

Compound **27a** was prepared from 2,6-dimethylcyclohexanone (**27**) through Wittig olefination according to the literature [65]. An inseparable mixture of *cis*/*trans* isomers (5.4:1.0) was formed. The structures of these compounds were assigned based on the most stable conformations of their respective chair conformations. The ***trans*-27a** isomer has an axial and an equatorial allylic hydrogen, while the ***cis*-27a** isomer has only axial allylic hydrogens. In ^{1}H NMR spectra, the signals for the axial allylic protons of ***cis*-27a** and ***trans*-27a** appear at 2.07–1.92 ppm, while the equatorial allylic proton of ***trans*-27a** appear at 2.43 ppm. Equatorial protons in the cyclohexane ring are typically shifted more downfield compared with axial ones, with the difference in chemical shift accounted for by the observed axial/equatorial integration of 11.8:1.0. Full NMR values are provided below because they are missing from the literature [65].

***cis*-78a**

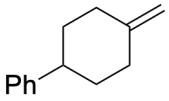
^{1}H NMR (400 MHz, $CDCl_3$) δ 4.64 (t, *J* = 1.6 Hz, 2H), 2.07–1.92 (m, 2H), 1.86–1.77 (m, 2H), 1.77–1.68 (m, 1H), 1.68–1.18 (m, 23), 1.07 (s, 3H), 1.05 (s, 3H)

^{13}C NMR (101 MHz, $CDCl_3$) δ 158.7, 101.1, 38.6, 37.7, 26.7, 18.8

***trans*-27a**

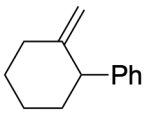
^{1}H NMR (400 MHz, $CDCl_3$) δ 4.64 (t, *J* = 1.6 Hz, 1H), 4.61 (t, *J* = 1.0 Hz, 1H), 2.43 (td, *J* = 6.9, 4.5 Hz, 1H), 2.07–1.92 (m, 1H), 1.86–1.77 (m, 2H), 1.77–1.68 (m, 1H), 1.68–1.18 (m, 2H), 1.07 (s, 3H), 1.05 (s, 3H)

^{13}C NMR (101 MHz, $CDCl_3$) δ 128.5, 103.8, 35.9, 35.8, 22.5, 21.2, 19.2, 14.2



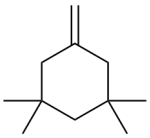
28a

Compound **28a** was prepared from 4-phenylcyclohexanone (**28**) according to a literature procedure [66].



29a

Compound **29a** was prepared from 2-phenylcyclohexanone (**29**) according to a literature procedure [67].



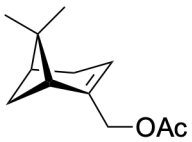
30a

Compound **30a** was prepared from 3,3,5,5-tetramethylcyclohexanone (**30**) according to a literature procedure [68].



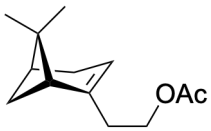
33a

Compound **33a** was prepared from norcamphor (**33**) according to a literature procedure [69].



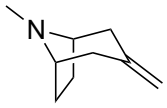
35a

(–)-*O*-Acetyl myrtenol (**35a**) was prepared from (–)-myrtenol (**35**) according to a literature procedure [70].



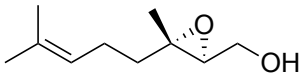
36a

(–)-*O*-Acetyl nopol (**36a**) was prepared from (–)-nopol (**36**) according to a literature procedure [71].



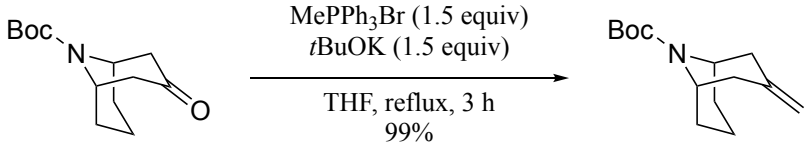
F2a

Compound **F2a** was prepared from tropinone (**F2**) according to a literature procedure [72].



F8a

Compound **F8a** was prepared through Sharpless asymmetric epoxidation of geraniol (**F8**) according to a literature procedure [73].



F10 **F10a**

Compound **F10a** was prepared from *N*-boc-norpseudopelletierine (**F10**).

Procedure: $MePPh_3Br$ (5.36 g, 15.0 mmol, 1.50 equiv) and TBuOK (1.68 g, 15.0 mmol, 1.50 equiv) were added to a flame-dried two-neck flask equipped with a condenser and a Teflon-coated magnetic stirrer bar. The system was evacuated and backfilled three times with argon, then dry THF (20 mL) was added. This mixture was stirred for 30 min at room temperature until a homogeneous canary-yellow color was observed. The ketone (**F10**, 2.39 g, 10.0 mmol, 1.00 equiv) was added to a separate flame-dried round bottom flask which was then purged with argon. Dry THF (5 mL) was added, and the solution was transferred dropwise to the first flask via cannula. Additional Et_2O (2 x 2.5 mL) was used to rinse the second flask. After complete addition, the reaction mixture was stirred under reflux until complete conversion had occurred (TLC, 3 h). The mixture was cooled,

and the reaction was quenched with acetone. The mixture was transferred to a separatory funnel washed with water. The aqueous layer was and extracted three times with EtOAc; the combined organic phases were washed with brine, dried (sodium sulfate), and concentrated. The residue purified through FCC (0–20% *v/v* acetone/hexanes) to give *tert*-butyl 3-methylene-9-azabicyclo[3.3.1]nonane-9-carboxylate (**F10a**) as a clear colorless oil (2.37 g, 99%).

Yield: 99%

Physical State: white solid

Melting Point: 26–28 ºC

Purification: SiO_2 (0–20% *v/v* acetone/hexanes)

$\boldsymbol{R_f}$ = 0.29 (3% *v/v* EtOAc/hexanes + vanillin stain)

IR (ATR, neat) $\tilde{\nu}_{max}$: 2973, 2930, 2850, 1686, 1475, 1439, 1407, 1363, 1348, 1324, 1287, 1252, 1218, 1173, 1112, 1090, 1066, 1011, 957, 942, 882, 869, 835,792, 769 cm^{-1}

GCMS–EI (*m/z*): $[M]^+$ calc'd for $C_{14}H_{23}NO_2$, 237.1723, found 237.17

^{1}H NMR (400 MHz, $CDCl_3$) δ 4.75 (t, *J* = 2.6 Hz, 2H), 4.46–4.22 (m, 2H), 2.63–2.42 (m, 2H), 2.31 (dt, *J* = 15.3, 1.4 Hz, 2H), 2.34–2.16 (m, 1H), 1.83–1.70 (m, 2H), 1.70–1.60 (m, 2H), 1.47 (s, 9H), 1.39–1.29 (m, 1H)

^{13}C NMR (126 MHz, $CDCl_3$) δ 154.3, 146.2, 109.0, 79.2, 47.9, 46.5, 38.5, 38.2, 30.7, 30.4, 28.5, 17.9

3.6.4 Ozonolysis

3.6.4.1 General Procedure for Ozonolysis

The alkene (1.00 equiv) and a magnetic stirrer bar were added to a round-bottom flask. Dry methanol and dichloromethane (4:1) were added and then the flask was cooled to –78 ºC in an acetone/dry ice bath. Oxygen was bubbled through a 16Gx4" needle at 1.0 L/min and then the ozone generator was turned on. TLC was used to track the reaction's progress (some reactions were complete before the reaction solution had turned pale blue, indicative of excess ozone). When the reaction was complete, excess ozone was removed using air or oxygen.

3.6.4.2 General Procedure for Hydrodealkenylation

The previously reported procedure for hydrodealkenylation was followed, combined with the procedure described above (Section 3.6.4.1) for the ozonolysis step [74].

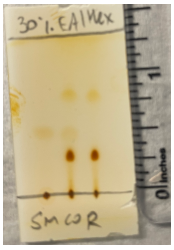
3.6.4.3 Thin Layer Chromatography (TLC) Analysis

Applying the anomalous trends for ozonolysis published in the literature to our selected alkenes (**3a**–**15a**, **17a**–**21a**) enabled us to predict the convoluted crude ozonolysis reaction profiles. To verify these hypotheses, we treated alkenes **3a**–**15a** and **17a**–**21a** according to the general procedure for ozonolysis in Section 3.6.4.1. Crude thin layer chromatography (TLC) allowed us to qualitatively observe the formation of compounds other than the predicted product(s), considered as evidence for ozone incompatibility. Figure S1 shows images of the TLC plates of the crude reaction mixtures after ozonolysis. The lanes marked as SM indicate starting material. The lanes marked as Co indicate the

co-spot. The lanes marked as R indicate the crude reaction mixture. Mobile phases and visualization methods are provided underneath each TLC plate.

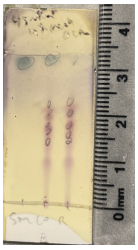
The alkene **3a** exhibited more than the one desired spot and was likely oxidized similarly to caffeine [75,76]. Rotenone (**4a**) exhibited many spots, which we attribute to electron-rich aryl oxidation as well as Grob fragmentation. We believe the aromatic ring of alkenes **5a**, **6a**, and **7a**, were quickly oxidized, providing the many products found on the TLC plates. The alkenes **8a**, **9a**, and **10a** revealed their corresponding aldehydes, as expected. The additional spots in the sample for **10a** may result from aldol reactions of the generated aldehyde. The alkene **11a** appears to have formed the corresponding peroxide, but additional UV-active spots which may have arisen from oxidative rearrangement reactions. (+)-Longifolene (**12a**) is sterically hindered and is known to be epoxidizable by ozone [77]. The vanillin-stained TLC plate featured two blue spots, suggesting *endo* and *exo* epoxide formation. Ozonolysis of cholesterol (**13**) is known to form an endoperoxide via cyclization of the hydroperoxide and the generated aldehyde [78]. Ozonolysis of *O*-triethylsilyl cholesterol (**13a**) led to many product spots on the TLC plate. (±)-4-Carvomenthenol (**14a**) forms a peroxide tethered to an internal nucleophile alcohol, creating a potentially equilibrating mixture; the streaks on TLC may be indicative of this phenomenon. The ozonolysis product of α-terpineol (**15a**) was complex, not only because of an internal nucleophile (alcohol), but also because of an internal electrophile (aldehyde). A similar equilibration to (±)-4-carvomenthenol was observed on the TLC plate. After ozonolysis, the peroxide from (±)-*trans*-sobrerol (**17a**) exhibited behavior similar to that of the ozonolysis product from α-terpineol (**15a**), as indicated by the streaking of the lower spots on the TLC plate. The allylic alcohol functionality provided an

avenue for Grob fragmentation, which may have led to the upper spots. (*S*)-*cis*-Verbenol (**18a**) created a cyclization product and a Grob fragmentation product, along with the standard Criegee ozonolysis product when reacted in DCM; the TLC plate featured three spots [79]. (–)-Isopulegone (**19a**), after treatment with ozone, generated an endoperoxy hemiketal with the β-carbonyl. We were able to isolate and characterize compound **19x** (see Section 3.6.9). There is a regioselectivity problem for reduction because of this ensuant cyclization. The alkene of carbic anhydride (**20a**) is known to form a peroxide that can open the anhydride [80]. Ozonolysis of steviol methyl ester (**21a**) has been reported to form a secosteroid after Grob fragmentation [81]. We attribute the green spot at the top of the reaction lane of the TLC plate to this product.



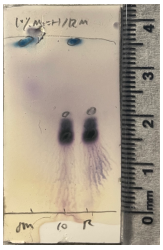
3a

10% *v/v* MeOH/DCM + UV/vanillin



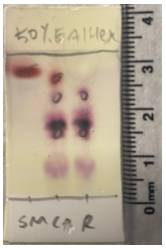
4a

10% *v/v* MeOH/DCM + UV/vanillin



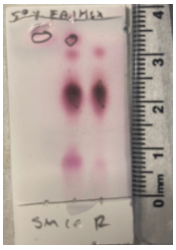
5a

10% *v/v* MeOH/DCM + UV/vanillin



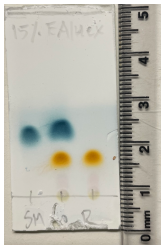
6a

50% *v/v* EtOAc/hexanes + UV/vanillin



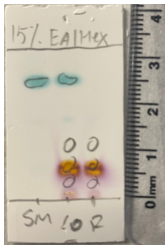
7a

50% *v/v* EtOAc/hexanes + UV/vanillin



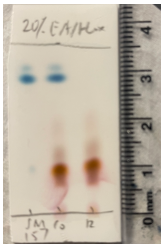
8a

15% *v/v* EtOAc/hexanes + UV/vanillin



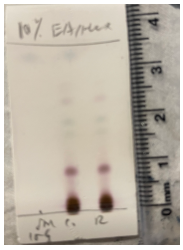
9a

15% *v/v* EtOAc/hexanes + UV/vanillin



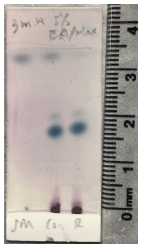
10a

20% *v/v* EtOAc/hexanes + vanillin



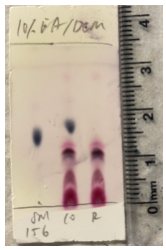
11a

10% *v/v* EtOAc/hexanes + vanillin



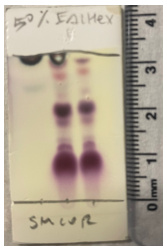
12a

5% *v/v* EtOAc/hexanes + vanillin



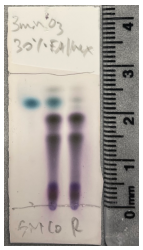
13

10% *v/v* EtOAc/DCM + vanillin



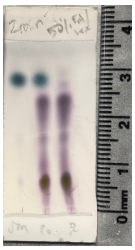
13a

50% *v/v* EtOAc/hexanes + vanillin



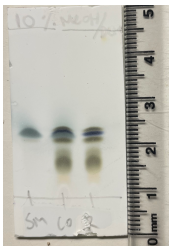
14a

30% *v/v* EtOAc/hexanes + vanillin



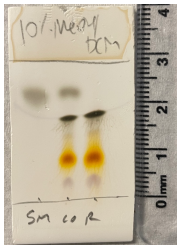
15a

50% *v/v* EtOAc/hexanes + vanillin



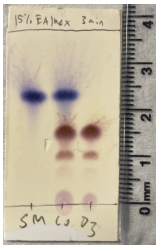
17a

10% *v/v* EtOAc/hexanes + vanillin



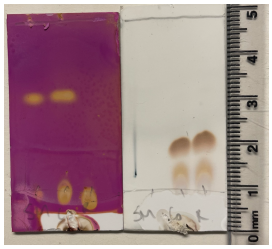
18a

10% *v/v* MeOH/DCM + vanillin



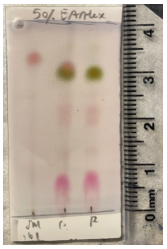
19a

15% *v/v* EtOAc/hexanes + vanillin



20a

50% *v/v* EtOAc/hexanes + $KMnO_4$ and 10% *v/v* EtOAc/hexanes + vanillin



21a

50% *v/v* EtOAc/hexanes + vanillin

Figure 3.12 TLC Analysis

3.6.5 Ozonolysis-Incompatible Alkene Examples

In this section we compile literature examples of anomalous ozonolysis reactions to aid the reader in visualizing the incompatibilities of each substrate class with ozone. References are cited for known ozonolysis reactions.

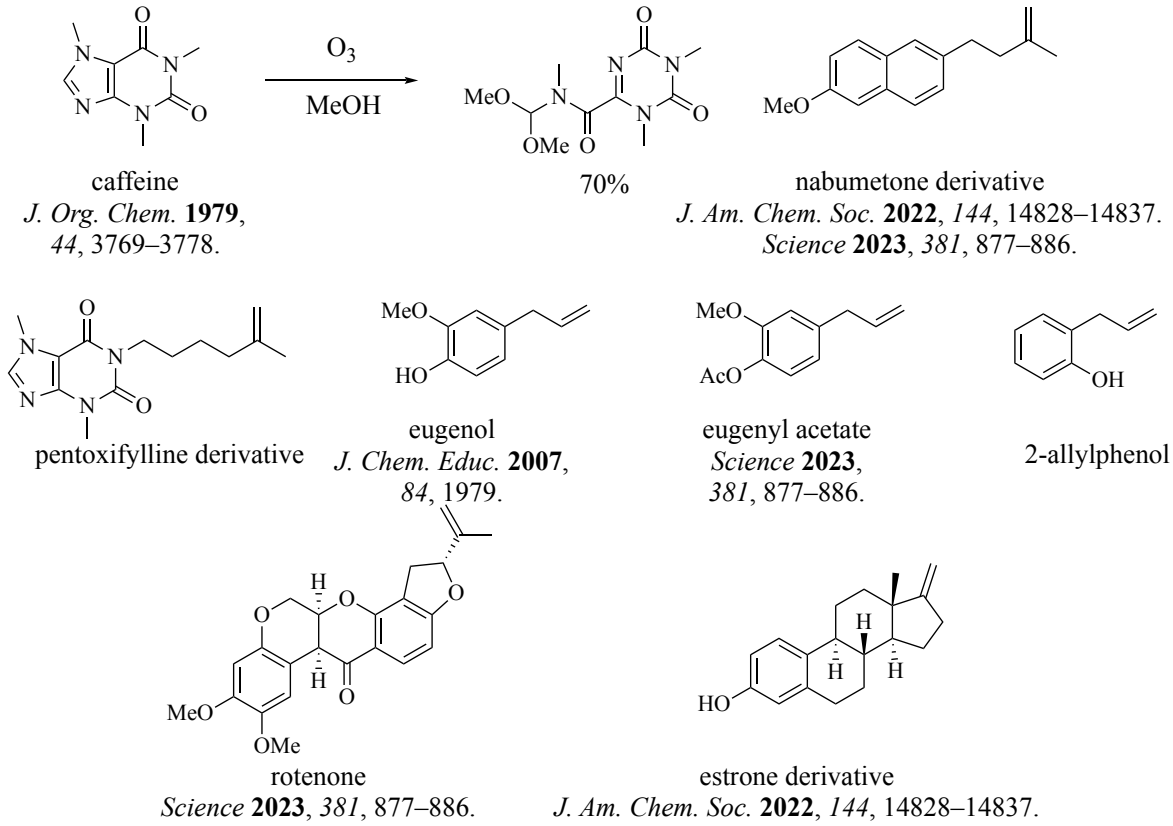
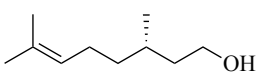
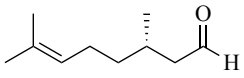


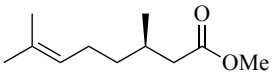
Figure 3.13 Electron-Rich Aromatics [53,75,82,83]



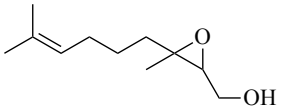
(–)-citronellol



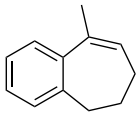
(–)-citronellal



(+)-methyl citronellate



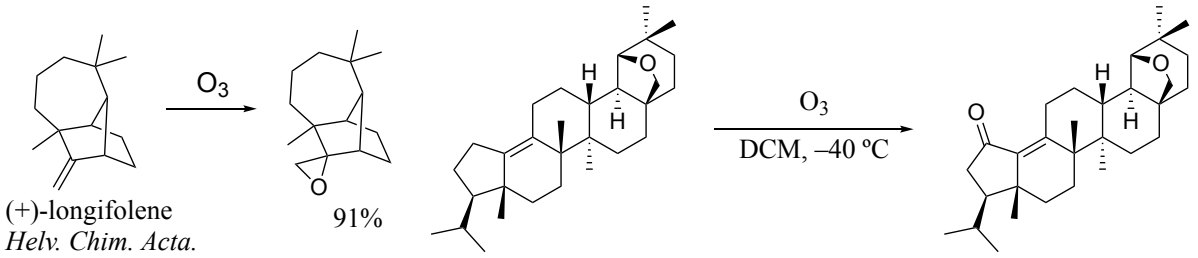
epoxygeraniol



benzosuberone derivative
Science **2019**, *364*, 681–685.

Figure 3.14 Electron-Rich Aromatics

[74]

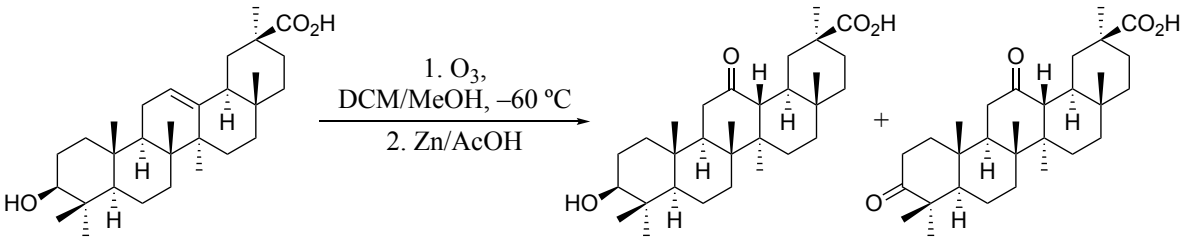


(+)-longifolene
Helv. Chim. Acta.
2003, *86*, 106–121.

91%

allobetulin derivative
Chem. Nat. Comp. **2011**, *47*, 579–582.

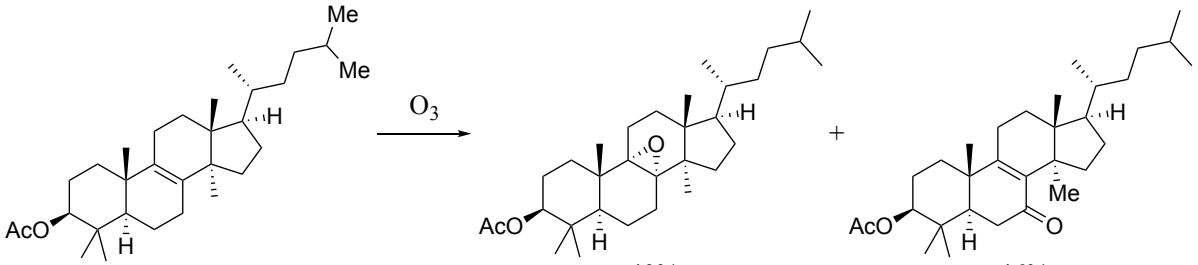
63%



11-deoxoglycyrrhizinic acid
Chem. Nat. Comp. **2007**, *43*, 571–575.

42%

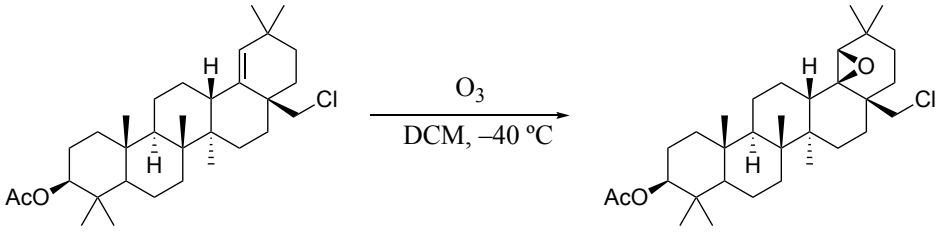
36%



dihydrolanosteryl acetate
Can. J. Chem. **1988**, *66*, 2130–2136.

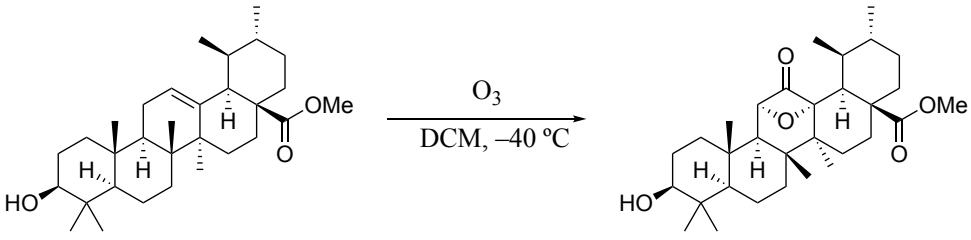
40%

46%



Chem. Nat. Comp. **2011**, *46*, 900–901.

92%

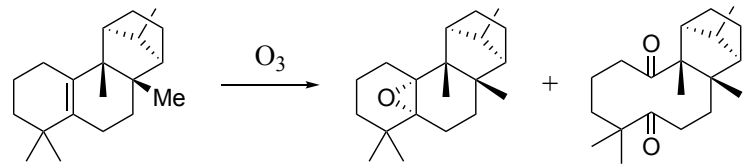


ursolic acid methyl ester
Chem. Nat. Comp. **2011**, *46*, 897–899.

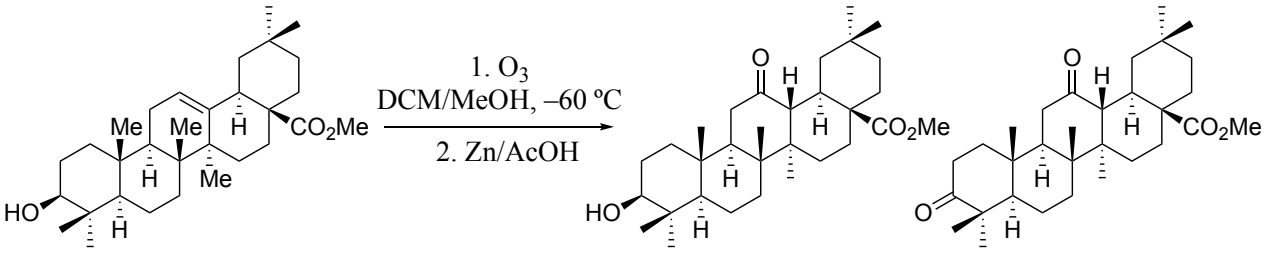
73% (x-ray)

Figure 3.15 Sterically Hindered

[77, 84–88]

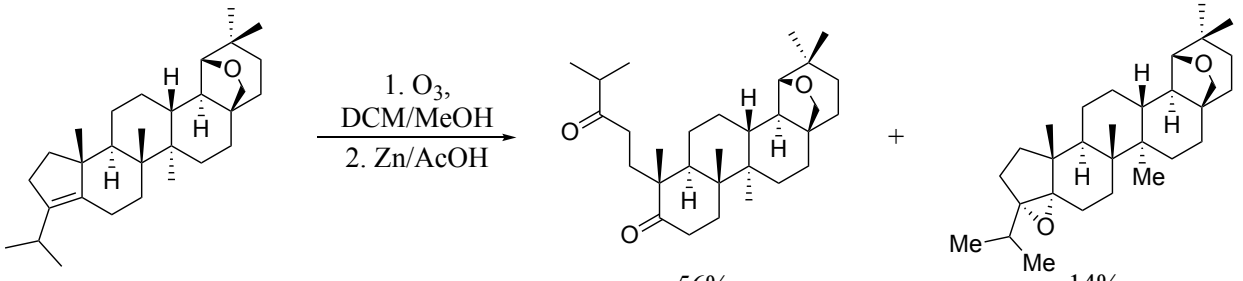


Chem. Nat. Comp. **1988**, *24*, 166–170. 66% 11%



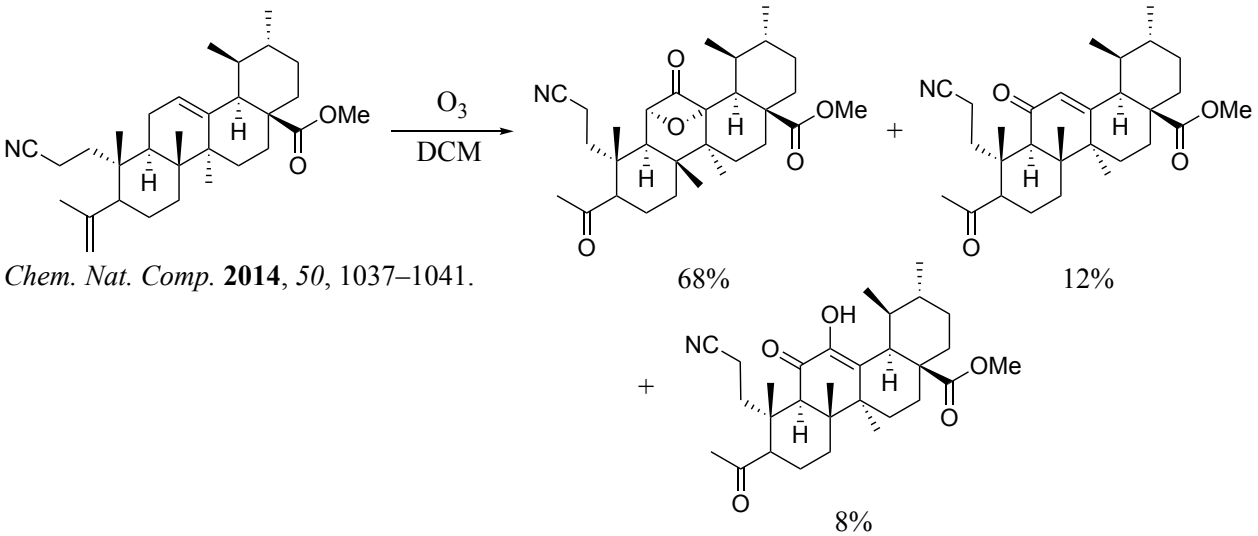
oleanolic acid methyl ester
Chem. Nat. Comp. **2010**, *46*, 397–399.

O_3 (2 equiv) 75% or O_3 (excess) 71%



allobetulin derivative
Chem. Nat. Comp. **2006**, *42*, 618–619.

56% 14%

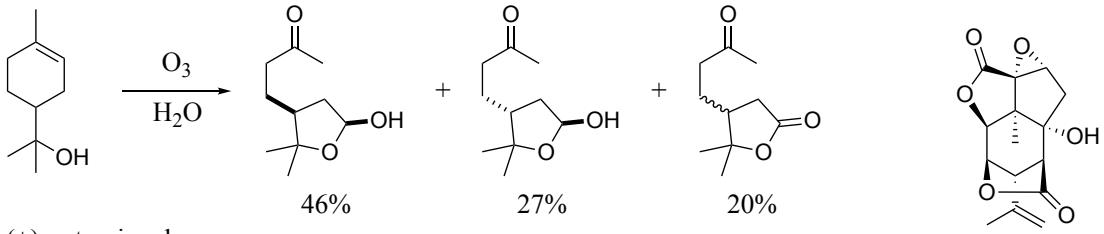


Chem. Nat. Comp. **2014**, *50*, 1037–1041.

68% 12% 8%

Figure 3.16 Sterically Hindered

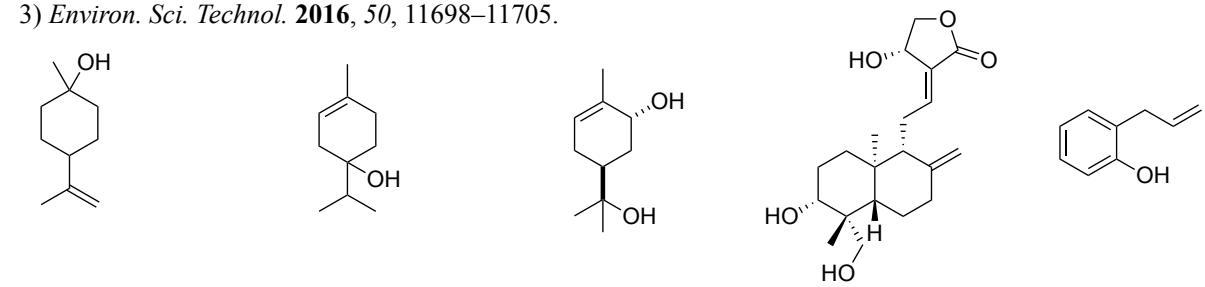
[89–92]



46% 27% 20%

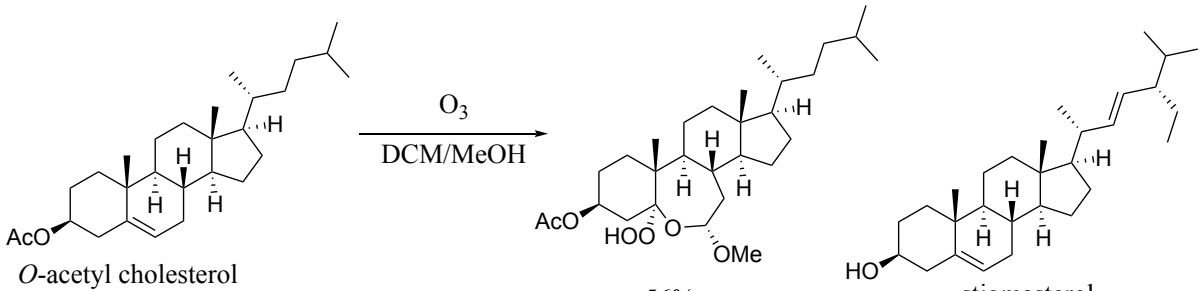
(±)-α-terpineol
1) *J. Chem. Soc. Chem. Comm.* **1974**, 1005–1006.
2) *Tetrahedron* **1986**, *42*, 3311–3321.
3) *Environ. Sci. Technol.* **2016**, *50*, 11698–11705.

picrotoxinin
Science **2023**, *381*, 877–886.



(±)-β-terpineol (±)-4-carvomenthenol *trans*-sobrerol andrographolide 2-allylphenol

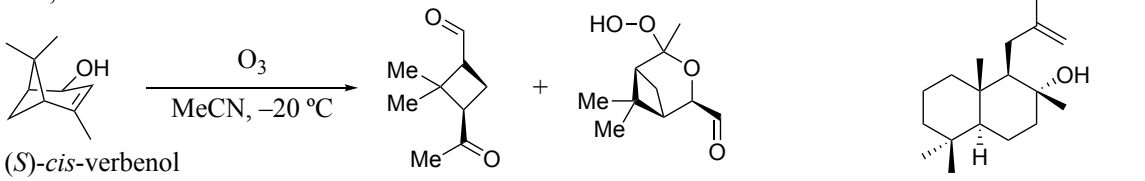
Angew. Chem. Intl. Ed. **2020**, *59*, 17575–17571.



O-acetyl cholesterol
J. Chem. Soc. Perkin Trans. 2. **1997**, 2313–2318.

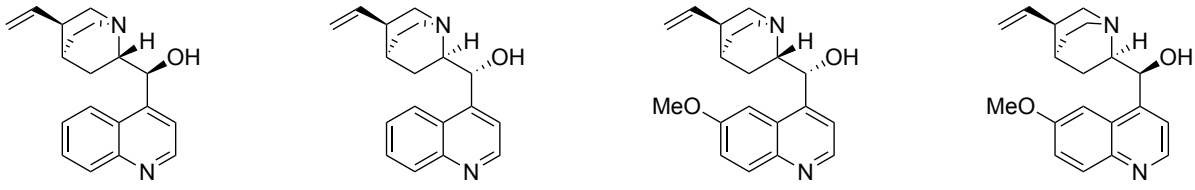
56%

stigmasterol



(*S*)-*cis*-verbenol
Russ. J. Org. Chem. **2010**, *46*, 1431–1449.

(+)-sclareolide derivative

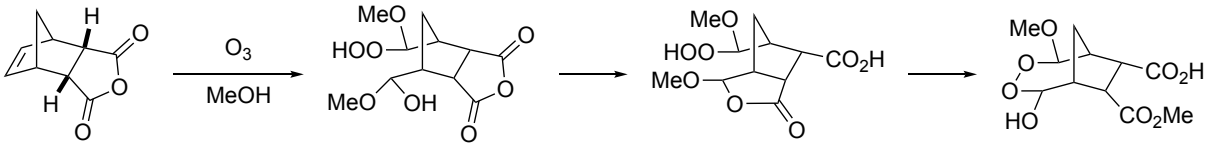


cinchonine cinchonidine quinine quinidine

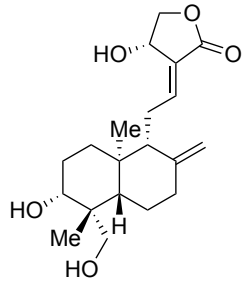
Rec. Trav. Chim. **1923**, *42*, 69.

Figure 3.17 Internal Nucleophiles

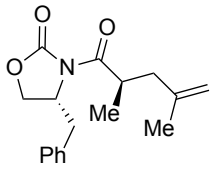
[53,78,80,93–95]



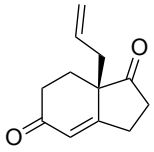
carbic anhydride
Zh. Org. Khim. **1977**, *13*, 2342–2353.



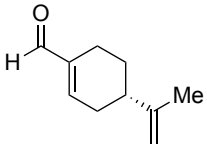
andrographolide



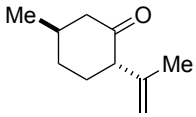
Evan's amide



Hajos-Parrish ketone derivative



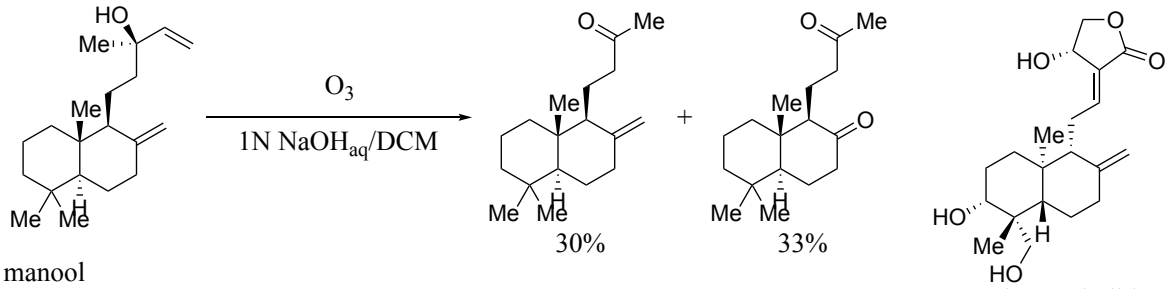
(*S*)-(–)-perillaldehyde



trans-isopulegone
J. Am. Chem. Soc. **2022**, *144*, 14828–14837.
Science **2023**, *381*, 877–886.

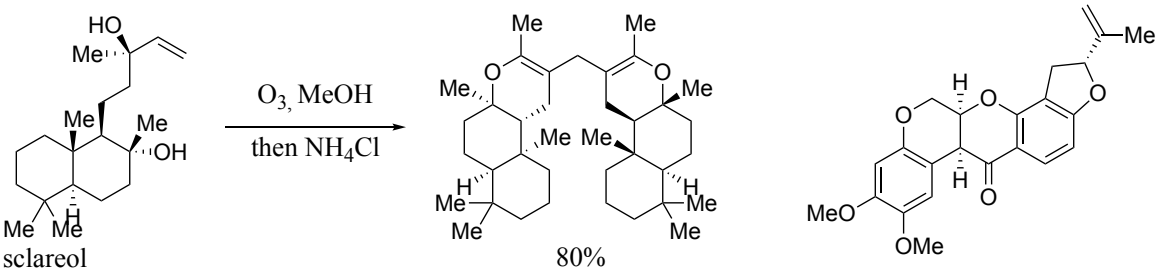
Figure 3.18 Internal Electrophiles

[53,80,82]



manool
Nat. Prod. Comm. **2014**, *9*, 355–358.

andrographolide



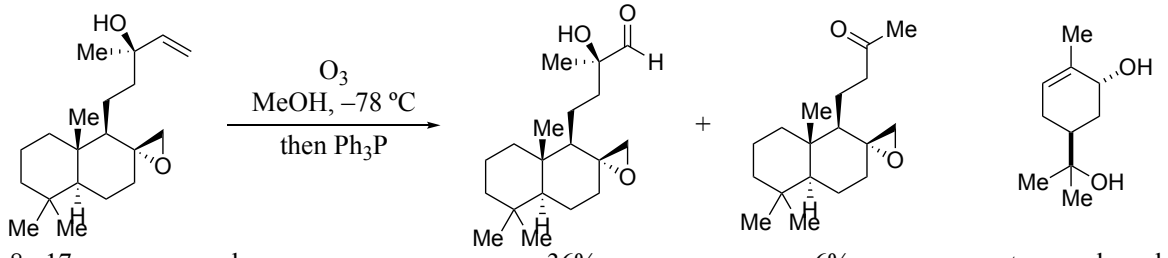
sclareol
Chem. Nat. Compd. **1991**, *27*, 436–443.

80%

rotenone
Science **2023**, *381*, 877–886.

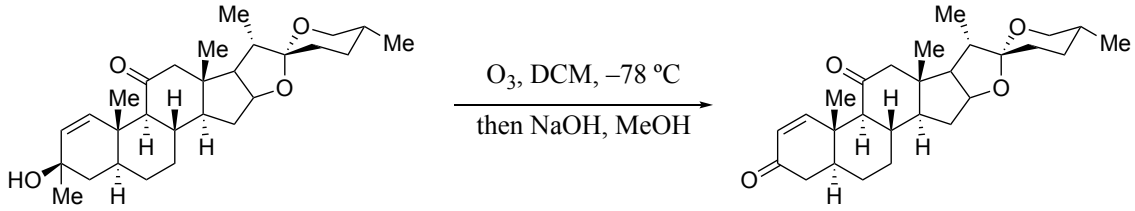
Figure 3.19 Allylic Alcohols and Ethers

[53,96,97]



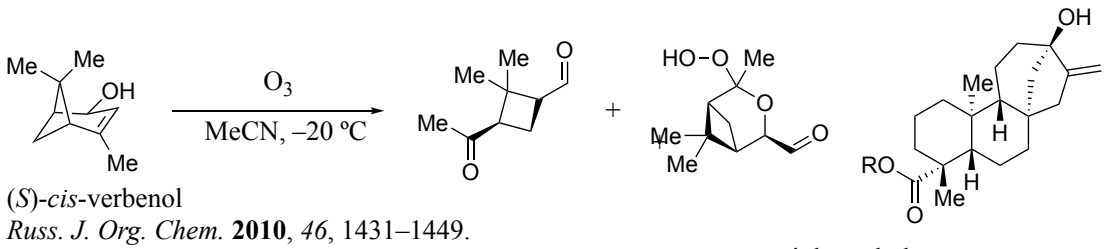
8a-17-epoxy-manool 36% 6% *trans*-sobrerol

Aust. J. Chem. **1988**, *41*, 1025–1035.



spirostanoid derivatives 40%

J. Am. Chem. Soc. **1995**, *117*, 9927–9928.



(*S*)-*cis*-verbenol

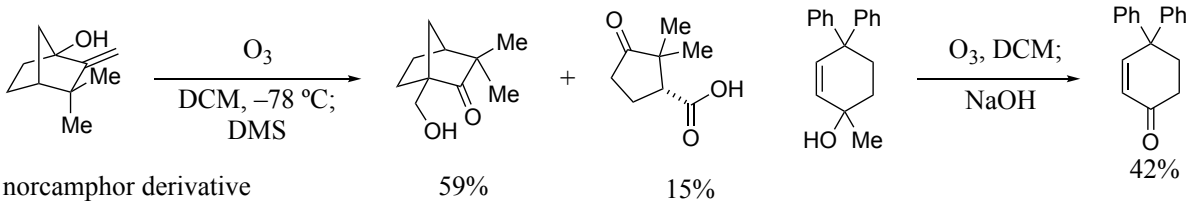
Russ. J. Org. Chem. **2010**, *46*, 1431–1449.

steviol, methyl ester

R = H, Me

J. Am. Chem. Soc. **1963**, *85*, 2305–2309.

J. Am. Chem. Soc. **2022**, *144*, 14828–14837.



norcamphor derivative 59% 15% 42%

Tetrahedron Let. **2005**, *46*, 5157–5159.

J. Am. Chem. Soc. **1995**, *117*, 9927–9928.

Figure 3.20 Allylic Alcohols and Ethers

[81,98–100]

3.6.6 Reaction Optimization

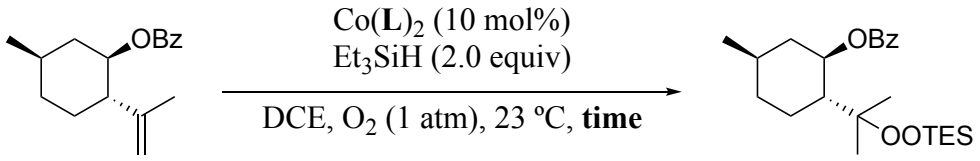
3.6.6.1 IMP Optimization

The previously optimized conditions reported by Isayama and Mukaiyama involved the use of $Co(modp)_2$ (10 mol%) with Et_3SiH (2.0 equiv) in DCE (5 mL/mmol) under O_2 (1 atm) at room temperature [51].

3.6.6.1.1 Co(II) Catalyst

We used (–)-*O*-benzoyl isopulegol (**1a**) to test the three most commonly applied ligands for this reaction, identifying modp as the best ligand (Table 3.2).

Table 3.2 Co(II) Catalyst Survey



1a **1b**

entry	L	time	1b
1	acac	7 h	83%
2	thd	1.5 h	94%
3	modp	1.5 h	95%

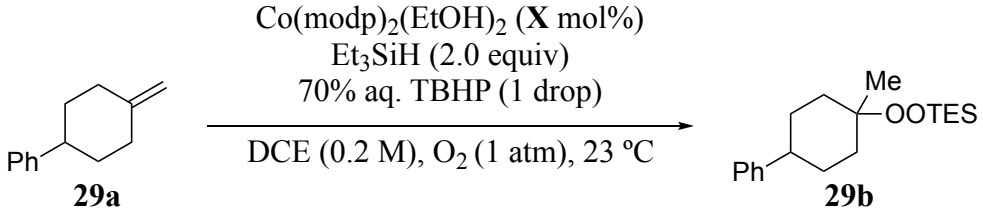
Procedure: A round bottom flask was charged with a magnetic stirring bar and (–)-*O*-benzoyl isopulegol (**1a**, 129 mg, 0.50 mmol, 1.0 equiv) and DCE (2.5 mL, 0.2 M). The catalyst [$Co(modp)_2(EtOH)_2$ (**C1**, 31.6 mg, 0.05 mmol, 10 mol%), $Co(thd)_2$ (**C2**, 21.3 mg, 0.05 mmol, 10 mol%), or $Co(acac)_2$ (**C3**, 12.9 mg, 0.05 mmol, 10 mol%)] was added and the contents was stirred/sonicated until completely dissolved. Triethylsilane (116 mg, 1.0 mmol, 2.0 equiv) was added. An oxygen balloon was affixed to the reaction vessel for continuous sparging with a 22G x 4” needle as the inlet and a 23G (0.06 mm x 30 mm)

needle as the outlet. 70% Aqueous *tert*-butyl hydroperoxide (TBHP, one drop) was added to initiate the catalytic cycle. The reaction was stirred at room temperature until the starting material had been consumed completely (TLC, 5% *v/v* EtOAc/hexanes + UV/vanillin stain). The solution was concentrated through rotatory evaporation and the residue purified through FCC (0–5% *v/v* EA/hexanes) to afford the triethylsilylperoxide **1b** as a clear oil.

3.6.6.1.2 Catalyst Loading

The optimal catalyst loading of 10 mol% was verified when using compound **29a** as the alkene (Table 3.3).

Table 3.3 Optimization of Catalyst Loading



29a **29b**

entry	X	29b
1	2.5	77%
2	5	93%
3	10	97%
4	20	86%

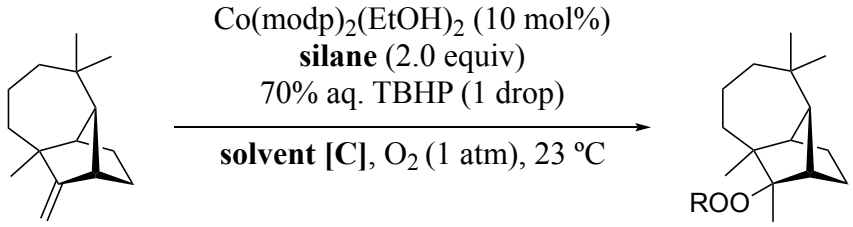
Procedure: A round bottom flask was charged with a magnetic stirring bar and (4-methylenecylcohexyl)benzene (**29a**, 173 mg, 1.00 mmol, 1.0 equiv) and DCE (5 mL, 0.2 M). $Co(modp)_2(EtOH)_2$ (**C1**, 15.9/31.7/63.4/127 mg, 0.025/0.05/0.10/0.20 mmol, 2.5/5.0/10/20 mol%) was added and then the mixture was stirred/sonicated until it had dissolved completely o form a red solution. Triethylsilane (234 mg, 2.00 mmol, 2.0 equiv) was added. An oxygen balloon was affixed to the reaction vessel for continuous sparging

with a 22G x 4” needle as the inlet and a 23G (0.06 mm x 30 mm) needle as the outlet. 70% Aqueous *tert*-butyl hydroperoxide (TBHP, one drop) was added to initiate the catalytic cycle. The solution became green during the course of the reaction. The reaction was stirred at room temperature until the starting material had been consumed completely (TLC, hexanes + UV/$KMnO_4$ stain). The solution was concentrated through rotatory evaporation and the residue was purified through FCC (0–5% *v/v* EtOAc/hexanes) to afford **29b**.

3.6.6.1.3 Reductant, Solvent, and Concentration Screening

Alternative *tri*-alkylsilane reductants, solvents, and concentrations were screened by using (+)-longifolene (**12a**) as the alkene (Table 3.4). The originally reported conditions from Isayama and Mukaiyama did indeed provide the highest yield of the triethylsilylperoxide **12b**.

Table 3.4 Optimization of Reductant, Solvent, and Concentration



12a **12b**

entry	R	reductant	solvent	[C]	12b
1	Et_3Si	Et_3SiH	DCE	0.2 M	17%
2	Et_3Si	Et_3SiH	DCE	0.4 M	16%
3	Et_3Si	Et_3SiH	DCE	1.0 M	15%
4	Et_3Si	Et_3SiH	Et_2O	0.2 M	6%
5	Et_3Si	Et_3SiH	EtOAc	0.2 M	10%
6	Et_3Si	Et_3SiH	Me_2CO	0.2 M	2%
7	$i Pr_3Si$	$i Pr_3SiH$	DCE	0.2 M	no rxn
8	$t BuMe_2Si$	$t BuMe_2SiH$	DCE	0.2 M	no rxn
9	Me_2PhSi	Me_2PhSiH	DCE	0.2 M	0%

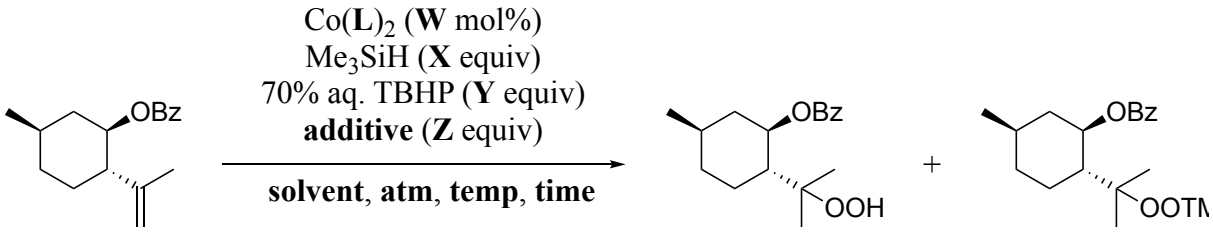
Procedure: A round bottom flask was charged with a magnetic stirring bar and (+)–longifolene (**12a**, 102 mg, 0.5 mmol, 1.0 equiv) and **solvent** (**[C]**). $Co(modp)_2(EtOH)_2$ (**C1**, 31.6 mg, 0.05 mmol, 5 mol%) was added and the mixture was stirred/sonicated until dissolved completely, forming a red solution. The **reductant** (2.0 equiv) was added. An oxygen balloon was affixed to the reaction vessel for continuous sparging with a 22G x 4" needle as the inlet and a 23G (0.06 mm x 30 mm) needle as the outlet. 70% Aqueous *tert*-butyl hydroperoxide (TBHP, one drop) was added initiate the catalytic cycle. The solution became green during the course of the reaction. The reaction was stirred at room temperature until the starting material had been consumed completely (TLC, hexanes + vanillin stain). The solution was then concentrated through rotatory evaporation and the residue was purified through FCC (hexanes) to afford **12b**.

3.6.6.1.4 IMP with Trimethylsilane

Because of the steric bulk of (+)-longifolene (**12a**), facile silylation of the peroxy-cobalt intermediate is prevented under standard IMP conditions. We sought to use trimethylsilane as a sterically less-demanding silane reductant. Trimethylsilane was synthesized from chlorotrimethylsilane and lithium aluminum hydride (LAH) according to a literature procedure [101]. (Note: slow addition of chlorotrimethylsilane is extremely important because the production of trimethylsilane does not commence until about a third of the chlorotrimethylsilane was added to the LAH solution.) We used (–)-*O*-benzoyl isopulegol (**1a**) as a model substrate for the development of this reaction before applying the condition to the reactions of (+)-longifolene (**12a**) and *O*-triethylsilyl cholesterol (**13a**) (Table 3.5). Substitution of Et_3SiH (2.0 equivalents) with Me_3SiH (2.0 equivalents) with the standard IMP conditions did not result in full conversion of the alkene. We added an additional 2 equivalents of trimethylsilane after 12 h, but TLC analysis of the reaction mixture did not reveal any change. We found 10% of hydroperoxide **1b'** from this experiment (entry 1). With acetone as the solvent, further consumption of the alkene was observed, and we noticed a 1% increase in **1b'**. The reaction did not proceed when using $Co(acac)_2$ as the catalyst (entry 3), but the addition of 2 equivalents of acetylacetonate ligand (entry 4) enabled full conversion and provided 7% of **1b"** and 93% of **1b'**. To avoid a super stoichiometric quantity of ligand, we returned to the $Co(modp)_2(EtOH)_2$ catalyst and added 2.0 equivalents of 70% aq. TBHP (entry 5). We observed comparable yields for both conditions (entries 4 and 5). Doubling the amount of catalyst to 20 mol% did not provide a better result (entry 6). In the absence of oxygen (entry 7) there was no reaction. When using TBHP (2.0 equiv) with Et_3SiH instead of Me_3SiH, the reaction provided **1b'**

as the major product in 92% yield with the triethylsilylperoxide **1b** formed in 8% yield (entry 8).

Table 3.5 Optimization of IMP with Trimethylsilane



1a **1b′** **1b″**

entry	L	W	X	Y	additive	Z	solvent	atm	temp (ºC)	time	1b'	1b"	1a
1	modp	10	4	0.08	–	–	DCE	O_2	–78 to 0	24 h	10%	–	90%
2	modp	10	2	0.08	–	–	Acetone	O_2	–78 to 0	20 h	11%	–	74%
3	acac	10	2	0.08	–	–	DCE	O_2	–78 to 0	3 h	–	–	100%
4	acac	10	2	0.08	acac	2	DCE	O_2	–78 to –20	53 h	93%	7%	–
5	modp	10	2	2	–	–	DCM	O_2	–78 to 0	3 h	92%	8%	–
6	modp	20	2	2	–	–	DCM	O_2	–78 to 0	1 h	85%	7%	–
7	modp	10	2	2	–	–	DCM	N_2	–78 to 0	24 h	–	–	100%
8	modp	10	0	2	Et_3SiH	2	DCE	O_2	23	15 min	92%	–	–

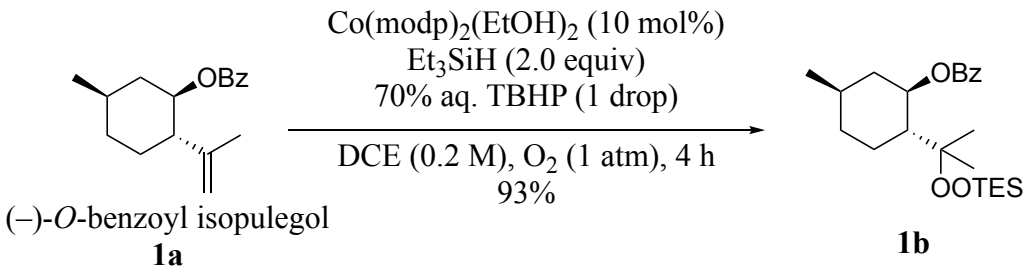
Procedure: A round-bottom flask was charged with a magnetic stirrer bar, (–)-*O*-benzoyl isopulegol (129 mg, 0.500 mmol, 1 equiv), and $Co(modp)_2(EtOH)_2$ (**C1**, 31.6/63.2 mg, 0.0500/0.100 mmol, 10/20 mol%) [or $Co(acac)_2$ (25.7 mg, 0.0500 mmol, 10 mol%)] and DCE/acetone/DCM (5 mL, 0.1 M). The reaction was sparged with O_2/N_2 for 15 minutes before a balloon was affixed with the corresponding gas using a 22G x 4" needle as the inlet. The mixture was cooled to –78 ºC in an acetone/dry ice bath. Trimethylsilane (116 µL, 1.00 mmol, 2 equiv) was added as a condensed liquid (cooled to –78 ºC) using a pre-chilled needle and syringe. Next, 70% aq. TBHP (143 µL, 1.00 mmol, 2 equiv) was added to the mixture. The reaction flask was transferred to an ice bath (0 ºC) or a brine bath (–20 ºC) and then stirred. The progress of the reaction was monitored using TLC (10% *v/v* EtOAc/hexanes + vanillin stain). Once the reaction had stopped, the crude mixture was

concentrated through rotatory evaporation and the residue purified through FCC (0–10% *v/v* EtOAc/hexanes) to afford **1b'** and **1b"** (and **1a**).

We hypothesize IMP with trimethylsilane deviates from the standard IMP mechanism at the transmetallation/σ-bond metathesis step. Judging from the comparative experiments of entries 5 and 8, the role of TBHP may be that of a ligand. TBHP may intercept the alkyl peroxy–Co^{III} intermediate to furnish the alkyl hydroperoxide. The formed *t*BuOOCo^{III} may interact with the silane to regenerate the Co^{III}–H for the reaction. GCMS analysis of the crude reaction mixture (entry 5) revealed the formation of a large quantity of *tert*-butyl trimethylsilylperoxide (EI: calc'd for $C_7H_{18}O_2Si$ $[M]^+$ *m/z* = 162.1076, found 162.1), supporting this mechanistic scenario. The generation of trimethylsilylperoxide **1b"** is also possible if the classical IMP mechanism is followed, or if the formed alkyl hydroperoxide desilylates *tert*-butyl trimethylsilylperoxide. Nevertheless, the parameters of the reaction make either of these pathways unfavorable because the alkyl hydroperoxide product **1b'** is quite sterically hindered, it is formed in low concentration, and a low reaction temperature is required (trimethylsilane boiling point is 6.7 ºC) [102]. Therefore it is more likely for TBHP to act as a ligand and exchange with the alkylperoxide to form the alkyl hydroperoxide.

3.6.6.1.5 Large Scale IMP Reaction

The optimized IMP conditions worked well on a large scale (2.01 g) using (–)-*O*-benzoyl isopulegol (**1a**) as the alkene.



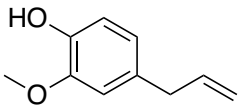
(–)-*O*-benzoyl isopulegol
1a

1b

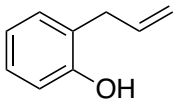
Procedure: A round bottom flask was charged with a magnetic stirring bar and (–)-*O*-benzoyl isopulegol (**1a**, 2.01 g, 7.78 mmol, 1.0 equiv) and DCE (38.9 mL, 0.2 M). $Co(modp)_2(EtOH)_2$ (**C1**, 491 mg, 0.10 mmol, 10 mol%) was added and the mixture was stirred/sonicated until it had dissolved completely, forming a red solution. Triethylsilane (1.81 g, 15.6 mmol, 2.0 equiv) was added. An oxygen balloon was affixed to the reaction vessel for continuous sparging with a 22G x 4" needle as the inlet and a 23G (0.06 mm x 30 mm) needle as the outlet. 70% Aqueous *tert*-butyl hydroperoxide (TBHP, 1 drop) was added to initiate the catalytic cycle. The solution became green during the course of the reaction. The reaction was stirred at room temperature until the starting material had been consumed completely (TLC, 5% *v/v* EtOAc/hexanes, UV + vanillin stain). The solution was concentrated through rotatory evaporation and purified through FCC (0%–5% *v/v* EA/hexanes) to afford the triethylsilylperoxide **1b** as a clear oil (2.93 g) in 93% yield.

3.6.6.1.6 Failed IMP Substrates

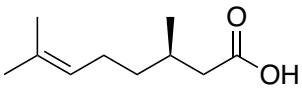
Figure 3.21 presents the alkene substrates that were tried in IMP but did not provide their products. The acidic phenolic units of eugenol (**6**) and 2-allylphenol (**7**) protonated the modp ligand and destroyed the catalyst. The carboxylic acid unit of (+)-citronellic acid (**10**) made it incompatible for the same reason as the phenol substrates. The allylic and homoallylic systems of (–)-myrtenol (**33**) and (–)-nopol (**34**) generated a complex mixture of products. The basic amino groups of cinchonidine (**F1a**) and the tropinone derivative **F2a** are incompatible with the catalyst for IMP. We believe the enonate of andrographolide (**F3a**) acted as an electrophile for the alkyl peroxycobalt intermediate (similar to the cyclization into the ketone of **19a**), as well as providing some interaction with the cobalt(III) hydride to promote the formation of a complex mixture. The aldehyde unit of (–)-citronellal (**F4a**) was oxidized during the course of the reaction and the peroxide unit of the product would oxidize the aldehyde after isolation. We detected approximately 42% of the corresponding triethylsilylperoxide from **F4a**, but it spontaneously decomposes on SiO_2 and was not distillable, even by Kugelrohr. The alkyl radical generated from (±)-sabinene (**F5a**) after MHAT may have undergone a cyclopropyl ring opening to create a new alkene an alkyl radical, inevitably resulting in a complex mixture of products. The quinone unit of Vitamin K1 (**F6a**) was reducible under these reaction conditions and prevented progress of the reaction [103].



eugenol
6



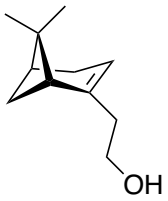
2-allylphenol
7



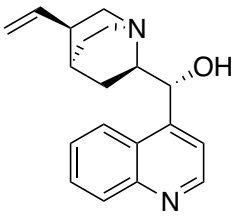
(+)-citronellic acid
10



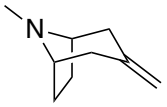
(–)-myrtenol
33



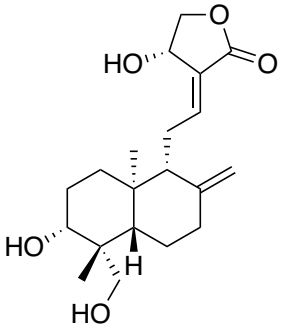
(–)-nopol
34



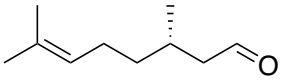
cinchonidine
F1a



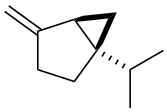
tropinone derivative
F2a



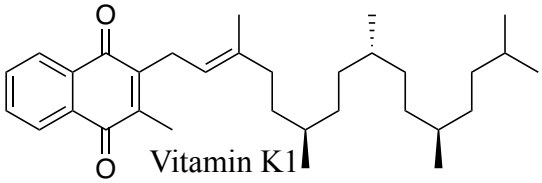
andrographolide
F3a



(–)-citronellal
F4a



(±)-sabinene
F5a



Vitamin K1
F6a

Figure 3.21 Failed IMP Substrates

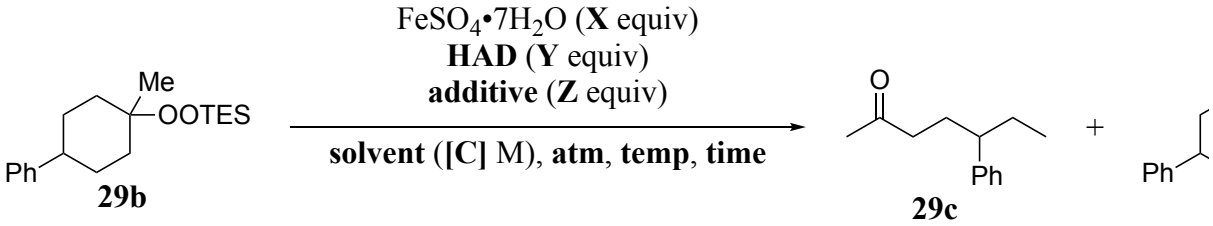
3.6.6.2 Optimization of Reductive Functionalization with HAD

3.6.6.2.1 Ferrous Reduction Optimization

We began probing for reductive hydrogenation conditions by using (4-methyl-4-triethylsilylperoxycyclohexyl)benzene (**29b**) as a model substrate and iron(II) sulfate heptahydrate as our electron source for SET. Table 3.6 summarizes the conditions screened for this transformation. With iron(II) sulfate heptahydrate (2.0 equiv) and benzenthiol (1.5 equiv), in methanol at room temperature, the previously reported ozonolysis–hydrodealkenylation condition, we observed (by NMR) 25% of the desired product **29c**, with the remaining mass attributed to alcohol **29d** (entry 1). Heating the reaction mixture under reflux with additional iron (3.0 equiv, entry 2) enhanced the yield of **29c**. We surveyed two other hydrogen atom donors, γ-terpinene and triethylsilane, but neither provided improved yields (entry 3, 72% and entry 4, 67%). Inverse addition, where the peroxide was added to the iron solution, also failed to improve the yield (entries 5 and 6). We tested alternative solvent mixtures, chosen to increase the reaction temperature, with γ-terpinene as the HAD. A 1:1 ratio of THF/H_2O as the solvent provided **29c** in 69% (entry 7) and a 1:1 ratio of MeCN/H_2O gave 79% (entry 8). We then transitioned to catalytic conditions involving vitamin C and observed an inverse ratio of **29c**/**29d**, primarily yielding the alcohol **29d** (70%, entry 9). A change of solvent from methanol to 1:1 THF/H_2O exacerbated the outcome of the reaction, forming alcohol **29d** in 77% (entry 10). When using vitamin C as both the reductant and the HAD, the amount of **29c** increased to 48% isolated yield (entry 11). Heating this reaction under reflux slightly improved the yield to 68% (entry 12). Having achieved some success in the catalytic loading of iron sulfate heptahydrate, we replaced vitamin C with γ-terpinene as the

stoichiometric reductant and HAD (entries 13–15). An elevated reflux temperature associated with 3:1 iPrOH/H_2O and the yield improved to 72% (entry 13). Doubling the amounts of iron sulfate heptahydrate and γ-terpinene (entries 14 and 15) led to outcomes identical to that of entry 13. Without an improvement in yield, we abandoned our iron(II) optimization and sought to develop iron(III) catalytic conditions (Table 3.7).

Table 3.6 Optimization of Ferrous Reductive Hydrogenation



29b **29c**

entry	X	HAD	Y	additive	Z	Solvent	[C]	atm	temp (°C)	time	29c	29d
1	1.2	PhSH	1.5	none	–	MeOH	0.1	N_2	23	4 d	25%[a]	75%[a]
2	3.0	PhSH	1.5	none	–	MeOH	0.1	air	reflux	15 min	75%[a]	25%[a]
3	3.0	g-T	1.5	none	–	MeOH	0.1	air	reflux	15 min	72%[a]	28%[a]
4	3.0	Et_3SiH	1.5	none	–	MeOH	0.1	air	reflux	15 min	67%[a]	18%[a]
5	3.0	PhSH	1.5	inv add'n	–	MeOH	0.1	air	reflux	15 min	69%[a]	30%[a]
6	3.0	g-T	1.5	inv add'n	–	MeOH	0.1	air	reflux	15 min	69%[a]	25%[a]
7	3.0	g-T	1.5	none	–	1:1 THF/H_2O	0.1	air	reflux	12 h	69%[a]	15%[a]
8	3.0	g-T	1.5	none	–	1:1 MeCN/H_2O	0.1	air	reflux	15 min	79%[a]	18%[a]
9	0.2	PhSH	1.5	Vit C.	2.0	MeOH	0.2	Ar	23	8 h	30%	70%
10	0.2	PhSH	1.5	Vit. C.	2.0	1:1 THF/H_2O	0.1	Ar	23	24 h	20%	77%
11	0.2	Vit. C.	2.0	none	–	MeOH	0.1	Ar	23	5 h	48%	–
12	0.2	Vit. C	2.0	none	–	MeOH	0.1	air	reflux	90 min	68%[a]	31%[a]
13	0.2	g-T	1.5	none	–	3:1 iPrOH/H_2O	0.1	air	reflux	30 min	72%[a]	25%[a]
14	0.2	g-T	3.0	none	–	3:1 iPrOH/H_2O	0.1	air	reflux	30 min	72%[a]	25%[a]
15	0.4	g-T	3.0	none	–	3:1 iPrOH/H_2O	0.1	air	reflux	30 min	71%[a]	29%[a]

[a]NMR Yield versus 1-chloro-2,4-dinitrobenzene; γ-T (γ-terpinene); Vit. C., Vitamin C.

Procedure for Line 1: A round-bottom flask was charged with a magnetic stirrer bar and (4-methyl-4-triethylsilylperoxycyclohexyl)benzene (**29b**, 52.1 mg, 0.163 mmol, 1.00

equiv). The flask was evaporated and backfilled three times with nitrogen before the contents were dissolved in the methanol (0.82 mL). A separate round bottom flask was charged with crushed iron(II) sulfate heptahydrate (54.2 mg, 1.95 mmol, 1.20 equiv) and evacuated and backfilled three times with nitrogen, and charged with methanol (0.82 mL). After dissolving completely, the solution of iron(II) sulfate heptahydrate was transferred via syringe to the reaction flask. Benzenethiol (26.9 mg, 25.1 μL, 0.244 mmol, 1.5 equiv) was added immediately after addition of the iron solution. The reaction was stirred (1000 RPM) until complete consumption of the starting material had occurred (4 days; TLC, hexanes, UV/vanillin stain). When the reaction was complete, the mixture was diluted with diethyl ether and an NMR spectral internal standard, 1-chloro-2,4-dinitrobenzene, was added. The mixture was filtered through a short silica plug, washing with Et_2O, and concentrated, with the NMR yield of the residue then measured in $CDCl_3$.

Procedure for Lines 2–8, 12–15: A round-bottom flask was charged with a magnetic stirring bar and (4-methyl-4-triethylsilylperoxycyclohexyl)benzene (**29b**, 106 mg, 0.330 mmol, 1.00 equiv) and **HAD** (**Y** equiv). The contents were dissolved in the **solvent**, then a condenser was affixed, and the flask was equilibrated to **temperature**. Crushed iron(II) sulfate heptahydrate (**Y** equiv) was directly added to the reaction flask at **temperature**. The reaction was stirred (1000 RPM) at the desired **temperature** until complete consumption of the starting material had occurred (TLC, hexanes, UV/vanillin stain). *Efficient mixing was necessary during the reaction period to avoid phase separation.* The completed reaction mixture was diluted with Et_2O and dried (sodium sulfate). The solids were crushed, then the reaction mixture was filtered through cotton wool or a short silica

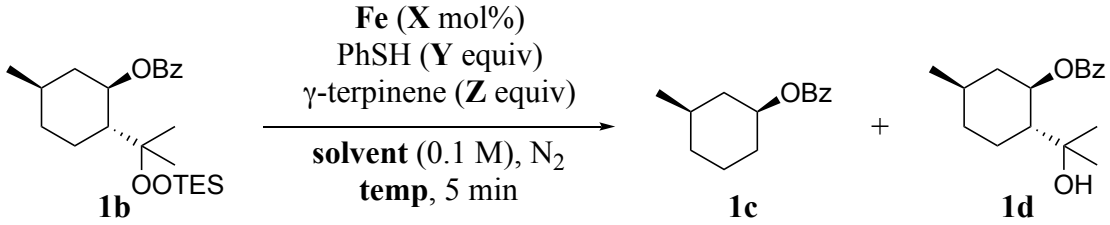
plug, washing with Et_2O. The crude mixture was concentrated and the residue was purified through FCC (0% to 20% *v/v* EA/hexanes + UV/vanillin stain); alternatively, the NMR spectral yield of the crude mixture was measured in $CDCl_3$ using 1-chloro-2,4-dinitrobenzene as the internal standard.

Procedure for Lines 9–11: A round-bottom flask was charged with a magnetic stirring bar and (4-methyl-4-triethylsilylperoxycyclohexyl)benzene (**29b**, 106 mg, 0.330 mmol, 1.00 equiv), **HAD** (**Y** equiv) and the additive (**Z** equiv), if applicable. The contents were dissolved in the organic solvent and equilibrated to temperature. A separate round bottom flask was charged with crushed iron(II) sulfate heptahydrate (**X** equiv) and evacuated and backfilled three times with argon before **solvent** was added (50% total volume). After complete dissolution, then the solution of iron(II) sulfate heptahydrate was transferred via syringe to the reaction flask. The reaction mixture was stirred (1000 RPM) at the desired **temperature** until complete consumption of the starting material had occurred (TLC, hexanes, UV/vanillin stain). *Efficient mixing was necessary during the reaction to avoid phase separation.* When the reaction was complete, it was diluted with water then transferred to a separatory funnel and extracted three times with Et_2O. The combined organic phases were washed with brine, dried (sodium sulfate), filtered, and concentrated through rotatory evaporation. The residue was purified through FCC (0% to 20% *v/v* EA/hexanes + UV/vanillin stain).

3.6.6.2.2 Ferric Reduction Optimization

The original conditions [stoichiometric iron(II) and PhSH] for hydrodealkenylation were inefficient, forming the product **1c** in only 57% yield (Table 3.7, entry 1). Garnering inspiration from our previous studies using catalytic iron(II) or copper(I) as well as other reductive methods concerning peroxides, we designed new reaction conditions to involve an iron(III) pre-catalyst, a thiol, and a stoichiometric reductant (γ-terpinene) (entries 2–18). Beginning with catalytic $FeCl_3$, we identified methanol as the best solvent, achieving 79% (by NMR) of the desired product **1c** and 18% of side-product **1d** (entries 2–6). When surveying iron(III) salts, the relatively weakly coordinating sulfate counter-ion was found to perform the best (entries 6–9). Heating under reflux dramatically favored **1c** to **1d** (entry 10). There was little effect across the tested iron quantities (entries 10–13). The amount of thiol was decreased, a catalytic quantity was found to be the best (entries 10, 14, and 15). Control experiments (entries 16–18) demonstrated that iron was required, and the use of a mixture of thiol and γ-terpinene provided the best result.

Table 3.7 Optimization of Reductive Hydrogenation



1b **1c** **1d**

entry	Fe	X	Y	Z	solvent	temp	1c[a]	1d[a]
1	$FeSO_4•7H_2O$[b]	120	1.5	–	MeOH	23 ºC	57	13
2	$FeCl_3$	10	1.5	1.5	MeCN	23 ºC	56	36
3	$FeCl_3$	10	1.5	1.5	EtOAc	23 ºC	59	38
4	$FeCl_3$	10	1.5	1.5	Acetone	23 ºC	57	36
5	$FeCl_3$	10	1.5	1.5	THF	23 ºC	68	32
6	$FeCl_3$	10	1.5	1.5	MeOH	23 ºC	79	18
7	$Fe(acac)_3$[c]	10	1.5	1.5	MeOH	23 ºC	72	12
8	$Fe(OTf)_3$	10	1.5	1.5	MeOH	23 ºC	81	17
9	$Fe_2(SO_4)_3•xH_2O$	5	1.5	1.5	MeOH	23 ºC	82	12
10	$Fe_2(SO_4)_3•xH_2O$	5	1.5	1.5	MeOH	reflux	91	9
11	$Fe_2(SO_4)_3•xH_2O$	10	1.5	1.5	MeOH	reflux	91	7
12	$Fe_2(SO_4)_3•xH_2O$	2.5	1.5	1.5	MeOH	reflux	91	7
13	$Fe_2(SO_4)_3•xH_2O$	0.05	1.5	1.5	MeOH	reflux	89	9
14	$Fe_2(SO_4)_3•xH_2O$	5	1.1	1.5	MeOH	reflux	92	5
15	$Fe_2(SO_4)_3•xH_2O$	5	0.1	1.5	MeOH	reflux	95	5
16	none	–	1.1	1.5	MeOH	reflux	–	–
17	$Fe_2(SO_4)_3•xH_2O$	5	–	3.0	MeOH	reflux	86	5
18	$Fe_2(SO_4)_3•xH_2O$	5	2.2	–	MeOH	reflux	88	5

[a]NMR yield with 1-chloro-2,4-dinitrobenzene as internal standard. [b]48 h reaction time. [c]1 h reaction time.

Procedure: A 1-dram vial was treated with triethylsilylperoxide (**1b**, 40.7 mg, 0.100 mmol, 1.00 equiv) and a magnetic stirrer bar. The vial was sealed with a rubber septum, evacuated and backfilled three times with nitrogen, and charged with γ-terpinene (**Z** equiv). A separate 1 dram-vial was treated with an iron salt and made into a solution in dry **solvent**. The iron solution was sparged for 1 minute with nitrogen then transferred to the vial containing the silylperoxide. Stirring was started (1000 RPM) with heating to **temperature**. PhSH (**Y** equiv) was added via Hamilton syringe. For reactions with $Fe_2(SO_4)_3•xH_2O$ we observed decolorization from yellow upon addition of the thiol. After

completion of the reaction (typically 5 min), the mixture was filtered through a silica plug washing with diethyl ether. 1-Chloro-2,4-dinitrobenzene was added as an NMR spectral internal standard, then the sample was evaporated. The NMR spectral yield was measured in $CDCl_3$.

3.6.6.2.3 Failed Reductive Hydrogenation Substrates

Some of our alkenes successfully generated the corresponding triethylsilylperoxide but were not amenable towards reductive hydrogenation (Figure 3.22). All attempts at reduction of peroxide **13b'** failed to provide ketone products. Beckith's 1983 study of the particularly reversible β-scission of the 9-decalinoxyl radical explains our issues related to reductive hydrogenation in the cholesterol system [104]. Alternative reductive strategies may be viable for the cholesterol hydroperoxide [105]. Under the radical hydrogenation condition, **17b** formed **17c** in 64% yield. Compound **17c** could have been generated by two mechanistic pathways, either SET–β-scission-[Fe^{III}]-oxidation or from Grob fragmentation. Since we are unable to ascertain the mechanism, we have included **17b** as a member of this table. Refluxing **21b** in methanol for the reduction provided a diketone **21c** which, like **17c**, may have arisen from SET–β-scission-[Fe^{III}]-oxidation or from Grob fragmentation [81,106]. We have included **21b** here for the same reason as **17b**. The complex caged structure of picrotoxinin (**F7a**) successfully underwent IMP to generate **F7b** in 68% yield. It was necessary to add ethyl acetate as an additional polar co-solvent (4:1 DCE/EtOAc) for this substrate to fully dissolve. Upon treatment of the silylperoxide under the optimum reduction conditions, a slow reaction took place, taking more than 12 times the usual time of 5 minutes. Analysis of the resulting mixture did not reveal the product. The epoxide of **F8a** survived the IMP condition, providing a 62% yield of **F8b**. Treatment of the resulting silylperoxide with the standard reduction conditions resulted in 15% of the desired product (yield determined using ^1H NMR, based on the resulting acetone CH_3 peak) which we were unable to isolate. Although basic amines are incompatible with IMP, the Boc-protected amines of **F9a** and **F10a** proved suitable for

IMP (96% and 70%, respectively), but less than 5% of the hydrogenation product was observed in each case.

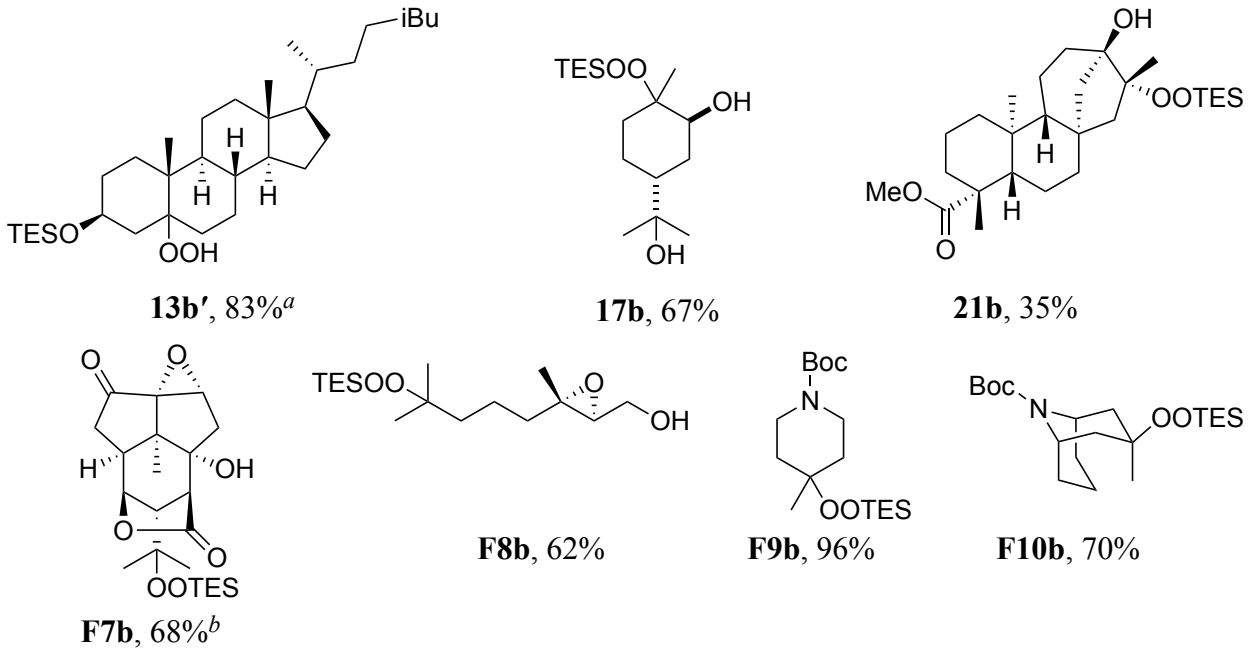
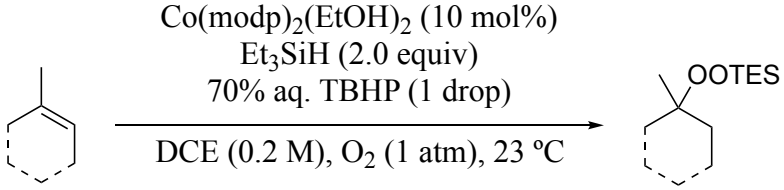


Figure 3.22 Failed Reductive Hydrogenation Substrates

See Section 3.6.7 for reaction conditions. [a]$Co(modp)_2(EtOH)_2$ (10 mol%), Et_3SiH (2.0 equiv), 70% aqueous TBHP (1.5 equiv), O_2 (1 atm), DCE (0.2 M), 23 ºC, 5 min. [b]4:1 DCE/EtOAc (0.2 M) as the solvent.

3.6.7 Experimental Procedures

3.6.7.1 General Procedure for IMP

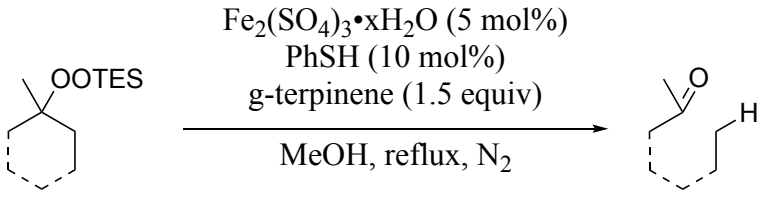


A round-bottom flask was charged with a magnetic stirring bar, the alkene (1.0 equiv), and DCE (5 mL/mmol) to form a solution. $Co(modp)_2(EtOH)_2$ (10 mol%) was added and the mixture was stirred/sonicated until homogeneous. Triethylsilane (2.0 equiv) was added. An oxygen balloon was affixed for continuous sparging using a 22G x 4" needle as the inlet and a 23G (0.06 mm x 30 mm) needle as the outlet. 70% Aqueous *tert*-butyl hydroperoxide (TBHP, 1 drop) was added to initiate the catalytic cycle. The solution became green during the course of the reaction. The reaction was stirred at room temperature until the starting material had been completely consumed (TLC). The mixture was concentrated through rotatory evaporation at 30 ºC (or at 0 ºC for volatile compounds) and the residue was purified through FCC.

It was best to stop and purify this reaction as soon as it was complete. If this reaction were allowed to continue past full consumption of the starting material, then the triethylsilylperoxide product began to be consumed by Co(II) and excess triethylsilane. We observed (by GCMS) an additional volatile silane-related impurity [$(Et_3Si)_2O$] forming after the alkene has been consumed. We typically observed this impurity by TLC as a pink spot, when visualized with vanillin stain, which travels near the solvent front in 10% *v/v* EtOAc/hexanes.

3.6.7.2 General Procedure for Reductive Functionalization

Deviations from the following procedure are noted for specific substrates.

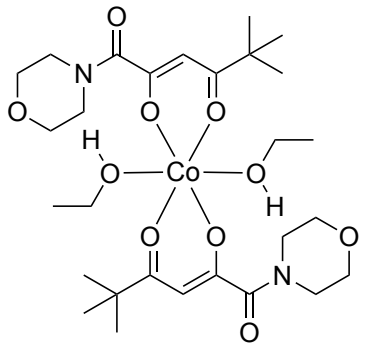


A round bottom flask was charged with triethylsilylperoxide (1.0 equiv) and a magnetic stirrer bar. The flask was sealed with a rubber septum then evacuated and backfilled three times with nitrogen (skip this step for volatile silylperoxides). γ-Terpinene (1.5 equiv) was added. In a separate flask, $Fe_2(SO_4)_3$•xH_2O (5.0 mol%) was dissolved in dry methanol (0.1 M based on silylperoxide). The iron solution was sparged for 1 minute with nitrogen then transferred via syringe to the vial containing the silylperoxide. Stirring was started (1000 RPM). (For volatile silylperoxides, the mixture of alkene, methanol, and $Fe_2(SO_4)_3$•xH_2O was sparged with nitrogen for 1 min.) Heated under reflux. PhSH (0.10 equiv) was added. Within a few seconds the reaction turned from yellow to colorless, and bubbles also formed rapidly. Upon completion of the reaction (typically 5 min), the mixture was cooled, the magnetic stirrer bar was removed, and the sample was concentrated through rotatory evaporation. The residue was purified through FCC.

For volatile ketone substrates, *p*-tolylsulfonylhydrazide (3.0 equiv) was added after completion of the reaction. The mixture was stirred for an additional 1 h then concentrated through rotatory evaporation. The hydrazone was purified through FCC. The hydrazone would partially hydrolyze on silica, so maximum flow rates for the chromatography step are recommended to achieve the yields reported.

3.6.8. Characterization Data

3.6.8.1 Co(II) Catalysts



C1

Complex **C1**: $Co(modp)_2(EtOH)_2$: Bis(1-morpholinocarbamoyl-4,4-dimethyl-1,3 pentanedionato)bis(ethanol) cobalt(II)

Yield: 94%

Physical state: red/orange crystals

Purification: filtration and recrystallization from absolute ethanol

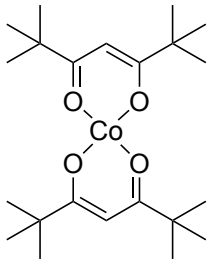
Melting point: 279–281 ºC

IR (ATR, neat) $\tilde{\nu}_{max}$: 3439, 2965, 2925, 2864, 2360, 2349, 2341, 2300, 1740, 1645, 1579, 1524, 1455, 1428, 1390, 1362, 1332, 1300, 1283, 1246, 1227, 1176, 1143, 1114, 1067, 1034, 960, 937, 908, 849, 833, 800, 776, 733, 703, 657, 634, 625, 614 cm^{-1}

HRMS–DART (*m/z*): $[M]^+$ calc'd for $C_{28}H_{48}CoN_2O_{10}$, 631.2635, found 631.2622

Elemental Analysis (EA): Anal. Calc'd for $C_{28}H_{48}CoN_2O_{10}$: C, 53.24; H, 7.66; Co, 9.33; N, 4.44; O, 25.33. Found C, 52.90; H, 7.69; N, 4.44

X-Ray Diffraction (XRD): CCDC deposition number 2395198. See Section 3.6.11.



C2

Complex **C2**: $Co(thd)_2$: Bis((*Z*)-2,2,6,6-tetramethyl-3,5-heptanedionato) cobalt(II)

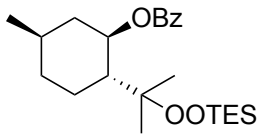
Yield: 82%

Physical state: purple crystals

Purification: vacuum sublimation at 1 mbar and 135 ºC (oil bath temperature)

Characterization data match literature values [52].

3.6.8.2 Alkylperoxides



1b

Compound **1b**: (1*R*,2*R*,5*R*)-5-Methyl-2-(2-((triethylsilyl)peroxy)propan-2-yl)cyclohexyl Benzoate

Scale: 0.50 mmol

Yield: 95%

Physical State: clear liquid

Purification: SiO_2 (0–5% *v/v* EtOAc/hexanes)

R_f = 0.41 (5% *v/v* EtOAc/hexanes + UV/vanillin stain)

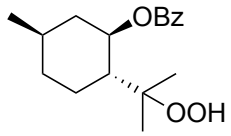
IR (ATR, neat) $\tilde{\nu}_{max}$: 2953, 2918, 2875, 1714, 1451, 1313, 1269, 1175, 1103, 1069, 1025, 1006, 975, 848, 833, 803, 740, 709 cm^{-1}

HRMS–ESI (*m/z*): $[M + H]^+$ calc'd for $C_{23}H_{39}O_4Si$, 407.2612, found 407.2606

Specific Rotation: $[\alpha]_D^{23.2}$ –62.0 (c 1.0, $CHCl_3$)

^{1}H NMR (400 MHz, $CDCl_3$) δ 8.11–8.01 (dd, *J* = 8.2, 1.4 Hz, 2H), 7.54 (tt, *J* = 6.7, 1.3 Hz, 1H), 7.44 (ddt, *J* = 8.3, 6.7, 1.3 Hz, 2H), 5.05 (td, *J* = 10.8, 4.4 Hz, 1H), 2.21–2.05 (m, 3H), 1.73 (ddt, *J* = 13.0, 3.5, 1.7 Hz, 1H), 1.63–1.50 (m, 1H), 1.33 (s, 3H), 1.19–1.05 (m, 5H), 0.99–0.90 (m, 13H), 0.64 (q, *J* = 8.1 Hz, 6H)

^{13}C NMR (101 MHz, $CDCl_3$) δ 165.8, 132.9, 131.0, 129.8, 128.4, 83.8, 74.7, 48.0, 41.8, 34.3, 31.7, 26.5, 25.6, 22.0, 21.0, 6.9, 4.0



1b′

Compound **1b'**: (1*R*,2*R*,5*R*)-2-(2-Hydroperoxypropan-2-yl)-5-methylcyclohexyl Benzoate

Procedure: As described above, (Section 3.6.7.1) exchange 1 drop of 70% aq. TBHP for 2.0 equivalents of 70% aq. TBHP. The solution will become brown then green once the reaction is complete (30 min at 0.500 mmol scale). Do not concentrate. Instead, directly transfer the reaction mixture for FCC.

Scale: 1.0 mmol

Yield: 92%

Physical State: white solid

Melting Point: 79–83 ºC

Purification: SiO_2 (0–10% *v/v* EtOAc/hexanes)

R_f = 0.22 (10% *v/v* EtOAc/hexanes + UV/vanillin stain)

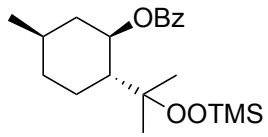
IR (ATR, neat) $\tilde{\nu}_{max}$: 3410, 2952, 2923, 2870, 1713, 1693, 1713, 1693, 1451, 1364, 1315, 1292, 1278, 1178, 1160, 1126, 1105, 1070, 1027, 959, 714 cm^{-1}

HRMS–ESI (*m/z*): $[M–OOH]^+$ calc'd for $C_{17}H_{23}O_2$, 259.1693, found 259.1696

Specific Rotation: $[\alpha]_D^{23.1}$ –74.0 (*c* 1.0, $CHCl_3$)

^{1}H NMR (400 MHz, $CDCl_3$) δ 8.08–7.99 (m, 2H), 7.58–7.52 (m, 1H), 7.44 (dd, *J* = 8.3, 7.0 Hz, 3H), 5.16 (td, *J* = 10.8, 4.5 Hz, 1H), 2.22 (ddd, *J* = 12.3, 10.6, 3.7 Hz, 1H), 2.12–2.04 (m, 1H), 1.94 (dq, *J* = 13.4, 3.5 Hz, 1H), 1.79–1.71 (m, 1H), 1.58 (tdq, *J* = 12.7, 6.4, 3.0 Hz, 1H), 1.24 (s, 6H), 1.22–1.12 (m, 2H), 1.05–0.96 (m, 1H), 0.94 (d, *J* = 6.5 Hz, 3H)

^{13}C NMR (101 MHz, $CDCl_3$) δ 166.0, 133.0, 131.0, 129.6, 128.6, 84.9, 74.2, 46.5, 41.6, 34.3, 31.6, 26.7, 23.3, 22.4, 22.0



1b″

Compound **1b"**: (1*R*,2*R*,5*R*)-5-Methyl-2-(2-((trimethylsilyl)peroxy)propan-2-yl)cyclohexyl Benzoate

Procedure: As described above, Section 3.6.6.1.4.

Scale: 0.50 mmol

Yield: 8%

Physical State: white solid

Melting Point: 52–55 ºC

Purification: SiO_2 (0–10% *v/v* EtOAc/hexanes)

$\boldsymbol{R_f}$ = 0.63 (10% *v/v* EtOAc/hexanes + UV/vanillin stain)

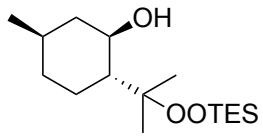
IR (ATR, neat) $\tilde{\nu}_{max}$: 2953, 2924, 2852, 1715, 1451, 1381, 1363, 1314, 1273, 1251, 1176, 1105, 1070, 1026, 894, 862, 846, 773, 712 cm^{-1}

HRMS–ESI (*m/z*): $[M–OOSiMe_3]^+$ calc'd for $C_{17}H_{23}O_2$, 259.1693, found 259.1693

Specific Rotation: $[\alpha]_D^{22.5}$ –54.0 (*c* 1.0, $CHCl_3$)

^{1}H NMR (400 MHz, $CDCl_3$) δ 8.09–8.02 (m, 2H), 7.58–7.50 (m, 1H), 7.48–7.37 (m, 2H), 5.05 (td, *J* = 10.7, 4.4 Hz, 1H), 2.19–2.03 (m, 3H), 1.76–1.67 (m, 1H), 1.59 (d, *J* = 8.6 Hz, 2H), 1.43 (s, 1H), 1.29 (s, 3H), 1.11 (s, 3H), 1.02–0.93 (m, 1H), 0.91 (d, *J* = 6.5 Hz, 3H), 0.11 (s, 9H).

^{13}C NMR (101 MHz, $CDCl_3$) δ 165.9, 132.9, 131.1, 129.9, 128.4, 84.2, 74.5, 47.8, 41.7, 34.3, 31.6, 25.8, 25.7, 22.0, 21.5, 0.0.



2b

Compound **2b**: (1*R*,2*R*,5*R*)-5-Methyl-2-(2-((triethylsilyl)peroxy)propan-2-yl)cyclohexan-1-ol

Scale: 1.0 mmol

Physical State: clear liquid

Purification: SiO_2 (0–10% *v/v* EtOAc/hexanes)

R_f = 0.19 (10% *v/v* EtOAc/hexanes + vanillin stain)

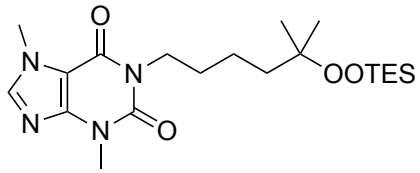
IR (ATR, neat) $\tilde{\nu}_{max}$: 3475, 2953, 2920, 2876, 1456, 1413, 1381, 1366, 1236, 1200, 1151, 1094, 1054, 1026, 1008, 975, 881, 845, 829, 797, 770, 738, 728, 711, 702, 693, 687, 676, 666, 660, 647, 635, 620, cm^{-1}

Specific Rotation: $[\alpha]_D^{24}$ +28.4 (*c* 1.0, $CHCl_3$)

HRMS–DART (*m/z*): $[M + H]^+$ calc'd for $C_{16}H_{35}O_3Si$, 303.2350, found 303.2356

^{1}H NMR (400 MHz, C_6D_6) δ 3.95 (s, *J* = 1.1 Hz, 1H), 3.68–3.57 (m, 1H), 2.12 (ddt, *J* = 12.2, 5.1, 2.1 Hz, 1H), 1.88–1.79 (m, 1H), 1.52–1.41 (m, 2H), 1.23 (s, 6H), 1.26–1.17 (m, 1H), 1.16–1.08 (m, 1H), 1.00 (t, *J* = 7.9 Hz, 9H), 0.83 (d, *J* = 6.3 Hz, 3H), 0.72–0.66 (m, 8H)

^{13}C NMR (101 MHz, C_6D_6) δ 88.4, 71.8, 49.8, 44.6, 34.9, 31.3, 27.0, 24.7, 22.3, 20.0, 7.0, 4.2



3b

Compound **3b**: 3,7-Dimethyl-1-(5-methyl-5-((triethylsilyl)peroxy)hexyl)-3,7-dihydro-1*H*-purine-2,6-dione

Scale: 1.0 mmol

Yield: 94%

Physical State: clear liquid

Purification: SiO_2 (iPrOH)

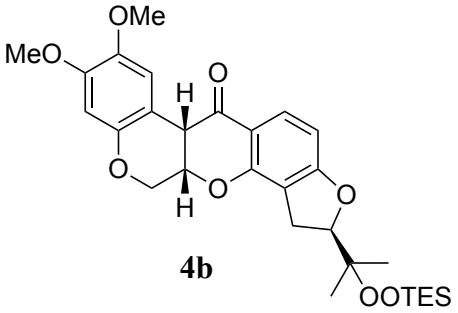
R_f = 0.33 (*i*PrOH + UV)

IR (ATR, neat) $\tilde{\nu}_{max}$: 2952, 2913, 2901, 2876, 1704, 1656, 1605, 1550, 1534, 1485, 1459, 1436, 1414, 1379, 1361, 1321, 1286, 1233, 1188, 1073, 1046, 1011, 948, 843, 830, 817, 806, 789, 779, 762, 741, 721, 706, 692, 663, 653 cm^{-1}

HRMS–DART (*m/z*): $[M + H]^+$ calc'd for $C_{20}H_{37}N_4O_4Si$, 425.2579, found 425.2585

^{1}H NMR (500 MHz, $CDCl_3$) δ 7.47 (s, 1H), 4.00–3.92 (m, 5H), 3.54 (s, 3H), 1.65–1.50 (m, 4H), 1.40–1.30 (m, 2H), 1.13 (s, 6H), 0.92 (t, *J* = 8.0 Hz, 9H), 0.61 (q, *J* = 7.9 Hz, 6H)

^{13}C NMR (126 MHz, $CDCl_3$) δ 155.4, 151.5, 148.8, 141.4, 107.8, 82.2, 41.4, 38.8, 33.6, 29.7, 28.6, 24.3, 21.5, 6.9, 3.9



4b

Compound **4b**: (2*R*,6a*S*,12a*S*)-8,9-Dimethoxy-2-(2-((triethylsilyl)peroxy)propan-2-yl)-1,2,12,12a-tetrahydrochromeno[3,4-*b*]furo[2,3-*h*]chromen-6(6a*H*)-one

***** Do not concentrate the crude reaction mixture. Directly transfer it for FCC. The compound decomposes upon concentration.

Scale: 1.0 mmol

Yield: 80%

Physical State: white solid

Purification: SiO_2 (0–20% *v/v* EtOAc/hexanes)

$\boldsymbol{R_f}$ = 0.80 (40% *v/v* EtOAc/hexanes + UV/vanillin stain)

Melting Point: 56–58 ºC

IR (ATR, neat) $\tilde{\nu}_{max}$: 2951, 2881, 1674, 1605, 1512, 1454, 1408, 1350, 1308, 1203, 1088, 1007, 964, 910, 802, 733, 675 cm^{-1}

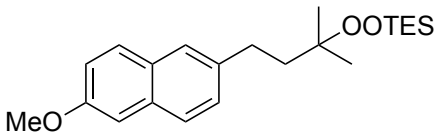
HRMS–ESI (*m/z*): $[M + H]^+$ calc'd for $C_{29}H_{39}O_8Si$, 543.2409, found 543.2418

Specific Rotation: $[\alpha]_D^{24.7}$ –108 (*c* 1.0, C_6H_6)

^{1}H NMR (500 MHz, C_6D_6) δ 8.15 (d, *J* = 8.5 Hz, 1H), 7.21 (s, 1H), 6.53 (s, 1H), 6.38 (d, *J* = 8.5 Hz, 1H), 4.75 (dd, *J* = 10.1, 7.9 Hz, 1H), 4.25 (dd, *J* = 12.1, 3.1 Hz, 1H), 4.10 (t, *J* = 3.4 Hz, 1H), 3.58 (d, *J* = 4.0 Hz, 1H), 3.47 (d, *J* = 12.1 Hz, 1H), 3.39 (s, 3H), 3.24 (s, 3H),

3.04 (dd, *J* = 16.0, 7.9 Hz, 1H), 2.74 (dd, *J* = 16.0, 10.1 Hz, 1H), 1.22 (s, 3H), 1.10 (s, 3H), 0.99 (t, *J* = 7.9 Hz, 9H), 0.66 (q, *J* = 8.0 Hz, 6H)

^{13}C NMR (126 MHz, C_6D_6) δ 188.6, 167.7, 158.2, 151.1, 148.2, 145.4, 130.2, 114.0, 113.8, 111.9, 105.5, 105.0, 102.2, 88.0, 83.2, 72.6, 66.2, 56.2, 55.4, 45.1, 27.7, 21.3, 19.5, 7.0, 4.2



5b

Compound **5b**: Triethyl((4-(6-methoxynaphthalen-2-yl)-2-methylbutan-2-yl)peroxy)silane

Scale: 1.0 mmol

Yield: 98%

Physical State: yellow solid

Purification: SiO_2 (0–5% *v/v* EtOAc/hexanes)

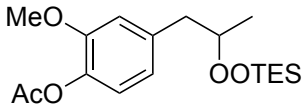
$\boldsymbol{R_f}$ = 0.81 (10% *v/v* EtOAc/hexanes)

IR (ATR, neat) $\tilde{\nu}_{max}$: 3056, 2953, 2936, 2913, 2876, 2841, 1635, 1607, 1506, 1484, 1461, 1440, 1415, 1391, 1378, 1363, 1343, 1262, 1228, 1210, 1195, 1174, 1160, 1134, 1120, 1035, 1018, 1008, 974, 935, 881, 849, 805, 785, 740, 728, 693, 683, 675, 662, 646, 637, 626, 616, 608 cm^{-1}

LCMS–DART (*m/z*): $[M + Na]^+$ calc'd for $C_{22}H_{34}O_3SiNa$, 397.2169, found 397.2174

^{1}H NMR (500 MHz, $CDCl_3$) δ 7.70–7.64 (m, 2H), 7.56 (s, 1H), 7.32 (dd, *J* = 8.5, 1.9 Hz, 1H), 7.12 (d, *J* = 7.8 Hz, 2H), 3.91 (s, 3H), 2.81–2.74 (m, 2H), 1.96–1.89 (m, 2H), 1.28 (s, 6H), 1.02 (t, *J* = 7.9 Hz, 9H), 0.71 (q, *J* = 8.0 Hz, 6H)

^{13}C NMR (126 MHz, CDCl3) δ 157.2, 138.4, 133.0, 129.3, 129.0, 128.1, 126.8, 126.2, 118.7, 105.8, 82.2, 55.4, 41.1, 30.5, 24.5, 7.0, 4.1



6b

Compound **6b**: 2-Methoxy-4-(2-((triethylsilyl)peroxy)propyl)phenyl Acetate

Scale: 1.00 mmol

Yield: 87%

Physical State: clear liquid

Purification: SiO_2 (0–5% *v/v* EtOAc/hexanes)

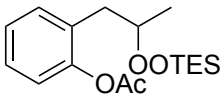
R_f = 0.40 (10% *v/v* EtOAc/hexanes + UV/vanillin stain)

IR (ATR, neat) $\tilde{\nu}_{max}$: 3037, 2956, 2937, 2913, 2877, 2842, 1767, 1605, 1510, 1464, 1418, 1369, 1311, 1289, 1269, 1215, 1197, 1152, 1123, 1088, 1069, 1037, 1009, 976, 933, 903, 875, 855, 813, 793, 740 cm^{-1}

GCMS–EI (*m/z*): $[M]^+$ calc'd for $C_{18}H_{30}O_5Si$, 354.1857, found 354.2

^{1}H NMR (500 MHz, $CDCl_3$) δ 6.93 (d, *J* = 7.9 Hz, 1H), 6.82 (d, *J* = 2.0 Hz, 1H), 6.76 (dd, *J* = 8.1, 2.0 Hz, 1H), 4.20 (q, *J* = 6.1 Hz, 1H), 3.82 (s, 3H), 2.99 (dd, *J* = 13.7, 5.8 Hz, 1H), 2.68 (dd, *J* = 13.7, 6.6 Hz, 1H), 2.30 (s, 3H), 1.18 (d, *J* = 6.1 Hz, 3H), 0.97 (t, *J* = 7.9 Hz, 9H), 0.65 (q, *J* = 7.9 Hz, 6H)

^{13}C NMR (126 MHz, $CDCl_3$) δ 169.3, 150.8, 138.3, 137.5, 122.5, 121.9, 113.9, 82.4, 55.9, 40.8, 20.8, 18.1, 6.9, 3.9



7b

Compound **7b**: 2-(2-((Triethylsilyl)peroxy)propyl)phenyl Acetate

Scale: 1.0 mmol

Yield: 90%

Physical State: clear liquid

Purification: SiO_2 (0–6% *v/v* EtOAc/hexanes)

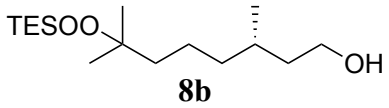
R_f = 0.58 (10% *v/v* EtOAc/hexanes + UV/vanillin stain)

IR (ATR, neat) $\tilde{\nu}_{max}$: 2956, 2936, 2913, 2877, 1767, 1489, 1455, 1412, 1369, 1201, 1172, 1145, 1115, 1093, 1008, 975, 945, 914, 897, 862, 831, 814, 793, 742, 673, 666, 661 cm^{-1}

GCMS–EI (*m/z*): $[M]^+$ calc'd for $C_{17}H_{28}O_4Si$, 324.1751, found 324.1

^{1}H NMR (500 MHz, CDCl3) δ 7.29–7.21 (m, 2H), 7.17 (td, *J* = 7.5, 1.4 Hz, 1H), 7.04 (dd, *J* = 7.9, 1.5 Hz, 1H), 4.26–4.11 (m, 1H), 3.11 (dd, *J* = 13.6, 5.3 Hz, 1H), 2.52 (dd, *J* = 13.6, 7.6 Hz, 1H), 2.32 (s, 3H), 1.14 (d, *J* = 6.3 Hz, 3H), 0.97 (t, *J* = 7.9 Hz, 9H), 0.65 (q, *J* = 7.9 Hz, 6H)

^{13}C NMR (126 MHz, CDCl3) δ 169.6, 149.4, 131.9, 130.4, 127.7, 126.1, 122.5, 81.4, 35.4, 21.1, 17.9, 6.9, 3.9



8b

Compound **8b**: (*S*)-3,7-Dimethyl-7-((triethylsilyl)peroxy)octan-1-ol

Scale: 1.0 mmol

Yield: 97%

Physical State: clear liquid

Purification: (SiO_2, 0–10% *v/v* EtOAc/hexanes)

$\boldsymbol{R_f}$ = 0.50 (20% *v/v* EtOAc/hexanes + vanillin stain)

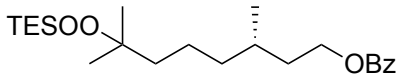
IR (ATR, neat) $\tilde{\nu}_{max}$: 3345, 2953, 2935, 2918, 2876, 2851, 1459, 1415, 1378, 1363, 1238, 1092, 1062, 1007, 974, 893, 847, 805, 739, 728 cm^{-1}

HRMS–DART (*m/z*): $[M + H]^+$ calc'd for $C_{16}H_{37}O_3Si$, 305.2506, found 305.2511

Optical Rotation: $[\alpha]_D^{25.6}$–2.00 (*c* 1.0, $CHCl_3$)

^{1}H NMR (400 MHz, $CDCl_3$) δ 3.95–3.39 (m, 2H), 1.71–1.19 (m, 9H), 1.19–1.10 (m, 1H), 1.17 (s, 6H), 0.98 (t, *J* = 7.9 Hz, 9H), 0.90 (d, *J* = 6.6 Hz, 3H), 0.66 (q, *J* = 8.0 Hz, 6H)

^{13}C NMR (101 MHz, $CDCl_3$) δ 82.5, 61.4, 40.2, 39.3, 37.8, 29.6, 24.39, 24.35, 21.5, 19.7, 7.0, 4.1



9b

Compound **9b**: (*S*)-3,7-Dimethyl-7-((triethylsilyl)peroxy)octyl benzoate

Scale: 4.0 mmol

Yield: 89%

Physical State: clear liquid

Purification: SiO_2 (0–5% *v/v* EtOAc/hexanes)

$\boldsymbol{R_f}$ = 0.50 (5% *v/v* EtOAc/hexanes + UV/vanillin stain)

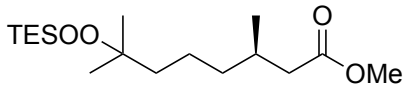
IR (ATR, neat) $\tilde{\nu}_{max}$: 2954, 2937, 2913, 2876, 1721, 1455, 1378, 1314, 1273, 1247, 1112, 1026, 806, 742, 729, 711 cm^{-1}

HRMS–ESI (*m/z*): $[M + Na]^+$ calc'd for $C_{23}H_{40}O_4SiNa$, 431.2588, found 431.2603

Specific Rotation: $[\alpha]_D^{23.3}$ –4.00 (*c* 1.0, $CHCl_3$)

^{1}H NMR (400 MHz, $CDCl_3$) δ 8.04 (dd, *J* = 8.4, 1.4 Hz, 2H), 7.62–7.48 (m, 1H), 7.44 (td, *J* = 7.0, 1.8 Hz, 2H), 4.36 (td, *J* = 6.5, 2.9 Hz, 2H), 1.87–1.76 (m, 1H), 1.72–1.43 (m, 4H), 1.42–1.08 (m, 10H), 0.98 (t, *J* = 7.8 Hz, 12H), 0.66 (q, *J* = 7.9 Hz, 6H)

^{13}C NMR (101 MHz, $CDCl_3$) δ 166.8, 132.9, 130.7, 129.7, 128.5, 82.4, 63.7, 39.3, 37.6, 35.7, 30.1, 24.41, 24.37, 21.4, 19.7, 7.0, 4.1



10b

Compound **10b**: methyl (*R*)-3,7-Dimethyl-7-((triethylsilyl)peroxy)octanoate

Scale: 5.0 mmol

Yield: 94%

Physical State: clear liquid

Purification: SiO_2 (0–10% *v/v* Et_2O/pentane)

$\boldsymbol{R_f}$ = 0.32 (10% *v/v* EtOAc/hexanes + vanillin stain)

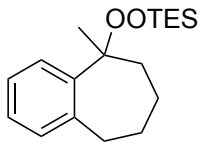
IR (ATR, neat) $\tilde{\nu}_{max}$: 2953, 2918, 2877, 2370, 2320, 1741, 1542, 1508, 1488, 1459, 1436, 1417, 1378, 1363, 1339, 1316, 1287, 1238, 1214, 1192, 1172, 1090, 1007, 974, 931, 895, 863, 846, 804, 770, 740, 728, 691, 678, 635, 626, 607 cm^{-1}

HRMS–DART (*m/z*): $[M + Na]^+$ calc'd for $C_{17}H_{36}O_4SiNa$, 355.2275, found 355.2275

Specific Rotation: $[\alpha]_D^{24.2}$ +6.00 (*c* 1.0, $CHCl_3$)

^{1}H NMR (400 MHz, $CDCl_3$) δ 3.66 (s, 3H), 2.31 (dd, *J* = 14.7, 5.9 Hz, 1H), 2.11 (ddd, *J* = 14.7, 8.3, 0.9 Hz, 1H), 1.97 (dp, *J* = 13.0, 6.3 Hz, 1H), 1.55–1.44 (m, 2H), 1.31 (dddd, *J* = 25.5, 16.6, 6.2, 4.2 Hz, 4H), 1.16 (s, 6H), 0.98 (dd, *J* = 8.4, 7.5 Hz, 9H), 0.93 (dd, *J* = 6.6, 0.7 Hz, 3H), 0.78–0.57 (m, 6H)

^{13}C NMR (101 MHz, $CDCl_3$) δ 173.9, 82.4, 51.5, 41.8, 39.1, 37.3, 30.4, 24.39, 24.36, 21.4, 19.8, 7.0, 4.1



11b

Compound **11b**: Triethyl((5-methyl-6,7,8,9-tetrahydro-5*H*-benzo[7]annulen-5-yl)peroxy)silane

Scale: 0.89 mmol

Yield: 95%

Physical State: clear liquid

Purification: SiO_2 (hexanes)

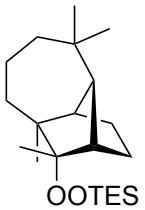
R_f = 0.52 (hexanes + UV/vanillin stain)

IR (ATR, neat) $\tilde{\nu}_{max}$: 3019, 2953, 2935, 2876, 1488, 1458, 1414, 1366, 1239, 1171, 1090, 1066, 1007, 973, 937, 910, 886, 863, 844, 803, 776, 743, 685, 666, 631, 601 cm^{-1}

HRMS–DART (*m/z*): $[M + H]^+$ calc'd for $C_{18}H_{30}O_2Si$, 306.2010, found 306.2003

^{1}H NMR (500 MHz, $CDCl_3$) δ 7.6–7.4 (m, 1H), 7.3–6.9 (m, 3H), 3.1 (ddd, *J* = 14.4, 8.7, 2.4 Hz, 1H), 2.9–2.6 (m, 1H), 2.2 (dddd, *J* = 16.9, 11.0, 8.5, 4.3 Hz, 1H), 2.0 (ttt, *J* = 13.0, 6.6, 3.2 Hz, 1H), 1.9–1.8 (m, 1H), 1.7 (tdd, *J* = 11.3, 4.7, 2.5 Hz, 2H), 1.7–1.5 (m, 4H), 1.0 (t, *J* = 7.9 Hz, 9H), 0.7 (q, *J* = 8.4 Hz, 6H)

^{13}C NMR (101 MHz, $CDCl_3$) δ 143.5, 141.2, 130.7, 127.4, 126.9, 125.9, 87.0, 37.5, 36.2, 27.9, 25.6, 25.2, 6.9, 4.0



12b

Compound **12b**: Triethyl(((1*S*,8a*R*,9*S*)-4,8,8,9-tetramethyldecahydro-1,4-methanoazulen-9-yl)peroxy)silane

Scale: 0.50 mmol

Yield: 17% (*endo*)

Physical State: clear liquid

Purification: SiO_2 (hexanes)

R_f = 0.67 (hexanes + vanillin stain)

IR (ATR, neat) $\tilde{\nu}_{max}$: 3006, 2953, 2913, 2876, 1456, 1379, 1364, 1220, 1007, 850, 802, 772, 743 cm^{-1}

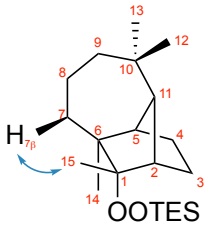
GCMS–EI (*m/z*): $[M–OSiEt_3]^-$ calc'd for $C_{15}H_{25}O$, 221.1911, found 221.2

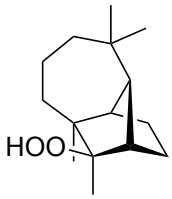
Specific Rotation: $[a]_D^{23.4}$ +32.0 (*c* 1.0, $CHCl_3$)

^{1}H NMR (400 MHz, $CDCl_3$) δ 2.23 (d, *J* = 3.9 Hz, 1H), 2.05–2.01 (m, 1H), 2.01–1.90 (m, 2H), 1.76–1.57 (m, 3H), 1.53 (s, 1H), 1.45 (s, 3H), 1.44–1.11 (m, 5H), 1.06–0.93 (m, 15H), 0.85 (s, 3H), 0.74–0.61 (m, 6H)

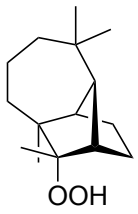
^{13}C NMR (126 MHz, $CDCl_3$) δ 91.0, 63.3, 49.6, 49.5, 45.2, 39.4, 39.1, 34.1, 33.1, 30.4, 25.0, 24.7, 23.0, 21.7, 21.6, 7.0, 4.1

HMBC, **HSQC**, and **NOESY** spectra are provided to support the configurational assignment. NOE correlations are presented below. See Section 3.6.10 for more details.


13
9
12
10
8
11
7
6
5
4
H7β
15
2
3
1
14
OOTES



***exo*-12b′**



***endo*-12b′**

Compound **12b'**: (1*S*,8a*R*)-9-hydroperoxy-4,8,8,9-tetramethyldecahydro-1,4-methanoazulene

Procedure: As described above, (Section 3.6.7) exchange 1 drop of 70% aq. TBHP for 1.5 equivalents of 70% aq. TBHP. The solution will become brown then green once the reaction is complete (10 min at 0.500 mmol scale). Do not concentrate. Instead, directly transfer the reaction mixture for FCC.

Scale: 0.50 mmol

Yield: 83% (*endo/exo = 2.8:1.0*)

Physical State: clear liquid

Purification: SiO_2 (0–3% *v/v* EtOAc/hexanes)

***exo*-12b'**: R_f = 0.53 (10% *v/v* EtOAc/hexanes + vanillin stain)

***endo*-12b'**: R_f = 0.46 (10% *v/v* EtOAc/hexanes + vanillin stain)

IR (ATR, neat) $\tilde{\nu}_{max}$: 3419, 3008, 2953, 2909, 2868, 1468, 1451, 1380, 1365, 1169, 1127, 1063, 913, 745 cm^{-1}

GCMS–EI (*m/z*): $[M–OH]^+$ calc'd for $C_{15}H_{25}O$, 221.1911, found 221.2

***endo*-12b'**

^{1}H NMR (500 MHz, C_6D_6) δ 6.36 (br, 1H), 2.20 (d, *J* = 4.4 Hz, 1H), 2.00 (ddd, *J* = 12.4, 9.1, 3.7 Hz, 1H), 1.90–1.83 (m, 1H), 1.75 (ddd, *J* = 13.7, 9.1, 4.5 Hz, 1H), 1.66–1.45 (m, 3H), 1.43 (s, 1H), 1.42 (s, 3H), 1.39–1.15 (m, 5H), 0.98 (s, 3H), 0.91 (s, 3H), 0.89 (s, 3H)

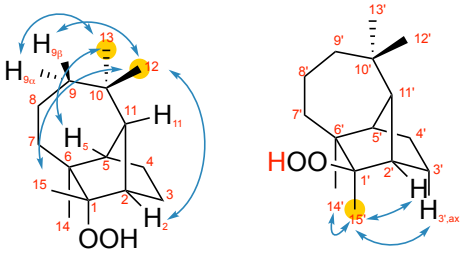
^{13}C NMR (126 MHz, C_6D_6) δ 90.8, 63.44, 49.8, 49.0, 45.4, 39.3, 39.2, 34.1, 33.0, 30.4, 25.2, 25.0, 23.5, 21.8, 21.5

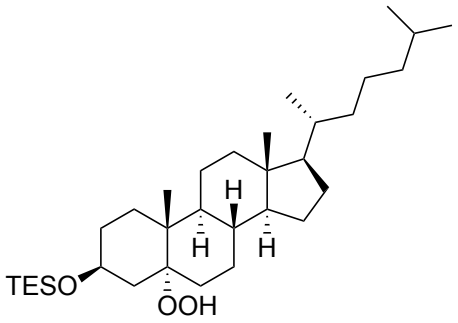
***exo*-12b'**

^{1}H NMR (500 MHz, C_6D_6) δ 6.45 (br, 1H), 2.49 (d, J = 5.2 Hz, 1H), 2.43 (t, J = 13.5 Hz, 1H), 2.23 (m, 1H), 1.96–1.85 (m, 1H), 1.73–1.49 (m, 2H), 1.43–1.19 (m, 9H), 1.14 (s, 3H), 1.13–1.10 (m, 1H), 1.08 (s, 3H), 0.82 (s, 3H)

^{13}C NMR (126 MHz, C_6D_6) δ 91.2, 63.37, 48.9, 46.4, 46.2, 38.4, 35.9, 35.0, 33.5, 30.7, 26.9, 25.9, 24.5, 22.2, 19.0

HMBC, **HSQC**, and **1D Selective Gradient NOESY** spectra are provided to support configurational assignments. NOE correlations are presented below. See Section 3.6.10 for more details.





13b′

Compound **13b'**: Triethyl(((3*S*,5*R*,8*S*,9*S*,10*R*,13*R*,14*S*,17*R*)-5-hydroperoxy-10,13-dimethyl-17-((*R*)-6-methylheptan-2-yl)hexadecahydro-1*H*-cyclopenta[*a*]phenanthren-3-yl)oxy)silane

Procedure: As described above, (Section 3.6.7) exchange 1 drop of 70% aq. TBHP for 2.0 equivalents of 70% aq. TBHP. The solution will become brown then green once the reaction is complete.

Scale: 0.50 mmol

Yield: 83%

Physical State: white solid

Melting Point: 161–163 ºC

Purification: SiO_2 (0–30% *v/v* DCM/hexanes)

$\boldsymbol{R_f}$ = 0.46 (50% *v/v* DCM/hexanes + vanillin stain)

IR (ATR, neat) $\tilde{\nu}_{max}$: 3368, 2954, 2935, 2868, 1467, 1449, 1382, 1238, 1199, 1170, 1106, 1039, 1009, 990, 960, 940, 922, 850, 811, 793, 778, 744, 727 cm^{-1}

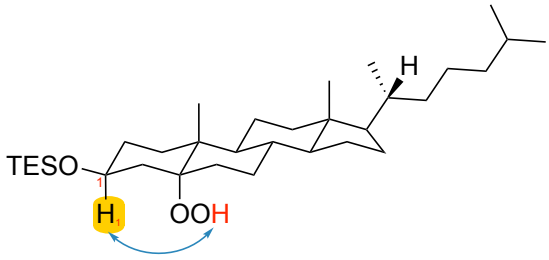
HRMS–ESI (*m/z*): $[M–OSiEt_3]^+$ calc'd for $C_{27}H_{47}O_2$, 403.3571, found 403.3578

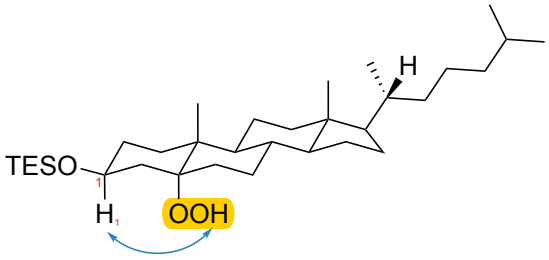
Specific Rotation: $[a]_D^{23.1}$ +4.00 (*c* 1.0, $CHCl_3$)

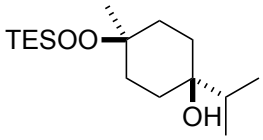
^{1}H NMR (600 MHz, $CDCl_3$) δ 6.71 (s, 1H), 3.98 (tt, *J* = 10.7, 5.1 Hz, 1H), 2.08 (ddd, *J* = 13.7, 5.0, 2.1 Hz, 1H), 1.94 (dt, *J* = 12.5, 3.3 Hz, 1H), 1.88–1.71 (m, 3H), 1.61–1.55 (m, 2H), 1.55–1.48 (m, 2H), 1.48–1.04 (m, 20H), 1.03 (s, 3H), 0.96 (t, *J* = 7.9 Hz, 10H), 0.89 (s, 3H), 0.89–0.83 (m, 6H), 0.64 (s, 3H), 0.61 (q, *J* = 8.0 Hz, 6H)

^{13}C NMR (126 MHz, $CDCl_3$) δ 86.9, 67.6, 56.4, 56.3, 45.5, 42.9, 40.2, 39.65, 39.57, 38.1, 36.3, 36.0, 35.2, 31.5, 31.0, 28.4, 28.15, 28.10, 26.2, 24.3, 24.0, 23.0, 22.7, 21.4, 18.8, 17.2, 12.3, 7.0, 4.9

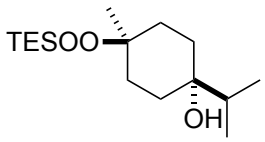
HMBC, **HSQC**, and **1D Selective Gradient NOESY** spectra are provided to support the configurational assignment. NOE correlations are presented below. See Section 3.6.10 for more details.







***cis*-14b**



***trans*-14b**

Compound **14b**: 1-Isopropyl-4-methyl-4-((triethylsilyl)peroxy)cyclohexan-1-ol

Scale: 3.0 mmol

Yield: 99% (*trans/cis* = *1.4:1.0*) [isolated as a mixture of diastereomers]

Physical State: clear liquid

Purification: SiO_2 (0–10% *v/v* EtOAc/Hex)

***cis*-14b**: R_f = 0.43 (10% *v/v* EtOAc/hexanes + vanillin stain)

***trans*-14b**: R_f = 0.32 (10% *v/v* EtOAc/hexanes + vanillin stain)

IR (ATR, neat) $\tilde{\nu}_{max}$: 3448, 2955, 2917, 2877, 1460, 1414, 1369, 1257, 1239, 1143, 1081, 1017, 1006, 978, 961, 941, 928, 909, 889, 848, 807, 741, 678, 626, 616, 603 cm^{-1}

HRMS–DART (*m/z*): $[M]^+$ calc'd for $C_{16}H_{34}O_3Si$, 302.2272, found 302.2285

***trans*-14b**

^{1}H NMR (400 MHz, $CDCl_3$) δ 1.80 (dt, *J* = 11.1, 2.9 Hz, 2H), 1.73–1.55 (m, 6H), 1.36–1.27 (m, 2H), 1.20 (s, 3H), 1.02–0.94 (m, 9H), 0.91 (d, *J* = 6.9 Hz, 6H), 0.72–0.62 (m, 6H)

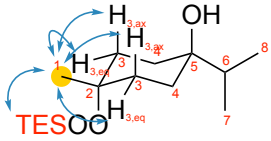
^{13}C NMR (101 MHz, $CDCl_3$) δ 80.1, 72.9, 38.8, 30.1, 29.3, 25.5, 17.0, 6.9, 4.0

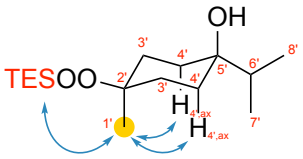
***cis*-14b**

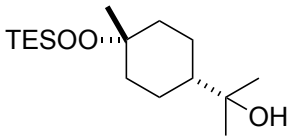
^{1}H NMR (400 MHz, $CDCl_3$) δ 1.95–1.85 (m, 2H), 1.73–1.43 (m, 8H), 1.21 (s, 3H), 1.02–0.94 (m, 9H), 0.91 (d, *J* = 6.9, Hz, 6H), 0.72–0.62 (m, 6H)

^{13}C NMR (101 MHz, $CDCl_3$) δ 81.7, 72.7, 35.9, 31.6, 30.6, 21.4, 16.9, 7.0, 4.1

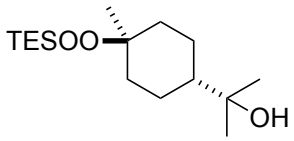
HSQC and **1D Selective Gradient NOESY** spectra are provided to support configurational assignments. NOE correlations are presented below. See Section 3.6.10 for more details.







***cis*-15b**



***trans*-15b**

Compound **15b**: 2-(4-Methyl-4-((triethylsilyl)peroxy)cyclohexyl)propan-2-ol

Scale: 1.0 mmol

Yield: 98% (*cis/trans* = *1.1:1.0*) [isolated as a mixture of diastereomers]

Physical State: clear liquid

Purification: SiO_2 (0–10% *v/v* EtOAc/hexanes)

$\boldsymbol{R_f}$ = 0.52 (10% *v/v* EtOAc/hexanes + vanillin stain) [incidental R_f]

IR (ATR, neat) $\tilde{\nu}_{max}$: 3520, 3369, 2953, 2940, 2915, 2876, 2804, 2368, 2359, 2344, 2331, 1507, 1460, 1444, 1413, 1366, 1347, 1333, 1310, 1272, 1238, 1197, 1163, 1144, 1130, 1084, 1017, 1007, 990, 975, 951, 931, 911, 863, 827, 805, 768, 740, 728, 683, 674, 650, 632, 620, 608, 599, 589, 581, 573, 554, 542, 533, 515, 503 cm^{-1}

GCMS–EI (*m/z*): $[M–H_2O]^+$ calc'd for $C_{16}H_{32}O_2Si$, 284.2166, found 284.2

***trans*-15b**

^{1}H NMR (400 MHz, $CDCl_3$) δ 2.09–2.00 (m, 2H), 1.64–1.52 (m, 2H), 1.46–1.11 (m, 15H), 1.08–0.92 (m, 9H), 0.81–0.60 (m, 6H)

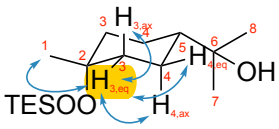
^{13}C NMR (151 MHz, $CDCl_3$) δ 79.8, 73.1, 48.6, 34.8, 27.0, 24.6, 22.6, 6.9, 4.0

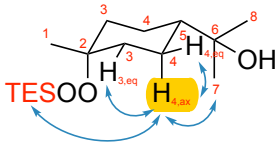
***cis*-15b**

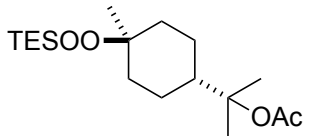
^{1}H NMR (400 MHz, $CDCl_3$) δ 1.89–1.71 (m, 4H), 1.64–1.51 (m, 2H), 1.46–1.10 (m, 13H), 1.08–0.92 (m, 9H), 0.81–0.60 (m, 6H)

^{13}C NMR (151 MHz, $CDCl_3$) δ 82.7, 72.7, 48.9, 35.0, 27.4, 25.8, 20.9, 7.0, 4.1

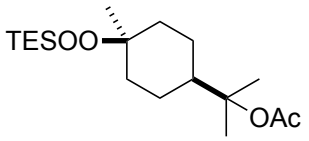
HMBC, **HSQC**, and **1D Selective Gradient NOESY** spectra are provided to support configurational assignments. NOE correlations are presented below for ***cis*-15b**. We were unable to measure **1D Selective Gradient NOESY** for ***trans*-15b** due to overlapping signals. See Section 3.6.10 for more details.







***trans*-16b**



***cis*-16b**

Compound **16b**: 2-(4-Methyl-4-((triethylsilyl)peroxy)cyclohexyl)propan-2-yl acetate

Scale: 1.0 mmol

Yield: 85% (*cis/trans* = *1.3:1.0*) [isolated as a mixture of diastereomers]

Physical State: clear liquid

Purification: SiO_2 (0–5 % *v/v* EtOAc/hexanes)

***trans*-16b**: R_f = 0.56 (3x 3% *v/v* EtOAc/hexanes + CAM stain)

***cis*-16b**: R_f = 0.61 (3x 3% *v/v* EtOAc/hexanes + CAM stain)

IR (ATR, neat) $\tilde{\nu}_{max}$: 2953, 2877, 1770, 1758, 1733, 1457, 1385, 1368, 1248, 1018, 851, 803, 743, 735, 720 cm^{-1}

HRMS–DART (*m/z*): $[M]^+$ calc'd for $C_{18}H_{36}O_4Si$, 344.2377, found 344.2369

***trans*-16b**

^{1}H NMR (500 MHz, C_6D_6) δ 2.08 (ddd, *J* = 14.5, 4.3, 2.5 Hz, 2H), 1.94 (tt, *J* = 12.2, 3.4 Hz, 1H), 1.72 (s, 3H), 1.57–1.41 (m, 4H), 1.45 (s, 6H), 1.22 (s, 3H), 1.14–0.97 (m, 11H), 0.82–0.69 (m, 6H)

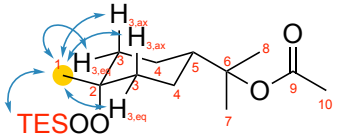
^{13}C NMR (126 MHz, C_6D_6) δ 169.6, 84.6, 80.1, 45.5, 34.7, 25.9, 23.7, 22.6, 22.1, 7.1, 4.37

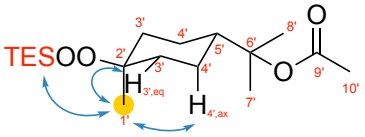
***cis*-16b**

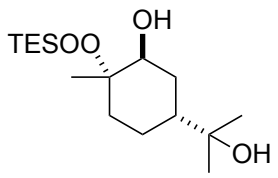
^{1}H NMR (500 MHz, C_6D_6) δ 1.81 (tt, *J* = 12.4, 3.6 Hz, 3H), 1.70–1.63 (m, 2H), 1.67 (s, 3H), 1.57–1.41 (m, 2H), 1.34 (s, 6H), 1.31 (s, 3H), 1.14–0.97 (m, 11H), 0.82–0.69 (m, 6H)

^{13}C NMR (126 MHz, C_6D_6) δ 169.5, 84.0, 82.7, 46.6, 35.2, 24.3, 23.5, 22.0, 21.0, 7.2, 4.44

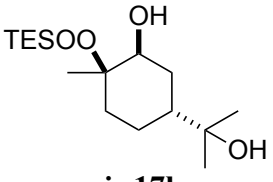
HMBC, **HSQC**, and **1D Selective Gradient NOESY** spectra are provided to support configurational assignments. NOE correlations are presented below. See Section 3.6.10 for more details.







***trans*-17b**



***cis*-17b**

Compound **17b**: (1,5-*trans*)-5-(2-Hydroxypropan-2-yl)-2-methyl-2-((triethylsilyl)peroxy)cyclohexan-1-ol

Scale: 1.0 mmol

Yield: 67% (*trans/cis* = *6.0:1.0*)

Physical State: white solid

Melting Point: 112–115 ºC

Purification: SiO_2 (0–90% *v/v* EtOAc/hexanes)

***cis*-17b**: R_f = 0.74 (80% *v/v* EtOAc/hexanes + vanillin stain)

***trans*-17b**: R_f = 0.58 (80% *v/v* EtOAc/hexanes + vanillin stain)

IR (ATR, neat) $\tilde{\nu}_{max}$: 3373, 3309, 2954, 2937, 2916, 2877, 1714, 1456, 1433, 1380, 1364, 1248, 1239, 1219, 1183, 1153, 1116, 1100, 1057, 1037, 1018, 1005, 975, 952, 912, 878, 846, 824, 806, 742, 635, 626, 615 cm^{-1}

HRMS–DART (*m/z*): $[M + Na]^+$ calc'd for $C_{16}H_{34}O_4SiNa$, 341.2119, found 341.2131

***cis*-17b**

^{1}H NMR (400 MHz, $CDCl_3$) δ 4.04 (s, 1H), 1.81–1.55 (m, 5H), 1.54–1.39 (m, 3H), 1.42–1.22 (m, 1H), 1.28 (s, 3H), 1.17 (d, *J* = 5.9 Hz, 6H), 0.98 (t, *J* = 7.9 Hz, 9H), 0.67 (q, *J* = 7.9 Hz, 6H)

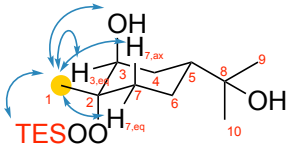
^{13}C NMR (101 MHz, $CDCl_3$) δ 82.0, 72.9, 70.2, 41.2, 30.5, 30.0, 27.4, 26.7, 22.0, 21.7, 6.9, 4.0

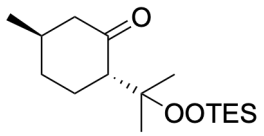
***trans*-17b**

^{1}H NMR (400 MHz, $CDCl_3$) δ 4.20–3.61 (m, 1H), 2.74 (br, 1H), 2.01 (dq, *J* = 14.1, 3.5 Hz, 1H), 1.86–1.65 (m, 3H), 1.40–1.27 (m, 2H), 1.27–1.23 (m, 4H), 1.23–1.13 (m, 1H), 1.18 (s, 6H), 0.98 (t, *J* = 7.9 Hz, 9H), 0.69 (qd, *J* = 7.9, 2.2 Hz, 6H)

^{13}C NMR (101 MHz, $CDCl_3$) δ 84.2, 72.4, 70.2, 41.5, 29.8, 29.3, 27.5, 27.4, 23.8, 19.9, 6.9, 4.0

HSQC and **1D Selective Gradient NOESY** spectra are provided to support the configurational assignment of ***trans*-17b**. NOE correlations are presented below for ***cis*-17b**. We were unable to measure **1D Selective Gradient NOESY** for ***cis*-17b** due to overlapping signals. See Section 3.6.10 for more details.





18b

Compound **18b**: (2*S*,5*R*)-5-Methyl-2-(2-((triethylsilyl)peroxy)propan-2-yl)cyclohexan-1-one

Scale: 1.0 mmol

Yield: 36%

Physical State: clear liquid

Purification: SiO_2 (0–5% *v/v* EtOAc/hexanes)

R_f = 0.77 (15% *v/v* EtOAc/hexanes + vanillin stain)

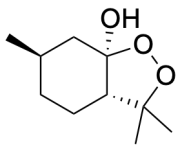
IR (ATR, neat) $\tilde{\nu}_{max}$: 3407, 2954, 2876, 1709, 1457, 1414, 1375, 1360, 1318, 1293, 1271, 1241, 1208, 1187, 1146, 1122, 1092, 1007, 977, 890, 876, 849, 833, 804, 728, 678, 622 cm^{-1}

HRMS–ESI (*m/z*): $[M + Na]^+$ calc'd for $C_{16}H_{32}O_3SiNa$, 323.2013, found 323.2018

Specific Rotation: $[\alpha]_D^{25}$ –80.0 (*c* 1.0, $CHCl_3$)

^{1}H NMR (600 MHz, $CDCl_3$) δ 2.91 (ddd, *J* = 12.5, 5.1, 1.3 Hz, 1H), 2.30 (tdt, *J* = 10.1, 4.2, 2.2 Hz, 2H), 2.04 (td, *J* = 12.7, 1.4 Hz, 1H), 1.96–1.80 (m, 2H), 1.45–1.36 (m, 5H), 1.14 (s, 3H), 1.01 (d, *J* = 6.4 Hz, 3H), 0.97 (t, *J* = 7.9 Hz, 9H), 0.66 (qd, *J* = 7.9, 3.1 Hz, 6H)

^{13}C NMR (101 MHz, $CDCl_3$): δ 211.3, 82.7, 55.4, 52.2, 36.4, 34.3, 27.7, 24.5, 22.5, 19.8, 6.9, 4.0



18b′

Compound **18b'**: (3a*S*,6*R*,7a*R*)-3,3,6-Trimethylhexahydro-7a*H*-benzo[*c*][1,2]dioxol-7a-ol

Scale: 1.0 mmol

Yield: 31%

Physical State: white solid

Melting Point: 77–80 ºC

Purification: SiO_2 (0–20% *v/v* EtOAc/hexanes)

$\boldsymbol{R_f}$ = 0.32 (15% *v/v* EtOAc/hexanes + vanillin stain)

IR (ATR, neat) $\boldsymbol{\tilde{\nu}_{max}}$: 3435, 3000, 2975, 2953, 2928, 2912, 2873, 2848, 1708, 1459, 1448, 1434, 1419, 1377, 1363, 1319, 1309, 1289, 1258, 1214, 1172, 1138, 1107, 1093, 1074, 1028, 1013, 990, 958, 950, 912, 852, 797, 734, 677 cm^{-1}

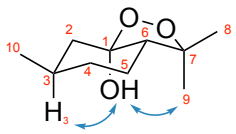
HRMS–ESI (*m/z*): $[M + H]^+$ calc'd for $C_{10}H_{19}O_3$, 187.1329, found 187.1333

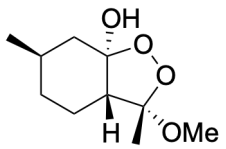
Specific Rotation: $[a]_D^{21.3}$ +66.0 (*c* 1.0, $CHCl_3$)

^{1}H NMR (600 MHz, $CDCl_3$) δ 3.54 (s, 1H), 2.39 (dd, *J* = 12.0, 6.3 Hz, 1H), 2.02 (ddd, *J* = 14.4, 4.8, 1.6 Hz, 1H), 1.78–1.62 (m, 2H), 1.53 (dtd, *J* = 10.8, 6.6, 4.4 Hz, 1H), 1.49 (s, 3H), 1.46–1.38 (m, 1H), 1.23 (s, 3H), 0.92 (ddd, *J* = 13.1, 7.9, 2.7 Hz, 1H), 0.88 (d, *J* = 6.6 Hz, 3H)

^{13}C NMR (126 MHz, $CDCl_3$) δ 106.0, 85.9, 59.5, 40.2, 31.9, 28.5, 28.0, 25.4, 23.3, 21.9

HSQC and **NOESY** spectra are provided to support the configurational assignment. NOE correlations are presented below. See Section 3.6.10 for more details.





18x

Compound **18x**: (3*S*,3a*R*,6*R*,7a*R*)-3-Methoxy-3,6-dimethylhexahydro-7a*H*-benzo[*c*][1,2]dioxol-7a-ol

Scale: 1.0 mmol

Yield: 59%

Physical State: white solid

Melting Point: 43–45 ºC

Purification: SiO_2 (0–10% *v/v* EtOAc/hexanes)

R_f = 0.34 (15% *v/v* EtOAc/hexanes + vanillin stain)

IR (ATR, neat) $\tilde{\nu}_{max}$: 3329, 2950, 2925, 2869, 1703, 1451, 1419, 1375, 1352, 1306, 1245, 1177, 1135, 1096, 1050, 1015, 958, 942, 915, 846, 746, 619 cm^{-1}

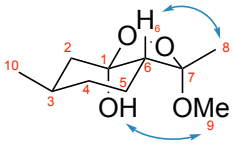
HRMS–ESI (*m/z*): $[M + H]^+$ calc'd for $C_{10}H_{19}O_4$, 203.1278, found 203.1283

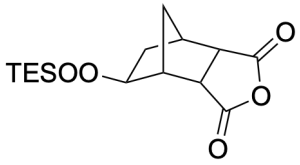
Specific Rotation: $[\alpha]_D^{20.8}$–60.0 (*c* 1.0, $CHCl_3$)

^{1}H NMR (600 MHz, $CDCl_3$) δ 5.98 (s, 1H), 3.42 (s, 3H), 2.56 (dd, *J* = 12.4, 6.4 Hz, 1H), 2.12 (ddd, *J* = 14.6, 4.0, 2.0 Hz, 1H), 1.86 (ddt, *J* = 13.2, 6.5, 3.3 Hz, 1H), 1.71 (dqd, *J* = 13.3, 3.4, 1.9 Hz, 1H), 1.59–1.49 (m, 1H), 1.42 (s, 3H), 1.36 (dd, *J* = 14.7, 12.5 Hz, 1H), 1.30 (tdd, *J* = 13.6, 12.3, 3.5 Hz, 1H), 0.97 (tdd, *J* = 13.5, 11.7, 3.1 Hz, 1H), 0.93 (d, *J* = 6.5 Hz, 3H)

^{13}C NMR (151 MHz, $CDCl_3$) δ 110.2, 105.4, 58.9, 49.3, 38.7, 32.2, 28.7, 26.1, 21.5, 13.8

HMBC, **HSQC**, and **NOESY** spectra are provided to support the configurational assignment. NOE correlations are presented below. See Section 3.6.10 for more details.





19b

Compound **19b**: (±)-(3a*R*,4*R*,5*S*,7*R*,7a*S*)-5-((Triethylsilyl)peroxy)hexahydro-4,7-methanoisobenzofuran-1,3-dione

Scale: 1.0 mmol

Yield: 44% (*exo*)

Physical State: clear liquid

Purification: SiO_2 (0–30% *v/v* EtOAc/hexanes)

R_f = 0.38 (30% *v/v* EtOAc/hexanes + I_2/vanillin stain)

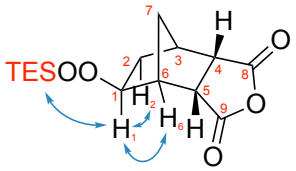
IR (ATR, neat) $\tilde{\nu}_{max}$: 2956, 2914, 2877, 1860, 1780, 1459, 1414, 1366, 1298, 1277, 1234, 1220, 1147, 1082, 1059, 1008, 989, 951, 903, 862, 835, 816, 784, 771, 741, 717 cm^{-1}

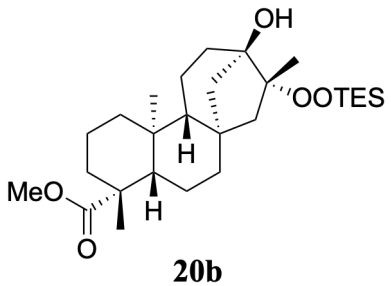
HRMS–ESI (*m/z*): $[M + H]^+$ calc'd for $C_{15}H_{25}O_5Si$, 313.1466, found 313.1470

^{1}H NMR (500 MHz, CDCl3) δ 4.16 (ddd, *J* = 7.3, 3.2, 1.7 Hz, 1H), 3.45 (dd, *J* = 10.1, 6.0 Hz, 1H), 3.37 (ddd, *J* = 10.1, 5.2, 1.8 Hz, 1H), 3.25–3.19 (m, 1H), 2.83 (tt, *J* = 4.9, 1.5 Hz, 1H), 1.91 (dt, *J* = 10.5, 1.5 Hz, 1H), 1.78 (ddd, *J* = 15.3, 7.2, 2.7 Hz, 1H), 1.54 (ddq, *J* = 10.5, 2.9, 1.6 Hz, 1H), 1.50–1.41 (m, 1H), 0.97 (t, *J* = 7.9 Hz, 9H), 0.66 (q, *J* = 7.8 Hz, 6H)

^{13}C NMR (126 MHz, CDCl3) δ 171.4, 170.9, 82.3, 49.1, 46.2, 43.4, 39.2, 38.7, 32.6, 6.8, 3.8

HSQC, **HMBC**, and **NOESY** spectra support the *exo* configuration. NOE correlations are presented below. See Section 3.6.10 for more details.


TESOO
H
O
O
O
H
H
H
H
1
2
3
4
5
6
7
8
9



20b

Compound **20b**: Methyl (4*R*,4a*S*,6a*S*,8*R*,9*S*,11a*R*,11b*S*)-9-hydroxy-4,8,11b-trimethyl-8-((triethylsilyl)peroxy)tetradecahydro-6a,9-methanocyclohepta[*a*]naphthalene-4-carboxylate

Scale: 190 mg

Yield: 35%

Physical State: white solid

Purification: SiO_2 (0–10% *v/v* EtOAc/hexanes)

Melting Point: 73–75 °C

R_f = 0.76 (30% *v/v* EtOAc/hexanes + vanillin stain)

IR (ATR, neat) $\tilde{\nu}_{max}$: 3512, 2938, 2876, 2848, 1725, 1461, 1444, 1412, 1373, 1334, 1281, 1238, 1230, 1208, 1188, 1152, 1122, 1097, 1066, 1046, 1017, 1004, 969, 958, 913, 887, 856, 807, 779, 680 cm^{-1}

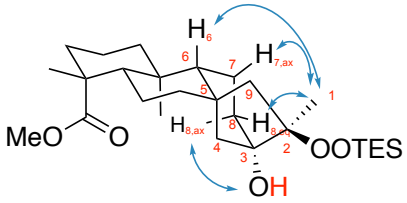
HRMS–ESI (*m/z*): $[M–OH]^+$ calc'd for $C_{27}H_{47}O_4Si$, 463.3238, found 463.3250

Specific Rotation: $[\alpha]_D^{23.0}$ –40.0 (*c* 1.0, $CHCl_3$)

^{1}H NMR (500 MHz, $CDCl_3$) δ 4.48 (s, 1H), 3.62 (s, 3H), 2.20–2.13 (m, 1H), 1.96–1.76 (m, 4H), 1.76–1.65 (m, 3H), 1.66–1.51 (m, 3H), 1.54–1.45 (m, 1H), 1.46–1.32 (m, 6H), 1.29 (dd, J = 13.1, 3.8 Hz, 1H), 1.24 (s, 1H), 1.14 (s, 3H), 0.97 (dt, J = 11.1, 8.0 Hz, 11H), 0.82 (d, J = 6.1 Hz, 5H), 0.69 (q, J = 8.0 Hz, 6H)

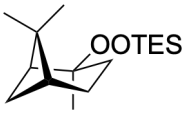
^{13}C NMR (126 MHz, $CDCl_3$) δ 178.1, 89.0, 82.6, 56.9, 54.5, 52.0, 51.2, 44.0, 43.9, 42.2, 40.9, 40.7, 39.3, 38.2, 34.2, 28.8, 22.1, 19.7, 19.1, 16.1, 15.3, 6.8, 3.9

HSQC, **HMBC**, and **NOESY** spectra are provided to support the configurational assignment. NOE correlations are presented below. See Section 3.6.10 for more details.





***exo*-21b**



***endo*-21b**

Compound **21b**: Triethyl(((1*S*,5*R*)-2,6,6-trimethylbicyclo[3.1.1]heptan-2-yl)peroxy)silane

Scale: 1.0 mmol

Yield: 79% (*exo/endo = 2.0:1.0*)

Physical State: clear liquid

Purification: SiO_2 (pentane)

***exo*-21b**: R_f = 0.58 (pentane + vanillin stain)

***endo*-21b**: R_f = 0.77 (pentane + vanillin stain)

IR (ATR, neat) $\tilde{\nu}_{max}$: 2953, 2874, 2854, 1462, 838 cm^{-1}

HRMS–DART (*m/z*): $[M + H]^+$ calc'd for $C_{16}H_{33}O_2Si$, 285.2244, found 285.2250

***exo*-21b**: **Specific Rotation**: $[\alpha]_D^{22.0}$ +28.0 (*c* 1.0, $CHCl_3$)

***endo*-21b**: **Specific Rotation**: $[\alpha]_D^{22.6}$ +4.00 (*c* 1.0, $CHCl_3$)

***exo*-21b**

^{1}H NMR (500 MHz, $CDCl_3$): δ 2.14 (t, *J* = 5.5 Hz, 1H), 2.12–2.04 (m, 1H), 1.90–1.69 (m, 4H), 1.64 (ddd, *J* = 15.6, 10.1, 5.0 Hz, 1H), 1.54 (s, 1H), 1.45 (d, *J* = 9.9 Hz, 1H), 1.34 (s, 3H), 1.25 (s, 3H), 1.05–0.90 (m, 2H), 1.05–0.90 (m, 9H), 0.65 (qd, *J* = 7.8, 3.3 Hz, 6H)

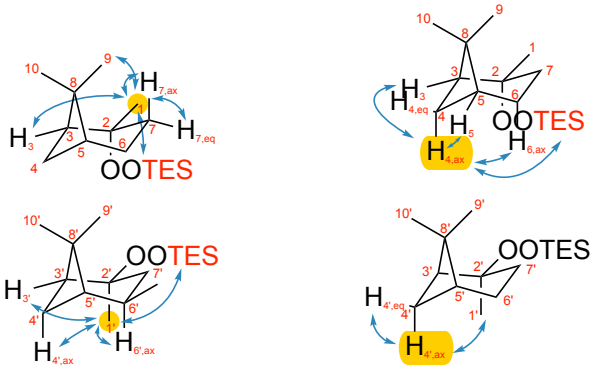
^{13}C NMR (126 MHz, $CDCl_3$): δ 86.5, 49.8, 40.7, 38.1, 28.0, 27.6, 26.8, 26.0, 24.9, 23.7, 7.0, 4.1

***endo*-21b**

^{1}H NMR (400 MHz, $CDCl_3$): δ 2.30–2.20 (m, 1H), 2.05 (dd, *J* = 6.6, 4.9 Hz, 1H), 2.01–1.84 (m, 3H), 1.79–1.69 (m, 1H), 1.69–1.60 (m, 1H), 1.27 (s, 3H), 1.18 (s, 3H), 1.05 (d, *J* = 10.2 Hz, 1H), 1.03–0.93 (m, 12H), 0.74–0.61 (m, 6H)

^{13}C NMR (101 MHz, $CDCl_3$): δ 87.9, 50.0, 41.2, 38.4, 28.1, 27.7, 27.1, 26.0, 24.4, 23.4, 6.9, 4.0

1D selective gradient NOESY spectrum is provided to support the configurational assignments. NOE correlations are presented below. See Section 3.6.10 for more details.





22b

Compound **22b**: *exo*-Triethyl(2,3,3-trimethylbicyclo[2.2.1]heptan-2-yl)peroxy)silane

Scale: 1.0 mmol

Yield: 74% (*exo*)

Physical state: clear liquid

Purification: SiO_2 (0–2% *v/v* EtOAc/hexanes)

$\boldsymbol{R_f}$ = 0.45 (hexanes + vanillin stain)

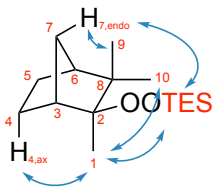
IR (ATR, neat) $\tilde{\nu}_{max}$: 2959, 2877, 1462, 1413, 1388, 1370, 1298, 1243, 1162, 1120, 1071, 1019, 971, 858, 827, 789, 742, 673, 665, 655, 647, 638, 621, 614, 605 cm^{-1}

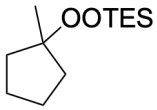
HRMS–DART (*m/z*): $[M]^+$ calc'd for $C_{16}H_{32}O_2Si$, 284.2166, found 284.2169

^{1}H NMR (400 MHz, $CDCl_3$) δ 2.50 (dq, *J* = 5.0, 1.7 Hz, 1H), 2.04–1.97 (m, 1H), 1.65 (dd, *J* = 3.6, 1.8 Hz, 1H), 1.60–1.50 (m, 1H), 1.49–1.37 (m, 1H), 1.37–1.24 (m, 2H), 1.22 (s, 3H), 1.01–0.93 (m, 1H), 0.98 (t, *J* = 7.9 Hz, 9H), 0.92 (s, 3H), 0.89 (s, 3H), 0.75–0.59 (m, 6H)

^{13}C NMR (101 MHz, $CDCl_3$) δ 91.3, 50.0, 45.9, 45.2, 34.5, 24.2, 24.1, 23.4, 23.4, 16.1, 6.9, 4.1

NOESY and **HSQC** spectra are provided to support the configurational assignments. NOE correlations are presented below. See Section 3.6.10 for more details.





23b

Compound **23b**: Triethyl((1-methylcyclopentyl)peroxy)silane

Scale: 1.0 mmol

Yield: 99%

Physical State: clear liquid

Purification: SiO_2 (pentane + vanillin stain)

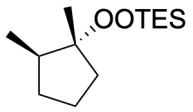
$\boldsymbol{R_f}$ = 0.61 (pentane)

IR (ATR, neat) $\tilde{\nu}_{max}$: 2956, 2937, 2916, 2877, 1459, 1441, 1414, 1370, 1238, 1213, 1018, 1007, 975, 882, 851, 809, 741, 731, 622 cm^{-1}

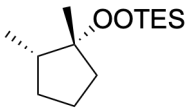
HRMS–DART (*m/z*): $[M + H]^+$ calc'd for $C_{12}H_{27}O_2Si$, 231.1775, found 231.1782

^{1}H NMR (400 MHz, $CDCl_3$): δ 2.00–1.86 (m, 2H), 1.75 - 1.64 (m, 2H), 1.62 - 1.50 (m, 2H), 1.47–1.37 (m, 2H), 1.34 (s, 3H), 0.98 (t, *J* = 8.0 Hz, 9H), 0.67 (q, *J* = 8.0 Hz, 6H)

^{13}C NMR (101 MHz, $CDCl_3$): δ 91.9, 37.0, 25.0, 24.0, 6.9, 4.1



***trans*-24b**



***cis*-24b**

Compound **24b**: ((1,2-Dimethylcyclopentyl)peroxy)triethylsilane

Scale: 0.40 mmol

Yield: 94% (*cis/trans = 1.7:1.0*)

Physical State: clear liquid

Purification: SiO_2 (pentane)

***trans*-24b**: R_f = 0.69 (pentane + vanillin stain)

***cis*-24b**: R_f = 0.55 (pentane + vanillin stain)

IR (ATR, neat) $\tilde{\nu}_{max}$: 2954, 2935, 2877, 2804, 1459, 1414, 1377, 1368, 1261, 1238, 1170, 1120, 1108, 1090, 1065, 1018, 1007, 975, 947, 931, 891, 864, 830, 810, 741, 729, 676, 628, 613 cm^{-1}

HRMS–DART (*m/z*): $[M + Na]^+$ calc'd for $C_{13}H_{28}O_2SiNa$, 267.1751, found 267.1744

***trans*-24b**

^{1}H NMR (400 MHz, $CDCl_3$) δ 2.19–1.78 (m, 3H), 1.65–1.49 (m, 2H), 1.50–1.39 (m, 1H), 1.20 (s, 3H), 1.18–1.11 (m, 1H), 0.98 (t, *J* = 7.9 Hz, 9H), 0.89 (d, *J* = 7.1 Hz, 3H), 0.66 (q, *J* = 7.7 Hz, 6H)

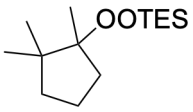
^{13}C NMR (101 MHz, $CDCl_3$) δ 93.2, 40.4, 36.1, 33.5, 22.0, 19.5, 16.5, 7.0, 4.1

***cis*-24b**

^{1}H NMR (400 MHz, $CDCl_3$) δ 2.27 (ddd, *J* = 13.4, 8.8, 4.4 Hz, 1H), 1.81–1.63 (m, 3H), 1.53–1.36 (m, 3H), 1.28 (s, 3H), 0.98 (t, *J* = 7.9 Hz, 9H), 0.92 (d, *J* = 6.8 Hz, 3H), 0.70–0.63 (m, 6H)

^{13}C NMR (101 MHz, $CDCl_3$) δ 90.8, 45.2, 35.6, 33.0, 29.9, 21.5, 12.4, 6.9, 4.1

The configurations for ***trans*-24b** and ***cis*-24b** were assigned based on the ^{1}H NMR spectral chemical shifts for the corresponding 1,2-dimethylcyclopentanols [107]. Compound ***cis*-24b** was the major diastereomer.



25b

Compound **25b**: Triethyl((1,2,2-trimethylcyclopentyl)peroxy)silane

Scale: 1.0 mmol

Yield: 80%

Physical State: clear liquid

Purification: SiO_2 (pentane)

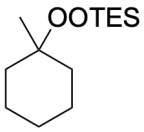
$\boldsymbol{R_f}$ = 0.63 (pentane + vanillin stain)

IR (ATR, neat) $\tilde{\nu}_{max}$: 2955, 2914, 2877, 1459, 1414, 1386, 1367, 1237, 1175, 1136, 1108, 1018, 1006, 974, 935, 921, 873, 838, 813, 741, 730, 685, 677 cm^{-1}

HRMS–DART (*m/z*): $[M + H]^+$ calc'd for $C_{14}H_{31}O_2Si$, 259.2088, found 259.2092

^{1}H NMR (400 MHz, $CDCl_3$) δ 2.35–2.26 (m, 1H), 1.77–1.49 (m, 4H), 1.43–1.37 (m, 1H), 1.19 (s, 3H), 0.98 (t, *J* = 7.8 Hz, 9H), 0.90 (s, 3H), 0.87 (s, 3H), 0.66 (q, *J* = 7.8 Hz, 6H)

^{13}C NMR (101 MHz, $CDCl_3$) δ 93.9, 45.5, 39.7, 33.2, 26.5, 21.1, 19.6, 17.2, 6.9, 4.1



26b

Compound **26b**: Triethyl((1-methylcyclohexyl)peroxy)silane

Scale: 1.0 mmol

Yield: 93%

Physical State: clear liquid

Purification: SiO_2 (pentane)

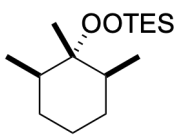
$\boldsymbol{R_f}$ = 0.53 (pentane + vanillin stain)

IR (ATR, neat) $\boldsymbol{\tilde{\nu}_{max}}$: 2953, 2936, 2877, 1460, 1446, 1414, 1370, 1280, 1260, 1238, 1166, 1143, 1118, 1090, 1039, 1018, 1007, 975, 963, 926, 905, 893, 867, 847, 820, 804, 741, 730, 695, 673, 641, 633, 607 cm^{-1}

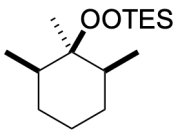
HRMS–DART (*m/z*): $[M + H]^+$ calc'd for $C_{13}H_{29}O_2Si$, 245.1931, found 245.1941

^{1}H NMR (400 MHz, $CDCl_3$) δ 1.81–1.71 (m, 2H), 1.64–1.50 (m, 2H), 1.50–1.23 (m, 6H), 1.18 (s, 3H), 0.99 (t, *J* = 7.9 Hz, 9H), 0.68 (q, *J* = 8.0 Hz, 6H)

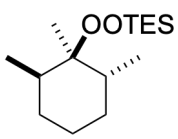
^{13}C NMR (101 MHz, $CDCl_3$) δ 81.3, 35.1, 26.0, 24.4, 22.6, 7.0, 4.1



27b1



27b2



27b3

Compound **27b**: Triethyl((1,2,6-trimethylcyclohexyl)peroxy)silane

Scale: 1.0 mmol

Yield: 73% (*1/2/3 = 2.9:1.7:1.0*)

Physical State: clear liquid

Purification: SiO_2 (pentane)

R_f = 0.88, 0.76, 0.66 (pentane + vanillin stain)

IR (ATR, neat) $\tilde{\nu}_{max}$: 2955, 2931, 2877, 2857, 1460, 1414, 1376, 1238, 1160, 1127, 1102, 1017, 1007, 975, 948, 907, 891, 851, 819, 809, 741, 731, 690, 682, 672, 625, 608 cm^{-1}

HRMS–DART (*m/z*): $[M + H]^+$ calc'd for $C_{15}H_{33}O_2Si$, 273.2244, found 273.2248

27b1

^{1}H NMR (500 MHz, $CDCl_3$) δ 2.10 (dqd, *J* = 13.4, 6.7, 3.8 Hz, 2H), 1.69–1.22 (m, 4H), 1.13–1.04 (m, 2H), 1.02–0.94 (m, 9H), 0.85 (d, *J* = 6.7 Hz, 6H), 0.77 (s, 3H), 0.72–0.62 (m, 6H)

^{13}C NMR (126 MHz, $CDCl_3$) δ 87.8, 36.5, 32.9, 26.1, 15.3, 10.3, 7.0, 4.0

27b2

^{1}H NMR (500 MHz, $CDCl_3$) δ 1.74–1.22 (m, 8H), 1.28 (s, 3H), 1.03 (d, *J* = 6.7 Hz, 6H), 1.02–0.94 (m, 9H), 0.72–0.62 (m, 6H)

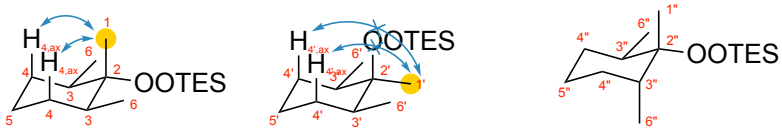
^{13}C NMR (126 MHz, $CDCl_3$) δ 83.8, 42.8, 31.1, 26.7, 19.7, 17.2, 7.0, 3.9

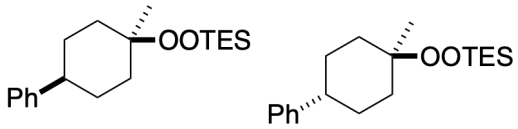
27b3

^{1}H NMR (500 MHz, $CDCl_3$) δ 2.06–2.00 (m, 1H), 1.94 (q, *J* = 6.1 Hz, 1H), 1.72–1.23 (m, 6H), 1.20 (s, 3H), 1.02–0.94 (m, 9H), 0.93 (d, *J* = 7.0 Hz, 3H), 0.85 (d, *J* = 4.3 Hz, 3H), 0.72–0.62 (m, 6H)

^{13}C NMR (126 MHz, $CDCl_3$) δ 85.4, 36.0, 33.1, 30.7, 30.4, 20.4, 19.5, 15.5, 14.5, 7.0, 4.0

HSQC and **1D selective gradient NOESY** spectra are provided to support the configurational assignment for 1/2/3. NOE correlations are presented below. See Section 3.6.10 for more details. The minor diastereomer is assigned to the *trans*-1,3-methyl substituents, based on the starting material **27a**.





***cis*-28b** ***trans*-28b**

Compound **28b**: Triethyl((1-methyl-4-phenylcyclohexyl)peroxy)silane

Scale: 1.0 mmol

Yield: 97% (*cis/trans* = *1.4:1.0*)

Physical State: clear liquid

Purification: SiO_2 (0–5% *v/v* EtOAc/hexanes)

***cis*-28b**: R_f = 0.38 (hexanes + UV/vanillin stain)

***trans*-28b**: R_f = 0.10 (hexanes + UV/vanillin stain)

IR (ATR, neat) $\tilde{\nu}_{max}$: 3083, 3061, 3028, 2953, 2936, 2876, 1604, 1541, 1527, 1507, 1494, 1458, 1414, 1369, 1348, 1328, 1295, 1282, 1260, 1238, 1186, 1146, 1131, 1115, 1096, 1019, 1009, 964, 929, 905, 880, 851, 806, 775, 742, 698, 675, 657, 649, 640, 628, 622, 608 cm^{-1}

HRMS–DART (*m/z*): $[M + H]^+$ calc'd for $C_{19}H_{33}O_2Si$, 321.2244, found 321.2252

***cis*-28b**

^{1}H NMR (400 MHz, $CDCl_3$): δ 7.34–7.27 (m, 2H), 7.25–7.16 (m, 3H), 2.46 (tt, *J* = 12.3, 3.6 Hz, 1H), 2.17–2.04 (m, 2H), 1.92–1.72 (m, 2H), 1.71–1.58 (m, 2H), 1.41 (td, *J* = 13.8, 4.1 Hz, 2H), 1.25 (s, 3H), 1.04 (t, *J* = 7.9 Hz, 9H), 0.73 (q, *J* = 7.9 Hz, 6H)

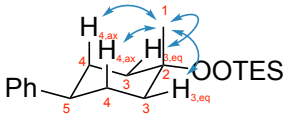
^{13}C NMR (101 MHz, $CDCl_3$): δ 147.8, 128.4, 127.0, 126.0, 79.6, 44.0, 35.1, 29.5, 25.9, 7.0, 4.1

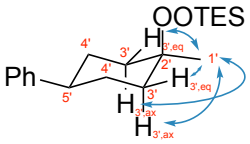
***trans*-28b**

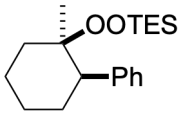
^{1}H NMR (400 MHz, $CDCl_3$): δ 7.31 (dddd, *J* = 8.2, 7.3, 1.8, 1.0 Hz, 2H), 7.26–7.17 (m, 3H), 2.56 (tt, *J* = 12.0, 3.7 Hz, 1H), 1.96–1.86 (m, 2H), 1.86–1.70 (m, 4H), 1.70–1.52 (m, 2H), 1.36 (s, 3H), 1.03 (t, *J* = 7.9 Hz, 9H), 0.73 (q, *J* = 7.9 Hz, 6H)

^{13}C NMR (101 MHz, $CDCl_3$): δ 146.8, 128.5, 126.9, 126.2, 82.4, 44.0, 35.2, 31.3, 21.1, 7.0, 4.1

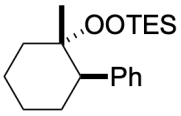
HSQC and NOESY spectra are provided to support the configurational assignments. NOE correlations are presented below. See Section 3.6.10 for more details.







***cis*-29b**



***trans*-29b**

Compound **29b**: Triethyl((1-methyl-2-phenylcyclohexyl)peroxy)silane

Scale: 1.0 mmol scale reaction

Yield: 95% (*cis*/*trans* = *1.1:1.0*)

Physical State: clear liquid

Purification: SiO_2 (0–4% *v/v* EtOAc/hexanes)

***cis*-29b**: R_f = 0.46 (hexanes + UV/vanillin stain)

***trans*-29b**: R_f = 0.23 (hexanes + UV/vanillin stain)

IR (ATR, neat) $\tilde{\nu}_{max}$: 3087, 3063, 3029, 2951, 2936, 2876, 2805, 1604, 1496, 1457, 1446, 1414, 1371, 1333, 1258, 1239, 1177, 1147, 1135, 1018, 1006, 975, 960, 934, 905, 875, 851, 807, 763, 741, 730, 699, 677, 634, 628, 617, 608 cm^{-1}

HRMS–DART (*m/z*): $[M + H]^+$ calc'd for $C_{19}H_{33}O_2Si$, 321.2244, found 321.2252

***cis*-29b**

^{1}H NMR (400 MHz, $CDCl_3$) δ 7.28–7.16 (m, 5H), 2.54 (dd, *J* = 13.2, 3.7 Hz, 1H), 2.44–2.35 (m, 1H), 2.02 (qd, *J* = 13.1, 3.7 Hz, 1H), 1.91–1.80 (m, 1H), 1.74 (tt, *J* = 13.3, 3.7 Hz, 1H), 1.61–1.49 (m, 2H), 1.44–1.28 (m, 1H), 1.18 (td, *J* = 13.6, 3.9 Hz, 1H), 1.00 (s, 3H), 0.94 (t, *J* = 7.9 Hz, 9H), 0.64 (qd, *J* = 8.0, 1.9 Hz, 6H)

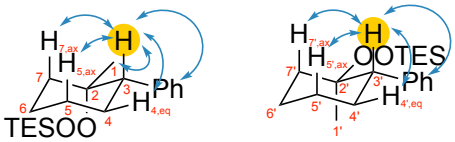
^{13}C NMR (101 MHz, $CDCl_3$) δ 142.8, 129.8, 127.6, 126.3, 82.3, 54.6, 35.0, 29.3, 26.9, 24.0, 21.8, 6.9, 4.0

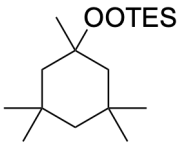
***trans*-29b**

^{1}H NMR (400 MHz, $CDCl_3$) δ 7.29–7.14 (m, 5H), 3.12 (dd, *J* = 10.8, 5.9 Hz, 1H), 2.02–1.72 (m, 6H), 1.51–1.31 (m, 2H), 0.95 (d, *J* = 0.7 Hz, 3H), 0.94 (t, *J* = 7.9 Hz, 9H), 0.67–0.58 (m, 6H)

^{13}C NMR (101 MHz, $CDCl_3$) δ 142.2, 129.7, 127.3, 126.1, 84.9, 47.9, 36.7, 29.4, 26.5, 24.2, 16.9, 6.9, 4.1

1D Selective Gradient NOESY spectrum is provided to support the configurational assignments. NOE correlations are presented below. See Section 3.6.10 for more details.





30b

Compound **30b**: Triethyl((1,3,3,5,5-pentamethylcyclohexyl)peroxy)silane

Scale: 1.0 mmol

Yield: 82%

Physical State: clear liquid

Purification: SiO_2 (pentane)

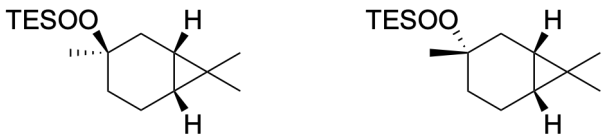
R_f = 0.78 (pentane)

IR (ATR, neat) $\tilde{\nu}_{max}$: 2953, 2913, 2895, 2878, 2832, 2805, 1507, 1483, 1457, 1417, 1387, 1366, 1354, 1316, 1255, 1239, 1223, 1112, 1069, 1019, 1008, 974, 954, 894, 877, 855, 805, 787, 740, 729, 674, 624, 608 cm^{-1}

HRMS–DART (*m/z*): $[M + H]^+$ calc'd for $C_{17}H_{37}O_2Si$, 301.2557, found 301.2562

^{1}H NMR (400 MHz, $CDCl_3$) δ 1.93–1.78 (m, 2H), 1.53 (s, 2H), 1.31 (dt, *J* = 13.7, 2.1 Hz, 1H), 1.17 (s, 3H), 1.11 (s, 6H), 1.07–0.93 (m, 12H), 0.86 (s, 6H), 0.66 (q, *J* = 7.9 Hz, 6H)

^{13}C NMR (101 MHz, $CDCl_3$) δ 83.7, 52.2, 46.1, 36.2, 31.2, 28.5, 28.0, 6.9, 4.0



***trans*-31b** ***cis*-31b**

Compound **31b**: Triethyl(((1*S*,6*R*)-3,7,7-trimethylbicyclo[4.1.0]heptan-3-yl)peroxy)silane

Scale: 1.0 mmol

Yield: From **31a**: 89% (*cis/trans* = *1.1:1.0*)

From **32a**: 99% (*cis/trans* = *1.1:1.0*)

Physical State: clear liquid

Purification: SiO_2 (pentane)

***trans*-31b**: R_f = 0.59 (pentane + vanillin stain)

***cis*-31b**: R_f = 0.38 (pentane + vanillin stain)

IR (ATR, neat) $\tilde{\nu}_{max}$: 2953, 2937, 2915, 2876, 2814, 2733, 1542, 1517, 1508, 1459, 1414, 1368, 1345, 1311, 1267, 1237, 1148, 1134, 1118, 1091, 1057, 1007, 971, 939, 876, 836, 811, 786, 729, 695, 673, 650, 643, 630, 615, 601 cm^{-1}

HRMS–DART (*m/z*): $[M + H]^+$ calc'd for $C_{16}H_{33}O_2Si$, 285.2244, found 285.2250

***cis*-31b**: **Specific Rotation**: $[\alpha]_D^{22.0}$ +4.00 (*c* 1.0, $CHCl_3$)

***trans*-31b**: **Specific Rotation**: $[\alpha]_D^{22.6}$ +18.0 (*c* 1.0, $CHCl_3$)

***cis*-31b**

^{1}H NMR (400 MHz, $CDCl_3$) δ 1.92–1.78 (m, 2H), 1.63 (dddd, *J* = 14.8, 6.7, 4.3, 2.4 Hz, 1H), 1.42–1.21 (m, 3H), 1.24 (s, 3H), 1.01–0.94 (m, 15H), 0.72–0.60 (m, 7H), 0.47 (ddd, *J* = 9.0, 7.8, 2.4 Hz, 1H)

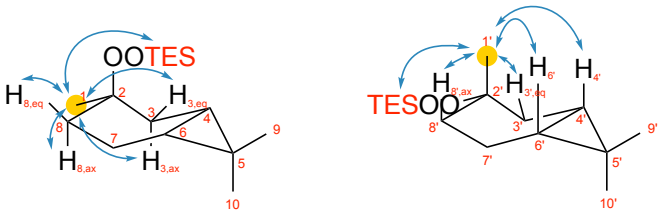
^{13}C NMR (101 MHz, $CDCl_3$) δ 82.5, 31.2, 29.2, 28.7, 22.6, 19.8, 18.8, 18.1, 17.7, 15.1, 7.0, 4.1

***trans*-32b**

^{1}H NMR (300 MHz, $CDCl_3$) δ 2.17 (ddd, *J* = 15.5, 9.1, 2.5 Hz, 1H), 1.88 (ddt, *J* = 14.2, 11.0, 7.4 Hz, 1H), 1.67 (ddt, *J* = 14.3, 7.7, 2.6 Hz, 1H), 1.48–1.34 (m, 1H), 1.13 (s, 3H), 1.06–0.94 (m, 14H), 0.91 (s, 3H), 0.68 (qd, *J* = 7.8, 1.0 Hz, 6H), 0.60–0.49 (m, 2H)

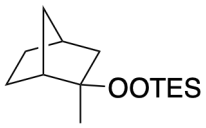
^{13}C NMR (126 MHz, $CDCl_3$) δ 79.1, 31.3, 29.3, 28.2, 25.6, 19.1, 18.0, 17.2, 16.3, 15.0, 7.0, 4.1

HSQC and **1D selective gradient NOESY** spectra are provided to support the configurational assignments. NOE correlations are presented below. See Section 3.6.10 for more details.





***endo*-33b**



***exo*-33b**

Compound **33b**: Triethyl((2-methylbicyclo[2.2.1]heptan-2-yl)peroxy)silane

Scale: 1.00 mmol

Yield: 99% (*exo/endo* = *3.3:1.0*) [isolated as a mixture of diastereomers]

Physical State: clear liquid

Purification: SiO_2 (pentane)

***endo*-33b**: R_f = 0.64 (pentane + vanillin stain)

***exo*-33b**: R_f = 0.44 (pentane + vanillin stain)

IR (ATR, neat) $\tilde{\nu}_{max}$: 2953, 2876, 1459, 1369, 1238, 1006, 833, 801, 741 cm^{-1}

HRMS–DART (*m/z*): $[M + H]^+$ calc'd for $C_{14}H_{29}O_2Si$, 257.1931, found 257.1938

***exo*-33b**

^{1}H NMR (400 MHz, $CDCl_3$) δ 2.42–2.35 (m, 1H), 2.21–2.11 (m, 1H), 1.77–1.70 (m, 1H), 1.58–1.01 (m, 10H), 1.02–0.94 (m, 9H), 0.74–0.62 (m, 6H)

^{13}C NMR (101 MHz, $CDCl_3$) δ 89.7, 44.5, 44.2, 37.3, 36.8, 28.6, 23.9, 20.7, 7.0, 4.1

***endo*-33b**

^{1}H NMR (400 MHz, $CDCl_3$) δ 2.24–2.21 (m, 1H), 2.20–2.12 (m, 1H), 1.97–1.87 (m, 1H), 1.58–1.01 (m, 10H), 0.98 (td, *J* = 8.0, 1.9 Hz, 9H), 0.74–0.62 (m, 6H)

^{13}C NMR (101 MHz, $CDCl_3$) δ 89.1, 46.5, 43.8, 38.7, 36.8, 28.5, 24.8, 22.3, 7.0, 4.1

HSQC, **HMBC**, and **1D selective gradient NOESY** spectra are provided to support the configurational assignments. NOE correlations are presented below. See Section 3.6.10 for more details.





***exo*-34b** ***endo*-34b**

Compound **34b**: Triethyl(((1*R*,5*S*)-2,6,6-trimethylbicyclo[3.1.1]heptan-2-yl)peroxy)silane

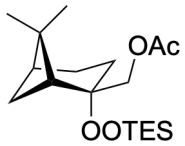
Scale: 1.0 mmol

Yield: 86% (*endo/exo = 2.0:1.0*)

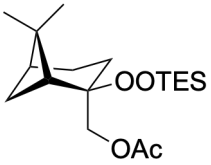
***exo*-34b**: **Specific Rotation**: $[\alpha]_D^{22.9}$ –28.0 (*c* 1.0, $CHCl_3$)

***endo*-34b**: **Specific Rotation**: $[\alpha]_D^{23.4}$ –4.00 (*c* 1.0, $CHCl_3$)

See **21b** for additional characterization.



***exo*-35b**



***endo*-35b**

Compound **35b**: ((1*R*,5*S*)-6,6-Dimethyl-2-((triethylsilyl)peroxy)bicyclo[3.1.1]heptan-2-yl)methyl acetate

Scale: 1.0 mmol

Yield: 94% (*exo/endo* = *2.3:1.0*)

Physical State: yellow liquid

Purification: SiO_2 (50% *v/v* DCM/pentane) [isolated as a mixture of diastereomers]

R_f = 0.55, 0.36 (50% *v/v* DCM/pentane)

IR (ATR, neat) $\tilde{\nu}_{max}$: 2952, 2916, 2877, 2359, 1697, 1419, 1365, 1285, 1262, 1243, 1154, 1140, 1087, 1006, 989, 966, 896, 851, 822, 804, 733, 675 cm^{-1}

HRMS–DART (*m/z*): $[M + H]^+$ calc'd for $C_{18}H_{35}O_4Si$, 343.2299, found 343.2305

***exo*-35b**

^{1}H NMR (500 MHz, CDCl3) δ 4.31 (d, *J* = 11.9 Hz, 1H), 4.19 (d, *J* = 11.9 Hz, 1H), 2.25–2.20 (m, 1H), 2.20–2.12 (m, 1H), 2.06 (s, 3H), 1.94–1.83 (m, 2H), 1.83–1.72 (m, 2H), 1.69–1.58 (m, 1H), 1.50 (d, *J* = 9.9 Hz, 1H), 1.25 (s, 3H), 1.0–0.9 (t, *J* = 8.0, 9H), 0.96 (s, 3H), 0.64 (qd, *J* = 7.9, 2.1 Hz, 6H)

^{13}C NMR (126 MHz, CDCl3) δ 171.5, 86.7, 65.8, 45.4, 40.8, 37.97, 27.8, 26.2, 24.5, 23.38, 22.7, 21.0, 6.8, 3.9

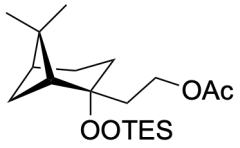
***endo*-35b**

^{1}H NMR (500 MHz, CDCl3) δ 4.26 (d, *J* = 11.6 Hz, 1H), 4.08 (d, *J* = 11.7 Hz, 1H), 2.25–2.20 (m, 1H), 2.20–2.12 (m, 1H), 2.06 (s, 3H), 1.94–1.83 (m, 2H), 1.83–1.72 (m, 2H), 1.69–1.58 (m, 1H), 1.21 (s, 3H), 1.10 (d, *J* = 10.4 Hz, 1H), 1.0–0.9 (t, *J* = 8.0, 9H), 0.96 (s, 3H), 0.64 (qd, *J* = 7.9, 2.1 Hz, 6H)

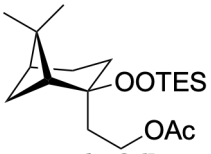
^{13}C NMR (126 MHz, CDCl3) δ 171.4, 87.8, 65.0, 45.0, 41.0, 38.0, 27.6, 27.4, 23.9, 23.41, 22.4, 21.1, 6.8, 3.9

1D Selective Gradient NOESY spectrum is provided to support the configurational assignments. NOE correlations are presented below. See Section 3.6.10 for more details.





***exo*-36b**



***endo*-36b**

Compound **36b**: 2-((1*R*,5*S*)-6,6-Dimethyl-2-((triethylsilyl)peroxy)bicyclo[3.1.1]heptan-2-yl)ethyl acetate

Scale: 1.0 mmol

Yield: 94% (*exo/endo = 4.0:1.0*)

Physical State: yellow liquid

Purification: SiO_2 (0–5% *v/v* Et_2O/pentane) [isolated as a mixture of diastereomers]

R_f = 0.50, 0.43 (5% *v/v* EtOAc/hexanes + vanillin stain)

IR (ATR, neat) $\tilde{\nu}_{max}$: 2953, 2937, 2915, 2876, 2368, 2320, 2310, 1745, 1698, 1689, 1542, 1508, 1488, 1459, 1416, 1380, 1363, 1313, 1288, 1236, 1161, 1093, 1043, 1020, 1007, 975, 917, 875, 839, 821, 803, 740, 730, 690, 674, 631, 603 cm^{-1}

HRMS–DART (*m/z*): $[M + H]^+$ calc'd for $C_{19}H_{37}O_4Si$, 357.2456, found 357.2460.

***exo*-36b**

^{1}H NMR (500 MHz, $CDCl_3$) δ 4.26–4.08 (m, 2H), 2.34–1.64 (m, 12H), 1.42 (d, *J* = 10.2 Hz, 1H), 1.26 (s, 3H), 1.03–0.90 (m, 12H), 0.73–0.59 (m, 6H)

^{13}C NMR (126 MHz, C_6D_6) δ 170.21, 87.7, 61.41, 48.9, 40.9, 38.1, 36.8, 27.89, 27.0, 25.9, 25.1, 23.5, 20.72, 7.1, 4.2

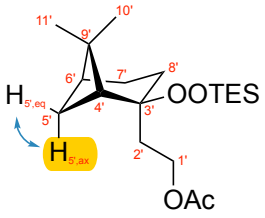
***endo*-36b**

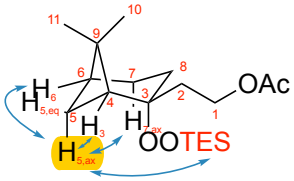
^{1}H NMR (500 MHz, $CDCl_3$) δ 4.26–4.08 (m, 2H), 2.34–1.64 (m, 12H), 1.19 (s, 3H), 1.08 (d, *J* = 10.4 Hz, 1H), 1.03–0.90 (m, 12H), 0.73–0.59 (m, 6H)

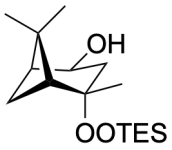
^{13}C NMR (126 MHz, C_6D_6) δ 170.23, 89.1, 61.43, 48.3, 41.2, 38.2, 36.5, 27.86, 27.78, 26.5, 24.5, 23.7, 20.68, 7.1, 4.2

1D selective gradient NOESY spectrum is provided to support the configurational assignments. NOE correlations are presented below. See Section 3.6.10 for more details.

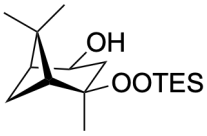
Note: When ^{13}C NMR spectrum was measured in $CDCl_3$, the signals at 61.7 and 38.1 were incidental.







***exo*-37b**



***endo*-37b**

Compound **37b**: (1*S*,2*S*,5*R*)-4,6,6-Trimethyl-4-((triethylsilyl)peroxy)bicyclo[3.1.1]heptan-2-ol

Scale: 1.0 mmol

Yield: 92% (*exo/endo* = *4.0:1.0*) [isolated as a mixture of diastereomers]

Physical State: white solid

Melting Point: 28 ºC

Purification: SiO_2 (0–10% *v/v* Et_2O/hexanes).

R_f = 0.27 (10% *v/v* EtOAc/hexanes + vanillin stain) [incidental R_f]

IR (ATR, neat) $\tilde{\nu}_{max}$: 3357, 2953, 2918, 2876, 1508, 1461, 1415, 1386, 1369, 1357, 1335, 1317, 1253, 1236, 1112, 1087, 1051, 1016, 1005, 975, 942, 913, 893, 875, 850, 814, 739, 729 cm^{-1}

HRMS–DART (*m/z*): $[M + H]^+$ calc'd for $C_{16}H_{33}O_3Si$, 301.2193, found 301.2185

***exo*-37b**

^{1}H NMR (400 MHz, $CDCl_3$) δ 4.20 (ddd, *J* = 9.2, 5.6, 2.6 Hz, 1H), 2.45–2.25 (m, 1H), 2.19–1.96 (m, 3H), 1.69 (dt, *J* = 11.4, 5.6 Hz, 2H), 1.37 (s, 3H), 1.30 (s, 3H), 1.12 (s, 3H), 1.02–0.90 (m, 9H), 0.79 (d, *J* = 10.9 Hz, 1H), 0.71–0.59 (m, 6H)

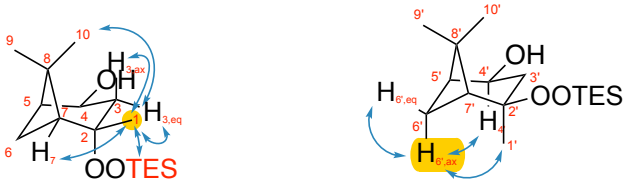
^{13}C NMR (101 MHz, $CDCl_3$) δ 85.0, 71.8, 50.3, 48.6, 39.4, 38.0, 28.8, 25.6, 25.2, 24.7, 6.9, 4.0

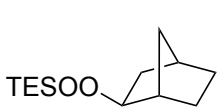
***endo*-37b**

^{1}H NMR (400 MHz, $CDCl_3$) δ 4.20 (ddd, *J* = 9.2, 5.6, 2.6 Hz, 1H), 2.50–2.22 (m, 1H), 2.22–1.93 (m, 3H), 1.69 (dt, *J* = 11.4, 5.6 Hz, 2H), 1.30 (s, 3H), 1.23 (s, 3H), 1.19 (s, 3H), 1.02–0.88 (m, 9H), 0.90–0.86 (m, 1H), 0.74–0.57 (m, 6H)

^{13}C NMR (101 MHz, $CDCl_3$) δ 86.3, 72.4, 50.0, 48.6, 40.4, 37.8, 28.3, 27.2, 25.9, 24.9, 6.9, 4.0

HMBC, **HSQC**, and **1D Selective Gradient NOESY** spectra are provided to support configurational assignments. NOE correlations are presented below. See Section 3.6.10 for more details.





***exo*-38b**



***endo*-38b**

Compound **38b**: ((Bicyclo[2.2.1]heptan-2-yl)peroxy)triethylsilane

Scale: 1.0 mmol

Yield: 65% (*exo/endo = 2.6:1.0*) [isolated as a mixture of diastereomers]

Physical State: clear liquid

Purification: SiO_2 (pentane)

***endo*-38b**: R_f = 0.36 (pentane + vanillin stain)

***exo*-38b**: R_f = 0.21 (pentane + vanillin stain)

IR (ATR, neat) $\tilde{\nu}_{max}$: 2954, 2913, 2875, 1458, 1414, 1378, 1349, 1238, 1182, 1158, 1084, 1017, 1006, 984, 976, 948, 935, 925, 913, 882, 851, 831, 817, 790, 728, 673, 627 cm^{-1}

HRMS–DART (*m/z*): $[M + H]^+$ calc'd for $C_{13}H_{27}O_2Si$, 243.1775, found 243.1779

***exo*-38b**

^{1}H NMR (400 MHz, $CDCl_3$) δ 3.98 (ddt, *J* = 7.2, 2.3, 1.2 Hz, 1H), 2.54 (d, *J* = 4.9 Hz, 1H), 2.26–2.18 (m, 1H), 1.58–1.38 (m, 4H), 1.38–1.12 (m, 1H), 1.13–0.93 (m, 12H), 0.79–0.61 (m, 6H)

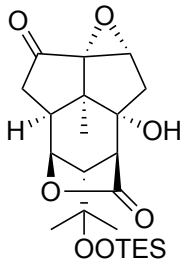
^{13}C NMR (101 MHz, $CDCl_3$) δ 88.1, 39.7, 36.9, 35.2, 34.6, 28.7, 24.2, 6.9, 4.0

endo-38b

^{1}H NMR (400 MHz, $CDCl_3$) δ 4.40 (dtd, *J* = 10.5, 3.8, 1.6 Hz, 1H), 2.51 (q, *J* = 2.8 Hz, 1H), 2.18–2.13 (m, 1H), 1.89–1.70 (m, 2H), 1.58–1.38 (m, 1H), 1.38–1.16 (m, 4H), 1.12–0.93 (m, 9H), 0.89 (dt, *J* = 13.3, 3.7 Hz, 1H), 0.76–0.62 (m, 6H)

^{13}C NMR (101 MHz, $CDCl_3$) δ 86.2, 40.2, 37.6, 36.6, 35.5, 29.8, 20.5, 6.9, 4.0

HSQC supports the ^{1}H and ^{13}C assignments. The chemical shift and coupling constants of 2º peroxide proton signal support an axial hydrogen for the major diastereomer, which is consistent with an *exo*-configuration for the peroxide. Reported ^{1}H NMR values for *endo*-norborneol and *exo*-norborneol also support this conclusion [108].



F7b

Compound **F7b**: (1a*R*,2a*R*,2a^1*R*,3*S*,6*S*,6a*S*,8a*S*,9*S*)-2a-Hydroxy-2a^1-methyl-9-(2-((triethylsilyl)peroxy)propan-2-yl)hexahydro-3,6-methanooxireno[2',3':3a,4]pentaleno[1,6-*cd*]oxepine-4,8(2a^1*H*,6*H*)-dione

*****Solvent used was 4:1 DCE/EtOAc

Scale: 28 mg

Yield: 68%

Physical State: white solid

Melting Point: 176–180 °C

Purification: (SiO_2, 0–30% *v/v* EtOAc/hexanes)

R_f = 0.711 (40% *v/v* EtOAc/hexanes)

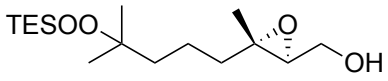
IR (ATR, neat) $\tilde{\nu}_{max}$: 3454, 2959, 2939, 2918, 2878, 1798, 1508, 1488, 1457, 1435, 1415, 1396, 1379, 1357, 1329, 1306, 1256, 1240, 1169, 1152, 1124, 1065, 1039, 1010, 992, 978, 940, 930, 913, 797, 779, 734 cm^{-1}

HRMS–DART (*m/z*): $[M + H]^+$ calc'd for $C_{21}H_{33}O_8Si$, 441.1939, found 441.1936

Specific Rotation: $[\alpha]_D^{26}$ –22.7 (*c*. 1.0, $CHCl_3$)

^{1}H NMR (500 MHz, $CDCl_3$): δ 4.95 (dd, *J* = 4.9, 3.2 Hz, 1H), 4.64 (d, *J* = 3.3 Hz, 1H), 4.16 (s, 1H), 3.73 (d, *J* = 3.3 Hz, 1H), 2.88–2.77 (m, 3H), 2.14 (d, *J* = 15.0 Hz, 1H), 1.54 (d, *J* = 7.3 Hz, 6H), 1.32 (s, 3H), 1.00 (t, *J* = 8.0 Hz, 9H), 0.75 (qd, *J* = 7.9, 2.0 Hz, 6H)

^{13}C NMR (126 MHz, $CDCl_3$): δ 173.4, 169.3, 85.3, 82.9, 79.7, 73.2, 62.0, 52.8, 50.1, 47.9, 43.1, 24.94, 24.89, 16.4, 6.7, 4.4



F8b

Compound **F8b**: ((2*S*,3*S*)-3-Methyl-3-(4-methyl-4-((triethylsilyl)peroxy)pentyl)oxiran-2-yl)methanol

Scale: 1.0 mmol

Yield: 62%

Physical State: clear liquid

Purification: SiO_2 (0–25% *v/v* EtOAc/hexanes)

R_f = 0.36 (30% *v/v* EtOAc/hexanes + vanillin stain)

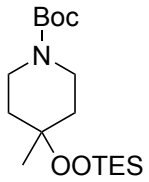
IR (ATR, neat) $\tilde{\nu}_{max}$: 3422, 2954, 2939, 2918, 2877, 2363, 1743, 1665, 1599, 1521, 1461, 1416, 1381, 1363, 1240, 1202, 1148, 1097, 1091, 1039, 1018, 973, 859, 851, 806, 774, 743, 687, 677, 662, 642, 635, 627, 616, 608 cm^{-1}

HRMS–DART (*m/z*): $[M + H]^+$ calc'd for $C_{16}H_{35}O_4Si$, 319.2299, found 319.2304

Specific Rotation: $[\alpha]_D^{24.8}$ +4.00 (*c* 1.0, $CHCl_3$)

^{1}H NMR (500 MHz, $CDCl_3$) δ 3.84 (dd, *J* = 12.2, 4.3 Hz, 1H), 3.70 (dd, *J* = 12.1, 6.7 Hz, 1H), 2.97 (dd, *J* = 6.6, 4.5 Hz, 1H), 1.63 (qd, *J* = 8.5, 3.4 Hz, 2H), 1.57–1.48 (m, 2H), 1.48–1.38 (m, 3H), 1.30 (d, *J* = 1.3 Hz, 3H), 1.17 (d, *J* = 1.9 Hz, 6H), 1.03–0.91 (m, 9H), 0.66 (q, *J* = 8.0 Hz, 6H)

^{13}C NMR (126 MHz, $CDCl_3$) δ 82.2, 62.9, 61.6, 61.4, 38.9, 38.7, 24.5, 24.3, 19.7, 16.8, 7.0, 4.0



F9b

Compound **F9b**: *tert*-Butyl 4-methyl-4-((triethylsilyl)peroxy)piperidine-1-carboxylate

Scale: 1.0 mmol

Yield: 96%

Physical State: clear liquid

Purification: SiO_2 (0–5% *v/v* EtOAc/hexanes)

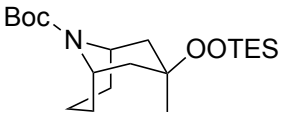
$\boldsymbol{R_f}$ = 0.52 (10 *v/v* EtOAc/hexanes + vanillin stain)

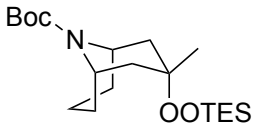
IR (ATR, neat) $\tilde{\nu}_{max}$: 3383, 2956, 2877, 2359, 1697, 1419, 1365, 1285, 1262, 1243, 1154, 1140, 1087, 1006, 989, 966, 896, 851, 822, 804, 733, 675 cm^{-1}

HRMS–DART (*m/z*): $[M]^+$ calc'd for $C_{17}H_{35}NO_4Si$, 345.2330, found 345.2320

^{1}H NMR (400 MHz, $CDCl_3$): δ 3.64 (d, *J* = 13.4 Hz, 2H), 3.18–3.06 (m, 2H), 1.89–1.77 (m, 2H), 1.44 (s, 11H), 1.21 (s, 3H), 0.97 (t, *J* = 7.9 Hz, 9H), 0.66 (q, *J* = 0.8 Hz, 6H)

^{13}C NMR (101 MHz, $CDCl_3$): δ 155.0, 79.4, 79.1, 40.1, 34.2, 28.6, 24.6, 6.9, 4.0





***exo*-F10b** ***endo*-F10b**

Compound **F10b**: *tert*-Butyl 3-methyl-3-((triethylsilyl)peroxy)-9-azabicyclo[3.3.1]nonane-9-carboxylate

Scale: 1.0 mmol

Yield: 70% (*exo/endo* = *2.3:1.0*)

Physical State: clear liquid

Purification: SiO_2 (0–10% *v/v* EtOAc/hexanes) [isolated as a mixture of diastereomers]

***endo*-F10b**: R_f = 0.61 (10% *v/v* EtOAc/hexanes + vanillin stain)

***exo*-F10b**: R_f = 0.53 (10% *v/v* EtOAc/hexanes + vanillin stain)

HRMS–DART (*m/z*): $[M + H]^+$ calc'd for $C_{20}H_{40}NO_4Si$, 386.2721, found 386.2729

IR (ATR, neat) $\tilde{\nu}_{max}$: 2958, 2944, 2933, 2907, 2878, 1692, 1470, 1456, 1446, 1424, 1365, 1335, 1328, 1317, 1264, 1255, 1178, 1139, 1101, 1086, 1011, 810, 797, 738, 722, 715, 703, 692, 676, 665, 656, 647, 633, 618 cm^{-1}

***exo*-F10b**

^{1}H NMR (400 MHz, $CDCl_3$): δ 4.32 (dd, *J* = 43.8, 9.3 Hz, 2H), 2.44–2.30 (m, 2H), 1.84–1.71 (m, 1H), 1.73–1.55 (m, 1H), 1.54–1.44 (m, 3H), 1.42 (s, 9H), 1.29 (ddd, *J* = 15.4, 10.2, 2.8 Hz, 3H), 1.24 (s, 3H), 0.93 (t, *J* = 7.9 Hz, 9H), 0.72–0.51 (m, 6H)

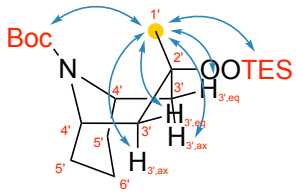
^{13}C NMR (101 MHz, $CDCl_3$): δ 153.9, 79.9, 78.6, 44.0, 42.6, 34.0, 33.6, 32.2, 31.6, 28.6, 26.7, 14.7, 6.9, 3.8

***endo*-F10b**

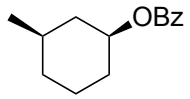
^{1}H NMR (400 MHz, $CDCl_3$): δ 4.28 (d, *J* = 50.0 Hz, 2H), 2.23 (ddt, *J* = 13.8, 11.8, 6.1 Hz, 1H), 1.96 (d, 2H), 1.87–1.59 (m, 4H), 1.56–1.46 (m, 2H), 1.45 (s, 9H), 1.38–1.30 (m, 1H), 1.19 (s, 3H), 0.98 (t, *J* = 7.9 Hz, 9H), 0.68 (q, 6H)

^{13}C NMR (101 MHz, $CDCl_3$): δ 154.3, 79.5, 79.2, 45.6, 44.1, 36.4, 36.1, 29.8, 29.4, 28.7, 28.6, 15.3, 6.9, 4.0

HSQC and **1D Selective Gradient NOESY** spectra are provided to support configurational assignments. NOE correlations are presented below. We were unable to measure **1D Selective Gradient NOESY** for ***exo*-F10b** due to overlapping signals. See Section 3.6.10 for more details.



3.6.8.3 Hydrodealkenylation Products



1c

Compound **1c**: (1*S*,3*R*)-3-Methylcyclohexyl Benzoate

Yield: 95%

Physical State: white solid

Melting Point: 64–66 ºC

Purification: SiO_2 (0–4% *v/v* EtOAc/hexanes)

R_f = 0.77 (15% *v/v* EtOAc/hexanes + UV)

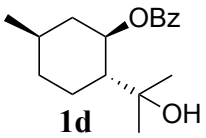
IR (ATR, neat) $\tilde{\nu}_{max}$: 2950, 2863, 1717, 1451, 1316, 1279, 1176, 1114, 1070, 1041, 1026, 973, 931, cm^{-1}

HRMS–ESI (*m/z*): $[M + H]^+$ calc'd for $C_{14}H_{19}O_2$, 219.1380, found 219.1391

Specific Rotation: $[\alpha]_D^{26.1}$ –12.0 (*c* 1.0, $CHCl_3$)

^{1}H NMR (500 MHz, $CDCl_3$) δ 8.06–8.01 (m, 2H), 7.58–7.50 (m, 1H), 7.46–7.39 (m, 2H), 4.95 (tt, *J* = 11.0, 4.4 Hz, 1H), 2.13–2.05 (m, 2H), 1.83 (dt, *J* = 13.0, 3.4 Hz, 1H), 1.73–1.64 (m, 1H), 1.64–1.50 (m, 1H), 1.47–1.30 (m, 2H), 1.13 (q, *J* = 12.1 Hz, 1H), 0.96 (d, *J* = 6.6 Hz, 3H), 0.88 (qd, *J* = 12.8, 4.0 Hz, 1H)

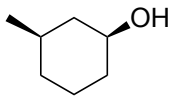
^{13}C NMR (126 MHz, $CDCl_3$) δ 166.2, 132.8, 131.1, 129.7, 128.4, 74.0, 40.7, 34.2, 31.7, 31.5, 24.1, 22.5



1d

Compound **1d**: 2-(2-Hydroxypropan-2-yl)-5-methylcyclohexyl Benzoate

Characterization data match those previously reported in the literature [109].



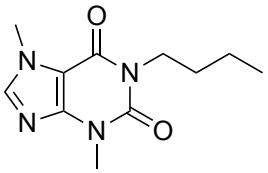
2c

Compound **2c**: (1*S*,3*R*)-3-Methylcyclohexan-1-ol

Scale: 1.00 mmol

Yield: 76%

Characterization data match those previously reported in the literature [74].



3c

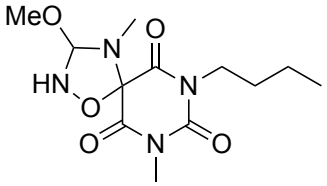
Compound **3c**: 1-Butyl-3,7-dimethyl-3,7-dihydro-1*H*-purine-2,6-dione

* 4:1 *n*PrOH/H_2O was used as the solvent

Scale: 110 mg

Yield: 64%

Characterization data match those previously reported in the literature [110].



3x

Compound **3x**: 7-butyl-3-methoxy-4,9-dimethyl-1-oxa-2,4,7,9-tetraazaspiro[4.5]decane-6,8,10-trione

Scale: 0.50 mmol

Yield: 42%

Physical State: clear liquid

Purification: SiO_2 (0–70% *v/v* EtOAc/hexanes)

$\boldsymbol{R_f}$ = 0.68 (10% *v/v* MeOH/DCM + UV)

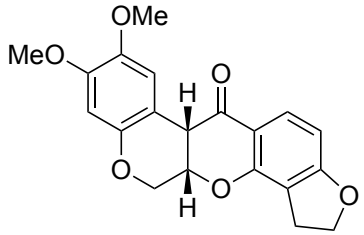
IR (ATR, neat) $\tilde{\nu}_{max}$: 3358, 2962, 2874, 1718, 1660, 1500, 1436, 1397, 1336, 1249, 1196, 1097, 1062, 976, 917, 763, 751, 732, 647, 629, 609 cm^{-1}

HRMS–ESI (*m/z*): $[M–OMe]^+$ calc'd for $C_{11}H_{17}N_4O_4$, 269.1244, found 269.1242

^{1}H NMR (500 MHz, CDCl3) δ 6.03 (s, 1H), 5.16 (s, 1H), 3.85 (ddd, *J* = 13.5, 10.3, 5.4 Hz, 1H), 3.64 (ddd, *J* = 13.5, 10.3, 5.4 Hz, 1H), 3.49 (s, 3H), 3.18 (s, 3H), 2.93 (s, 3H), 1.56 (ddtd, *J* = 13.5, 10.3, 7.5, 5.4 Hz, 1H), 1.40 (ddtd, *J* = 13.5, 10.3, 7.5, 5.4 Hz, 1H), 1.29 (sext, *J* = 7.5 Hz, 2H), 0.89 (t, *J* = 7.5 Hz, 3H)

^{13}C NMR (126 MHz, CDCl3) δ 164.6, 151.8, 149.9, 93.1, 86.1, 53.5, 42.7, 31.4, 28.6, 27.0, 20.1, 13.8

HSQC spectrum indicates the singlet at 6.03 ppm is a C–H. See Section 3.6.10.



4c

Compound **4c**: (6a*S*,12a*S*)-8,9-Dimethoxy-1,2,12,12a-tetrahydrochromeno[3,4-*b*]furo[2,3-*h*]chromen-6(6a*H*)-one

Scale: 50 mg

Yield: 97%

Physical State: white solid

Purification: SiO_2 (0–25% *v/v* EtOAc/hexanes)

Melting Point: 188 ºC (decomposition)

$\boldsymbol{R_f}$ = 0.28 (30% *v/v* EtOAc/hexanes + UV/vanillin stain)

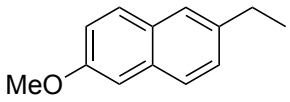
IR (ATR, neat) $\tilde{\nu}_{max}$: 2920, 2858, 1670, 1605, 1508, 1454, 1408, 1350, 1308, 1246, 1203, 1084, 1045, 1007, 910, 868, 818, 779, 725, 652 cm^{-1}

HRMS–ESI (*m/z*): $[M + H]^+$ calc'd for $C_{20}H_{19}O_6$, 355.1176, found 355.1193

Specific Rotation: $[\alpha]_D^{24.5}$ –16.0 (*c* 1.0, $CHCl_3$)

^{1}H NMR (500 MHz, C_6D_6) δ 8.13 (d, *J* = 8.4 Hz, 1H), 7.20 (s, 1H), 6.51 (s, 1H), 6.36 (d, *J* = 8.5 Hz, 1H), 4.24 (dd, *J* = 12.1, 2.9 Hz, 1H), 4.07 (t, *J* = 3.4 Hz, 1H), 3.96–3.88 (m, 1H), 3.81 (dt, *J* = 10.4, 8.3 Hz, 1H), 3.58 (d, *J* = 4.0 Hz, 1H), 3.48 (d, *J* = 12.1 Hz, 1H), 3.39 (s, 3H), 3.23 (s, 3H), 2.56 (ddd, *J* = 15.3, 10.5, 7.9 Hz, 1H), 2.42 (ddd, *J* = 15.3, 10.3, 6.9 Hz, 1H)

^{13}C NMR (126 MHz, C6D6) δ 188.6, 168.1, 158.3, 151.0, 148.2, 145.4, 114.0, 113.6, 111.9, 105.5, 105.2, 102.1, 72.7, 72.5, 66.2, 56.2, 55.4, 45.1, 26.4



5c

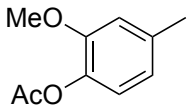
Compound **5c**: 2-Ethyl-6-methoxynaphthalene

* 4:1 *n*PrOH/H_2O was used as the solvent

Scale: 240 mg

Yield: 13%

Characterization data match those previously reported in the literature [111].



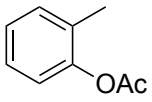
6c

Compound **6c**: 2-Methoxy-4-methylphenyl acetate

Scale: 50 mg

Yield: 61% (NMR yield versus 1-chloro-2,4-dinitrobenzene)

Characterization data match those previously reported in the literature [112].



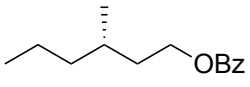
7c

Compound **7c**: *o*-Tolyl acetate

Scale: 100 mg

Yield: 50% (NMR yield versus 1-chloro-2,4-dinitrobenzene)

Characterization data match those previously reported in the literature [113].



9c

Compound **9c**: (*S*)-3-Methylhexyl benzoate

Scale: 0.50 mmol

Yield: 40%

Physical State: clear liquid

Purification: aqueous extraction then SiO_2 (0–4% *v/v* EtOAc/hexanes)

R_f = 0.71 (15% *v/v* EtOAc/hexanes + UV/vanillin stain)

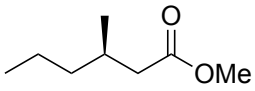
HRMS–ESI (*m/z*): $[M + H]^+$ calc'd for $C_{14}H_{21}O_2$, 221.1536, found 221.1537

IR (ATR, neat) $\tilde{\nu}_{max}$: 3068, 2928, 2871, 2845, 1718, 1682, 1602, 1585, 1452, 1381, 1314, 1269, 1175, 1109, 1070, 1026, 947, 708 cm^{-1}

Specific Rotation: $[\alpha]_D^{23.0}$ +10.0 (*c* 1.0, $CHCl_3$)

^{1}H NMR (500 MHz, $CDCl_3$) δ 8.27–7.95 (dd, *J* = 8.3, 1.3 Hz, 2H), 7.58–7.51 (m, 1H), 7.43 (t, *J* = 7.8 Hz, 2H), 4.43–4.30 (m, 2H), 1.87–1.75 (m, 1H), 1.73–1.61 (m, 1H), 1.61–1.53 (m, 1H), 1.45–1.24 (m, 3H), 1.25–1.12 (m, 1H), 0.95 (d, *J* = 6.6 Hz, 3H), 0.90 (t, *J* = 7.1 Hz, 3H)

^{13}C NMR (126 MHz, $CDCl_3$) δ 166.8, 132.9, 130.7, 129.6, 128.4, 63.7, 39.3, 35.7, 29.8, 20.1, 19.7, 14.4



10c

Compound **10c**: Methyl (*R*)-3-Methylhexanoate

Scale: 50 mg

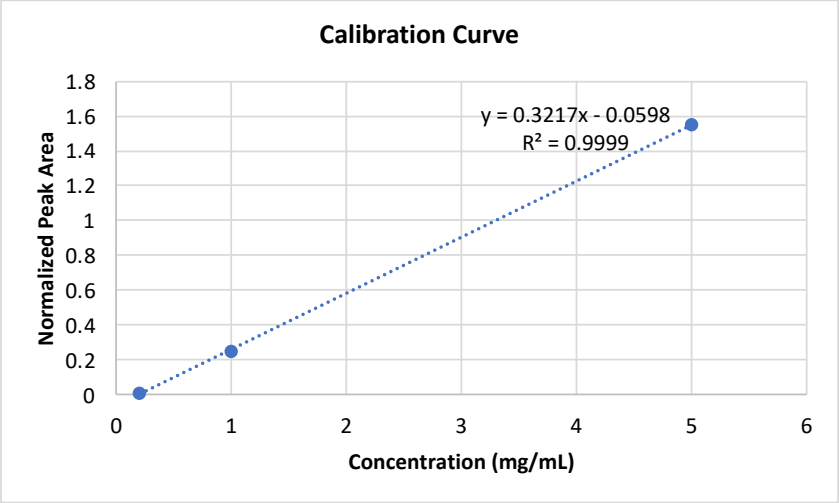
Yield: 67% (GCMS)

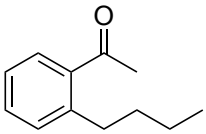
Characterization data are available in the literature for the enantiomeric compound [114].

GCMS yield was conducted using cyclododecanone as an internal standard (IS) with methyl hexanoate as a reference. A 50 mL stock solution of cyclododecanone (50.0 mg) in MeOH (1 mg/mL) was prepared in a volumetric flask. Methyl hexanonate (100.0 mg) was administered into a 10-mL volumetric flask and was dissolved using the stock solution of IS. The 10 mg/mL reference solution was serially diluted to concentrations of 1 and 0.2 mg/mL using the IS stock solution. Samples were prepared and measured in triplicate. A calibration curve was generated by plotting normalized peak area versus concentration, providing a linear regression equation,

$$y = 0.3217x - 0.0598$$

with a variance of R^2 = 0.9999. The crude reaction mixture was transferred to a 3-mL volumetric flask containing cyclododecanone (3.00 mg) and diluted with methanol. A normalized peak area value of 1.5795 was measured (3.918 min retention time versus 6.670 min IS), corresponding to a concentration of 5.0958 mg/mL. Multiplying by the known volume (3.00 mL), provided a mass of 15.3 mg. The calculated yield based on this mass was 67%.





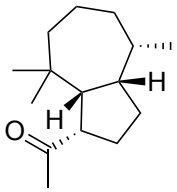
11c

Compound **11c**: 1-(2-Butylphenyl)ethan-1-one

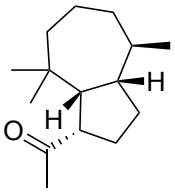
Scale: 150 mg

Yield: 75%

Characterization data match those previously reported in the literature [115].



***cis*-12c**



***trans*-12c**

Compound **12c**: 1-((1*S*,3a*S*,8a*R*)-4,8,8-Trimethyldecahydroazulen-1-yl)ethan-1-one

* 2.2 equivalents of PhSH were used, instead of γ-terpinene (1.5 equiv) and PhSH (10 mol%)

Scale: 0.41 mmol

Yield: 86% (*cis/trans* = *1.0:1.0*) [isolated as a mixture of diastereomers]

Physical State: clear liquid

Purification: SiO_2 (0–2% *v/v* EtOAc/hexanes)

$\boldsymbol{R_f}$ = 0.64, 0.63 (10% *v/v* EtOAc/hexanes + vanillin stain)

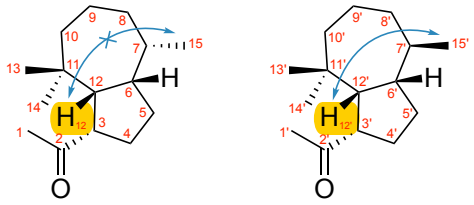
IR (ATR, neat) $\tilde{\nu}_{max}$: 2952, 2930, 2869, 1706, 1471, 1456, 1391, 1363, 1350, 1157, 772 cm^{-1}

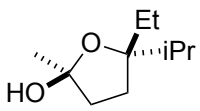
HRMS–DART (*m/z*): $[M]^+$ calc'd for $C_{15}H_{26}O$, 222.1978, found 222.1968

^{1}H NMR (500 MHz, $CDCl_3$) δ 3.15–2.85 (m, 1H), 2.40–1.74 (m, 8H), 1.66–1.29 (m, 7H), 1.28–1.18 (m, 1H), 1.04–0.84 (m, 9H).

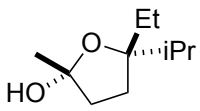
^{13}C NMR (126 MHz, $CDCl_3$) δ 212.8, 212.2, 58.7, 57.8, 56.7, 56.4, 54.3, 54.1, 53.2, 49.8, 45.9, 39.4, 38.1, 37.7, 37.6, 33.9, 33.8, 32.7, 31.7, 30.4, 28.6, 28.1, 27.1, 26.8, 26.0, 25.2, 24.6, 24.3, 23.44, 23.41

HSQC and **1D Selective Gradient NOESY** spectra are provided to support configurational assignments. NOE correlations are presented below. See Section 3.6.10 for more details.

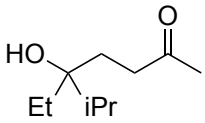




***cis*-14c**



***trans*-14c**



14c′

Compound **14c** and **14c'**: 5-Ethyl-5-isopropyl-2-methyltetrahydrofuran-2-ol and 5-Ethyl-5-hydroxy-6-methylheptan-2-one

Scale: 100 mg

Yield: 69% (*cis/trans/**14c'*** = *1.1:0.9:1.0*) [isolated as a mixture]

Physical State: yellow liquid

Purification: SiO_2 (0–15% *v/v* Et_2O/pentane)

***cis/trans*-14c**: R_f = 0.59 (10% *v/v* EtOAc/hexanes + vanillin stain)

14c': R_f = 0.12 (10% *v/v* EtOAc/hexanes + vanillin stain)

IR (ATR, neat) $\tilde{\nu}_{max}$: 3418, 2960, 2930, 2877, 1717, 1465, 1378, 1244, 1195, 1130, 1110, 1095, 1069, 1057, 1014, 1002, 970, 934, 885, 841, 737, 691, 681, 669 cm^{-1}

HRMS–ESI (*m/z*): $[M–OH]^+$ calc'd for $C_{10}H_{19}O$, 155.1430, found 155.1434

GCMS–EI (*m/z*): $[M–OH]^+$ calc'd for $C_{10}H_{19}O$, 155.1430, found 155.1

***trans*-14c**

^{1}H NMR (600 MHz, D_2O) δ 1.91–1.52 (m, 6H), 1.44–1.30 (m, 2H), 1.34 (s, 3H), 0.82–0.66 (m, 9H)

^{13}C NMR (126 MHz, D_2O) δ 105.22, 91.8, 38.28, 36.3, 31.0, 27.1, 25.8, 16.9, 16.4, 7.5

***cis*-14c**

^{1}H NMR (600 MHz, D_2O) δ 1.91–1.52 (m, 8H), 1.35 (s, 3H), 0.82–0.66 (m, 9H)

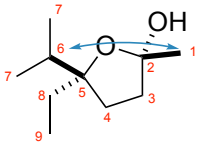
^{13}C NMR (126 MHz, D_2O) δ 105.15, 91.6, 38.32, 33.2, 31.6, 30.2, 26.14, 17.1, 16.8, 7.2

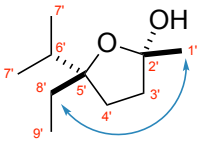
14c'

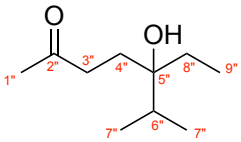
^{1}H NMR (600 MHz, D_2O) δ 2.49–2.44 (m, 2H), 2.08 (s, 3H), 1.73–1.56 (m, 4H), 1.44–1.37 (m, 2H), 0.82–0.66 (m, 9H)

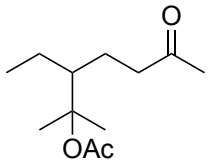
^{13}C NMR (126 MHz, D_2O) δ 216.8, 76.8, 37.5, 32.1, 29.3, 28.3, 26.15, 16.1, 16.0, 6.6

HSQC, **HMBC**, **COSY**, **NOESY**, **DEPT–90**, and **DEPT–135** spectra are provided to support structural assignments. NOE correlations are presented below. See Section 3.6.10 for more details.









16c

Compound **16c**: 3-Ethyl-2-methyl-6-oxoheptan-2-yl acetate

Scale: 0.33 mmol

Yield: 73% (NMR yield vs 1-chloro-2,4-dinitrobenzene), 65% isolated

Physical State: clear liquid

Purification: SiO_2 (0–20% *v/v* EtOAc/hexanes)

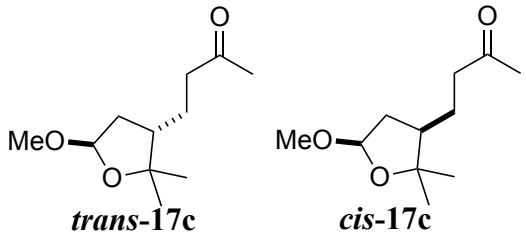
R_f = 0.30 (20% *v/v* EtOAc/hexanes + vanillin stain)

IR (ATR, neat) $\tilde{\nu}_{max}$: 2968, 2878, 1462, 1367, 1257, 1165, 1140, 1018, 944, 875, 783, 736 cm^{-1}

HRMS–DART (*m/z*): $[M + H]^+$ calc'd for $C_{12}H_{23}O_3$, 215.1642, found 215.1632

^{1}H NMR (400 MHz, $CDCl_3$): δ 2.60–2.38 (m, 2H), 2.12 (s, 3H), 1.94 (s, 3H), 1.83–1.64 (m, 2H), 1.58–1.32 (m, 2H), 1.42 (s, 3H), 1.39 (s, 3H), 1.21–1.07 (m, 1H), 0.92 (t, *J* = 7.5 Hz, 3H)

^{13}C NMR (101 MHz, $CDCl_3$): δ 209.0, 170.5, 85.9, 47.9, 43.5, 30.0, 24.1, 24.0, 23.5, 23.4, 22.8, 13.7



***trans*-17c** ***cis*-17c**

Compound **17c**: 4-(5-Methoxy-2,2-dimethyltetrahydrofuran-3-yl)butan-2-one

Scale: 100 mg

Yield: 64% (*cis/trans* = *35:65*) (inseparable isomers)

Physical State: clear liquid

Purification: SiO_2 (0–50% *v/v* Et_2O/pentane)

R_f = 0.39 (50% *v/v* EtOAc/hexanes + vanillin stain) [incidental R_f]

IR (ATR, neat) $\tilde{\nu}_{max}$: 2972, 2828, 1716, 1446, 1368, 1104, 1037, 971, 909, 729 cm^{-1}

HRMS–ESI (*m/z*): $[M + Na]^+$ calc'd for $C_{11}H_{20}O_3Na$, 223.1305, found 223.1307

***trans*-17c**

^{1}H NMR (300 MHz, $CDCl_3$) δ 4.83 (d, *J* = 4.8 Hz, 1H), 3.27 (s, 3H), 2.54–2.26 (m, 2H), 2.11 (s, 3H), 2.08–1.90 (m, 1H), 1.79–1.58 (m, 2H), 1.58–1.33 (m, 2H), 1.29 (s, 3H), 1.01 (s, 3H)

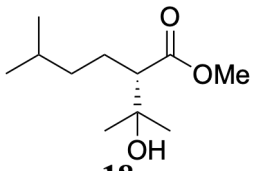
^{13}C NMR (75 MHz, $CDCl_3$) δ 208.2, 103.0, 83.9, 54.2, 45.3, 42.9, 38.8, 30.0, 29.7, 23.8, 23.7

***cis*-17c**

^{1}H NMR (300 MHz, $CDCl_3$) δ 4.91 (dd, *J* = 6.2, 4.4 Hz, 1H), 3.30 (s, 3H), 2.54–2.26 (m, 2H), 2.11 (s, 3H), 2.08–1.90 (m, 1H), 1.79–1.58 (m, 2H), 1.58–1.33 (m, 2H), 1.21 (s, 3H), 1.12 (s, 3H)

^{13}C NMR (75 MHz, $CDCl_3$) δ 208.3, 104.3, 83.0, 55.4, 47.8, 42.8, 39.0, 30.4, 28.1, 24.1, 23.1

Characterization data match those previously reported in the literature [93b].



18c

Compound **18c**: Methyl (*S*)-2-(2-Hydroxypropan-2-yl)-5-methylhexanoate

* 2.2 equivalents of PhSH were used instead of γ-terpinene (1.5 equiv) and PhSH (10 mol%)

Scale: 94 mg

Yield: 54%

Physical State: yellow solid

Melting Point: 68–70 ºC

Purification: SiO_2 (0–15% *v/v* EtOAc/hexanes)

$\boldsymbol{R_f}$ = 0.17 (10% *v/v* EtOAc/hexanes + vanillin stain)

IR (ATR, neat) $\tilde{\nu}_{max}$: 3281, 3216, 2967, 2954, 2901, 2871, 2847, 1724, 1536, 1462, 1438, 1383, 1354, 1328, 1297, 1253, 1222, 1197, 1166, 1137,1066, 996, 949, 904, 868, 830, 777, 732 cm^{-1}

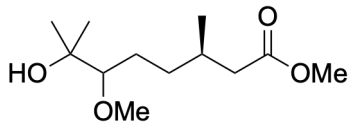
HRMS–ESI (*m/z*): $[M–OH]^+$ calc'd for $C_{11}H_{21}O_2$, 185.1536, found 185.1540

Specific Rotation: $[\alpha]_D^{20.9}$ –6.00 (*c* 1.0, $CHCl_3$)

^{1}H NMR (500 MHz, $CDCl_3$) δ 3.70 (s, 3H), 2.73 (s, 1H), 2.33 (dd, *J* = 11.4, 3.7 Hz, 1H), 1.71 (dtd, *J* = 13.4, 11.1, 5.0 Hz, 1H), 1.63–1.47 (m, 2H), 1.21 (d, *J* = 2.1 Hz, 6H), 1.17–1.00 (m, 2H), 0.85 (t, *J* = 6.5 Hz, 6H)

^{13}C NMR (126 MHz, $CDCl_3$) δ 176.7, 71.2, 56.2, 51.6, 37.3, 29.3, 28.1, 26.8, 25.6, 22.8, 22.3

HSQC spectrum is provided to support structural assignment. See Section 3.6.10.



18c′

Compound **18c'**: Methyl (3*R*)-7-Hydroxy-6-methoxy-3,7-dimethyloctanoate

* 2.2 equivalents of PhSH were used instead of γ-terpinene (1.5 equiv) and PhSH (10 mol%)

Scale: 94 mg

Yield: 21% (*d.r. = 1.9:1.0*) [isolated as a mixture of diastereomers]

Physical State: yellow liquid

Purification: SiO_2 (0–15% *v/v* EtOAc/hexanes)

$\boldsymbol{R_f}$ = 0.09 (10% *v/v* EtOAc/hexanes + vanillin stain) [indistinguishable by TLC]

IR (ATR, neat) $\tilde{\nu}_{max}$: 3448, 2953, 2876, 1736, 1536, 1460, 1437, 1381, 1364, 1296, 1247, 1153, 1076, 1009, 962, 913, 867, 835, 748 cm^{-1}

HRMS–ESI (*m/z*): $[M + Na]^+$ calc'd for $C_{12}H_{24}O_4Na$, 255.1567, found 255.1578

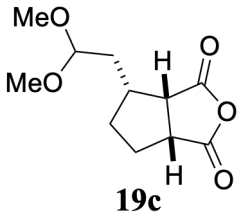
***Major*–^{1}H NMR** (500 MHz, $CDCl_3$) δ 3.657 (s, 3H), 3.48–3.35 (m, 1H), 3.215 (s, 3H), 2.49 (br, 1H), 2.35 (dd, *J* = 14.6, 5.5 Hz, 1H), 2.11 (dd, *J* = 14.7, 8.6 Hz, 1H), 2.03–1.92 (m, 1H), 1.77–1.58 (m, 1H), 1.55–1.18 (m, 3H), 1.12 (s, 3H), 1.077 (s, 3H), 0.95 (d, *J* = 6.5 Hz, 3H)

***Major* –^{13}C NMR** (126 MHz, $CDCl_3$) δ 173.9, 77.6, 77.1, 51.5, 49.2, 41.6, 34.3, 30.7, 28.80, 20.9, 20.1, 18.90

***Minor*–^{1}H NMR** (500 MHz, $CDCl_3$) δ 3.659 (s, 3H), 3.48–3.35 (m, 1H), 3.212 (s, 3H), 2.49 (br, 1H), 2.32 (dd, *J* = 15.0, 6.0 Hz, 1H), 2.15 (dd, *J* = 15.0, 6.0 Hz, 1H), 2.03–1.92 (m, 1H), 1.55–1.18 (m, 4H), 1.11 (s, 3H), 1.081 (s, 3H), 0.94 (d, *J* = 7.0 Hz, 3H)

***Minor*–^{13}C NMR** (126 MHz, $CDCl_3$) δ 173.9, 77.3, 76.8, 51.5, 49.2, 41.9, 34.1, 30.5, 28.77, 20.9, 19.7, 18.94

HSQC and **HMBC spectra** are provided to support structural assignment, but differentiation of the identity of each diastereomer was not possible. See Section 3.6.10.



19c

Compound **19c**: (±)-(3a*S*,4*R*,6a*R*)-4-(2,2-Dimethoxyethyl)tetrahydro-1*H*-cyclopenta[*c*]furan-1,3(3a*H*)-dione

Scale: 130 mg

Yield: 39%

Physical State: clear liquid

Purification: SiO_2 (0–40% *v/v* EtOAc/hexanes)

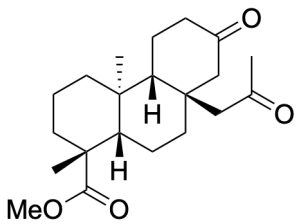
R_f = 0.35 (40% *v/v* EtOAc/hexanes + vanillin stain)

IR (ATR, neat) $\tilde{\nu}_{max}$: 2995, 2834, 1856, 1774, 1723, 1453, 1252, 1220, 1170, 1128, 1053, 1011, 970, 928, 793 cm^{-1}

GCMS–EI (*m/z*): $[M - OMe]^+$ calc'd for $C_{10}H_{13}O_4$, 197.0808, found 197.0

^{1}H NMR (500 MHz, $CDCl_3$) δ 4.57 (t, *J* = 5.6 Hz, 1H), 3.45 (t, *J* = 8.7 Hz, 1H), 3.42–3.36 (m, 1H), 3.36 (s, 3H), 3.35 (s, 3H), 2.42–2.24 (m, 2H), 2.13–1.91 (m, 3H), 1.71 (ddd, *J* = 14.0, 7.6, 6.1 Hz, 1H), 1.23–1.10 (m, 1H)

^{13}C NMR (126 MHz, $CDCl_3$) δ 174.7, 171.7, 103.3, 53.7, 53.2, 47.8, 46.0, 40.6, 33.2, 31.5, 30.7



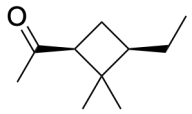
20c

Compound **20c**: methyl (1R,4aS,4bR,8aR,10aS)-1,4a-dimethyl-7-oxo-8a-(2-oxopropyl)tetradecahydrophenanthrene-1-carboxylate

Scale: 36.8 mg

Yield: 78%

Characterization data match with those previously reported in the literature [106].

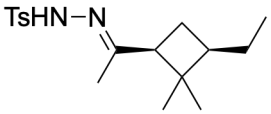


21c

Compound **21c**: 1-((1*S*,3*R*)-3-Ethyl-2,2-dimethylcyclobutyl)ethan-1-one

Scale: 100 mg

Yield: Not determined because the compound is volatile and overlapping signals in the crude NMR prevented quantification.



21e

Isolated as the *p*-toluenesulfonylhydrazone (**21e**): *N*'-((*E*)-1-((1*S*,3*R*)-3-Ethyl-2,2-dimethylcyclobutyl)ethylidene)-4-methylbenzenesulfonohydrazide

Yield: 68% (E isomer)

Physical State: white wax

Purification: SiO_2 (0–30% V/V Et_2O/hexanes)

$\boldsymbol{R_f}$ = 0.68 (40% V/V EtOAc/hexanes + UV/vanillin stain)

HRMS–ESI (*m/z*): $[M]^+$ calc'd for $C_{17}H_{26}N_2O_2S$, 322.1710, found 322.1712

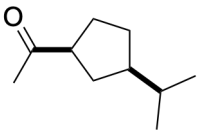
IR (ATR, neat) $\tilde{\nu}_{max}$: 3225, 3215, 2953, 2925, 2873, 2858, 1460, 1385, 1366, 1333, 1307, 1235, 1186, 1091, 1032, 1021, 913, 813, 728, 671, 666 cm^{-1}

21e–Specific Rotation: $[\alpha]_D^{22.8}$ +67.3 (*c* 1.0, $CHCl_3$)

^{1}H NMR (400 MHz, $CDCl_3$) δ 7.85 (d, *J* = 8.4 Hz, 2H), 7.48 (s, 1H), 7.29 (d, *J* = 8.6 Hz, 2H), 2.51–2.43 (m, 1H), 2.42 (s, 3H), 1.88–1.66 (m, 3H), 1.65 (s, 3H), 1.34–1.16 (m, 2H), 1.12 (s, 3H), 0.78 (t, *J* = 7.4 Hz, 3H), 0.45 (s, 3H)

^{13}C NMR (101 MHz, $CDCl_3$) δ 157.6, 144.0, 135.5, 129.4, 128.3, 50.0, 43.9, 42.8, 30.9, 24.3, 23.1, 21.7, 16.5, 16.4, 12.1

Only a single diastereomer was isolated.



22c

Compound **22c**: *cis*–1-(3-Isopropylcyclopentyl)ethan-1-one

* 2.2 equivalents of PhSH were used instead of γ-terpinene (1.5 equiv) and PhSH (10 mol%)

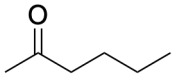
Scale: 100 mg

Yield: 88%

^{1}H NMR (500 MHz, CDCl3) δ 2.88 (tt, J = 9.8, 7.2 Hz, 1H), 2.14 (s, 3H), 2.00 (dt, J = 13.3, 7.2 Hz, 1H), 1.92–1.71 (m, 3H), 1.61–1.49 (m, 1H), 1.40 (dp, J = 8.7, 6.6 Hz, 1H), 1.31 (dt, J = 12.4, 10.5 Hz, 1H), 1.27–1.16 (m, 1H), 0.89 (dd, J = 6.7, 4.6 Hz, 6H)

^{13}C NMR (126 MHz, CDCl3) δ 211.3, 52.4, 48.7, 34.3, 33.4, 30.2, 28.9, 27.7, 21.73, 21.69

Other characterization data match those previously reported in the literature [116].

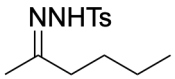


23c

Compound **23c**: Hexan-2-one

Scale: 170 mg scale

Yield: 79% (NMR yield vs 1-chloro-2,4-dinitrobenzene)

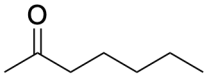


23e

Isolated as the *p*-toluenesulfonylhydrazone (**23e**): *N*'-(Hexan-2-ylidene)-4-methylbenzenesulfonohydrazide

Yield: 44% (*E/Z = 3.2:1.0*)

Characterization data match those previously reported in the literature [117].



24c

Compound **24c**: Heptan-2-one

From **24b**

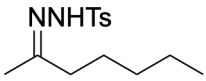
Scale: 37 mg

Yield: 87% (NMR yield vs 1-chloro-2,4-dinitrobenzene)

From **26b**

Scale: 50 mg

Yield: 79% (NMR yield vs 1-chloro-2,4-dinitrobenzene)

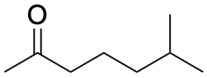


24e

Isolated as the *p*-toluenesulfonylhydrazone (**45e**): *N*'-(Heptan-2-ylidene)-4-methylbenzenesulfonohydrazide

Yield: 68% (*E/Z = 4.1:1.0*)

Characterization data match those previously reported in the literature [118].

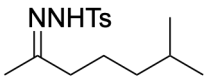


25c

Compound **25c**: 6-Methylheptan-2-one

Scale: 180 mg

Yield: 86% (NMR Yield vs 1-chloro-2,4-dinitrobenzene)



25e

Isolated as the *p*-toluenesulfonylhydrazone (**25e**): 4-Methyl-*N*'-(6-methylheptan-2-ylidene)benzenesulfonohydrazide

Yield: 75% (*E/Z = 4.0:1.0*)

Physical State: white solid

Melting Point: 83–85 ºC

Purification: SiO_2 (0–25% *v/v* Et_2O/hexanes)

***E*-25e**: R_f = 0.70 (40% *v/v* EtOAc/hexanes + UV/vanillin stain)

***Z*-25e**: R_f = 0.74 (40% *v/v* EtOAc/hexanes + UV/vanillin stain)

IR (ATR, neat) $\tilde{\nu}_{max}$: 3225, 2955, 2931, 1386, 1332, 1164, 1093, 1042, 667 cm^{-1}

HRMS–DART (*m/z*): $[M]^+$ calc'd for $C_{15}H_{24}N_2O_2S$, 296.1553, found 296.1545

***E*-25e**

^{1}H NMR (500 MHz, $CDCl_3$) δ 8.10 (br, 1H), 7.96–7.71 (m, 2H), 7.43–7.04 (m, 2H), 2.36 (d, *J* = 3.8 Hz, 3H), 2.10 (t, *J* = 7.6 Hz, 2H), 1.73 (s, 3H), 1.48–1.28 (m, 3H), 1.03–0.85 (m, 2H), 0.74 (dd, *J* = 6.7, 2.3 Hz, 6H)

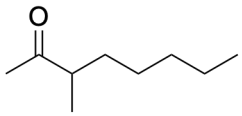
^{13}C NMR (126 MHz, $CDCl_3$) δ 158.7, 143.7, 135.5, 129.4, 128.0, 38.8, 38.0, 27.6, 23.7, 22.4, 21.5, 15.7

***Z*-25e**

^{1}H NMR (500 MHz, $CDCl_3$) δ 8.23 (br, 1H), 7.96–7.71 (m, 2H), 7.43–7.04 (m, 2H), 2.36 (d, *J* = 3.8 Hz, 3H), 2.10 (t, *J* = 7.6 Hz, 2H), 1.83 (s, 3H), 1.48–1.28 (m, 3H), 1.08–0.99 (m, 2H), 0.74 (dd, *J* = 6.7, 2.3 Hz, 6H)

^{13}C NMR (126 MHz, $CDCl_3$) δ 159.6, 143.7, 135.7, 129.5, 127.9, 38.4, 30.6, 30.2, 29.6, 27.7, 23.1, 22.9

The minor diastereomer was assigned to the less stable *Z*-isomer.

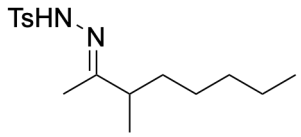


27c

Compound **27c**: 3-Methyloctan-2-one

Scale: 140 mg

Yield: 86% (NMR Yield vs 1-chloro-2,4-dinitrobenzene)



27e

Isolated as the *p*-toluenesulfonylhydrazone (**27e**): (*E*)-4-Methyl-*N*'-(3-methylheptan-2-ylidene)benzenesulfonohydrazide

Yield: 57% (*E* isomer)

Physical State: white solid

Melting Point: 102–104 ºC

Purification: SiO_2 (0–25% *v/v* Et_2O/hexanes)

$\boldsymbol{R_f}$ = 0.69 (40% *v/v* EtOAc/hexanes + UV/vanillin stain)

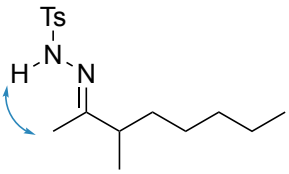
IR (ATR, neat) $\boldsymbol{\tilde{\nu}_{max}}$: 3227, 2954, 2925, 2850, 1467, 1394, 1326, 1290, 1166, 1118, 1092, 1012, 964, 910, 812, 770, 732, 706, 662 cm^{-1}

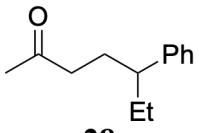
HRMS–ESI (*m/z*): $[M + H]^+$ calc'd for $C_{16}H_{27}N_2O_2S$, 311.1788, found 311.1804

^{1}H NMR (500 MHz, $CDCl_3$) δ 7.85–7.81 (m, 2H), 7.80 (s, 1H), 7.27 (d, *J* = 8.1 Hz, 2H), 2.39 (s, 3H), 2.31 (dt, *J* = 8.1, 6.6 Hz, 1H), 1.66 (s, 3H), 1.33 (dddd, *J* = 13.4, 10.1, 8.1, 5.3 Hz, 1H), 1.27–0.83 (m, 10H), 0.79 (t, *J* = 7.0 Hz, 3H)

^{13}C NMR (126 MHz, $CDCl_3$) δ 161.7, 143.7, 135.5, 129.4, 128.0, 42.1, 33.8, 31.7, 26.7, 22.5, 21.5, 17.8, 14.0, 12.7

NOESY spectrum supports the *E*-isomer assignment. NOE correlations are presented below. See Section 3.6.10 for more details.





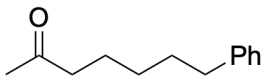
28c

Compound **28c**: 5-Phenylheptan-2-one

Scale: 1.0 mmol

Yield: 89%

Characterization data match those previously reported in the literature [119].



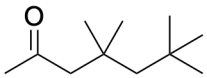
29c

Compound **29c**: 7-Phenylheptan-2-one

Scale: 50 mg

Yield: 61%

Characterization data match those previously reported in the literature [120].

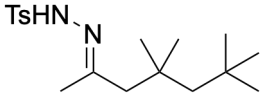


30c

Compound **31c**: 4,4,6,6-Tetramethylheptan-2-one

Scale: 210 mg

Yield: 10% (NMR Yield vs 1-chloro-2,4-dinitrobenzene)



30e

Isolated as the *p*-tosylhydrazone (**30e**): (*E*)-4-Methyl-*N*'-(4,4,6,6-tetramethylheptan-2-ylidene)benzenesulfonohydrazide

Yield: 7%

Physical State: thin film

Purification: SiO_2 (0–25% *v/v* Et_2O/hexanes)

$\boldsymbol{R_f}$ = 0.53 (40% *v/v* EtOAc/hexanes + UV/vanillin stain)

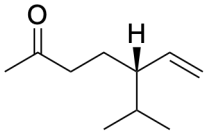
IR (ATR, neat) $\tilde{\nu}_{max}$: 3224, 2957, 2904, 2873, 1716, 1599, 1458, 1366, 1337, 1186, 1166, 1093, 1053, 917, 813, 732, 670 cm^{-1}

HRMS–ESI (*m/z*): $[M + Na]^+$ calc'd for $C_{18}H_{30}N_2O_2SNa$, 361.1920, found 361.1927

^{1}H NMR (500 MHz, $CDCl_3$) δ 7.84 (d, *J* = 8.4 Hz, 2H), 7.29 (d, *J* = 8.4 Hz, 2H), 7.14 (s, 1H), 2.41 (s, 3H), 2.20 (s, 2H), 1.79 (s, 3H), 1.25 (s, 3H), 1.17 (s, 2H), 0.90 (s, 9H), 0.86 (s, 6H)

^{13}C NMR (126 MHz, $CDCl_3$) δ 157.2, 144.1, 135.6, 129.6, 128.3, 55.0, 53.0, 36.3, 32.4, 32.1, 29.9, 29.1, 21.7, 18.6

Only a single diastereomer was isolated.

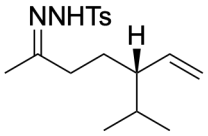


31c

Compound **31c**: 1-((1*S*,3*R*)-3-Isopropylcyclopentyl)ethan-1-one

Scale: 210 mg

Yield: 80% (NMR Yield vs 1-chloro-2,4-dinitrobenzene)



31e

Isolated as the *p*-toluenesulfonylhydrazone (**31e**): (*S*)-*N*'-(5-Isopropylhept-6-en-2-ylidene)-4-methylbenzenesulfonohydrazide

Yield: 66% (*E/Z = 3.5:1.0*)

Physical State: white solid

Melting Point: 77–79 ºC

Purification: SiO_2 (DCM)

R_f = 0.68 (40% *v/v* EtOAc/hexanes + UV/vanillin stain) [incidental R_f]

R_f = 0.20 (DCM + UV/vanillin stain) [incidental R_f]

IR (ATR, neat) $\tilde{\nu}_{max}$: 3216, 2956, 2926, 2895, 2871, 1455, 1386, 1367, 1334, 1307, 1291, 1163, 1093, 1000, 913, 812, 665 cm^{-1}

HRMS–ESI (*m/z*): $[M + H]^+$ calc'd for $C_{17}H_{27}N_2O_2S$, 323.1788, found 323.1790

***E*-31e**

^{1}H NMR (500 MHz, $CDCl_3$) δ 7.85 (dd, *J* = 8.2, 3.0 Hz, 2H), 7.53 (s, 1H), 7.29 (dd, *J* = 8.3, 3.0 Hz, 2H), 5.44 (ttd, *J* = 20.0, 9.9, 3.1 Hz, 1H), 4.96 (d, *J* = 10.2 Hz, 1H), 4.80 (d, *J* = 17.1 Hz, 1H), 2.42 (s, 3H), 2.26–1.98 (m, 2H), 1.73 (s, 3H), 1.65–1.45 (m, 3H), 1.37–1.22 (m, 1H), 0.79 (dd, *J* = 16.7, 6.9 Hz, 6H)

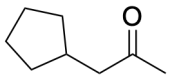
^{13}C NMR (126 MHz, $CDCl_3$) δ 159.1, 144.0, 140.2, 135.57, 129.56, 128.3, 116.1, 50.2, 37.0, 31.7, 28.1, 21.71, 20.62, 19.1, 16.1

***Z*-31e**

^{1}H NMR (500 MHz, $CDCl_3$) δ 7.85 (dd, *J* = 8.2, 3.0 Hz, 2H), 7.53 (s, 1H), 7.29 (dd, *J* = 8.3, 3.0 Hz, 2H), 5.44 (ttd, *J* = 20.0, 9.9, 3.1 Hz, 1H), 5.08 (d, *J* = 10.2 Hz, 1H), 4.91 (d, *J* = 17.2 Hz, 1H), 2.44 (s, 3H), 2.26–1.98 (m, 2H), 1.89 (s, 3H), 1.65–1.45 (m, 3H), 1.37–1.22 (m, 1H), 0.92–0.85 (m, 6H)

^{13}C NMR (126 MHz, $CDCl_3$) δ 159.7, 140.3, 139.9, 135.60, 129.62, 128.2, 117.4, 50.5, 31.9, 28.7, 27.4, 23.3, 21.72, 20.58, 19.0

The minor diastereomer was assigned as the less stable *Z*-isomer.

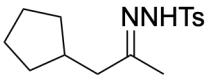


33c

Compound **33c**: 1-Cyclopentylpropan-2-one

Scale: 210 mg

Yield: 80% (NMR Yield vs 1-chloro-2,4-dinitrobenzene)



33e

Isolated as the *p*-toluenesulfonylhydrazone (**33e**): *N*'-(1-Cyclopentylpropan-2-ylidene)-4-methylbenzenesulfonohydrazide

Yield: 58% (*E/Z = 4.6:1.0*)

Physical State: white solid

Melting Point: 132–134 ºC

Purification: SiO_2 (0–25% *v/v* Et_2O/hexanes)

R_f = 0.64 (40% *v/v* Et_2O/hexanes + UV/vanillin stain) [incidental R_f]

IR (ATR, neat) $\tilde{\nu}_{max}$: 3214, 2947, 2865, 1738, 1641, 1598, 1494, 1449, 1388, 1324, 1304, 1289, 1217, 1184, 1183, 1092, 1034, 1019, 910, 811, 730, 680 cm^{-1}

HRMS–ESI (*m/z*): $[M + Na]^+$ calc'd for $C_{15}H_{22}N_2O_2SNa$, 317.1294, found 317.1300

***E*-33e**

^{1}H NMR (500 MHz, $CDCl_3$) δ 7.84 (d, *J* = 8.2 Hz, 2H), 7.46 (br, 1H), 7.29 (d, *J* = 8.2 Hz, 2H), 2.41 (s, 3H), 2.18 (d, *J* = 7.5 Hz, 2H), 1.98 (p, *J* = 7.8 Hz, 1H), 1.75 (s, 3H), 1.72–1.37 (m, 6H), 1.15–0.83 (m, 2H)

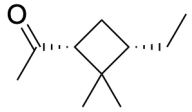
^{13}C NMR (126 MHz, $CDCl_3$) δ 158.8, 144.01, 135.6, 129.64, 128.22, 44.8, 37.0, 32.9, 32.2, 25.0, 24.9, 21.71, 15.9

***Z*-33e**

^{1}H NMR (500 MHz, $CDCl_3$) δ 7.80 (d, *J* = 8.2 Hz, 2H), 7.55 (br, 1H), 7.36 (d, *J* = 8.2 Hz, 2H), 2.45 (s, 3H), 2.13 (d, *J* = 4.6 Hz, 2H), 1.98 (p, *J* = 7.8 Hz, 1H), 1.91 (s, 3H), 1.72–1.37 (m, 6H), 1.15–0.83 (m, 2H)

^{13}C NMR (126 MHz, $CDCl_3$) δ 159.4, 144.03, 135.5, 129.55, 128.15, 50.2, 36.8, 36.3, 35.7, 32.7, 25.1, 24.1, 21.74

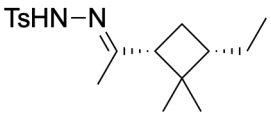
The minor diastereomer was assigned as the less stable *Z*-isomer.



34c

Compound **34c**: 1-((1*R*,3*S*)-3-Ethyl-2,2-dimethylcyclobutyl)ethan-1-one

Scale: 210 mg



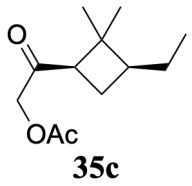
34e

Isolated as the *p*-toluenesulfonylhydrazone (**34e**): *N*'-((*E*)-1-((*1R*,3*S*)-3-Ethyl-2,2-dimethylcyclobutyl)ethylidene)-4-methylbenzenesulfonohydrazide

See compound **22e** for characterization.

Yield: 68% (*E* isomer)

34e–Specific Rotation: $[\alpha]_D^{23.8}$ –70.0 (*c* 1.0, $CHCl_3$)



35c

Compound **35c**: 2-((1*R*,3*S*)-3-ethyl-2,2-dimethylcyclobutyl)-2-oxoethyl acetate

Scale: 100 mg

Yield: 62% (NMR Yield vs 1-chloro-2,4-dinitrobenzene), 58% isolated

Physical State: clear liquid

Purification: SiO_2 (0–3% *v/v* EtOAc/hexanes)

R_f = 0.24 (10% *v/v* EtOAc/hexanes + vanillin stain)

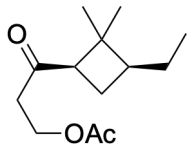
IR (ATR, neat) $\tilde{\nu}_{max}$: 2957, 2877, 1752, 1723, 1462, 1415, 1371, 1268, 1229, 1151, 1064 cm^{-1}

GCMS–EI (*m/z*): $[M]^+$ calc'd for $C_{12}H_{20}O_3$, 212.1407, found 211.9

Specific Rotation: $[\alpha]_D^{24.1}$ –44.0 (c 1.0, $CHCl_3$)

^{1}H NMR (500 MHz, $CDCl_3$) δ 4.54 (s, 2H), 2.82 (dd, *J* = 10.2, 7.2 Hz, 1H), 2.16 (s, 3H), 1.99–1.79 (m, 3H), 1.37–1.28 (m, 1H), 1.27 (s, 3H), 1.26–1.16 (m, 1H), 0.87 (s, 3H), 0.80 (t, *J* = 7.4 Hz, 3H)

^{13}C NMR (126 MHz, $CDCl_3$) δ 202.6, 170.1, 68.3, 49.7, 44.1, 43.9, 30.8, 22.8, 22.0, 20.4, 16.9, 11.7



36c

Compound **36c**: 3-((1*R*,3*S*)-3-Ethyl-2,2-dimethylcyclobutyl)-3-oxopropyl Acetate

Scale: 100 mg

Yield: 82%

Physical State: yellow liquid

Purification: SiO_2 (0–2% *v/v* EtOAc/hexanes)

$\boldsymbol{R_f}$ = 0.18 (10% *v/v* EtOAc/hexanes + vanillin stain)

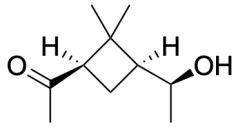
IR (ATR, neat) $\boldsymbol{\tilde{\nu}_{max}}$: 2956, 2874, 1740, 1704, 1461, 1383, 1366, 1234, 1147, 1091, 1038 cm^{-1}

GCMS–EI (*m/z*): $[M–AcOH]^+$ calc'd for $C_{11}H_{18}O$, 166.1352, found 166.1

Specific Rotation: $[\alpha]_D^{23.5}$ –70.0 (c 1.0, $CHCl_3$)

^{1}H NMR (500 MHz, $CDCl_3$) δ 4.38–4.24 (m, 2H), 2.83–2.74 (m, 1H), 2.67–2.49 (m, 2H), 2.00 (s, 3H), 1.93–1.74 (m, 3H), 1.39–1.29 (m, 1H), 1.28 (s, 3H), 1.23–1.14 (m, 1H), 0.83 (s, 3H), 0.79 (t, *J* = 7.4 Hz, 3H)

^{13}C NMR (101 MHz, $CDCl_3$) δ 207.0, 171.0, 59.3, 53.6, 44.2, 43.8, 41.7, 31.0, 23.0, 22.8, 21.0, 17.1, 11.9



37c

Compound **37c**: 1-((1*R*,3*S*)-3-((*S*)-1-Hydroxyethyl)-2,2-dimethylcyclobutyl)ethan-1-one

Scale: 140 mg

Yield: 38% (NMR yield vs 1-chloro-2,4-dinitrobenzene), 29% isolated

Physical state: clear liquid

Purification: SiO_2 (0–60% *v/v* Et_2O/pentane)

IR (ATR, neat) $\tilde{\nu}_{max}$: 3457, 2961, 2919, 2886, 2850, 2839, 1696, 1465, 1372 cm^{-1}

HRMS–DART (*m/z*): $[M + H]^+$ calc'd for $C_{10}H_{19}O_2$, 171.1380, found 171.1384

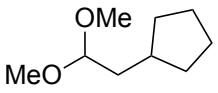
***R*f** = 0.28 (50% *v/v* EtOAc/hexanes + vanillin stain)

Specific Rotation: $[\alpha]_D^{25.2}$ –56.0 (*c* 0.5, $CHCl_3$)

^{1}H NMR (500 MHz, $CDCl_3$) δ 3.66 (dq, J = 9.0, 6.5 Hz, 1H), 2.82 (dd, J = 10.3, 7.4 Hz, 1H), 2.10 (q, J = 9.5 Hz, 1H), 2.05 (s, 3H), 1.91 (ddd, J = 11.1, 8.1, 7.3 Hz, 1H), 1.81 (ddd, J = 10.7, 9.4, 8.0 Hz, 1H), 1.32 (s, 3H), 1.27 (br, 1H), 1.12 (d, J = 6.1 Hz, 3H), 0.89 (s, 3H)

^{13}C NMR (126 MHz, $CDCl_3$) δ 208.0, 68.9, 53.6, 49.1, 42.7, 31.0, 30.5, 22.8, 20.8, 17.3

Signals for the other regioisomeric product formed from a cyclobutene radical were also present in the crude NMR, but it was not isolated.



38c

Compound **38c**: (2,2-Dimethoxyethyl)cyclopentane

Scale: 130 mg

Yield: 80% (NMR Yield vs 1-chloro-2,4-dinitrobenzene), 59% isolated

Physical State: clear liquid

Purification: SiO_2 (0–1% *v/v* Et_2O/pentane)

R_f = 0.66 (10% *v/v* EtOAc/hexanes + vanillin stain)

IR (ATR, neat) $\tilde{\nu}_{max}$: 2943, 2970, 2828, 1450, 1385, 1365, 1192, 1165, 1125, 1053, 995, 967, 935, 909 cm^{-1}

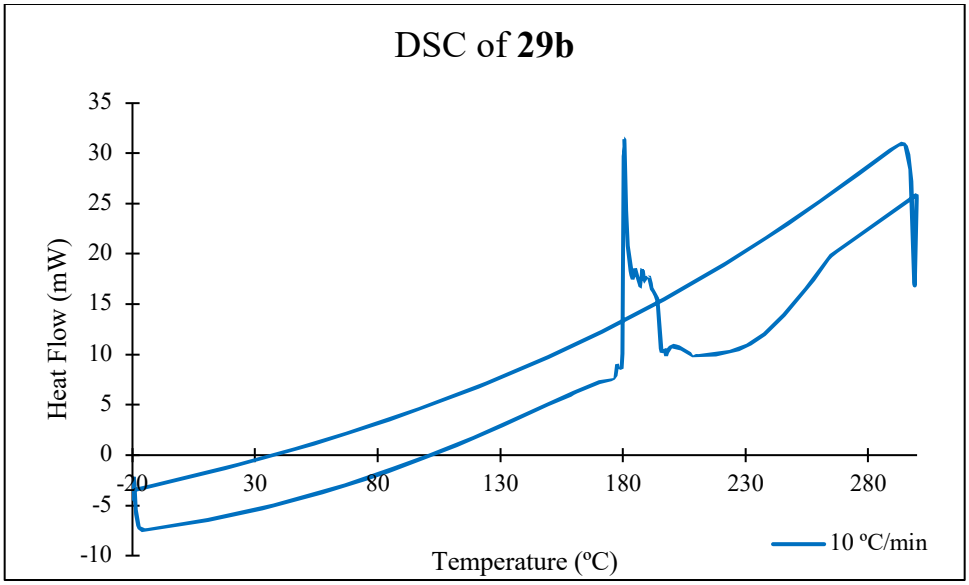
GCMS–EI (*m/z*): $[M–H]^+$ calc'd for $C_9H_{17}O_2$, 157.1223, found 157.1

^{1}H NMR (500 MHz, $CDCl_3$) δ 4.39 (s, 1H), 3.30 (s, 6H), 1.91–1.73 (m, 3H), 1.67–1.51 (m, 4H), 1.49 (dd, *J* = 8.2, 3.9 Hz, 2H), 1.10 (qd, *J* = 8.3, 4.0 Hz, 2H)

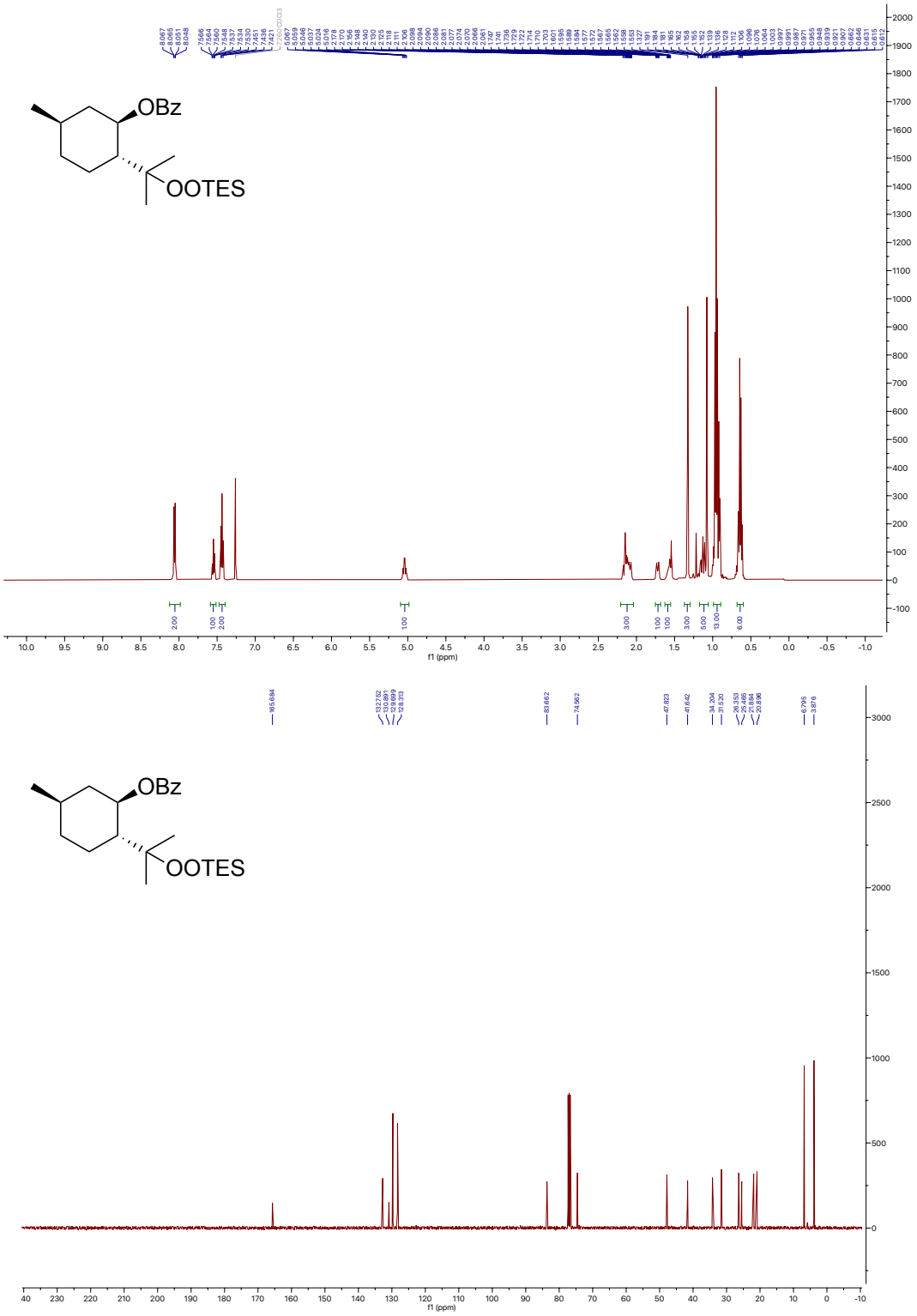
^{13}C NMR (101 MHz, $CDCl_3$) δ 104.2, 52.6, 38.6, 36.2, 32.9, 25.0

5.6.9 Differential Scanning Calorimetry (DSC)

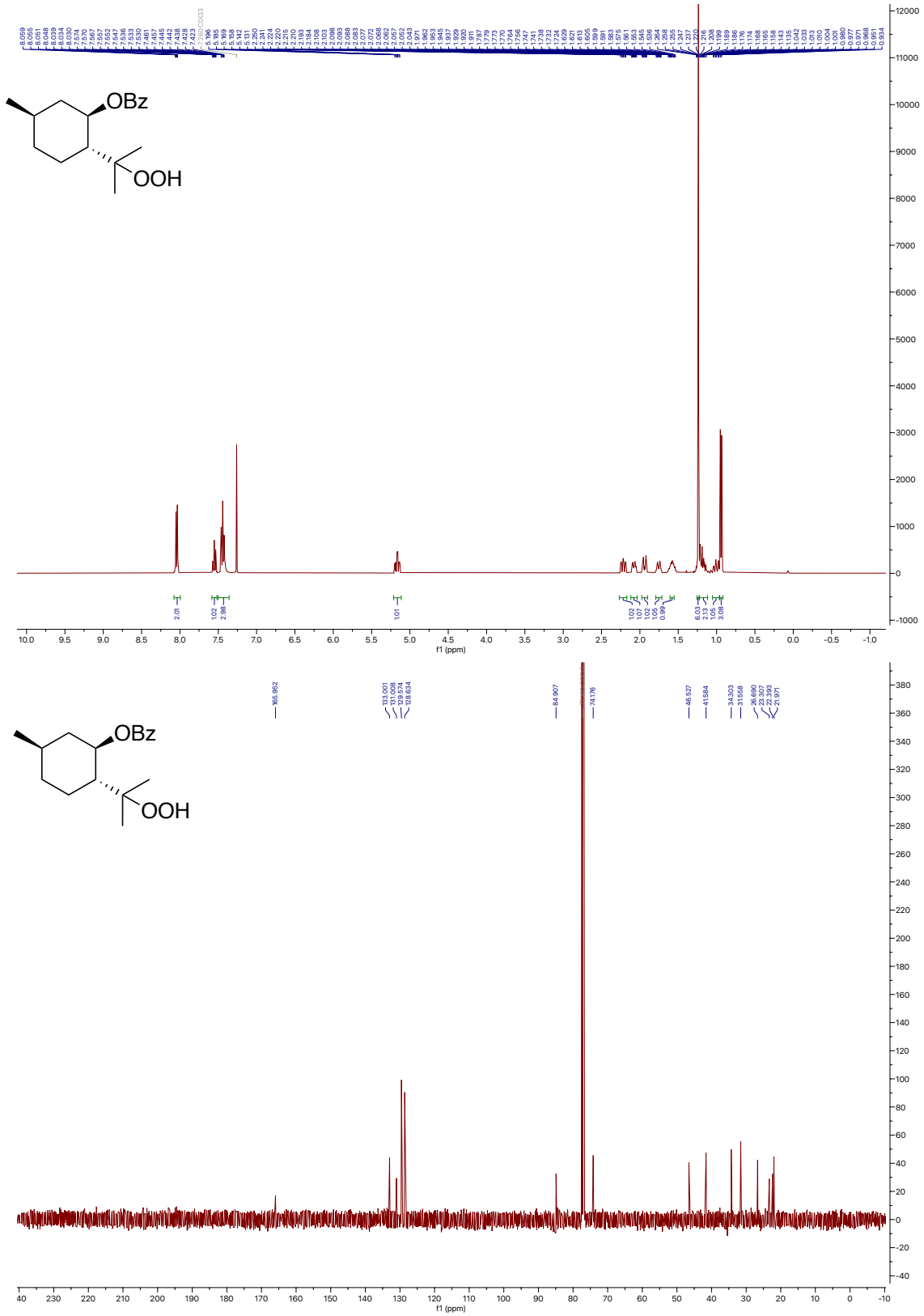
To derive thermal safety parameters, we assessed the thermal stability of the triethylsilylperoxide (**29b**) through differential scanning calorimetry (DSC). Beginning at –20 ºC we slowly warmed a sample of **29b** at a rate of 10 ºC min^{-1} to a maximum temperature of 300 ºC then cooled the sample back down to –20 ºC. We observed an abrupt increase in heat flow (mW) at a sample temperature of 179.4 ºC. The peak increase in heat flow was 22.28 mW over a 0.979 ºC increase in temperature. It is known that the decomposition temperature for peroxides are typically around 180 ºC; our experimental measurement matches such a value [121].



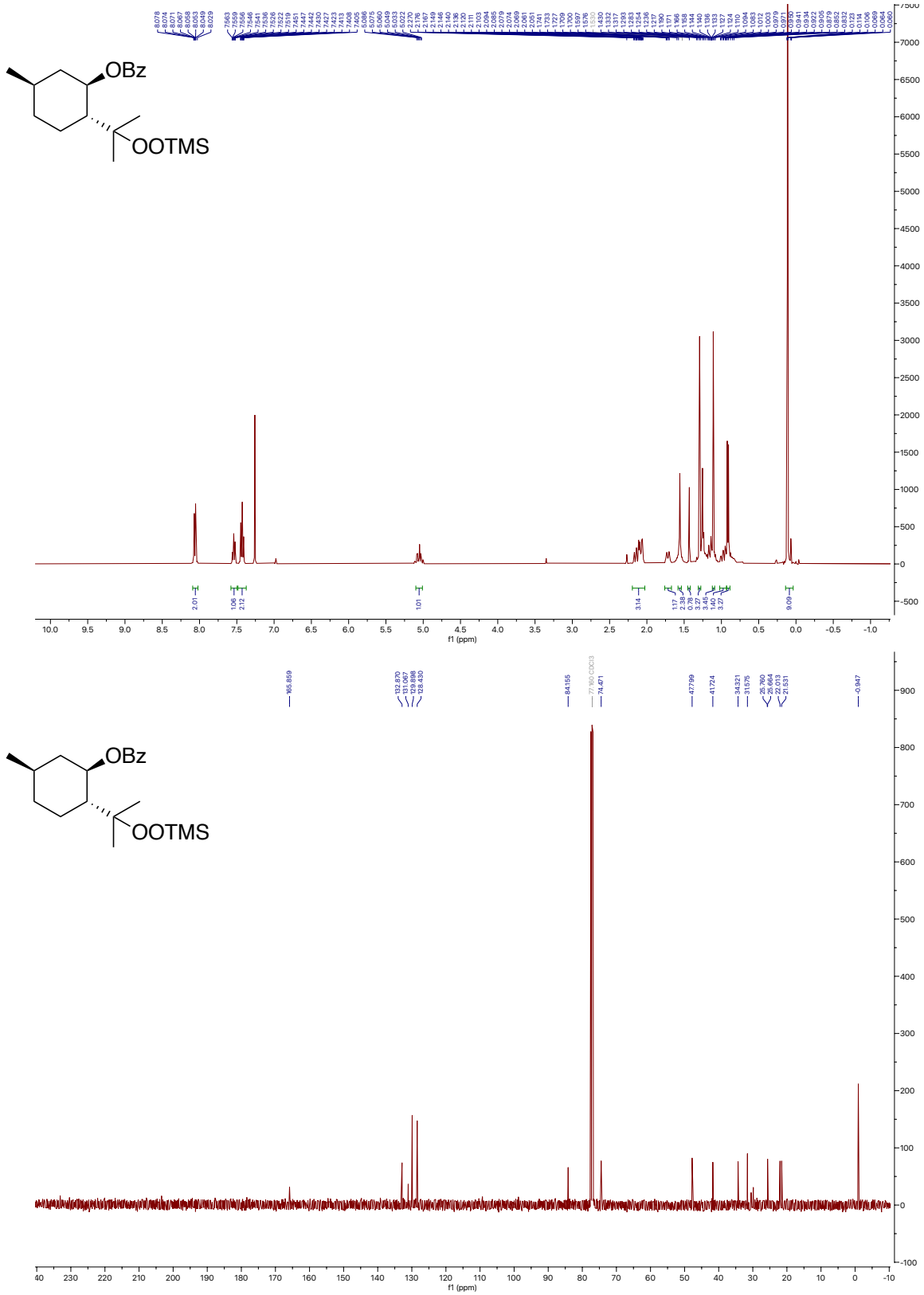
3.6.10 Copies of NMR Spectra



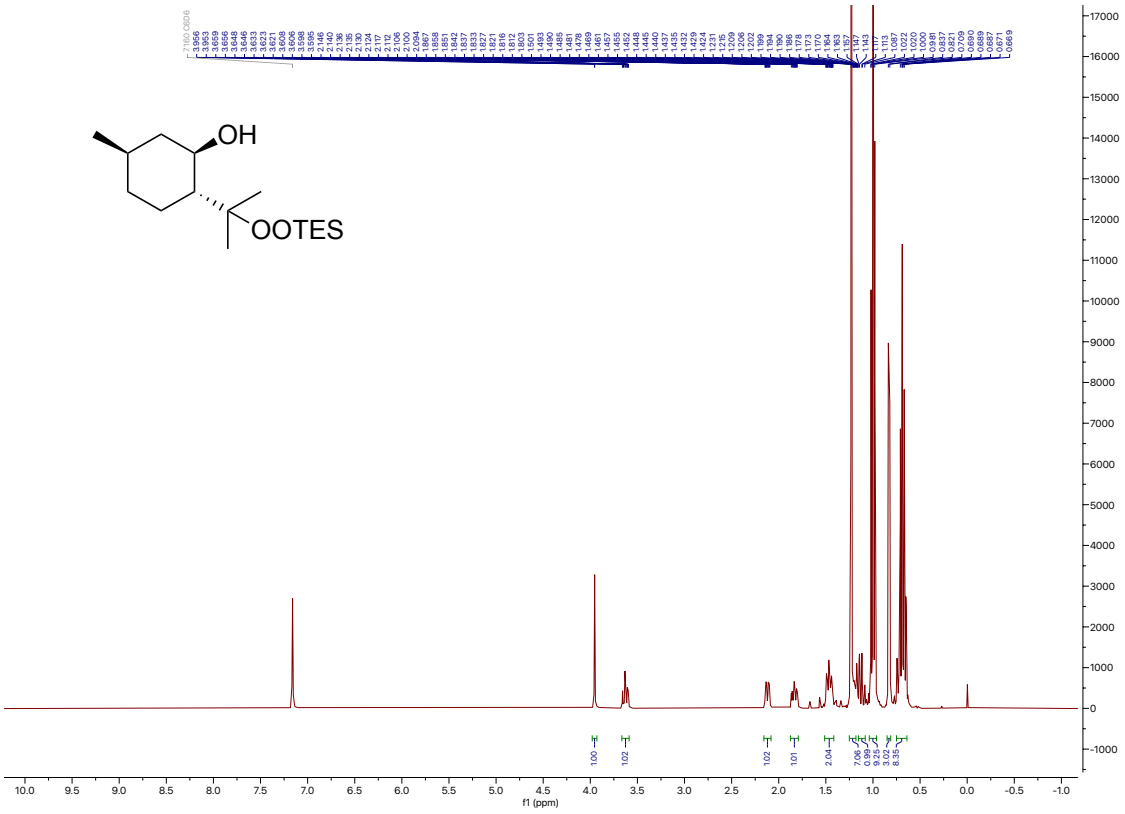
^{1}H NMR (400 MHz, $CDCl_3$) and ^{13}C NMR (101 MHz, $CDCl_3$) of **1b**

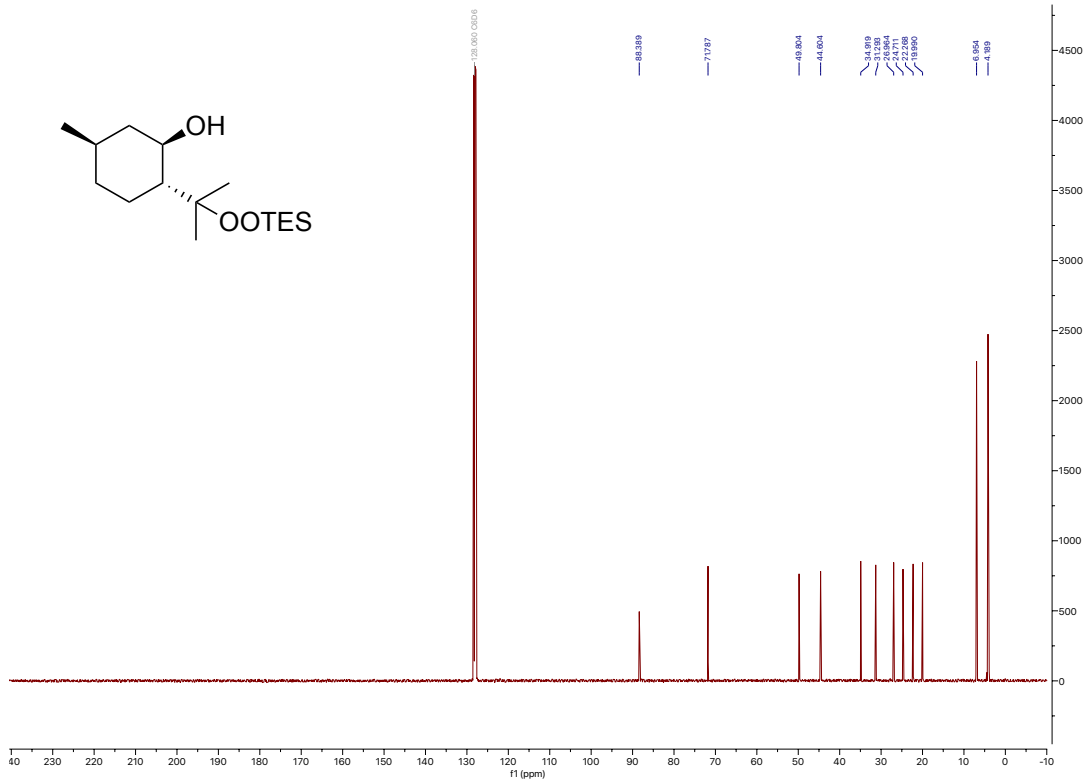


^{1}H NMR (400 MHz, $CDCl_3$) and ^{13}C NMR (101 MHz, $CDCl_3$) of **1b'**

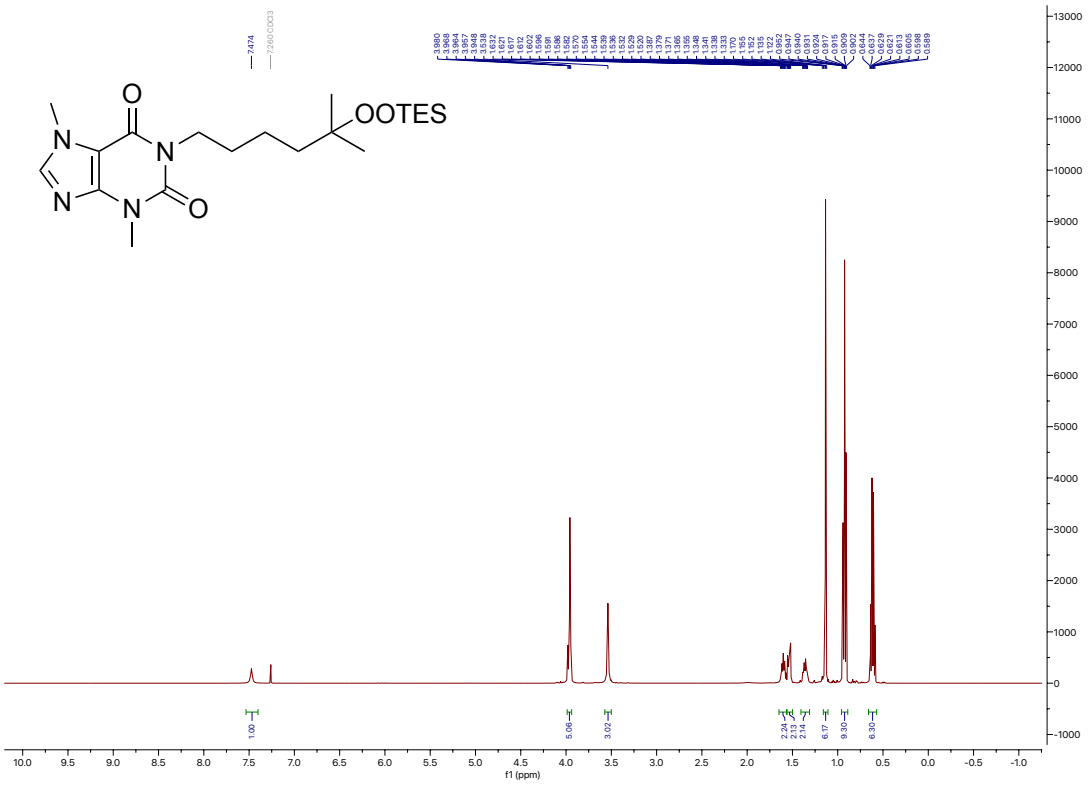


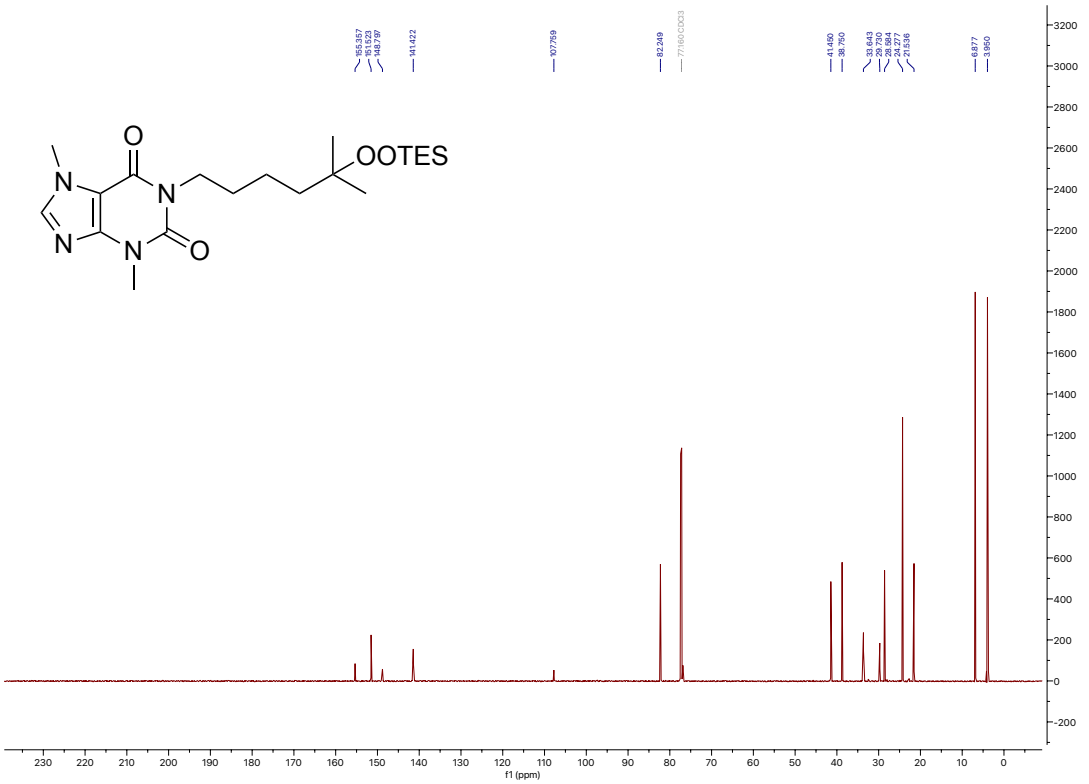
^{1}H NMR (400 MHz, $CDCl_3$) and ^{13}C NMR (101 MHz, $CDCl_3$) of **1b"**



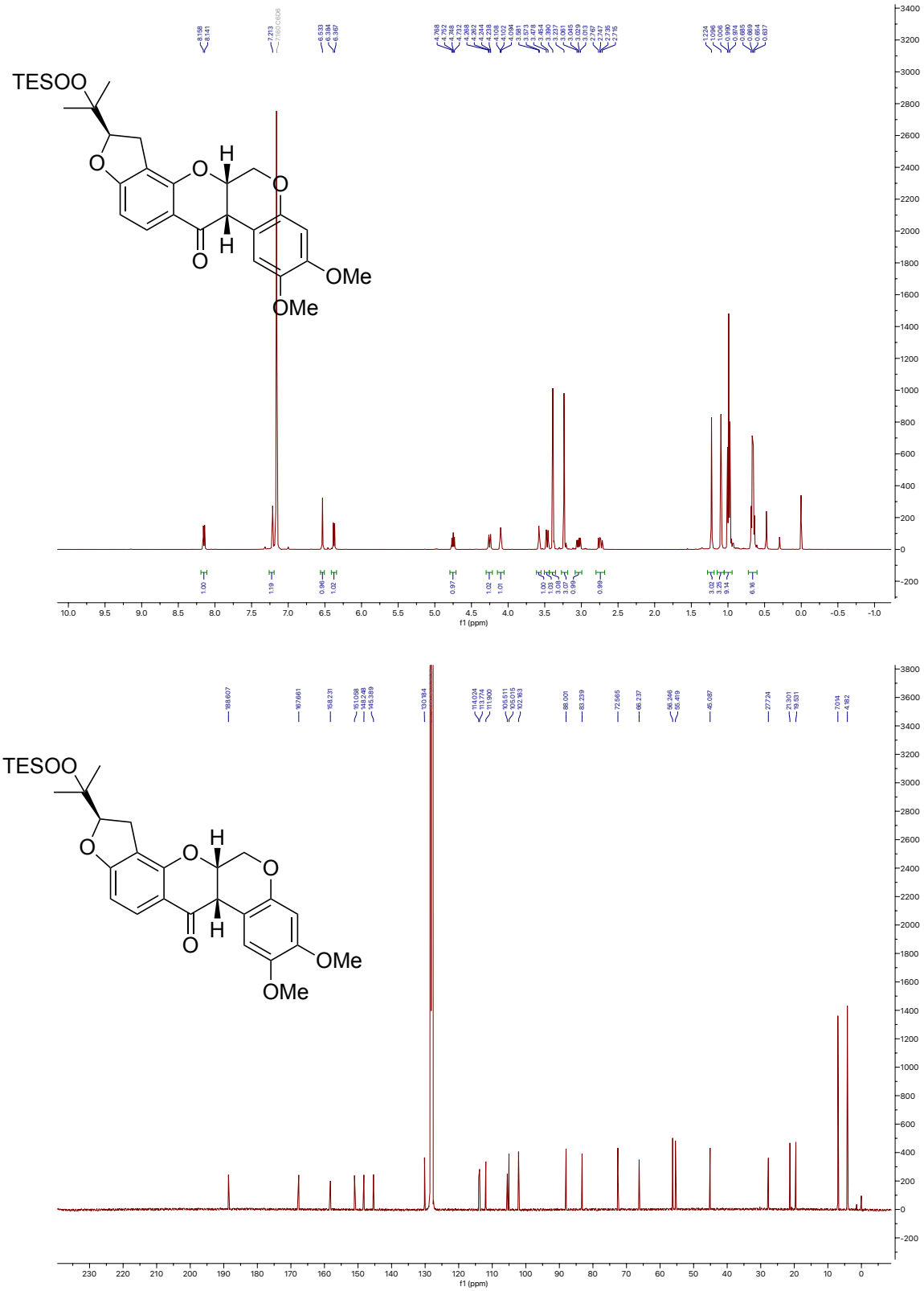


^{1}H NMR (400 MHz, C_6D_6) and ^{13}C NMR (101 MHz, C_6D_6) of **2b**

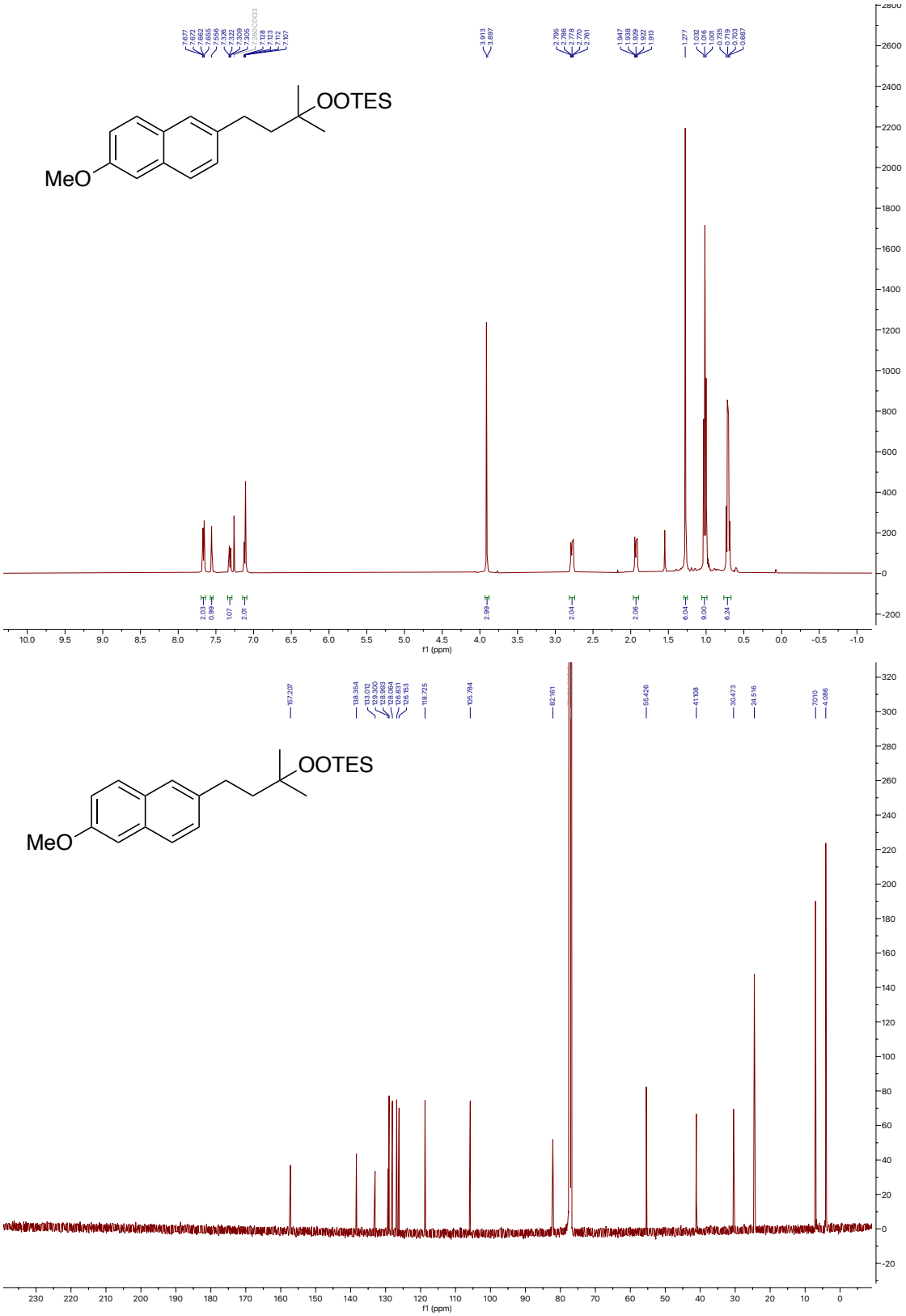




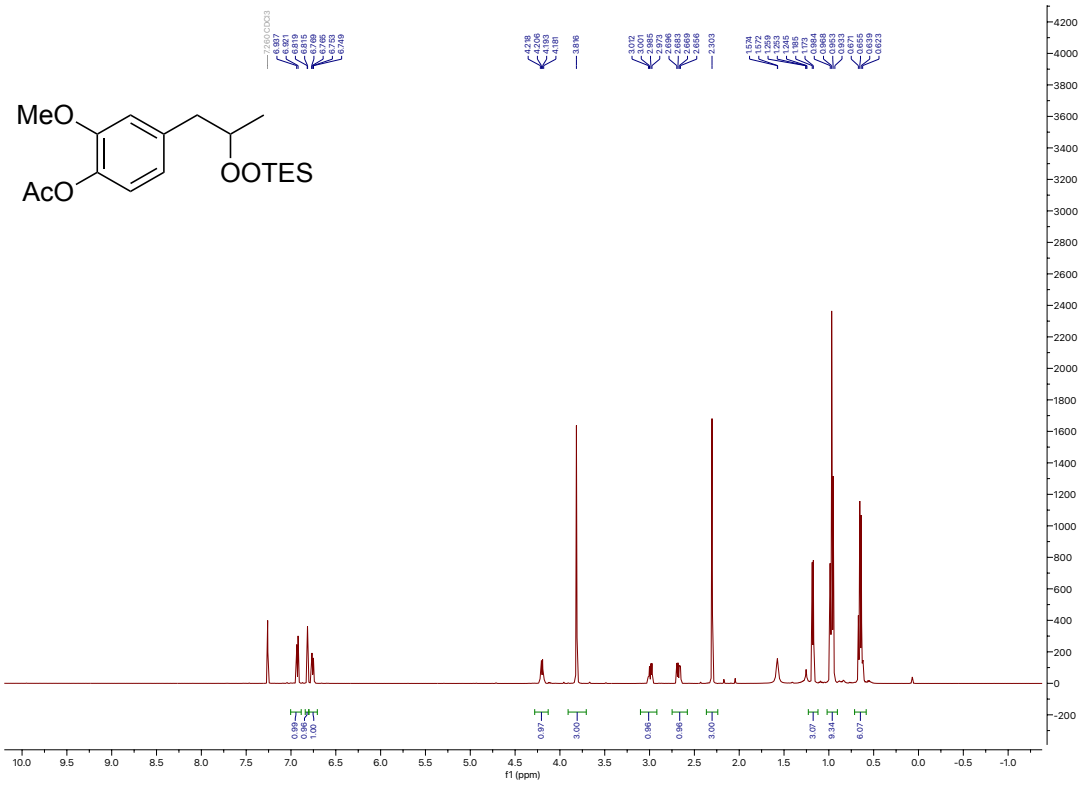
^{1}H NMR (500 MHz, $CDCl_3$) and ^{13}C NMR (126 MHz, $CDCl_3$) of **3b**

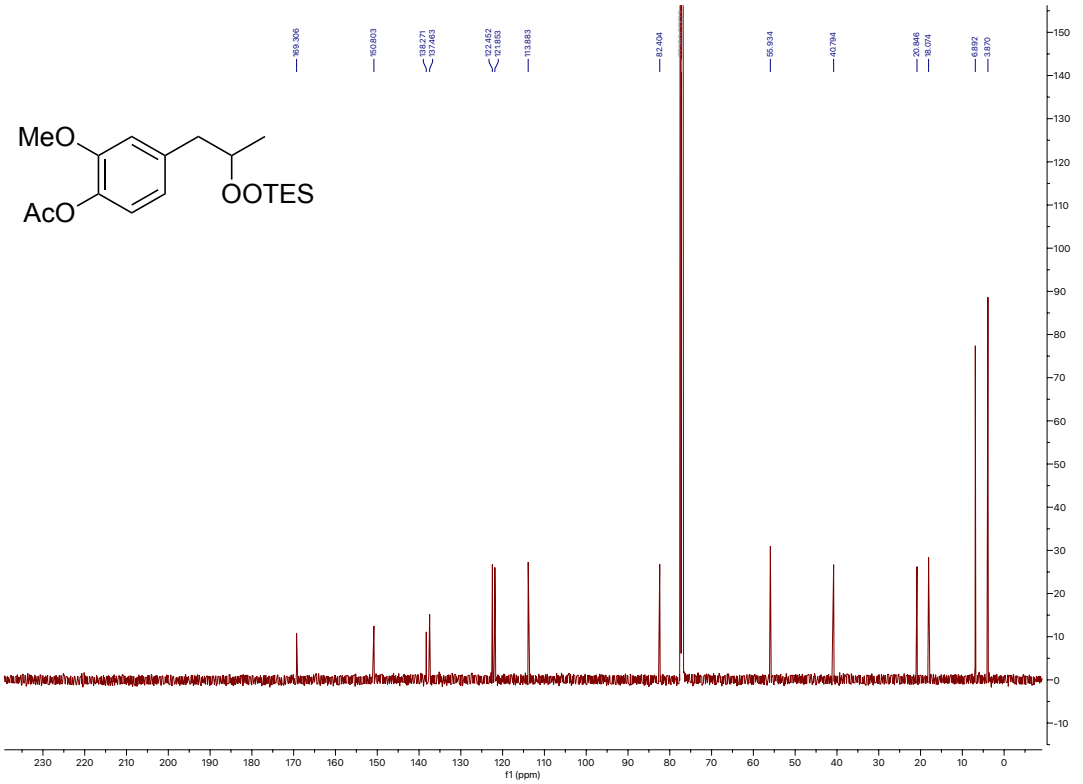


^{1}H NMR (500 MHz, C_6D_6) and ^{13}C NMR (126 MHz, C_6D_6) of **4b**

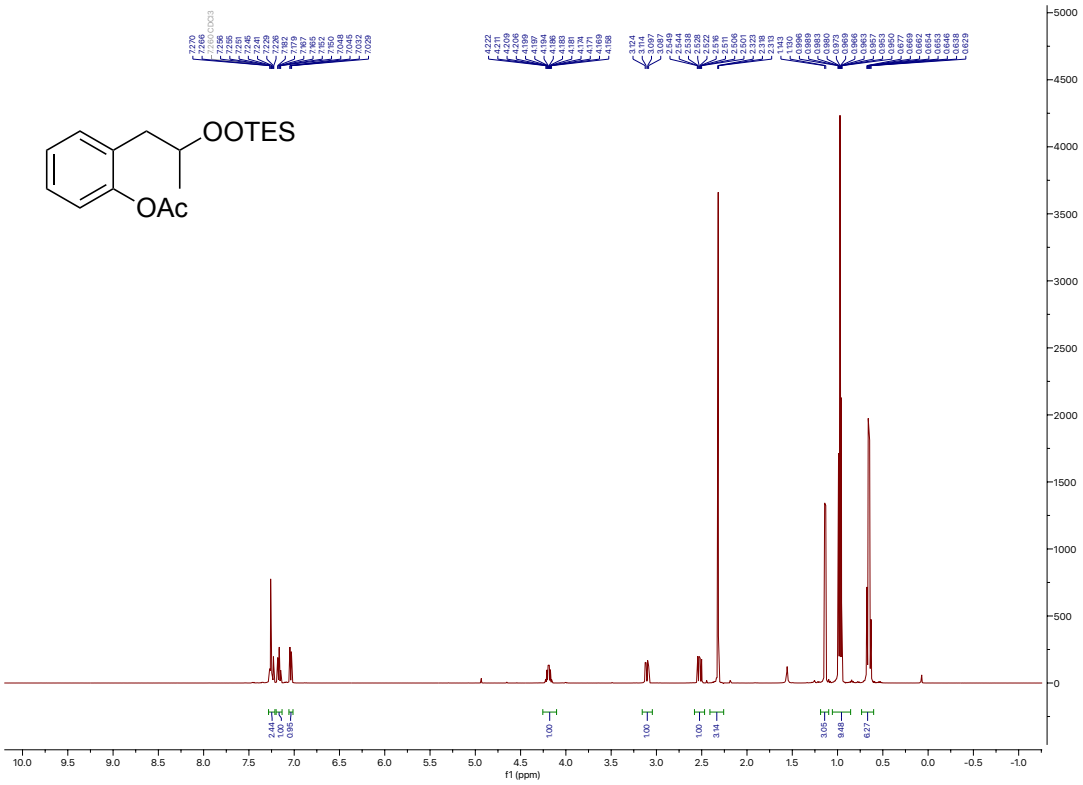


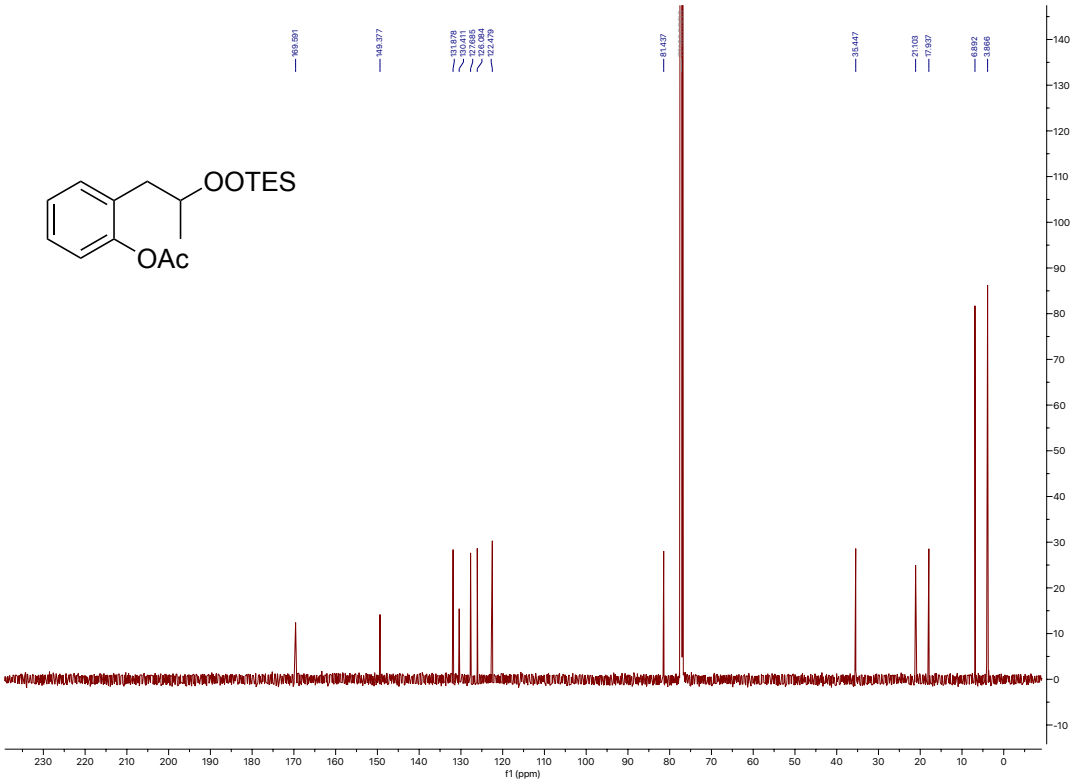
^{1}H NMR (500 MHz, $CDCl_3$) and ^{13}C NMR (126 MHz, $CDCl_3$) of **5b**



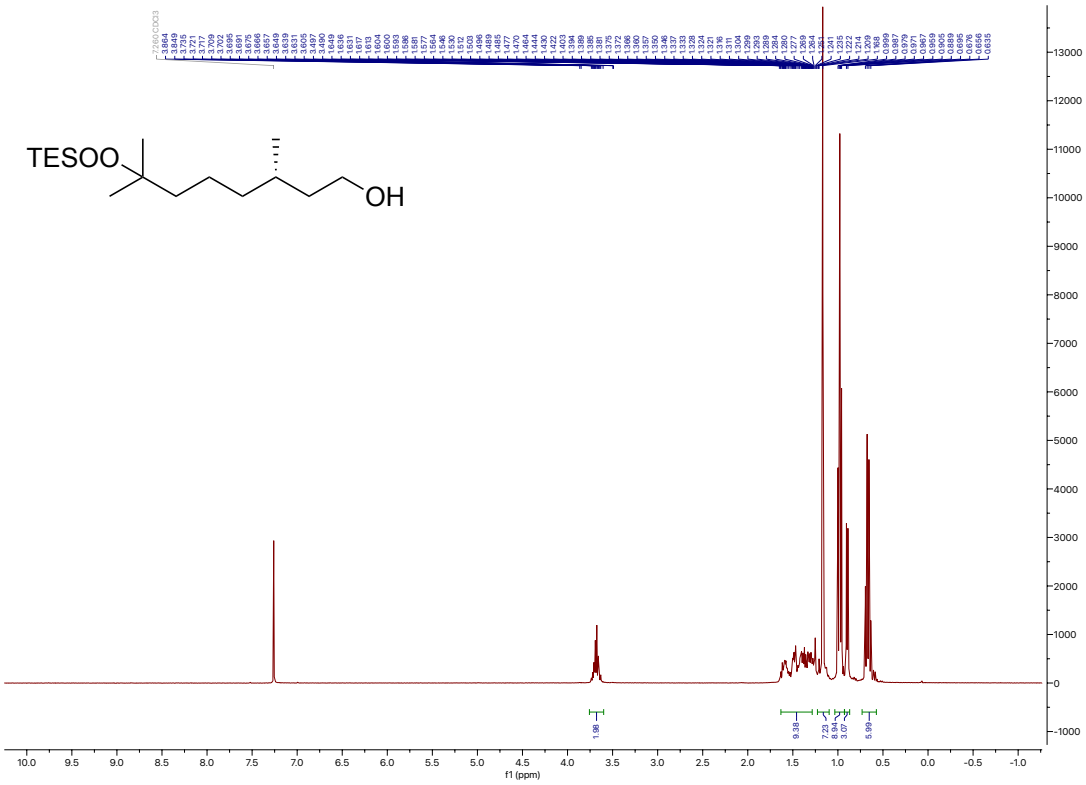


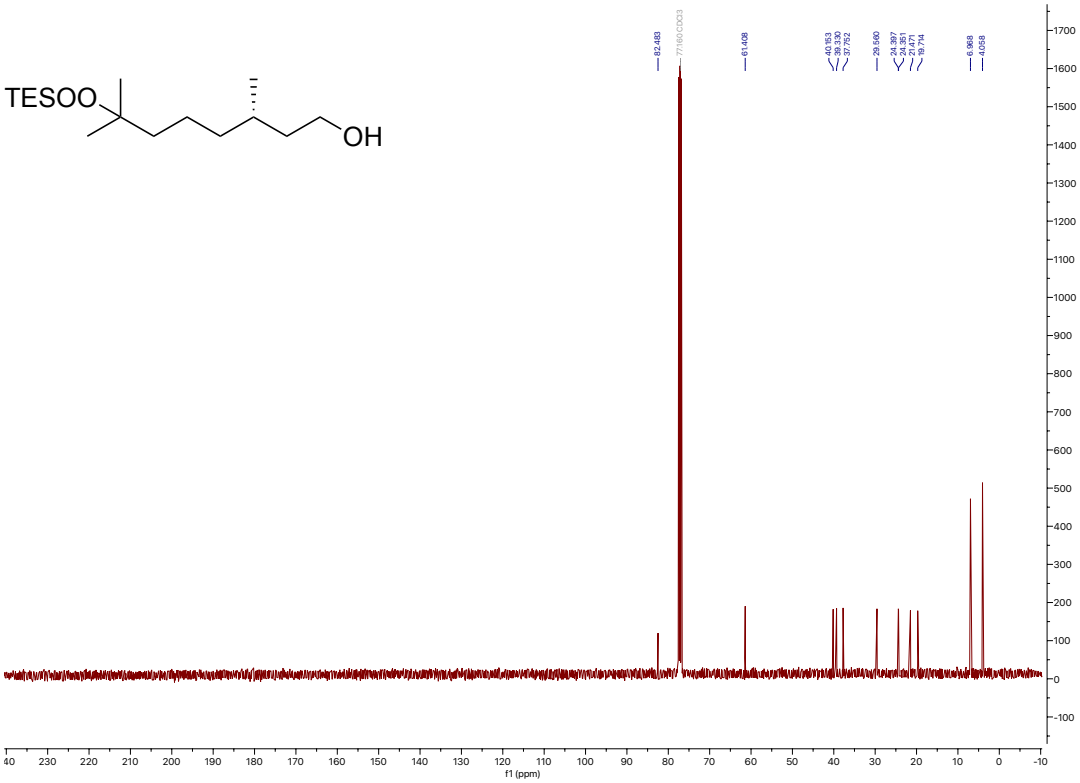
^{1}H NMR (500 MHz, $CDCl_3$) and ^{13}C NMR (126 MHz, $CDCl_3$) of **6b**



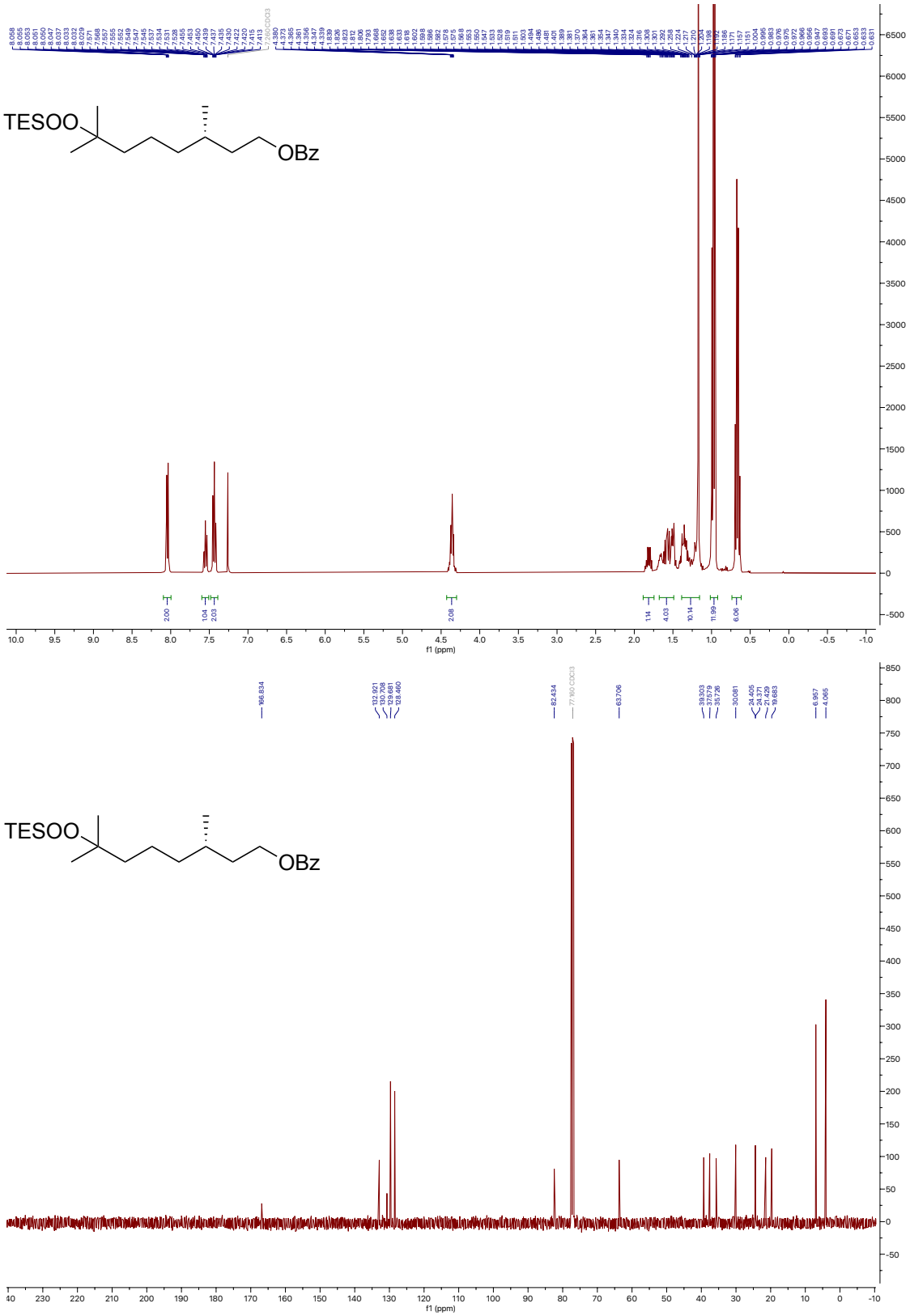


^{1}H NMR (500 MHz, $CDCl_3$) and ^{13}C NMR (126 MHz, $CDCl_3$) of **7b**

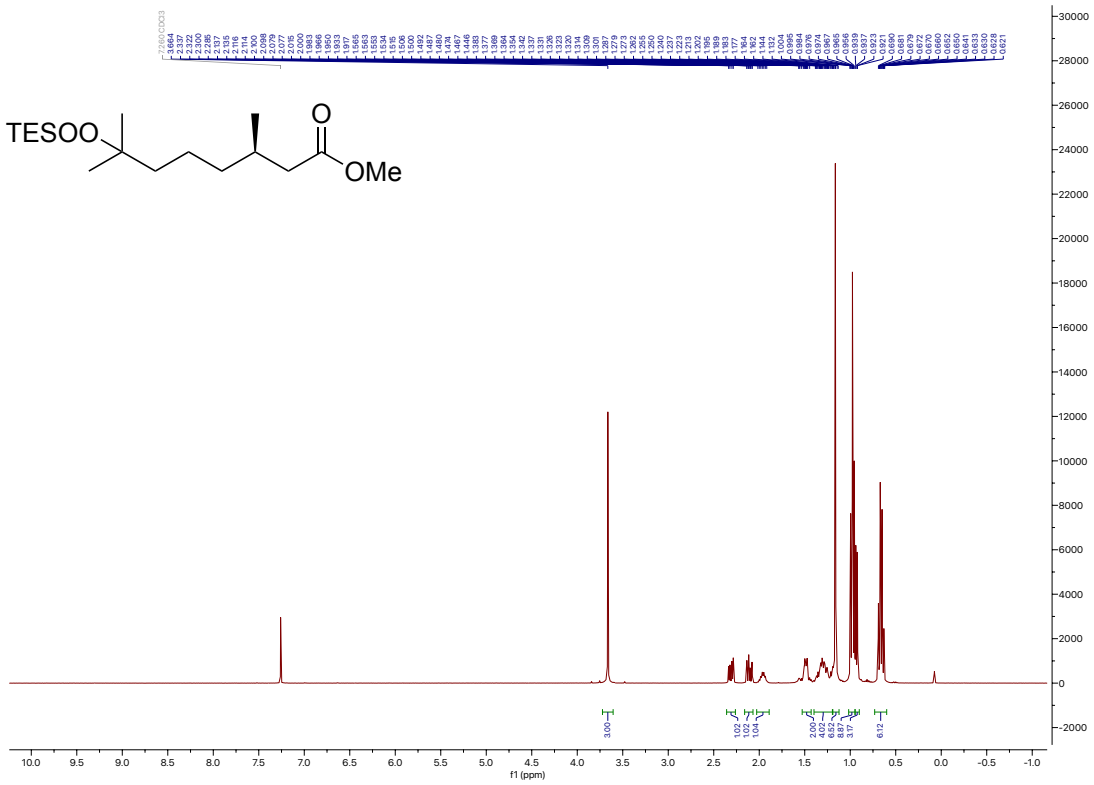


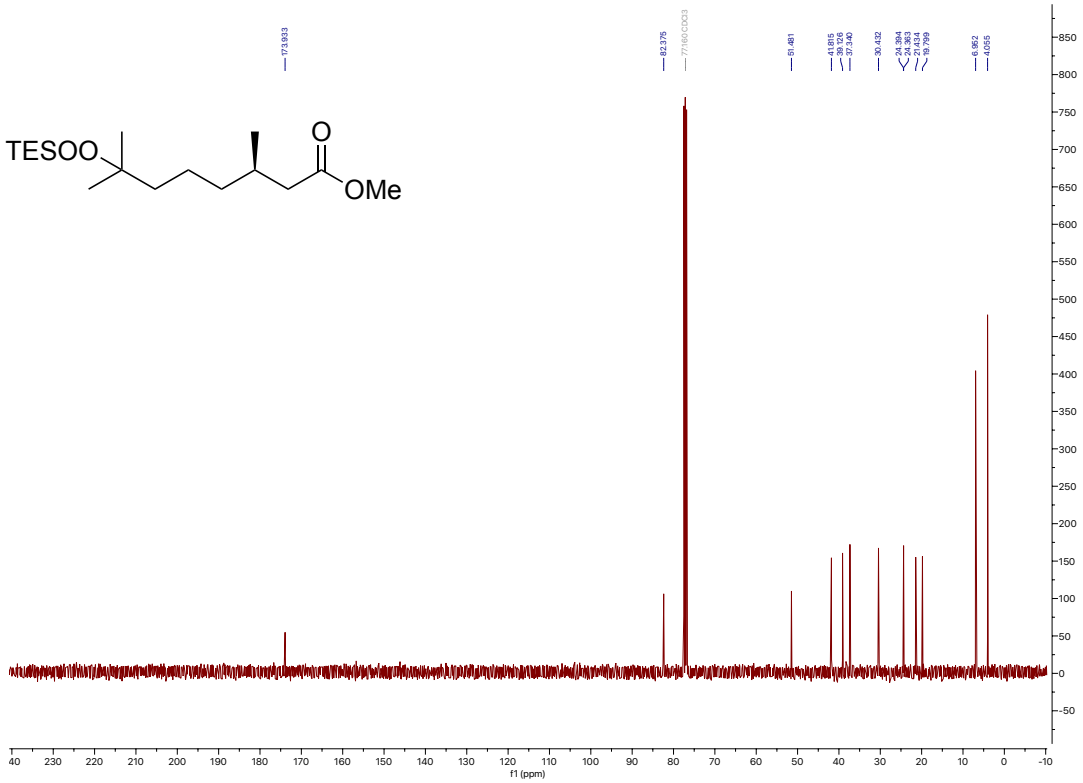


^{1}H NMR (400 MHz, $CDCl_3$) and ^{13}C NMR (101 MHz, $CDCl_3$) of **8b**

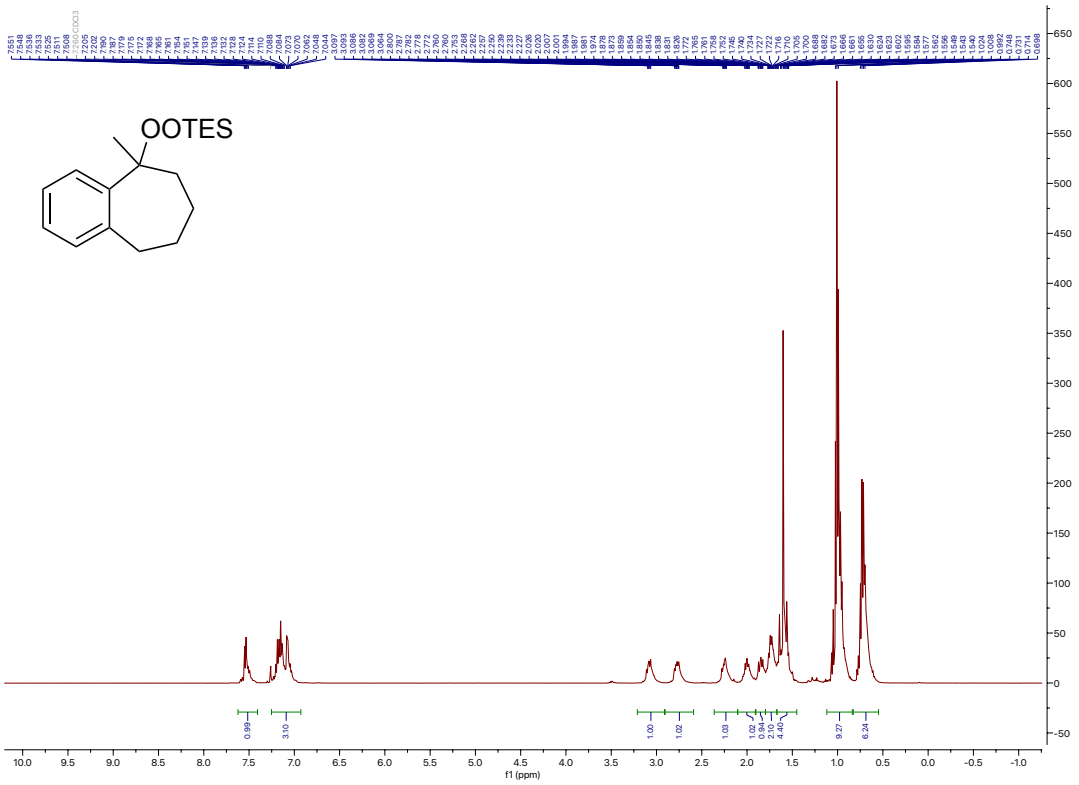


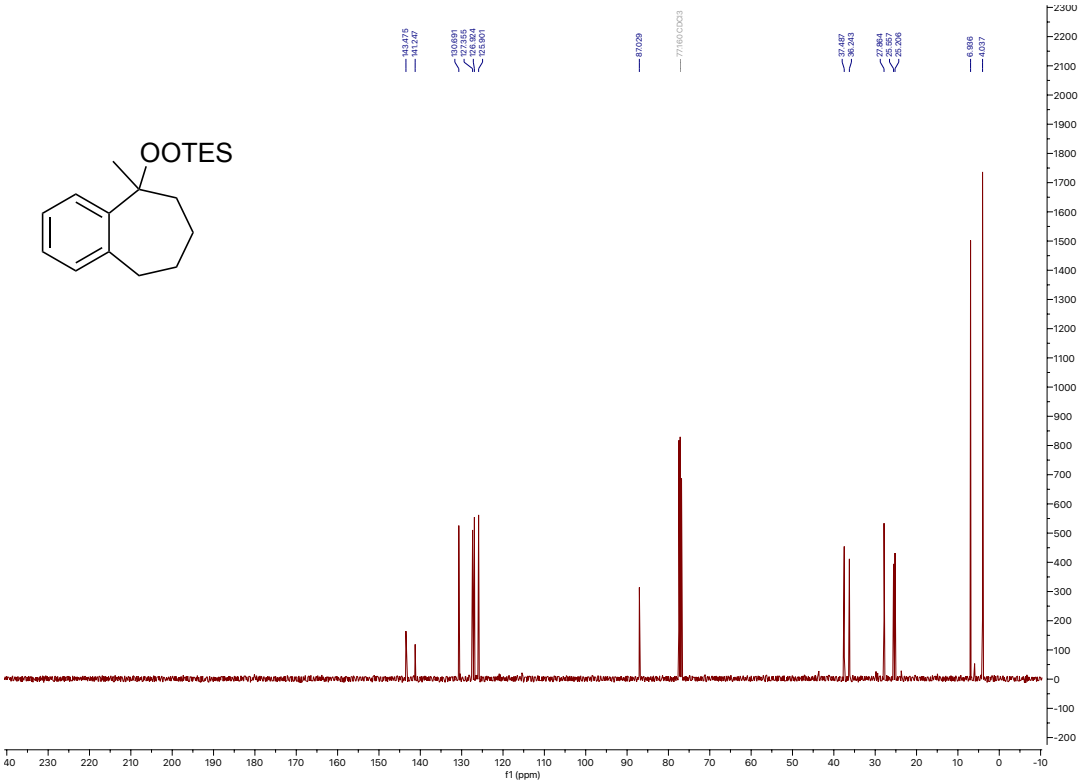
^{1}H NMR (400 MHz, $CDCl_3$) and ^{13}C NMR (101 MHz, $CDCl_3$) of **9b**



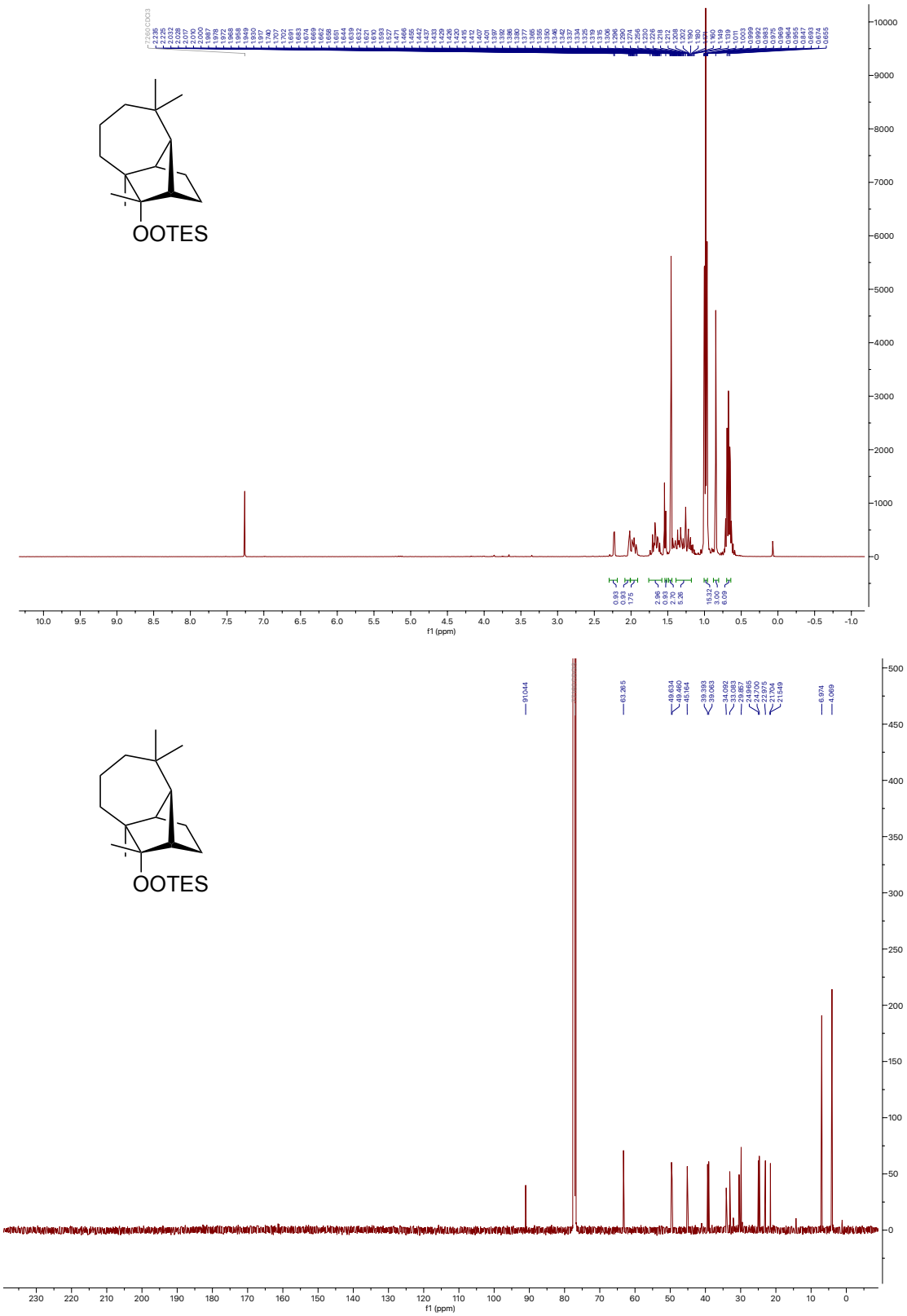


^{1}H NMR (400 MHz, $CDCl_3$) and ^{13}C NMR (101 MHz, $CDCl_3$) of **10b**

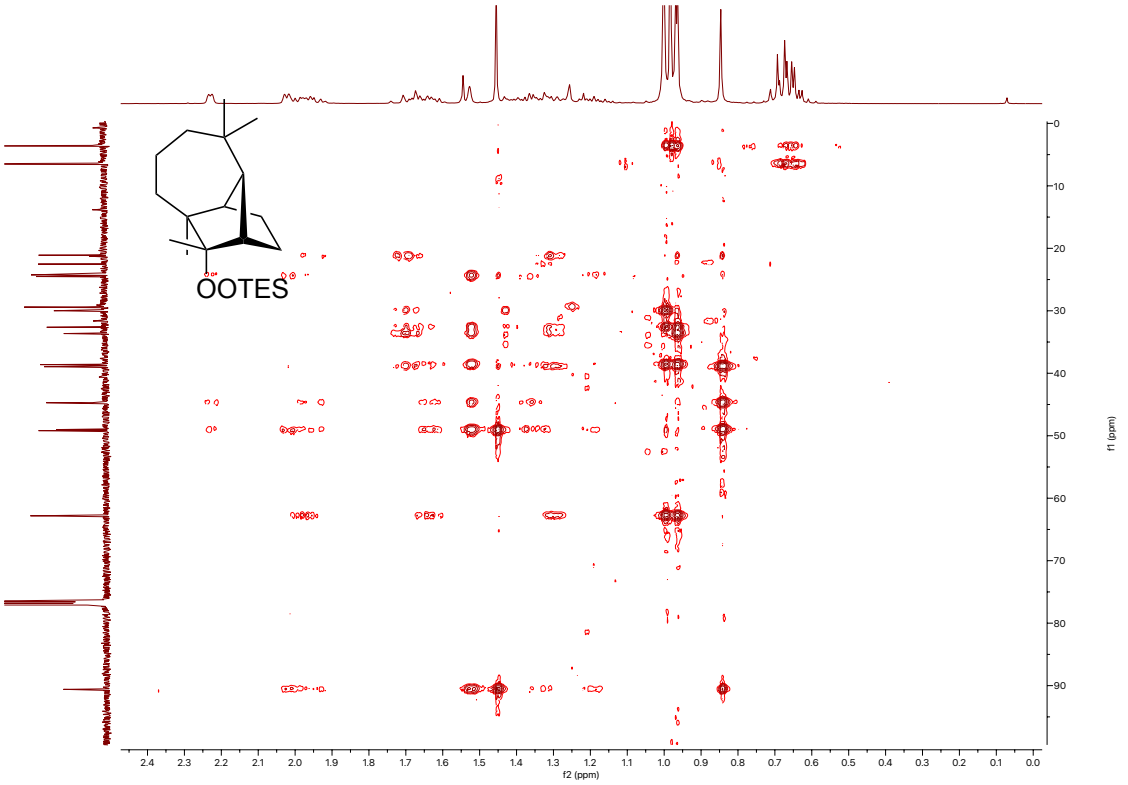


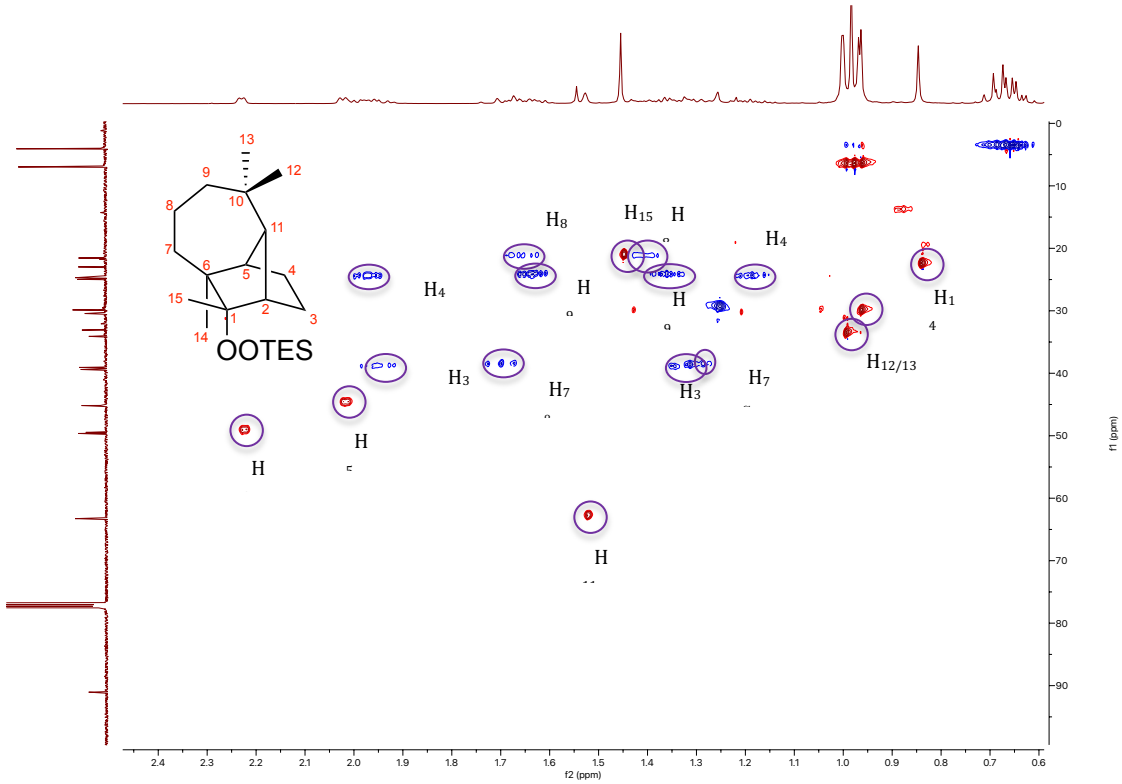


^{1}H NMR (500 MHz, $CDCl_3$) and ^{13}C NMR (101 MHz, $CDCl_3$) of **11b**

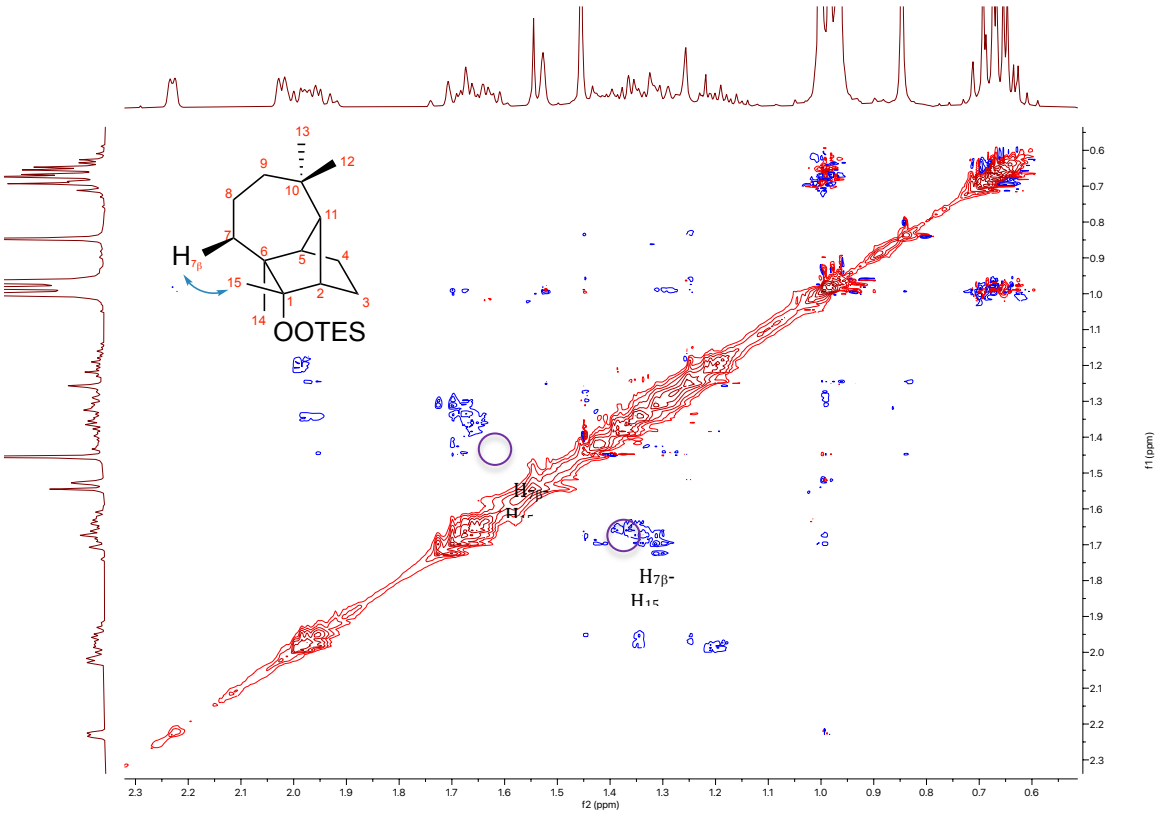


^{1}H NMR (400 MHz, $CDCl_3$) and ^{13}C NMR (126 MHz, $CDCl_3$) of **12b**

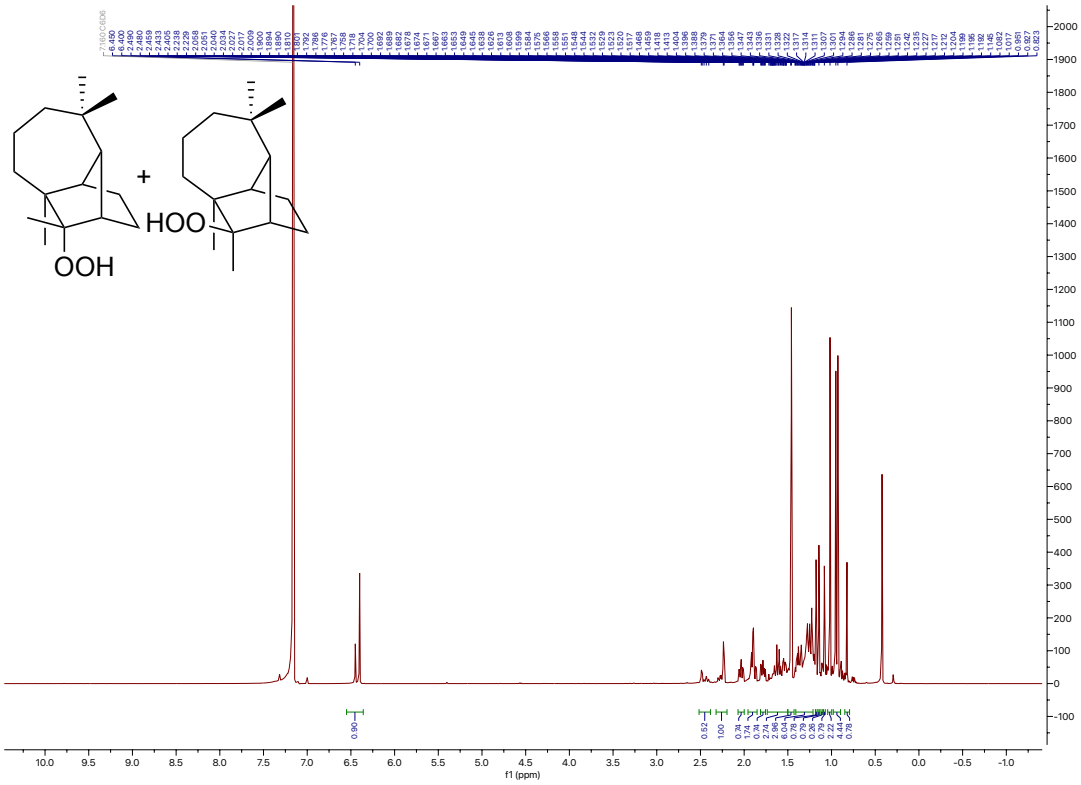


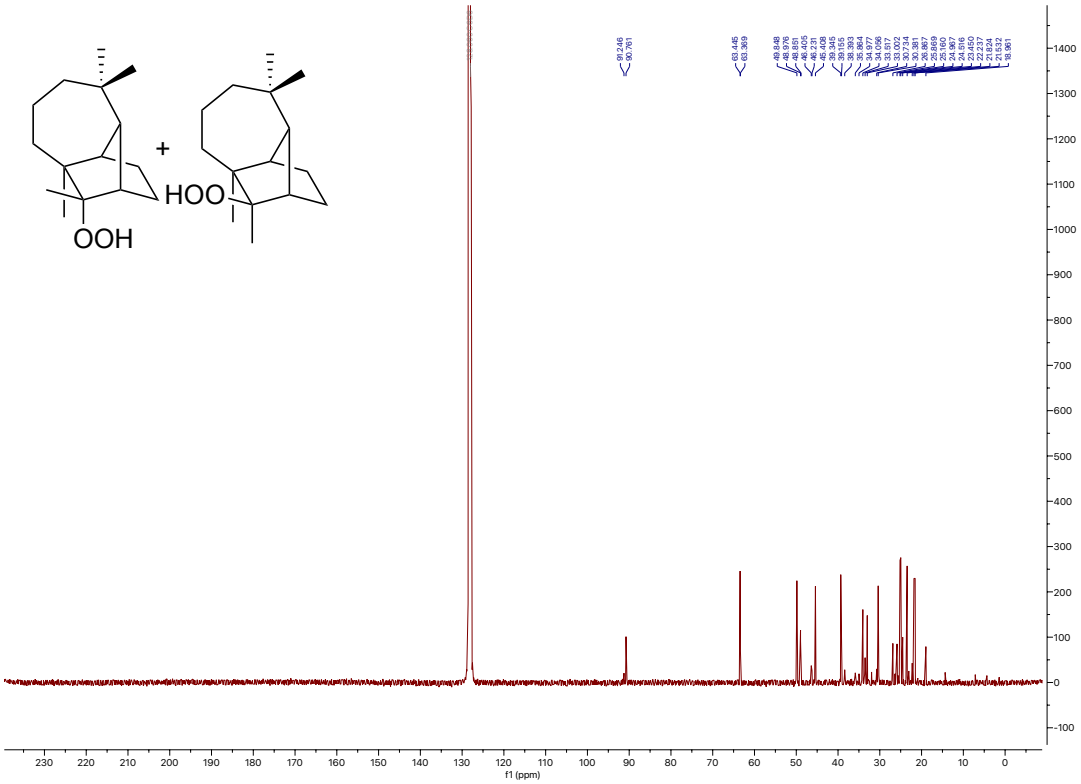


HMBC and HSQC of **12b**

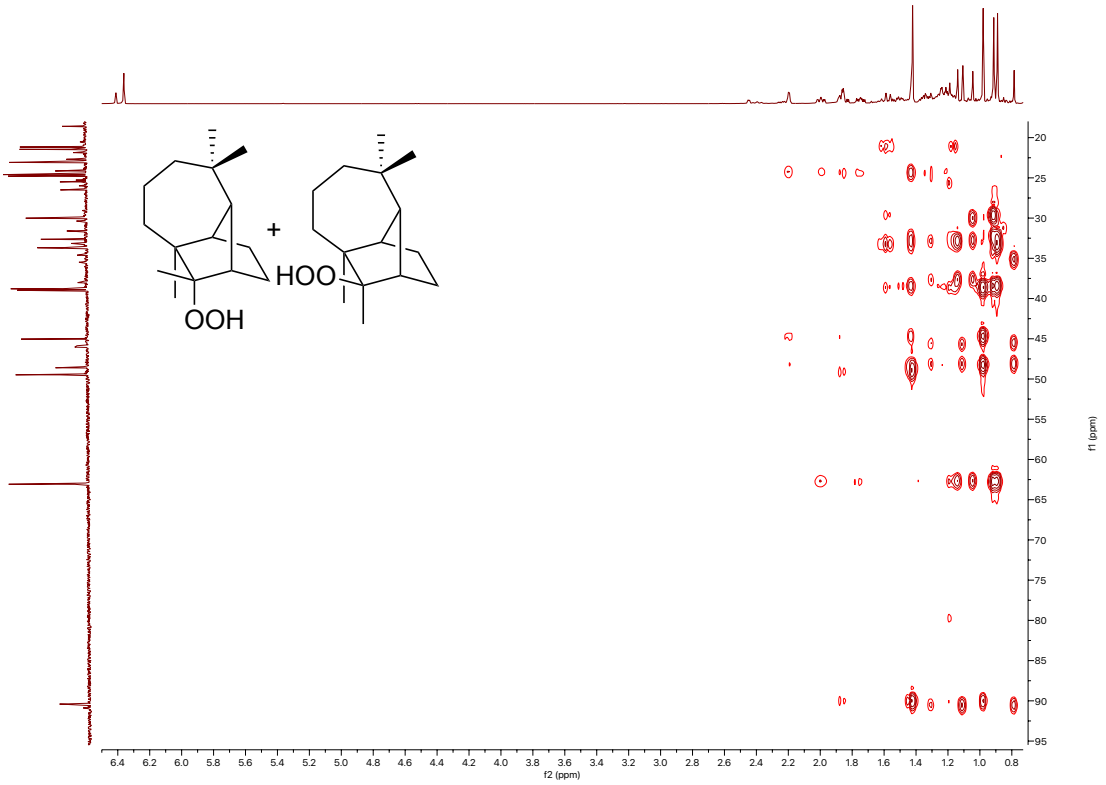

13
9
12
8
10
11
7
6
5
4
15
1
2
3
14
OOTES
H7β
H7β-
H15
H7β-
H15
f2 (ppm)
f1 (ppm)

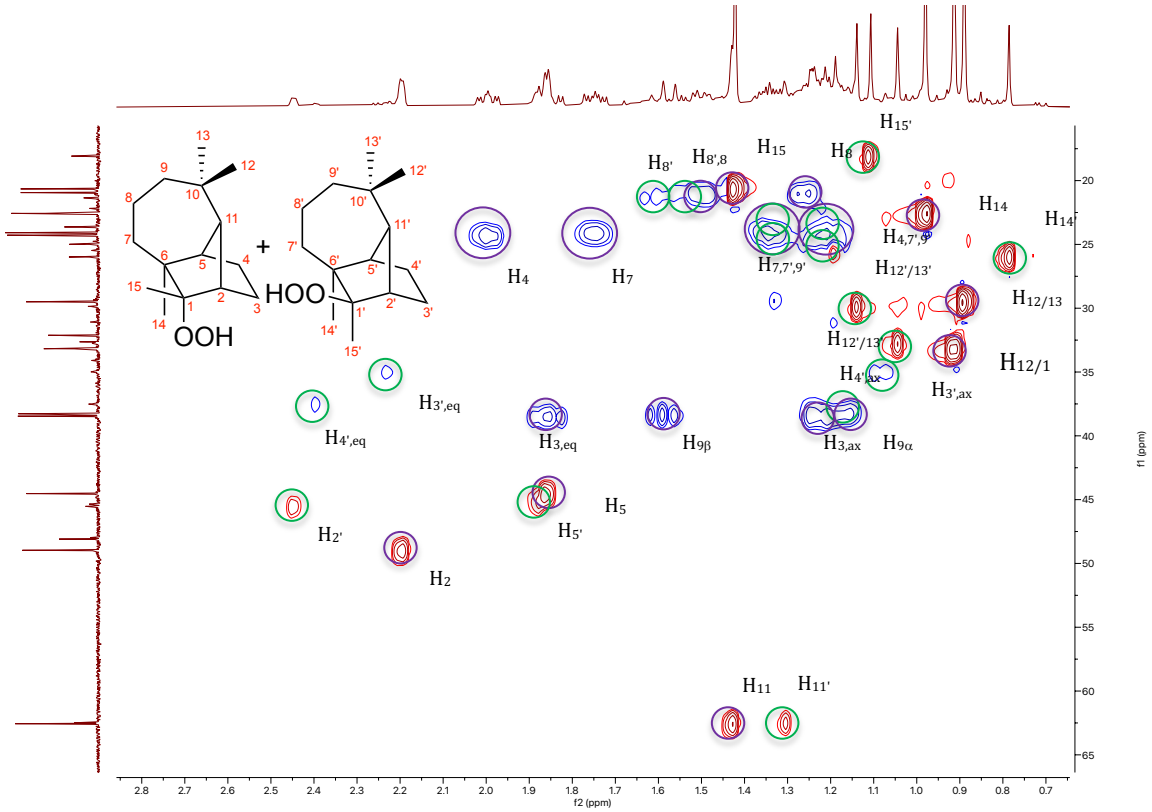
NOESY of **12b**



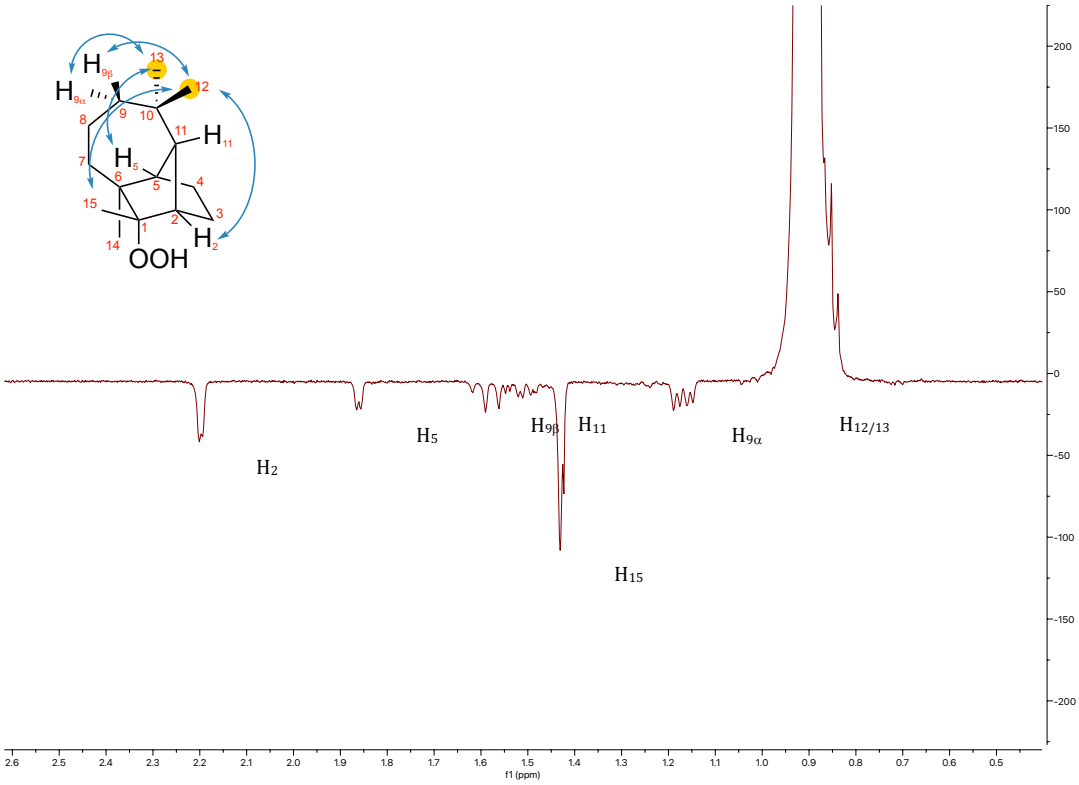


^{1}H NMR (500 MHz, C_6D_6) and ^{13}C NMR (126 MHz, C_6D_6) of **12b'**

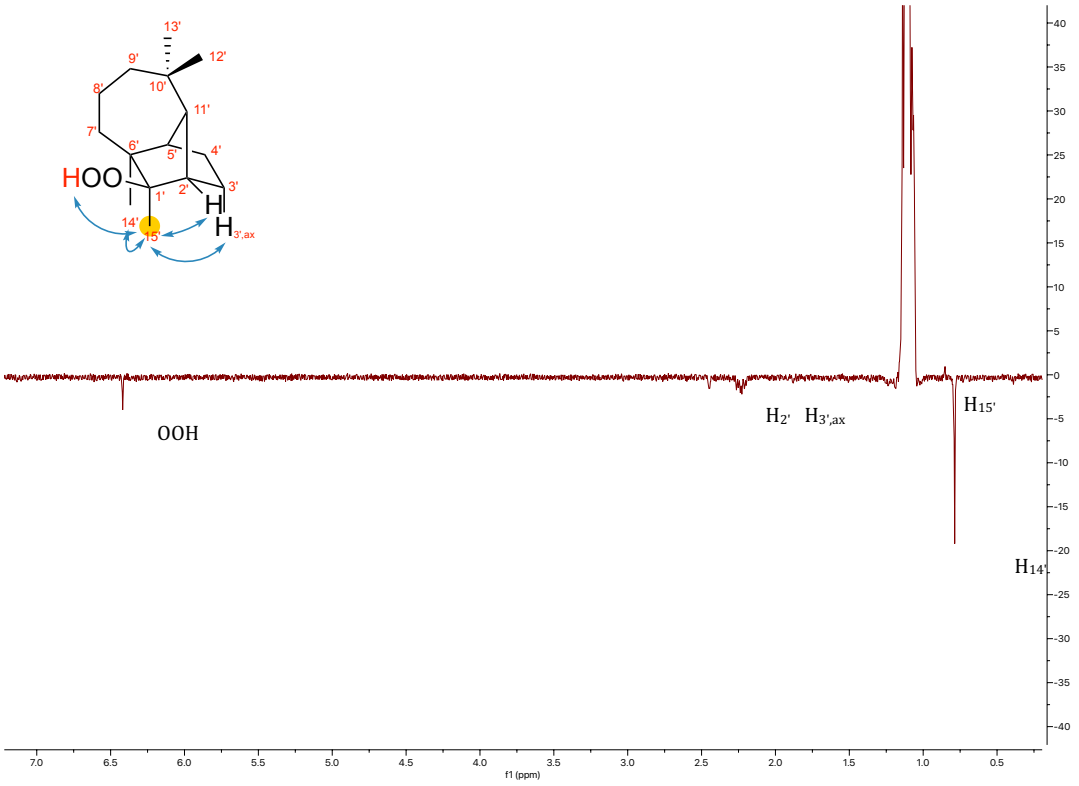




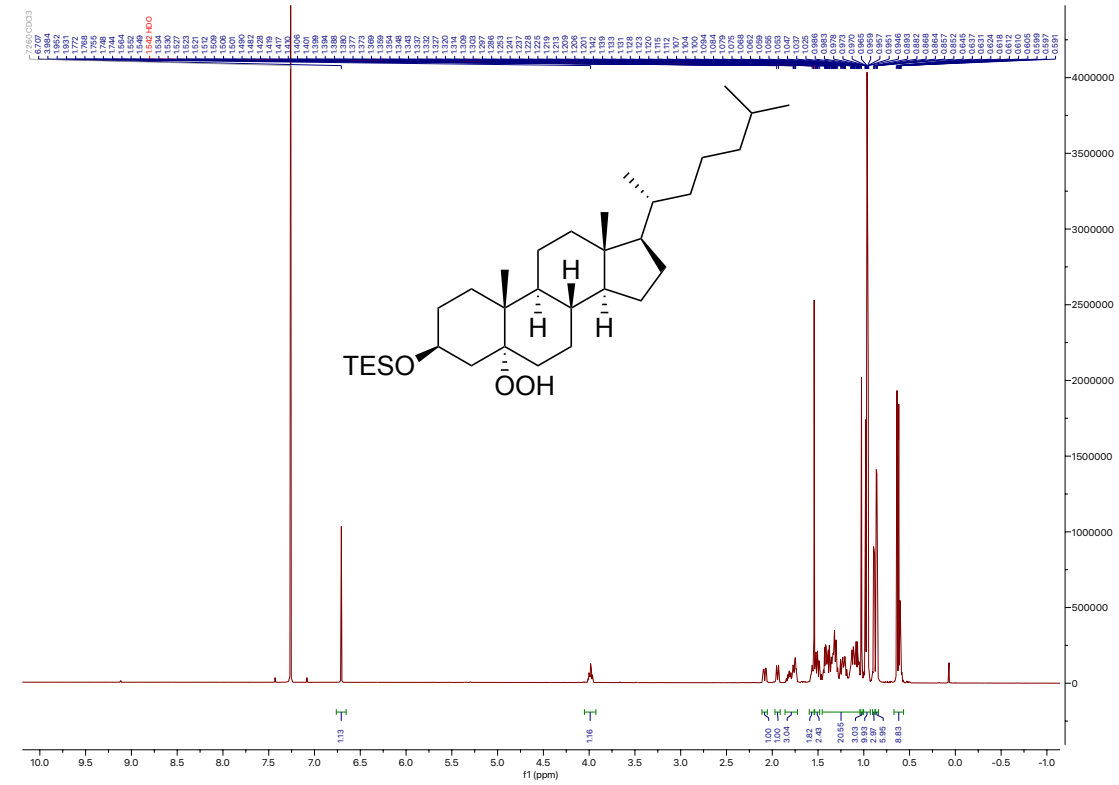
HMBC and HSQC of **12b'**

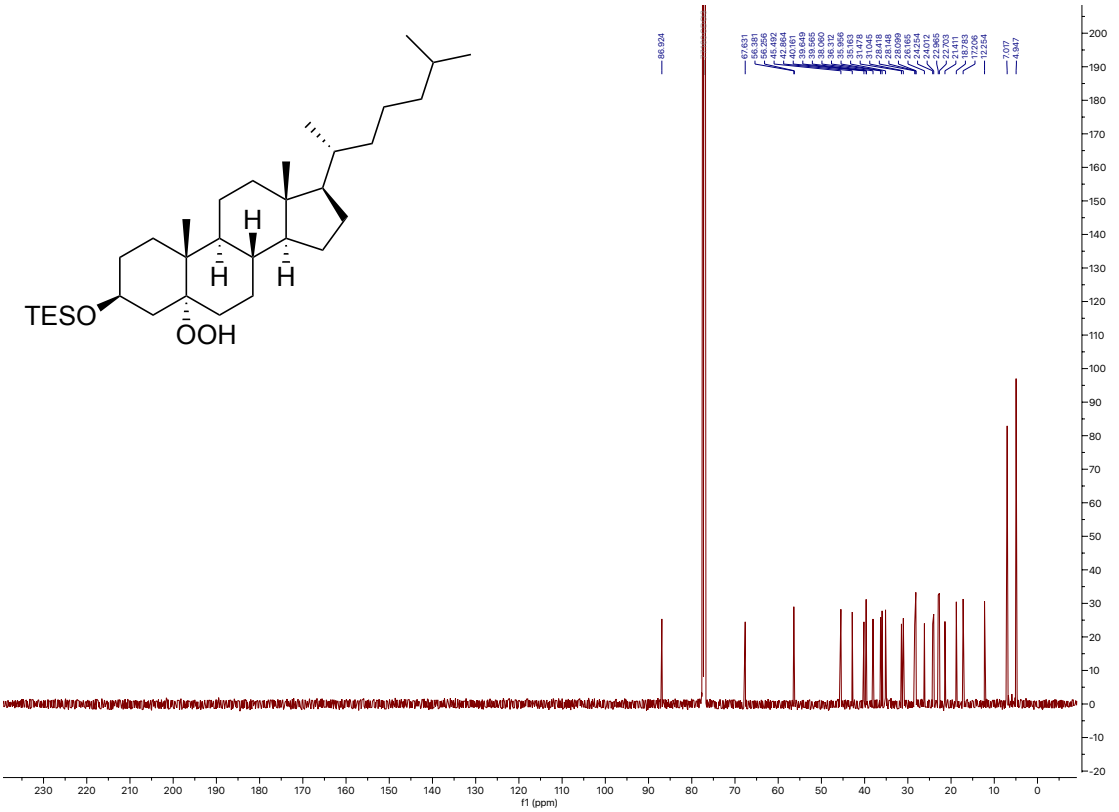


1D Selective Gradient NOESY frequency 0.926 ppm of ***endo*-12b'**

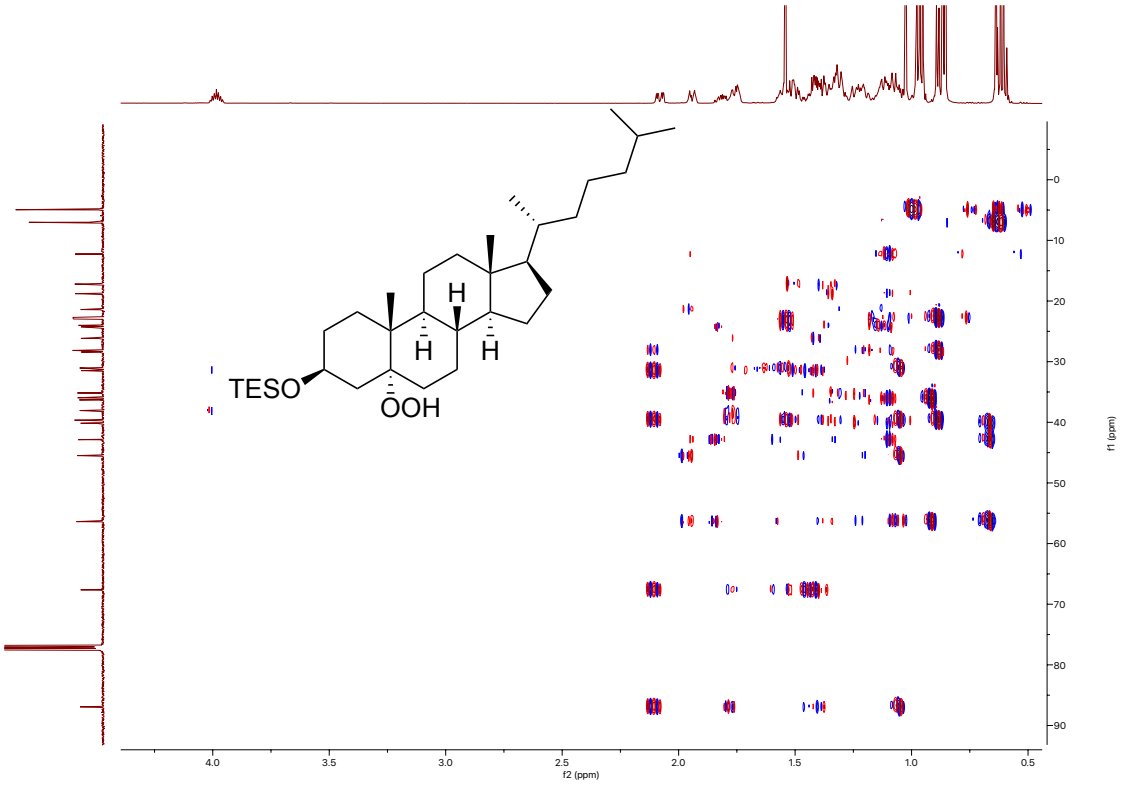


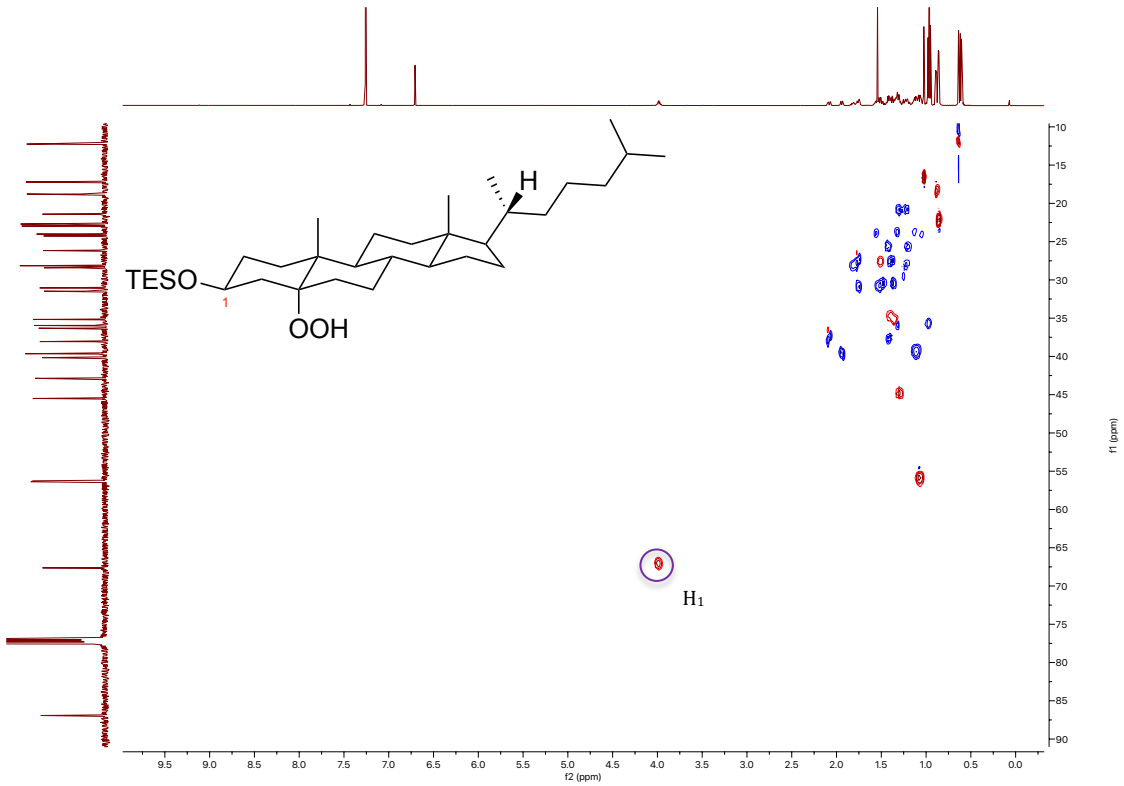
and 1D Selective Gradient NOESY frequency 1.138 ppm of ***exo*-12b'**



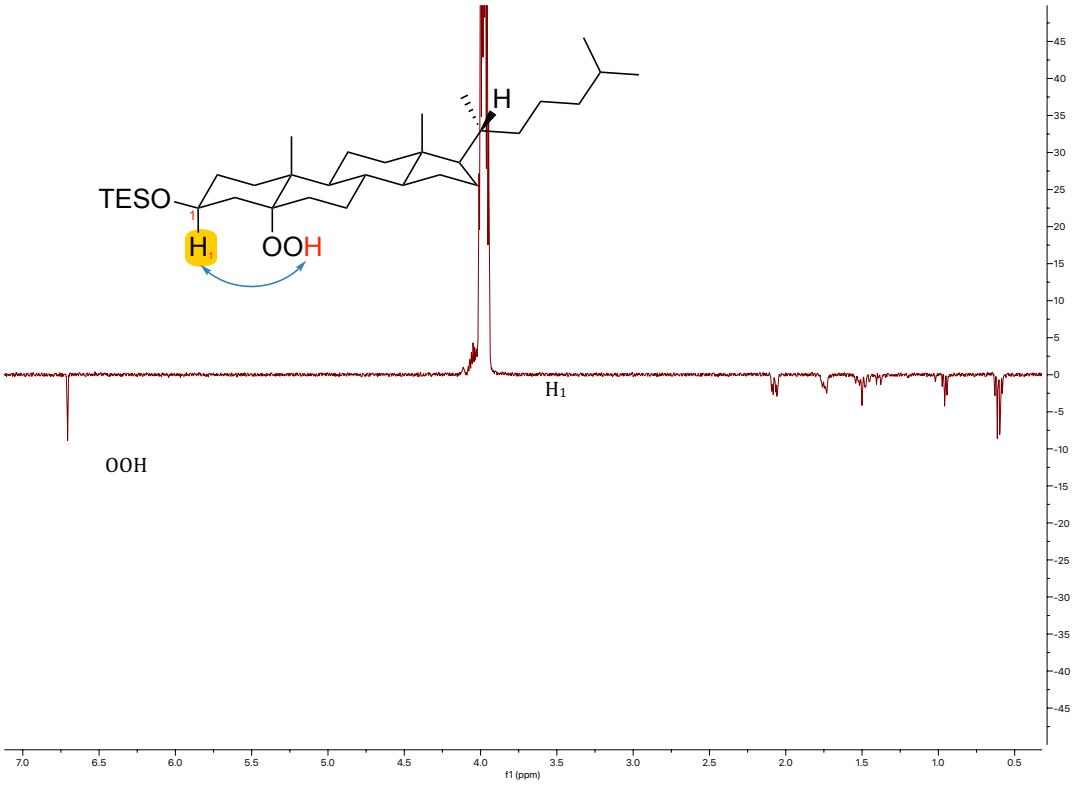


^{1}H NMR (600 MHz, $CDCl_3$) and ^{13}C NMR (126 MHz, $CDCl_3$) of **13b'**

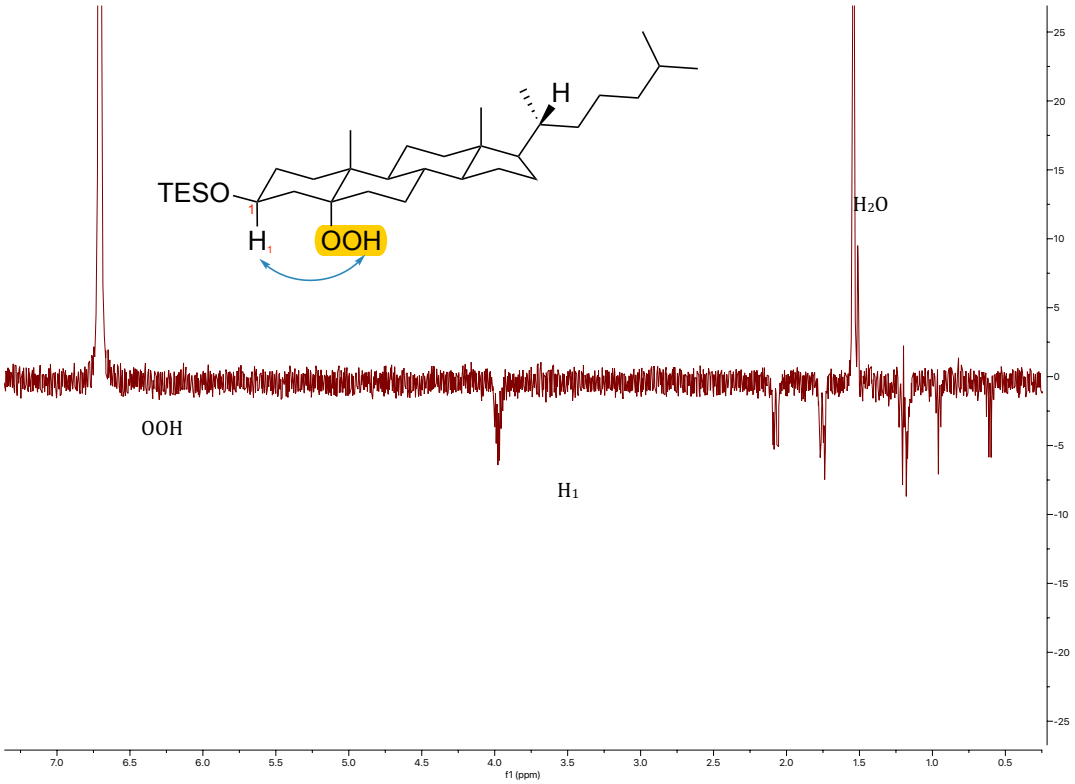




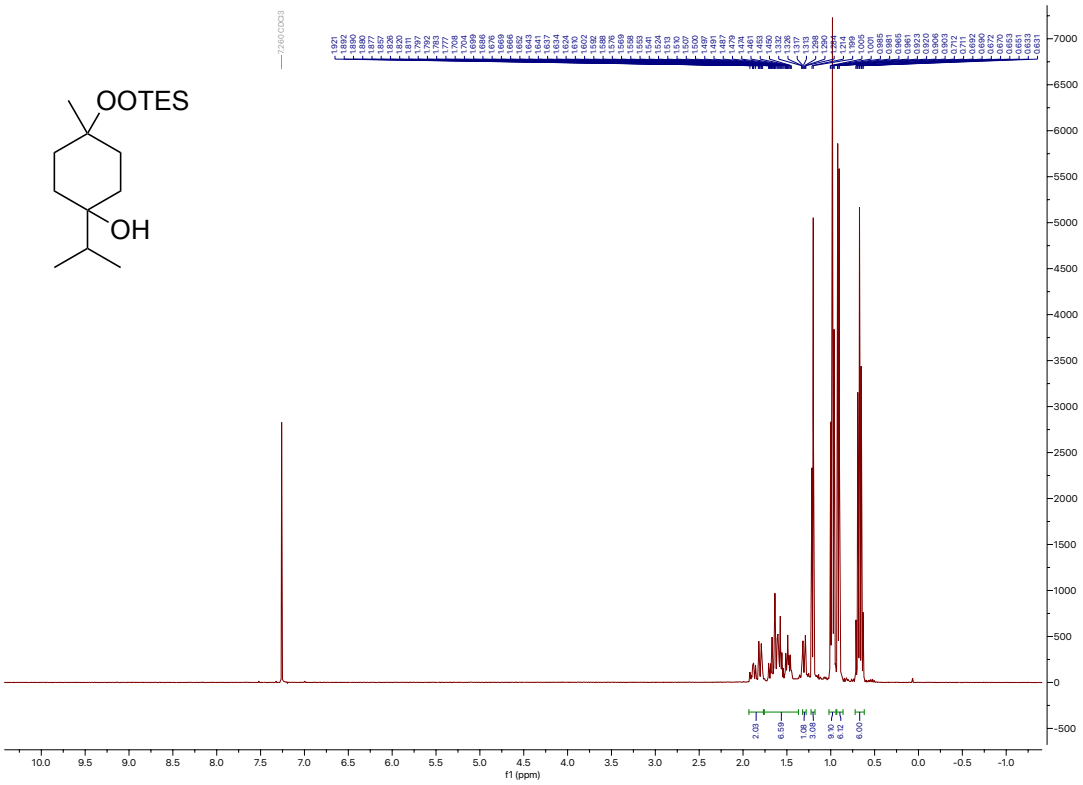
HMBC and HSQC of **13b'**

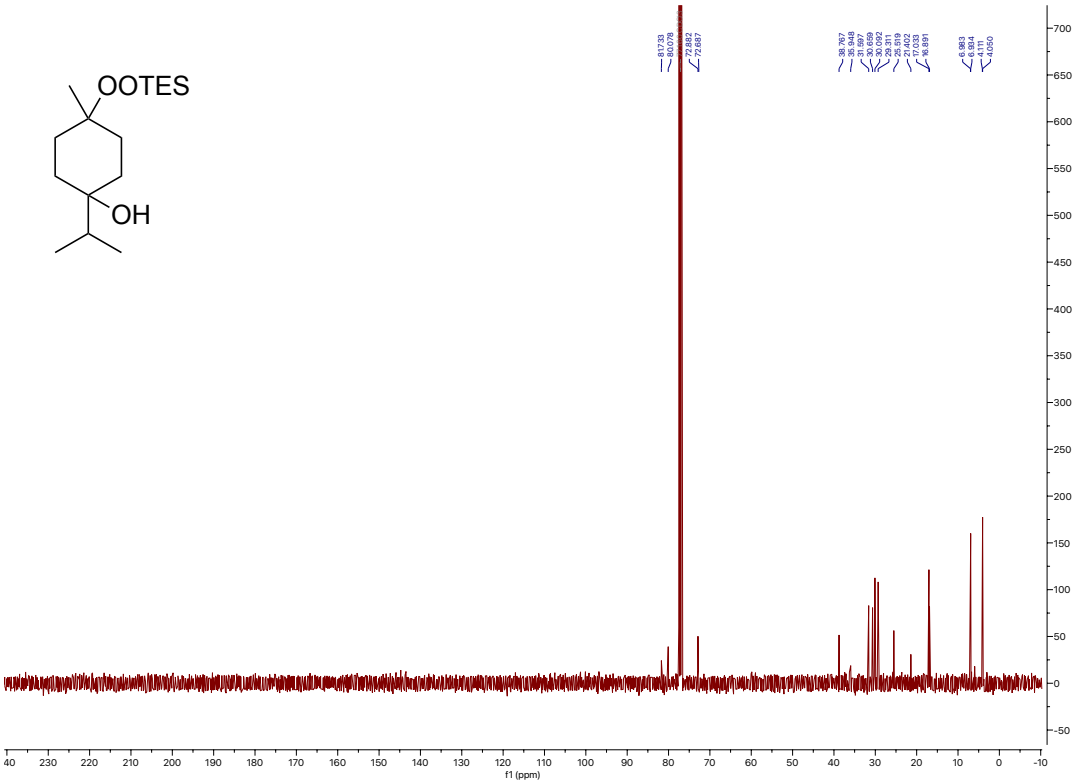


1D Selective Gradient NOESY frequency 4.021 ppm of **13b'**

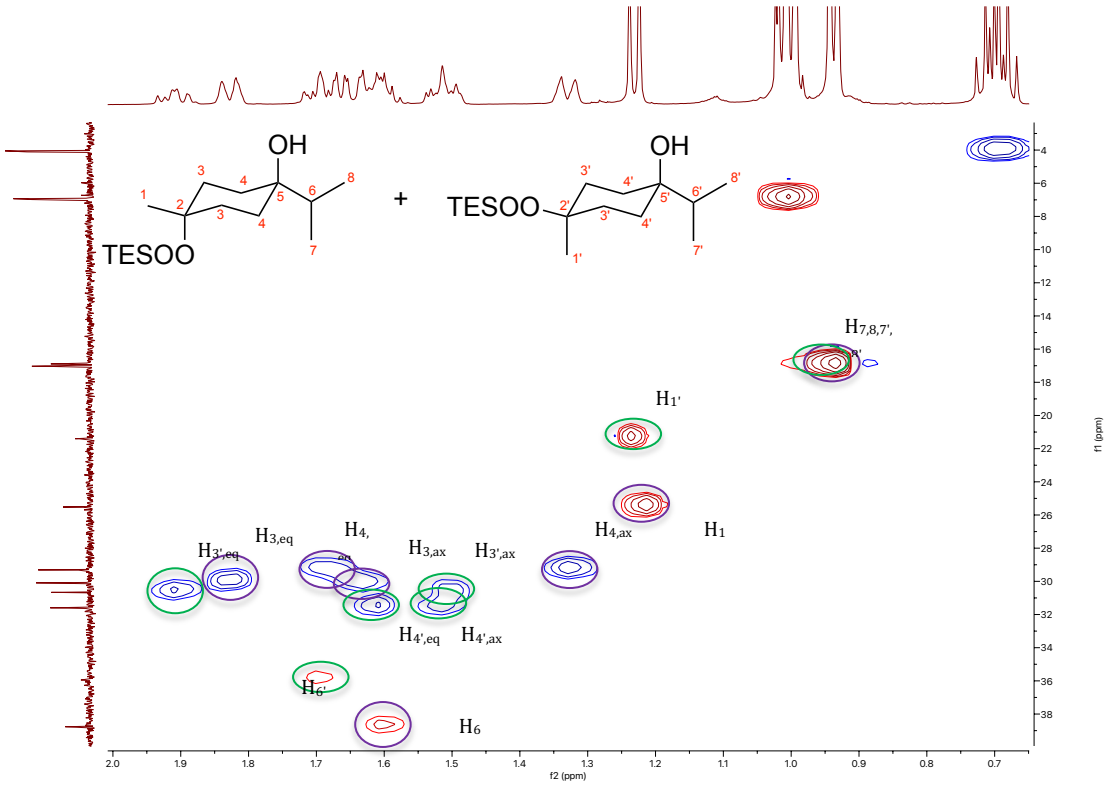


1D Selective Gradient NOESY frequency 6.734 ppm of **13b'**

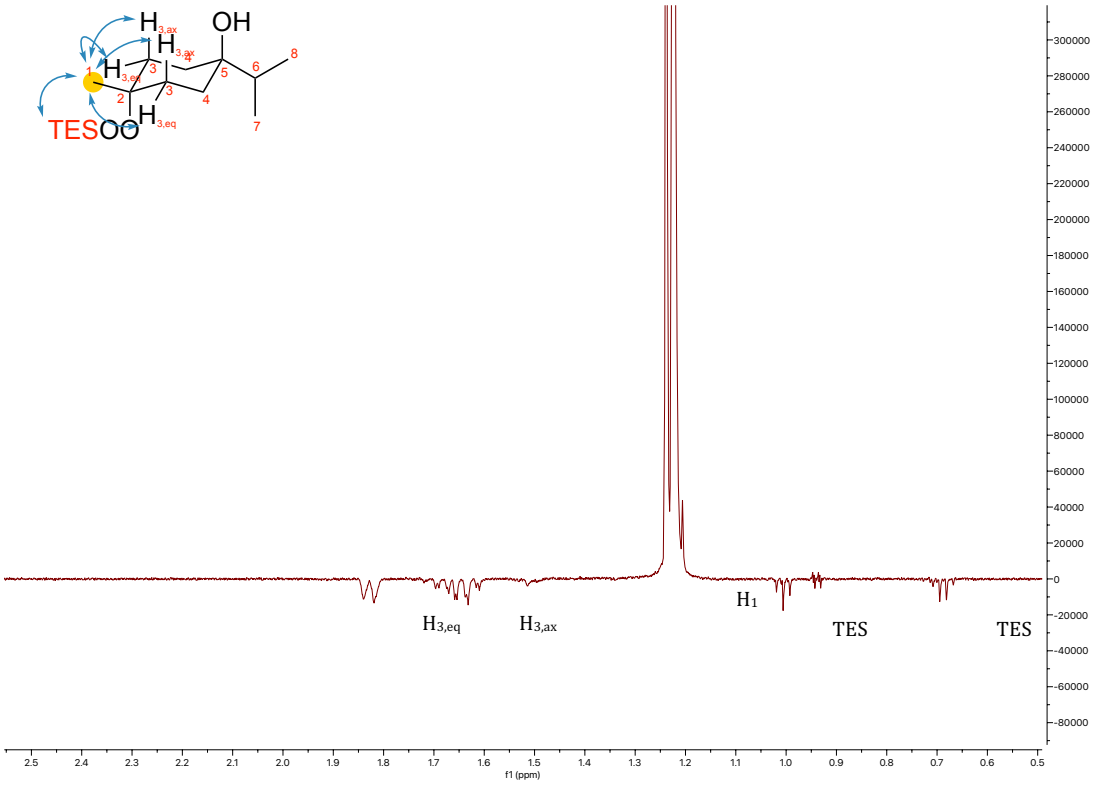




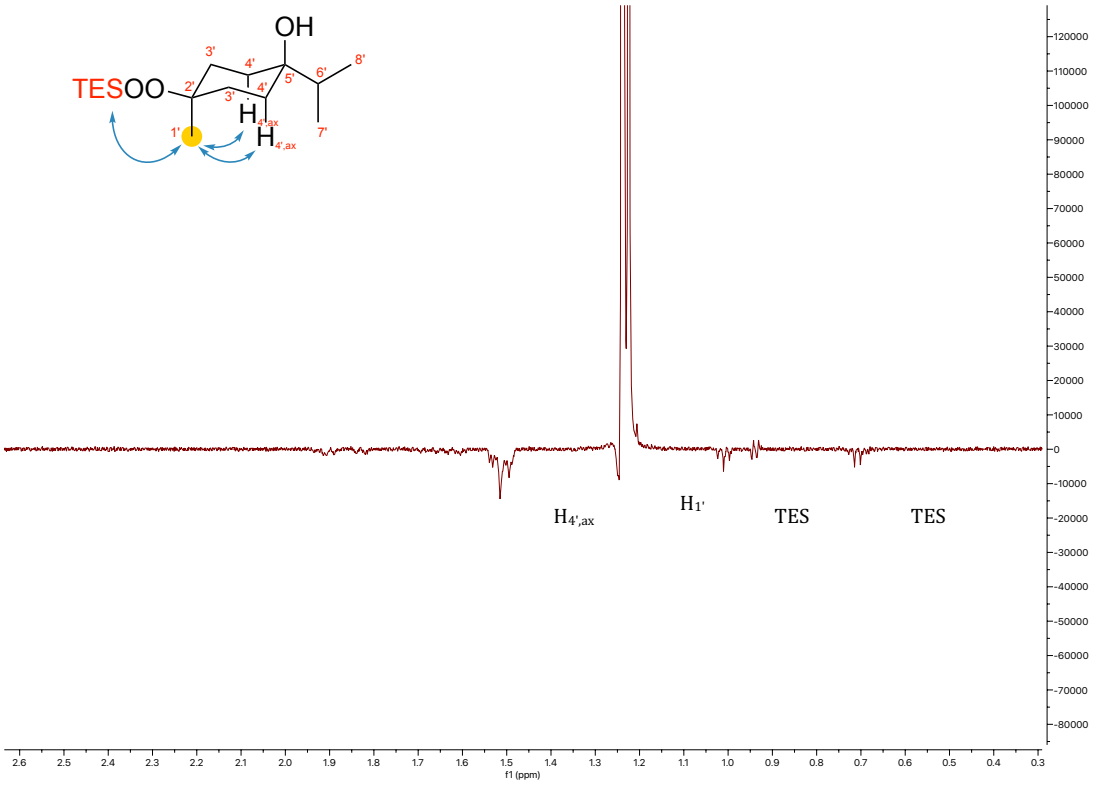
^{1}H NMR (400 MHz, $CDCl_3$) and ^{13}C NMR (101 MHz, $CDCl_3$) of **14b**


OH
TESOO
+
OH
TESOO
H7,8,7',
H1'
H4,ax
H1
H3,eq
H4,
H3,ax
H3',ax
H3',eq
H4',eq
H4',ax
H6'
H6
f2 (ppm)
f1 (ppm)

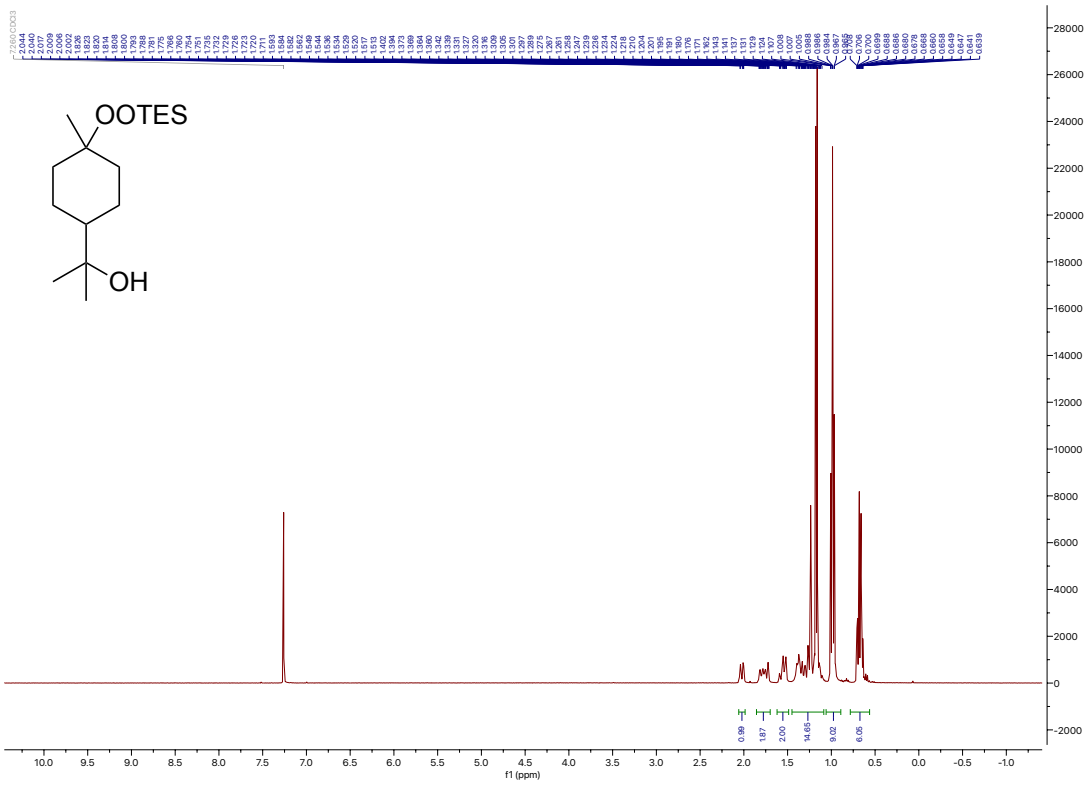
HSQC of **14b**

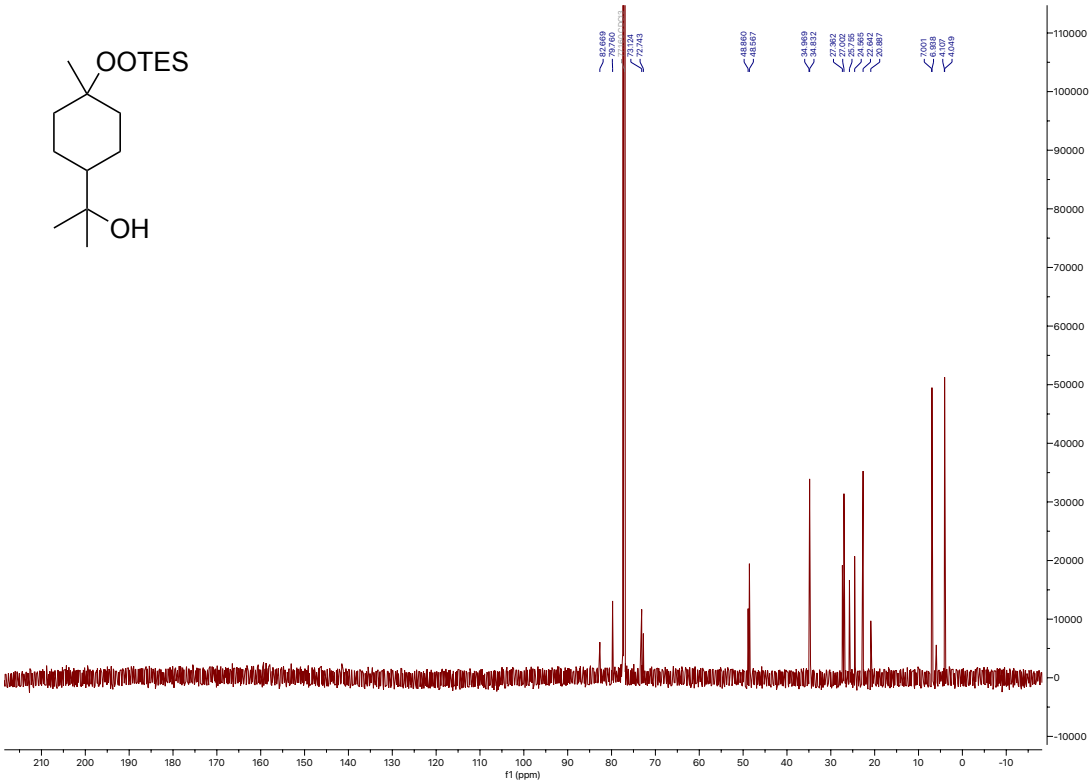


1D Selective Gradient NOESY of ***trans*-14b**, frequency 1.200 ppm

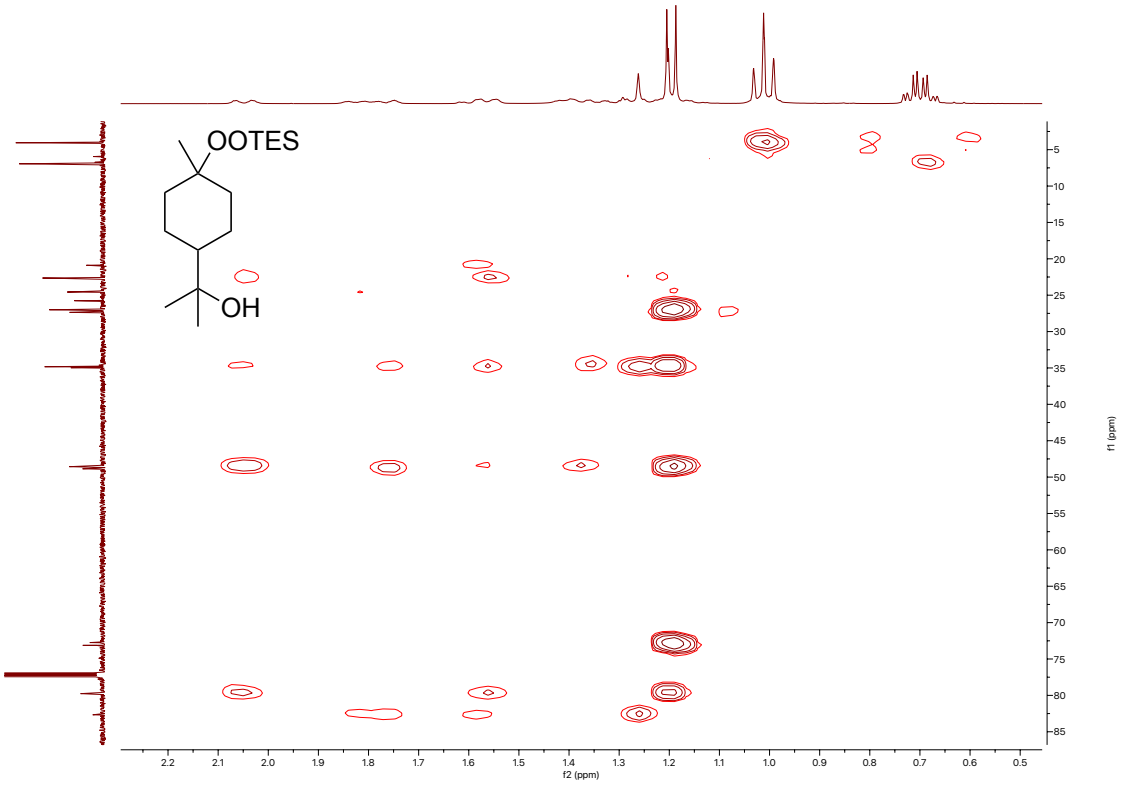


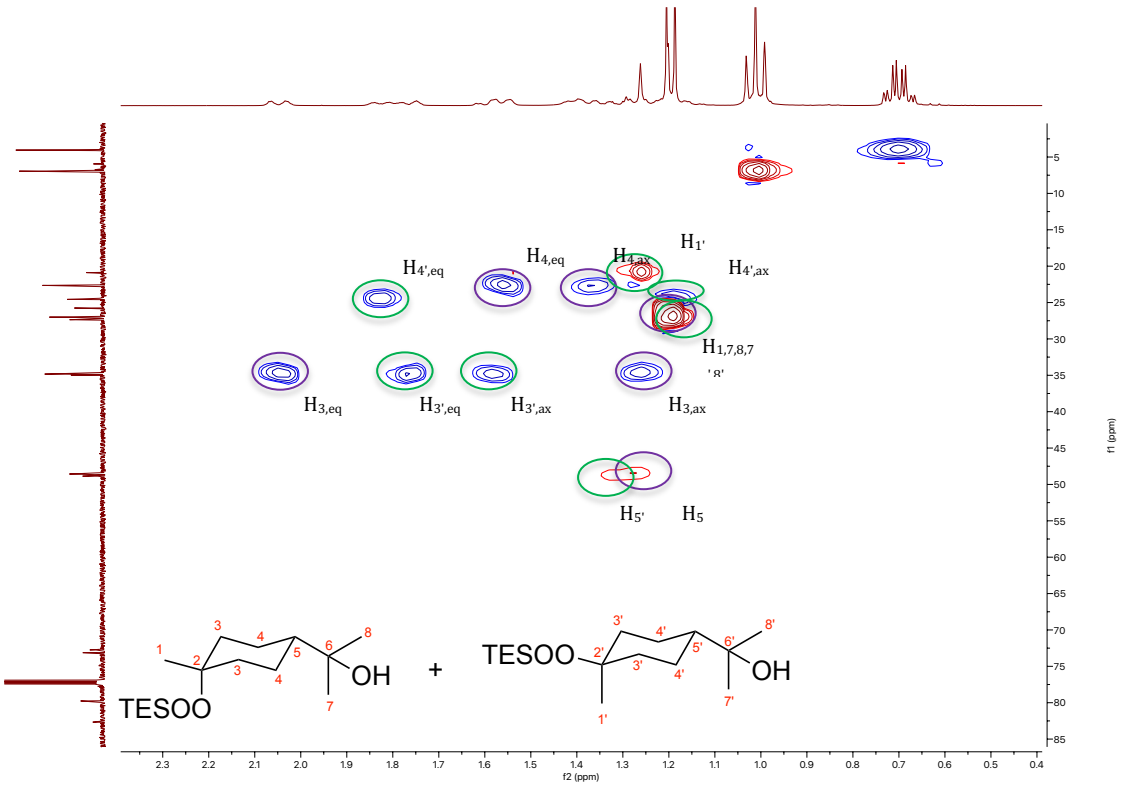
1D Selective Gradient NOESY frequency 1.214 ppm of ***cis*-14b**



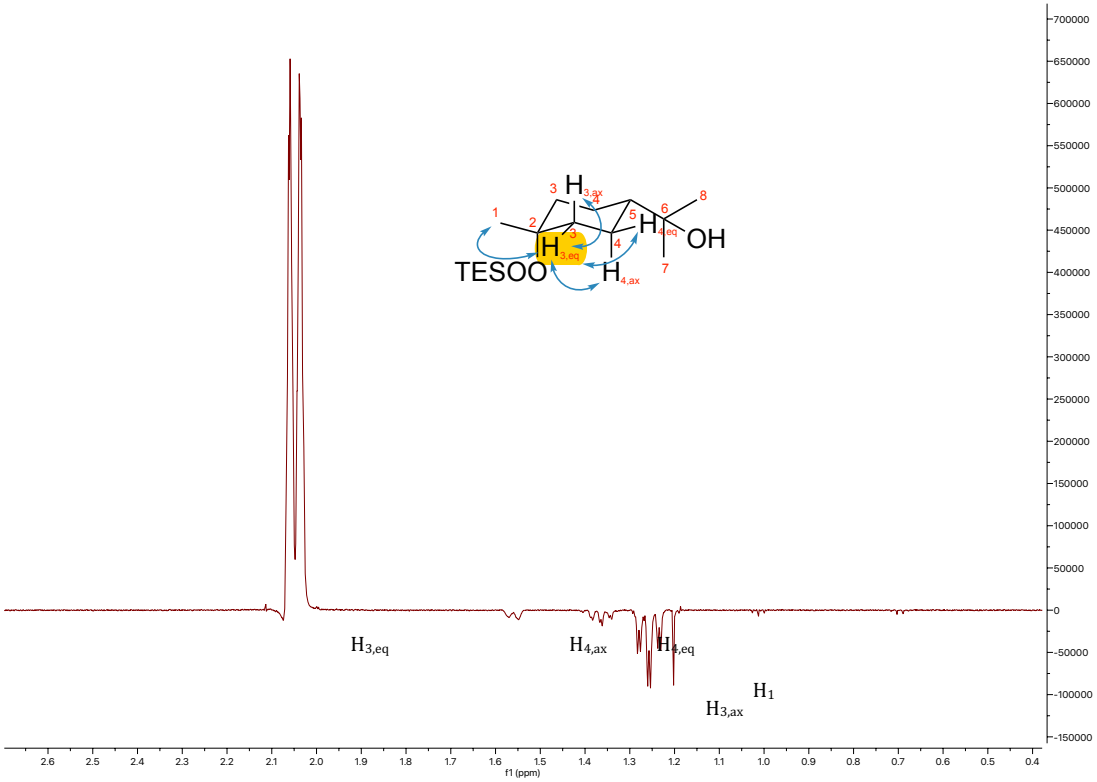


^{1}H NMR (400 MHz, $CDCl_3$) and ^{13}C NMR (151 MHz, $CDCl_3$) of **15b**

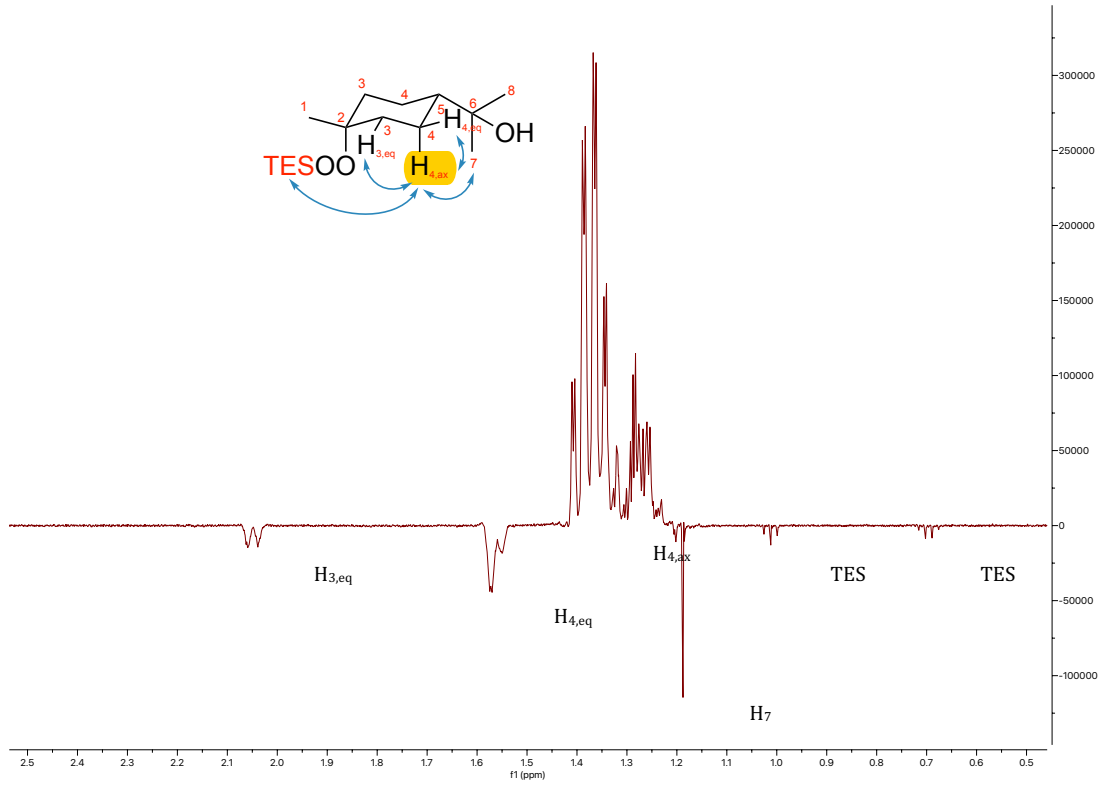




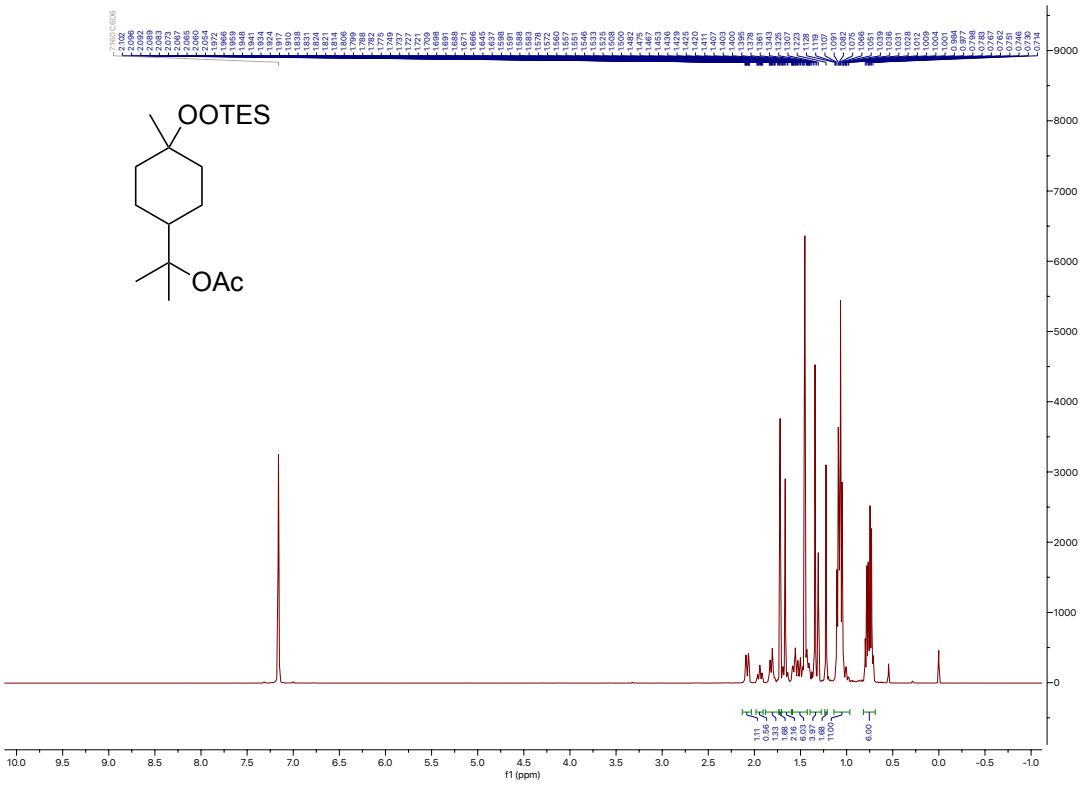
HMBC of and HSQC of **15b**

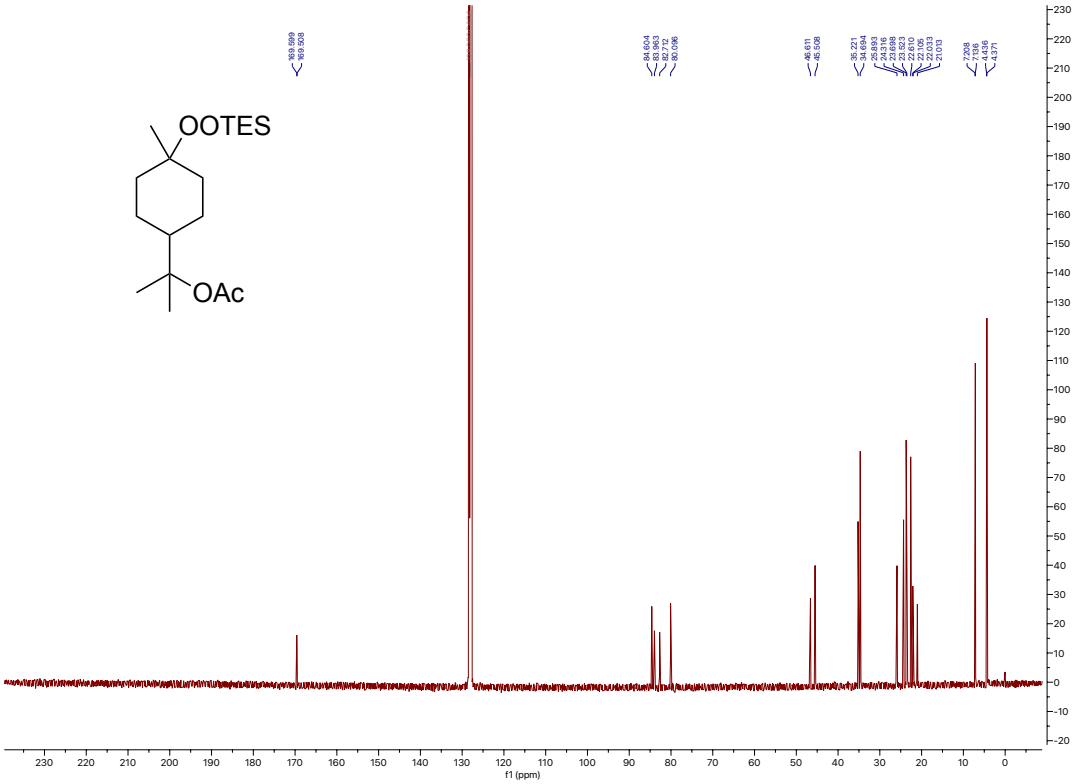


1D Selective Gradient NOESY frequency 2.047 ppm of ***cis*-15b**

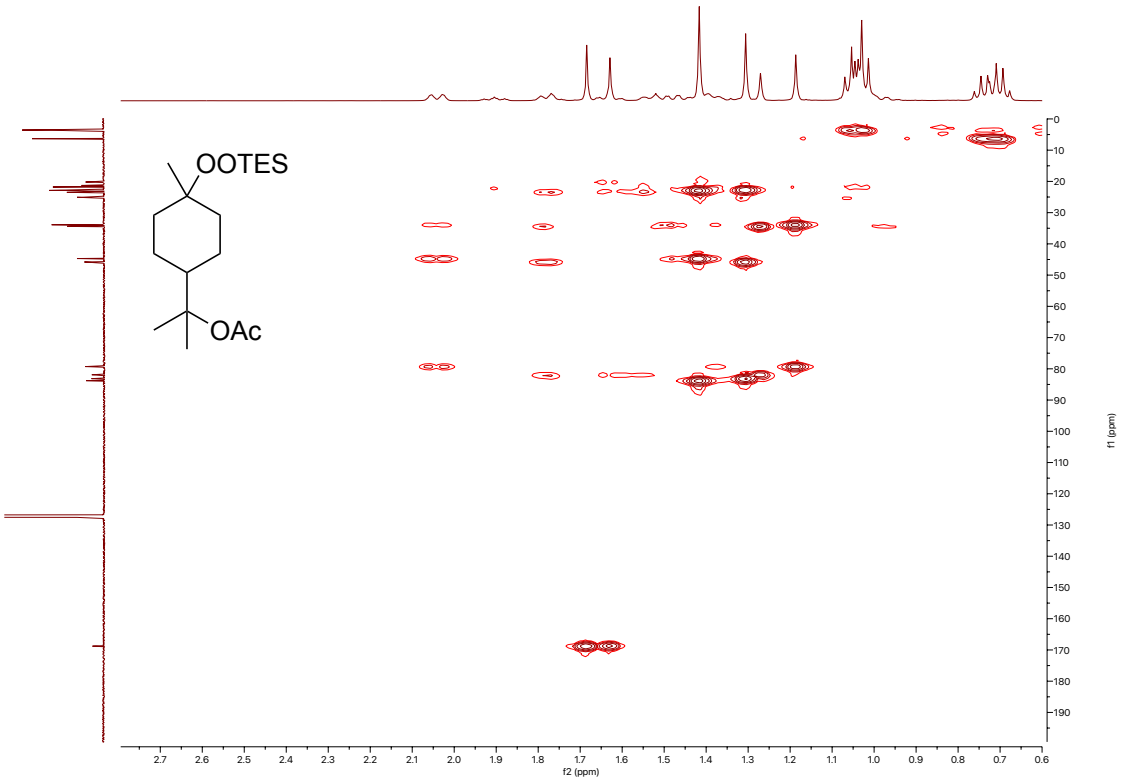


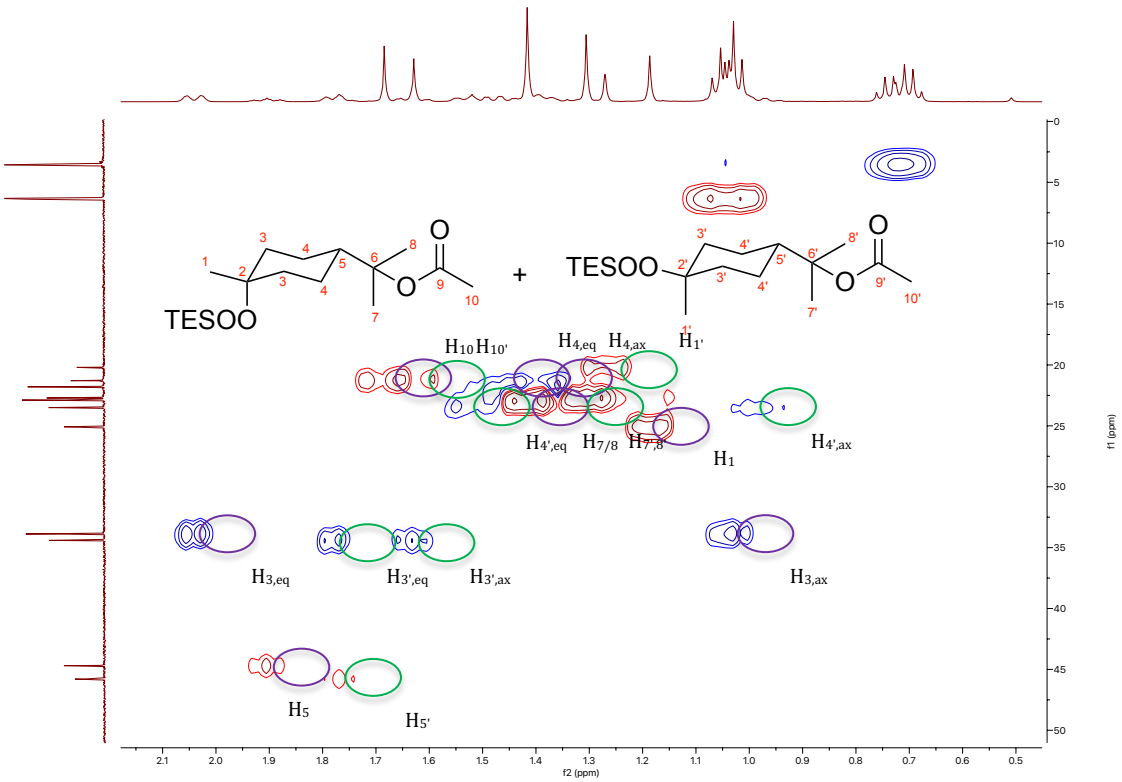
1D Selective Gradient NOESY frequency 1.389 ppm of ***cis*-15b**



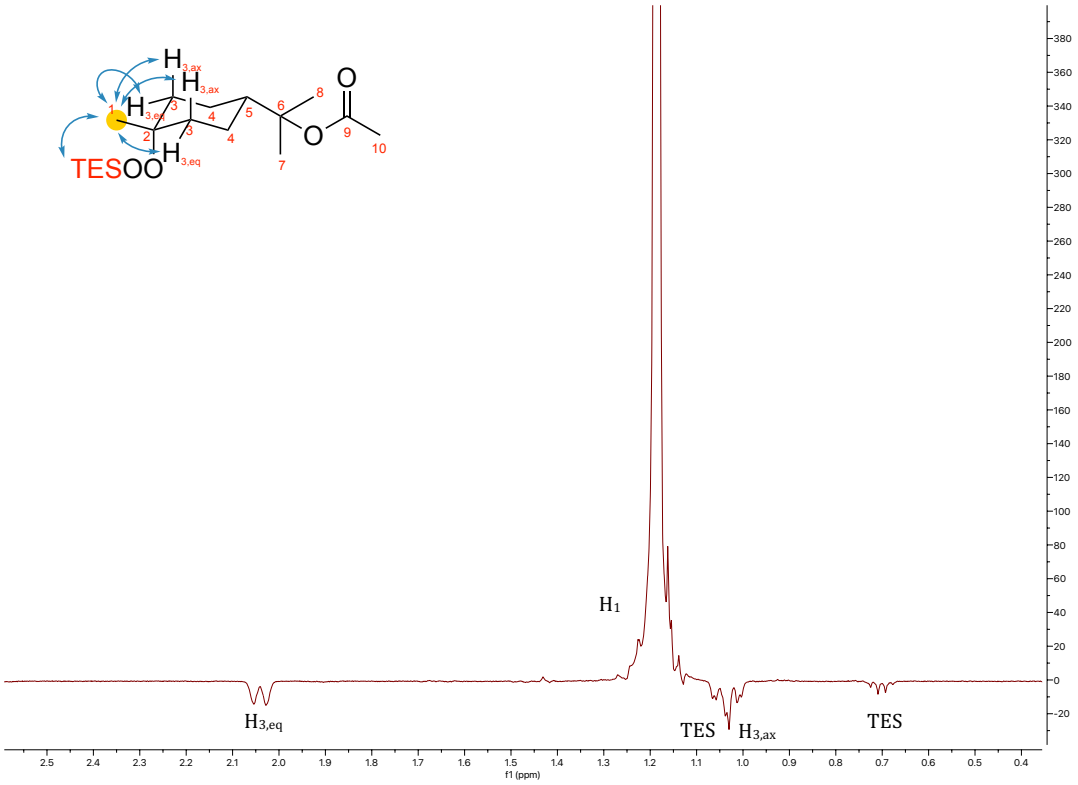


^{1}H NMR (500 MHz, C_6D_6) and ^{13}C NMR (126 MHz, C_6D_6) of **16b**

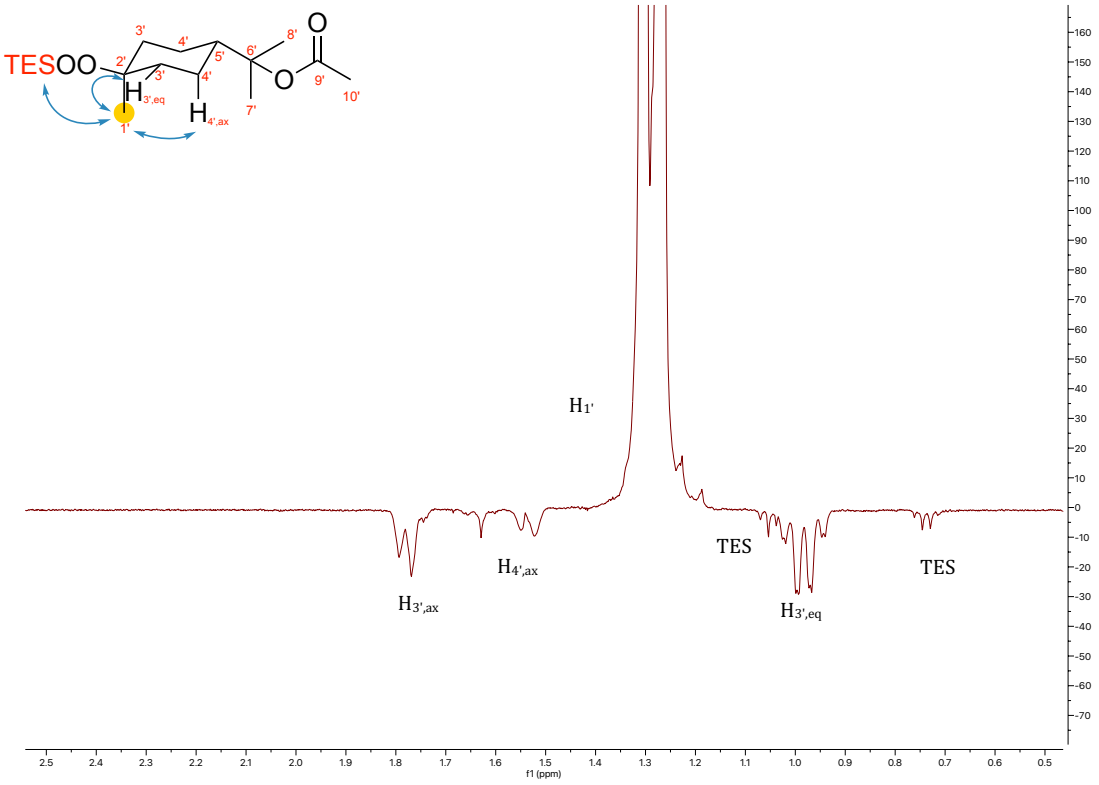




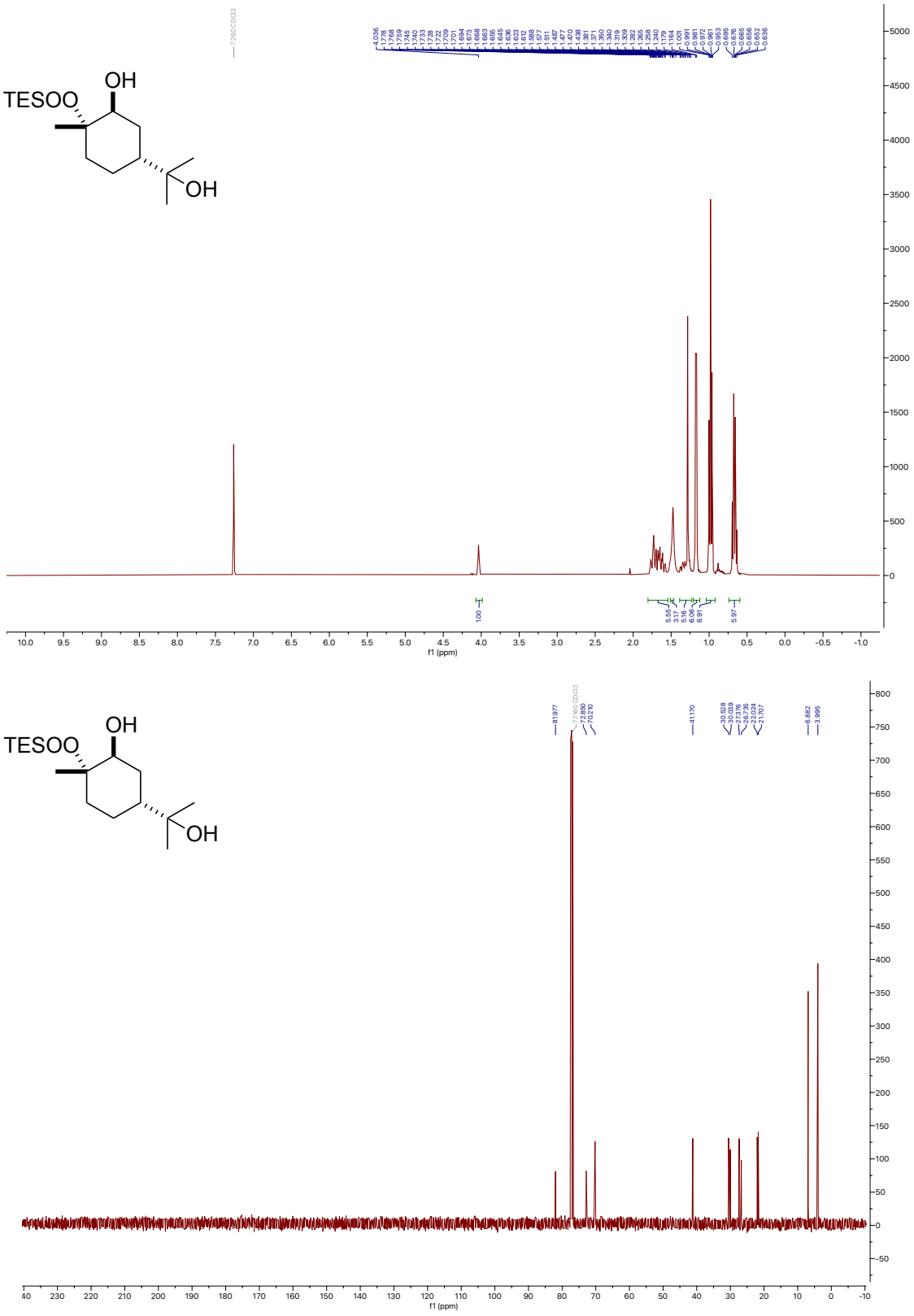
HMBC and HSQC of **16b**



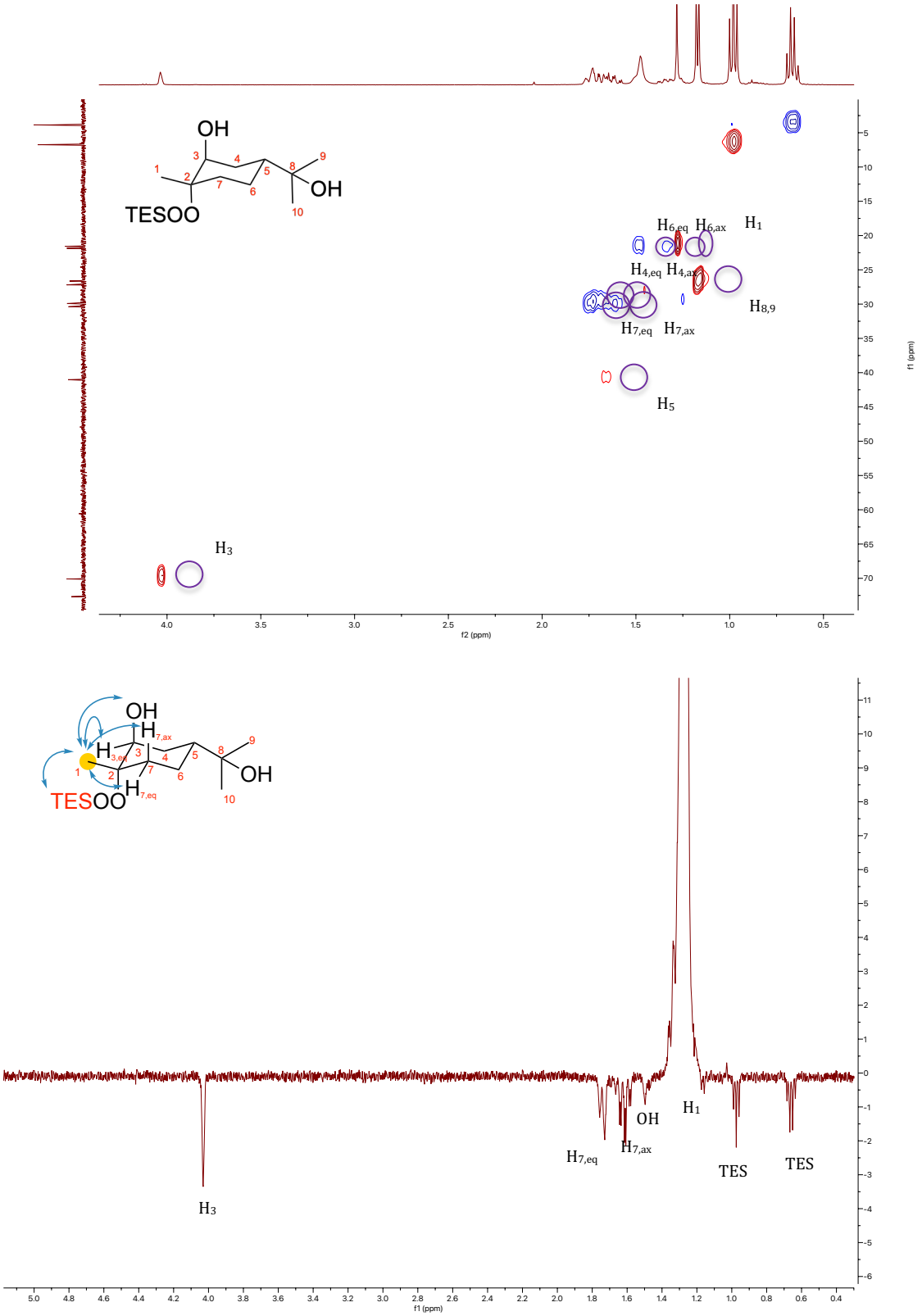
1D Selective Gradient NOESY frequency 1.217 ppm of ***cis*-16b**



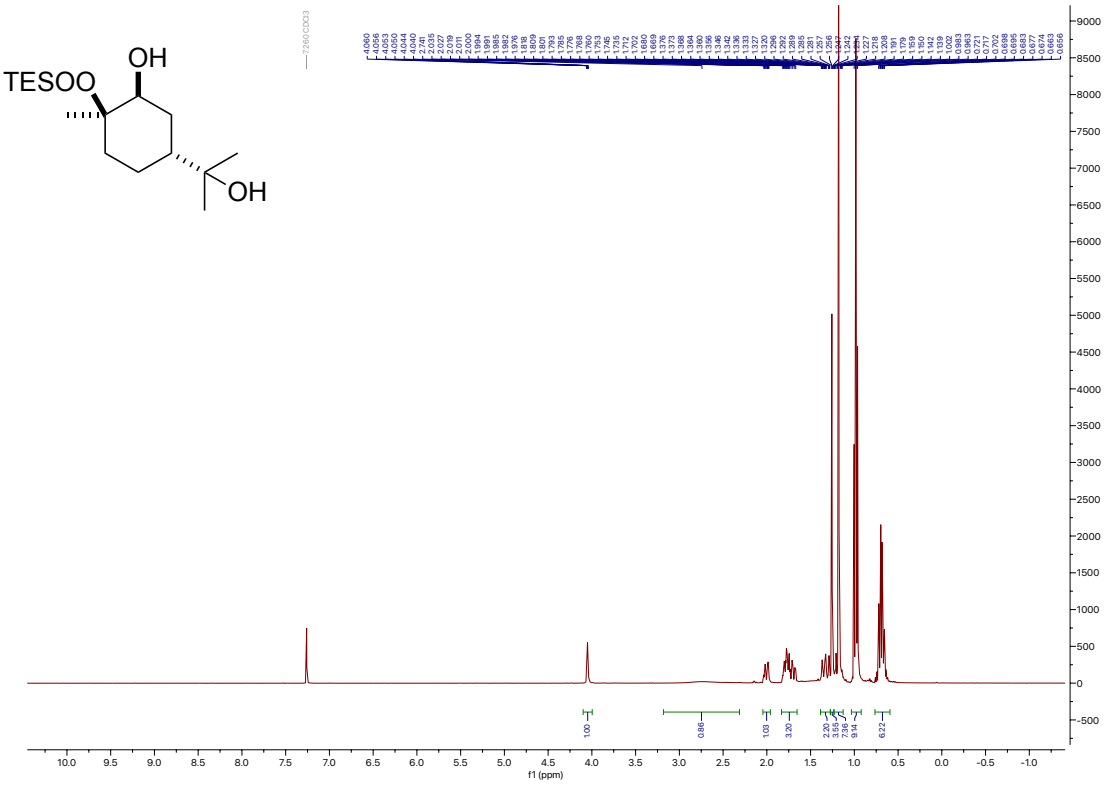
and 1D Selective Gradient NOESY of frequency 1.300 ppm of ***trans*-16b**

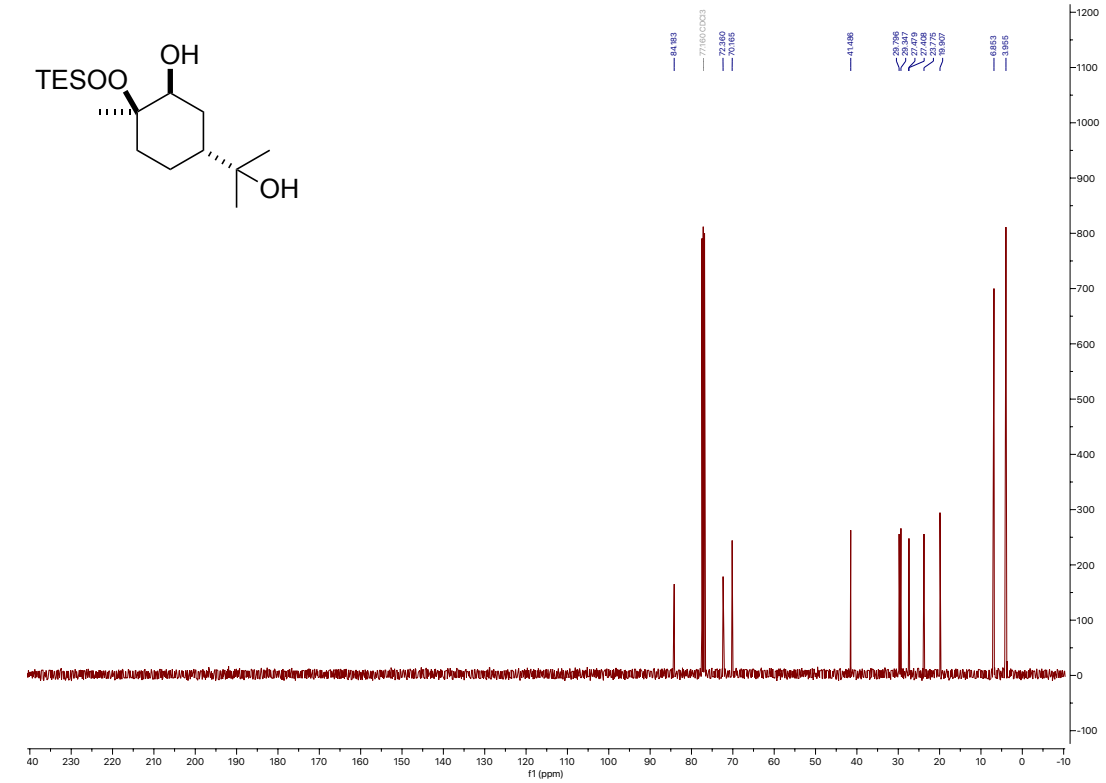


^{1}H NMR (400 MHz, $CDCl_3$) and ^{13}C NMR (101 MHz, $CDCl_3$) of ***trans*-17b**

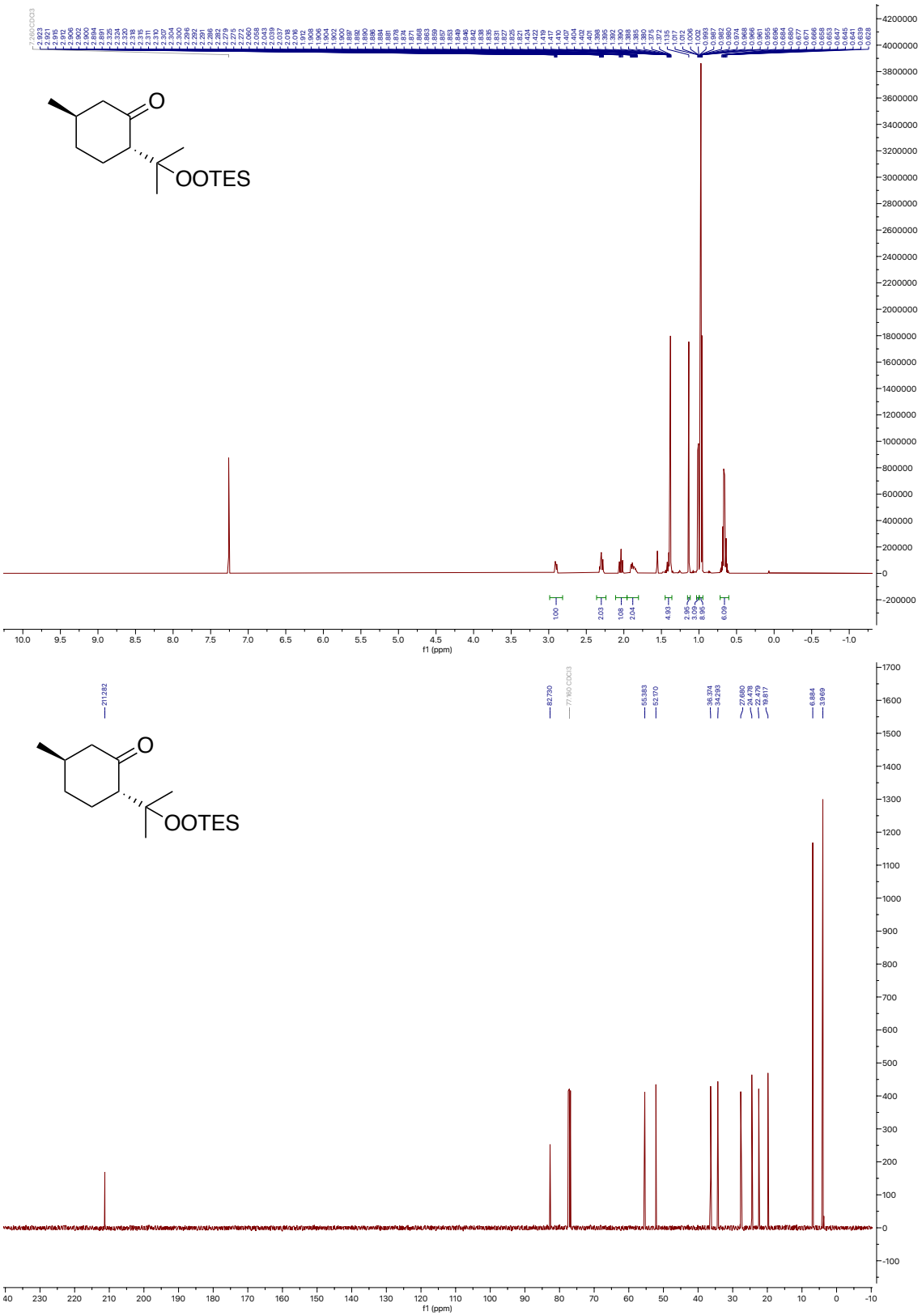


HSQC and Selective Gradient NOESY frequency 1.305 ppm of ***trans*-17b**

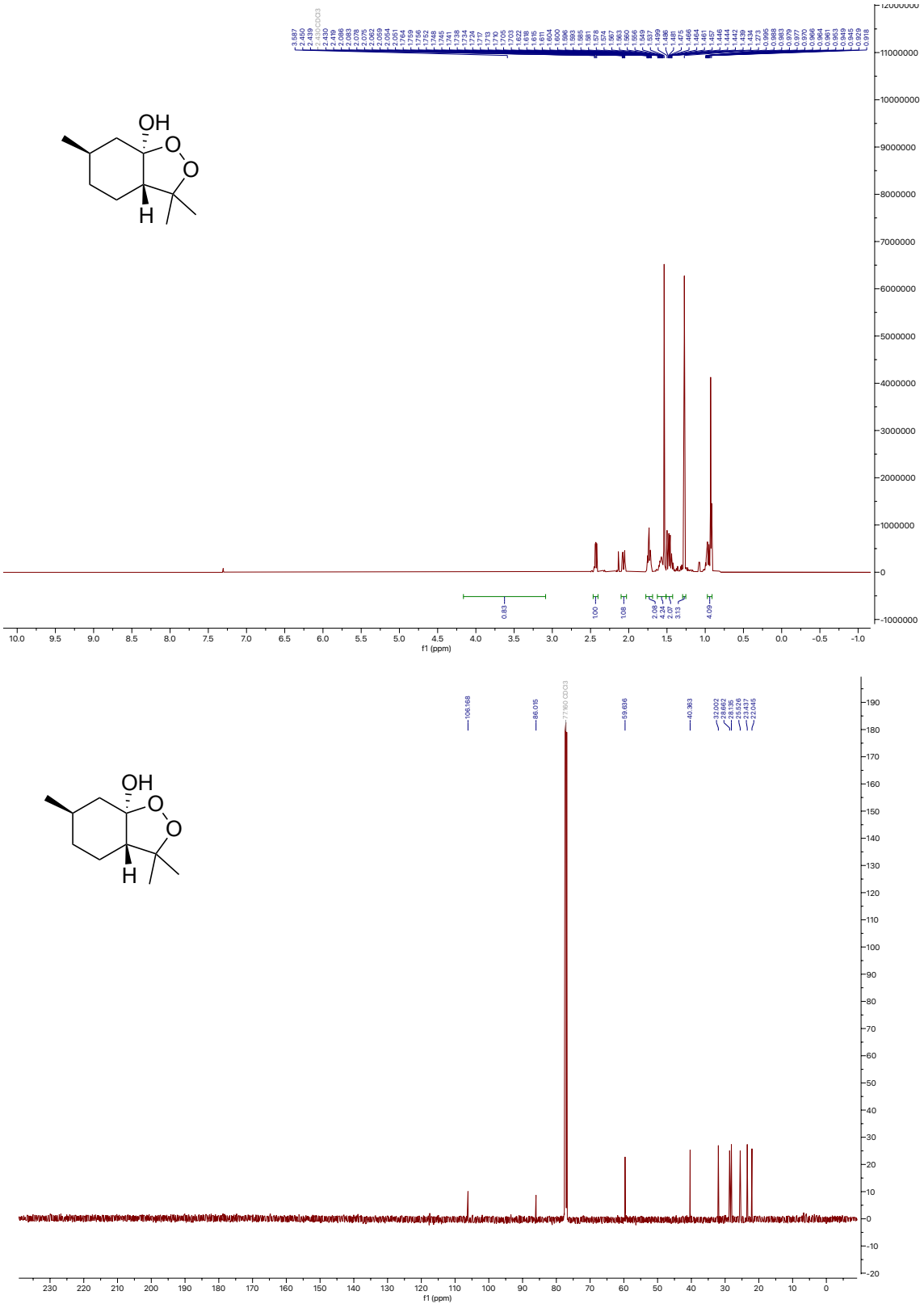




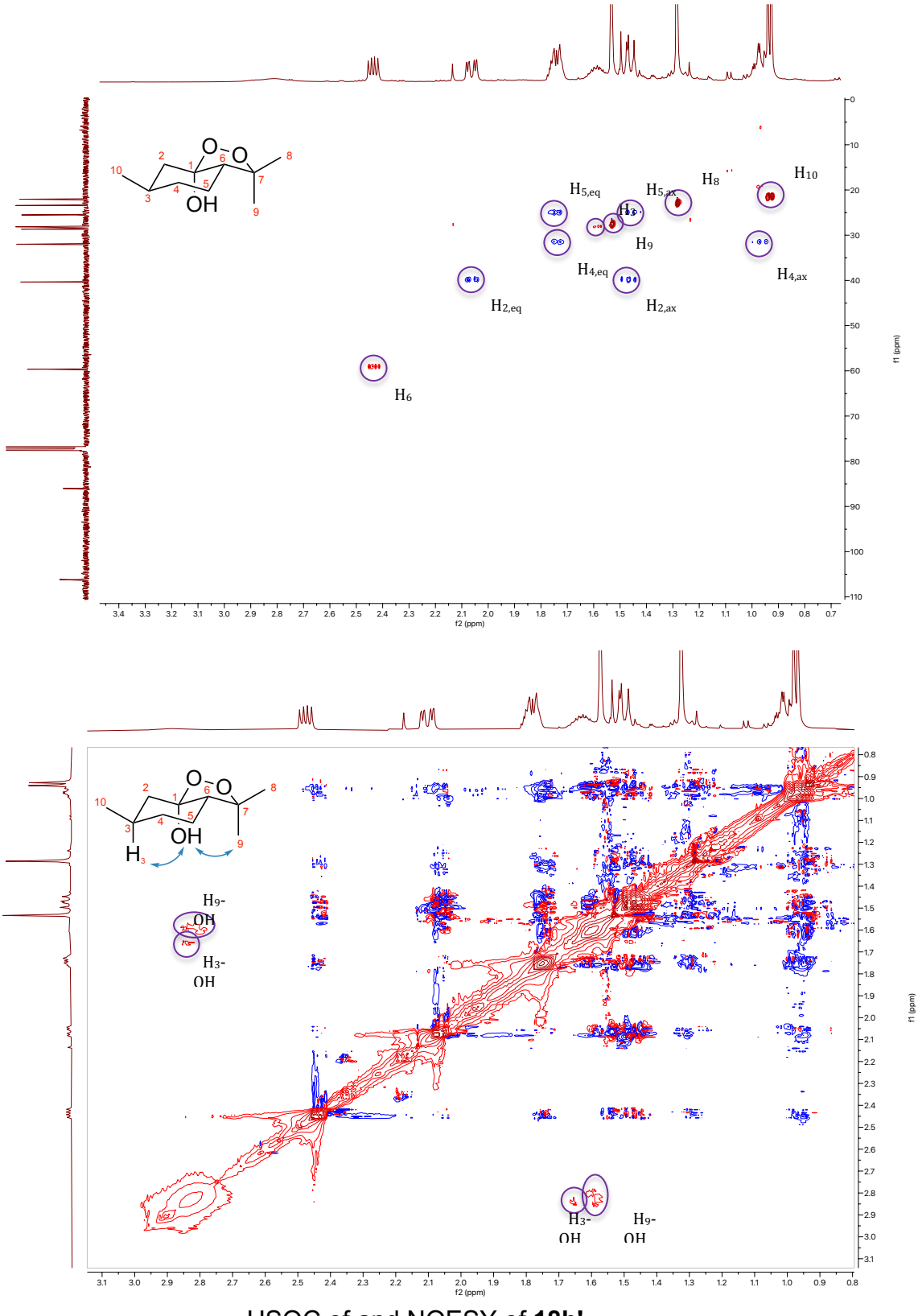
^{1}H NMR (400 MHz, $CDCl_3$) and ^{13}C NMR (101 MHz, $CDCl_3$) of ***cis*-17b**



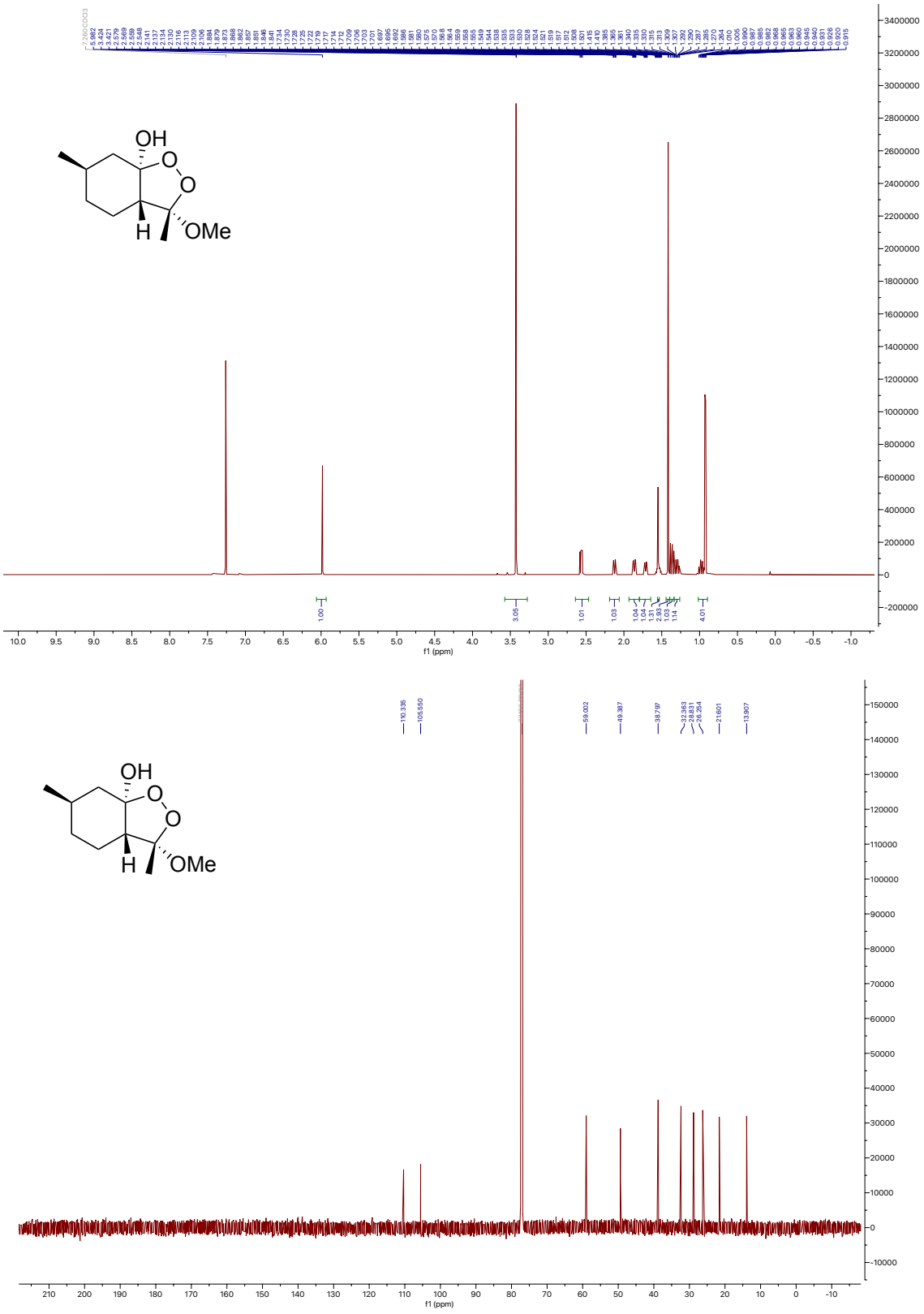
^{1}H NMR (400 MHz, $CDCl_3$) and ^{13}C NMR (101 MHz, $CDCl_3$) of **18b**



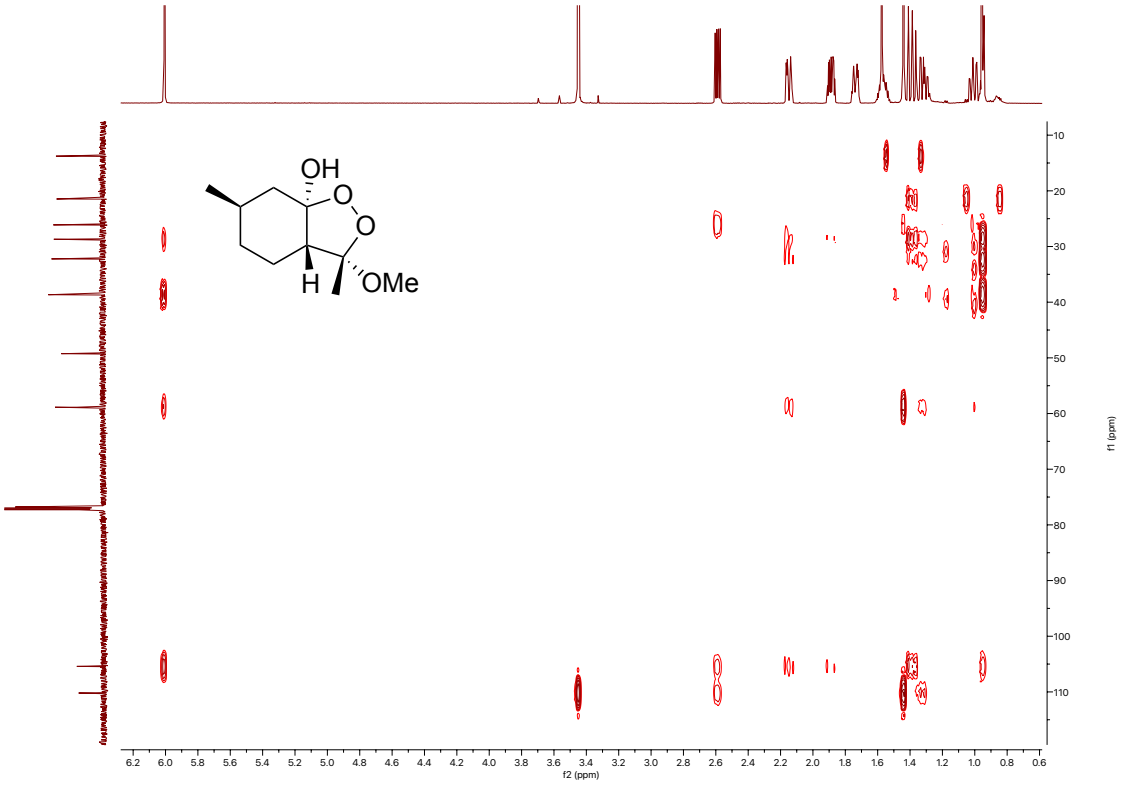
^{1}H NMR (600 MHz, $CDCl_3$) and ^{13}C NMR (126 MHz, $CDCl_3$) of **18b'**

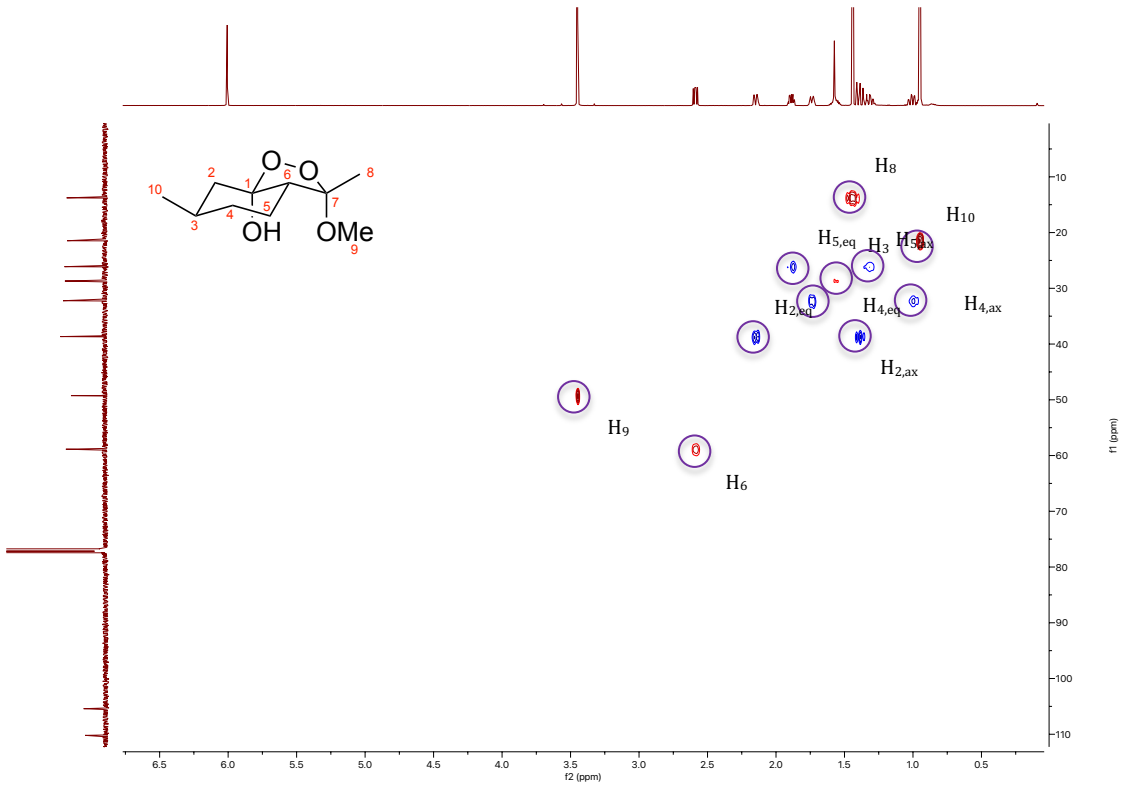


HSQC of and NOESY of **18b'**

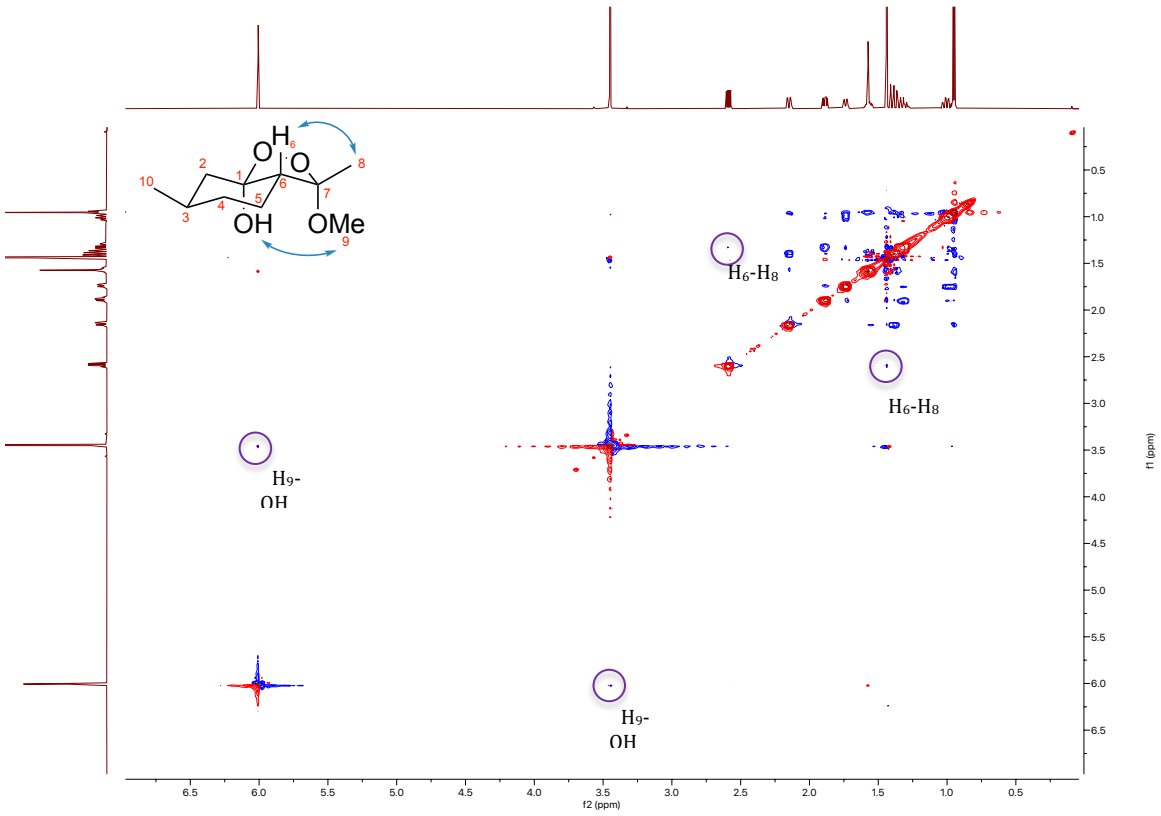


^{1}H NMR (600 MHz, $CDCl_3$) and ^{13}C NMR (151 MHz, $CDCl_3$) of **18x**

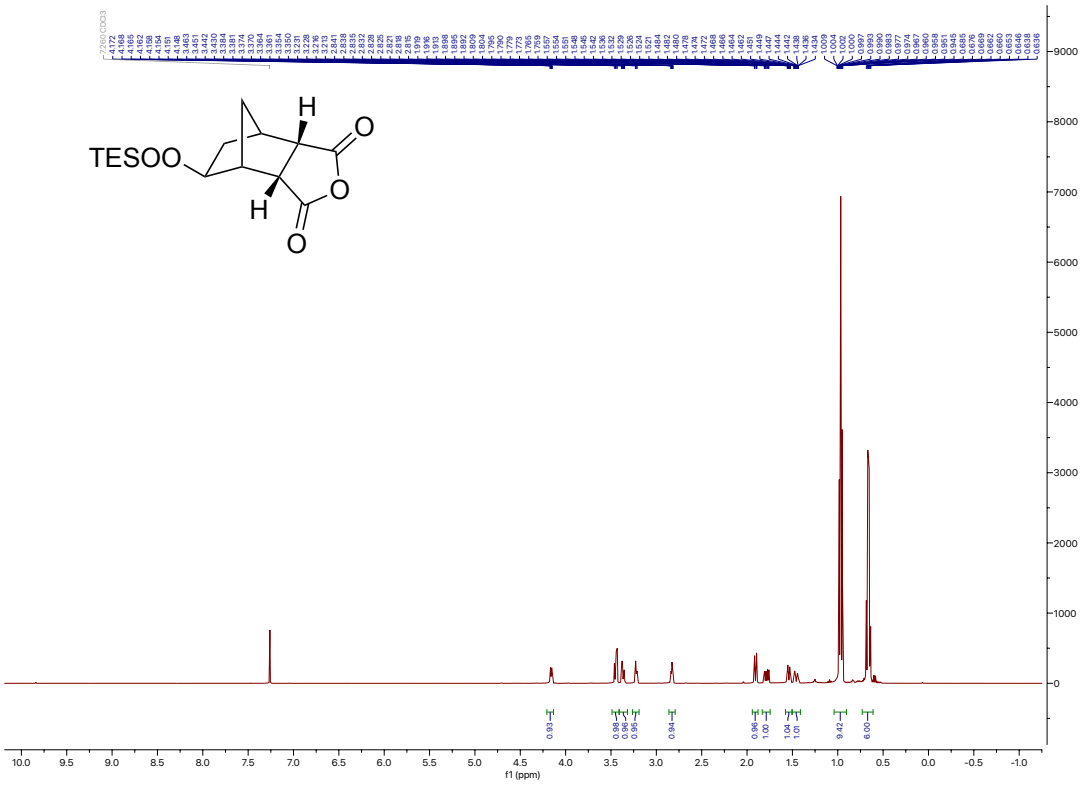


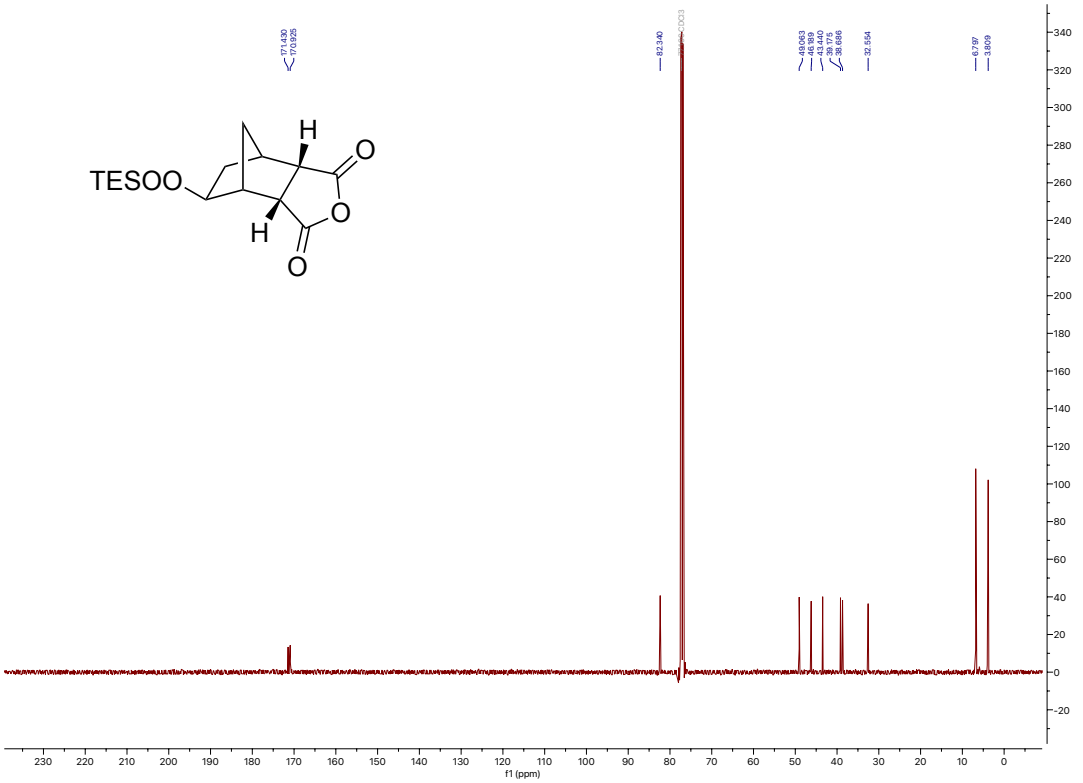


HMBC and HSQC of **18x**

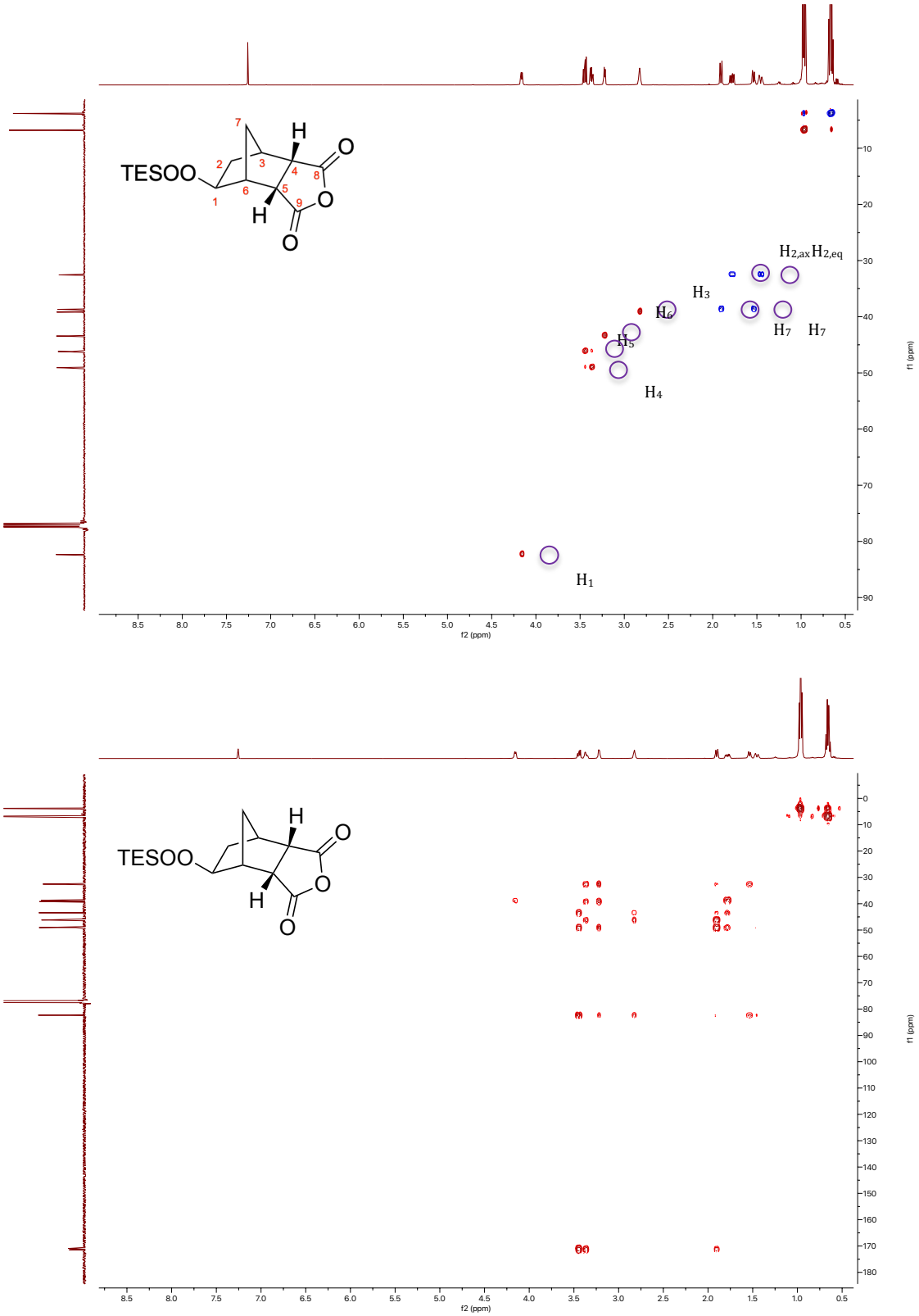


NOESY of **18x**

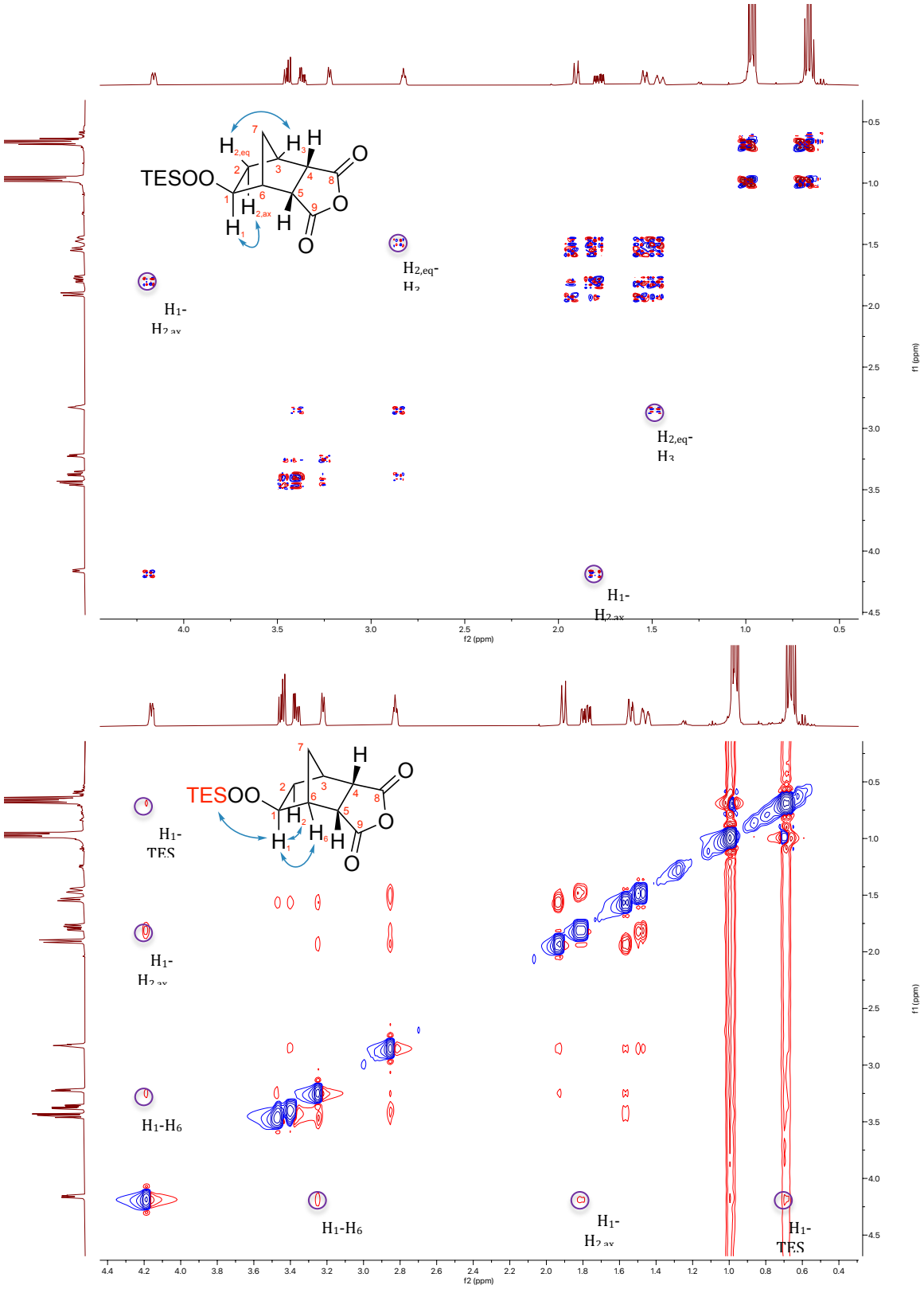




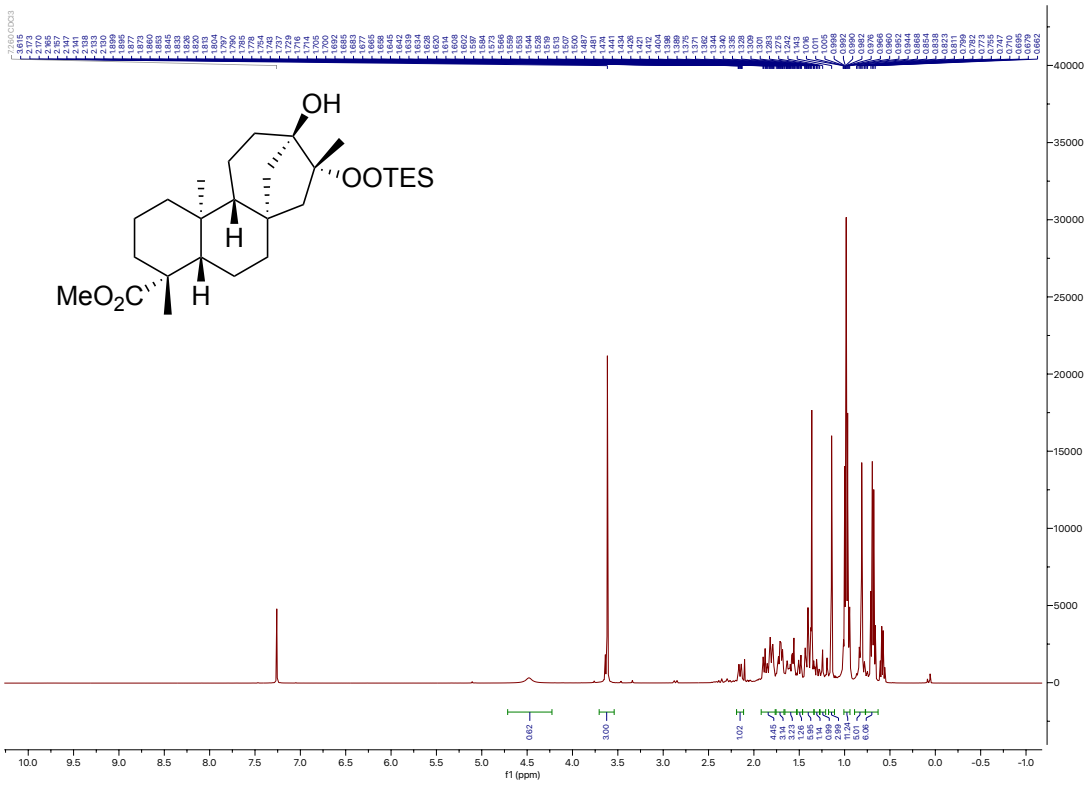
^{1}H NMR (500 MHz, $CDCl_3$) and ^{13}C NMR (126 MHz, $CDCl_3$) of **19b**

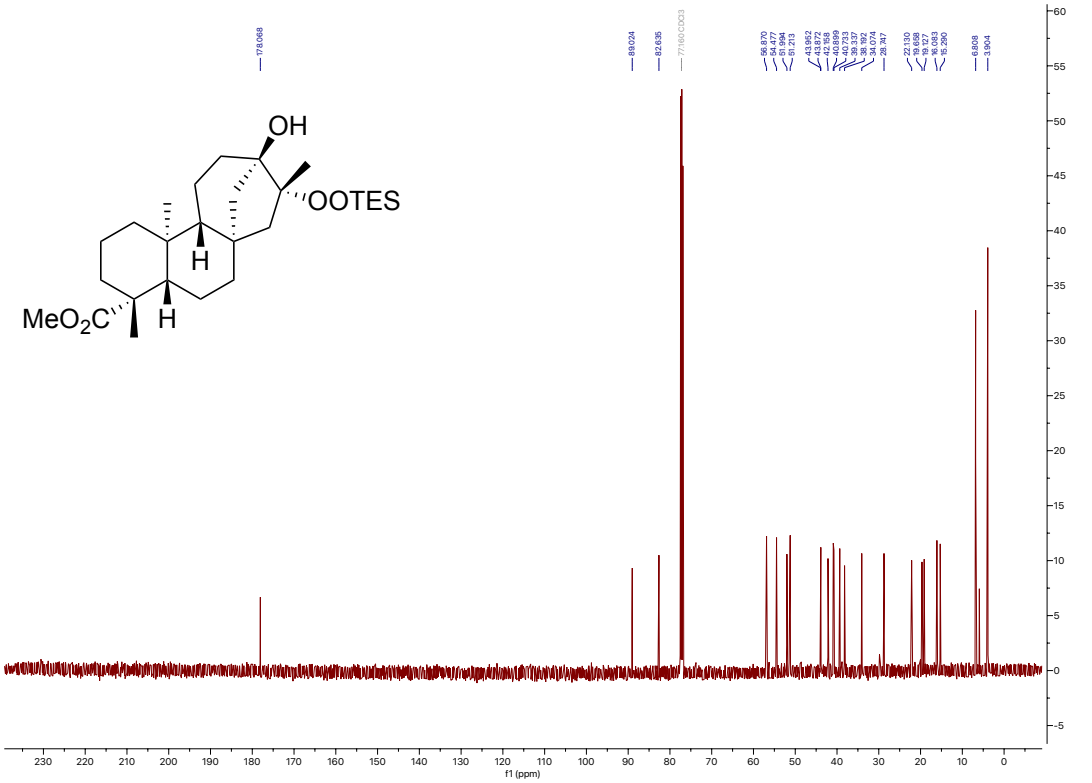


HSQC and HMBC of **19b**

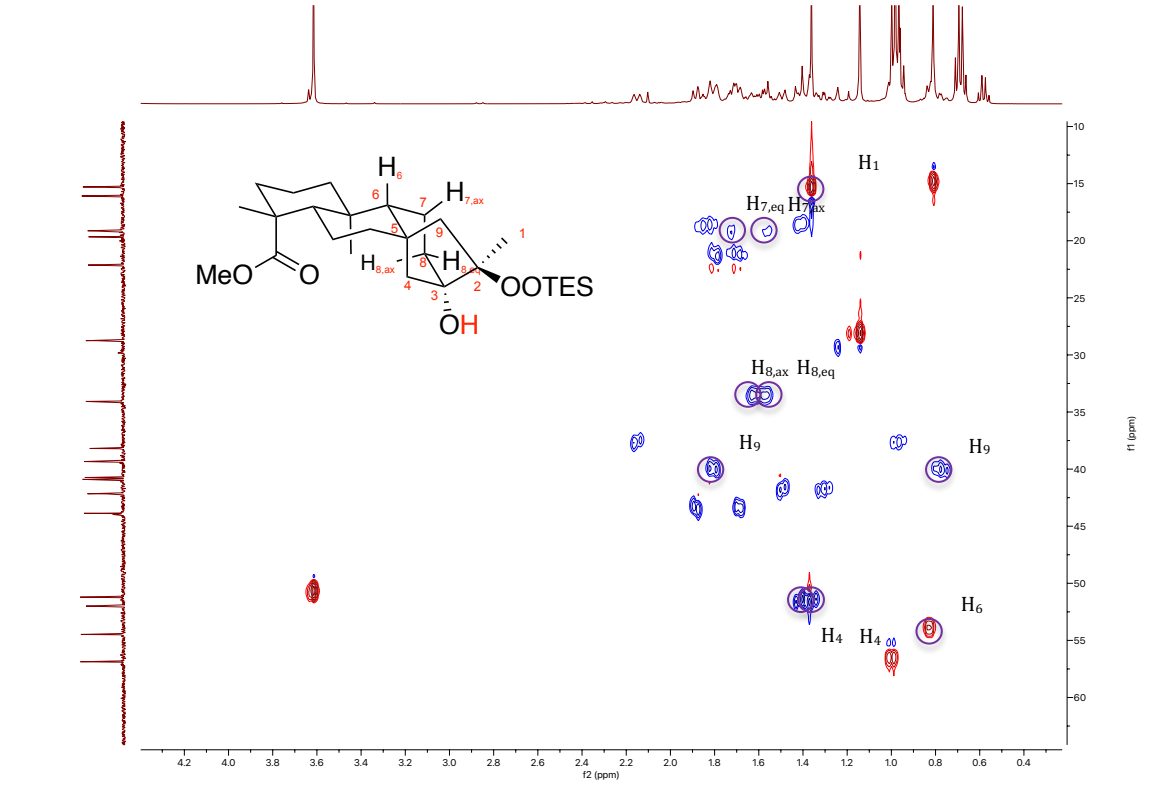


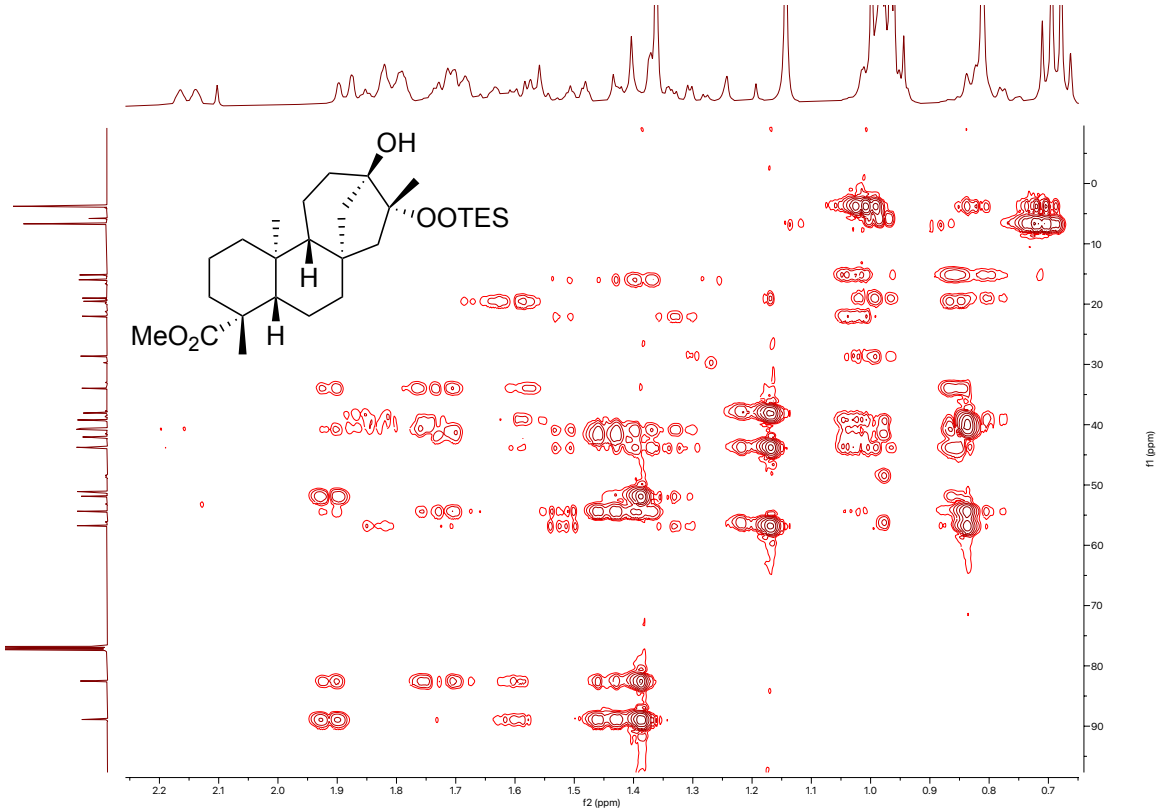
COSY and NOESY of **19b**



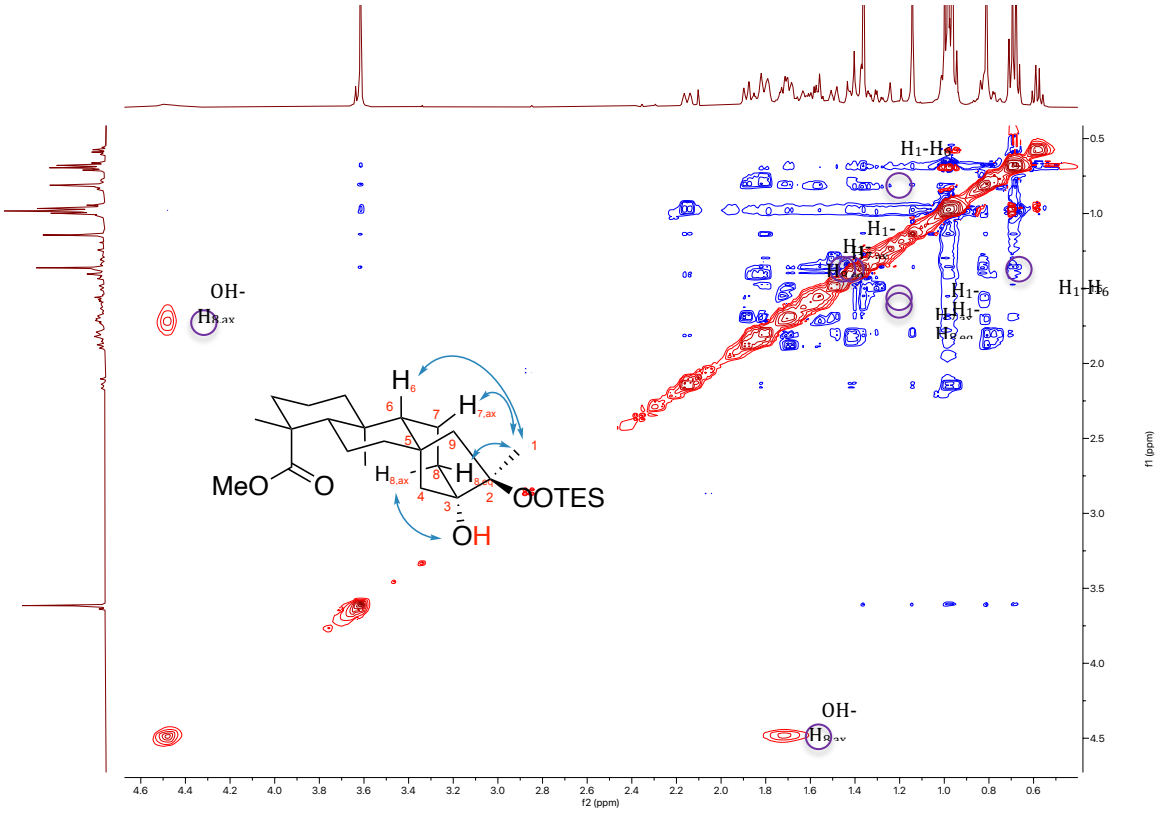


^{1}H NMR (500 MHz, $CDCl_3$) and ^{13}C NMR (126 MHz, $CDCl_3$) of **20b**

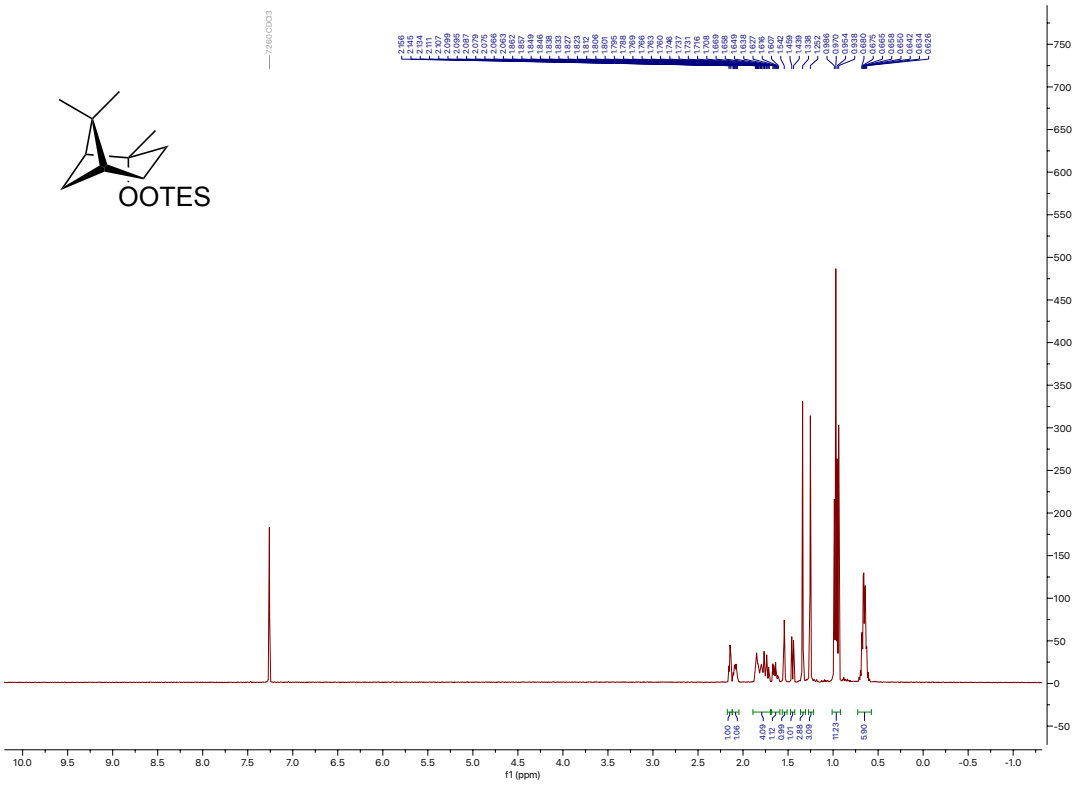


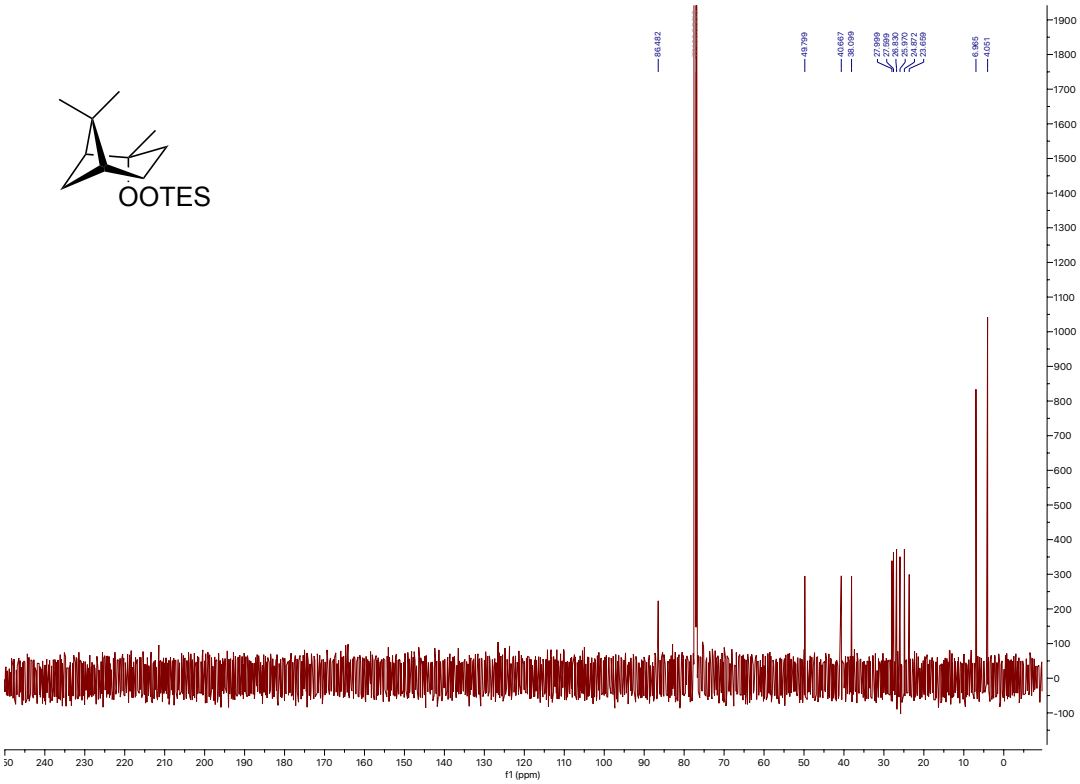


HSQC and HMBC of **20b**

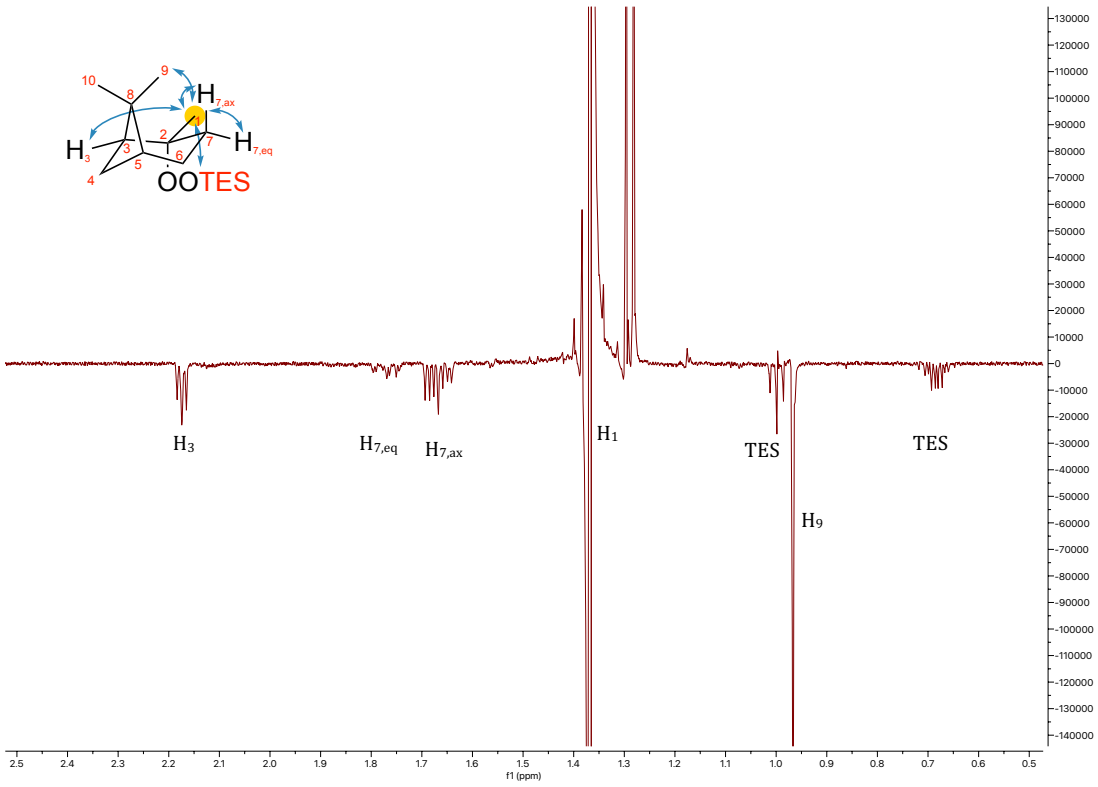

OH-
H8,ax
H6
H7,ax
H8,ax
H8,eq
MeO
O
OTES
OH
H1-H6
H1-
H1-
H1-H6
OH-
H8,ax
f2 (ppm)
f1 (ppm)

NOESY of **20b**

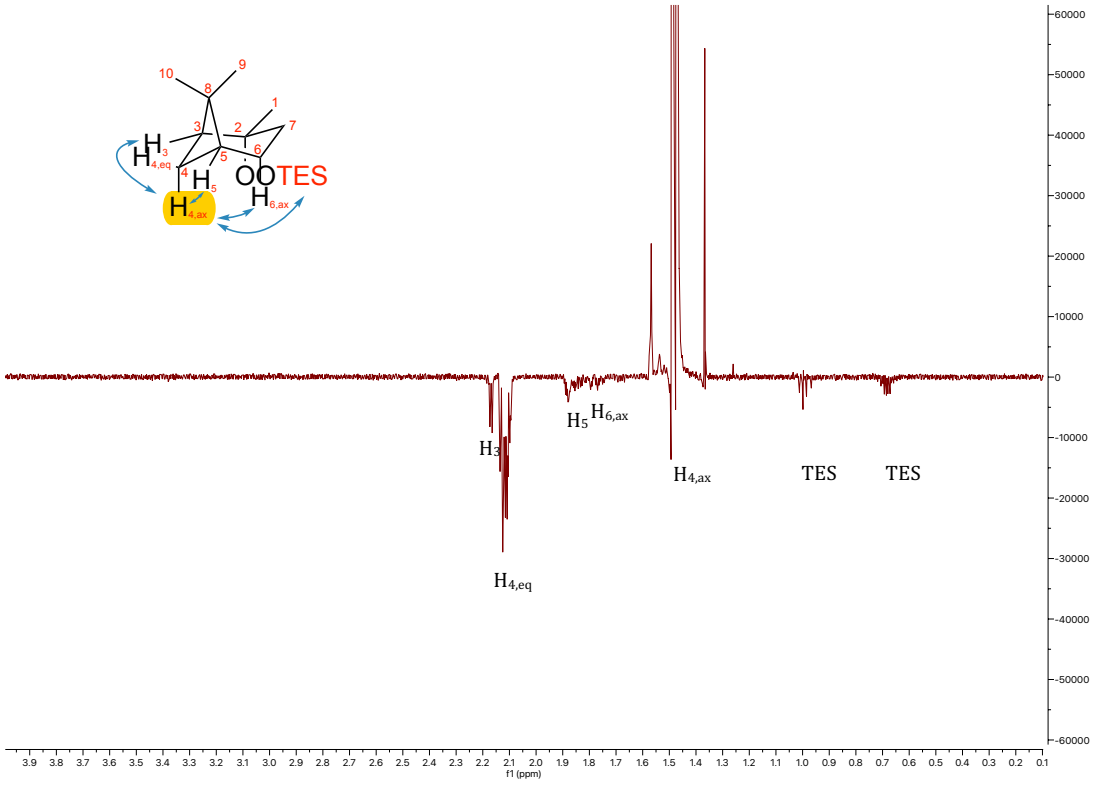




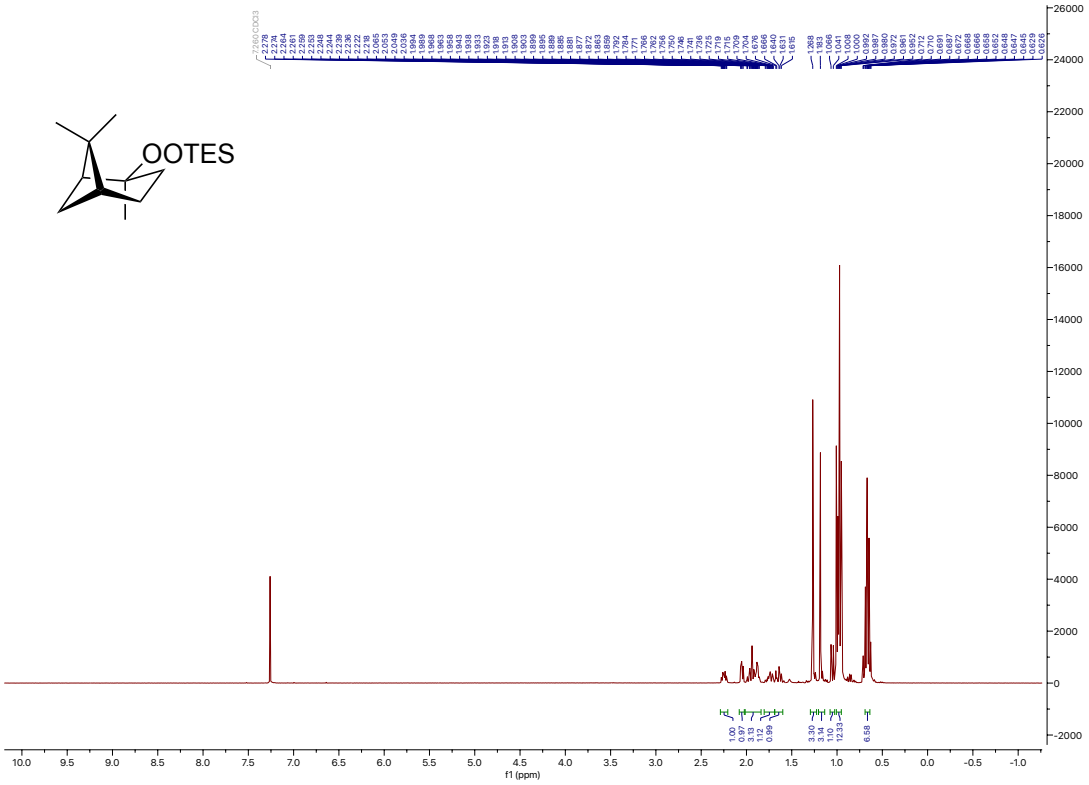
^{1}H NMR (500 MHz, $CDCl_3$) and ^{13}C NMR (126 MHz, $CDCl_3$) of ***exo*-21b**

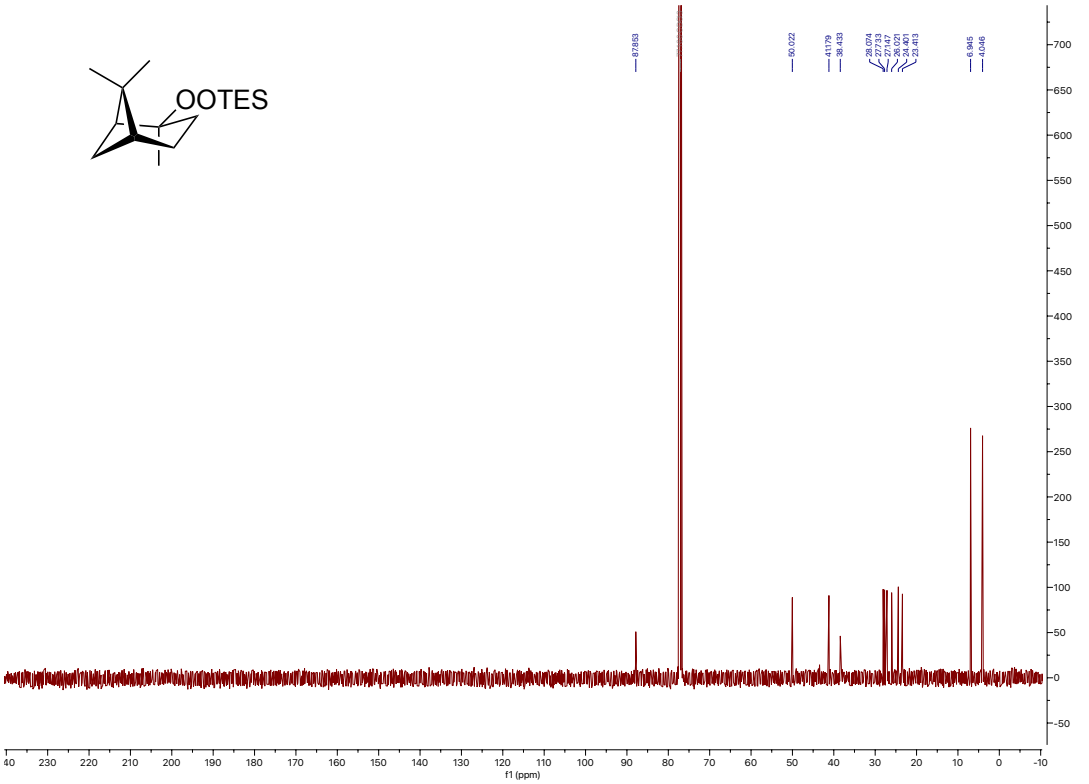


1D Selective Gradient NOESY, frequency 1.367 ppm of ***exo*-21b**

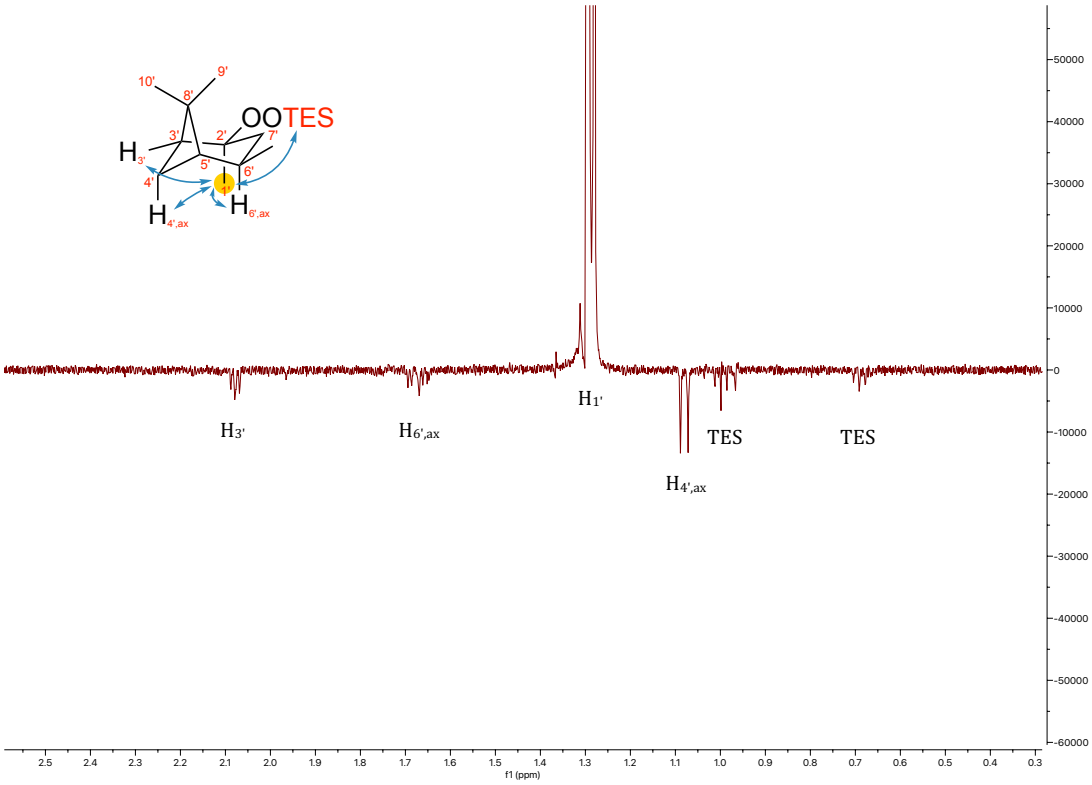


1D Selective Gradient NOESY, frequency 1.480 ppm of ***exo*-21b**

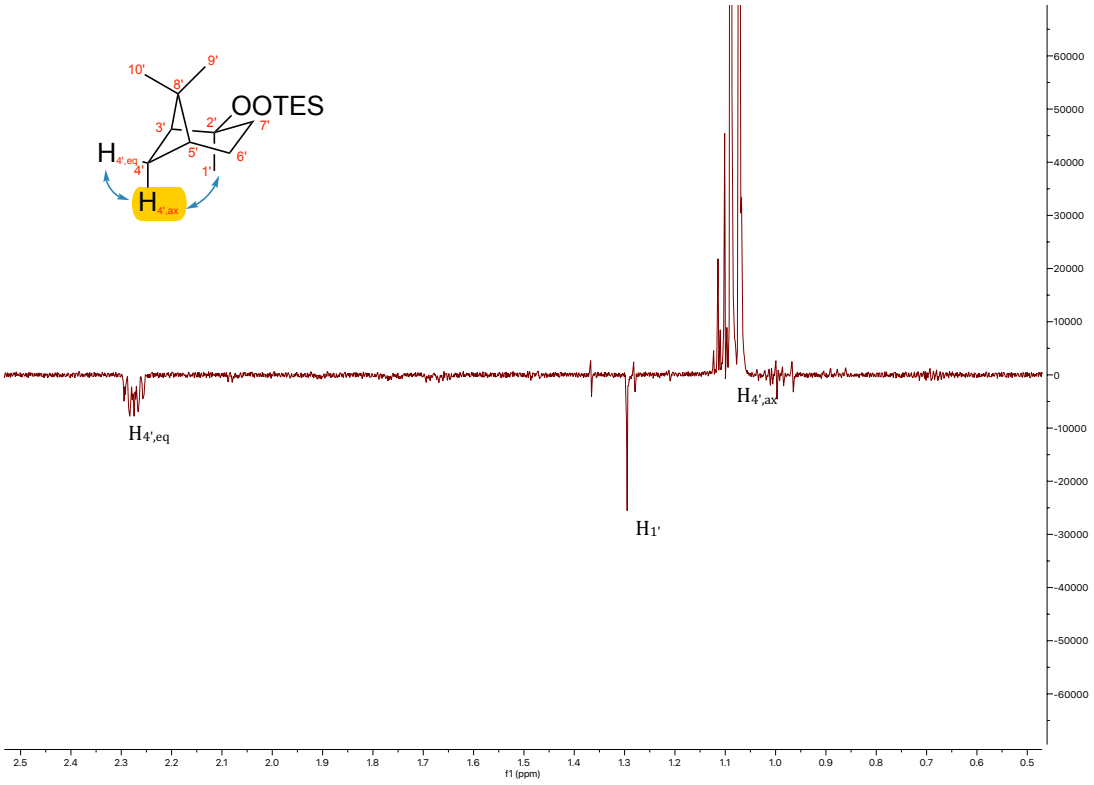




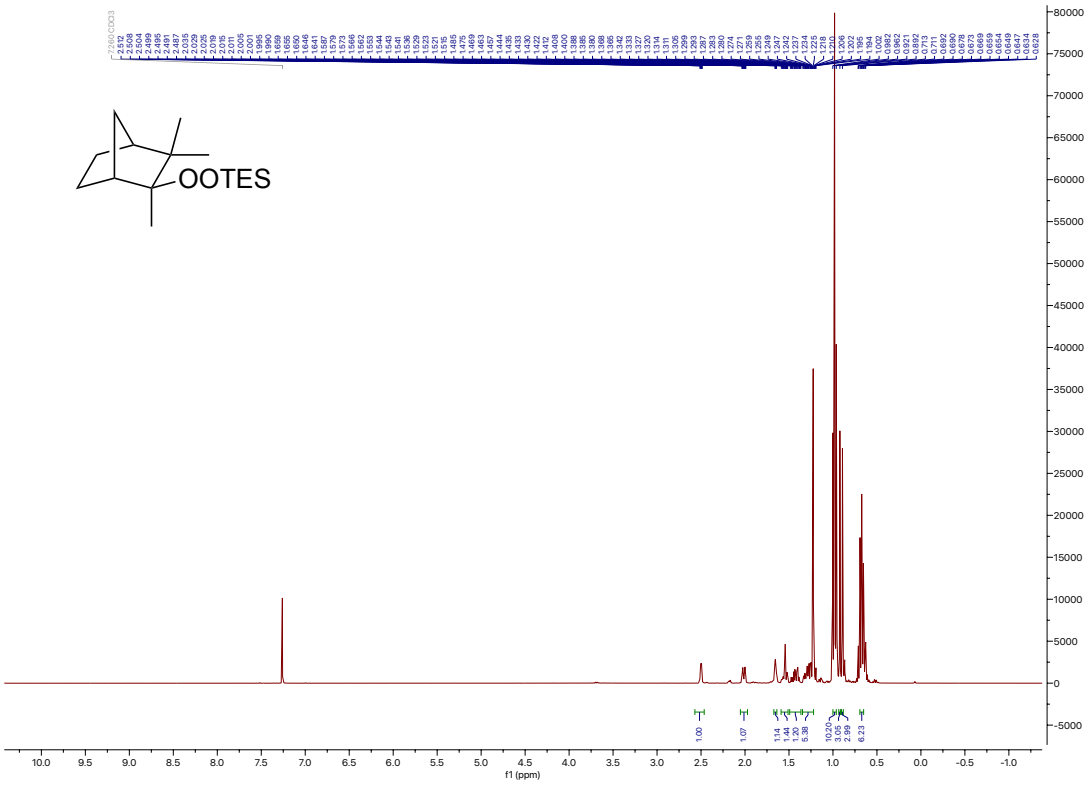
^{1}H NMR (400 MHz, $CDCl_3$) and ^{13}C NMR (101 MHz, $CDCl_3$) of ***endo*-21b**

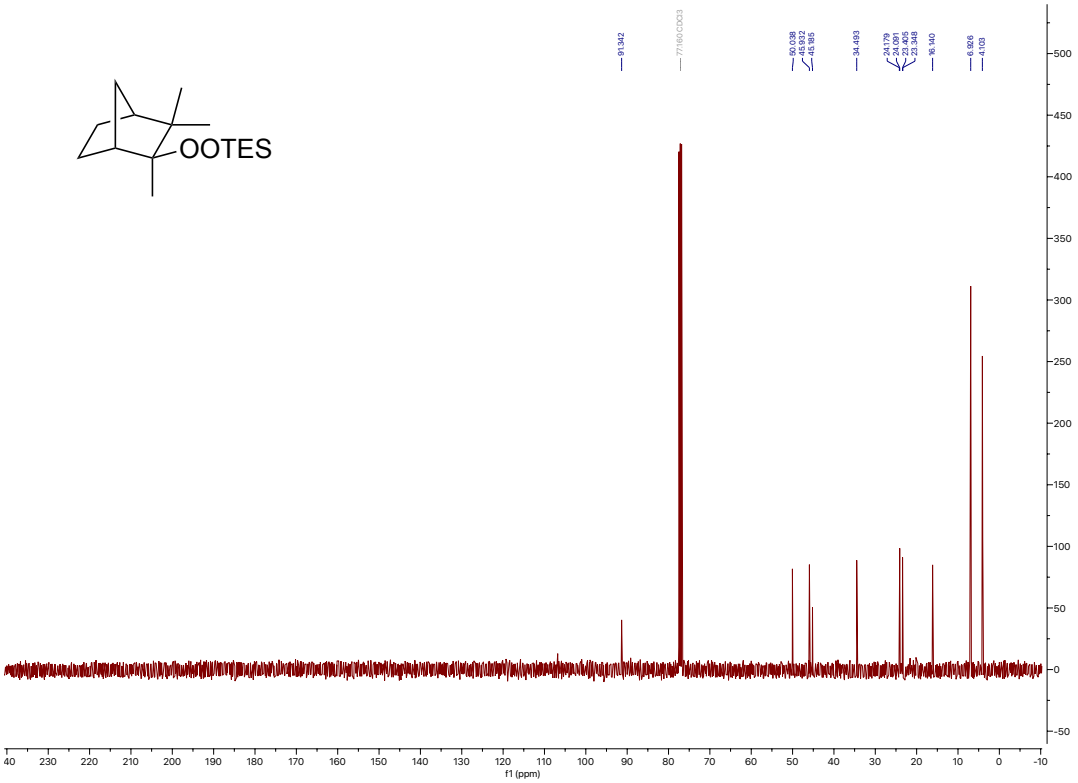


1D Selective Gradient NOESY, frequency 1.300 ppm of ***endo*-21b**

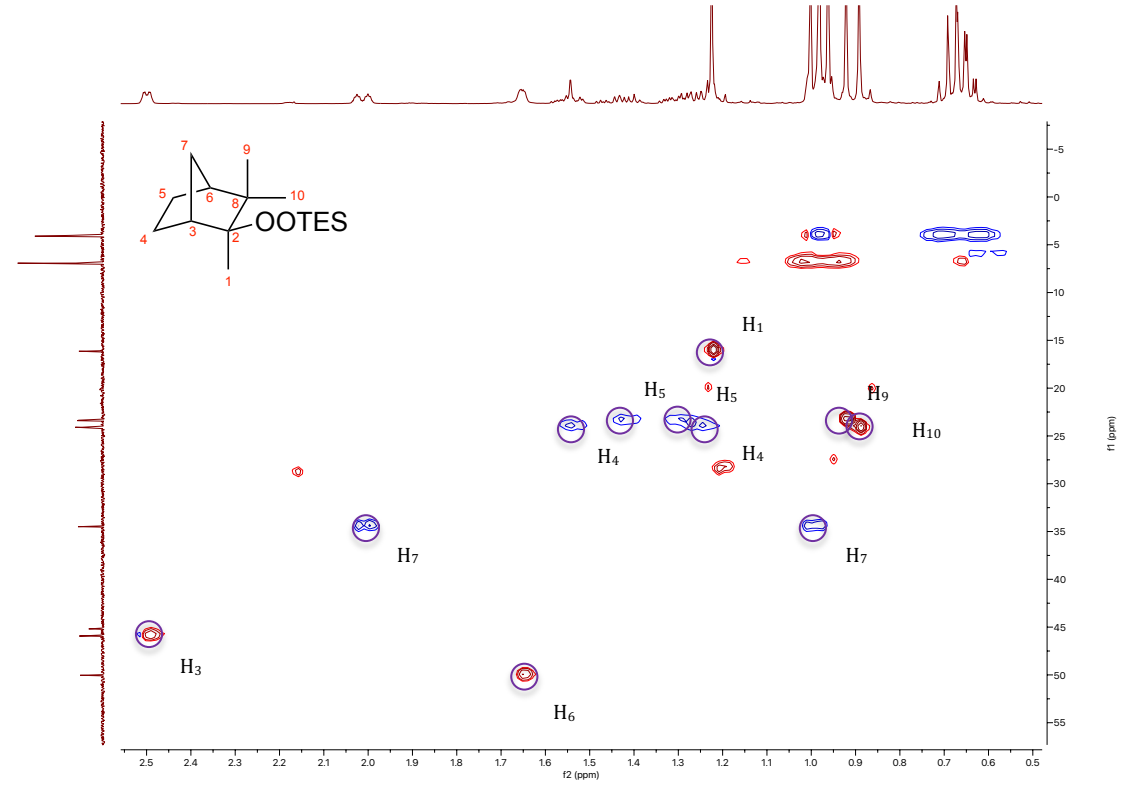


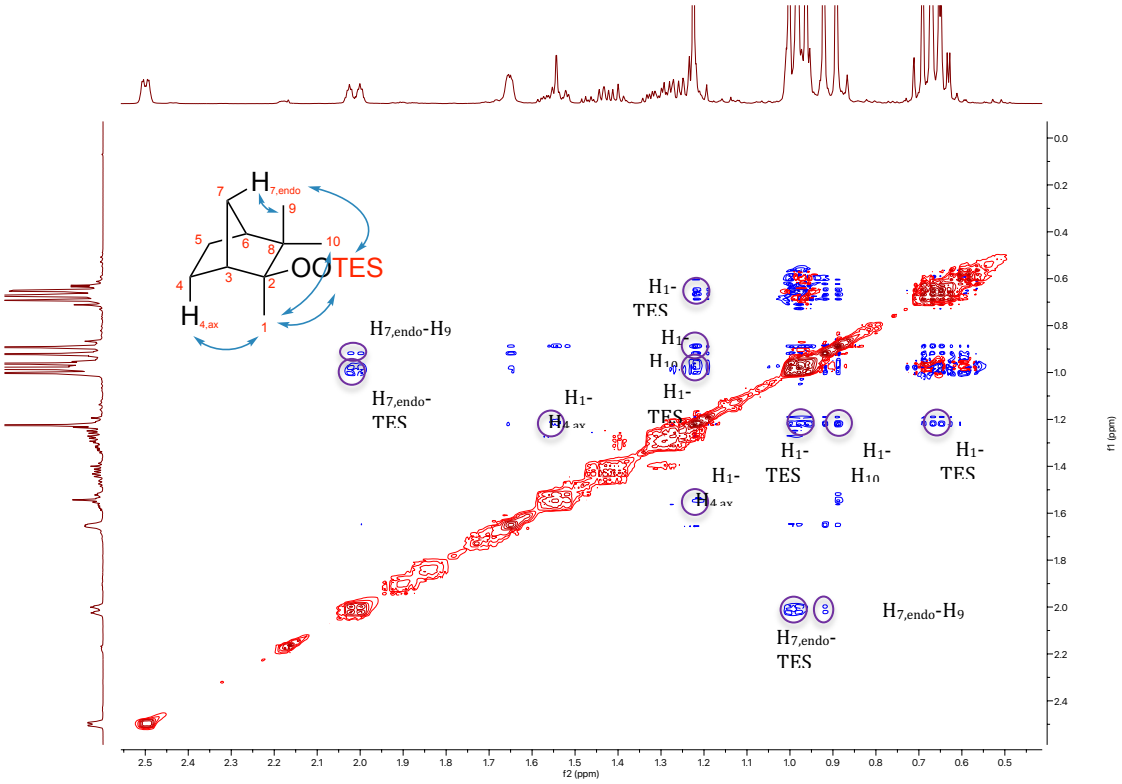
1D Selective Gradient NOESY, frequency 1.082 ppm of ***endo*-21b**



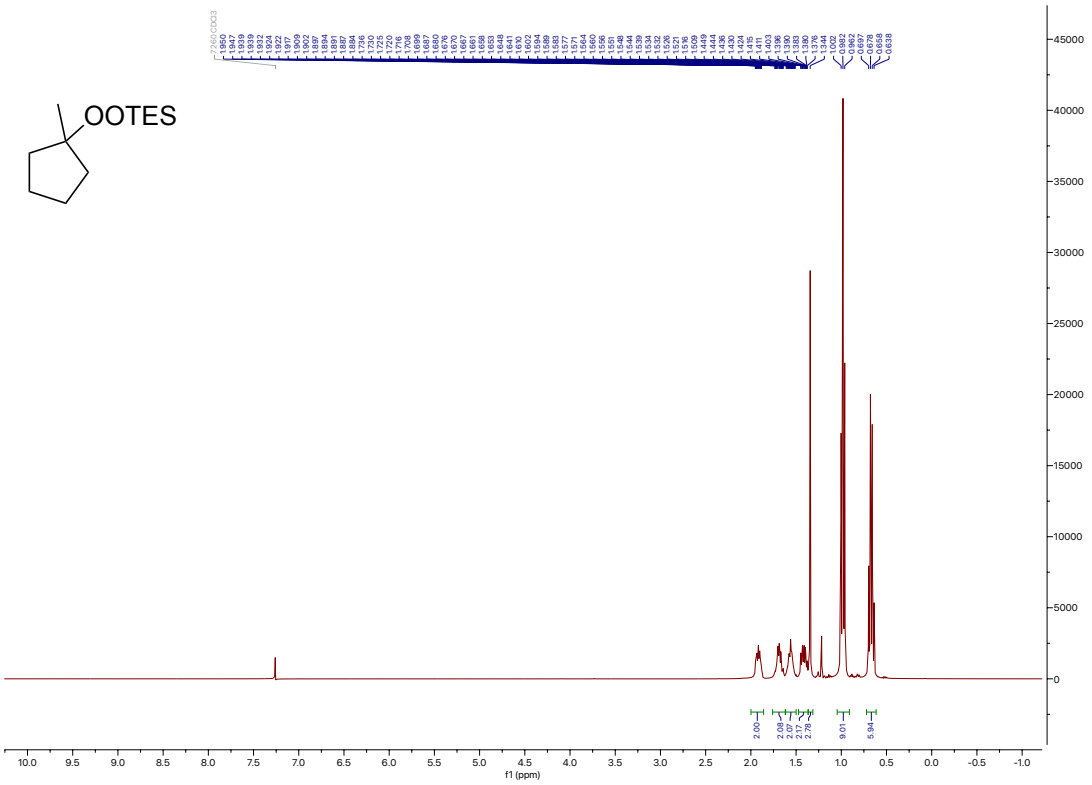


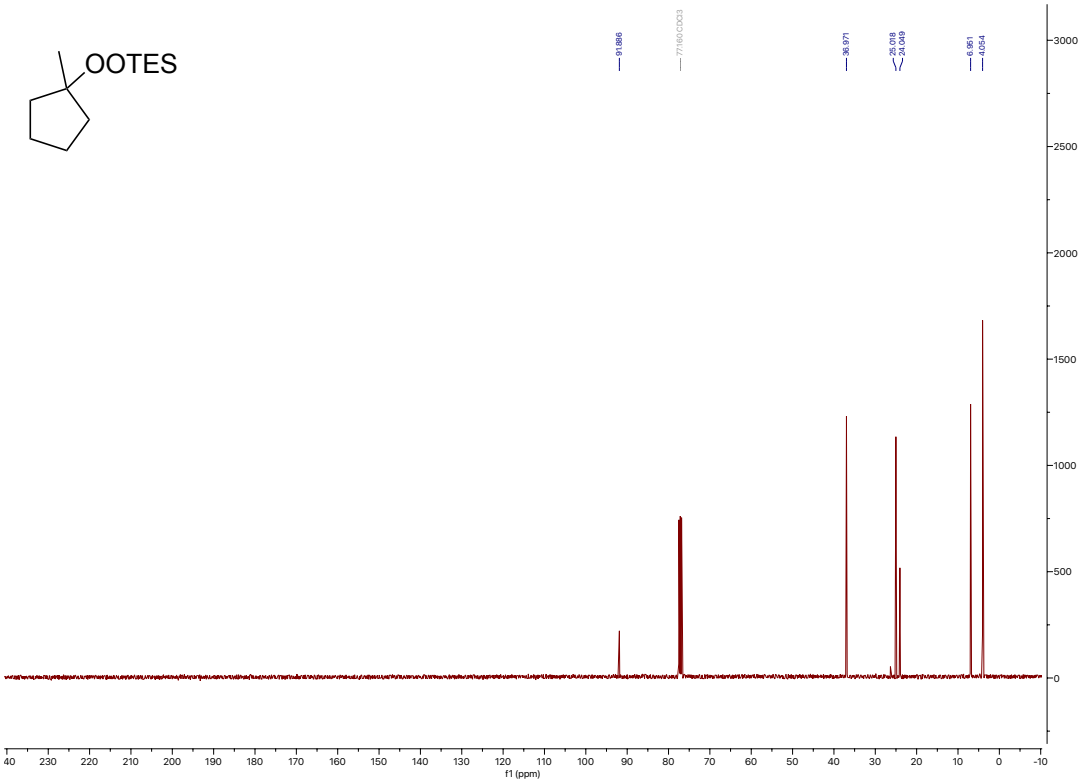
^{1}H NMR (400 MHz, $CDCl_3$) and ^{13}C NMR (101 MHz, $CDCl_3$) of **22b**



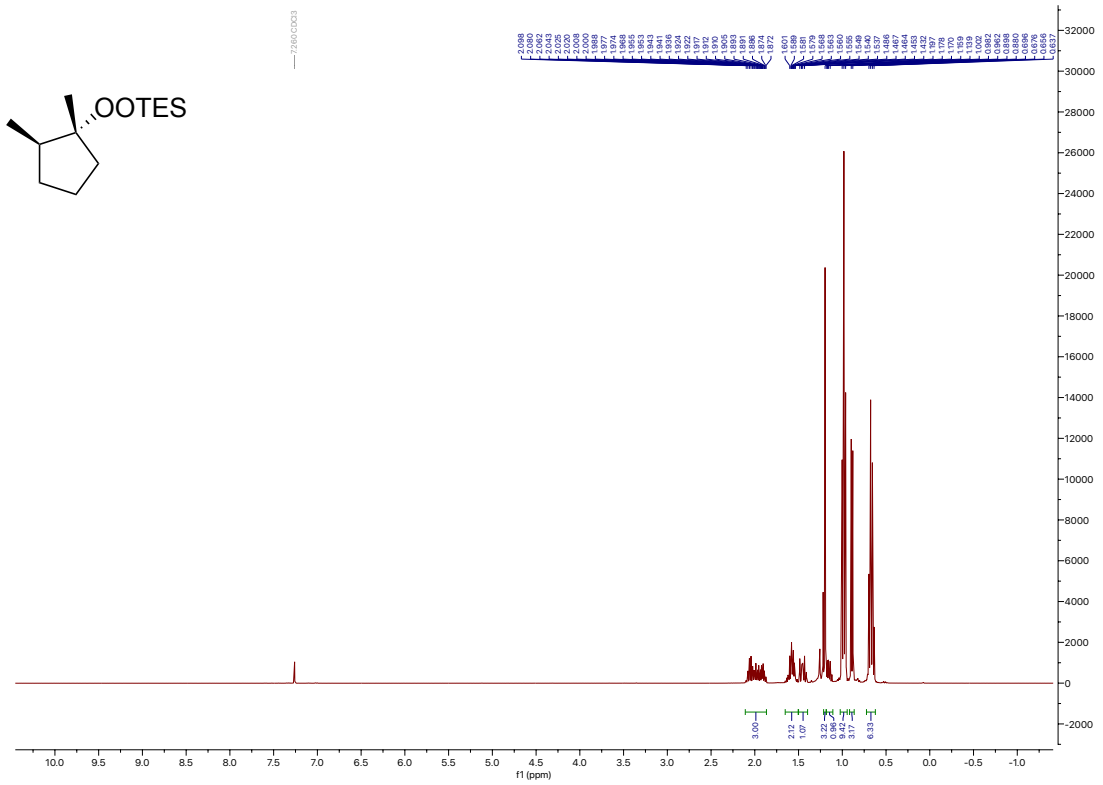


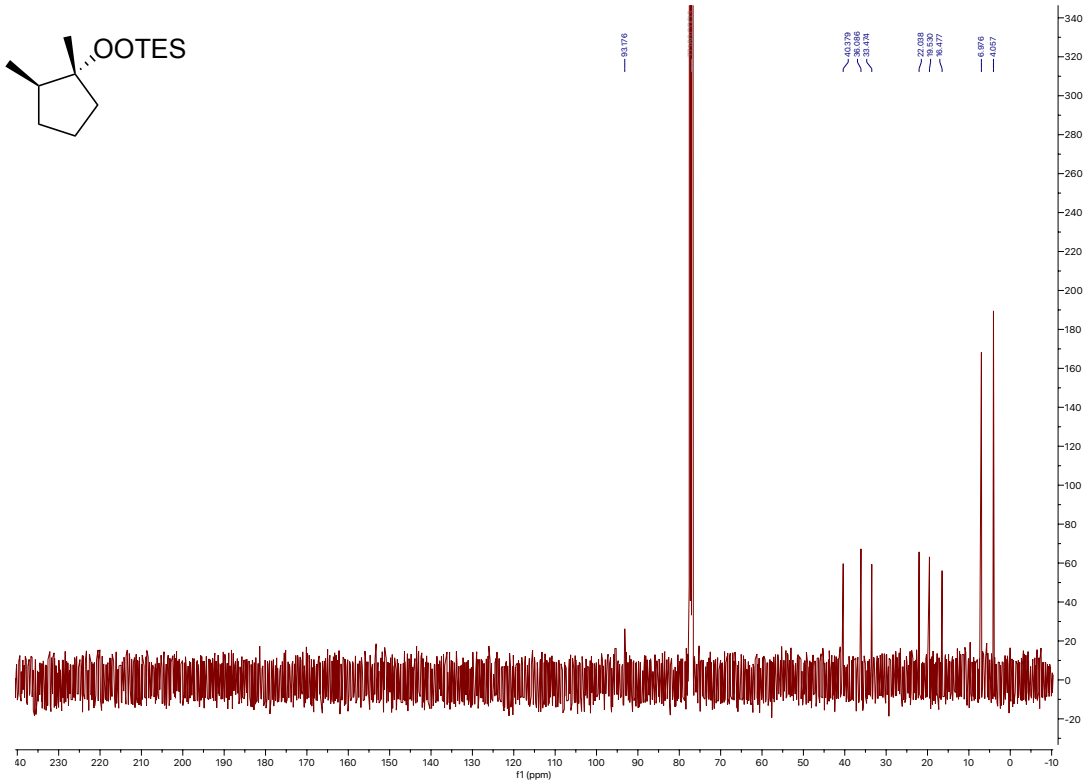
HSQC and NOESY of **22b**



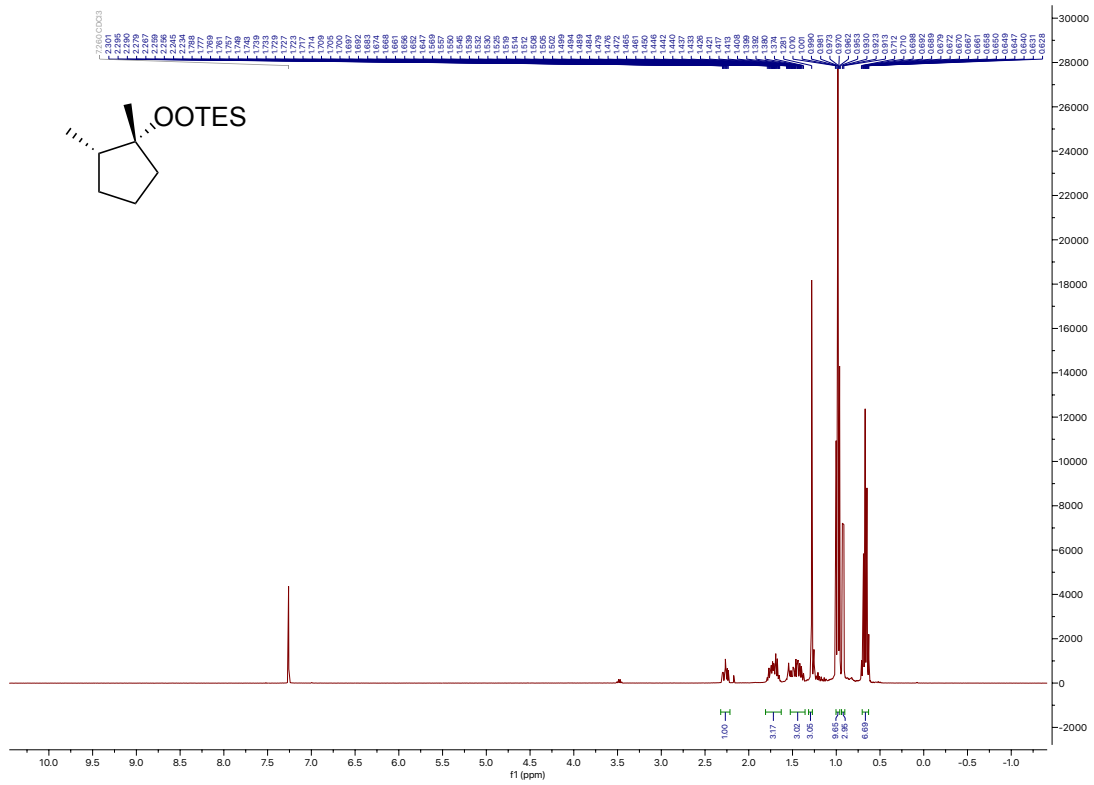


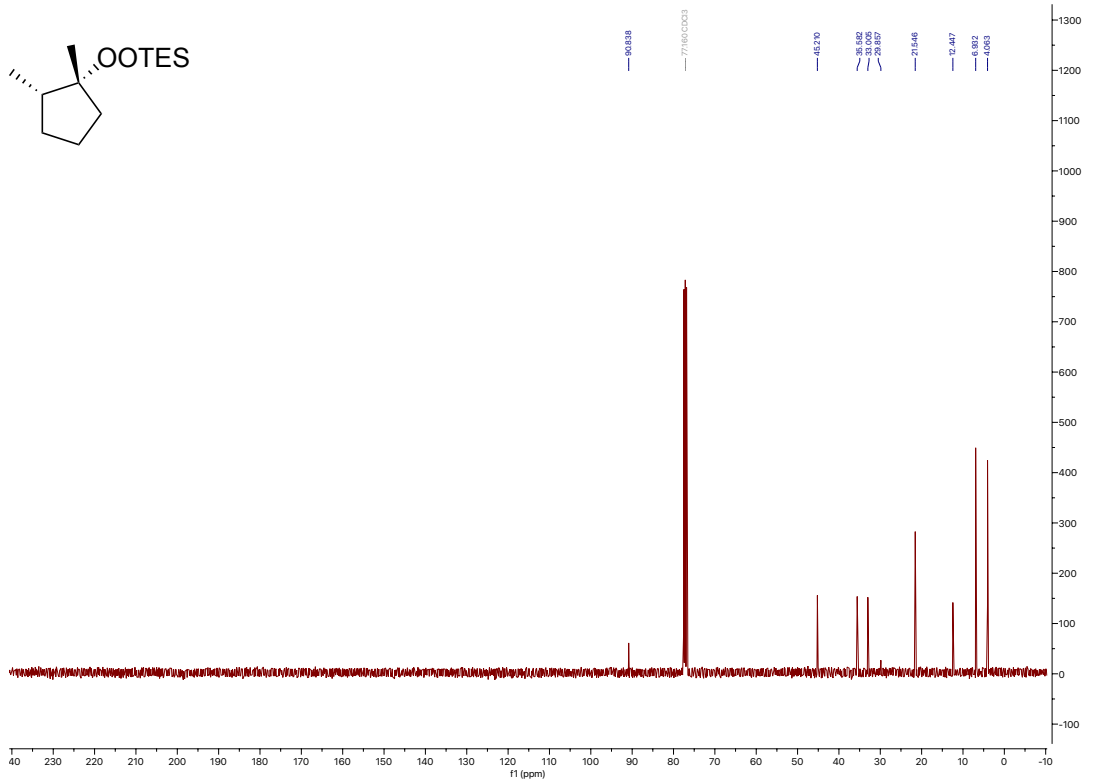
^{1}H NMR (400 MHz, $CDCl_3$) and ^{13}C NMR (101 MHz, $CDCl_3$) of **23b**



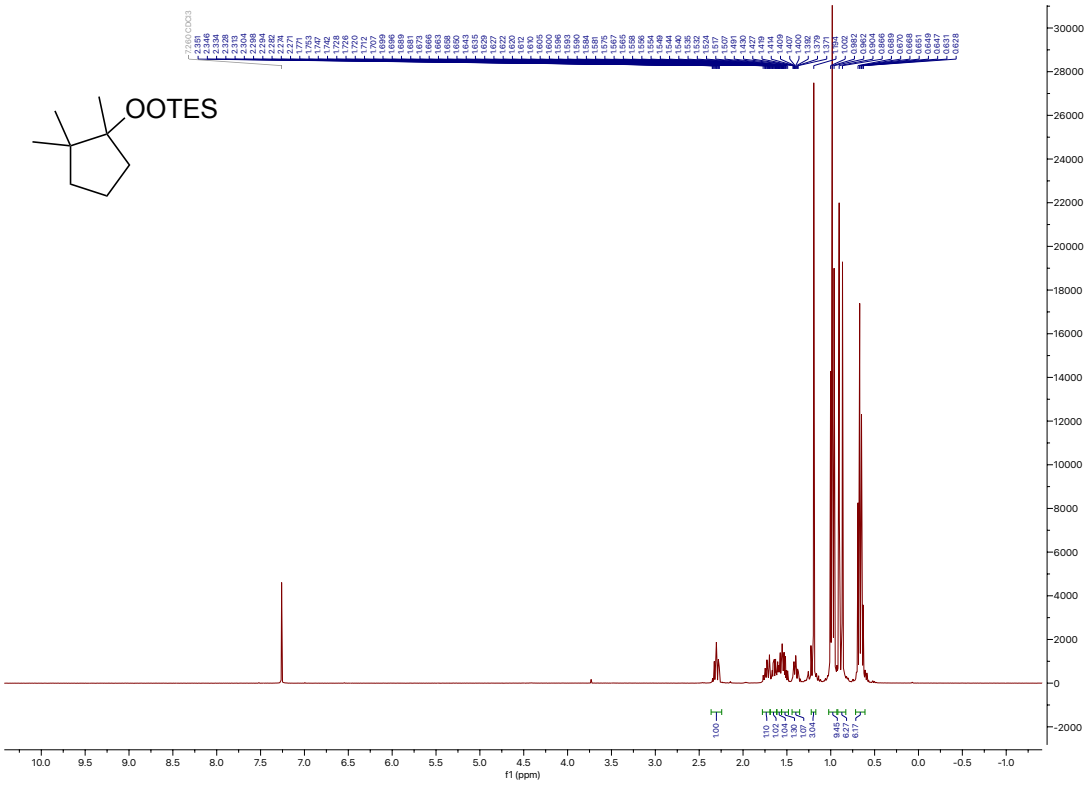


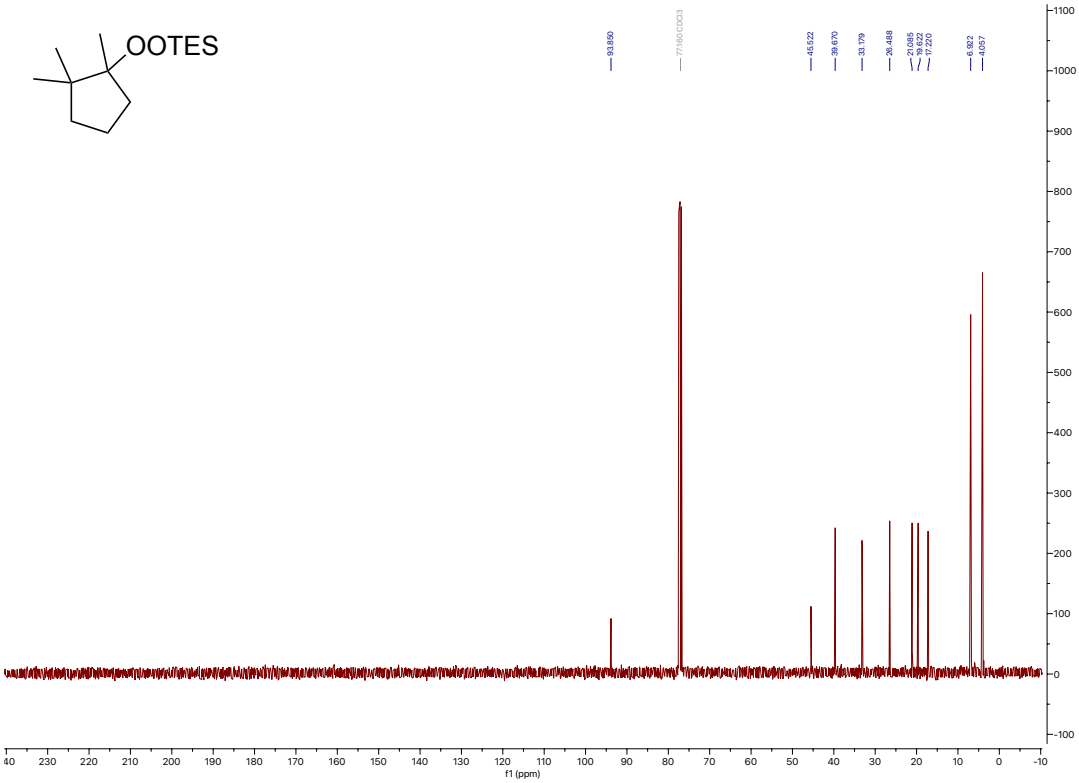
^{1}H NMR (400 MHz, $CDCl_3$) and ^{13}C NMR (101 MHz, $CDCl_3$) of ***trans*-24b**



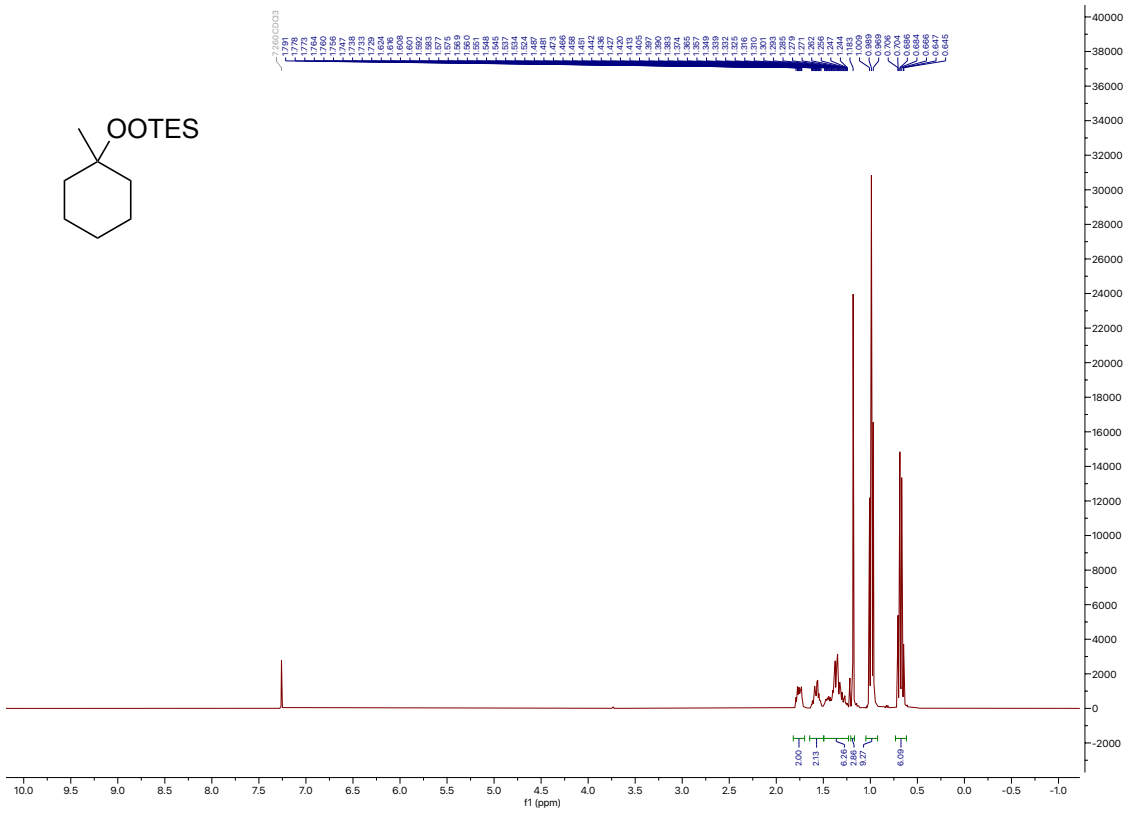


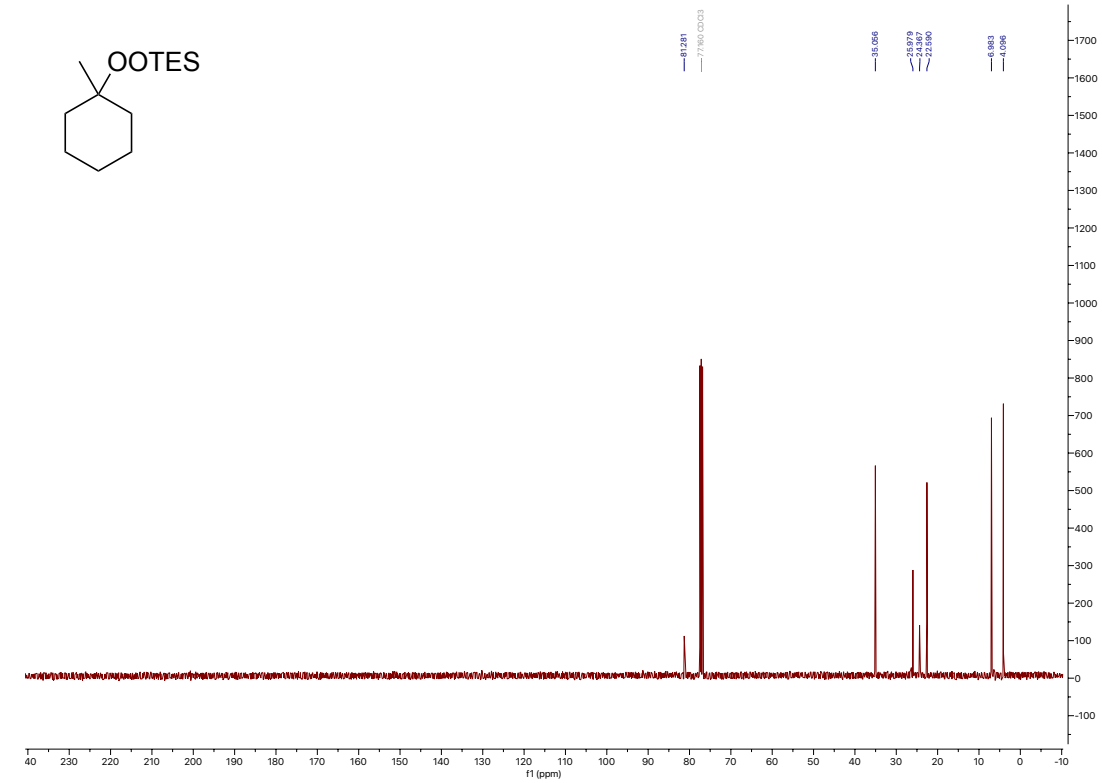
^{1}H NMR (400 MHz, $CDCl_3$) and ^{13}C NMR (101 MHz, $CDCl_3$) of ***cis*-24b**



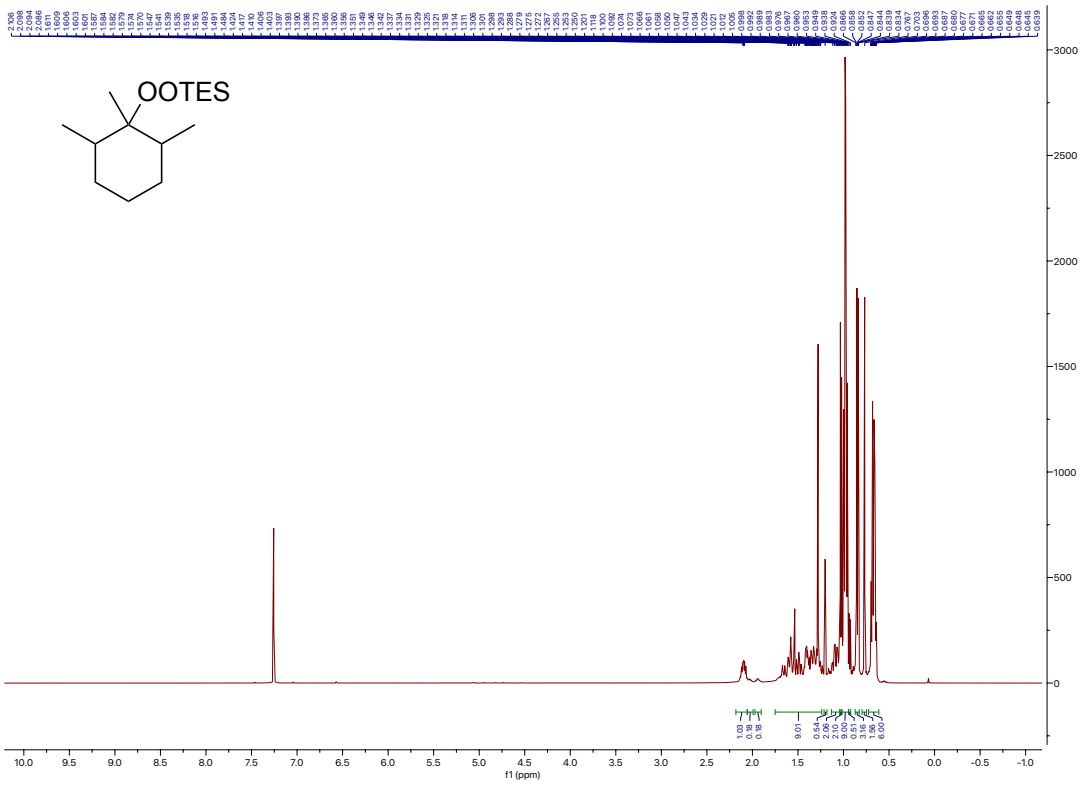


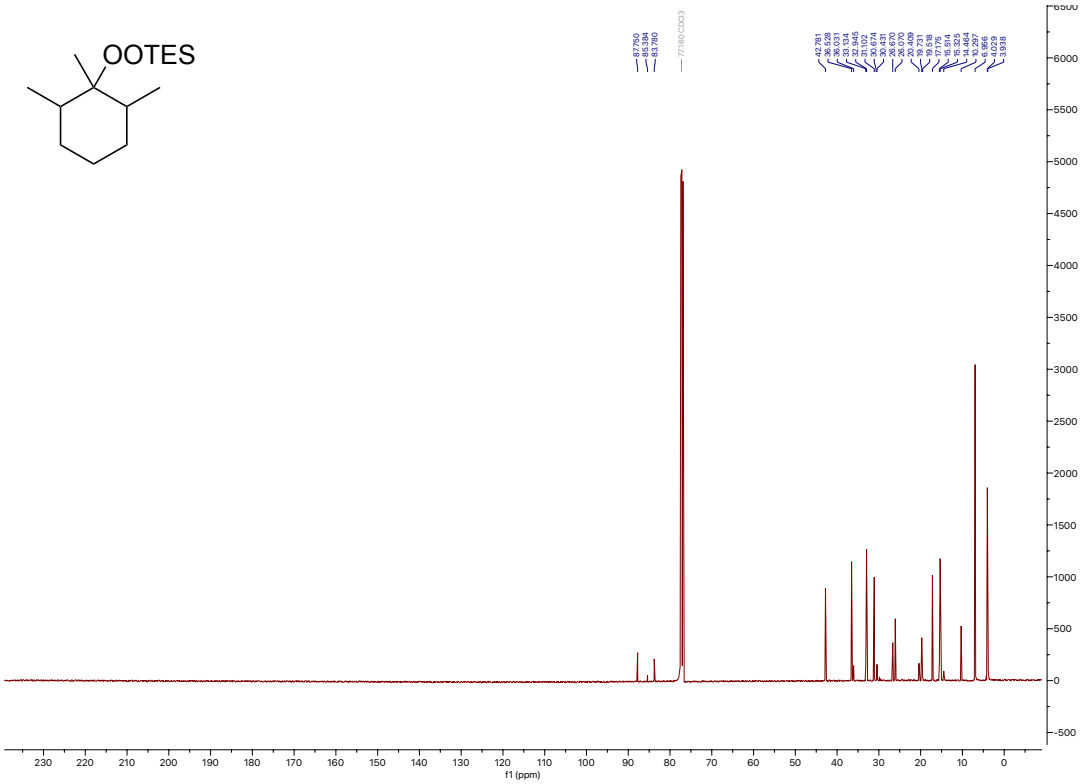
^{1}H NMR (400 MHz, $CDCl_3$) and ^{13}C NMR (101 MHz, $CDCl_3$) of **25b**



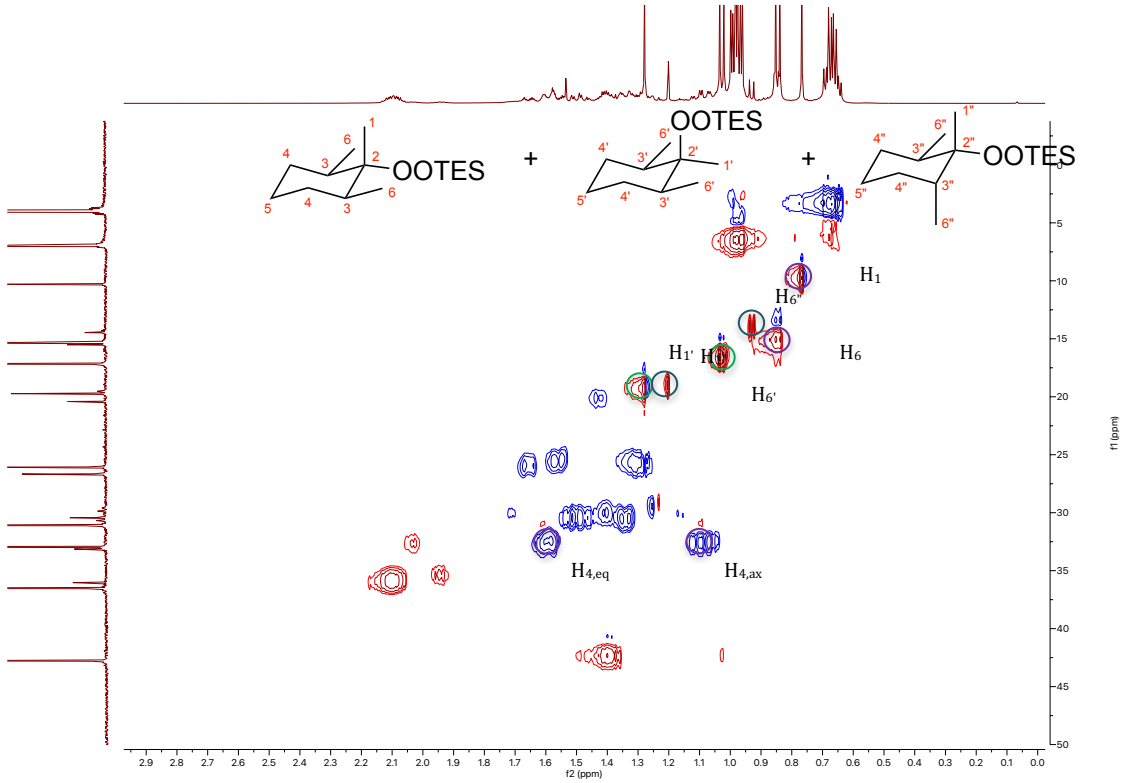


^{1}H NMR (400 MHz, $CDCl_3$) and ^{13}C NMR (101 MHz, $CDCl_3$) of **26b**

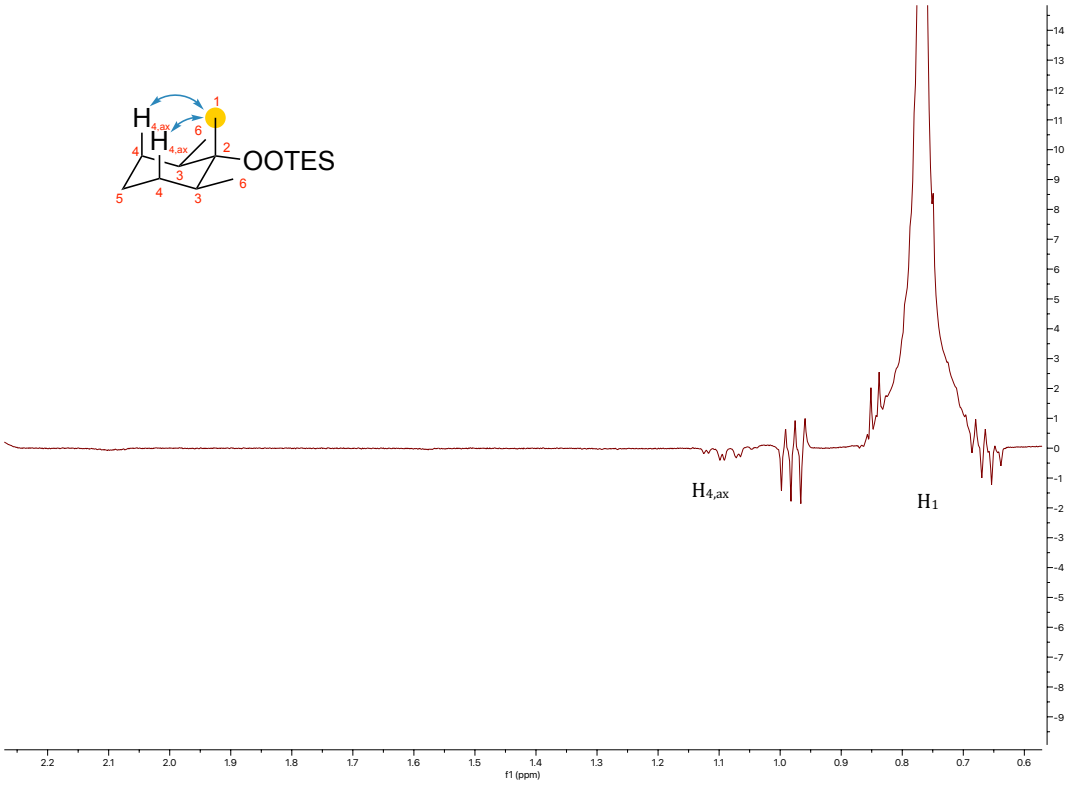




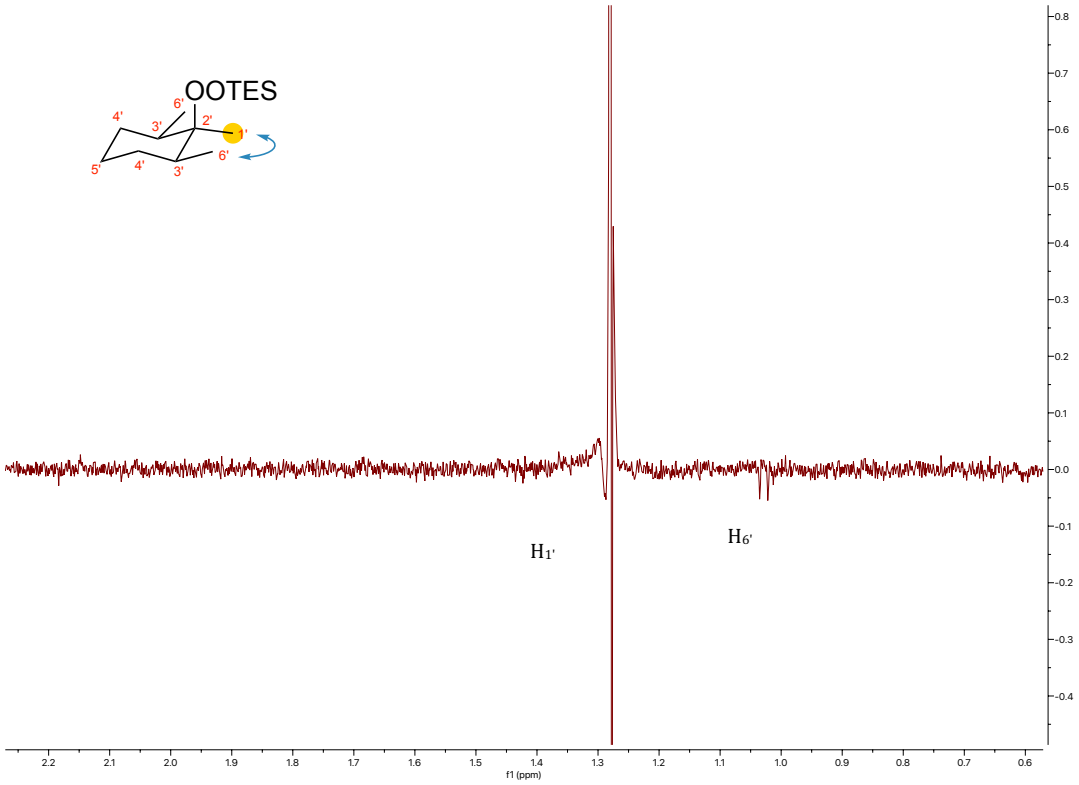
^{1}H NMR (500 MHz, $CDCl_3$) and ^{13}C NMR (126 MHz, $CDCl_3$) of **27b**



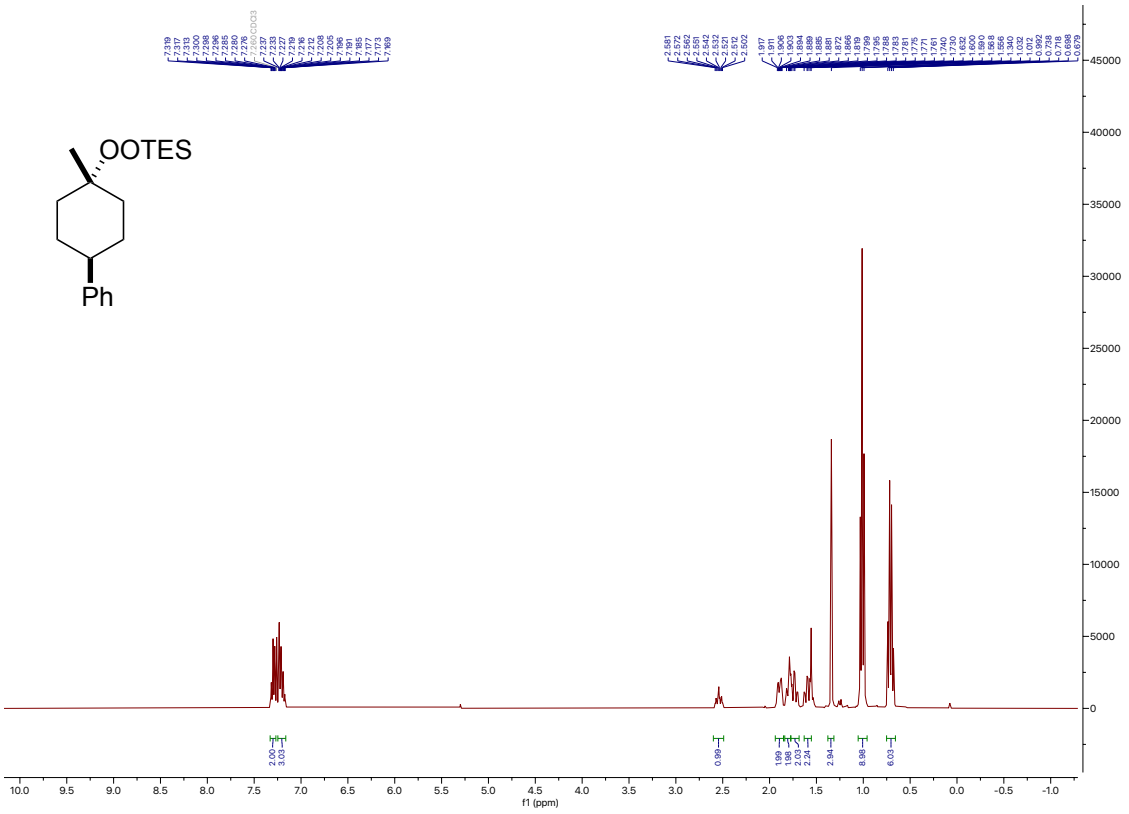
HSQC ($CDCl_3$) of **27b**

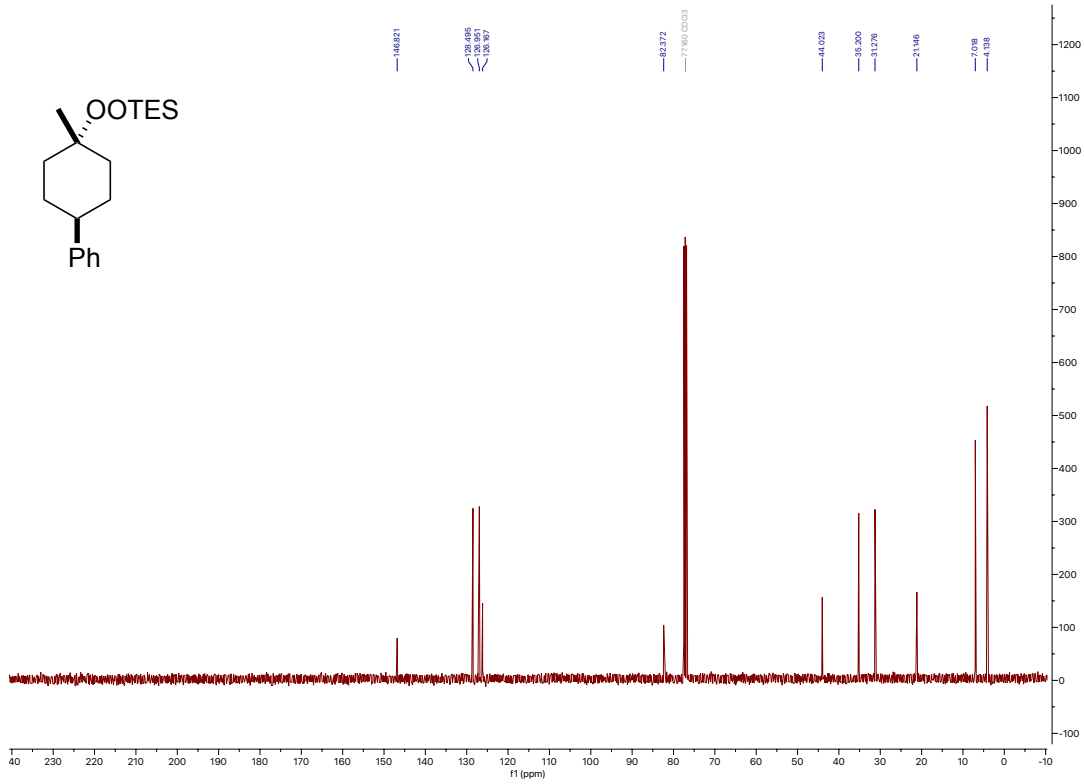


1D Selective Gradient NOESY of **27b1**, frequency 0.799 ppm

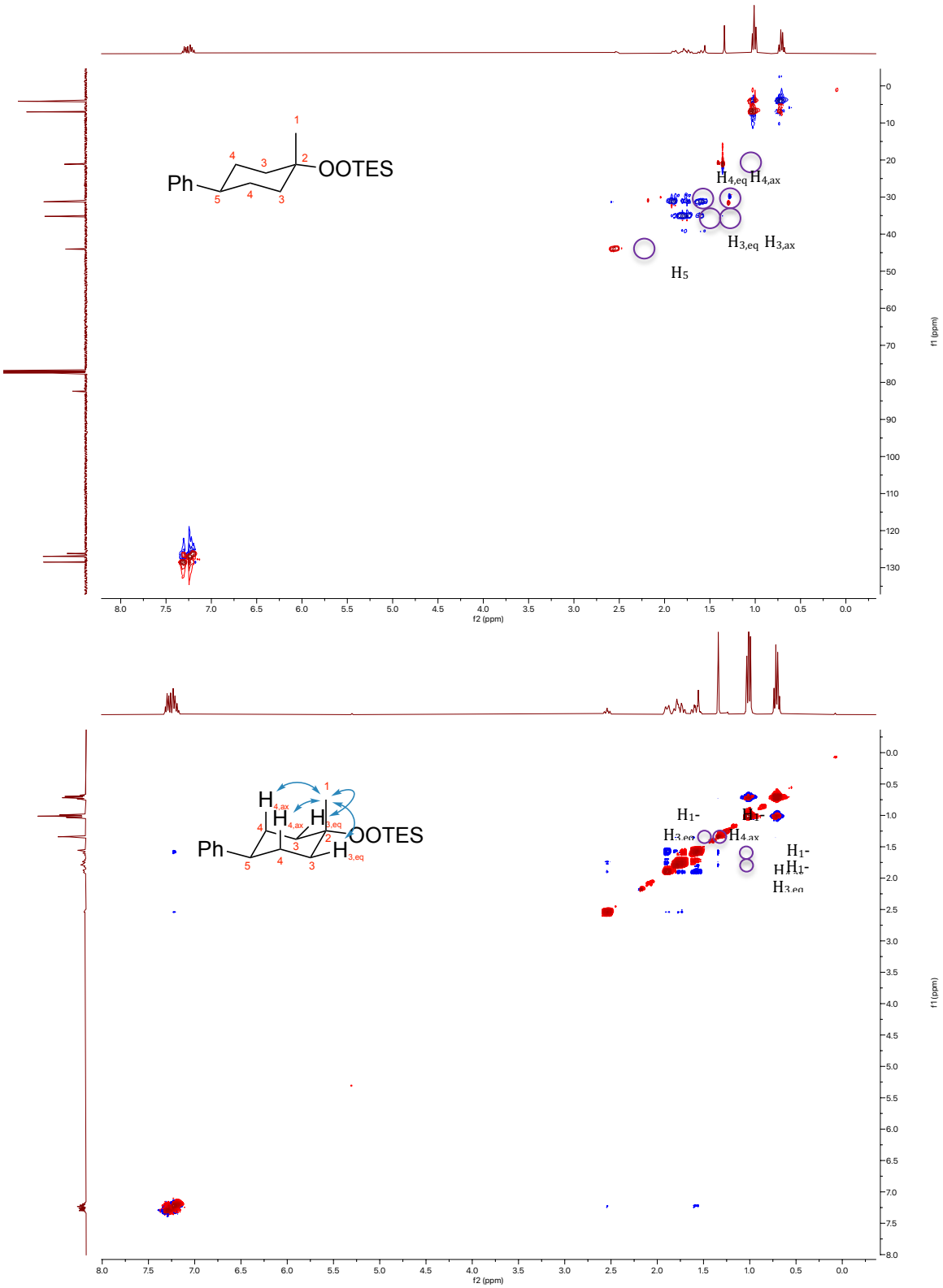


1D Selective Gradient NOESY of **27b2**, frequency 1.308 ppm

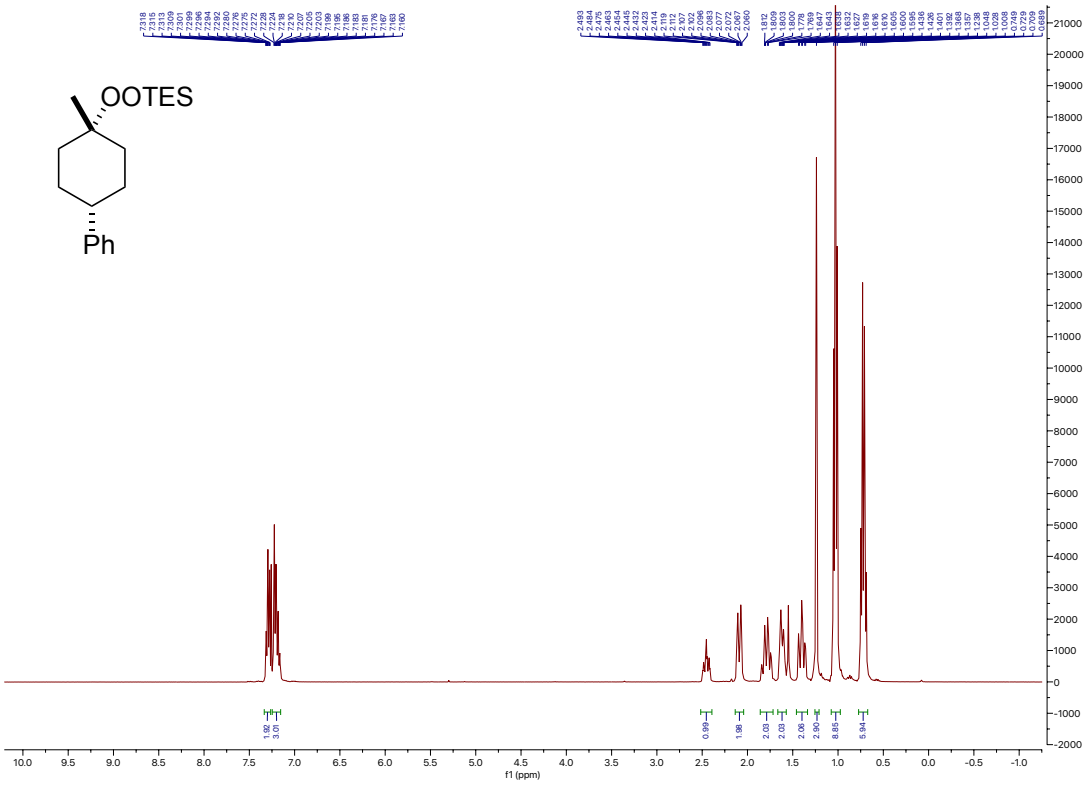


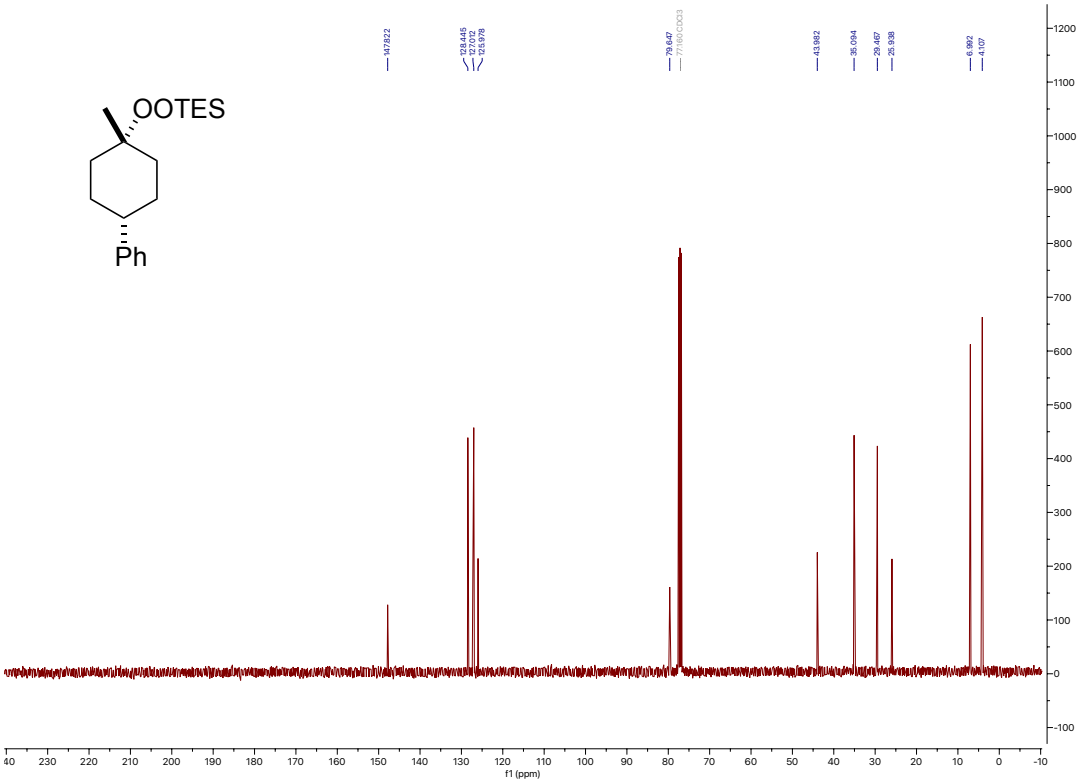


^{1}H NMR (400 MHz, $CDCl_3$) and ^{13}C NMR (101 MHz, $CDCl_3$) of ***trans*-28b**

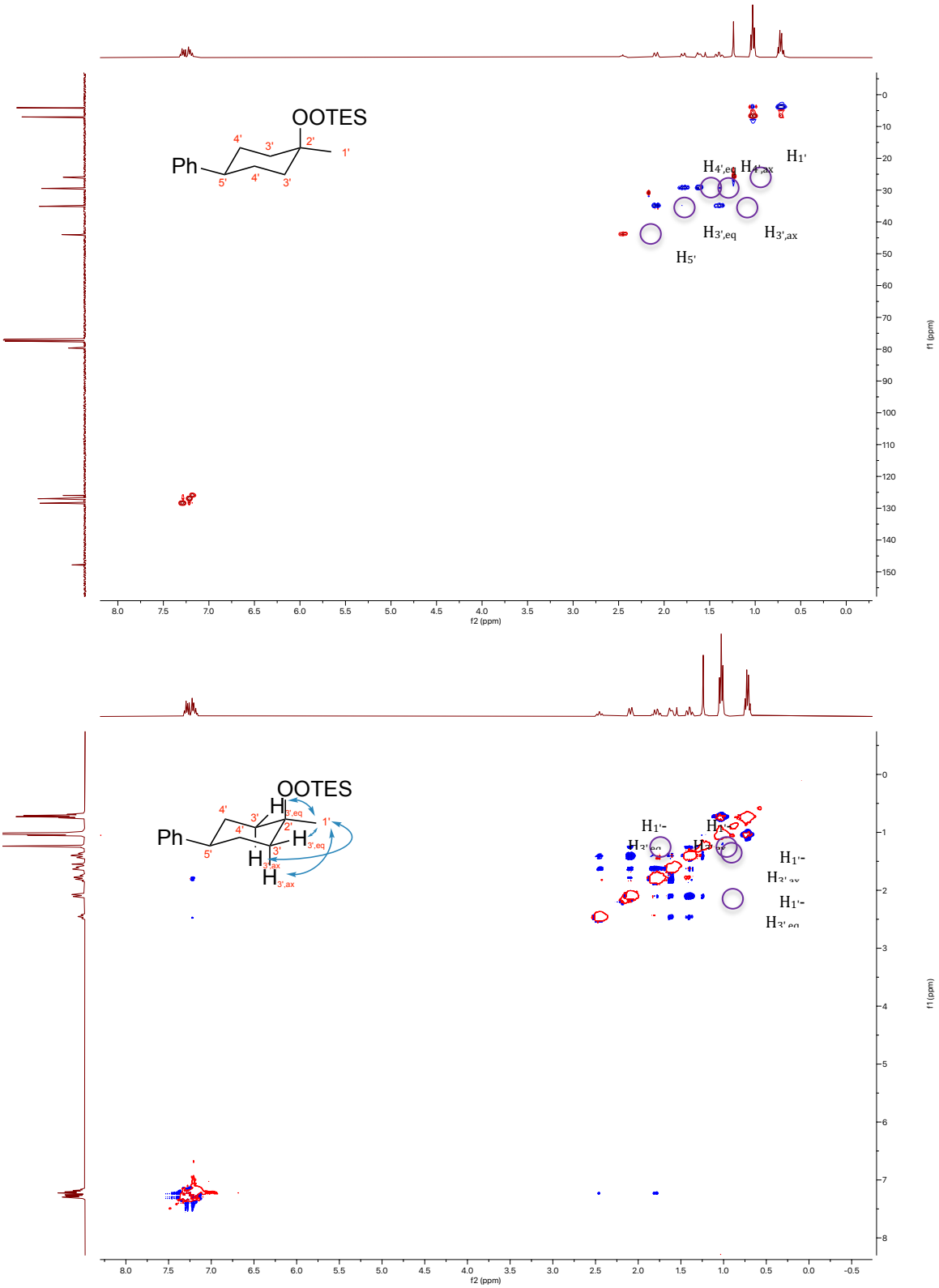


HSQC and NOESY of ***trans*-28b**

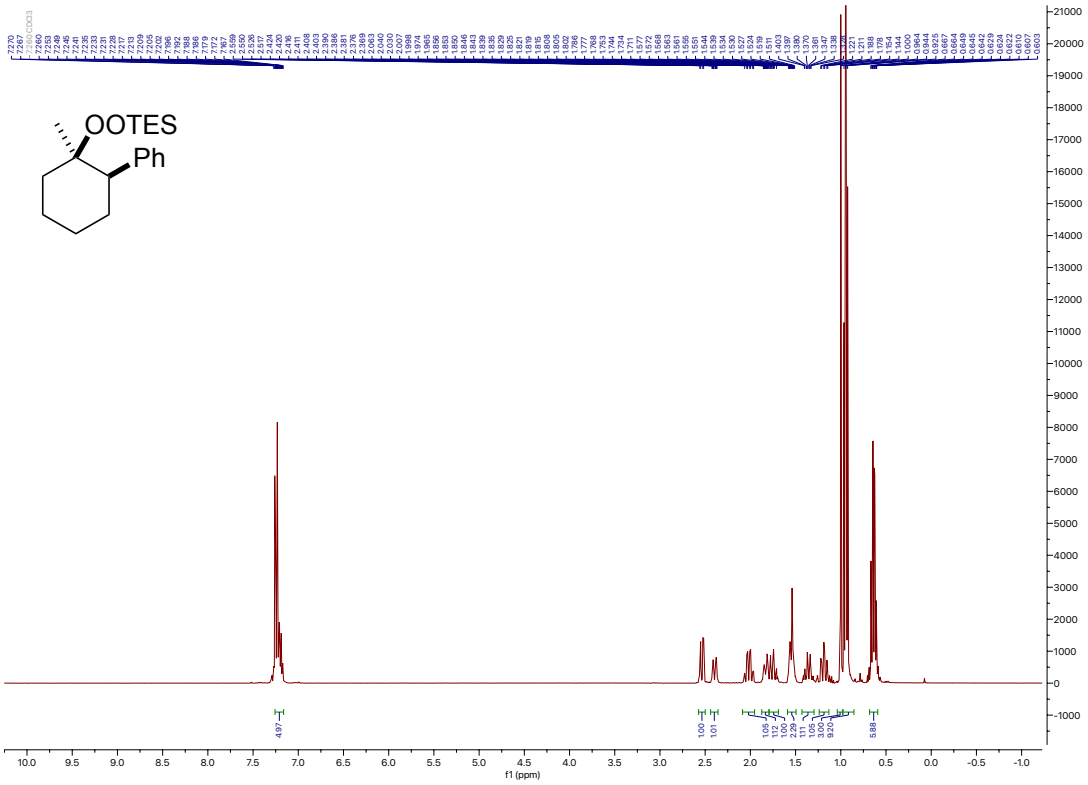


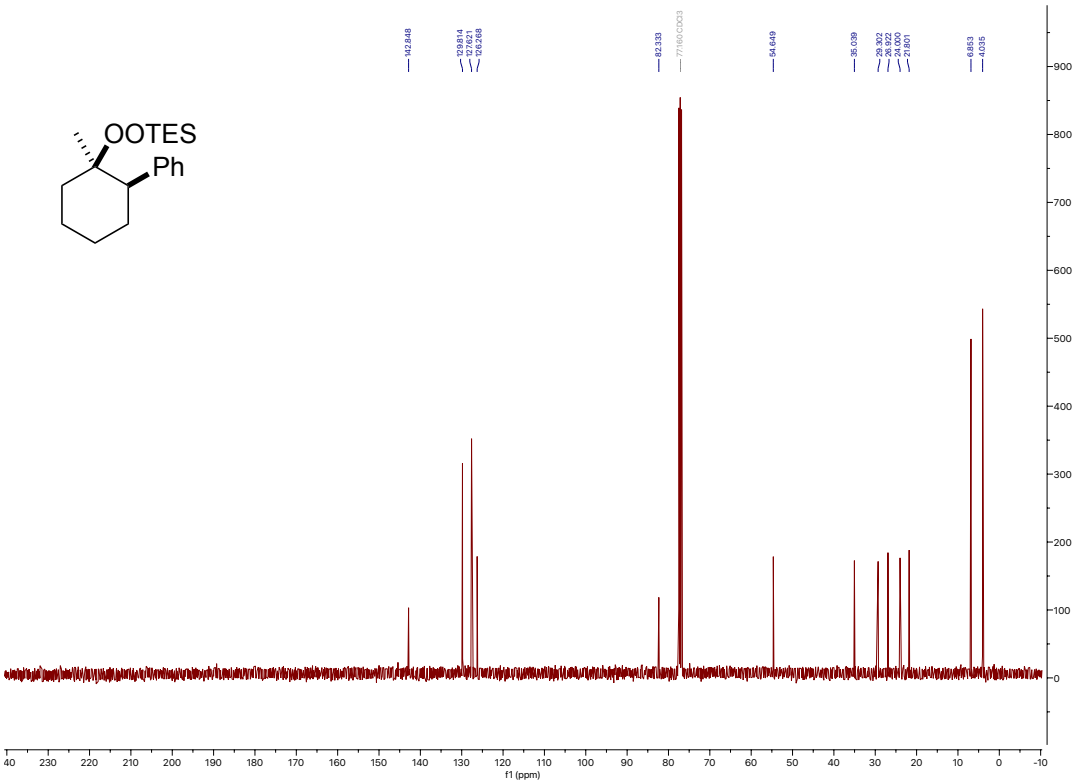


^{1}H NMR (400 MHz, $CDCl_3$) and ^{13}C NMR (101 MHz, $CDCl_3$) of ***cis*-28b**

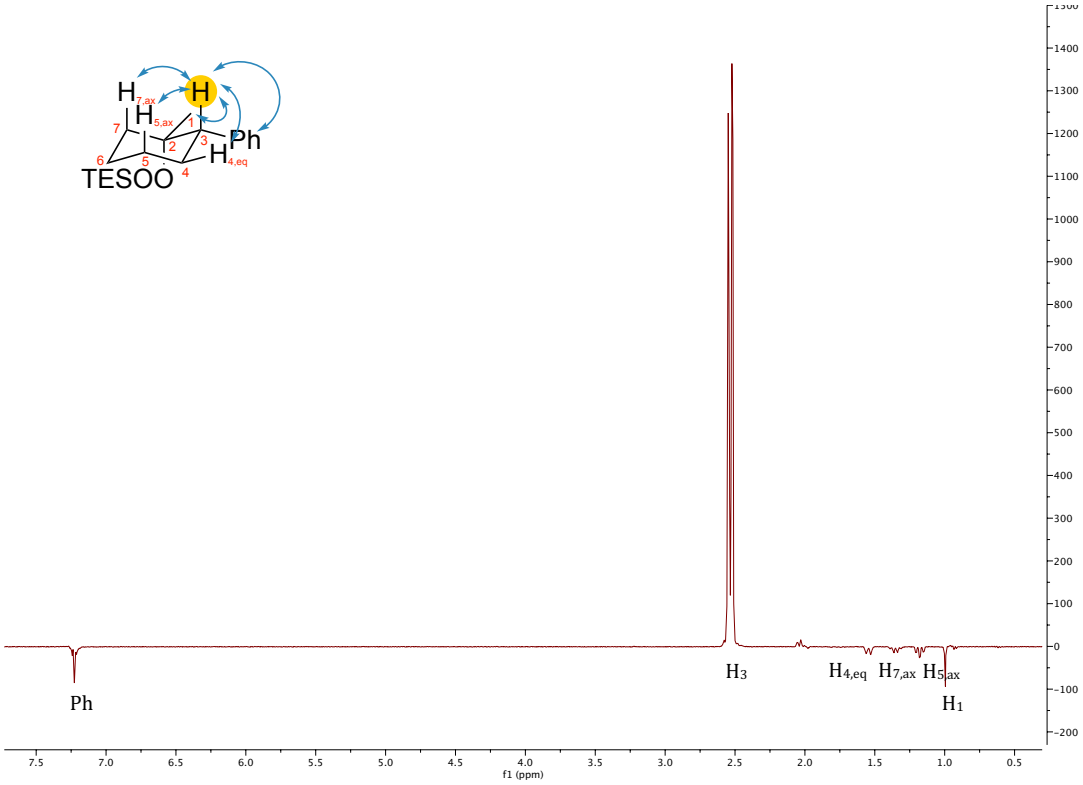


HSQC and NOESY of ***cis*-28b**

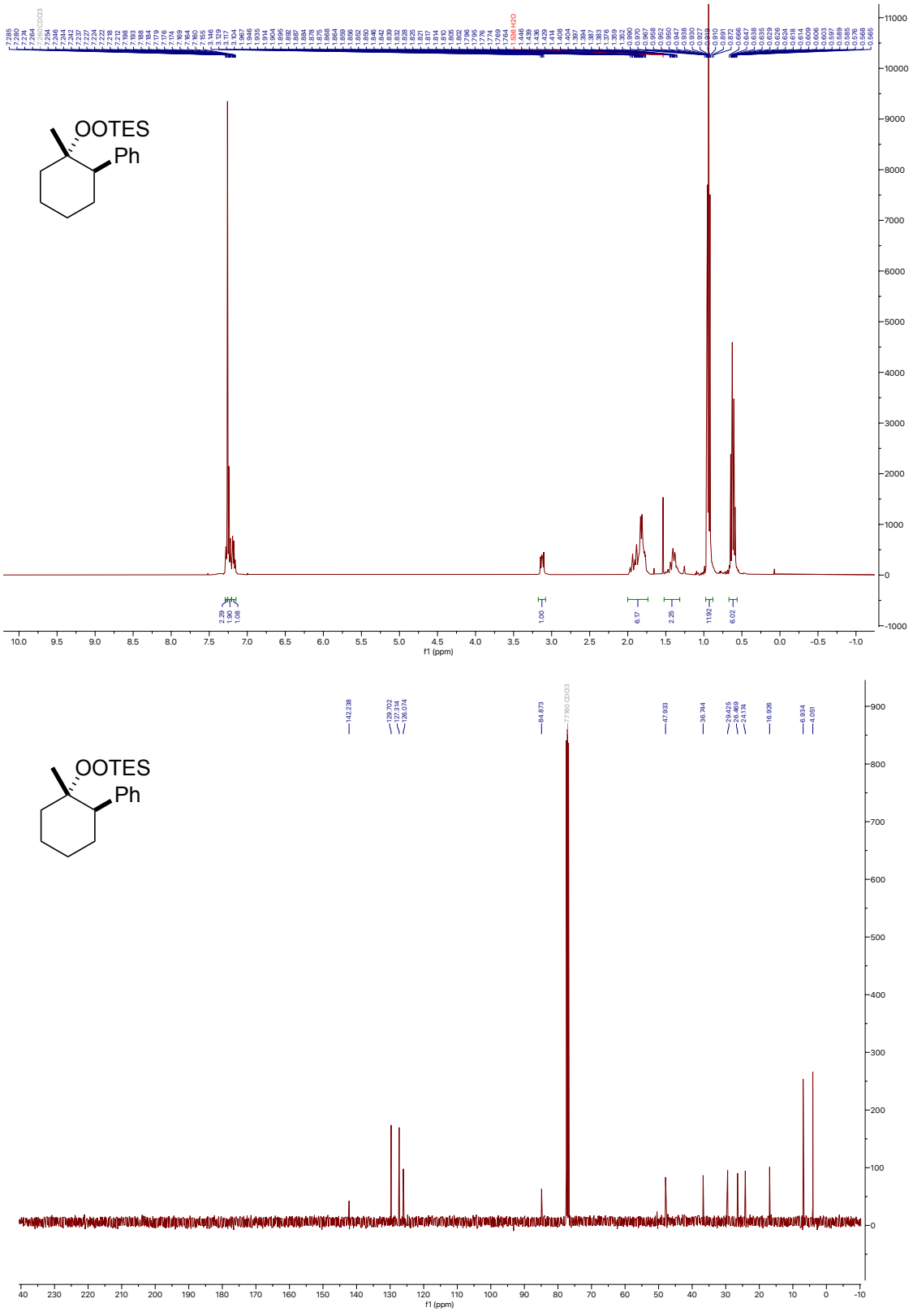




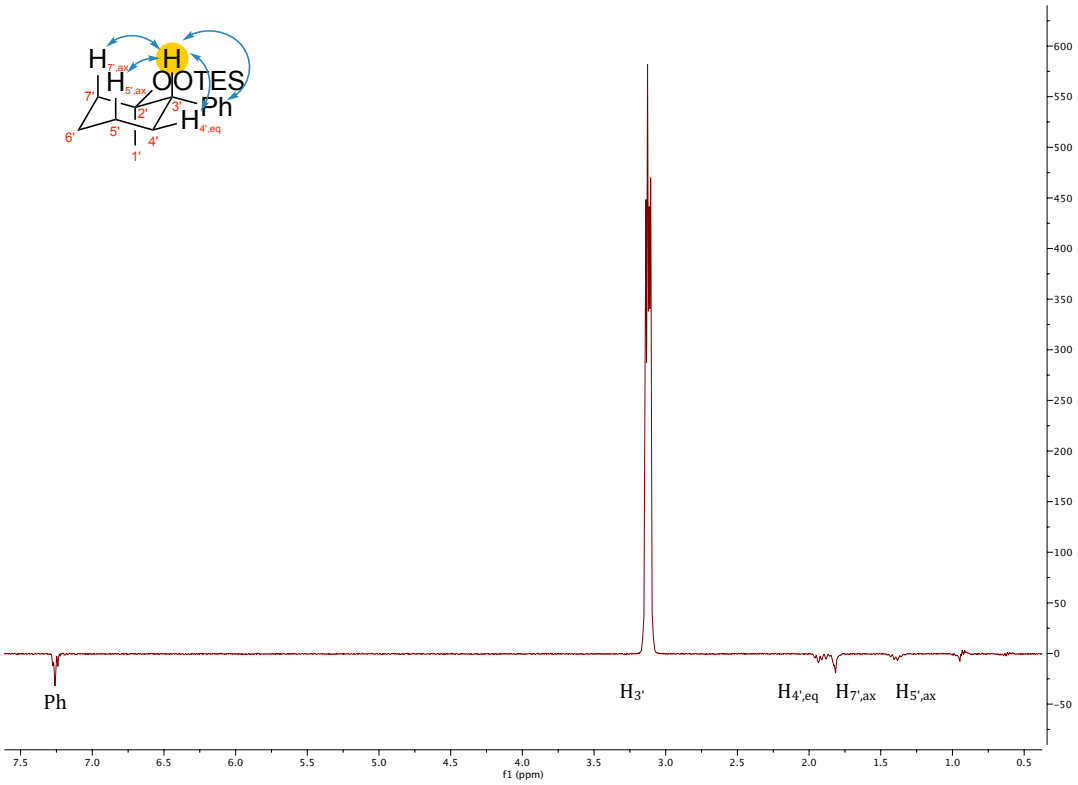
^{1}H NMR (400 MHz, $CDCl_3$) and ^{13}C NMR (101 MHz, $CDCl_3$) of ***cis*-29b**



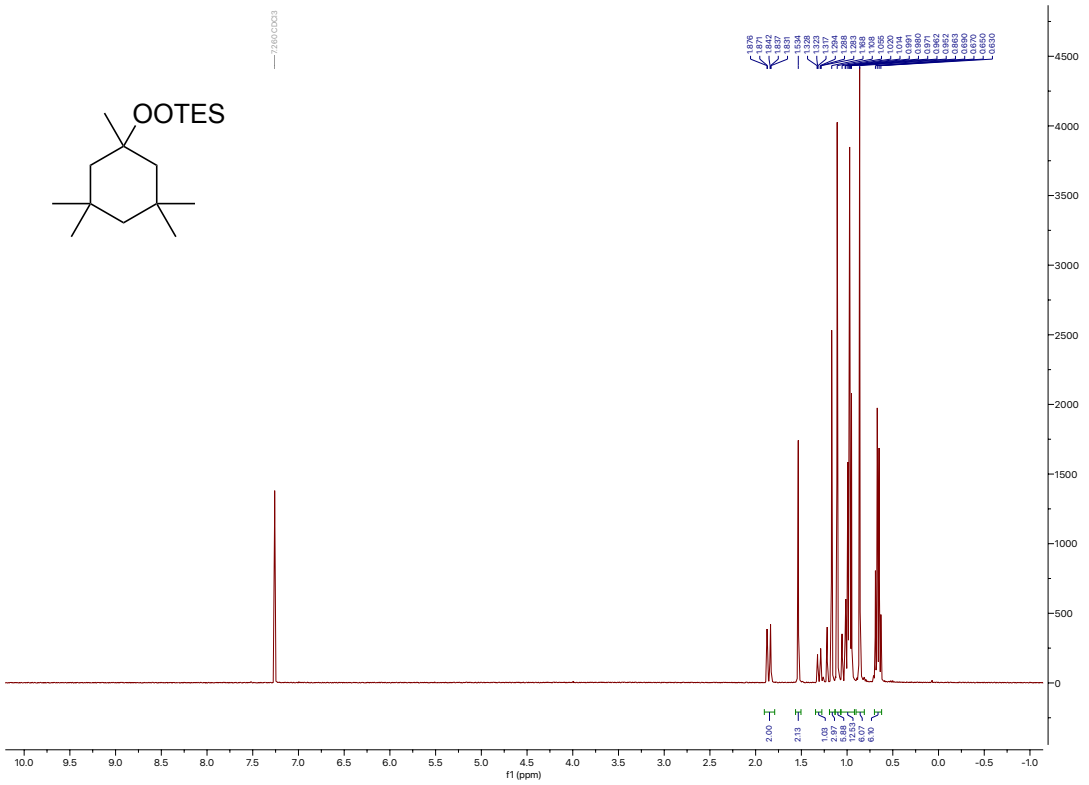
1D Selective Gradient NOESY, frequency 2.554 ppm of of ***cis*-29b**

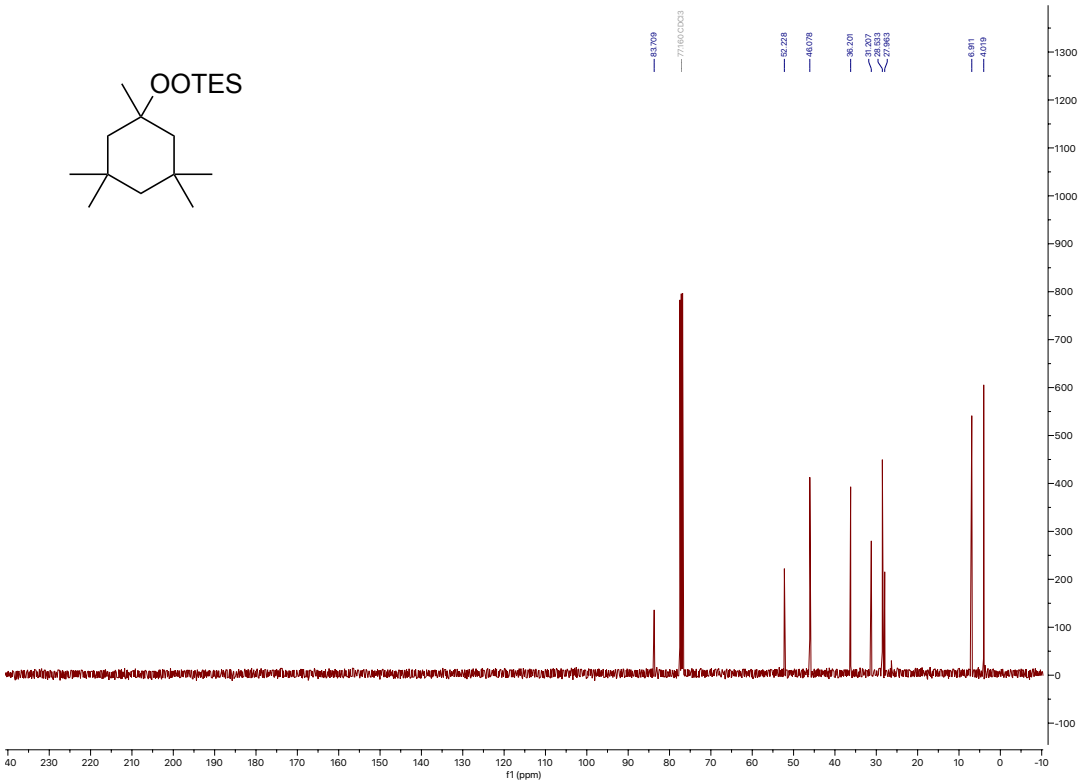


^{1}H NMR (400 MHz, $CDCl_3$) and ^{13}C NMR (101 MHz, $CDCl_3$) of ***trans*-29b**

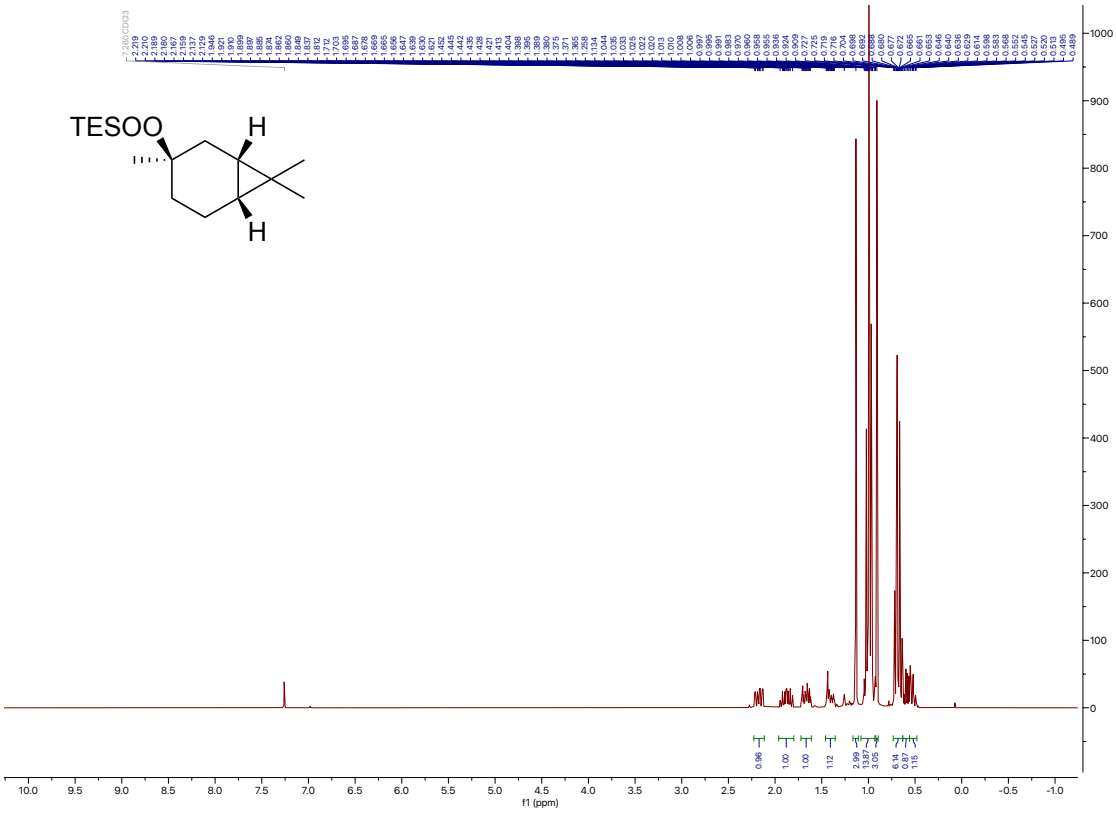


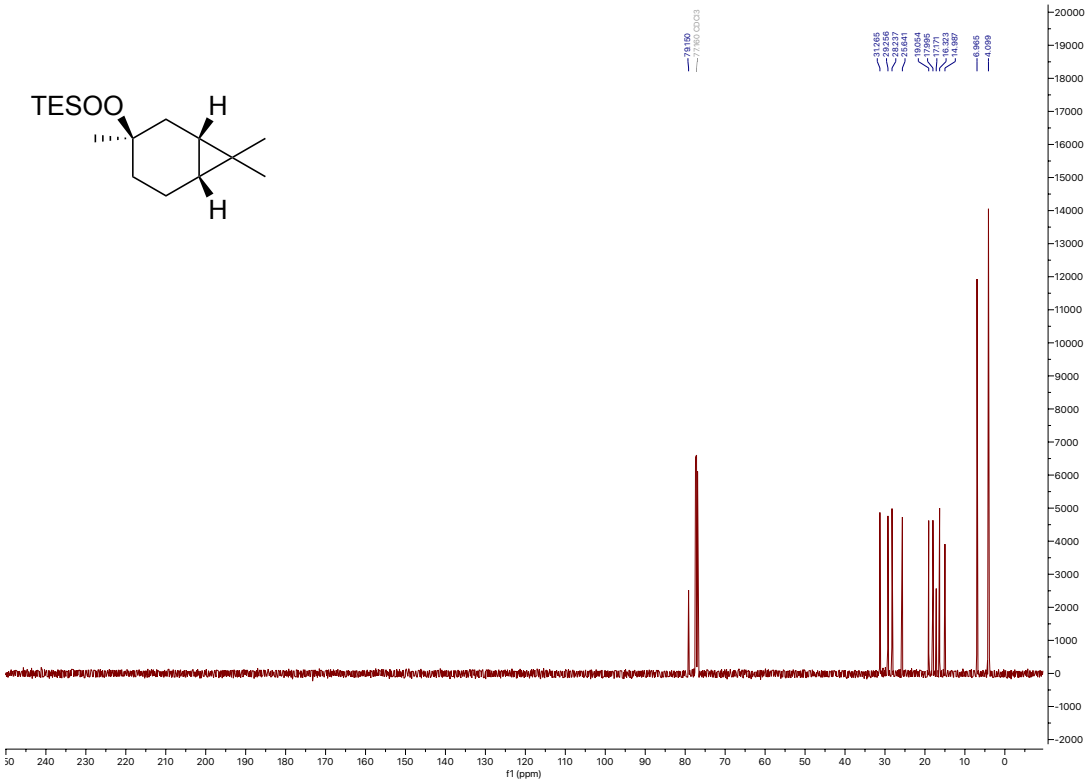
1D Selective Gradient NOESY, frequency 3.155 ppm of ***trans*-29b**



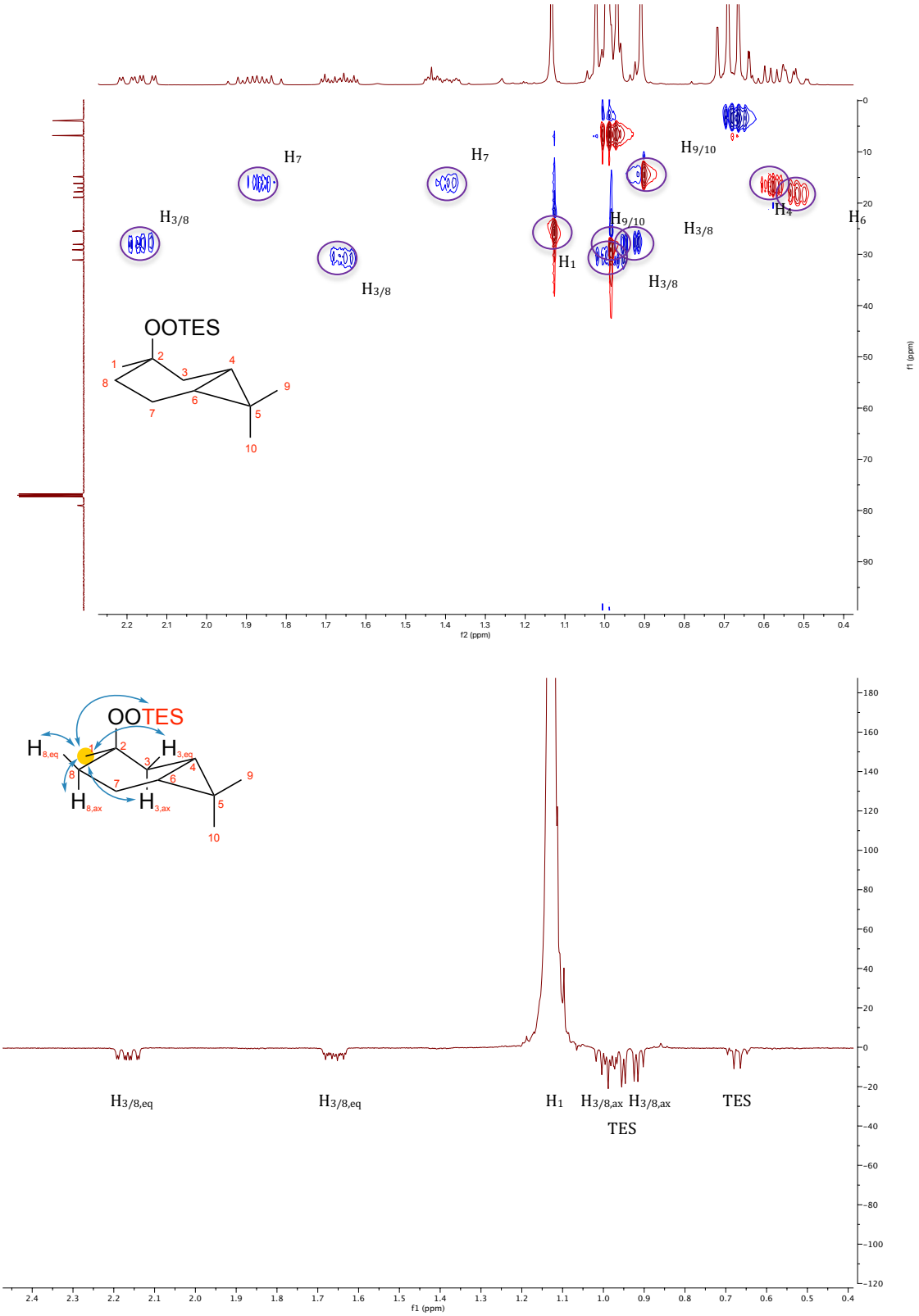


^{1}H NMR (400 MHz, $CDCl_3$) and ^{13}C NMR (101 MHz, $CDCl_3$) of **30b**

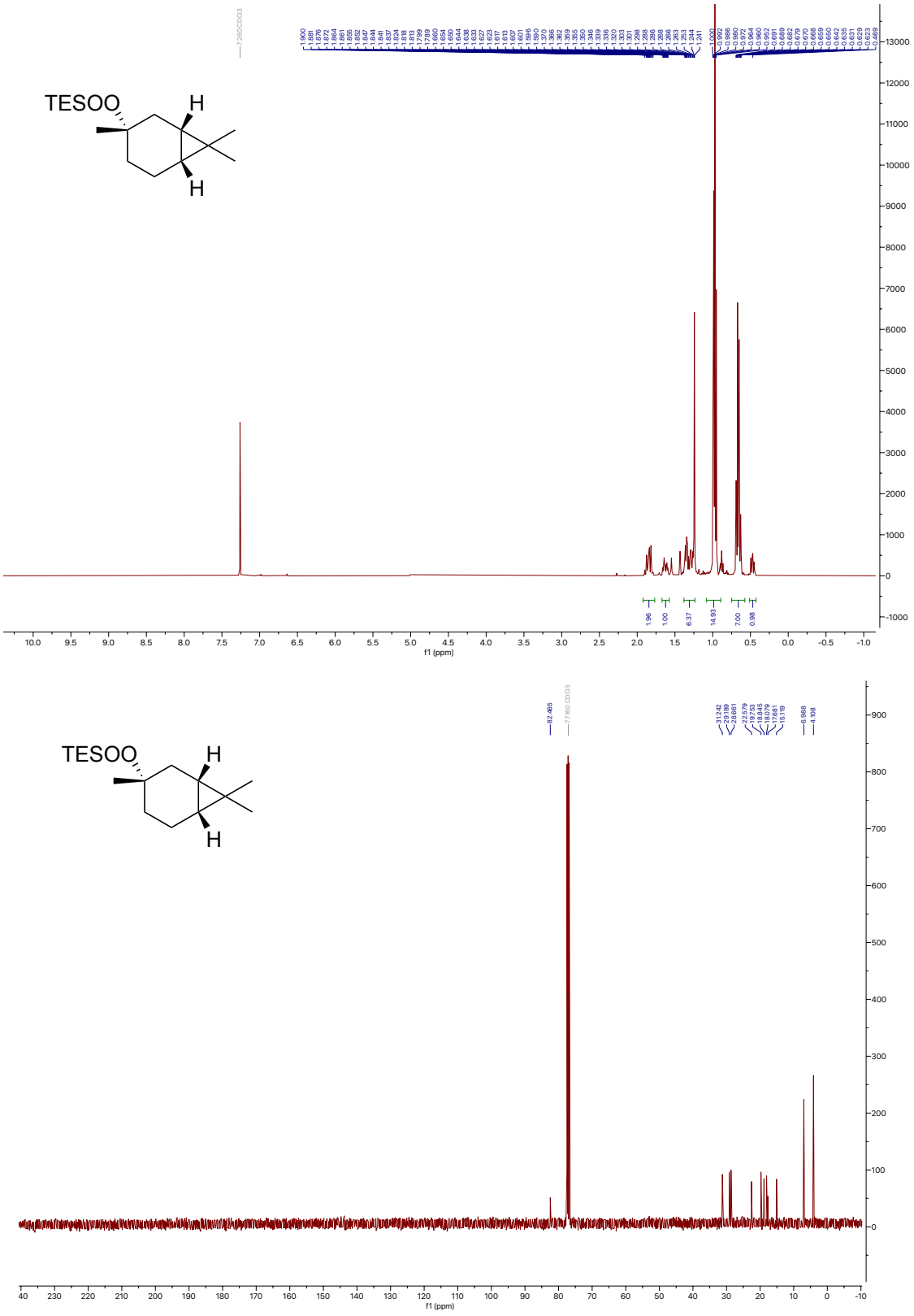




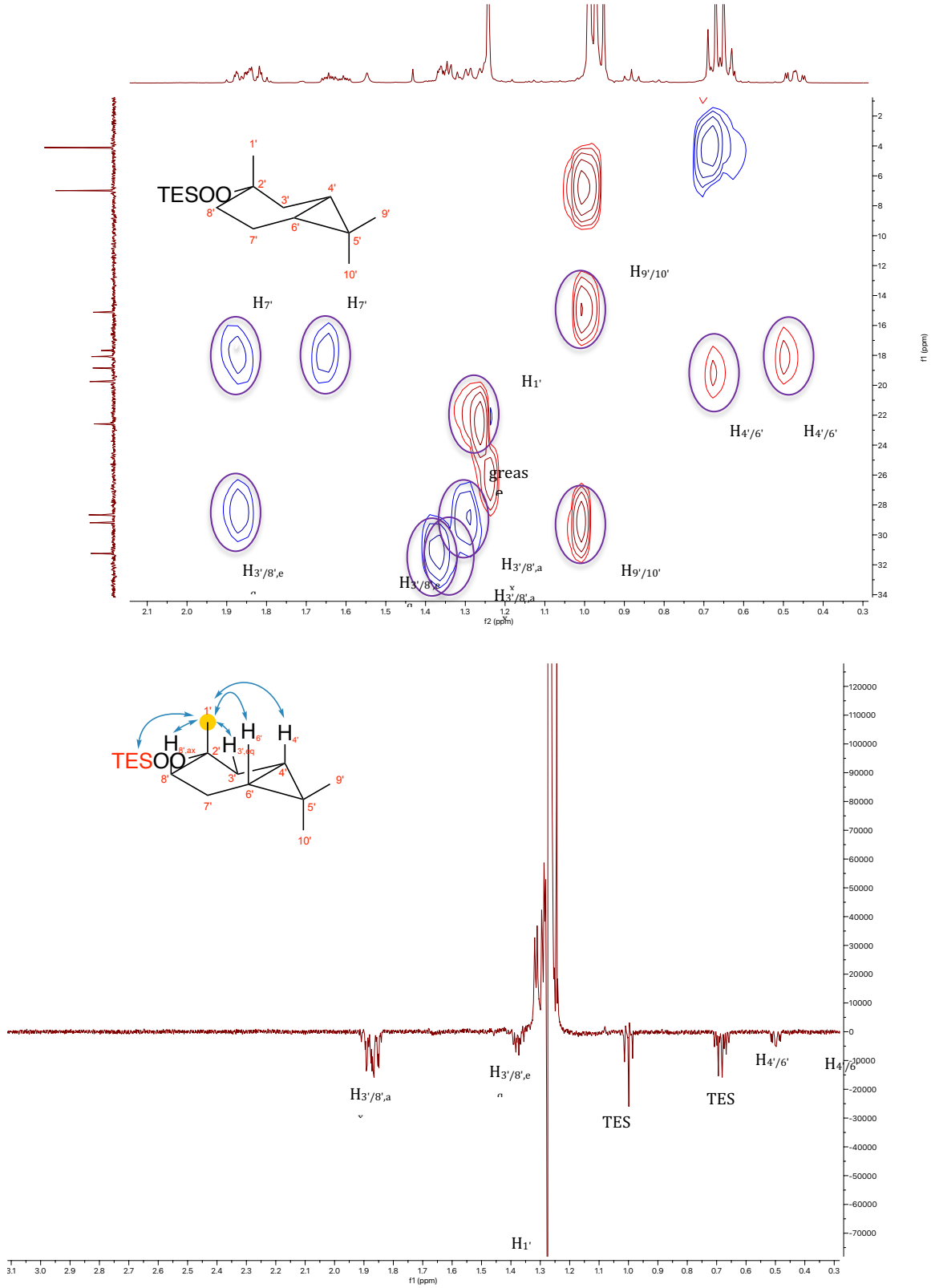
^{1}H NMR (300 MHz, $CDCl_3$) and ^{13}C NMR (126 MHz, $CDCl_3$) of ***trans*-31b**



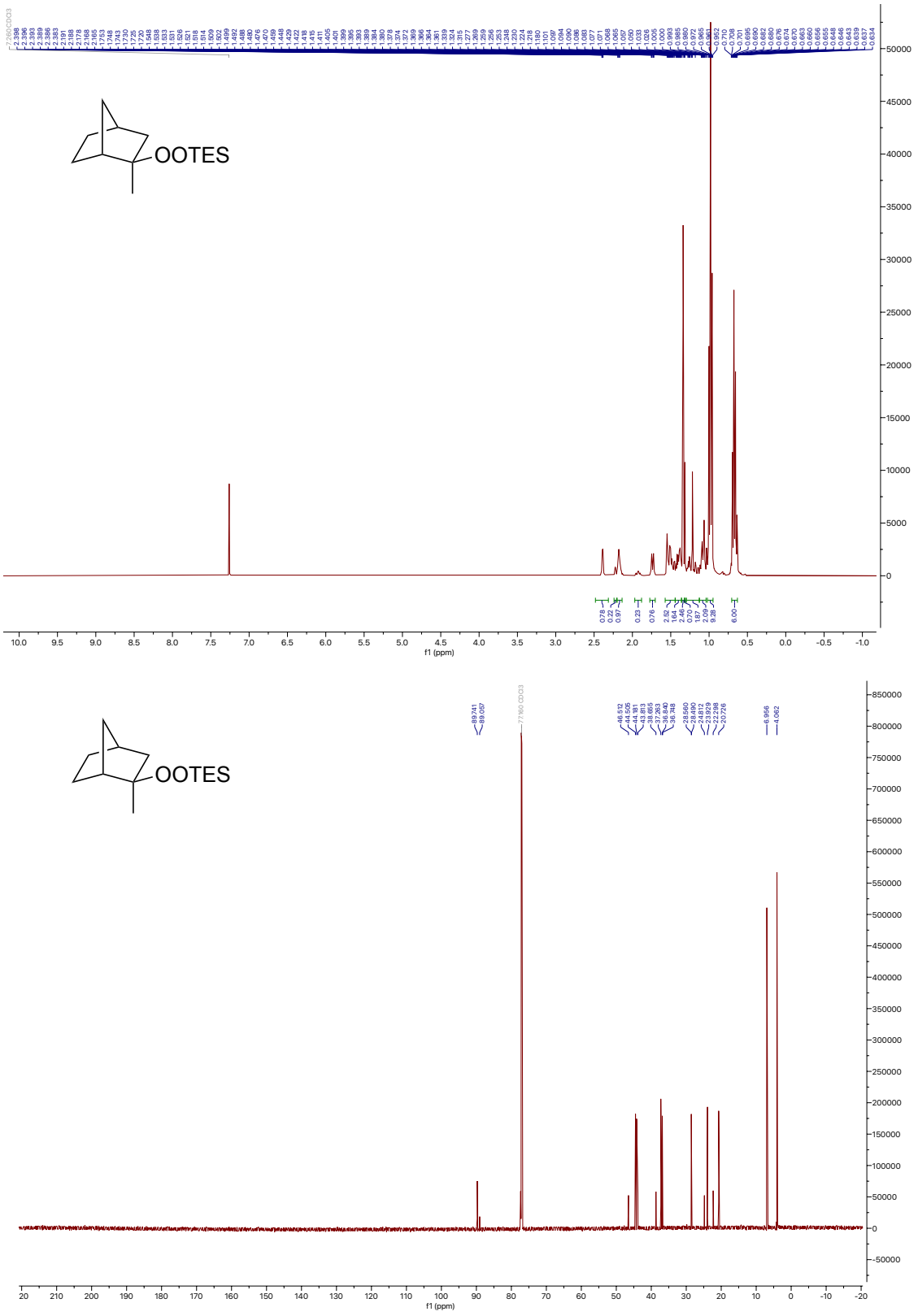
HSQC and 1D Selective Gradient NOESY, frequency 1.159 ppm of ***trans*-31b**



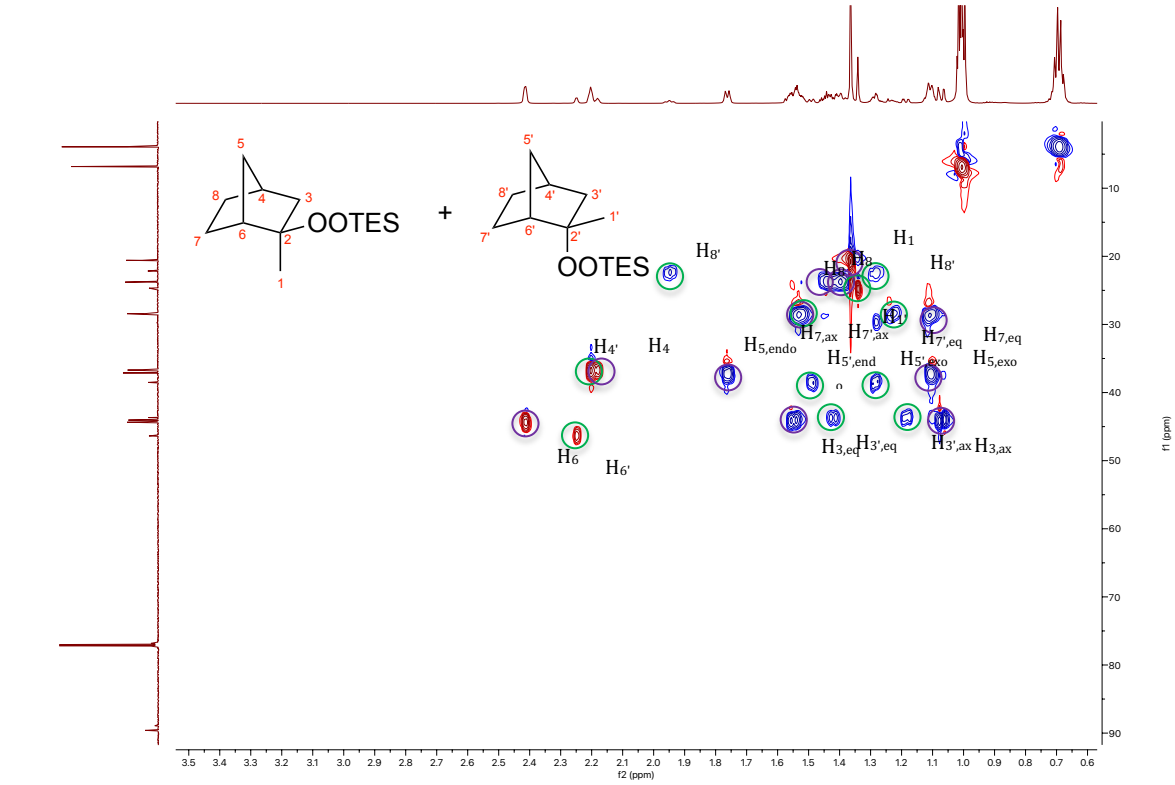
^{1}H NMR (400 MHz, $CDCl_3$) and ^{13}C NMR (101 MHz, $CDCl_3$) of ***cis*-31b**

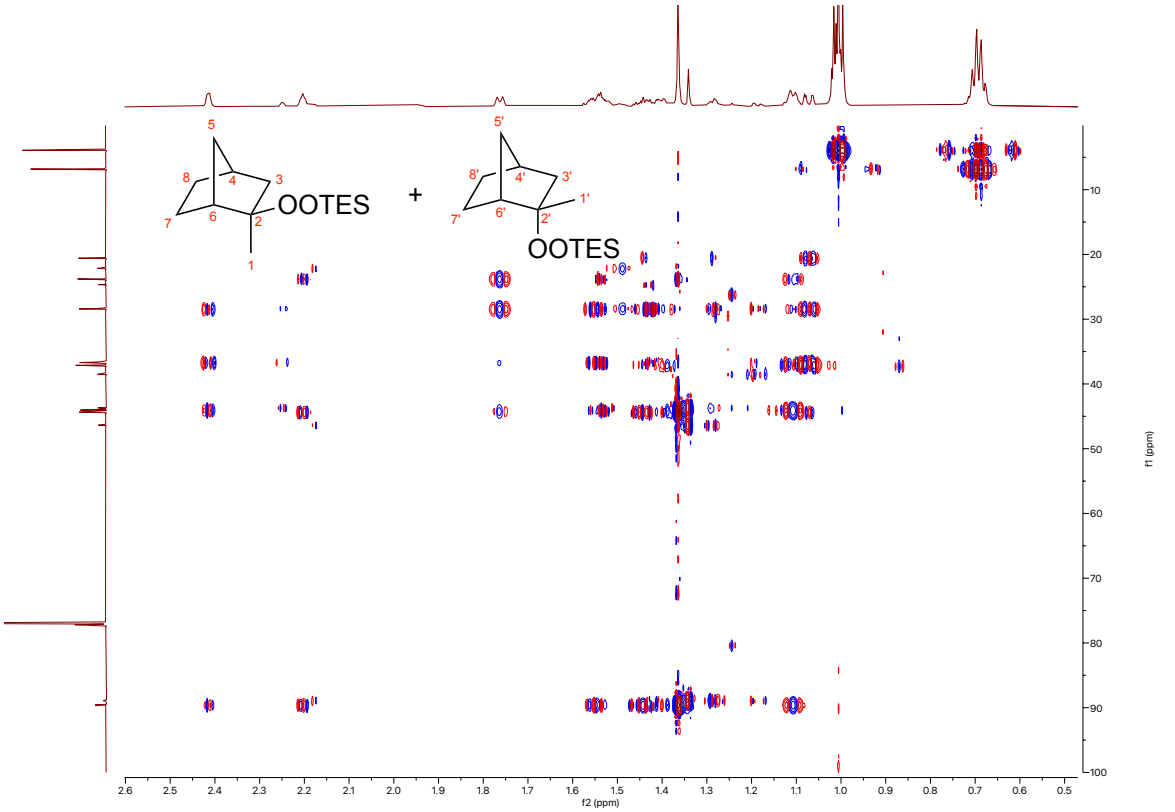


HSQC and 1D Selective Gradient NOESY, frequency 1.244 ppm of ***cis*-31b**

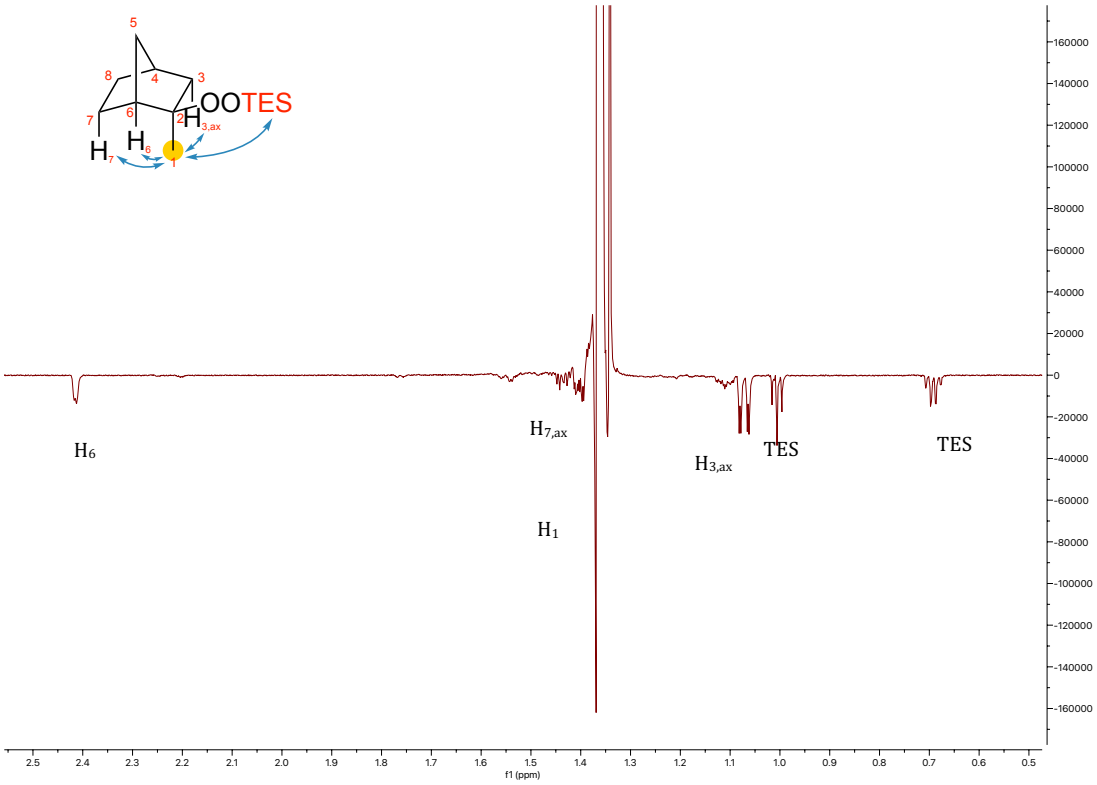


^{1}H NMR (400 MHz, $CDCl_3$) and ^{13}C NMR (101 MHz, $CDCl_3$) of **33b**

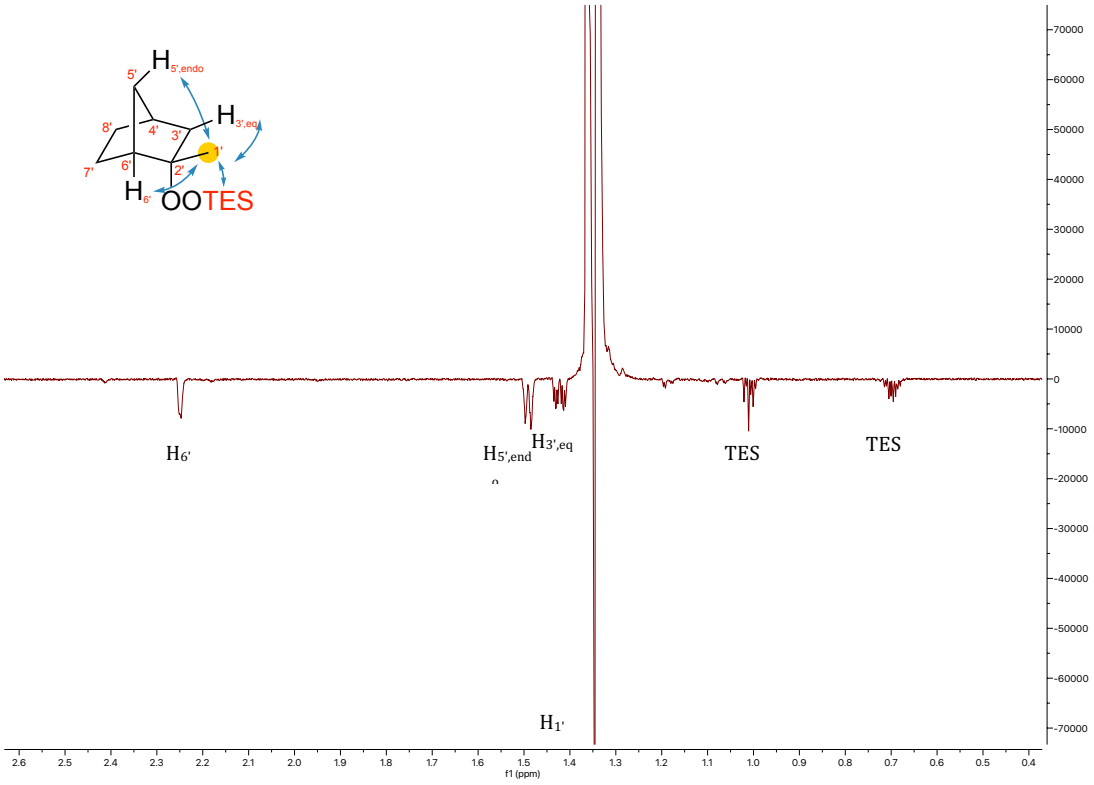




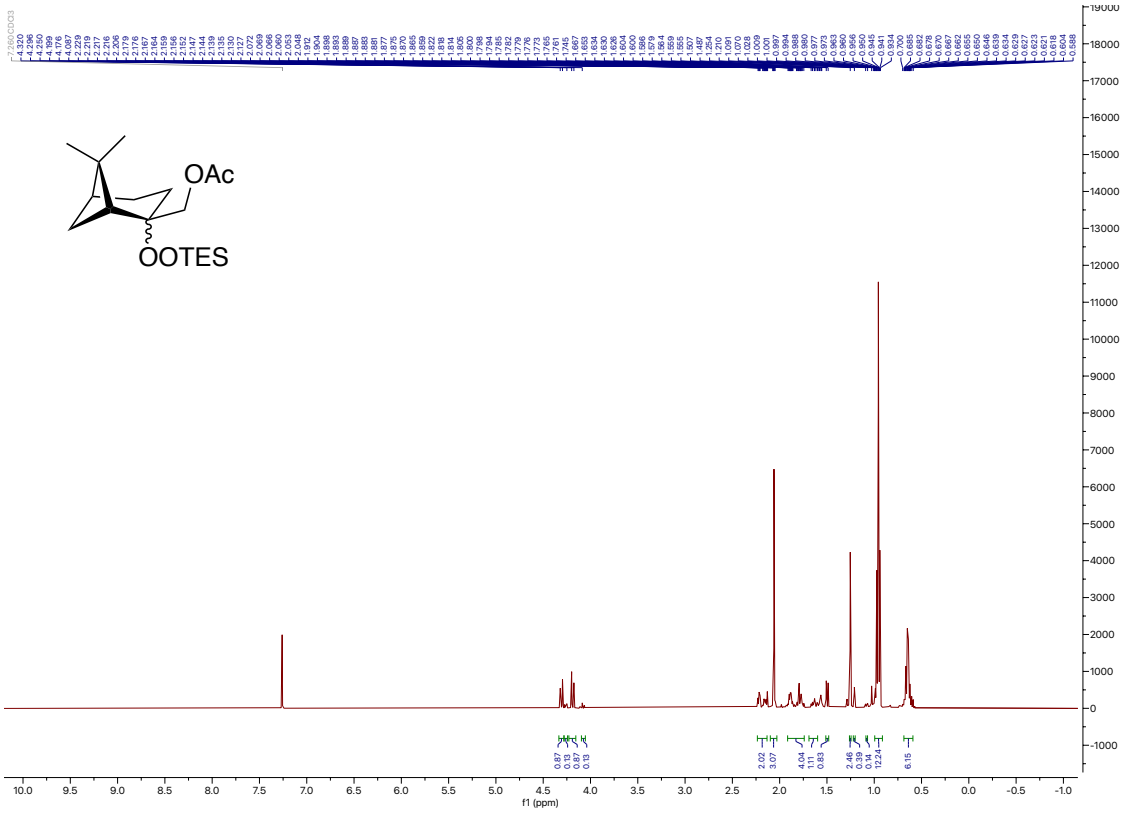
HSQC and HMBC of Compound **33b**

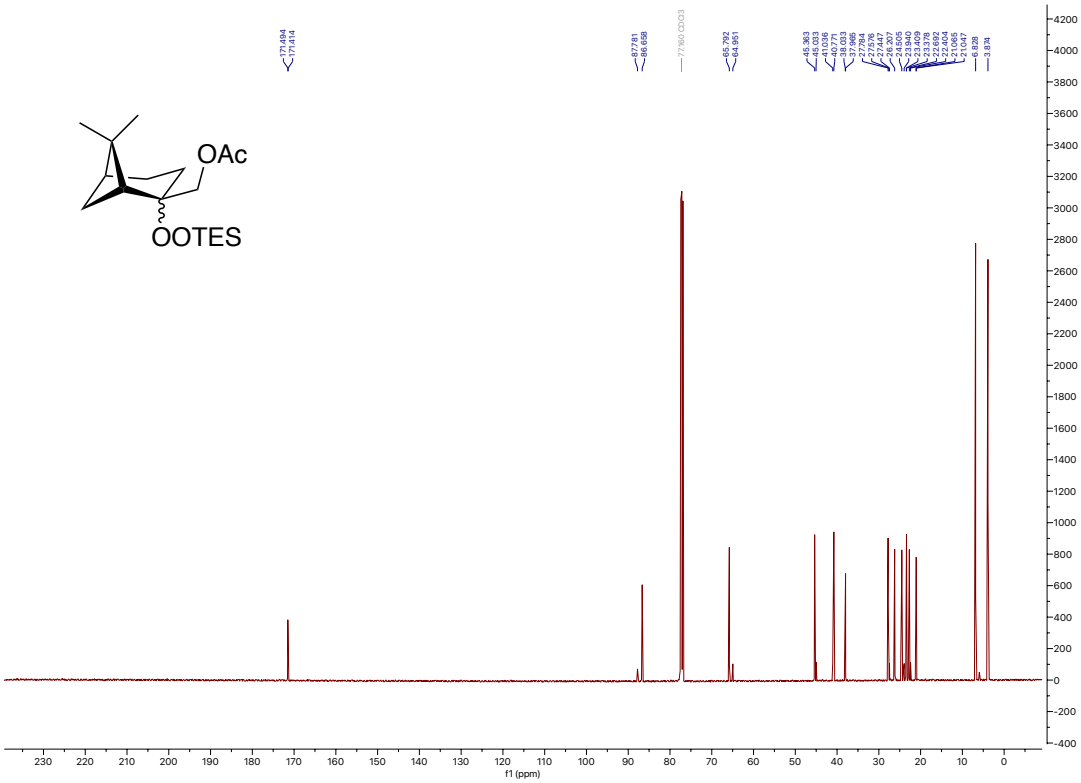


1D Selective Gradient NOESY, frequency 1.359 ppm of **33b**

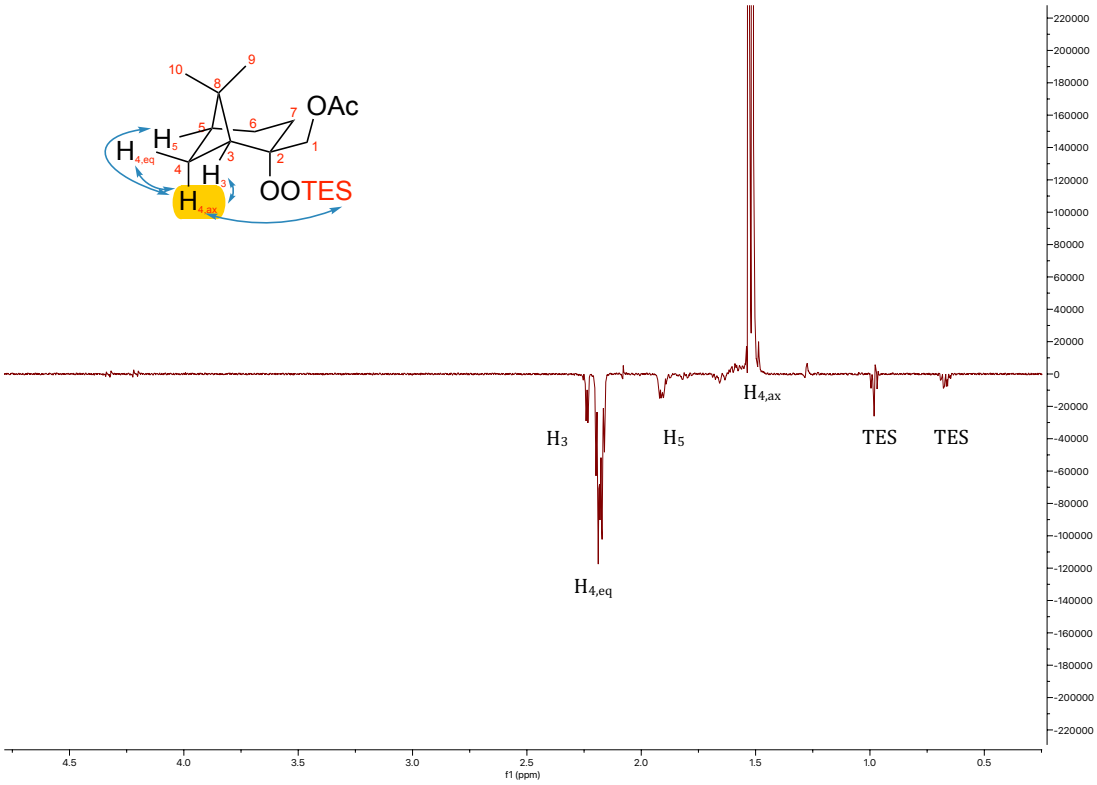


1D Selective Gradient NOESY, frequency 1.340 ppm of **33b**

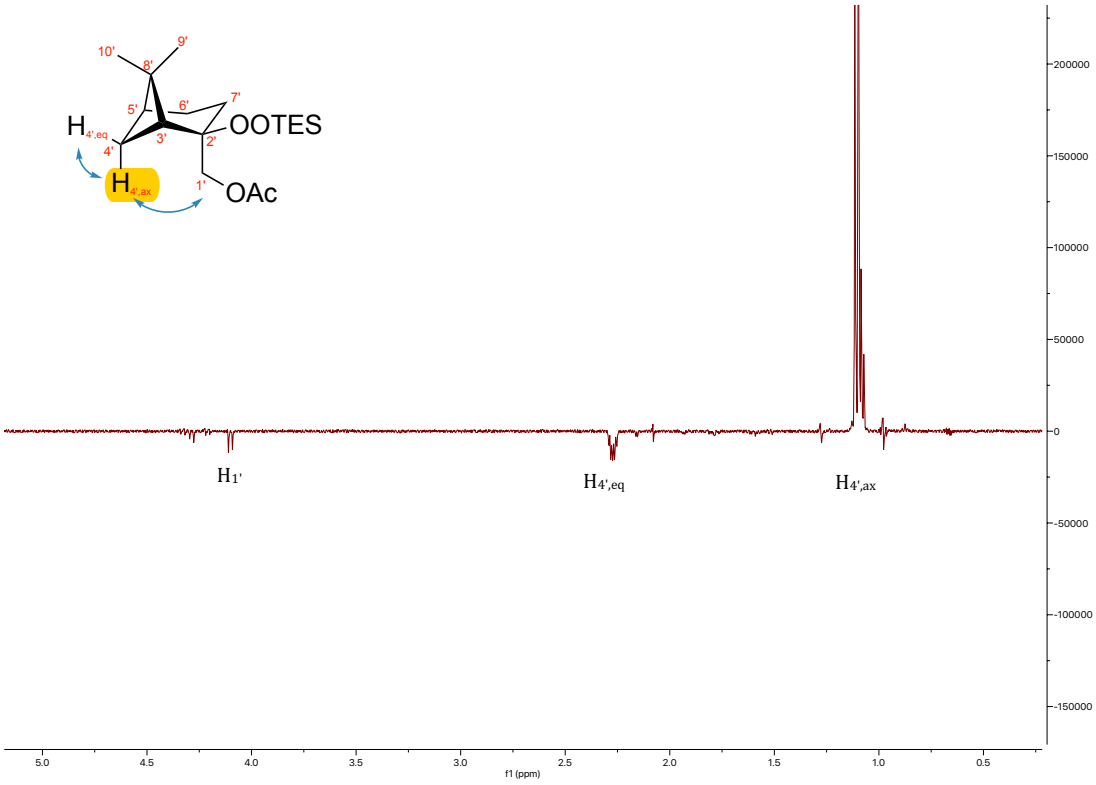




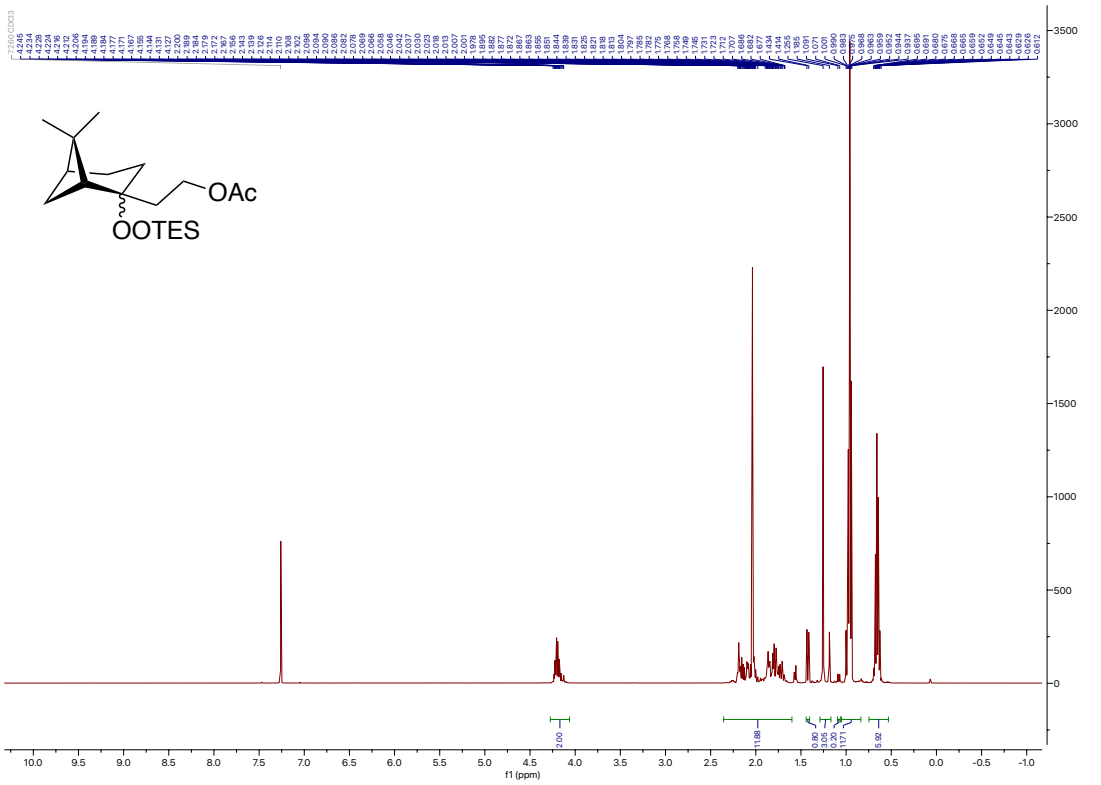
^{1}H NMR (500 MHz, $CDCl_3$) and ^{13}C NMR (126 MHz, $CDCl_3$) of **35b**

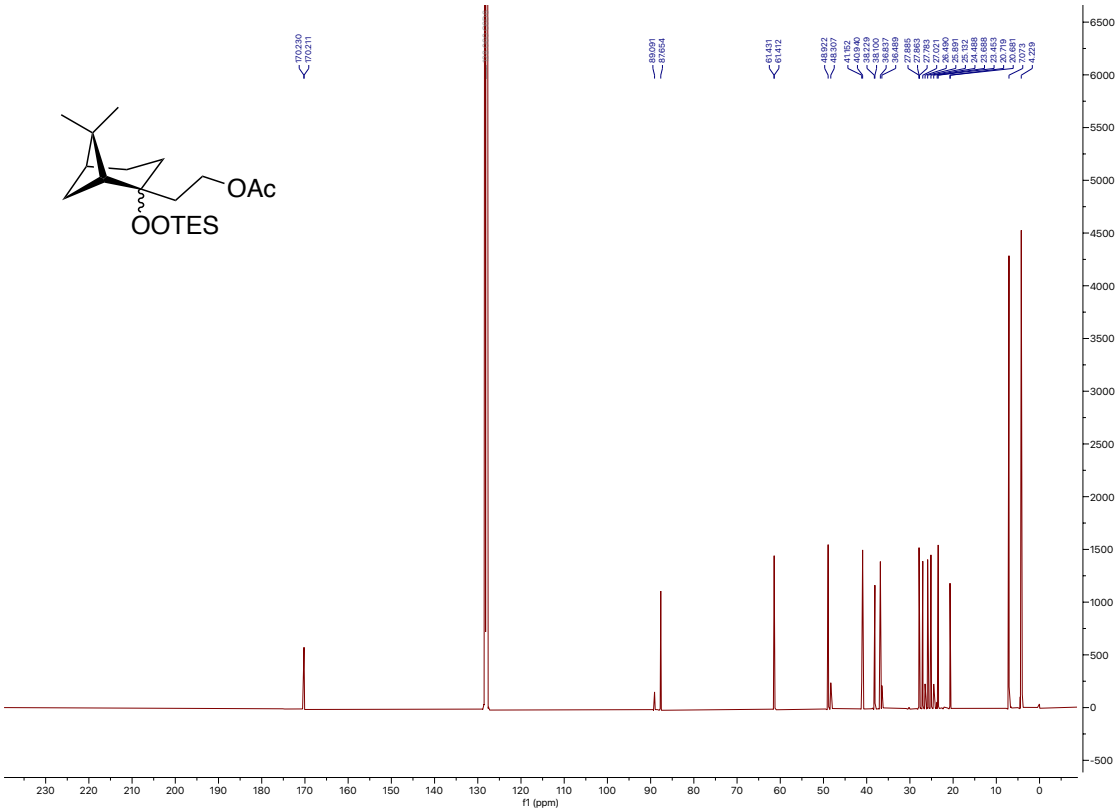


1D Selective Gradient NOESY, frequency 1.520 ppm of ***endo*-36b**

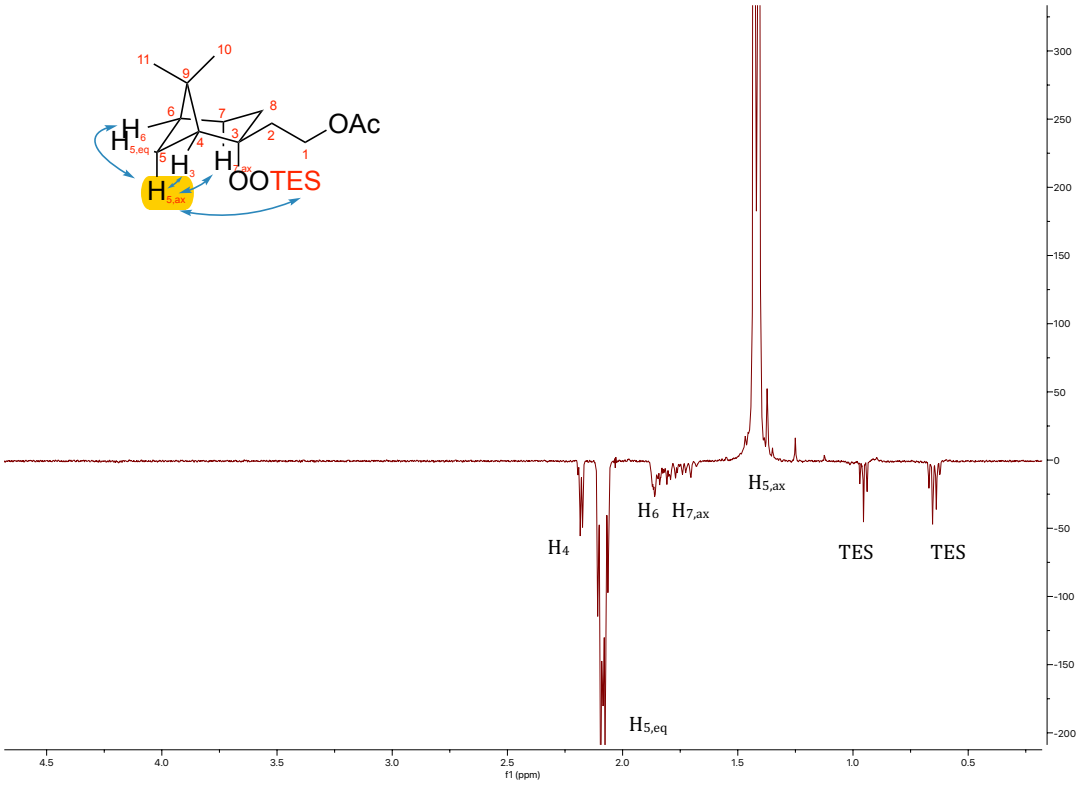


1D Selective Gradient NOESY, frequency 1.107 ppm of ***endo*-35b**

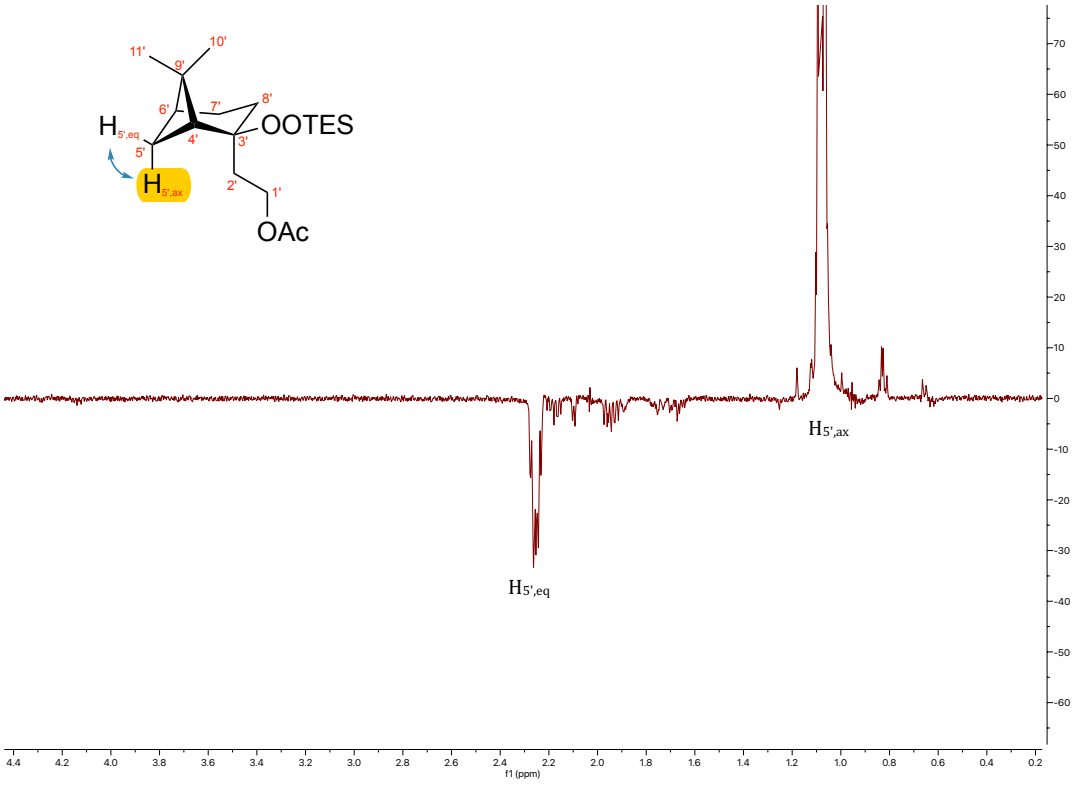




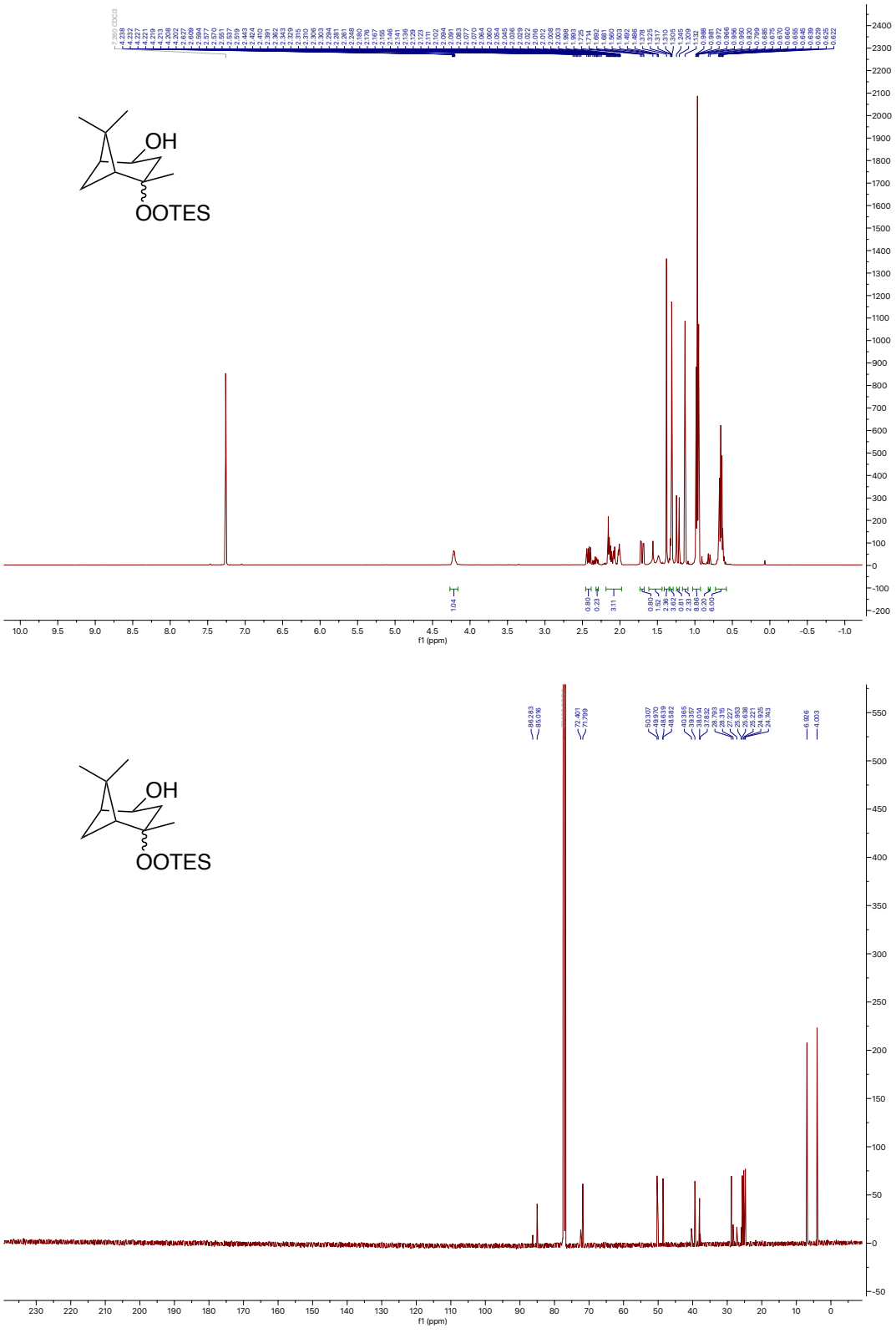
^{1}H NMR (500 MHz, $CDCl_3$) and ^{13}C NMR (126 MHz, C_6D_6) of **36b**



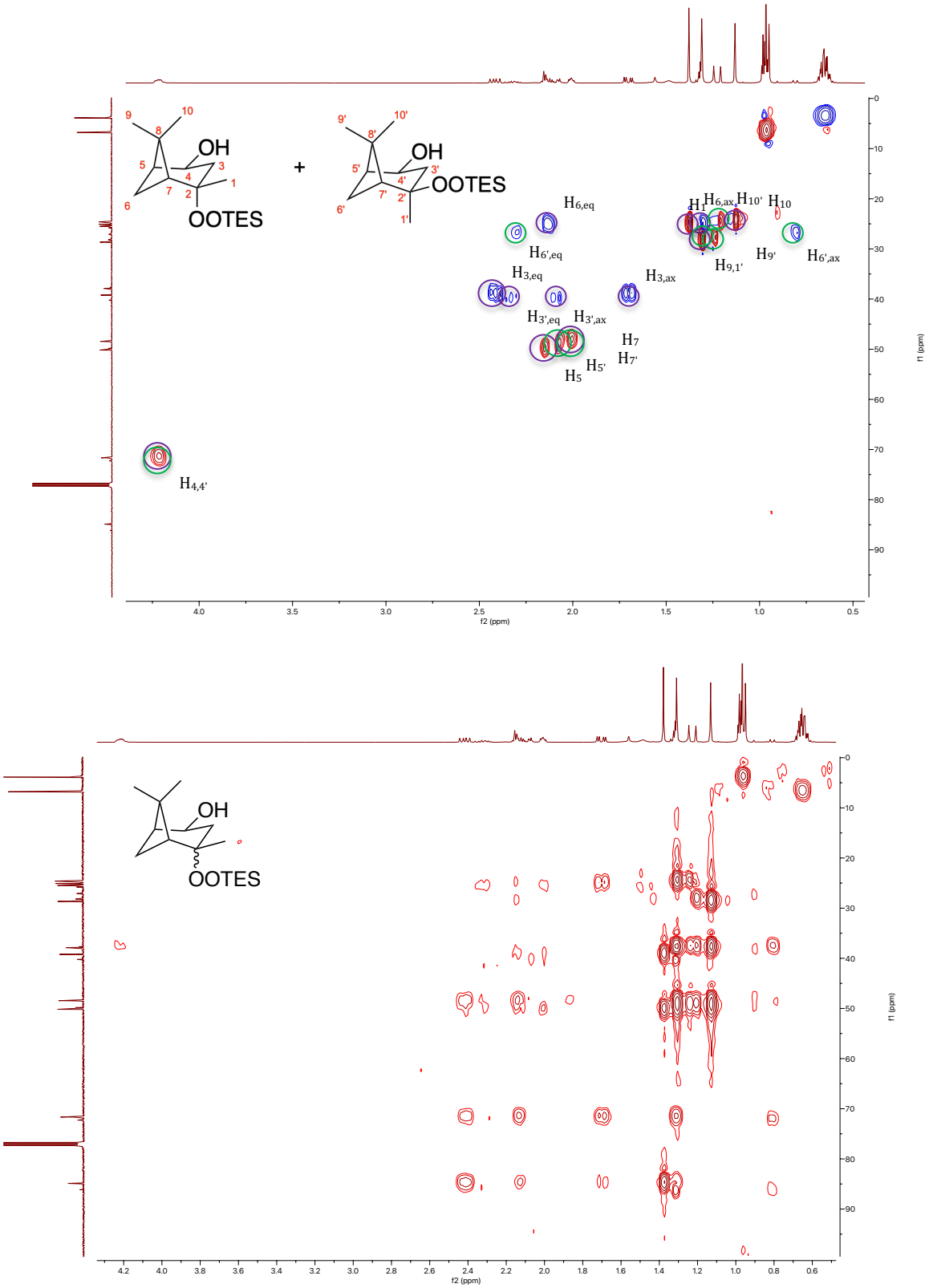
1D Selective Gradient NOESY, frequency 1.451 ppm of ***exo*-36b**



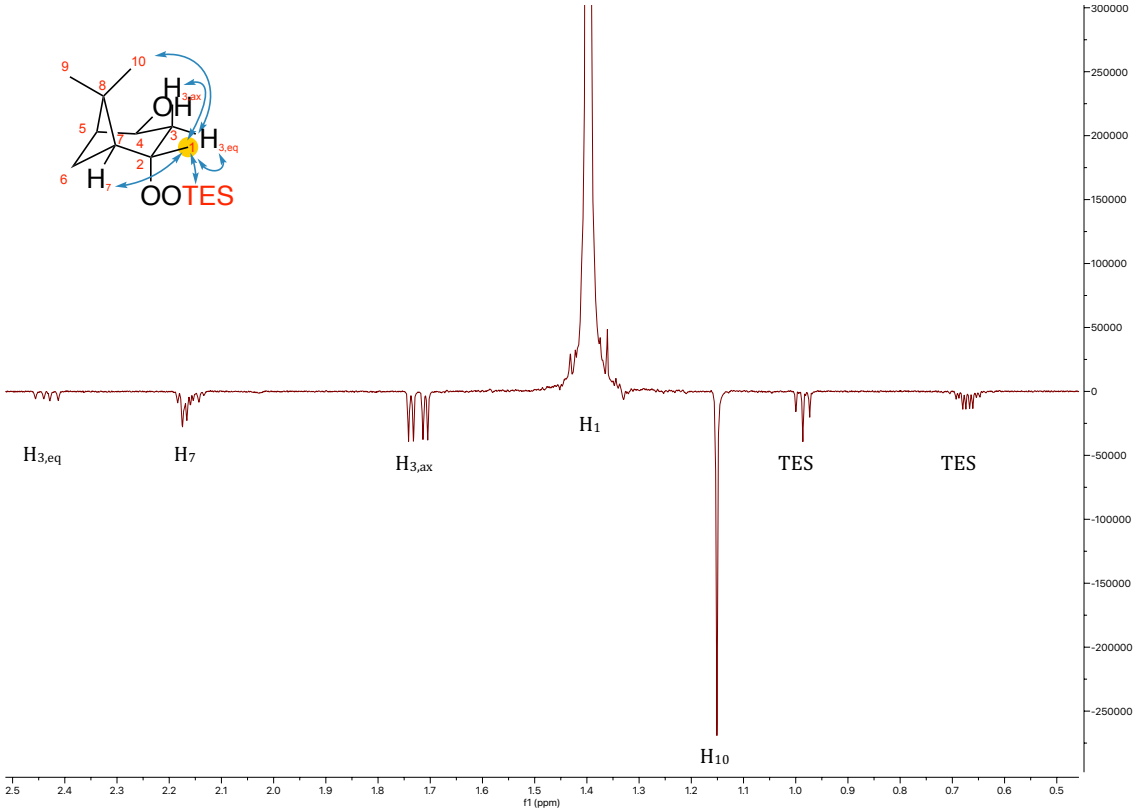
1D Selective Gradient NOESY, frequency 1.103 ppm of ***endo*-36b**



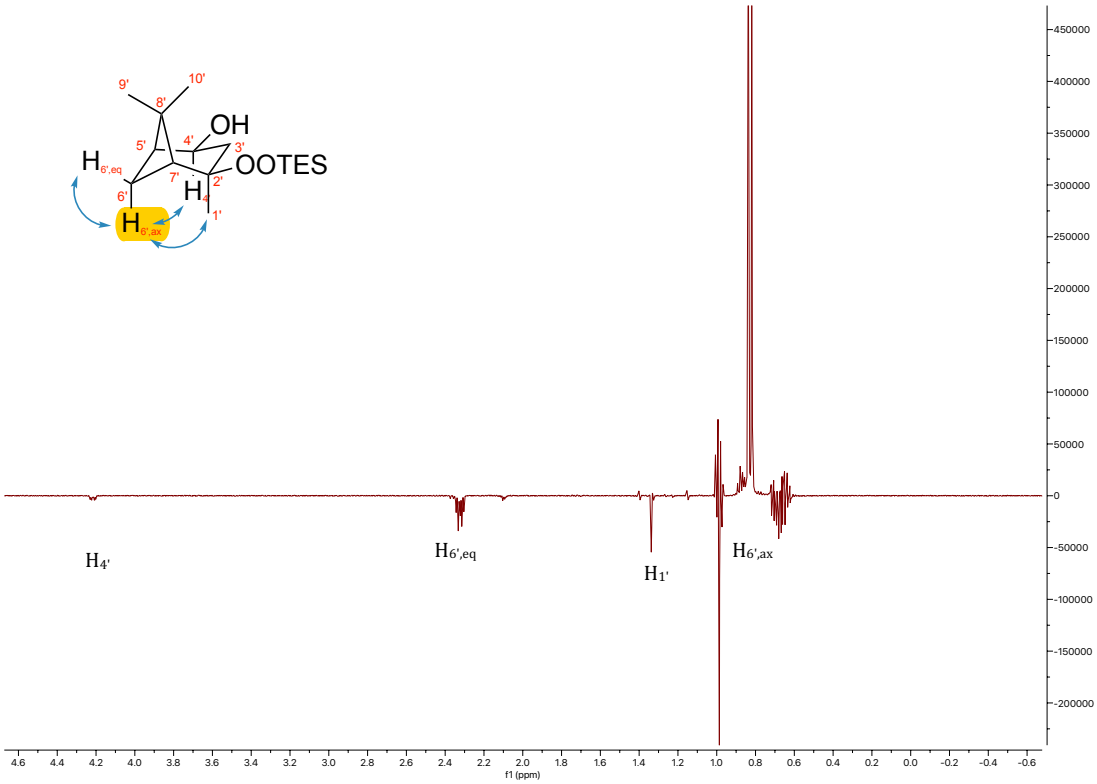
^{1}H NMR (400 MHz, $CDCl_3$) and ^{13}C NMR (101 MHz, $CDCl_3$) of **37b**



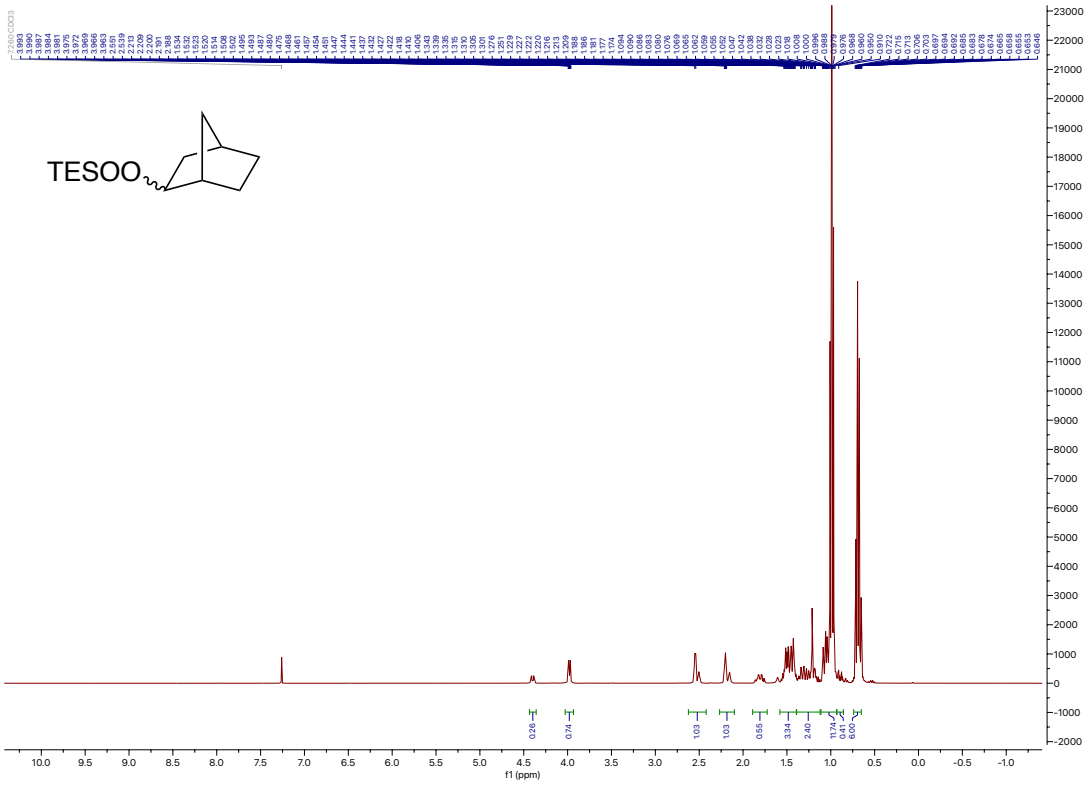
HSQC and HMBC of Compound **37b**

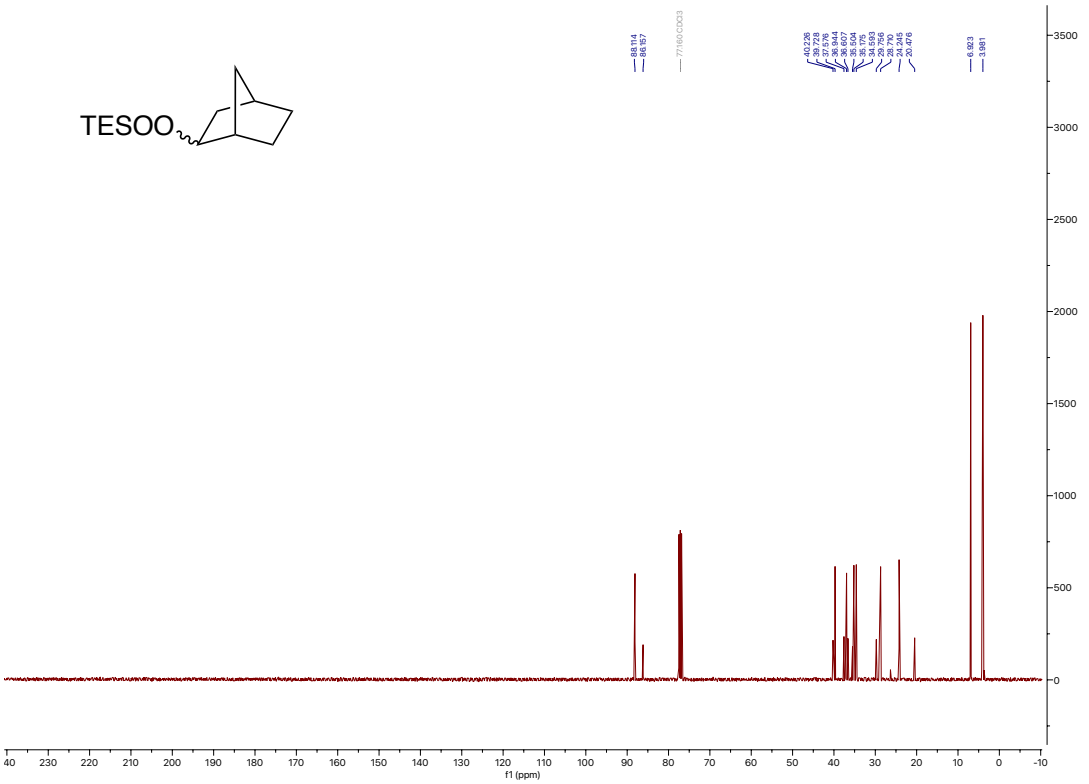


1D Selective Gradient NOESY frequency 1.401 ppm of ***exo*-37b**

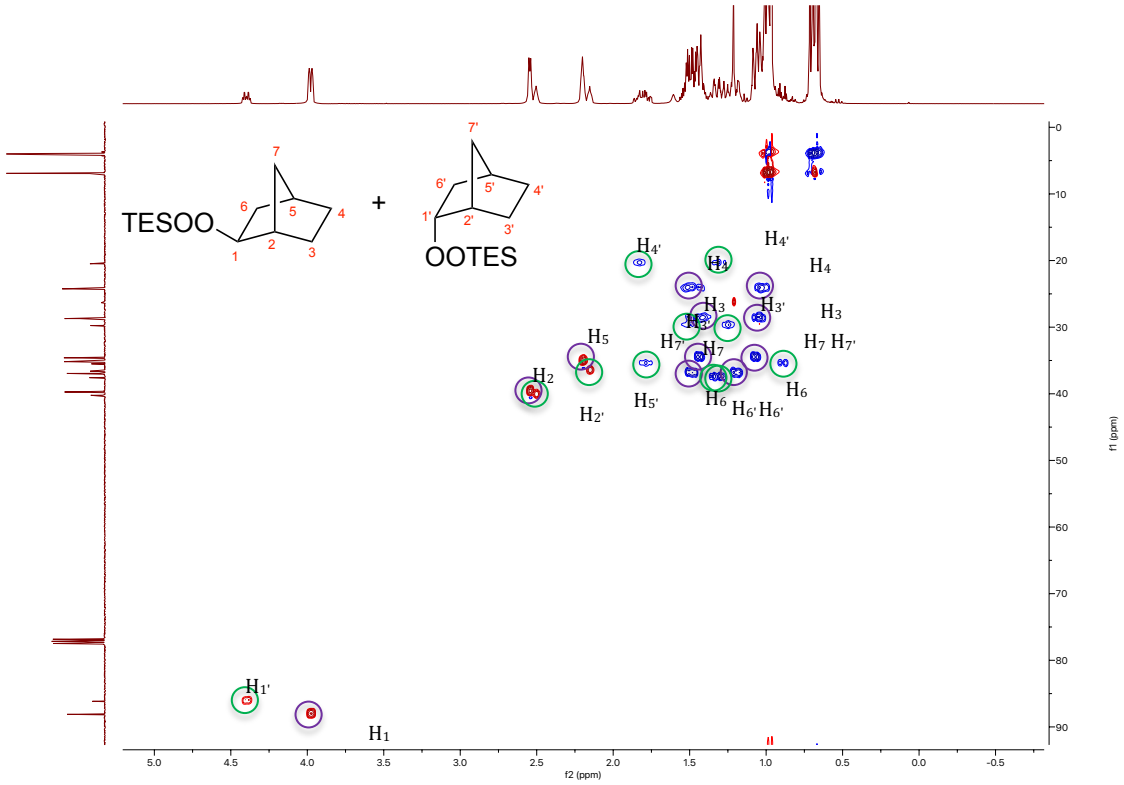


1D Selective Gradient NOESY frequency 1.401 ppm of ***endo*-37b**

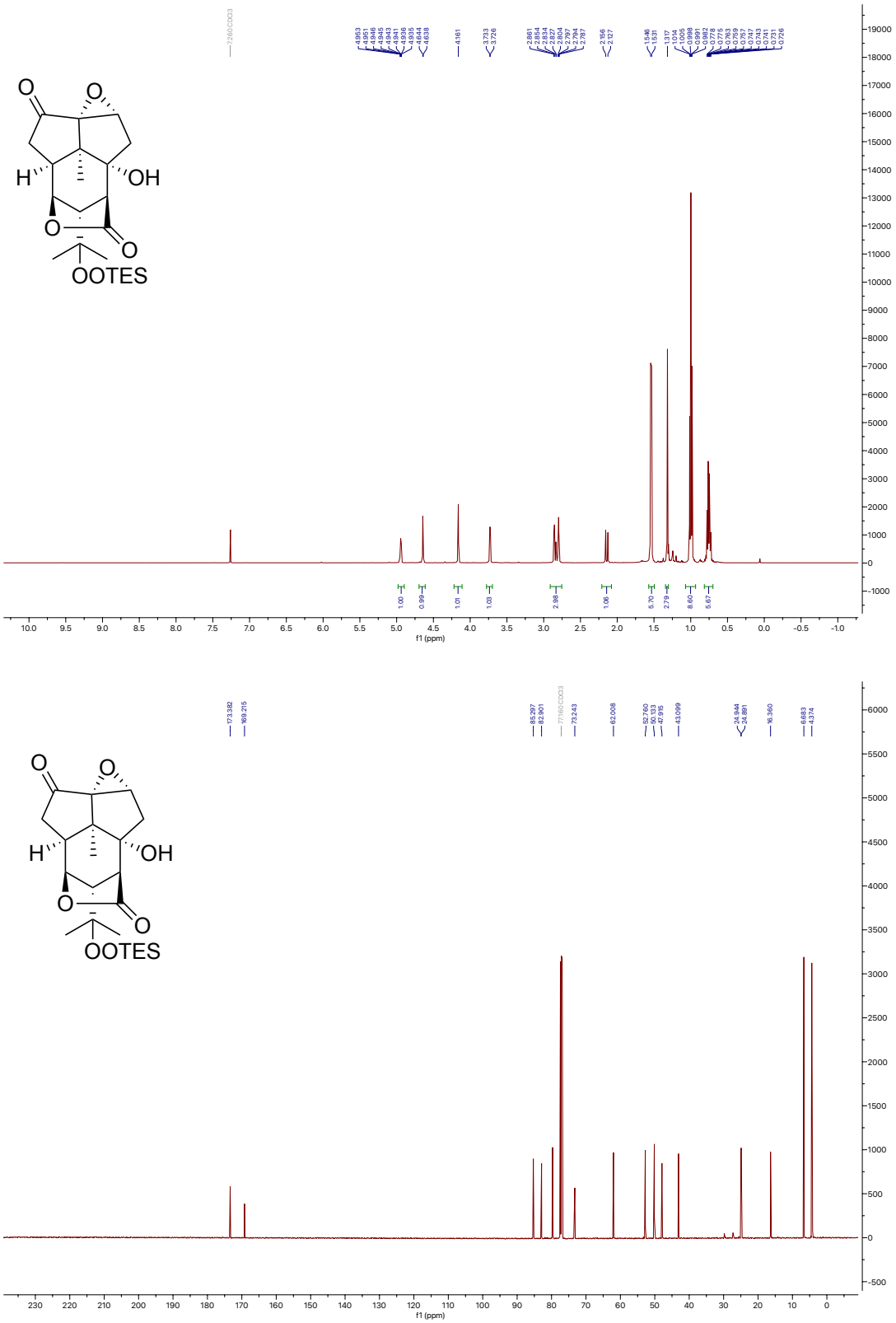




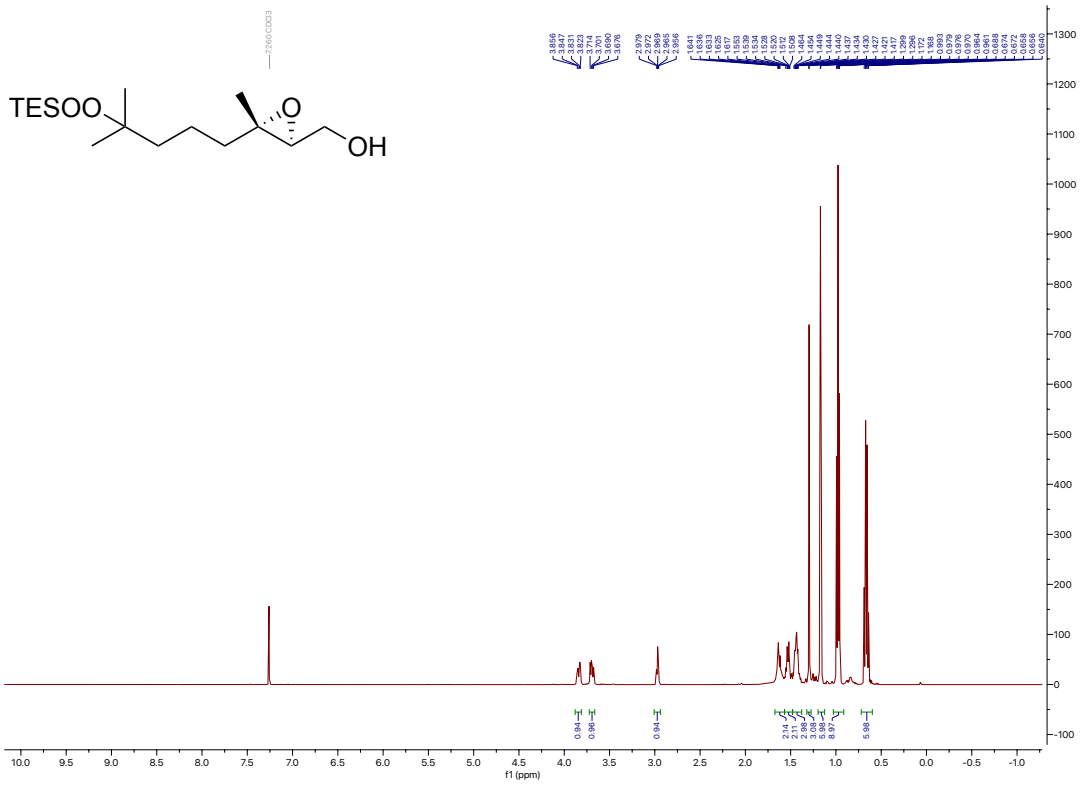
^{1}H NMR (400 MHz, $CDCl_3$) and ^{13}C NMR (101 MHz, $CDCl_3$) of **38b**

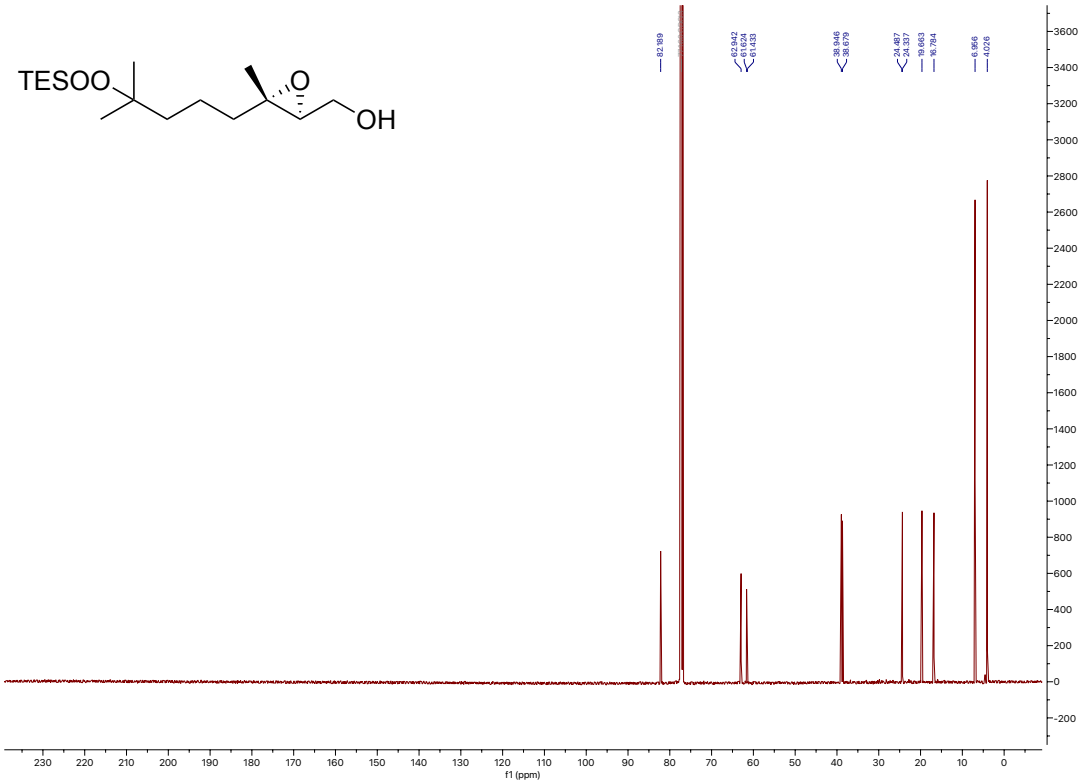


HSQC of **38b**

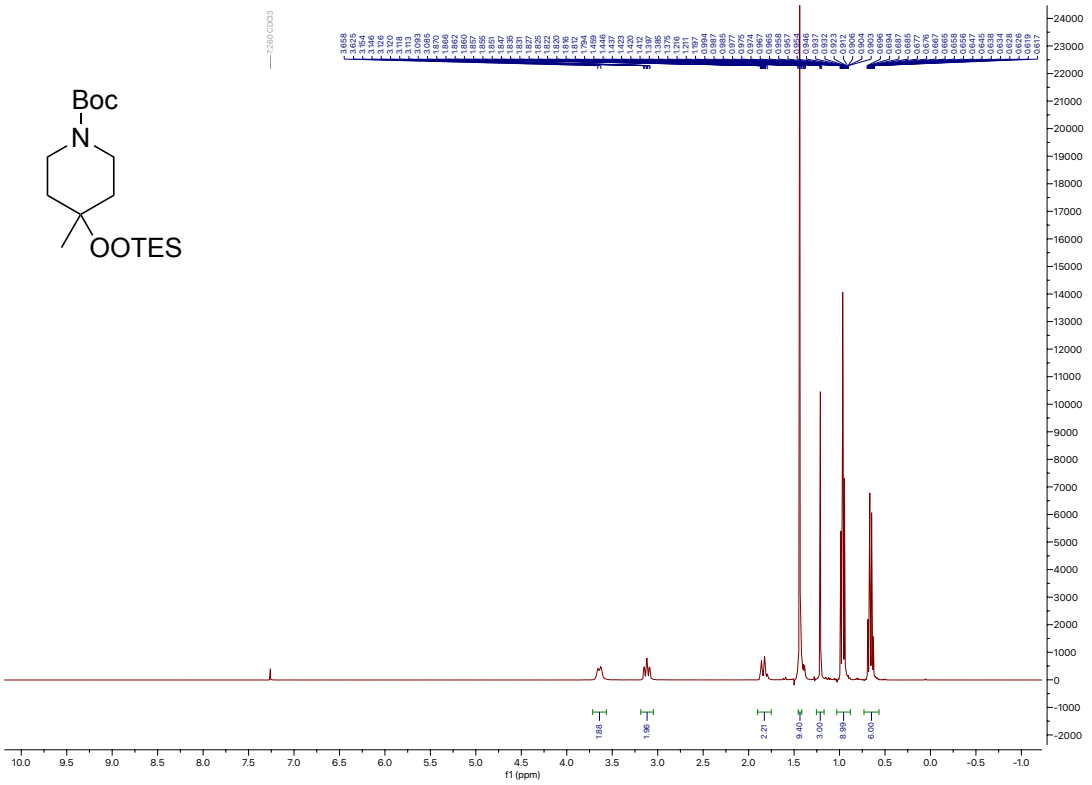


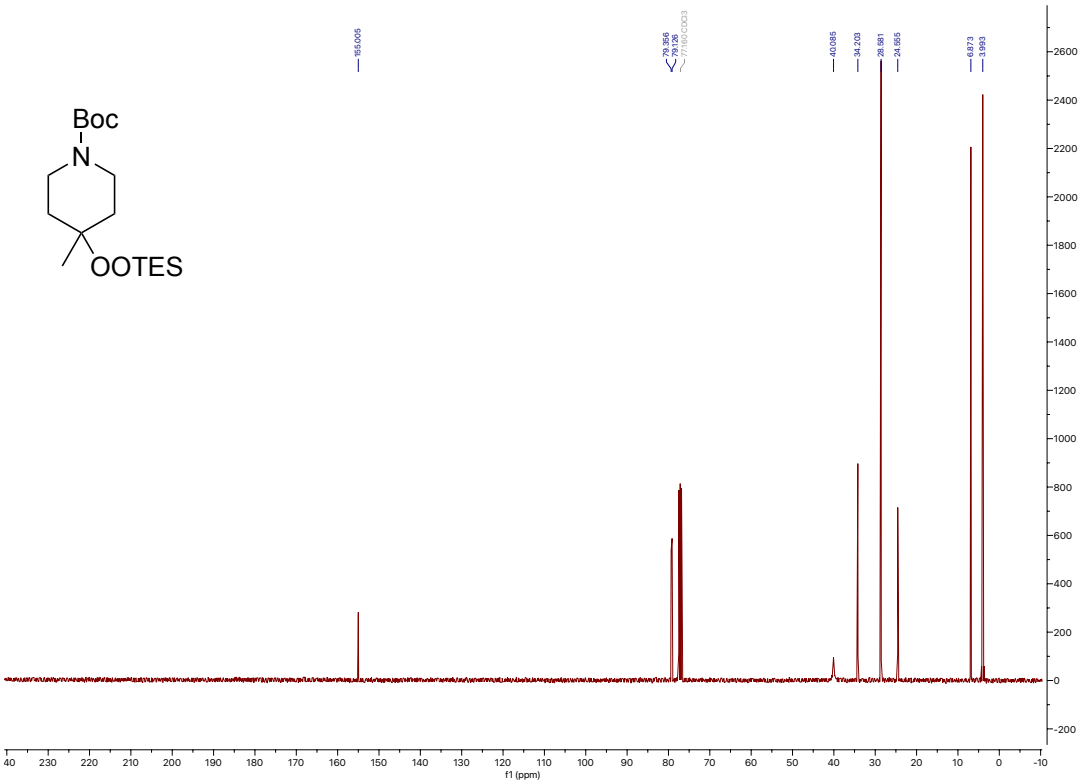
^{1}H NMR (500 MHz, $CDCl_3$) and ^{13}C NMR (126 MHz, $CDCl_3$) of **F7b**



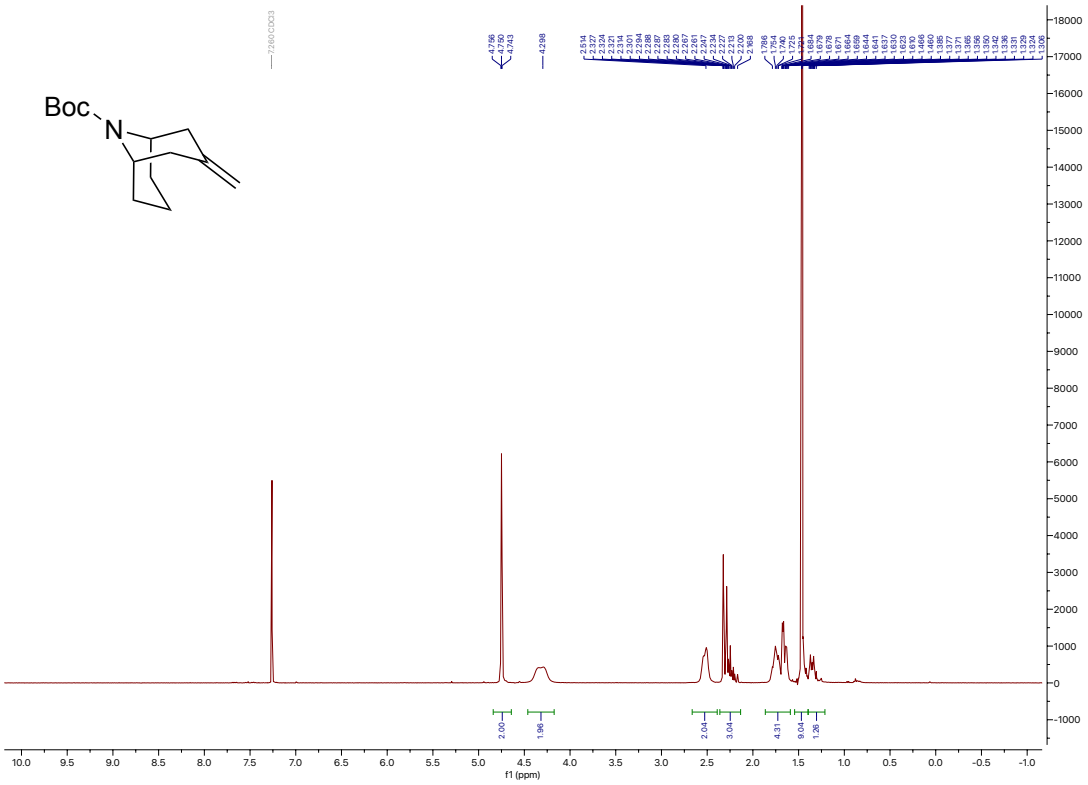


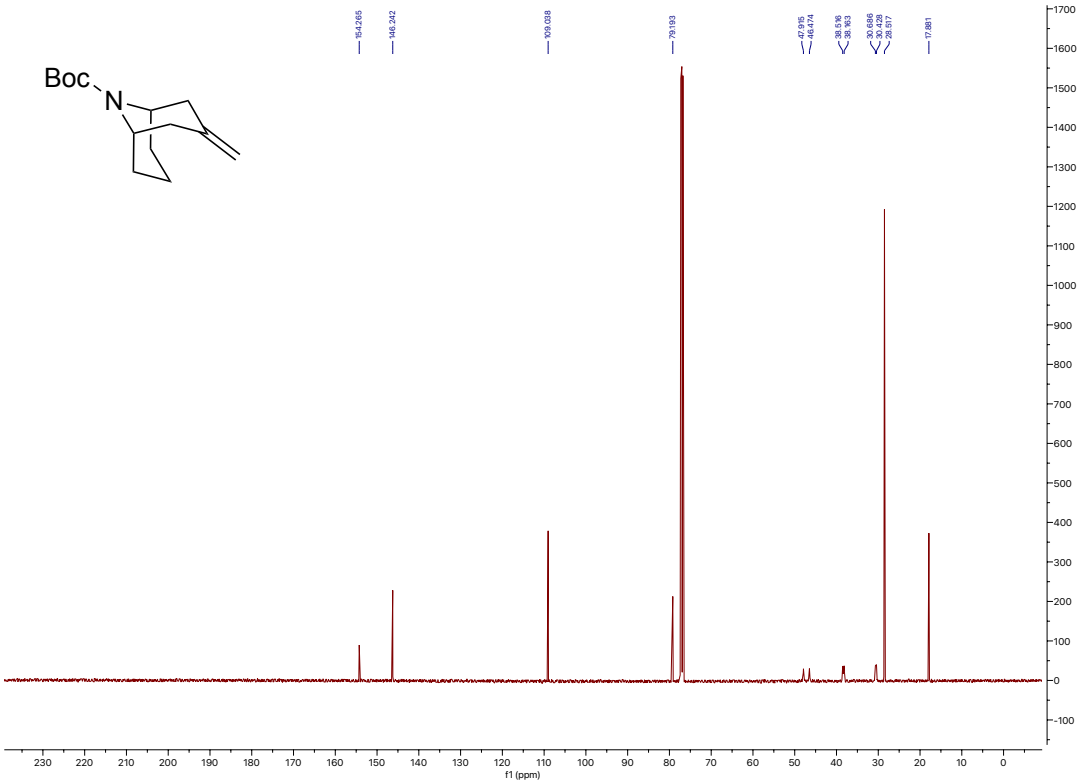
^{1}H NMR (500 MHz, $CDCl_3$) and ^{13}C NMR (126 MHz, $CDCl_3$) of Compound **F8b**



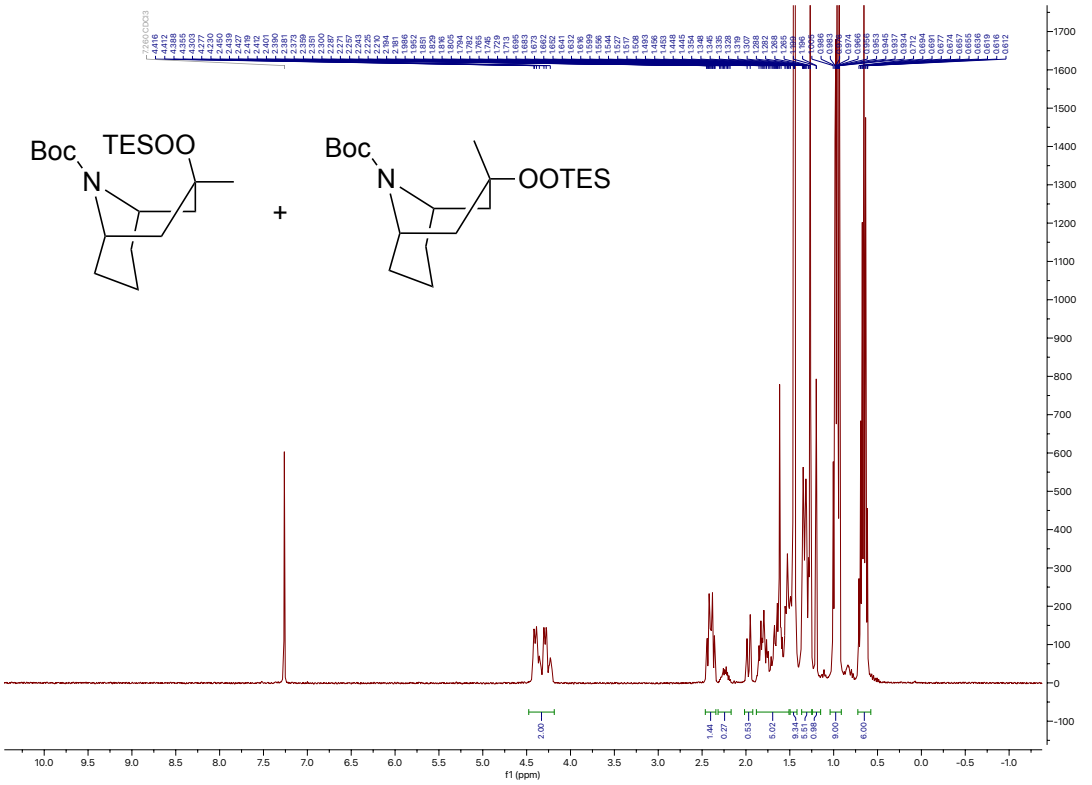


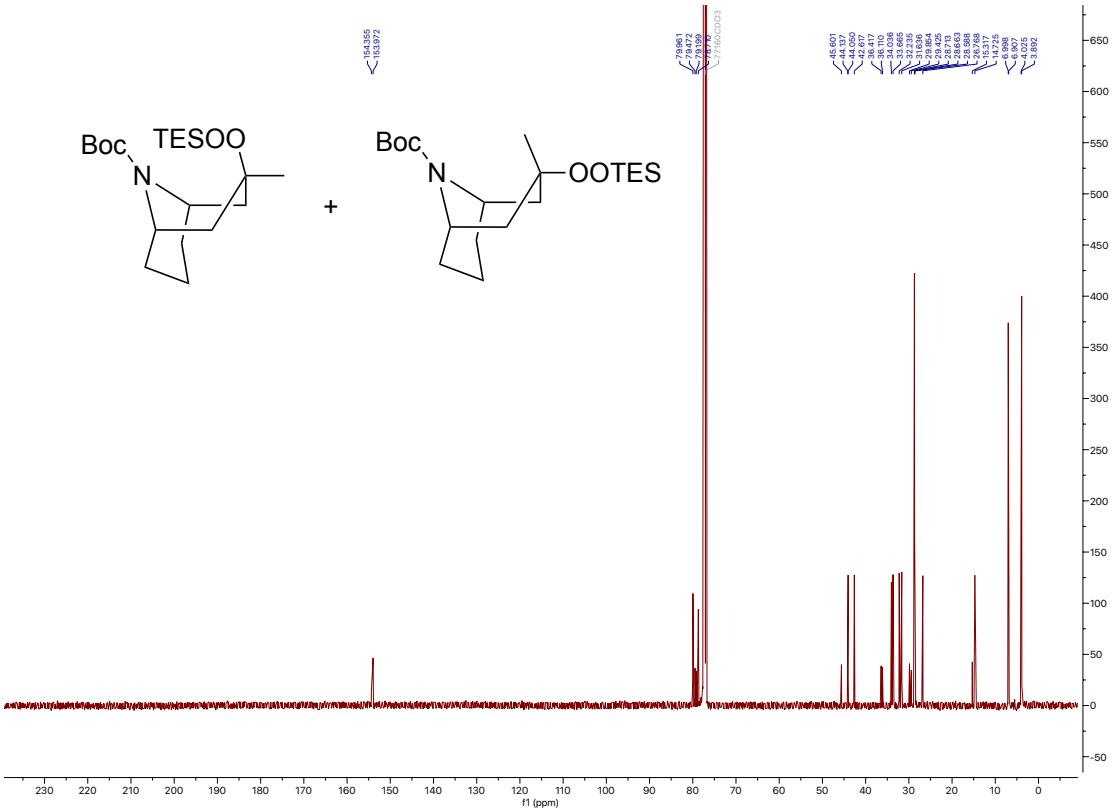
^{1}H NMR (400 MHz, $CDCl_3$) and ^{13}C NMR (101 MHz, $CDCl_3$) of **F9b**



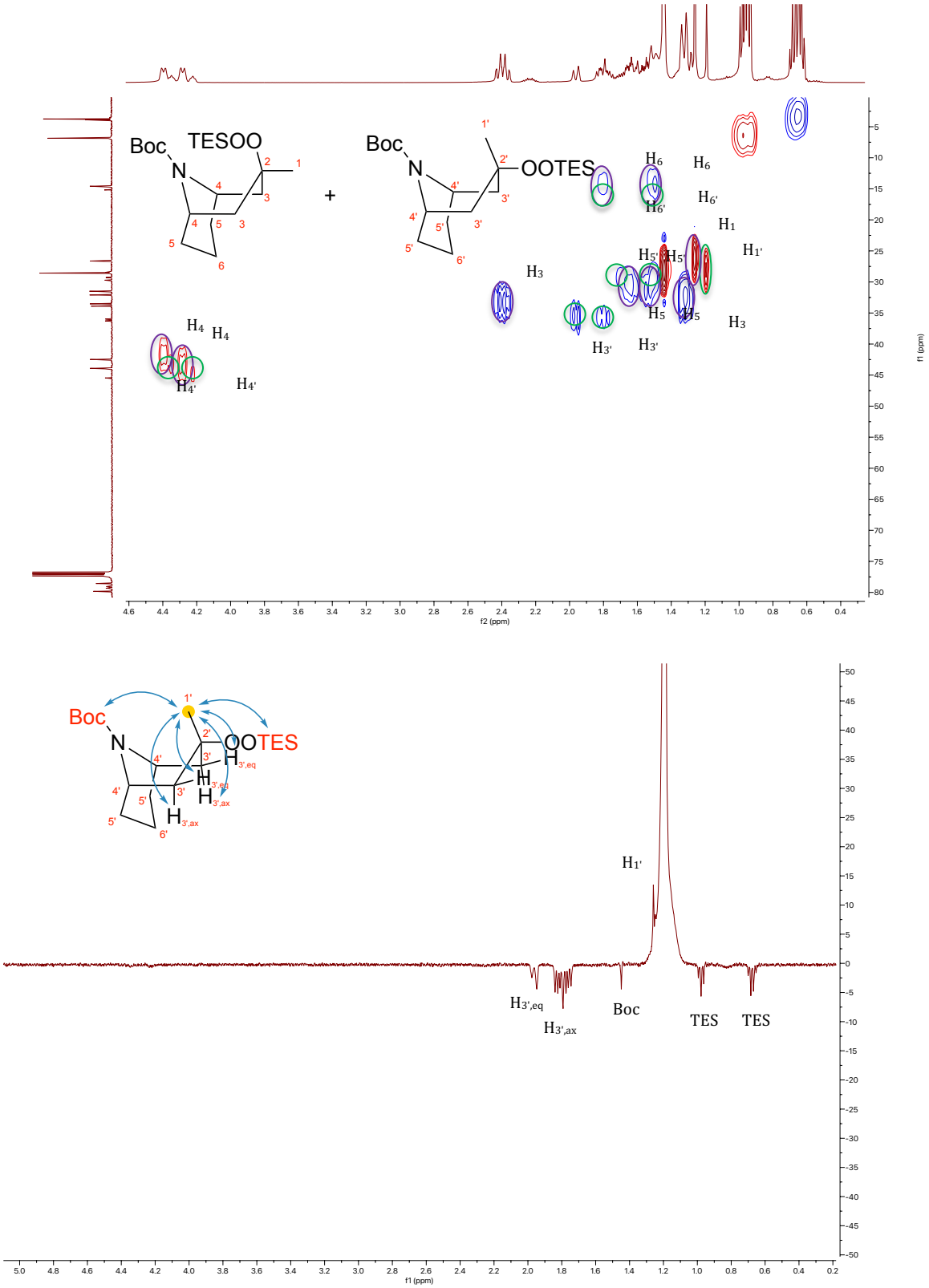


^{1}H NMR (400 MHz, $CDCl_3$) and ^{13}C NMR (126 MHz, $CDCl_3$) of Compound **F10a**

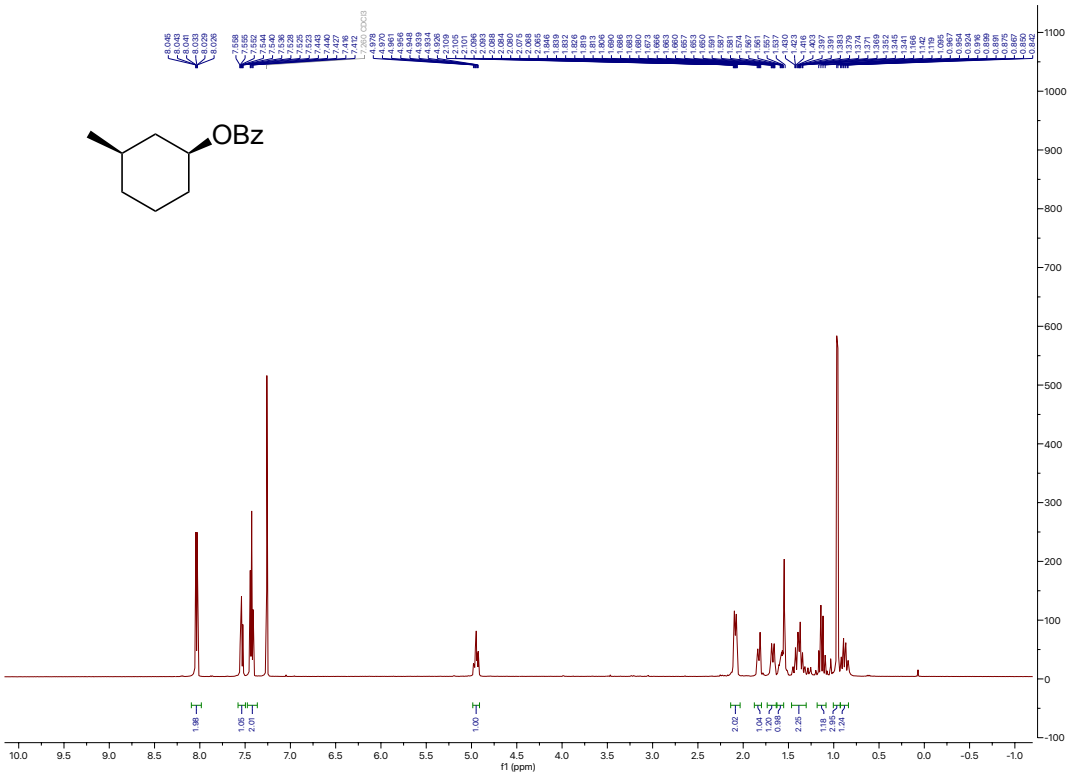


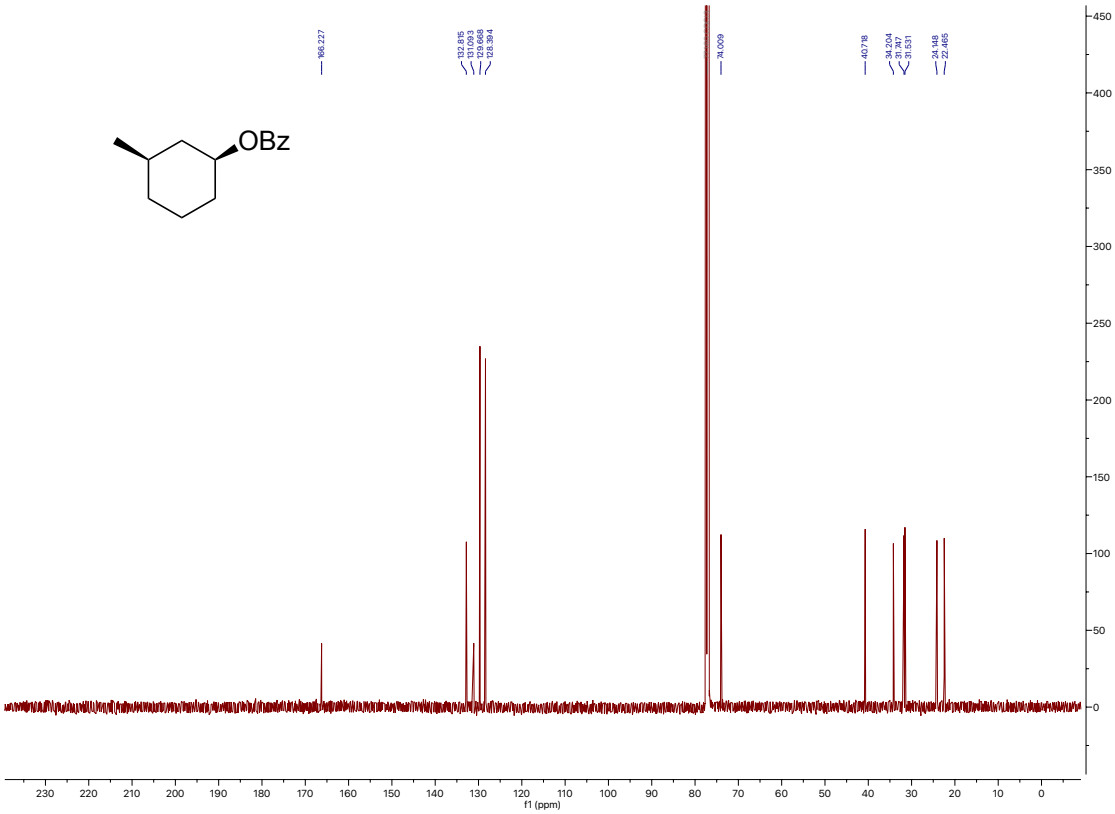


^{1}H NMR (400 MHz, $CDCl_3$) and ^{13}C NMR (126 MHz, $CDCl_3$) of Compound **F10b**

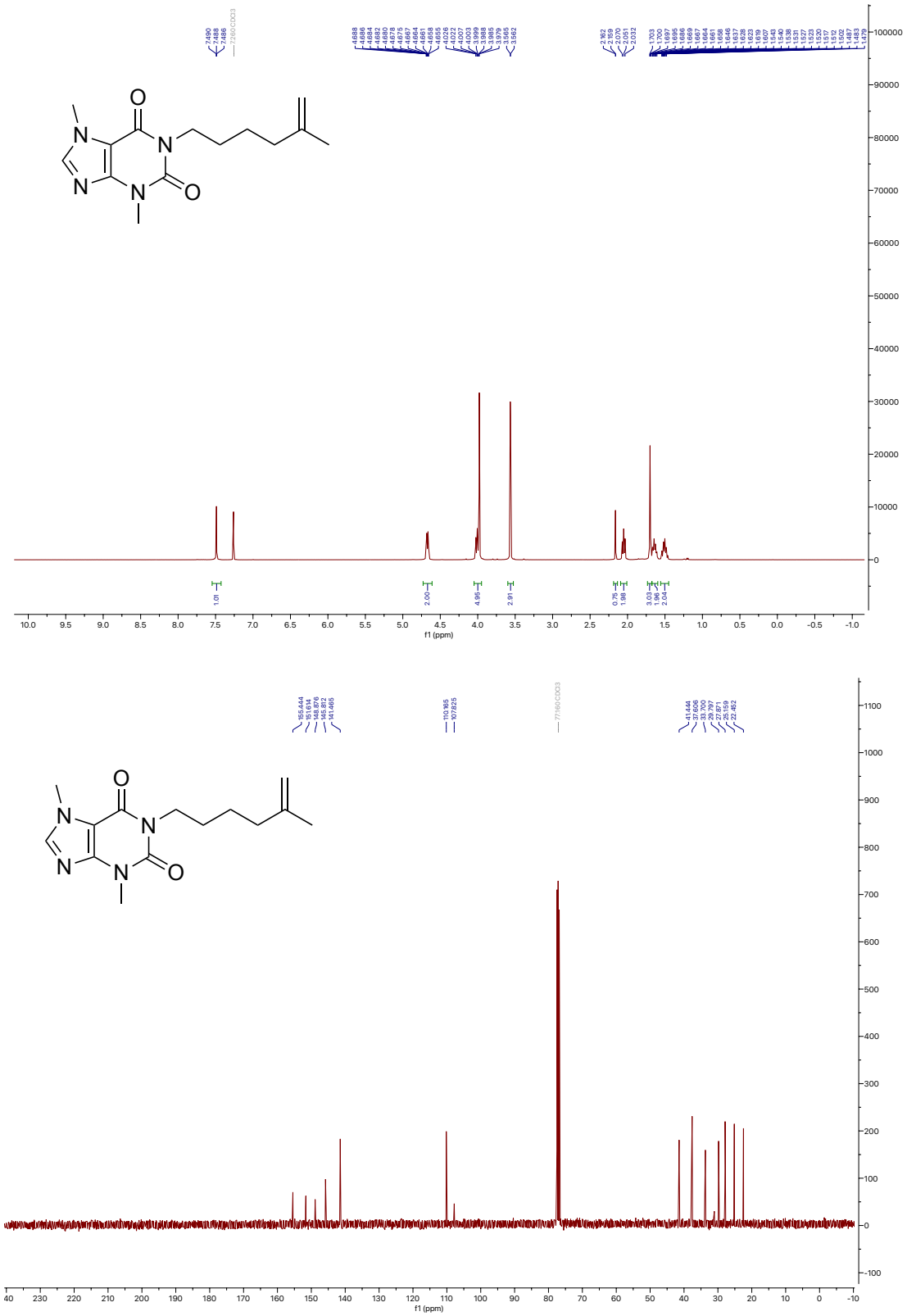


HSQC of **F10b** and 1D Selective Gradient NOESY, frequency 1.190 ppm of ***endo*-F10b**

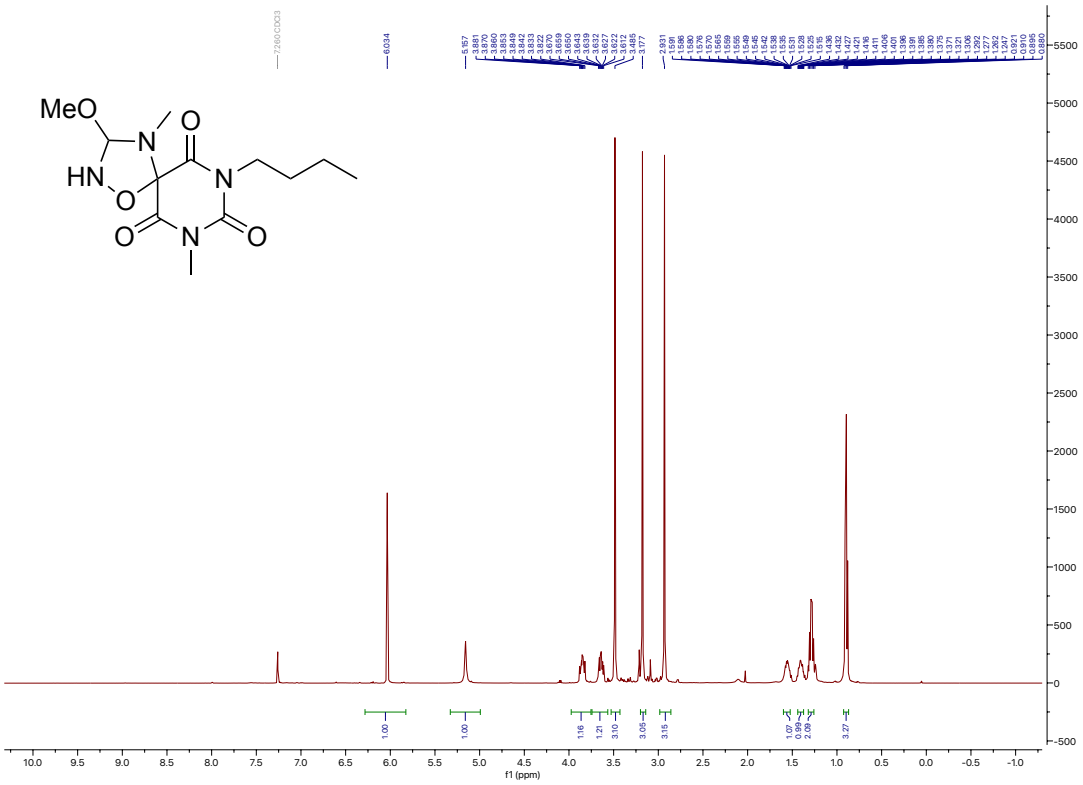


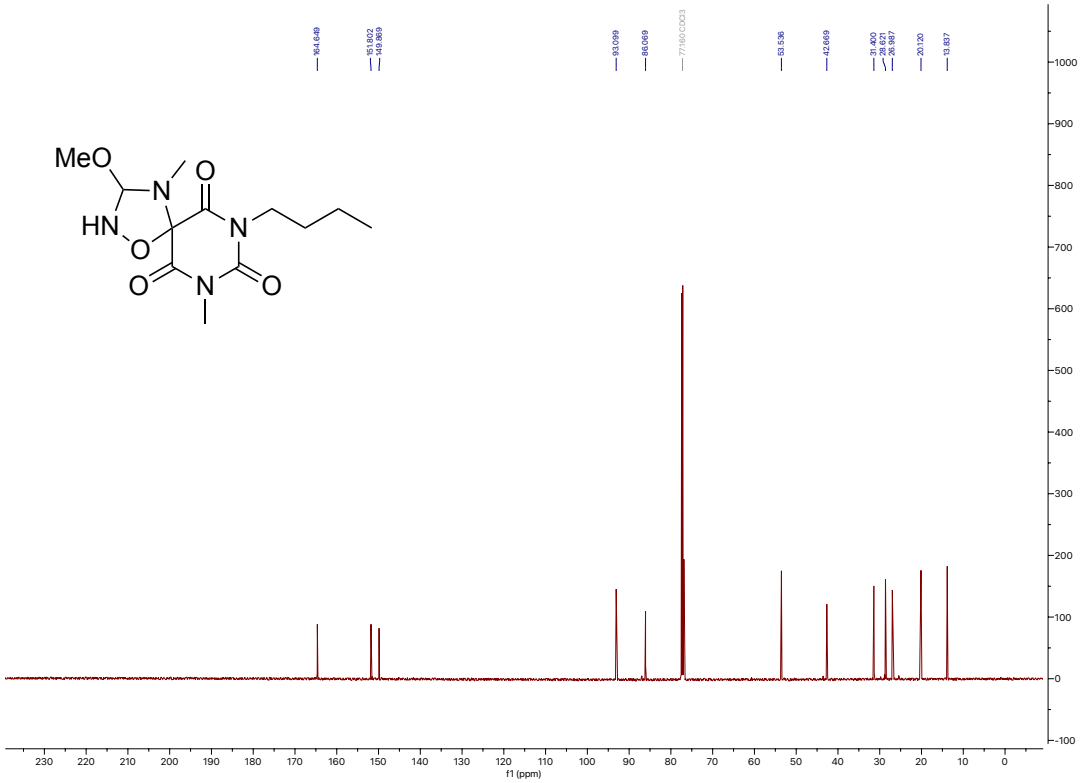


^{1}H NMR (500 MHz, $CDCl_3$) and ^{13}C NMR (126 MHz, $CDCl_3$) of **1c**

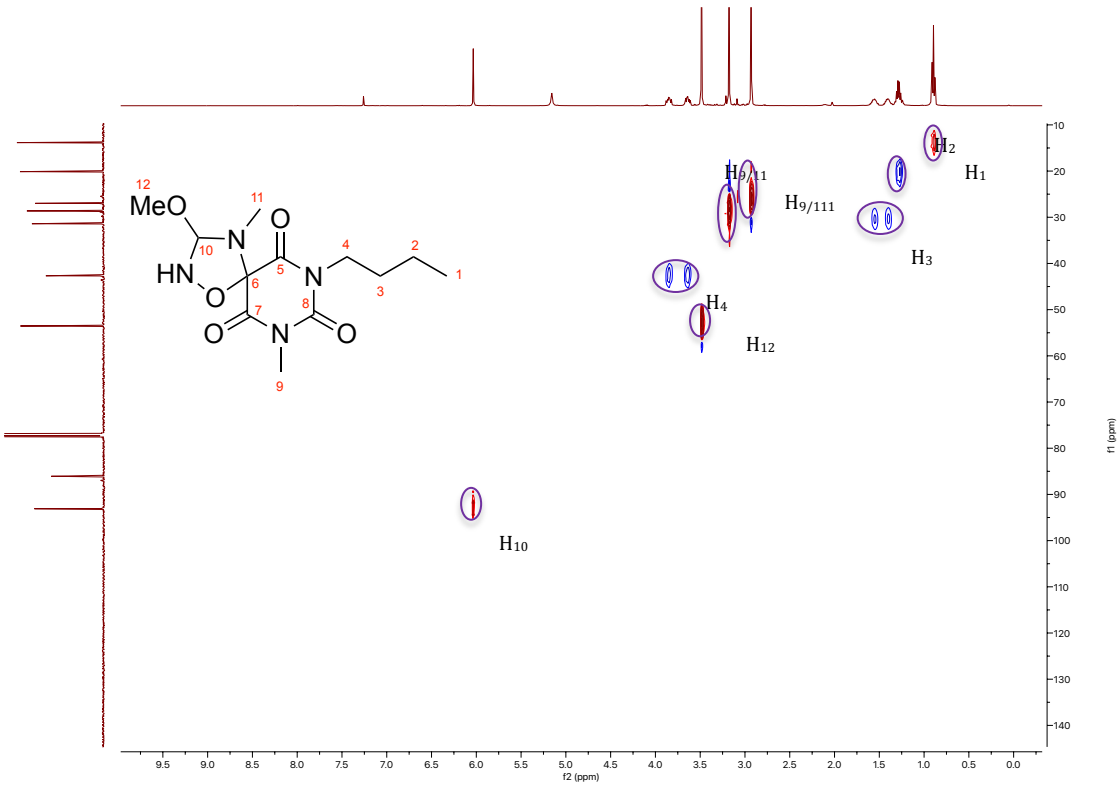


^{1}H NMR (400 MHz, $CDCl_3$) and ^{13}C NMR (101 MHz, $CDCl_3$) of **3a**

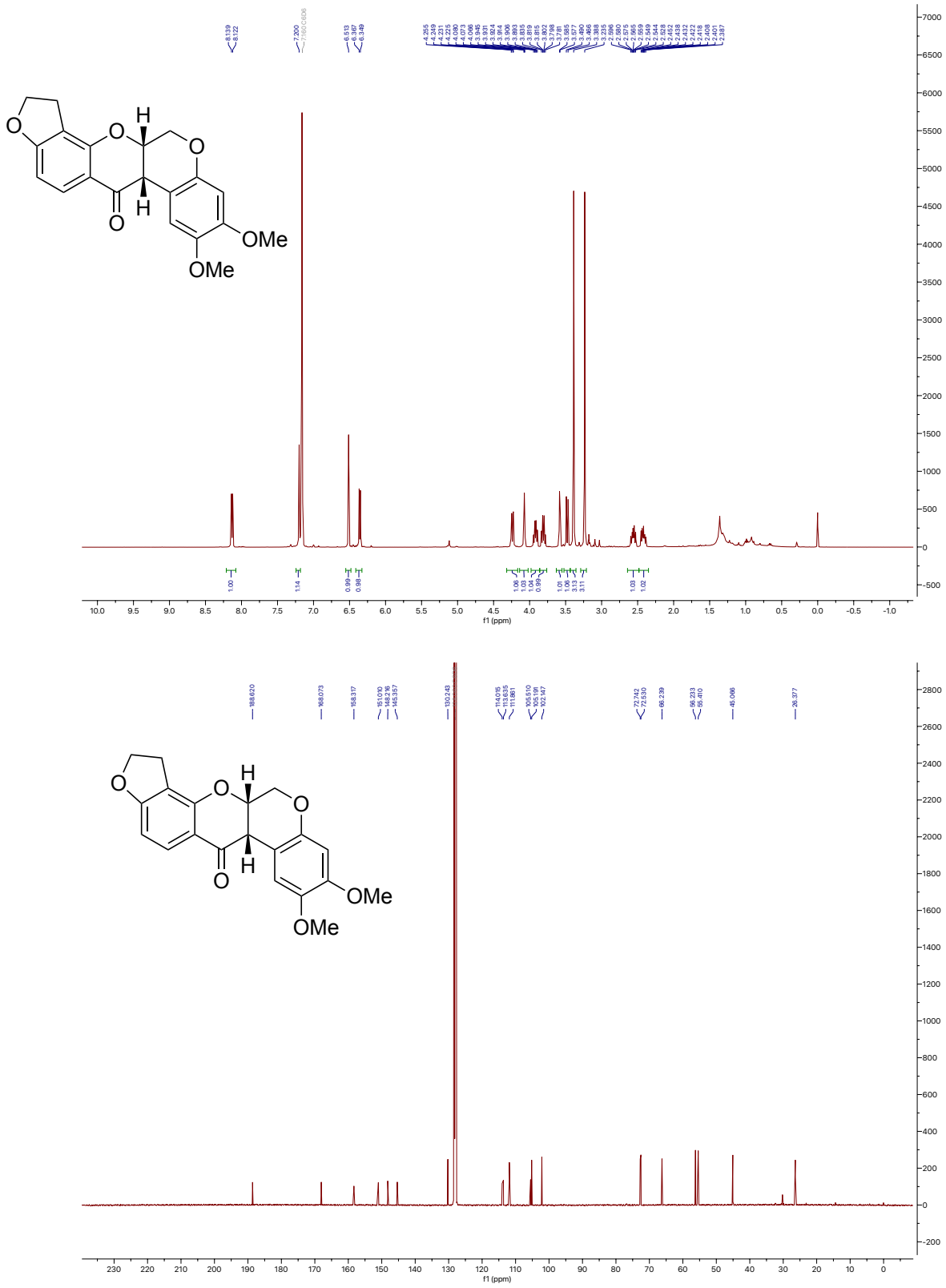




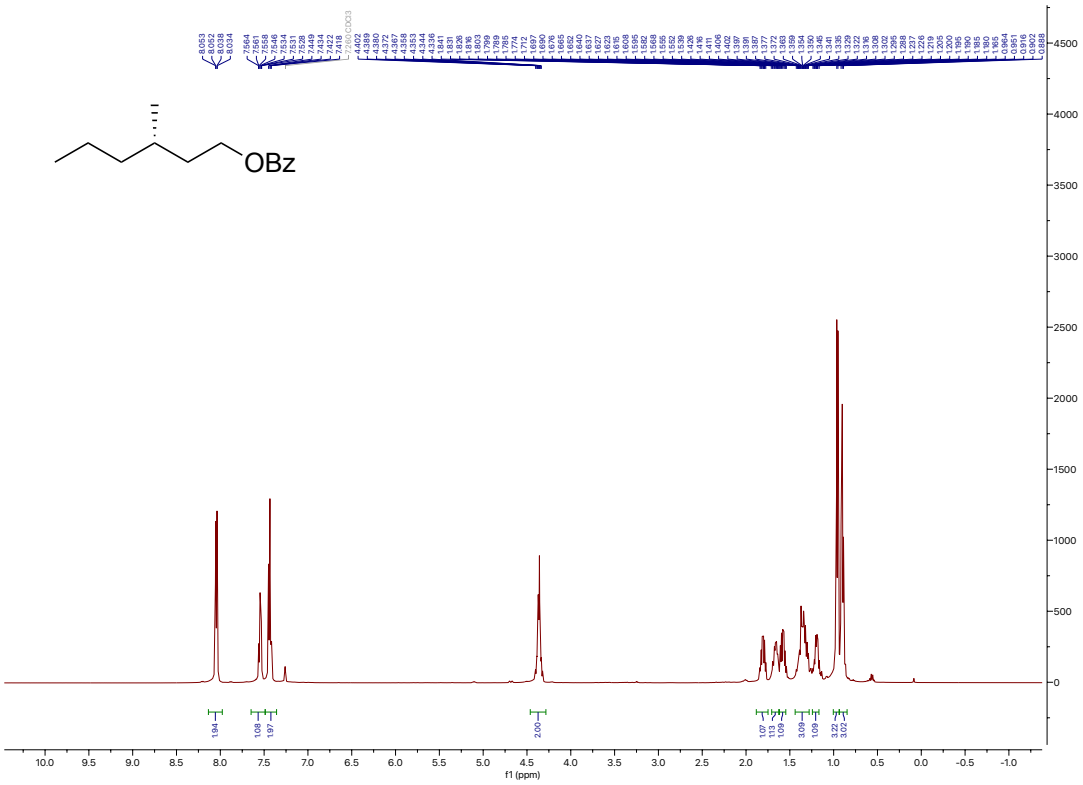
^{1}H NMR (500 MHz, $CDCl_3$) and ^{13}C NMR (126 MHz, $CDCl_3$) of **3x**

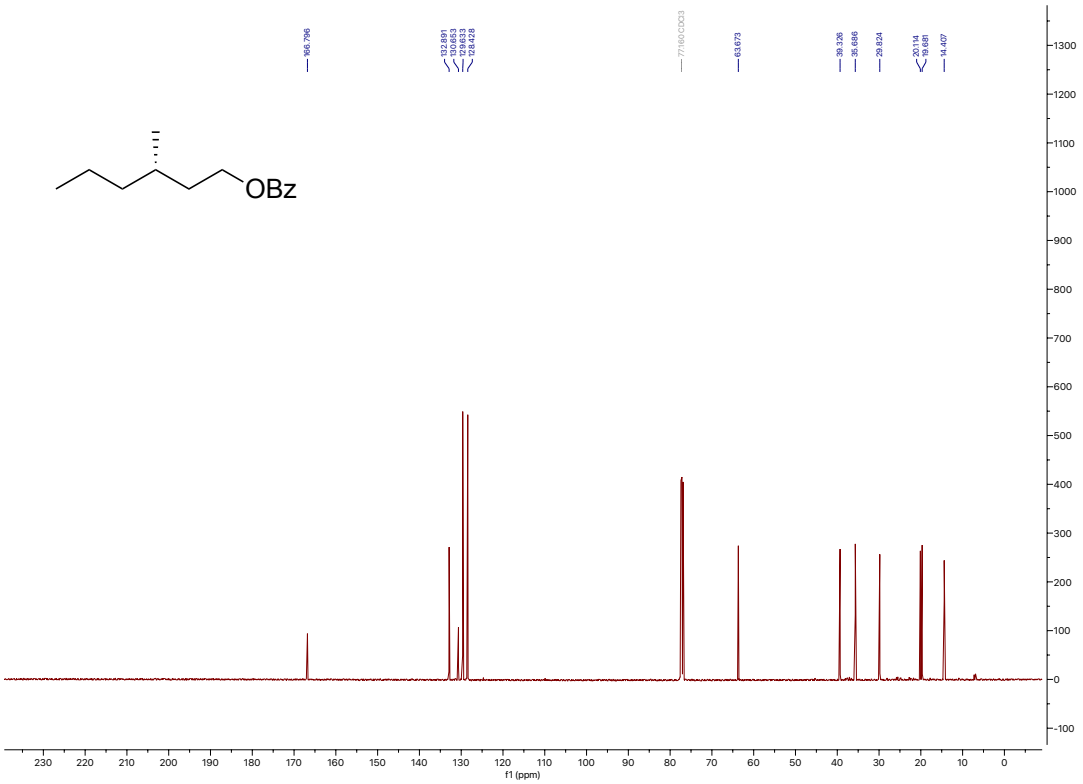

MeO
HN
O
N
O
O
N
O
N
O
12
11
10
6
5
4
2
1
3
7
8
9
H10
H4
H12
H9/11
H9/111
H3
H2
H1
f2 (ppm)
f1 (ppm)

HSQC of **3x**

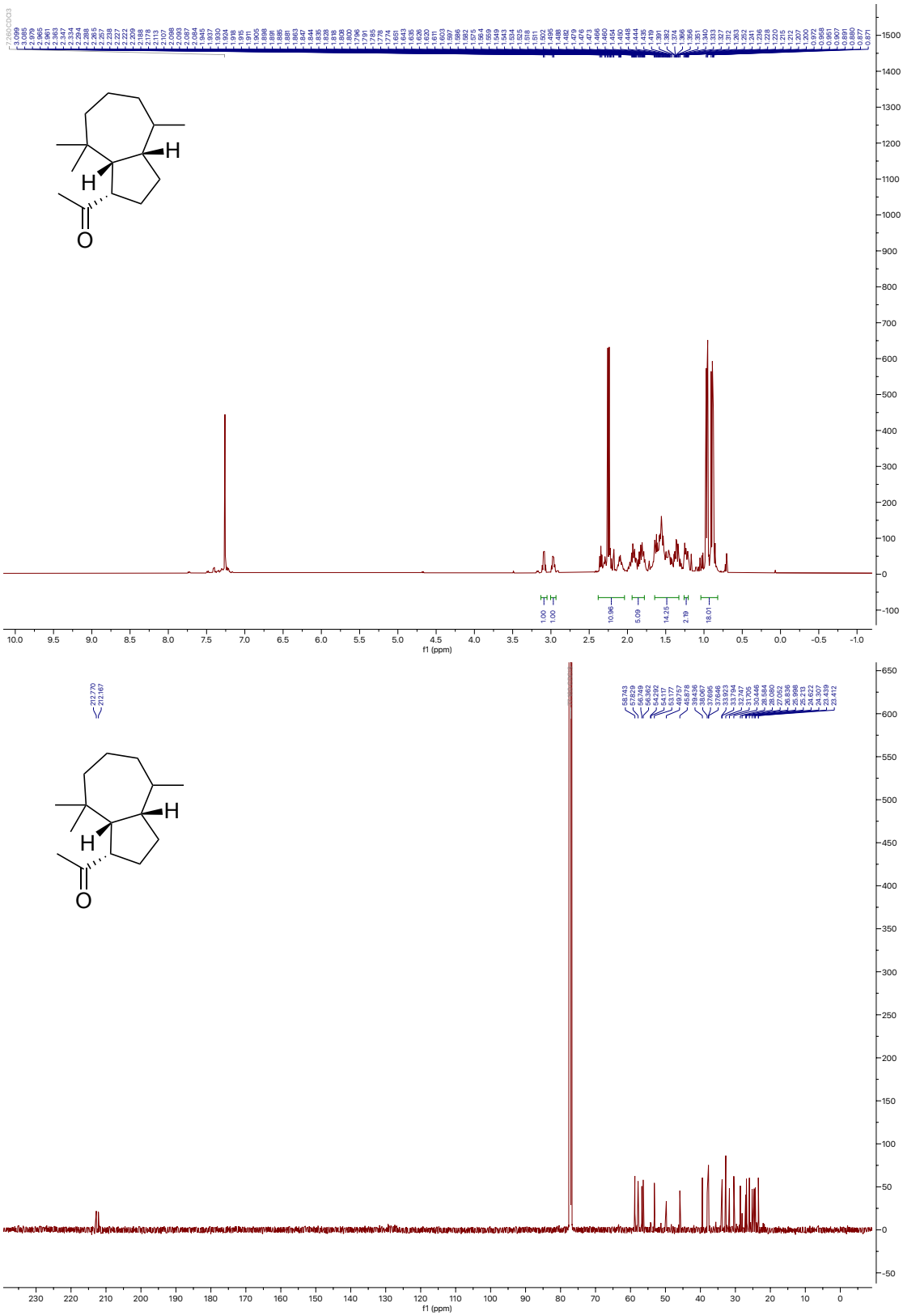


^{1}H NMR (500 MHz, C_6D_6) and ^{13}C NMR (126 MHz, C_6D_6) of **4c**

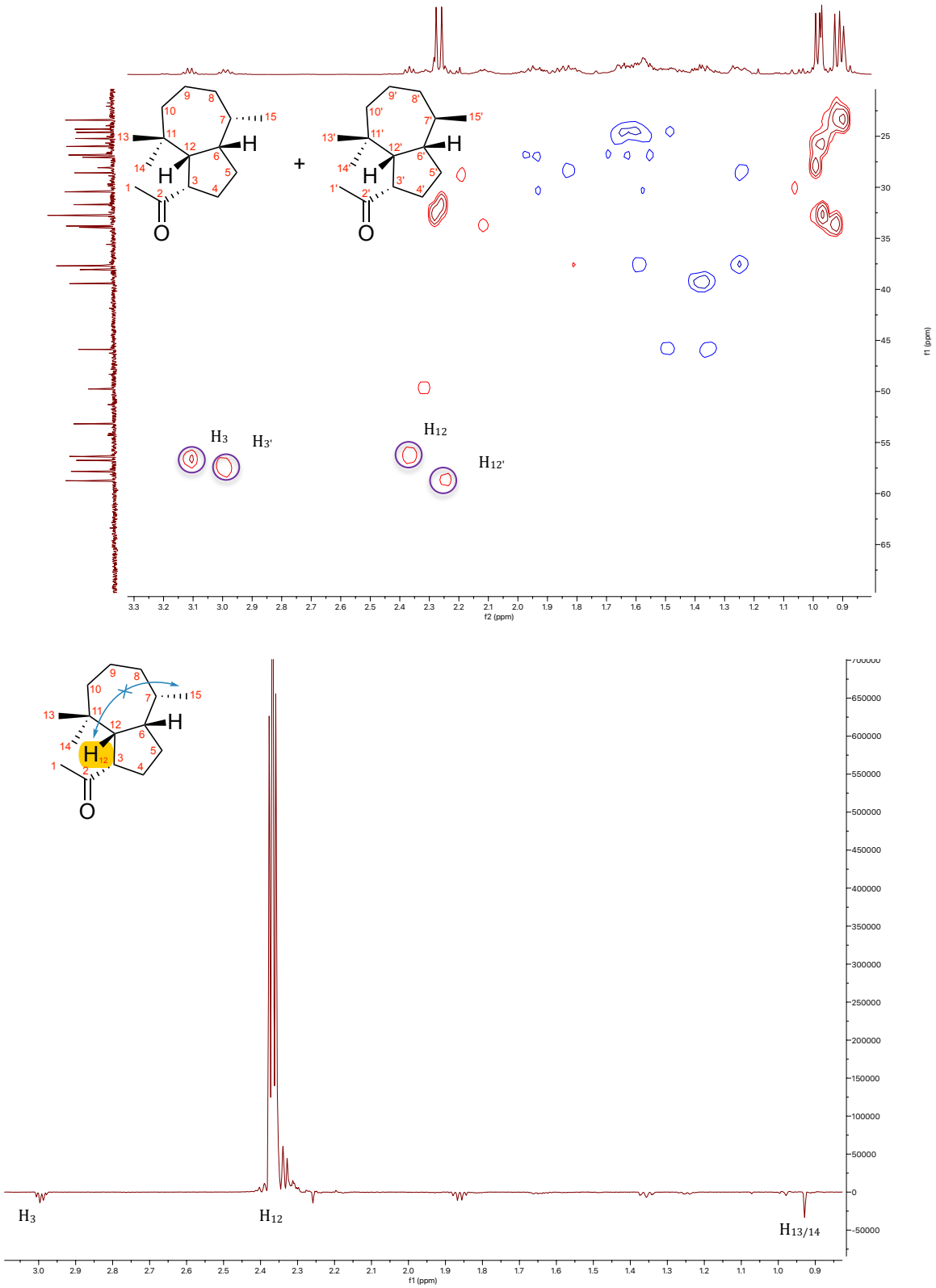




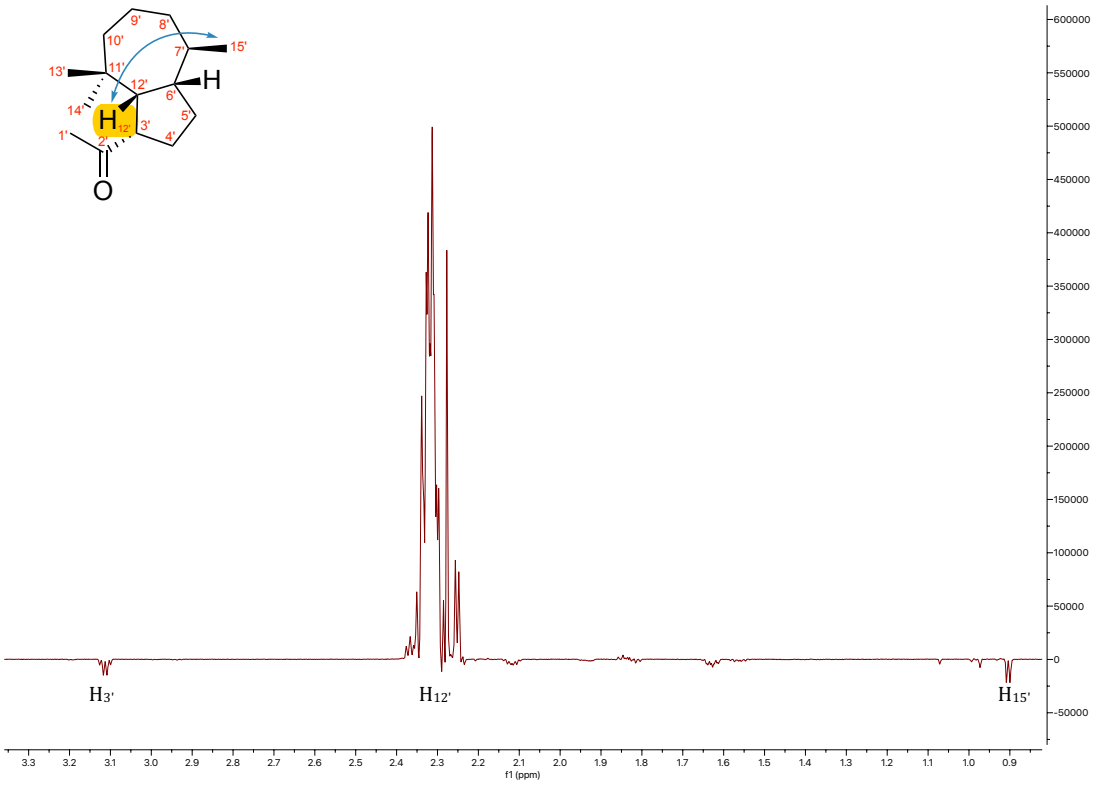
^{1}H NMR (500 MHz, $CDCl_3$) and ^{13}C NMR (126 MHz, $CDCl_3$) of **9c**



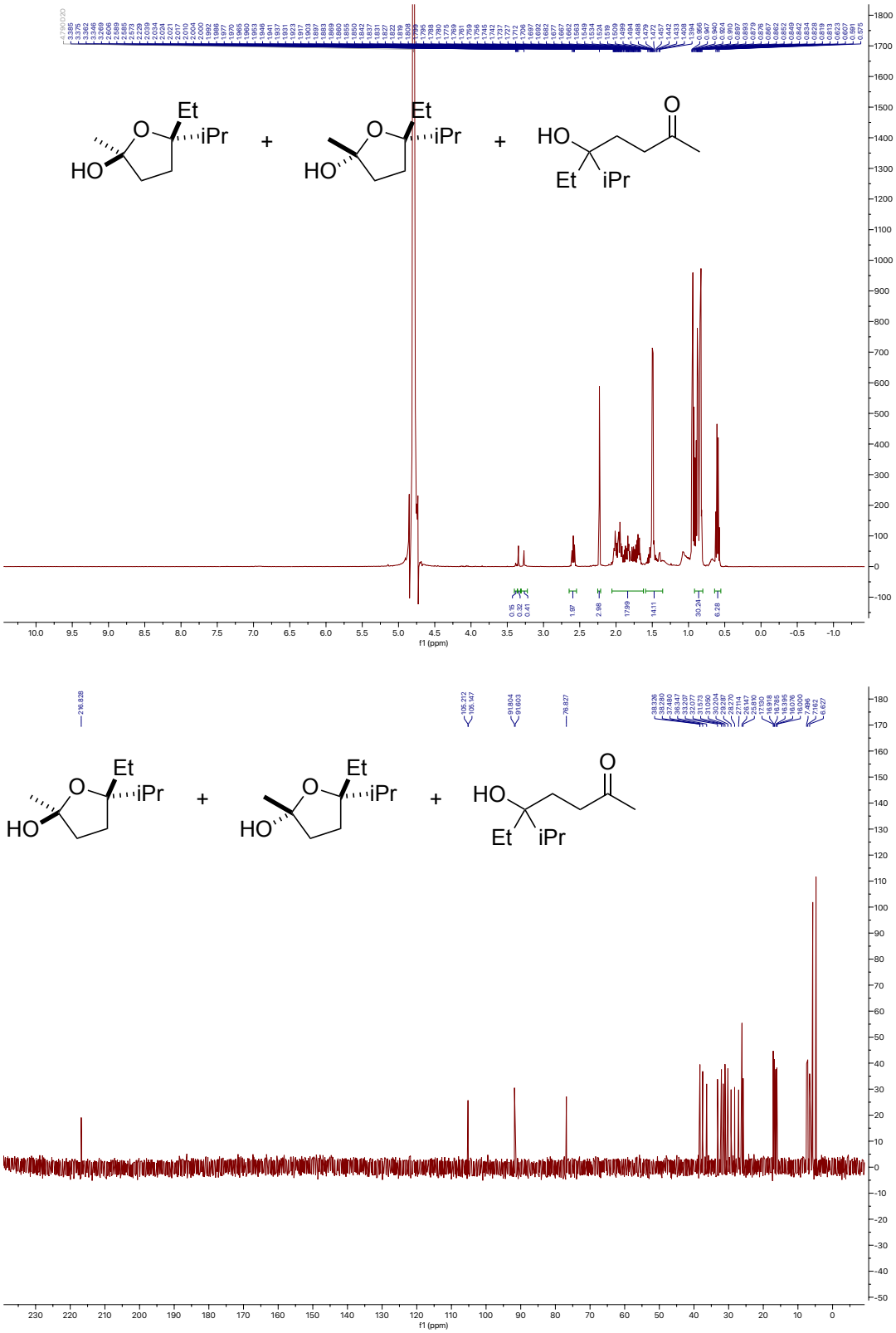
^{1}H NMR (500 MHz, $CDCl_3$) and ^{13}C NMR (126 MHz, $CDCl_3$) of **12c**



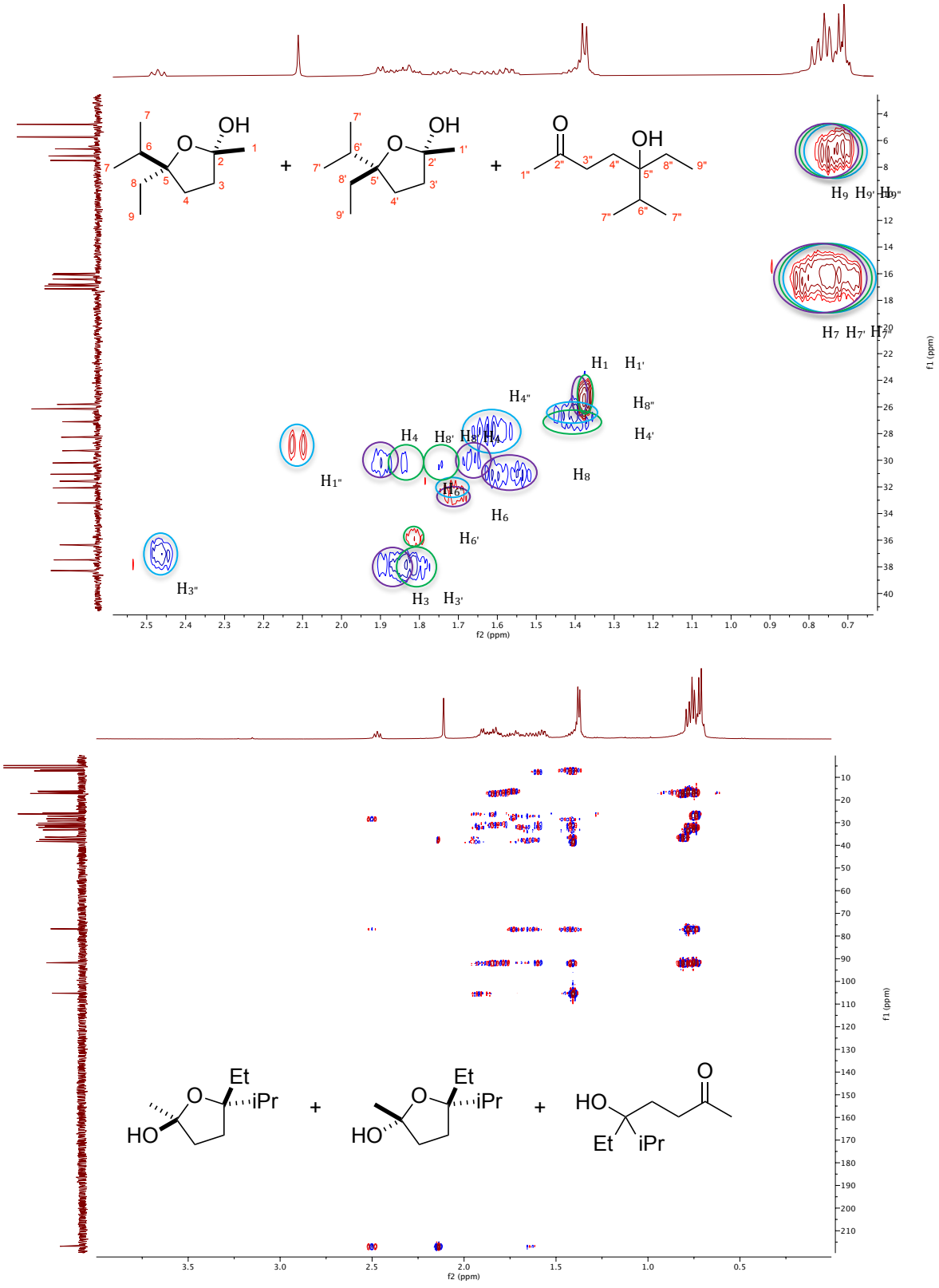
HSQC of **12c** and 1D Selective Gradient NOESY of ***cis*-12c**, frequency 2.369 ppm



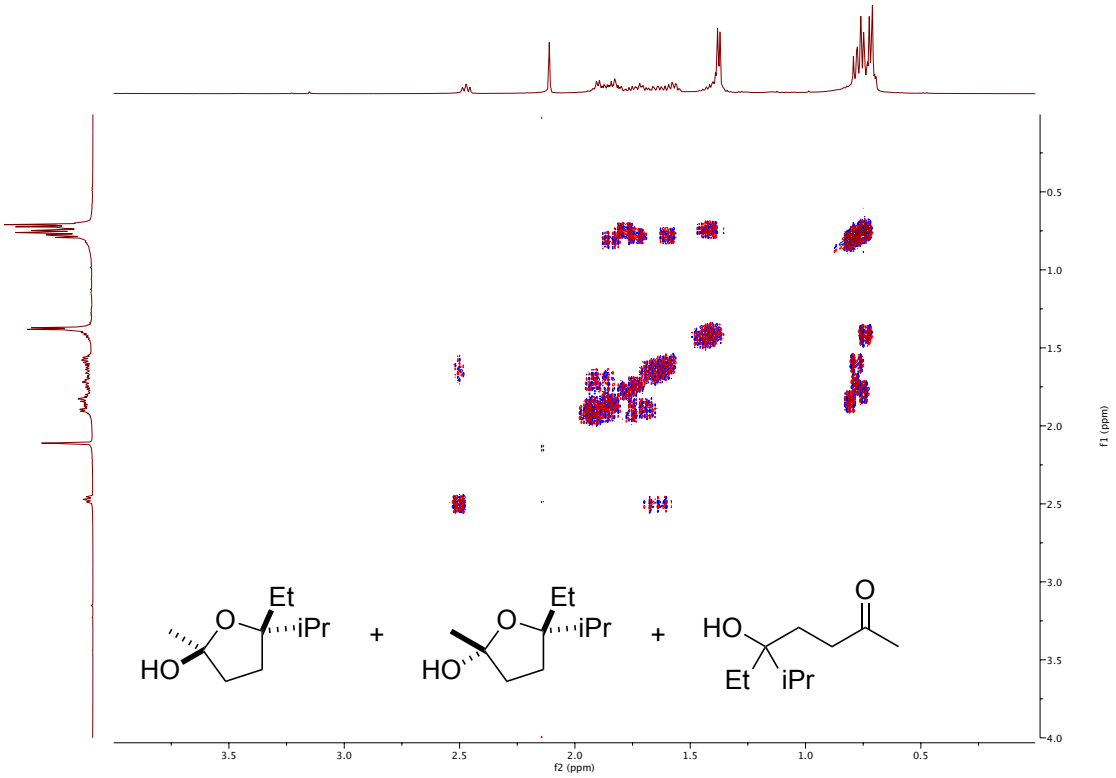
1D Selective Gradient NOESY of Compound ***trans*-12c**, frequency 2.319 ppm

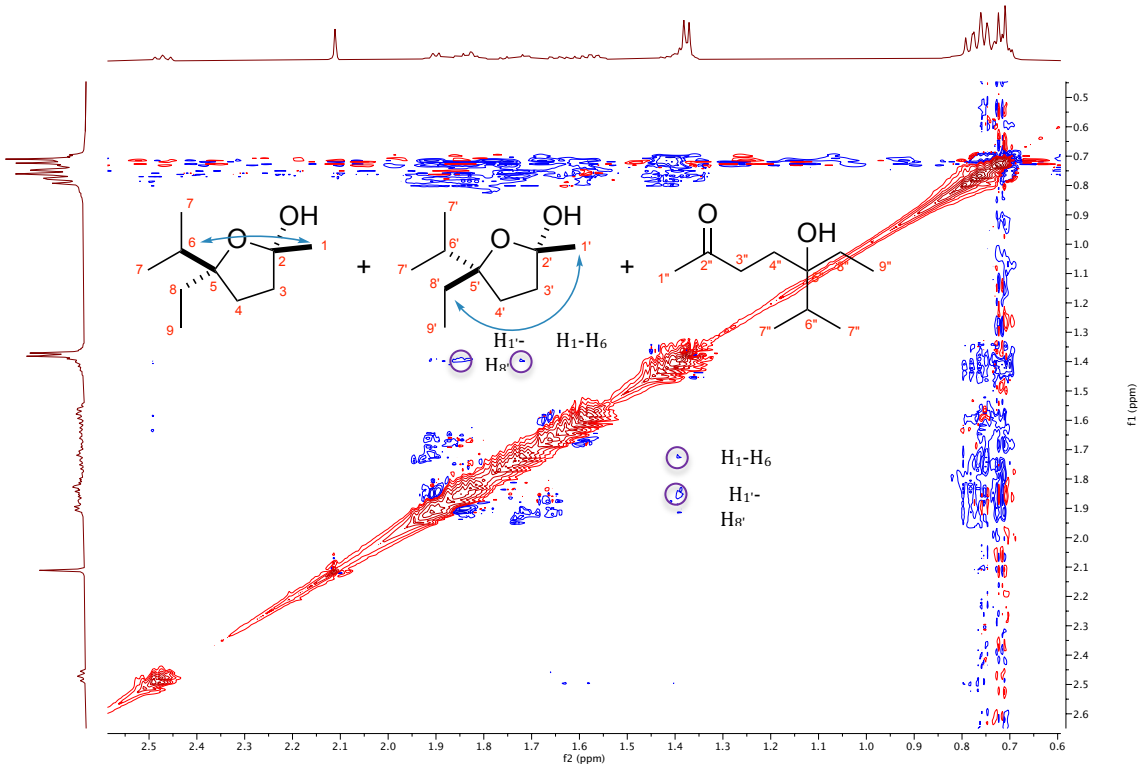


^{1}H NMR (600 MHz, D_2O) and ^{13}C NMR (126 MHz, D_2O) of **14c** and **14c'**

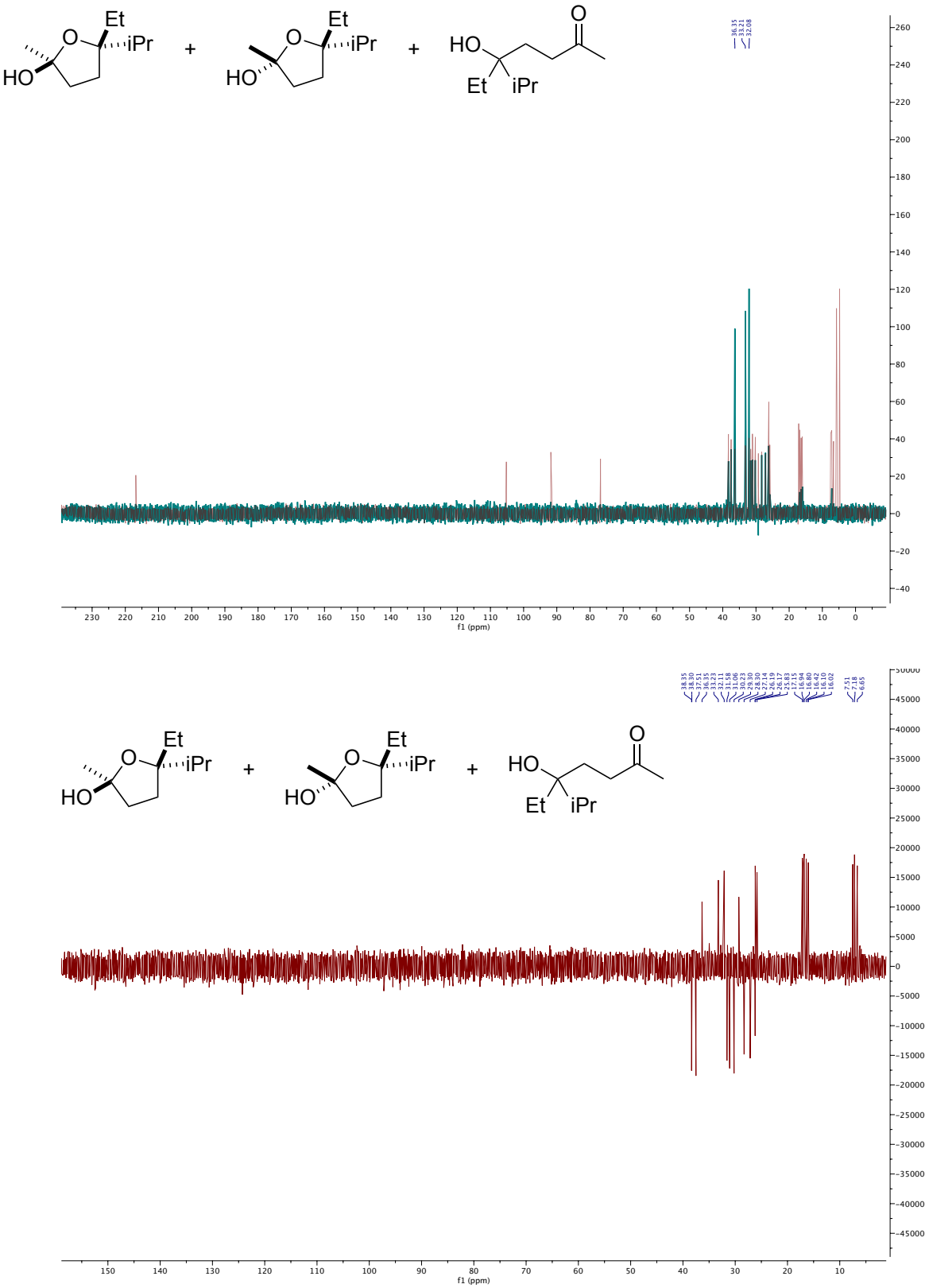


HSQC and HMBC of **14c** and **14c'**

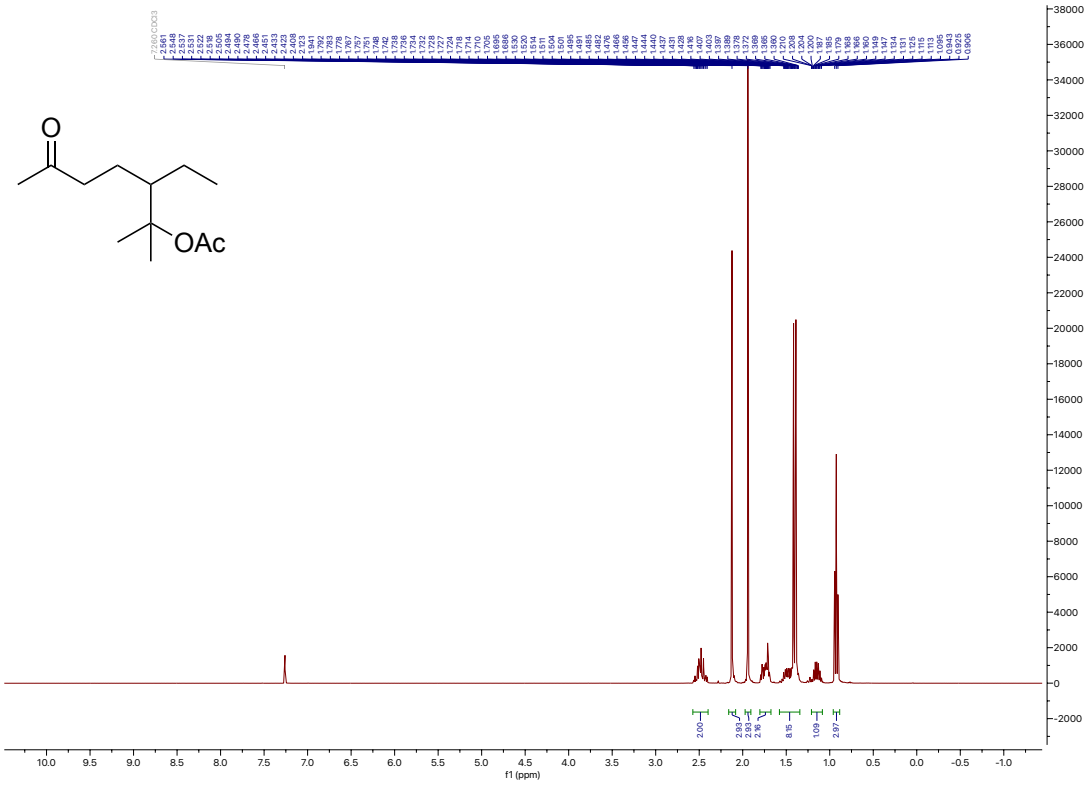


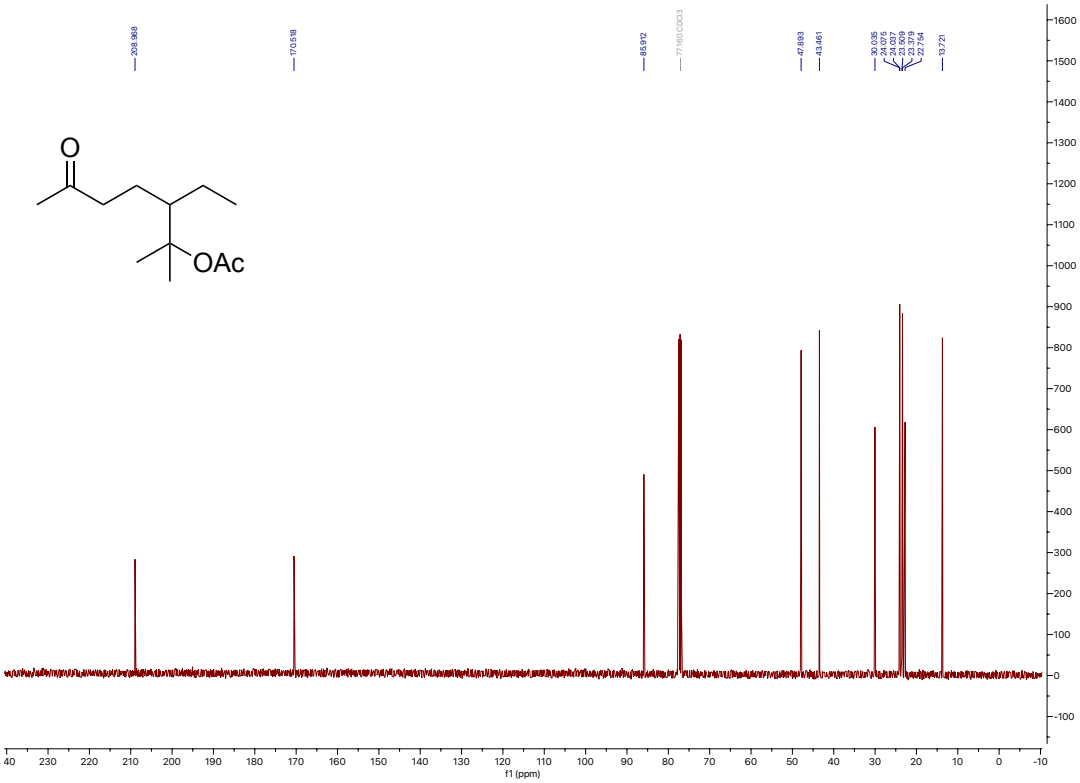


COSY and NOESY of **14c** and **14c'**

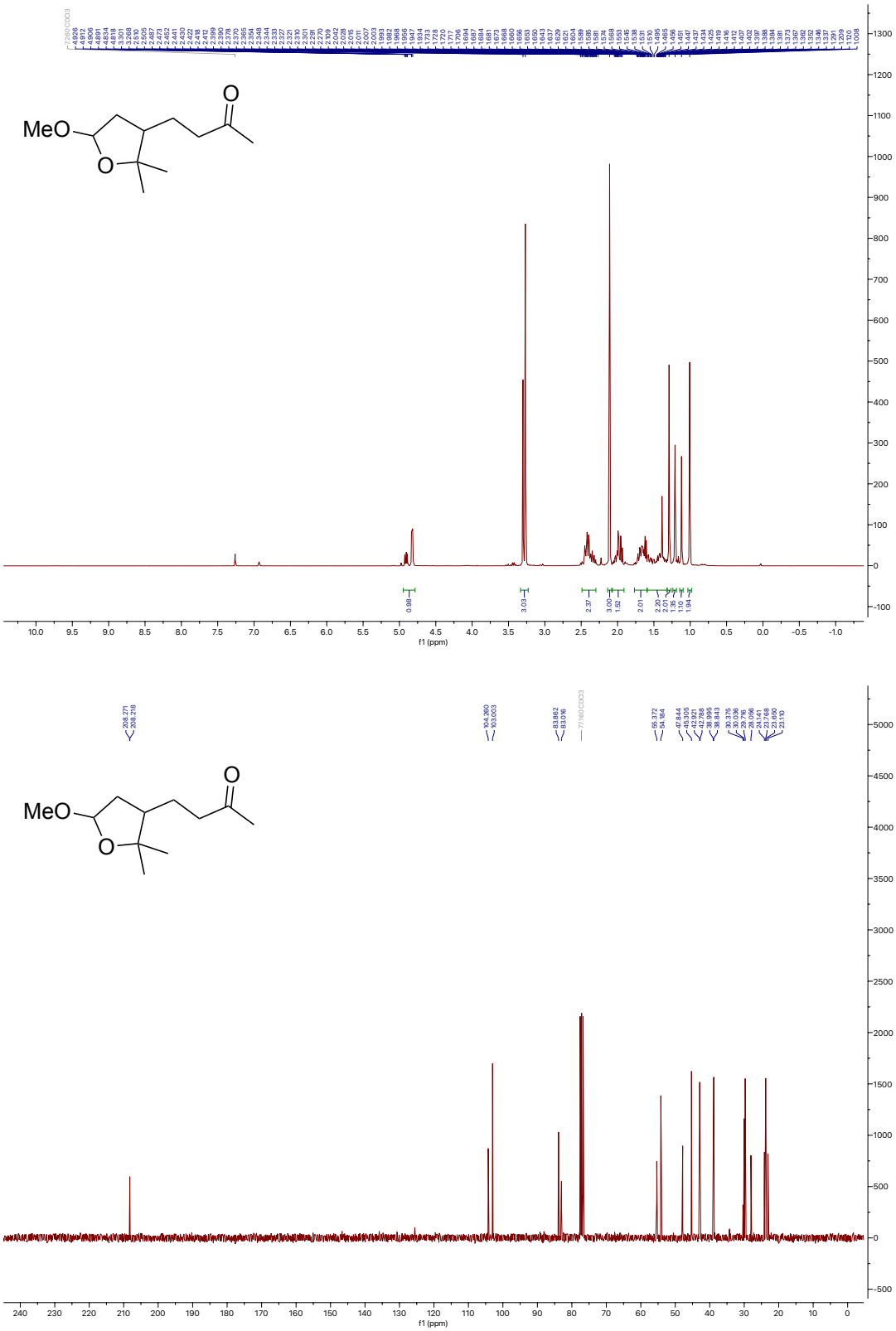


DEPT–90 superimposed over ^{13}C NMR and DEPT–135 of **14c** and **14c'**

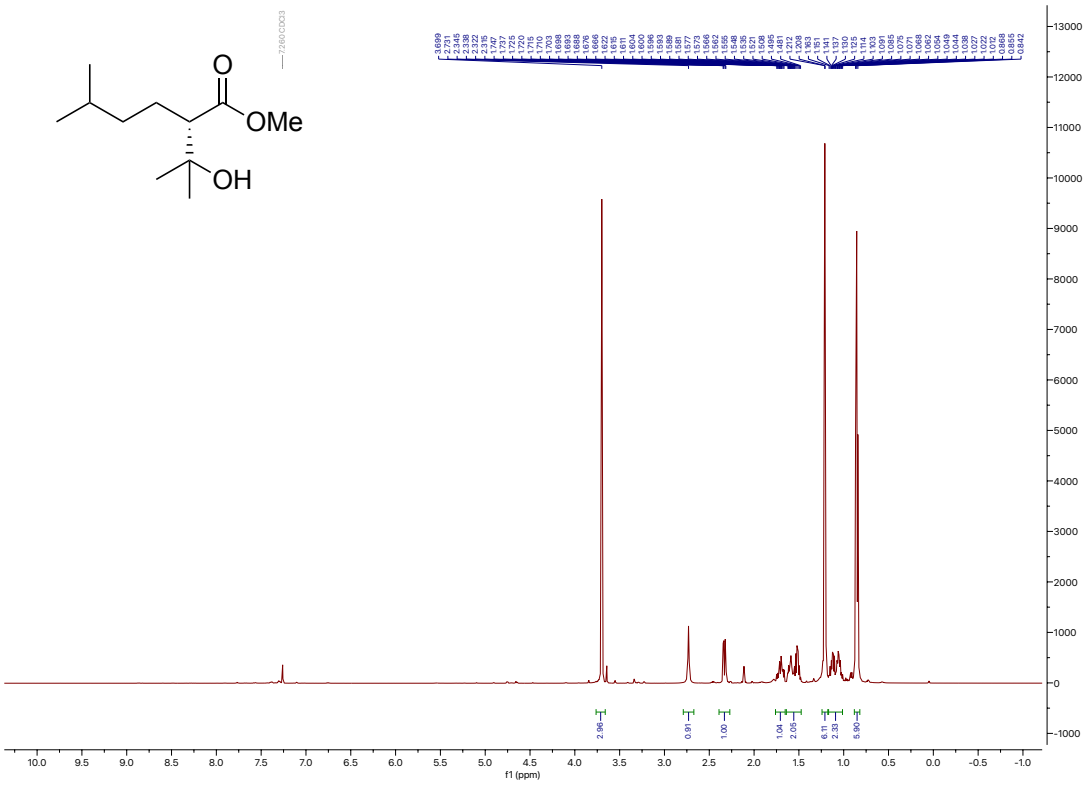


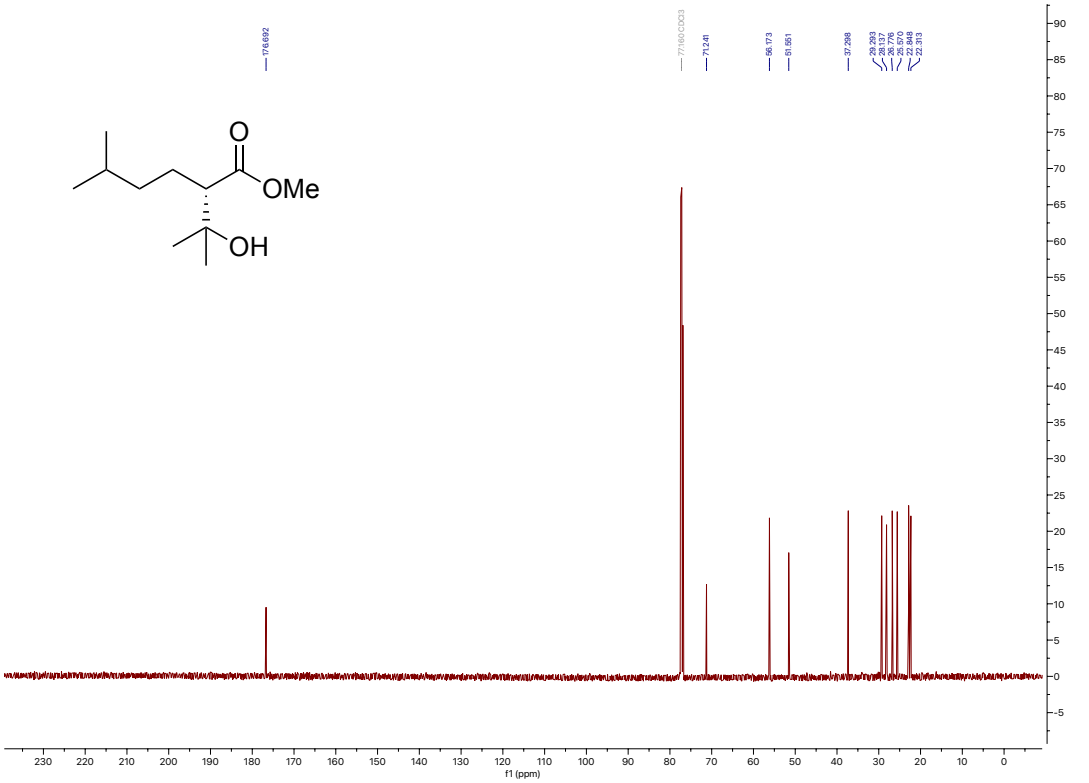


^{1}H NMR (400 MHz, $CDCl_3$) and ^{13}C NMR (101 MHz, $CDCl_3$) of **16c**

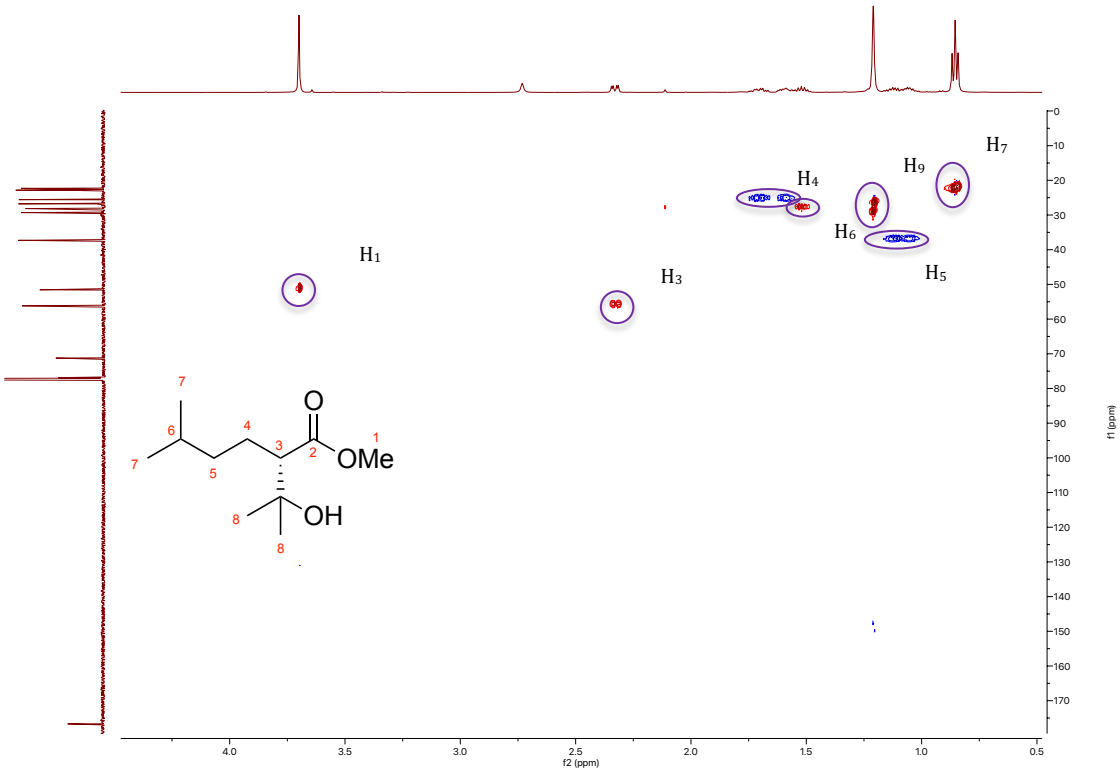


^{1}H NMR (300 MHz, $CDCl_3$) and ^{13}C NMR (75 MHz, $CDCl_3$) of **17c**

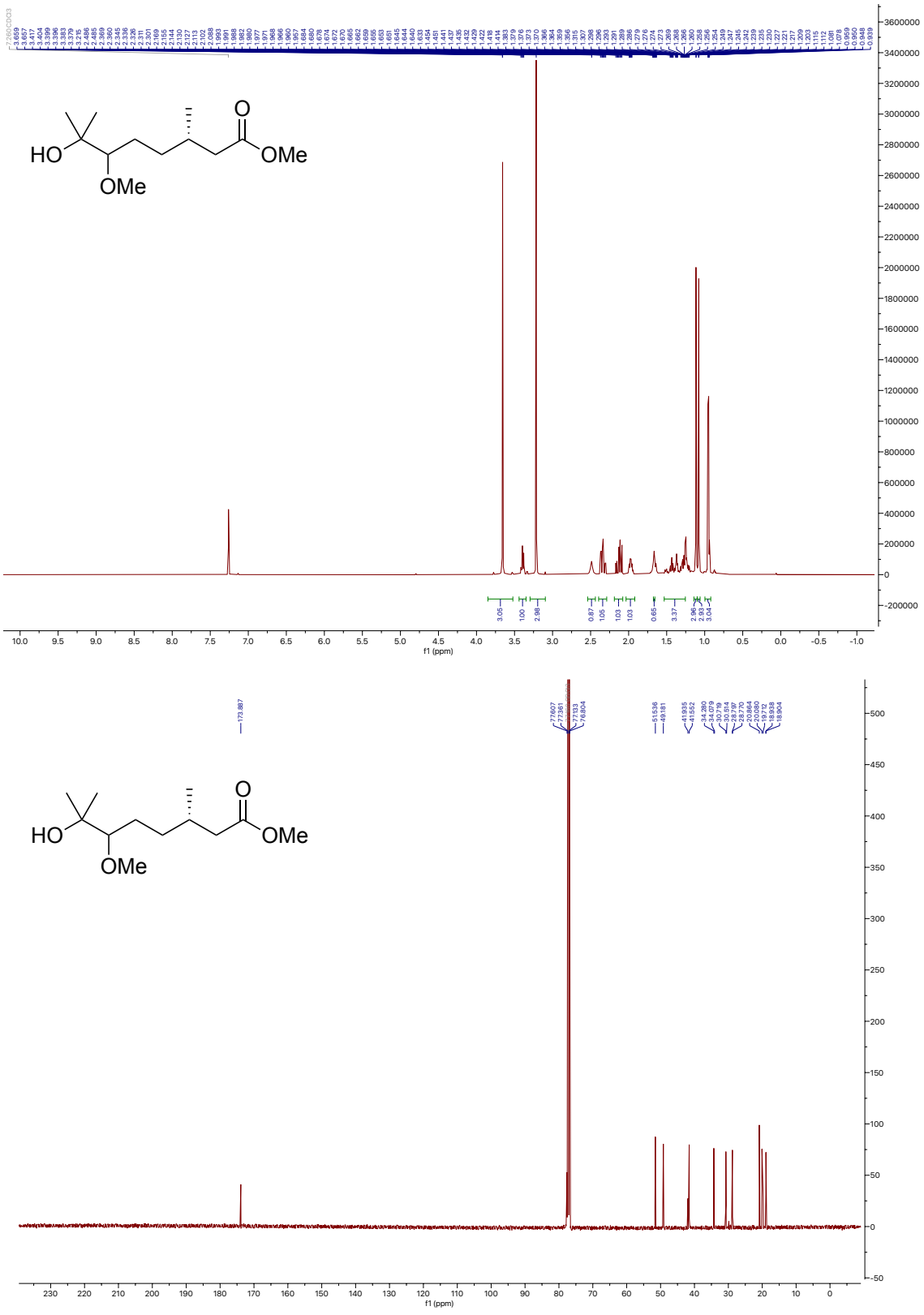




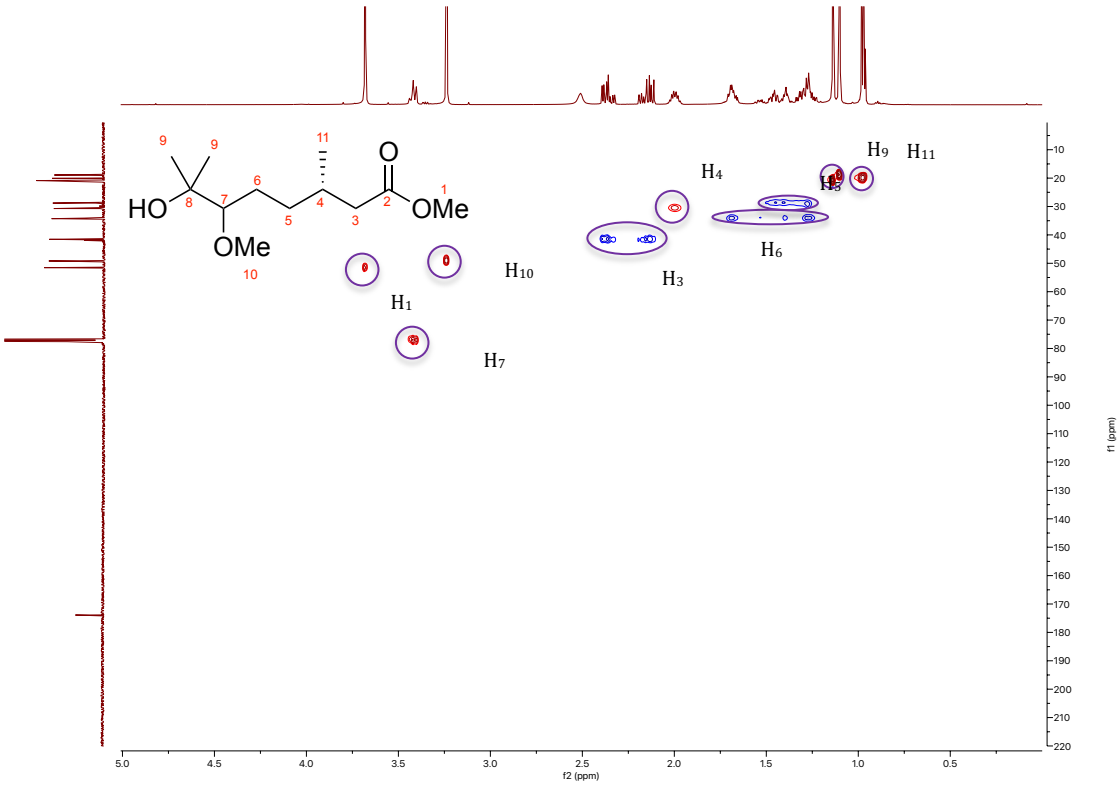
^{1}H NMR (500 MHz, $CDCl_3$) and ^{13}C NMR (126 MHz, $CDCl_3$) of **18c**



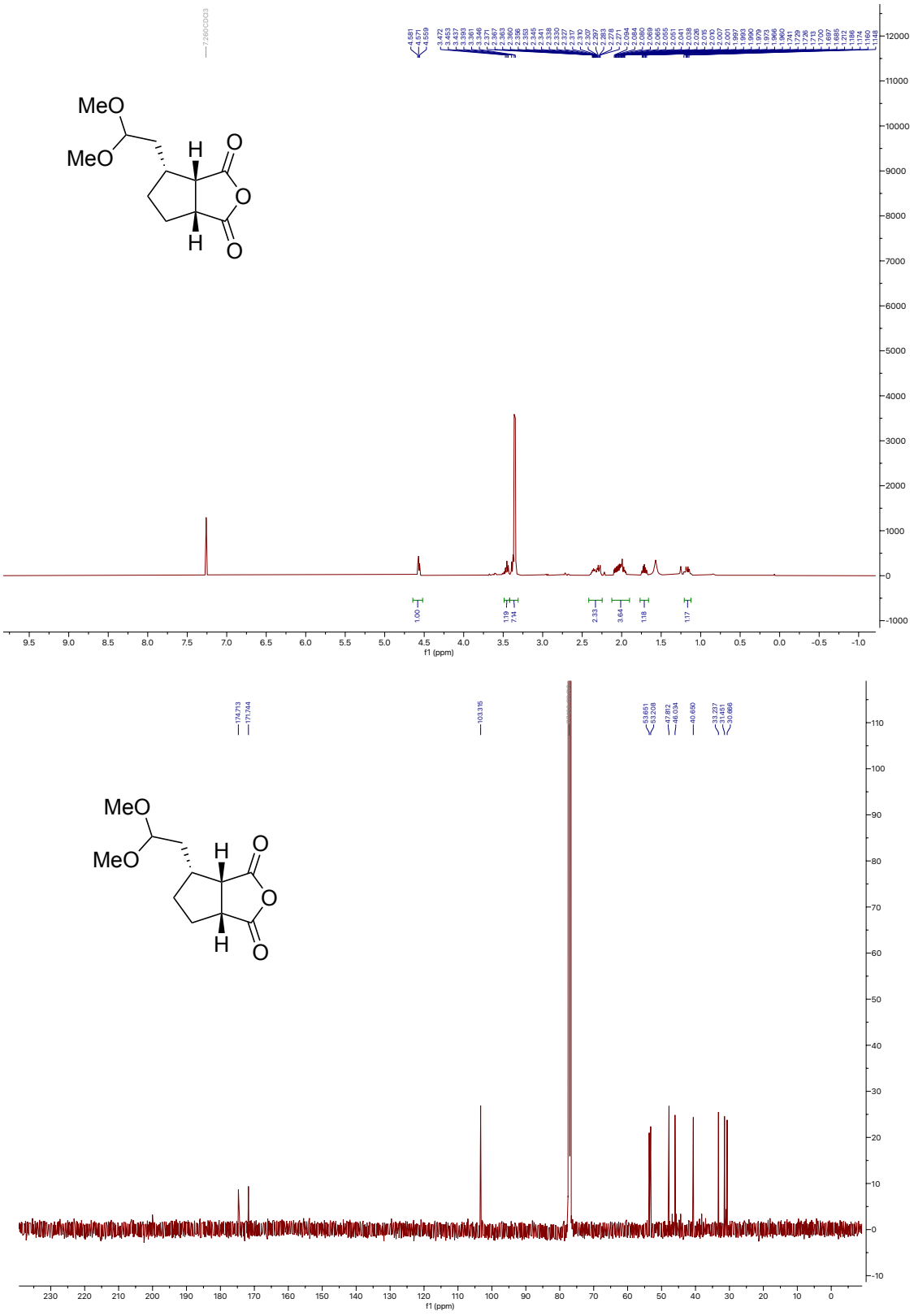
HSQC of **18c**



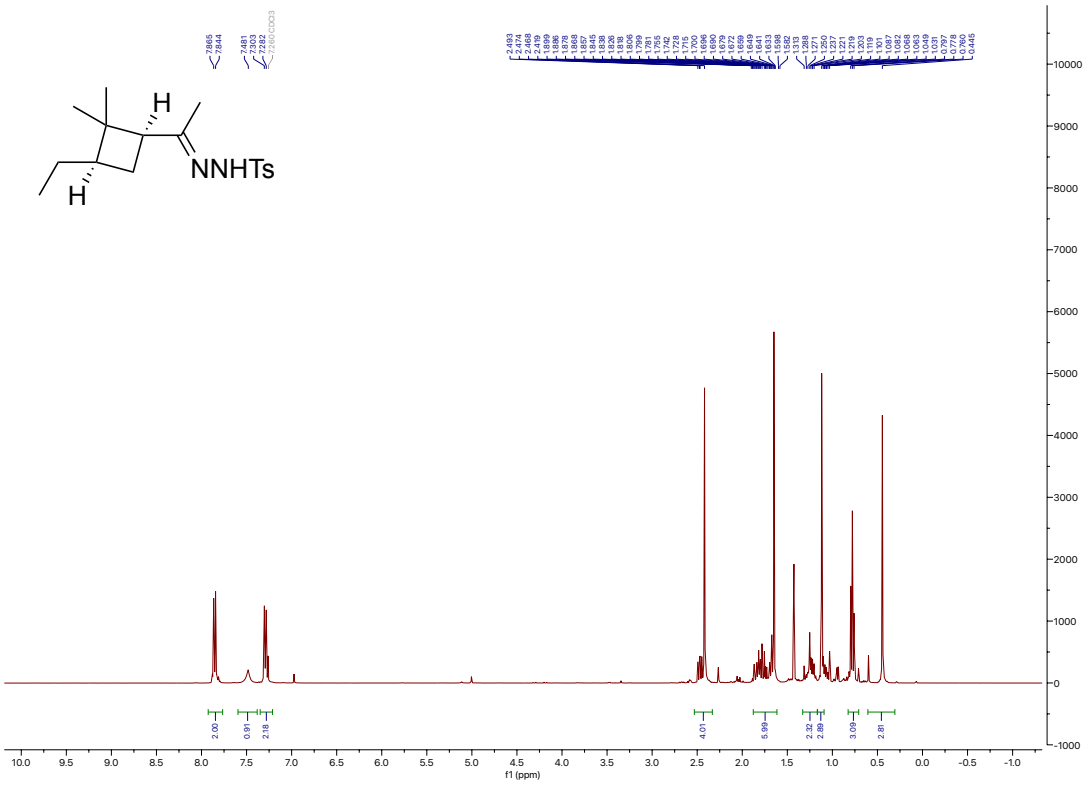
^{1}H NMR (500 MHz, $CDCl_3$) and ^{13}C NMR (126 MHz, $CDCl_3$) of **18c'**

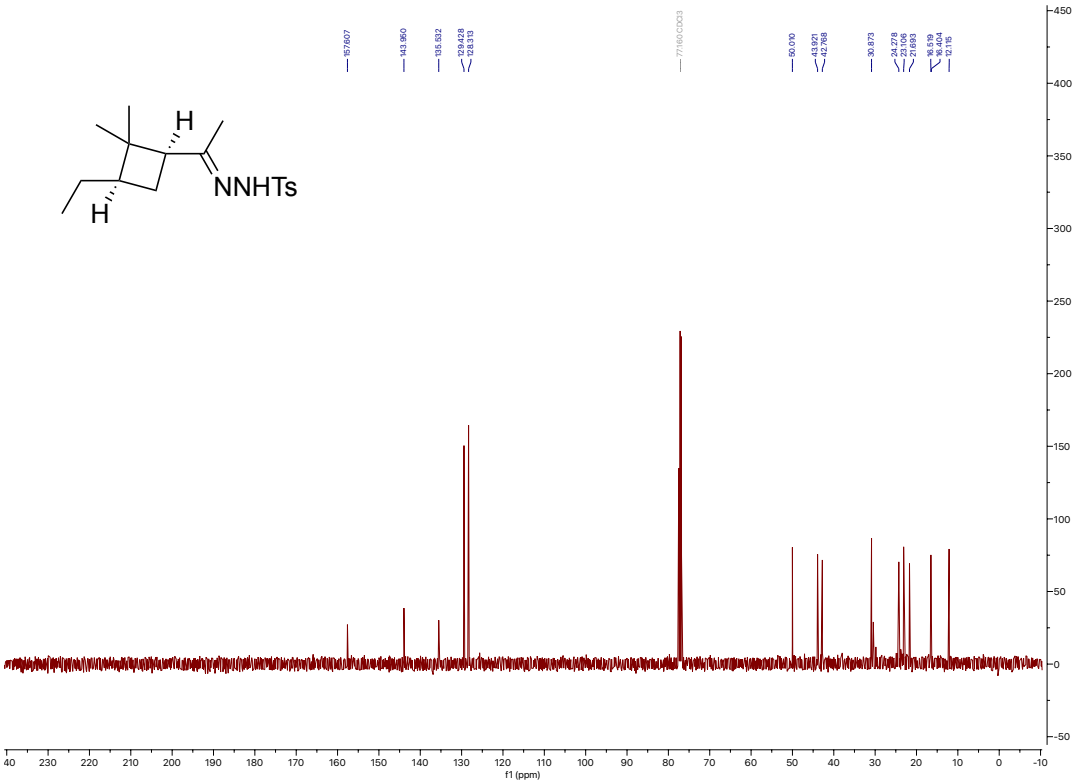


HSQC of **18c'**

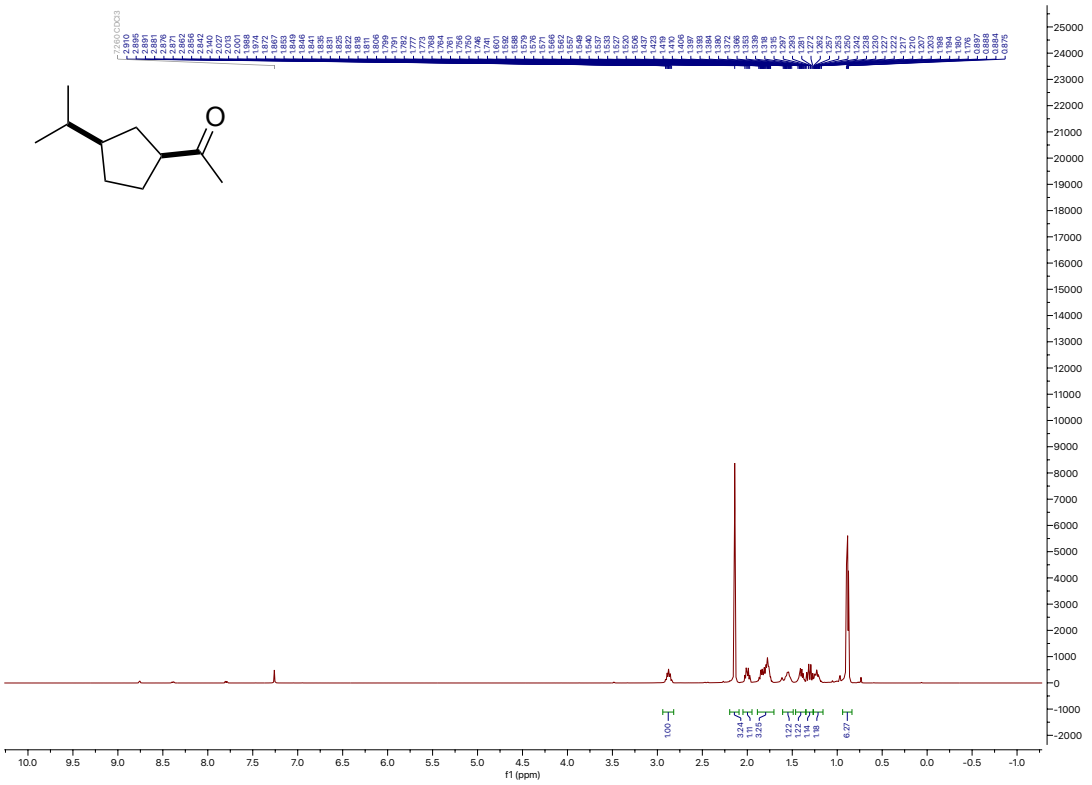


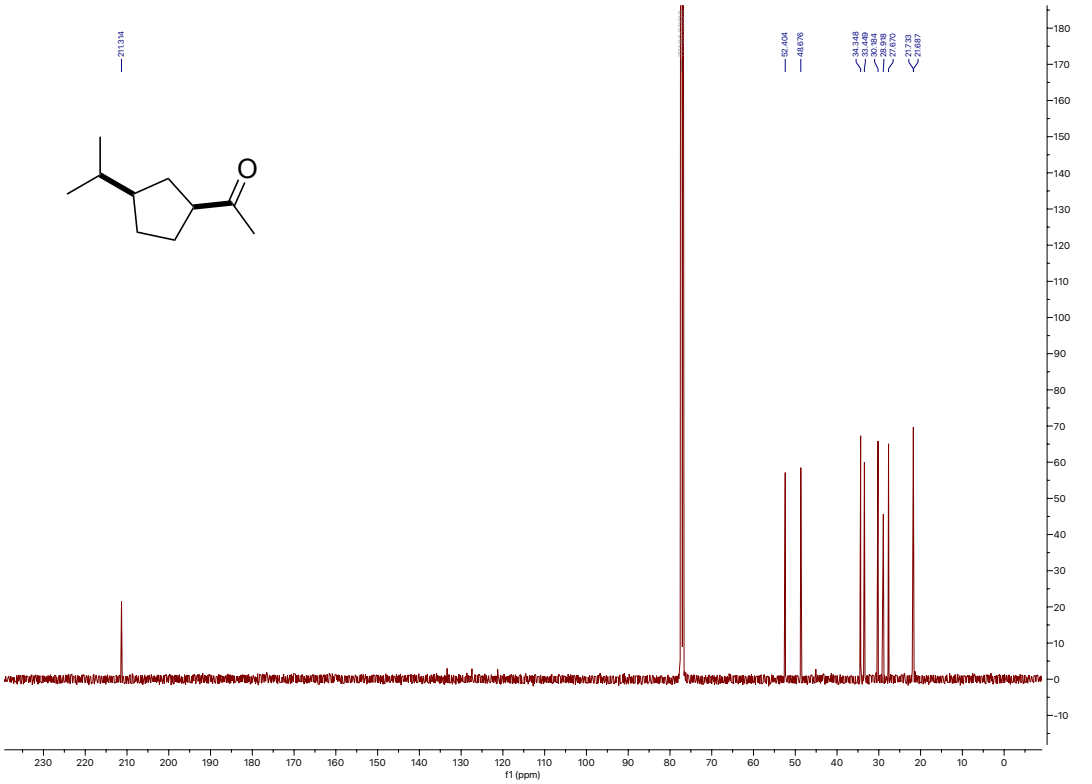
^{1}H NMR (500 MHz, $CDCl_3$) and ^{13}C NMR (126 MHz, $CDCl_3$) of **19c**



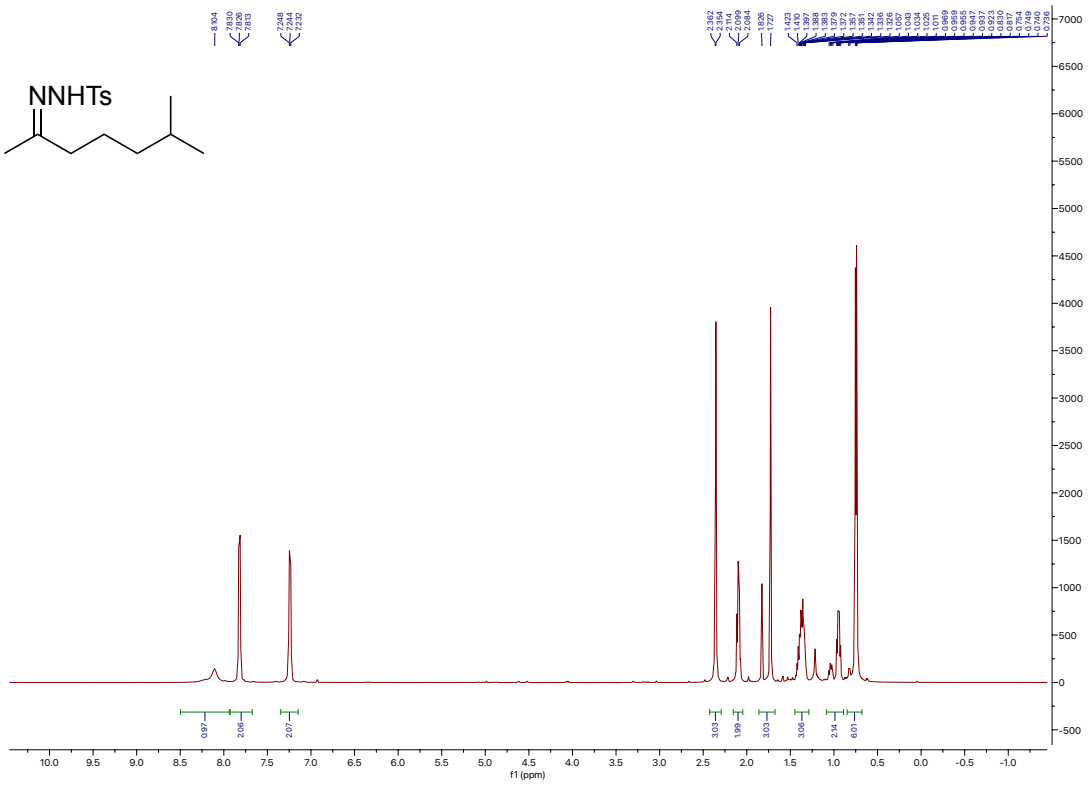


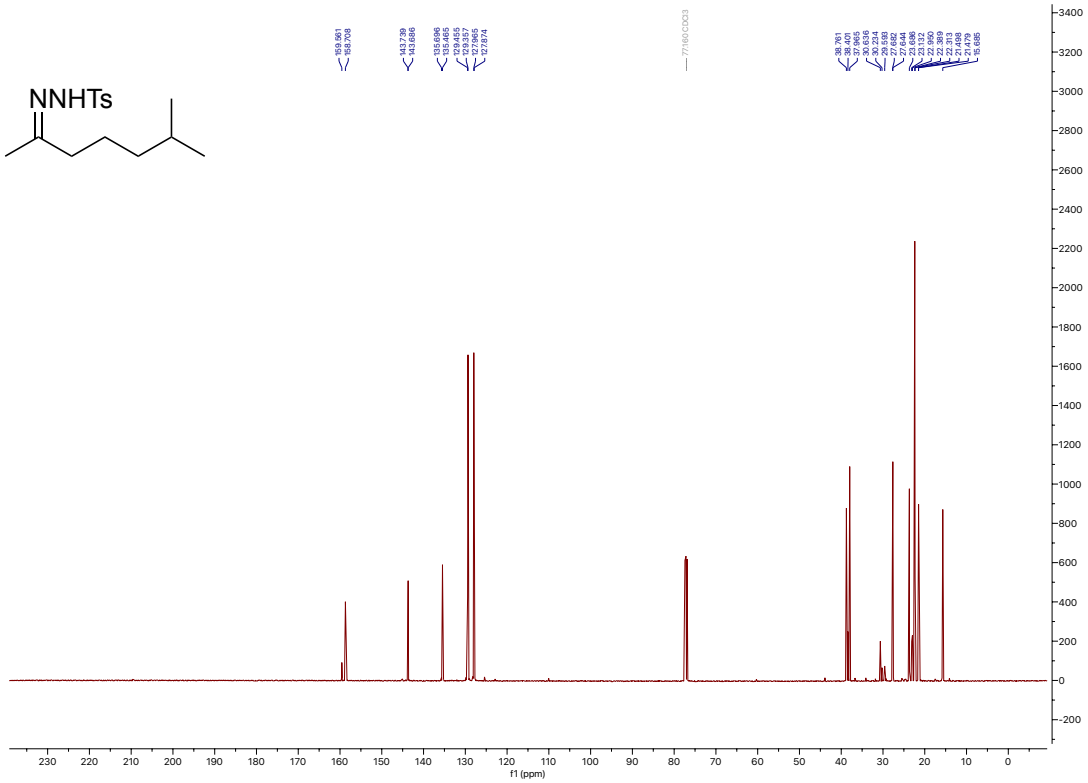
^{1}H NMR (400 MHz, $CDCl_3$) and ^{13}C NMR (101 MHz, $CDCl_3$) of **21e**



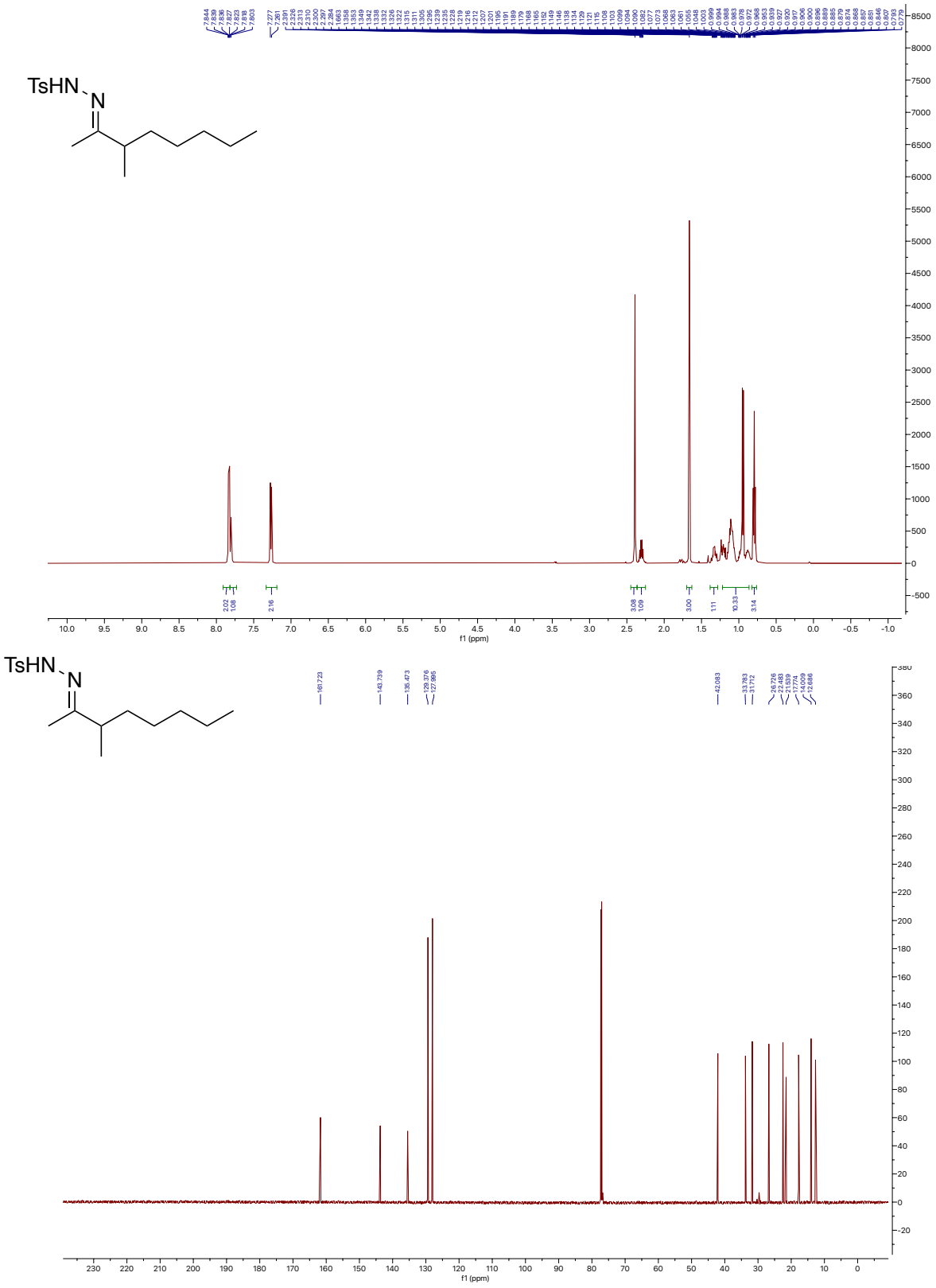


^{1}H NMR (500 MHz, $CDCl_3$) and ^{13}C NMR (126 MHz, $CDCl_3$) of **22c**

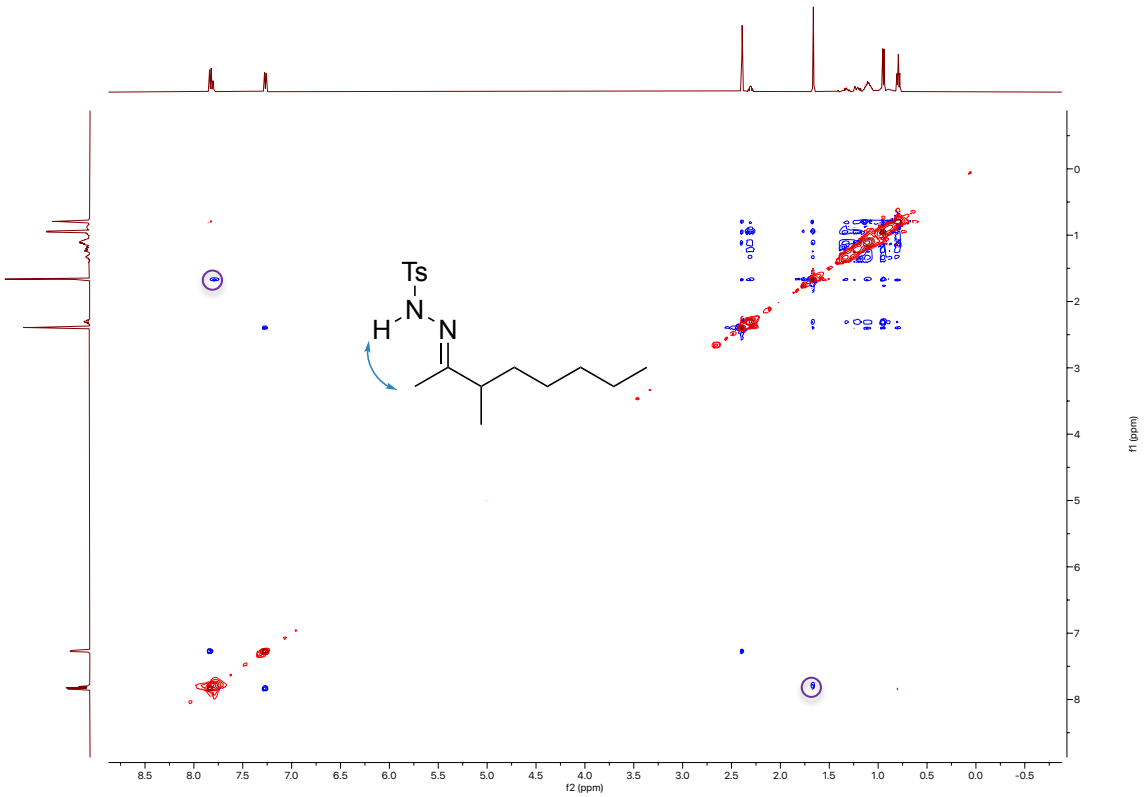




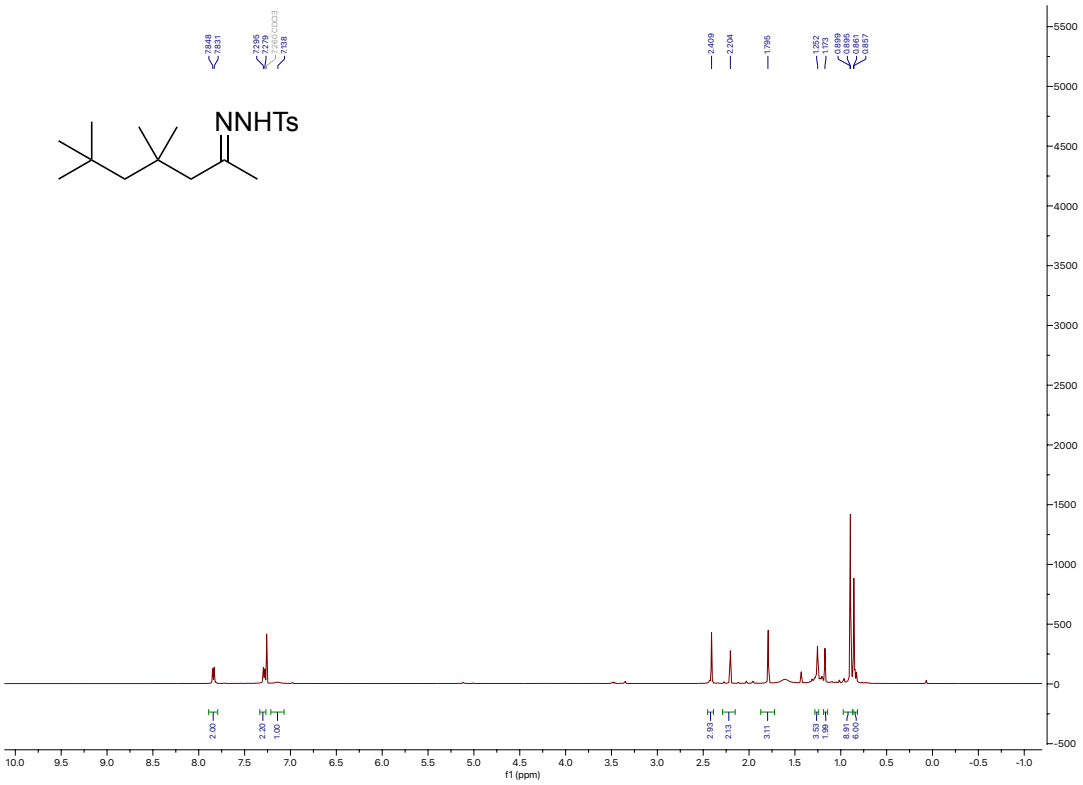
^{1}H NMR (500 MHz, $CDCl_3$) and ^{13}C NMR (126 MHz, $CDCl_3$) of **25e**

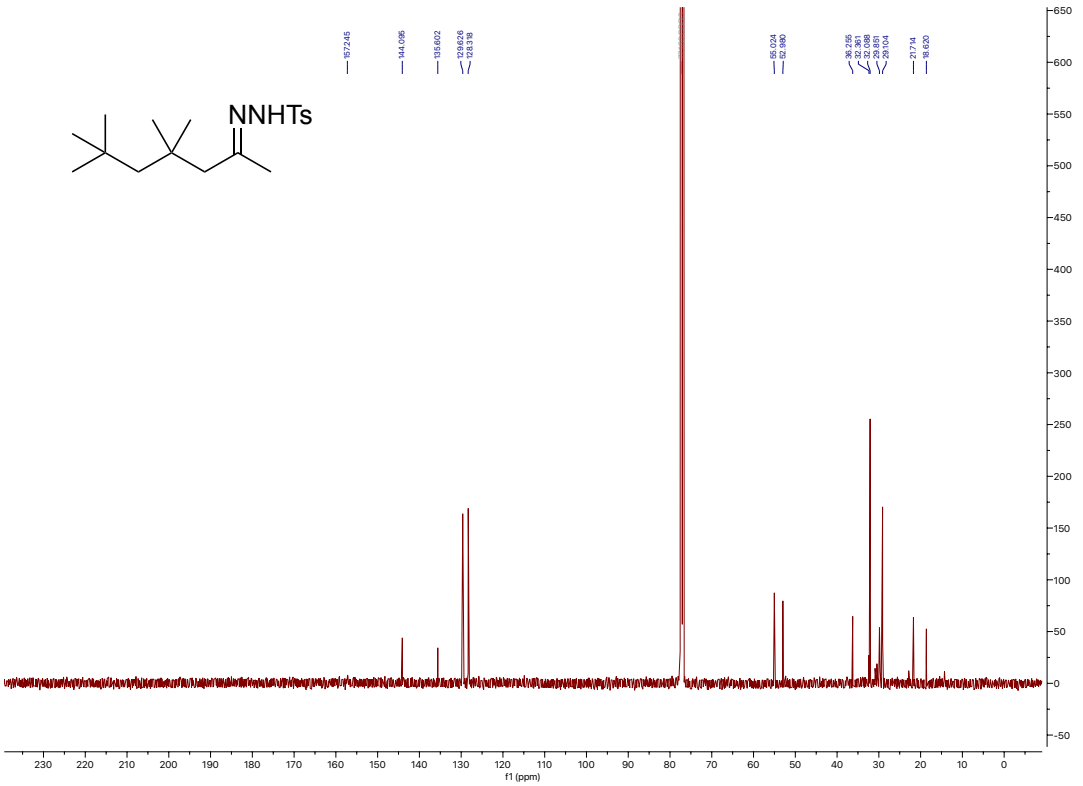


^{1}H NMR (500 MHz, $CDCl_3$) and ^{13}C NMR (126 MHz, $CDCl_3$) of **27e**

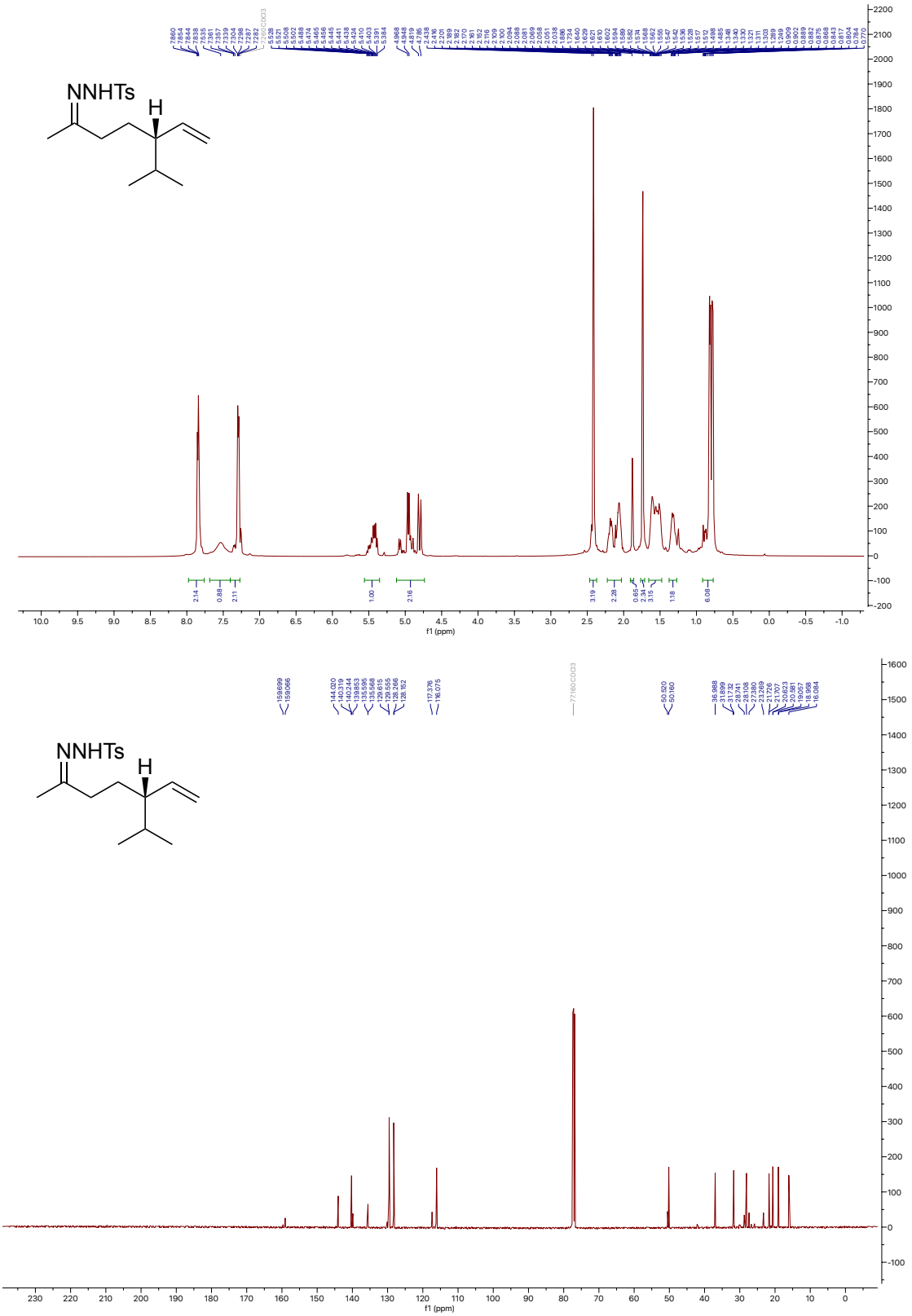


NOESY of Compound **27e**

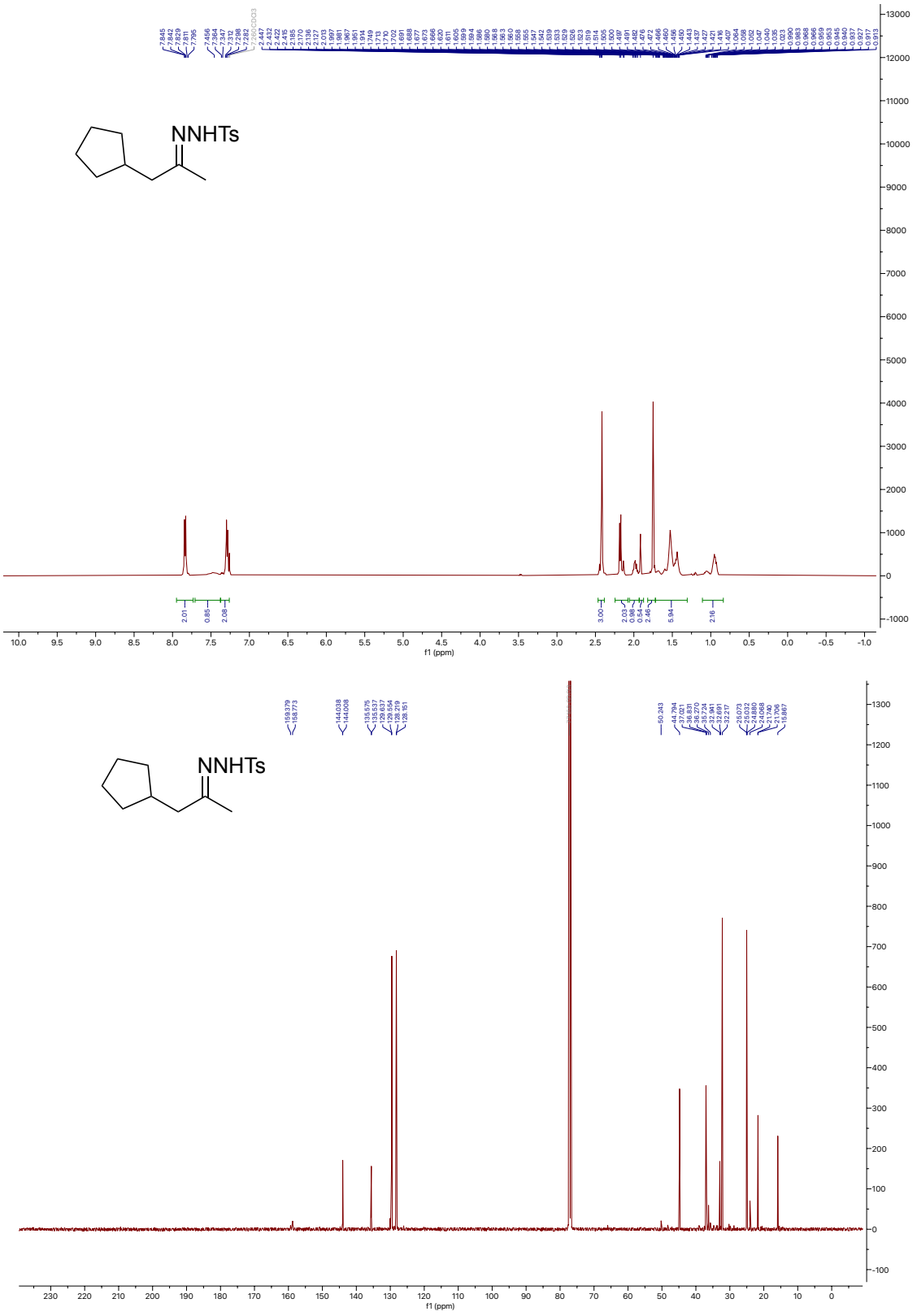




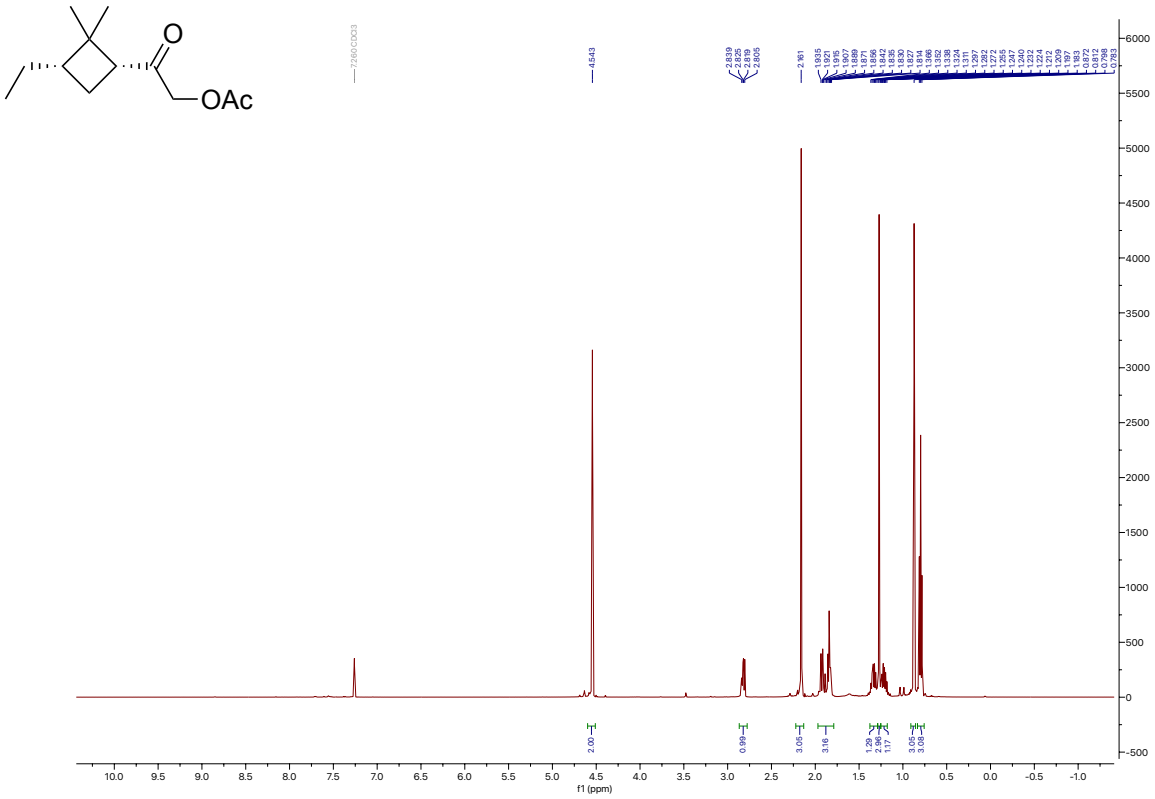
^{1}H NMR (500 MHz, $CDCl_3$) and ^{13}C NMR (126 MHz, $CDCl_3$) of **30e**

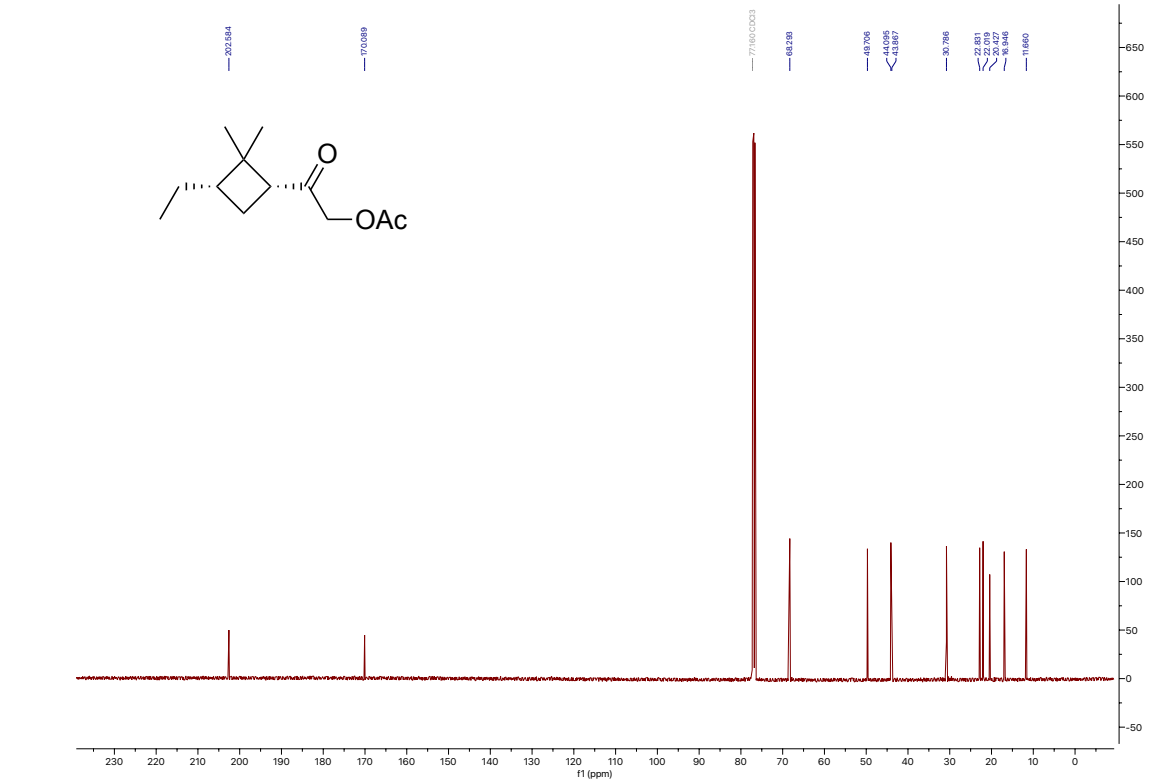


^{1}H NMR (500 MHz, $CDCl_3$) and ^{13}C NMR (126 MHz, $CDCl_3$) of **31e**

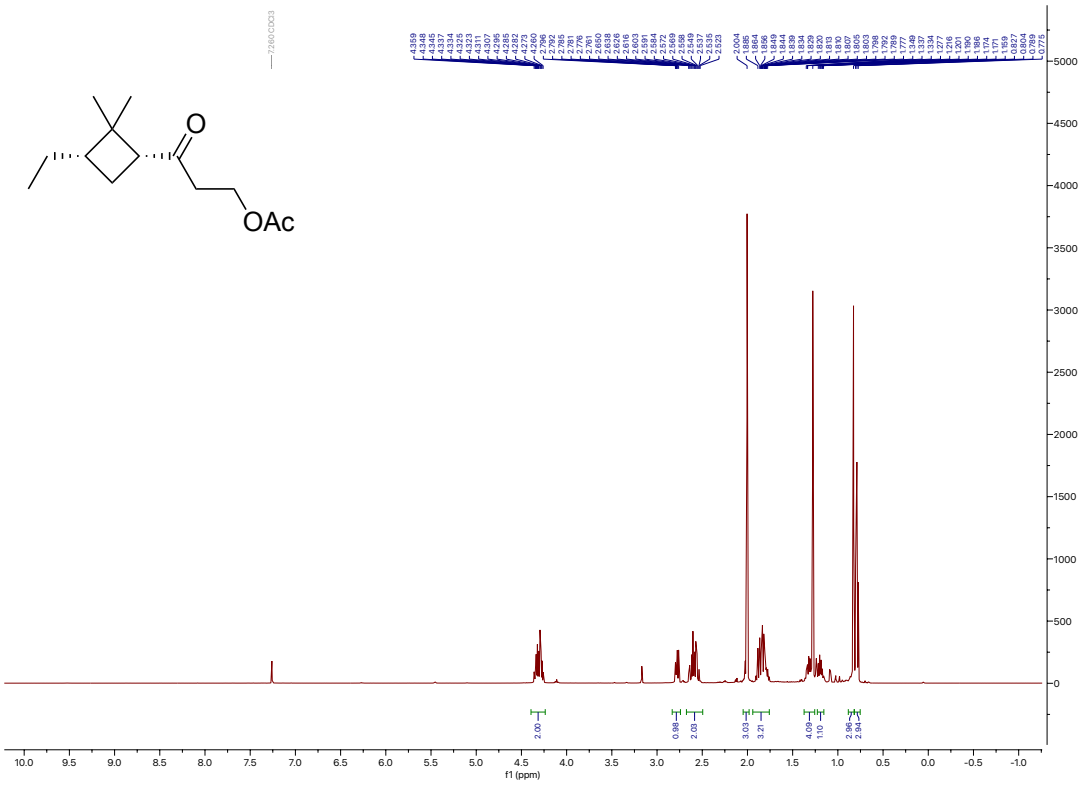


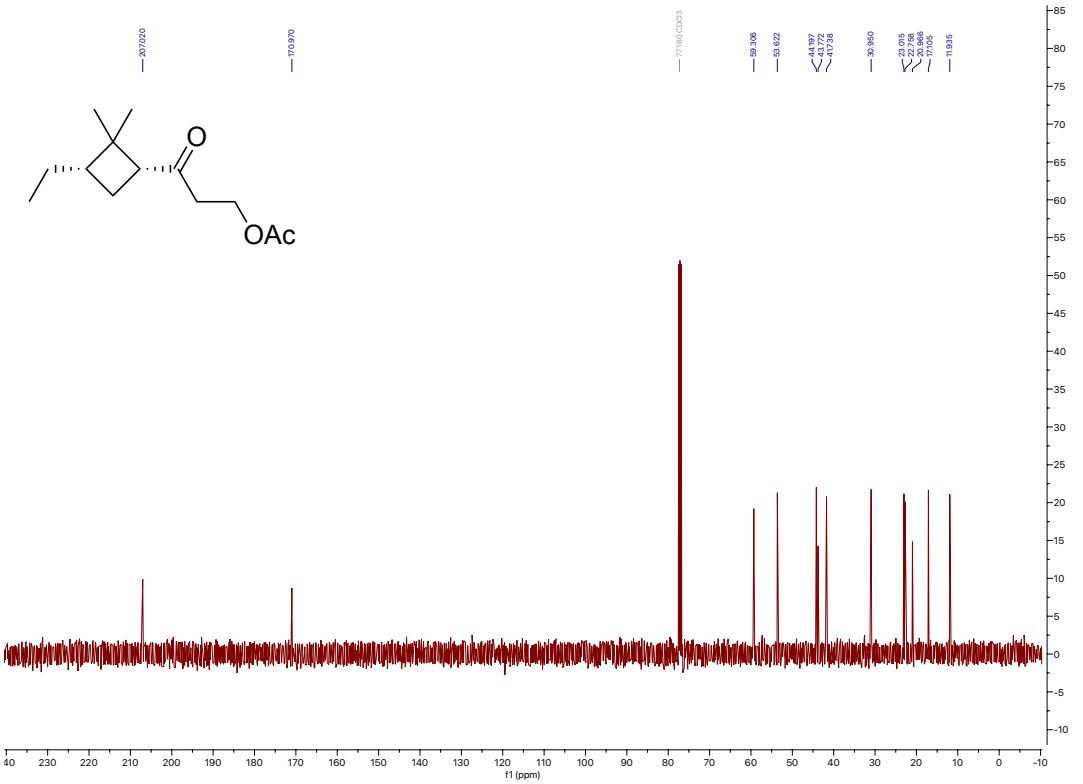
^{1}H NMR (500 MHz, $CDCl_3$) and ^{13}C NMR (126 MHz, $CDCl_3$) of **33e**



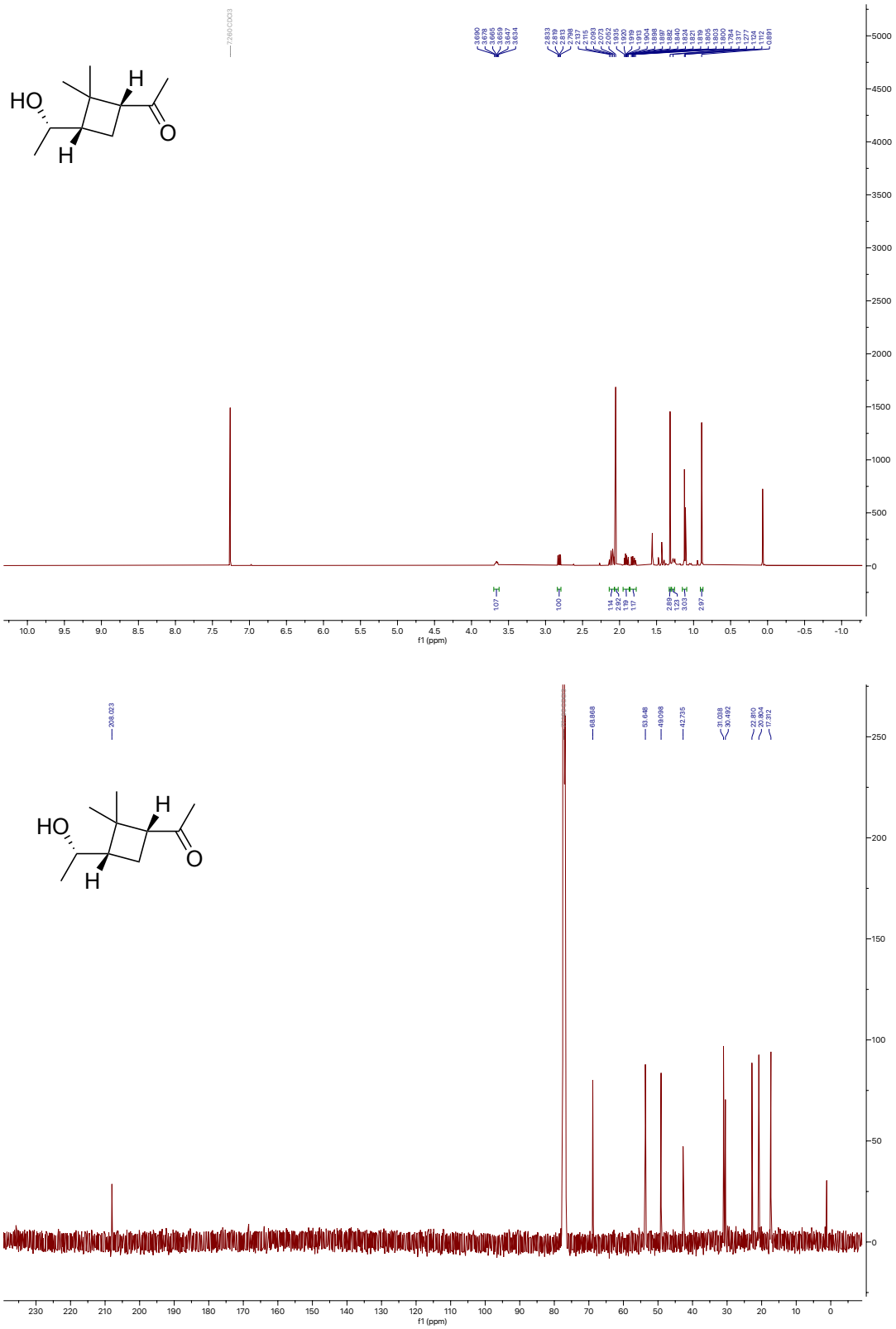


^{1}H NMR (500 MHz, $CDCl_3$) and ^{13}C NMR (126 MHz, $CDCl_3$) of **35c**

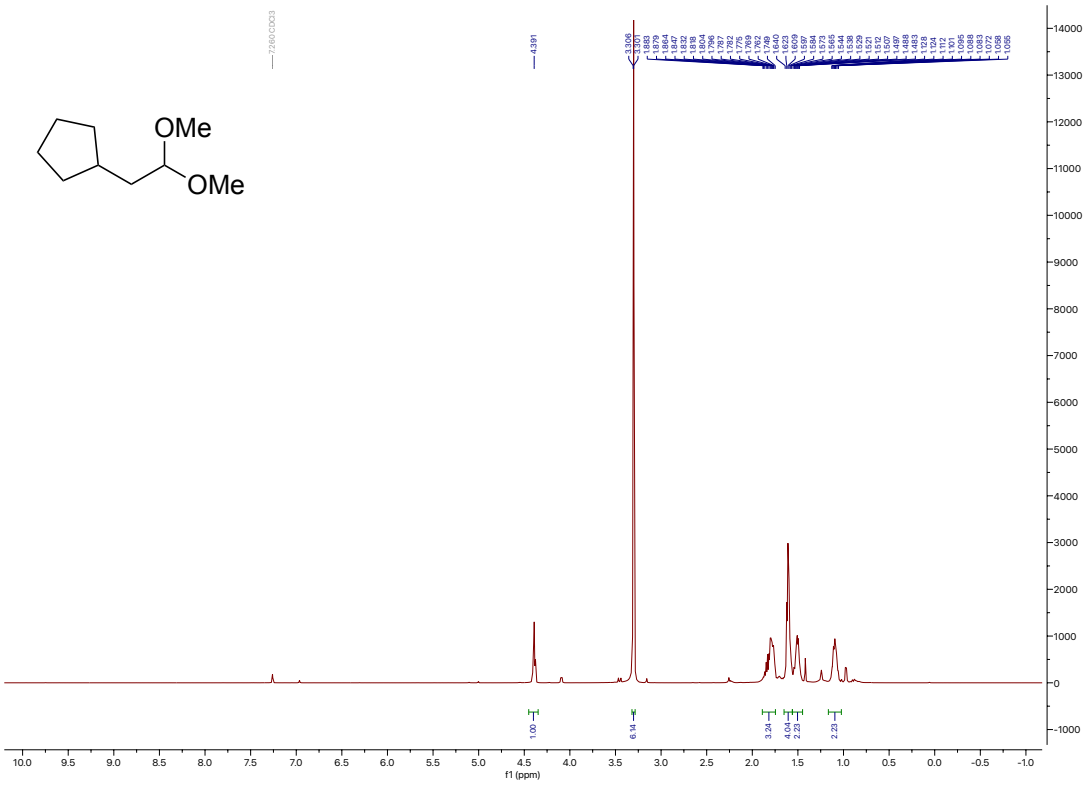


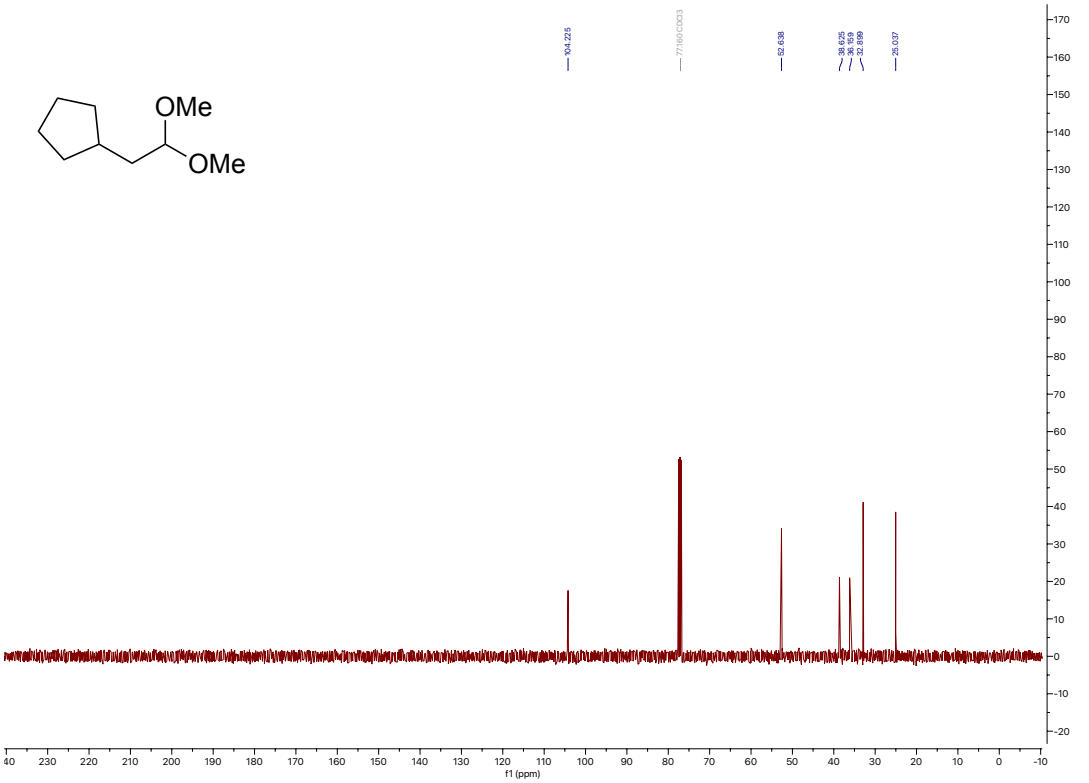


^{1}H NMR (500 MHz, $CDCl_3$) and ^{13}C NMR (101 MHz, $CDCl_3$) of **36c**



^{1}H NMR (500 MHz, $CDCl_3$) and ^{13}C NMR (126 MHz, $CDCl_3$) of **37c**





^{1}H NMR (500 MHz, $CDCl_3$) and ^{13}C NMR (101 MHz, $CDCl_3$) of **38c**

3.6.11. X-Ray Diffraction

$Co(modp)_2(EtOH)_2$ **C1**
CCDC deposition number 2395198.

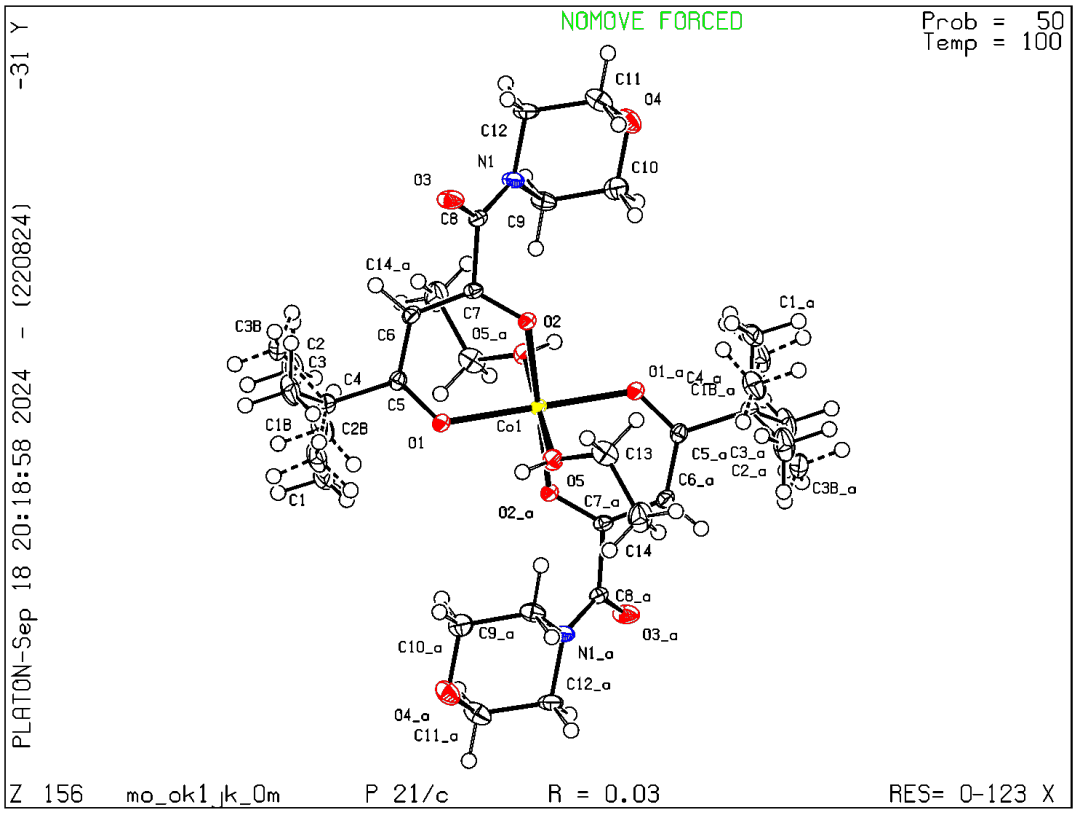


Figure 3.23 X-Ray Structure of $Co(modp)_2(EtOH)_2$

The crystal was formed by within absolute ethanol. An orange, block-shaped crystal of **C1** was mounted on the goniometer. Data were collected from a shock-cooled single crystal at 100(2) K on a Bruker D8 three-axis goniometer three-circle diffractometer with a sealed X-ray tube using a Bruker Apex-II CCD detector. The diffractometer was equipped with an Oxford Cryostream 700 low temperature device and used MoK_α radiation (λ = 0.71073 Å). All data were integrated with SAINT and a multi-scan absorption correction using SADABS was applied [122,123]. The structure was solved by direct methods using SHELXT and refined by full-matrix least-squares methods against F^2 by

SHELXL-2019/1 using ShelXle [124–126]. All non-hydrogen atoms were refined with anisotropic displacement parameters. All C-bound hydrogen atoms were refined with isotropic displacement parameters. Some were refined freely and some on calculated positions using a riding model with their U_{iso} values constrained to 1.5 times the U_{eq} of their pivot atoms for terminal sp^3 carbon atoms and 1.2 times for all other carbon atoms. Disordered moieties were refined using bond lengths restraints and displacement parameter restraints. This report and the CIF file were generated using FinalCif [127].

Refinement Details: All non-hydrogen atoms were refined as anisotropic ellipsoids with no restraints or constraints. All C-H hydrogen atoms were refined along riding positions. The single O-H hydrogen atom position was refined freely with its displacement parameter linked to the connecting oxygen.

Table 3.8 Crystal Data and Structure Refinement for **C1**

CCDC number	
Empirical formula	$C_{28}H_{48}CoN_2O_{10}$
Formula weight	631.61
Temperature [K]	100(2)
Crystal system	monoclinic
Space group (number)	$P2_1/c$ (14)
a [Å]	9.030(5)
b [Å]	14.068(7)
c [Å]	12.424(6)
α [°]	90
β [°]	104.907(11)
γ [°]	90
Volume [Å^3]	1525.2(14)
Z	2
ρ_{calc} [gcm^{-3}]	1.375
μ [mm^{-1}]	0.620
$F(000)$	674
Crystal size [mm^3]	0.247×0.210×0.120
Crystal colour	orange
Crystal shape	block
Radiation	MoK_α (λ=0.71073 Å)
2θ range [°]	4.46 to 56.78 (0.75 Å)
Index ranges	−12 ≤ h ≤ 11 −18 ≤ k ≤ 18 −16 ≤ l ≤ 16
Reflections collected	23658
Independent reflections	3820 R_{int} = 0.0207 R_{sigma} = 0.0135
Completeness to θ = 25.242°	100.0 %
Data / Restraints / Parameters	3820/0/226
Absorption correction T_{min}/T_{max} (method)	0.7002/0.7457 1.065(multi-scan)
Goodness-of-fit on F^2	1.044
Final R indexes [I≥2σ(I)]	R_1 = 0.0263 wR_2 = 0.0680
Final R indexes [all data]	R_1 = 0.0301 wR_2 = 0.0703
Largest peak/hole [eÅ^{-3}]	0.44/−0.25

Table 3.9 Atomic Coordinates and U_{eq} [Å^2] for **C1**

Atom	x	y	z	U_{eq}
Co1	0.500000	0.500000	0.500000	0.01165(7)
N1	0.44497(12)	0.65628(7)	0.82148(8)	0.01743(19)
O1	0.66908(9)	0.58908(5)	0.48442(6)	0.01545(16)
O2	0.42789(9)	0.60044(5)	0.59169(6)	0.01440(15)
O3	0.43641(12)	0.79761(6)	0.73108(7)	0.0256(2)
O4	0.27964(11)	0.53327(6)	0.92650(8)	0.02459(19)
O5	0.35844(10)	0.55775(6)	0.34678(7)	0.01751(16)
H5	0.3919(19)	0.5984(12)	0.3191(13)	0.026(4)
C4	0.86858(13)	0.70375(8)	0.52872(10)	0.0188(2)
C5	0.72283(12)	0.65793(7)	0.54666(9)	0.0139(2)
C6	0.65614(13)	0.69395(7)	0.62963(9)	0.0157(2)
H6	0.709314	0.742646	0.677145	0.019
C7	0.51809(12)	0.66258(7)	0.64588(8)	0.0133(2)
C8	0.46317(13)	0.71152(8)	0.73846(9)	0.0160(2)
C9	0.48147(14)	0.55495(8)	0.83333(9)	0.0194(2)
H9A	0.562802	0.543726	0.902616	0.023
H9B	0.519290	0.532863	0.769555	0.023
C10	0.33918(16)	0.50098(8)	0.83719(10)	0.0235(2)
H10A	0.260631	0.509375	0.765800	0.028
H10B	0.363360	0.432370	0.846801	0.028
C11	0.24461(15)	0.63175(9)	0.91550(11)	0.0252(3)
H11A	0.205841	0.652647	0.979303	0.030
H11B	0.162356	0.642296	0.846548	0.030
C12	0.38227(15)	0.69094(8)	0.91123(9)	0.0222(2)
H12A	0.351925	0.758422	0.898057	0.027
H12B	0.460897	0.686488	0.983159	0.027
C13	0.19510(14)	0.56281(9)	0.31135(10)	0.0244(2)
H13A	0.163054	0.630295	0.303450	0.029
H13B	0.151176	0.533598	0.368736	0.029
C14	0.13336(16)	0.51245(11)	0.20193(12)	0.0313(3)
H14A	0.174699	0.542243	0.144544	0.047
H14B	0.021288	0.516900	0.180337	0.047
H14C	0.163922	0.445442	0.209762	0.047
C1	0.9070(3)	0.66286(16)	0.4241(2)	0.0312(6)
H1A	0.818753	0.671064	0.359668	0.047
H1B	0.930858	0.595055	0.435259	0.047
H1C	0.995657	0.696452	0.410799	0.047
C2	0.9978(3)	0.69436(19)	0.6279(2)	0.0347(6)
H2A	1.019239	0.626855	0.644222	0.052
H2B	0.971734	0.724907	0.691478	0.052
H2C	1.088555	0.725034	0.614026	0.052
C3	0.8355(3)	0.81312(14)	0.5014(2)	0.0279(5)

H3A	0.927243	0.843245	0.488499	0.042
H3B	0.808255	0.844167	0.564263	0.042
H3C	0.750412	0.819471	0.434449	0.042
C1B	0.8412(4)	0.7328(3)	0.4168(3)	0.0317(9)
H1BA	0.798896	0.679501	0.367698	0.048
H1BB	0.937644	0.753524	0.401917	0.048
H1BC	0.767977	0.785638	0.402861	0.048
C2B	0.9919(4)	0.6163(2)	0.5528(3)	0.0274(8)
H2BA	0.954701	0.564881	0.499396	0.041
H2BB	1.003783	0.592545	0.628671	0.041
H2BC	1.091001	0.638968	0.544599	0.041
C3B	0.9398(4)	0.7762(3)	0.6177(3)	0.0326(9)
H3BA	1.043149	0.792120	0.611962	0.049
H3BB	0.945565	0.749427	0.691478	0.049
H3BC	0.876627	0.833784	0.607009	0.049

U_{eq} is defined as 1/3 of the trace of the orthogonalized U_{ij} tensor.

Table 3.10 Anisotropic Displacement Parameters [Å2] for **C1**.
The anisotropic displacement factor exponent takes the form:
$-2\pi^2[\, h^2(a^*)^2U_{11} + k^2(b^*)^2U_{22} + \ldots + 2hka^*b^*U_{12}\,]$

Atom	U_{11}	U_{22}	U_{33}	U_{23}	U_{13}	U_{12}
Co1	0.01611(11)	0.00907(10)	0.01027(10)	−0.00138(7)	0.00428(7)	−0.00287(7)
N1	0.0255(5)	0.0158(4)	0.0134(4)	−0.0011(3)	0.0094(4)	−0.0002(4)
O1	0.0193(4)	0.0128(3)	0.0152(4)	−0.0026(3)	0.0062(3)	−0.0038(3)
O2	0.0175(4)	0.0127(3)	0.0136(3)	−0.0022(3)	0.0049(3)	−0.0026(3)
O3	0.0465(6)	0.0127(4)	0.0234(4)	−0.0027(3)	0.0193(4)	−0.0013(4)
O4	0.0292(5)	0.0217(4)	0.0266(4)	0.0059(3)	0.0140(4)	0.0006(4)
O5	0.0217(4)	0.0151(4)	0.0152(4)	0.0032(3)	0.0037(3)	−0.0016(3)
C4	0.0165(5)	0.0194(5)	0.0224(5)	−0.0060(4)	0.0086(4)	−0.0045(4)
C5	0.0148(5)	0.0117(4)	0.0145(5)	0.0009(4)	0.0024(4)	−0.0008(4)
C6	0.0196(5)	0.0130(5)	0.0141(5)	−0.0026(4)	0.0039(4)	−0.0035(4)
C7	0.0192(5)	0.0107(4)	0.0099(4)	0.0010(3)	0.0038(4)	0.0006(4)
C8	0.0208(5)	0.0148(5)	0.0130(5)	−0.0035(4)	0.0055(4)	−0.0038(4)
C9	0.0261(6)	0.0188(5)	0.0149(5)	0.0042(4)	0.0079(4)	0.0060(4)
C10	0.0327(7)	0.0172(5)	0.0209(6)	0.0012(4)	0.0077(5)	−0.0007(4)
C11	0.0286(6)	0.0256(6)	0.0258(6)	0.0054(5)	0.0148(5)	0.0070(5)
C12	0.0362(7)	0.0190(5)	0.0146(5)	−0.0031(4)	0.0127(5)	−0.0009(5)
C13	0.0223(6)	0.0274(6)	0.0239(6)	0.0059(5)	0.0062(5)	0.0071(5)
C14	0.0230(6)	0.0389(7)	0.0278(7)	0.0056(5)	−0.0014(5)	−0.0052(5)
C1	0.0317(12)	0.0307(12)	0.0401(13)	−0.0143(9)	0.0254(10)	−0.0116(9)
C2	0.0209(10)	0.0470(14)	0.0308(12)	0.0142(10)	−0.0031(9)	−0.0104(9)
C3	0.0259(10)	0.0152(9)	0.0482(13)	0.0049(8)	0.0195(9)	−0.0020(7)
C1B	0.0255(17)	0.043(2)	0.0246(16)	0.0135(15)	0.0035(13)	−0.0131(15)
C2B	0.0196(15)	0.0285(17)	0.0368(19)	0.0045(14)	0.0122(13)	0.0018(12)
C3B	0.0280(18)	0.0330(18)	0.042(2)	−0.0180(16)	0.0193(16)	−0.0163(14)

Table 3.11 Torsion Angles for **C1**

Atom–Atom–Atom–Atom	Torsion Angle [°]
Co1–O1–C5–C6	−10.35(15)
Co1–O1–C5–C4	169.89(7)
C1B–C4–C5–O1	56.2(2)
C2–C4–C5–O1	−117.24(16)
C3B–C4–C5–O1	−171.3(2)
C1–C4–C5–O1	7.95(17)
C3–C4–C5–O1	122.20(13)
C2B–C4–C5–O1	−60.32(18)
C1B–C4–C5–C6	−123.6(2)
C2–C4–C5–C6	62.99(18)
C3B–C4–C5–C6	8.9(2)
C1–C4–C5–C6	−171.82(14)
C3–C4–C5–C6	−57.56(16)
C2B–C4–C5–C6	119.91(17)
O1–C5–C6–C7	−5.32(17)
C4–C5–C6–C7	174.43(10)
Co1–O2–C7–C6	21.49(15)
Co1–O2–C7–C8	−161.01(7)
C5–C6–C7–O2	−1.41(18)
C5–C6–C7–C8	−178.87(10)
C12–N1–C8–O3	3.57(19)
C9–N1–C8–O3	−177.66(11)
C12–N1–C8–C7	−175.16(10)
C9–N1–C8–C7	3.62(16)
O2–C7–C8–O3	−116.03(12)
C6–C7–C8–O3	61.79(15)
O2–C7–C8–N1	62.77(13)
C6–C7–C8–N1	−119.41(11)
C8–N1–C9–C10	−121.87(12)
C12–N1–C9–C10	57.02(12)
C11–O4–C10–C9	58.73(13)
N1–C9–C10–O4	−57.90(12)
C10–O4–C11–C12	−57.57(14)
C8–N1–C12–C11	123.42(12)
C9–N1–C12–C11	−55.50(13)
O4–C11–C12–N1	55.40(14)
Co1–O5–C13–C14	−122.11(10)

Table 3.12 Bond Lengths for **C1**

Atom–Atom	Length [Å]
Co1–O1$^{\#1}$	2.0227(11)
Co1–O1	2.0227(11)
Co1–O2$^{\#1}$	2.0248(10)
Co1–O2	2.0248(10)
Co1–O5	2.1600(11)
Co1–O5$^{\#1}$	2.1601(11)
N1–C8	1.3349(15)
N1–C12	1.4584(15)
N1–C9	1.4620(16)
O1–C5	1.2564(13)
O2–C7	1.2645(13)
O3–C8	1.2338(15)
O4–C11	1.4198(17)
O4–C10	1.4261(16)
O5–C13	1.4285(17)
O5–H5	0.768(17)
C4–C1B	1.409(3)
C4–C2	1.468(2)
C4–C3B	1.519(4)
C4–C5	1.5324(16)
C4–C1	1.540(2)
C4–C3	1.588(2)
C4–C2B	1.635(4)
C5–C6	1.4147(15)
C6–C7	1.3853(16)
C6–H6	0.9500
C7–C8	1.5286(15)
C9–C10	1.5038(18)
C9–H9A	0.9900
C9–H9B	0.9900
C10–H10A	0.9900
C10–H10B	0.9900
C11–C12	1.5085(19)
C11–H11A	0.9900
C11–H11B	0.9900
C12–H12A	0.9900
C12–H12B	0.9900
C13–C14	1.507(2)
C13–H13A	0.9900
C13–H13B	0.9900
C14–H14A	0.9800
C14–H14B	0.9800
C14–H14C	0.9800

C1–H1A	0.9800
C1–H1B	0.9800
C1–H1C	0.9800
C2–H2A	0.9800
C2–H2B	0.9800
C2–H2C	0.9800
C3–H3A	0.9800
C3–H3B	0.9800
C3–H3C	0.9800
C1B–H1BA	0.9800
C1B–H1BB	0.9800
C1B–H1BC	0.9800
C2B–H2BA	0.9800
C2B–H2BB	0.9800
C2B–H2BC	0.9800
C3B–H3BA	0.9800
C3B–H3BB	0.9800
C3B–H3BC	0.9800

Table 3.13 Bond Ancles for **C1**

Atom–Atom–Atom	Angle [°]
O1$^{\#1}$–Co1–O1	180.00(3)
O1$^{\#1}$–Co1–O2$^{\#1}$	88.94(4)
O1–Co1–O2$^{\#1}$	91.06(4)
O1$^{\#1}$–Co1–O2	91.07(4)
O1–Co1–O2	88.93(4)
O2$^{\#1}$–Co1–O2	180.0
O1$^{\#1}$–Co1–O5	91.56(4)
O1–Co1–O5	88.44(4)
O2$^{\#1}$–Co1–O5	88.27(5)
O2–Co1–O5	91.73(5)
O1$^{\#1}$–Co1–O5$^{\#1}$	88.44(4)
O1–Co1–O5$^{\#1}$	91.56(4)
O2$^{\#1}$–Co1–O5$^{\#1}$	91.73(5)
O2–Co1–O5$^{\#1}$	88.27(5)
O5–Co1–O5$^{\#1}$	180.00(4)
C8–N1–C12	123.04(10)
C8–N1–C9	125.18(9)
C12–N1–C9	111.77(9)
C5–O1–Co1	126.90(7)
C7–O2–Co1	121.71(8)
C11–O4–C10	110.81(9)
C13–O5–Co1	128.35(7)
C13–O5–H5	108.6(12)
Co1–O5–H5	117.6(12)
C1B–C4–C3B	117.2(2)
C1B–C4–C5	109.05(16)
C2–C4–C5	111.53(13)
C3B–C4–C5	113.27(15)
C2–C4–C1	111.81(17)
C5–C4–C1	110.72(11)
C2–C4–C3	109.40(15)
C5–C4–C3	108.49(11)
C1–C4–C3	104.61(15)
C1B–C4–C2B	109.7(2)
C3B–C4–C2B	103.4(2)
C5–C4–C2B	103.11(15)
O1–C5–C6	123.71(10)
O1–C5–C4	116.43(9)
C6–C5–C4	119.86(9)
C7–C6–C5	124.04(10)
C7–C6–H6	118.0
C5–C6–H6	118.0
O2–C7–C6	128.55(10)

O2–C7–C8	115.01(10)
C6–C7–C8	116.39(9)
O3–C8–N1	124.63(10)
O3–C8–C7	118.78(10)
N1–C8–C7	116.57(10)
N1–C9–C10	108.85(10)
N1–C9–H9A	109.9
C10–C9–H9A	109.9
N1–C9–H9B	109.9
C10–C9–H9B	109.9
H9A–C9–H9B	108.3
O4–C10–C9	111.12(10)
O4–C10–H10A	109.4
C9–C10–H10A	109.4
O4–C10–H10B	109.4
C9–C10–H10B	109.4
H10A–C10–H10B	108.0
O4–C11–C12	112.13(11)
O4–C11–H11A	109.2
C12–C11–H11A	109.2
O4–C11–H11B	109.2
C12–C11–H11B	109.2
H11A–C11–H11B	107.9
N1–C12–C11	109.14(10)
N1–C12–H12A	109.9
C11–C12–H12A	109.9
N1–C12–H12B	109.9
C11–C12–H12B	109.9
H12A–C12–H12B	108.3
O5–C13–C14	111.58(10)
O5–C13–H13A	109.3
C14–C13–H13A	109.3
O5–C13–H13B	109.3
C14–C13–H13B	109.3
H13A–C13–H13B	108.0
C13–C14–H14A	109.5
C13–C14–H14B	109.5
H14A–C14–H14B	109.5
C13–C14–H14C	109.5
H14A–C14–H14C	109.5
H14B–C14–H14C	109.5
C4–C1–H1A	109.5
C4–C1–H1B	109.5
H1A–C1–H1B	109.5
C4–C1–H1C	109.5

H1A–C1–H1C	109.5
H1B–C1–H1C	109.5
C4–C2–H2A	109.5
C4–C2–H2B	109.5
H2A–C2–H2B	109.5
C4–C2–H2C	109.5
H2A–C2–H2C	109.5
H2B–C2–H2C	109.5
C4–C3–H3A	109.5
C4–C3–H3B	109.5
H3A–C3–H3B	109.5
C4–C3–H3C	109.5
H3A–C3–H3C	109.5
H3B–C3–H3C	109.5
C4–C1B–H1BA	109.5
C4–C1B–H1BB	109.5
H1BA–C1B–H1BB	109.5
C4–C1B–H1BC	109.5
H1BA–C1B–H1BC	109.5
H1BB–C1B–H1BC	109.5
C4–C2B–H2BA	109.5
C4–C2B–H2BB	109.5
H2BA–C2B–H2BB	109.5
C4–C2B–H2BC	109.5
H2BA–C2B–H2BC	109.5
H2BB–C2B–H2BC	109.5
C4–C3B–H3BA	109.5
C4–C3B–H3BB	109.5
H3BA–C3B–H3BB	109.5
C4–C3B–H3BC	109.5
H3BA–C3B–H3BC	109.5
H3BB–C3B–H3BC	109.5

Symmetry transformations used to generate equivalent atoms: #1: 1-X, 1-Y, 1-Z

3.7 References

[1] For the development of dealkenylative functionalization, see: (a) Smaligo, A. J.; Vardhineedi, S.; Kwon, O. Carvone-Derived *P*-Stereogenic Phosphines: Design, Synthesis, and Use in Allene–Imine [3+2] Annulation. *ACS Catal.* **2018**, *8*, 5188–5192. (b) Smaligo, A. J.; Swain, M.; Quintana, J. C.; Tan, M. F.; Kim, D. A.; Kwon, O. Hydrodealkenylative C(sp^3)–C(sp^2) Bond Fragmentation. *Science* **2019**, *364*, 681–685, (c) Smaligo, A. J.; Kwon, O. Dealkenylative Thiylation of C(sp3)–C(sp2) Bonds. *Org. Lett.* **2019**, *21*, 8592–8597. (d) Smaligo, A. J.; Wu, J.; Burton, N. R.; Hacker, A. S.; Shaikh, A. C.; Quintana, J. C.; Wang, R.; Xie, C.; Kwon, O. Oxodealkenylative Cleavage of Alkene C(sp^3)–C(sp^2) Bonds: A Practical Method for Introducing Carbonyls into Chiral Pool Materials. *Angew. Chem., Int. Ed.* **2020**, *59*, 1211–1215. (e) Swain, M.; Sadykhov, G.; Wang, R.; Kwon, O. Dealkenylative Alkenylation: Formal π-Bond Metathesis of Olefins. *Angew. Chem., Int. Ed.* **2020**, *59*, 17565–17571. (f) Swain, M.; Bunnell, T. B.; Kim, J.; Kwon, O. Dealkenylative Alkynylation Using Catalytic Fe(II) and Vitamin C. *J. Am. Chem. Soc.* **2022**, *144*, 14828–14837. (g) He, Z.; Moreno, J. A.; Swain, M.; Wu, J.; Kwon, O. Aminodealkenylation: Ozonolysis and Copper Catalysis Convert C(sp^3)–C(sp^2) Bonds to C(sp^3)–N Bonds. *Science* **2023**, *381*, 877–886. (h) Dehnert, B. W.; Yin, Y.; Kwon, O. Halodealkenylation: Ozonolysis and Catalytic Fe with Vitamin C Convert C(sp^3)–C(sp^2) Bonds to C(sp^3)–Halide Bonds. *Org. Lett.* **2024**, *26*, 10921–10927. (i) Dehnert, B. W.; Dworkin, J. H.; Kwon, O. Dealkenylative Functionalizations: Conversion of Alkene C(sp^3)–C(sp^2) Bonds into C(sp^3)–X Bonds via Redox-Based Radical Processes. *Synthesis* **2024**, *56*, 71–86.

[2] For applications of hydrodealkenylation, see: (a) Ji, J.; Chen, J.; Qin, S.; Li, W.; Zhao, J.; Li, G.; Song, H.; Liu, X.-Y.; Qin, Y. Total Synthesis of Vilmoraconitine. *J. Am. Chem. Soc.* **2023**, *145*, 3903–3908. (b) Kim, D. E.; Zhu, Y.; Harada, S.; Aguilar, I.; Cuomo, A. E.; Wang, M.; Newhouse, T. R. Total Synthesis of (+)-Shearilicine. *J. Am. Chem. Soc.* **2023**, *145*, 4394–4399. (c) Kobayashi, T.; Sugitate, R.; Uchida, K.; Kawamoto, Y.; Ito, H. Asymmetric Total Synthesis of (–)-Lemnalemanane A. *Org. Lett.* **2024**, *26*, 1803–1806. (d) Gu, X.; Zhang, Y.-A.; Zhang, S.; Wang, L.; Ye, X.; Occhialini, G.; Barbour, J.; Pentelute, B. L.; Wendlandt, A. E. Synthesis of Non-Canonical Amino Acids Through Dehydrogenative Tailoring. *Nature* **2024**, *634*, 352–358.

[3] Ertl, P.; Schuhmann, T. A Systematic Cheminformatics Analysis of Functional Groups Occurring in Natural Products. *J. Nat. Prod.* **2019**, *82*, 1258–1263.

[4] (a) Young, W. G.; McKinnis, A. C.; Webb, I. D.; Roberts, J. D. Allylic Rearrangements. XIX. Studies of the Ozonization of Allylic Systems. *J. Am. Chem. Soc.* **1946**, *68**, 293–296. (b) Mosettig, E.; Beglinger, U.; Dolder, F.; Lichti, H.; Quitt, P.; Waters, J. A. The Absolute Configuration of Steviol and Isosteviol. *J. Am. Chem. Soc.* **1963**, *85*, 2305–2309. (c) Bailey, P. S. Chapter IX. Anomalous Ozonolysis of Olefins. In *Ozonation in Organic Chemistry, Volume 1: Olefinic Compounds*; Academic Press, Inc., **1978**; pp 147–184. (d) Odinokov, V. N.; Tolstikov, G. A. Ozonolysis—A Modern Method in the Chemistry of Olefins. *Russ. Chem. Rev.* **1981**, *50*, 636–656. (e) Everest, D. J.; Grant, P. K.; Slim, G. C.; Yeo, I. K. L. A Mechanism for Anomalous Ozonolysis. *Aust. J. Chem.* **1988**, *41*, 1025–1035. (f) DeNinno, M. P. "Anomalous" Ozonolysis of Cyclic Allylic Alcohols: Mechanism and Synthetic Utility. *J. Am. Chem. Soc.* **1995**, *117*, 9927–9928. (g) Zvereva, T. I.; Kasradze, V. G.; Kazakova, O. B.; Kukovinets, O. S. Ozonolysis of

Unsaturated Carbonyl Compounds and Alcohols. *Russ. J. Org. Chem.* **2010**, *46*, 1431–1451. (h) Hanson, J. R. The Ozonolysis of Terpenoids, A Pandora's Box of By-Products. *J. Chem. Res.* **2017**, *41*, 557–563. (i) Fisher, T. J.; Dussault, P. H. Alkene Ozonolysis. *Tetrahedron* **2017**, *73*, 4233–4258.

[5] Ozonolysis incompatible alkenes 3a–20a were treated with ozone at –78 °C in 4:1 methanol/dichloromethane. Thin layer chromatography (TLC) of each crude reaction mixture is provided as qualitative evidence to support the predicted incompatibility (see Figure 3.13). Examples of additional anomalous ozonolysis substrates are compiled from the literature (Figure 3.14–3.20) as supplemental details for pattern recognition.

[6] For references related to non-ozone alkyl peroxide synthesis from alkenes, see: (a) Isayama, S. Development of Novel Methodology in Organic Synthesis Using Cobalt(II) Catalyst. *J. Synth. Org. Chem., Jpn.* **1992**, *50*, 190–201. (b) Shinkai, I.; Alberti, M. N.; Montagnon, T.; Baader, W. J.; Orfanopoulos, M.; Bastos, E. L.; Scarso, A.; Bergsträßer, U.; Shi, Y.; DellaGreca, M.; Stratakis, M.; Hartung, J.; Strukul, G.; Heydt, H.; Tzirakis, M. D.; Iesce, M. R.; Vassilikogiannakis, G.; Lykakis, I. N.; Wang, B. Product Class 1: Alkyl and Cycloalkyl Hydroperoxides. In *Science of Synthesis 5: Compounds with One Saturated Carbon Heteroatom Bond*, 1st ed.; Thieme, **2009**; Vol. 38, pp 9–71. (c) Terent'ev, A. O.; Platonov, M. M.; Levitsky, D. O.; Dembitsky, V. M. Organosilicon and Organogermanium Peroxides: Synthesis and Reactions. *Russ. Chem. Rev.* **2011**, *80*, 807–828. (d) Crossley, S. W. M.; Obradors, C.; Martinez, R. M.; Shenvi, R. A. Mn-, Fe-, and Co-Catalyzed Radical Hydrofunctionalizations of Olefins. *Chem. Rev.* **2016**, *116*, 8912–9000. (e) Gandhi, H.; O'Reilly, K.; Gupta, M. K.; Horgan, C.; O'Leary, E. M.; O'Sullivan, T. P. Advances in the Synthesis of Acyclic Peroxides. *RSC Adv.* **2017**, *7*,

19506–19556. (f) Shevick, S. L.; Wilson, C. V.; Kotesova, S.; Kim, D.; Holland, P. L.; Shenvi, R. A. Catalytic Hydrogen Atom Transfer to Alkenes: A Roadmap for Metal Hydrides and Radicals. *Chem. Sci.* **2020**, *11*, 12401–12422. (g) Yaremenko, I. A.; Radulov, P. S.; Belyakova, Y. Y.; Fomenkov, D. I.; Tsogoeva, S. B.; Terent'ev, A. O. Lewis Acids and Heteropoly Acids in the Synthesis of Organic Peroxides. *Pharmaceuticals* **2022**, *15*, 472. (h) Zhang, K.; Liu, C.; Abdukerem, D.; Mao, Z.; Zhu, W.; Kia, K.; Abdukader, A. Synthesis of α/β-Aromatic Peroxy Thiols Mediated by Iodine Source. *J. Org. Chem.* **2024**, *89*, 3049–3057. (i) Bityukov, O. V.; Serdyuchenko, P. Y.; Kirillov, A. S.; Nikishin, G. I.; Vil, V. A.; Terent'ev, A. O. Advances in Radical Peroxidation with Hydroperoxides. *Beilstein J. Org. Chem.* **2024**, *20*, 2959–3006.

[7] For selected examples of IMP discovery and development, see: (a) Isayama, S.; Mukaiyama, T. A New Method for Preparation of Alcohols from Olefins with Molecular Oxygen and Phenylsilane by the Use of Bis(acetylacetonato)cobalt(II). *Chem. Lett.* **1989**, *18*, 1071–1074. (b) Isayama, S. An Efficient Method for the Direct Peroxygenation of Various Olefinic Compounds with Molecular Oxygen and Triethylsilane Catalyzed by a Cobalt(II) Complex. *Bull. Chem. Soc. Jpn.* **1990**, *63*, 1305–1310. (c) Matsusita, Y.-i.; Sugamoto, K.; Matsui, T. One-Pot Preparation of Alcohols from Aromatic Olefins and Acrylic Acid Derivatives by Cobalt(II) Porphyrin-Catalyzed Reductive Oxygenation Followed by Reduction with Trimethyl Phosphite. *Chem. Lett.* **1993**, *22*, 925–928. (d) Magnus, P.; Payne, A. H.; Waring, M. J.; Scott, D. A.; Lynch, V. Conversion of α,β-Unsaturated Ketones into α-Hydroxy Ketones using an Mn Catalyst, Phenylsilane and Dioxygen: Acceleration of Conjugate Hydride Reduction by Dioxygen. *Tetrahedron Lett.* **2000**, *41*, 9725–9730. (e) O'Neill, P. M.; Hindley, S.; Pugh, M. D.; Davies, J.; Bray, P. G.;

Park, B. K.; Kapu, D. S.; Ward, S. A.; Stocks, P. A. $Co(thd)_2$: A Superior Catalyst for Aerobic Epoxidation and Hydroperoxysilylation of Unactivated Alkenes: Application to the Synthesis of Spiro-1,2,4-Trioxanes. *Tetrahedron Lett.* **2003**, *44*, 8135–8138. (f) Liu, W.; Li, Y.; Liu, K.; Li, Z. Iron-Catalyzed Carbonylation–Peroxidation of Alkenes with Aldehydes and Hydroperoxides. *J. Am. Chem. Soc.* **2011**, *133*, 10756–10759. (g) Peralta-Neel, Z.; Woerpel, K. A. Hydroperoxidations of Alkenes Using Cobalt Picolinate Catalysts. *Org. Lett.* **2021**, *23*, 5002–5006. (h) Bityukov, O. V.; Serdyuchenko, P. Y.; Vil', V. A.; Nikishin, G. L.; He, L.-N.; Terent'ev, A. O. Co-Catalyzed Peroxidation of Cyclic β-Dicarbonyls. *Eur. J. Org. Chem.* **2024**, *27*, No. e202400078.

[8] For examples of IMP in total synthesis, see: (a) Tokuyasu, T.; Kunikawa, S.; Abe, M.; Masuyama, A.; Nojima, M.; Kim, H.-S.; Begum, K.; Wataya, Y. Synthesis of Antimalarial Yingzhaosu A Analogues by the Peroxidation of Dienes with Co(II)/O2/Et3SiH. *J. Org. Chem.* **2003**, *68*, 7361–7367. (b) Hu, X.; Maimone, T. J. Four-Step Synthesis of the Antimalarial Cardamom Peroxide via an Oxygen Stitching Strategy. *J. Am. Chem. Soc.* **2014**, *136*, 5287–5290. (c) Cherney, E. C.; Lopchuk, J. M.; Green, J. C.; Baran, P. S. A Unified Approach to ent-Atisane Diterpenes and Related Alkaloids: Synthesis of (–)-Methyl Atisenoate, (–)-Isoatisine, and the Hetidine Skeleton. *J. Am. Chem. Soc.* **2014**, *136*, 12592–12595. (d) Hilf, J. A.; Witthoft, L. W.; Woerpel, K. A. An SN1-Type Reaction to Form the 1,2-Dioxepane Ring: Synthesis of 10,12-Peroxycalamenene. *J. Org. Chem.* **2015**, *80*, 8262–8267. (e) Gazal, S.; Gupta, P.; Gunturu, S. R.; Isherwood, M.; Voss, M. E. Application of Isayama–Mukaiyama Cobalt Catalyzed Hydroperoxysilylation for the Preparation of Ritonavir Hydroperoxide. *Tetrahedron Lett.* **2016**, *57*, 5099–5102. (f) Xuan, J.; Zhu, A.; Ma, B.; Ding, H.

Diastereoselective Synthesis of the Hydroperoxide–Keto Form of (–)-Steenkrotin B. *Org. Lett.* **2018**, *20*, 4153–4156. (g) Sennari, G.; Gardner, K. E.; Wiesler, S.; Haider, M.; Eggert, A.; Sarpong, R. Unified Total Syntheses of Benzenoid Cephalotane-Type Norditerpenoids: Cephanolides and Ceforalides. *J. Am. Chem. Soc.* **2022**, *144*, 19173–19185. (h) Watanabe, A.; Hikone, Y.; Nagatomo, M.; Inoue, M. Conversion of Phorbol into Des-D-Ring Tricycle and Crotonianoid B via Peroxidation Reaction. *Org. Lett.* **2024**, *26*, 4335–4339.

[9] (a) Johansson, S. G. H.; Emilsson, K.; Grøtli, M.; Börje, A. Structural Influence on Radical Formation and Sensitizing Capacity of Alkylic Limonene Hydroperoxide Analogues in Allergic Contact Dermatitis. *Chem. Res. Toxicol.* **2010**, *23*, 677–688. (b) Nagano, S.; Maeda, N.; Kato, T.; Matsumoto, A.; Maruoka, K. Visible Light-Promoted Alkylation of Electron-Deficient Alkenes with Alkylsilyl Peroxides. *Tetrahedron Lett.* **2023**, *122*, No. 154486. (c) Xie, J.-H.; Kato, T.; Maruoka, K. Carbon-Chain Elongation by Co-Catalyzed Selective C–C Bond Cleavage and Subsequent Silylperoxidation of Alkene Substrates. *ACS Catal.* **2024**, *14*, 14754–14761.

[10] (a) Matsumoto, A.; Maruoka, K. Development of Organosilicon Peroxides as Practical Alkyl Radical Precursors and Their Applications to Transition Metal Catalysis. *Bull. Chem. Soc. Jpn.* **2021**, *94*, 513–524. (b) Gao, P.; Niu, Y.-J.; Yang, F.; Guo, L.-N.; Duan, X.-H. Three-component 1,2-Dicarbofunctionalization of Alkene Involving Alkyl Radicals. *Chem. Commun.* **2022**, *58*, 730–746. (c) Dworkin, J. H.; Dehnert, B. W.; Kwon, O. When All C–C Breaks LO-Ose. *Trends Chem.* **2023**, *5*, 174–200. (d) Harada, S.; Cantrell, R.; Tyler, T.; Newman, J.; Aguilar, I.; Wang, M.; Kim, D.; Zhu, Y.; Newhouse, T.

Ozone-Free Protocol for Hydrodealkenylation via Peroxide Formation and Fragmentation. *ChemRxiv*, **2025**, DOI: 10.26434/chemrxiv-2025-xwbdj.

[11] Vreshch, V. D.; Yang, J.-H.; Zhang, H.; Filatov, A. S.; Dikarev, E. V. Monomeric Square-Planar Cobalt(II) Acetylacetonate: Mystery or Mistake? *Inorg. Chem.* **2010**, *49*, 8430–8434.

[12] Olson, A. S.; Jameson, A. J.; Kyasa, S. K.; Evans, B. W.; Dussault, P. H. Reductive Cleavage of Organic Peroxides by Iron Salts and Thiols. *ACS Omega* **2018**, *3*, 14054–14063.

[13] (a) Kolonko, K. J.; Shapiro, R. H.; Barkley, R. M.; Sievers, R. E. Ozonation of Caffeine in Aqueous Solution. *J. Org. Chem.* **1979**, *44*, 3769–3778,. (b) Tentscher, P. R.; Bourgin, M.; von Gunten, U. Ozonation of Para-Substituted Phenolic Compounds Yields p-Benzoquinones, Other Cyclic α,β-Unsaturated Ketones, and Substituted Catechols. *Environ. Sci. Technol.* **2018**, *52*, 4763–4773.

[14] Zimmer, H.; Amer, A.; Ho, D.; Koch, K.; Schumacher, C.; Wingfield, R. C. A Novel Oxidative Skeleton Rearrangement of the Caffeine System. *J. Org. Chem.* **1990**, *55*, 4988–4989.

[15] (a) Fliszár, S.; Granger, M. A Quantitative Investigation of the Ozonolysis Reaction. VIII. On the Direction of Cleavage of Primary Ozonides of Selected Unsymmetrical Olefins. *J. Am. Chem. Soc.* **1969**, *91*, 3330–3337. (b) Fliszár, S.; Carles, J. Quantitative Investigation of the Ozonolysis Reaction. IX. On the Mechanism of Ozonide Formation. *Can. J. Chem.* **1969**, *47*, 3921–3929. (c) Fliszár, S.; Granger, M. A Quantitative Investigation of the Ozonolysis Reaction. XI. On the Effects of Substituents

in Directing Ozone Cleavage of trans-1,2-Disubstituted Ethylenes. *J. Am. Chem. Soc.* **1970**, *92*, 3361–3369.

[16] Dimitrov, V.; Rentsch, G. H.; Linden, A.; Hesse, M. The Ozonolysis of Longifolene: A Tool for the Preparation of Useful Chiral Compounds. Configuration Determination of New Stereogenic Centers by NMR Spectroscopy and X-Ray Crystallography. *Helv. Chim. Acta* **2003**, *86*, 106–121.

[17] Tannenbaum, S.; Kaye, S.; Lewenz, G. F. Synthesis and Properties of Some Alkylsilanes. *J. Am. Chem. Soc.* **1953**, *75*, 3753–3757.

[18] Data were obtained from the "Hazardous Substances Data Bank", National Library of Medicine (US).

[19] Gumulka, J.; Smith, L. L. Ozonization of Cholesterol. *J. Am. Chem. Soc.* **1983**, *105*, 1972–1979.

[20] (a) Leifert, D.; Studer, A. The Persistent Radical Effect in Organic Synthesis. *Angew. Chem., Int. Ed.* **2020**, *59*, 74–108. (b) Mei, R.; Dhawa, U.; Samanta, R. C.; Ma, W.; Wencel-Delord, J.; Ackermann, L. Cobalt-Catalyzed Oxidative C–H Activation: Strategies and Concepts. *ChemSusChem* **2020**, *13*, 3306–3356. (c) Reese, P. B. Remote Functionalization Reactions in Steroids: Discovery and Application. *Steroids* **2024**, *204*, No. 109362.

[21] Beckwith, A. L. J.; Kazlauskas, R.; Syner-Lyons, M. R. β-Fission of 9-Decalinoxyl Radicals: Reversible Formation of 6-Ketocyclodecyl Radical. *J. Org. Chem.* **1983**, *48*, 4718–4722.

[22] (a) Bozzato, G.; Bachmann, J.-P.; Pesaro, M. Stereoselective Addition of Methylcuprates to a 2-Formyl-cyclohexa-2,5-dienone System. A Stereoselective Total Synthesis of Racemic β-Vetivone. *J. Chem. Soc., Chem. Commun.* **1974**, *23*, 1005–1006. (b) Paryzek, Z.; Rychlewska, U. Ozonolysis of Cholesterol and other Δ^5-Steroids in the Presence of Alcohols: A Revised Mechanism and Hydroperoxide Structure of the Solvent-Participated Product, Confirmed by X-ray Analysis. *J. Chem. Soc., Perkin Trans. 2* **1997**, 2313–2318. (c) Thomas, A. F.; Perret, C. 4-(1-Hydroperoxy-1-methylethyl)-1,3-cyclopentadienyl Methyl Ketone: Its Formation from α-Terpineol and Behaviour as a Dimethylfulvene Epoxide. *Tetrahedron* **1986**, *42*, 3311–3321. (d) Leviss, D. H.; Van Ry, D. A.; Hinrichs, R. Z. Multiphase Ozonolysis of Aqueous α-Terpineol. *Environ. Sci. Technol.* **2016**, *50*, 11698–11705.

[23] (a) Deng, M.; Chu, M.; Li, N.; Sun, G.; Li, F.; Guo, D.; Kang, G.; Ji, B. Aerobic C–C Bond Cleavage of Allylic Alcohols via Co-Catalyzed Hydrogen Atom Transfer. *Org. Lett.* **2023**, *25*, 2420–2425. (b) Bagkavou, G. G.; Stathakis, C. I. Iron(III) Catalyzed Aerobic $C_\alpha - C_\beta$ Cleavage of Allylic Alcohols. *Eur. J. Org. Chem.* **2024**, *27*, No. e202400556.

[24] (a) Cieplak, A. S. Stereochemistry of Nucleophilic Addition to Cyclohexanone. The Importance of Two-Electron Stabilizing Interactions. *J. Am. Chem. Soc.* **1981**, *103*, 4540–4552. (b) Giese, B. The Stereoselectivity of Intermolecular Free Radical Reactions. *Angew. Chem., Int. Ed. Engl.* **1989**, *28*, 969–1146.

[25] Gemma, S.; di Cerbo, L.; Relitti, N.; Vallone, A.; Brindisi, M.; Brogi, S.; Chemi, G.; Novellino, E.; Campiani, G.; Butini, S. Synthetic Studies Toward Bicyclic Endoperoxides Presenting Polar Side Chains. *Tetrahedron Lett.* **2018**, *59*, 4330–4333.

[26] Odinokov, V. N. Ozonolysis of Alkenes and Study of Reactions of Polyfunctional Compounds. X. Peroxide Products of the Ozonolysis of Derivatives of bicyclo[2.2.1]hept-5-en-2,3-di- and -2-carboxylic acids. *Zh. Org. Khim.* **1977**, *13*, 2342–2353.

[27] Beesley, R. M.; Ingold, C. K.; Thorpe, J. F. CXIX.—The Formation and Stability of spiro-Compounds. Part I. spiro-Compounds from Cyclohexane. *J. Chem. Soc., Trans.* **1915**, *107*, 1080–1106.

[28] Acharya, S. P. Conformations of 3-Carene and 2-Carene. Their Conformational Preference and the Reactivity of the Double Bond. *Tetrahedron Lett.* **1966**, *7*, 4117–4122.

[29] Kochi's comparison of *t*-butyl hydroperoxide, α-butoxyethyl hydroperoxide, and cumyl hydroperoxide, quantifies alkoxyl radical fragmentation which occurred with 48–55%, 90%, and quantitative conversions, respectively: Kochi, J. K. Chemistry of Alkoxy Radicals: Cleavage Reactions. *J. Am. Chem. Soc.* **1962**, *84*, 1193–1197.

[30] Salamone, M.; Bietti, M. Reaction Pathways of Alkoxy Radicals. The Role of Solvent Effects on C–C Bond Fragmentation and Hydrogen Atom Transfer Reactions. *Synlett* **2014**, *25*, 1803–1816.

[31] (a) Fittschen, C.; Hippler, H.; Viskolcz, B. The C–C Bond Scission in Alkoxy Radicals: Thermal Unimolecular Decomposition of *t*-Butoxy Radicals. *Phys. Chem. Chem. Phys.* **2000**, *2*, 1677–1683. (b) Vereecken, L.; Peeters, J. Decomposition of Substituted Alkoxy Radicals—Part I: A Generalized Structure–Activity Relationship for Reaction Barrier Heights. *Phys. Chem. Chem. Phys.* **2009**, *11*, 9062–9074.

[32] This value was derived taking into consideration the common pre-exponential factor (A) for the β-C–C bond scission rate constants of alkoxyl radicals ($A = 10^{14}$ s^{-1}, ref

31a) and the activation energy (E) for the β-scission of the α-methoxy-isopropoxyl radical (7.1 kcal mol^{-1}, ref 31b).

[33] Baciocchi, E.; Bietti, M.; Salamone, M.; Steenken, S. Spectral Properties and Absolute Rate Constants for β-Scission of Ring Substituted Cumyloxy Radicals. A Laser Flash Photolysis Study. *J. Org. Chem.* **2002**, *67*, 2266–2270.

[34] This value was derived taking into consideration the common pre-exponential factor (A) for the β-C–C bond scission rate constants of alkoxyl radicals ($A = 10^{14}$ s^{-1}, ref 31a) and the activation energy (E) for the β-scission of the *t*-butoxyl radical (13.9 kcal mol^{-1}, ref 31b).

[35] This value was derived taking into consideration the common pre-exponential factor (A) for the β-C–C bond scission rate constants of alkoxyl radicals ($A = 10^{14}$ s^{-1}, ref 31a) and the activation energy (E) for the β-scission of the *iso*-propoxyl radical (15.1 kcal mol^{-1}, ref 31b).

[36] This value was derived taking into consideration the common pre-exponential factor (A) for the β-C–C bond scission rate constants of alkoxyl radicals ($A = 10^{14}$ s^{-1}, ref 31a) and the activation energy (E) for the β-scission of the ethoxyl radical (18.8 kcal mol^{-1}, ref 31b).

[37] This value was derived taking into consideration the common pre-exponential factor (A) for the β-C–C bond scission rate constants of alkoxyl radicals ($A = 10^{14}$ s^{-1}, ref 31a) and the activation energy (E) for the β-scission of the 2-methylbutan-2-oxyl radical (9.7 kcal mol^{-1}, ref 31b).

[38] This value was derived taking into consideration the common pre-exponential factor (A) for the β-C–C bond scission rate constants of alkoxyl radicals ($A = 10^{14}$ s^{-1}, ref 31a) and the activation energy (E) for the β-scission of the 2,3-dimethylbutan-2-oxyl radical (6.6 kcal mol^{-1}, ref 31b).

[39] This value was derived taking into consideration the common pre-exponential factor (A) for the β-C–C bond scission rate constants of alkoxyl radicals ($A = 10^{14}$ s^{-1}, ref 31a) and the activation energy (E) for the β-scission of the 2,3,3-trimethylbutan-2-oxyl radical (4.2 kcal mol^{-1}, ref 31b).

[40] (a) Beckwith, A. L. J.; Hay, B. P. Kinetics of the Reversible β-Scission of the Cyclopentyloxy Radical. *J. Am. Chem. Soc.* **1989**, *111*, 230–234. (b) Beckwith, A. L. J.; Hay, B. P. Kinetics and Mechanism of the Exo Cyclizations of ω-Formylalkyl Radicals. *J. Am. Chem. Soc.* **1989**, *111*, 2674–2681.

[41] Fordham, J. W. L.; Williams, H. L. The Decomposition of Cumene Hydroperoxide by Ferrous Iron in the Presence of Oxygen. *J. Am. Chem. Soc.* **1950**, *72*, 4465–4469.

[42] (a) Huston, P.; Espenson, J. H.; Bakac, A. Kinetics of Formation and Reactions of Thiyl Radicals in Aqueous Solution. *Inorg. Chem.* **1992**, *31*, 720–722. (b) Denisov, E.; Chatgilialoglu, C.; Shestakov, A.; Denisova, T. Rate Constants and Transition-State Geometry of Reactions of Alkyl, Alkoxyl, and Peroxyl Radicals with Thiols. *Int. J. Chem. Kinet.* **2009**, *41*, 284–293. (c) Dénès, F.; Pichowicz, M.; Povie, G.; Renaud, P. Thiyl Radicals in Organic Synthesis. *Chem. Rev.* **2014**, *114*, 2587–2693.

[43] (a) Hawari, J. A.; Engel, P. S.; Griller, D. Rate Constants for the Reactions of Alkyl Radicals with 1,4-Cyclohexadiene. *Int. J. Chem. Kinet.* **1985**, *17*, 1215–1219. (b) Atkinson, R. Gas-Phase Tropospheric Chemistry of Volatile Organic Compounds: 1.

Alkanes and Alkenes. *J. Phys. Chem. Ref. Data* **1997**, *26*, 215–290. (c) Martínez, E.; Cabañas, B.; Aranda, A.; Martín, P.; Salgado, S. Absolute Rate Coefficients for the Gas-Phase Reactions of NO3 Radical with a Series of Monoterpenes at $T = 298$ to 433 K. *J. Atmos. Chem.* **1999**, *33*, 265–282. (d) Fouqueau, A.; Cirtog, M.; Cazaunau, M.; Pangui, E.; Doussin, J.-F.; Picquet-Varrault, B. A Comparative and Experimental Study of the Reactivity with Nitrate Radical of Two Terpenes: α-Terpinene and γ-Terpinene. *Atmos. Chem. Phys.* **2020**, *20*, 15167–15189. (e) Bhunia, A.; Studer, A. Recent Advances in Radical Chemistry Proceeding Through Pro-Aromatic Radicals. *Chem* **2021**, *7*, 2060–2100.

[44] Adewuyi, Y. G.; Carmichael, G. R. Kinetics of Oxidation of Dimethyl Sulfide by Hydrogen Peroxide in Acidic and Alkaline Medium. *Environ. Sci. Technol.* **1986**, *20*, 1017–1022.

[45] Buzsaki, S. R.; Mason, S. M.; Kattamuri, P. V.; Serviano, J. M. L.; Rodriguez, D. N.; Wilson, C. V.; Hood, D. M.; Ellefsen, J. D.; Lu, Y.-C.; Kan, J.; West, J. G.; Miller, S. J.; Holland, P. L. Fe/Thiol Cooperative Hydrogen Atom Transfer Olefin Hydrogenation: Mechanistic Insights That Inform Enantioselective Catalysis. *J. Am. Chem. Soc.* **2024**, *146*, 17296–17310.

[46] (a) Baignée, A.; Howard, J. A.; Scaiano, J. C.; Stewart, L. C. Absolute Rate Constants for Reactions of Cumyloxy in Solution. *J. Am. Chem. Soc.* **1983**, *105*, 6120–6123. (b) Avila, D. V.; Brown, C. E.; Ingold, K. U.; Lusztyk, J. Solvent Effects on the Competitive β-Scission and Hydrogen Atom Abstraction Reactions of the Cumyloxy Radical: Resolution of a Long-Standing Problem. *J. Am. Chem. Soc.* **1993**, *115*, 466–470.

[47] Szuppa, T.; Stolle, A.; Ondruschka, B.; Hopfe, W. Solvent-Free Dehydrogenation of γ-Terpinene in a Ball Mill: Investigation of Reaction Parameters. *Green Chem.* **2010**, *12*, 1288–1294.

[48] Neutral, protic ligands are stronger acids when bound to the metal than unbound: (a) Parkin, G. Synthetic Analogues Relevant to the Structure and Function of Zinc Enzymes. *Chem. Rev.* **2004**, *104*, 699–767. (b) Salazar-Salinas, K.; Baldera-Aguayo, P. A.; Encomendero-Risco, J. J.; Orihuela, M.; Sheen, P.; Seminario, J. M.; Zimic, M. Metal-Ion Effects on the Polarization of Metal-Bound Water and Infrared Vibrational Modes of the Coordinated Metal Center of Mycobacterium tuberculosis Pyrazinamidase via Quantum Mechanical Calculations. *J. Phys. Chem. B* **2014**, *118*, 10065–10075.

[49] MeOH, $\mathrm{p}K_\mathrm{a} = 16$; Me3SiOH, $\mathrm{p}K_\mathrm{a} = 11$; PhSH, $\mathrm{p}K_\mathrm{a} = 6.81$: (a) West, R.; Baney, R. H. Hydrogen Bonding Studies. II. The Acidity and Basicity of Silanols Compared to Alcohols. *J. Am. Chem. Soc.* **1959**, *81*, 6145–6148. (b) Kagiya, T.; Sumida, Y.; Tachi, T. An Infrared Spectroscopic Study of Hydrogen Bonding Interaction. Structural Studies of Proton-Donating and -Accepting Powers. *Bull. Chem. Soc. Jpn.* **1970**, *43*, 3716–3722. (c) Chuchani, G.; Frohlich, A. The $\mathrm{p}K_\mathrm{a}$ Values of Mono-Substituted Phenols and Benzenethiols and the Conjugation of Substituents Having a Strong +K Effect. *J. Chem. Soc. B* **1971**, 1417–1420.

[50] Despite the unfavorable acid equilibrium constants (ref 49) for an exchange of methanol and silanol, the resulting decrease in cone angle and the statistical excess of methanol can provide some compensation for this substitution. Furthermore, with GCMS we observed triethyl(methoxy)silane and bis(triethylsilyl)ether as secondary reaction analytes which serves as evidence for the removal of triethylsilanol from iron.

[51] Isayama, S. An Efficient Method for the Direct Peroxygenation of Various Olefinic Compounds with Molecular Oxygen and Triethylsilane Catalyzed by a Cobalt(II) Complex. *Bull. Chem. Soc. Jpn.* **1990**, *63* (5), 1305–1310.

[52] O'Neill, P. M.; Hindley, S.; Pugh, M. D.; Davies, J.; Bray, P. G.; Park, B. K.; Kapu, D. S.; Ward, S. A.; Stocks, P. A. $Co(thd)_2$: A Superior Catalyst for Aerobic Epoxidation and Hydroperoxysilylation of Unactivated Alkenes: Application to the Synthesis of Spiro-1,2,4-Trioxanes. *Tetrahedron Lett.* **2003**, *44* (44), 8135–8138.

[53] He, Z.; Moreno, J. A.; Swain, M.; Wu, J.; Kwon, O. Aminodealkenylation: Ozonolysis and Copper Catalysis Convert $C(sp^3)$–$C(sp^2)$ Bonds to $C(sp^3)$–N Bonds. *Science* **2023**, *381* (6660), 877–886.

[54] Selmani, A.; Schoenebeck, F. Anti-Markovnikov Hydrogermylation of Alkenes via Lewis Acid Catalysis. *Synthesis* **2023**, *55* (11), 1792–1798.

[55] Gresser, M. J.; Wales, S. M.; Keller, P. A. The Attempted Stereoselective Synthesis of Chiral 2,2'-biindoline. *Tetrahedron* **2010**, *66* (34), 6965–6976.

[56] García, C.; León, L. G.; Pungitore, C. R.; Ríos-Luci, C.; Daranas, A. H.; Montero, J. C.; Pandiella, A.; Tonn, C. E.; Martín, V. S.; Padrón, J. M. Enhancement of Antiproliferative Activity by Molecular Simplification of Catalpol. *Bioorg. Med. Chem.* **2010**, *18* (7), 2515–2523.

[57] Djerassi, C.; Krakower, G. W. Optical Rotatory Dispersion Studies. XXI. Effect of Ring Size. *J. Am. Chem. Soc.* **1959**, *81* (1), 237–242.

[58] (a) Kelley, B. T.; Walters, J. C.; Wengryniuk, S. E. Access to Diverse Oxygen Heterocycles via Oxidative Rearrangement of Benzylic Tertiary Alcohols. *Org. Lett.* **2016**,

18 (8), 1896–1899. (b) Friedfeld, M. R.; Shevlin, M.; Margulieux, G. W.; Campeau, L.-C.; Chirik, P. J. Cobalt-Catalyzed Enantioselective Hydrogenation of Minimally Functionalized Alkenes: Isotopic Labeling Provides Insight into the Origin of Stereoselectivity and Alkene Insertion Preferences. *J. Am. Chem. Soc.* **2016**, *138* (10), 3314–3324.

[59] Marković, D.; Tchawou, W. A.; Novosjolova, I.; Laclef, S.; Stepanovs, D.; Turks, M.; Vogel, P. Synthesis and Applications of Silyl 2-Methylprop-2-ene-1-sulfinates in Preparative Silylation and GC-Derivatization Reactions of Polyols and Carbohydrates. *Chem. Eur. J.* **2016**, *22* (12), 4196–4205.

[60] Barrett, R. R. G.; Campbell, D. A.; Gleason, J. L. An Organocatalytic Oxy-Cope/Michael Cascade Reaction. *Org. Lett.* **2023**, *25* (5), 777–781.

[61] (a) Ogawa, T.; Nozaki, M.; Matsui, M. Total Synthesis of Stevioside. *Tetrahedron* **1980**, *36* (19), 2641–2648. (b) Khaibullin, R. N.; Strobykina, I. Y.; Kataev, V. E.; Lodochnikova, O. A.; Gubaidullin, A. T.; Musin, R. Z. New Synthesis of Diterpenoid (16S)-Dihydrosteviol. *Russ. J. Gen. Chem.* **2009**, *79* (5), 967–971.

[62] Ukiya, M.; Sawada, S.; Kikuchi, T.; Kushi, Y.; Fukatsu, M.; Akihisa, T. Cytotoxic and Apoptosis-Inducing Activities of Steviol and Isosteviol Derivatives Against Human Cancer Cell Lines. *Chem. Biodiversity* **2013**, *10* (2), 177–188.

[63] Zou, Y.; Wang, D.; Wurst, K.; Kühnel, C.; Reinhardt, I.; Decker, U.; Gurram, V.; Camadanli, S.; Buchmeiser, M. R. Group 4 Dimethylsilylenebisamido Complexes Bearing the 6-[2-(Diethylboryl)phenyl]pyrid-2-yl Motif: Synthesis and Use in Tandem Ring Opening Metathesis/Vinyl-Insertion Copolymerization of Cyclic Olefins with Ethylene. *Chem. Eur. J.* **2011**, *17* (49), 13832–13846.

[64] Barfield, M.; Dean, A. M.; Fallick, C. J.; Spear, R. J.; Sternhell, S.; Westerman, P. W. Conformational Dependence and Mechanisms for Long-Range H–H Coupling Constants Over Four Bonds. *J. Am. Chem. Soc.* **1975**, *97* (6), 1482–1492.

[65] Pine, S_ H.; Shen, G. S.; Hoang, H. Ketone Methylenation Using the Tebbe and Wittig Reagents – A Comparison. *Synthesis* **1991**, *1991* (2), 165–167.

[66] Soulard, V.; Villa, G.; Vollmar, D. P.; Renaud, P. Radical Deuteration with D2O: Catalysis and Mechanistic Insights. *J. Am. Chem. Soc.* **2018**, *140* (1), 155–158.

[67] Zefirov, N. S.; Baranekov, I. V. Stereochemical Studies—XXVIII. Conformational Equilibria of 2-OCH3, 2OCOCH3 and 2-Br Derivatives of ω-Substituted Methylenecyclohexanes. *Tetrahedron* **1983**, *39* (10), 1769–1775.

[68] Bank, S.; Rowe, C. A., Jr.; Schriesheim, A.; Naslund, L. A. Base-Catalyzed Isomerization of Bicyclic Olefins. *J. Am. Chem. Soc.* **1967**, *89* (26), 6897–6904.

[69] Bennani, Y. L.; Bunnelle, W. H.; Chang, S.-J.; Chembrukar, S. R.; Chen, J.; Dart, M. J.; Fernando, D.; Ku, Y.-Y.; Lockwood, M.; Wang, L. Spirocyclopropylamides and Acids and Their Therapeutic Applications. U.S. Patent 2004/0204396, October 14, 2004.

[70] Zanato, C.; Pelagalli, A.; Marwick, K. F. M.; Piras, M.; Dall'Angelo, S.; Spinaci, A.; Pertwee, R. G.; Wyllie, D. J. A.; Hardingham, G. E.; Zanda, M. Synthesis, Radio-Synthesis and in vitro Evaluation of Terminally Fluorinated Derivatives of HU-210 and HU-211 as Novel Candidate PET Tracers. *Org. Biomol. Chem.* **2017**, *15* (9), 2086–2096.

[71] Baggio, R. F.; Sparks, A. L.; Juo, R.-R.; Arenas, J. F. Constrained Cis-Diol-Borate Bioconjugation System. WO 2005/119255 A2, December 15, 2005.

[72] Spanka, G.; Rademacher, P. Transannular Interactions in Difunctional Medium Rings. 1. n/π Interactions in Cyclic Amino Ketones and Aminoalkenes Studied by Photoelectron Spectroscopy. *J. Org. Chem.* **1986**, *51* (5), 592–596.

[73] Du, X.-L.; Chen, H.-L.; Feng, H.-J.; Li, Y.-C. Stereoselective Total Synthesis of Natural (S)-Bakuchiol and Its Enantiomer. *Helv. Chim. Acta* **2008**, *91* (2), 371–378.

[74] Smaligo, A. J.; Swain, M.; Quintana, J. C.; Tan, M. F.; Kim, D. A.; Kwon, O. Hydrodealkenylative $C(sp^3)$–$C(sp^2)$ Bond Fragmentation. *Science* **2019**, *364* (6441), 681–685.

[75] Kolonko, K. J.; Shapiro, R. H.; Barkley, R. M.; Sievers, R. E. Ozonation of Caffeine in Aqueous Solution. *J. Org. Chem.* **1979**, *44* (22), 3769–3778.

[76] Zimmer, H.; Amer, A.; Ho, D.; Koch, K.; Schumacher, C.; Wingfield, R. C. A Novel Oxidative Skeleton Rearrangement of the Caffeine System. *J. Org. Chem.* **1990**, *55* (16), 4988–4989.

[77] Dimitrov, V.; Rentsch, G. H.; Linden, A.; Hesse, M. The Ozonolysis of Longifolene: A Tool for the Preparation of Useful Chiral Compounds. Configuration Determination of New Stereogenic Centers by NMR Spectroscopy and X-Ray Crystallography. *Helv. Chim. Acta* **2003**, *86* (1), 106–121.

[78] Paryzek, Z.; Rychlewska, U. Ozonolysis of Cholesterol and other Δ5-Steroids in the Presence of Alcohols: A Revised Mechanism and Hydroperoxide Structure of the Solvent-Participated Product, Confirmed by X-ray Analysis. *J. Chem. Soc., Perkin Trans. 2* **1997**, (11), 2313–2318.

[79] Zvereva, T. I.; Kasradze, V. G.; Kazakova, O. B.; Kukovinets, O. S. Ozonolysis of Unsaturated Carbonyl Compounds and Alcohols. *Russ. J. Org. Chem.* **2010**, *46* (10), 1431–1451.

[80] Odinokov, V. N. Ozonolysis of Alkenes and Study of Reactions of Polyfunctional Compounds. X. Peroxide Products of the Ozonolysis of Derivatives of bicyclo[2.2.1]hept-5-en-2,3-di- and -2-carboxylic acids. *Zh. Org. Khim.* **1977**, *13* (11), 2342–2353.

[81] Mosettig, E.; Beglinger, U.; Dolder, F.; Lichti, H.; Quitt, P.; Waters, J. A. The Absolute Configuration of Steviol and Isosteviol. *J. Am. Chem. Soc.* **1963**, *85* (15), 2305–2309.

[82] Swain, M.; Bunnell, T. B.; Kim, J.; Kwon, O. Dealkenylative Alkynylation Using Catalytic FeII and Vitamin C. *J. Am. Chem. Soc.* **2022**, *144* (33), 14828–14837.

[83] Branan, B. M.; Butcher, J. T.; Olsen, L. R. Using Ozone in Organic Chemistry Lab: The Ozonolysis of Eugenol. *J. Chem. Educ.* **2007**, *84* (12), 1979–1981.

[84] Kazakova, O. B.; Khusnutdinova, E. F.; Lobov, A. N.; Medvedeva, N. I.; Spirikhin, L. V. Allylic Oxidation of 19β,28-Epoxy-A-neo-5β-methyl-25-nor-18α-olean-9-ene. *Chem. Nat. Compd.* **2011**, *47* (4), 579–582.

[85] Mikhailova, L. R.; Khudobko, M. V.; Baltina, L. A.; Kukovinets, O. S.; Mavrodiev, V. K.; Galin, F. Z. Ozonolysis of 11-Desoxoglycyrrhetic Acid and its Derivatives. *Chem. Nat. Compd.* **2007**, *43* (5), 571–575.

[86] Paryzek, Z.; Martynow, J. Tetracyclic Triterpenes. X. Solvent Effect in Reactions of Tetrasubstituted Triterpenoidal Olefins with Ozone. An Allylic Oxidation. *Can. J. Chem.* **1988**, *66* (9), 2130–2136.

[87] Kazakova, O. B.; Khusnutdinova, E. F.; Korlyukov, A. A. Stereospecific Epoxidation of an Olean-18(19)-Ene-Type Triterpenoid. *Chem. Nat. Compd.* **2011**, *46* (6), 900–901.

[88] Kazakova, O. B.; Khusnutdinova, E. F.; Lobov, A. N.; Zvereva, T. I.; Suponitskii, K. Y. Oxidation of Ursolic Acid by Ozone. *Chem. Nat. Compd.* **2011**, *46* (6), 897–899.

[89] Vlad, P. F.; Ungur, N. D.; Barba, A. N.; Korchagina, D. V.; Bagryanskaya, I. Y.; Gatilov, Y. V.; Gatilov, V. P.; Barkhash, V. A. Cyclization of Some Labdane Alcohols with a Hydroxy Group at C-13 by a Superacid. *Chem. Nat. Compd.* **1988**, *24* (2), 166–170.

[90] Kazakova, O. B.; Medvedeva, N. I.; Kukovinets, O. S.; Tolstikov, G. A.; Khusnutdinova, E. F.; Zaprutko, L.; Bednarczyk-Cwynar, B.; Paryzek, Z. Chemoselective Oxidation of Oleanolic Acid Derivatives with Ozone. *Chem. Nat. Compd.* **2010**, *46* (3), 397–399.

[91] Medvedeva, N. I.; Flekhter, O. B. Structure of the Minor Ozonolysis Product of 19β,28-Epoxy-A-neo-18α-olean-3(5)-ene. *Chem. Nat. Compd.* **2006**, *42* (5), 618–619.

[92] Khusnutdinova, E. F.; Kazakova, O. B.; Lobov, A. N.; Kukovinets, O. S. Oxidation of Methyl 2-Cyano-3,4-seco-4(23)-ene-ursolate by Ozone. *Chem. Nat. Compd.* **2014**, *50* (6), 1037–1041.

[93] (a) Bozzato, G.; Bachmann, J.-P.; Pesaro, M. Stereoselective Addition of Methylcuprates to a 2-Formyl-cyclohexa-2,5-dienone System. A Stereoselective Total Synthesis of Racemic β-Vetivone. *J. Chem. Soc., Chem. Commun.* **1974**, (23), 1005–1006. (b) Thomas, A. F.; Perret, C. 4-(1-Hydroperoxy-1-methylethyl)-1,3-cyclopentadienyl Methyl Ketone: Its Formation from α-Terpineol and Behaviour as a Dimethylfulvene Epoxide. *Tetrahedron* **1986**, *42* (12), 3311–3321. (c) Leviss, D. H.; Van

Ry, D. A.; Hinrichs, R. Z. Multiphase Ozonolysis of Aqueous α-Terpineol. *Environ. Sci. Technol.* **2016**, *50* (21), 11698–11705.

[94] Smaligo, A. J.; Wu, J.; Burton, N. R.; Hacker, A. S.; Shaikh, A. C.; Quintana, J. C.; Wang, R.; Xie, C.; Kwon, O. Oxodealkenylative Cleavage of Alkene $C(sp^3)$–$C(sp^2)$ Bonds: A Practical Method for Introducing Carbonyls into Chiral Pool Materials. *Angew. Chem. Int. Ed.* **2020**, *59* (3), 1211–1215.

[95] Seekles, L. Aldéhydes Dérivées de la Cinchonine et de la Quinine et de Leurs Composés Acyliques. *Rec. Trav. Chim. Pays-Bas* **1923**, *42* (1), 69–104.

[96] Nóvoa, M. L.; Salazar, F. J.; Gámez, C.; Angarita, A. Y.; Tropper, E.; Canudas, N.; Villamizar, J. E. Facile Access to Optically Active Ring C Aromatic Diterpene Derivatives from (+)-Manool. First Synthesis of 13,14-Dihydroxy-8,11,13-podocarpatrien-7-one. *Nat. Prod. Commun.* **2014**, *9* (3), 355–358.

[97] Vlad, P. F.; Aryku, A. N.; Koltsa, M. N. Investigation of the Products of the Ozonolysis of Sclareol and the Pathways for their Formation. *Chem. Nat. Compd.* **1991**, *27* (4), 436–443.

[98] Everest, D. J.; Grant, P. K.; Slim, G. C.; Yeo, I. K. L. A Mechanism for Anomalous Ozonolysis. *Aust. J. Chem.* **1988**, *41* (7), 1025–1035.

[99] DeNinno, M. P. “Anomalous” Ozonolysis of Cyclic Allylic Alcohols: Mechanism and Synthetic Utility. *J. Am. Chem. Soc.* **1995**, *117* (39), 9927–9928.

[100] Martínez, A. G.; Vilar, E. T.; Fraile, A. G.; Cerero, S. d. l. M.; Maroto, B. L. A New Type of Anomalous Ozonolysis in Strained Allylic Bicycloalkan-1-ols. *Tetrahedron Lett.* **2005**, *46* (31), 5157–5159.

[101] Ogawa, T.; Muramatsu, Y.; Ohashi, M. Method for Producing Organosilane. European Patent EP 1688422 A1, September 6, 2005.

[102] Tannenbaum, S.; Kaye, S.; Lewenz, G. F. Synthesis and Properties of Some Alkylsilanes. *J. Am. Chem. Soc.* **1953**, *75* (15), 3753–3757.

[103] (a) Lecea, B.; Aizpurua, J. M.; Palomo, C. Reagents and Synthetic Methods 52. Silane Reduction of Carbonyl Compounds in the Presence of Iodine. *Tetrahedron* **1985**, *41* (20), 4657–4665. (b) Fukuzumi, S.; Kitano, T.; Ishikawa, M.; Matsuda, Y. Electron Transfer Chemistry of Hydride and Carbanion Donors. Hydride and Carbanion Transfer via Electron Transfer. *Chem. Phys.* **1993**, *176* (2–3), 337–347. (c) Zuleta, E. C.; Goenaga, G. A.; Zawodzinski, T. A.; Elder, T.; Bozell, J. J. Deactivation of Co-Schiff Base Catalysts in the Oxidation of para-Substituted Lignin Models for the Production of Benzoquinones. *Catal. Sci. Technol.* **2020**, *10* (2), 403–413.

[104] Beckwith, A. L. J.; Kazlauskas, R.; Syner-Lyons, M. R. β-Fission of 9-Decalinoxyl Radicals: Reversible Formation of 6-Ketocyclodecyl Radical. *J. Org. Chem.* **1983**, *48* (24), 4718–4722.

[105] (a) Matsumoto, A.; Maruoka, K. Development of Organosilicon Peroxides as Practical Alkyl Radical Precursors and Their Applications to Transition Metal Catalysis. *Bull. Chem. Soc. Jpn.* **2021**, *94* (2), 513–524. (b) Gao, P.; Niu, Y.-J.; Yang, F.; Guo, L.-N.; Duan, X.-H. Three-component 1,2-Dicarbofunctionalization of Alkene Involving Alkyl Radicals. *Chem. Commun.* **2022**, *58* (5), 730–746. (c) Dworkin, J. H.; Dehnert, B. W.; Kwon, O. When All C–C Breaks LO–Ose. *Trends Chem.* **2023**, *5* (3), 174–200.

[106] Cherney, E. C.; Lopchuk, J. M.; Green, J. C.; Baran, P. S. A Unified Approach to ent-Atisane Diterpenes and Related Alkaloids: Synthesis of (–)-Methyl Atisenoate, (–)-Isoatisine, and the Hetidine Skeleton. *J. Am. Chem. Soc.* **2014**, *136* (36), 12592–12595.

[107] (a) Canonne, P.; Bernatchez, M. A Highly Stereoselective Synthesis of Trans-1,2-Disubstituted Cycloalkanols. *J. Org. Chem.* **1987**, *52* (18), 4025–4031. (b) Courtemanche, G.; Normant, J.-F. Carbocyclisation of ω-Ethylenic Propargylic Zinc Reagents. *Tetrahedron Lett.* **1991**, *32* (39), 5317–5320. (c) Molander, G. A.; McKie, J. A. Samarium(II) Iodide-Induced Reductive Cyclization of Unactivated Ketones. Sequential Radical Cyclization/Intermolecular Nucleophilic Addition and Substitution Reactions. *J. Org. Chem.* **1992**, *57* (11), 3132–3139.

[108] de Koning, P. D.; Jackson, M.; Lennon, I. C. Use of Achiral (Diphosphine)RuCl2(Diamine) Precatalysts as a Practical Alternative to Sodium Borohydride for Ketone Reduction. *Org. Process Res. Dev.* **2006**, *10* (5), 1054–1058.

[109] Litvinas, N. D.; Brodsky, B. H.; Du Bois, J. C–H Hydroxylation Using a Heterocyclic Catalyst and Aqueous H2O2. *Angew. Chem. Int. Ed.* **2009**, *48* (25), 4513–4516.

[110] Larsen, A. T.; May, E. M.; Auclair, K. Predictable Stereo- and Chemo-Selective Hydroxylations and Epoxidations with P450 3A4. *J. Am. Chem. Soc.* **2011**, *133* (20), 7853–7858.

[111] Guan, B.-T.; Xiang, S.-K.; Wang, B.-Q.; Sun, Z.-P.; Wang, Y.; Zhao, K.-Q.; Shi, Z.-J. Direct Benzylic Alkylation via Ni-Catalyzed Selective sp3 C–O Activation. *J. Am. Chem. Soc.* **2008**, *130* (11), 3268–3269.

[112] De Smet, G.; Bai, X.; Mensch, C.; Sergeyev, S.; Evano, G.; Maes, B. U. W. Selective Nickel-Catalyzed Hydrodeacetoxylation of Aryl Acetates. *Angew. Chem. Int Ed.* **2022**, *61* (27), e202201751.

[113] Merkel, M.; Müller, F. K.; Krebs, B. Novel Iron(III) Complexes with Phenolate Containing Tripodal Tetradentate Ligands as Model Systems for Catechol 1,2-Dioxygenases. *Inorg. Chim. Acta* **2002**, *337*, 308–316.

[114] Lum, T.-K.; Wang, S.-Y.; Loh, T.-P. A Highly Catalytic Asymmetric Conjugate Addition: Synthesis of the C14–C20 Fragment of Antibiotic TMC-151A, Siphonarienal and Siphonarienone. *Org. Lett.* **2008**, *10* (5), 761–764.

[115] Cahiez, G.; Luart, D.; Lecomte, F. Unexpected Substitution of Ortho-chloro Arylketones by Organomanganese Reagents. *Org. Lett.* **2004**, *6* (24), 4395–4398.

[116] Settine, R. L.; Parks, G. L.; Hunter, G. L. K. The Rearrangement of Limonene and Carvomenthene Epoxides. *J. Org. Chem.* **1964**, *29* (3), 616–618.

[117] Zimmer, O.; Meier, H. Die Regioselektivität der Ringschlußreaktionen zu 1,2,3-Thiadiazolen und 1,2,3-Selenadiazolen. *Chem. Ber.* **1981**, *114* (8), 2938–2946.

[118] Paquette, L. A.; Fristad, W. E.; Dime, D. S.; Bailey, T. R. Silanes in Organic Synthesis. 8. Preparation of Vinylsilanes from Ketones and Their Regiospecific Cyclopentenone Annulation. *J. Org. Chem.* **1980**, *45* (15), 3017–3028.

[119] Ansell, M. F.; Mahmud, S. A. Friedel–Crafts Reactions of Alkenones with Benzene. *J. Chem. Soc., Perkin Trans. 1* **1973**, (22), 2789–2795.

[120] Aragón, J.; Sun, S.; Pascual, D.; Jaworski, S.; Lloret-Fillol, J. Photoredox Activation of Inert Alkyl Chlorides for the Reductive Cross-Coupling with Aromatic Alkenes. *Angew. Chem. Int. Ed.* **2022**, *61* (9), e202114365.

[121] Prana, V.; Rotureau, P.; Fayet, G.; Andre, D.; Hub, S.; Vicot, P.; Rao, L.; Adamo, C. Prediction of the Thermal Decomposition of Organic Peroxides by Validated QSPR Models. *J. Hazard. Mater.* **2014**, *276*, 216–224.

[122] Bruker, SAINT, V8.40B, Bruker AXS Inc., Madison, Wisconsin, USA.

[123] Krause, L.; Herbst-Irmer, H.; Sheldrick, G. M.; Stalke, D. Comparison of Silver and Molybdenum Microfocus X-ray Sources for Single-Crystal Structure Determination. *J. Appl. Crystallogr.* **2015**, *48* (1), 3–10.

[124] Sheldrick, G. M. SHELXT – Integrated Space-Group and Crystal-Structure Determination. *Acta Crystallogr., Sect. A: Found. Adv.* **2015**, *71* (1), 3–8.

[125] Sheldrick, G. M. Crystal Structure Refinement with SHELXL. *Acta Crystallogr., Sect. C: Struct. Chem.* **2015**, *71* (1), 3–8.

[126] Hübschle, C. B.; Sheldrick, G. M.; Dittrich, B. ShelXle: A QT Graphical User Interface for SHELXL. *J. Appl. Crystallogr.* **2011**, *44* (6), 1281–1284.

[127] Kratzert, D. FinalCif, V137, **https://dkratzert.de/finalcif.html**.

CHAPTER FOUR

Synthesis through C(sp^3)–C(sp^2) Bond Scission in Alkenes and Ketones

Adapted from Šimek, M.; Dworkin, J. H.; Kwon, O.

Acc. Chem. Res. **2025**, *58*, 1547–1561.

4.1 Conspectus

The homolytic cleavage of C–C bonds adjacent to functional groups has recently become a popular strategy for restructuring the skeletons of complex organic molecules. In contrast to the traditional reactivity profiles of polar bond disconnections, homolytic scission furnishes carbon-centered free radicals primed for controlled termination with a diverse range of radicophiles. Beyond standard radical capture, transition-metal catalysis facilitates sophisticated C–C and C–heteroatom bond-forming reactions. Intensive efforts have been focused over many years into the cleavage of the neighboring C–C bonds of carboxylic acids and alcohols. Despite the ubiquity of alkenes and ketones in natural products, feedstock chemicals, and common synthetic intermediates, much less attention has been paid to exploiting their potential in diversifying chiral pool materials, such as terpenes and terpenoids. Defunctionalization in this manner is a powerful approach for synthesizing high-value chemicals and advanced synthetic intermediates because of the possibility to reconstruct and further decorate chirality-bearing carbon skeletons.

Motivated by synthetic necessity, since 2018 our group has focused on developing ozonolysis-based dealkenylative molecular diversification, and we expanded into deacylation in 2025. In this Account, we chronicle our initial motivation, describe the historical background, and summarize our research into dealkenylative and deacylative synthesis. Our dealkenylative approach capitalizes on the ozonolysis of alkenes in MeOH to generate α-methoxyhydroperoxides primed for a reaction with reducing agents. Their reduction through single-electron transfer, mediated by a transition metal, leads to the formation of an alkoxyl radical that undergoes rapid β-scission, furnishing both a carbon-centered free radical and an ester group derived from the acetal carbon atom. The

produced free radical can be strategically terminated by radicophiles, thereby delivering remodeled chiral molecules.

Using this concept, we have developed hydrodealkenylation (through hydrogen atom transfer from benzenethiol) [1], dealkenylative thiylation (through thiyl group transfer from diaryl disulfides) [40], alkenylation (through addition/elimination with nitrostyrenes) [43], and oxodealkenylation (through treatment with TEMPO followed by oxidation) [2]. Furthermore, kinetic analysis has enabled the development of a catalytic Fe(II)/vitamin C system for dealkenylative alkynylation [53] and halodealkenylation [56]. Synergizing ozonolysis and copper catalysis has recently enabled aminodealkenylation through net-redox-neutral C–C cleavage followed by C–N bond formation [3]. Although the high oxidation potential of ozone relative to organic compounds makes alkene-to-peroxide conversion possible, it also limits the applicability of dealkenylative techniques for substrates featuring ozone-sensitive functional groups. We recently overcame this constraint by first applying Isayama–Mukaiyama peroxidation to olefins and then using a novel catalytic system—catalytic Fe and PhSH with stoichiometric γ-terpinene for ozone-free hydrodealkenylation [65]. Beyond alkenes, we have developed a straightforward methodology for the homolytic deacylative cleavage of ketones as well, including cycloalkanones [4]. This process is applicable in total syntheses and in the late-stage modifications of complex ketone-containing natural products.

4.2 Initial Discoveries

Organic compounds have skeletal frameworks composed of carbon atoms with occasional heteroatoms, commonly O, N, S, and P. For this reason, the principal approaches for the synthesis of organic molecules have involved constructing C–C bonds and C–heteroatom bonds. In contrast, the cleavage of C–C bonds appears to be unorthodox, usually suggesting decomposition or degradation. When executed in a controlled manner, however, C–C bond scission can facilitate the synthesis of complex molecules and other significant synthetic building blocks, especially when applying readily available feedstock chemicals and chiral natural products (NPs). Synthesis based on C–C bond cleavage, when conducted under mild conditions that are compatible with common molecular functional groups, also allows late-stage modification of complex synthetic intermediates.

Methodological advancement in chemical research can come about through serendipitous discoveries and rational reaction design or through genuine synthetic needs that unveil unforeseen technological potential. In our laboratory, we initiated our endeavors into dealkenylative synthesis because we needed to skeletally modify a carvone-based phosphine organocatalyst. In 2012, we made progress in the enantioselective [3+2] annulations of allenoates and imines to form pyrrolines, mediated by [2.2.1] bicyclic phosphines, so-called HypPhos catalysts, derived from 4-hydroxy-L-proline (Hyp, Figure 4.1A). While both the *exo*- and *endo*-phenyl-HypPhos catalysts **1a** and **1b** served superbly in a wide array of phosphine organocatalysis processes, they are affordable only in one enantiomeric form and posed a potential pitfall for cases in which the L-Hyp-derived HypPhos would produce the unwanted enantiomer of the target

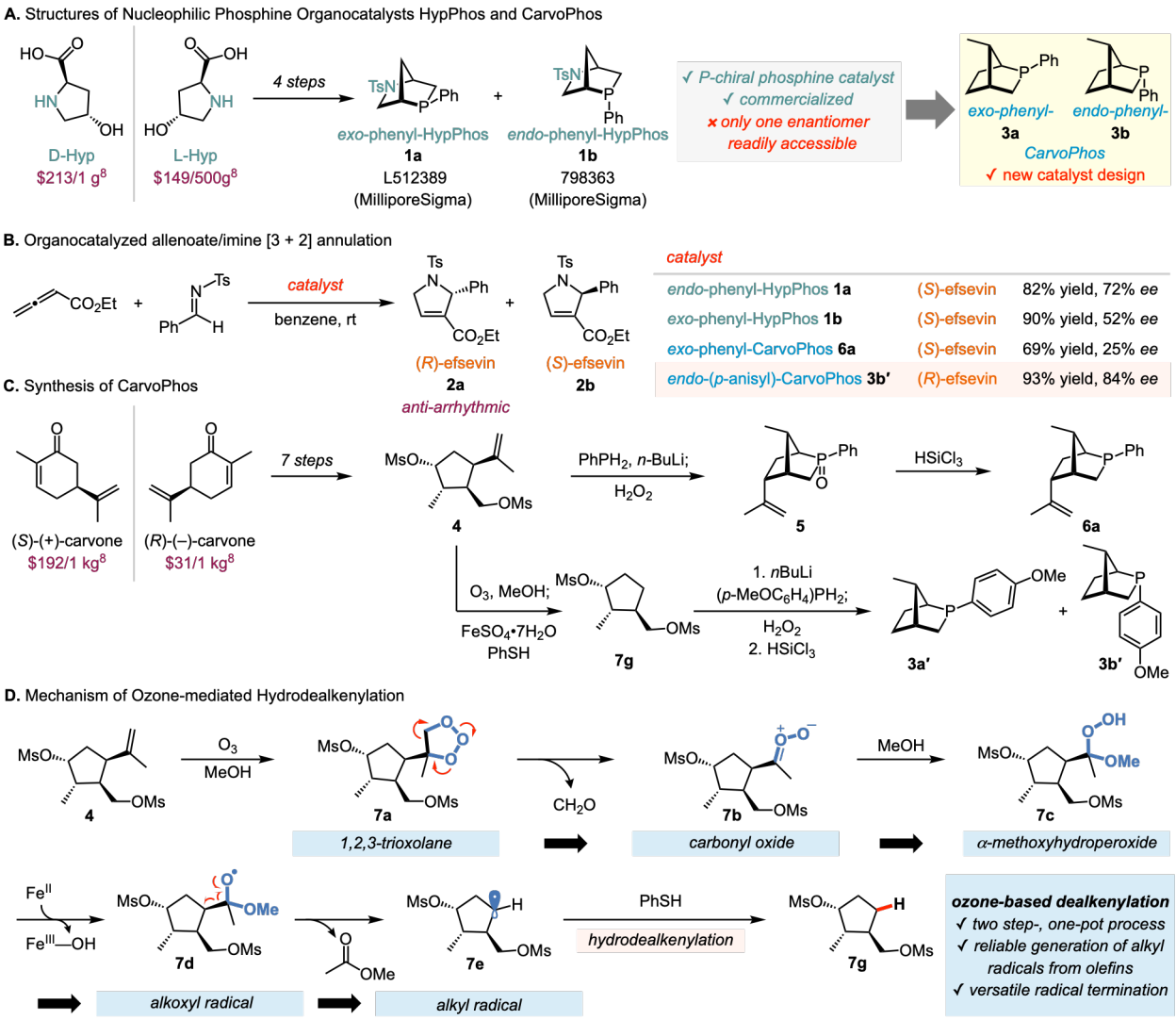


Figure 4.1 From Synthetic Needs to the Discovery of New Methodology

product. For instance, we had identified (*R*)-efsevin **2a** as an antiarrhythmic drug from multiple animal models; the HypPhos catalysts **1a,b** both produced (*S*)-efsevin **2b** in 82% yield with 72% ee and in 90% yield with 52% ee, respectively (Figure 4.1B). Production of the desired (*R*)-efsevin enantiomer necessitated the use of D-Hyp, which costs approximately 100 times more than its natural enantiomer.

Efforts to prepare both enantiomers of the [2.2.1] bicyclic P-stereogenic chiral phosphines from readily available starting materials led to a structural redesign toward

carbon analogues **3a,b** derived from the natural terpenoids (*R*)- and (*S*)-carvone. Both enantiomers are commercially available and affordable (Figure 4.1C). We transformed (*R*)-carvone into the dimesylate **4**. Dialkylation with dilithium phenylphosphide and oxidative workup with H_2O_2 provided the phosphine oxide **5**. Reduction with trichlorosilane gave the phosphine **6a**. The isopropenyl group cis to the mesyloxymethyl unit in **4**, however, prevented the formation of the desired *endo*-phenyl-CarvoPhos while the *exo*-phenyl-CarvoPhos **6a** provided (*S*)-efsevin **2b** in 69% yield with 25% ee. We decided to remove the isopropenyl group, sparking further catalyst development and a completely new research program.

Our chosen strategy to eliminate the isopropenyl group was inspired by chemistry popularized by Schreiber in 1980 [10]. His findings exemplify an early skeletal editing reaction on NPs and an application in total synthesis. Mechanistically, [3+2] cycloaddition of the olefin **4** forms 1,2,3-trioxolane **7a**, which cycloreverts to the carbonyl oxide **7b** (Figure 4.1D). Interception by MeOH provides the α-methoxyhydroperoxide **7c**. Treatment with Fe(II) generates an alkoxyl radical **7d**, fragmenting the neighboring C–C bond to give the alkyl radical **7e**. Driven by our objective to synthesize an isopropenyl-free CarvoPhos catalyst, we investigated the use of hydrogen atom transfer (HAT) to form the cyclopentane **7g**. Indeed, when we subjected the α-methoxyhydroperoxide **7c** to reduction, using $FeSO_4 \cdot 7H_2O$ and benzenethiol, we obtained the desired cycloalkane **7g** in 80% yield on a 10 g scale, thereby securing access to the CarvoPhos catalyst **3**, whose anisyl derivative **3b** [7] provided good stereocontrol in the preparation of (*R*)-efsevin **2a** (Figure 4.1B).

4.3 Historical Background

The history of the generation of organic peroxides, and their homolytic scission, is summarized elsewhere [11]. Here we highlight only the most relevant milestones (Figure 4.2). It has been known since the 19th century that copper and iron salts decompose H_2O_2 into water and an oxidized metal salt. Planche (1810) added fresh horseradish root to guaiac tincture and observed a blue coloration, indicating a peroxidase-catalyzed oxidation of α-guaiaconic acid [12]. Thénard (1818), credited with the discovery of hydrogen peroxide, mixed barium peroxide with various acids, including nitric, hydrochloric, and sulfuric acids, before reacting with copper oxide and noting an olive-green color [13]. Schönbein, credited with the discovery and naming of ozone, observed an intense blue coloration upon preparing a solution of H_2O_2 with KI and starch or guaiac tincture and adding blood corpuscles (1856) [14] or iron sulfate (1857) [15]. The same reports described a similar observation when using an ozonized turpentine oil instead of H_2O_2, marking one of the first combinations of ozonation and ferrous oxidation. Brodie and Parnell corroborated these observations when using ferrocyanide and the oxidation of other metals [16, 17]. The combination of H_2O_2 and Fe(II) would later be popularized by Fenton after his oxidation of tartaric acid in 1894 [18]. In 1932, Haber and Weiss unveiled the mechanism of H_2O_2/Fe(II) decomposition and proposed the presence of hydroxyl radicals [19].

With the large amount of information on organic peroxide decomposition gathered in the early 20th century, George and Walsh (1946) proposed that the decomposition of tertiary alkyl peroxides occurs first at the O–O bond and then through fission of the weakest adjacent α-carbon C–C bond [20]. Studies by Milas were in agreement with this

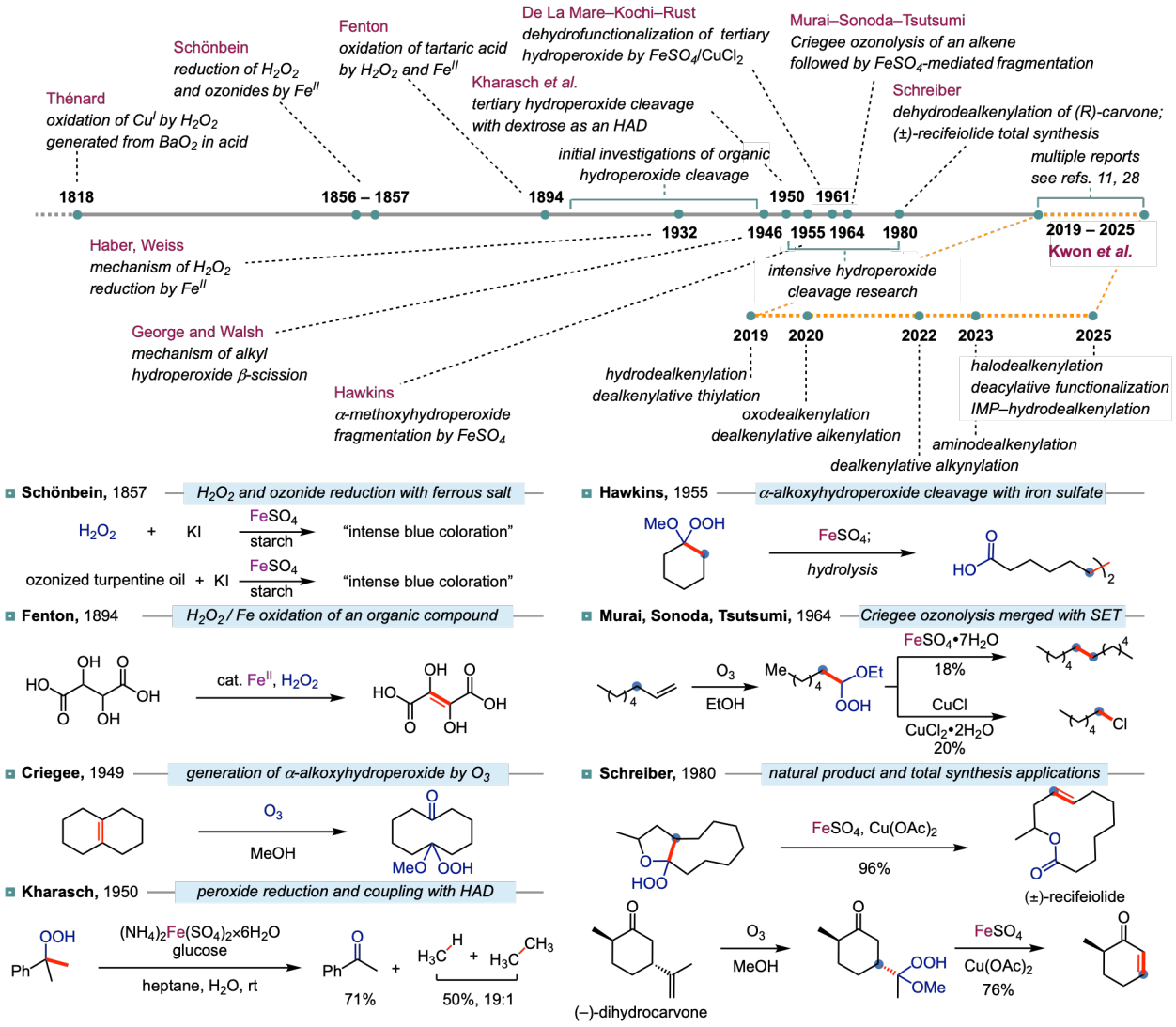


Figure 4.2 Historical Milestones Leading to Peroxide-Based Deconstructive Synthetic Strategies

explanation [21]. This realization sparked further studies into the thermal or low-valent-metal-mediated decompositions of dialkyl or monoalkyl peroxides without rational radical termination [21–25]. In 1950, Kharasch demonstrated the Fe(II)-mediated decomposition of cumene hydroperoxide in the presence of dextrose, a feasible hydrogen atom donor (HAD), into acetophenone and hydrocarbon gases [25]. In 1955, Hawkins disclosed the $FeSO_4$-mediated dimerization of a cyclohexanone-derived α-methoxyhydroperoxide,

which was synthesized inefficiently through autoxidation of cyclohexyl methyl ether by air [26].

The α-methoxyhydroperoxide intermediate critical for dealkenylative methodologies is efficiently generated through the ozonolysis of olefins in MeOH, as demonstrated by Criegee in 1949 [27]. Early examples of ozonolysis-derived peroxide fragmentations were facilitated under thermolysis. The first Fe(II)- or Cu(I)-mediated fragmentation of α-alkoxyhydroperoxides produced by Criegee ozonolysis was demonstrated by Murai, Sonoda, and Tsutsumi in 1964 [29]. In their investigation, the ozonolysis of 1-octene in ethanol yielded heptyl α-ethoxyhydroperoxide, which was subjected to reaction with ferrous sulfate to deliver dodecane or to reaction with CuCl/CuCl2 to furnish hexyl chloride [29]. These pioneering studies provided the basis for rationally designed skeletal modifications induced through peroxide-based C–C bond cleavage.

In 1980, Schreiber used De La Mare, Kochi, and Rust's (1961) Fe(II)/Cu(II) conditions [30] to reduce an α-perhydroxytetrahydrofuran, yielding the macrolide (±)-recifeiolide [10]. Furthermore, the same study described the dehydrodealkenylation of (–)-dihydrocarvone to give access to (*R*)-6-methylcyclohex-2-en-1-one [10]. We believe that this example is the first showcase of the transformation of a chiral pool NP into an unnatural building block with broad synthetic utility. Since 1980, the use of peroxides for deconstructive synthesis has remained limited, with only scattered reports demonstrating analogous tactics, applications, or improvements. Momentous progress in photoredox catalysis, coupled with the use of transition metals in the second decade of the 21st century, revitalized the field of free radical chemistry along with peroxide-based C–C bond cleavage strategies [31].

4.4 Hydrodealkenylation

In 2018, out of synthetic necessity, we reported the first example of hydrodealkenylation [1]. By achieving our goal of removing the isopropenyl group from the CarvoPhos core, we realized the immense potential that dealkenylative synthesis would have in allowing chiral pool feedstock olefins to synthesize diverse, and otherwise inaccessible, enantiomerically pure molecules. Furthermore, we envisioned that this methodology would provide a new retrosynthetic disconnection for total synthesis and enable late-stage diversification of biologically active molecules.

In our standard hydrodealkenylation, we dissolve an olefin in MeOH, ozonolyze it at −78 °C, treat the intermediate with benzenethiol (1.5 equiv) and $FeSO_4 \cdot 7H_2O$ (1.2 equiv), and warm the mixture to room temperature. Removal of the isopropenyl group from (+)-dihydrocarvone yielded the chiral (*R*)-2-methylcyclohexanone **8a** (Figure 4.3). A carvone-derived bicyclic endione was smoothly converted to the enantiopure Wieland–Mischer ketone **8b**. The bioactive sesquiterpenoid (+)-nootkatone and the triterpene betulinic acid were successfully engaged in hydrodealkenylation, yielding the simplified analogs **8c,d**. A striking example is of the inexpensive terpenoid (–)-isopulegol ($14/mol) giving the high-value cyclohexanol **8e** ($193 K/mol), which is used in the preparation of an androgen receptor modulator [32].

The method is highly suitable for the total synthesis of NPs, exemplified by the one-step conversion, previously six, of **8f'** to **8f**, which has been used in the synthesis of (–)-2-pupukeanone [33]. Similarly, we transformed compound **8g'** into the cyclohexanone **8g**, which has been used in the synthesis of (–)-7-epibakkenolide-A [34]. To date,

hydrodealkenylation has been applied in several total syntheses of NPs and peptide modifications [35–39].

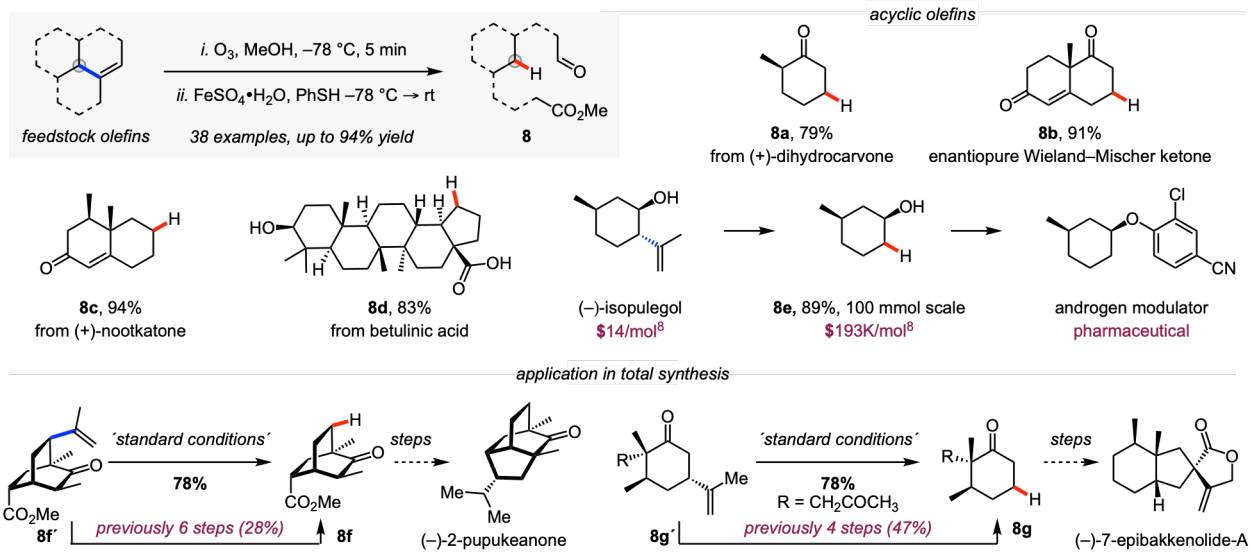


Figure 4.3 Hydrodealkenylation

4.5 Thiodealkenylation

The versatility of radical couplings allows the formation of bonds with various heteroatoms. Sulfur atoms are frequently found in drugs and various intermediates. Therefore, direct access to thioethers from feedstock olefins is desirable. We hypothesized that trapping an alkyl radical with a disulfide would directly yield thioethers [40]. Our survey revealed the optimal reaction conditions: ozonolysis of the olefin at –78 °C, addition of an aryl disulfide (3.0 equiv), and treatment with $FeSO_4•7H_2O$ (1.2 equiv) at 0 °C. The excess $(ArS)_2$ relative to the amount of PhSH in the previous case, compensated for the lower rate of thiylation (less than 10^5 M^{-1} s^{-1}) of the alkyl radical compared to HAT from PhSH (1.3×10^8 M^{-1} s^{-1}) [41, 42].

The terpenoids (+)-dihydrocarvone, (–)-limonene-1,2-diol, and (+)-nootkatone all provided good yields of their phenyl thioethers **9a–c** (Figure 4.4). Both electron-rich and -poor diaryl disulfides were viable, yielding the products **9d** and **9e**. Furthermore, (+)-2-carene and sabinene, which are cyclic olefins with internal and exocyclic double bonds, respectively, yielded the cyclopropyl-containing thioethers **9f,g** adorned with aldehyde/methyl ester units.

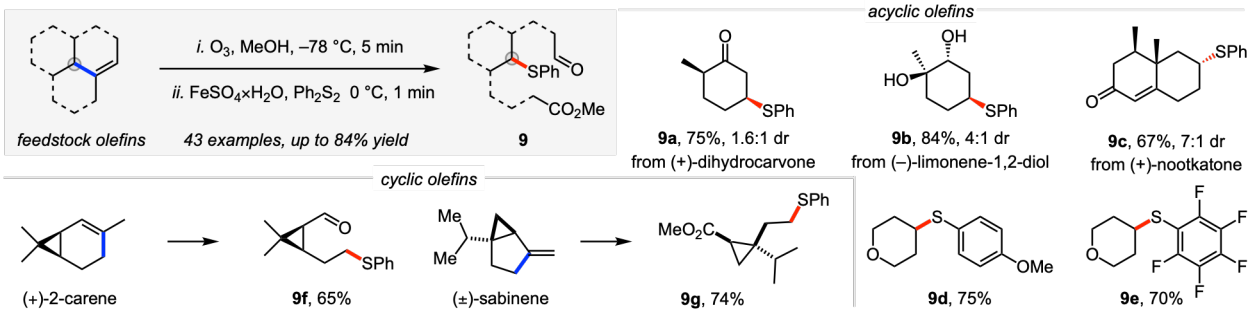


Figure 4.4 Thiodealkenylation

4.6 Dealkenylative Alkenylation

Olefins play pivotal roles in nature, organic synthesis, and material sciences. Traditional methods to introduce alkenes include the olefination of carbonyls, semihydrogenation of alkynes, eliminations, and cross-couplings as well as such direct alkene-to-alkene conversions as metathesis and the Heck reaction. The reactivity of nucleophilic alkyl radicals toward polarized C=C double bonds motivated us to explore ways to convert ubiquitous olefins into a new set of alkenes through a formal π-bond metathesis. We envisioned alkyl radicals produced by the β-scission of α-methoxyhydroperoxides to be added to olefins with a radical leaving group to regenerate the π-system upon elimination [43].

To test the feasibility of this idea, we subjected (–)-isopulegol to ozonolysis in MeOH and treated the resulting intermediate with alkenylating agents and a reducing metal salt. Nitrostyrene proved an optimal alkenylating agent when applied as the limiting substrate with 2.2 equiv of the alkene and 1.2 equiv of $FeSO_4 \bullet 7H_2O$ at 0 °C. Using the nitroalkene as the limiting reagent stemmed from the lower rate of addition to an olefin (less than 7.6×10^5 M^{-1} s^{-1}) [44], thus kinetically competing with other side reactions *(vide infra)*. The isopropenyl group of (–)-isopulegol underwent a metathesis to *p*-anisylstyrene adduct **10a** in 78% isolated yield on a 5.0 mmol scale (Figure 4.5). Benzylic alcohols are tolerated, as demonstrated by the styrene derivative **10b**. Dehydroleucine was converted to the styrene **10c**. Carbamate-protected amines are tolerated, as exemplified by the synthesis of (*E*)-metanicotine **10d** after Boc-deprotection. The skeletal reconstruction of cyclic alkenes was also possible: methylene indane yielded the styrene-decorated benzoate **12e**, while sabinene generated the cyclopropane **10f**.

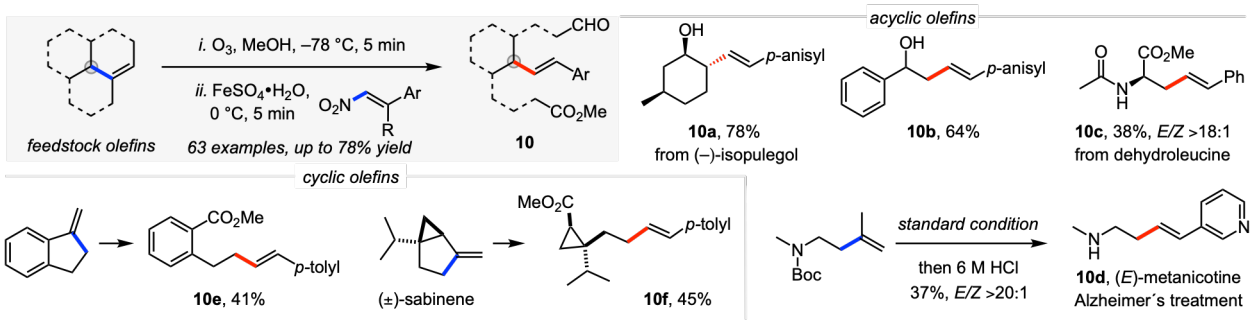


Figure 4.5 Dealkenylative Alkenylation

4.7 Oxodealkenylation

The coupling of transient and persistent radicals is a highly favorable kinetic and thermodynamic process with almost diffusion-controlled reaction rates. In this respect, (2,2,6,6-tetramethylpiperidin-1-yl)oxyl (TEMPO) is commonly used to detect radical intermediates by giving corresponding aminoxides (TEMPO adducts). The fast rate of TEMPO coupling with alkyl radicals (greater than 7.6×10^8 M^{-1} s^{-1}) facilitated the development of reaction conditions that were analogous to kinetically competent HAT: ozonolysis of the alkene in MeOH at –78 °C followed by the addition of 1.5 equiv of TEMPO and 1.2 equiv of an aqueous $FeSO_4 \cdot 7H_2O$ solution [2,45]. The reaction was complete within minutes after adding the reductant and provided excellent yields of TEMPO adducts. For conversion to carbonyls, we performed *in situ* treatment with magnesium bis(monoperoxyphthalate) hexahydrate (MMPP). We introduced carbonyl functionalities into various alkenes (Figure 4.6).

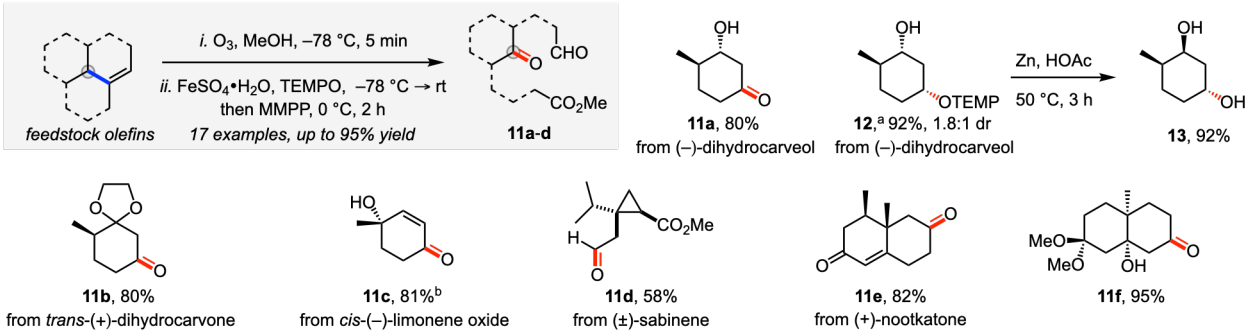


Figure 4.6 Oxodealkenylation

(–)-Dihydrocarveol, with a free hydroxyl group, smoothly underwent the three-step, one-pot sequence, giving the ketone **11a**. Omitting the oxidation step in the same sequence, we isolated the TEMPO adduct **12** and deprotected the major diastereoisomer using zinc in acetic acid, revealing the diol **13**. The ethylene glycol ketal of *trans*-(+)-

dihydrocarvone provided the ketone **11b**. We accessed the enone **11c** from *cis*-(–)-limonene oxide by adding triethylamine to the crude mixture after oxidation with MMPP to induce β-elimination of the epoxide. (±)-Sabinene underwent β-scission to give the ester **11d**. (+)-Nootkatone, despite its exposed enone functionality, provided the desired enedione product **11e**. The dimethyl ketal from the annulated dihydrocarvone survived, providing ketone **11f**.

4.8 Mechanistic Discussion

While developing various dealkenylative reactions, we made several crucial observations. In the hydrodealkenylative and oxodealkenylative cleavages, only a slight excess of the radicophile was necessary, and only traces of possible byproducts were formed. In radical thiylation, however, 3 equiv of a disulfide was necessary to obtain a good yield; more severely, in dealkenylative alkenylation, an excess of the starting olefin was used. This behavior can be rationalized by comparing the rate constants of the operating radical processes (Figure 4.7). Initially, the α-methoxyhydroperoxide **A** undergoes rapid SET reduction by Fe(II) with a rate constant k_1 of 1.2×10^7 M^{-1} s^{-1} (at 298 K) [46]. The formed alkoxyl radical **B** undergoes rapid β-scission (greater than 10^8 s^{-1}) [47] into an alkyl radical **C** while eliminating methyl acetate. The alkyl radical **C**, in addition to the desired pathways, can also undergo oxidation/elimination, disproportionation, or dimerization, giving the byproduct **E**, **F**, or **G**. We barely observed those byproducts, however, during hydrodealkenylation or aminoxylation, even with stoichiometric Fe(II) because the rate constants for 1°, 2°, and 3° radicals undergoing HAT from benzenethiol are 1.3×10^8, 1.0×10^8, and 1.4×10^8 M^{-1} s^{-1}, respectively, at 298 K [41, 42], and the rate constants for TEMPO capture of *n*-nonyl and *tert*-butyl radicals are 1.2×10^9 and 7.6×10^8 M^{-1} s^{-1}, respectively [45]. The situation is different for thiylation and alkenylation processes, whose rate constants are less than or equal to 7.6×10^5 M^{-1} s^{-1} [44]. These rate constants are lower than those for Fe-mediated oxidation of the radical **C** to the alkene **E** (less than 4.0×10^9 M^{-1} s^{-1}) [48], for the disproportionation of a pair of alkyl radicals **C** to the alkene **E** and the alkane **F** (1.8×10^8 M^{-1} s^{-1}), and even for dimerization to **G** (1.7×10^8 M^{-1} s^{-1}) [49–51]. The ketone **H**, the commonly observed

byproduct, is formed either through Fe(II)-mediated over-reduction of the alkoxyl radical **B** to alkoxide or through HAT (greater than 1.2 × 10^6 M^{-1} s^{-1}) [52] followed by hydrolysis. From this kinetic analysis, we concluded that high concentrations of both Fe(II) and Fe(III) as well as the radical species could promote byproduct formation. We hypothesized that the combination of a catalytic amount of iron and a stoichiometric amount of reductant could thwart kinetically unfavorable processes.

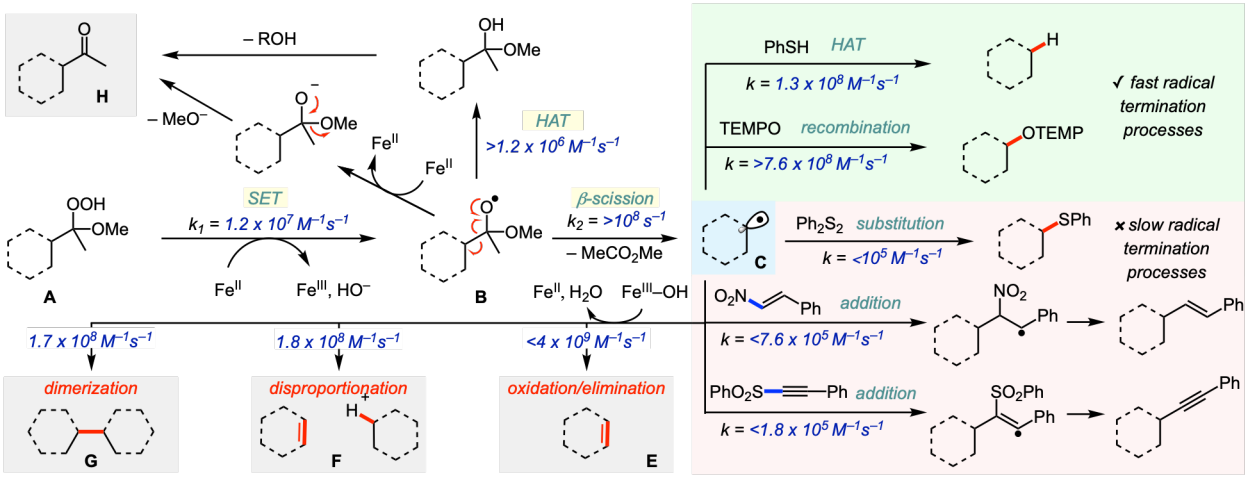


Figure 4.7 Kinetic Analysis

4.9 Dealkenylative Alkynylation with Catalytic Iron(II) and Vitamin C

Alkyne functionalities are found in many NPs, with several displaying promising biological activities. They are versatile as functional groups in chemical synthesis, structural motifs in bioactive molecules, and organic materials. They are also used in fossil fuel industries, materials science, and pharmaceuticals, and as tags for selective bioconjugation. This versatility inspired us to investigate methods for incorporating alkynes into ubiquitous olefin feedstocks.

Analogous to dealkenylative alkenylation, we envisioned an addition/elimination mechanism with alkynyl sulfones [53,54]. The low rate of alkyl radical addition to alkynyl sulfones (less than 1.8×10^5 M^{-1} s^{-1}) suggested potential byproduct formation with stoichiometric Fe(II) (Figure 4.7) [54]. Thus, we applied catalytic Fe(II) with a stoichiometric reductant. Alkynylation occurred using 20 mol % $FeSO_4 \cdot 7H_2O$ and 2 equiv of vitamin C, with 2 equiv of the olefin and the alkynyl sulfone as the limiting reagent.

We tested the scope of the olefins and alkynyl donors under the developed catalytic conditions (Figure 4.8). (–)-Isopulegol provided the desired alkyne **14a**. (–)-Dihydrocarveol provided **14b** unselectively. A thiophene-substituted alkynyl sulfone was also viable and enabled access to **14c**. The method is suited to reconstructing and introducing alkynes into cyclic olefins. For example, methylene adamantane delivered the bicyclic alkynylated ester **14d**. *N*-Boc-protected 4-methylene piperidine was reconstructed into the polyfunctional alkyne **14e**. Finally, we converted the homopropargyl alcohol **14a** into the alkoxyquinoline **15**, demonstrating the synthetic potential of these compounds in complex syntheses [55].

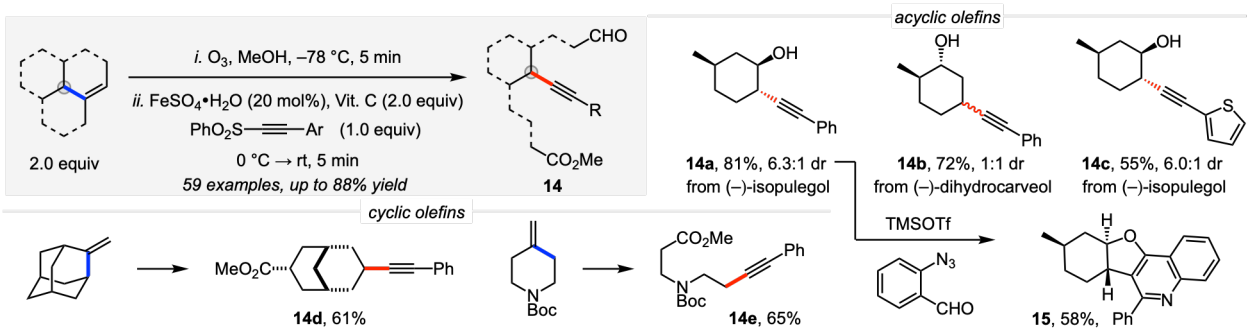


Figure 4.8 Dealkenylative Alkynylation

4.10 Halodealkenylation

Organic halides are a crucial part of organic synthesis because of their diverse reactivity profiles. Approximately 8400 naturally occurring halide-containing compounds have been identified, with organochlorides constituting around 1.84% and bromides about 1.45% of all NPs, including chlorine atoms in drug candidates that can significantly enhance their potency, the so-called "magic chloro effect". This disparity between the high utility and low occurrence of halides continues to drive the development of new strategies for their incorporation into NPs.

Considering the slow rate of chlorine atom abstraction from *para*-toluenesulfonyl chloride (*p*-TsCl) by carbon radicals, we employed our catalytic conditions to prevent potential side reactions [56]. Our optimal reaction conditions entailed subjecting 2 equiv of an olefin to Criegee ozonolysis in MeOH at −78 °C, warming the mixture to 0 °C, and then treatment with 1 equiv of the halogenating agent (*p*-TsCl, NBS, or NIS), 20 mol % FeSO4•7H2O, and 2 equiv of ascorbic acid.

Reactions of (–)-isopulegol produced good yields of chlorinated, brominated, and iodinated derivatives **16aa–ac** (Figure 4.9). (+)-Nootkatone gave high yields of **16ba–bc**. 1-Methylcyclohex-1-ene produced 5-chloro-, 5-bromo-, and 5-iodopentenals **16ca–cc**, but isolation of the ethylene glycol dioxolane was warranted for **16ca,cb** due to volatility. Methylene cyclohexane consistently yielded the 6-halogenated hexanoates **16da–dc**. Finally, we applied our method to the formal synthesis of the antioxidant α-tocopherol. Bromodealkenylation of phytol produced 72% of the bromide **16eb**, which has been used in α-tocopherol synthesis. Access to this bromide previously required four synthetic steps [61].

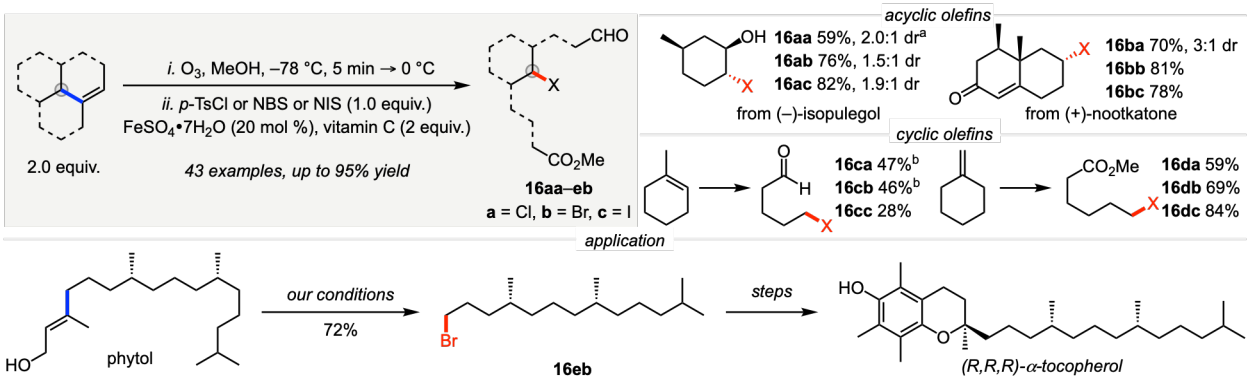


Figure 4.9 Halodealkenylation

Thorough kinetic analysis of our process enabled us to engage a slower radical generation and capture modality in dealkenylative functionalization using catalytic Fe^{II} with vitamin C. Dealkenylative functionalization as a net redox neutral catalytic process, however, was yet to come.

4.11 Aminodealkenylation

Aliphatic amines and nitrogen heterocycles are widespread in NPs, biomolecules, and pharmaceuticals. Approximately 43% of candidate drugs contain aliphatic amine fragments. The increasing demand for more complex three-dimensional architectures and for optically active amines in medicinal research has spurred the development of diverse methodologies for constructing *C*(sp^3)–N bonds [3].

A significant bottleneck in new C–N bond preparation lies in the availability of suitable starting materials. Inspired by the potential to transform ubiquitous olefins to alkaloids, we developed a redox-neutral catalytic system using copper(I) to couple amines with olefin-derived peroxides. The optimal amination conditions for the C–C cleavage followed by C–N coupling involved 20 mol % CuCl and 20 mol % 1,10-phenanthroline (phen) in MeCN at room temperature. Complete consumption of the amine, the limiting reagent, required 2 equiv of the alkene.

Subsequently, we investigated several nitrogen nucleophiles in the aminodealkenylation of (–)-isopulegol (Figure 4.10A). Our procedure successfully introduced various indoles into (–)-isopulegol, yielding the products **17a** and **17b** as indole scaffolds suitable for drug development. Notably, the aryl iodide in **17a**, which can engage in the copper-catalyzed Ullmann–Goldberg reaction, was tolerated. Furthermore, phthalimide, commonly used as a primary amine protecting group, was successfully coupled to yield the adduct **17c**. The drugs dexibuprofen amide and celecoxib, bearing a primary amide and a sulfonamide, were modified to produce the analogs **17d,e**. The antiretroviral lamivudine was also N-alkylated to form **17f**. The efficiency of the reactions

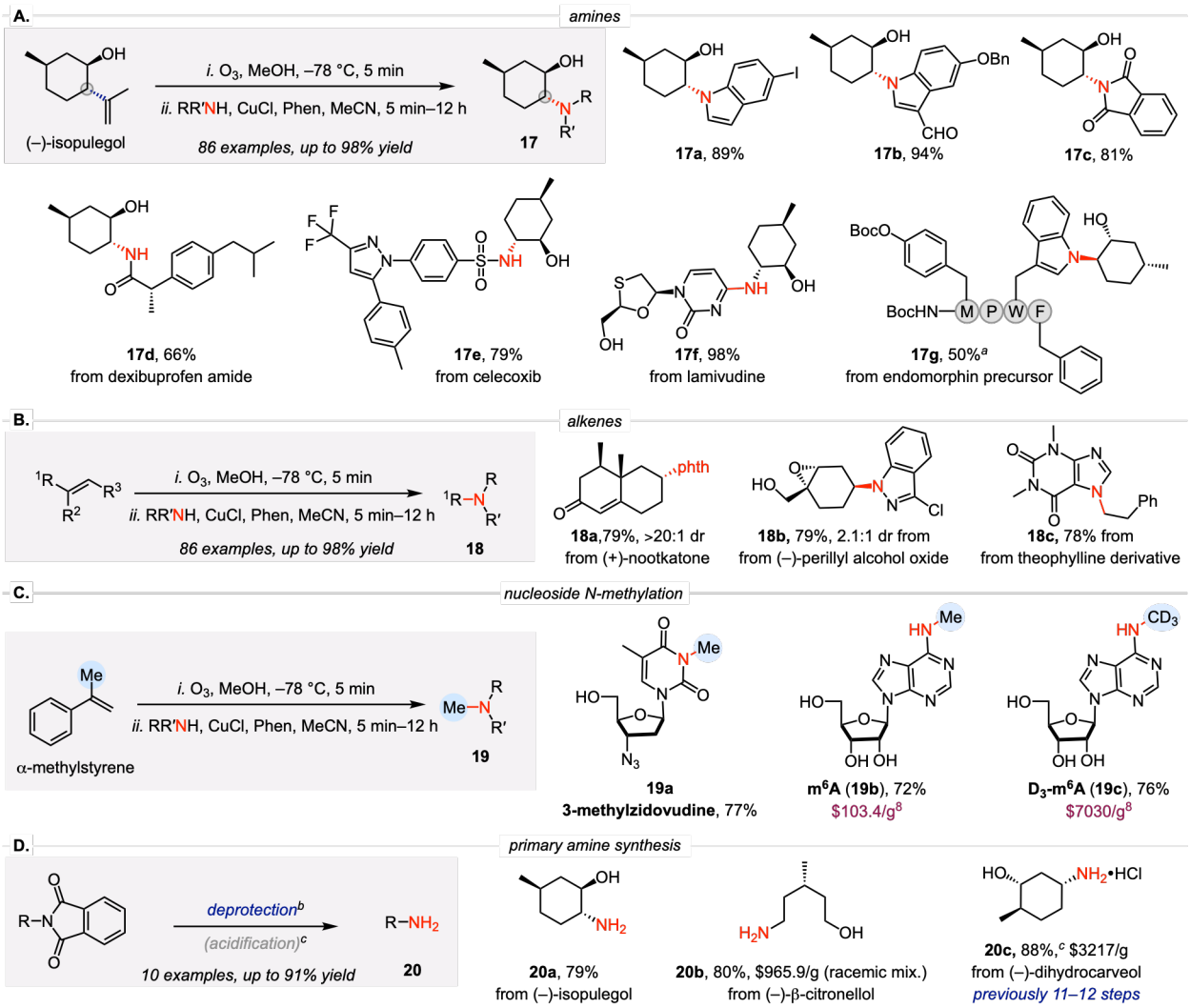


Figure 4.10 Aminodealkenylation and Primary Amine Synthesis

with indoles suggested an application in modifying tryptophan residues in peptides; in this context, the endomorphin tetrapeptide precursor yielded the (–)-isopulegol analog **17g**.

Natural terpenoids coupled well (Figure 4.10B). (+)-Nootkatone led to the adduct **18a**. The (–)-perillyl alcohol oxide coupled with indazole to give the adduct **18b**. Furthermore, primary alkyl radicals could be incorporated, exemplified by the theophylline derivative 18c.

The cumene process produces annually over 292,000 tons of α-methylstyrene (AMS) as a byproduct [62]. After Criegee ozonolysis in MeOH and reduction by Cu(I), AMS can be a useful methyl radical source because the stability of the methyl radical (BDE: 105.0 kcal/mol for Me–H) is greater than that of the phenyl radical (BDE: 112.9 kcal/mol for Ph–H) [63]. We N-methylated nucleoside bases without the need for any protecting groups (Figure 4.10C). Zidovudine, an anti-HIV drug, produced **19a**. We also prepared methyladenosine (m6A, **19b**) directly from adenosine. Although access to m^6A (**19b**) is desirable ($103.40/g), its trideuteromethyl analogue (D_3-m^6A) is 70-fold more valuable. Using D_3-AMS, prepared from acetophenone and deuterium oxide in two steps, we *N6*-trideuteromethylated adenosine to provide D_3-m^6A (**19c**).

Introducing phthalimide through aminodealkenylation opens the possibility of synthesizing primary amines upon deprotection (Figure 4.10D). Indeed, we converted (–)-isopulegol to the primary amine **20a** and (–)-β-citronellol to **20b**, previously available at $965.9/g for a racemic mixture. Aminodealkenylation/deprotection of (+)-dihydrocarveol ($3.10/g) furnished the amine **20c** ($3217/g), which has served as a precursor to a JNK inhibitor [64]. Previous syntheses of **20c** required 11 or 12 steps. We achieved a streamlined two-step synthesis of this compound using readily available feedstock.

Based on the gathered experimental data (see the original publication [3]), we proposed a mechanism involving cooperative catalysis by $[CuCl_2]^-$ and $[(Phen)_2Cu]^+$ (Figure 4.11). The amination is initiated with SET reduction of the peroxide **A** by the copper(I) complex **B**, generating the alkoxyl radical **C**. Its β-scission produces the alkyl radical **D** and methyl acetate. The generated $Cu(II)Cl_2$ complex **E** oxidizes the cationic complex **F**, leading to the formation of the copper(II) complex **G**. This species associates

with deprotonated phthalimide to form the complex **H** while releasing one phenanthroline ligand. This complex then captures the generated alkyl radical, resulting in the C–N coupled product; this process can occur through either an inner-sphere (I) or outer-sphere (**J**) pathway, ultimately yielding the copper(I) phenanthroline complex **K**. Reassociation of a phenanthroline ligand regenerates the cationic complex **F**. Electron transfer between complexes **K** and **E** is possible, ultimately providing the complex **H**.

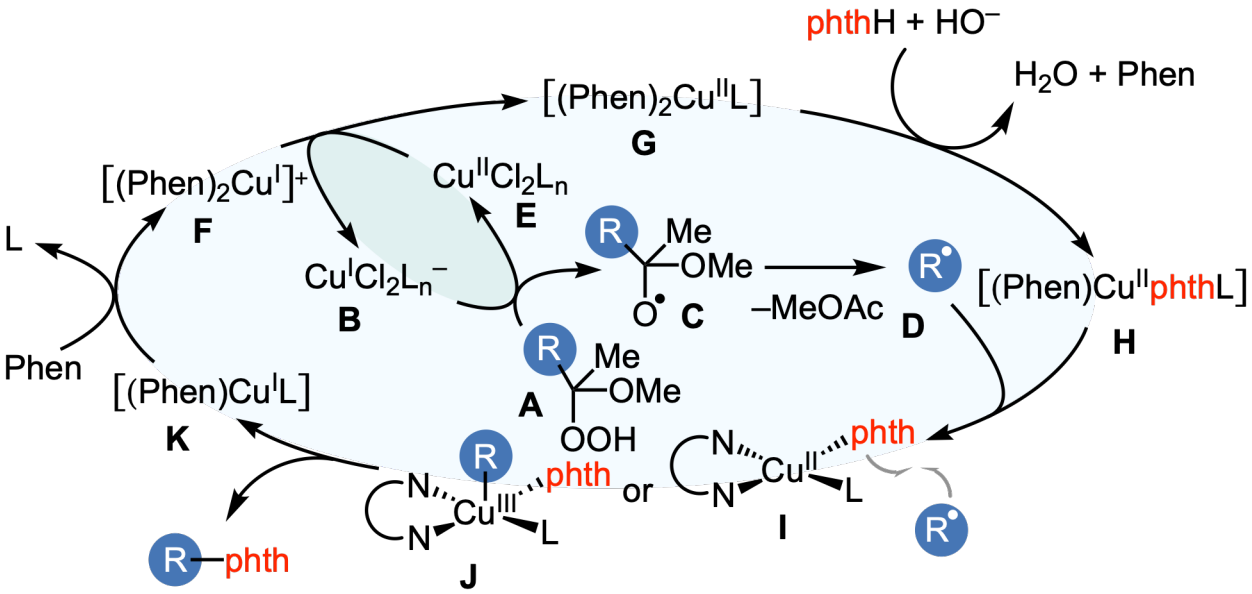


Figure 4.11 Mechanism for Hydroperoxide–Amine C(sp^3)–N Cross-Coupling

4.12 IMP–Hydrodeakenylation

Ozonolysis-based dealkenylation strategies offer robust molecular diversification, yielding products with new functional groups and carbon skeletons. Nevertheless, the high reactivity of ozone and various alkene structural features limits the universal application of ozonolysis to all olefins [65,66]. Notably, (1) ozone destructively affects electron-rich aromatic rings [67]; (2) Criegee ozonolysis directs the carbonyl oxide to the most electron-rich carbon atom of the alkene; (3) sterically hindered olefins do not produce hydroperoxides [68]; (4) internal electrophiles or nucleophiles near the double bond can lead to side reactions; and (5) allylic alcohols can induce Grob fragmentation (Figure 4.12).

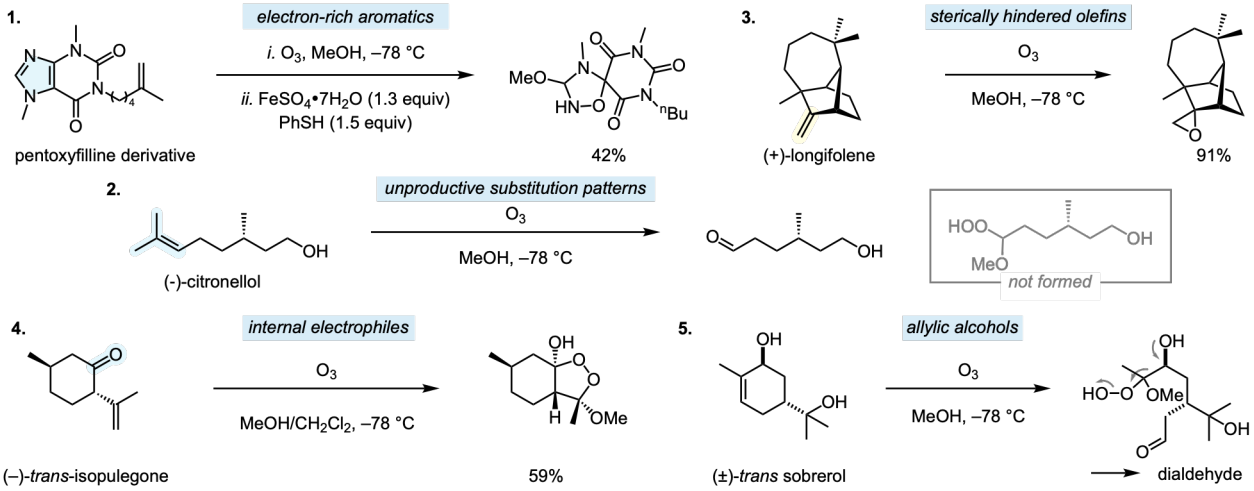


Figure 4.12 Ozone-Incompatible Alkene Classes

Therefore, we searched for an alternative strategy for activating alkenes for homolytic defunctionalization. The Isayama–Mukaiyama peroxidation (IMP) of alkenes employs a cobalt (or manganese) catalyst in the presence of a trialkylsilane to generate a metal hydride. Addition across the alkene, oxygen insertion, and transmetalation with the silane yields alkylsilylperoxides under mild and safe ozone-free conditions [66]. We found that

this reaction effectively activates olefins for SET cleavage, with IMP of Alkenes occurring using 10 mol % [$Co(modp)_2(EtOH)_2$], 2 equiv of Et3SiH, a drop of *t*-butylhydroperoxide (TBHP), and O_2 (1 atm) in DCE (0.2 M) at room temperature. We then focused on the reductive radical hydrogenation step. Treatment of triethylsilylperoxide with $FeSO_4 \cdot 7H_2O$ and PhSH in MeOH, the established conditions for ozonolysis–hydrodealkenylation, resulted in only a 57% yield of the cleavage product. Given that the rate of β-scission of trialkylalkoxyl radicals is 5 orders of magnitude lower than that of α-methoxydialkylalkoxyl radicals, over-reduction by Fe(II) to the alkoxide or HAT was likely (cf. Figure 4.7). Therefore, we developed unprecedented conditions using 5 mol % $Fe_2(SO_4)_3 \cdot xH_2O$, 10 mol % PhSH, and 1.5 equiv of γ-terpinene as the stoichiometric reductant in refluxing MeOH. These conditions allowed us to rescue ozone-incompatible substrates for hydrodealkenylative cleavage (Figure 4.13). The pentoxifylline-derived alkene **21a** underwent IMP, yielding 94% of silylperoxide **22a**, which gave a good yield of product **23a** upon reductive radical hydrogenation. An unproductively substituted alkene, (+)-methyl citronellate (**21b**), was converted to the peroxide **22b**, which we then reduced to the chiral ester **23b** in 67% GCMS yield. The sterically hindered olefin (+)-longifolene (**21c**) reacted under slightly modified reaction conditions to form the hydroperoxide **22c**. Its reductive cleavage with 2.2 equiv of PhSH furnished the bicyclic ketone **23c**. IMP of the carbic anhydride **21d**, bearing an internal electrophile, exclusively yielded the *exo*-configured triethylsilylperoxide **22d**, whose reductive radical hydrogenation gave the bicyclic anhydride **23d**. Allylic alcohols and internal nucleophiles were also "rescued" substrates when using IMP. For example, *trans*-sobrerol **21e** was peroxidized to give **22e**.

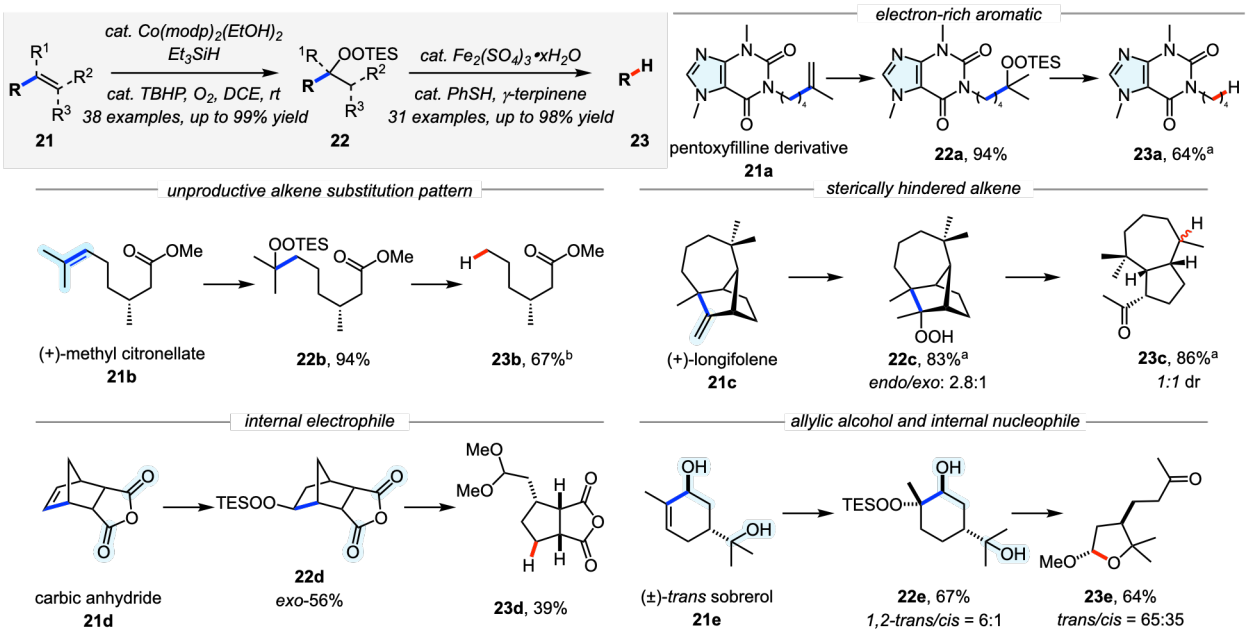


Figure 4.13 IMP–Hydrodealkenylation

Upon hydrodealkenylation, the aldehyde product underwent ketalization by the tertiary alcohol and MeOH, forming the tetrahydrofuran **23e**. The unusual catalytic cycle for the reductive radical hydrogenation of silylperoxides merits an explanation (Figure 4.14). The ferric sulfate hydrate precatalyst **I**, abbreviated as [Fe^{III}]–(H_2O), undergoes a ligand exchange in MeOH, forming the catalyst **II**. Another ligand exchange with thiophenol, a stronger ligand, generates the complex **III**, which, upon deprotonation, yields the covalent iron(III) complex **IV**. Disproportionation leads to the generation of the reducing iron(II) complex **V**, with concomitant production of a thiyl radical [70]. Complex **V** mediates SET reduction of the silylperoxide **VI**, producing the alkoxyl radical **VII**. After β-scission, HAT from thiophenol yields the product **VIII**. The newly formed [Fe^{III}]–$OSiEt_3$ species **IX** can regenerate the complex **II** upon return of a proton and MeOH, or the complex **IV** can be regenerated upon direct ligand exchange with thiophenol, producing silanol as a byproduct. The regeneration of PhSH occurs through HAT from γ-terpinene, yielding a

pentadienyl radical that, in an alternative scenario, reduces iron(III) complexes to iron(II), closing the catalytic cycle and producing *p*-cymene.

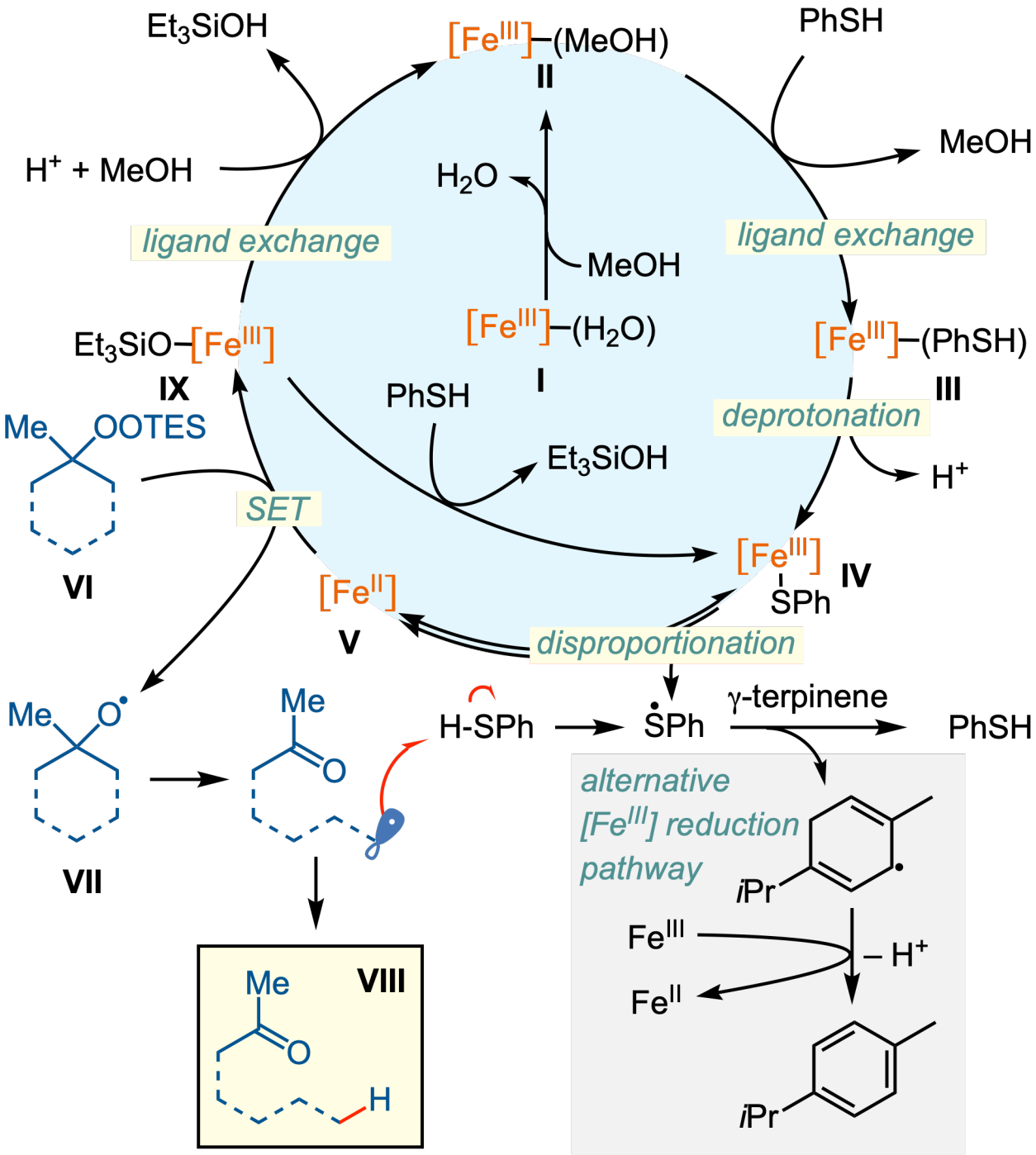


Figure 4.14 Silylperoxide Radical Hydrogenation Mechanism

4.13 Deacylative Homolysis of Ketone C(sp^3)–C(sp^2) Bonds

Since 2019, our laboratory has expanded the range of dealkenylative synthesis and has leveraged the abundance of olefins in chiral pool NPs (39.9%) to facilitate the synthesis of a diverse array of high-value compounds [11]. Ketones are also prevalent in NPs (15.9%) and commodity chemicals, and they serve as versatile synthetic handles because of their nucleophilic and electrophilic reactivity. Thus, we sought a generalized approach for ketone C–C bond homolysis, analogous to our dealkenylation strategy [4].

Current deacylation methods typically rely on the conversion of ketones to prearomatic intermediates (e.g., dihydrotriazoles and dihydroquinazolinones) that undergo SET oxidation, leading to C–C bond fragmentation and aromatic heterocycles [71]. While effective for acyclic ketones, with cyclic ketones the aromatic heterocycle remains integrated within the carbon skeleton of the fragmented product, limiting further modifications. This behavior has hindered the application of cycloalkanone C–C bond cleavage, highlighting the need for alternative strategies.

We evaluated ketone activation methods that could yield useful functional groups upon C–C bond scission of cycloalkanones, while not requiring intermediate purification. Recognizing that the α-methoxyhydroperoxides derived from Criegee ozonolysis of olefins are, in fact, peroxyacetals, we pursued the condensation of ketones with H_2O_2 and MeOH. We achieved only low conversions of the starting ketones, however, due to substrate-dependent equilibria. Therefore, we explored *gem*-dihydroperoxide formation from carbonyls through condensation with H_2O_2. Ultimately, we found that treating aliphatic ketones with anhydrous H_2O_2, prepared *in situ* via azeotropic drying of its 32–50% solution, consistently yielded *gem*-dihydroperoxides (Figure 4.15) [72].

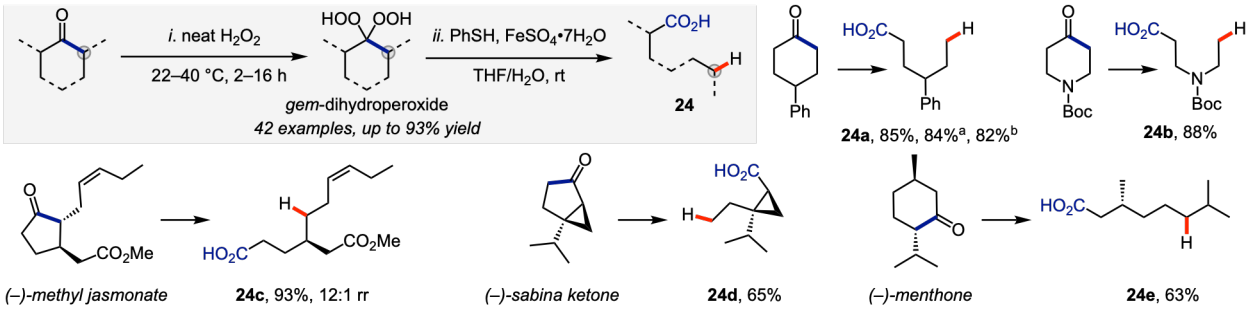


Figure 4.15 Hydrodeacylation of Cycloalkanones

Optimization of the cleavage step, using HAT for radical termination, revealed that slow addition of the *gem*-dihydroperoxide to a solution of benzenethiol and $FeSO_4$•$7H_2O$ in a THF/H_2O mixture efficiently provided reconstructed carboxylic acids from cycloalkanones. We tested a range of ketones in the optimized hydrodeacylative cleavage sequence. 4-Phenylcyclohexanone and *N*-Boc-4-piperidone underwent high-yielding conversions to the open-chain aliphatic carboxylic acids **24a,b**. The chiral pool terpenoids (–)-methyl jasmonate, (–)-sabina ketone, and (–)-menthone delivered the enantiopure carboxylic acids **24c–e**.

Next, we explored the utility of our deacylative methodology in the total synthesis of NPs (Figure 4.16). The versatility of the alkyl radical intermediate enabled a range of deacylative functionalizations, allowing the total synthesis of 14 NPs, 1 analog, and 2 drugs starting from readily available NPs. For example, we hydrodeacylated the ketone **25**, prepared in a single step from sclareol in 97% yield, to afford the decalinol **26**, previously synthesized in seven steps from sclareolide for clerodane biosynthesis investigations [73]. Notably, omitting benzenethiol redirected the reaction toward deacylative etherification, yielding the fragrance ambroxide (**27**). Deacylative aminoxylation of cholestenone (**28**) in the presence of TEMPO yielded the allylic

alkoxyamine **29**, which we converted in five steps to the nor-ring A steroid phorbasterone B (**30**), marking its first total synthesis [74]. Deacylative scission of methyl betulonate (**31**) with TEMPO, this time acting as a hydrogen atom abstractor, resulted in dehydrodeacylation, generating the C=C double bond of methyl sessiloside (**32**), previously synthesized in six steps [75]. Moreover, deacylative allylation of benzyloxycarbonyl-protected nortropinone with allylphenylsulfone resulted in the 2,5-disubstituted pyrrolidine **33**. Subsequent hydrogenation yielded the product **34**, which served as an intermediate in the synthesis of the alkaloid monomorine I (**35**) and the ant venom alkaloid from *Monomorium smithii* (**36**) [76,77].

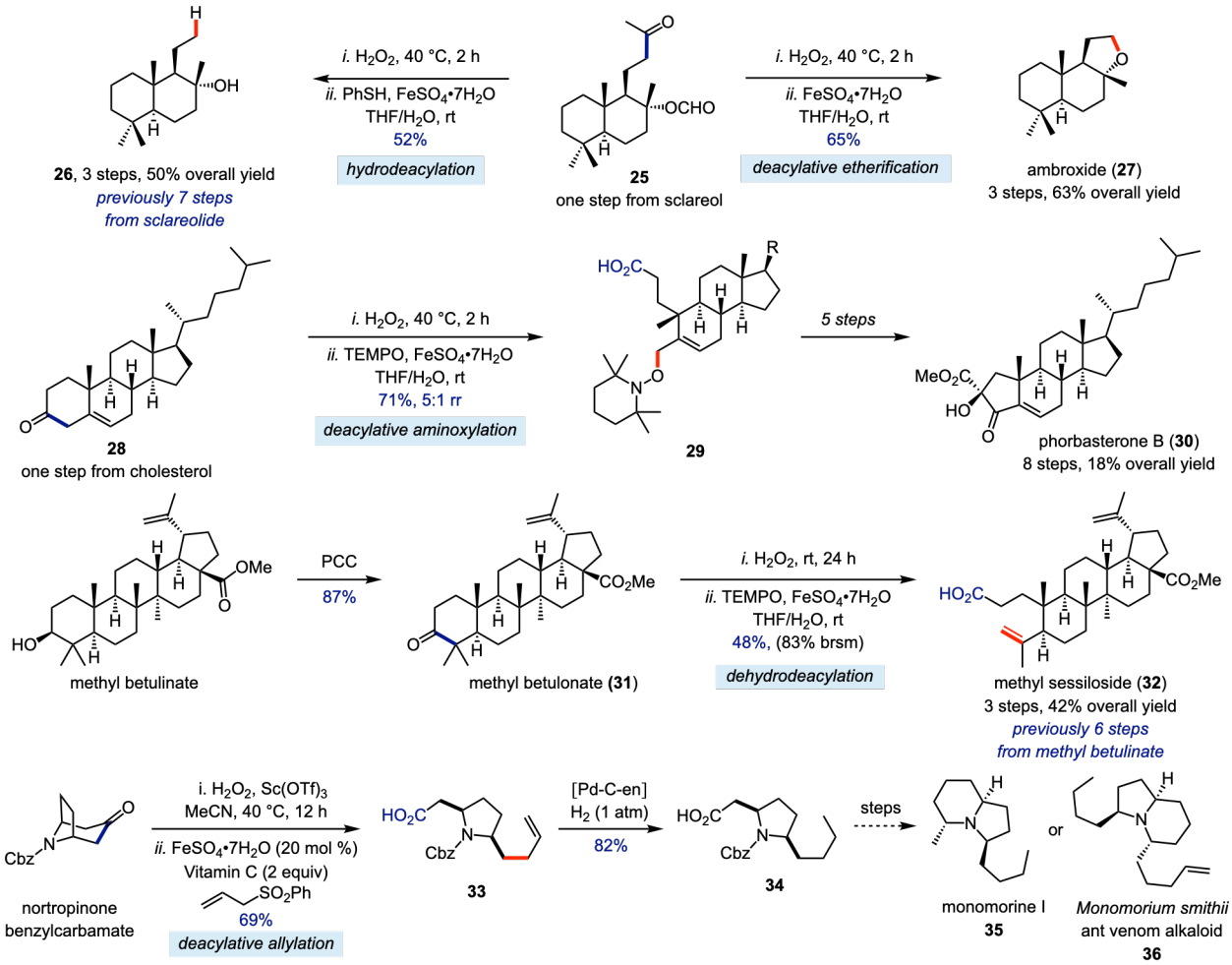


Figure 4.16 Selected Applications of Homolytic Deacylation in the Total Synthesis of NPs

4.14 Conclusions and Outlook

Investigations into the O–O bond cleavage of H_2O_2 by reducing metals has a rich history spanning over two centuries. However, it was not until the 1950s that chemists realized the potential of combining organic peroxides with SET reduction for synthetic applications. These insights enabled the rational design of reaction sequences involving C–C cleavage and functionalization. The resurgence of radical chemistry in the early 2000s also impacted peroxide-based deconstructive synthetic strategies.

Our exploration of this area was ignited by identifying technological gaps that required bridging for our synthetic needs. Since 2019, we have addressed these gaps by developing diverse peroxide-based deconstructive synthetic strategies that facilitate the conversion of readily available starting materials to advanced synthetic intermediates and high-value products. Chronologically, we have developed ozone-based processes: hydrodealkenylation, dealkenylative thiylation and alkenylation, oxodealkenylation, dealkenylative alkynylation, aminodealkenylation, and halodealkenylation. To overcome the limitations of ozonolysis, we applied IMP to convert alkenes to silylperoxides under mild reaction conditions. Recently, we successfully engaged ketones as another essential functional group in these methodologies, utilizing anhydrous H_2O_2 to transform readily available chiral-pool ketones into distinct NPs.

Looking ahead, the strategic combination of multiple reaction steps in a single pot, alongside peroxide-based functionalization, holds the potential for transformations reminiscent of alchemy, including molecular and single-atom editing technologies and profound skeletal remodeling. Ongoing investigations into several intriguing transformations are underway in our laboratory, promising many exciting advancements.

4.15 References

[1] Smaligo, A. J.; Swain, M.; Quintana, J. C.; Tan, M. F.; Kim, D. A.; Kwon, O. Hydrodealkenylative C(sp^3)–C(sp^2) Bond Fragmentation. *Science* **2019**, *364* (6441), 681–685.

[2] Smaligo, A. J.; Wu, J.; Burton, N. R.; Hacker, A. S.; Shaikh, A. C.; Quintana, J. C.; Wang, R.; Xie, C.; Kwon, O. Oxodealkenylative Cleavage of Alkene C(sp^3)–C(sp^2) Bonds: A Practical Method for Introducing Carbonyls into Chiral Pool Materials. *Angew. Chem. Int. Ed.* **2020**, *59* (3), 1211–1215.

[3] He, Z.; Moreno, J. A.; Swain, M.; Wu, J.; Kwon, O. Aminodealkenylation: Ozonolysis and Copper Catalysis Convert C(sp^3)–C(sp^2) Bonds to C(sp^3)–N Bonds. *Science* **2023**, *381* (6660), 877–886.

[4] Šimek, M.; Mahato, S.; Dehnert, B. W.; Kwon, O. Deacylative Homolysis of Ketone C(sp^3)–C(sp^2) Bonds: Streamlining Natural Product Transformations. *J. Am. Chem. Soc.* **2025**, *147* (7), 2664–2674.

[5] Henry, C. E.; Xu, Q.; Fan, Y. C.; Martin, T. J.; Belding, L.; Dudding, T.; Kwon, O. Hydroxyproline-Derived Pseudoenantiomeric [2.2.1] Bicyclic Phosphines: Asymmetric Synthesis of (+)- and (–)-Pyrrolines. *J. Am. Chem. Soc.* **2014**, *136* (34), 11890–11893.

[6] Xie, C.; Smaligo, A. J.; Song, X.-R.; Kwon, O. Phosphorus-Based Catalysis. *ACS Cent. Sci.* **2021**, *7* (4), 536–558.

[7] Shimizu, H.; Schredelseker, J.; Huang, J.; Lu, K.; Naghdi, S.; Lu, F.; Franklin, S.; Fiji, H. D.; Wang, K.; Zhu, H.; Tian, C.; Lin, B.; Nakano, H.; Ehrlich, A.; Nakai, J.; Stieg, A. Z.; Gimzewski, J. K.; Nakano, A.; Goldhaber, J. L.; Vondriska, T. M.; Hajnoczky, G.;

Kwon, O.; Chen, J.-N. Mitochondrial Ca^{2+} Uptake by the Voltage-Dependent Anion Channel 2 Regulates Cardiac Rhythmicity. *eLife* **2015**, *4*, No. e04801.

[8] All prices are indicated from the time of each original publication.

[9] Smaligo, A. J.; Vardhineedi, S.; Kwon, O. Carvone-Derived P-Stereogenic Phosphines: Design, Synthesis, and Use in Allene-Imine $[3 + 2]$ Annulation. *ACS Catal.* **2018**, *8* (6), 5188–5192.

[10] Schreiber, S. L. Fragmentation Reactions of α-Alkoxy Hydroperoxides and Application to the Synthesis of the Macrolide (±)-Recifeiolide. *J. Am. Chem. Soc.* **1980**, *102* (19), 6163–6165.

[11] Dehnert, B. W.; Dworkin, J. H.; Kwon, O. Dealkenylative Functionalizations: Conversion of Alkene C(sp^3)–C(sp^2) Bonds into C(sp^3)–X Bonds via Redox-Based Radical Processes. *Synthesis* **2024**, *56* (5), 71–86.

[12] Planche, L. A. Note sur la sophistication de la resine de jalap et sur les moyens de la reconnaitre, etc. *Bull. Pharmacie* **1810**, *2*, 578–580.

[13] Thénard, L. J. Nouvelles Observations sur les Acides et les Oxides Oxigénés. *Ann. Chim. Phys.* **1818**, *9*, 51–56.

[14] Schönbein, C. F. Ueber chemische Berührungswirkungen. *Verhand. Naturf. Ges. Basel* **1857**, 1–16.

[15] Schönbein, C. F. Ueber die Gleichheit des Einflusses, welchen in gewissen Fällen die Blutkörperchen und Eisenoxidulsalze auf die chemische Thätigkeit des gebundenen Sauerstoffes ausüben. *Verhand. Naturf. Ges. Basel* **1860**, 9–15.

[16] Brodie, B. C. XXXIII. On the Oxidation and Disoxidation Effected by the Alkaline Peroxides. *Philos. Trans. R. Soc.* **1862**, *152*, 837–859.

[17] Parnell, J. XXXVIII. On the Reducing Action of Peroxide of Hydrogen and Carbolic Acid. *J. Chem. Soc.* **1868**, *21*, 356–357.

[18] Fenton, H. J. H. LXXIII. Oxidation of Tartaric Acid in Presence of Iron. *J. Chem. Soc., Trans.* **1894**, *65*, 899–910.

[19] Haber, F.; Weiss, J. Über die Katalyse des Hydroperoxydes. *Naturwissenschaften* **1932**, *20*, 948–950.

[20] George, P.; Walsh, A. D. A Note on the Decomposition of Tertiary Alkyl Peroxides. *Trans. Faraday Soc.* **1946**, *42*, 94–97.

[21] Milas, N. A.; Surgenor, D. M. Studies in Organic Peroxides. VIII. t-Butyl Hydroperoxide and Di-t-butyl Peroxide. *J. Am. Chem. Soc.* **1946**, *68* (2), 205–208.

[22] Raley, J. H.; Rust, F. F.; Vaughan, W. E. Decompositions of Di-t-alkyl Peroxides. III. Kinetics in Liquid Phase. *J. Am. Chem. Soc.* **1948**, *70* (4), 1336–1338.

[23] Hawkins, E. G. E. The Reactions of Organic Peroxides. Part I. 2-phenyl-2-butyl Hydroperoxide. *J. Chem. Soc.* **1949**, 2076–2077.

[24] Rust, F. F.; Seubold, F. H., jr.; Vaughan, W. E. Decompositions of Di-t-alkyl Peroxides. V. Relative Stabilities of Alkoxy Radicals Derived from Unsymmetrical Dialkyl Peroxides. *J. Am. Chem. Soc.* **1950**, *72* (1), 338–340.

[25] Kharasch, M. S.; Fono, A.; Nudenberg, W. The Chemistry of Hydroperoxides. III. The Free-Radical Decomposition of Hydroperoxides. *J. Org. Chem.* **1950**, *15* (4), 763–774.

[26] Hawkins, E. G. E. Reactions of Organic Peroxides. Part VII. Reaction of 1-Hydroxycycloalkyl Hydroperoxides with Ferrous Compounds. *J. Chem. Soc.* **1955**, 3463–3467.

[27] Criegee, R.; Wenner, G. Die Ozonisierung des 9,10-Oktalins. *Justus Liebigs Annalen der Chemie* **1949**, *564* (1), 9–15.

[28] Bailey, P. S.; Bath, S. S. Ozonolyses of 1,2-Dibenzoylpropene and 1,2-Dibenzoylethylene. Markownikoff's Rule and the Initial Attack of Ozone on an Unsaturated System. *J. Am. Chem. Soc.* **1957**, *79* (12), 3120–3124.

[29] Murai, S.; Sonoda, N.; Tsutsumi, S. The Redox Reaction of 1-Ethoxy-n-heptyl Hydroperoxide. *Bull. Chem. Soc. Jpn.* **1964**, *37* (8), 1187–1190.

[30] De La Mare, H. E.; Kochi, J. K.; Rust, F. F. The Oxidation of Free Radicals by Metal Ions. *J. Am. Chem. Soc.* **1961**, *83* (8), 2013.

[31] Dworkin, J. H.; Dehnert, B. W.; Kwon, O. When All C–C Breaks LO–Ose. *Trends Chem.* **2023**, *5* (3), 174–200.

[32] Hu, L.-Y.; Lefker, B. A.; Du, D. Y.; Smith, Y. D.; Lei, H.; Harter, W. G.; Downs, V. L.; Boys, M. L.; Lula, D. M. Androgen Modulators. US Patent Application US20060009427A1, 2006.

[33] Srikrishna, A.; Kumar, P. R.; Gharpure, S. J. An Enantiospecific Synthesis of (–)-2-Pupukeanone via a Rhodium Carbenoid C-H Insertion Reaction. *Tetrahedron Lett.* **2001**, *42* (23), 3929–3931.

[34] Srikrishna, A.; Reddy, T. J. Enantiospecific Synthesis of (+)-(1*S*,2*R*,6*S*)-1,2-Dimethylbicyclo[4.3.0]nonan-8-one and (–)-7-Epibakkenolide-A. *Tetrahedron* **1998**, *54* (38), 11517–11524.

[35] Ji, J.; Chen, J.; Qin, S.; Li, W.; Zhao, J.; Li, G.; Song, H.; Liu, X.-Y.; Qin, Y. Total Synthesis of Vilmoraconitine. *J. Am. Chem. Soc.* **2023**, *145* (6), 3903–3908.

[36] Kim, D. E.; Zhu, Y.; Harada, S.; Aguilar, I.; Cuomo, A. E.; Wang, M.; Newhouse, T. R. Total Synthesis of (+)-Shearilicine. *J. Am. Chem. Soc.* **2023**, *145* (7), 4394–4399.

[37] Gu, X.; Zhang, Y.-A.; Zhang, S.; Wang, L.; Ye, X.; Occhialini, G.; Barbour, J.; Pentelute, B. L.; Wendlandt, A. E. Synthesis of Non-canonical Amino Acids Through Dehydrogenative Tailoring. *Nature* **2024**, *634*, 352–358.

[38] Kobayashi, T.; Sugitate, R.; Uchida, K.; Kawamoto, Y.; Ito, H. Asymmetric Total Synthesis of (–)-Lemnalemnane A. *Org. Lett.* **2024**, *26* (9), 1803–1806.

[39] Schaaf, R. E.; Quirke, J. C. K.; Ghavami, M.; Tonogai, E. J.; Yeon Lee, H.; Barlock, S. L.; Trzupek, T. R.; Abo, K. R.; Rees, M. G.; Ronan, M. M.; Roth, J. A.; Hergenrother, P. J. Identification of a Selective Anticancer Agent from a Collection of Complex-And-Diverse Compounds Synthesized from Stevioside. *J. Am. Chem. Soc.* **2025**, *147* (28), 10647–10661.

[40] Smaligo, A. J.; Kwon, O. Dealkenylative Thiylation of C(sp^3)–C(sp^2) Bonds. *Org. Lett.* **2019**, *21* (21), 8592–8597.

[41] Huston, P.; Espenson, J. H.; Bakac, A. Kinetics of Formation and Reactions of Thiyl Radicals in Aqueous Solution. *Inorg. Chem.* **1992**, *31* (5), 720–722.

[42] Dénès, F.; Pichowicz, M.; Povie, G.; Renaud, P. Thiyl Radicals in Organic Synthesis. *Chem. Rev.* **2014**, *114* (5), 2587–2693.

[43] Swain, M.; Sadykhov, G.; Wang, R.; Kwon, O. Dealkenylative Alkenylation: Formal π-Bond Metathesis of Olefins. *Angew. Chem., Int. Ed.* **2020**, *59* (40), 17565–17571.

[44] (a) Fischer, H. Substituent Effects in Radical Chemistry. In *Substituent Effects in Radical Chemistry*; Viehe, H. G., Janousek, Z., Merenyi, R., Eds.; Reidel: Dordrecht, 1986; pp 123–142. (b) Wong, M. W.; Radom, L. Radical Addition to Alkenes: An Assessment of Theoretical Procedures. *J. Phys. Chem.* **1995**, *99* (21), 8582–8588. (c) Zytowski, T.; Fischer, H. Absolute Rate Constants for the Addition of Methyl Radicals to Alkenes in Solution: New Evidence for Polar Interactions. *J. Am. Chem. Soc.* **1996**, *118* (2), 437–439. (d) Rubin, H.; Fischer, H. The Addition of tert-Butyl (Me_3C) and (*tert*-butoxy)carbonyl Methyl Radicals to Alkynes in Solution Studied by ESR Spectroscopy. *Helv. Chim. Acta* **1996**, *79* (6), 1670–1682. (e) Fischer, H.; Radom, L. Factors Controlling the Addition of Carbon-Centered Radicals to Alkenes: An Experimental and Theoretical Perspective. *Angew. Chem., Int. Ed.* **2001**, *40* (8), 1340–1371. (f) Newcomb, M. Radical Kinetics and Clocks. In *Encyclopedia of Radicals in Chemistry, Biology and Materials*; Chatgilialoglu, C., Studer, A., Eds.; John Wiley & Sons: Chichester, 2012; pp 107–124. (g) Wille, U. Radical Cascades Initiated by Intermolecular Radical Addition to Alkynes and Related Triple Bond Systems. *Chem. Rev.* **2013**, *113* (1), 813–853.

[45] Chateauneuf, J.; Lusztyk, J.; Ingold, K. U. Absolute Rate Constants for the Reactions of Some Carbon-Centered Radicals with 2,2,6,6-Tetramethyl-1-piperidinoxyl. *J. Org. Chem.* **1988**, *53* (7), 1629–1632.

[46] Fordham, J. W. L.; Williams, H. L. The Decomposition of Cumene Hydroperoxide by Ferrous Iron in the Presence of Oxygen. *J. Am. Chem. Soc.* **1950**, *72* (10), 4465–4469.

[47] (a) Fittschen, C.; Hippler, H.; Viskolcz, B. The β C-C Bond Scission in Alkoxy Radicals: Thermal Unimolecular Decomposition of t-Butoxy Radicals. *Phys. Chem. Chem. Phys.* **2000**, *2* (8), 1677–1683. (b) Vereecken, L.; Peeters, J. Decomposition of Substituted Alkoxyradicals—Part I: A Generalized Structure-Activity Relationship for Reaction Barrier Heights. *Phys. Chem. Chem. Phys.* **2009**, *11* (40), 9062–9074.

[48] Neta, P.; Grodkowski, J.; Ross, A. B. Rate Constants for Reactions of Aliphatic Carbon-Centered Radicals in Aqueous Solution. *J. Phys. Chem. Ref. Data* **1996**, *25* (3), 709–1050.

[49] Basco, N.; James, D. G. L.; Suart, R. D. A Quantitative Study of Alkyl Radical Reactions by Kinetic Spectroscopy. Part 1. Mutual Combination of Methyl Radicals and Combination of Methyl Radicals with Nitric Oxide. *Int. J. Chem. Kinet.* **1970**, *2* (3), 215–234.

[50] Gibian, M. J.; Corley, R. C. Organic Radical-Radical Reactions. Disproportionation vs. Combination. *Chem. Rev.* **1973**, *73* (5), 441–464.

[51] LaVerne, J. A.; Wojnarovits, L. Rates of Alkyl Radical-Radical, Alkyl Radical-Iodine, and Iodine Atom-Atom Reactions in Normal Alkanes and Cycloalkanes. *J. Phys. Chem.* **1994**, *98* (48), 12635–12640.

[52] Avila, D. V.; Brown, C. E.; Ingold, K. U.; Lusztyk, J. Solvent Effects on the Competitive β-Scission and Hydrogen Atom Abstraction Reactions of the Cumyloxyl Radical. Resolution of a Long-Standing Problem. *J. Am. Chem. Soc.* **1993**, *115* (2), 466–470.

[53] Swain, M.; Bunnell, T. B.; Kim, J.; Kwon, O. Dealkenylative Alkynylation Using Catalytic Fe and Vitamin C. *J. Am. Chem. Soc.* **2022**, *144* (32), 14828–14837.

[54] García Ruano, J. L.; Alemán, J.; Parra, A.; Marzo, L. Sulfonyl Acetylenes as Alkynylating Reagents Under Radical or Anionic Conditions. *Eur. J. Org. Chem.* **2014**, *2014* (8), 1577–1588.

[55] Gharpure, S. J.; Nanda, S. K.; Adate, P. A.; Shelke, Y. G. Lewis Acid Promoted Oxonium Ion Driven Carboamination of Alkynes for the Synthesis of 4-Alkoxy Quinolines. *J. Org. Chem.* **2017**, *82* (4), 2067–2080.

[56] Dehnert, B. W.; Yin, Y.; Kwon, O. Halodealkenylation: Ozonolysis and Catalytic Fe with Vitamin C Convert C(sp^3)–C(sp^2) Bonds to C(sp^3)–Halide Bonds. *Org. Lett.* **2024**, *26* (24), 10921–10927.

[57] Gribble, G. W. A Survey of Recently Discovered Naturally Occurring Organohalogen Compounds. *J. Nat. Prod.* **2024**, *87* (5), 1285–1305.

[58] Ertl, P.; Schuhmann, T. A Systematic Cheminformatics Analysis of Functional Groups Occurring in Natural Products. *J. Nat. Prod.* **2019**, *82* (5), 1258–1263.

[59] Chiodi, D.; Ishihara, Y. "Magic Chloro": Profound Effects of the Chlorine Atom in Drug Discovery. *J. Med. Chem.* **2023**, *66* (8), 5305–5331.

[60] Dneprovskii, A. S.; Eliseenkov, E. V.; Chulkova, T. G. Rate Constants of Halogen Abstraction from Halogenating Agents by Alkyl Radicals. *Russ. J. Org. Chem.* **2002**, *38* (3), 338–343.

[61] Wu, Z.; Harutyunyan, S. R.; Minnaard, A. J. Total Synthesis of (R,R,R)-γ-Tocopherol through Cu-Catalyzed Asymmetric 1,2-Addition. *Chem. Eur. J.* **2014**, *20* (44), 14250–14255.

[62] Wood, L. Alpha-Methylstyrene Market Global Forecast to 2024. Research and Markets, 2019.

[63] Luo, Y.-R. *Comprehensive Handbook of Chemical Bond Energies*; Taylor & Francis Group: Boca Raton, FL, 2007.

[64] Man, H.-W.; Xu, J.; Beauchamps, M. G.; Kothare, M. A.; Zou, N.; Li, Y.; Huang, L. Solid Forms of 2-(*tert*-Butylamino)-4-((1R,3R,4R)-3-hydroxy-4-methylcyclohexylamino)-pyrimidine-5-carboxamide, Compositions Thereof and Methods of Their Use. US Patent US9365524B2, 2016.

[65] Dworkin, J. H.; Chen, Z. M.; Cheasty, K. C.; Rubio, A. V.; Kwon, O. Hydrodealkenylative $C(sp^3)$–$C(sp^2)$ Bond Fragmentation Using Isayama-Mukaiyama Peroxidation. *J. Am. Chem. Soc.* **2025**, *147*, ahead of print.

[66] Zvereva, T. I.; Kasradze, V. G.; Kazakova, O. B.; Kukovinets, O. S. Ozonolysis of Unsaturated Carbonyl Compounds and Alcohols. *Russ. J. Org. Chem.* **2010**, *46* (10), 1431–1451.

[67] Zimmer, H.; Amer, A.; Ho, D.; Koch, K.; Schumacher, C.; Wingfield, R. C. A Novel Oxidative Skeleton Rearrangement of the Caffeine System. *J. Org. Chem.* **1990**, *55* (16), 4988–4989.

[68] Dimitrov, V.; Hopp Rentsch, G.; Linden, A.; Hesse, M. The Ozonolysis of Longifolene: A Tool for the Preparation of Useful Chiral Compounds. Configuration

Determination of New Stereogenic Centers by NMR Spectroscopy and X-Ray Crystallography. *Helv. Chim. Acta* **2003**, *86* (1), 106–121.

[69] Isayama, S. An Efficient Method for the Direct Peroxygenation of Various Olefinic Compounds with Molecular Oxygen and Triethylsilane Catalyzed by a Cobalt (II) Complex. *Bull. Chem. Soc. Jpn.* **1990**, *63* (5), 1305–1310.

[70] Buzsaki, S. R.; Mason, S. M.; Kattamuri, P. V.; Serviano, J. M. L.; Rodriguez, D. N.; Wilson, C. V.; Hood, D. M.; Ellefsen, J. D.; Lu, Y.-C.; Kan, J.; et al. Fe/Thiol Cooperative Hydrogen Atom Transfer Olefin Hydrogenation: Mechanistic Insights That Inform Enantioselective Catalysis. *J. Am. Chem. Soc.* **2024**, *146* (25), 17296–17310.

[71] Xu, Y.; Qi, X.; Zheng, P.; Berti, C. C.; Liu, P.; Dong, G. Deacylative Transformations of Ketones via Aromatization-Promoted C-C Bond Activation. *Nature* **2019**, *567* (7748), 373–378.

[72] Starkl Renar, K.; Pečar, S.; Iskra, J. Activation of Aqueous Hydrogen Peroxide for Non-Catalyzed Dihydroperoxidation of Ketones by Azeotropic Removal of Water. *Org. Biomol. Chem.* **2015**, *13* (36), 9369–9372.

[73] George, J. H.; McArdle, M.; Baldwin, J. E.; Adlington, R. M. Biomimetic Rearrangements of Simplified Labdane Diterpenoids. *Tetrahedron* **2010**, *66* (32), 6321–6330.

[74] Masuno, M. N.; Pawlik, J. R.; Molinski, T. F. Phorbasterones A-D, Cytotoxic Nor-Ring A Steroids from the Sponge Phorbas amaranthus. *J. Nat. Prod.* **2004**, *67* (5), 731–733.

[75] Klinot, J.; Šumanová, J.; Vystrčil, A. 3,4-Seco Derivatives of Betulinic Acid. *Collect. Czechoslov. Chem. Commun.* **1972**, *37* (2), 603–609.

[76] Saliou, C.; Fleurant, A.; Célérier, J. P.; Lhommet, G. Total Synthesis of (+)-Monomorine I from Chiral Cyclic β-Enamino Ester. *Tetrahedron Lett.* **1991**, *32* (29), 3365–3368.

[77] Takahata, H.; Bandoh, H.; Momose, T. An Asymmetric Synthesis of the Ant Venom Alkaloid (3S,5S,8aR)-3-Butyl-5-(4-pentenyl)indolizidine via the Sharpless Asymmetric Dihydroxylation. *Heterocycles* **1996**, *42* (1), 39–42.

CHAPTER FIVE

Ozonolysis of Alkenes Containing Amines, Allylic Alcohols, and Electron-Rich Arenes for Dealkenylation

Adapted from Dworkin, J. H.; Chen, Z. M.; Prout, E. S.; Kwon, O.

Org. Lett. **2025**, *27*, 7833–7839

5.1 Abstract

Dealkenylative synthesis generates alkyl radicals through ozonolysis of alkenes in MeOH and subsequent low valent metal–mediated reduction of the resulting α-methoxyhydroperoxide intermediates. The net transformation cleaves alkene $C(sp^3)$–$C(sp^2)$ bonds and forms new $C(sp^3)$–X bonds. While broadly effective, the presence of amine, allylic alcohol, or electron-rich aromatic functionalities can cause undesired side-reactions during ozonolysis. Herein, we demonstrate that in situ protonation of amines, acylation of allylic alcohols, and controlling the number of ozone equivalents can be used to address these challenges.

5.2 Introduction

Several common organic functional groups—namely carboxylic acids, alcohols, and amines—have been used recently to generate alkyl radicals, extending beyond traditional alkyl radical precursors (e.g., alkyl halides) [1–4]. In turn, these alkyl radicals enable the formation of new chemical bonds through direct radical capture, radical–polar crossover, or metal-mediated coupling [5]. Dealkenylative synthesis invokes radical chemistry to break the $C(sp^3)$–$C(sp^2)$ σ-bond of an alkene and install a new $C(sp^3)$–X bond [6]. This method expands the sources of alkyl radicals to olefins, which are abundant in natural products (40%) and feedstock chemicals [7]. Dealkenylation uses Fe(II)- or Cu(I)-mediated single-electron reduction of peroxides formed from alcohol-intercepted Criegee ozonolysis of alkenes to access alkyl radicals after β-scission [6]. Both processes—ozonolysis and base metal-mediated reduction—require minimal preparation, are quick to enact, and can be performed open-to-air, making dealkenylation an invaluable tool for constructing complex molecules. Overall, dealkenylative synthesis opens up new possibilities in synthetic chemistry—for example, enabling the derivatization of ubiquitous alkenes, particularly those from Nature's chiral pool, into useful chiral building blocks.

Ozone is an eco-friendly, atom-economical oxidant that is operationally simple to handle and exceptionally potent. These benefits directly facilitate the tandem two-step protocol for dealkenylation, which hinges on efficient Criegee ozonolysis of alkenes in MeOH to produce α-methoxyhydroperoxides (Figure 5.1) [8]. Mechanistically, a given alkene, in this case *O*-benzoyl-isopulegol (**1a**), forms a 1,2,3-trioxolane **I** after initial (3+2)-cycloaddition with ozone. *Retro*-(3+2)-cycloaddition of **I** ejects formaldehyde and provides the carbonyl oxide II, the so-called Criegee intermediate. Capture of **II** with MeOH

quantitatively forms the α-methoxyhydroperoxide **III** [8]. Addition of iron(II) sulfate heptahydrate initiates single electron transfer (SET) to reduce the peroxide O–O bond. The alkoxyl radical **IV** and iron(III) hydroxysulfate are formed after SET. Rapid β-scission of **IV** extrudes methyl acetate and provides the alkyl radical **V**. Finally, hydrogen atom transfer (HAT) from benzenethiol furnishes the hydrodealkenylation product **1b**.

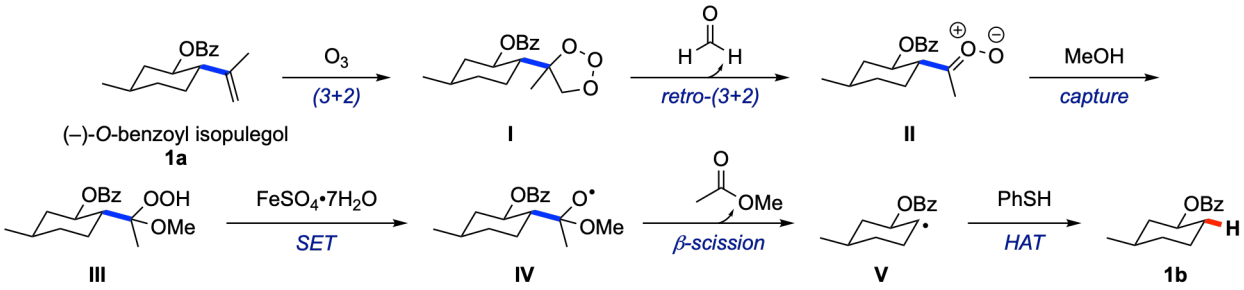


Figure 5.1 Hydrodealkenylation Mechanism

While many alkenes are compatible with ozonolysis in this manner, those possessing amine, allylic alcohol, and electron-rich arene (ERA) functionalities tend to obstruct efficient production of the α-methoxyhydroperoxide. An amine may be oxidized to the *N*-oxide prior to ozone reacting with the intended alkene (Figure 5.2a) [9]. The peroxide **2x** formed from steviol methyl ester (2a), an allylic alcohol, is destroyed through Grob fragmentation (Figure 5.2b) [10]. ERAs can react with ozone at a rate comparable to or faster than their unactivated alkene substituents [11,12]. For example, isoeugenol is oxidized to muconic acid derivatives at the arene instead of to homovanillin at the alkene (Figure 5.2c) [11,12]. In addition to the effects of these three functionalities, some olefinic compounds are insoluble in MeOH, preventing the formation of α-methoxyhydroperoxides. In this paper we provide solutions to "rescue" alkenes bearing

these molecular features, allowing them to become suitable substrates for dealkenylation chemistry.

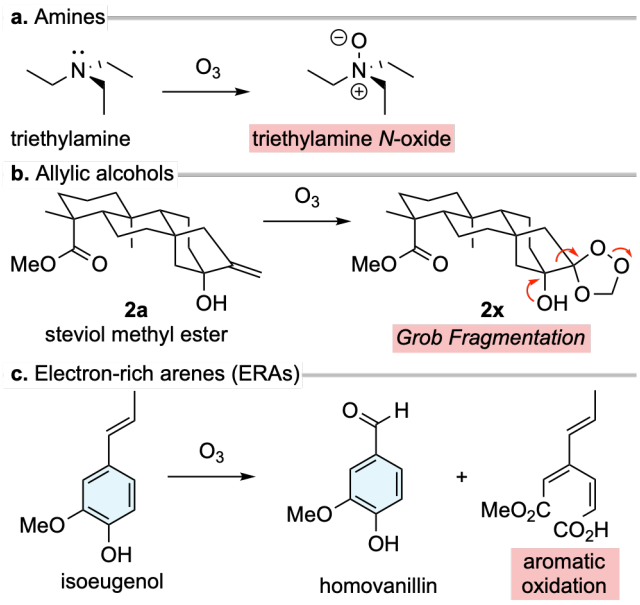


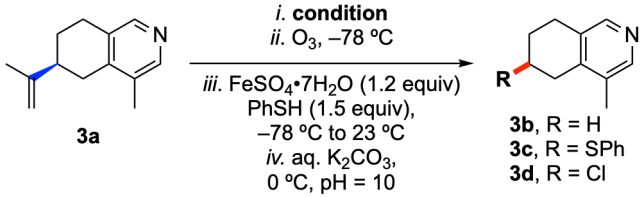
Figure 5.2 Ozone Incompatible Functionalities

5.3 Alkenes with Amines

The wide representation of amine functionalities in natural products, pharmaceuticals, agrochemicals, and other bioactive compounds elicits their status as a privileged functional group [13]. Direct ozonolysis of compounds containing basic amines or pyridines is challenging because they readily form *N*-oxides at rates comparable to alkene ozonolysis [6,12,14]. In dealkenylation, this side reaction complicates the ozonolysis mixture and obstructs reaction monitoring, as zwitterionic *N*-oxides remain stationary on SiO_2 thin-layer-chromatography plates. Although postreduction of *N*-oxides [e.g., using a transition metal or bis(pinacolato)diboron] can regenerate the amine, it lowers overall yield [6b,16]. Protonated amines, on the other hand, are generally unreactive toward ozone, with *N*-oxide formation inversely related to the acid–base equilibrium constant [6b,16]. To incorporate substrates bearing amines, we opted to form ammonium ions in situ to prevent amine oxidation [17]. Other modes of protection, such as *tert*-butyloxycarbonyl (Boc) or *p*-toluenesulfonyl (Ts), have previously been demonstrated for dealkenylation [6e–g]. In our prior study, the hydrochloride salt of an amino alcohol from (+)-trans-limonene oxide gave the hydrodealkenylation product in 62% yield after basic workup [6g]. Based on this observation, we opted to further pursue *in situ* conjugate acid formation to streamline amine hydrodealkenylation into a one-pot procedure.

We prepared the model pyridine substrate **3a** in 71% yield via condensation of propargylamine with (–)-perillaldehyde (**3**), followed by lithium *tert*-butoxide mediated isomerization, 6π-electrocyclization, and aromatization [18]. Initial optimization began with conditions from our prior report (Table 5.1) [6b]. Treatment of **3a** in MeOH (0.1 M) at 0 ºC with 1.0 equiv HCl formed the pyridinium hydrochloride. Ozonolysis in MeOH,

Table 5.1 Optimization of Hydrodealkenylation for Amino-Alkenes



	condition	3b	3c	3d
1	HCl (1.0 equiv), MeOH, 0 ºC	74%	14%	10%
2	HCl (2.0 equiv), MeOH, 0 ºC	61%	2%	29%
3	1:4 AcOH/MeOH, 0 ºC	57%	20%	
4	1:4 TFA/MeOH, 0 ºC	90%		

followed by addition of $FeSO_4•7H_2O$ (1.2 equiv) and benzenethiol (1.5 equiv), then aqueous K_2CO_3 workup (pH 10, 0 °C), delivered the hydrodealkenylation product. This one-pot, four-step process gave 74% of **3b**, 14% of thiylation product **3c**, and 10% of chloride **3d** (entry 1). Doubling HCl to 2.0 equiv lowered **3b** to 61% and **3c** to 2%, while increasing **3d** to 29% (entry 2). To avoid the chloride **3d**, we replaced HCl with alternative acids. Using 1:4 AcOH/MeOH gave 57% of **3b** and 20% of **3c** (entry 3), likely due to the small ΔpK_a between AcOH (4.76) and the pyridinium ion (5.21) [19], yielding an equilibrium constant (K_{eq}) of $10^{0.45}$. Using trifluoroacetic acid (TFA; pK_a = –0.25) [19] increased K_{eq} to $10^{5.46}$, improving the yield of **3b** to 90% (entry 4). As such, TFA/MeOH became our standard condition for *in situ* amine protection. In applying this condition to other amino-alkenes, we obtained hydrodealkenylation products **4b** and **5b** from tertiary amine substrates **4a** and **5a** in 63% and 70% yields, respectively (Figure 5.3). Our method also enabled three formal syntheses (Figure 5.4) [20–22]. Wittig olefination of *N*-Boc norpseudopelletierine (**6**) gave **6a** in 99% yield. Boc deprotection (1:4 TFA/DCM, 0 °C) provided the ammonium trifluoroacetate, which underwent hydrodealkenylation in 1:4 TFA/MeOH followed by K_2CO_3 workup to afford **6b** in 85% yield—an intermediate in the

synthesis of (±)-pinidinone, Galbulimima alkaloid GB17, and a nonpeptide GnRH antagonist.

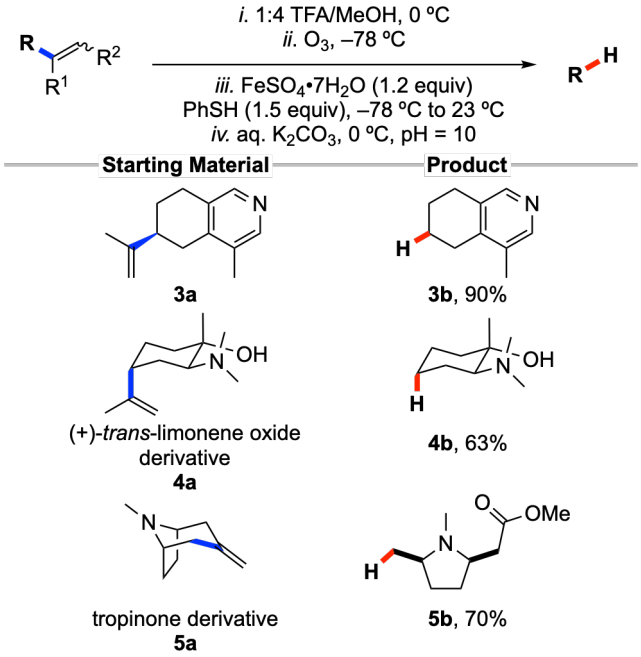


Figure 5.3 Hydrodealkenylation of Amino-Alkenes

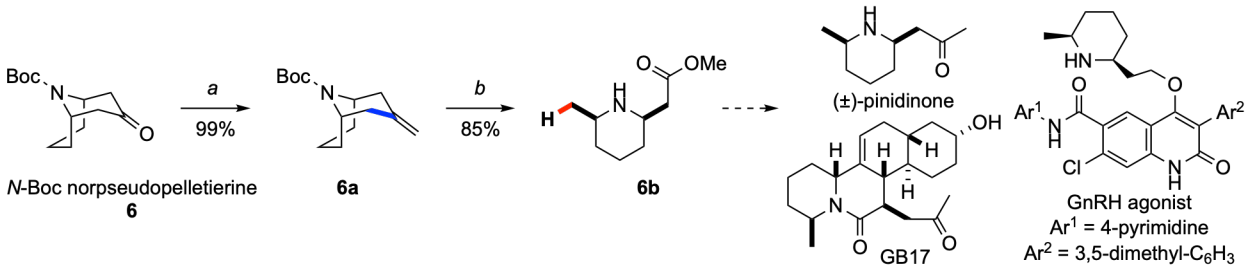


Figure 5.4 Formal Syntheses of (±)-Pinidinone, GB17, and GnRH Agonist from *N*-Boc Norpseudopelletierine

(a) Ph_3PMeBr (1.5 equiv), *t*BuOK (1.5 equiv), THF, reflux, 3 h, 99%; (b) i. 1:4 TFA/DCM, 0 ºC; ii. O_3, 1:4 TFA/MeOH, –78 ºC; iii. $FeSO_4$•$_7$H2O (1.2 equiv), PhSH (1.5 equiv), from –78 to 23 ºC; iv. aq. K_2CO_3, 0 ºC, pH 10; 85%

5.4 Allylic Alcohols

Allylic alcohols are valuable in organic synthesis and are commonly used in asymmetric oxidations and metal-mediated substitutions [23]. However, this motif has not previously been compatible with dealkenylation due to undesired Grob fragmentation, which cleaves the peroxide O–O and allyl σ-C(sp^3)–C(sp^2) and exchanges them for two π-C=O bonds [10b]. We hypothesized that decreasing the nucleophilicity of the allylic alcohol would reduce Grob fragmentation of β-oxyalkylperoxides. Since acylation is known to suppress this pathway, we pursued it as a strategy for enabling dealkenylation [10a].

Indeed, acylation of allylic alcohols enabled hydrodealkenylation. From *O*-acetyl steviol methyl ester (**2a'**), we obtained compound **2b** in 67% yield via secondary alkyl radical hydrogenation, with a 1.0:7.8 axial-to-equatorial ratio (Figure 5.5), and compound **2b'** in 25% yield via the primary radical. A similar outcome was observed for *O,O*-diacetyl gibberellic acid derivative **7a**, yielding **7b** in 52% (1.0:5.7 axial-to-equatorial ratio) and **7b'** in 15%. Methyl shikimate triacetate (**8a**) gave **8b** in 65% yield after β-elimination of an acetoxy group. From (±)-*trans*-sobrerol, the diacetate **9a** yielded aldehyde **9b** (51%) and ketone **9b'** (26%). In comparison, the dibenzoate **10a** gave higher yields of **10b** and **10b'** (66% and 34%, respectively), reflecting the stronger electron-withdrawing effect of the benzoyl group in suppressing Grob fragmentation. These results collectively demonstrate that acylation facilitates hydrodealkenylation of allylic alcohols.

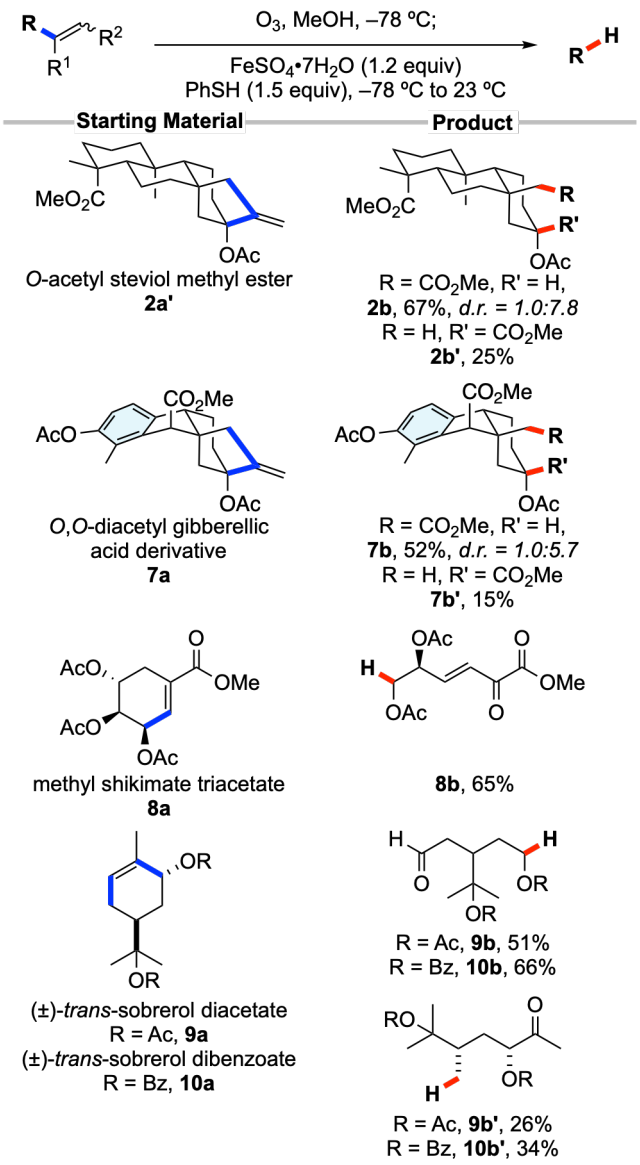


Figure 5.5 Hydrodealkenylation of Allylic Alcohols

5.5 Alkenes with Electron-Rich Aromatics

In 2009, the "escape from flatland" concept argued increased molecular saturation correlated with higher clinical success rates for drug candidates [24]. Now, 15 years later, a "return to flatland" trend has emerged, marked by a decline of saturation for approved drugs and a surging trend toward aromatic, planar scaffolds [25]. This shift highlights a key limitation of ozonolysis—and thus dealkenylation—since ozone reacts with aromatics at rates comparable to those of unactivated alkenes [11,26].

Electron-poor aromatics react slowly with ozone, but ERAs can react with rates (10^2 to 10^6 M^{-1} s^{-1}) comparable to those for unactivated alkenes (10^4–10^5 M^{-1} s^{-1}, Figure 5.6a) [11,12]. These rates were, however, measured in H_2O for ERAs and CCl_4 for unactivated alkenes, thus they cannot be directly compared. We reasoned that dipolar cycloaddition of ozone with the unactivated alkene may be accelerated in methanol to support the formation of our desired α-methoxyhydroperoxides prior to arene oxidation. Therefore, we aimed to selectively oxidize alkenes without concomitant oxidation of the aromatic ring. To do so, we titrated ozone absorption over time to control its addition to the reaction mixture to prevent overoxidation.

We applied two methods to titrate ozone from our generator: standard iodometry and quantitative NMR (qNMR) spectroscopy (see Chapter 5.8 for details). In iodometry, ozone oxidizes aqueous KI to produce I_2, forming an orange/red solution alongside KOH and O_2. The amount of I_2 is then quantified by reductive titration with sodium thiosulfate [27]. A known limitation of this method is the side reaction of I_2 with KOH to form KIO_3, KI, and H_2O [28]. Although pH buffering can suppress this reaction, we instead added 1 M aq. H_2SO_4 after ozonation to regenerate I_2 for accurate titration [27,28]. To avoid the

iodometry complications, we developed a qNMR-based titration method. We ozonized (–)-*O*-benzoyl isopulegol (**1a**) in the presence of 1-chloro-2,4-dinitrobenzene, an electron-poor aromatic internal standard, and took timed aliquots for NMR analysis. Alkene C–H signals were integrated relative to the standard and quantified over time. Both methods gave comparable results, but qNMR proved more straightforward, rapid, and operationally simpler for calibrating ozone output.

With the ozone generator calibrated, we targeted selective oxidation of alkenes in the presence of ERAs. The estrone derivative **11a**, previously unresponsive toward dealkenylative alkynylation [6f], underwent hydrodealkenylation with 2.0 equiv of ozone to furnish secosteroid **11b** in 89% yield and a 3.0:1.0 diastereomeric ratio, with no oxidation of the 3,4-dialkylphenolic A-ring (Figure 5.6b). *O*-Methyl estrone derivative (**12a**) was also smoothly hydrodealkenylated, forming secosteroids **12b** and **12b'** in 49% $(\text{d.r.} = 1.8{:}\,1.0)$ and 29%, respectively, from the corresponding tertiary or primary alkyl radicals. The stark difference in D-ring opening of **11a** and **12a** is puzzling and we are unable to rationalize their respective formations at this time. The ERA and alkene of eugenol (**13**) were competitively oxidized by ozone (Figure 5.12). Eugenol acetate (**13a**) is more electron-rich than the A-ring of estrone, but it is less activated than eugenol (**13**) with the phenol acetylated. It had failed in prior aminodealkenylation attempts [6g], however, it survived ozonation with 1.65 equiv of O_3. Treatment of that Criegee ozonolysis product with our catalytic radical hydrogenation condition [6i] enabled capture of the benzylic radical to access **13b** in 41% yield. Realizing hydrodealkenylation struggles with benzylic radical hydrogenation, we also performed dealkenylative aminoxylation to better assess alkyl radical formation from eugenol acetate (**13a**). We isolated the TEMPO

adduct **13b'** in 66% yield. The *O,O*-diacetyl gibberellic acid derivative **7a** (Figure 5.5), bearing both an allylic acetate and an ERA unit (1-acetyloxy-2,3,4-trialkylbenzene), required 1.2 equiv of ozone for full consumption. This suggests that acetylation of the phenol significantly reduced the ERA ozonation rate. Based on the data from these tested ERAs, we conclude that two or more hydroxy/methoxy activating substituents are an approximate threshold for competitive alkene and ERA oxidation.

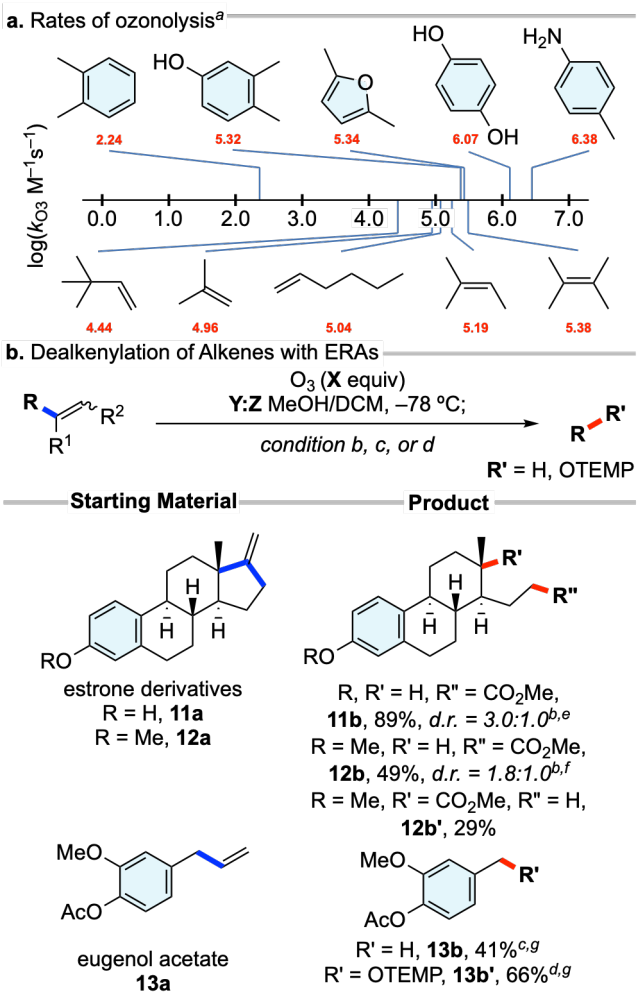


Figure 5.6 Dealkenylation of Alkenes with ERAs

[a]Arene ozonolysis rates were measured in water [11], while alkene ozonolysis rates were measured in CCl_4 [12]. [b]$FeSO_4$•$7H_2O$ (1.2 equiv), PhSH (1.5 equiv), –78 ºC to 23 ºC. [c]$Fe_2(SO_4)_3$•xH_2O (5 mol%), PhSH (10 mol%), γ-terpinene (1.5 equiv), 10:1 MeOH/DCM, reflux. [d]$FeSO_4$•$7H_2O$ (1.2 equiv), TEMPO (1.5 equiv), –78 ºC to 23 ºC. [e]X = 2.0, Y:Z = 4:1. [f]X = 4.0, Y:Z = 2:1. [g]X = 1.65, Y:Z = 3:1.

5.6 Insoluble Alkenes

Finally, alkenes that are insoluble in methanol have posed a challenge for hydrodealkenylation. In the absence of MeOH, α-methoxyhydroperoxides are not accessible via ozonolysis. Even with DCM added as a nonpolar, MeOH-miscible cosolvent, the low reaction temperature (–78 ºC) promotes precipitation for some substrates. In this study, however, we identified conditions that enabled successful hydrodealkenylation of these insoluble compounds. Sonication allowed initial dissolution of isosteviol derivative **14a** in 2:1 MeOH/DCM. Upon cooling to –78 ºC a white precipitate formed, but continuous ozonation produced a characteristic blue solution within minutes, indicating excess ozone. By Le Chatelier's principle, the alkene dissolved as it was consumed, allowing the reaction to proceed slowly. We isolated the hydrodealkenylation products **14b** and **14b'** in 61% and 22% yields, respectively (Figure 5.7). Compound **14b** was formed with a 1.0:1.8 diastereomeric ratio of axial-to-equatorial radical hydrogenation. For an inseparable mixture of methyl enol ethers of 5α-cholestanone (**15a**), 1:1 MeOH/DCM was required for initial dissolution. Similar to **14a**, a precipitate formed during ozonation of **15a** but was eventually consumed during the reaction. After radical hydrogenation, we observed **15b** from the kinetic enol ether ($\Delta^{2,3}$-**15a**) in 76% yield and **15b'** from the thermodynamic enol ether ($\Delta^{3,4}$-**15a**) in 6%. The *tert*-butyldimethylsilyl enol ether from 4-phenylcyclohexanone (**16a**) was initially soluble in MeOH but precipitated out of solution at –78 ºC. The alkene was consumed with constant ozonation, and we isolated acid **16b** in 67% after radical hydrogenation where the silyl ester was deprotected during aqueous work up. These results suggest that other poorly soluble

alkenes lacking ozone-sensitive functionalities may also be amenable to dealkenylation under similar conditions [10c,29].

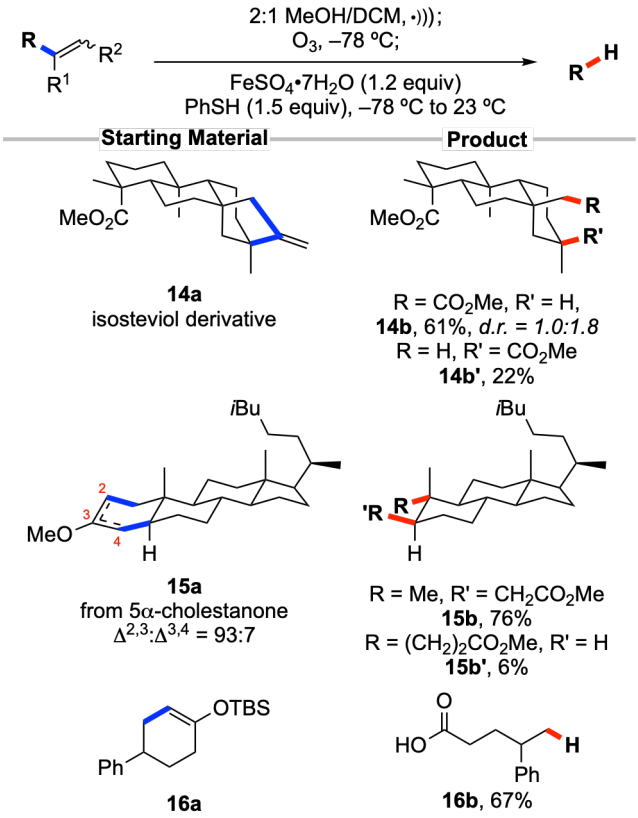


Figure 5.7 Hydrodealkenylation of Insolubles

[a]X:Y = 2:1. [b]X:Y = 1:1. [c]X:Y = 1:0.

5.7 Conclusion

In conclusion, we developed complementary ozonolysis strategies for alkenes bearing amine, allylic alcohol, and ERA functionalities. Amines were protected in situ as ammonium ions using trifluoroacetic acid, enabling formal syntheses of (±)-pinidinone, (±)-GB17, and a GnRH agonist from *N*-Boc-norpseudopelletierine. For allylic alcohols, acylation suppressed Grob fragmentation by reducing OH nucleophilicity. Acetylation was effective, but benzoylation was better. Despite similar rate constants, alkenes were selectively oxidized in the presence of ERAs through controlled ozone delivery. We also developed conditions for poorly soluble alkenes in MeOH at –78 ºC where ozone-mediated oxidation drove dissolution by Le Chatelier's principle. Overall, our strategies expand the scope of dealkenylation.

5.8 Supporting Information and Experimental Details

5.8.1 Materials and Methods

Unless otherwise stated, all reactions were conducted in glassware that had been washed sequentially with 12 M HCl and Alconox, oven-dried, and fitted with rubber septa; the reaction mixtures were stirred with Teflon-coated magnetic stirrer bars. For dry or air-free reactions, standard Schlenk techniques were used to transfer liquid reagents and solvents. Tetrahydrofuran (THF) and toluene were distilled over sodium/benzophenone ketyl under an argon atmosphere. All other solvents and reagents were used as received from commercial sources, unless otherwise noted. Reaction temperatures above room temperature (23 ºC) and below 80 ºC refer to water bath temperatures, unless otherwise stated. Reaction temperatures above 80 ºC refer to silicone oil bath temperatures. Thin layer chromatography (TLC) was performed using SiliCycle silica gel 60 F-254 precoated plates (0.25 mm) with visualization under UV irradiation and with a silica-iodine (SiO_2–I_2), cerium ammonium molybdate (CAM), potassium permanganate ($KMnO_4$), or vanillin stain. SiliCycle Silica-P silica gel (particle size: 40–63 μm) was used for flash column chromatography (FCC). ^1H, ^{13}C, and 2D NMR spectra were recorded using NEO-600, AV-500, AV-400, or AV-300 MHz spectrometers, with ^{13}C NMR spectroscopic operating frequencies of 126, 101, or 75 MHz, respectively. Chemical shifts (δ) are reported in parts per million (ppm) relative to the (residual protonated) signal of the solvent $CDCl_3$ (choloroform-*d*, δ = 7.26 for ^1H NMR; δ = 77.2 for ^{13}C NMR) or C_6D_6 (benzene-d_6, δ = 7.16 for ^1H NMR; δ = 128.1 for ^{13}C NMR). Data for ^1H NMR spectra are reported as follows: chemical shift, multiplicity, coupling constants (Hz), and number of hydrogen atoms. Data for ^{13}C NMR spectra are reported in terms of chemical shift. The following

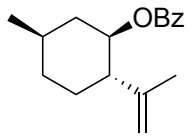
abbreviations are used to describe the multiplicities: s = singlet; d = doublet; t = triplet; q = quartet; m = multiplet; br = broad. Some structural assignments were made with additional information from HMBC, HSQC, COSY, and NOESY experiments. Melting points are uncorrected and were recorded using an Electrothermal® capillary melting point apparatus. Infrared (IR) spectra were recorded using a Jasco FTIR-4100 spectrometer with an ATR attachment. High-resolution mass spectrometry (HRMS) was performed using a Thermo Fisher Scientific Exactive Plus spectrometer equipped with an IonSense ID-CUBE DART source or an Agilent 6545 Q-TOF LC/MS with 1260 Infinity LC. Low-resolution mass spectrometry was performed with an Agilent 7250 Q-TOF GC/MS with low energy EI or an Agilent Intuvo 9000 GC with a 5977B GC/MSD. Specific rotations were measured using an Autopol IV polarimeter and a 50 mm cell, at concentrations of 0.1 g/100 mL. Ozone was synthesized using a Globalozone GO-D3G ozone generator set to 0.74 amps.

5.8.2 Safety

Caution: Organic peroxides are typically high-risk shock-sensitive compounds prone to explosion. Although we have not encountered any peroxide-related safety issues in our lab, the peroxides generated using the reported methods should be handled only by properly trained individuals and the isolated compounds should be stored at cryogenic temperatures. The use of a blast-shield is also recommended, especially for reactions performed on larger scales.

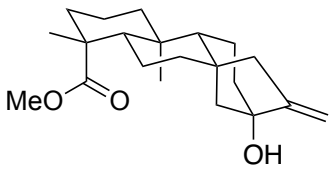
5.8.3 Preparation of Alkene Starting Materials

Stevioside (**2**), (+)-limonene oxide (**4**), tropinone (**5**), *N*-Boc-norpseudopelletierine (**6**), gibberellic acid (**7**), shikimic acid (**8**), estrone (**11**), eugenol (**13**), 5α-cholesterol (**15**), 4-phenylcyclohexanone (**16**), cinchonine (**F1**), cinchonidine (**F2**), quinidine (**F3**), vindoline (**F4**), *N*,*N*-dimethyl-*p*-phenylenediamine (**F5a**), and 5-hexenoic acid (**F5b**) were purchased from a commercial source. (–)-Isopulegol (**1**) and (–)-perillaldehyde (**3**) were purchased from a commercial source and distilled under reduced pressure prior to use. Propargylamine (**3'**) was purchased from a commercial source and distilled over calcium hydride prior to use. (±)-*trans*-Sobrerol (**9**) was purchased from a commercial source and recrystallized from dichloromethane (DCM) prior to use.



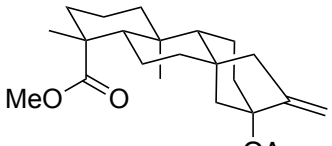
1a

O-Benzoyl isopulegol (**1a**) was prepared from isopulegol (**1**) according to a literature procedure [30].



2a

Steviol methyl ester (**2a**) was prepared in two steps from stevioside (**2**). Stevioside (**2**) was oxidized and saponified according to a literature procedure, providing steviol after recrystallization from MeOH [31]. Steviol was esterified by treatment with $TMSCHN_2$ (2.0 equiv) according to a literature procedure [32].



2a'

O-Acetyl steviol methyl ester (**2a'**) was prepared from steviol methyl ester (**2a**) according to a literature procedure for the acetylation of steviol (**2**) [33].

Scale: 1.13 mmol.

Yield: 233 mg, 75%.

Physical State: Clear colorless oil.

Purification: SiO_2 (0–30% *v*/*v* EtOAc/hexanes), then SiO_2 (15% *v*/*v* Et_2O/hexanes), then SiO_2 (10% *v*/*v* Et_2O/hexanes).

R_f = 0.60 (20% *v*/*v* EtOAc/hexanes + vanillin stain).

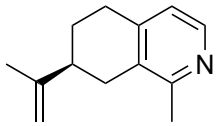
IR (ATR, neat): 2989, 2945, 849, 1725, 1666, 1463, 1447, 1366, 1253, 1235, 1207, 1190, 1170, 1149, 1128, 1107, 1078, 1066, 1047, 1022, 966, 882 cm^{-1}.

HRMS (ESI): calc'd for $C_{21}H_{33}O_3$ $[M + H]^+$ *m*/*z* = 333.2430, found 333.2445.

Specific Rotation: $[a]_D^{24.8}$ = –47.0 (*c* 1.0, $CHCl_3$).

^{1}H NMR (500 MHz, $CDCl_3$) δ 4.90 (t, *J* = 2.7 Hz, 1H), 4.86 (t, *J* = 2.3 Hz, 1H), 3.63 (s, 3H), 2.58 (dd, *J* = 10.9, 2.8 Hz, 1H), 2.34–2.21 (m, 2H), 2.22–2.13 (m, 1H), 2.02 (s, 3H), 2.07–1.98 (m, 1H), 1.90–1.80 (m, 3H), 1.80–1.71 (m, 3H), 1.68–1.61 (m, 1H), 1.58 (dt, *J* = 13.1, 3.3 Hz, 1H), 1.52–1.38 (m, 3H), 1.16 (s, 3H), 1.10–1.02 (m, 1H), 1.02–0.94 (m, 2H), 0.86 (s, 3H), 0.85–0.76 (m, 1H) ppm.

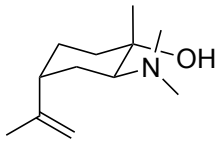
^{13}C NMR (126 MHz, $CDCl_3$) δ 178.1, 170.1, 152.2, 103.6, 87.8, 57.0, 53.9, 51.4, 47.0, 43.9, 42.7, 42.2, 41.3, 40.9, 39.3, 38.2, 36.9, 28.8, 22.4, 21.9, 20.2, 19.2, 15.3 ppm.



3a

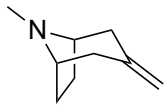
Compound **3a** was prepared from (–)-perillaldehyde (**3**) and propargylamine (**3'**).

Procedure: A bomb flask was charged with a magnetic stirrer bar, (–)-perillaldehyde (**3**, 965 mg, 6.42 mmol, 1.00 equiv), propargylamine (**3'**, 531 mg, 9.64 mmol, 1.50 equiv), and activated 4-Å molecular sieves (2.0 g). The mixture was stirred for 12 h before toluene (50 mL) was added and the flask sealed and heated at 140 ºC for 12 h. The flask was cooled to room temperature before opening and adding LiO*t*Bu (771 mg, 9.64 mmol, 1.5 equiv). The flask was sealed and heated at 140 ºC for 12 h. After cooling to room temperature, the flask was opened and the mixture was diluted with water (50 mL). The mixture was transferred to a separatory funnel and the aqueous layer was extracted with EtOAc (3 x 50 mL). The organics were combined, washed with brine (25 mL), dried (Na_2SO_4), filtered through cotton, and concentrated. The residue was purified through FCC (30% *v*/*v* EtOAc/hexanes) then distilled (bp: 114 ºC, 1 mmHg) to yield **3a** as a transparent pale-yellow oil (854 mg) in 71% yield. Characterization data matched the literature values [34].



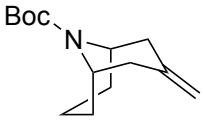
4a

(1*S*,2*S*,4*R*)-2-(Dimethylamino)-1-methyl-4-(prop-1-en-2-yl)cyclohexan-1-ol **4a** was prepared from (+)-limonene oxide (**4**) according to a literature procedure [35].



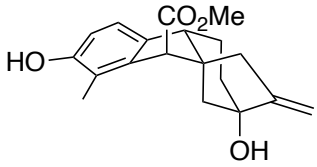
5a

The tropinone derivative **5a** was prepared from tropinone (**5**) according to a literature procedure [36].



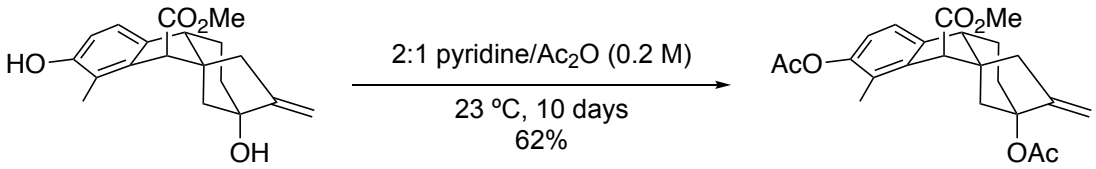
6a

The *N*-Boc-norpseudopelletierine derivative **6a** was prepared from *N*-Boc-norpseudopelletierine according to a literature procedure [30].



7'

Compound **7'** was prepared from gibberellic acid (**7**) according to a literature procedure [37].



7' **7a**

The gibberellic acid derivative **7a** was prepared from compound **7'**.

Procedure: A solution of compound **7'** (1.1 g, 3.5 mmol, 1.0 equiv) in dry pyridine/Ac_2O (2:1, 0.2 M) in a round-bottom flask equipped with a magnetic stirrer bar was stirred at room temperature for 10 days. The solvent was evaporated through distillation (50 ºC, 5 mmHg) and the residue diluted with EtOAc (100 mL). This solution was transferred to a separatory funnel; washed sequentially with aq. 1 M HCl (3 x 15 mL), sat. aq. $NaHCO_3$ (2 x 25 mL), and brine (2 x 25 mL); dried (Na_2SO_4); filtered through cotton; and concentrated. The mixture was purified through FCC (0–45% *v*/*v* EtOAc/hexanes) to yield the gibberellic acid derivative **7'** as a white solid (868 mg) in 62% yield.

Scale: 3.5 mmol.

Yield: 868 mg, 62%.

Physical State: Amorphous white solid.

R_f = 0.41 (30% *v*/*v* EtOAc/hexanes + UV/CAM stain).

Purification: SiO_2 (0–45% *v*/*v* EtOAc/hexanes).

Melting Point: 100–102 ºC.

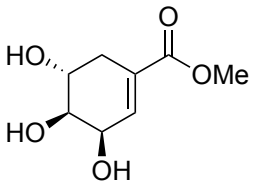
IR (ATR, neat) $\tilde{\nu}_{max}$: 2947, 2867, 1761, 1733, 1236, 1213, 1185 $cm^{-1.}$

HRMS–DART (*m*/*z*): $[M + H]^+$ calc'd for $C_{23}H_{27}O_6$ 399.1802, found 399.1794.

Specific Rotation: $[a]_D^{21.8}$ = +48.0 (*c* 1.0, $CHCl_3$).

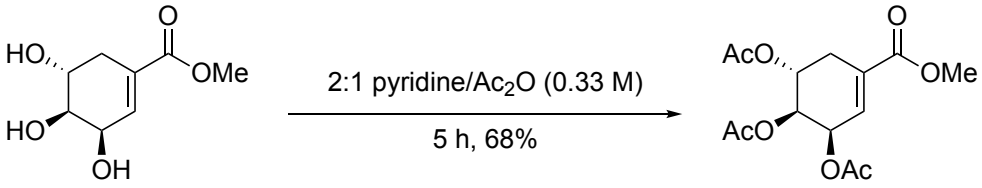
^{1}H NMR (400 MHz, $CDCl_3$) δ 7.01–6.96 (m, 1H), 6.92 (d, *J* = 8.1 Hz, 1H), 5.13–5.01 (m, 2H), 3.70 (s, 1H), 3.66 (s, 3H), 3.47–3.40 (m, 1H), 2.84 (dt, *J* = 15.9, 2.9 Hz, 1H), 2.50 (dq, *J* = 15.9, 1.5 Hz, 1H), 2.31 (s, 3H), 2.23–1.93 (m, 11H), 1.78–1.67 (m, 1H) ppm.

^{13}C NMR (126 MHz, $CDCl_3$) δ 172.2, 169.9, 169.6, 151.6, 148.2, 144.2, 141.1, 127.4, 121.5, 120.7, 106.8, 85.2, 56.6, 54.7, 51.9, 48.1, 43.8, 38.6, 36.5, 22.3, 21.0, 21.0, 12.9 ppm.



8'

Methyl shikimate **8'** was prepared from shikimic acid (**8**) according to a literature procedure [38].

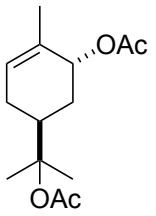


8' **8a**

Triacetyl methyl shikimate **8a** was prepared from methyl shikimate **8'**.

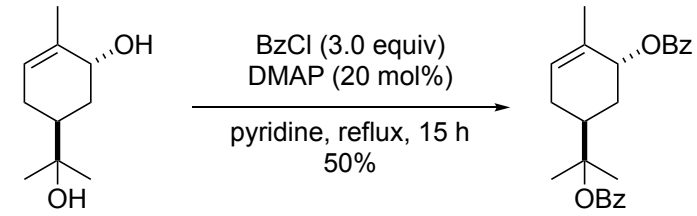
Procedure: A round-bottom flask was charged with a magnetic stirrer bar, methyl shikimate (**8'**, 508 mg, 2.70 mmol, 1.00 equiv), pyridine (5.45 mL), and acetic anhydride (2.72 mL). The mixture was stirred for 4 h at room temperature and then concentrated under reduced pressure, using toluene to remove the pyridine through co-distillation. The residue was diluted with EtOAc. This solution was washed with 1 M HCl (3 x 10 mL) and

brine (10 mL), dried (anhydrous Na_2SO_4), filtered through cotton, and concentrated under reduced pressure. The residue was purified twice through FCC (0–50% *v*/*v* EtOAc/hexanes) to yield triacetyl methyl shikimate **8a** as a transparent clear colorless oil (574 mg) in 68% yield. Characterization data matched the literature values [39].



9a

(±)-*trans*-(*O*,*O*)-Diacetyl sobrerol **9a** was prepared from (±)-*trans*-sobrerol (**9**) according to a literature procedure [40].



trans-sobrerol
9

10a

(±)-*trans*-(*O*,*O*)-Dibenzoyl sobrerol **10a** was prepared from (±)-*trans*-sobrerol (**9**).

Procedure: A round-bottom flask was charged with a magnetic stirring bar, *trans*-sobrerol (**9**, 1.00 equiv, 1.98 g, 11.6 mmol), dry pyridine (38.8 mL), and dimethylaminopyridine (DMAP, 20.0 mol%, 284 mg, 2.33 mmol). The solution was heated under reflux for 15 h before cooling to room temperature and diluting with Et_2O (100 mL). The solution was cooled further to 0 ºC in an ice bath and then the reaction was quenched through the slow addition of aq. 1 M HCl (20 mL). The mixture was stirred for 30 min at 0 ºC and then transferred to a separatory funnel. The aqueous phase was removed and then the organic

phase was washed twice with aq. 1 M HCl, twice with sat. aq. $NaHCO_3$, and once with brine. The organic phase was dried (Na_2SO_4), filtered, and concentrated. The residue was purified through FCC (0–10% *v*/*v* EtOAc/hexanes) to afford **10a** as an amorphous white solid (2.20 g) in 50% yield.

Scale: 11.6 mmol.

Yield: 2.20 g, 50%.

Physical State: Amorphous white solid.

Purification: SiO_2 (0–10% *v*/*v* EtOAc/hexanes).

Melting Point: 76–78 ºC.

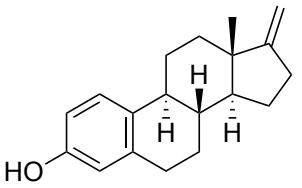
R_f = 0.60 (10% *v*/*v* EtOAc/hexanes + UV/CAM).

IR (ATR, neat) $\tilde{\nu}_{max}$: 2974, 2937, 1712, 1313, 1268, 1108, 710 cm^{-1}.

HRMS–DART (*m*/*z*): $[M + Na]^+$ calc'd for $C_{24}H_{26}O_4Na$ 401.1723, found 401.1713.

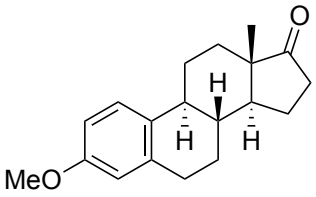
^{1}H NMR (300 MHz, $CDCl_3$) δ 8.14–8.04 (m, 2H), 7.85 (dd, *J* = 8.4, 1.3 Hz, 2H), 7.64–7.52 (m, 1H), 7.46 (ddt, *J* = 8.3, 7.5, 0.7 Hz, 3H), 7.29–7.24 (m, 2H), 5.81 (d, *J* = 5.7 Hz, 1H), 5.55 (s, 2H5), 2.55–2.39 (m, 1H), 2.31–2.21 (m, 2H), 2.05–1.95 (m, 1H), 1.80–1.76 (m, 3H), 1.75–1.63 (m, 1H), 1.59 (d, *J* = 4.2 Hz, 6H) ppm.

^{13}C NMR (126 MHz, $CDCl_3$) δ 166.6, 165.6, 133.0, 132.6, 131.9, 131.5, 130.8, 129.8, 129.4, 128.5, 128.3, 127.9, 84.6, 71.4, 39.0, 30.5, 26.9, 23.8, 23.0, 20.9 ppm.



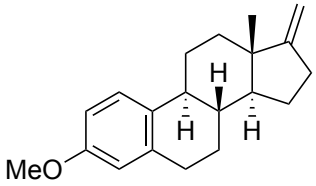
11a

The estrone derivative **11a** was prepared from estrone (**11**) according to a literature procedure [41].



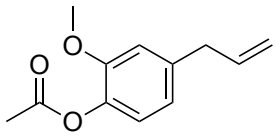
12

O-methyl estrone (**12**) was prepared from estrone (**11**) according to a literature procedure [42].



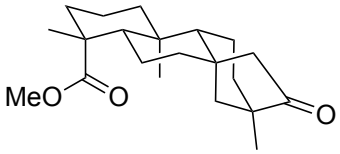
12a

O-methyl estrone derivative **12a** was prepared from *O*-methyl estrone (**12**) according to a literature procedure [43].



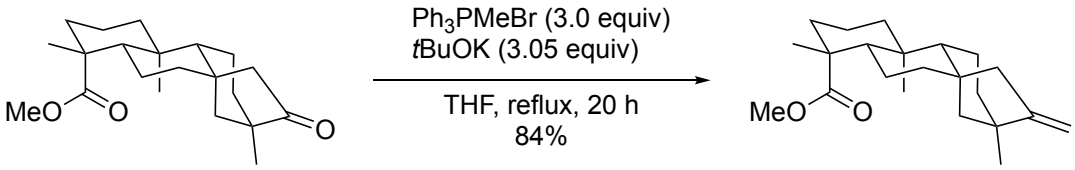
13a

Eugenol acetate (**13a**) was prepared from eugenol (**13**) according to a literature procedure [44].



14

Isosteviol methyl ester (**14**) was prepared in two steps from stevioside (**2**) according to a literature procedure [32].



14 **14a**

The isosteviol methyl ester derivative **14a** was prepared from isosteviol methyl ester (**14**).

Procedure: A flame-dried two-neck round-bottom flask equipped with a water condenser was charged with Ph_3PMeBr (3.0 equiv, 3.52 g, 9.85 mmol) and *t*BuOK (3.05 equiv, 1.12 g, 10.0 mmol). The flask was evacuated and backfilled with argon three times, then dry THF (40 mL) was added. A solution of isosteviol methyl ester (**14**, 1.00 equiv, 1.09 g, 3.29 mmol) in dry THF (5 mL) was added dropwise via cannula; this flask was rinsed with dry THF (5 mL) and the rinsing added to the reaction flask. The mixture was heated under reflux for 20 h and then cooled to room temperature. The reaction was quenched through the addition of sat. aq. NH_4Cl. The mixture was transferred to a separatory funnel and the aqueous layer was extracted with Et_2O (3 x 75 mL). The organic phase was washed with brine, dried (Na_2SO_4), filtered, and concentrated under reduced pressure. The residue

was purified through FCC (0–3% v/v EtOAc/hexanes) to obtain a white solid (1.15 g) in 84% yield.

Scale: 3.29 mmol.

Yield: 1.15 g, 84%.

Physical State: Amorphous white solid.

Purification: SiO_2 (0–3% *v*/*v* EtOAc/hexanes).

Melting Point: 100–102 ºC.

$\boldsymbol{R_f}$ = 0.71 (10% *v*/*v* EtOAc/hexanes + CAM stain).

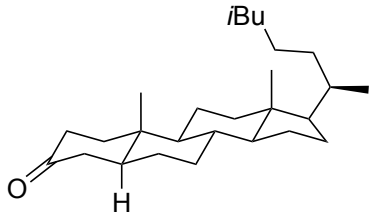
IR (ATR, neat) $\tilde{\nu}_{max}$: 2944, 2870, 2842, 1725, 1449, 1232, 1217, 1187, 1172, 1149 cm^{-1}.

HRMS–DART (*m*/*z*): $[M + H]^+$ calc'd for $C_{22}H_{35}O_2$ 331.2632, found 331.2624.

Specific Rotation: $[a]_D^{23.3}$ = –48 (*c* 1.0, $CHCl_3$).

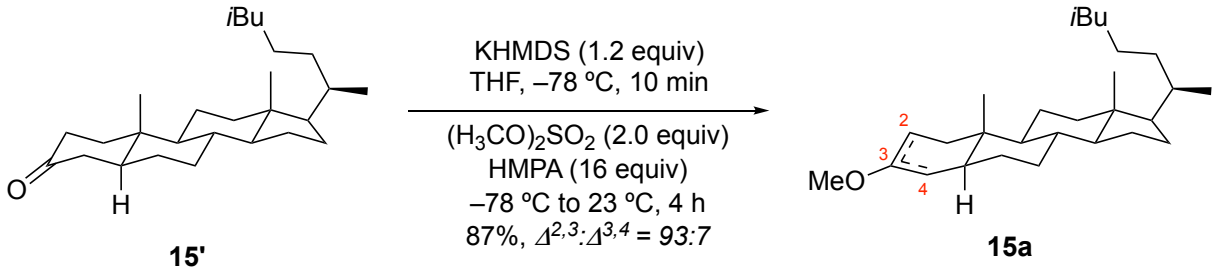
^{1}H NMR (400 MHz, $CDCl_3$) δ 4.70 (td, *J* = 1.7, 0.9 Hz, 1H), 4.59 (td, *J* = 2.1, 1.0 Hz, 1H), 3.63 (d, *J* = 0.6 Hz, 3H), 2.92–2.43 (m, 1H), 2.28–2.03 (m, 1H), 1.92 (dt, *J* = 17.1, 2.9 Hz, 1H), 1.86–1.77 (m, 2H), 1.75–1.69 (m, 1H), 1.62 (tdd, *J* = 13.8, 12.0, 3.3 Hz, 1H), 1.57–1.48 (m, 2H), 1.46–1.23 (m, 6H), 1.17 (s, 3H), 1.12–0.94 (m, 7H), 0.86 (td, *J* = 13.1, 4.2 Hz, 1H), 0.73 (s, 3H) ppm.

^{13}C NMR (101 MHz, $CDCl_3$) δ 178.3, 160.6, 101.2, 57.50, 57.48, 55.6, 51.3, 43.98, 43.96, 42.4, 41.6, 41.4, 41.3, 40.2, 38.22, 38.17, 29.0, 24.0, 22.0, 20.8, 19.2, 13.4 ppm.



15'

5α-Cholestanone (**15'**) was prepared from 5α-cholesterol (**15**) according to a literature procedure [45].



15' **15a**

The 5α-cholestanone methyl enol ethers **15a** were prepared from 5α-cholestanone (**15'**).

Procedure: The 5α-cholestanone methyl enol ether **15a** was synthesized using a modified literature procedure [46]. A flame-dried round-bottom flask equipped with a teflon-coated magnetic stirrer bar was evacuated and backfilled 3x with argon. Dry THF (3.0 mL) and KHMDS (1.0 molar in THF, 1.80 mmol, 1.80 mL, 1.2 equiv) were added and the reaction mixture was cooled to –78 ºC using a dry ice/acetone bath. To a separate flame-dried round-bottom flask equipped with a teflon-coated magnetic stirrer bar was added cholestanone (**15'**, 1.50 mmol, 0.580 g, 1.0 equiv), which was evacuated and backfilled 3x with argon then dissolved in dry THF (7.0 mL). The ketone solution was then added dropwise to the solution of KHMDS, and the resulting mixture was allowed to stir for 10 minutes. HMPA (24.0 mmol, 4.2 mL, 16.0 equiv) was added, and the reaction mixture was allowed to stir for 10 minutes before dimethyl sulfate (3.00 mmol, 290 µL, 2.0 equiv) was added. The reaction mixture was slowly allowed to warm to room temperature over the course of 4 hours (conversion was monitored by TLC). The reaction mixture was quenched with saturated aqueous $NaHCO_3$ (10 mL) and water (6 mL) then extracted with 1:1 pentane/diethyl ether (4 x 20 mL). The combined organics were washed with water and brine, dried over sodium sulfate, filtered, and concentrated *in vacuo*. The crude material was purified through FCC using basified SiO_2 (1% *v/v* Et_3N/hexanes) to afford

the methyl enol ether products **15a** as a white solid (521 mg) in 87% yield as a $\Delta^{2,3}$:$\Delta^{3,4}$ mixture of 93:7.

Scale: 1.50 mmol.

Yield: 521 mg, 87%, $\Delta^{2,3}$:$\Delta^{3,4}$ = 93:7.

Physical State: Amorphous white solid.

$\boldsymbol{R_f}$ = 0.80 (5% *v/v* EtOAc/hexanes + vanillin stain).

Purification: SiO_2 (1% *v/v* Et_3N/hexanes).

Melting Point: 88–90 ºC.

IR (ATR, neat) $\tilde{\nu}_{max}$: 3055, 2931, 2907, 2866, 2836, 1673, 1466, 1442, 1377, 1208, 1170, 1016, 786 cm^{-1}.

HRMS–DART (*m/z*): $[M + H]^+$ calc'd for $C_{28}H_{49}O$ 401.3778, found 401.3784.

15a$^{\Delta2,3}$

^{1}H NMR (400 MHz, $CDCl_3$) δ 4.48 (dt, *J* = 5.9, 1.9 Hz, 1H), 3.49 (s, 3H), 2.04–1.94 (m, 2H), 1.86–1.76 (m, 3H), 1.69–1.62 (m, 1H), 1.60–1.49 (m, 2H), 1.47–0.95 (m, 19H), 0.92–0.85 (m, 10H), 0.75 (s, 3H), 0.73–0.67 (m, 1H), 0.66 (s, 3H).

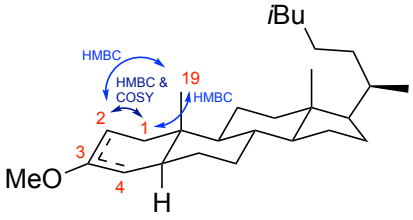
^{13}C NMR (151 MHz, $CDCl_3$) δ 154.0, 91.8, 56.6, 56.5, 54.0, 53.9, 42.7, 41.9, 40.2, 39.7, 38.4, 36.3, 35.96, 35.75, 34.9, 32.4, 31.9, 28.73, 28.40, 28.2, 24.40, 24.0, 23.0, 22.7, 21.4, 18.9, 12.1, 11.8.

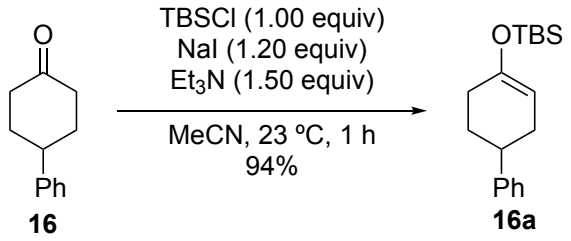
15a$^{\Delta3,4}$

^{1}H NMR (400 MHz, $CDCl_3$) δ 4.20 (s, 1H), 3.50 (s, 3H), 2.04–1.94 (m, 2H), 1.86–1.76 (m, 3H), 1.69–1.62 (m, 1H), 1.60–1.49 (m, 2H), 1.47–0.95 (m, 19H), 0.92–0.85 (m, 10H), 0.75 (s, 3H), 0.73–0.67 (m, 1H), 0.65 (s, 3H).

^{13}C NMR (151 MHz, $CDCl_3$) δ 154.2, 97.7, 60.5, 56.1, 54.1, 53.2, 44.9, 42.9, 42.8, 42.6, 40.3, 36.4, 35.97, 35.78, 35.6, 34.7, 32.2, 28.70, 28.44, 25.6, 24.37, 22.4, 21.6, 21.2, 18.8, 14.4, 12.3, 12.0.

HMBC, **HSQC**, and **COSY** spectra are provided to support the structural assignment. See Section 5.8.10 for more details. The relative chemical shift for the alkene C–H signal of **15a**$^{\Delta 2,3}$ and **15a**$^{\Delta 3,4}$ match the literature for relative chemical shifts of the alkene C–H signals for the trimethylsilylenol ethers from cholestanone [47].





16 **16a**

tert-Butyldimethyl((1,2,5,6-tetrahydro-[1,1'-biphenyl]-4-yl)oxy)silane (**16a**) was synthesized from 4-phenylcyclohexanone (**16**).

Procedure: To a 100 mL flame-dried round-bottom flask equipped with a teflon-coated magnetic stirrer bar was added 4-phenylcyclohexanone (**16**, 2.02 g, 11.6 mmol, 1.00 equiv) and sodium iodide (2.09 g, 13.9 mmol, 1.20 equiv) then evacuated and backfilled 3x with argon. Note: The water content of the sodium iodide is directly related to the overall yield of the reaction. Dry acetonitrile (11.6 mL) was added, and stirring was commenced at room temperature. Next, triethylamine (1.76 g, 17.4 mmol, 1.50 equiv) was added, followed by the dropwise addition of *tert*-butyldimethylsilylchloride (1.75 g, 11.6 mmol, 1.00 equiv). The reaction was stirred for one hour at room temperature then diluted with hexanes (50 mL) and quenched with saturated aqueous sodium bicarbonate (25 mL). The biphasic mixture was transferred to a separatory funnel and the aqueous layer was removed. The aqueous layer was extracted with hexanes (3 x 50 mL) and the combined organics were washed with brine, dried over sodium sulfate, and evaporated. The crude oil was purified through FCC (hexanes) to afford the product **16a** as a clear colorless oil (3.15 g) in 94% yield.

Scale: 11.6 mmol.

Yield: 3.15 g, 94%

Physical State: Clear colorless liquid.

Purification: SiO_2 (hexanes).

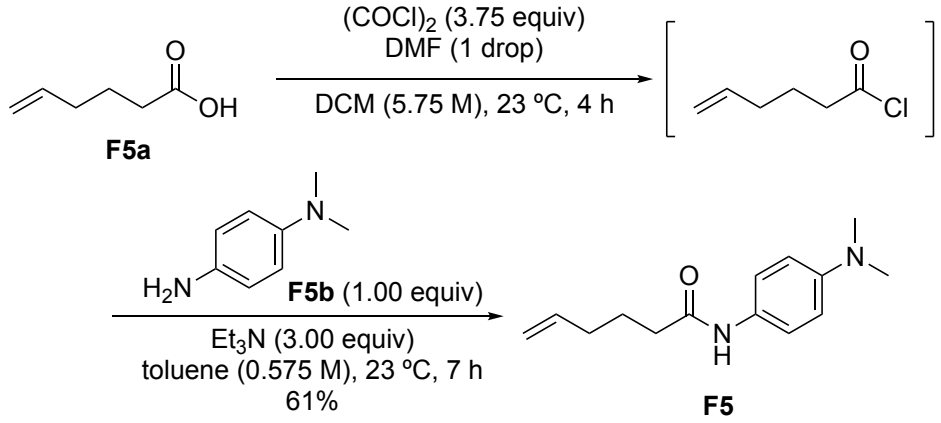
R_f = 0.57 (hexanes + UV/vanillin stain).

IR (ATR, neat) $\tilde{\nu}_{max}$: 3084, 3060, 3026, 2953, 2928, 2891, 2856, 1670, 1493, 1472, 1462, 1441, 1388, 1361, 1251, 1216, 1191, 1176, 1143, 893, 863, 836, 819, 794, 776, 756, 697, 677 cm^{-1}.

HRMS–DART (*m/z*): $[M + H]^+$ calc'd for $C_{18}H_{29}OSi$ 289.1982, found 289.1988.

^{1}H NMR (600 MHz, $CDCl_3$) δ 7.33–7.28 (m, 2H), 7.25 (dd, *J* = 8.3, 1.4 Hz, 2H), 7.22–7.19 (m, 1H), 5.06–4.88 (m, 1H), 2.76 (tdd, *J* = 11.8, 5.2, 2.9 Hz, 1H), 2.32–2.17 (m, 3H), 2.11–2.04 (m, 1H), 1.99–1.93 (m, 1H), 1.91–1.85 (m, 1H), 0.95 (s, 9H), 0.173 (s, 3H), 0.170 (s, 3H).

^{13}C NMR (151 MHz, $CDCl_3$) δ 150.6, 146.8, 128.5, 127.0, 126.2, 103.9, 40.2, 32.1, 30.3, 30.3, 25.9, 18.2, –4.1, –4.3.



N-(4-(dimethylamino)phenyl)hex-5-enamide (**F5**) was prepared from 5-hexenoic acid (**F5a**) and *N*,*N*-dimethyl-*p*-phenylenediamine (**F5b**).

Procedure: To a flame-dried round-bottom flask with a teflon-coated magnetic stirrer bar added hex-5-enoic acid (**F5a**, 656 mg, 5.75 mmol, 1.00 equiv), dry DCM (1.00 mL) and 1 drop of DMF. Dropwise added oxalyl chloride (2.74 g, 1.89 mL, 21.55 mmol, 3.75 equiv). Stirred for 4 hours at room temperature then evaporated at room temperature and 100 mbar by rotatory evaporation for one hour. Backfilled with argon and added dry toluene (10 mL). Added *N*,*N*-dimethylbenzene-1,4-diamine (**F5b**, 783 mg, 5.74 mmol, 1.00 equiv) in small portions, followed by triethylamine (1.74 g, 2.40 mL, 17.2 mmol, 3.00 equiv). A cloud of gas formed and the reaction darkened. Stirred at room temperature for 7 hours then diluted with toluene 25 mL and washed with aq. potassium carbonate (3 x 15 mL). Washed the organic layer with brine (25 mL) then dried over sodium sulfate, filtered through cotton, and evaporated. Purified through FCC (SiO_2, 30–40% *v/v* EtOAc/hexanes) to afford *N*-(4-(dimethylamino)phenyl)hex-5-enamide (**F5**) (814 mg) as a green solid.

Scale: 5.75 mmol.

Yield: 814 mg, 61%.

Physical State: Amorphous green solid.

Purification: SiO_2 (30–40% *v/v* EtOAc/hexanes).

Melting Point: 86–90 ºC.

$\boldsymbol{R_f}$ = 0.20 (30% *v/v* EtOAc/hexanes + UV/$KMnO_4$ stain).

IR (ATR, neat) $\tilde{\nu}_{max}$: 3283, 2974, 2925, 2862, 2802, 1647, 1617, 1597, 1532, 1458, 1445, 1409, 1355, 1340, 1316, 1258, 1226, 1176, 1167, 1062, 991, 915, 815 cm^{-1}.

HRMS–DART (*m/z*): $[M]^+$ calc'd for $C_{14}H_{20}N_2O$ 232.1570, found 323.1571.

^1H NMR (400 MHz, $CDCl_3$) δ 7.40–7.29 (m, 2H), 7.00 (br s, 1H), 6.70 (d, *J* = 9.2 Hz, 2H), 5.81 (ddt, *J* = 16.9, 10.1, 6.7 Hz, 1H), 5.12–4.97 (m, 2H), 2.91 (s, 6H), 2.36–2.28 (m, 2H), 2.15 (qt, *J* = 7.0, 1.4 Hz, 2H), 1.90–1.78 (m, 2H).

^{13}C NMR (101 MHz, $CDCl_3$) δ 170.9, 148.2, 138.1, 127.9, 121.9, 115.5, 113.2, 41.1, 36.9, 33.3, 24.9.

5.8.4 Ozone Generator Calibration

The absorbance rate of ozone (mmol O_3 per L O_2 per min) from the generator was measured so that the number of equivalents of ozone added could be calculated as a function of time. Two titration methods were applied: iodometry and qNMR spectroscopy. See Section 5.8.4.3 for the results.

5.8.4.1 Iodometric Titration [48]

The principle of iodometric titration of ozone is governed by the following equations:

(1) $$2KI + O_3 + H_2O \rightarrow 2KOH + O_2 + I_2$$

(2) $$2Na_2S_2O_3 + I_2 \rightarrow Na_2S_4O_6 + 2NaI$$

As the concentration of KOH increases, a third equation applies, representing the consumption of I_2 as colorless KIO_3:

(3) $$6KOH + 3I_2 \rightarrow KIO_3 + 5KI + 3H_2O$$

The addition of sulfuric acid after ozonation can reverse equation 3 by way of equation 4:

(4) $$KIO_3 + 5KI + 6H_2SO_4 \rightarrow 6KHSO_4 + 3H_2O + 3I_2$$

Therefore, to titrate the formation of I_2 from ozonation of KI using sodium thiosulfate, H_2SO_4 must be added after ozonation to reform the I_2 required to react with the sodium thiosulfate. Typically, a pH of 2 is used.

Procedure

A stock solution of 0.2 M aq. KI was prepared by adding KI (830 mg, 50.0 mmol) to a 250-mL volumetric flask, dissolving it in deionized (DI) H_2O, and diluting the solution to the mark with DI H_2O. A stock solution of 0.1 M aq. $Na_2S_2O_3$ by prepared by adding $Na_2S_2O_3 \cdot 5H_2O$ (6.205 g, 25.0 mmol) to a 250-mL volumetric flask, dissolving it in DI H_2O, and diluting the solution to the mark with DI H_2O. A solution of 1 M H_2SO_4 was prepared by adding H_2SO_4 (9.8 g) to DI H_2O (50 mL) in a 100-mL volumetric flask and diluting the solution to the mark with DI H_2O.

From the stock solution, nine samples were prepared. To each of three 25-mL round-bottom flasks was added a magnetic stirrer bar and the 0.2 M aq. KI solution (5 mL), using a 5-mL volumetric pipette. To each of three 50-mL pear-shaped flasks was added a magnetic stirrer bar and the 0.2 M aq. KI solution (10 mL), using a 5-mL volumetric pipette. To each of three 50-mL pear-shaped flasks was added a magnetic stirrer bar and the 0.2 M aq. KI solution (15 mL), using a 5-mL volumetric pipette.

To each of the three 25-mL round-bottom flasks, O_2 was bubbled through a 4” 16G needle at 1.0 L/min and then the ozone generator was turned on. After 30 s, the ozone generator was turned off, the oxygen tank was shut off, and the excess O_2 in the line was bubbled through the solution. The ozonized sample was treated with 1 M aq. H_2SO_4 (1.0 mL), turning the solution red. 0.1 M aq. $Na_2S_2O_3$ was added dropwise through a burette until the solution decolorized. In the event of precipitation of iodine, the addition of 0.1 M aq. $Na_2S_2O_3$ was paused after the solution turned yellow and resumed when dissolution was

achieved. The final volume of added 0.1 M aq. $Na_2S_2O_3$ was recorded. The procedure was repeated for each of the three 50-mL flasks containing 0.2 M aq. KI (10 mL) with ozonation occurring for 60 s and adding 1 M aq. H_2SO_4 (2.0 mL). The procedure was also repeated for each of the three 50-mL flasks containing 0.2 M aq. KI (15 mL) with ozonation occurring for 90 s and adding 1 M aq. H_2SO_4 (3.0 mL). The results of these experiments are presented in Table 5.2.

Table 5.2 Experimental Values for Iodometric Titration of Ozone

		0.1 M aq. $Na_2S_2O_3$ added	O_3	Average	Standard Deviation
30 s	Trial 1	3.20 mL	0.160 mmol	0.167 mmol	7.64×10^{-3}
	Trial 2	3.50 mL	0.175 mmol		
	Trial 3	3.30 mL	0.165 mmol		
60 s	Trial 1	6.40 mL	0.320 mmol	0.322 mmol	2.89×10^{-3}
	Trial 2	6.40 mL	0.320 mmol		
	Trial 3	6.50 mL	0.325 mmol		
90 s	Trial 1	10.0 mL	0.500 mmol	0.515 mmol	1.32×10^{-3}
	Trial 2	10.5 mL	0.525 mmol		
	Trial 3	10.4 mL	0.520 mmol		

The O_3 (mmol) values from Table 5.2 were plotted with respect to time (s) (Figure 5.8, blue dots). The average O_3 (mmol) values are plotted in gold. A linear regression (gold) was applied to the average values, setting the *y*-intercept to 0. The slope indicated an absorbance of 0.0056 mmol of O_3 per second (at 1 L O_2/min feed gas), or a rate of 0.336 mmol of O_3 per minute. The coefficient of determination (R^2) was 0.9992.

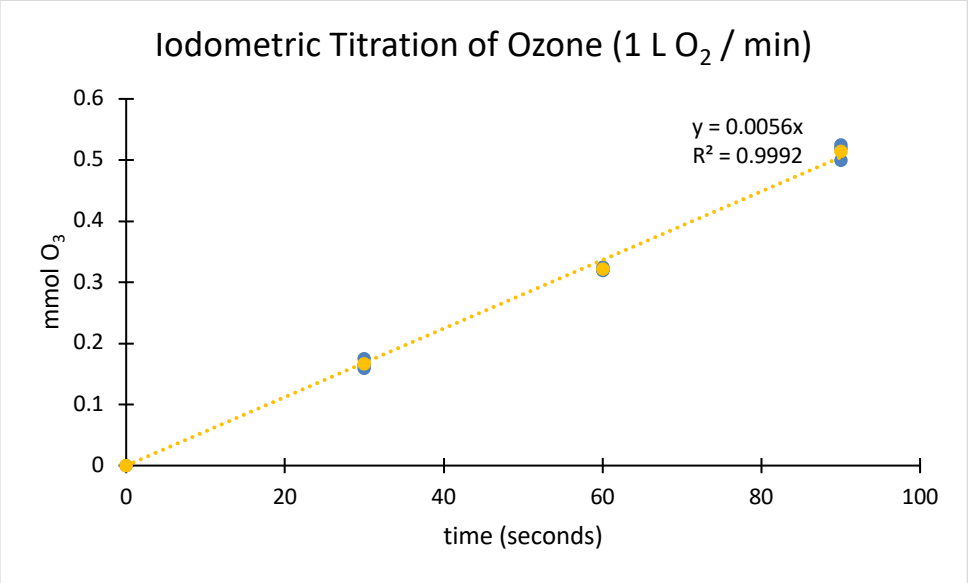


Figure 5.8 Plot of Iodometric Titration of Ozone

5.8.4.2 qNMR Spectroscopic Titration

Procedure

Ozonolysis of *O*-benzoyl isopulegol (**1a**) was conducted on a 1.00 mmol scale in dry MeOH (10.0 mL) at a temperature of –78 ºC. The NMR spectral internal standard (1-chloro-2,4-dinitrobenzene) was added to the reaction mixture at the beginning of the experiment. Ozone was bubbled from an oxygen gas feed source at a rate of 1 L/min. Aliquots were removed every 30 s for 300 s by dipping a clean pipette tip into the reaction mixture. The contents were expelled from the pipette into an NMR tube using $CDCl_3$ (0.7 mL). The ^1H NMR spectrum for each aliquot was then measured.

For data analysis, standard baseline and phase corrections were applied. The residual solvent peak was set to 7.260 ppm and the doublet of doublets at 7.78 ppm was integrated from 7.672 to 7.865 ppm and normalized to a value of 1.00. The singlet at 4.76 ppm, corresponding to one of the alkene hydrogen atoms, was monitored by integrating from 4.750 to 4.770 ppm and recording the corresponding value. The measured values are compiled in Table 5.3. The number of millimoles of ozone delivered is equal to one minus the observed integral for the remaining alkene.

The O_3 (mmol) values from Table 5.3 were plotted with respect to time (s) (Figure 5.8, blue dots). The average O_3 (mmol) values are plotted in gold. A linear regression (gold) was applied to the average values for the first 90 s, setting the *y*-intercept to 0. The slope indicated an absorbance of 0.0053 mmol of O_3 per second (at 1 L O_2/min feed gas), or a rate of 0.318 mmol of O_3 per minute. The coefficient of determination (R^2) was 0.9984.

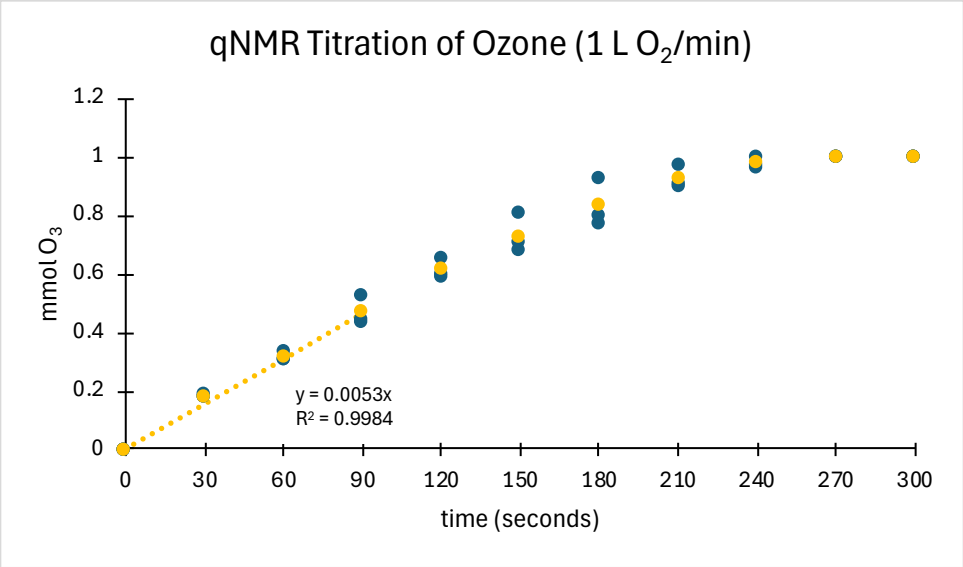


Figure 5.9 Plot of qNMR Spectroscopic Titration of Ozone

Table 5.3 Experimental Values for qNMR Spectroscopic Titration of Ozone

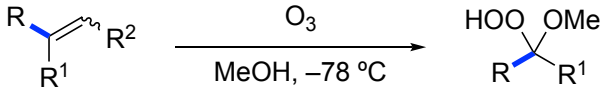
		Normalized Integral 4.750 to 4.770 ppm	mmol O_3	Average O_3	Standard Deviation
30 s	Trial 1	0.820	0.180	0.183 mmol	0.577×10^{-3}
	Trial 2	0.810	0.190		
	Trial 3	0.820	0.180		
60 s	Trial 1	0.660	0.340	0.320 mmol	1.73×10^{-2}
	Trial 2	0.690	0.310		
	Trial 3	0.690	0.310		
90 s	Trial 1	0.470	0.530	0.473 mmol	4.93×10^{-2}
	Trial 2	0.560	0.440		
	Trial 3	0.550	0.450		
120 s	Trial 1	0.340	0.660	0.617 mmol	3.79×10^{-2}
	Trial 2	0.400	0.600		
	Trial 3	0.410	0.590		
150 s	Trial 1	0.190	0.810	0.733 mmol	6.81×10^{-2}
	Trial 2	0.320	0.680		
	Trial 3	0.290	0.710		
180 s	Trial 1	0.070	0.930	0.837 mmol	8.15×10^{-2}
	Trial 2	0.220	0.780		
	Trial 3	0.200	0.800		
210 s	Trial 1	0.020	0.980	0.930 mmol	4.36×10^{-2}
	Trial 2	0.100	0.900		
	Trial 3	0.090	0.910		
240 s	Trial 1	0.000	> 1.00	0.983 mmol	1.53×10^{-2}
	Trial 2	0.020	0.980		
	Trial 3	0.030	0.970		
270 s	Trial 1	0.000	> 1.00	> 1.00 mmol	0.00
	Trial 2	0.000	> 1.00		
	Trial 3	0.000	> 1.00		
300 s	Trial 1	0.000	> 1.00	> 1.00 mmol	0.00
	Trial 2	0.000	> 1.00		
	Trial 3	0.000	> 1.00		

5.8.4.3 Calibration Conclusion

The iodometric titration method indicated delivery of 0.0056 mmol of O_3 per second; the qNMR spectroscopic titration method indicated delivery of 0.0053 mmol of O_3 per second with a 1 L O_2/min feed-gas. The average value from each of these methods was 0.00545 mmol of O_3 per second, corresponding to 0.33 mmol of O_3 per minute absorbed into solution. This value was used to calculate the number of equivalents of O_3 delivered for each ozonolysis reaction performed in this study.

5.8.5 Experimental Procedures

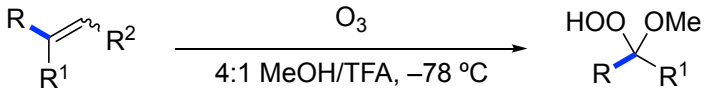
5.8.5.1 Ozonolysis



The following procedure is written for a 1.00 mmol scale reaction:

To a 25 mL round-bottom flask equipped with a Teflon-coated magnetic stirrer bar, added the alkene (1.00 mmol, 1.00 equiv) and methanol or a mixture of MeOH/DCM as indicated (10 mL, 0.1 M). The flask was cooled to –78 ºC in an acetone/dry ice bath (ozonolysis temperatures differing from –78 ºC are specified in their corresponding section). The flask was open to the air and no cap was used to seal the system. Oxygen was bubbled through a 16G x 4" needle at 1.0 L/min and then the ozone generator was turned on. The desired number of equivalents of O_3 was added according to the calibrated delivery quantity for the ozone generator (0.33 mmol per minute; see Section 5.8.4). TLC was used to track the reaction's progress (some reactions were complete before the reaction solution had turned pale blue, indicative of excess O_3). When the reaction was complete, excess O_3 was removed by bubbling air or O_2 into the reaction mixture for at least 30 seconds. The formed peroxide was not isolated.

Modification for alkenes containing basic amines



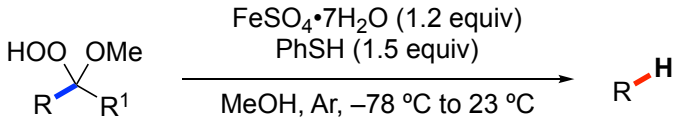
Instead of MeOH or MeOH/DCM solvent, the alkene was dissolved in methanol (8 mL) and cooled to 0 ºC. TFA (2 mL) was then added slowly. The flask was then cooled to –78 ºC for ozonolysis and the general ozonolysis procedure mentioned above was followed.

Modification for insoluble alkenes

In the event that the alkene precipitated out of solution during ozonolysis, ozone was continuously bubbled until the solution became blue, the alkene fully dissolved, and was completely consumed. To check for precipitation and full dissolution, the flask was removed from the acetone/dry ice bath and briefly warmed in ambient atmosphere.

5.8.5.2 Hydrodealkenylation

Stoichiometric Fe(II)

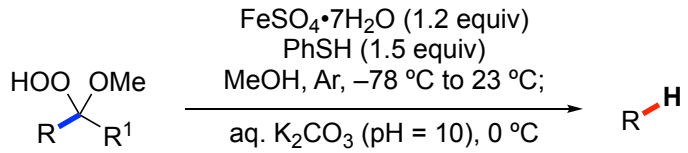


crude ozonolysis solution

The previously reported procedure for hydrodealkenylation was followed, combined with the procedure described above (Section 5.8.5.1) for the ozonolysis step [49]. The following procedure is written for a 1.00 mmol scale reaction:

To the sparged ozonolysis mixture at –78 ºC was added benzenethiol (165 mg, 154 μL, 1.50 mmol, 1.50 equiv), followed immediately by powdered iron(II) sulfate heptahydrate (334 mg, 1.20 mmol, 1.20 equiv). The acetone/dry ice bath was removed, and the reaction was allowed to stir until it reached room temperature. The solution was diluted with water (10 mL) and extracted with ethyl acetate (3 x 10 mL). The combined organic layers were washed with brine (10 mL), dried over sodium sulfate, gravity filtered through cotton, and concentrated. The crude residue was then purified. Isolated yields and purification methods are specified in Section 5.8.9.

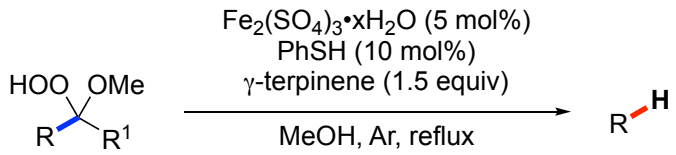
Modification for alkenes containing basic amines



crude ozonolysis solution

Following the above procedure for stoichiometric hydrodealkenylation, instead of diluting with water, the crude hydrodealkenylation reaction was cooled to 0 ºC and aqueous potassium carbonate was added dropwise until the phases separated and bubbling of carbon dioxide ceased. The reaction was then extracted with ethyl acetate (3 x 10 mL). The combined organic layers were washed with brine (10 mL), dried over sodium sulfate, gravity filtered through cotton, and concentrated. The crude residue was then purified. Isolated yields and purification methods are specified in Section 5.8.9.

Catalytic Fe(III)



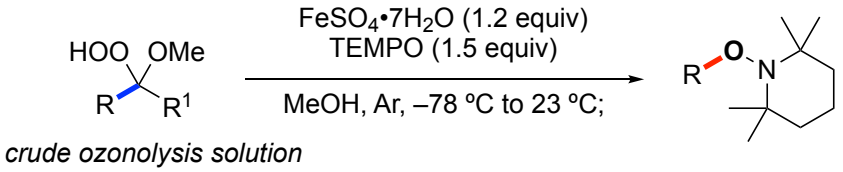
crude ozonolysis solution

The previously reported procedure for catalytic hydrodealkenylation was followed, replacing the IMP reaction with the procedure described above (Section 5.8.5.1) for the ozonolysis [30]. The following procedure is written for a 1.00 mmol scale reaction:

A 50 mL round-bottom flask equipped with a Teflon-coated magnetic stirrer bar was evacuated and backfilled 3x with argon. Then a solution of iron(III) sulfate hydrate (20.8 mg, 0.500 mmol, 5.00 mol%) in methanol (3–4 mL) was added, followed by additional methanol to reach a total volume of 10 mL. Note: The iron(III)/MeOH solution was initially prepared by microwave dissolution because iron(III) sulfate hydrate does not easily dissolve into methanol at room temperature. The yellow solution was heated to reflux using a water bath. Next, γ-terpinene (144 μL, 204 mg, 1.50 mmol, 1.50 equiv) and benzenethiol (10.2 μL, 11.0 mg, 0.100 mol, 10.0 mol%) were pre-measured into separate Hamilton syringes and set aside. This was done to ensure these reagents could be added immediately after the other. The crude ozonolysis solution was sealed and sparged with argon for 30 seconds. A cannula needle was inserted into both the iron(III)/MeOH and α-methoxyhydroperoxide/MeOH flasks to prepare for immediate transfer after addition of the γ-terpinene and benzenethiol. Finally, the γ-terpinene was dispensed into the iron(III)/methanol solution, followed by the benzenethiol, and then the ozonolysis solution

was transferred via cannula. After the yellow solution became colorless, it was cooled to room temperature and the methanol was evaporated. The crude mixture was then purified. Isolated yields and purification methods are specified in Section 5.8.9.

5.8.5.3 Aminoxyldealkenylation



crude ozonolysis solution

The previously reported procedure for oxodealkenylation was followed, combined with the procedure described above (Section 5.8.5.1) for the ozonolysis step, although the addition of MMPP of oxodealkenylation was omitted [50]. The following procedure is written for a 1.00 mmol scale reaction:

To the sparged ozonolysis mixture at –78 ºC was added TEMPO (234 mg, 1.50 mmol, 1.50 equiv) followed immediately by powdered iron sulfate heptahydrate (334 mg, 1.20 mmol, 1.20 equiv). The acetone/dry ice bath was removed, and the reaction was allowed to stir until it reached room temperature. The solution was diluted with water (10 mL) and extracted with ethyl acetate (3 x 10 mL). The combined organic layers were washed with brine (10 mL), dried over sodium sulfate, gravity filtered through cotton, and concentrated. The crude residue was then purified. Isolated yields and purification methods are specified in Section 5.8.9.

5.8.6 Mechanism of Hydrodealkenylation

A given alkene, in this case *O*-benzoyl-isopulegol (**1a**), forms a 1,2,3-trioxolane **I** after initial (3+2)-cycloaddition with ozone (Figure 5.10). *Retro*-(3+2)-cycloaddition of **I** ejects formaldehyde and provides the carbonyl oxide **II**, the so-called Criegee intermediate. Capture of **II** with MeOH quantitatively forms the α-methoxyhydroperoxide **III**. Addition of iron(II) sulfate heptahydrate initiates single electron transfer (SET) to reduce the peroxide O–O bond. The alkoxyl radical **IV** and iron(III) hydroxysulfate are formed after SET. Rapid β-scission of **IV** extrudes methyl acetate and provides the alkyl radical **V**. Finally, hydrogen atom transfer (HAT) from benzenethiol furnishes the hydrodealkenylation product **1b**.

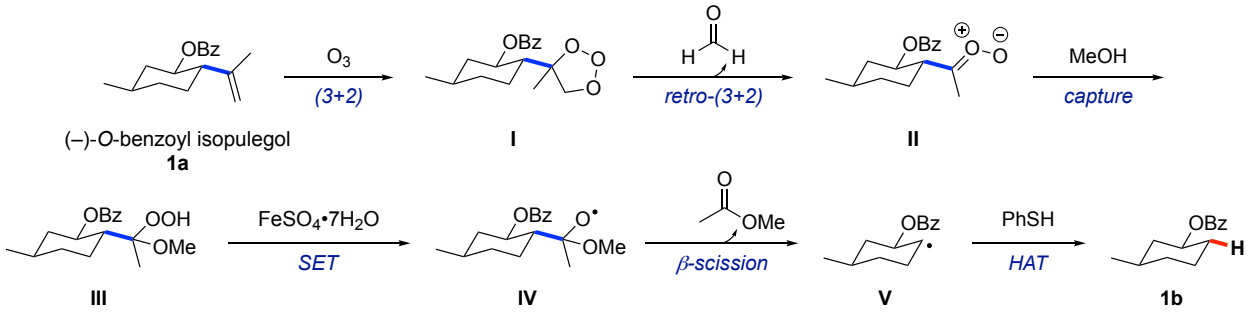
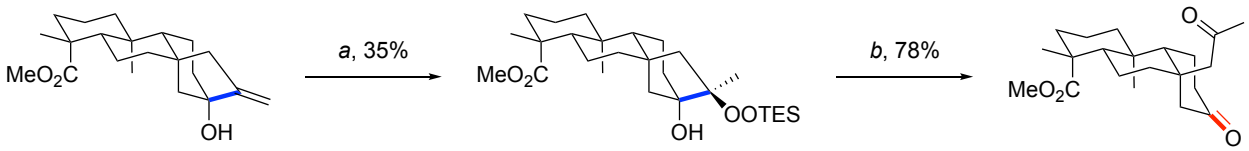


Figure 5.10 Hydrodealkenylation Mechanism

5.8.7 Isayama–Mukaiyama Peroxidation Hydrodealkenylation

We previously attempted Isayama–Mukaiyama peroxidation (IMP) to access the hydrodealkenylation product from steviol methyl ester (**2a**). We generated the silylperoxide intermediate **2y** in 35% yield by treating the alkene with 10 mol% of $Co(modp)_2(EtOH)_2$ and triethyl silane (2.0 equiv) in DCE (0.2 M) under an oxygen atomosphere (1 atm) at 23 ºC (Figure 5.11) [30]. One drop of 70% aqueous *tert*-butyl hydroperoxide was added to initiate the reaction. We reasoned the triethylsilylperoxide may be used for radical functionalization. With altered hydrodealkenylation conditions, [$Fe_2(SO_4)_3$•xH_2O (5 mol%), PhSH (10 mol%), γ-terpinene (1.5 equiv), MeOH, reflux] we observed the formation of the diketone **2z** in 78% yield from the silylperoxide **2y**. We were unable to differentiate between a Grob mechanism and a SET–β-scission–[Fe^{III}]-oxidation pathway for the formation of **2z**.



2a
steviol methyl ester

2y

2z

Figure 5.11 IMP–Hydrodealkenylation of Steviol Methyl Ester

(a) $Co(modp)_2(EtOH)_2$ (10 mol%), Et_3SiH (2.0 equiv), O_2 (1 atm), DCE (0.2 M), 70% aq. TBHP (1 drop), 23 ºC; 35%. (b) $Fe_2(SO_4)_3$•xH_2O (5 mol%), PhSH (10 mol%), γ-terpinene (1.5 equiv), MeOH, reflux; 78%.

5.8.8 Failed Substrates

The ERA from eugenol (**13**) began to be oxidized by ozone immediately as indicated by the multiple UV-active spots on the thin-layer-chromatography plate (Figure 5.12). We tested other amino-alkenes (Figure 5.13). The cinchona alkaloids [cinchonine (**F1**), cinchonidine (**F2**), and quinidine (**F3**)] were tested using the *in situ* ammonium condition we developed. Unfortunately, no hydrodealkenylation products were observed and only the corresponding aldehydes were isolated. Applying the *in situ* ammonium protection of vindoline (**F4**) did not enable product formation either. We found aromatic oxidation to dominate during the ozonolysis of vindoline (**F4**), leading to a 4-hydroxycyclohexa-2,5-dien-1-one motif. Ammonium protection of *N*-(4-(dimethylamino)phenyl)hex-5-enamide (**F5**) did not enable ozonolysis. We observed a complex mixture after hydrodealkenylation. For all of these amino-alkenes, we hypothesize that α-methoxyhydroperoxides with an α-hydrogen may be decomposed more easily than α-methoxyhydroperoxides without an α-hydrogen as in some of our other substrates.

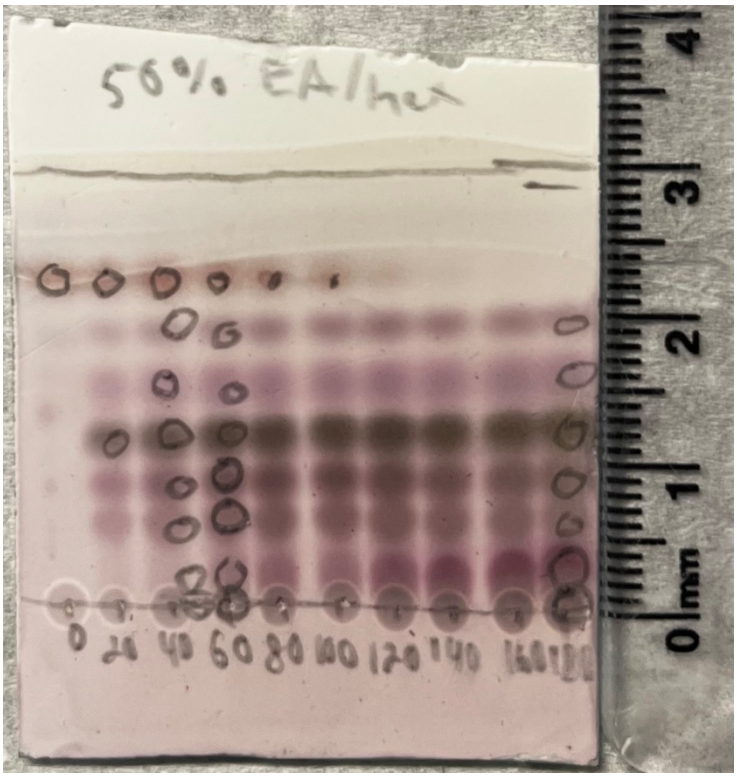
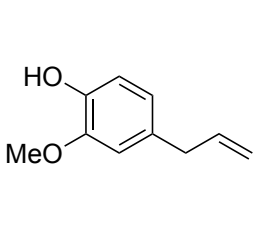
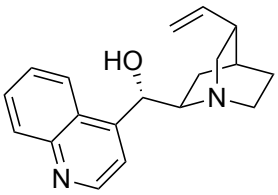


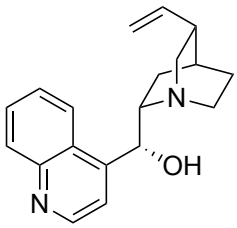
Figure 5.12 TLC (50% v/v EtOAc/hexanes + UV/vanillin stain) of the ozonolysis of eugenol (**13**) in methanol (0.1 M) at –78 ºC with lanes spotted every 30 seconds.



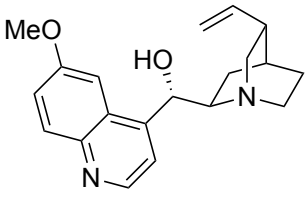
eugenol
13



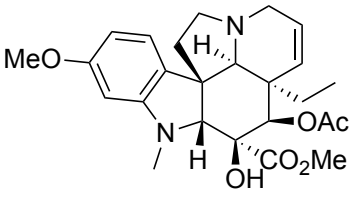
cinchonine
F1



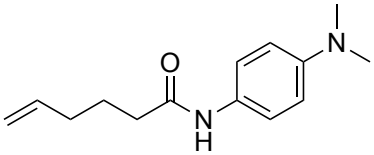
cinchonidine
F2



quinidine
F3



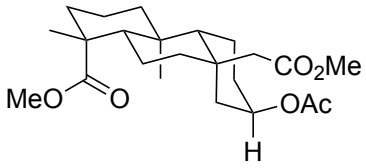
vindoline
F4



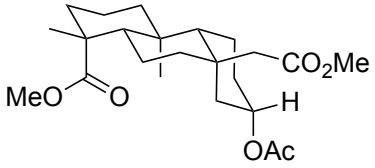
F5

Figure 5.13 Failed Substrates

5.8.9 Characterization Data



2b-1



2b-2

Compound **2b-1**: Methyl (1*R*,4a*S*,4b*R*,7*R*,8a*S*,10a*S*)-7-Acetoxy-8a-(2-methoxy-2-oxoethyl)-1,4a-dimethyltetradecahydrophenanthrene-1-carboxylate

Compound **2b-2**: Methyl (1*R*,4a*S*,4b*R*,7*S*,8a*S*,10a*S*)-7-Acetoxy-8a-(2-methoxy-2-oxoethyl)-1,4a-dimethyltetradecahydrophenanthrene-1-carboxylate

Scale: 50 mg.

Yield: 37 mg, 67%; **2b-1**/**2b-2** = 7.8:1.0.

Physical State: Amorphous white solid.

Purification: SiO_2 (0–15% *v*/*v* Et_2O/hexanes).

$\boldsymbol{R_f}$ = 0.30 (20% *v*/*v* Et_2O/hexanes + CAM) [incidental].

IR (ATR, neat) $\tilde{\nu}_{max}$: 2948, 2874, 2852, 1723, 1463, 1435, 1377, 1364, 1330, 1298, 1238, 1021, 1190, 1163, 1149, 1114, 1105, 1095, 1073, 1033, 1022, 992, 963, 953, 915, 775, 730 cm^{-1}.

HRMS–ESI (*m*/*z*): $[M + Na]^+$ calc'd for $C_{23}H_{36}O_6Na$ 431.2410, found 431.2414.

2b-1

^{1}H NMR (600 MHz, $CDCl_3$) δ 5.14 (s, 1H), 3.634 (s, 3H), 3.628 (s, 3H), 2.99 (d, *J* = 14.1 Hz, 1H), 2.21 (dd, *J* = 14.3, 9.8 Hz, 2H), 2.01 (s, 3H), 1.97–1.67 (m, 9H), 1.66–1.48 (m, 2H), 1.48–1.37 (m, 2H), 1.19–1.14 (m, 4H), 1.05 (dd, *J* = 12.1, 2.0 Hz, 1H), 1.00 (td, *J* = 13.5, 4.2 Hz, 1H), 0.95–0.85 (m, 1H), 0.85 (s, 3H) ppm.

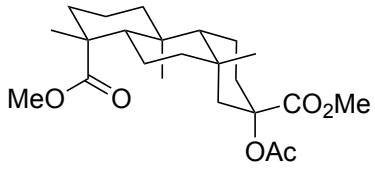
^{13}C NMR (126 MHz, $CDCl_3$) δ 178.3, 173.0, 170.6, 69.9, 56.9, 51.4, 51.2, 51.1, 47.7, 43.8, 42.3, 40.9, 39.6, 37.9, 35.2, 33.3, 28.9, 26.6, 21.8, 20.1, 19.4, 18.0, 16.8 ppm.

2b-2

^{1}H NMR (600 MHz, $CDCl_3$) δ 5.10 (tt, *J* = 11.3, 5.4 Hz, 1H), 3.634 (s, 3H), 3.628 (s, 3H), 2.57 (d, *J* = 14.1 Hz, 1H), 2.21 (dd, *J* = 14.3, 9.8 Hz, 2H), 2.01 (s, 3H), 1.97–1.67 (m, 9H), 1.66–1.48 (m, 2H), 1.48–1.37 (m, 2H), 1.19–1.14 (m, 4H), 1.05 (dd, *J* = 12.1, 2.0 Hz, 1H), 1.00 (td, *J* = 13.5, 4.2 Hz, 1H), 0.95–0.85 (m, 1H), 0.85 (s, 3H) ppm.

^{13}C NMR (126 MHz, $CDCl_3$) δ 177.9, 172.3, 170.7, 70.2, 56.8, 53.1, 52.9, 49.7, 46.0, 43.9, 42.2, 40.7, 39.0, 36.6, 33.9, 32.1, 28.4, 22.8, 21.6, 20.3, 19.9, 18.3, 14.3 ppm.

The signal having the larger chemical shift and the “smaller” coupling constant was assigned to the α-acetoxy equatorial-C–H unit (5.14 ppm, s) of compound **1b-1**. The signal having the smaller chemical shift and larger coupling constants was assigned to the α-acetoxy axial-C–H unit (5.10 ppm, tt, *J* = 11.3, 5.4 Hz) of compound **1b-2** [51].



2b'

Compound **2b'**: Dimethyl (1*R*,4a*S*,4b*R*,7*S*,8a*S*,10a*S*)-7-Acetoxy-1,4a,8a-trimethyltetradecahydrophenanthrene-1,7-dicarboxylate

Scale: 50 mg.

Yield: 14 mg, 25%.

Physical State: Amorphous white solid.

Melting Point: 128–130 ºC.

Purification: SiO_2 (0–15% *v*/*v* EtOAc/hexanes).

R_f = 0.40 (20% *v*/*v* EtOAc/hexanes + CAM).

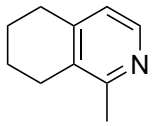
IR (ATR, neat) $\tilde{\nu}_{max}$: 2946, 2874, 2851, 1739, 1723, 1467, 1435, 1370, 1326, 1295, 1245, 1222, 1193, 1169, 1162, 1148, 1134, 1100, 1089, 1076, 1035, 1021, 983, 966, 914, 805, 774, 736 cm^{-1}.

HRMS–DART (*m*/*z*): $[M + Na]^+$ calc'd for $C_{23}H_{36}O_6Na$ 431.2410, found 431.2415.

Specific Rotation: $[a]_D^{26.1}$ = –4.0 (*c* 1.0, $CHCl_3$).

^{1}H NMR (500 MHz, $CDCl_3$) δ 3.72 (s, 3H), 3.65 (s, 3H), 2.71 (ddt, *J* = 13.9, 5.0, 2.4 Hz, 1H), 2.24–2.17 (m, 1H), 2.13 (d, *J* = 13.9 Hz, 1H), 2.10–2.02 (m, 1H), 2.00 (s, 3H), 1.96–1.89 (m, 1H), 1.84–1.66 (m, 5H), 1.66–1.51 (m, 3H), 1.45 (q, *J* = 4.0 Hz, 1H), 1.28–1.20 (m, 2H), 1.18 (s, 3H), 1.04 (dd, *J* = 11.6, 2.4 Hz, 1H), 1.01–0.93 (m, 2H), 0.92–0.88 (m, 2H), 0.86 (s, 3H) ppm.

^{13}C NMR (126 MHz, $CDCl_3$) δ 178.4, 174.1, 170.3, 80.6, 57.1, 52.4, 51.5, 51.3, 44.9, 43.9, 42.3, 42.2, 39.3, 38.0, 34.6, 31.2, 30.5, 29.4, 29.0, 21.4, 20.3, 19.9, 19.4, 18.1 ppm.



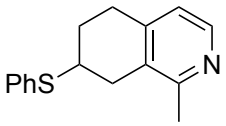
3b

Compound **3b**: 1-Methyl-5,6,7,8-tetrahydroisoquinoline

Scale: 0.500 mmol.

Yield: 66.3 mg, 90.1%.

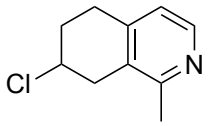
Characterization data match those previously reported in the literature [52].



3c

Compound **3c**: 1-Methyl-7-(phenylthio)-5,6,7,8-tetrahydroisoquinoline

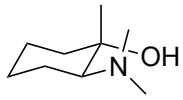
Identified in the crude reaction mixture by its diagnostic ^{1}H NMR spectral signal (500 MHz, $CDCl_3$) at δ 3.46 (tdd, J = 8.7, 5.5, 2.9 Hz, 1H) and from its mass spectrum: GCMS (m/z) $[M]^+$ calc'd for $C_{16}H_{17}NS$ 255.1076, found 255.0998.



3d

Compound **3d**: 7-Chloro-1-methyl-5,6,7,8-tetrahydroisoquinoline

Identified in the crude reaction by its diagnostic ^{1}H NMR spectral signal (500 MHz, $CDCl_3$) at δ 4.37 (dddd, J = 8.4, 6.9, 5.2, 2.9 Hz, 1H) and from the presence of both isotopes of chlorine identified in the mass spectrum: GCMS (m/z) $[M]^+$ calc'd for $C_{10}H_{12}NCl$ 181.0653/183.0623, found 181.0700/183.1000 in a 3:1 ratio.



4b

Compound **4b**: (1*S*,2*S*)-2-(Dimethylamino)-1-methylcyclohexan-1-ol

Scale: 0.50 mmol.

Yield: 50 mg, 63%. After extraction from the hydrodealkenylation reaction, the residue was purified through FCC [0–5% *v*/*v* (7 N NH_3/MeOH)/DCM] to afford an inseparable mixture of the hydrodealkenylation product **3b** and 1-((1*R*,3*S*,4*S*)-3-(dimethylamino)-4-hydroxy-4-methylcyclohexyl)ethan-1-one. This mixture was treated with $NaBH_4$ (0.500 mmol) in dry MeOH (0.1 M) for 2 h at room temperature and then for 1 h at 30 ºC to reduce the ketone functionality. The solution was concentrated directly under reduced pressure at 0 ºC and then the residue was purified through FCC [0–4% *v*/*v* (7N NH_3/MeOH)/DCM] to afford (1*S*,2*S*)-2-(dimethylamino)-1-methylcyclohexan-1-ol **3b** as a yellow oil.

Physical State: Yellow oil.

Purification: SiO_2 [0–4% *v*/*v* (7 N NH_3/MeOH)/DCM].

R_f = 0.74 [10% *v*/*v* (7 N NH_3/MeOH)/DCM + $KMnO_4$].

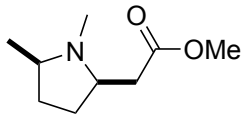
IR (ATR, neat) $\tilde{\nu}_{max}$: 2957, 2923, 2853, 2357, 2339, 1738, 1709, 1687, 1639, 1440, 1371, 1300, 1211, 1152, 1120, 1077, 1044, 975, 857, 828, 794 cm^{-1}.

HRMS–DART (*m/z*): $[M + H]^+$ calc'd for $C_9H_{20}NO$ 158.1539, found 158.1532.

Specific Rotation: $[a]_D^{22.4}$ = +6.0 (*c* 1.0, $CHCl_3$).

^{1}H NMR (400 MHz, $CDCl_3$) δ 3.63 (s, 1H), 2.30 (d, *J* = 1.0 Hz, 7H), 1.91–1.68 (m, 3H), 1.67–1.53 (m, 1H), 1.43–1.16 (m, 7H) ppm.

^{13}C NMR (101 MHz, $CDCl_3$) δ 77.4, 72.4, 71.9, 44.1, 40.4, 26.4, 23.4, 22.1, 21.7 ppm.



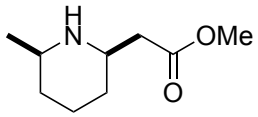
5b

Compound **5b**: Methyl 2-(*cis*-1,5-Dimethylpyrrolidin-2-yl)acetate

Scale: 0.50 mmol.

Yield: 60 mg, 70%.

Characterization data matched the literature values [53].



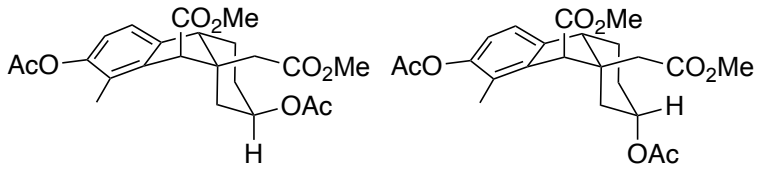
6b

Compound **6b**: Methyl 2-((2*R*,6*R*)-6-Methylpiperidin-2-yl)acetate

Scale: 0.397 mmol.

Yield: 57.8 mg, 85%.

Characterization data matched the literature values [54].



7b-1 **7b-2**

Compound **7b-1**: (2*R*,4a*R*,9*R*,9a*R*)-9a-(2-Methoxy-2-oxoethyl)-9-(methoxycarbonyl)-8-methyl-2,3,4,4a,9,9a-hexahydro-1*H*-fluorene-2,7-diyl Diacetate

Compound **7b-2**: (2*S*,4a*R*,9*R*,9a*R*)-9a-(2-Methoxy-2-oxoethyl)-9-(methoxycarbonyl)-8-methyl-2,3,4,4a,9,9a-hexahydro-1*H*-fluorene-2,7-diyl Diacetate

Scale: 50.0 mg.

Yield: 28.3 mg, 52%; **7b-1**/**7b-2** = 5.7:1.0.

Physical State: Thin white film.

Purification: SiO_2 (0–40% *v*/*v* EtOAc/hexanes) [inseparable from **7b'** with SiO_2]

An analytical standard was prepared using preparative HPLC. A 20-min gradient from 25 to 85% MeCN/H_2O + 1% formic acid was applied at a rate of 40 mL/min through an Agilent

10 Prep-C18 column (150 x 30.00 mm, PN 413910-302). Peaks were monitored at a wavelength of 210 nm. Compounds **7b-1** and **7b-2** eluted together with a retention time of 13.940 min. The combined fractions were extracted three times with Et_2O. The combined organic phases were washed with brine, dried (Na_2SO_4), filtered through cotton, and concentrated to provide **7b-1** and **7b-2** as a thin film.

R_f = 0.33 (40% *v*/*v* EtOAc/hexanes + UV/CAM) [incidental R_f].

IR (ATR, neat) $\tilde{\nu}_{max}$: 2949, 2932, 2871, 2850, 1761, 1735, 1472, 1435, 1369, 1345, 1264, 1237, 1210, 1185, 1062, 1013 cm^{-1}.

HRMS–LC-QTOF (*m*/*z*): $[M + Na]^+$ calc'd for $C_{23}H_{28}O_8Na$ 455.1676, found 455.1681.

7b-1

^{1}H NMR (500 MHz, $CDCl_3$) δ 7.01 (d, *J* = 8.1 Hz, 1H), 6.94 (d, *J* = 8.1 Hz, 1H), 4.88 (p, *J* = 3.4 Hz, 1H), 3.81 (s, 1H), 3.68 (s, 3H), 3.65 (s, 3H), 3.61 (t, *J* = 4.1 Hz, 1H), 3.24 (d, *J* = 15.6 Hz, 1H), 2.96 (dd, *J* = 15.7, 1.8 Hz, 1H), 2.30 (s, 3H), 2.12 (s, 3H), 2.09 (s, 3H), 2.08–1.97 (m, 3H), 1.65 (dt, *J* = 14.5, 3.1 Hz, 1H), 1.39 (dddd, *J* = 15.9, 13.1, 5.3, 2.3 Hz, 1H), 1.23–1.20 (m, 1H) ppm.

^{13}C NMR (126 MHz, $CDCl_3$) δ 172.7, 172.1, 170.3 (incidental), 169.3, 148.4 (incidental), 141.6, 141.5, 128.3, 121.7 (incidental), 121.2, 69.2, 58.6, 51.6, 51.3, 47.2, 47.2, 38.1, 32.7, 24.0, 21.5, 20.9, 17.4, 12.6 ppm.

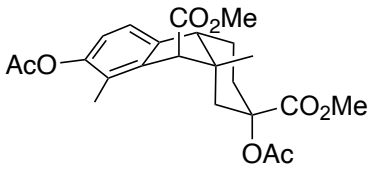
7b-2

^{1}H NMR (500 MHz, $CDCl_3$) δ 7.01 (d, *J* = 8.1 Hz, 1H), 6.94 (d, *J* = 8.1 Hz, 1H), 4.81 (ddd, *J* = 11.7, 7.6, 4.0 Hz, 1H), 3.88 (s, 1H), 3.71 (s, 3H), 3.64 (s, 3H), 3.61 (t, *J* = 4.1 Hz, 1H),

2.96 (dd, *J* = 15.7, 1.8 Hz, 1H), 2.85 (d, *J* = 16.2 Hz, 1H), 2.31 (s, 3H), 2.12 (s, 3H), 2.09 (s, 3H), 2.08–1.97 (m, 3H), 1.65 (dt, *J* = 14.5, 3.1 Hz, 1H), 1.39 (dddd, *J* = 15.9, 13.1, 5.3, 2.3 Hz, 1H), 1.23–1.20 (m, 1H) ppm.

^{13}C NMR (126 MHz, $CDCl_3$) δ 172.2, 172.0, 170.3 (incidental), 169.3, 148.4 (incidental), 141.7, 141.1, 128.3, 121.7 (incidental), 121.2, 69.5, 58.2, 51.7, 49.8, 47.2, 46.9, 36.8, 35.4, 31.9, 26.4, 22.7, 21.4, 21.3, 14.1 ppm.

The signal having the larger chemical shift and smaller coupling constant was assigned to the α-acetoxy equatorial-C–H unit (4.88 ppm, p, *J* = 3.4 Hz) of compound **6b-1**. The signal having the smaller chemical shift and the larger coupling constant was assigned to the α-acetoxy axial-C–H unit (4.81 ppm, ddd, *J* = 11.7, 7.6, 4.0 Hz) of compound **6b-2** [51].



7b'

Compound **7b'**: Dimethyl (2*S*,4a*R*,9*R*,9a*S*)-2,7-Diacetoxy-8,9a-dimethyl-2,3,4,4a,9,9a-hexahydro-1*H*-fluorene-2,9-dicarboxylate

Scale: 50.0 mg.

Yield: 8.03 mg, 15%.

Physical State: Thin white film.

Purification: SiO_2 (0–40% *v*/*v* EtOAc/hexanes) [inseparable from **7b-1** and **7b-2** with SiO_2].

An analytical standard was prepared by preparative HPLC. A 20-min gradient from 25 to 85% MeCN/H_2O + 1% formic acid was applied at a rate of 40 mL/min through an Agilent 10 Prep-C18 column (150 x 30.00 mm, PN 413910-302). Peaks were monitored at a wavelength of 210 nm. Compound **7b'** eluted with a retention time of 14.279 min. The combined fractions were extracted three times with Et_2O. The combined organic phases were washed with brine, dried (Na_2SO_4), filtered through cotton, and concentrated to provide **7b'** as a thin film.

R_f = 0.33 (40% *v*/*v* EtOAc/hexanes + UV/CAM).

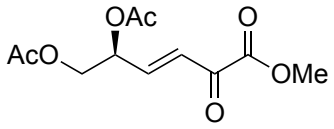
IR (ATR, neat) $\tilde{\nu}_{max}$: 2954, 2925, 1739, 1470, 1461, 1370, 1242, 1213, 1193, 1059, 1032 cm^{-1}.

HRMS–DART (*m*/*z*): $[M + H]^+$ calc'd for $C_{23}H_{29}O_8$ 433.1857, found 433.1867.

Specific Rotation: $[a]_D^{23.0}$ = +16.0 (*c* 1.0, $CHCl_3$).

^{1}H NMR (400 MHz, $CDCl_3$) δ 7.02 (d, *J* = 8.1 Hz, 1H), 6.93 (d, *J* = 8.0 Hz, 1H), 3.85 (s, 1H), 3.75 (s, 3H), 3.68 (s, 3H), 3.08 (t, *J* = 5.7 Hz, 1H), 2.32 (s, 4H), 2.22–2.13 (m, 1H), 1.99 (s, 9H), 1.89 (dtd, *J* = 15.0, 6.8, 4.2 Hz, 1H), 1.67–1.61 (m, 1H), 1.08 (s, 3H) ppm.

^{13}C NMR (101 MHz, $CDCl_3$) δ 172.8, 172.0, 169.9, 169.5, 148.3, 143.7, 140.3, 127.8, 121.5, 121.4, 79.3, 59.1, 52.4, 51.7, 48.3, 46.9, 40.2, 28.6, 23.0, 22.6, 21.2, 20.9, 13.0 ppm.



8b

Compound **8b**: (*S*,*E*)-6-Methoxy-5,6-dioxohex-3-ene-1,2-diyl Diacetate

Scale: 0.500 mmol.

Yield: 83.9 mg, 65%.

Physical State: Yellow oil.

Purification: SiO_2 (0–30% *v*/*v* EtOAc/hexanes).

R_f = 0.58 (50% *v*/*v* EtOAc/hexanes + vanillin stain).

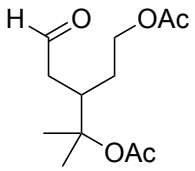
IR (ATR, neat) $\tilde{\nu}_{max}$: 2957, 2924, 2953, 1737, 1706, 1634, 1436, 1371, 1211, 1076, 1042, 973 cm^{-1}.

HRMS–DART (*m*/*z*): $[M + H]^+$ calc'd for $C_{11}H_{15}O_7$ 259.0812, found 259.0801.

Specific Rotation: $[a]_D^{23.7}$ = +4.0 (*c* 1.0, $CHCl_3$).

^{1}H NMR (400 MHz, $CDCl_3$) δ 7.07 (dd, *J* = 16.0, 4.7 Hz, 1H), 6.90 (dd, *J* = 15.9, 1.7 Hz, 1H), 5.74–5.68 (m, 1H), 4.35 (dd, *J* = 12.0, 4.0 Hz, 1H), 4.16 (dd, *J* = 11.9, 6.2 Hz, 1H), 3.91 (s, 3H), 2.16 (s, 3H), 2.07 (s, 3H) ppm.

^{13}C NMR (101 MHz, $CDCl_3$) δ 181.8, 170.6, 169.8, 161.9, 145.6, 125.6, 70.5, 63.8, 53.3, 20.9, 20.8 ppm.



9b

Compound **9b**: 4-Methyl-3-(2-oxoethyl)pentane-1,4-diyl Diacetate

Scale: 0.50 mmol.

Yield: 62 mg, 51%.

Physical State: Clear colorless oil.

Purification: SiO_2 (0–35% *v*/*v* Et_2O/pentane).

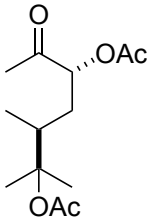
$\boldsymbol{R_f}$ = 0.54 (40% *v*/*v* EtOAc/hexanes + vanillin stain)

IR (ATR, neat) $\tilde{\nu}_{max}$: 2982, 2728, 1722, 1367, 1228, 1138, 1018, 940, 774, 610 cm^{-1}.

HRMS–DART (*m*/*z*): $[M + H]^+$ calc'd for $C_{12}H_{21}O_5$ 245.1384, found 245.1387.

^{1}H NMR (400 MHz, $CDCl_3$) δ 9.69 (t, *J* = 2.1 Hz, 1H), 4.15–4.01 (m, 2H), 2.64–2.43 (m, 2H), 2.43–2.27 (m, 1H), 2.02 (s, 3H), 1.91 (d, *J* = 1.2 Hz, 3H), 1.47 (s, 3H), 1.40 (s, 3H) ppm.

^{13}C NMR (101 MHz, $CDCl_3$) δ 201.3, 171.0, 170.1, 84.0, 62.7, 45.0, 39.5, 29.5, 24.0, 22.4, 22.3, 21.0 ppm.



9b'

Compound **9b'**: (3*S*,5*R*)-2,3-Dimethyl-6-oxoheptane-2,5-diyl Diacetate

Scale: 0.50 mmol.

Yield: 34 mg, 26%.

Physical State: Clear colorless oil.

Purification: SiO_2 (0–35% *v*/*v* Et_2O/pentane).

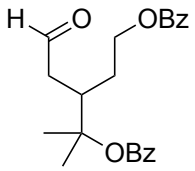
R_f = 0.61 (40% *v*/*v* EtOAc/hexanes + vanillin stain).

IR (ATR, neat) $\tilde{\nu}_{max}$: 2980, 2930, 1725, 1433, 1367, 1243, 1228, 1140, 1096, 1019, 939, 825, 609 cm^{-1}.

HRMS–DART (*m*/*z*): $[M + H]^+$ calc'd for $C_{13}H_{23}O_5$ 259.1540, found 259.1542.

^{1}H NMR (400 MHz, $CDCl_3$) δ 4.96 (dd, *J* = 7.5, 6.1 Hz, 1H), 2.20–2.11 (m, 7H), 2.06–1.97 (m, 1H), 1.94 (s, 3H), 1.49–1.41 (m, 4H), 1.35 (s, 3H), 0.94 (d, *J* = 6.9 Hz, 3H) ppm.

^{13}C NMR (101 MHz, $CDCl_3$) δ 205.4, 170.6, 170.4, 85.0, 78.8, 38.6, 32.4, 26.1, 23.9, 22.6, 21.9, 20.8, 15.6 ppm.



10b

Compound **10b**: 4-Methyl-3-(2-oxoethyl)pentane-1,4-diyl Dibenzoate

Scale: 0.500 mmol.

Yield: 122 mg, 66%.

Physical State: Clear colorless oil.

Purification: SiO_2 (0–15% *v*/*v* EtOAc/hexanes).

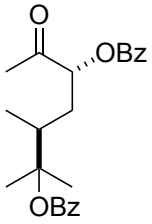
R_f = 0.64 (40% *v*/*v* EtOAc/hexanes + UV/vanillin stain).

IR (ATR, neat) $\tilde{\nu}_{max}$: 3062, 3032, 2981, 2823, 2720, 1707, 1450, 1313, 1269, 1175, 1138, 1107, 1097, 1069. 1025, 706, 689 cm^{-1}.

HRMS–DART (*m*/*z*): $[M + K]^+$ calc'd for $C_{22}H_{24}O_5K$ 407.1255, found 407.1237.

^{1}H NMR (500 MHz, $CDCl_3$) δ 9.84 (t, *J* = 1.8 Hz, 1H), 8.08–7.99 (m, 2H), 7.97–7.89 (m, 2H), 7.61–7.48 (m, 2H), 7.48–7.34 (m, 4H), 4.45 (ddd, *J* = 11.3, 7.0, 5.3 Hz, 1H), 4.36 (ddd, *J* = 11.3, 8.2, 6.3 Hz, 1H), 2.94 (qd, *J* = 5.8, 3.1 Hz, 1H), 2.81 (ddd, *J* = 17.5, 5.3, 1.9 Hz, 1H), 2.55 (ddd, *J* = 17.5, 6.4, 2.0 Hz, 1H), 2.21 (dtt, *J* = 13.7, 6.6, 3.4 Hz, 1H), 1.75–1.67 (m, 1H), 1.66 (s, 3H), 1.63 (s, 3H) ppm.

^{13}C NMR (126 MHz, $CDCl_3$) δ 201.2, 166.5, 165.5, 133.1, 132.9, 131.4, 130.1, 129.6, 129.4, 128.5, 128.4, 115.9, 84.8, 63.3, 45.4, 39.0, 30.1, 24.1, 23.5 ppm.



10b'

Compound **10b'**: (3*S*,5*R*)-2,3-Dimethyl-6-oxoheptane-2,5-diyl Dibenzoate

Scale: 0.500 mmol.

Yield: 65.0 mg, 34%.

Physical State: Clear colorless oil.

Purification: SiO_2 (0–15% *v*/*v* EtOAc/hexanes).

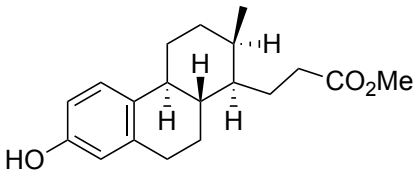
R_f = 0.78 (40% *v*/*v* EtOAc/hexanes + UV/vanillin stain).

IR (ATR, neat) $\tilde{\nu}_{max}$: 2979, 2949, 2937, 1716, 1282, 1110, 710 cm^{-1}.

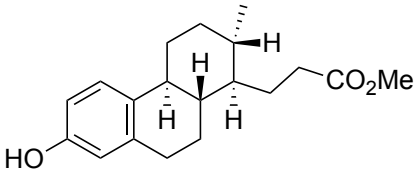
HRMS–DART (*m*/*z*): $[M + K]^+$ calc'd for $C_{23}H_{26}O_5K$ 421.1412, found 421.1398.

^{1}H NMR (500 MHz, $CDCl_3$) δ 8.07 (dt, *J* = 6.9, 1.5 Hz, 2H), 7.94 (dt, *J* = 7.0, 1.5 Hz, 2H), 7.56 (dt, *J* = 41.7, 7.5 Hz, 1H), 7.43 (dt, *J* = 40.3, 7.8 Hz, 3H), 5.26 (td, *J* = 6.0, 1.5 Hz, 1H), 2.46 (dddd, *J* = 11.1, 8.5, 5.7, 2.8 Hz, 1H), 2.35–2.25 (m, 1H), 2.20 (s, 3H), 1.73 (dddd, *J* = 15.4, 6.3, 5.0, 1.7 Hz, 1H), 1.63 (s, 3H), 1.57 (s, 4H), 1.13 (dd, *J* = 7.0, 1.7 Hz, 3H) ppm.

^{13}C NMR (126 MHz, $CDCl_3$) δ 205.4, 166.0, 165.5, 133.5, 132.6, 131.7, 129.8, 129.3, 129.2, 128.5, 128.3, 85.6, 79.2, 39.3, 32.5, 26.0, 23.9, 22.3, 15.6 ppm.



11b-1



11b-2

Compound **11b-1**: Methyl 3-((1*R*,2*R*,4a*S*,10a*S*)-7-Hydroxy-2-methyl-1,2,3,4,4a,9,10,10a-octahydrophenanthren-1-yl)propanoate

Compound **11b-2**: Methyl 3-((1*R*,2*S*,4a*S*,10a*S*)-7-Hydroxy-2-methyl-1,2,3,4,4a,9,10,10a-octahydrophenanthren-1-yl)propanoate

Scale: 0.250 mmol.

Yield: 67.3 mg, 89%; **11b-1**/**11b-2** = 3.0:1.0.

Physical State: Amorphous white solid.

Purification: SiO_2 (0–30% *v*/*v* EtOAc/hexanes).

R_f = 0.59 (30% *v*/*v* EtOAc/hexanes + UV/vanillin stain) [incidental R_f].

IR (ATR, neat) $\tilde{\nu}_{max}$: 3405, 3022, 2950, 2919, 2854, 1739, 1712, 1611, 1586, 1502, 1440, 1360, 1314, 1287, 1245, 1219, 1024, 914, 868, 820, 787, 737 cm^{-1}.

HRMS–DART (*m*/*z*): $[M + H]^+$ calc'd for $C_{19}H_{27}O_3$ 303.1955, found 303.1964.

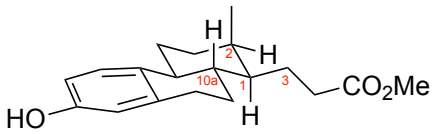
11b-1

^{1}H NMR (500 MHz, $CDCl_3$) δ 7.15 (d, *J* = 8.4 Hz, 1H), 6.62 (dd, *J* = 8.4, 2.9 Hz, 1H), 6.55 (d, *J* = 2.9 Hz, 1H), 4.69 (s, 1H), 3.68 (s, 3H), 2.78 (dt, *J* = 6.6, 3.9 Hz, 2H), 2.38 (dt, *J* = 9.2, 3.4 Hz, 1H), 2.32–2.13 (m, 2H), 2.13–2.05 (m, 1H), 2.00–1.82 (m, 3H), 1.39–1.18 (m,

5H), 1.13 (qd, *J* = 10.8, 2.9 Hz, 1H), 1.00 (tt, *J* = 9.9, 3.4 Hz, 1H), 0.96 (d, *J* = 7.2 Hz, 3H) ppm.

^{13}C NMR (126 MHz, $CDCl_3$) δ 175.0, 153.4 [incidental with **11b-2**], 138.4, 133.1, 126.9, 115.0, 112.9, 51.78, 47.4, 43.1, 42.6, 35.8, 34.6, 31.3, 30.3, 29.4, 26.5, 23.6, 20.5 ppm.

The dihedral angle for the axial C_{10a}/C_1 hydrogen atoms is different from that of the axial-C_1/equatorial-C_2 hydrogen atoms. The axial-C_1/equatorial-C_2 hydrogen atoms are gauche, which are closer in dihedral angle for the C_1/C_3 hydrogen atoms. These different dihedral angles make the splitting for C_1 hydrogen atom appear in the ^{1}H NMR spectrum as a doublet-of-quartets (dq, C_1/C_{10a} x $C_1/C_2/2C_3$) at 1.13 ppm.

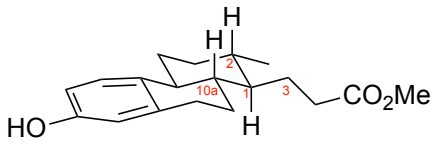


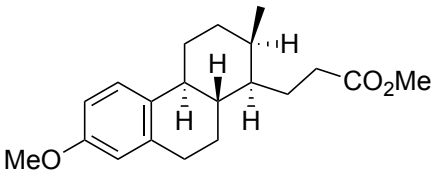
11b-2

^{1}H NMR (500 MHz, $CDCl_3$) δ 7.15 (d, *J* = 8.4 Hz, 1H), 6.62 (dd, *J* = 8.4, 2.9 Hz, 1H), 6.55 (d, *J* = 2.9 Hz, 1H), 4.69 (s, 1H), 3.70 (s, 3H), 2.78 (dt, *J* = 6.6, 3.9 Hz, 2H), 2.38 (dt, *J* = 9.2, 3.4 Hz, 1H), 2.32–2.13 (m, 2H), 2.13–2.05 (m, 1H), 2.00–1.82 (m, 3H), 1.39–1.18 (m, 5H), 1.13 (qd, *J* = 10.8, 2.9 Hz, 1H), 1.00 (tt, *J* = 9.9, 3.4 Hz, 1H), 0.84 (d, *J* = 7.2 Hz, 3H) ppm.

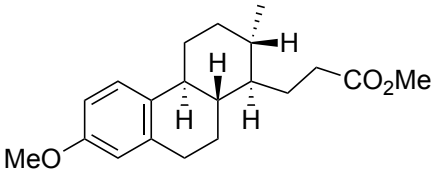
^{13}C NMR (126 MHz, $CDCl_3$) δ 174.9, 153.4 [incidental with **11b-1**], 138.4, 133.3, 126.7, 116.9, 112.8, 51.75, 44.3, 43.6, 38.9, 33.3, 32.1, 30.1, 29.8, 29.1, 26.5, 25.4, 12.3 ppm.

The dihedral angles for the axial C_1/C_2 and the C_{10a}/C_1 hydrogen atoms are roughly the same (anti, 180º). These similar dihedral angles make the splitting for the C_1 hydrogen atom appear in the ^{1}H NMR spectrum as a triplet-of-triplets (tt, C_1/C_{10a}/C_2 x C_1/2C_3) at 1.00 ppm.





12b-1



12b-2

Compound **12b-1**: Methyl 3-((1*R*,2*R*,4a*S*,10a*S*)-7-methoxy-2-methyl-1,2,3,4,4a,9,10,10a-octahydrophenanthren-1-yl)propanoate

Compound **12b-2**: Methyl 3-((1*R*,2*S*,4a*S*,10a*S*)-7-methoxy-2-methyl-1,2,3,4,4a,9,10,10a-octahydrophenanthren-1-yl)propanoate

Scale: 0.250 mmol

Yield: 39.0 mg, 49%, *d.r = 1.8:1.0*

Physical State: Clear colorless oil

R_f = 0.25 (5% *v/v* EtOAc/hexanes + CAM)

Purification: SiO_2 (0.5% *v/v* EtOAc/hexanes to 2.0% *v/v* EtOAc/hexanes)

IR (ATR, neat) $\tilde{\nu}_{max}$: 2947, 2917, 2853, 1735, 1500, 1434, 1279, 1255, 1237, 1191, 1163, 1040 cm^{-1}.

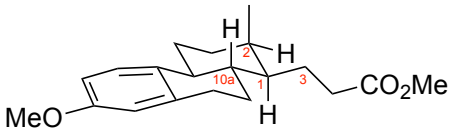
HRMS–DART (*m/z*): $[M + H]^+$ calc'd for $C_{20}H_{29}O_3$ 317.2111, found 317.2119.

12b-1

^{1}H NMR (500 MHz, $CDCl_3$) δ 7.22–7.19 (m, 1H), 6.76–6.68 (m, 1H), 6.66–6.60 (m, 1H), 3.78 (s, 3H), 3.68 (s, 3H), 2.83 (dq, *J* = 6.6, 3.7 Hz, 2H), 2.49–2.35 (m, 1H), 2.35–1.82 (m, 7H), 1.49–1.20 (m, 5H), 1.14 (qd, *J* = 10.5, 2.7 Hz, 1H), 0.97 (d, *J* = 6.3 Hz, 2H).

^{13}C NMR (126 MHz, $CDCl_3$) δ 174.8, 157.5 [incidental with **12b-2**], 138.08, 133.0, 126.7, 113.4, 111.8, 55.32 [incidental with **12b-2**], 51.71, 43.1, 42.7, 35.8, 34.6, 31.3, 30.5, 29.4, 26.5, 25.4, 23.6, 20.5.

The dihedral angle for the axial C_{10a}/C_1 hydrogen atoms is different from that of the axial-C_1/equatorial-C_2 hydrogen atoms. The axial-C_1/equatorial-C_2 hydrogen atoms are gauche, which are closer in dihedral angle for the C_1/C_3 hydrogen atoms. These different dihedral angles make the splitting for C_2 hydrogen atom appear in the ^{1}H NMR spectrum as a doublet-of-quartets (qd, C_1/C_{10a} x $C_1/C_2/2C_3$) at 0.93 ppm.

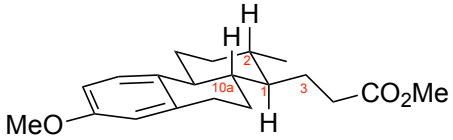


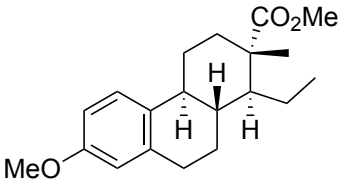
12b-2

^{1}H NMR (500 MHz, $CDCl_3$) δ 7.22–7.19 (m, 1H), 6.76–6.68 (m, 1H), 6.66–6.60 (m, 1H), 3.78 (s, 3H), 3.69 (s, 3H), 2.83 (dq, *J* = 6.6, 3.7 Hz, 2H), 2.49–2.35 (m, 1H), 2.35–1.82 (m, 7H), 1.82–1.66 (m, 2H), 1.49–1.20 (m, 3H), 1.02 (tt, *J* = 10.4, 3.6 Hz, 1H), 0.85 (d, *J* = 7.2 Hz, 1H).

^{13}C NMR (126 MHz, $CDCl_3$) δ 174.7, 157.5 [incidental with **12b-1**], 138.10, 133.2, 126.5, 113.5, 111.7, 55.32 [incidental with **12b-1**], 51.68, 47.4, 44.3, 43.6, 38.9, 33.3, 32.1, 30.3, 29.8, 29.1, 26.6, 12.3.

The dihedral angles for the axial C_1/C_2 and the C_{10a}/C_1 hydrogen atoms are roughly the same (anti, 180º). These similar dihedral angles would make the splitting for the C_1 hydrogen atom appear in the ^{1}H NMR spectrum as a triplet-of-triplets (tt, $C_1/C_{10a}/C_2$ x $C_1/2C_3$) at 1.02 ppm.





12b'

Compound **12b'**: Methyl (1*S*,2*S*,4a*S*,10a*R*)-1-ethyl-7-methoxy-2-methyl-1,2,3,4,4a,9,10,10a-octahydrophenanthrene-2-carboxylate

Scale: 0.250 mmol.

Yield: 22.9 mg, 29%.

Physical State: Clear colorless oil.

R_f = 0.31 (5% *v/v* EtOAc/hexanes + CAM).

Purification: SiO_2 (0.5% *v/v* EtOAc/hexanes to 2.0% *v/v* EtOAc/hexanes).

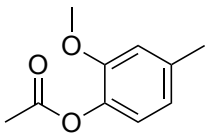
IR (ATR, neat) $\tilde{\nu}_{max}$: 2946, 2921, 2863, 1727, 1500, 1281, 1236, 1161, 1120, 1042 cm^{-1}.

HRMS–DART (*m/z*): $[M + H]^+$ calc'd for $C_{20}H_{29}O_3$ 317.2111, found 317.2117.

Specific Rotation: $[a]_D^{24.0}$ = 64.00 (*c* 1.0, $CHCl_3$).

^{1}H NMR (600 MHz, $CDCl_3$) δ 7.20 (d, *J* = 8.5 Hz, 1H), 6.72 (dd, *J* = 8.6, 2.8 Hz, 1H), 6.63 (d, *J* = 2.8 Hz, 1H), 3.78 (s, 3H), 3.71 (s, 3H), 2.86 (dt, *J* = 10.1, 4.5 Hz, 2H), 2.39 (td, *J* = 11.4, 3.8 Hz, 1H), 2.29 (dq, *J* = 13.4, 3.8 Hz, 1H), 2.12 (ddt, *J* = 11.9, 5.1, 2.4 Hz, 1H), 1.95 (td, *J* = 13.4, 4.0 Hz, 1H), 1.75 (dt, *J* = 13.0, 3.4 Hz, 1H), 1.70 (ddd, *J* = 10.9, 5.4, 3.6 Hz, 1H), 1.44–1.32 (m, 4H), 1.21 (ddd, *J* = 10.9, 7.5, 3.8 Hz, 1H), 1.14 (s, 3H), 0.94 (t, *J* = 7.5 Hz, 3H).

^{13}C NMR (151 MHz, $CDCl_3$) δ 179.4, 157.7, 138.0, 132.5, 126.6, 113.6, 111.8, 55.3, 51.8, 48.1, 47.9, 43.2, 41.2, 37.3, 30.5, 27.2, 26.1, 24.3, 15.3, 15.1.



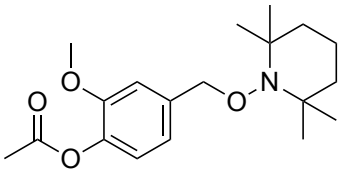
13b

Compound **13b**: 2-methoxy-4-methylphenyl acetate

Scale: 0.500 mmol.

Yield: 37 mg, 41%.

Characterization data match those previously reported in the literature [55].



13b'

Compound **13b'**: 2-Methoxy-4-(((2,2,6,6-tetramethylpiperidin-1-yl)oxy)methyl)phenyl Acetate

Scale: 0.40 mmol.

Yield: 89 mg, 66%.

Physical State: Clear colorless solid.

Melting Point: 59–61 ºC.

Purification: SiO_2 (0–15% *v*/*v* EtOAc/hexanes).

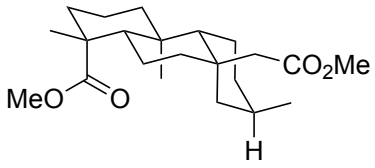
R_f = 0.38 (15% *v*/*v* EtOAc/hexanes + UV/vanillin stain).

IR (ATR, neat) $\tilde{\nu}_{max}$: 3004, 2974, 2934, 2872, 2843, 1767, 1605, 1509, 1466, 1417, 1361, 1312, 1281, 1264, 1245, 1195, 1151, 1120, 1036, 1010, 925, 902, 853, 825 cm^{-1}.

HRMS–DART (*m*/*z*): [M + Na]$^+$ calc'd for $C_{19}H_{29}NO_4Na$ 358.1989, found 358.1976.

^{1}H NMR (500 MHz, $CDCl_3$) δ 7.29–7.22 (m, 2H), 7.19 (dd, *J* = 8.1, 1.8 Hz, 1H), 5.07 (s, 2H), 4.10 (s, 3H), 2.57 (s, 3H), 1.91–1.71 (m, 5H), 1.65–1.57 (m, 1H), 1.51 (s, 6H), 1.42 (s, 6H) ppm.

^{13}C NMR (126 MHz, $CDCl_3$) δ 169.2, 150.8, 138.8, 137.4, 122.5, 119.4, 111.4, 78.3, 60.0, 55.8, 39.7, 33.1, 20.7, 20.3, 17.1 ppm.



14b-1

Compound **14b-1**: Methyl (1*R*,4a*S*,4b*R*,7*R*,8a*S*,10a*S*)-8a-(2-Methoxy-2-oxoethyl)-1,4a,7-trimethyltetradecahydrophenanthrene-1-carboxylate

Scale: 0.500 mmol.

Yield: 70.6 mg, 39%.

Physical State: Amorphous white solid.

Purification: SiO_2 (0–30% *v*/*v* EtOAc/hexanes).

***R*$_f$** = 0.33 (5% *v*/*v* EtOAc/hexanes + CAM).

IR (ATR, neat) $\tilde{\nu}_{max}$: 2949, 2850, 1728, 1466, 1371, 1287, 1233, 1194, 1151, 1095, 1026, 996, 908, 736 cm^{-1}.

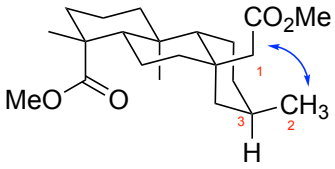
HRMS–DART (*m*/*z*): [M + H]$^+$ calc'd for $C_{22}H_{37}O_4$ 365.2686, found 365.2690.

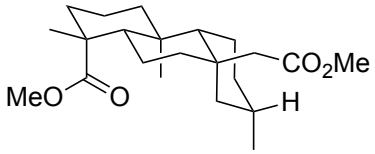
Specific Rotation: $[a]_D^{23.0}$ = –36.0 (*c* 3.0, $CHCl_3$).

^{1}H NMR (300 MHz, $CDCl_3$) δ 3.63 (s, 6H), 2.67 (dd, *J* = 15.5, 1.6 Hz, 1H), 2.54 (dd, *J* = 15.5, 2.0 Hz, 1H), 2.26 (dt, *J* = 13.4, 3.3 Hz, 1H), 2.14 (dd, *J* = 13.3, 4.1 Hz, 1H), 1.97–1.80 (m, 3H), 1.80–1.68 (m, 2H), 1.55–1.38 (m, 4H), 1.35–1.18 (m, 2H), 1.16 (s, 3H), 1.14–0.74 (m, 6H), 0.99 (d, *J* = 7.3 Hz, 3H), 0.65 (s, 3H) ppm.

^{13}C NMR (101 MHz, $CDCl_3$) δ 178.0, 173.5, 59.5, 57.9, 51.3, 51.1, 44.3, 44.0, 41.2, 40.3, 38.3, 37.9, 37.3, 36.8, 33.2, 28.7, 27.1, 21.5, 19.7, 19.2, 16.5, 14.3 ppm.

HSQC and **NOESY** spectra are provided to support the configurational assignment. NOE correlations are presented below. See Section 5.8.10 for more details.





14b-2

Compound **14b-2**: Methyl (1*R*,4a*S*,4b*R*,7*S*,8a*S*,10a*S*)-8a-(2-Methoxy-2-oxoethyl)-1,4a,7-trimethyltetradecahydrophenanthrene-1-carboxylate

Scale: 0.500 mmol.

Yield: 39.2 mg, 22%.

Physical State: Amorphous white solid.

Purification: SiO_2 (0–30% *v*/*v* EtOAc/hexanes).

R_f = 0.29 (5% *v*/*v* EtOAc/hexanes + CAM).

IR (ATR, neat) $\tilde{\nu}_{max}$: 2990, 2948, 2870, 2848, 1728, 1456, 1376, 1324, 1285, 1256, 1229, 1198, 1151, 1115, 1098, 1024, 977, 910, 737 cm^{-1}.

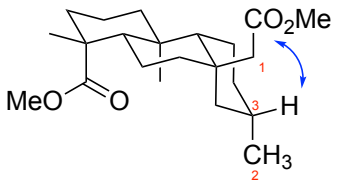
HRMS–DART (*m*/*z*): $[M + H]^+$ calc'd for $C_{22}H_{37}O_4$ 365.2686, found 365.2690.

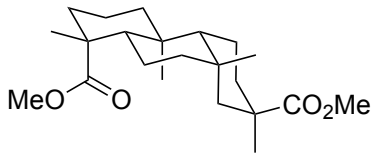
Specific Rotation: $[a]_D^{23.0}$ = –36.0 (*c* 3.0, $CHCl_3$).

^{1}H NMR (500 MHz, $CDCl_3$) δ 3.63 (s, 6H), 2.53 (qd, *J* = 13.3, 1.4 Hz, 2H), 2.14 (dt, *J* = 13.4, 3.2 Hz, 2H), 1.96–1.67 (m, 5H), 1.58 (ddq, *J* = 13.3, 9.9, 3.1 Hz, 2H), 1.47–1.37 (m, 1H), 1.20 (dd, *J* = 12.9, 3.7 Hz, 1H), 1.17 (s, 3H), 1.10 (dd, *J* = 12.4, 2.9 Hz, 1H), 1.00 (td, *J* = 13.6, 4.4 Hz, 1H), 0.92 (tdd, *J* = 13.3, 3.7, 1.5 Hz, 1H), 0.84 (ddd, *J* = 12.5, 6.3, 3.3 Hz, 3H), 0.78 (d, *J* = 6.4 Hz, 3H), 0.66–0.55 (m, 1H), 0.60 (s, 3H) ppm.

^{13}C NMR (126 MHz, $CDCl_3$) δ 178.0, 173.5, 59.0, 57.8, 51.3, 51.2, 49.4, 44.0, 40.2, 39.7, 38.3, 38.1, 37.7, 36.3, 35.7, 28.8, 27.4, 22.8, 20.7, 19.9, 19.2, 14.0 ppm.

HSQC and **NOESY** spectra are provided to support the configurational assignment. NOE correlations are presented below. See Section 5.8.10 for more details.





14b'

Compound **14b'**: Dimethyl (1*R*,4a*S*,4b*R*,7*R*,8a*S*,10a*S*)-1,4a,7,8a-Tetramethyltetradecahydrophenanthrene-1,7-dicarboxylate

Scale: 0.500 mmol.

Yield: 40.0 mg, 22%.

Physical State: Amorphous white solid.

Purification: SiO_2 (0–30% *v*/*v* EtOAc/hexanes).

***R*f** = 0.38 (5% *v*/*v* EtOAc/hexanes + CAM).

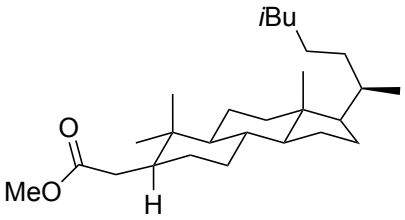
IR (ATR, neat) $\tilde{\nu}_{max}$: 2999, 2942, 2924, 2888, 2838, 1728, 1467, 1445, 1427, 1384, 1326, 1253, 1231, 1215, 1196, 1187, 1152, 1104, 1094, 1043, 1025, 1016, 1002, 986, 973, 935, 903, 881, 851, 824, 793, 771, 737 cm^{-1}.

HRMS–DART (*m*/*z*): $[M + H]^+$ calc'd for $C_{22}H_{37}O_4$ 365.2686, found 365.2691.

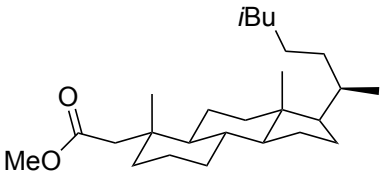
Specific Rotation: $[a]_D^{23.0}$ = –33.0 (*c* 3.0, $CHCl_3$).

^{1}H NMR (500 MHz, $CDCl_3$) δ 3.62 (s, 3H), 3.61 (s, 3H), 2.34 (dq, *J* = 13.4, 3.2 Hz, 1H), 2.18–2.08 (m, 1H), 1.98 (dd, *J* = 13.4, 2.6 Hz, 1H), 1.91–1.76 (m, 2H), 1.72 (dq, *J* = 14.3, 3.6 Hz, 2H), 1.54–1.46 (m, 2H), 1.46–1.33 (m, 2H), 1.14 (s, 3H), 1.07 (s, 4H), 1.06–0.91 (m, 5H), 0.81 (td, *J* = 13.0, 4.4 Hz, 1H), 0.76 (s, 3H), 0.72 (dd, *J* = 12.2, 2.7 Hz, 1H), 0.57 (s, 3H) ppm.

^{13}C NMR (101 MHz, $CDCl_3$) δ 178.8, 178.0, 58.4, 57.7, 55.2, 51.5, 51.2, 44.0, 43.6, 41.5, 40.2, 38.3, 37.6, 37.0, 35.4, 30.3, 28.8, 19.9, 19.4, 19.3, 19.1, 13.8 ppm.



15b



15b'

Compound **15b**: Methyl 2-((3*R*,3a*R*,5a*S*,7*S*,9a*R*,9b*S*)-3a,6,6-trimethyl-3-((*R*)-6-methylheptan-2-yl)dodecahydro-1*H*-cyclopenta[*a*]naphthalen-7-yl)acetate

Compound **15b'**: Methyl 2-((3*R*,3a*R*,5a*S*,6*R*,9a*R*,9b*S*)-3a,6-dimethyl-3-((*R*)-6-methylheptan-2-yl)dodecahydro-1*H*-cyclopenta[*a*]naphthalen-6-yl)acetate

Scale: 0.120 mmol.

Yield: **15b**: 36.7 mg, 76%.

15b': 2.8 mg, 6%.

Physical State: Yellow oil.

Purification: SiO_2 (0.5% *v/v* EtOAc/hexanes to 2.0% *v/v* EtOAc/hexanes) [inseparable].

R_f = 0.45 (5% *v/v* EtOAc/hexanes + CAM) [incidental R_f].

IR (ATR, neat) $\tilde{\nu}_{max}$: 2932, 2868, 2850, 1741, 1466, 1367, 1169, 1155 cm^{-1}.

HRMS–DART (*m/z*): $[M + H]^+$ calc'd for $C_{27}H_{49}O_2$ 405.3727, found 405.3733.

15b

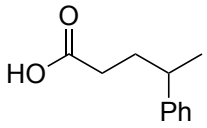
^{1}H NMR (600 MHz, $CDCl_3$) δ 3.68–3.63 (m, 3H), 2.52 (dd, *J* = 14.9, 3.1 Hz, 1H), 1.99–1.91 (m, 2H), 1.85–1.77 (m, 1H), 1.67–1.59 (m, 2H), 1.59–1.48 (m, 4H), 1.38–0.82 (m, 28H), 0.80–0.73 (m, 1H), 0.70 (s, 3H), 0.64 (s, 3H).

^{13}C NMR (126 MHz, $CDCl_3$) δ 175.0, 56.7, 56.4, 53.2, 51.6, 45.0, 42.4, 40.3, 39.7, 36.5, 36.3, 36.0, 35.9, 35.7, 31.7, 28.42, 28.41, 28.2, 26.6, 24.3, 24.0, 23.0, 22.7, 22.1, 18.8, 14.9, 12.1.

15b'

^{1}H NMR (600 MHz, $CDCl_3$) δ 3.68–3.63 (m, 3H), 2.23 (dd, *J* = 9.5, 7.5 Hz, 2H), 1.99–1.91 (m, 1H), 1.85–1.77 (m, 1H), 1.67–0.82 (m, 37H), 0.80–0.73 (m, 1H), 0.65 (s, 3H).

^{13}C NMR (126 MHz, $CDCl_3$) δ 175.3, 56.54, 56.48, 51.7, 49.9, 42.7, 40.2, 39.5, 37.7, 37.3, 35.8, 35.0, 32.1, 32.0, 31.9, 28.64, 28.55, 28.3, 26.7, 24.4, 24.2, 22.8, 21.9, 21.7, 19.4, 14.3, 12.2.



16b

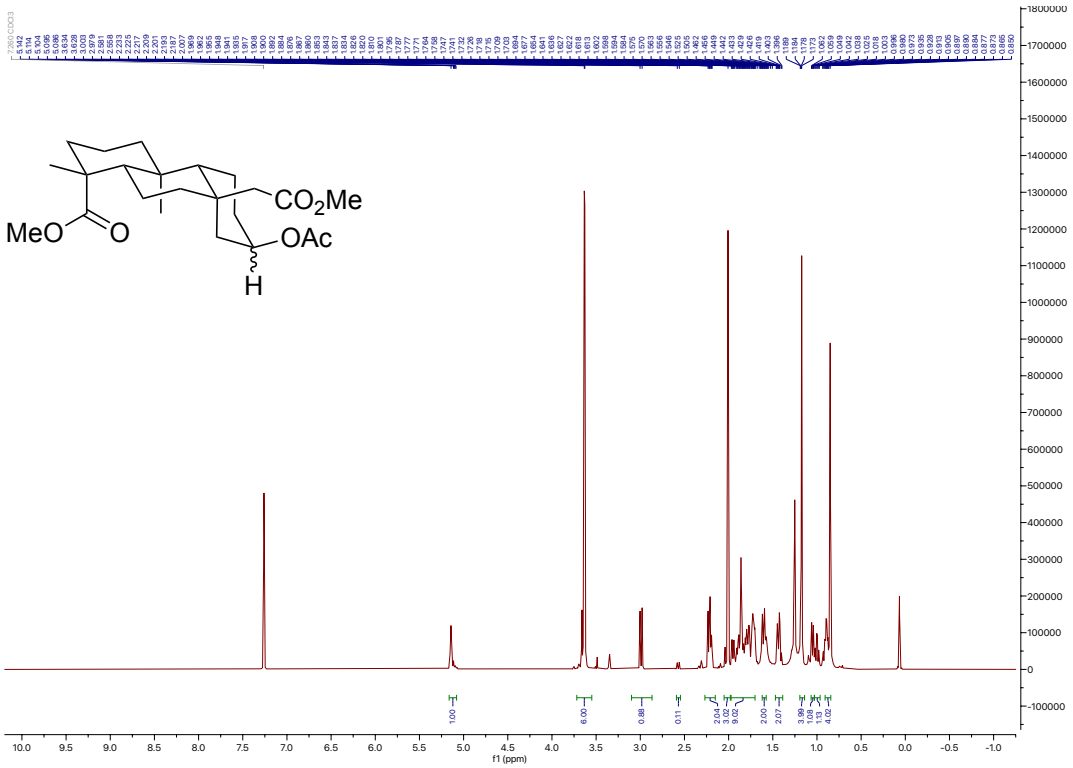
Compound **16b**: 4-Phenylpentanoic acid

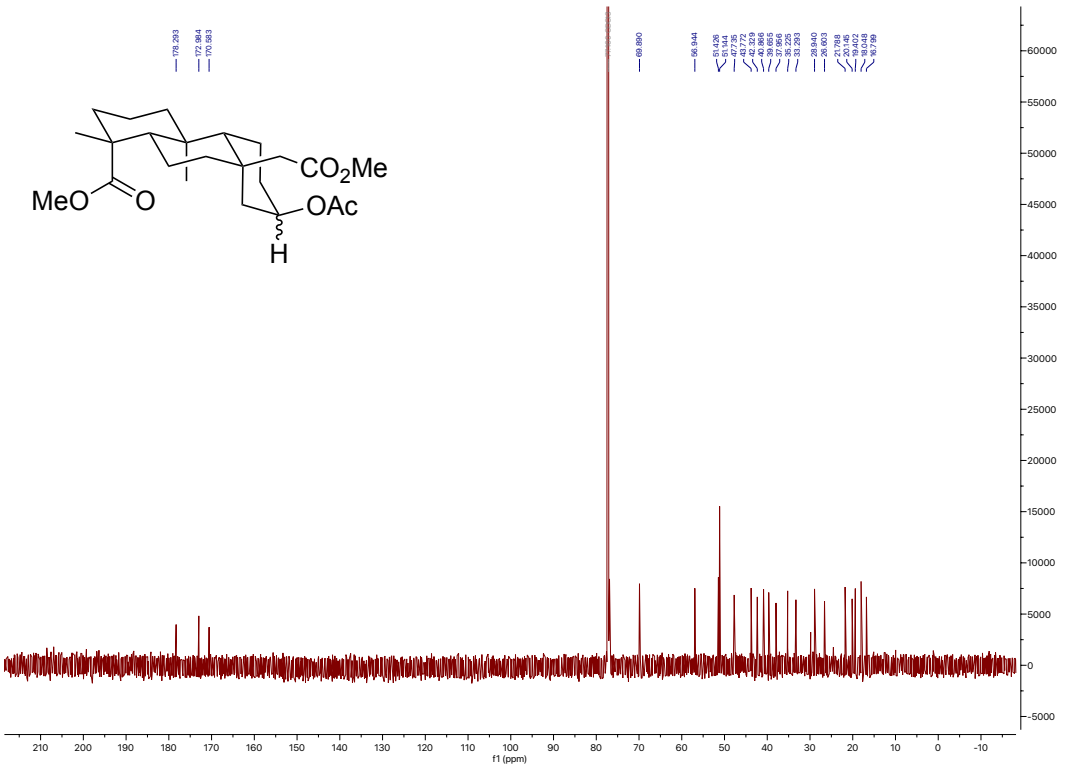
Scale: 0.459 mmol.

Yield: 55.1 mg, 67%.

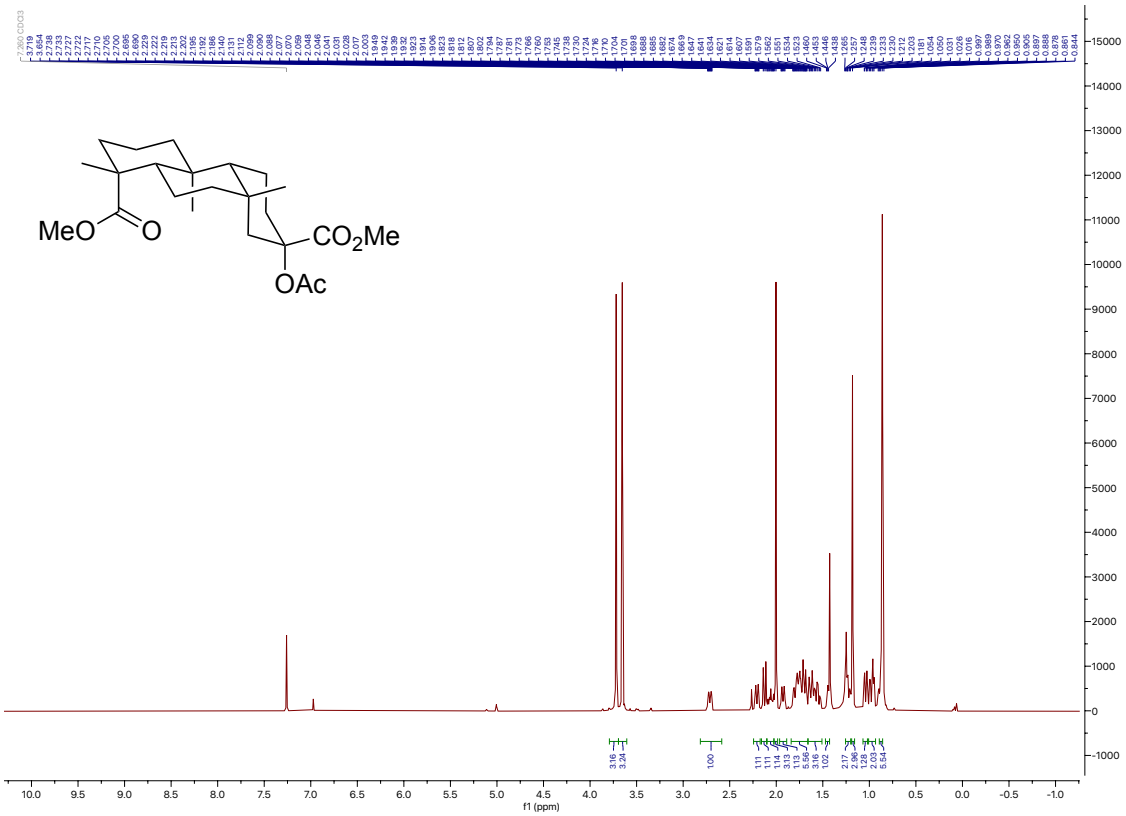
Characterization matches those previously reported in the literature [56].

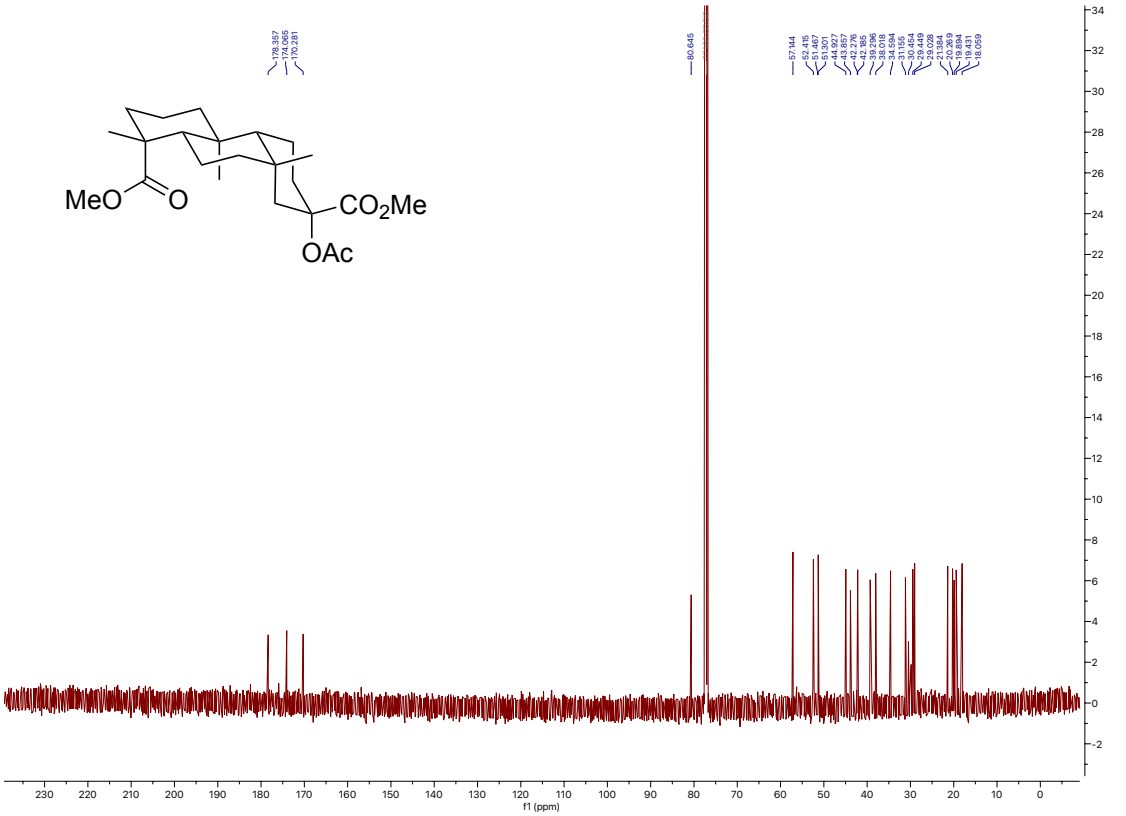
5.8.10 Copies of NMR Spectra



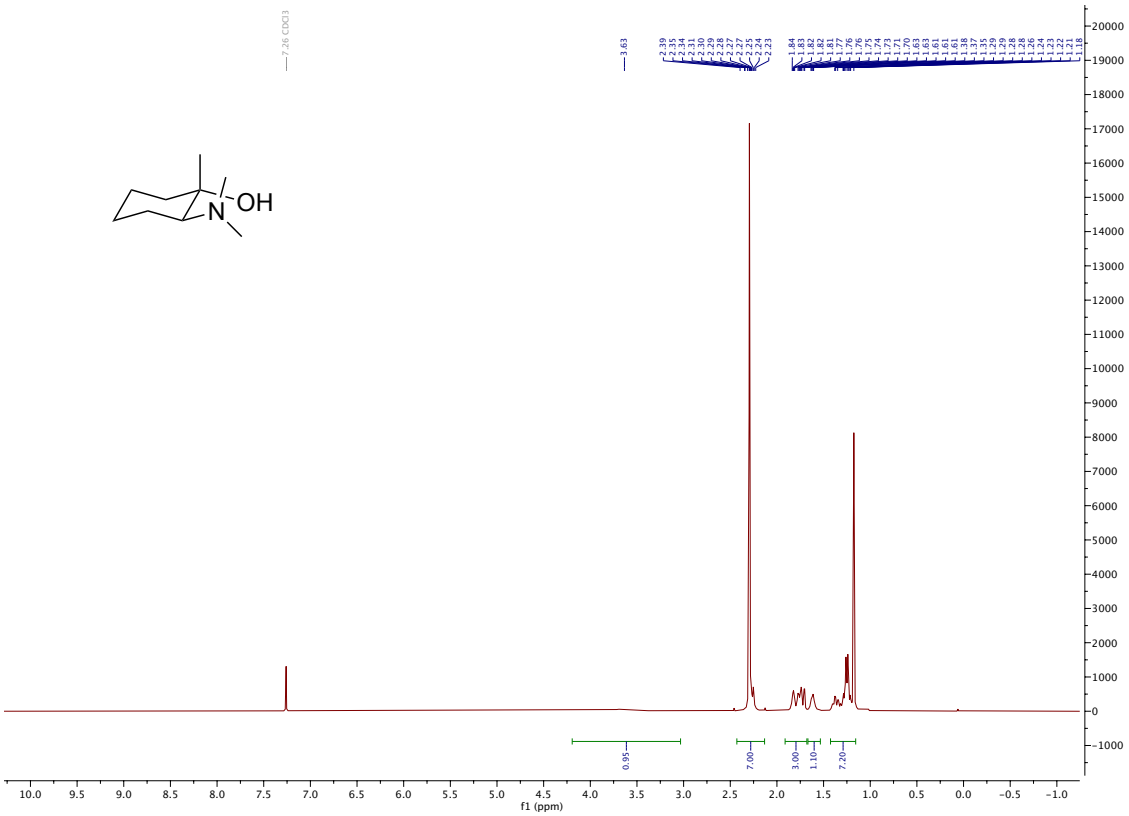


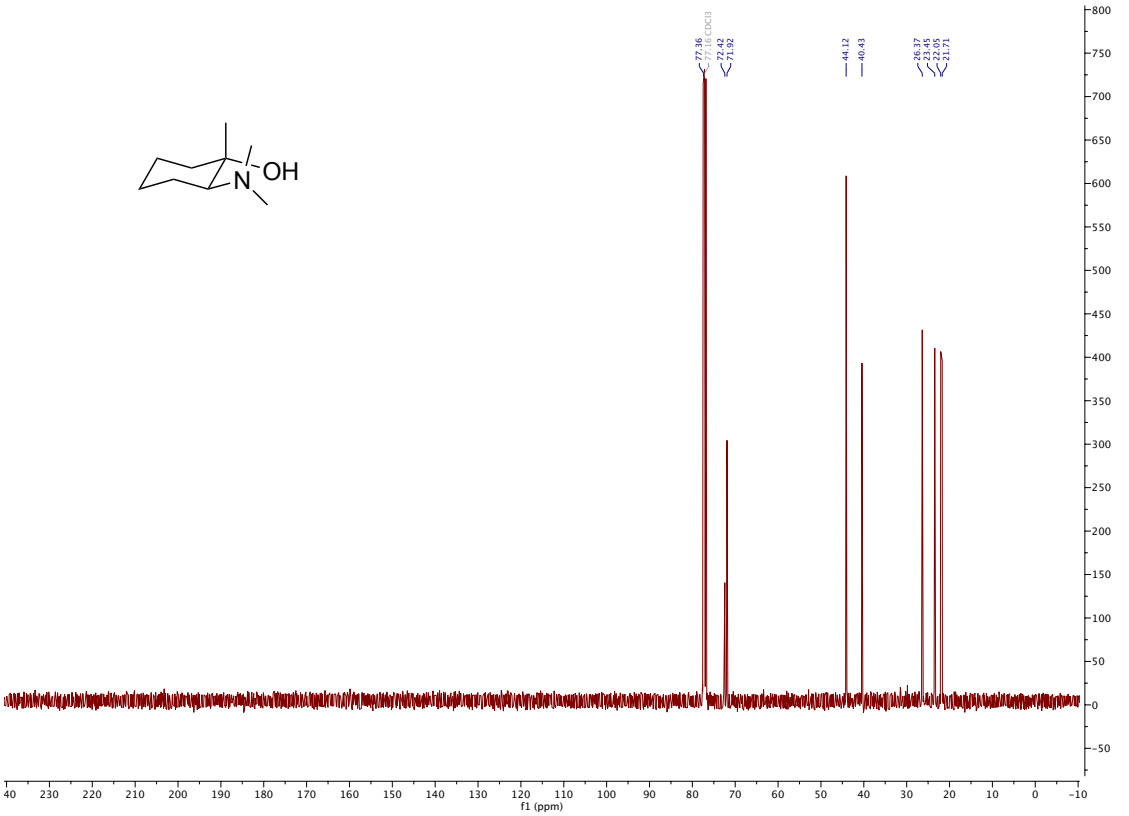
^{1}H NMR (600 MHz, $CDCl_3$) and **^{13}C NMR** (126 MHz, $CDCl_3$) of **2b-1** and **2b-2**



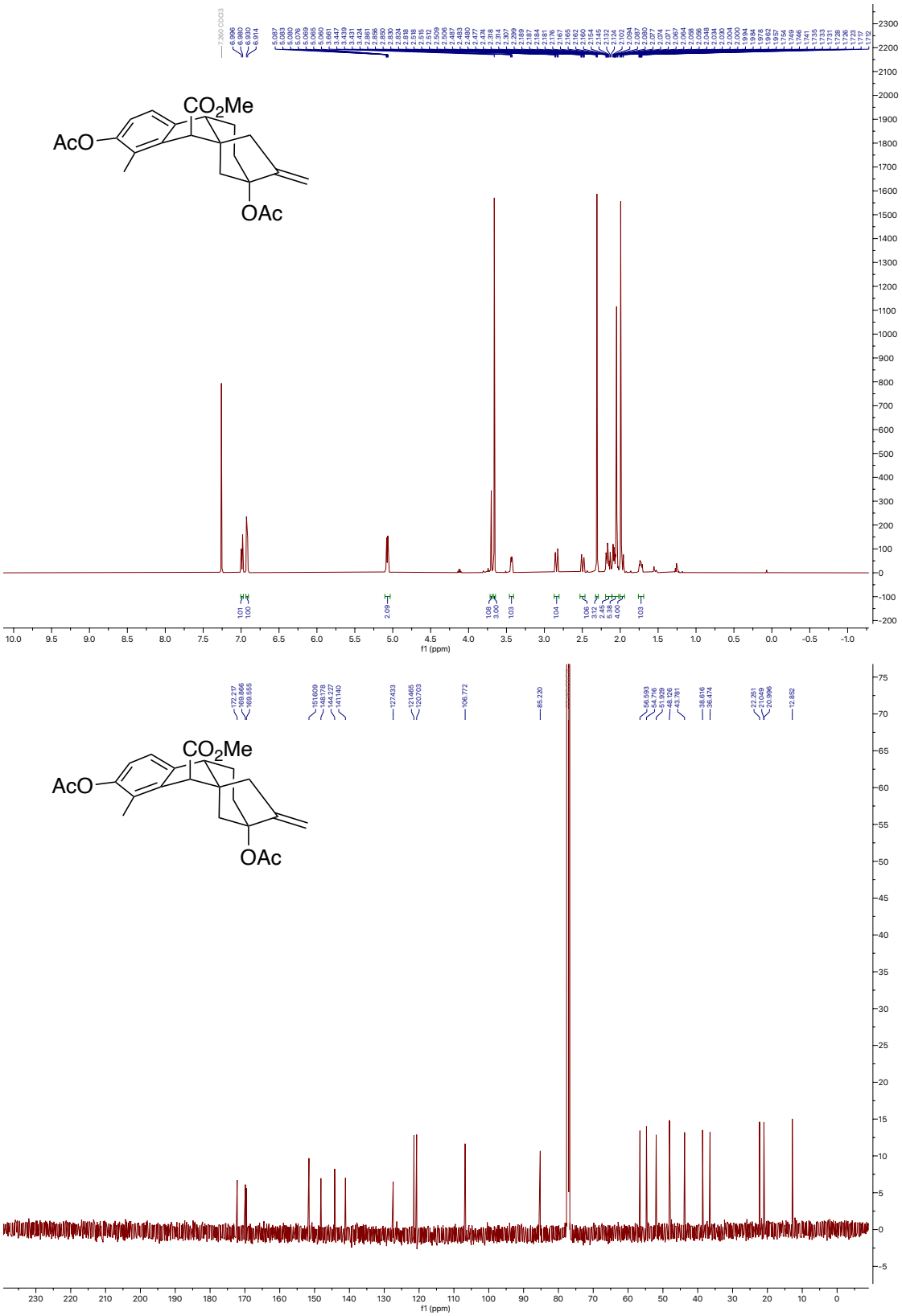


^{1}H NMR (500 MHz, $CDCl_3$) and **^{13}C NMR** (126 MHz, $CDCl_3$) of Compound **2b'**

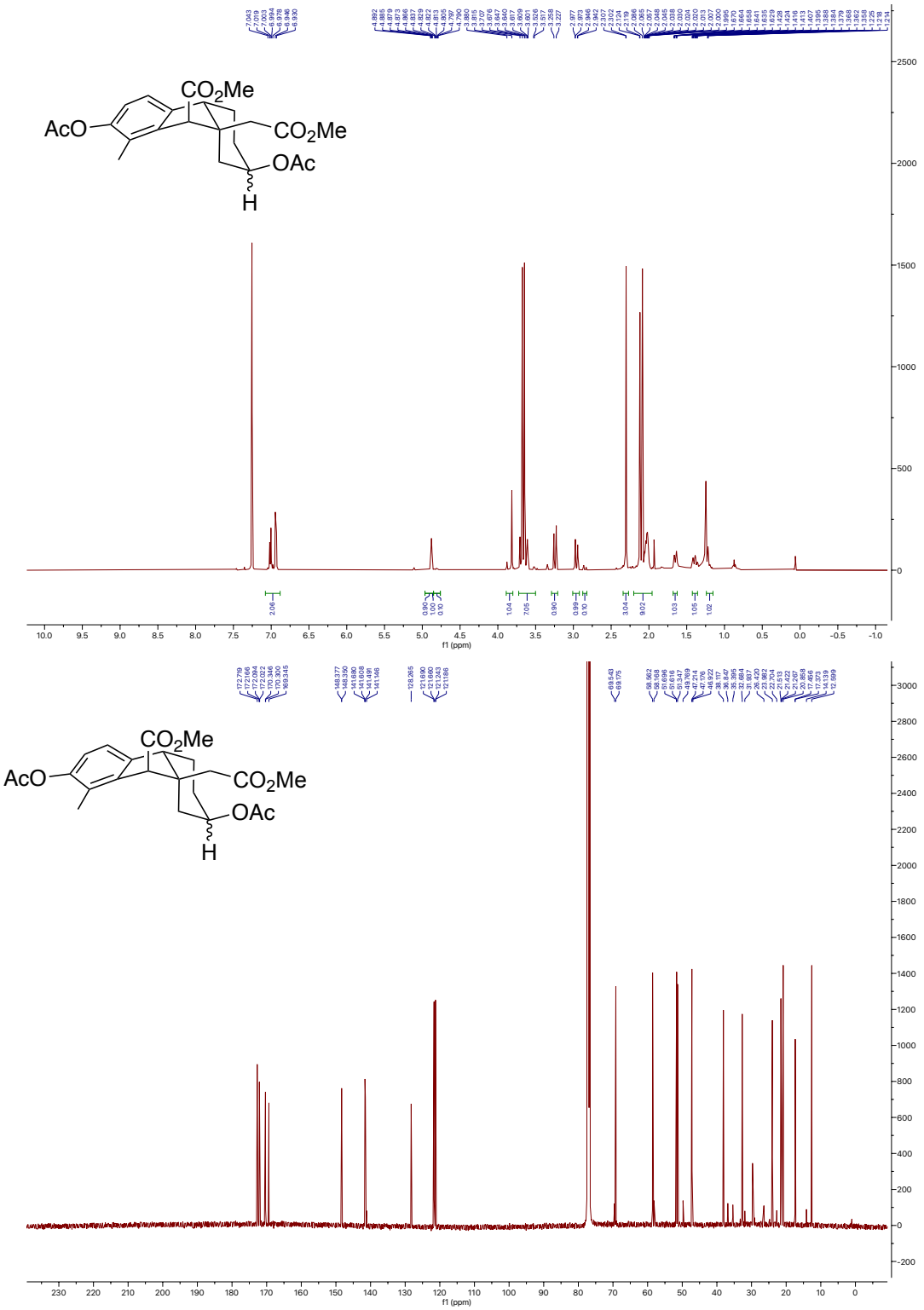




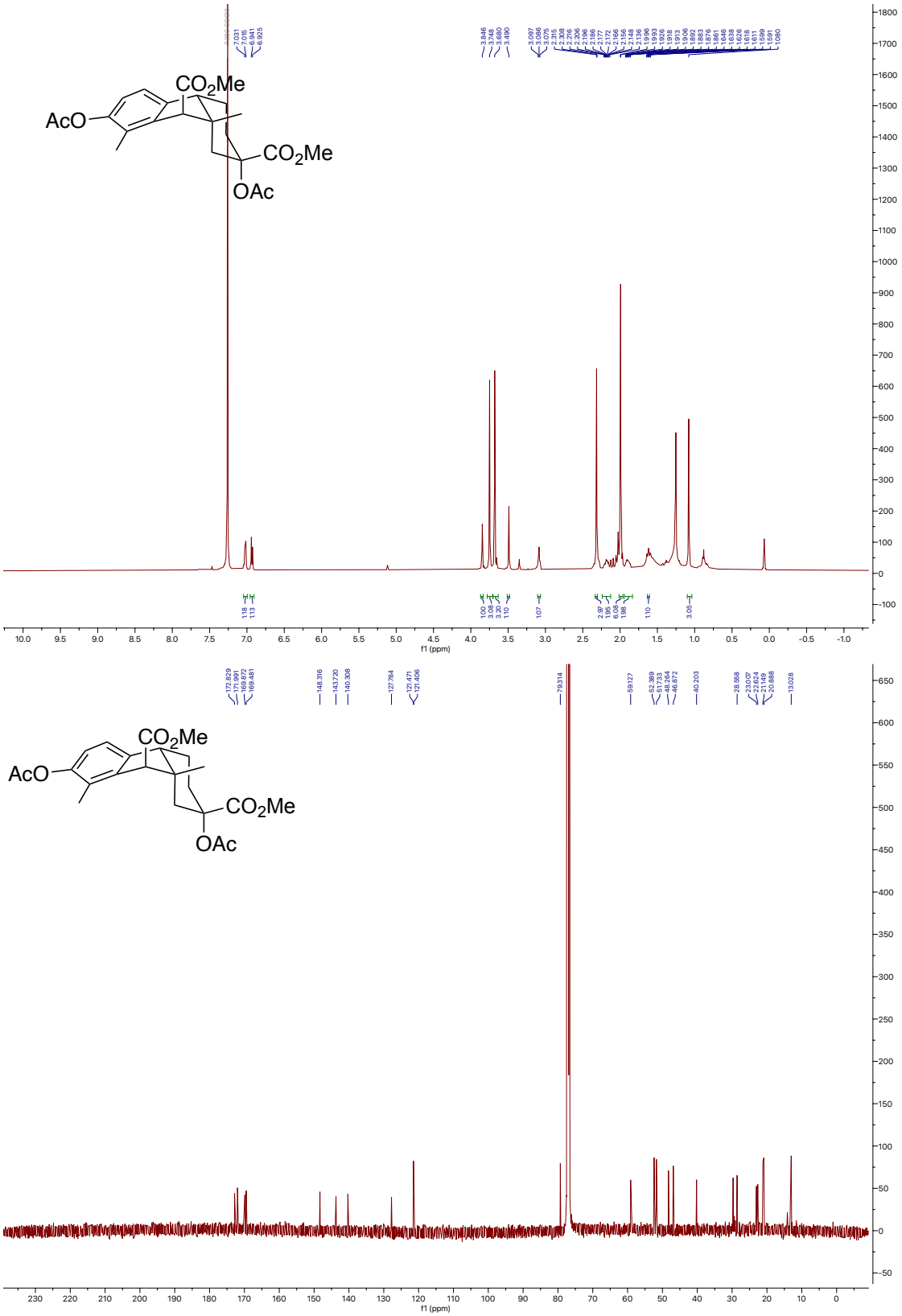
^{1}H NMR (400 MHz, $CDCl_3$) and **^{13}C NMR** (101 MHz, $CDCl_3$) of Compound **4b**



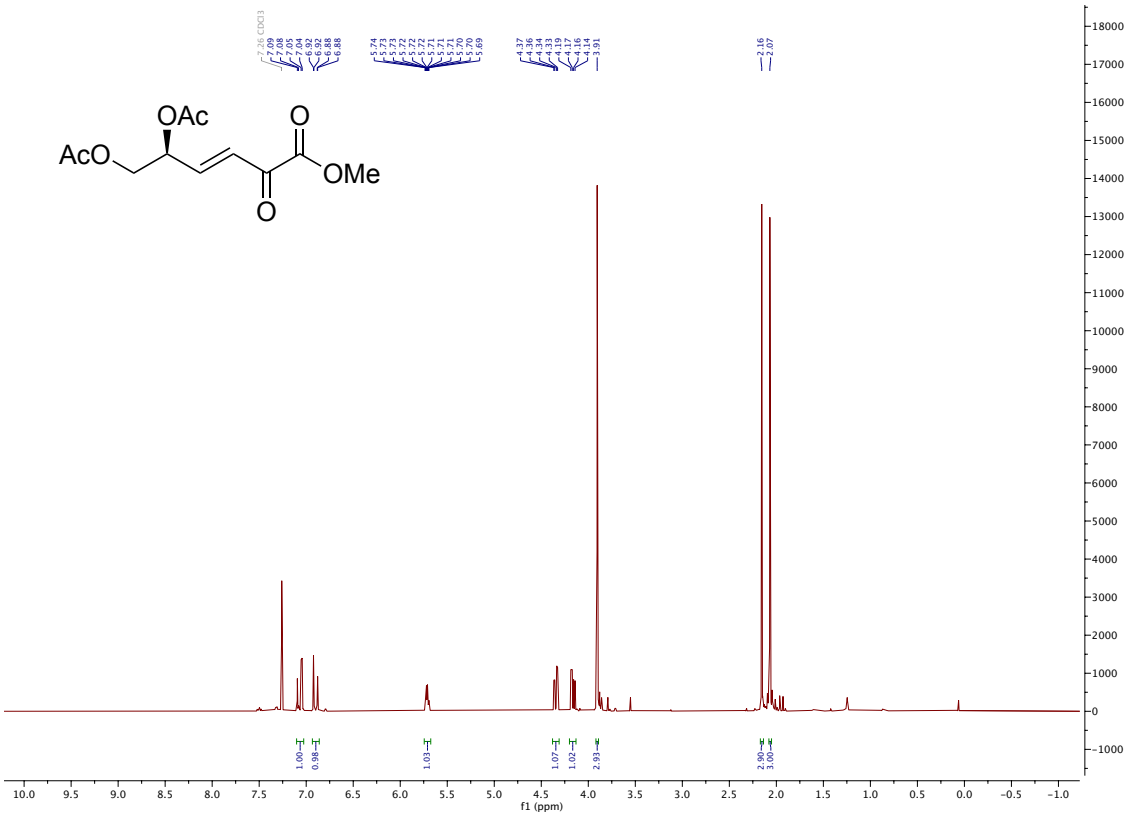
^{1}H NMR (400 MHz, $CDCl_3$) and **^{13}C NMR** (126 MHz, $CDCl_3$) of Compound **7a**

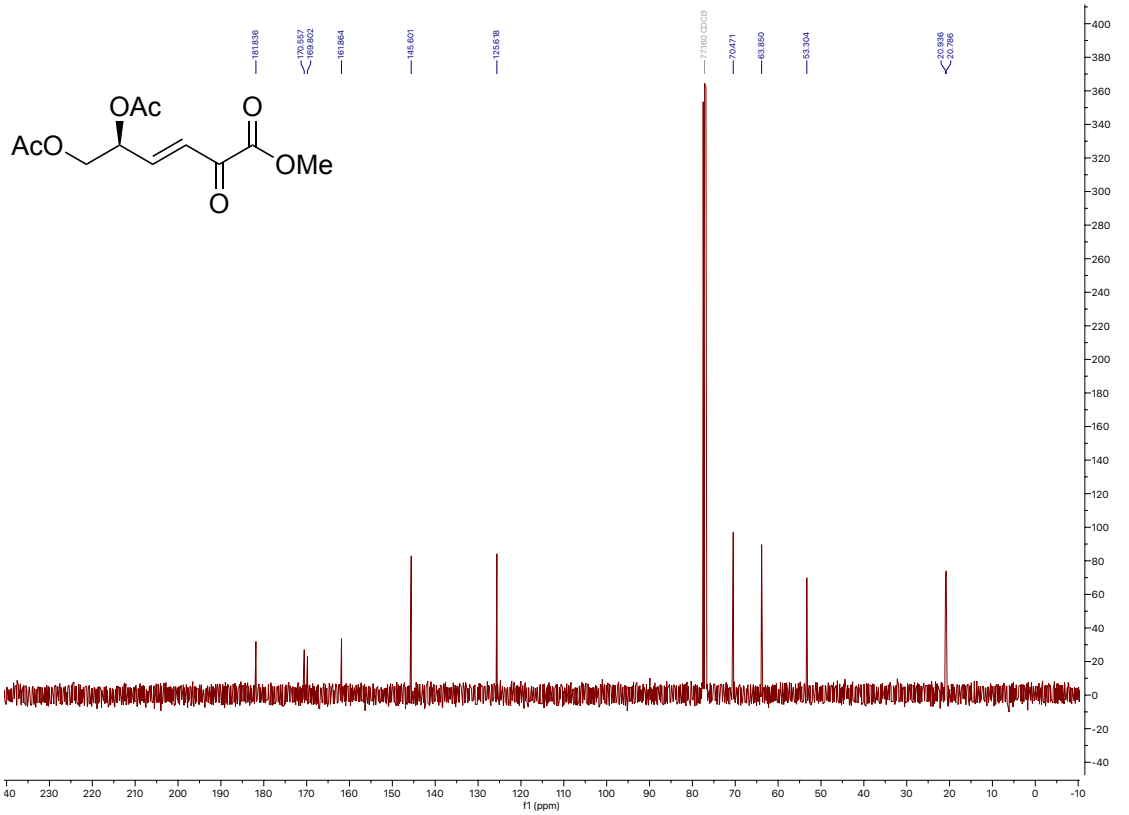


^{1}H NMR (500 MHz, $CDCl_3$) and **^{13}C NMR** (126 MHz, $CDCl_3$) of Compound **7b-1** and **7b-2**

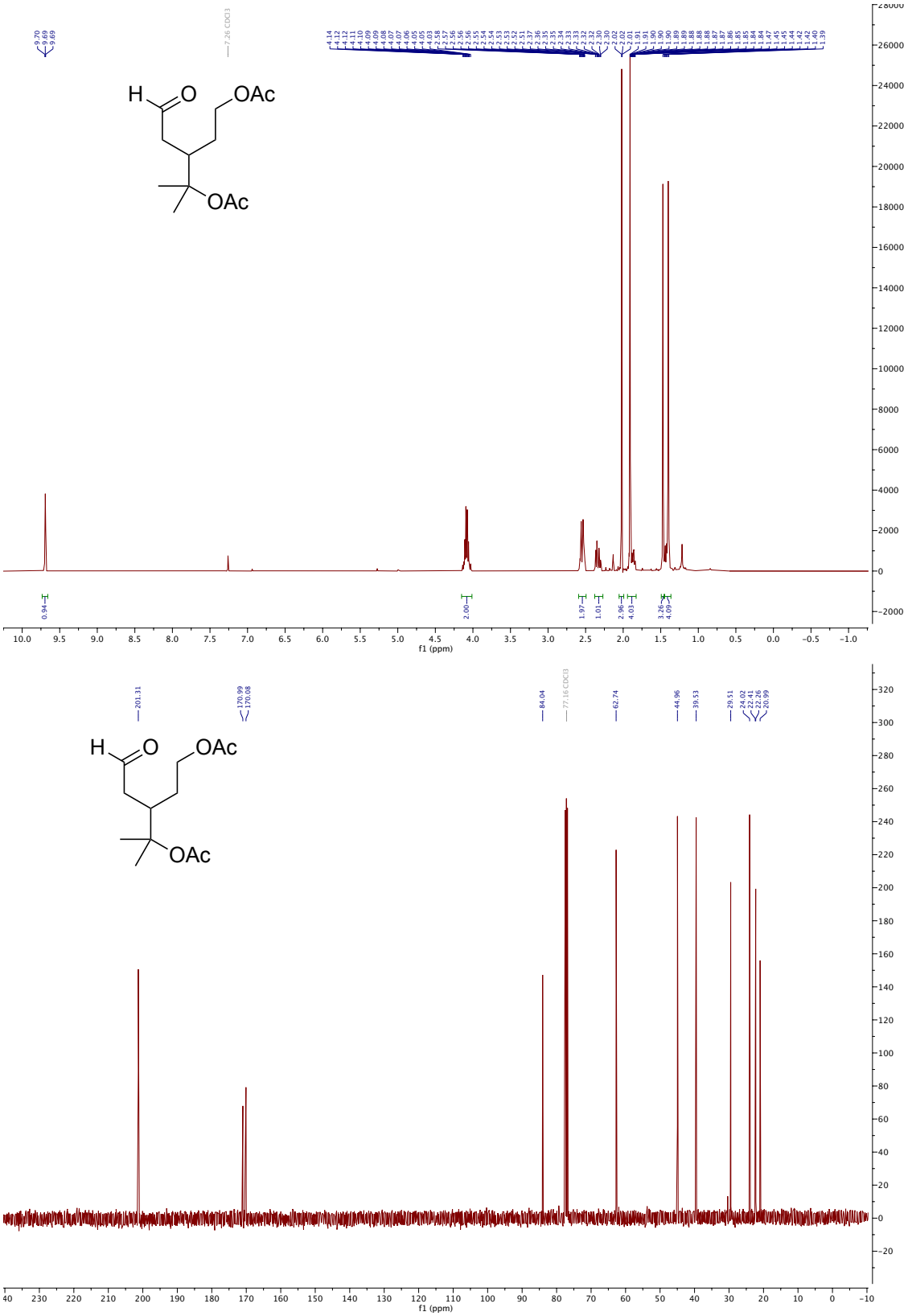


^{1}H NMR (400 MHz, $CDCl_3$) and **^{13}C NMR** (101 MHz, $CDCl_3$) of Compound **7b'**

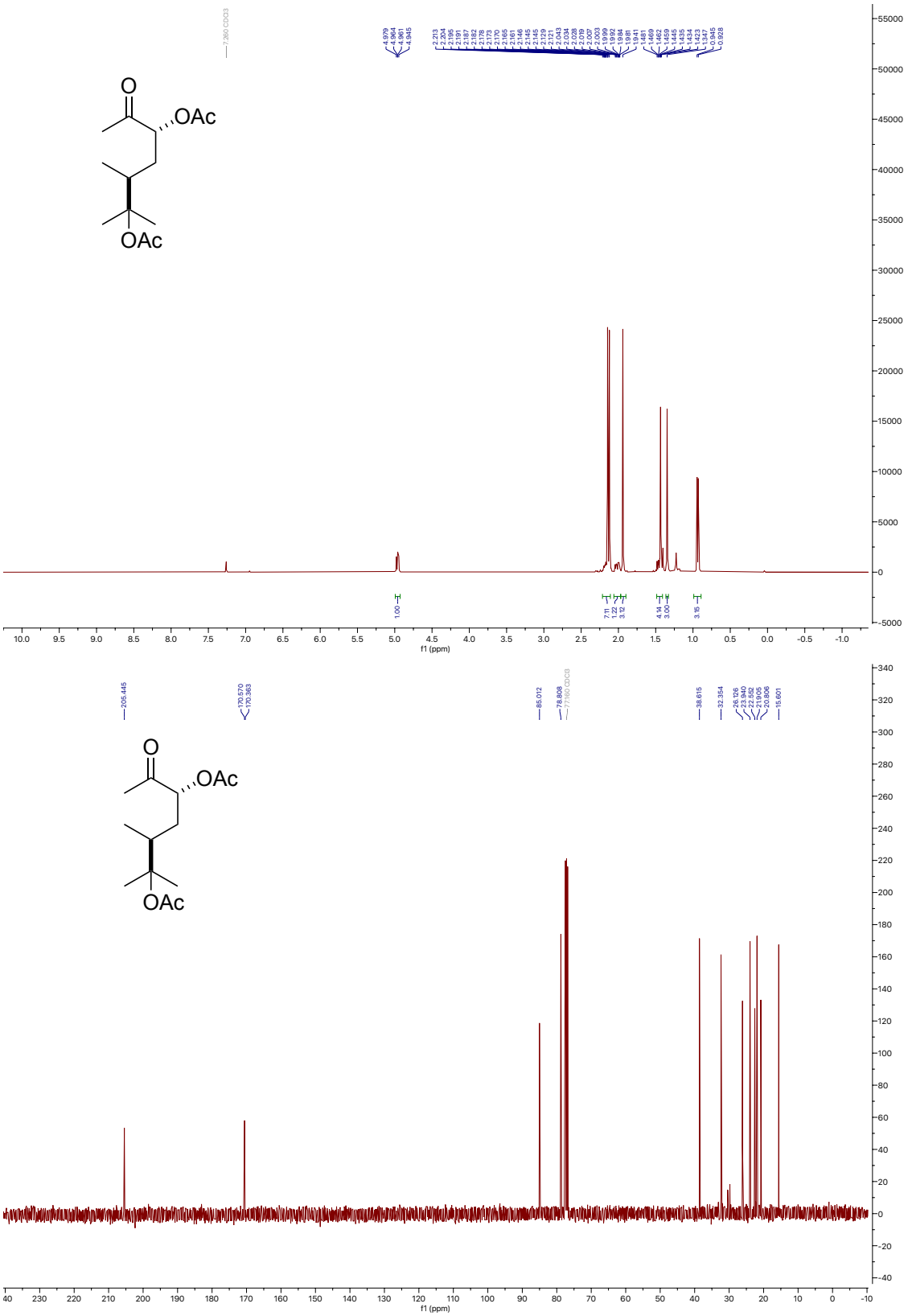




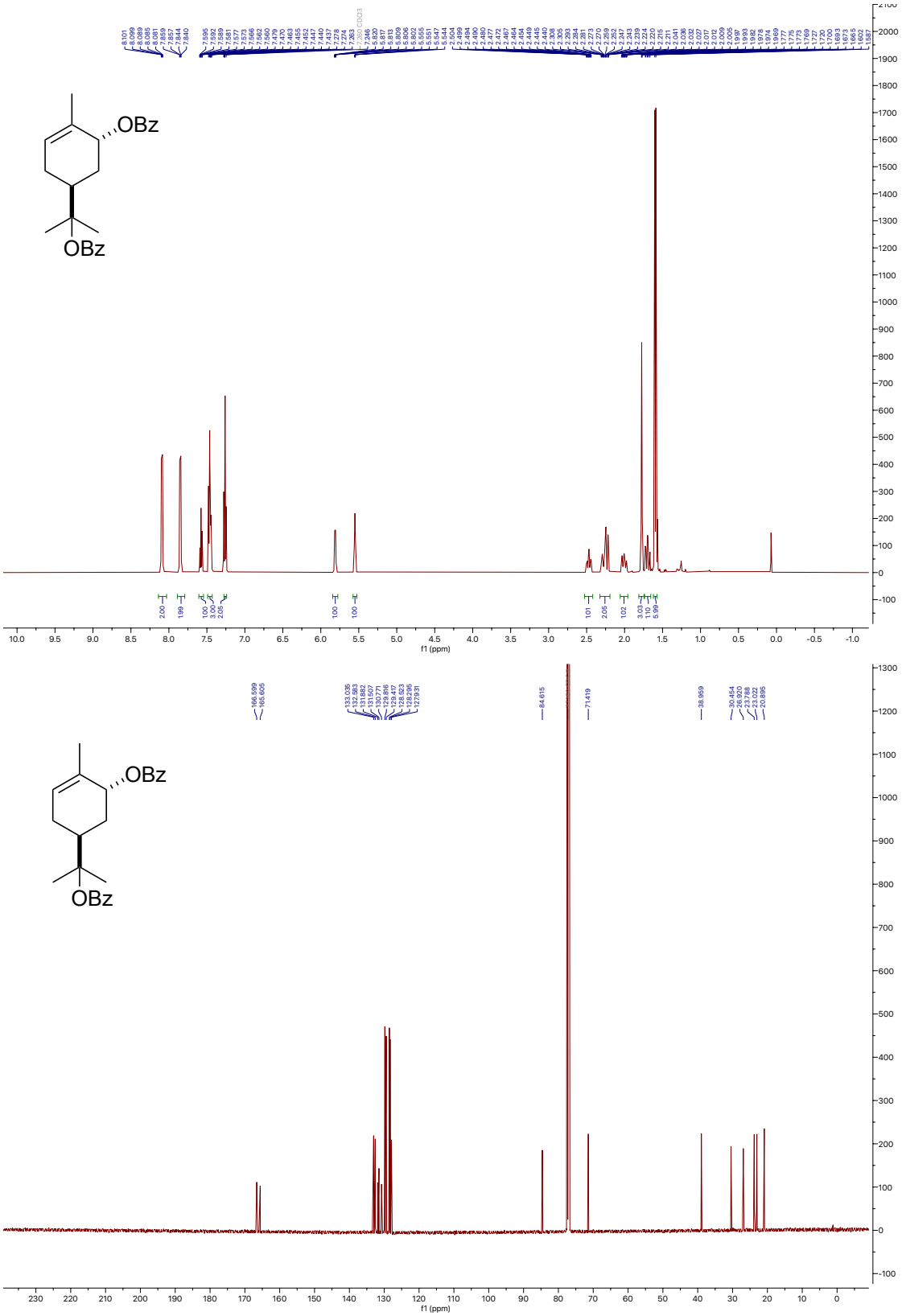
^{1}H NMR (400 MHz, $CDCl_3$) and **^{13}C NMR** (101 MHz, $CDCl_3$) of Compound **8b**



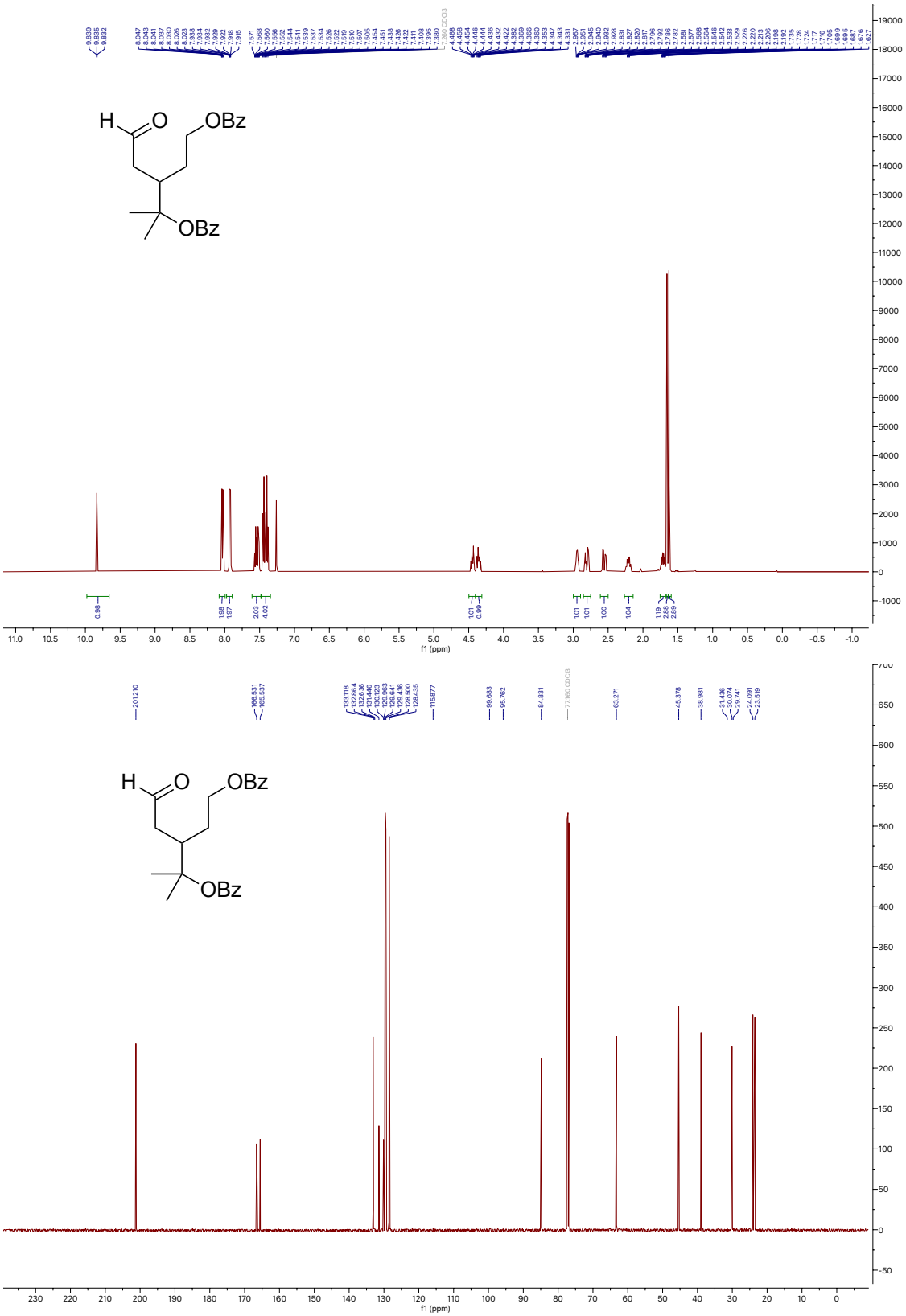
^{1}H NMR (400 MHz, $CDCl_3$) and **^{13}C NMR** (101 MHz, $CDCl_3$) of Compound **9b**



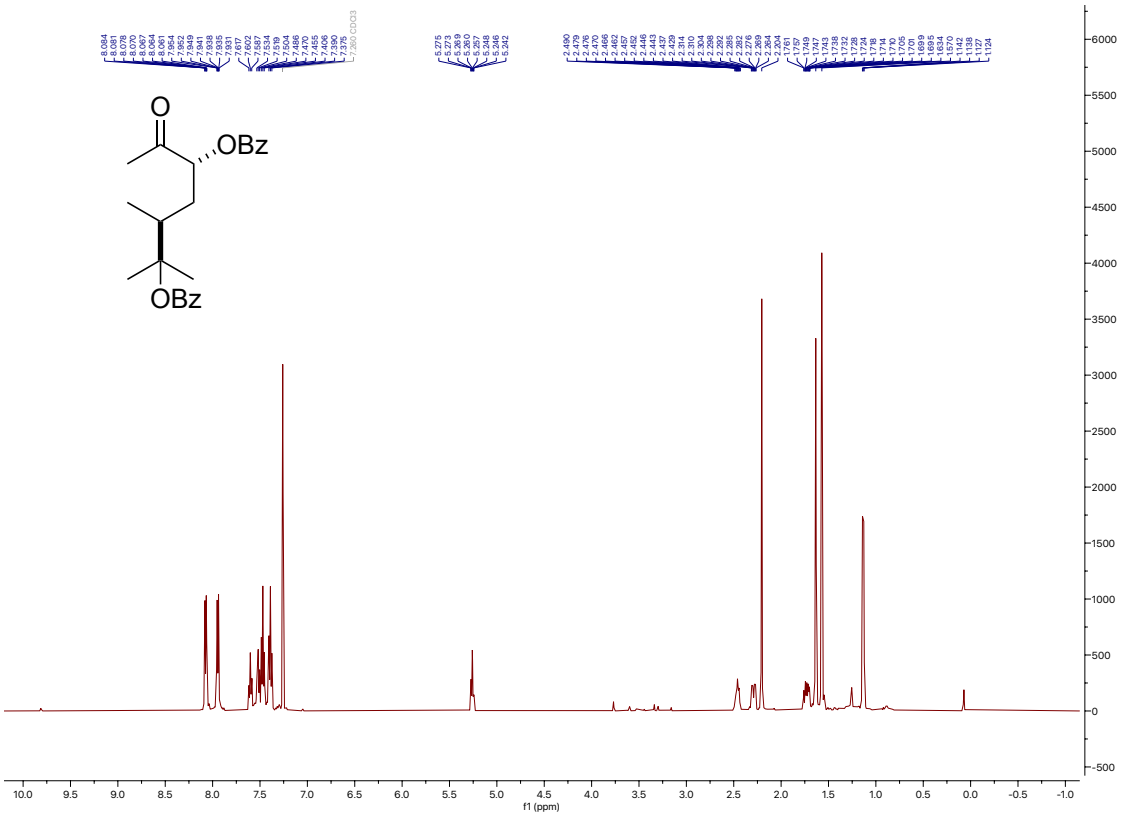
^{1}H NMR (400 MHz, $CDCl_3$) and **^{13}C NMR** (101 MHz, $CDCl_3$) of Compound **9b'**

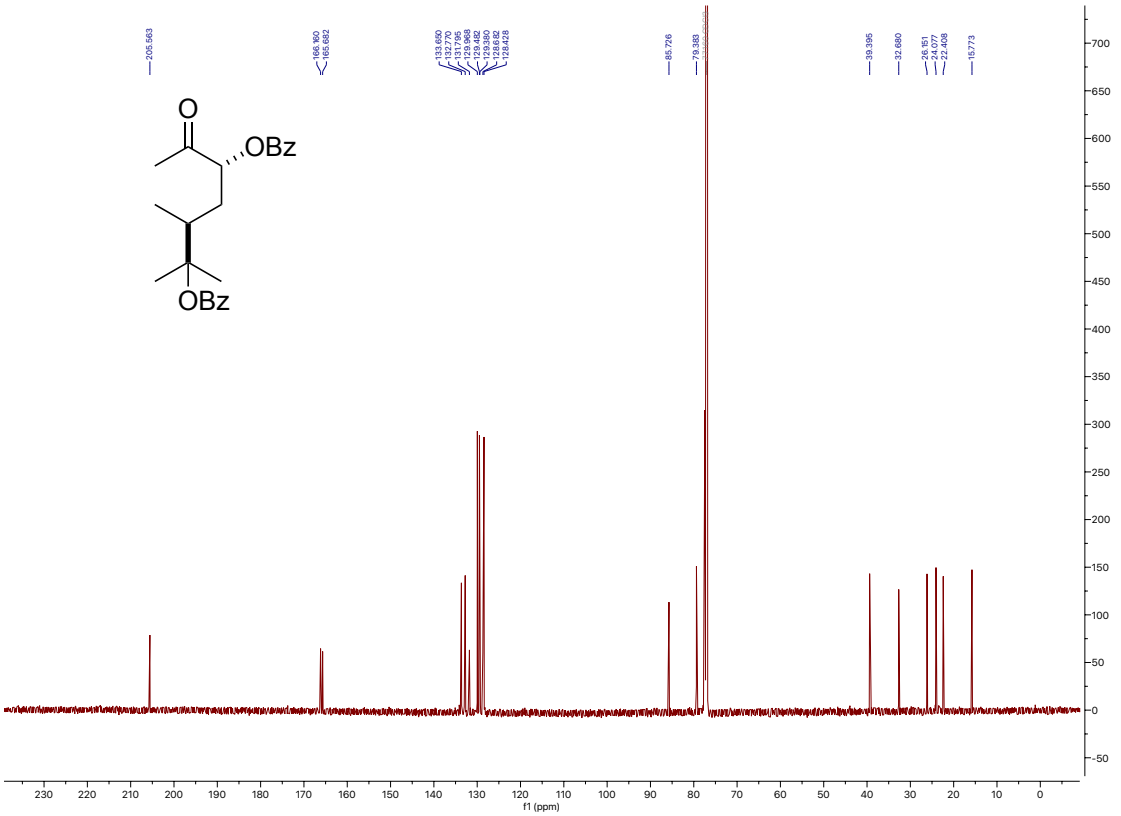


^{1}H NMR (300 MHz, $CDCl_3$) and **^{13}C NMR** (126 MHz, $CDCl_3$) of Compound **10a**

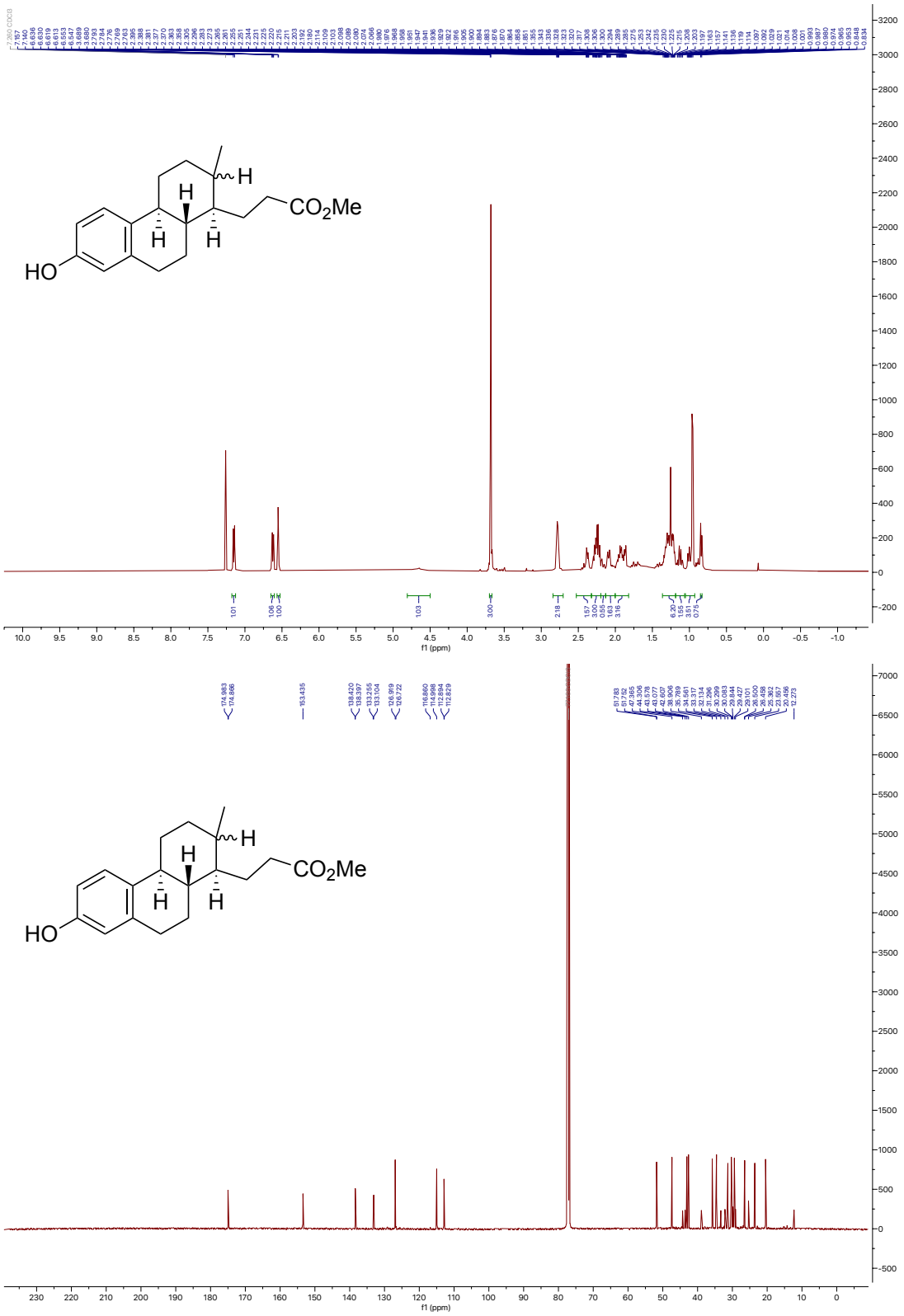


^{1}H NMR (500 MHz, $CDCl_3$) and **^{13}C NMR** (126 MHz, $CDCl_3$) of Compound **10b**

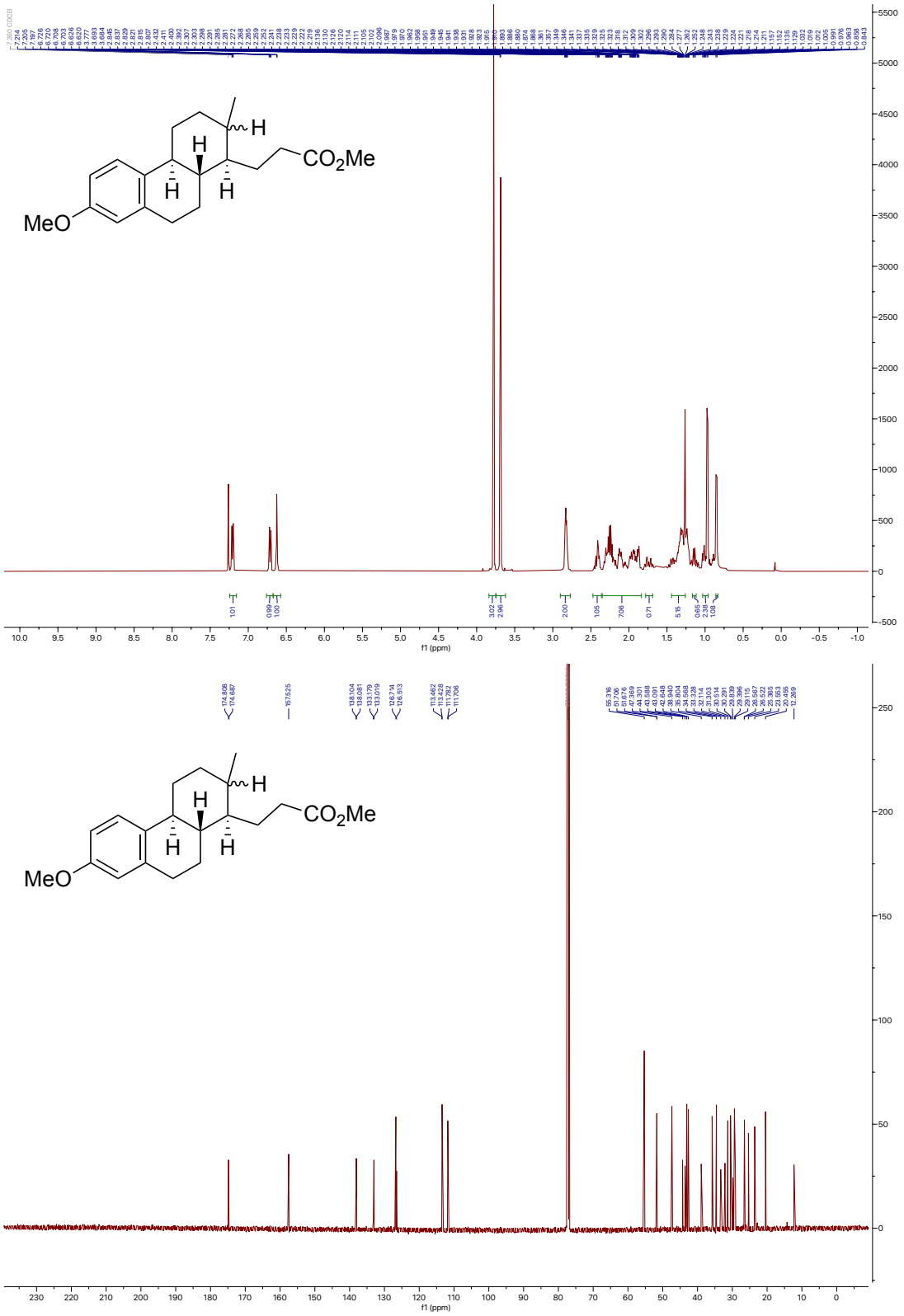




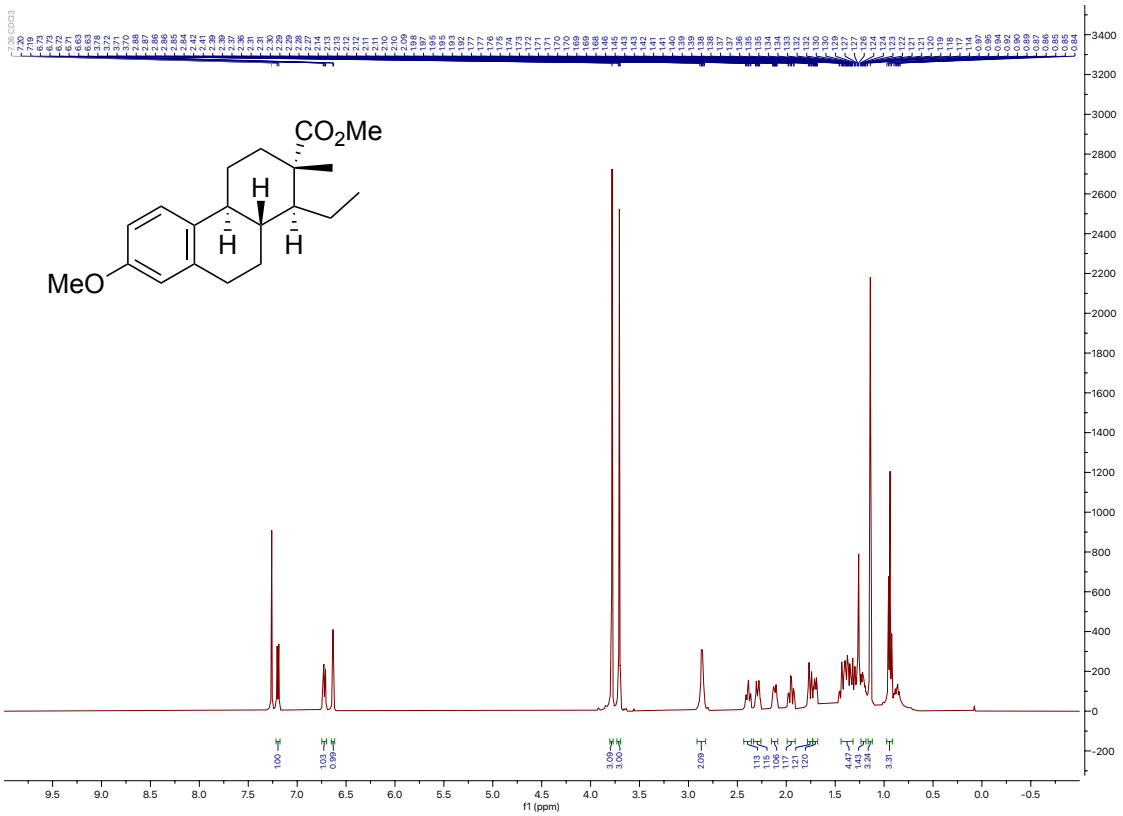
^{1}H NMR (500 MHz, $CDCl_3$) and **^{13}C NMR** (126 MHz, $CDCl_3$) of Compound **10b'**

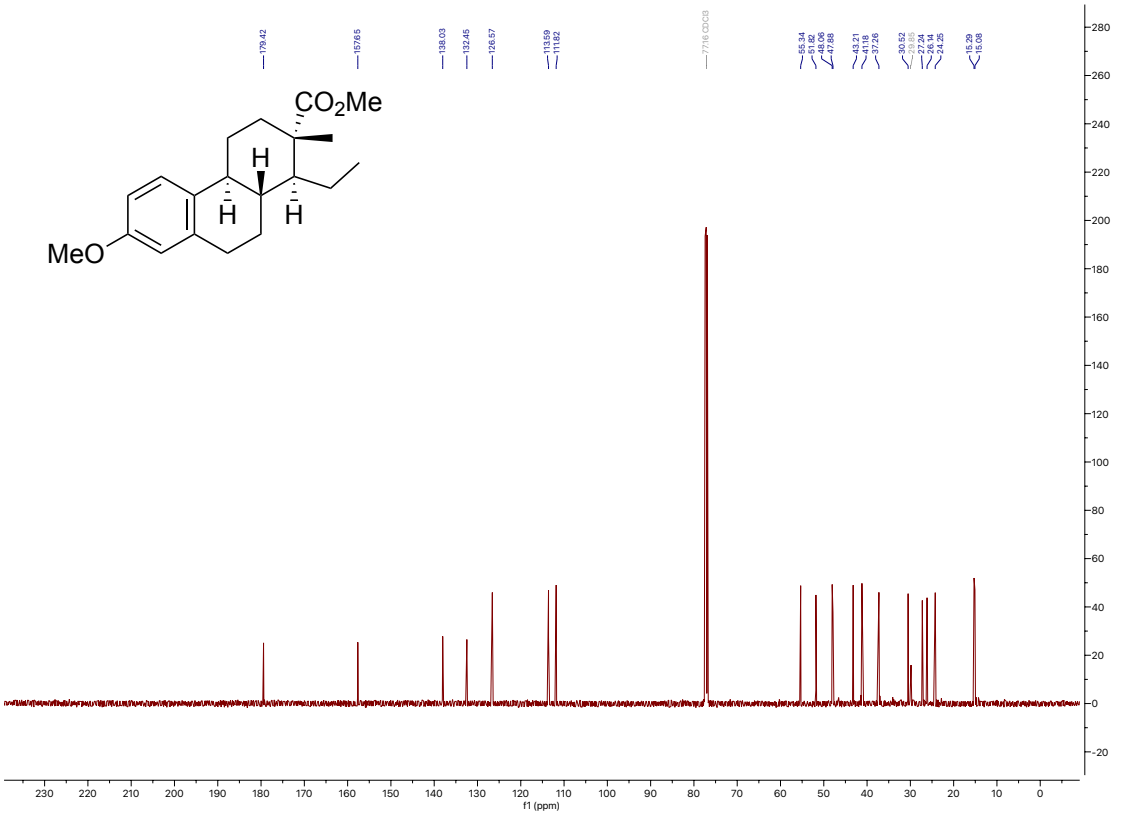


^{1}H NMR (500 MHz, $CDCl_3$) and **^{13}C NMR** (126 MHz, $CDCl_3$)
of Compound **11b-1** and **11b-2**

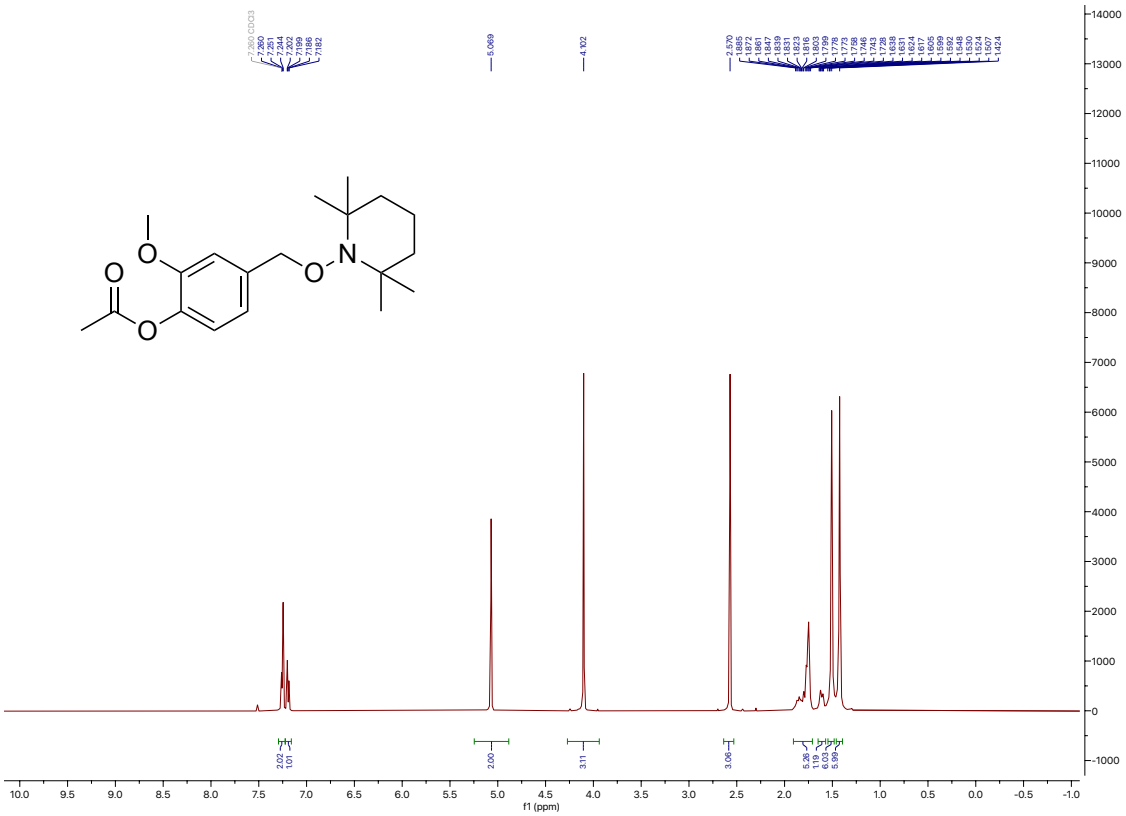


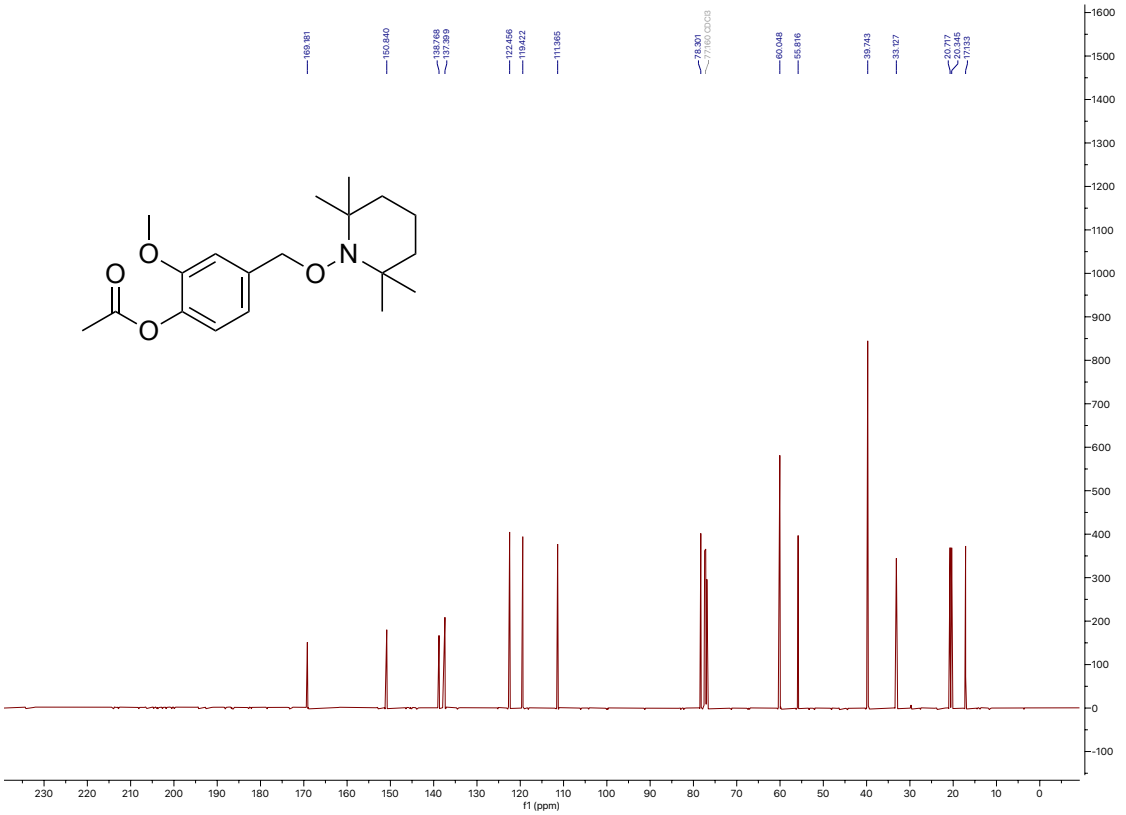
^{1}H NMR (500 MHz, $CDCl_3$) and **^{13}C NMR** (126 MHz, $CDCl_3$)
of Compounds **12b-1** and **12b-2**



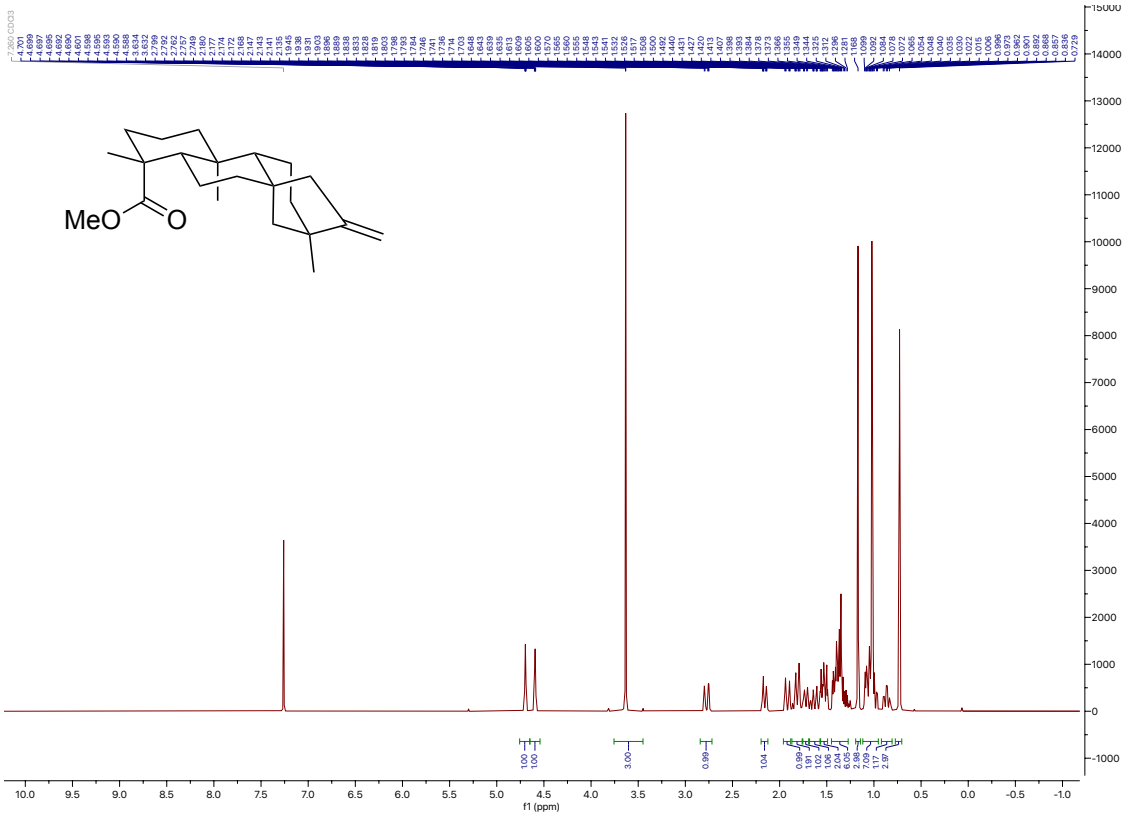


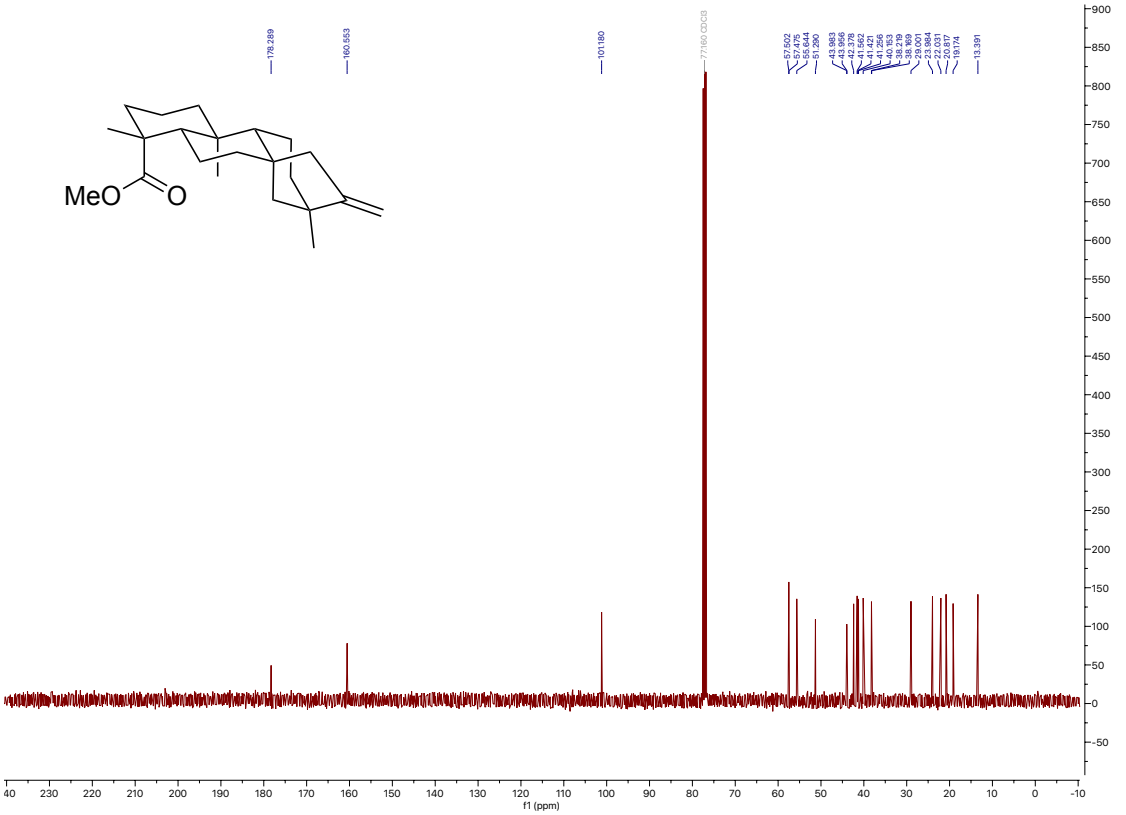
^{1}H NMR (600 MHz, $CDCl_3$) and **^{13}C NMR** (151 MHz, $CDCl_3$) of Compound **12b'**



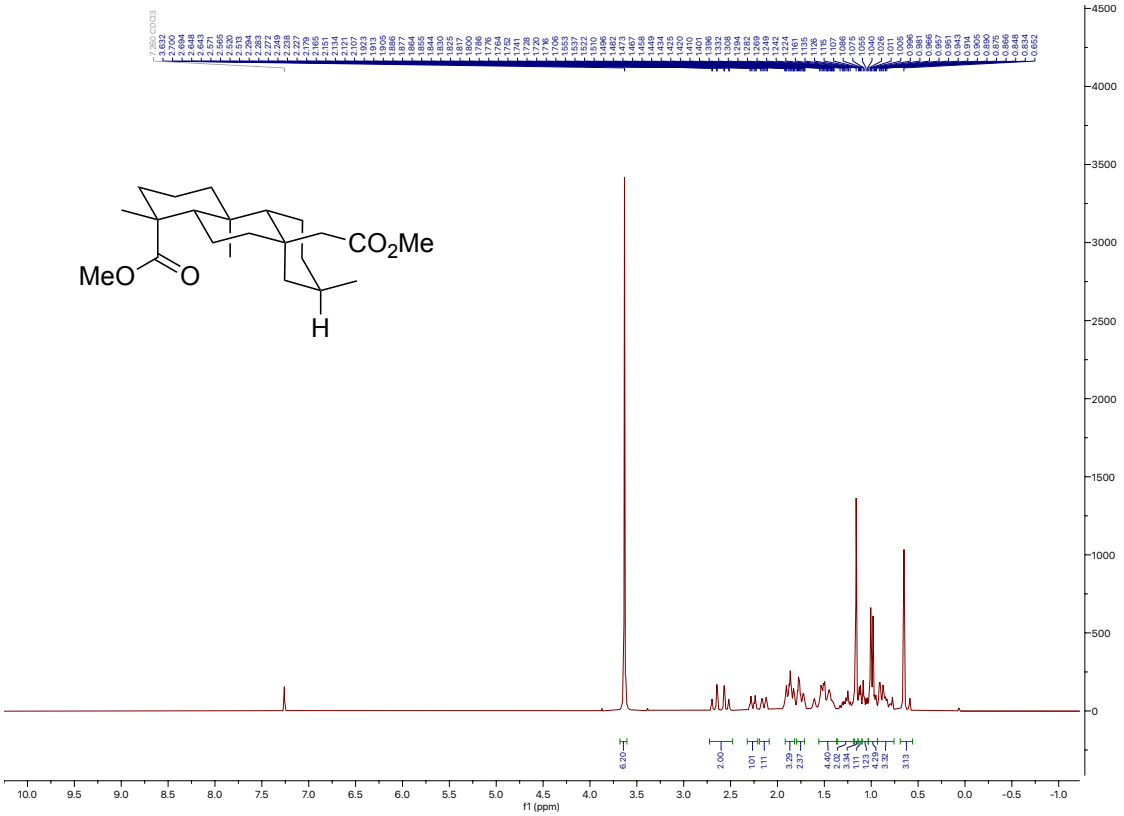


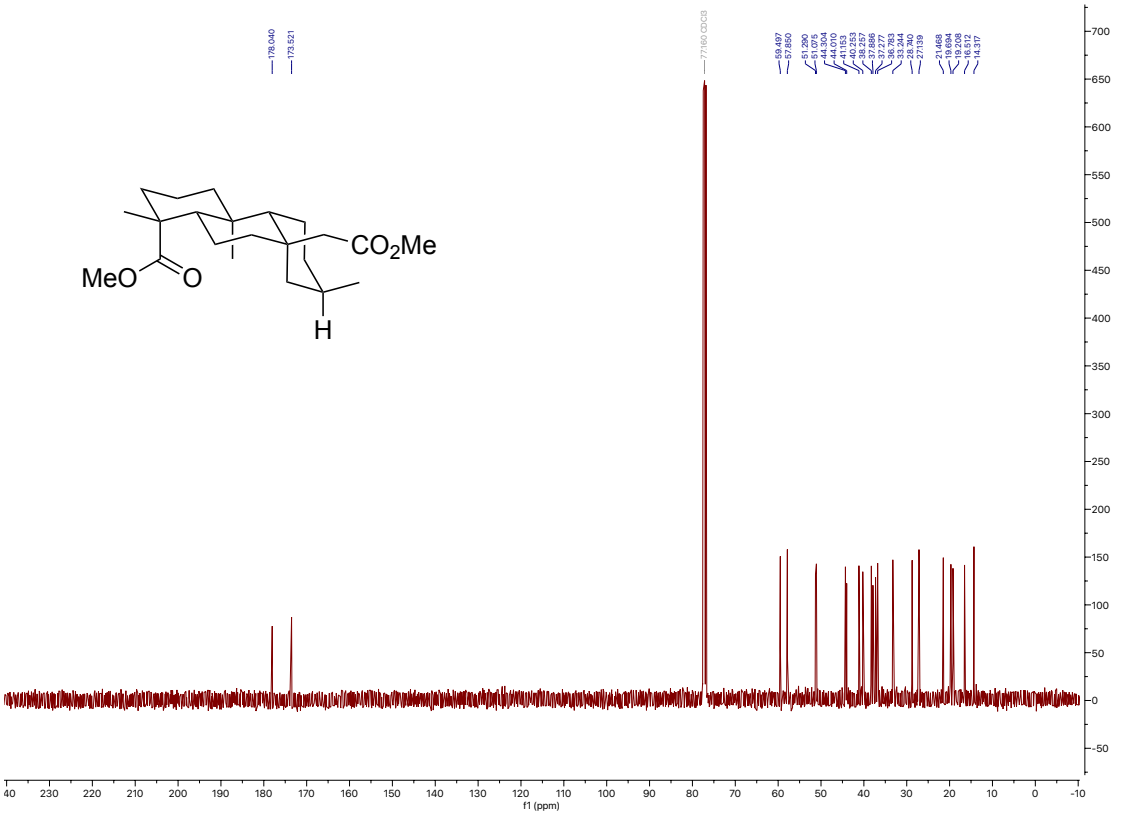
^{1}H NMR (500 MHz, $CDCl_3$) and **^{13}C NMR** (126 MHz, $CDCl_3$) of Compound **13b'**



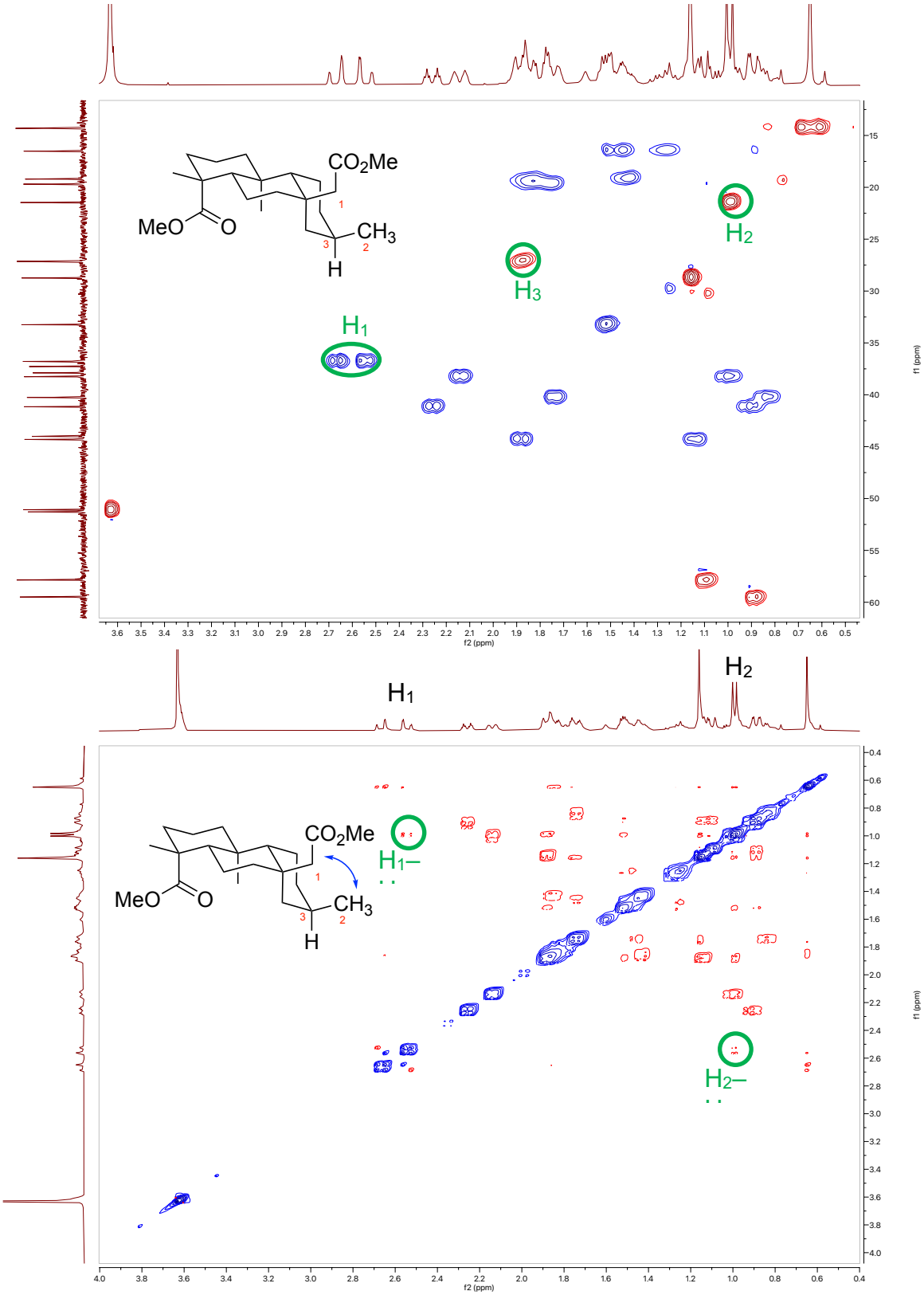


^{1}H NMR (400 MHz, $CDCl_3$) and **^{13}C NMR** (101 MHz, $CDCl_3$) of Compound **14a**

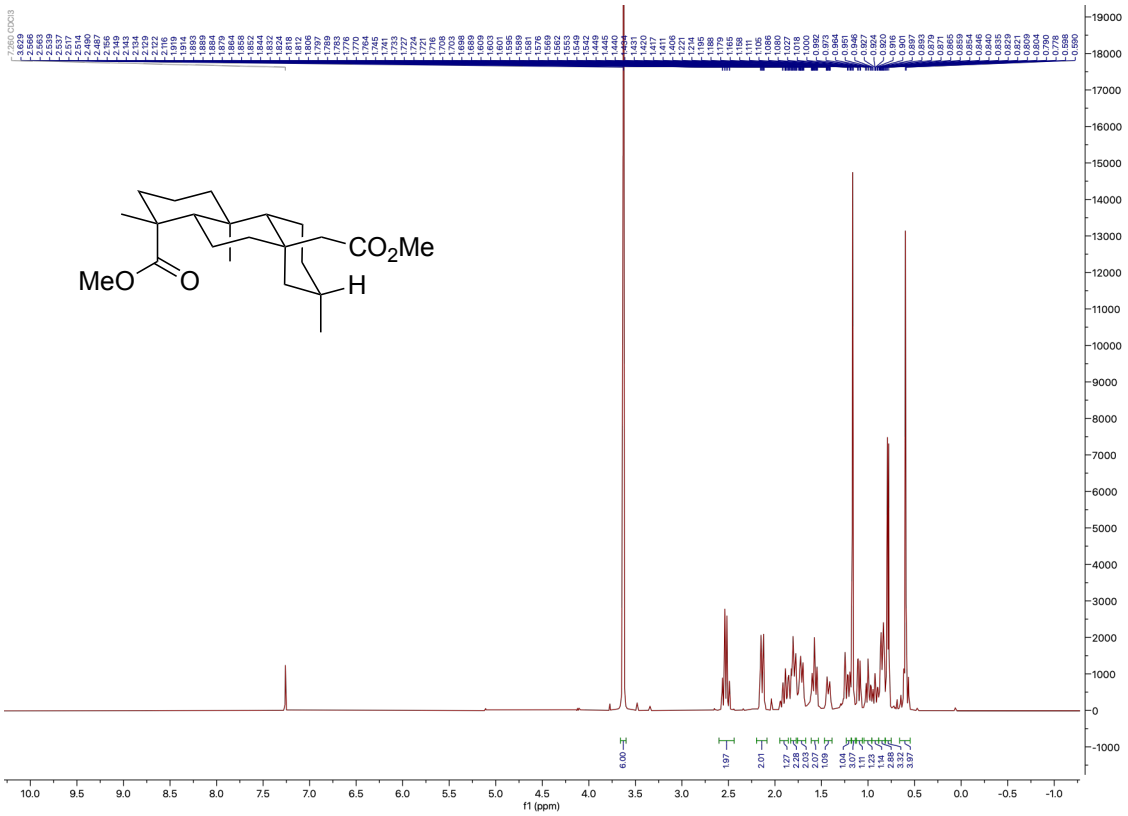


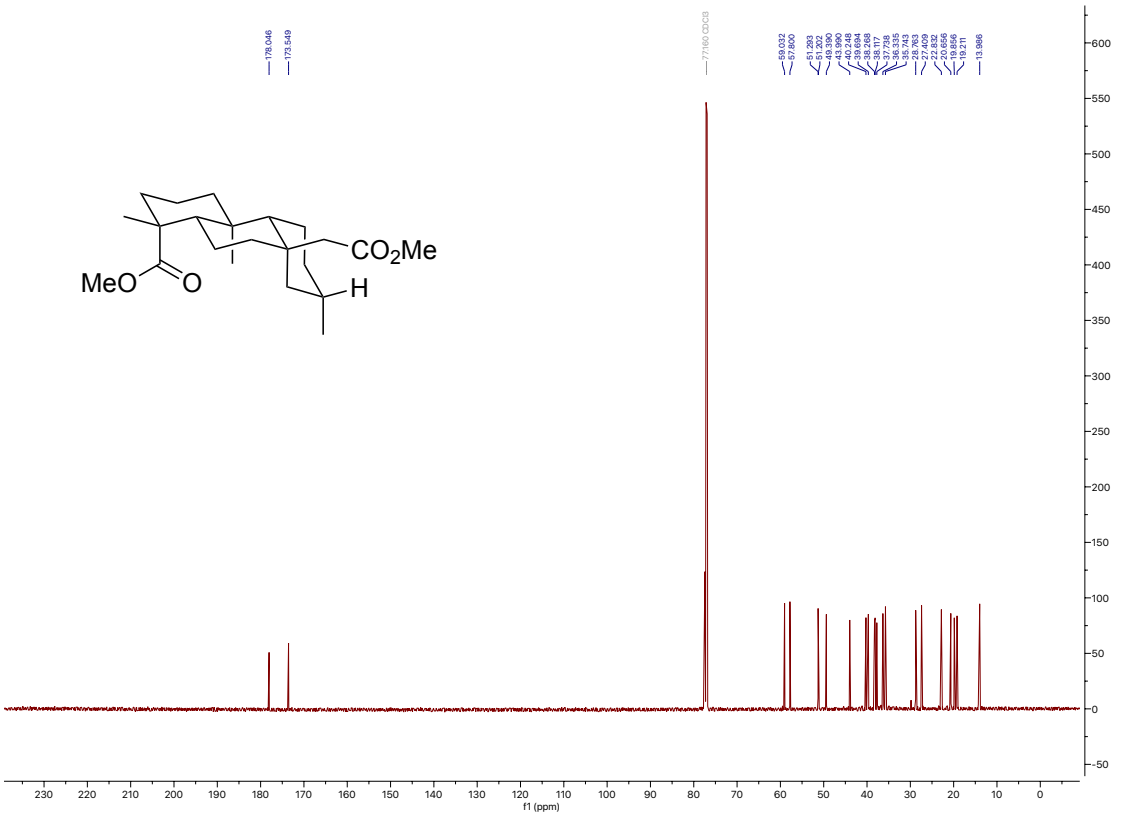


^{1}H NMR (300 MHz, $CDCl_3$) and **^{13}C NMR** (101 MHz, $CDCl_3$) of Compound **14b-1**

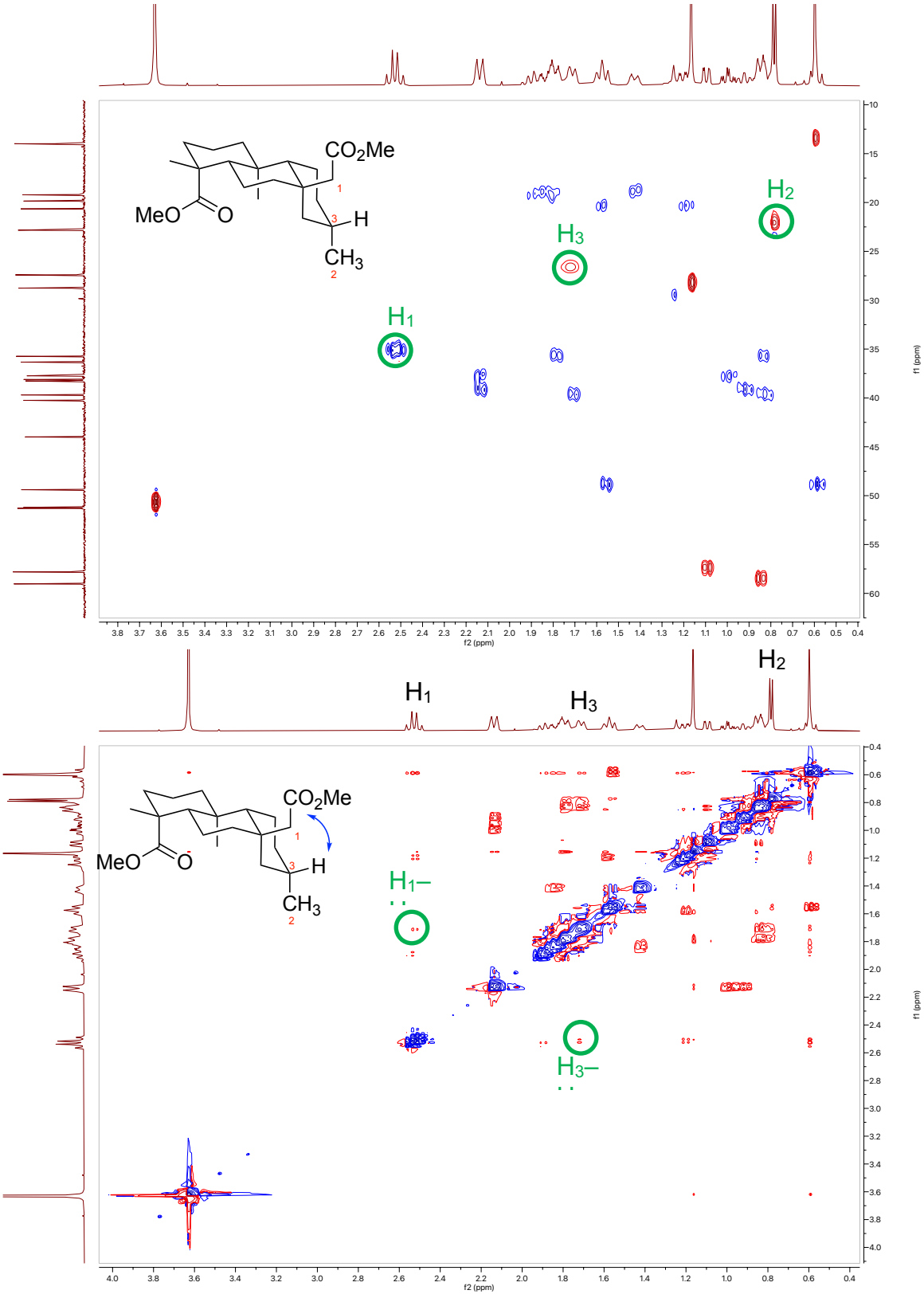


HSQC and **NOESY** of Compound **14b-1**

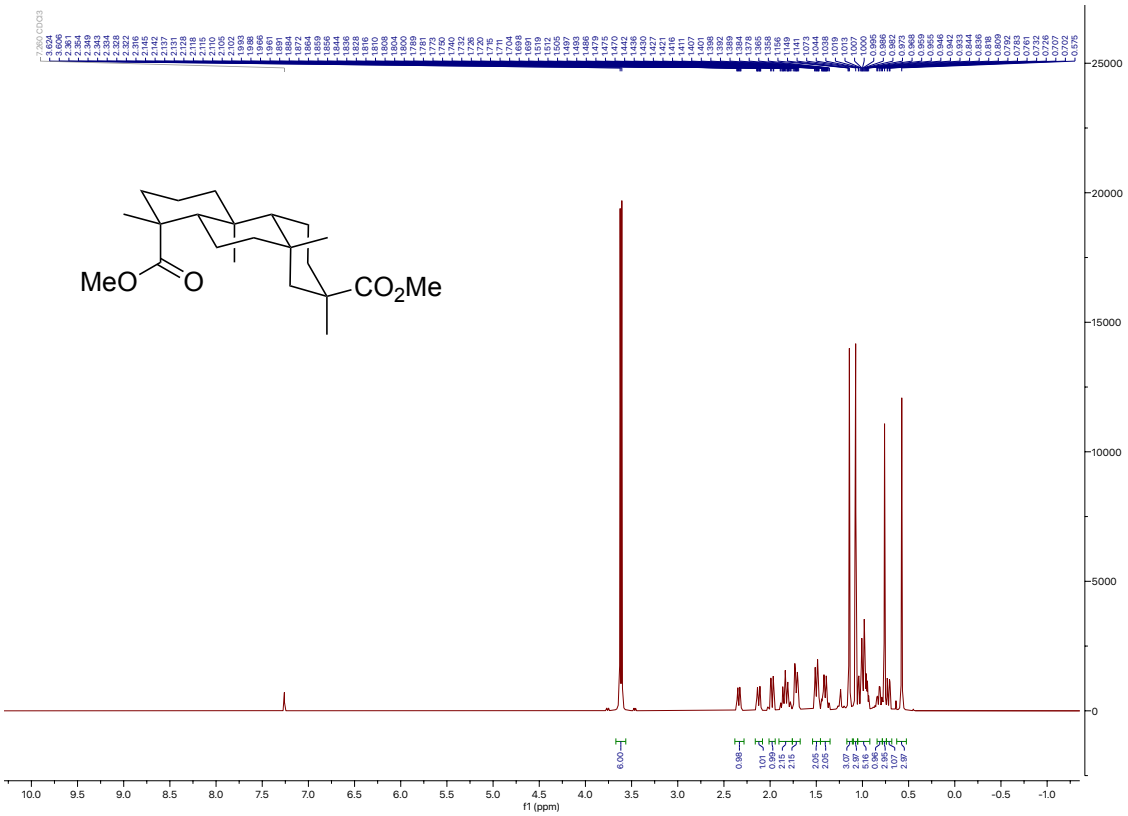


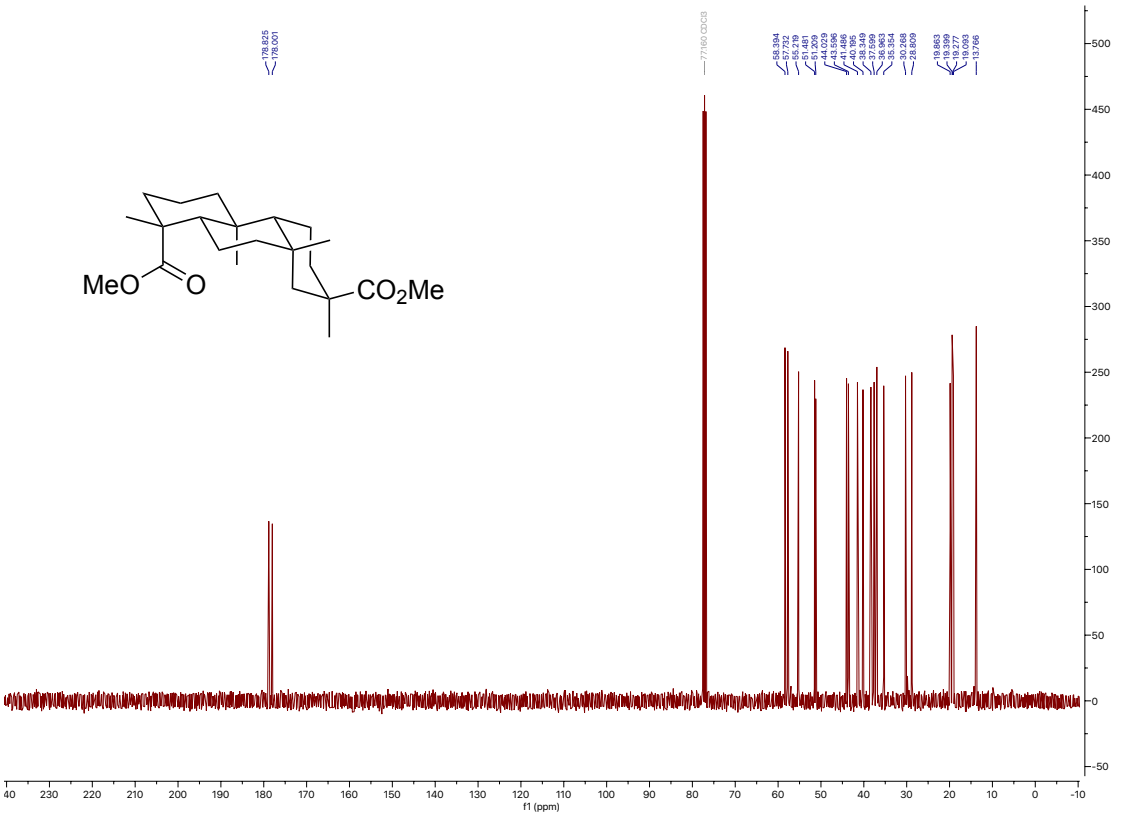


^{1}H NMR (500 MHz, $CDCl_3$) and **^{13}C NMR** (126 MHz, $CDCl_3$) of Compound **14b-2**

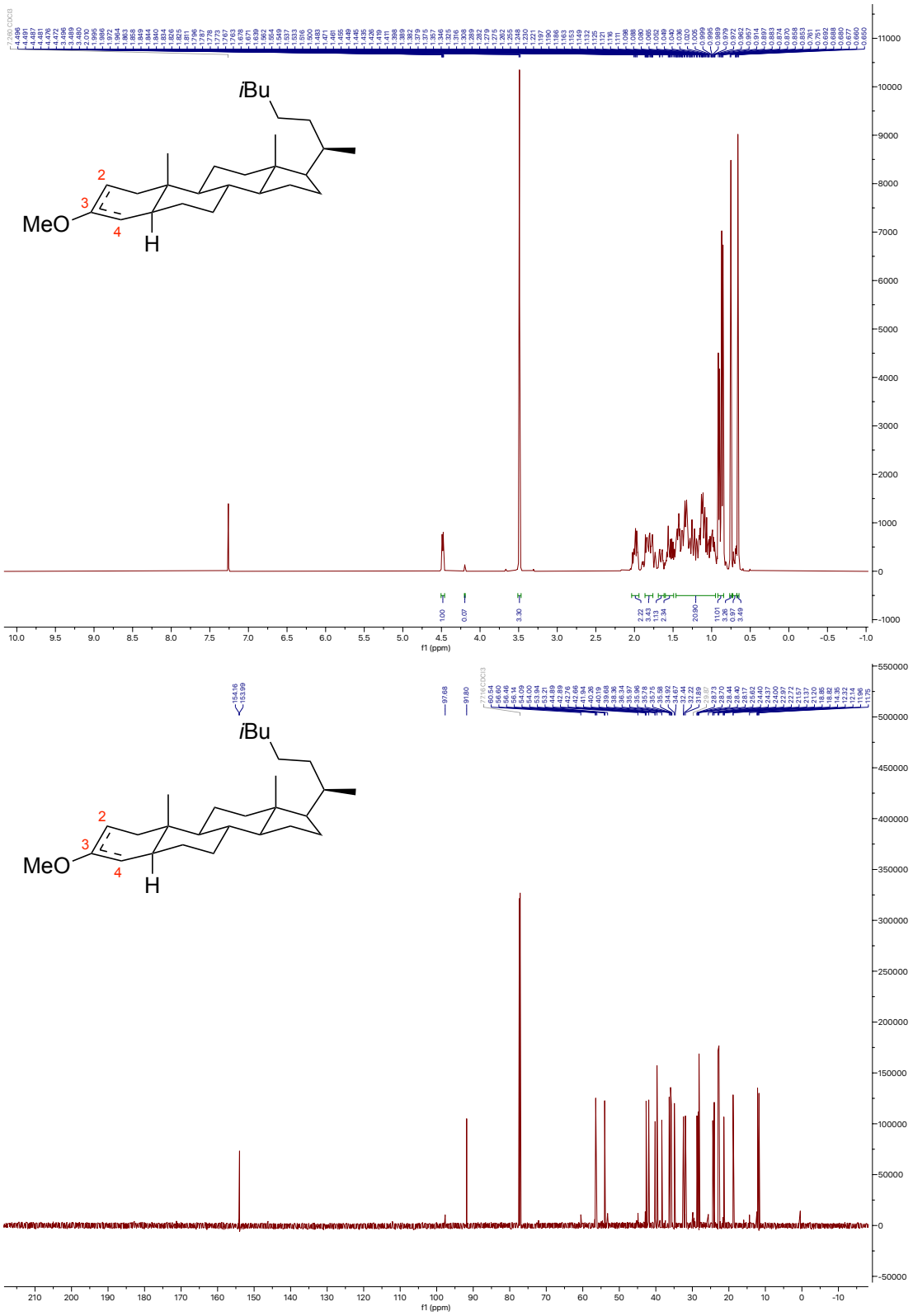


HSQC and **NOESY** of Compound **14b-2**

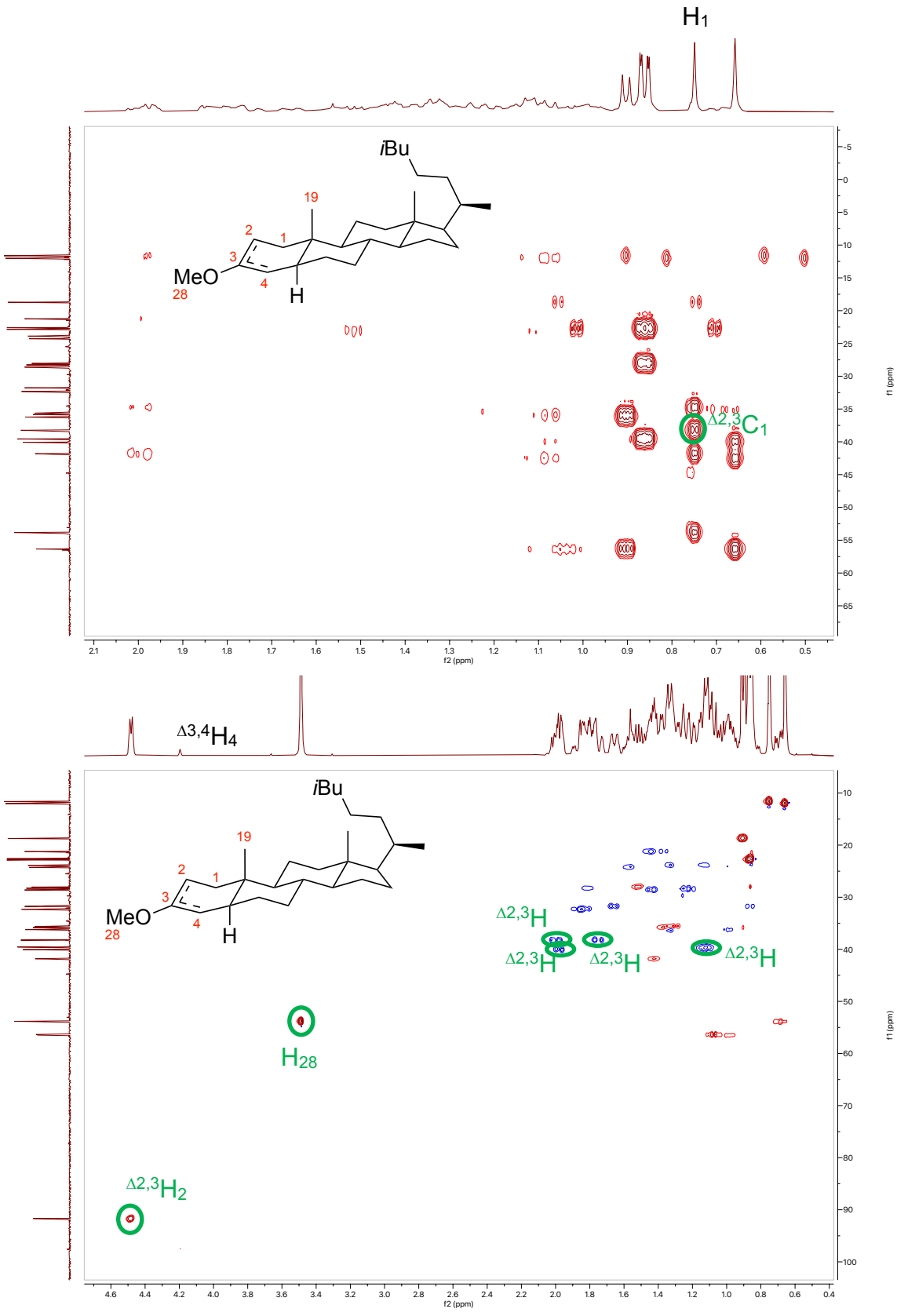




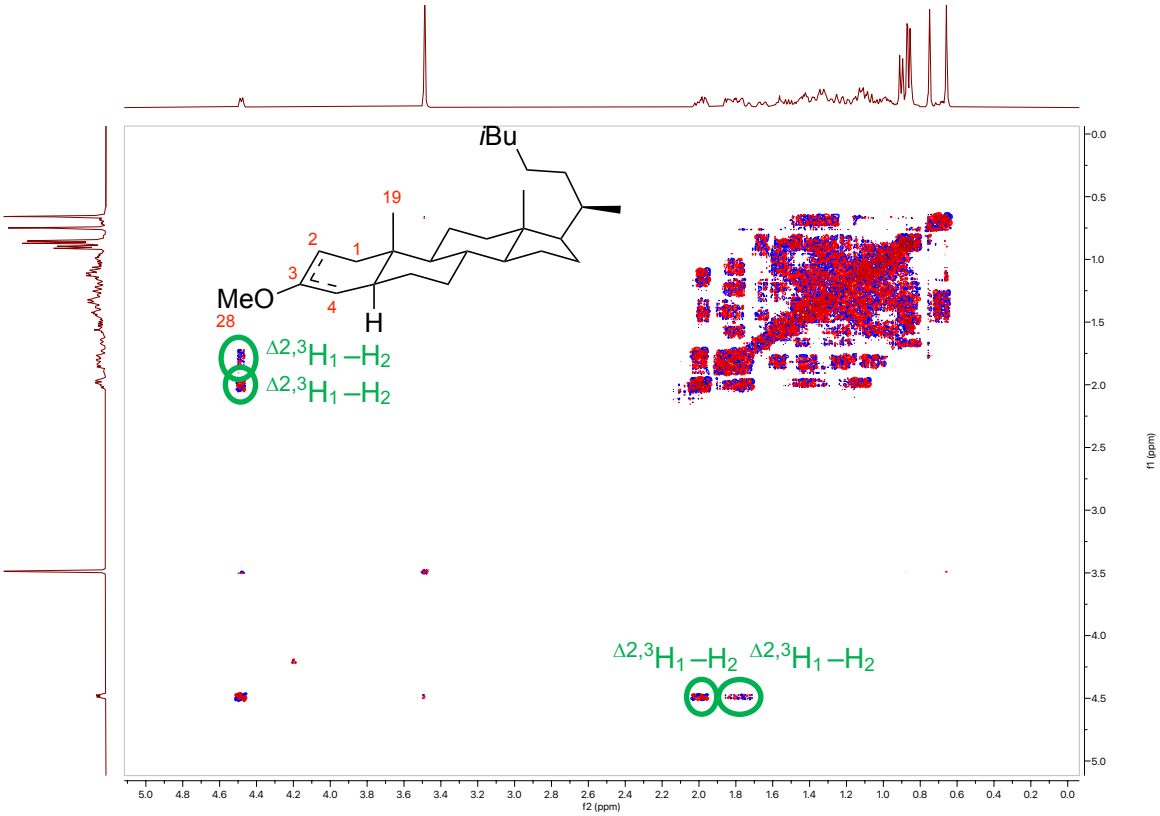
^{1}H NMR (500 MHz, $CDCl_3$) and **^{13}C NMR** (101 MHz, $CDCl_3$) of Compound **14b'**



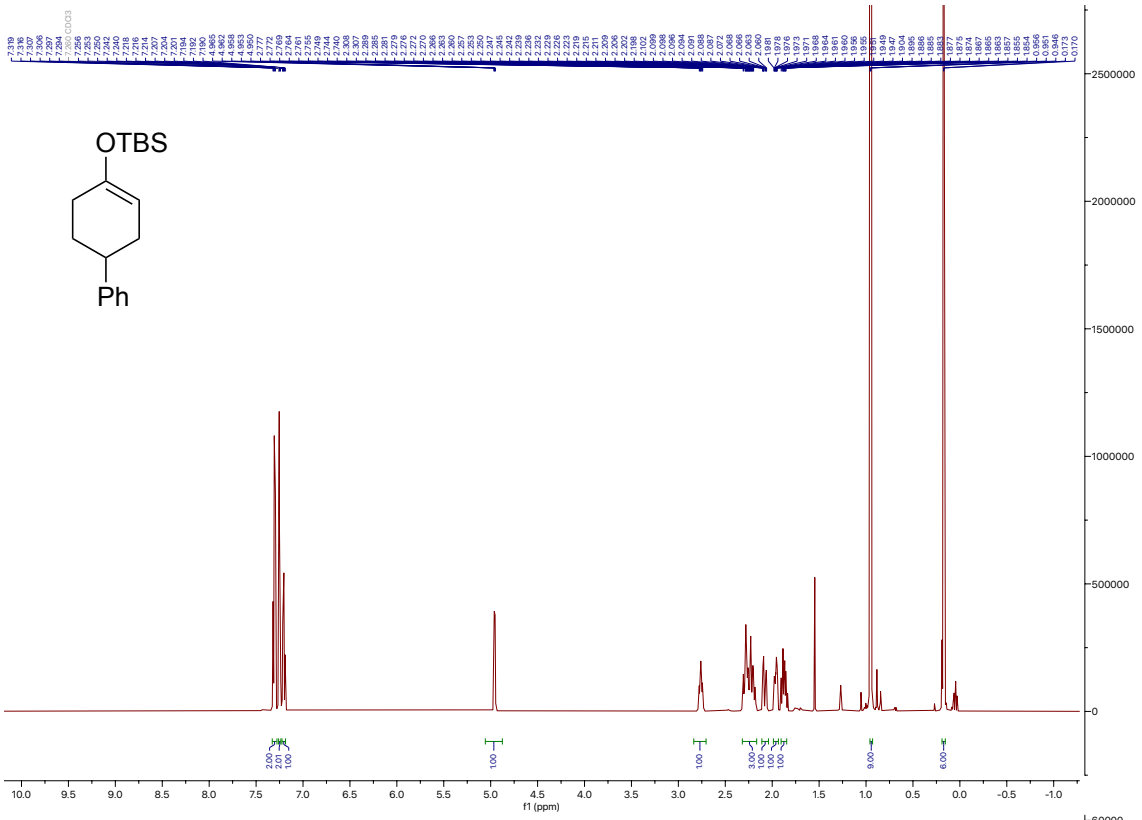
^{1}H NMR (400 MHz, $CDCl_3$) and **^{13}C NMR** (151 MHz, $CDCl_3$)
of Compound **15a** ($\Delta^{2,3}$:$\Delta^{3,4}$ = *93:7*)

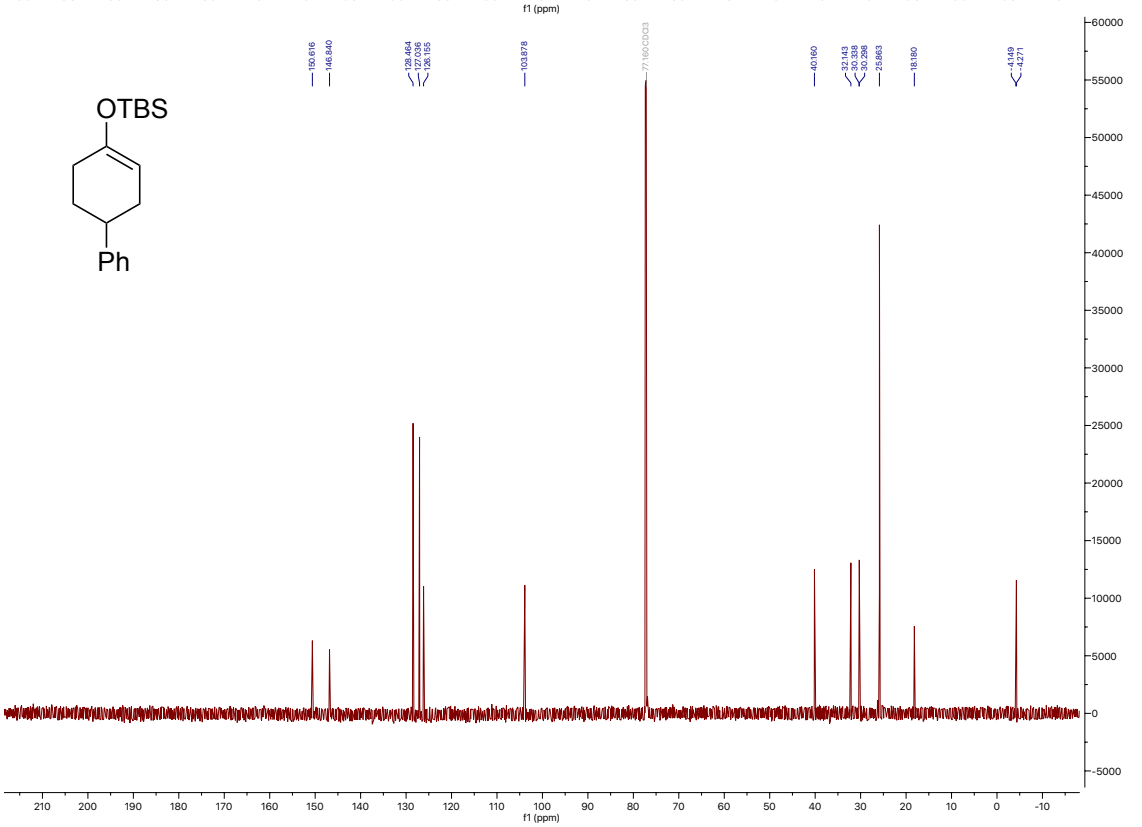


HMBC and **HSQC** of Compound **15a** ($\Delta^{2,3}$:$\Delta^{3,4}$ = *93:7*)



COSY of Compound **15a** ($\Delta^{2,3}$:$\Delta^{3,4}$ = *93:7*)





^{1}H NMR (600 MHz, $CDCl_3$) and **^{13}C NMR** (151 MHz, $CDCl_3$) of Compound **16a**

5.9 References

[1] Crespi, S.; Fagnoni, M. Generation of Alkyl Radicals: From the Tyranny of Tin to the Photon Democracy. *Chem. Rev.* **2020**, *120*, 9790–9833.

[2] Ji, C.-L.; Lu, Y.-N.; Xia, S.; Zhu, C.; Zhu, C.; Li, W.; Xie, J. Photoinduced Late-Stage Radical Decarboxylative and Deoxygenative Coupling of Complex Carboxylic Acids and Their Derivatives. *Angew. Chem., Int. Ed.* **2025**, *64*, No. e202423113.

[3] (a) McCombie, S. W.; Motherwell, W. B.; Tozer, M. J. Chapter 2: The Barton-McCombie Reaction. *Organic Reactions*; John Wiley & Sons: 2012; pp 161–591. (b) Pang, X.; Shu, X.-Z. Titanium: A Unique Metal for Radical Dehydroxylative Functionalization of Alcohols. *Synlett* **2021**, *32*, 1269–1274. (c) Mandal, T.; Mallick, S.; Islam, M.; De Sarkar, S. D. Alcohols as Alkyl Synthons Enabled by Photoredox-Catalyzed Deoxygenative Activation. *ACS Catal.* **2024**, *14*, 13451–13496.

[4] (a) Rössler, S. L.; Jelier, B. J.; Magnier, E.; Dagousset, G.; Carreira, E. M.; Togni, A. Pyridinium Salts as Redox-Active Functional Group Transfer Reagents. *Angew. Chem., Int. Ed.* **2020**, *59*, 9264–9280. (b) Berger, K. J.; Levin, M. D. Reframing Primary Alkyl Amines as Aliphatic Building Blocks. *Org. Biomol. Chem.* **2021**, *19*, 11–36.

[5] (a) Yan, M.; Lo, J. C.; Edwards, J. T.; Baran, P. S. Radicals: Reactive Intermediates with Translational Potential. *J. Am. Chem. Soc.* **2016**, *138*, 12692–12714. (b) Smith, J. M.; Harwood, S. J.; Baran, P. S. Radical Retrosynthesis. *Acc. Chem. Res.* **2018**, *51*, 1807–1817. (c) Wiles, R. J.; Molander, G. A. Photoredox-Mediated Net-Neutral Radical/Polar Crossover Reactions. *Isr. J. Chem.* **2020**, *60*, 281–293.

[6] (a) Smaligo, A. J.; Vardhineedi, S.; Kwon, O. Carvone-Derived *P*-Stereogenic Phosphines: Design, Synthesis, and Use in Allene-Imine [3+2] Annulation. *ACS Catal.*

2018, *8*, 5188–5192. (b) Smaligo, A. J.; Swain, M.; Quintana, J. C.; Tan, M. F.; Kim, D. A.; Kwon, O. Hydrodealkenylative C(sp^3)–C(sp^2) Bond Fragmentation. *Science* **2019**, *364*, 681–685. (c) Smaligo, A. J.; Kwon, O. Dealkenylative Thiylation of C(sp^3)–C(sp^2) Bonds. *Org. Lett.* **2019**, *21*, 8592–8597. (d) Smaligo, A. J.; Wu, J.; Burton, N. R.; Hacker, A. S.; Shaikh, A. C.; Quintana, J. C.; Wang, R.; Xie, C.; Kwon, O. Oxodealkenylative Cleavage of Alkene C(sp^3)–C(sp^2) Bonds: A Practical Method for Introducing Carbonyls into Chiral Pool Materials. *Angew. Chem., Int. Ed.* **2020**, *59*, 1211–1215. (e) Swain, M.; Sadykhov, G.; Wang, R.; Kwon, O. Dealkenylative Alkenylation: Formal σ-Bond Metathesis of Olefins. *Angew. Chem., Int. Ed.* **2020**, *59*, 17565–17571. (f) Swain, M.; Bunnell, T. B.; Kim, J.; Kwon, O. Dealkenylative Alkynylation Using Catalytic Fe^{II} and Vitamin C. *J. Am. Chem. Soc.* **2022**, *144*, 14828–14837. (g) He, Z.; Moreno, J. A.; Swain, M.; Wu, J.; Kwon, O. Aminodealkenylation: Ozonolysis and Copper Catalysis Convert C(sp^3)–C(sp^2) Bonds to C(sp^3)–N Bonds. *Science* **2023**, *381*, 877–886. (h) Dehnert, B. W.; Yin, Y.; Kwon, O. Halodealkenylation: Ozonolysis and Catalytic Fe^{II} with Vitamin C Convert C(sp^3)–C(sp^2) Bonds to C(sp^3)–Halide Bonds. *Org. Lett.* **2024**, *26*, 10921–10927. (i) Dworkin, J. H.; Chen, Z. M.; Cheasty, K. C.; Rubio, A. V.; Kwon, O. Hydrodealkenylative C(sp^3)–C(sp^2) Bond Fragmentation Using Isayama–Mukaiyama Peroxidation. *J. Am. Chem. Soc.* **2025**, *147*, 13531–13544. (j) Dehnert, B. W.; Dworkin, J. H.; Kwon, O. Dealkenylative Functionalizations: Conversion of Alkene C(sp^3)–C(sp^2) Bonds into C(sp^3)–X Bonds via Redox-Based Radical Processes. *Synthesis* **2024**, *56*, 71–86.

[7] Ertl, P.; Schuhmann, T. A Systematic Cheminformatics Analysis of Functional Groups Occurring in Natural Products. *J. Nat. Prod.* **2019**, *82*, 1258–1263.

[8] Fliszár, S.; Granger, M. A. Quantitative Investigation of the Ozonolysis Reaction. XI. On the Effects of Substituents in Directing the Ozone Cleavage of *trans*-1,2-Disubstituted Ethylenes. *J. Am. Chem. Soc.* **1970**, *92*, 3361–3369.

[9] (a) Bailey, P. S.; Keller, J. E.; Mitchard, D. A.; White, H. M. Ozonation of Amines. Oxidation of Organic Compounds. *Adv. Chem.* **1968**, *77*, 58–64. (b) Muñoz, F.; von Sonntag, C. The Reactions of Ozone with Tertiary Amines Including the Complexing Agents Nitrilotriacetic Acid (NTA) and Ethylenediaminetetraacetic Acid (EDTA) in Aqueous Solution. *J. Chem. Soc., Perkin Trans. 2* **2000**, 2029–2033. (c) Lim, S.; McArdell, C. S.; von Gunten, U. Reactions of Aliphatic Amines with Ozone: Kinetics and Mechanisms. *Water Res.* **2019**, *157*, 514–528. (d) Skrotzki, E. A.; Vandavasi, J. K.; Newman, S. G. Ozone-Mediated Amine Oxidation and Beyond: A Solvent-Free Flow-Chemistry Approach. *J. Org. Chem.* **2021**, *86*, 14169–14176.

[10] (a) Young, W. G.; McKinnis, A. C.; Webb, I. D.; Roberts, J. D. Allylic Rearrangements. XIX. Studies of the Ozonization of Allylic Systems. *J. Am. Chem. Soc.* **1946**, *68*, 293–296. (b) Mosettig, E.; Beglinger, U.; Dolder, F.; Lichti, H.; Quitt, P.; Waters, J. A. The Absolute Configuration of Steviol and Isosteviol. *J. Am. Chem. Soc.* **1963**, *85*, 2305–2309. (c) Bailey, P. S. Chapter IX. Anomalous Ozonolysis of Olefins. In *Ozonation in Organic Chemistry*, Vol. 1, Olefinic Compounds; Academic Press: 1978; pp 147–184. (d) Fisher, T. J.; Dussault, P. H. Alkene Ozonolysis. *Tetrahedron* **2017**, *73*, 4233–4258.

[11] (a) Brus, G.; Peyresblanques, G. Sur la Fixation de l'ozone par les Liasons Benzeniques et les Liaisons Acetyléniques. *C. R. Hebd. Seances Acad. Sci.* **1930**, *190*, 685–686. (b) Hoigné, J.; Bader, H. Rate Constants of Reactions of Ozone with Organic and Inorganic Compounds in Water—I. Non-Dissociating Organic Compounds. *Water*

Res. **1983**, *17*, 173–183. (c) Gurol, M. D.; Nekouinaini, S. Kinetic Behavior of Ozone in Aqueous Solutions of Substituted Phenols. *Ind. Eng. Chem. Fundamen.* **1984**, *23*, 54–60. (d) O'Neill, E. M.; Kawam, A. Z.; Van Ry, D. A.; Hinrichs, R. Z. Ozonolysis of Surface-Adsorbed Methoxyphenols: Kinetics of Aromatic Ring Cleavage vs. Alkene Side-Chain Oxidation. *Atmos. Chem. Phys.* **2014**, *14*, 47–60. (e) Tekle-Röttering, A.; von Sonntag, C.; Reisz, E.; vom Eyster, C.; Lutze, H. V.; Türk, J.; Naumov, S.; Schmidt, W.; Schmidt, T. C. Ozonation of anilines: Kinetics, Stoichiometry, Product Identification and Elucidation of Pathways. *Water Res.* **2016**, *98*, 147–159. (f) Bhosale, G. S.; Vaidya, P. D.; Joshi, J. B.; Patil, R. N. Kinetics of Ozonation of Phenol and Substituted Phenols. *Ind. Eng. Chem. Res.* **2019**, *58*, 7461–7466. (g) Zoumpouli, G. A.; Zhang, Z.; Wenk, J.; Prasse, C. Aqueous Ozonation of Furans: Kinetics and Transformation Mechanisms Leading to the Formation of α,β-Unsaturated Dicarbonyl Compounds. *Water Res.* **2021**, *203*, 117487. (h) Bhosale, G. S.; Vaidya, P. D.; Gogate, P. R.; Joshi, J. B.; Patil, R. N. Ozonation of Phenol and Substituted Phenols: Dependency of the Reaction Rate Constant on the Molecular Structure. *Can. J. Chem. Eng.* **2022**, *100*, 317–324.

[12] (a) Williamson, D. G.; Cvetanovic, R. J. Rates of Ozone-Olefin Reactions in Carbon Tetrachloride Solutions. *J. Am. Chem. Soc.* **1968**, *90*, 3668–3672. (b) Pryor, W. A.; Giamalva, D.; Church, D. F. Kinetics of Ozonation. 3. Substituent Effects on the Rates of Reaction of Alkenes. *J. Am. Chem. Soc.* **1985**, *107*, 2793–2797. (c) Komissarov, V. D.; Shafikov, N. Ya.; Zimin, Yu. S. Kinetics of the Reactions of Ozone with Substituted Ethylenes. *Kinet. Catal.* **2004**, *45*, 483–487. (d) Arriaga, D. K.; Kang, S.; Thomas, A. A. Effect of Solvent on the Rate of Ozonolysis: Development of a Homogeneous Flow Ozonolysis Protocol. *J. Org. Chem.* **2023**, *88*, 13720–13726.

[13] (a) Vitaku, E.; Smith, D. T.; Njardarson, J. T. Analysis of the Structural Diversity, Substitution Patterns, and Frequency of Nitrogen Heterocycles Among U.S. FDA Approved Pharmaceuticals. *J. Med. Chem.* **2014**, *57*, 10257–10274. (b) Peplow, M. "Almost Magical": Chemists Can Now Move Single Atoms In and Out of a Molecule's Core. *Nature* **2023**, *618*, 21–24. (c) Masand, V. H.; Al-Hussain, S.; Alzahrani, A. Y.; El-Sayed, N. N. E.; Yeo, C. I.; Tan, Y. S.; Zaki, M. E. A. Leveraging Nitrogen Occurrence in Approved Drugs to Identify Structural Patterns. *Expert Opin. Drug Discovery* **2024**, *19*, 111–124.

[14] The rate of ozonolysis of ethylamine in water at pH 7 and room temperature is 2.1×10 $M^{-1}s^{-1}$; see ref 9d.

[15] Kokatla, H. P.; Thomson, P. F.; Bae, S.; Doddi, V. R.; Lakshman, M. K. Reduction of Amine N-Oxides by Diboron Reagents. *J. Org. Chem.* **2011**, *76*, 7842–7848.

[16] Hoigné, J.; Bader, H. Rate Constants of Reactions of Ozone with Organic and Inorganic Compounds in Water—II: Dissociating Organic Compounds. *Water Res.* **1983**, *17*, 185–192.

[17] Gross, B. M.; Stoltz, B. M. Concise Syntheses of Lycojapomine Alkaloids Enabled by Radical Dearomatization of a Pyrrole. *J. Am. Chem. Soc.* **2025**, *147*, 20200–20204.

[18] Uredi, D.; Motati, D. R.; Watkins, E. B. A Simple Tandem Approach to the Construction of Pyridine Derivatives Under Metal-Free Conditions: A One-Step Synthesis of the Monoterpene Natural Product, (–)-Actinidine. *Chem. Commun.* **2019**, *55*, 3270–3273.

[19] The values of pK_a originate from the D. H. Ripin and D. A. Evans pK_a table at https://organicchemistrydata.org/hansreich/resources/pka/pka_data/evans_pKa_table.pdf.

[20] Munchhof, M. J.; Meyers, A. I. A Novel Asymmetric Route to Chiral, Nonracemic *cis*-2,6-Disubstituted Piperidines. Synthesis of (+)-Pinidinone and (+)-Monomorine. *J. Am. Chem. Soc.* **1995**, *117*, 5399–5400.

[21] Larson, R. T.; Clift, M. D.; Thomson, R. J. Total Synthesis of the Galbulimima Alkaloid (–)-GB17. *Angew. Chem., Int. Ed.* **2012**, *51*, 2481–2484.

[22] Jiang, J.; DeVita, R. J.; Goulet, M. T.; Wyvratt, M. J.; Lo, J.-L.; Ren, N.; Yudkovitz, J. B.; Cui, J.; Yang, Y. T.; Cheng, K.; Rohrer, S. P. Synthesis and Structure-Activity Relationship Studies of Piperidine-Substituted Quinolones as Nonpeptide Gonadotropin Releasing Hormone Antagonists. *Bioorg. Med. Chem. Lett.* **2004**, *14*, 1795–1798.

[23] (a) Lumbroso, A.; Cooke, M. L.; Breit, B. Catalytic Asymmetric Synthesis of Allylic Alcohols and Derivatives and their Applications in Organic Synthesis. *Angew. Chem., Int. Ed.* **2013**, *52*, 1890–1932. (b) Zhang, J.; Liao, J.; Wei, Y.-F.; Cheng, G.; Luo, R. Recent Advance of Allylic Alcohol Reagents in Organic Synthesis. *Mini-Rev. Org. Chem.* **2018**, *15*, 476–478. (c) Alonso, D. A.; Maciá, B.; Pastor, I. M.; Baeza, A. Recent Advances on the Catalytic Asymmetric Allylic α-Alkylation of Carbonyl Derivatives Using Free Allylic Alcohols. *ACS Org. Inorg. Au* **2024**, *4*, 269–286. (d) Bera, S.; Kabadwal, L. M.; Banerjee, D. Harnessing Alcohols as Sustainable Reagents for Late-Stage Functionalisation: Synthesis of Drugs and Bio-Inspired Compounds. *Chem. Soc. Rev.* **2024**, *53*, 4607–4647.

[24] Lovering, F.; Bikker, J.; Humblet, C. Escape from Flatland: Increasing Saturation as an Approach to Improving Clinical Success. *J. Med. Chem.* **2009**, *52*, 6752–6756.

[25] Churcher, I.; Newbold, S.; Murray, C. W. Return to Flatland. *Nat. Rev. Chem.* **2025**, *9*, 140–141.

[26] Bailey, P. S. Chapter III. Ozonation of Aromatic Compounds: Benzene and Substituted Benzenes. *Ozonation in Organic Chemistry* **1982**, *2*, 18–42.

[27] (a) Briner, E.; Patry, R.; de Luserna, E. Recherches sur l'Oxydation au Moyen de l'Ozone I. Etude de la Préparation de la Vanilline. *Helv. Chim. Acta* **1924**, *7*, 62–74. (b) Birdsall, C. M.; Jenkins, A. C.; Spadinger, E. Iodometric Determination of Ozone. *Anal. Chem.* **1952**, *24*, 662–664.

[28] (a) Gordon, G.; Rakness, K.; Vornehm, D.; Wood, D. Limitations of the Iodometric Determination of Ozone. *Journal AWWA* **1989**, *81*, 72–76. (b) Tjahjanto, R. T.; R, D. H.; Wardani, S. Ozone Determination: A Comparison of Quantitative Analysis Methods. *J. Pure Appl. Chem. Res.* **2012**, *1*, 18–25. (c) Chasanah, U.; Yulianto, E.; Zain, A. Z.; Sasmita, E.; Restiwijaya, M.; Kinandana, A. W.; Arianto, F.; Nur, M. Evaluation of Titration Method on Determination of Ozone Concentration Produced by Dielectric Barrier Discharge Plasma (DBDP) Technology. *J. Phys.: Conf. Ser.* **2019**, *1153*, 012086.

[29] Bailey, P. S.; Chapter IX. Ozone Attack at sp^3 Carbon Centers: Ozonation of Carbon-Hydrogen Bonds. *Ozonation in Organic Chemistry*, Vol. 2: Nonolefinic Compounds; Academic Press: 1982; pp 255–328.

[30] Dworkin, J. H.; Chen, Z. M.; Cheasty, K. C.; Rubio, A. V.; Kwon, O. Hydrodealkenylative C(sp3)–C(sp2) Bond Fragmentation Using Isayama–Mukaiyama Peroxidation. *J. Am. Chem. Soc.* **2025**, *147* (23), 13531–13544.

[31] (a) Ogawa, T.; Nozaki, M.; Matsui, M. Total Synthesis of Stevioside. *Tetrahedron* **1980**, *36* (19), 2641–2648.

(b) Khaibullin, R. N.; Strobykina, I. Y.; Kataev, V. E.; Lodochnikova, O. A.; Gubaidullin, A. T.; Musin, R. Z. New Synthesis of Diterpenoid (16S)-Dihydrosteviol. *Russ. J. Gen. Chem.* **2009**, *79* (5), 967–971.

[32] Ukiya, M.; Sawada, S.; Kikuchi, T.; Kushi, Y.; Fukatsu, M; Akihisa, T. Cytotoxic and Apoptosis-Inducing Activities of Steviol and Isosteviol Derivatives Against Human Cancer Cell Lines. *Chem. Biodiversity* **2013**, *10* (2), 177–188.

[33] Sai Prakash Chaturvedula, V.; Kinger, K. P.; Campbell, M.; Prakash, I. NMR Spectral Assignments of Steviol and Steviol Monoacetate. *J. Chem. Pharm. Res.* **2012**, *4* (5), 2666–2670.

[34] Uredi, D.; Reddy Motati, D.; Blake Watkins, E. A Simple Tandem Approach to the Construction of Pyridine Derivatives Under Metal-free Conditions: A One-Step Synthesis of Monoterpene Natural Product (–)-Actinidine. *Chem. Commun.* **2019**, *55* (22), 3270–3273.

[35] Wilkinson, S. M.; Price, J.; Kassiou, M. Improved Accessibility to the Desoxy Analogues of Δ9-Tetrahydrocannabinol and Cannabidiol. *Tetrahedron Lett.* **2013**, *54* (1), 52–54.

[36] Spanka, G.; Rademacher, P. Transannular Interactions in Difunctional Medium Rings. 1. n/π Interactions in Cyclic Amino Ketones and Aminoalkenes Studied by Photoelectron Spectroscopy. *J. Org. Chem.* **1986**, *51* (5), 592–596.

[37] Wu, M.-J.; Wu, D.-M.; Chen, J.-B.; Zhao, J.-F.; Gong, L.; Gong, Y.-X.; Li, Y.; Yang, X.-D.; Zhang, H. Synthesis and Anti-Proliferatice Activity of Allogibberic Acid Derivatives Containing 1,2,3-Triazole Pharmacophore. *Bioorg. Med. Chem. Lett.* **2018**, *28* (14), 2543–2549.

[38] Padala, A. K.; Saikam, S.; Ali, A.; Naveed Ahmed, Z. Efficient and Practical Approach to Esters from Acids, 2-Oxoacids, 2-Oxoaldehydes & 2-Oxoesters. *Tetrahedron* **2015**, *71* (49), 9388–9395.

[39] Hamada, M.; Higashi, T.; Shoji, M.; Umezawa, K.; Sugai, T. Lipase-Catalyzed Enantio- and Regioselective Transformation of 3-epi-Shikimic Acid Derivatives as the Key Step for the Entry of Polyoxygenated Carbacycles. *J. Mol. Catal. B: Enzym.* **2010**, *67* (1–2), 78–84.

[40] Ott, A. A.; Goshey, C. S.; Topczewski, J. J. Dynamic Kinetic Resolution of Allylic Azides via Asymmetric Dihydroxylation. *J. Am. Chem. Soc.* **2017**, *139* (23), 7737–7740.

[41] Pettersson, L. Steroids for Cancer Treatment. WO 2005/077968 A2, August 25, 2005.

[42] Li, H.; Wang, K.; Wan, Q.; Chen, Y. Design, Synthesis and Anti-Tumor Evaluation of Novel Steroidal Gylcoconjugate with Furoxan Derivatives. *Steroids* **2019**, *141*, 81–95.

[43] Green, S. A.; Huffman, T. R.; McCourt, R. O.; van der Puyl, V.; Shenvi, R. A. Hydroalkylation of Olefins to Form Quatenary Carbons. *J. Am. Chem. Soc.* **2019**, *141* (20), 7709–7714.

[44] Álvarez-Calero, J. M.; Jorge, Z. D.; Massanet, G. M. TiCl4/Et3N-Mediated Condensation of Acetate and Formate Esters: Direct Access to β-Alkoxy- and β-Aryloxyacrylates. *Org. Lett.* **2016**, *18* (24), 6344–6347.

[45] Yang, C.; Shi, L.; Wang, F.; Su, Y.; Xia, J.-B.; Li, F. Rhodium-Catalyzed Asymmetric (3 + 2 + 2) Annulation via N–H/C–H Dual Activation and Internal Alkyne Insertion Toward N-Fused 5/7 Bicycles. *ACS Catal.* **2022**, *12* (22), 14194–14208.

[46] Waller, D. L.; Stephenson, C. R. J.; Wipf, P. Spiroketals via Oxidative Rearrangement of Enol Ethers. *Org. Biomol. Chem.* **2007**, *5* (1), 58–60.

[47] Sobukawa, M.; Koga, K. Determination of the Protons Eliminated in the Regioselective Deprotonation of Some Optically Active 3-Keto Steroids by a Chiral Lithium Amide. *Tetrahedron Lett.* **1993**, *34* (32), 5101–5104.

[48] (a) Briner, E.; Patry, R.; de Luserna, E. Recherches sur l'Oxydation au Moyen de l'Ozone I. Etude de la Préparation de la Vanilline. *Helv. Chim. Acta* **1924**, *7* (1), 62–74.

(b) Birdsall, C. M.; Jenkins, A. C.; Spadinger, E. Iodometric Determination of Ozone. *Anal. Chem.* **1952**, *24* (4), 662–664.

(c) Gordon, G.; Rakness, K.; Vornehm, D.; Wood, D. Limitations of the Iodometric Determination of Ozone. *J. Am. Water Works Assoc.* **1989**, *81* (6), 72–76.

(d) Tjahjanto, R. T.; R., D. H.; Wardani, S. Ozone Determination: A Comparison of Quantitative Analysis Methods. *J. Pure App. Chem. Res.* **2012**, *1* (1), 18–25.

(e) Chasanah, U.; Yulianto, E.; Zain, A. Z.; Sasmita, E.; Restiwijaya, M.; Kinandana, A. W.; Arianto, F.; Nur, M. Evaluation of Titration Method on Determination of Ozone Concentration Produced by Dielectric Barrier Discharge Plasma (DBDP) Technology. *J. Phys.: Conf. Ser.* **2019**, *1153*, 012086.

[49] Smaligo, A. J.; Swain, M.; Quintana, J. C.; Tan, M. F.; Kim, D. A.; Kwon, O. Hydrodealkenylative C(sp^3)–C(sp^2) Bond Fragmentation. *Science* **2019**, *364* (6441), 681–685.

[50] Smaligo, A. J.; Wu, J.; Burton, N. R.; Hacker, A. S.; Shaikh, A. C.; Quintana, J. C.; Wang, R.; Xie, C.; Kwon, O. Oxodealkenylative Cleavage of Alkene C(sp3)–C(sp2)

Bonds: A Practical Method for Introducing Carbonyls into Chiral Pool Materials. *Angew. Chem. Int. Ed.* **2020**, *59* (3), 1211–1215.

[51] Franklin, N. C.; Feltkamp, H. Conformational Analysis of Cyclohexane Derivatives by Nuclear Magnetic Resonance Spectroscopy. *Angew. Chem. Int. Ed.* **1965**, *4* (9), 774–783.

[52] Hilf, J. A.; Holzwarth, M. S.; Rychnovsky, S. D. Route to Highly Substituted Pyridines. *J. Org. Chem.* **2016**, *81* (21), 10376–10382.

[53] Cheruvallath, Z.; Green J.; Johnson, B.; Jones, B.; Schleicher, K.; Sun, H.; Tang, M. N-Heteroarylalkyl-2-(heterocyclyl and heterocyclylmethyl) Acetamide Derivatives as SSTR4 Agonists. WO 2021/202781 A1, October 7, 2021.

[54] Munchhof, M. J.; Meyers, A. I. A Novel Asymmetric Route to Chiral, Nonracemic cis-2,6-Disubstituted Piperidines. Synthesis of (+)-Pinidinone and (+)-Monomorine. *J. Am. Chem. Soc.* **1995**, *117* (19), 5399–5400.

[55] De Smet, G.; Bai, X.; Mensch, C.; Sergeyev, S.; Evano, G.; Maes, B. U. W. Selective Nickel-Catalyzed Hydrodeacetoxylation of Aryl Acetates. *Angew. Chem. Int. Ed.* **2022**, *61* (27), e202201751.

[56] Weix, D. J.; Dreher, S. D.; Katz, T. J. [5]HELOL Phosphite: A Helically Grooved Sensor of Remote Chirality. *J. Am. Chem. Soc.* **2000**, *122* (41), 10027–10032.

CHAPTER SIX

An Ab Initio Machine Learned Model to Predict Molozonide retro-(3+2) Cycloaddition Selectivity for Dealkenylation

Unpublished results to be submitted in collaboration with the Xin Hong group as Dworkin, J. H.; Li, J.-Q.; Foker, E. A.; Dehnert, B. W.; Prout, E. S.; Silva, T. G.; Tuermer-Lee, J. X.; Leung, C. B.; Chen, Z. M.; Yu Liao, L. Wang, J. M. Hong, X.; Kwon, O. An *Ab Initio* Machine Learned Model to Predict Molozonide *Retro*-(3+2) Cycloaddition Selectivity for Dealkenylation. The dissertation author originated the idea for the project, was the primary researcher and co-first author of this manuscript.

6.1 Abstract

Despite its status as a foundational method for C–C bond oxidative cleavage, Criegee ozonolysis remains traditionally governed by the unpredictable regioselectivity of primary ozonide fragmentation. While this transformation is essential for generating critical reactive intermediates—such as the α-methoxyhydroperoxides used in modern dealkenylative radical cascades—the lack of control over the *retro*-(3+2)-cycloaddition of unsymmetrical alkenes can lead to complex mixtures and reduced synthetic efficiency. To transition this classical reaction from empirical trial-and-error to a predictive science, we developed a machine learning model that quantitatively forecasts the directionality of molozonide fragmentation. Validated against a dataset of 54 diverse substrates, this tool provides an *in silico* framework to predict the ratios of resulting carbonyl oxides and carbonyl fragments. By providing an algorithmic roadmap for C–C σ-bond severance, this approach enhances the precision of ozonolysis across its entire range of applications, from the synthesis of functionalized peroxides to the strategic remodeling of complex molecular architectures.

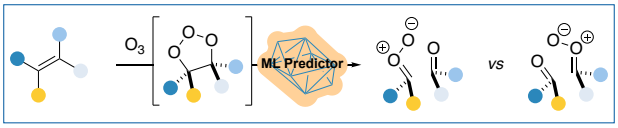


Figure 6.1 Abstract

6.2 Introduction

Since its discovery, the Criegee ozonolysis of alkenes has remained a cornerstone of organic synthesis, representing one of the most powerful and atom-economical methods for the oxidative cleavage of carbon-carbon double bonds. As a staple of both introductory pedagogy and complex natural product synthesis, the reaction's ability to disassemble olefins into carbonyl-based fragments is often perceived as a finalized chapter in the annals of chemical methodology. However, this familiarity belies a persistent and fundamental challenge: the lack of precise control over the fragmentation of the primary ozonide. Despite decades of mechanistic study, the *retro*-(3+2)-cycloaddition of unsymmetrical molozonides continues to be governed by empirical observations rather than rigorous predictive frameworks [*1*]. As modern synthetic design moves toward a new frontier defined by the strategic cleavage of C–C bonds to remodel molecular architectures, revisiting this classical transformation is not merely a matter of historical refinement, but a necessity for the advancement of precision synthesis [*2*].

Synthetic design has recently advanced toward a new frontier defined by the strategic cleavage of C–C bonds to remodel molecular architectures [2]. Within this context, dealkenylative synthesis has unlocked access to a broad chemical space, converting the $C(sp^3)$–$C(sp^2)$ bonds of alkenes into $C(sp^3)$–H, –S, –O, –N, –C, and –X bonds, through redox-based radical processes [3]. The utility of this "dump-and-stir" methodology lies in its operational simplicity and mild conditions, often proceeding in open-to-air vessels with high efficiency and stereoselectivity. By leveraging the Criegee ozonolysis of alkenes in methanol, stable α-methoxyhydroperoxides can be generated *in situ* and subsequently engaged in iron- or copper-mediated radical cascades to restructure carbon skeletons.

While dealkenylation has witnessed significant innovations for radical coupling, the broad applicability of the tandem two-step protocol is intrinsically linked to the first step—the selective and efficient formation of the α-methoxyhydroperoxide intermediate.

Classically, Criegee ozonolysis of an alkene **I** in methanol proceeds through an initial (3+2)-dipolar cycloaddition between ozone and the C–C π-bond to form a 1,2,3-trioxolane **II**, also known as the molozonide or primary ozonide (POZ) (Figure 6.2) [4]. This initial, exergonic reaction is immediately followed by *retro*-(3+2)-cycloaddition of the POZ into a carbonyl oxide **IIIa**/**IIIb** (Criegee intermediate, CI) and a carbonyl **IVa**/**IVb**. This fragmentation step is the pivotal moment where the alkene C–C σ-bond is irreversibly severed. For unsymmetrical alkenes, it is chemically decisive. The POZ can fragment in two possible directions, dictating the regiochemistry of the resulting Criegee intermediate. Consequently, high-selectivity in this fragmentation is desirable to yield synthetically useful quantities of α-methoxyhydroperoxide intermediates **Va**/**Vb** after quantitative capture of the carbonyl oxide **IIIa**/**IIIb** by methanol.

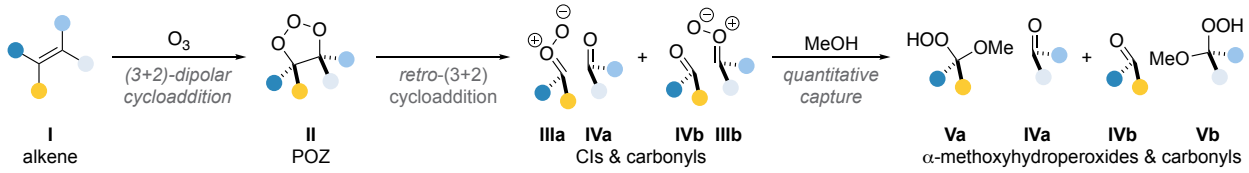


Figure 6.2 Mechanism of Criegee Ozonolysis in Methanol

6.3 Regiochemical Considerations

While the directionality of molozonide fragmentation can often be qualitatively anticipated, quantitative prediction has remained largely speculative. Canonically, three

major molecular features play into the regiochemical outcome: mesomeric effects, inductive effects, and hyperconjugation (Figure 6.3A) [5–7]. To assess these contributions, three categories were analyzed: intuitive (*mono*-, *gem*-, *tri*-), ambiguous (*trans*-, *cis*-, *tetra*-), and polarized (enols and α,β-unsaturated carbonyls) (Figure 6.3B). For the *mono*-substituted, *gem*-disubstituted, and *tri*-substituted alkenes, hyperconjugative stabilization reliably directs fragmentation toward the more-substituted Criegee intermediate. However, these qualitative 'rules' become complex and unintuitive when electronic effects compete, such as in 1,2-*di*-substituted and *tetra*-substituted systems. α-Position substituents capable of resonance often behave paradoxically. For example, while an aromatic ring is expected to stabilize a benzylic Criegee intermediate, the homobenzylic position is frequently favored (Figure 6.3C). Similarly, in the case of enol ethers, the expected resonance stabilization of an α-alkoxy Criegee intermediate is typically overridden, and fragmentation preferentially yields the alkoxy-substituted carbonyl fragment. In these environments, typical mesomeric donors may instead function as inductive withdrawers, destabilizing the adjacent positive character. This complexity persists as the β-position is considered, where a purely inductive model often fails to account for the observed regioselectivity. In aliphatic series with increasing β-branching, the regiochemical outcome is frequently dominated not by the inductive donation of the bulky alkyl group, but by a concomitant decrease in hyperconjugative stabilization (Figure 6.3D). As C–C bonds replace C–H bonds at the β-carbon, the loss of effective hyperconjugative overlap creates a competitive electronic environment that is difficult to weigh through qualitative reasoning alone. These discrepancies underscore a

fundamental limitation in current synthetic logic and emphasize the necessity of a unified, algorithmic framework to balance these competing rules.

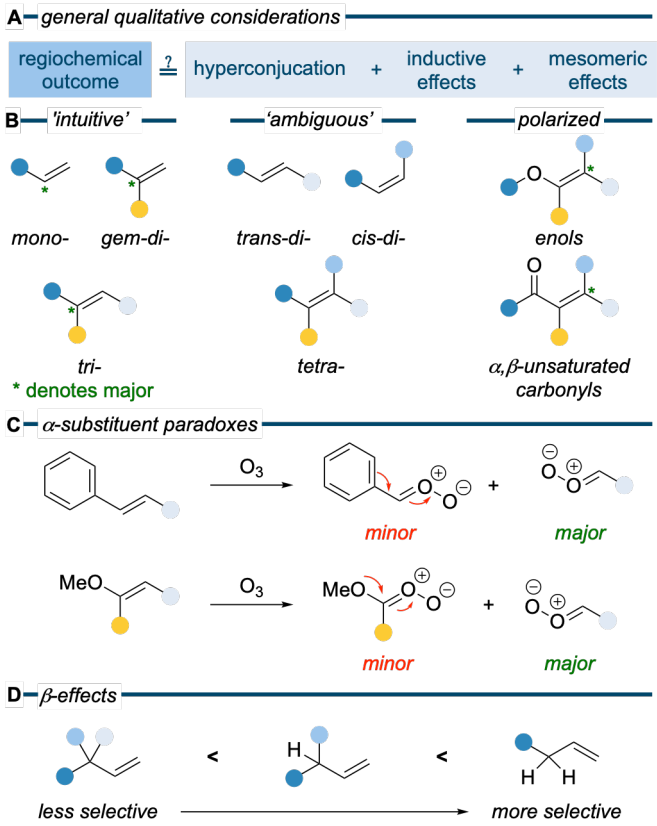


Figure 6.3 Scope and Qualitative Regiochemical Considerations

6.4 Computational Design

This workflow circumvents traditional bottlenecks by providing access to hypothesized transition state (TS) ensembles at a significantly reduced computational cost, integrating state-of-the-art generative and ranking tools such as TSDiff for 3D coordinate generation and ConfRank+ for energetic inference. Validated against 54 experimental data points, this end-to-end model offers an algorithmic avenue to screen substrates *in silico*, delivering regiochemical insights with the nuance of quantum mechanical calculations at a fraction of the temporal and computational expense.

The current pipeline employs a diffusion-based generative model to hypothesize chemically plausible 3D transition state structures directly from 2D SMILES strings (Figure 6.4). It was hypothesized that by bypassing iterative optimizations and instead sampling the structural manifold via TSDiff, regiochemical outcomes could be predicted with a degree of accuracy comparable to DFT-level features but at a fraction of the temporal cost.



Figure 6.4 Computational Pipeline

To validate this featurization strategy, the pipeline was applied to a chemical space curated from the ZINC20 library, restricted to organic compounds containing H, C, N, O, F, Si, P, S, Cl, and Br. Following the removal of symmetric and multi-alkene species, a representative subset of 1,000 alkenes was selected via Morgan Fingerprint analysis to ensure maximal structural and electronic diversity. For each candidate, the relative stability of competing transition state ensembles (Site A vs. Site B) was evaluated using

the ConfRank+ interatomic potential. This ranking allows for the determination of the activation energy differential without absolute energy calculation for each TS, which is subsequently mapped to quantitative product ratios via a Boltzmann distribution. This end-to-end approach effectively reduces the time required for regioselectivity screening from months to minutes, enabling real-time *de novo* reaction design.

To ensure the predictive accuracy of the pipeline, a multi-stage training protocol was implemented, utilizing high-level quantum mechanical calculations as the ground truth. The initial dataset was constructed by performing DFT optimizations on a diverse set of transition state geometries. For each reaction in the training set, first-order saddle points were located, providing the definitive 3D coordinates and associated Gibbs free energies required for model calibration.

The structural generation component, TSDiff, was trained as a conditional diffusion model. During this phase, the optimized 3D coordinates from the DFT dataset were subjected to a forward diffusion process, gradually introducing Gaussian noise until the structural information was fully obscured. The model was then trained to reverse this process, learning to hypothesize the original 3D transition state geometry by denoising the atomic distribution while conditioned on the 2D molecular graph of the starting alkene. The objective function prioritized the minimization of root-mean-square deviation (RMSD) between the hypothesized and DFT-optimized coordinates, ensuring that the generative output remained physically grounded.

The energetic evaluation component, ConfRank+, was trained utilizing a pairwise ranking objective within a graph neural network (GNN) architecture. Rather than performing absolute energy regression, the model was presented with pairs of transition

state conformers and tasked with identifying the lower-energy species. This ranking approach allows the model to capture the subtle electronic and steric factors governing regioselectivity, such as secondary orbital interactions and transannular strain, without the systematic errors often associated with predicting absolute magnitudes of total electronic energy. By pre-training the GNN on a broad chemical space before fine-tuning on ozonolysis-specific transition states, the model inherited a robust understanding of interatomic potentials, which was then specialized for the potential energy surface of 1,3-dipolar cycloadditions.

While initial modeling efforts utilized selectivity values reported in the literature, these data points failed to provide a cohesive correlation with our computational predictions [5–7]. Further investigation revealed that traditional analytical techniques, such as infrared spectroscopy (IR), gas chromatography (GC), and titration, rely on a simplified model of ozonolysis that assumes a binary product distribution. However, our *in situ* quantitative NMR (qNMR) studies demonstrated that these assumptions are mechanically and mechanistically flawed. We hypothesize that IR often lacks the necessary spectral resolution to distinguish between closely related intermediates, and titration methods are prone to mis-calibration due to the confounding presence of secondary ozonides. Furthermore, the volatilization required for GCMS analysis can skew the results, as the thermal energy involved may trigger the adventitious oxidation of sensitive aldehyde products. These legacy methods also fail to account for competitive pathways such as epoxidation, ozonide formation, or secondary reactions between carbonyl fragments and solvent/intermediates to form acetals [*1*].

6.5 Experimental Results

To address these discrepancies, we established a rigorous experimental protocol using internal standard-based qNMR to ensure the integrity of the model's training set (Figure 6.6). For each substrate, a stock solution (0.1 M in CD_3OD) containing the alkene and a known quantity of an internal standard was prepared and divided into a blank and three analytical replicates. The blank was utilized to precisely calibrate the initial molar ratio between the internal standard and the analyte, providing a baseline for quantitative tracking. The subsequent replicates were then subjected to ozonolysis, enabling for the direct observation of product partitioning and ensuring statistical reproducibility across the dataset. This approach enabled the full accounting of all species within the reaction mixture for simple substrates, ensuring that minor pathways did not obscure the primary regiochemical data. For substrates exhibiting high mechanistic complexity, we deduced the ratios from diagnostic signals consistent with other substrates within the dataset.

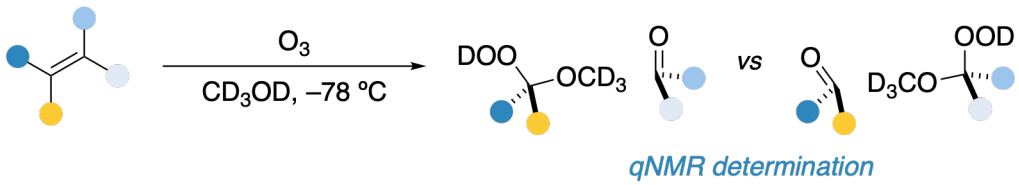


Figure 6.5 Experimental Pipeline

The selection of the validation substrates was anchored by the inclusion of complex, biologically relevant alkenes to demonstrate the practical utility of the model in synthetic chemistry. This subset featured polycyclic terpenes and terpenoids, vitamins, mono-unsaturated fatty acids, and steroids, presenting architecture with intricate ring systems and distal functional groups. Despite the structural density of these natural products, the predicted regioselectivity remained consistent with our qNMR-measured outcomes. To systematically evaluate the drivers of this performance, the remainder of the dataset was

strategically designed across a gradient of steric and electronic environments, beginning with alkyl-substituted alkenes to establish a baseline for increasingly crowded transition states and various electronic factors.

The 'intuitive' regioselectivity for *mono*-substiuted alkenes matched with both the experimental and computational values. Doubling alkyl-substitutent chain length from 4 in 1-hexene (**1**) to 8 in 1-decene (**2**) resulted in only a marginal increase in preference from 89% to 92%, respectively (Figure 6.6). This baseline performance was further tested against steric perturbations at the β-position. Vinylcyclohexane (**3**) and 3,3-dimethylbutene (4) led to a systematic decrease in selectivity that scaled with degree of β-branching (89% and 82%, respectively). Furthermore, the inductive influence of a distal halogen was found to be highlight distance-dependent. The proximity of the bromine atom in 4-bromobutene (**5**) caused a significant attenuation in preference to 61%. Conversely, the insertion of two additional methylene units in 6-bromohexene (**6**) effectively insulated the reaction center and almost completely restored selectivity (85%).

In the analysis of *gem*-substituted alkenes, a slight trend emerged between acyclic and cyclic frameworks. While acyclic *gem*-substituted alkenes provided high selectivity (2-methylbutene **7**), 95%), cyclic analogs demonstrated an incremental increase in regiochemical control, with methylenecycloheptene (**8**) reaching 96% and the methylenecyclododecene (**9**) achieving 98% (Figure 6.6). This enhanced selectivity in larger cyclic systems is likely driven flexibility of the ring scaffold to promote ideal orbital alignment for hyperconjugative stabilization of the developing positive charge.

To investigate a potential resonance contribution during the transition state, three α-phenyl-*gem*-alkenes were measured. There was a one percent experimental difference

of selectivity between α-methylstyrene (**10**, 93%) and α-(methyl-d_3) styrene (**11**, 92%). A significant decrease of selectivity (67%) was observed for α-trifluoromethylstyrene (**12**) because of a strong electron withdrawing effect of the CF_3-group. Surprisingly, the introduction of branching groups to the styrene system inverted selectivity. The α-cyclobutyl styrene (**14**) more strongly inverted the selectivity (90%) than α-cyclopentyl styrene (**13**, 83%).

A specific case study was conducted on allylic and homoallylic carboxylates to investigate how inductive effects and proximity dictate product ratios. The electronic influence of the substituent was clearly visible in the allylic series, where the strongly electron-withdrawing *p*-CF_3-benzoate **15** yielded 69% selectivity, compared to 71% for the *p*-Br-benzoate **16** and 79% for the ibuprofen derivative **17**. This trend illustrates the varying degrees of inductive destabilization exerted by the carboxylate on the proximal carbon during transition state formation. The impact of distance was even more pronounced. When transitioning from allylic ibuprofen **17** (79%) to its homoallylic counterpart **18** (93%), selectivity increased significantly as the withdrawing group was moved further from the reaction center, allowing the inherent electronic preference of the alkene to dominate.

Investigations of the *tri*-substituted series began with assessing selectivity for the simplest *tri*-substituted alkene, 2-methyl-2-butene (**19**) (Figure 6.6). It was measured at 94%, falling within 1% of its *gem*-di-substituted isomer. The monoterpenoid (–)-β-citronellol (**20**), showed a slightly diminished ratio of which the change in magnitude was accurately captured by the computation. More complex, cyclic environments resulted in an attenuation of selectivity. The diterpene, (–)-α-cedrene (**21**), exhibited only 80%

selectivity, a trend that became more pronounced with the kobusone derivative **22** (63%) and (*E*)-1-methylcyclododecene (**23**) (50%). This reduction in regiochemical control is likely governed by the reactivity-selectivity principle (RSP), where increasing ring strain crates a more reactive alkene and a correspondingly less selective transition state. Conversely, the allylic alcohol in the diterpenoid (+)-phytol (**24**) strengthened the selectivity (99%) through the impartation of an inductive effect.

Across all three of these 'intuitive' alkene categories [*mono*-, *gem*-, and *tri*-] the measured ratios closely mirrored the predicted values, confirming that the model architecture can navigate both the structural complexity of natural products and the subtle nuances of hyperconjugative, mesomeric, and inductive effects to deliver precise regiochemical insights. Furthermore, a distinct correlation was observed regarding molecular strain, wherein regioselectivity was attenuated as alkene strain increased. This suggests the ground-state destabilization of strained systems leads to a more-reactive, less-selective transition state of which the model captured with high fidelity.

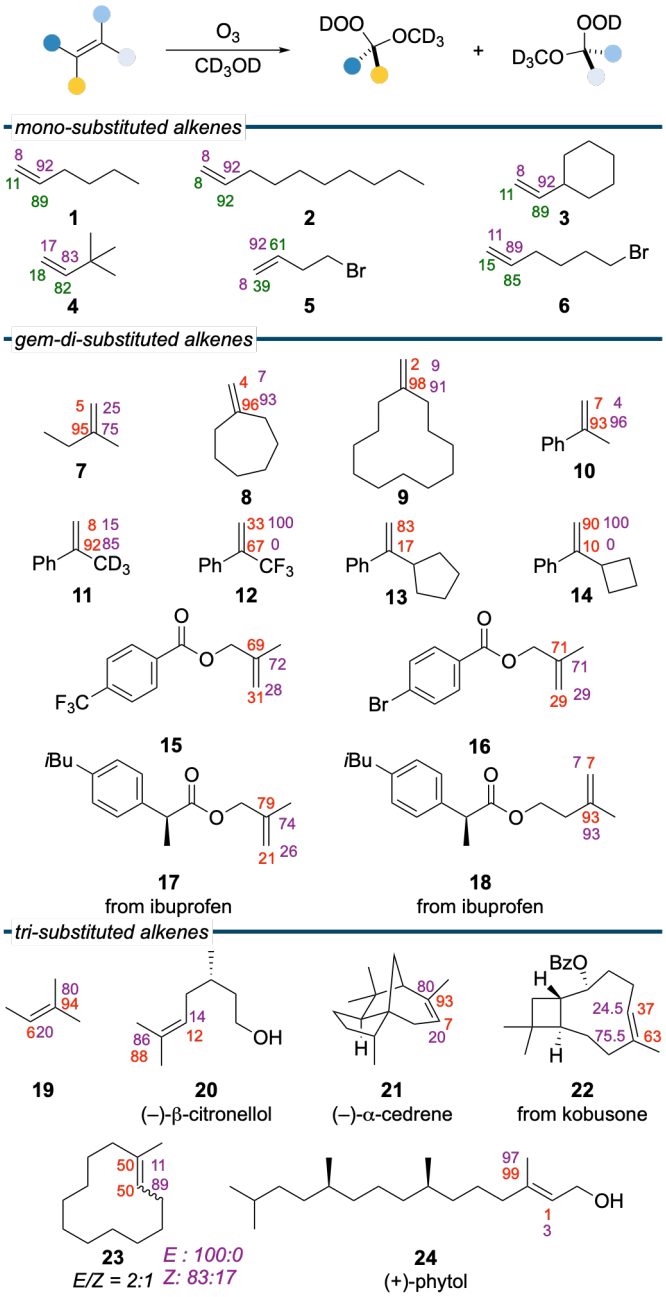


Figure 6.6 *retro*-(3+2) Cycloaddition Selectivity for 'Intuitive' Alkenes

Purple numbers refer to computationally predicted values. Red numbers refer to experimentally measured values with qNMR. Green numbers refer to experimentally measured values with qNMR corrected to account for ozonide formation.

The three remaining ‘ambiguous’ alkene categories [*trans*-, *cis*-, and *tetra*-] present a more complex regiochemical landscape because they lack a single, dominant geminal stabilizing group to anchor the regiochemical outcome. In turn, the model must resolve a much tighter competition between subtle effects. In these cases where human intuition may fail to provide a clear qualitative prediction, the model’s ability to quantify minor energetic differences in POZ *retro*-(3+2)-cycloaddition becomes essential.

The *trans*-1,2-*di*-substituted series provided the first rigorous test of this predictive resolution. Generally, RSP supports greater selectivity of *trans*-alkenes compared to their *cis*-isomers because of a lower ground-state energy. The first alkene in this class, (*E*)-2,2-dimethyl-3-hexene (**25**) compares primary and tertiary β-branching (Chart 2). The 4-position, proximal to the primary β-branch, was favored at 84%, an outcome accurately captured by the computation. Inductive effects remained a powerful driver as well, with the allylic alcohol of (*E*)-2-pentenol (**26**) pushing selectivity to the 3-position at 91%. Potential mesomeric stabilization from the electron rich anisole ring of *trans*-anethole (**27**) was insufficient to favor the benzylic position. The homobenzylic position was favored in a at 71%. These three datapoints suggest the ‘intuitive’ α- and β-position hyperconjugative and inductive are applicable for analyzing *trans*-*di*-substituted alkenes.

When applied to more complex natural products and steroids, the model correctly captured regiochemical directionality even when absolute accuracy slightly deviated. In capsaicin (**28**), the model resolved competition between primary and secondary β-branching to favor the primary side at 62:38, a significant finding because the “warhead” portion of the molecule effectively retains the peroxide. For the oxygenated stigmasterol derivative **29**, experimental measurements required a $CDCl_3$ co-solvent to improve

dissolution. The solvent shift may have impacted the experimental ratio away from the computational ideal, but the directionality was in agreement. Given that this alkene has secondary β-branching on both sides, we hypothesize the outcome is biased either by the greater inductive effect of the ethyl versus methyl, or the oxygenated steroid skeleton serves as London dispersion inductive sink to provide long-range electronic destabilization [8].

The investigation into the *cis*-*di*-substituted class began with 1,2-dihydronapthalene (**30**), which provided critical details about the α-substituent interplay between inductive and mesomeric effects (Figure 6.7). An overwhelming 94:6 preference for the homobenzylic position was observed, suggesting the inductive destabilization of the aryl group dominates the regiochemical outcome. This result is particularly illuminating when compared to *trans*-anethole (**27**) because both favor the homobenzylic position, but the 1,2-dihydronaphthalene (**30**) does so with much higher ratio. The disparity is likely due to the stronger mesomeric stabilization imparted by the presence of the *p*-methoxy group in *trans*-anethole (**27**), which imparts enough mesomeric stabilization to the benzylic position to partially offset the inductive bias. This comparison indicates that mesomeric stabilization is operative in a subordinate role to inductive effects.

The impact of β-substituents was clearly resolved in 3-methylcyclohexene (**31**), which was surprisingly selective at 81:19 in favor of the position with less β-branching. The high degree of regiocontrol is notable within a *cis*-geometry because the eclipsing interactions inherent to the *cis*-POZ may attenuate selectivity through a higher energy ground state. The stereoelectronic influence of β-substituents was realized in the comparison of two natural product diastereomers: (+)-*trans*-p-menth-2-ene (**32**) and (–)-*cis*-p-menth-2-ene

(**33**). While the *trans*-isomer exhibited a robust 78:22 preference for the less β-branched position, the *cis*-isomer saw selectivity drop to 64:36. This disparity confirms the relative stereochemistry of the diastereomers governs the efficacy of hyperconjugative stabilization, with the *trans*-orientation enabling superior alignment. Furthermore, the more sterically congested *cis*-geometry likely contributes to a ground state destabilization diminishes regioselectivity, a trend consistent with the RSP.

Finally, long-chain fatty acids demonstrated the reach of distal functional groups through the aliphatic backbone. Oleic acid (**34**) showed a nearly statistical preference away from the carboxylate (53:47), indicating the inductive influence of the terminal acid is largely insulated by the intervening carbon chain and plays a minimal role in affecting selectivity. In contrast, ricinoleic acid (**35**) exhibited a more pronounced 39:61 preference distal to the homoallylic alcohol. This reversal underscores that the closer proximity of the hydroxyl group provides a more significant inductive perturbation than the distant carboxylate. Both of these nuances were accurately resolved by the model's assessment.

The investigation into *tetra*-substituted alkenes began with 1,2-dimethyl-1-phenylpropene (**36**) to assess the impact of a direct α-aryl substituent (Figure 6.7). Despite the high degree of substitution, an overwhelming 94:6 preference for the homobenzylic position was observed. This result is consistent with the strong inductive destabilization seen in less substituted aryl alkenes and confirms the α-aryl influence for fully substituted systems.

To systematically evaluate more nuanced β-effects, the study moved to a series of isopropylidene-substituted cyclohexanes. To establish a baseline, the unsubstituted isopropylidenecyclohexane (**37**) was first evaluated, yielding a distinct preference for the

isopropylidene carbon (72%). This result confirms that the β-branching inherent within the cyclohexane framework is significant in directing regioselectivity. The system was then perturbed by adding additional substituents at the β-position of the cyclohexane ring. The introduction of a methyl group in **38** resulted in a surprisingly lower selectivity (58%). Swapping the methyl of **38** for a phenyl group in **39** restored and improved selectivity to 82%. The attenuation of selectivity for **38** with the methyl substituent suggests a conformational lock that optimizes alignment of the bonds for hyperconjucative stabilization from the cyclohexane ring. Although the phenyl group of **39** is likely to also create a conformational lock, the electron-withdrawing nature of the phenyl ring relative to the methyl group effectively overrides any localized hyperconjugative gains.

The predictive model performed well with these 'ambiguous' alkene classes [*trans*, *cis*, *tetra*] and successfully resolved subtle electronic gradients. However, two specific examples, (–)-*cis*-p-menth-2-ene (**33**) and isopropylidenecyclohexane (**37**), exhibited particularly poor accuracy and the model predicted the incorrect directionality for both. These outliers are concerning because they represent cases where the electronic tropes of the model architecture fail to account for the experimental reality. Nonetheless, the fundamental influences of hyperconjugative, mesomeric effects, and induction were adequately captured across the majority of the 'ambiguous' library. Overall, the rules derived from the 'intuitive' class remain remarkably robust at deriving the results for the 'ambiguous' class.

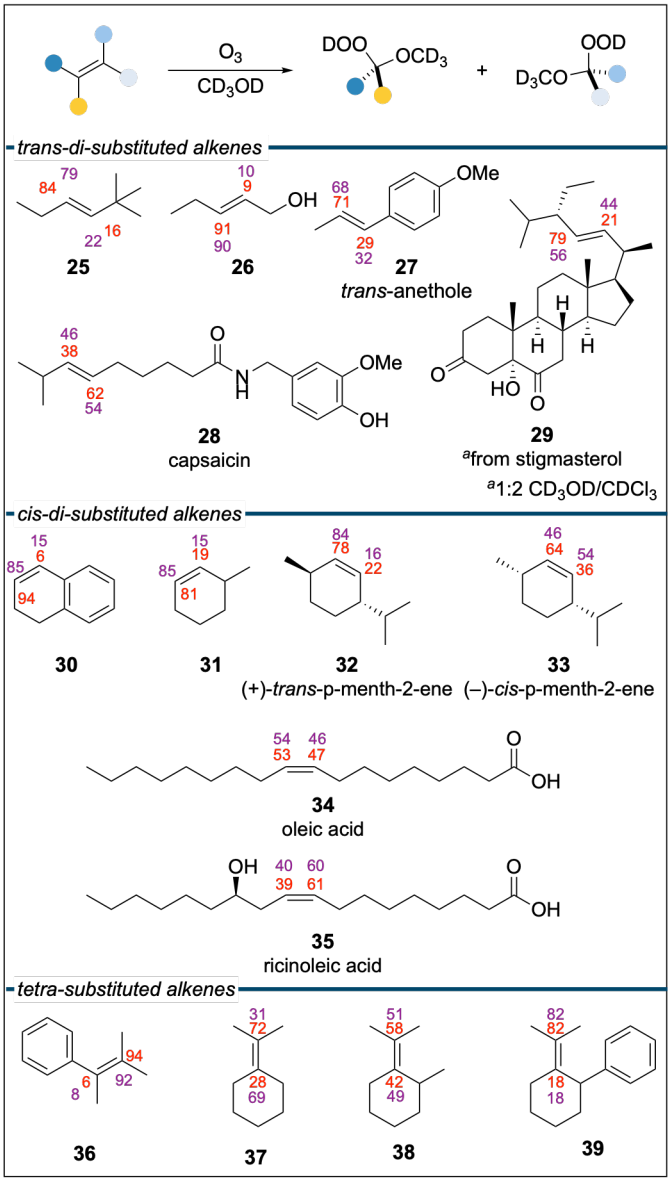


Figure 6.7 *retro*-(3+2) Cycloaddition Selectivity for 'Ambiguous' Alkenes

Purple numbers refer to computationally predicted values. Red numbers refer to experimentally measured values with qNMR.

The final assessment of the predictive architecture focused on polarized substrates, specifically enol derivatives and α,β-unsaturated carbonyls. Unlike the previous classes where a multitude of factors affected regioselectivity, the extreme electronic gradients imparted by heteroatom substitution govern these systems despite the potential mesomeric stabilization. In both cases, position distal to the electron withdrawing group is favored [9].

Polarized, electron-rich olefins were initially assessed with enol derivatives of 4-phenylcyclohexanone. A scaling effect emerged as the electron-withdrawing character of the substituent was increased. The methyl enol ether **40** and 2-trimethylsiloxylethyl-enol ether **41** were the most electron donating and showed a preference of 82% and 84%, respectively (Figure 6.8). The enol acetate **42** intensified the preference to 96%, and the enol phosphate **43** reached nearly absolute selectivity. This trend suggests that as the oxygen-based substituent becomes more electron-deficient, the inductive effect on the proximal carbon becomes so severe that *retro*-cycloaddition occurred exclusively at the distal position.

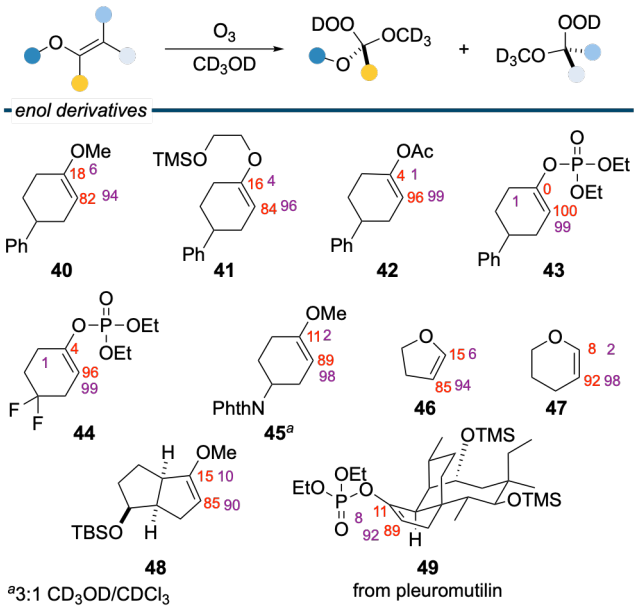


Figure 6.8 *retro*-(3+2) Cycloaddition Selectivity for Polarized, Electron-Rich Enol Derivatives

Purple numbers refer to computationally predicted values. Red numbers refer to experimentally measured values with qNMR

Inductive competition *trans*-annularly was scrutinized by introducing stronger electron-withdrawing groups at the 4-position of the cyclohexane ring. Despite the additional pull from a 4,4-difluoro enol phosphate **44** or a 4-phthalimide methyl enol ether **45**, the distal preference remained the governing factor (96% and 89%, respectively). The fact that the proximal inductive penalty of the enol oxygen overrides competing influence across the ring highlights its potency as a regiochemical driver.

Analysis of cyclic enol ethers demonstrated the dependability of the inductive effect in these systems. Both 2,3-dihydrofuran (**46**) and 3,4-dihydro-2H-pyran (**47**) favored attack at the β-carbon in 85% and 92%, respectively. The larger strain of the 5-membered ring is likely to have led to the slight decrease in selectivity due to ground-state

destabilization. Polycyclic architectures that present significant steric and electronic complexity make up the final category of this class. The pentalene methyl enol ether of **48** formed the peroxide at the β-carbon in 85% and the enol phosphate of the natural product pleuromutilin derivative **49** was 89% β-selective. The model performed well in both of these cases despite the intricate bridging.

The analysis of electron-deficient α,β-unsaturated carbonyls completed the study of polarized substrates. A systematic analysis of cinnamic acid derivatives established a baseline for differing carbonyl substituents. Across all electron-withdrawing groups, the alkene β-position was preferred (Figure 6.9). Methyl styryl ketone (**50**) yielded a 72% preference for the distal carbon. Cinnamic acid (**51**) resulted in 89% selectivity. Methyl cinnamate (**52**) formed the β-peroxide in 87%. Assuming the small quantity of ozonide formed (5%) originates from the β-carbonyl oxide, the ratio is then increased to 95%. Cinnamonitrile (**53**) showed an 84% preference with no side-products. This dataset reveals a clear hierarchy of inductive influence based on number of electron withdrawing substituents: methyl styryl ketone (**50**) < cinnamonitrile (**53**) < methyl cinnamate (**52**) < cinnamic acid (**51**). Cyclohexenone (**54**), a cyclic system, showed an 84% preference for the β-carbon, a slight increase over the methyl styryl ketone (**50**) likely due to the lack of the phenyl electron-withdrawing substituent.

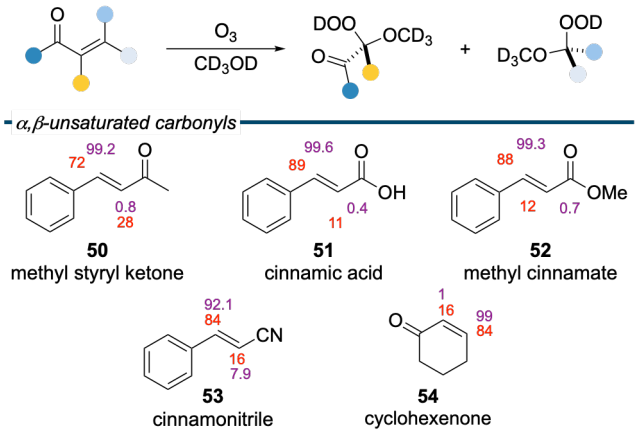


Figure 6.9 *retro*-(3+2) Cycloaddition Selectivity for Polarized, Electron-Deficient α,β-Unsaturated Carbonyl Derivatives

Purple numbers refer to computationally predicted values. Red numbers refer to experimentally measured values with qNMR

Collectively, these results for polarized alkenes underscore a unifying theme of architecture. Whether the system is electron-rich (enols) or electron-poor (α,β-unsaturated carbonyls), the inductive profile of the substituent is the most reliable predictor of regioselectivity. In every case studied, the inductive effect effectively directed *retro*-cycloaddition to position distal to the electron-withdrawing functional group. While the model successfully captured these overarching trends, it tended to over-estimate the severity of the induction. For now, the precise calibration to accommodate these electronic gradients remains a significant limitation of the model, signaling a need for future parameterization.

6.6 Results and Discussion

With the individual assessments of the 'intuitive', 'ambiguous', and 'polarized' alkene classes complete, global, holistic evaluation of the predictive model is now possible. The primary indicator of the model's performance is parity of experimental and computational values. To assess this parameter, these values were graphed with the experimental results on the x-axis and the computational predictions on the y-axis (Figure 6.10). An ideal model would match the experimental value with computation, aggregating all datapoints on the y = x line. The strengths and weaknesses of the model emerge by breaking down the model for each category.

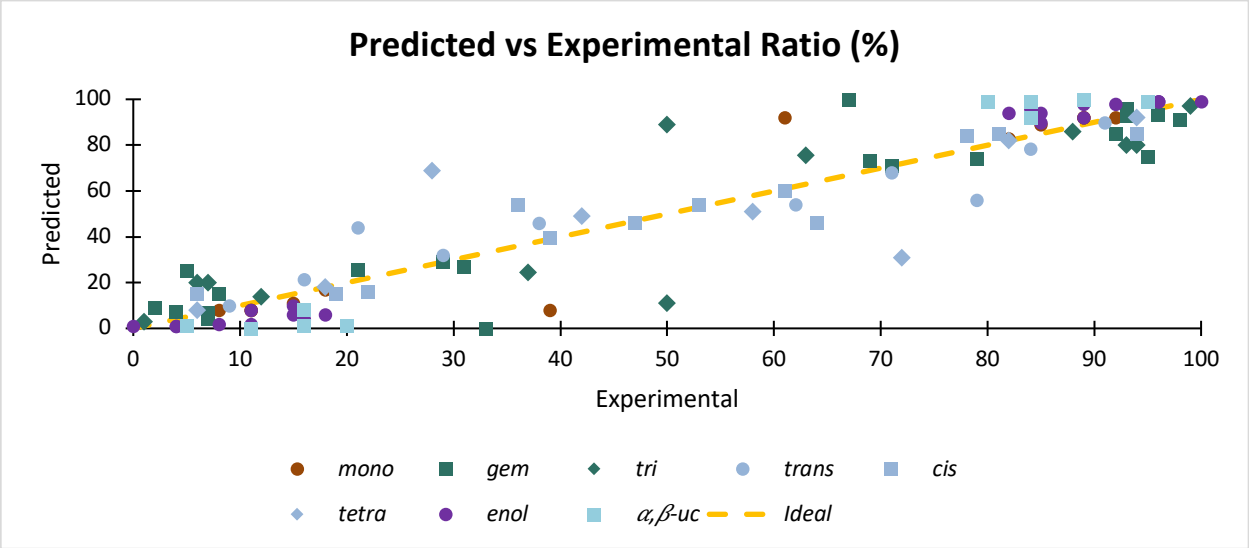


Figure 6.10 Model Performance per Category

The model performed well with the 'intuitive' alkene class as a whole. Notably, the mono-substituted alkenes formed small quantities of secondary ozonide despite the excess of methanol in the reaction. Mono-substituted alkenes create the most reactive carbonyl oxide and carbonyl possible, out of all alkene classes, because of the lone substituent, minimized sterics, and minimal electronic stabilization. Such a phenomenon is not accounted for by the model which may have affected the results. The 'ambiguous'

alkene class performed satisfactorily. The general trends in reactivity were accounted for, but the higher ground state destabilization energy of the *cis*-alkenes was translated into the transition states and subsequently led to decreased regiochemical selectivity. The model was able to capture these smaller ratio differences with slightly lower accuracy than other alkene classes. Polarized alkenes posed a significant challenge for the model because the larger dipole moments were over-compensated. As a result, the model predicts extreme selectivity for all of these alkenes, which was not the experimental reality. Regardless, the model was able to determine the correct directionality for the regioselectivity, a feat which had created an issue when these systems were initially studied decades ago [*9*].

This first generation of the computational model demonstrated an average regiochemical assignment accuracy of 88%±16% (Figure 6.11), successfully identifying the major product across a broad range of substitution patterns with an absolute error centered within ±5% (Figure 6.12). The model consistently identified the dominant isomer with few exceptions, reflecting its ability to resolve significant energetic differences. Further refinement is required to boost the accuracy and will be attempted prior to submission for publication.

Intriguingly, predicted ^{13}C NMR chemical shifts of the molozonide also track with regioselectivity, where the alkenes of the 'ambiguous' category show preference for the carbonyl oxide formation at the smaller ^{13}C NMR chemical shift. We were unable to determine any quantification based on this technique. Nevertheless, ^{13}C NMR chemical shift could serve as a secondary validation should the qualitative rules outlined in section 6.3 breakdown.

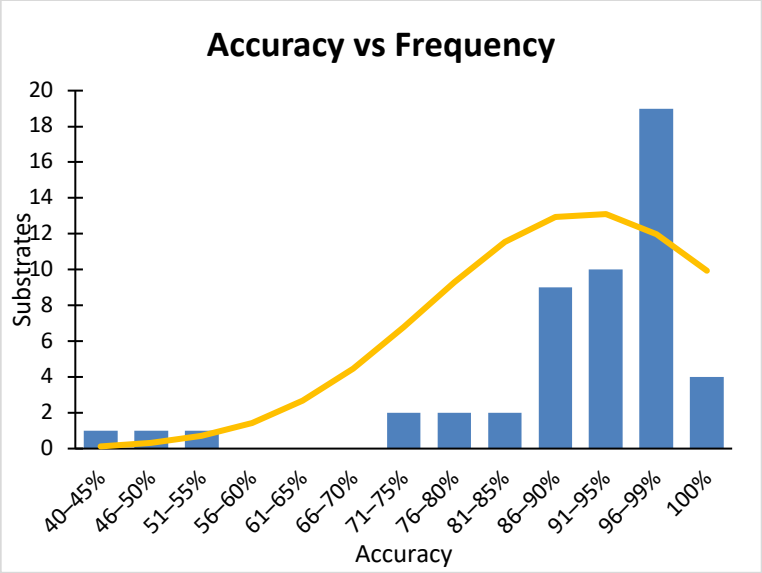


Figure 6.11 ML Model Accuracy vs Frequency

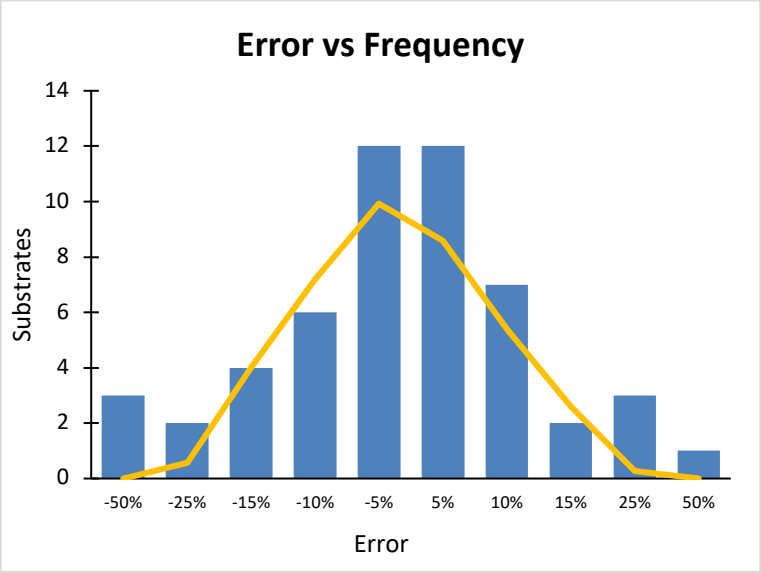


Figure 6.12 ML Model Error vs Frequency

6.7 Conclusions

In conclusion, we have developed a machine learning pipeline to predict the regioselective fragmentation of primary ozonides during Criegee ozonolysis through a collaborative experimental and computational approach. By utilizing an internal standard-based qNMR protocol to analyze crude reaction mixtures, we accounted for competitive pathways and provided a refined set of training data. These experimental values allowed for the development of a robust model, capable of accurately balancing hyperconjugative, inductive, and mesomeric effects across a variety of alkene substrates, to minimize empirical trial-and-error for future studies involving Criegee ozonolysis.

6.8 Supporting Information and Experimental Section

6.8.1 Materials and Methods

Glassware

Unless otherwise stated, all reactions were conducted in glassware that had been washed sequentially with 12 M HCl and Alconox, oven-dried, and fitted with rubber septa; the reaction mixtures were stirred with Teflon-coated magnetic stir bars.

Solvents and Reagents

For dry or air-free reactions, standard Schlenk techniques were used to transfer liquid reagents and solvents. Argon was used as the gas for inert atmosphere reactions. Methanol (MeOH) was distilled over magnesium under an argon atmosphere. Dichloromethane (DCM) and acetonitrile (MeCN) were distilled over calcium hydride under an argon atmosphere. Tetrahydrofuran (THF) and diethyl ether (Et_2O) were distilled over sodium/benzophenone ketyl under an argon atmosphere. All other solvents and reagents were used as received from commercial sources, unless otherwise noted.

Reaction Temperatures

Reaction temperatures above room temperature (23 ºC) and below 50 ºC refer to water bath temperatures, unless otherwise stated. Reaction temperatures above 50 ºC refer to silicone oil bath temperatures.

SiO_2 Chromatography

Thin layer chromatography (TLC) was performed using SiliCycle silica gel 60 F-254 precoated plates (0.25 mm) with visualization under UV irradiation and with a bromocresol green, ceric ammonium molybdate (CAM), potassium permanganate ($KMnO_4$), or vanillin stain. SiliCycle Silica-P silica gel (particle size: 40–63 μm) was used for flash column chromatography (FCC).

Melting Point

Melting points are uncorrected and were recorded using an Electrothermal® capillary melting point apparatus.

Infrared (IR) Spectroscopy

IR spectra were recorded using a Jasco FTIR-4100 spectrometer with a Zirconium–Selenium crystal ATR attachment or an Agilent Cary 630 FTIR with a diamond ATR attachment.

High Resolution Mass Spectrometry (HRMS)

HRMS was performed using a Thermo Fisher Scientific Exactive Plus spectrometer equipped with an IonSense ID-CUBE DART source or an Agilent 6545 Q-TOF LC/MS with 1260 Infinity LC.

Gas Chromatography Mass Spectrometry (GCMS)

GCMS was performed with an Agilent 7250 Q-TOF GC/MS with low energy EI or an Agilent Intuvo 9000 GC with a 5977B GC/MSD.

Liquid Chromatography Mass Spectrometry (LCMS)

LCMS was performed with an Agilent 1260 Infinity II LC using a poroshell 120 EC-C18 (2.7 μm, 4.6x100 mm) column coupled to a low resolution 6120 Quadrupole MSD. The mobile phase consisted of H_2O/MeCN mixtures spiked with 0.1% formic acid.

Nuclear Magnetic Resonance Spectroscopy

Samples were prepared in $CDCl_3$ saturated with K_2CO_3 as a desiccant or MeOD-*d*$_4$ which was used as received. ^1H, ^{13}C, and 2D NMR spectra were recorded using AV-800, NEO-600, AV-500, AV-400, or AV-300 MHz spectrometers, with ^{13}C NMR spectroscopic operating frequencies of 201, 151, 126, 101, or 75 MHz, respectively. NMR spectra were analyzed using the MestReNova software application (v.14.2.3-29241). Standard auto-baseline and auto-phase corrections were applied to all spectra prior to manual integration and manual peak picking. Chemical shifts (δ) are reported in parts per million (ppm) relative to the (residual protonated) signal of the solvent $CDCl_3$ (choloroform-*d*, δ = 7.26 for ^1H NMR; δ = 77.2 for ^{13}C NMR) or CD_3OD (MeOD-d_4, δ = 3.31 for ^1H NMR; δ = 49.0 for ^{13}C NMR). Data for ^1H NMR spectra are reported as follows: chemical shift, multiplicity, coupling constants (Hz), and number of hydrogen atoms. Data for ^{13}C NMR spectra are reported in terms of chemical shift. The following abbreviations are used to

describe the multiplicities: s = singlet; d = doublet; t = triplet; q = quartet; m = multiplet; br = broad.

6.8.2 Safety

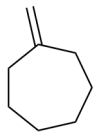
Caution: Organic peroxides are typically high-risk shock-sensitive compounds prone to explosion. Although we have not encountered any peroxide-related safety issues in our lab, the peroxides generated using the reported methods should be handled only by properly trained individuals and the isolated compounds should be stored at cryogenic temperatures. The use of a blast-shield is also recommended, especially for reactions performed on larger scales.

6.8.3 Preparation of Starting Materials

6.8.3.1 Alkenes

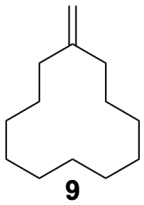
The preparation for alkenes **8**, **9**, **11**–**18**, **22**, **23**, **25**, **29**, **32**, **33**, **36**–**45**, **48**, and **49** are described herein. Alkenes **1**–**7**, **10**, **19–21**, **24**, **26**–**28**, **30**, **31**, **34**, **35**, **46**, **47**, **50**–**54** were purchased from commercial sources and used as received. α-Methyl styrene (**10**) was purchased from a commercial vendor and filtered through SiO_2 (pentane) to remove polymers prior to use. Ricinoleic acid (**35**) was purchased from a commercial vendor and purified through FCC (20% *v/v* EtOAc/hexanes) prior to use.

6.8.3.2 Alkene Syntheses



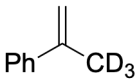
8

Methylenecycloheptane (**8**) was prepared from cycloheptanone according to a literature procedure [10].



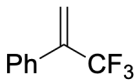
9

Methylenecyclododecane (**9**) was prepared from cyclododecanone according to a literature procedure [11].



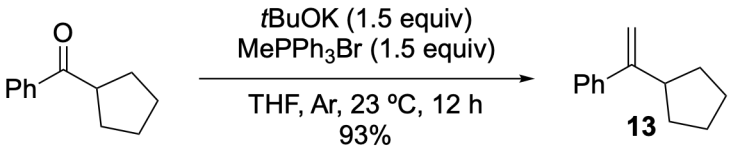
11

(prop-1-en-2-yl-3,3,3-d_3)benzene (**11**) was prepared from acetophenone according to a literature procedure [12].



12

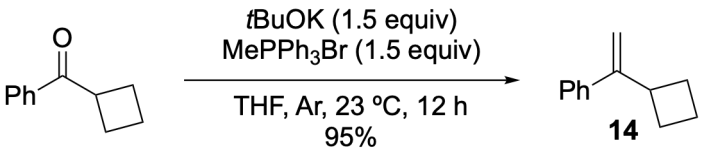
(3,3,3-trifluoroprop-1-en-2-yl)benzene (**12**) was prepared from 2,2,2-trifluoro-1-phenylethan-1-one according to a literature procedure [13].



13

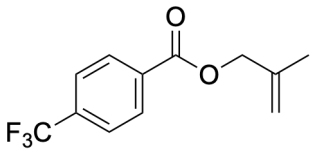
(1-Cyclopentylvinyl)benzene (**13**) was prepared from cyclopentyl(phenyl)methanone on a 5.00 mmol scale in 93% yield (802 mg) according to a literature procedure [14].

Characterization matched with literature values [15].



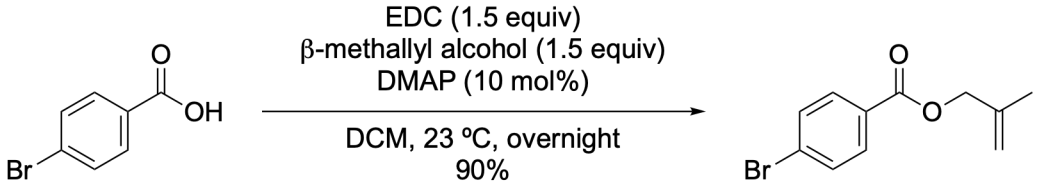
14

(1-Cyclobutylvinyl)benzene (**14**) was prepared from cyclobutyl(phenyl)methanone on a 5.00 mmol scale in 95% yield (751 mg) according to a literature procedure [16]. Characterization matched with literature values [17].



15

2-methylallyl 4-(trifluoromethyl)benzoate (**15**) was prepared from 4-(trifluoromethyl)benzoic acid according to a literature procedure [18].



16

2-methylallyl 4-bromobenzoate (**16**) was prepared from 4-bromobenzoic acid.

Procedure: To a 100 mL round bottom flask equipped with a Teflon-coated magnetic stirrer bar was added 4-bromobenzoic acid (1.61 g, 8.01 mmol, 1.00 equiv), 1-ethyl-3-(3'-dimethylaminopropyl)carbodiimide hydrochloride (2.30 g, 12.0 mmol, 1.50 equiv), and DMAP (97.8 mg, 0.801 mmol, 1.50 equiv). The contents were dissolved in DCM (40 mL) then β-methallyl alcohol (866 mg, 12.00 mmol, 1.50 equiv) was added. The reaction was stirred at room temperature overnight. After complete conversion, the reaction mixture was diluted with DCM (20 mL) and transferred to a separatory funnel and sat. aq. NH_4Cl (20 mL) was added. The aqueous layer was extracted with DCM (2 x 10 mL). The combined organics were dried over sodium sulfate, filtered through cotton, and evaporated. The residue was purified through FCC (SiO_2, 0–5% *v/v* EtOAc/hexanes) to afford 2-methylallyl 4-bromobenzoate as a clear colorless oil in 90% (1.84 g, 7.21 mmol).

Scale: 8.01 mmol

Yield: 90% (1.84 g)

R_f = 0.45 (0–5% *v/v* EtOAc/hexanes + UV/vanillin stain)

Purification: SiO_2 (5% *v/v* EtOAc/hexanes)

Physical State: clear colorless oil

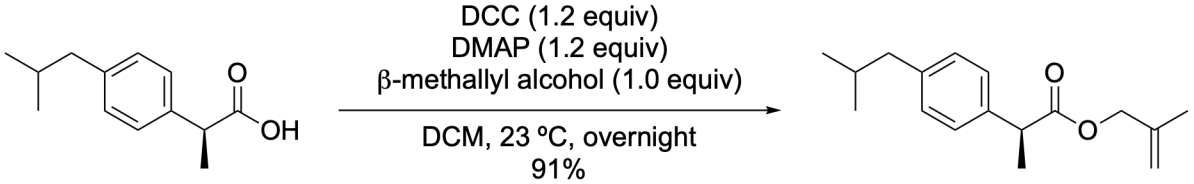
IR (ATR, neat) $\tilde{\nu}_{max}$: 3083. 2974, 2928, 2876, 1722, 1591, 1483, 1452, 1397, 1363, 1265, 1246, 1172, 1114, 1101, 1069, 1012, 986, 950, 908, 846, 755, 682 cm^{-1}

HRMS–DART (*m/z*): $[M + H]^+$ calc'd for $C_{11}H_{11}O_2Br^{79}$ 255.0015, found 255.0008

$[M + H]^+$ calc'd for $C_{11}H_{11}O_2Br^{81}$ 256.9995, found 256.9989

^{1}H NMR (500 MHz, $CDCl_3$) δ 7.93 (d, *J* = 8.7 Hz, 2H), 7.59 (d, *J* = 8.7 Hz, 2H), 5.03 (ddd, *J* = 36.9, 2.4, 1.4 Hz, 2H), 4.74 (s, 2H), 1.83 (s, 3H).

^{13}C NMR (126 MHz, $CDCl_3$) δ 165.7, 139.9, 131.9, 131.3, 129.2, 128.3, 113.3, 68.5, 19.7.



17

The synthesis of 2-methylallyl (*S*)-2-(4-isobutylphenyl)propanoate (**17**) from (*S*)-ibuprofen was adapted from a literature procedure [19].

Procedure: To a 50 mL round bottom flask equipped with a Teflon-coated magnetic stirrer bar was added (*S*)-ibuprofen (1.03 g, 5.00 mmol, 1.00 equiv), dicyclohexylcarbodiimide (1.24 g, 6.00 mmol, 1.20 equiv), and DMAP (733 mg, 6.00 mmol, 1.20 equiv). The contents were dissolved in DCM (17 mL) then β-methallyl alcohol (361 mg, 5.00 mmol, 1.00 equiv) was added. The reaction was stirred at room temperature overnight. The precipitated solids were removed by vacuum filtration and the filtrate was concentrated *in vacuo*. The residue was purified through FCC (SiO_2, 5% *v/v* EtOAc/hexanes) to afford 2-methylallyl (*S*)-2-(4-isobutylphenyl)propanoate as a clear colorless oil in 91 % (1.18 g, 4.53 mmol)

Scale: 5.00 mmol

Yield: 91% (1.18 g)

R_f = 0.63 (10% *v/v* EtOAc/hexanes + UV/vanillin stain)

Purification: SiO_2 (5% *v/v* EtOAc/hexanes)

Physical State: clear colorless oil

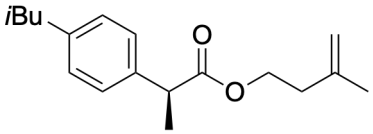
IR (ATR, neat) $\tilde{\nu}_{max}$: 2952, 2930, 2868, 2118, 1735, 1512, 1450, 1376, 1321, 1199, 1159, 1093, 950, 901, 848 cm^{-1}

HRMS–DART (*m/z*): $[M + H]^+$ calc'd for $C_{17}H_{25}O_2$ 261.1849, found 261.1851

Specific Rotation: $[\alpha]_D^{28}$= +20 (*c* = 1.0, $CHCl_3$)

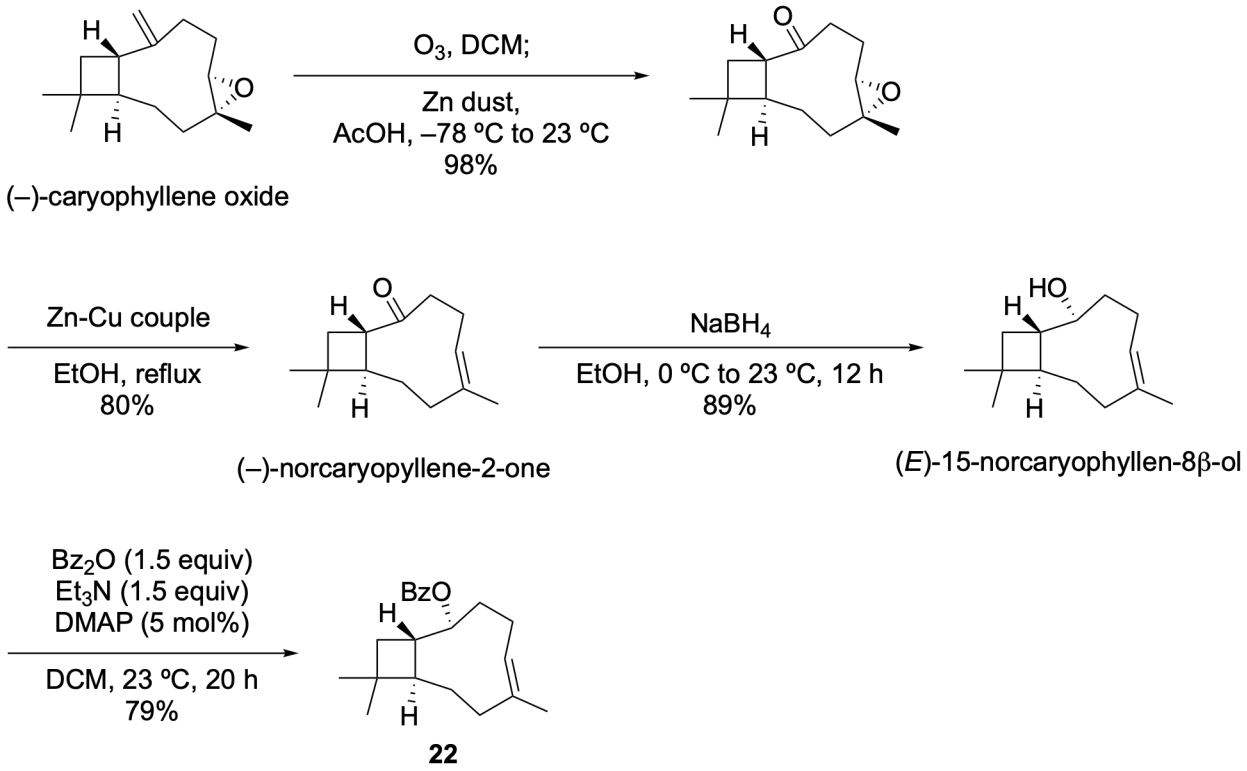
^{1}H NMR (800 MHz, $CDCl_3$) δ 7.25 – 7.19 (m, 2H), 7.09 (dd, *J* = 8.2, 2.0 Hz, 2H), 4.83 (ddd, *J* = 9.7, 2.8, 1.4 Hz, 2H), 4.57 – 4.42 (m, 2H), 3.74 (qd, *J* = 7.3, 2.1 Hz, 1H), 2.45 (dd, *J* = 7.3, 2.1 Hz, 2H), 1.84 (dtd, *J* = 13.5, 6.8, 2.1 Hz, 1H), 1.64 (q, *J* = 1.3 Hz, 3H), 1.52 (dd, *J* = 7.2, 1.8 Hz, 3H), 0.89 (dd, *J* = 6.6, 2.1 Hz, 6H).

^{13}C NMR (201 MHz, $CDCl_3$) δ 174.5, 140.7, 140.1, 137.8, 129.4, 127.4, 112.6, 67.8, 45.3, 45.2, 30.3, 22.5, 19.5, 18.5.



18

3-methylbut-3-en-1-yl (*S*)-2-(4-isobutylphenyl)propanoate (**18**) was prepared from (*S*)-ibuprofen according to a literature procedure [20].



22

(–)-Caryophyllene oxide was transformed into (–)-norcaryophyllene-2-one according to a literature procedure [21]. (–)-norcaryophyllene-2-one was reduced to (*E*)-norcaryophyllen-8β-ol with sodium borohydride according to a literature procedure [22].

(1*S*,2*S*,9*R*,*E*)-6,10,10-trimethylbicyclo[7.2.0]undec-5-en-2-yl benzoate (**22**) was prepared from (*E*)-15-norcaryophyllen-8β-ol.

Procedure: To a 100 mL round bottom flask equipped with a Teflon-coated magnetic stirrer bar was added (*E*)-norcaryophyllen-8β-ol (950 mg, 4.56 mmol, 1.00 equiv) and DCM (45.6 mL) to dissolve. Next, triethylamine (692 mg, 0.953 mL, 6.84 mmol, 1.50 equiv) was added, followed by DMAP (27.9 mg, 0.228 mmol, 5.0 mol%). The mixture was stirred for 5 minutes, then benzoic anhydride (1.55 g, 6.84 mmol, 1.50 equiv) was added portionwise. The solution was stirred at room temperature for 20 h, then quenched with sat. aq. $NaHCO_3$ (75 mL) and transferred to a separatory funnel. The aqueous layer was extracted with DCM (4 x 30 mL). The combined organics were washed with brine (50 mL), dried over sodium sulfate, filtered, and evaporated. The residue was purified through FCC (5% *v/v* EtOAc/hexanes) to afford the product as a clear colorless oil (79% yield) which precipitated under high vacuum at –78 ºC (1.129 g, 3.61 mmol).

Scale: 4.56 mmol

Yield: 79% (1.129 g)

R_f = 0.43 (5% *v/v* EtOAc/hexanes + UV/vanillin stain)

Purification: SiO_2 (5% *v/v* EtOAc/hexanes)

Physical State: crystalline white solid

Melting Point: 69–70 ºC

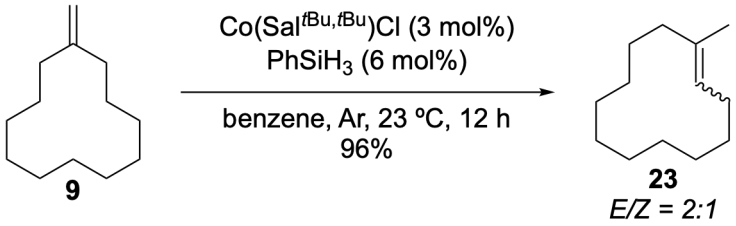
IR (ATR, neat) $\tilde{\nu}_{max}$: 2496, 2924, 2856, 1716, 1450, 1365, 1312, 1271, 1241, 1174, 1113, 1097, 1069, 1026, 710 cm^{-1}

HRMS–DART (*m/z*): $[M + H]^+$ calc'd for $C_{21}H_{28}O_2$ 313.2162, found 313.2164

Specific Rotation: $[\alpha]_D^{22}$= –104 (*c* = 1.0, $CHCl_3$)

^{1}H NMR (800 MHz, $CDCl_3$) δ 8.14 (d, *J* = 8.0 Hz, 2H), 7.59 (t, *J* = 7.4 Hz, 1H), 7.49 (t, *J* = 7.6 Hz, 2H), 5.54 (t, *J* = 8.2 Hz, 1H), 4.99 (d, *J* = 8.4 Hz, 1H), 2.31 (p, *J* = 8.1 Hz, 1H), 2.26 – 2.20 (m, 1H), 2.13 (d, *J* = 12.2 Hz, 1H), 2.05 (h, *J* = 9.8 Hz, 3H), 1.80 (hept, *J* = 6.3 Hz, 1H), 1.71 – 1.64 (m, 2H), 1.68 (s, 3H), 1.58 – 1.54 (m, 1H), 1.47 (q, *J* = 12.6 Hz, 2H), 0.96 (s, 3H), 0.95 (s, 3H).

^{13}C NMR (201 MHz, $CDCl_3$) δ 166.4, 135.4, 133.0, 130.9, 129.7, 128.6, 123.1, 76.6, 46.5, 45.8, 40.1, 38.4, 33.0, 31.0, 30.3, 29.0, 23.1, 22.8, 16.1.



1-Methylcyclododecene (**23**) was prepared from methylenecyclododecane (**9**). The procedure was adapted from a literature protocol [21].

Procedure: To a flame-dried single-neck round bottom flask equipped with a stir bar, methylenecyclododecane (**9**, 1.80 g, 10.00 mmol, 1 equiv.) and dry benzene (50 mL) were sequentially added. In another flame-dried single-neck round bottom flask, Co(Sal^{tBu,tBu})Cl (192 mg, 0.30 mmol, 0.03 equiv.) and dry benzene (50 mL) were added sequentially. Both solutions were sparged with argon for 10 minutes with stirring. After degassing, the Co(Sal^{tBu,tBu})Cl solution was cannulated to the solution of methylenecyclododecane (**9**) and then charged with phenylsilane ($PhSiH_3$, 74.0 µL, 0.60 mmol, 0.06 equiv.). The red-orange solution was allowed to stir at room temperature for 12 hours (completion monitored by ^{1}H NMR). Upon completion, the reaction mixture was concentrated by rotary evaporation. The resulting residue was passed through a silica plug eluting with pentane to afford 1-methylcyclododecene (**23**, 1.73 g, 9.60 mmol, 96%) as a clear colorless oil.

Scale: 10 mmol

Yield: 96%

R_f = 0.98 (pentane, $KMnO_4$)

Purification: SiO_2 (pentane)

Physical State: clear colorless oil

IR (ATR, neat) $\tilde{\nu}_{max}$: 2921, 2850, 1459, 1444 cm^{-1}

HRMS–DART (*m/z*): $[M + H]^+$ calc'd for $C_{13}H_{25}$ 181.1951, found 181.1949

(*E*)-1-methylcyclododec-1-ene (**23*E***)

^{1}H NMR (800 MHz, $CDCl_3$) δ 5.54 – 5.11 (m, 1H), 2.08 (td, *J* = 7.3, 3.2 Hz, 2H), 1.64 (d, *J* = 1.5 Hz, 3H), 1.51 (td, *J* = 7.4, 4.7 Hz, 2H), 1.44 – 1.25 (m, 16H).

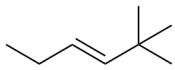
^{13}C NMR (201 MHz, $CDCl_3$) δ 133.6, 128.0, 38.6, 27.92, 27.3, 26.6, 26.3, 25.6, 24.9, 24.4, 24.3, 24.0, 15.2.

(*Z*)-1-methylcyclododec-1-ene (**23*Z***)

^{1}H NMR (800 MHz, $CDCl_3$) δ 5.13 (t, *J* = 7.8 Hz, 1H), 2.07 (q, *J* = 7.1 Hz, 2H), 1.79 – 1.66 (m, 3H), 1.57 – 1.48 (m, 2H), 1.47 – 1.35 (m, 10H), 1.31 – 1.24 (m, 4H).

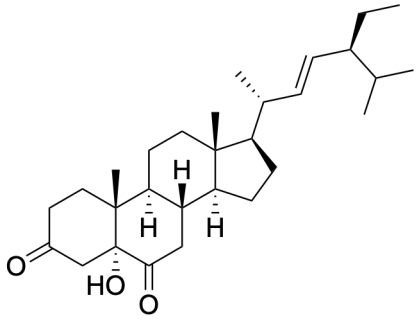
^{13}C NMR (201 MHz, $CDCl_3$) δ 135.4, 126.4, 27.93, 27.5, 25.12, 25.07, 24.9, 24.7, 24.5, 24.1, 23.2, 22.6, 22.4.

Characterization for the (*Z*)-1-methylcyclododec-1-ene matched with literature values [22].



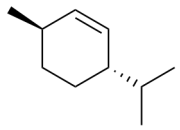
25

(*E*)-2,2-dimethylhex-3-ene (**25**) was prepared from 2-ethyloxirane and *tert*-butyllithium according to a literature procedure [23]. Characterization matched with literature values [24].



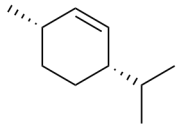
29

(22*R*,23*R*)-5α-hydroxy-22,23-stigmasten-3,6-dione (**29**) was prepared from stigmasterol according to a literature protocol [25,26].



32

(+)-*trans*-p-menth-2-ene (**32**) was prepared from (–)-menthol according to a literature procedure [27].



33

(–)-*cis*-p-menth-2-ene (**33**) was prepared from (+)-2-carene according to a literature procedure [28].

It is important that the (+)-2-carene, catecholborane, and 4-*tert*-butylcatechol required for the alkene synthesis are of good quality and purity to ensure the success of the reaction and ease of purification. For these reasons, (+)-2-carene, catecholborane, and 4-*tert*-butylcatechol were all distilled prior to use. Full characterization of (–)-*cis*-p-menth-2-ene (**33**) was missing from the literature so we have provided it below.

Scale: 8.5 mmol scale

Yield: 46% (541 mg, 86% pure)

Physical State: clear colorless oil

Purification: Al_2O_3 (pentane) then short path vacuum distillation

Boiling Point: 47 ºC, 10 mmHg

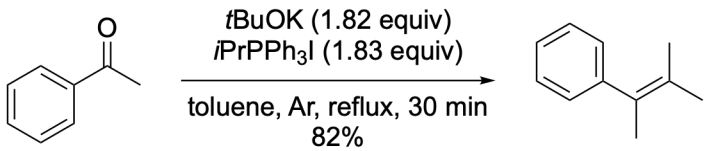
IR (ATR, neat) $\tilde{\nu}_{max}$: 3015, 2955, 2926, 2869, 1457, 1383, 1366, 970, 814, 803, 726, 700 cm^{-1}

GCMS (*m/z*): $[M]^+$ calc'd for $C_{10}H_{18}$ 138.1403, found 138.1.

Specific Rotation: $[\alpha]_D^{24}$ = –36 (c = 1.0, $CHCl_3$)

^{1}H NMR (500 MHz, $CDCl_3$) δ 5.65–5.52 (m, 2H), 2.22–2.10 (m, 1H), 1.85 (tdt, *J* = 8.1, 6.0, 2.4 Hz, 1H), 1.72–1.62 (m, 1H), 1.62–1.33 (m, 4H), 0.97 (d, *J* = 7.2 Hz, 3H), 0.91 (d, *J* = 6.9 Hz, 3H), 0.88 (d, *J* = 6.7 Hz, 3H).

^{13}C NMR (126 MHz, $CDCl_3$) δ 133.6, 130.0, 41.6, 32.3, 29.5, 29.0, 22.1, 21.4, 20.1, 19.9.



36

(3-methylbut-2-en-2-yl)benzene (**36**) was prepared from acetophenone.

Procedure: A 250 mL 2-neck round bottom flask equipped with a water condenser and a Teflon-coated magnetic stirrer bar was flame dried under vacuum. To the flask was added solid potassium *tert*-butoxide (1.12 g, 9.98 mmol, 1.82 equiv) and solid isopropyltriphenylphosphonium iodide (4.32 g, 9.99 mmol, 1.83 equiv). The vessel was evacuated and backfilled three times with argon. At room temperature, dry toluene (40.0 mL) was added, and the heterogeneous mixture was stirred for 5 min. The heterogeneous mixture was then heated to 60 ºC for 30 minutes to form the ylide as a homogeneous red solution. A separate 25 mL round bottom flask was flame-dried under vacuum. To the 25 mL flask was added neat acetophenone (657.6 mg, 5.473 mmol, 1.00 equiv) followed by dry toluene (6 mL). The acetophenone/toluene solution was cannulated dropwise into the 60 ºC ylide solution. Dry toluene (2 x 2 mL) was used to rinse the 25 mL flask to ensure full transfer. The reaction vessel was heated to reflux for 30 minutes, then cooled and quenched for 30 minutes after the dropwise addition of acetone (2 mL). Next, the reaction was filtered through silica (29 g) eluting with hexanes (250 mL). The solvent was removed by rotatory evaporation with a bath temperature of 30 ºC. The residue was transferred to a 50 mL kugelrohr boiling flask. The residue was purified using a Büchi Glass Oven B-585 with two-bulb fractionation. The glass oven was set to 90 ºC and the system pressure was set to 16 mmHg. After one hour at 90 ºC and 16 mmHg, distillation was stopped, and

the material was collected to yield a colorless liquid (654 mg, 82% yield). Characterization matched with the literature values [29,30].

Scale: 5.47 mmol

Yield: 82%

Physical State: colorless liquid

Purification: SiO_2 (29g, hexanes) then kugelrohr distillation (Büchi Glass Oven B-585, 90 ºC oven temperature, 16 mmHg)

Boiling Point: 85–86 ºC, 16 torr [29]

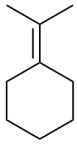
R_f = 0.78 (10% *v/v* EtOAc/hexanes + UV/I_2 stain)

IR (ATR, neat) $\tilde{\nu}_{max}$: 3075, 3055, 3019, 2987, 2913, 2857, 1599, 1490, 1441, 1372, 1207, 1131, 1072, 1025, 909, 764, 700 cm^{-1}

HRMS–DART (*m/z*): $[M + H]^+$ calc'd for $C_{11}H_{15}$ 147.1168 , found 147.1170

^{1}H NMR (400 MHz, $CDCl_3$) δ 7.32 (tt, *J* = 7.3, 0.9 Hz, 2H), 7.20 (ddt, *J* = 7.8, 6.5, 1.2 Hz, 1H), 7.14 (dd, *J* = 8.2, 1.2 Hz, 2H), 1.98 (s, 3H), 1.83 (s, 3H), 1.61 (s, 3H).

^{13}C NMR (101 MHz, $CDCl_3$) δ 145.5, 130.1, 128.6, 128.1, 127.3, 125.8, 22.2, 20.9, 20.7.

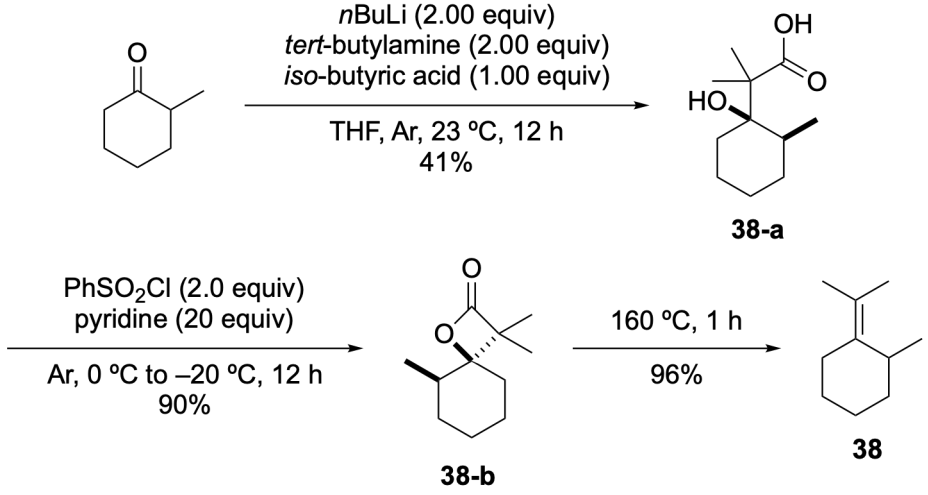


37

Propan-2-ylidenecyclohexane (**37**) was prepared from cyclohexanone according to a literature procedure [31]. The ^{1}H and ^{13}C NMR were missing from the literature, so they are provided below.

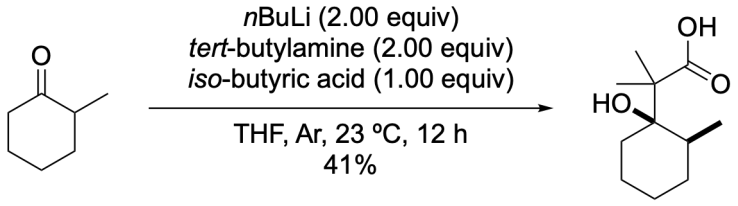
^{1}H NMR (500 MHz, $CDCl_3$) δ 2.23 – 2.10 (m, 4H), 1.66 (s, 6H), 1.58 – 1.46 (m, 6H).

^{13}C NMR (126 MHz, $CDCl_3$) δ 132.3, 120.2, 30.5, 28.2, 27.1, 20.0.



The 3-step synthesis of 1-methyl-2-(propan-2-ylidene)cyclohexane (**38**) from 2-methylcyclohexanone was adapted from a literature procedure [31].

Step 1: Aldol



38-a

A flame-dried 250 mL round-bottom flask equipped with a magnetic stir bar was evacuated and backfilled with argon (3x). The *t*BuNH$_2$ (2.93 g, 4.20 mL, 40.0 mmol, 2.00 equiv) and anhydrous THF (15.8 mL) were added to make a 1.0 M solution. While stirring magnetically, a stoichiometric amount (equal to the quantity of amine) of *n*-butyllithium in hexane (2.5 M, 2.56 g, 16.0 mL, 40.0 mmol, 2.00 equiv) was added dropwise. After 15 min, a stoichiometric amount (half the amount of amine) of *iso*-butyric acid (1.76 g, 1.86 mL, 20.0 mmol, 1.00 equiv) to be converted into its lithium *n*-lithiocarboxylate was injected as a 1.0 M solution in anhydrous THF and allowed to stir for 1.0 hr. Subsequently, a stoichiometric amount (equal to the quantity of carboxylic acid) of the 2-methylcyclohexanone (2.24 g, 20.0 mmol, 1.00 equiv, in 8 mL THF) as a 2.5 M solution in anhydrous THF was added at room temperature and the mixture allowed to stir overnight. After 12 hours, the reaction mixture was poured on ice and transferred to a separatory funnel using ethyl acetate. After 4 extractions with ethyl acetate (25 mL each), the aqueous layer was acidified with 6 N aqueous hydrochloric acid (8 mL). The aqueous layer was then extracted with ethyl acetate (3 x 20 mL). Those organic layers were combined, washed with brine (20 mL), dried over sodium sulfate, filtered through cotton, and evaporated. Excess *iso*-butyric acid was removed at 40 ºC under high vacuum (1 mmHg). The crude material was then purified by recrystallization from chloroform to afford

2-((1*R**,2*S**)-1-hydroxy-2-methylcyclohexyl)-2-methylpropanoic acid as white cubic crystals. The first crop contained 1.26 g (32%) second crop contained 372 mg (9%).

Scale: 20.0 mmol

Yield: 41% (1.63 g)

Physical State: white cubic crystals

Purification: recrystallization from chloroform

Melting Point: 123–125 ºC

R_f = 0.61 (50% *v/v* EtOAc/hexanes + vanillin stain)

IR (ATR, neat) $\tilde{\nu}_{max}$: 3228, 2984, 2929, 2855, 1698, 1451, 1268, 1164, 1097, 1062, 1022, 984, 957, 911, 887 cm^{-1}

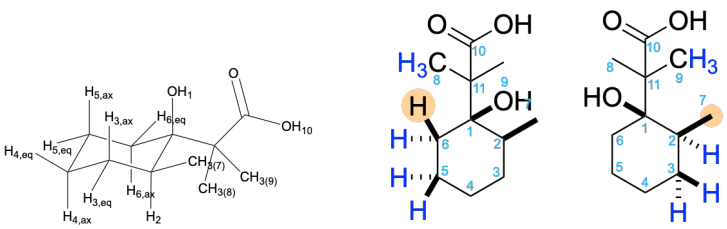
HRMS–DART (*m/z*): $[M + H]^+$ calc'd for $C_{11}H_{21}O_3$ 201.1485, found 201.1486

$[M – H]^–$ calc'd for $C_{11}H_{19}O_3$ 199.1340, found 199.1334

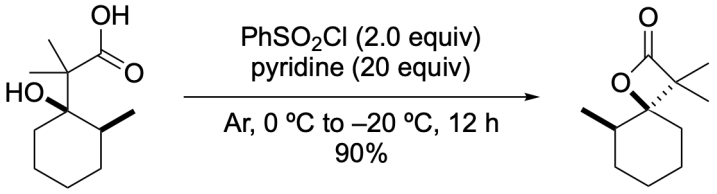
^{1}H NMR (800 MHz, $CDCl_3$) δ 10.13 (br, 1H), 4.31 (br, 1H), 1.81 (d, *J* = 13.0 Hz, 1H), 1.76 – 1.62 (m, 3H), 1.52 – 1.37 (m, 4H), 1.26 (d, *J* = 23.4 Hz, 7H), 0.87 (d, *J* = 7.0 Hz, 3H).

^{13}C NMR (201 MHz, $CDCl_3$) δ 181.8, 78.1, 48.1, 37.4, 32.2, 31.6, 25.8, 23.3, 21.5, 20.8, 16.3.

2D NMR (HSQC) and **1D Selective Gradient NOESY** were used to determine the relative configuration. The methyl (C_7) was assigned as equatorial because there was no NOE correlation between $H_{5,ax}$ and H_7. $H_{5,ax}$ can be clearly seen in the 1D Selective Gradient NOESY irradiation of $H_{6,eq}$. The same signal for $H_{5,ax}$ is missing from the 1D selective Gradient NOESY irradiation of H_7.



Step 2. Mixed Anhydride Lactonization



38-a **38-b**

Procedure: To a 50 mL RBF was added 2-((1*R**,2*S**)-1-hydroxy-2-methylcyclohexyl)-2-methylpropanoic acid (1.25 g, 6.24 mmol, 1.00 equiv). The flask was sealed and evacuated/backfilled 3x with argon. Then dry pyridine (9.87 g, 10.1 mL, 125 mmol, 20.0 equiv) was added and the flask was manipulated until the solution was homogeneous. The flask was then placed in an ice bath and cooled to 0 ºC before addition of benzenesulfonyl chloride (2.20 g, 1.60 mL, 12.5 mmol, 2.00 equiv). The solution was swirled to ensure full mixing then placed in the freezer at –20 ºC overnight. After completion, the reaction was transferred to a separatory funnel and water was added (50 mL). The aqueous layer was extracted with diethyl ether (4 x 15 mL) and the combined organics were washed with 1M aq. HCl (3 x 10 mL), sat. aq. $NaHCO_3$ (3 x 10 mL), brine (15 mL), dried over sodium sulfate, filtered through cotton and evaporated. The residue was further purified through Al_2O_3 (25% V/V Et_2O/hexanes) to afford the product as a clear colorless oil (1.03 g, 90% yield).

Scale: 6.24 mmol

Yield: 90% (1.03 g)

***R*$_f$** = 0.27 (10% *v/v* EtOAc/hexanes + vanillin stain)

Purification: Al_2O_3 (0 – 25% *v/v* Et_2O/hexanes)

Physical State: clear colorless oil

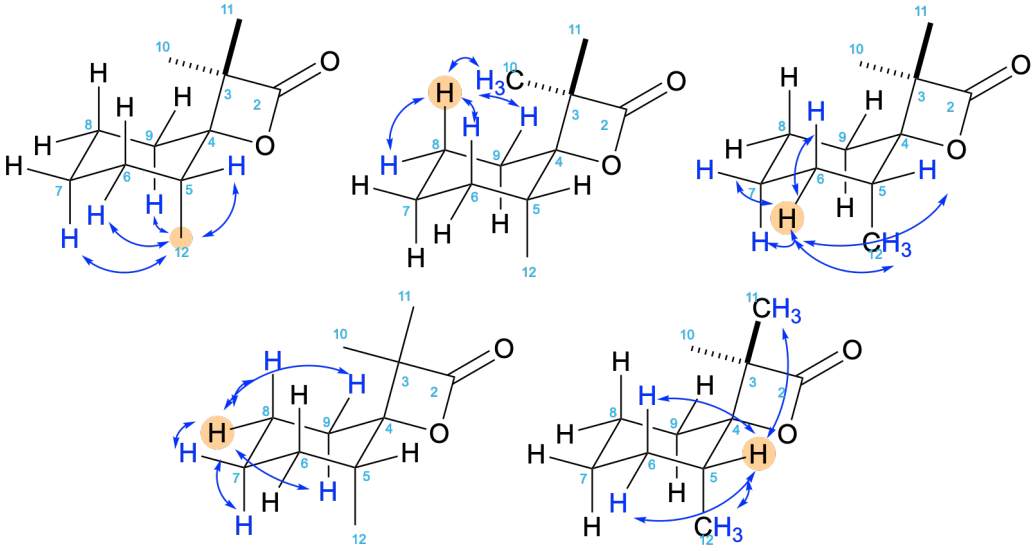
IR (ATR, neat) $\tilde{\nu}_{max}$: 2972, 2937, 2866, 1811, 1469, 1446, 1398, 1375, 1192, 1120, 1038, 1011, 997, 899, 838 cm^{-1}

HRMS–DART (*m/z*): $[M + H]^+$ calc'd for $C_{11}H_{19}O_2$ 183.1380, found 183.1372

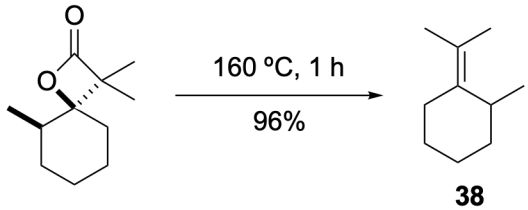
^{1}H NMR (800 MHz, $CDCl_3$) δ 2.47 – 2.29 (m, 1H), 1.99 – 1.90 (m, 2H), 1.80 (ddt, *J* = 13.7, 3.6, 1.6 Hz, 1H), 1.69 – 1.63 (m, 1H), 1.51 – 1.38 (m, 9H), 1.24 – 1.17 (m, 1H), 1.09 (dd, *J* = 7.0, 1.5 Hz, 3H).

^{13}C NMR (201 MHz, $CDCl_3$) δ 176.2, 87.7, 54.6, 33.4, 30.5, 27.7, 24.5, 19.2, 18.7, 18.5, 13.8.

2D NMR (COSY and HSQC) and **1D Selective Gradient NOESY** were used to assign configuration.



Step 3: Pyrolysis



38-b **38**

Procedure: To a 25 mL RBF was added (4R*,5S*)-3,3,5-trimethyl-1-oxaspiro[3.5]nonan-2-one (725 mg, 3.98 mmol, 1.00 equiv). A Hickman condenser was attached, and the vessel was insulated with aluminum foil. The condenser was cooled with acetone-soaked cotton. The apparatus was evacuated and backfilled 3x with argon then placed into an oil bath. The reaction was heated to 160 ºC for 1 hour. During this time, the CO_2 off-gassing was observable. After 1 hour, the bath temperature was raised to 210 ºC and the 1-methyl-2-(propan-2-ylidene)cyclohexane was distilled (bp: 190–192 ºC) to provide a clear colorless oil (529 mg) in 96% yield.

Scale: 3.98 mmol

Yield: 96% (529 mg)

R_f = 0.80 (hexanes + $KMnO_4$ stain)

Purification: Hickman distillation, 1 atm, Ar

Physical State: clear colorless oil

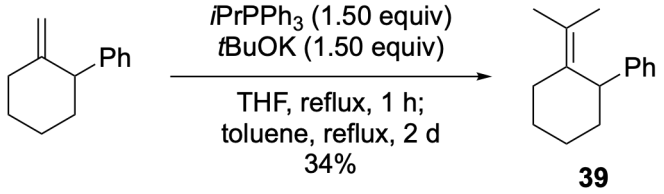
Boiling Point: 190–192 ºC, 1 atm

IR (ATR, neat) $\tilde{\nu}_{max}$: 2964, 2923, 2858, 1458, 1371, 1052, 1024, 917, 859 cm^{-1}

HRMS–DART (*m/z*): $[M + H]^+$ calc'd for $C_{10}H_{19}$ 139.1481, found 139.1478

^{1}H NMR (500 MHz, $CDCl_3$) δ 2.93 (td, *J* = 7.6, 4.5 Hz, 1H), 2.49 (dt, *J* = 14.2, 3.7 Hz, 1H), 1.86 (tdt, *J* = 14.0, 4.0, 2.0 Hz, 1H), 1.76 – 1.70 (m, 1H), 1.66 (d, *J* = 2.3 Hz, 3H), 1.64 (d, *J* = 1.8 Hz, 3H), 1.60 – 1.45 (m, 4H), 1.22 – 1.12 (m, 1H), 1.01 (d, *J* = 7.2 Hz, 3H).

^{13}C NMR (126 MHz, $CDCl_3$) δ 135.4, 120.3, 33.4, 31.3, 27.8, 25.1, 21.0, 20.3, 19.8, 18.2.



39

(Methylenecyclohexyl)benzene was prepared from 2-phenylcyclohexanone according to a literature procedure [32]. The synthesis of (2-(propan-2-ylidene)cyclohexyl)benzene (**39**) from (methylenecyclohexyl)benzene was adapted from a literature procedure [33].

Procedure: To a 250 mL RBF equipped with a Teflon-coated magnetic stirrer bar was added isopropyl triphenylphosphonium bromide (2.49 g, 6.46 mmol, 1.00 equiv) and potassium *tert*-butoxide (724 mg, 6.46 mmol, 1.00 equiv) in the glovebox. The flask was sealed and transferred to the Schlenk line. Dry THF (22 mL) was added, and the solution was stirred at 23 ºC for 10 min. The solution became red. 2-phenylcyclohexanone (750 mg, 4.30 mmol, 1.00 equiv) was added as a solution in THF (4 mL + 3 x 2 mL rinse). The reaction was heated to 50 ºC for 1 hour and there was no conversion. The THF was distilled off (27 mL) through a distillation head and replaced with toluene (20 mL). A reflux condenser was attached then the reaction was heated to reflux for 2 days. After 2 days, the reaction was cooled to room temperature and filtered through SiO_2 (hexanes). The residue was further purified through FCC (hexanes) to afford (2-(propan-2-ylidene)cyclohexyl)benzene (**39**) as a clear colorless liquid (295 mg, 34% yield).

Scale: 4.30 mmol

Yield: 34% (295 mg)

R_f = 0.61 (hexanes + UV/$KMnO_4$ stain)

Purification: SiO_2 (hexanes)

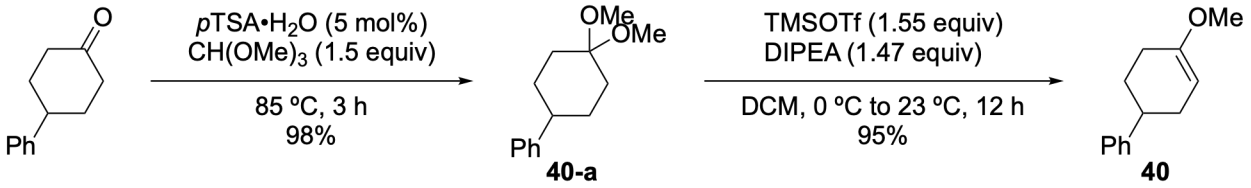
Physical State: clear colorless liquid

IR (ATR, neat) $\tilde{\nu}_{max}$: 3083, 3058, 3021, 2926, 2856, 1495, 1446, 1032, 747, 704 cm^{-1}

HRMS–DART (*m/z*): $[M]^+$ calc'd for $C_{15}H_{20}$ 200.1560, found 200.1565

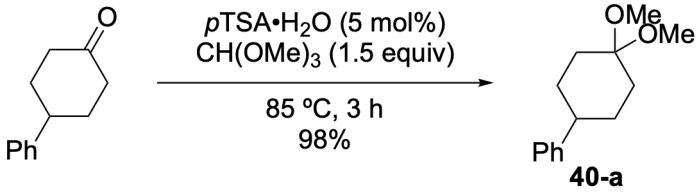
^{1}H NMR (400 MHz, $CDCl_3$) δ 7.32 – 7.26 (m, 4H), 7.19 – 7.13 (m, 1H), 4.06 (t, *J* = 4.2 Hz, 1H), 2.64 – 2.53 (m, 1H), 2.43 – 2.35 (m, 1H), 1.83 – 1.65 (m, 9H), 1.53 – 1.38 (m, 2H), 1.35 – 1.26 (m, 1H).

^{13}C NMR (101 MHz, $CDCl_3$) δ 143.7, 133.0, 128.3, 127.7, 125.4, 124.2, 41.0, 30.6, 27.7, 26.6, 21.6, 20.4, 20.3.



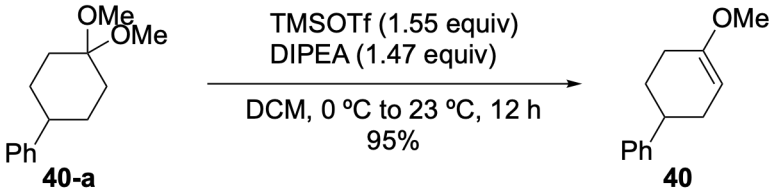
4-Methoxy-1,2,3,6-tetrahydro-1,1'-biphenyl (**40**) was synthesized in 2-steps from 4-phenylcyclohexanone.

Step 1: Ketalization



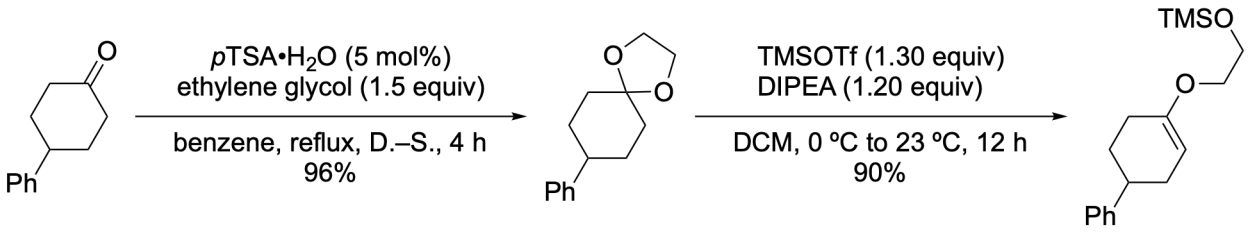
Procedure: To a 25 mL round bottom flask equipped with a Teflon-coated magnetic stirrer bar was added 4-phenylcyclohexanone (5.00 g, 28.7 mmol, 1.00 equiv) and *p*-toluenesulfonic acid monohydrate (*p*TSA•H_2O, 273 mg, 1.43 mmol, 5 mol%). The contents were dissolved in trimethylorthoformate (4.57 g, 4.71 mL, 43.0 mmol, 1.50 equiv). To the flask was added a Vigureaux column (7 cm) and a distillation head. The reaction was heated to 85 ºC until methanol ceased to distill (~3 h). The crude was cooled to room temperature, diluted with diethyl ether, filtered through SiO_2 (eluting with diethyl ether) and evaporated to provide an orange solid. The residue was purified through FCC (SiO_2, 25% DCM/hexanes) to afford (4,4-dimethoxycylohexyl)benzene (**40-a**) as a white solid (6.20 g, 98%). Characterization matched with the literature values [34].

Step 2: Enolization



The synthesis of 4-methoxy-1,2,3,6-tetrahydro-1,1'-biphenyl (**40**) was adapted from a literature procedure [35].

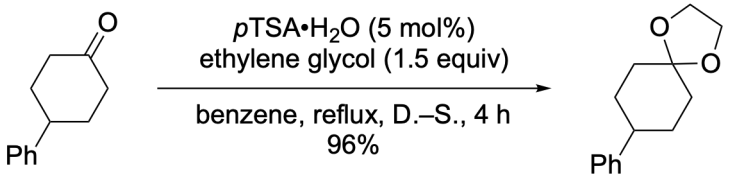
Procedure: To a flame dried RBF equipped with a Teflon-coated magnetic stirrer bar, was added (4,4-dimethoxycyclohexyl)benzene (1.10 g, 5.00 mmol, 1.00 equiv) and dissolved in dry DCM (8.20 mL). The solution was cooled to 0 ºC in an ice/water bath then freshly distilled dry DIPEA (1.00 g, 1.35 mL, 7.75 mmol, 1.55 eqiv) was added drop-wise. Next, TMSOTf (1.64 g, 1.36 mL, 7.37 mmol, 1.47 equiv) was added dropwise. A cloud of gas formed within the reaction vessel and slowly disappeared. The reaction was stirred overnight at room temperature. Approximately half of the DCM was removed by rotatory evaporation then pentane was added to precipitate the DIPEA•HOTf. The mixture was cooled to –20 ºC for 3 hours, then the cold supernatant was loaded onto an SiO_2 column packed with hexanes + 0.5% (v/v) Et_3N. The solids were triturated with pentane (3 x 1 mL) and also added to the column. The product was then purified through FCC (hexanes + 0.5% *v/v* Et_3N) to afford 4-methoxy-1,2,3,6-tetrahydro-1,1'-biphenyl (**40**) in 95% yield (893 mg) as a clear colorless liquid. Characterization matched with literature values [36].



41-a **41**

Trimethyl(2-((1,2,3,6-tetrahydro-[1,1'-biphenyl]-4-yl)oxy)ethoxy)silane (**41**) was synthesized in 2-steps from 4-phenylcyclohexanone.

Step 1: Ketalization



41-a

8-Phenyl-1,4-dioxaspiro[4.5]decane (**41-a**) was prepared through an adapted literature procedure [17]. Full characterization was missing from the literature, so we have provided it below.

Procedure: To a 100 mL round bottom flask equipped with a Teflon-coated magnetic stirrer bar was added 4-phenylcyclohexanone (3.93 g, 22.6 mmol, 1.00 equiv) and *p*-toluenesulfonic acid monohydrate (21.5 mg, 0.113 mmol, 0.500 mol%). Next, dry benzene was added (45 mL) and the mixture was stirred until it was homogeneous. Ethylene glycol (1.68 g, 1.51 mL, 27.1 mmol, 1.20 equiv) was added via syringe. A Dean–Stark apparatus was affixed, and the mixture was refluxed for 4 hours. The reaction mixture was cooled to room temperature, and then half of the volume was removed by rotatory evaporation. The remaining solution was directly loaded to a column packed with SiO_2/hexanes and

eluted with 5% *v/v* EtOAc/hexanes. The pure fractions were collected and evaporated to provide 8-phenyl-1,4-dioxaspiro[4.5]decane (**41-a**) as a white amorphous solid (4.71 g) in 96% yield.

Scale: 22.6 mmol (3.93 g)

Yield: 96% (4.71 g)

R_f = 0.45 (15% *v/v* EtOAc/hexane + UV/vanillin stain)

Purification: SiO_2 (0–5% *v/v* EtOAc/hexanes)

Physical State: white amorphous solid

Melting Point: 54–56 ºC

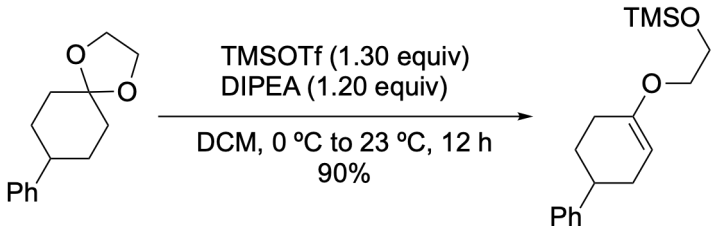
IR (ATR, neat) $\tilde{\nu}_{max}$: 2930, 2872, 1493, 1445, 1373, 1363, 1282, 1239, 1171, 1128, 1096, 1034, 964, 943, 924, 904, 867, 799, 755, 698, 664 cm^{-1}

HRMS–DART (*m/z*): $[M + H]^+$ calc'd for $C_{14}H_{19}O_2$ 219.1380, found 219.1377

^{1}H NMR (600 MHz, $CDCl_3$) δ 7.33 (t, *J* = 7.6 Hz, 2H), 7.31–7.26 (m, 2H), 7.26–7.19 (m, 1H), 4.02 (s, 4H), 2.60 (tt, *J* = 11.8, 3.6 Hz, 1H), 1.95–1.80 (m, 6H), 1.74 (td, *J* = 12.9, 4.9 Hz, 2H).

^{13}C NMR (151 MHz, $CDCl_3$) δ 146.7, 128.4, 127.0, 126.2, 108.6, 64.4, 64.4, 43.4, 35.2, 31.7.

Step 2: Enolization



41-a **41**

Trimethyl(2-((1,2,3,6-tetrahydro-[1,1'-biphenyl]-4-yl)oxy)ethoxy)silane (**41**) was prepared through an adapted literature procedure [35].

Procedure: To a flame-dried round bottom flask equipped with a Teflon-coated magnetic stirrer bar was added 8-phenyl-1,4-dioxaspiro[4.5]decane (0.990 g, 4.54 mmol, 1.00 equiv) followed by dry DCM (7.4 mL) and stirred until homogeneous. The mixture was cooled to 0 ºC in an ice-water bath and DIPEA (0.762 g, 1.03 mL, 5.90 mmol, 1.30 equiv), was added. TMSOTf (1.21 g, 1.00 mL, 5.4 mmol, 1.2 equiv) was added via syringe to the stirred solution dropwise over a period of approximately 5 min. The solution was allowed to warm to, and was subsequently stirred at, ambient temperature for 12 hours. After completion, approximately 70% of the solvent was removed by distillation at atmospheric pressure and replaced with a roughly equal volume of pentane, added dropwise with vigorous stirring. The resulting slurry was sealed and cooled to –20 ºC overnight for 2 hours to assist in precipitating the DIPEA•HOTf salt. After the supernatant solution was removed, the residual salt was rinsed with three 100-mL portions of pentane. The filtrate was directly loaded onto an SiO_2 column and purified by FCC (1% *v/v* EtOAc/hexanes) to afford trimethyl(2-((1,2,3,6-tetrahydro-[1,1'-biphenyl]-4-yl)oxy)ethoxy)silane (**41**) as a clear colorless oil (1.18 g, 4.06 mmol) in 90% yield.

Scale: 4.54 mmol

Yield: 90% (1.18 g)

Physical State: clear colorless liquid

Purification: FCC (1% *v/v* EtOAc/hexanes)

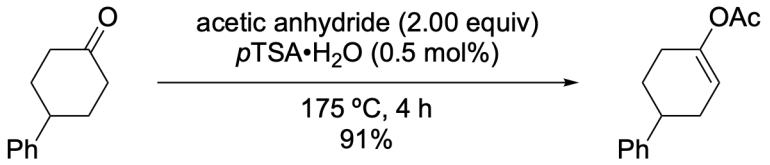
R_f = 0.34 (5% *v/v* / + UV/vanillin stain)

IR (ATR, neat) $\tilde{\nu}_{max}$: 3061, 3027, 2953, 2927, 2872, 2842, 1249, 1217, 1185, 1134, 1107, 874, 840, 754, 699 cm^{-1}

HRMS–DART (*m/z*): $[M + H]^+$ calc'd for $C_{17}H_{27}O_2Si$ 291.1775, found 291.1771

^{1}H NMR (600 MHz, $CDCl_3$) δ 7.31 (t, *J* = 7.5 Hz, 2H), 7.26 – 7.23 (m, 2H), 7.20 (td, *J* = 7.0, 1.4 Hz, 1H), 4.75 – 4.62 (m, 1H), 3.86 (t, *J* = 5.2 Hz, 2H), 3.75 (qt, *J* = 10.2, 5.1 Hz, 2H), 2.77 (tdd, *J* = 11.2, 5.1, 3.0 Hz, 1H), 2.38 – 2.28 (m, 2H), 2.26 – 2.14 (m, 2H), 1.98 (ddt, *J* = 15.3, 5.5, 2.5 Hz, 1H), 1.87 (qd, *J* = 12.2, 5.6 Hz, 1H), 0.16 (d, *J* = 0.9 Hz, 9H).

^{13}C NMR (151 MHz, $CDCl_3$) δ 154.5, 146.9, 128.5, 127.0, 126.2, 93.6, 67.9, 61.6, 40.6, 32.0, 29.9, 28.4.



42

1,2,3,6-tetrahydro-[1,1'-biphenyl]-4-yl acetate (**42**) was prepared from 4-phenylcyclohexanone through an adapted a literature procedure [37].

Procedure: To a 25 mL round-bottom flask equipped with a Teflon-coated magnetic stirrer bar was added 4-phenylcyclohexanone (3.49 g, 20.0 mmol, 1.00 equiv) and *p*-toluenesulfonic acid monohydrate (*p*TSA•H_2O, 19.0 mg, 0.500 mol%), and acetic anhydride (4.08 g, 3.77 mL, 40.0 mmol, 2.00 equiv). The vessel was capped with a 7 cm Vigureaux column and a distillation head then heated to a bath temperature of 175 ºC until distillation of AcOH ceased (~4 hours). The reaction was then cooled to room temperature and diluted with diethyl ether. The solution was transferred to a separatory funnel and washed with sat. aq. $NaHCO_3$ (4 x 25 mL), water (2 x 25 mL), brine (25 mL), dried over sodium sulfate, filtered through cotton, and evaporated. The orange solid was adsorbed onto SiO_2 and purified through SiO_2 (0–5% *v/v* Et_2O/hexanes) to afford 1,2,3,6-tetrahydro-[1,1'-biphenyl]-4-yl (**25**) as a pale-yellow solid (3.94 g, 91%).

Scale: 20.0 mmol

Yield: 91% (3.94 g)

R_f = 0.56 (15% *v/v* EtOAc/hexanes + UV/vanillin stain)

Purification: SiO_2 (adsorbed onto SiO_2 then 0–5% *v/v* Et_2O/hexanes)

Physical State: pale-yellow solid

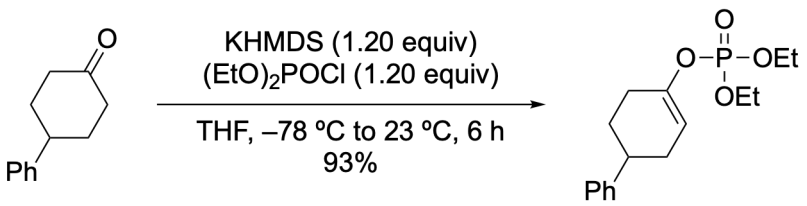
Melting Point: 66–68 ºC

IR (ATR, neat) $\tilde{\nu}_{max}$: 3087, 3061, 3028, 3002, 2925, 2894, 2840, 1753, 1692, 1495, 1453, 1368, 1225, 1207, 1118, 1039, 912, 759, 700, 632, 616 cm^{-1}

HRMS–DART (*m/z*): $[M + Na]^+$ calc'd for $C_{14}H_{16}O_2Na$ 239.1048, found 239.1041.

^{1}H NMR (500 MHz, CDCl3) δ 7.34 – 7.28 (m, 2H), 7.25 – 7.18 (m, 3H), 5.46 (dt, J = 4.6, 2.3 Hz, 1H), 2.91 – 2.82 (m, 1H), 2.49 – 2.34 (m, 2H), 2.28 (dddd, J = 17.1, 13.1, 4.3, 2.4 Hz, 1H), 2.23 – 2.09 (m, 4H), 2.04 – 1.88 (m, 2H).

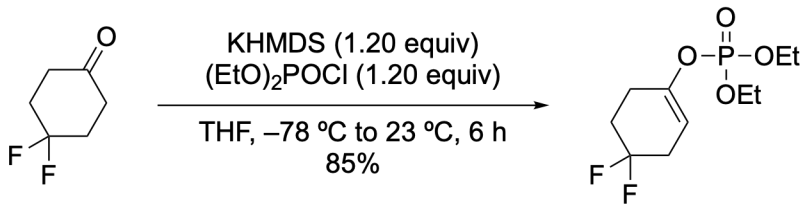
^{13}C NMR (126 MHz, CDCl3) δ 169.7, 148.4, 146.1, 128.6, 127.0, 126.4, 113.9, 39.6, 31.8, 29.8, 27.4, 21.3.



43

Diethyl (1,2,3,6-tetrahydro-[1,1'-biphenyl]-4-yl) phosphate (**43**) was prepared from 4-phenylcyclohexanone according to modified literature procedure [38].

Procedure: A flame-dried round-bottom flask equipped with a Teflon-coated magnetic stirrer bar was evacuated and backfilled with argon (3x) then charged with THF (10.0 ml) and KHMDS (1.20 g, 8.00 mL, 0.75 M, 1.2 equiv, 6.00 mmol). The reaction mixture was cooled to –78 °C. A separate flame-dried round-bottom flask equipped with a Teflon-coated magnetic stirrer bar was evacuated and backfilled with argon (3x) then charged with 4-phenylcyclohexan-1-one (871 mg, 1.0 equiv, 5.00 mmol) and THF (10.0 mL). The ketone solution was added to the reaction mixture dropwise via cannula. The ketone flask was washed with THF (2 x 2.5 mL). The reaction mixture was allowed to stir at –78 °C for 20 minutes then 1-[chloro(ethoxy)phosphoryl]oxyethane (1.04 g, 870 µL, 1.2 equiv, 6.00 mmol) was added. The reaction mixture was allowed to slowly warm to room temperature over the course of 6 hours (as the cold bath warmed). The reaction mixture was diluted with ether (20 mL) and quenched with 25% aq. $NaHCO_3$ (25 mL). The aqueous layer was extracted with ether (3 x 25 mL). The combined organics were washed with water then brine, dried over sodium sulfate, filtered, and concentrated *in vacuo*. The residue was purified through FCC (15%–30% *v/v* EtOAc/hexanes) to afford diethyl (1,2,3,6-tetrahydro-[1,1'-biphenyl]-4-yl) phosphate as a yellow liquid in 93% yield (1.44 g, 4.64 mmol). Characterization matches with what is previously described in the literature [39].



44

4,4-Difluorocyclohex-1-en-1-yl diethyl phosphate (**44**) was prepared from 4-phenylcyclohexanone according to modified literature procedure [38].

Procedure: A 50 mL flame-dried round-bottom flask equipped with a Teflon-coated magnetic stirrer bar was evacuated and backfilled with argon (3x) then charged with THF (10.0 ml) and KHMDS (718 mg, 1.2 equiv, 3.60 mmol) in a glovebox. The flask was removed from the glovebox and placed under a positive pressure of argon on the Schlenk line. THF (8.0 mL) was added to the flask to dissolve the KHMDS and the reaction mixture was cooled to –78 °C. A separate 25 mL flame-dried round-bottom flask equipped with a Teflon-coated magnetic stirrer bar was evacuated and backfilled with argon (3x) then charged with 4,4-difluorocyclohexanone (402 mg, 1.0 equiv, 3.00 mmol) and THF (12.0 mL). The ketone solution was added to the reaction mixture dropwise via cannula. The ketone flask was washed with THF (2 x 2.0 mL). The reaction mixture was allowed to stir at –78 °C for 30 minutes then 1-[chloro(ethoxy)phosphoryl]oxyethane (621 mg, 520 µL, 1.2 equiv, 3.60 mmol) was added. The reaction mixture was allowed to slowly warm to room temperature over the course of 6 hours (as the cold bath warmed). The reaction mixture was diluted with ether (15 mL) and quenched with 25% aq. $NaHCO_3$ (10 mL). The aqueous layer was extracted with ether (3 x 15 mL). The combined organics were washed with water then brine, dried over sodium sulfate, filtered, and concentrated *in vacuo*. The

residue was purified through FCC (40% *v/v* EtOAc/hexanes) to afford the 4,4-difluorocyclohex-1-en-1-yl diethyl phosphate (**44**) as a yellow liquid in 85% yield (687 mg, 2.54 mmol).

Scale: 3.00 mmol

Yield: 85% (687 mg)

R_f = 0.47 (60% *v/v* / + Vanillin stain)

Purification: SiO_2 (40% *v/v* EtOAc/hexanes)

Physical State: yellow liquid

IR (ATR, neat) $\tilde{\nu}_{max}$: 2984, 2936, 1685, 1440, 1381, 1349, 1268, 1155, 1118, 1022, 957, 886, 822 cm^{-1}

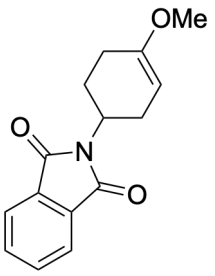
HRMS–DART (*m/z*): $[M + H]^+$ calc'd for $C_{10}H_{17}O_4F_2P$ 271.0905, found 271.0895

^{1}H NMR (600 MHz, $CDCl_3$) δ 5.37 (dddq, *J* = 4.9, 3.9, 2.5, 1.3 Hz, 1H), 4.20 – 4.10 (m, 4H), 2.58 (t, *J* = 13.9 Hz, 2H), 2.46 (dtq, *J* = 6.8, 4.5, 2.2 Hz, 2H), 2.12 (dq, *J* = 13.4, 6.9 Hz, 2H), 1.37 – 1.32 (m, 6H).

^{13}C NMR (151 MHz, $CDCl_3$) δ 146.4 (d, *J* = 8.7 Hz), 121.7 (t, *J* = 240.5 Hz), 105.7 (q, *J* = 6.0 Hz), 64.6 (d, *J* = 6.3 Hz), 33.0 (t, *J* = 27.8 Hz), 30.2 (t, *J* = 25.5 Hz), 25.7 (q, *J* = 5.7 Hz), 16.2 (d, *J* = 6.8 Hz).

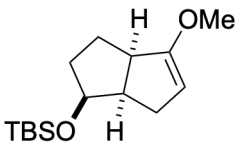
^{19}F NMR (565 MHz, $CDCl_3$) δ -97.00 – -99.60 (m).

^{31}P NMR (243 MHz, $CDCl_3$) δ -6.46.



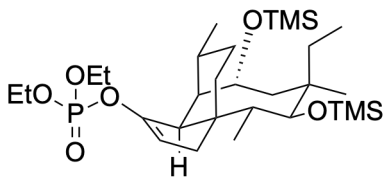
45

2-(4-methoxycyclohex-3-en-1-yl)isoindoline-1,3-dione (**45**) was prepared according to a literature procedure [36].



48

tert-butyl(((1*S*,3a*R*,6a*R*)-4-methoxy-1,2,3,3a,6,6a-hexahydropentalen-1-yl)oxy)dimethylsilane (**48**) was prepared according to a literature procedure [36].



49

Compound **49a** was prepared according to a literature procedure [36]. Diethyl ((3a*S*,4*R*,5*S*,7*R*,8*S*,9*R*,9a*S*,12*R*)-7-ethyl-7,9,12-trimethyl-5,8-bis((trimethylsilyl)oxy)-1,3a,4,5,6,7,8,9-octahydro-4,9a-propanocyclopenta[8]annulen-3-yl) phosphate (**49**) was prepared from compound **49-a** according to a modified literature procedure [38].

Scale: 1.25 mmol.

Yield: 88% (0.661 g).

Physical State: White solid.

R_f = 0.17 (15% *v/v* EtOAc/hexanes + vanillin).

Purification: SiO_2 (8% *v/v* EtOAc/hexanes to 15% *v/v* EtOAc/hexanes).

Melting Point: 56–58 ºC.

IR (ATR, neat) $\tilde{\nu}_{max}$: 2951, 2932, 1249, 1056, 1032, 987, 951, 898, 887, 857, 833 cm^{-1}.

HRMS–ESI (*m/z*): $[M + H]^+$ calc'd for $C_{30}H_{60}O_6PSi_2$ 603.3661, found 603.3674.

Specific Rotation: $[a]_D^{23.6\,°C}$ = –16.00 (*c* 1.0, $CHCl_3$).

^{1}H NMR (500 MHz, $CDCl_3$) δ 5.26 (dq, *J* = 3.3, 1.5 Hz, 1H), 4.43 (d, *J* = 8.3 Hz, 1H), 4.24–4.13 (m, 4H), 3.70 (d, *J* = 6.2 Hz, 1H), 2.82 (d, *J* = 2.9 Hz, 1H), 2.13–1.99 (m, 2H), 1.91 (dq, *J* = 15.1, 7.7 Hz, 1H), 1.75 (dd, *J* = 16.1, 8.4 Hz, 1H), 1.69–1.62 (m, 2H), 1.60–1.46 (m, 3H), 1.36 (tt, *J* = 7.1, 0.9 Hz, 6H), 1.32–1.22 (m, 3H), 1.16 (s, 3H), 0.93 (t, *J* = 7.6 Hz, 3H), 0.90–0.85 (m, 6H), 0.80 (d, *J* = 7.1 Hz, 3H), 0.13 (s, 9H), 0.08 (s, 9H).

^{13}C NMR (126 MHz, $CDCl_3$) δ 152.9 (d, *J* = 10.0 Hz), 107.5 (d, *J* = 3.3 Hz), 78.4, 67.9, 64.4 (dd, *J* = 8.7, 6.1 Hz), 52.0 (d, *J* = 6.0 Hz), 48.2, 46.7, 42.5, 41.5, 38.7, 35.83, 35.76, 31.9, 27.9, 27.6, 24.9, 18.8, 16.8, 16.3 (t, *J* = 6.4 Hz), 13.3, 10.3, 1.7, 1.2.

^{31}P NMR (243 MHz, $CDCl_3$) δ –6.6.

6.8.4 Direct Quantitative NMR (qNMR) Measurement of Alkene Ozonolysis

6.8.4.1 General Procedure

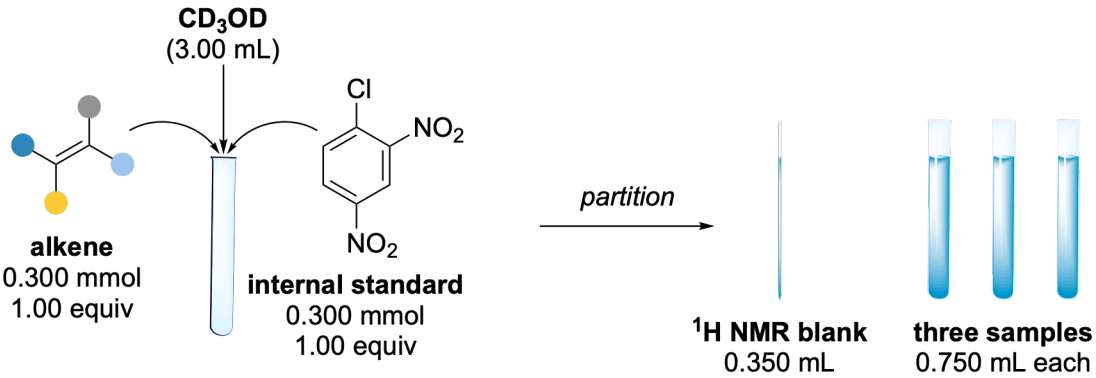


Figure 6.13 Sample Preparation

Step 1: Sample Preparation (Figure 6.13)

1. Stock Solution: Combine the alkene (0.300 mmol, 1.00 equiv) and 1-chloro-2,4-dinitrobenzene (60.8 mg, 0.300 mmol, 1.00 equiv) in a 10 mL test tube. Add CD_3OD (3.00 mL) and sonicate it until completely homogeneous.
2. Blank Sample: Remove a 0.35 mL aliquot and transfer it to an NMR tube to be the blank.
3. Partitioning: Divide the remaining mixture into three separate 10 mL test tubes (0.750 mL each). Cap all tubes with a rubber septum and cool to –78 ºC in an acetone/dry ice bath.

Step 2: ^{1}H NMR Baseline Acquisition

1. Spectrometer Optimization: Use the blank sample to establish the solvent lock, tuning and matching, shimming, and all other acquisition parameters on the spectrometer. Establishing these settings beforehand eliminates instrument delays between ozonation and measurement to enable rapid measurement of samples.

Significant delay between sample ozonation and sample measurement was observed to skew results in some cases.

2. Pre-ozonation measurement: Acquire the ^{1}H NMR spectrum (relaxation delay, D1 = 10 s, 32 scans) of the blank sample.

Step 3: Ozonolysis

1. Open one tube to air and bubble oxygen through a 16G x 4” needle at 1.0 L/min.
2. Turn on the ozone generator (Globazone GO-D3G) at 0.74 A (maximum value).
3. Run the reaction for the designated time. Some reactions are intentionally stopped short of full conversion to prevent over-oxidation of generated aldehydes.
4. Turn off the ozone generator and immediately purge excess ozone and oxygen by sparging with air through the needle into the solution for 10 seconds. Failure to completely remove excess ozone or oxygen will cause severe shimming issues during ^{1}H NMR acquisition due to the presence of paramagnetic species.

Step 4: ^{1}H NMR Acquisition of Ozonized Samples

1. Warm the sample to room temperature in a water bath for 10 seconds.
2. Transfer the entire solution to a clean NMR tube.
3. Measure the ^{1}H NMR (relaxation delay, D1 = 10 s, 32 scans) immediately. These samples are prone to decomposition at room temperature and must be loaded and scanned without delay. Only shimming and receiver gain optimization should need to be performed prior to acquisition because the spectrometer should already be optimized from the blank sample measurement.

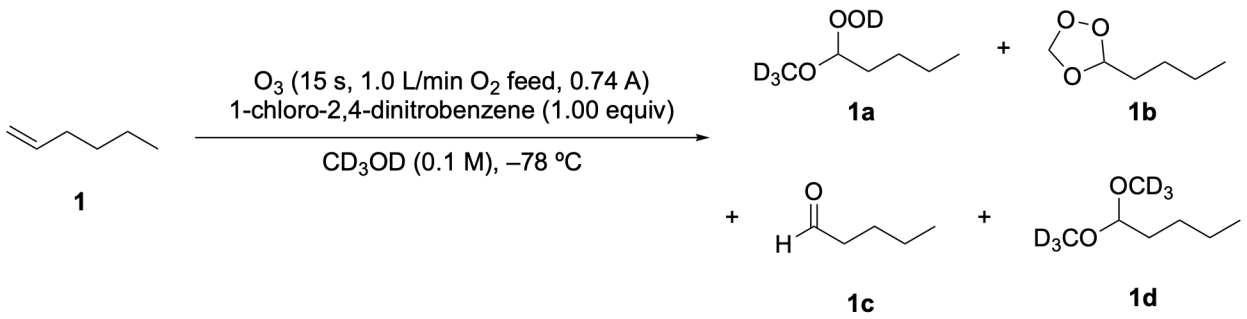
4. Iteration: Repeat this sequential ozonolysis and measurement process individually for the remaining two tubes.

Step 5: Advanced NMR and Data Processing

1. 1D selective gradient NMR and 2D NMR were collected on the crude mixtures as needed to assist in peak assignment. 1D selective gradient NMR was preferred over traditional 2D NMR due to the shorter acquisition times required to collect readable data.
2. Baseline and Phase Correction: All spectra were processed in MestReNova (14.2.3-29241). Standard automatic baseline and automatic phase corrections were applied to each spectrum.
3. Reference: The residual solvent peak (CD_3OD) was referenced to 3.310 ppm.
4. Internal Standard (IS) Calibration: Non-overlapping internal standard (1-chloro-2,4-dinitrobenzene) peaks were integrated to a value of 1.00 according to the following signal domains:
    a. C_3–H at 8.83 ppm (d, J = 2.7 Hz, 1H)
    b. C_4–H at 8.48 ppm (dd, J = 8.8, 2.6 Hz, 1H)
    c. C_5–H at 7.96 ppm (d, J = 8.9 Hz, 1H)
5. Alkene-to-IS Ratio Calibration: Peak signals in the blank sample were integrated to establish the baseline ratio between the internal standard and the alkene, accounting for initial alkene purity and experimental error in stock solution preparation.

6. Quantification: In addition to the 10 second scan delay for each sample to account for differences in relaxation times across protons on the molecule, as many non-overlapping peaks corresponding to the same analyte were integrated and averaged to maximize possible accuracy. The alkene-to-IS ratio determined from the blank sample was used to normalize sample values. Representative crude ^{1}H NMR spectra are provided and annotated for each substrate.

6.8.4.2 *mono*-Substituted Alkene qNMR

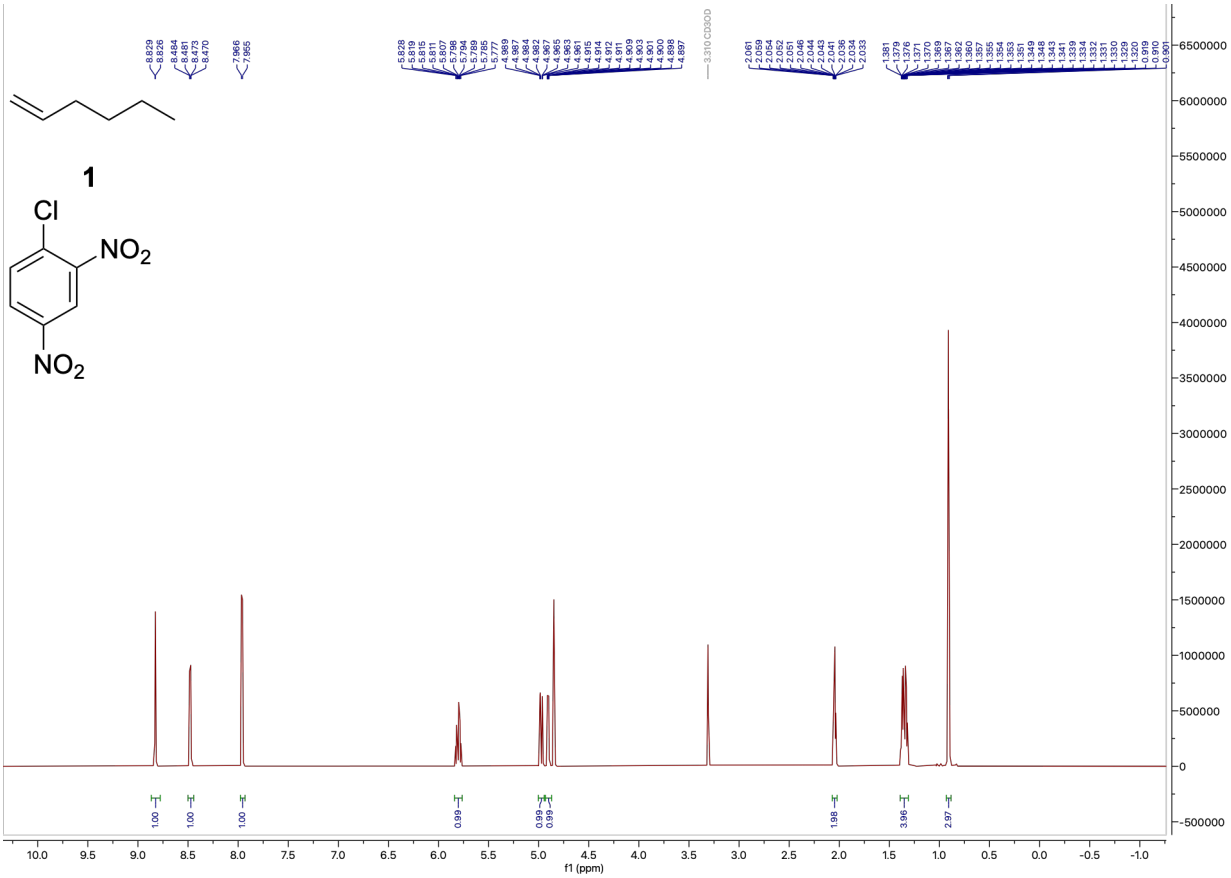


1-hexene (**1**)

Reaction Time: 15 seconds

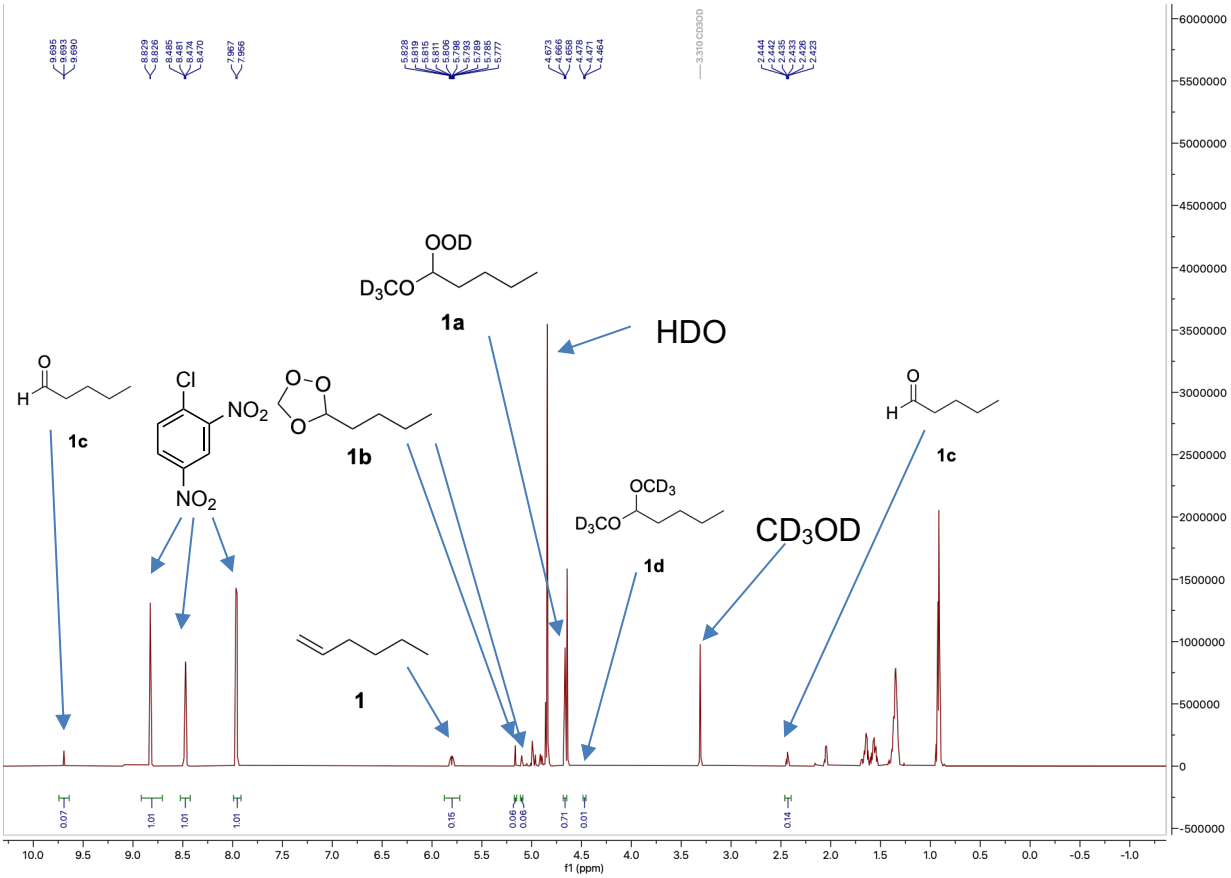
Alkene-to-IS Ratio: 0.99:1.00

Blank Sample: 1-hexene (**1**) and 1-chloro-2,4-dinitrobenzene (**IS**)



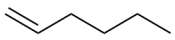
^{1}H NMR (800 MHz, CD_3OD), D1 = 10 s, 32 scans

Representative ^{1}H NMR: 1-hexene (**1**) ozonolysis



^{1}H NMR (800 MHz, CD_3OD), D1 = 10 s, 32 scans

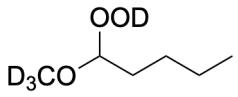
Characterization Data: 1-hexene (**1**)



1

1-hexene (**1**)

^{1}H NMR (800 MHz, MeOD) δ 5.80 (ddt, *J* = 17.0, 10.1, 6.7 Hz, 1H), 4.97 (dq, *J* = 17.1, 1.6 Hz, 1H), 4.91 (ddt, *J* = 10.2, 2.3, 1.2 Hz, 1H), 2.16 – 1.94 (m, 2H), 1.50 – 1.25 (m, 4H), 0.91 (t, *J* = 7.2 Hz, 3H).

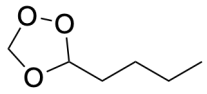


1a

1-deuteroperoxy-1-(methoxy-d_3)pentane (**1a**)

^{1}H NMR (800 MHz, MeOD) δ 4.68 (t, *J* = 5.9 Hz, 1H), 1.70 – 1.63 (m, 1H), 1.61 – 1.55 (m, 1H), 1.43 – 1.32 (m, 4H), 0.95 – 0.91 (m, 3H).

The peroxide α-CH peak was measured from the ^{1}H NMR of the crude reaction mixture. The other peaks were deduced from the 1D selective gradient TOCSY spectrum.

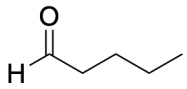


1b

3-butyl-1,2,4-trioxolane (**1b**)

^{1}H NMR (800 MHz, MeOD) δ 5.16 (s, 1H), 5.10 (t, *J* = 5.0 Hz, 1H), 4.99 (s, 1H), 1.75 – 1.67 (m, 2H), 1.51 – 1.36 (m, 4H), 1.00 – 0.86 (m, 3H).

The trioxolane CH and CH_2 signals were measured from the ^{1}H NMR of the crude reaction mixture. The remaining signals were deduced from the 1D selective gradient TOCSY spectrum.

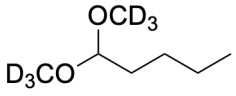


1c

pentanal (**1c**)

^{1}H NMR (800 MHz, MeOD) δ 9.73 – 9.70 (m, 1H), 2.50 – 2.41 (m, 2H), 1.61 (dtd, *J* = 9.1, 7.4, 6.0 Hz, 2H), 1.38 (h, *J* = 7.4 Hz, 2H), 0.95 – 0.86 (m, 3H).

The aldehyde CHO and carbonyl α-CH_2 signals were measured from the ^{1}H NMR of the crude reaction mixture. The remaining signals were deduced from the 1D selective gradient TOCSY spectrum.



1d

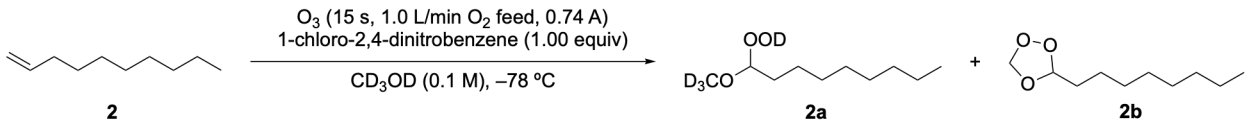
1,1-bis(methoxy-d_3)pentane (**1d**)

^{1}H NMR (800 MHz, MeOD) δ 4.47 (t, *J* = 5.5 Hz, 1H), 1.75 – 1.48 (m, 2H), 1.46 – 1.28 (m, 4H), 0.95 – 0.85 (m, 3H).

The acetal α-CH signal was measured from the ^{1}H NMR of the crude reaction mixture. The remaining signals were deduced from the ^{1}H NMR of the crude reaction mixture.

Table 6.1 1-hexene (**1**) ozonolysis qNMR Data

Trial	% conversion	%1a	%1b	%1c	%1d	normalized %1a	normalized %1b	normalized %(1c+1d)
1	85	71	5	6	3	84	5.9	11
2	91	75	7	7	2	82	7.7	9.9
3	85	71	6	7	1	84	7.1	9.4
average						83	6.9	10
st. dev.						0.64	0.92	0.59

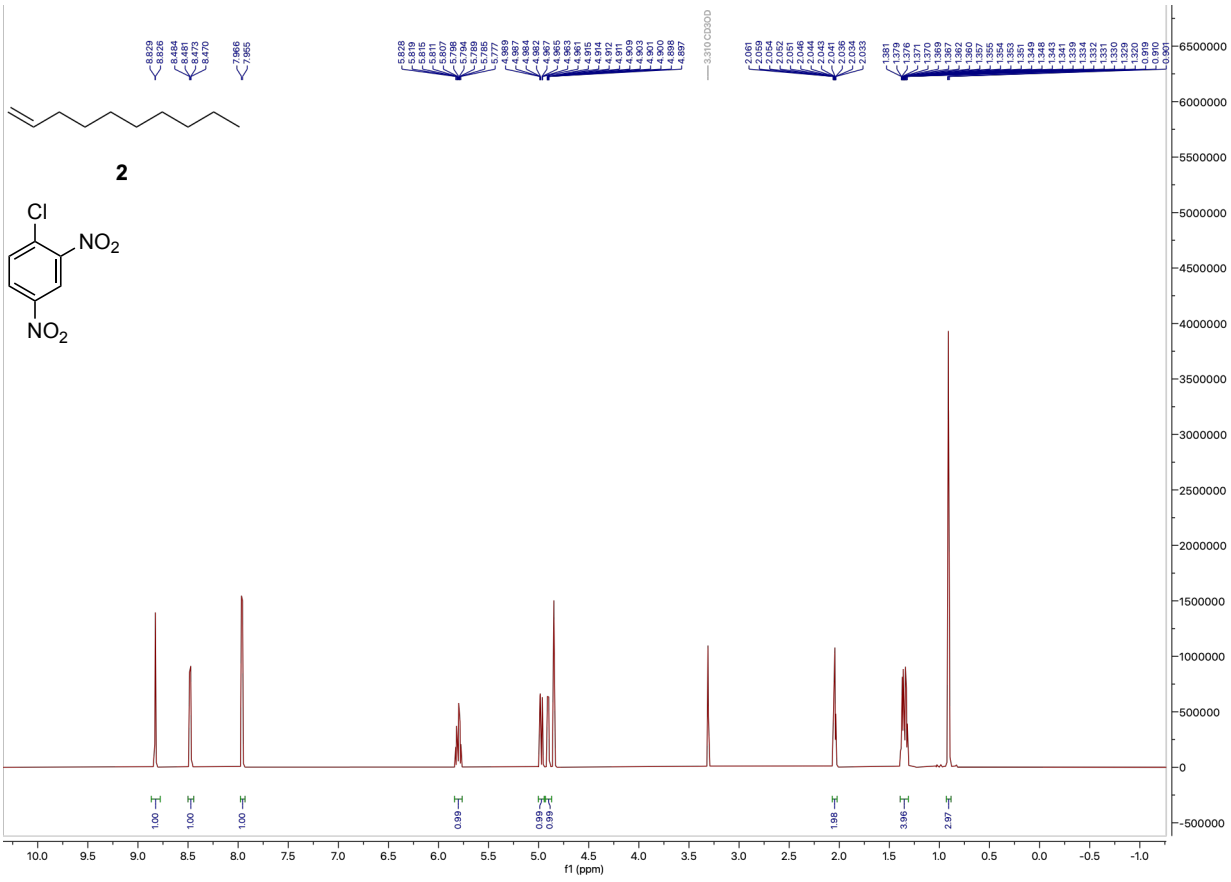


1-decene (**2**)

Reaction Time: 15 seconds

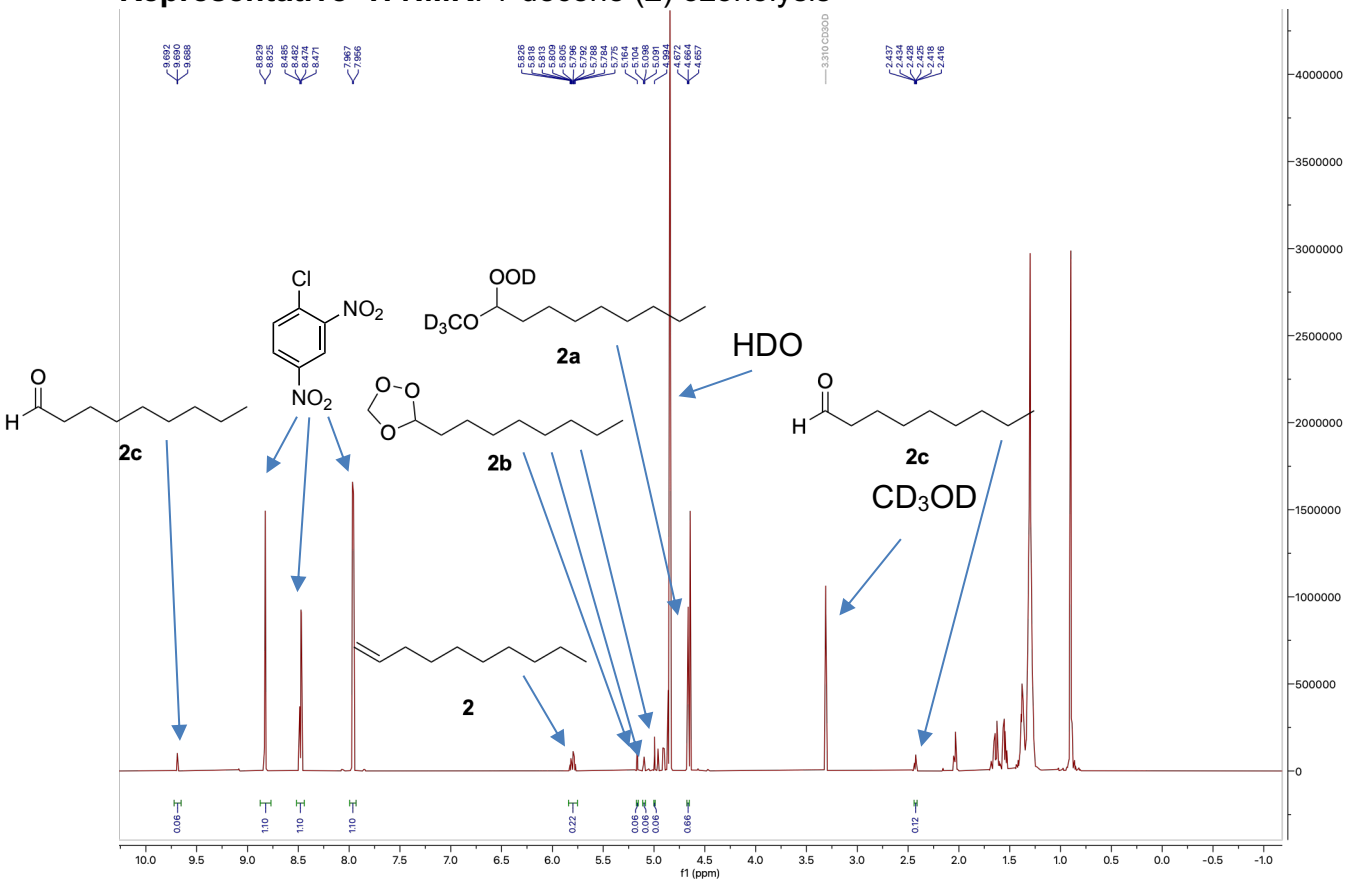
Alkene-to-IS Ratio: 0.90:1.00

Blank Sample: 1-decene (**2**) and 1-chloro-2,4-dinitrobenzene (**IS**)



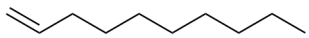
^{1}H NMR (800 MHz, CD_3OD), D1 = 10 s, 32 scans

Representative ^{1}H NMR: 1-decene (**2**) ozonolysis



^{1}H NMR (800 MHz, CD_3OD), D1 = 10 s, 32 scans

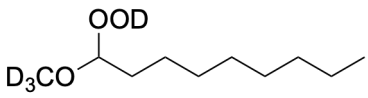
Characterization Data: 1-decene (**2**)



2

1-decene (**2**)

^{1}H NMR (800 MHz, MeOD) δ 5.80 (ddt, *J* = 17.0, 10.2, 6.7 Hz, 1H), 4.97 (dt, *J* = 17.1, 1.8 Hz, 1H), 4.91 (dq, *J* = 10.2, 1.5 Hz, 1H), 2.17 – 1.89 (m, 2H), 1.46 – 1.21 (m, 12H), 0.90 (t, *J* = 7.1 Hz, 3H).

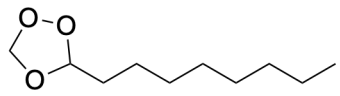


2a

1-deuteroperoxy-1-(methoxy-d_3)nonane (**2a**)

^{1}H NMR (800 MHz, MeOD) δ 4.68 (t, *J* = 5.8 Hz, 1H), 1.66 (ddt, *J* = 13.8, 9.6, 6.0 Hz, 1H), 1.57 (ddt, *J* = 13.9, 9.2, 6.0 Hz, 1H), 1.43 – 1.39 (m, 10H), 1.38 – 1.29 (m, 2H), 0.90 (t, *J* = 7.1 Hz, 3H).

The peroxide α-CH peak was measured from the ^{1}H NMR of the crude reaction mixture. The other peaks were deduced from the 1D selective gradient TOCSY spectrum.

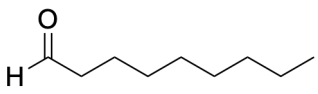


2b

3-octyl-1,2,4-trioxolane (**2b**)

^{1}H NMR (800 MHz, MeOD) δ 5.16 (s, 1H), 5.10 (t, *J* = 5.0 Hz, 1H), 4.99 (s, 1H), 1.72 – 1.67 (m, 2H), 1.48 – 1.29 (m, 12H), 0.92 (t, *J* = 7.1 Hz, 3H).

The trioxolane CH and CH_2 signals were measured from the ^{1}H NMR of the crude reaction mixture. The remaining signals were deduced from the 1D selective gradient TOCSY spectrum.



2c

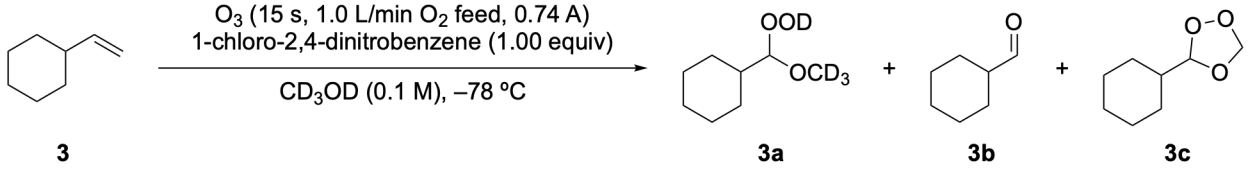
nonanal (**2c**)

^{1}H NMR (800 MHz, MeOD) δ 9.69 (t, *J* = 1.8 Hz, 1H), 2.43 (td, *J* = 7.3, 1.7 Hz, 2H), 1.73 – 1.16 (m, 12H), 0.90 (t, *J* = 7.1 Hz, 3H).

The aldehyde CHO and carbonyl α-CH_2 signals were measured from the ^{1}H NMR of the crude reaction mixture. The remaining signals were deduced from the ^{1}H NMR of the crude reaction mixture.

Table 6.2 1-decene (**2**) ozonolysis

Trial	**% conversion**	**%2a**	**%2b**	**%2c**	**normalized %2a**	**normalized %2b**	**normalized %2c**
1	86	73	6	7	85	7.0	8.1
2	78	66	6	6	85	7.7	7.7
3	86	73	6	7	85	7.0	8.1
average					85	7.2	8.0
st. dev.					0.15	0.41	0.26

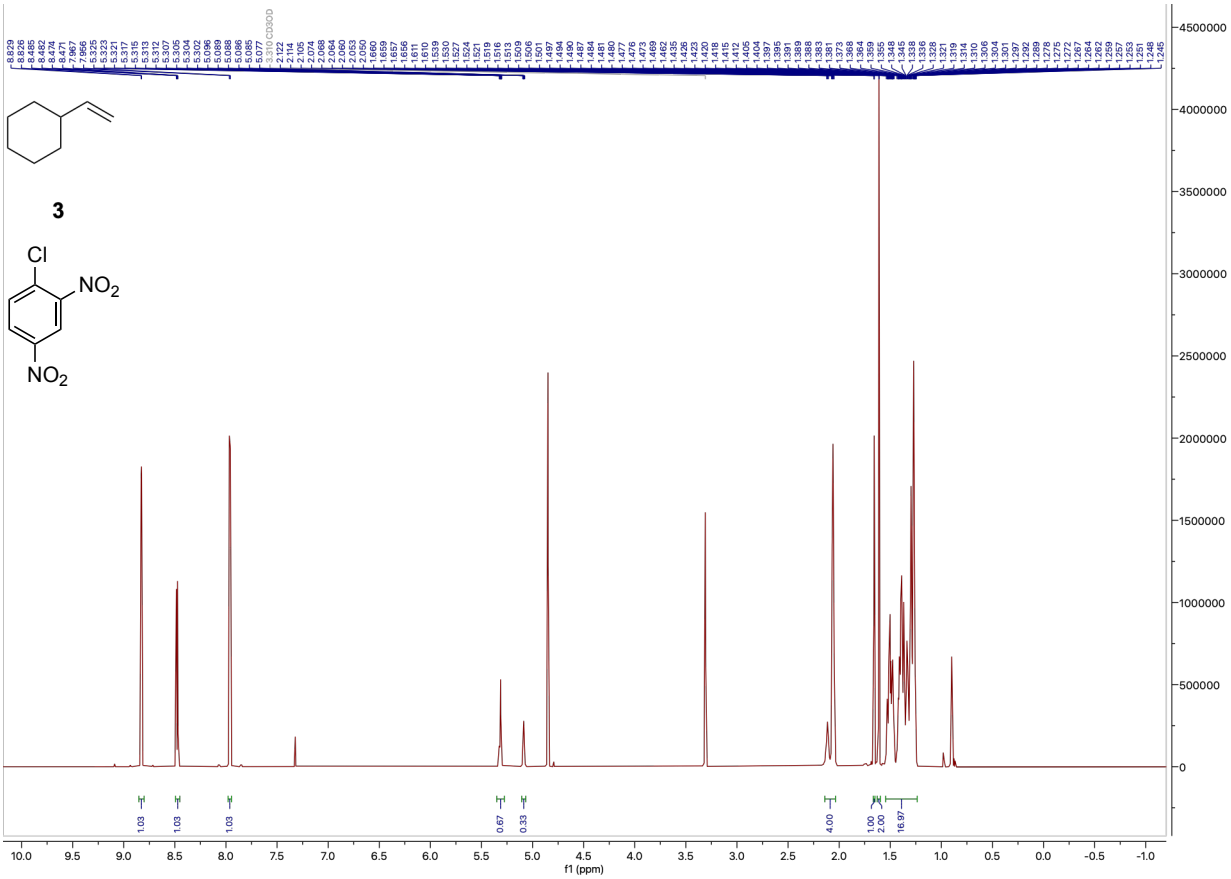


vinylcyclohexane (**3**)

Reaction Time: 15 seconds

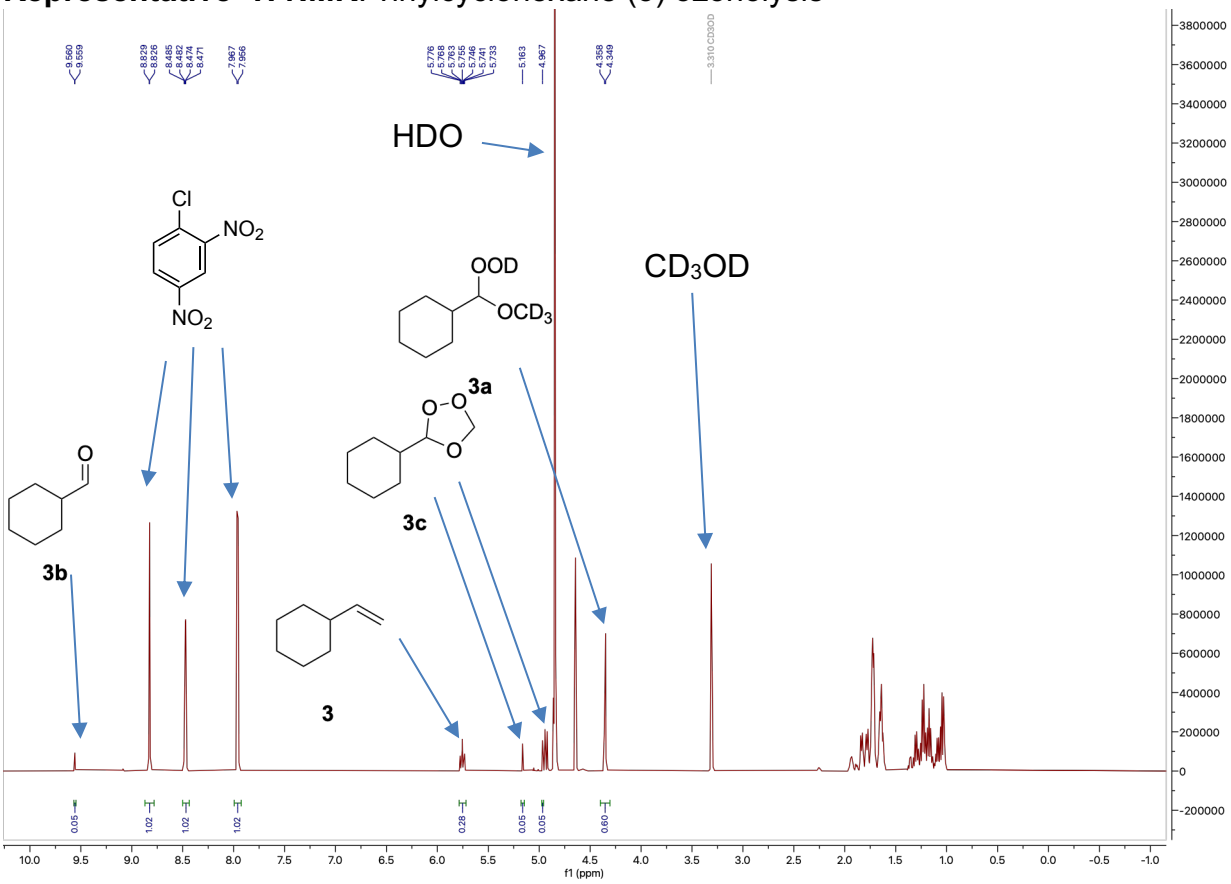
Alkene-to-IS Ratio: 0.98:1.00

Blank Sample: vinylcyclohexane (**3**) and 1-chloro-2,4-dinitrobenzene (**IS**)



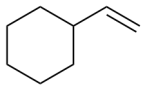
^{1}H NMR (800 MHz, CD_3OD), D1 = 10 s, 32 scans

Representative ^{1}H NMR: vinylcyclohexane (**3**) ozonolysis



^{1}H NMR (800 MHz, CD_3OD), D1 = 10 s, 32 scans

Characterization Data: vinylcyclohexane (**3**)

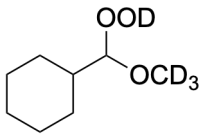


3

vinylcyclohexane (**3**)

^{1}H NMR (800 MHz, MeOD) δ 5.75 (ddd, *J* = 17.2, 10.5, 6.6 Hz, 1H), 4.93 (dt, *J* = 17.2, 1.7 Hz, 1H), 4.85 (ddd, *J* = 10.5, 2.0, 1.2 Hz, 1H), 1.94 (dtdd, *J* = 13.4, 6.8, 3.1, 1.7 Hz,

1H), 1.82 – 1.69 (m, 4H), 1.66 (dtd, *J* = 14.6, 3.4, 1.6 Hz, 1H), 1.30 (qt, *J* = 13.8, 3.6 Hz, 2H), 1.18 (qt, *J* = 12.8, 3.5 Hz, 1H), 1.13 – 1.01 (m, 2H).

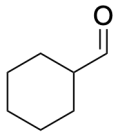


3a

(deuteroperoxy(methoxy-*d*3)methyl)cyclohexane (**3a**)

^{1}H NMR (800 MHz, MeOD) δ 4.37 (d, *J* = 7.1 Hz, 1H), 1.89 – 1.83 (m, 1H), 1.82 – 1.77 (m, 1H), 1.77 – 1.72 (m, 1H), 1.65 (dddd, *J* = 15.1, 11.7, 7.2, 3.6 Hz, 3H), 1.25 (qt, *J* = 12.4, 3.6 Hz, 2H), 1.18 (qt, *J* = 12.7, 3.3 Hz, 1H), 1.06 (qd, *J* = 12.7, 3.6 Hz, 2H).

The peroxide α-CH peak was determined from the ^{1}H NMR of the crude reaction mixture. The remaining peaks were deduced from the 1D TOCSY spectrum.

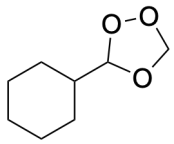


3b

cyclohexanecarbaldehyde (**3b**)

^{1}H NMR (800 MHz, MeOD) δ 9.56 (d, *J* = 1.2 Hz, 1H), 2.28 – 2.22 (m, 1H), 1.98 – 1.56 (m, 5H), 1.44 – 0.95 (m, 5H).

The aldehyde CHO and α-CH_2 peaks were determined from the ^{1}H NMR of the crude reaction mixture. The remaining peaks were deduced from the ^{1}H NMR of the crude reaction mixture.



3c

3-cyclohexyl-1,2,4-trioxolane (**3c**)

^{1}H NMR (800 MHz, MeOD) δ 5.16 (s, 1H), 4.97 (s, 1H), 4.83 (m, 1H), 1.99 – 1.57 (m, 6H), 1.49 – 0.96 (m, 5H).

The peroxide α-CH_2 peaks were determined from the ^{1}H NMR of the crude reaction mixture. The remaining peaks were deduced from the ^{1}H NMR of the crude reaction mixture.

Table 6.3 vinylcyclohexane (**3**) ozonolysis

Trial	**%conversion**	**%3a**	**%3b**	**%3c**	**normalized %3a**	**normalized %3b**	**normalized %3c**
1	74	61	6	6	82	8	8
2	85	70	6	6	82	7	7
3	72	60	5	5	83	7	7
average					83	7.4	7.4
st. dev.					0.54	0.64	0.64

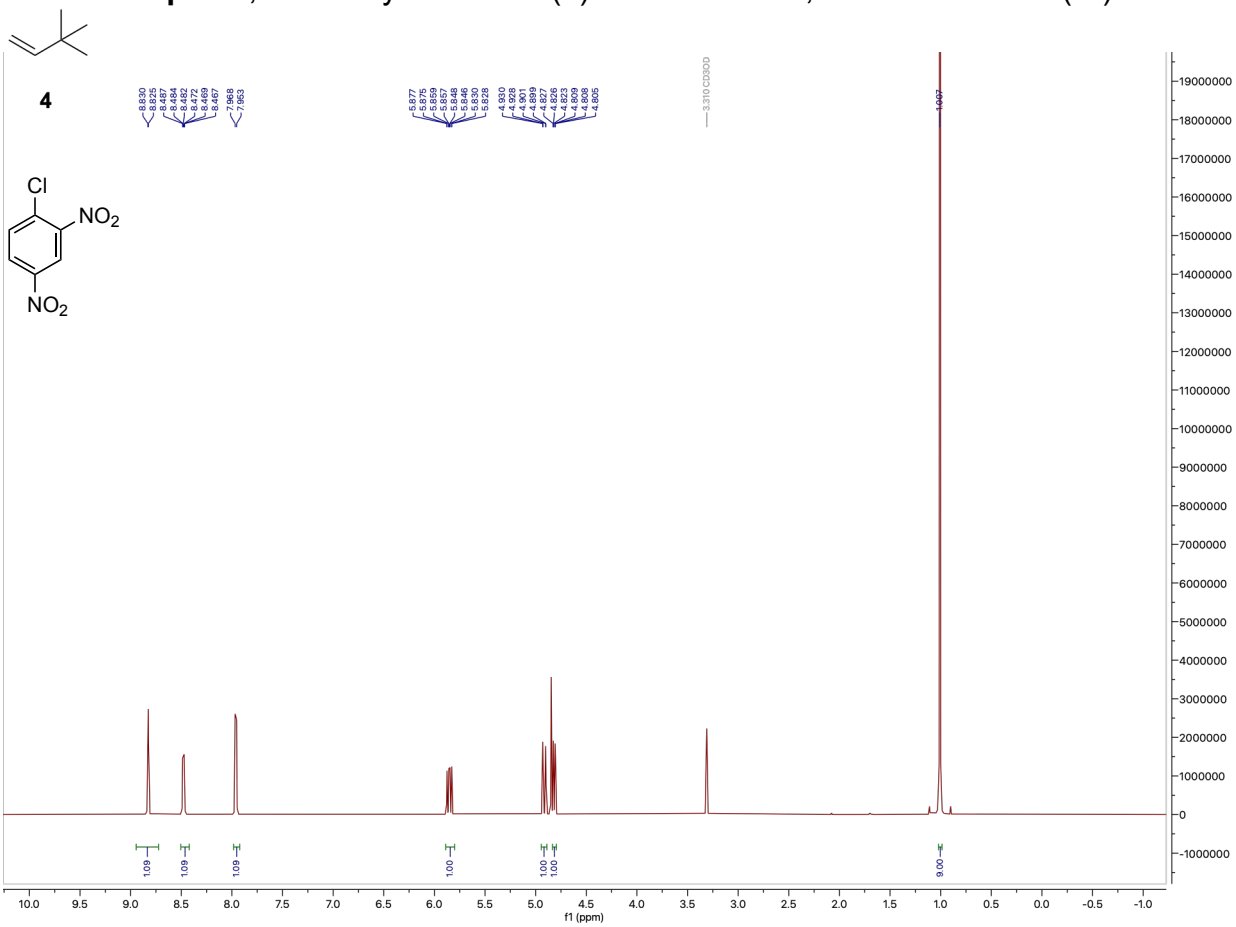


3,3-dimethyl-1-butene (**4**)

Reaction Time: 15 seconds

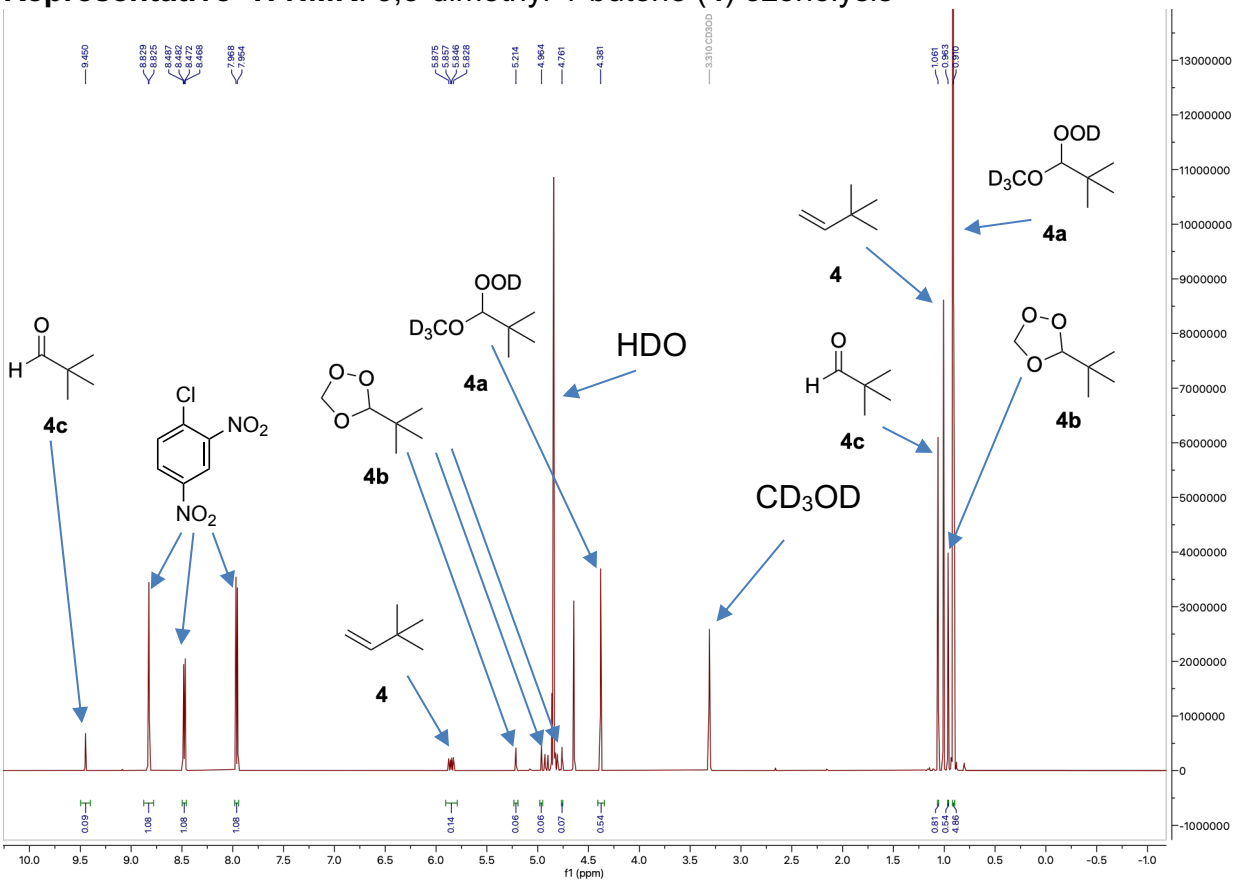
Alkene-to-IS Ratio: 0.91:1.00

Blank Sample: 3,3-dimethyl-1-butene (**4**) and 1-chloro-2,4-dinitrobenzene (**IS**)



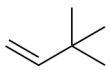
^{1}H NMR (600 MHz, CD_3OD), D1 = 10 s, 32 scans

Representative ^{1}H NMR: 3,3-dimethyl-1-butene (**4**) ozonolysis



^{1}H NMR (600 MHz, CD_3OD), D1 = 10 s, 32 scans

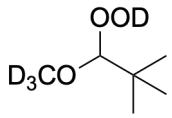
Characterization Data: 3,3-dimethyl-1-butene (**4**)



4

3,3-dimethyl-1-butene (**4**)

^{1}H NMR (600 MHz, MeOD) δ 5.85 (ddd, *J* = 17.5, 10.7, 0.9 Hz, 1H), 4.91 (dd, *J* = 17.5, 1.4 Hz, 1H), 4.82 (dt, *J* = 10.7, 1.2 Hz, 1H), 1.01 (s, 9H).

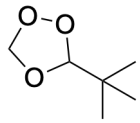


4a

1-deuteroperoxy-1-(methoxy-d_3)-2,2-dimethylpropane (**4a**)

^{1}H NMR (600 MHz, MeOD) δ 4.38 (s, 1H), 0.91 (s, 9H).

The signals were measured from the ^{1}H NMR of the crude reaction mixture.

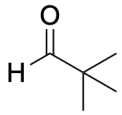


4b

3-(*tert*-butyl)-1,2,4-trioxolane (**4b**)

^{1}H NMR (600 MHz, MeOD) δ 5.21 (s, 1H), 4.96 (s, 1H), 4.76 (s, 1H), 0.96 (s, 9H).

The signals were measured from the ^{1}H NMR of the crude reaction mixture.



4c

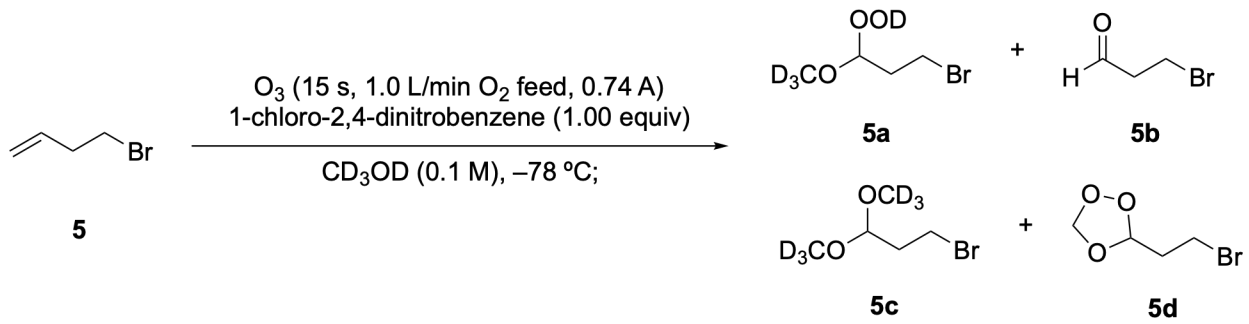
pivaldehyde (**4c**)

^{1}H NMR (600 MHz, MeOD) δ 9.45 (s, 1H), 1.06 (s, 9H).

The signals were measured from the ^{1}H NMR of the crude reaction mixture.

Table 6.4 3,3-dimethyl-1-butene (**4**) ozonolysis qNMR Data

Trial	**% conversion**	**%4a**	**%4b**	**%4c**	**normalized %4a**	**normalized %4b**	**normalized %4c**
1	67	50	6	8	75	9.0	12
2	74	56	6	10	76	8.1	14
3	84	63	7	11	75	8.3	13
average					75	8.5	13
st. dev.					0.53	0.44	0.81

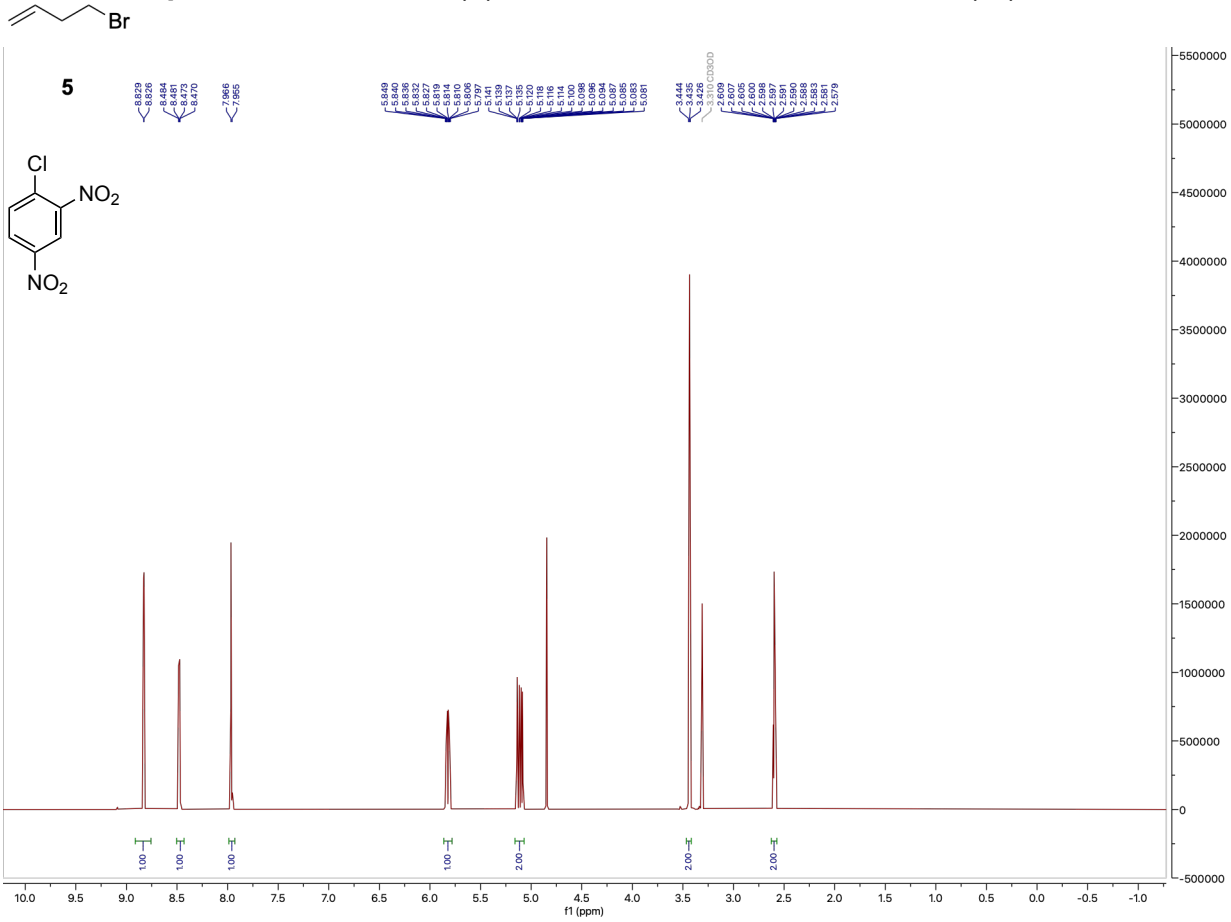


4-bromobutene (**5**)

Reaction Time: 15 seconds

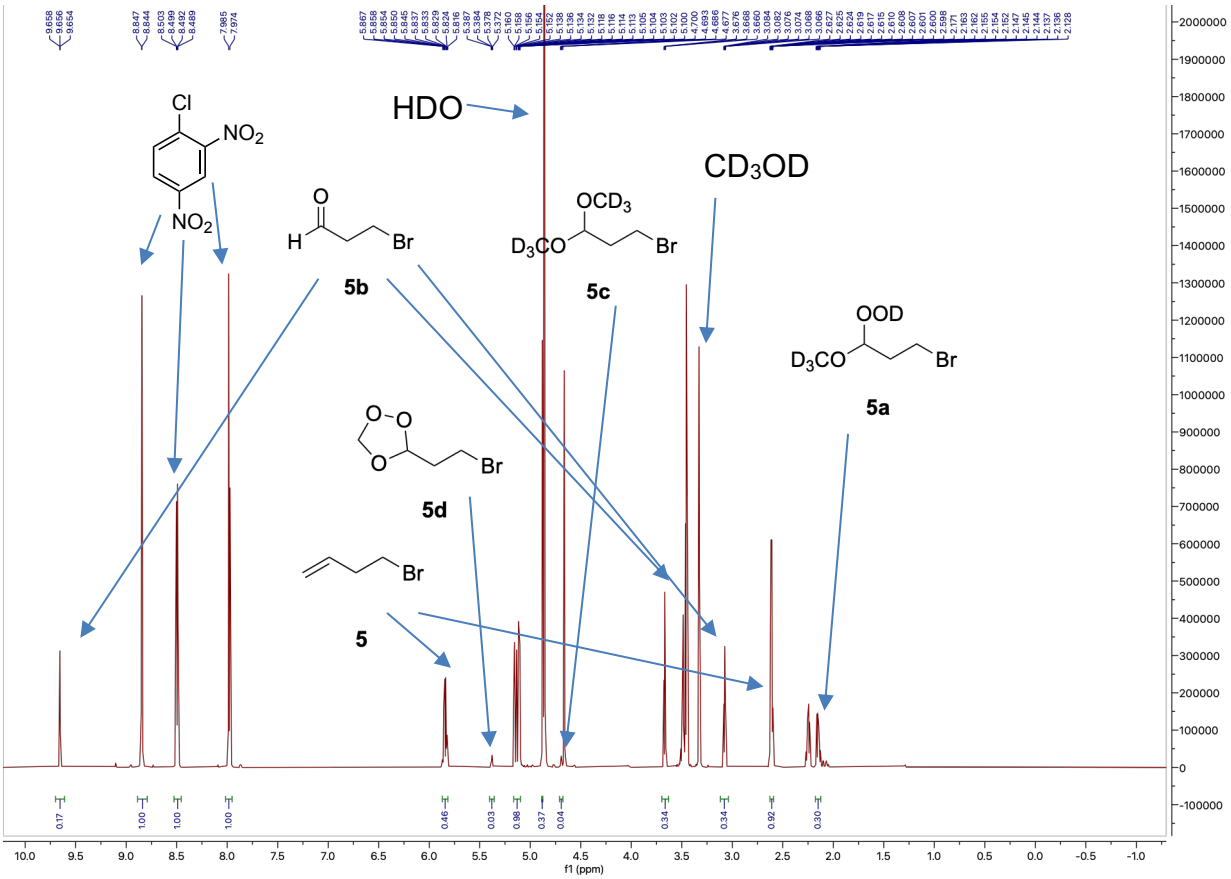
Alkene-to-IS Ratio: 1.00:1.00

Blank Sample: 4-bromobutene (**5**) and 1-chloro-2,4-dinitrobenzene (**IS**)



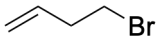
^{1}H NMR (800 MHz, CD_3OD)

Representative ^{1}H NMR: 4-bromobutene (**5**) ozonolysis



^{1}H NMR (800 MHz, CD_3OD), D1 = 10 s, 32 scans

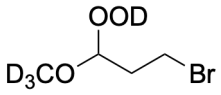
Characterization Data: 4-bromobutene (**5**)



5

4-bromobutene (**5**)

^{1}H NMR (800 MHz, MeOD) δ 5.82 (ddt, *J* = 17.1, 10.3, 6.8 Hz, 1H), 5.13 (dq, *J* = 17.2, 1.6 Hz, 1H), 5.09 (ddd, *J* = 10.2, 3.1, 1.2 Hz, 1H), 3.44 (t, *J* = 7.0 Hz, 2H), 2.59 (qt, *J* = 6.9, 1.4 Hz, 2H).

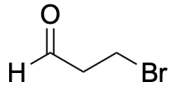


5a

3-bromo-1-deuteroperoxy-1-(methoxy-*d*3)propane (**5a**)

^{1}H NMR (800 MHz, MeOD) δ 4.86 (td, *J* = 5.8, 1.7 Hz, 1H), 3.49 (td, *J* = 6.8, 2.8 Hz, 2H), 2.53 – 2.18 (m, 1H), 2.18 – 2.07 (m, 1H).

The non-overlapping peroxide β-CH_2 peak (1H) from 2.18–2.07 ppm was measured from the ^{1}H NMR of the crude reaction mixture. The remaining peaks were deduced from the 1D selective gradient TOCSY spectrum.

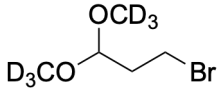


5b

3-bromopropanal (**5b**)

^{1}H NMR (800 MHz, MeOD) δ 9.66 (t, *J* = 1.3 Hz, 1H), 3.67 (t, *J* = 6.4 Hz, 2H), 3.08 (td, *J* = 6.4, 1.4 Hz, 2H).

The signals were measured from the ^{1}H NMR of the crude reaction mixture.

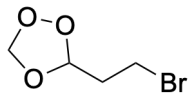


5c

3-bromo-1,1-bis(methoxy-*d*3)propane (**5c**)

^{1}H NMR (800 MHz, MeOD) δ 4.78 – 4.68 (m, 1H), 3.48 (t, *J* = 6.8 Hz, 2H), 2.14 – 2.03 (m, 2H).

The acetal methine peak (1H) was measured from the ^{1}H NMR of the crude reaction mixture. The remaining peaks were deduced from the 1D selective gradient TOCSY spectrum.



5d

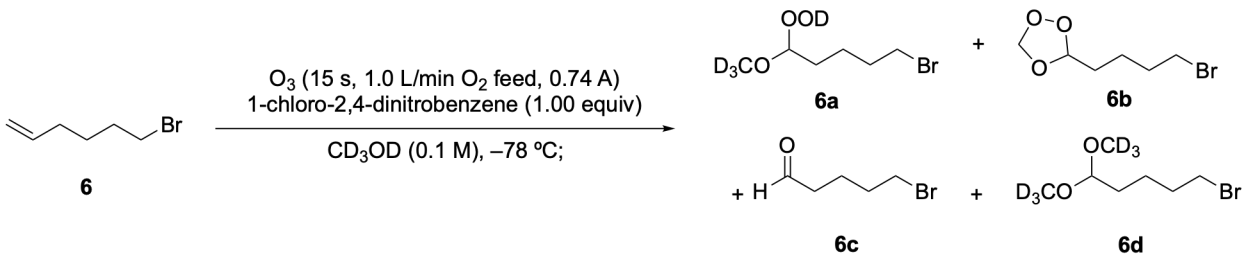
3-(2-bromoethyl)-1,2,4-trioxolane (**5d**)

^{1}H NMR (800 MHz, MeOD) δ 5.38 (t, *J* = 4.8 Hz, 1H), 5.17 – 5.08 (m, 2H), 3.54 – 3.44 (m, 2H), 2.28 – 2.22 (m, 2H).

The ozonide methine peak (1H) was measured from the ^{1}H NMR of the crude reaction mixture. The remaining peaks were deduced from the 1D selective gradient TOCSY spectrum.

Table 6.5 4-bromobutene (**5**) ozonolysis qNMR Data

Trial	% conversion	%H_{5a}	%H_{5b}	%H_{5c}	%H_{5d}	normalized %H_{5a}	normalized %H_{5b}	normalized %H_{5c}	normalized %H_{5d}
1	54	30	17	3	4	56	31	5.6	7.4
2	56	32	18	3	3	57	32	5.4	5.4
3	63	36	20	4	3	57	32	6.3	4.8
average						57	32	5.8	5.8
st. dev.						0.92	0.33	0.52	1.4

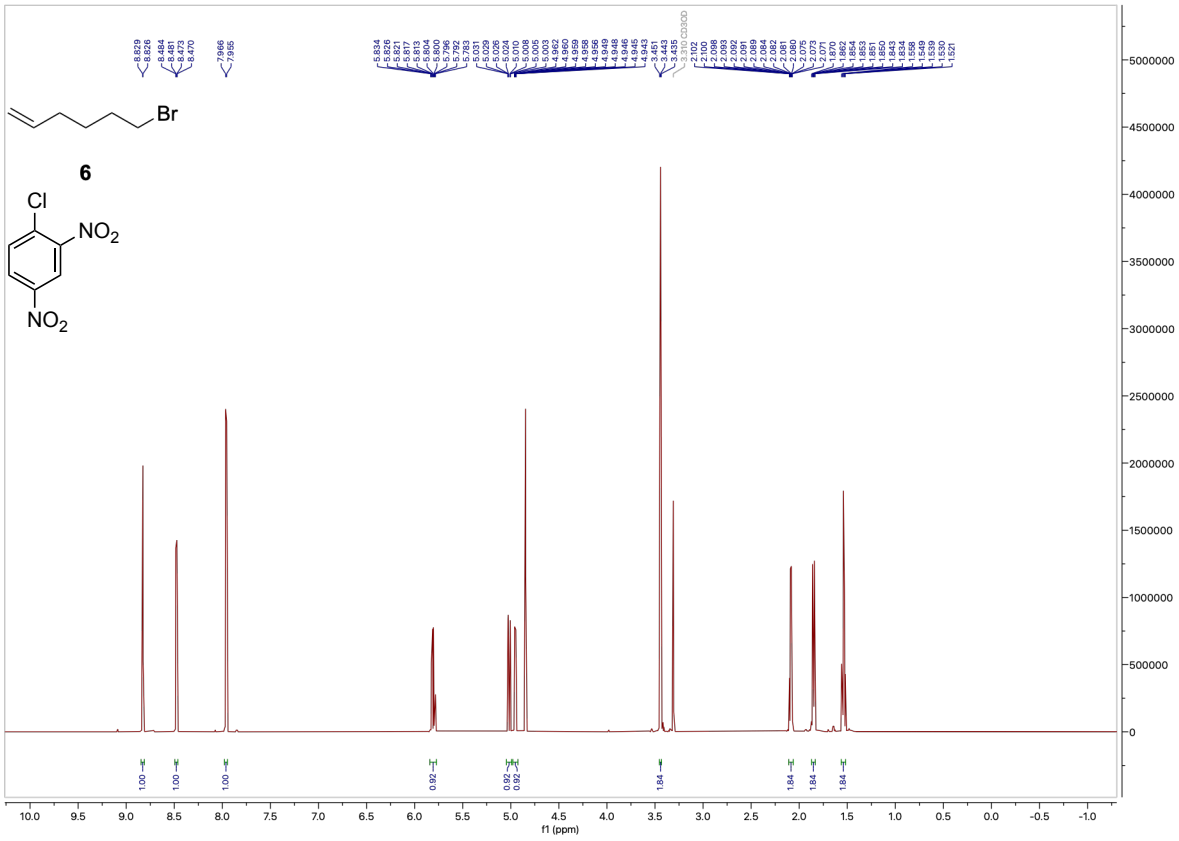


6-bromohexene (**6**)

Reaction Time: 15 seconds

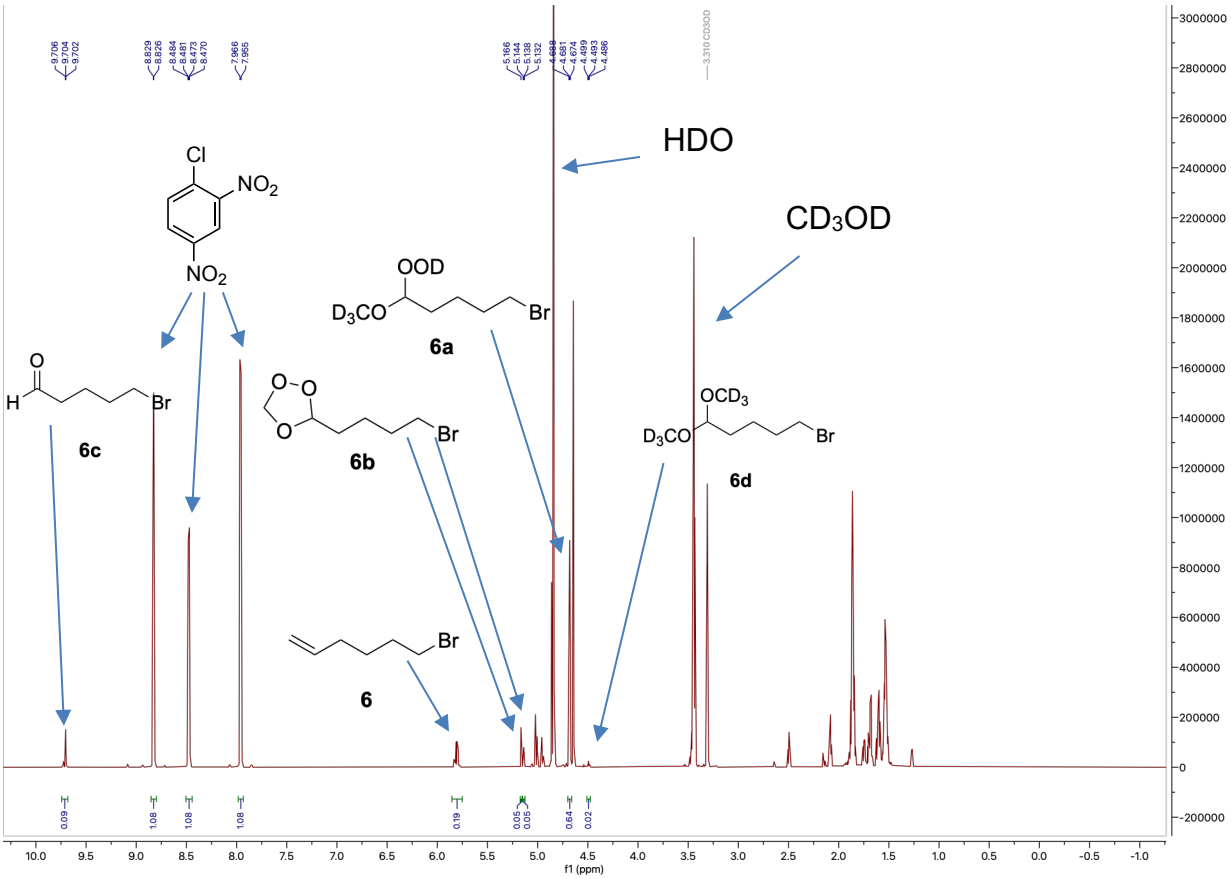
Alkene-to-IS Ratio: 0.92:1.00

Blank Sample: 4-bromohexene (**6**) and 1-chloro-2,4-dinitrobenzene (**IS**)



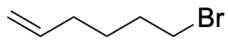
^{1}H NMR (800 MHz, CD_3OD)

Representative ^{1}H NMR: 6-bromohexene (**6**) ozonolysis



^{1}H NMR (800 MHz, CD_3OD), D1 = 10 s, 32 scans

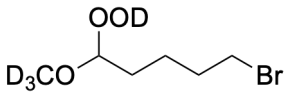
Characterization Data: 6-bromohexene (**6**)



6

6-bromo-1-hexene (**6**)

^{1}H NMR (800 MHz, MeOD) δ 5.81 (ddt, *J* = 17.0, 10.2, 6.8 Hz, 1H), 5.02 (dq, *J* = 17.1, 1.6 Hz, 1H), 4.95 (ddt, *J* = 10.2, 2.2, 1.2 Hz, 1H), 3.44 (t, *J* = 6.7 Hz, 2H), 2.09 (tdt, *J* = 7.5, 6.6, 1.4 Hz, 2H), 1.97 – 1.74 (m, 2H), 1.54 (p, *J* = 7.6 Hz, 2H).

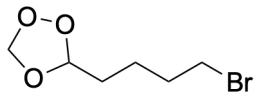


6a

5-bromo-1-deuteroperoxy-1-(methoxy-d_3)pentane (**6a**)

^{1}H NMR (800 MHz, MeOD) δ 4.68 (t, *J* = 5.8 Hz, 1H), 3.48 – 3.44 (m, 2H), 1.91 – 1.85 (m, 2H), 1.71 (ddt, *J* = 13.5, 9.2, 6.0 Hz, 1H), 1.65 – 1.59 (m, 1H), 1.59 – 1.51 (m, 2H).

The peroxide a-CH peak was measured from the ^{1}H NMR of the crude reaction mixture. The other peaks were deduced from the 1D selective gradient TOCSY spectrum.

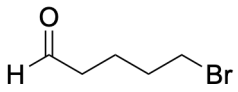


6b

3-(4-bromobutyl)-1,2,4-trioxolane (**6b**)

^{1}H NMR (800 MHz, MeOD) δ 5.17 (s, 1H), 5.14 (t, *J* = 4.9 Hz, 1H), 5.02 (s, 1H), 3.49 – 3.42 (m, 2H), 1.95 – 1.87 (m, 2H), 1.75 (td, *J* = 7.8, 4.8 Hz, 2H), 1.65 – 1.54 (m, 2H).

The trioxolane CH and CH_2 signals were measured from the ^{1}H NMR of the crude reaction mixture. The remaining signals were deduced from the 1D selective gradient TOCSY spectrum.

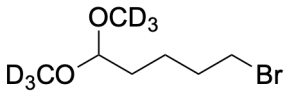


6c

5-bromo-pentanal (**6c**)

^{1}H NMR (800 MHz, MeOD) δ 9.70 (t, *J* = 1.5 Hz, 1H), 3.50 – 3.44 (m, 2H), 2.50 (td, *J* = 7.3, 1.5 Hz, 2H), 1.92 – 1.86 (m, 2H), 1.77 (dtd, *J* = 10.1, 7.4, 5.5 Hz, 2H).

The aldehyde CHO and carbonyl a-CH_2 signals were measured from the ^{1}H NMR of the crude reaction mixture. The remaining signals were deduced from the 1D selective gradient TOCSY spectrum.



6d

5-bromo-1,1-bis(methoxy-d_3)pentane (**6d**)

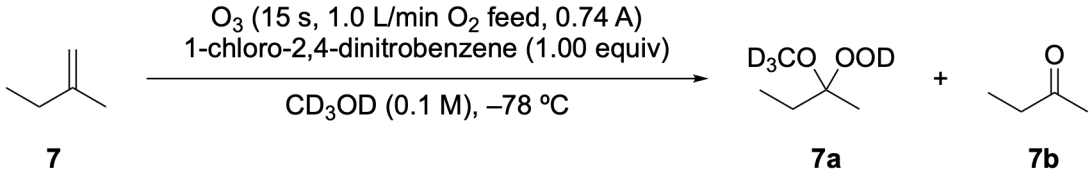
^{1}H NMR (800 MHz, MeOD) δ 4.49 (t, *J* = 5.2 Hz, 1H), 3.46 – 3.39 (m, 2H), 1.85 (dt, *J* = 14.0, 6.8 Hz, 2H), 1.68 – 1.42 (m, 4H).

The acetal a-CH signal was measured from the ^{1}H NMR of the crude reaction mixture. The remaining signals were deduced from the 1D selective gradient TOCSY spectrum.

Table 6.6 6-bromohexene (**6**) ozonolysis qNMR Data

Trial	% conversion	%6a	%6b	%6c	%6d	normalized %6a	normalized %6b	normalized %(6c+6d)
1	89	71	1	6	11	80	6.7	13
2	81	64	9	5	2	79	6	14
3	85	67	9	6	3	79	7	14
average						79	7	14
st. dev.						0.50	0.45	0.34

6.8.4.3 *gem*-1,1-Disubstituted Alkenes



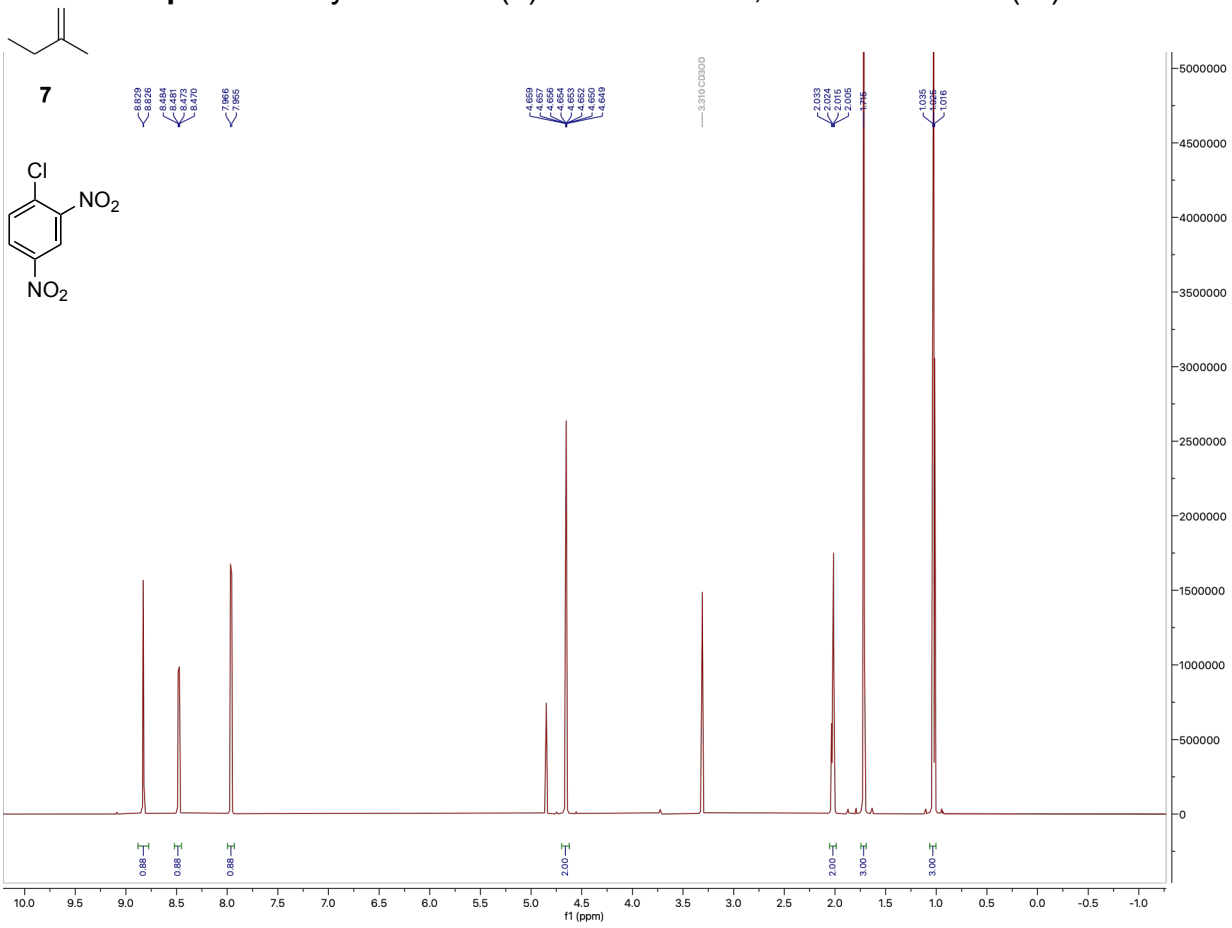
7 **7a** **7b**

2-methyl-1-butene (**7**)

Reaction Time: 15 seconds

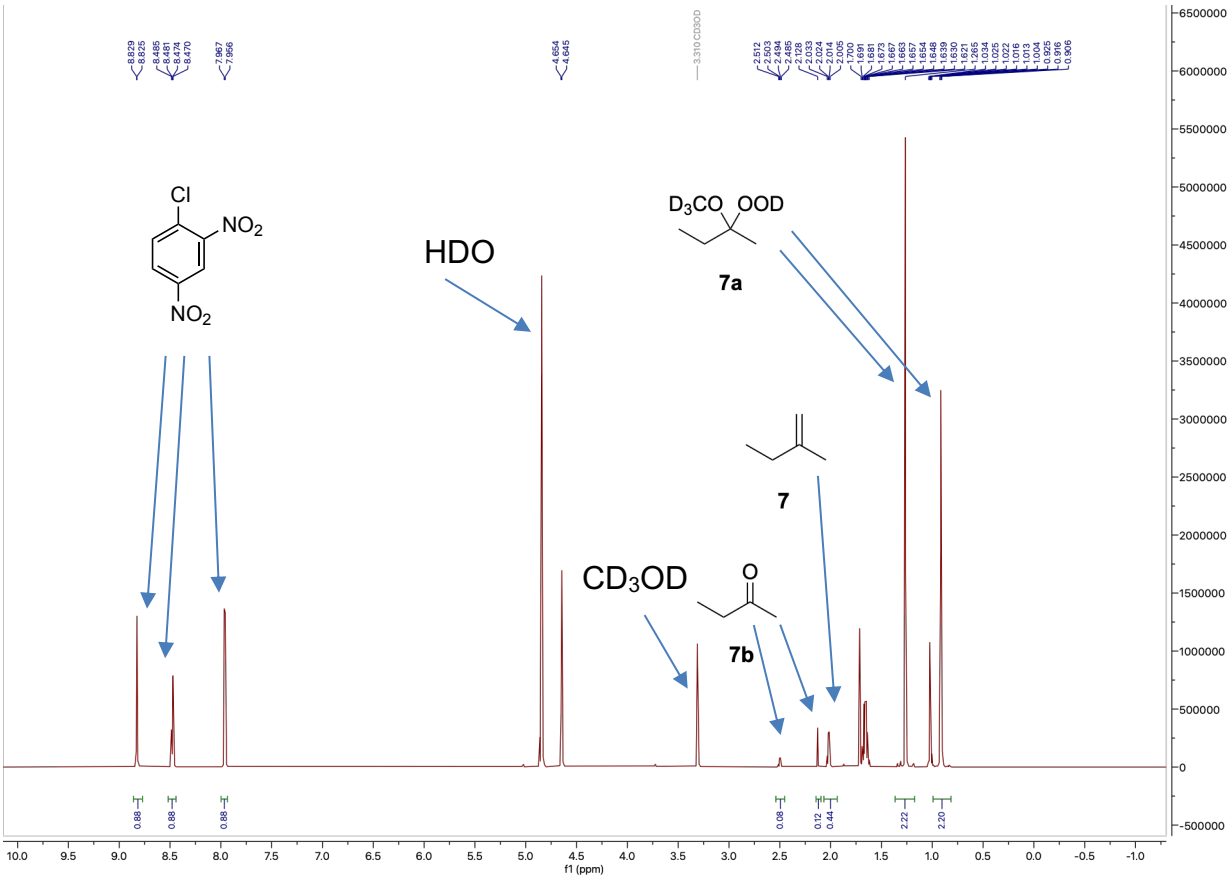
Alkene-to-IS Ratio: 1.12:1.00

Blank Sample: 2-methyl-1-butene (**7**) and 1-chloro-2,4-dinitrobenzene (**IS**)



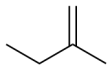
^{1}H NMR (800 MHz, CD_3OD), D1 = 10 s, 32 scans

Representative ^{1}H NMR: 2-methyl-1-butene (**7**) ozonolysis



^{1}H NMR (800 MHz, CD_3OD), D1 = 10 s, 32 scans

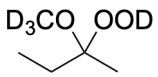
Characterization Data: 2-methyl-1-butene (**7**)



7

2-methyl-1-butene (**7**)

^{1}H NMR (800 MHz, MeOD) δ 4.65 (tq, *J* = 2.3, 1.1 Hz, 2H), 2.02 (q, *J* = 7.5 Hz, 2H), 1.71 (s, 3H), 1.03 (t, *J* = 7.5 Hz, 3H).

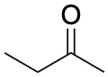


7a

2-deuteroperoxy-2-(methoxy-d_3)butane (**7a**)

^{1}H NMR (800 MHz, MeOD) δ 1.70 – 1.62 (m, 2H), 1.26 (s, 3H), 0.92 (t, *J* = 7.6 Hz, 3H).

The signals were measured from the ^{1}H NMR of the crude reaction mixture.



7b

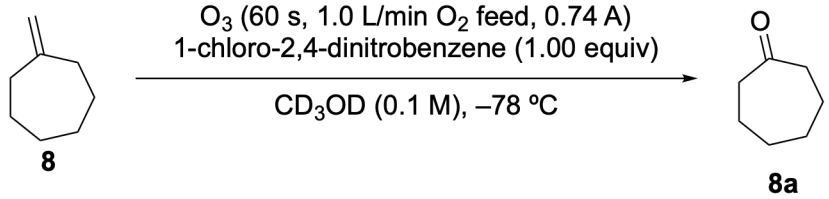
ethyl methyl ketone (**7b**)

^{1}H NMR (800 MHz, MeOD) δ 2.50 (q, *J* = 7.3 Hz, 2H), 2.13 (s, 3H), 1.02 (t, *J* = 7.4 Hz, 3H).

The signals were measured from the ^{1}H NMR of the crude reaction mixture.

Table 6.7 2-methyl-1-butene (**7**) ozonolysis qNMR Data

Trial	% conversion	%7a	%7b	normalized %7a	normalized %7b
1	78	74	4	94	5.1
2	81	77	4	95	4.9
3	87	82	4	95	4.6
average				95	4.9
st. dev.				0.11	0.27

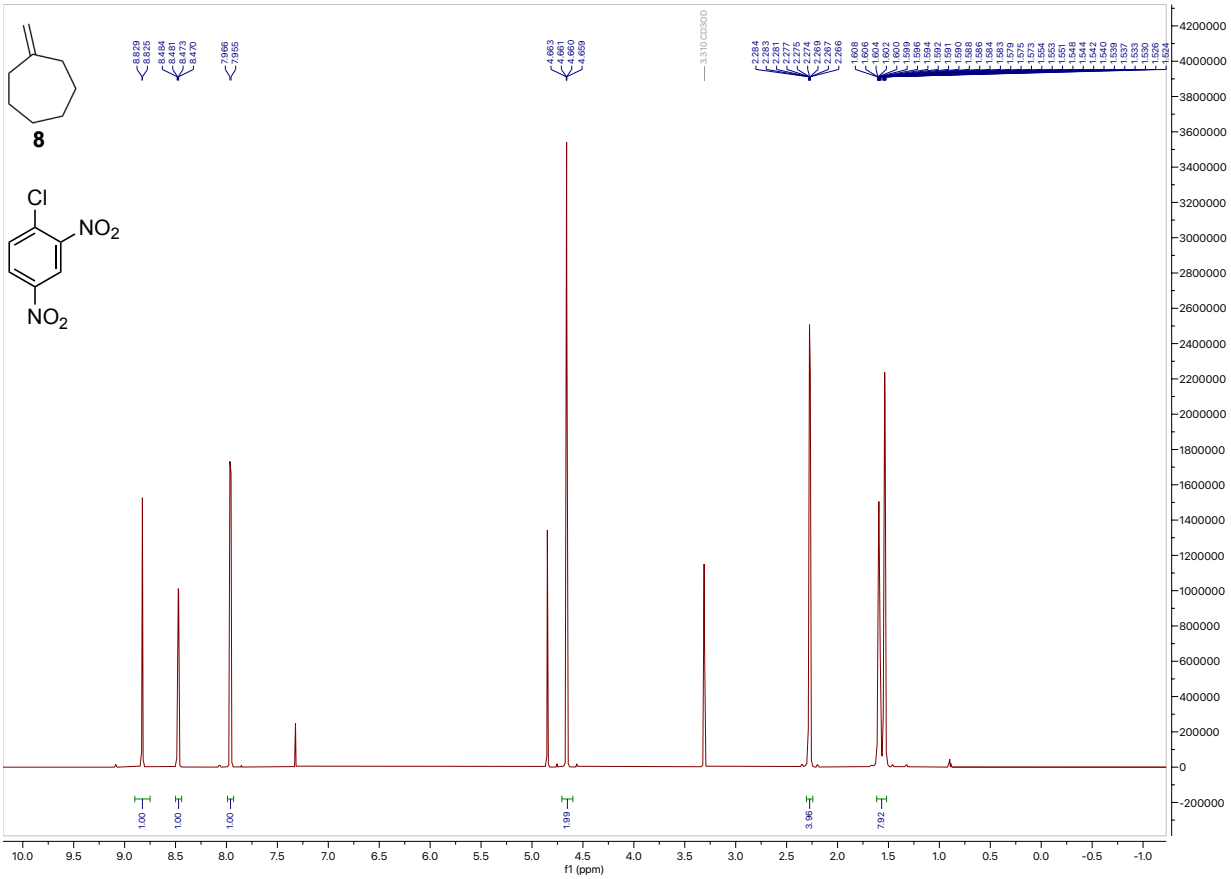


methylencycloheptane (**8**)

Reaction Time: 60 seconds

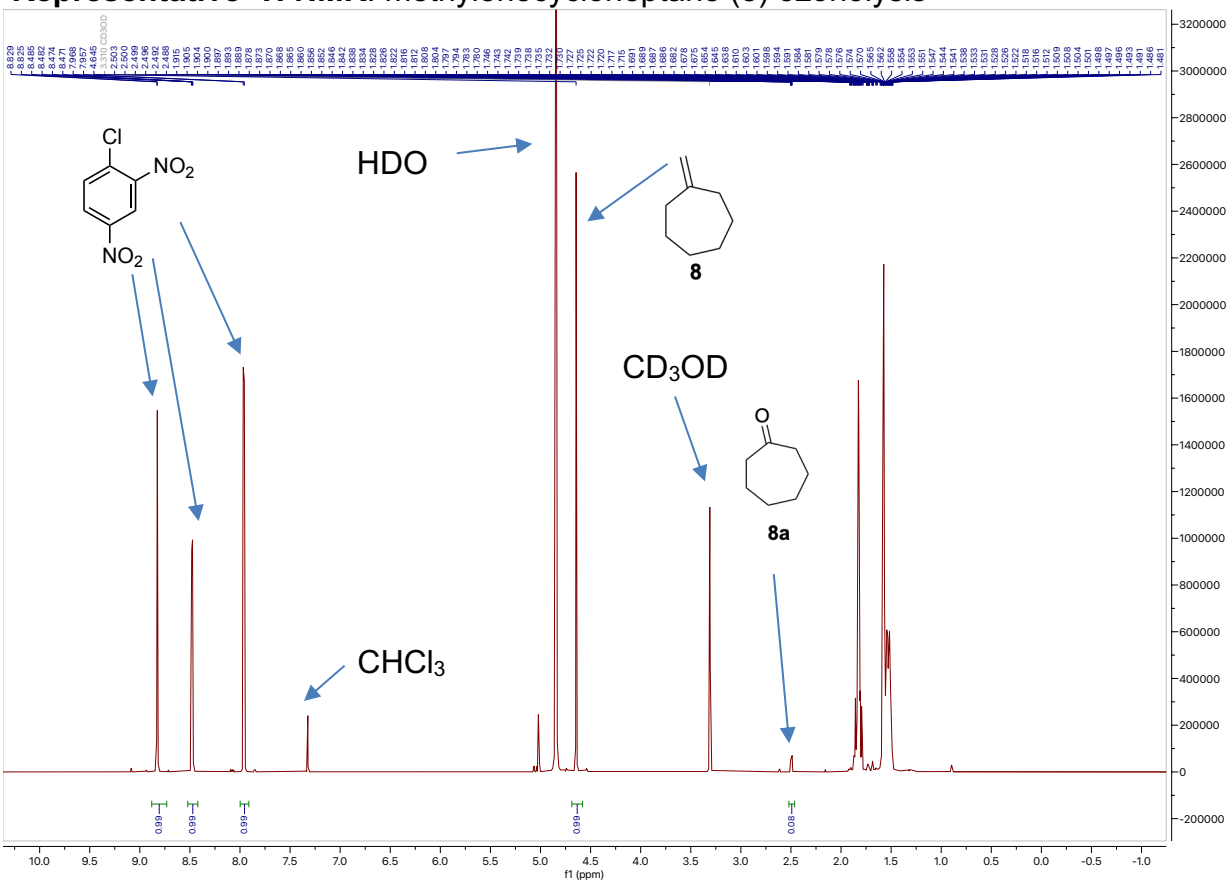
Alkene-to-IS Ratio: 0.99:1.00

Blank Sample: methylenecycloheptane (**8**) and 1-chloro-2,4-dinitrobenzene (**IS**)



^{1}H NMR (800 MHz, CD_3OD), D1 = 10 s, 32 scans

Representative ^{1}H NMR: methylenecycloheptane (**8**) ozonolysis



^{1}H NMR (800 MHz, $CDCl_3$), D1 = 10 s, 32 scans

Characterization Data: methylenecycloheptane (**8**)

methylenecycloheptane (**8**)

^{1}H NMR (800 MHz, MeOD) δ 4.73 – 4.41 (m, 2H), 2.54 – 1.88 (m, 4H), 1.68 – 1.56 (m, 4H), 1.56 – 1.45 (m, 4H).

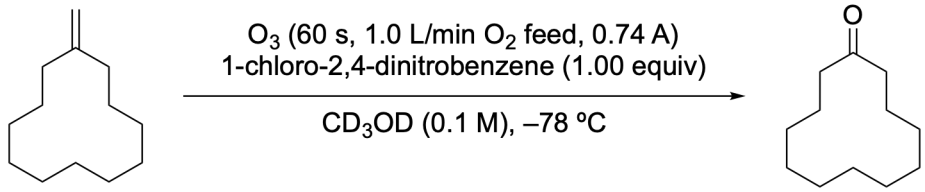
cycloheptanone (**8a**)

^{1}H NMR (800 MHz, MeOD) δ 2.53 – 2.45 (m, 4H), 1.92 – 1.38 (m, 8H).

The signals were deduced from the ^{1}H NMR of the crude reaction mixture.

Table 6.8 methylenecycloheptane (**8**) ozonolysis qNMR Data

Trial	**%conversion**	**%8a**	**normalized %8a**
1	50	2.0	4.0
2	54	2.0	3.7
3	47	2.0	4.3
average			4.0
st. dev.			0.30



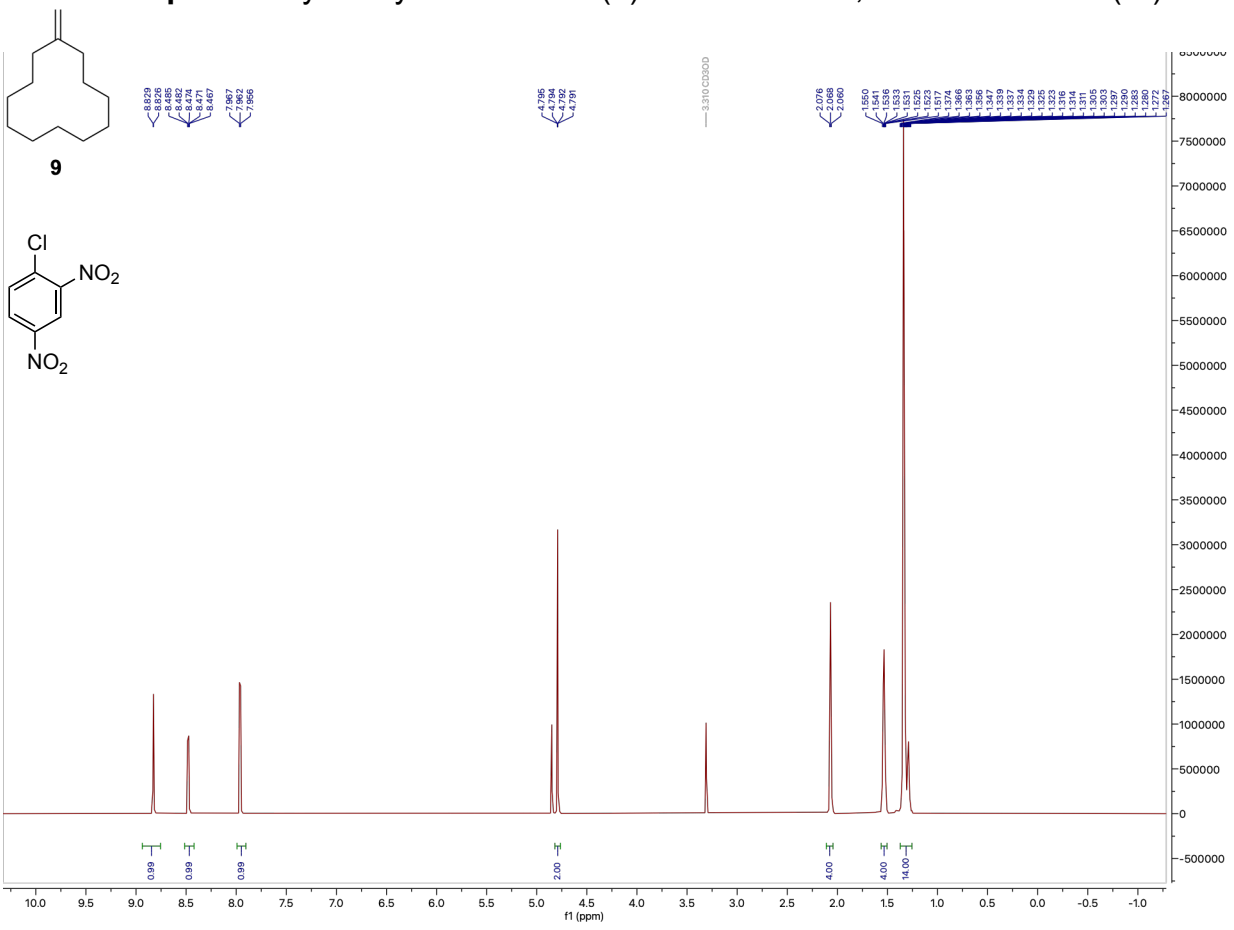
9 **9a**

methylencyclododecane (**9**)

Reaction Time: 60 seconds

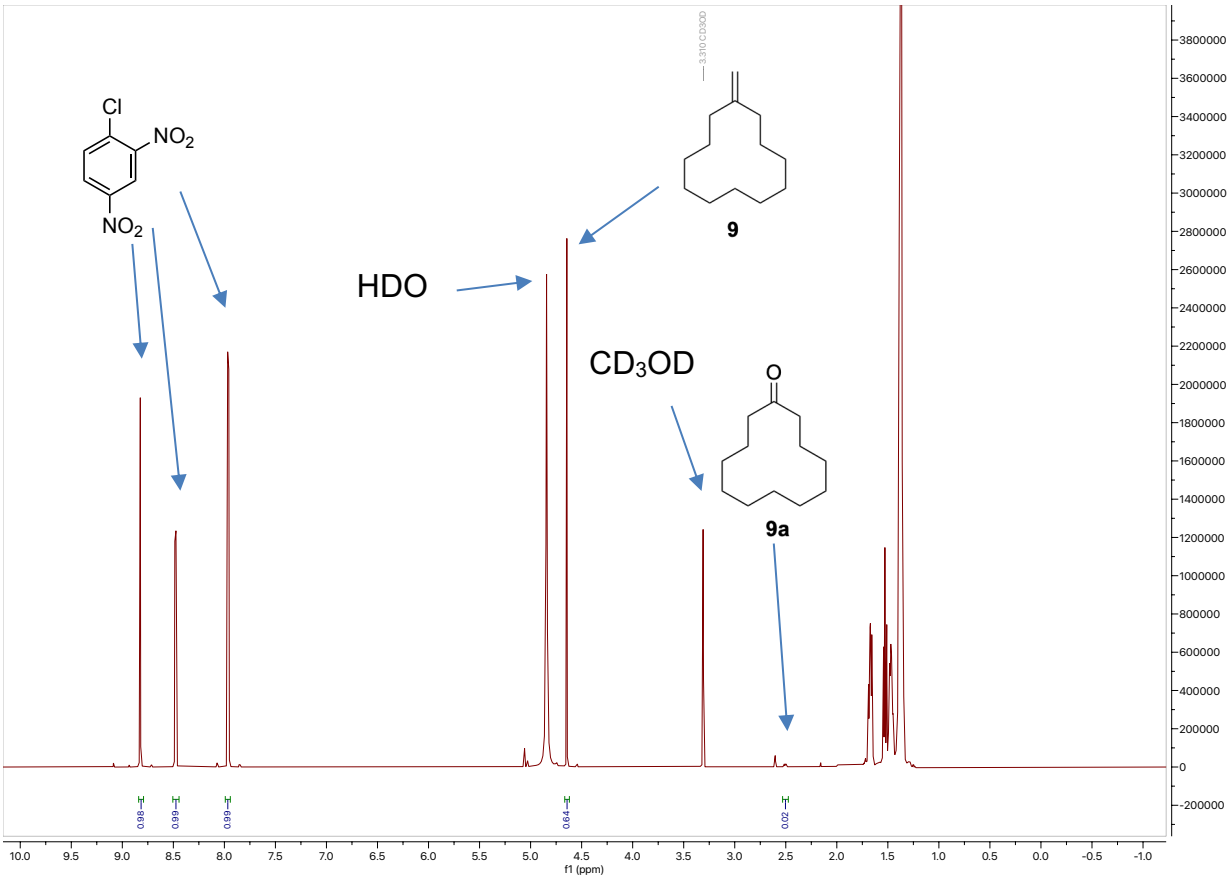
Alkene-to-IS Ratio: 0.99:1.00

Blank Sample: methylenecyclododecane (**9**) and 1-chloro-2,4-dinitrobenzene (**IS**)



^{1}H NMR (800 MHz, CD_3OD), D1 = 10 s, 32 scans

Representative ^{1}H NMR: methylenecyclododecane (**9**) ozonolysis



^{1}H NMR (800 MHz, $CDCl_3$), D1 = 10 s, 32 scans

Characterization Data: methylenecyclododecane (**9**)

methylenecyclododecane (**9**)

^{1}H NMR (800 MHz, MeOD) δ 4.85 – 4.62 (m, 2H), 2.24 – 1.87 (m, 4H), 1.61 – 1.45 (m, 4H), 1.41 – 1.19 (m, 14H).

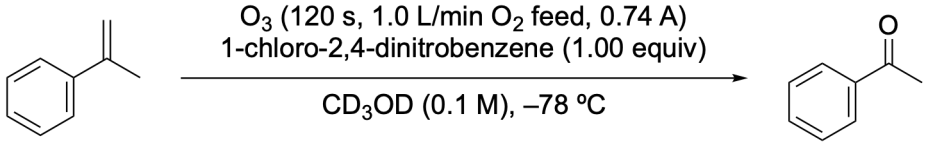
cyclododecanone (**9a**)

^{1}H NMR (800 MHz, MeOD) δ 2.56 – 2.48 (m, 4H), 1.78 – 1.23 (m, 18H).

The signals were deduced from the ^{1}H NMR of the crude reaction mixture.

Table 6.9 methylenecycloheptane (**9**) ozonolysis qNMR Data

Trial	**%conversion**	**%9a**	**normalized %9a**
1	68	1.0	1.5
2	84	1.8	2.2
3	87	1.8	2.0
average			1.9
st. dev.			0.36

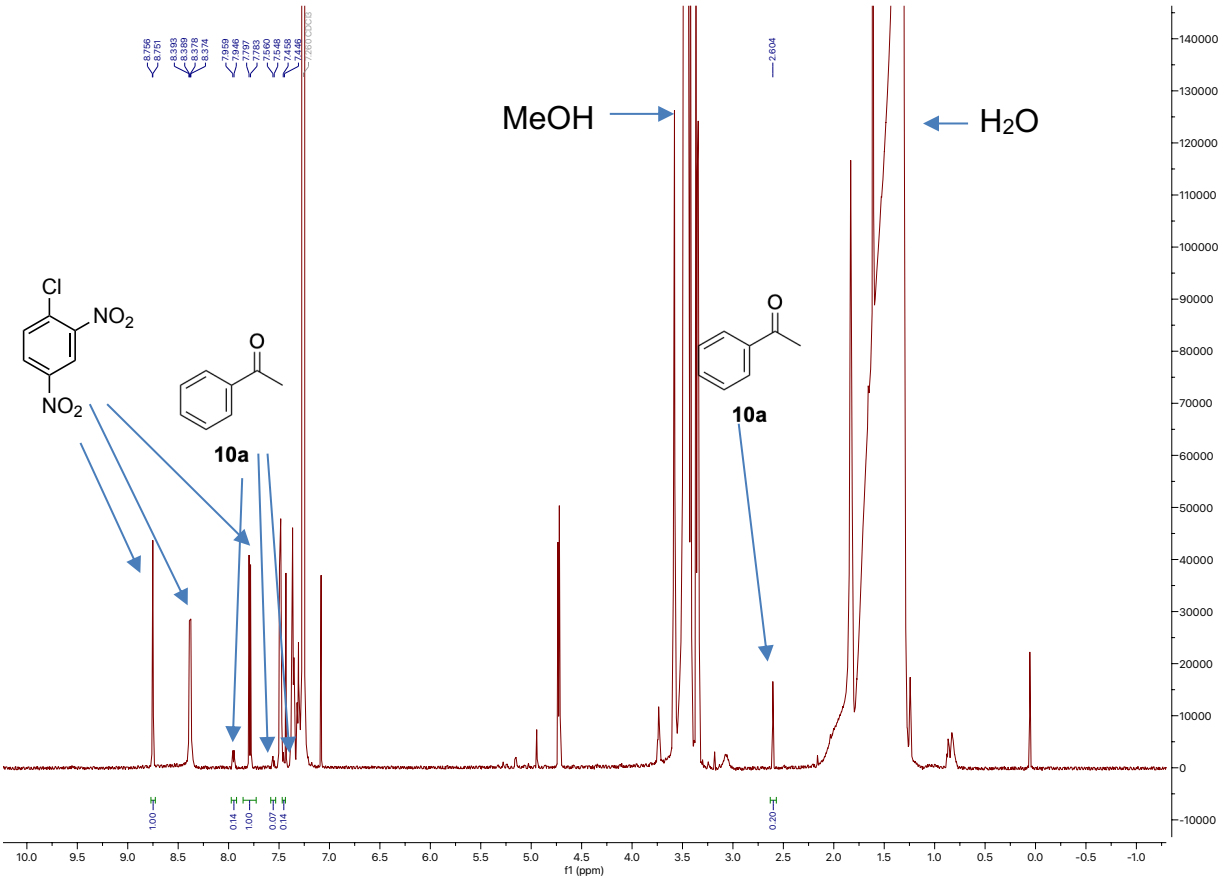


α-methyl styrene (**10**)

Three individual samples (0.333 mmol scale each) were prepared for α-methyl styrene (**10**) using MeOH as the solvent. After warming to room temperature, a 0.1 mL aliquot was taken from each reaction sample and diluted with $CDCl_3$ (0.6 mL) to measure ^1H NMR.

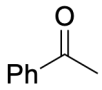
Reaction Time: 120 seconds

Representative ^1H NMR: α-methyl styrene (**10**) ozonolysis



^1H NMR (600 MHz, $CDCl_3$), D1 = 10 s, 32 scans

Characterization Data: α-methyl styrene (**10**)

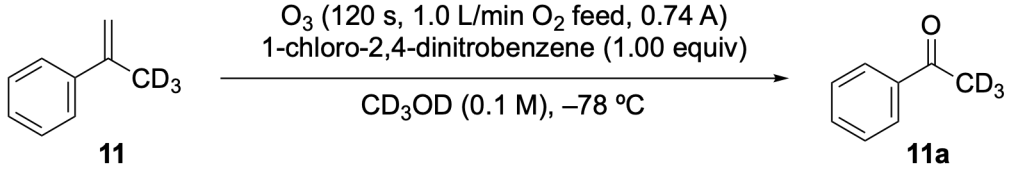


acetophenone (**10a**)

^{1}H NMR (600 MHz, $CDCl_3$) δ 7.95 (d, *J* = 7.4 Hz, 2H), 7.55 (t, *J* = 7.5 Hz, 1H), 7.45 (t, *J* = 7.3 Hz, 2H), 2.60 (s, 3H).

Table 6.10 α-methyl styrene (**10**) ozonolysis qNMR Data

Trial	**%10a**
1	6.8
2	7.1
3	6.9
average	6.9
St. Dev.	0.13



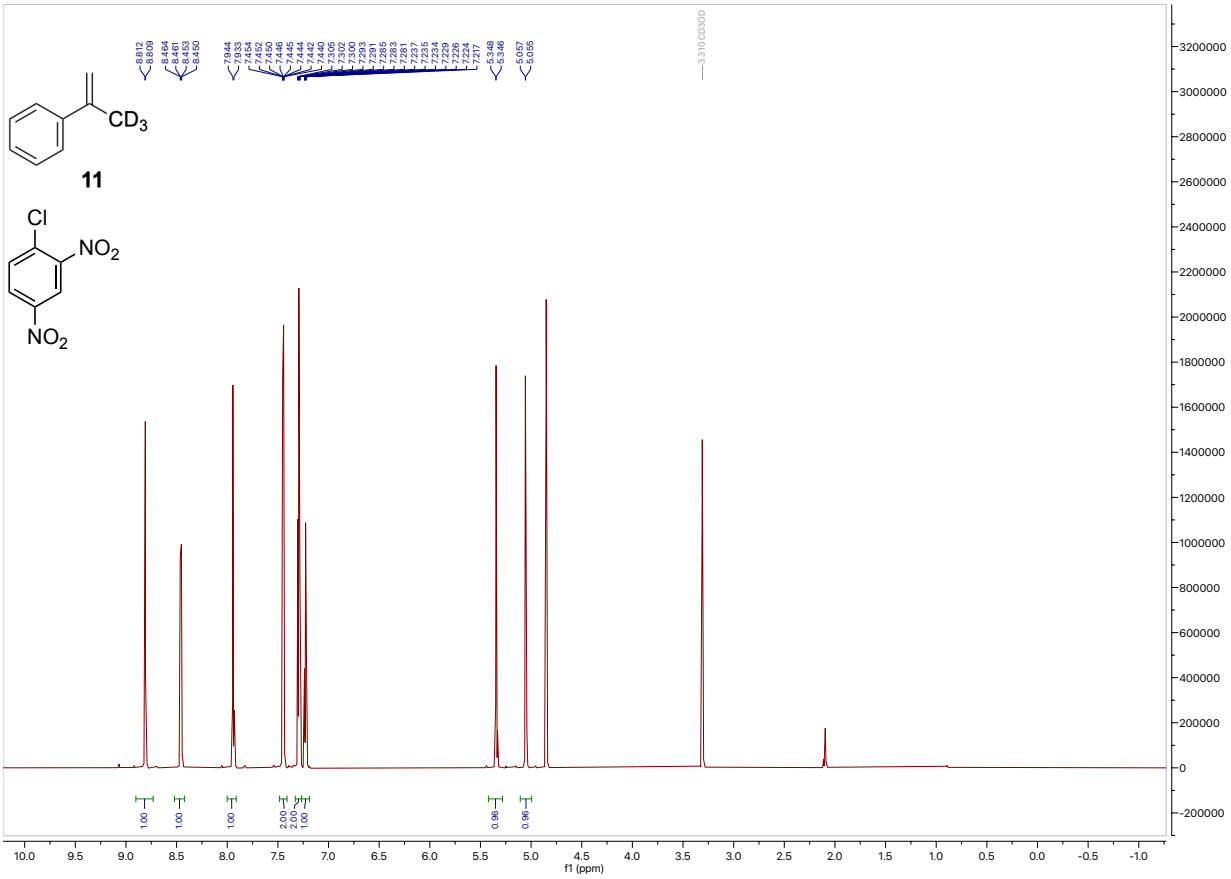
11 **11a**

(prop-1-en-2-yl-3,3,3-*d3*)benzene (**11**)

Reaction Time: 120 seconds

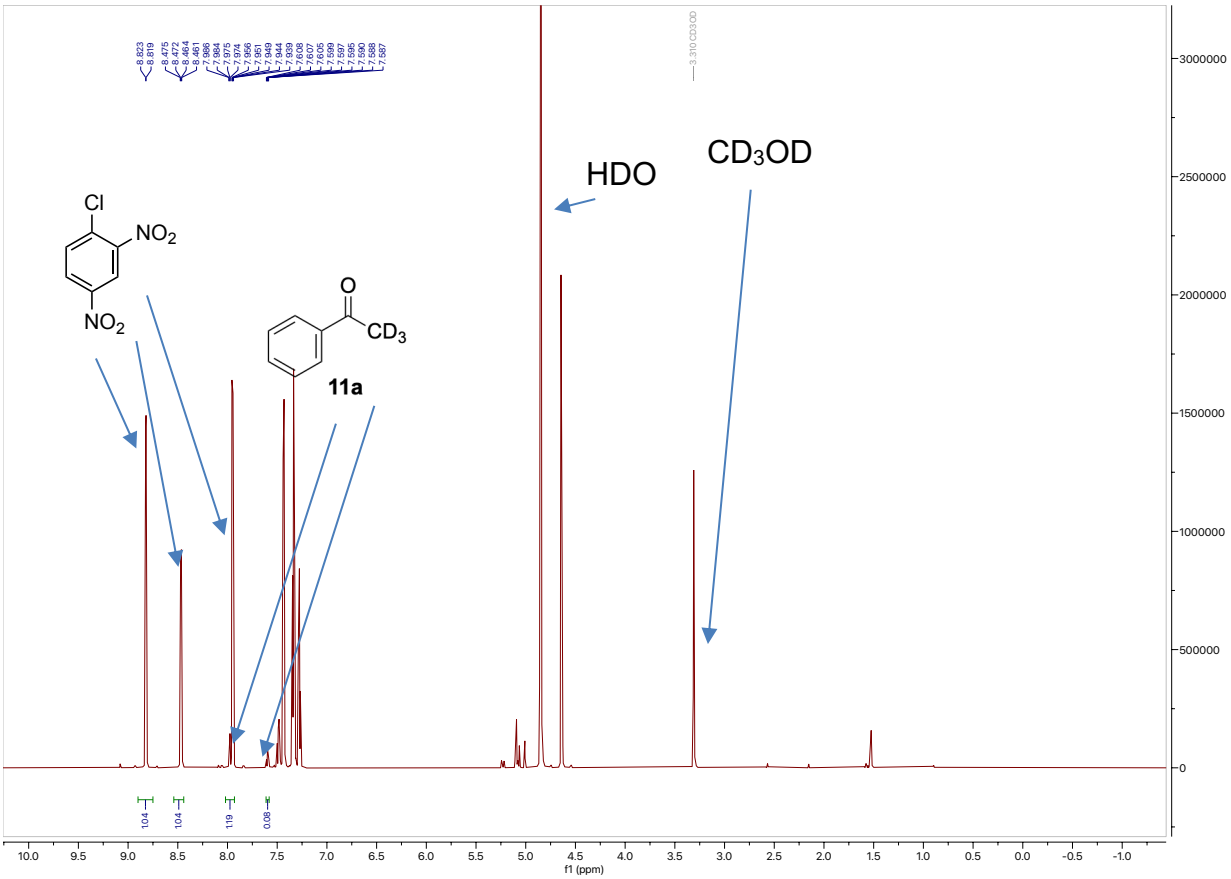
Alkene-to-IS Ratio: 0.96:1.00

Blank Sample: (prop-1-en-2-yl-3,3,3-*d3*)benzene (**11**) and 1-chloro-2,4-dinitrobenzene (**IS**)



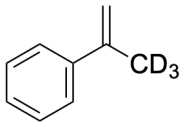
^{1}H NMR (800 MHz, CD_3OD), D1 = 10 s, 32 scans

Representative ^{1}H NMR: (prop-1-en-2-yl-3,3,3-*d3*)benzene (**11**) ozonolysis



^{1}H NMR (800 MHz, $CDCl_3$), D1 = 10 s, 32 scans

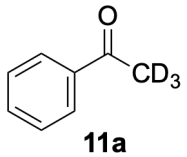
Characterization Data: (prop-1-en-2-yl-3,3,3-*d3*)benzene (**11**)



11

(prop-1-en-2-yl-3,3,3-d_3)benzene (**11**)

^{1}H NMR (800 MHz, MeOD) δ 7.50 – 7.40 (m, 2H), 7.38 – 7.26 (m, 2H), 7.25 – 7.20 (m, 1H), 5.35 (d, *J* = 1.6 Hz, 1H), 5.06 (d, *J* = 1.6 Hz, 1H).



11a

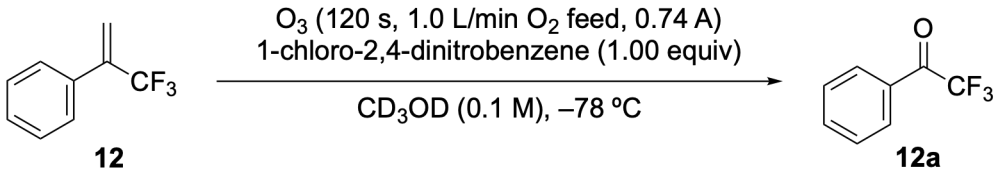
trideuteroacetophenone (**11a**)

^{1}H NMR (800 MHz, MeOD) δ 8.00 (dd, *J* = 8.4, 1.4 Hz, 2H), 7.68 – 7.57 (m, 1H), 7.54 – 7.42 (m, 2H).

The signals were measured from the ^{1}H NMR of the crude reaction mixture.

Table 6.11 (prop-1-en-2-yl-3,3,3-d_3)benzene (**11**) ozonolysis qNMR Data

Trial	**%11a**
1	7.8
2	8.0
3	7.8
average	7.9
st. dev.	0.12



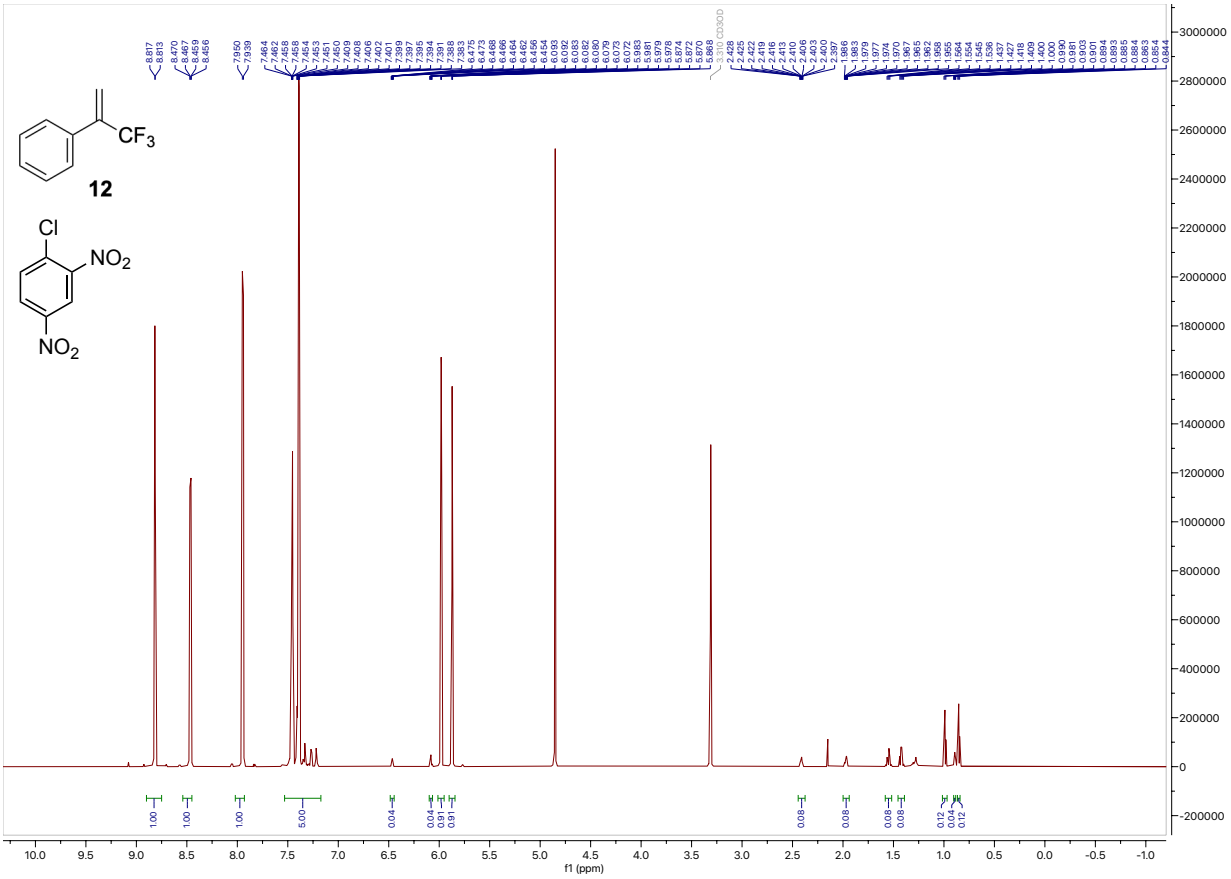
12 **12a**

(3,3,3-trifluoroprop-1-en-2-yl)benzene (**12**)

Reaction Time: 120 seconds

Alkene-to-IS Ratio: 0.91:1.00

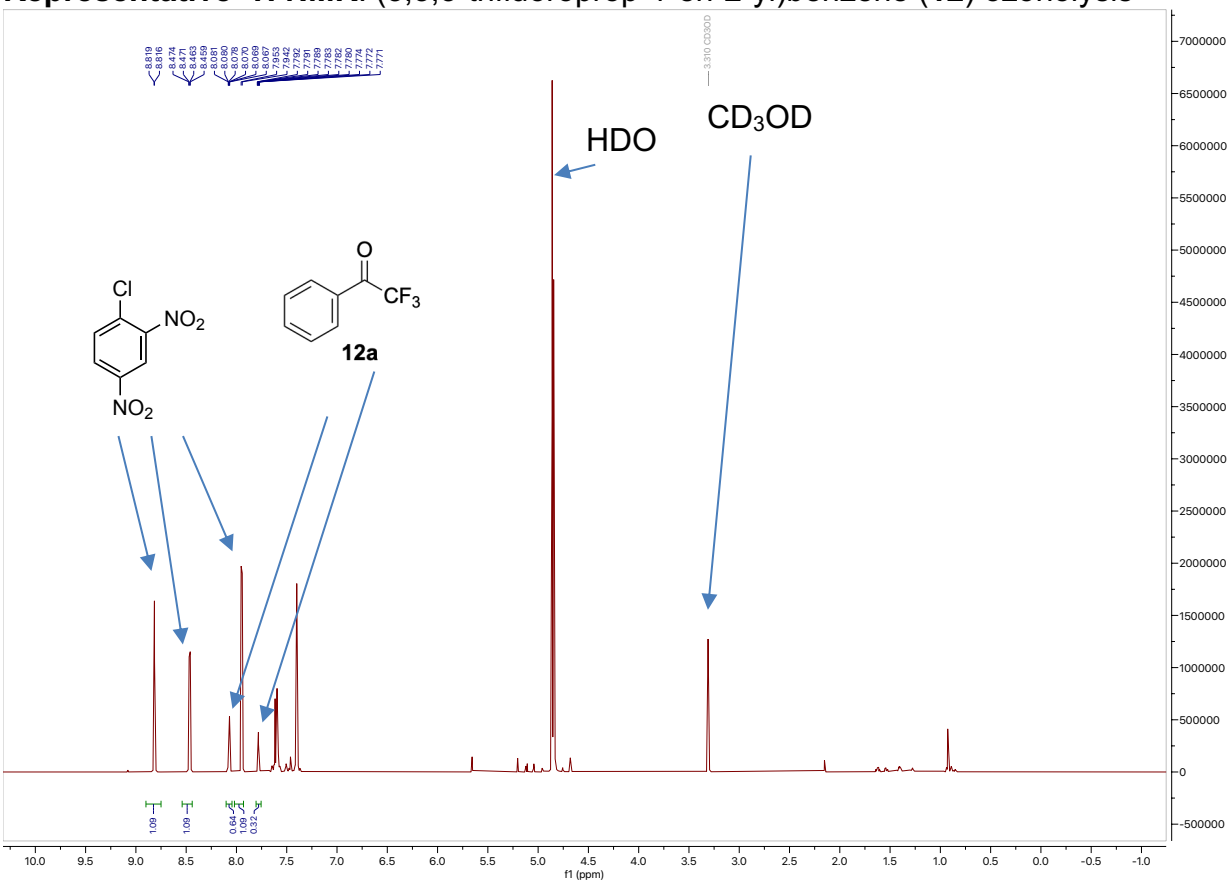
Blank Sample: (3,3,3-trifluoroprop-1-en-2-yl)benzene (**12**) and 1-chloro-2,4-dinitrobenzene (**IS**)



^{1}H NMR (800 MHz, CD_3OD)

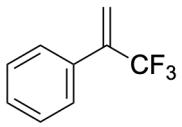
The sample of (3,3,3-trifluoroprop-1-en-2-yl)benzene (**12**) was contaminated with (1,1,1-trifluorohex-2-en-2-yl)benzene which formed from *n*BuLi addition to trifluoroacetophenone then loss of water during the synthesis of **12**.

Representative ^{1}H NMR: (3,3,3-trifluoroprop-1-en-2-yl)benzene (**12**) ozonolysis



^{1}H NMR (800 MHz, CD_3OD), D1 = 10 s, 32 scans

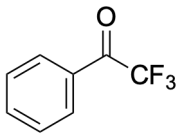
Characterization Data: (3,3,3-trifluoroprop-1-en-2-yl)benzene (**12**)



12

(3,3,3-trifluoroprop-1-en-2-yl)benzene (**12**)

^{1}H NMR (800 MHz, MeOD) δ 7.48 – 7.44 (m, 2H), 7.42 – 7.38 (m, 3H), 5.98 (q, *J* = 1.4 Hz, 1H), 5.87 (q, *J* = 1.7 Hz, 1H).



12a

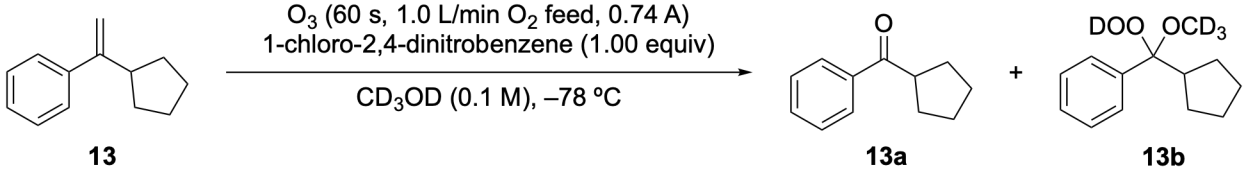
trifluoroacetophenone (**12a**)

^{1}H NMR (800 MHz, MeOD) δ 8.15 – 8.02 (m, 2H), 7.89 – 7.68 (m, 1H), 7.68 – 7.59 (m, 2H).

The *o*-CH and *p*-CH signals were measured from the ^{1}H NMR of the crude reaction mixture. The *m*-CH signal was deduced from the 1D Selective Gradient TOCSY spectrum.

Table 6.12 (3,3,3-trifluoroprop-1-en-2-yl)benzene (**12**)

Trial	**%12a**
1	32
2	32.3
3	33.3
average	32.5
st. dev.	0.68



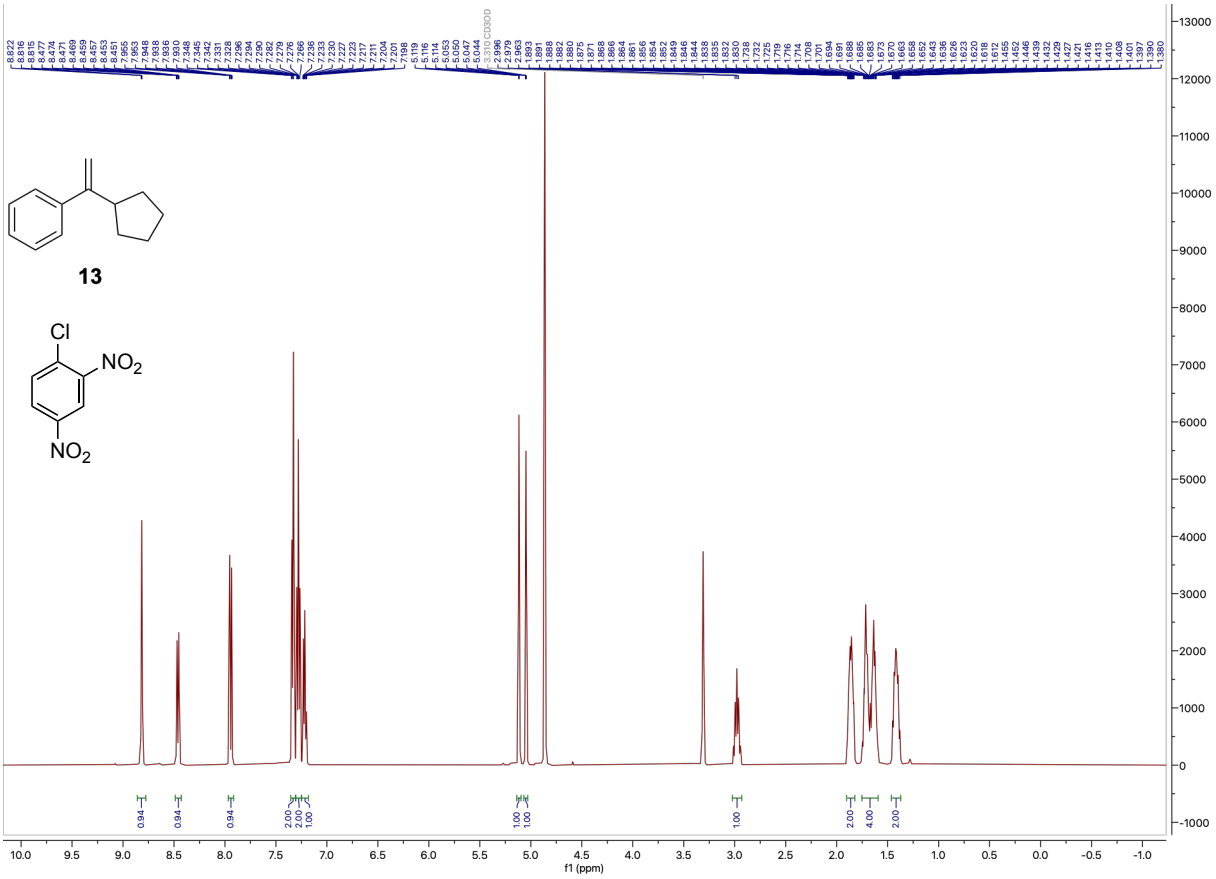
13 **13a** **13b**

(1-cyclopentylvinyl)benzene (**13**)

Reaction Time: 60 seconds

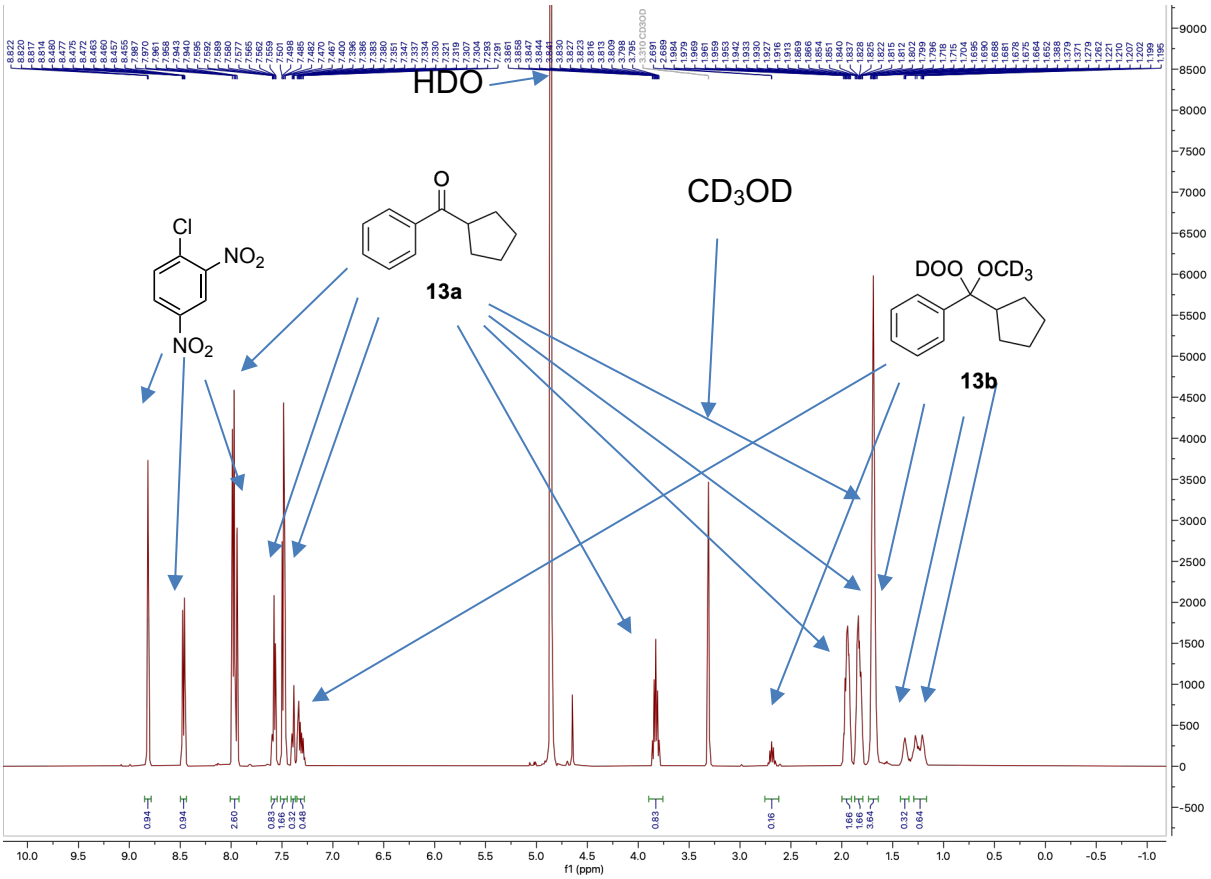
Alkene-to-IS Ratio: 1.00:0.94

Blank Sample: (1-cyclopentylvinyl)benzene (**13**) and 1-chloro-2,4-dinitrobenzene (**IS**)



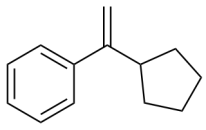
^{1}H NMR (500 MHz, CD_3OD), D1 = 10 s, 32 scans

Representative ^{1}H NMR: (1-cyclopentylvinyl)benzene (**13**) ozonolysis



^{1}H NMR (500 MHz, CD_3OD), D1 = 10 s, 32 scans

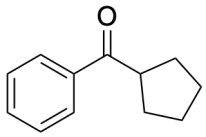
Characterization Data: (1-cyclopentylvinyl)benzene (**13**)



13

(1-cyclopentylvinyl)benzene (**13**)

^{1}H NMR (500 MHz, MeOD) δ 7.34 (dd, *J* = 7.1, 1.3 Hz, 2H), 7.31 – 7.24 (m, 2H), 7.24 – 7.18 (m, 1H), 5.18 – 5.08 (m, 1H), 5.05 (q, *J* = 1.4 Hz, 1H), 2.98 (p, *J* = 8.2 Hz, 1H), 1.98 – 1.78 (m, 2H), 1.78 – 1.57 (m, 4H), 1.42 (dddd, *J* = 15.1, 14.0, 6.6, 3.4 Hz, 2H).

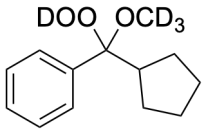


13a

cyclopentyl(phenyl)methanone (**13a**)

^{1}H NMR (500 MHz, MeOD) δ 8.05 – 7.92 (m, 2H), 7.58 (td, *J* = 7.2, 1.4 Hz, 1H), 7.48 (td, *J* = 7.6, 1.4 Hz, 2H), 3.83 (dddd, *J* = 13.7, 8.5, 6.9, 1.4 Hz, 1H), 2.00 – 1.89 (m, 2H), 1.83 (dtd, *J* = 11.4, 6.7, 1.3 Hz, 2H), 1.76 – 1.58 (m, 4H).

The signals were measured from the ^{1}H NMR of the crude reaction mixture.



13b

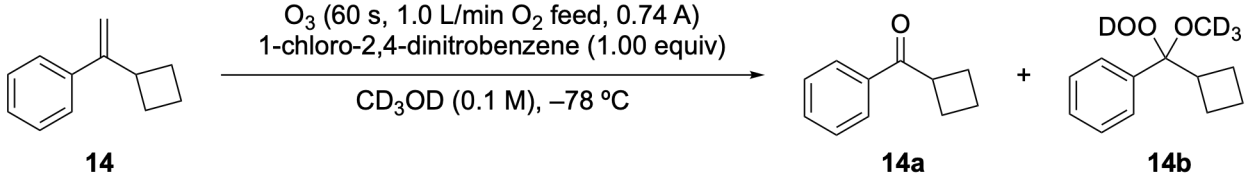
(cyclopentyl(deuteroperoxy)(methoxy-d_3)methyl)benzene (**13b**)

^{1}H NMR (500 MHz, MeOD) δ 7.42 – 7.36 (m, 2H), 7.32 (dtd, *J* = 15.4, 6.9, 1.4 Hz, 3H), 2.74 – 2.64 (m, 1H), 1.76 – 1.62 (m, 2H), 1.45 – 1.33 (m, 2H), 1.33 – 1.12 (m, 4H).

The signals were measured and deduced from the ^{1}H NMR of the crude reaction mixture.

Table 6.13 (1-cyclopentylvinyl)benzene (**13**) qNMR Data

Trial	%13a	%13b
1	83	16
2	83	17
3	83	17
average	83	17
st. dev.	0	0.47



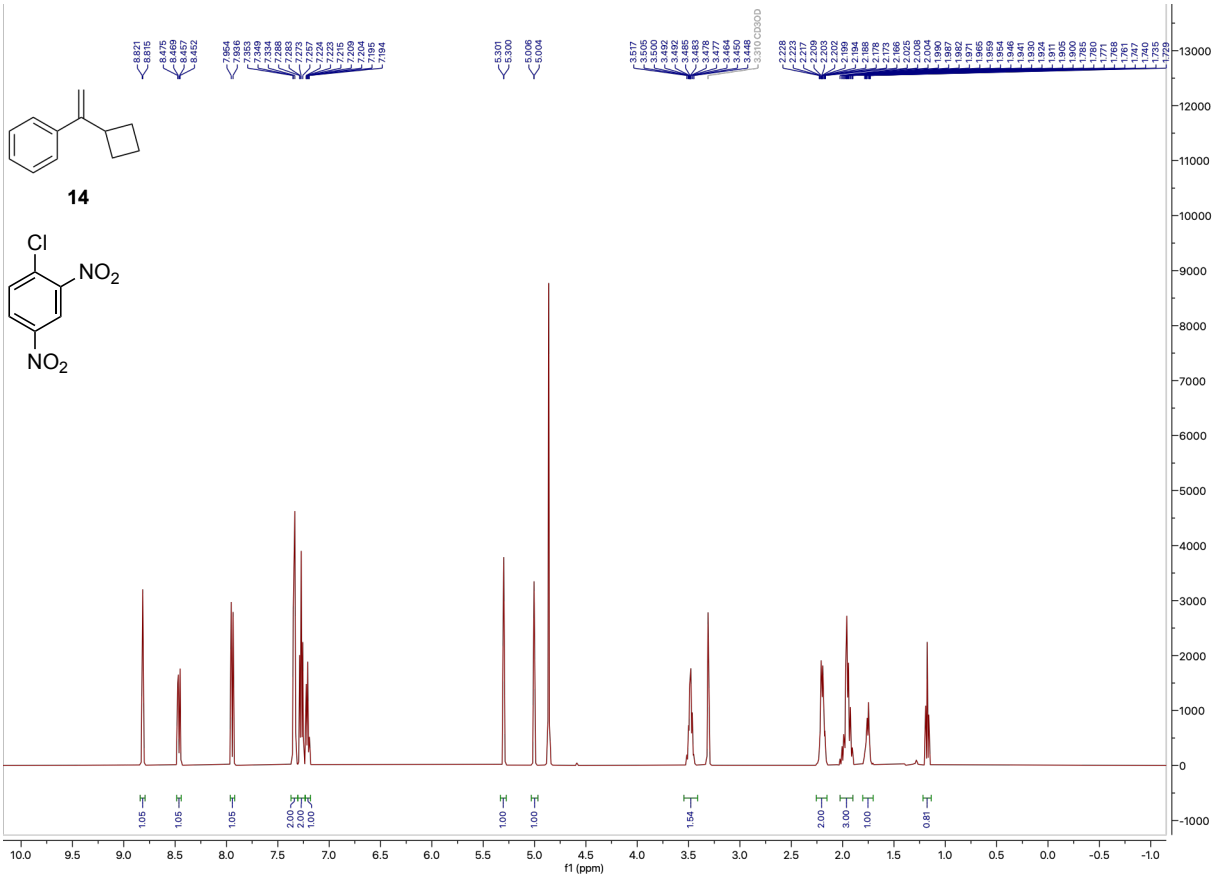
14 **14a** **14b**

(1-cyclobutylvinyl)benzene (**14**)

Reaction Time: 60 seconds

Alkene-to-IS Ratio: 0.95:1.00

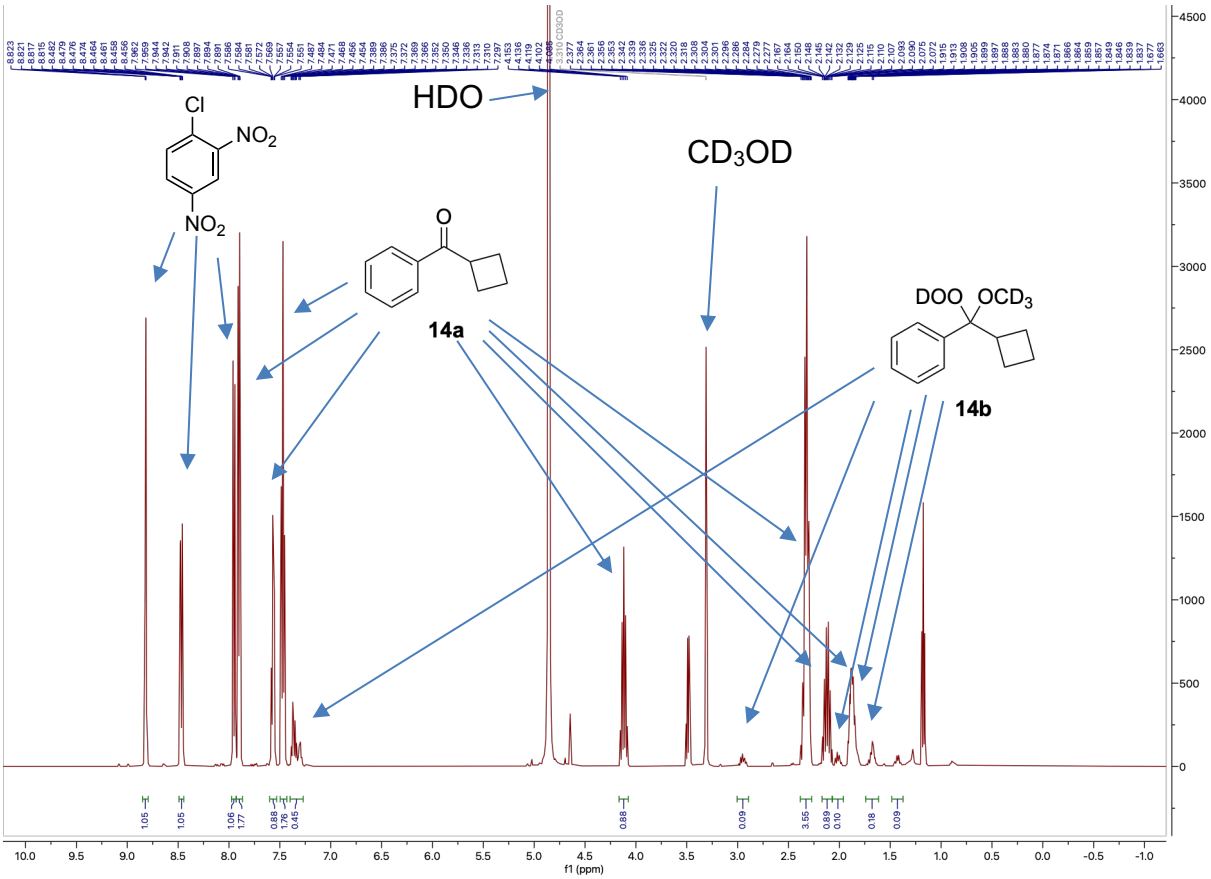
Blank Sample: (1-cyclobutylvinyl)benzene (**14**) and 1-chloro-2,4-dinitrobenzene (**IS**)



^{1}H NMR (500 MHz, CD_3OD)

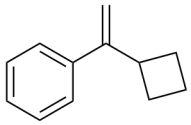
There was a small amount of diethyl ether remaining in the sample.

Representative ^{1}H NMR: (1-cyclobutylvinyl)benzene (**14**) ozonolysis



^{1}H NMR (500 MHz, CD_3OD), D1 = 10 s, 32 scans

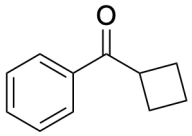
Characterization Data: (1-cyclobutylvinyl)benzene (**14**)



14

(1-cyclobutylvinyl)benzene (**14**)

^{1}H NMR (500 MHz, MeOD) δ 7.34 (d, *J* = 7.6 Hz, 2H), 7.27 (t, *J* = 7.6 Hz, 2H), 7.25 – 7.18 (m, 1H), 5.39 – 5.14 (m, 1H), 5.01 (d, *J* = 1.2 Hz, 1H), 3.54 – 3.39 (m, 1H), 2.55 – 2.09 (m, 2H), 2.06 – 1.86 (m, 3H), 1.85 – 1.68 (m, 1H).

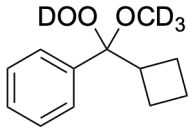


14a

cyclobutyl(phenyl)methanone (**14a**)

^{1}H NMR (500 MHz, MeOD) δ 7.93 – 7.83 (m, 2H), 7.57 (td, *J* = 7.4, 1.2 Hz, 1H), 7.51 – 7.43 (m, 2H), 4.12 (p, *J* = 8.5 Hz, 1H), 2.40 – 2.24 (m, 4H), 2.20 – 2.06 (m, 1H), 1.96 – 1.77 (m, 1H).

The signals were measured and deduced from the ^{1}H NMR of the crude reaction mixture.



14b

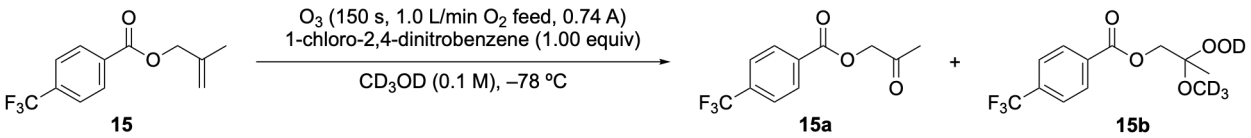
(cyclobutyl(deuteroperoxy)(methoxy-d_3)methyl)benzene (**14b**)

^{1}H NMR (500 MHz, MeOD) δ 7.40 – 7.26 (m, 5H), 3.01 – 2.88 (m, 1H), 2.01 (h, *J* = 8.2 Hz, 1H), 1.92 – 1.75 (m, 2H), 1.75 – 1.61 (m, 2H), 1.47 – 1.32 (m, 1H).

The signals were measured and deduced from the ^{1}H NMR of the crude reaction mixture.

Table 6.14 (1-cyclobutylvinyl)benzene (**14**) qNMR Data

Trial	%14a	%14b
1	88	9.0
2	91	9.0
3	90	9.0
average	90	9.0
st. dev.	1.5	0

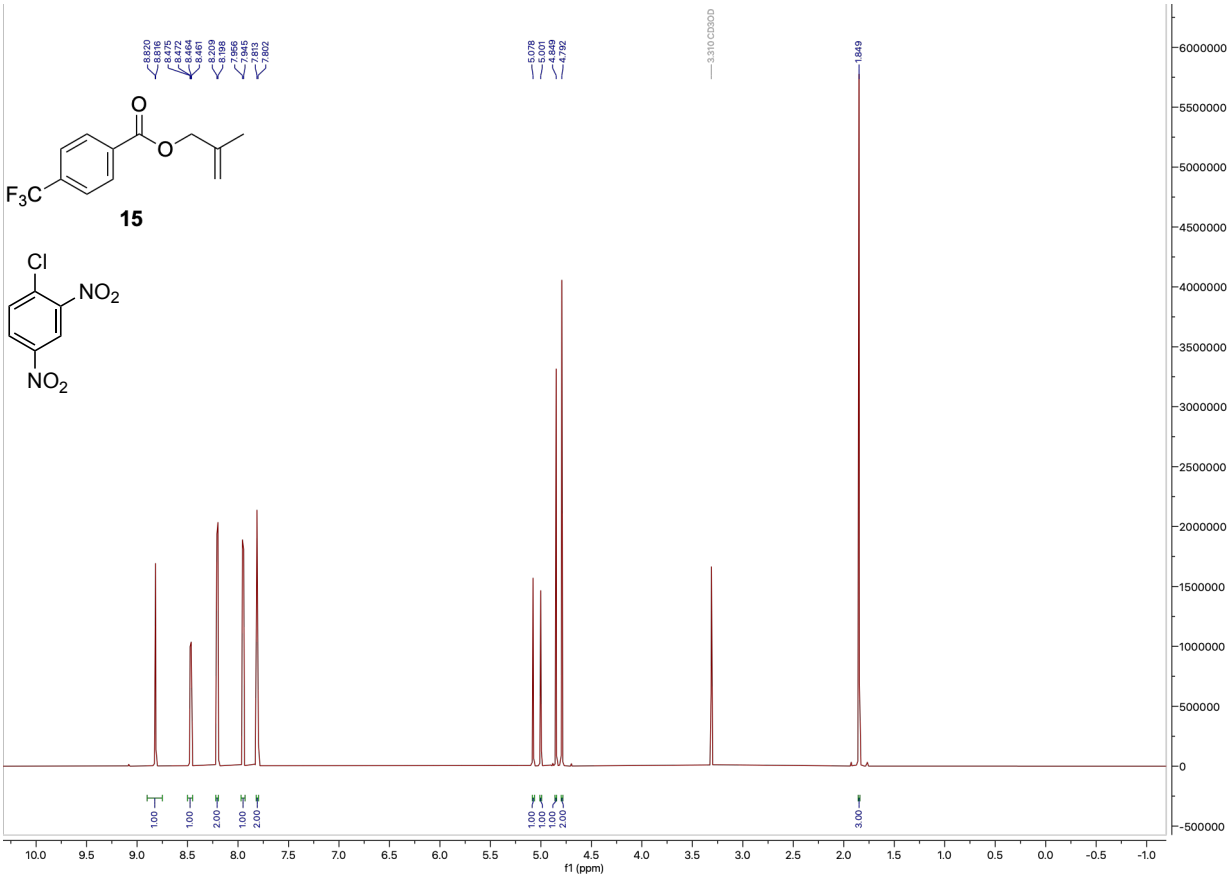


2-methylallyl 4-(trifluoromethyl)benzoate (**15**)

Reaction Time: 150 seconds

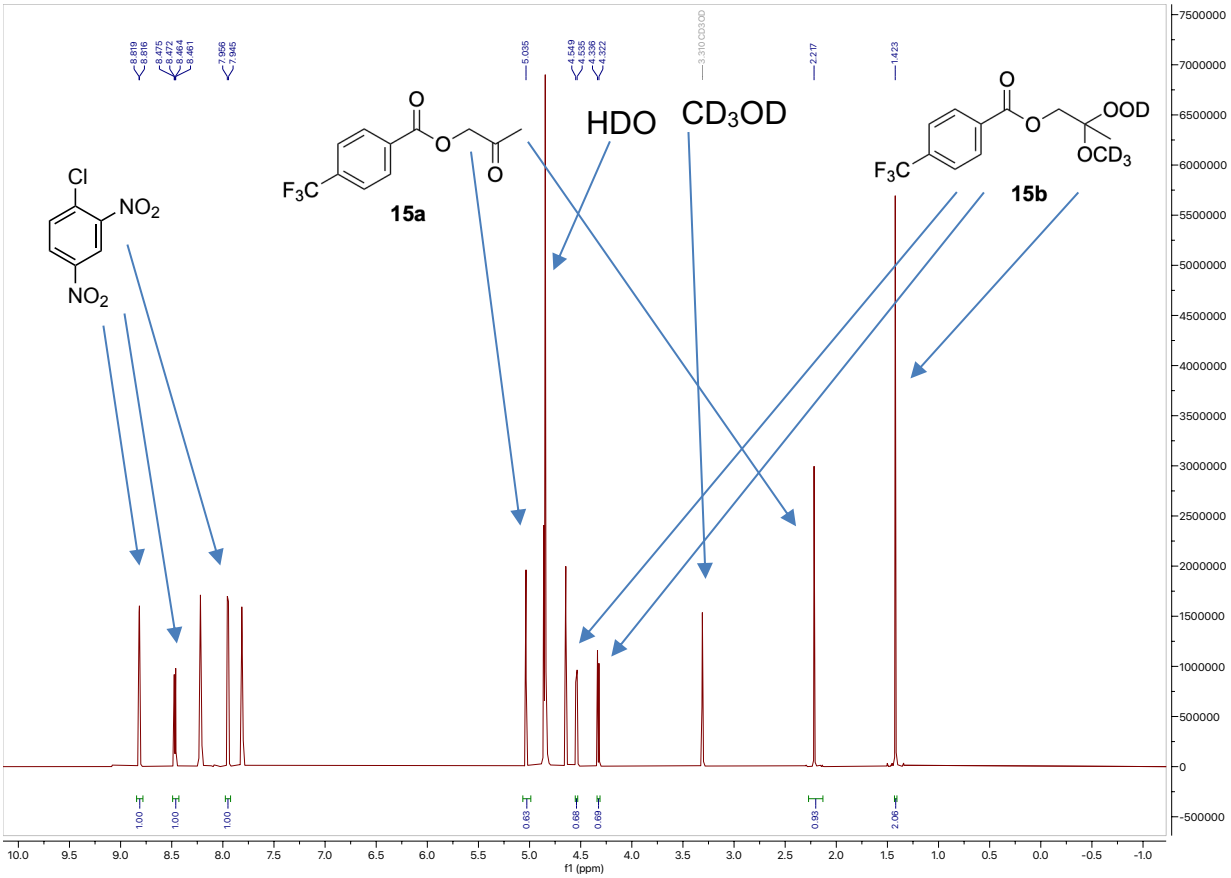
Alkene-to-IS Ratio: 1.00:1.00

Blank Sample: 2-methylallyl 4-(trifluoromethyl)benzoate (**15**) and 1-chloro-2,4-dinitrobenzene (**IS**)



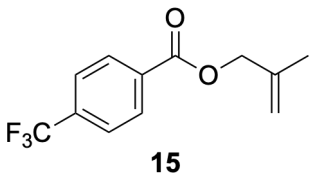
^{1}H NMR (800 MHz, CD_3OD), D1 = 10 s, 32 scans

Representative ^{1}H NMR: 2-methylallyl 4-(trifluoromethyl)benzoate (**15**) ozonolysis



^{1}H NMR (800 MHz, CD_3OD), D1 = 10 s, 32 scans

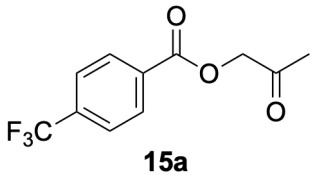
Characterization Data: 2-methylallyl 4-(trifluoromethyl)benzoate (**15**)



15

2-methylallyl 4-(trifluoromethyl)benzoate (**15**)

^{1}H NMR (800 MHz, MeOD) δ 8.20 (d, *J* = 8.2 Hz, 2H), 7.81 (d, *J* = 8.4 Hz, 2H), 5.08 (s, 1H), 5.00 (s, 1H), 4.85 (s, 1H), 4.79 (s, 2H), 1.85 (s, 3H).

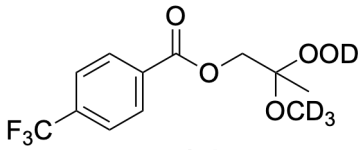


15a

2-oxopropyl 4-(trifluoromethyl)benzoate (**15a**)

^{1}H NMR (800 MHz, MeOD) δ 8.25 – 8.17 (m, 2H), 7.85 – 7.78 (m, 2H), 5.04 (s, 2H), 2.22 (s, 3H).

The signals were measured and deduced from the ^{1}H NMR of the crude reaction mixture.



15b

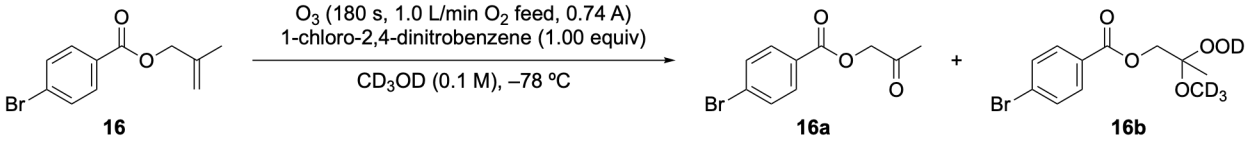
2-deuteroperoxy-2-(methoxy-d_3)propyl 4-(trifluoromethyl)benzoate (**15b**)

^{1}H NMR (800 MHz, MeOD) δ 8.25 – 8.17 (m, 2H), 7.85 – 7.78 (m, 2H), 4.54 (d, *J* = 11.2 Hz, 1H), 4.33 (d, *J* = 11.3 Hz, 1H), 1.42 (s, 3H).

The signals were measured and deduced from the ^{1}H NMR of the crude reaction mixture.

Table 6.15 2-methylallyl 4-(trifluoromethyl)benzoate (**15**) qNMR Data

Trial	%15a	%15b
1	31.3	70
2	31.3	68.5
3	31.3	68.5
average	31.3	68.7
st. dev.	0	1.18

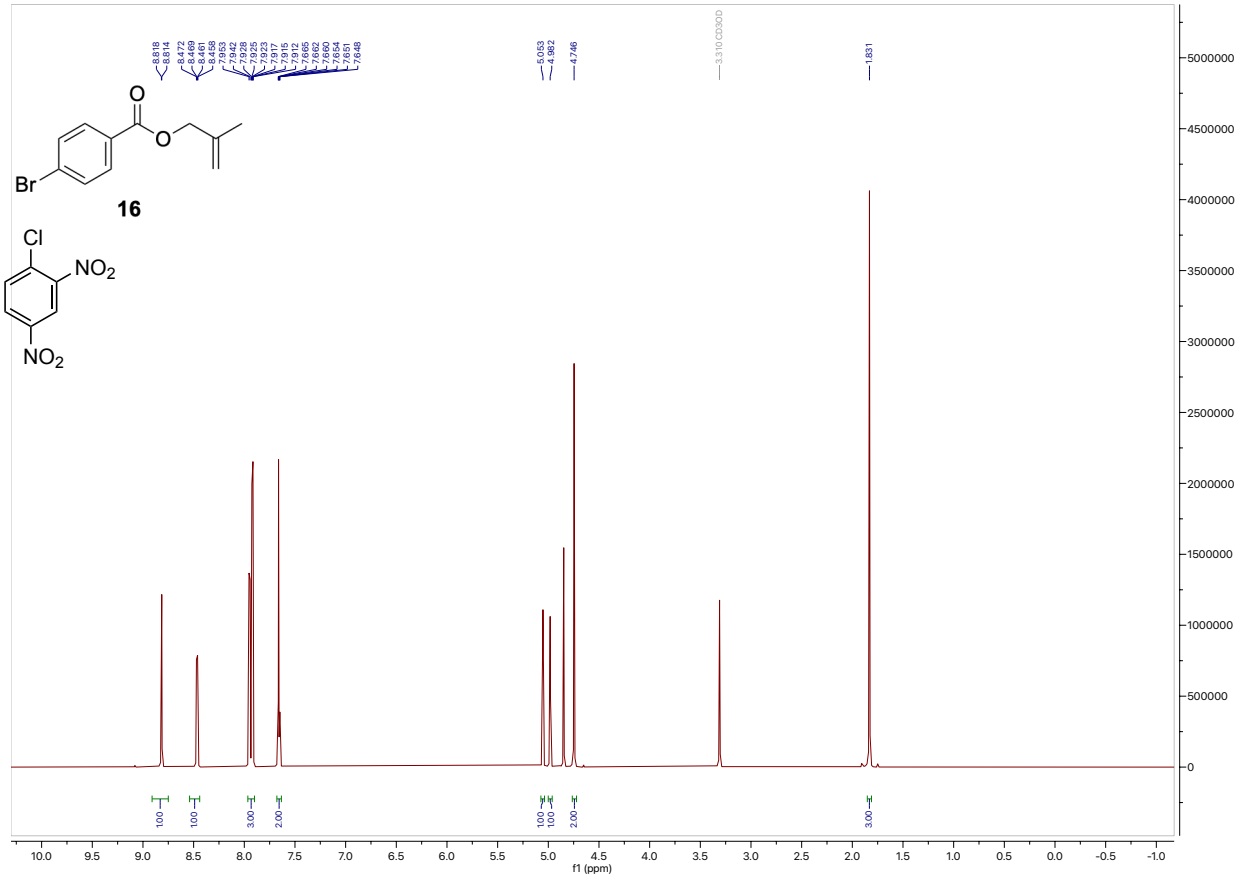


2-methylallyl 4-bromobenzoate (**16**)

Reaction Time: 180 seconds

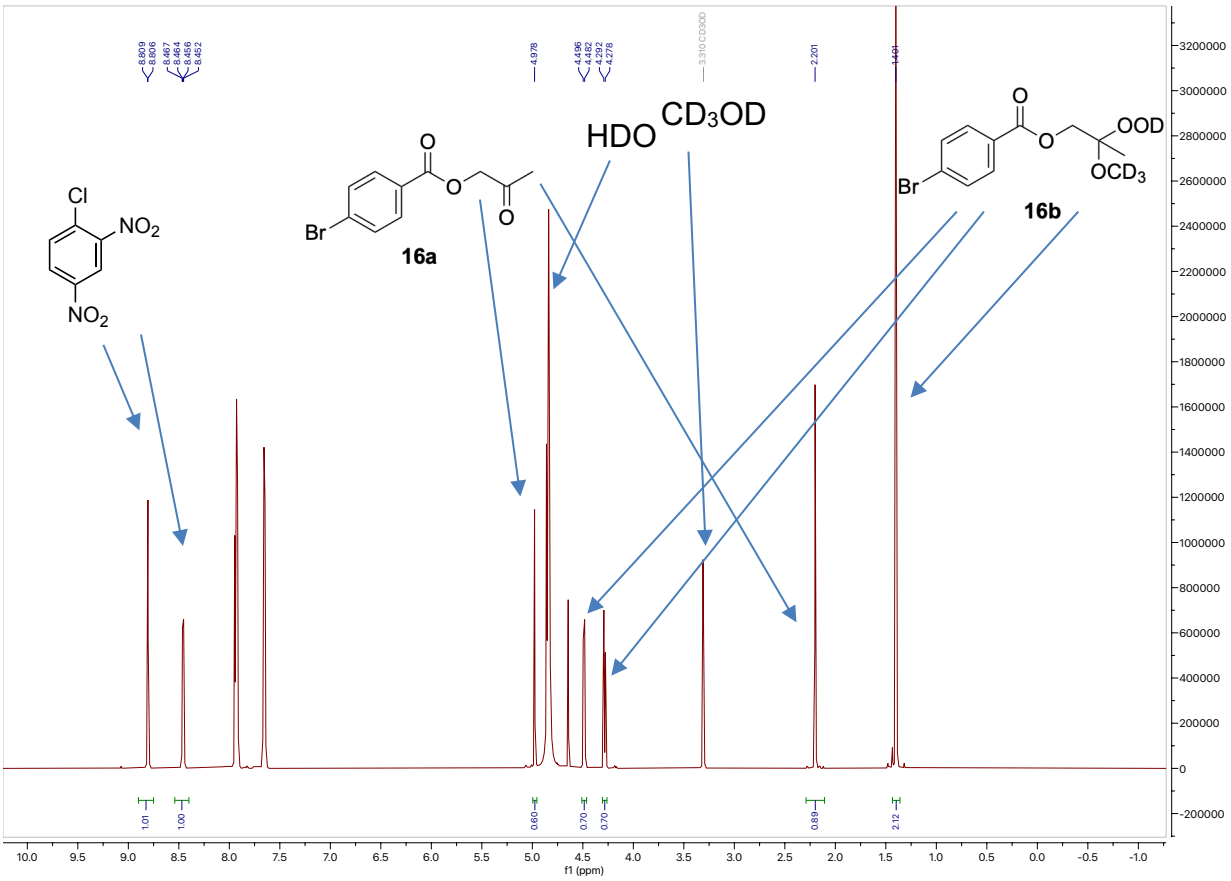
Alkene-to-IS Ratio: 1.00:1.00

Blank Sample: 2-methylallyl 4-bromobenzoate (**16**) and 1-chloro-2,4-dinitrobenzene (**IS**)



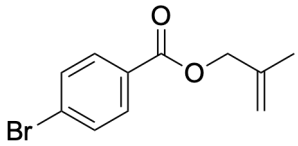
^{1}H NMR (800 MHz, CD_3OD)

Representative ^{1}H NMR: 2-methylallyl 4-bromobenzoate (**16**) ozonolysis



^{1}H NMR (800 MHz, CD_3OD), D1 = 10 s, 32 scans

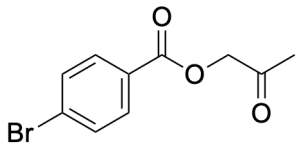
Characterization Data: 2-methylallyl 4-bromobenzoate (**16**)



16

2-methylallyl 4-bromobenzoate (**16**)

^{1}H NMR (800 MHz, MeOD) δ 7.94 – 7.89 (m, 2H), 7.70 – 7.61 (m, 2H), 5.05 (s, 1H), 4.98 (s, 1H), 4.75 (s, 2H), 1.83 (s, 3H).

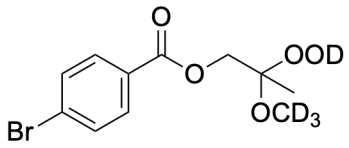


16a

2-oxopropyl 4-bromobenzoate (**16a**)

^{1}H NMR (800 MHz, MeOD) δ 7.99 – 7.87 (m, 2H), 7.72 – 7.60 (m, 2H), 4.98 (s, 2H), 2.20 (s, 3H).

The signals were measured and deduced from the ^{1}H NMR of the crude reaction mixture.



16b

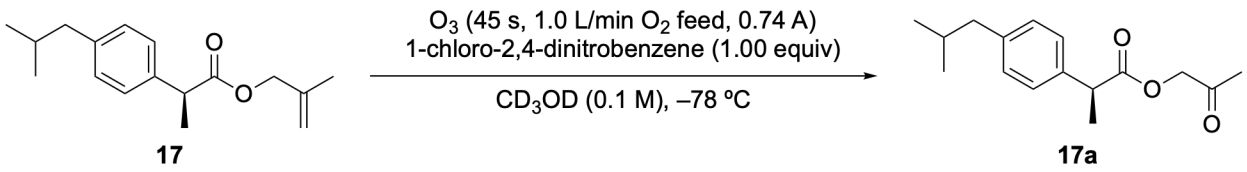
2-deuteroperoxy-2-(methoxy-d_3)propyl 4-bromobenzoate (**16b**)

^{1}H NMR (800 MHz, MeOD) δ 7.98 – 7.87 (m, 2H), 7.69 – 7.61 (m, 2H), 4.49 (d, *J* = 11.2 Hz, 1H), 4.28 (d, *J* = 11.3 Hz, 1H), 1.40 (s, 3H).

The signals were measured and deduced from the ^{1}H NMR of the crude reaction mixture.

Table 6.16 2-methylallyl 4-bromobenzoate (**16**) qNMR Data

Trial	**%16a**	**%16b**
1	29.2	70.8
2	28.8	71.1
3	29.9	70.2
average	29.3	70.7
st. dev.	0.557	0.437

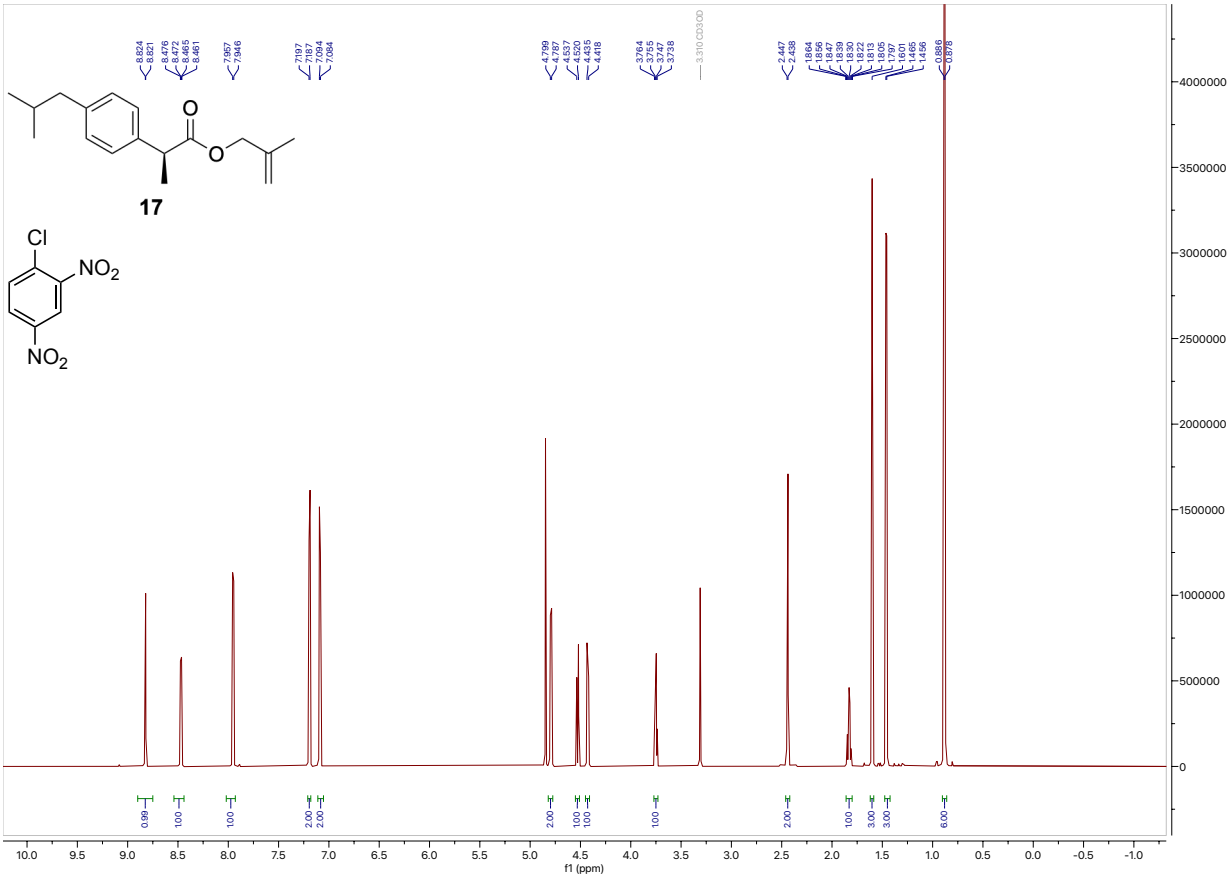


2-methylallyl (*S*)-2-(4-isobutylphenyl)propanoate (**17**)

Reaction Time: 45 seconds

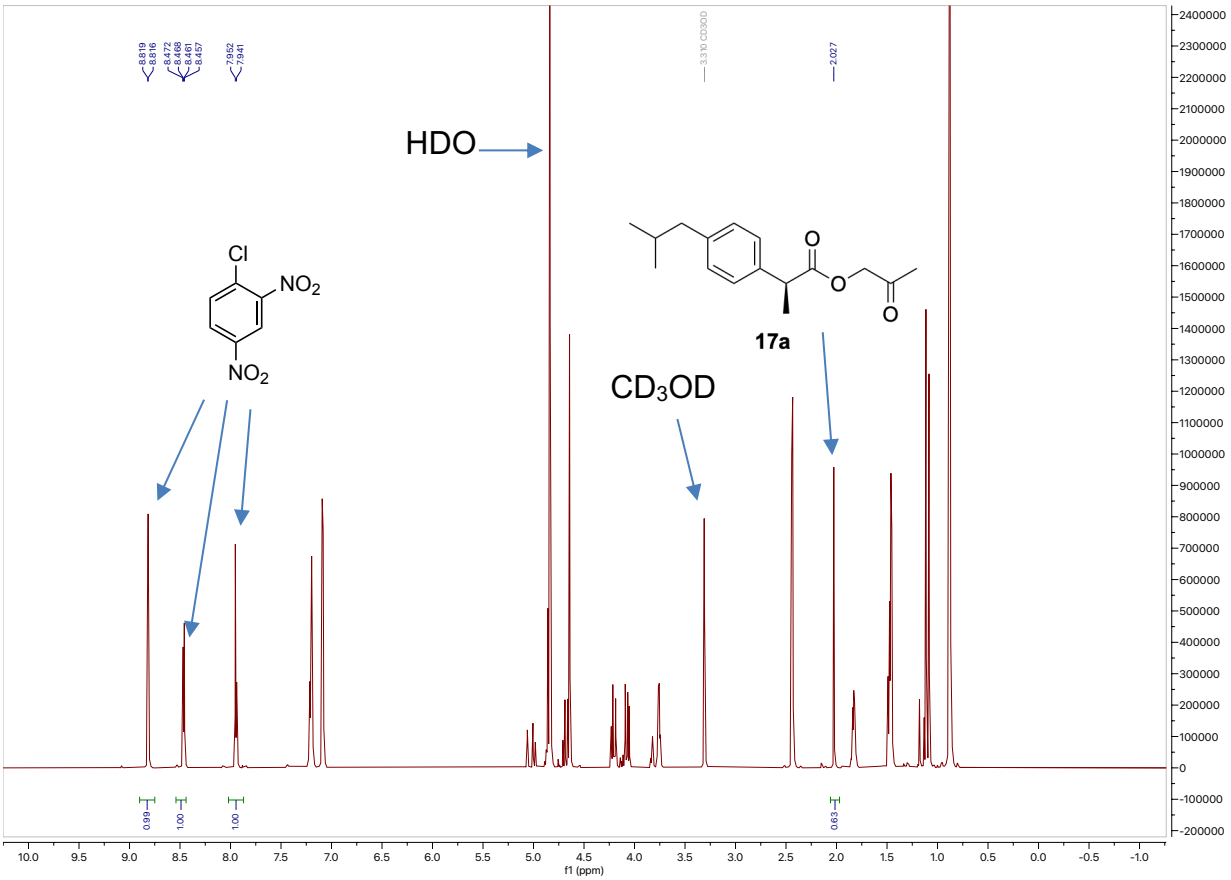
Alkene-to-IS Ratio: 1.00:1.00

Blank Sample: 2-methylallyl (*S*)-2-(4-isobutylphenyl)propanoate (**17**) and 1-chloro-2,4-dinitrobenzene (**IS**)



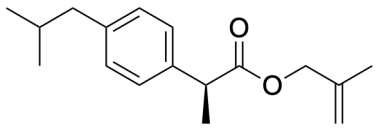
^{1}H NMR (800 MHz, CD_3OD)

Representative ^{1}H NMR: 2-methylallyl (*S*)-2-(4-isobutylphenyl)propanoate (**17**) ozonolysis



^{1}H NMR (800 MHz, CD_3OD), D1 = 10 s, 32 scans

Characterization Data: 2-methylallyl (*S*)-2-(4-isobutylphenyl)propanoate (**17**)

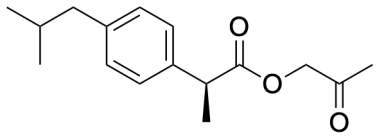


17

2-methylallyl (*S*)-2-(4-isobutylphenyl)propanoate (**17**)

^{1}H NMR (800 MHz, MeOD) δ 7.19 (d, *J* = 8.1 Hz, 2H), 7.09 (d, *J* = 8.2 Hz, 2H), 4.80 (s, 1H), 4.79 (s, 1H), 4.53 (d, *J* = 13.3 Hz, 1H), 4.43 (d, *J* = 13.3 Hz, 1H), 3.75 (q, *J* = 7.1

Hz, 1H), 2.44 (d, *J* = 7.3 Hz, 2H), 1.83 (nonet, *J* = 6.7 Hz, 1H), 1.60 (s, 3H), 1.46 (d, *J* = 7.1 Hz, 3H), 0.88 (d, *J* = 6.6 Hz, 6H).



17a

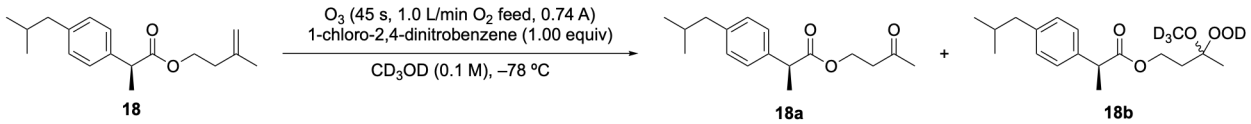
2-oxopropyl (*S*)-2-(4-isobutylphenyl)propanoate (**17a**)

^{1}H NMR (800 MHz, MeOD) δ 7.25 – 7.16 (m, 2H), 7.12 – 7.04 (m, 2H), 4.70 (d, *J* = 17.0 Hz, 1H), 4.65 (d, *J* = 17.0 Hz, 1H), 3.83 (q, *J* = 7.1 Hz, 1H), 2.44 (d, *J* = 7.3 Hz, 2H), 2.03 (s, 3H), 1.83 (nonet, *J* = 6.8 Hz, 1H), 1.53 –1.37 (m, 3H), 0.88 (d, *J* = 4.1 Hz, 6H).

The signals were measured and deduced from the ^{1}H NMR of the crude reaction mixture.

Table 6.17 2-methylallyl (*S*)-2-(4-isobutylphenyl)propanoate (**17**) qNMR Data

Trial	**%17a**
1	21
2	21
3	22
average	21.3
standard deviation	0.577

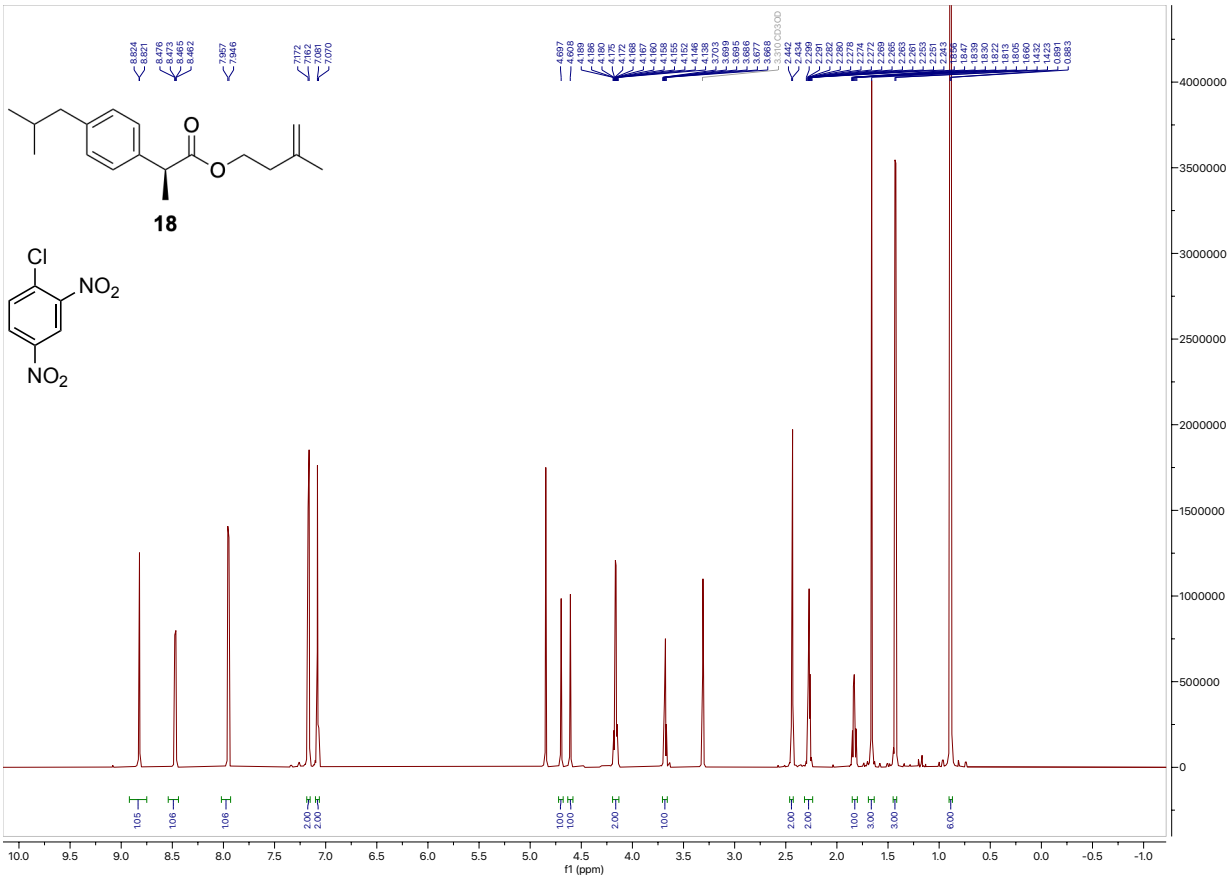


3-methylbut-3-en-1-yl (*S*)-2-(4-isobutylphenyl)propanoate (**18**)

Reaction Time: 45 seconds

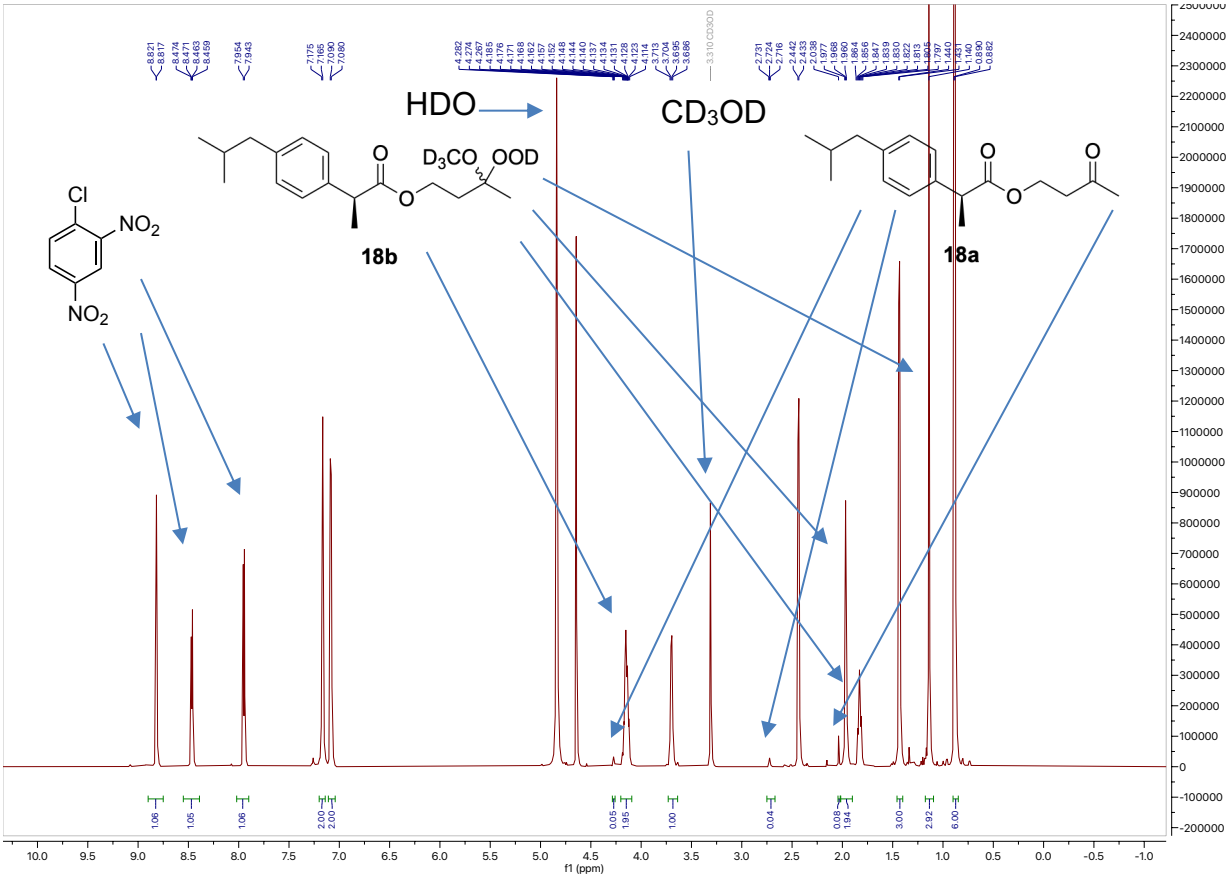
Alkene-to-IS Ratio: 0.94:1.00

Blank Sample: 2-methylallyl 3-methylbut-3-en-1-yl (*S*)-2-(4-isobutylphenyl)propanoate (**18**) and 1-chloro-2,4-dinitrobenzene (**IS**)



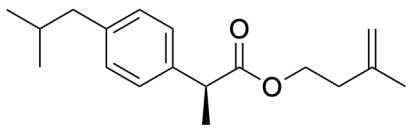
^{1}H NMR (800 MHz, CD_3OD)

Representative ^{1}H NMR: 2-methylallyl 3-methylbut-3-en-1-yl (*S*)-2-(4-isobutylphenyl)propanoate (**18**) ozonolysis



^{1}**H NMR** (800 MHz, $CDCl_3$), D1 = 10 s, 32 scans

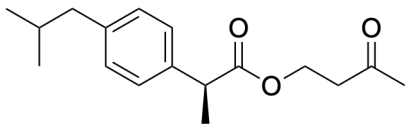
Characterization Data: 2-methylallyl 3-methylbut-3-en-1-yl (*S*)-2-(4-isobutylphenyl)propanoate (**18**)



18

3-methylbut-3-en-1-yl (*S*)-2-(4-isobutylphenyl)propanoate (**18**)

^{1}H NMR (800 MHz, MeOD) δ 7.17 (d, *J* = 8.1 Hz, 2H), 7.08 (d, *J* = 8.2 Hz, 2H), 4.70 (s, 1H), 4.61 (s, 1H), 4.20 – 4.13 (m, 2H), 3.68 (q, *J* = 7.2 Hz, 1H), 2.44 (d, *J* = 7.1 Hz, 2H), 2.27 (tt, *J* = 6.5, 1.7 Hz, 2H), 1.83 (nonet, *J* = 6.8 Hz, 1H), 1.66 (s, 3H), 1.43 (d, *J* = 7.1 Hz, 3H), 0.89 (d, *J* = 6.6 Hz, 6H).

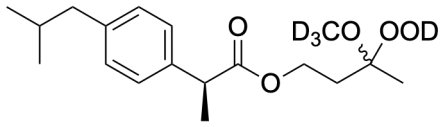


18a

2-oxopropyl (*S*)-2-(4-isobutylphenyl)propanoate (**18a**)

^{1}H NMR (800 MHz, MeOD) δ 7.17 (d, *J* = 8.1 Hz, 2H), 7.08 (d, *J* = 8.0 Hz, 2H), 4.27 (t, *J* = 6.2 Hz, 2H), 3.70 (q, *J* = 7.1 Hz, 1H), 2.72 (t, *J* = 6.1 Hz, 2H), 2.44 (d, *J* = 7.1 Hz, 2H), 2.04 (s, 3H), 1.87 – 1.77 (m, *J* = 6.6 Hz, 1H), 1.44 (d, *J* = 7.3 Hz, 3H), 0.89 (d, *J* = 6.6 Hz, 6H).

The signals were measured and deduced from the ^{1}H NMR of the crude reaction mixture.



18b

3-deuteroperoxy-3-(methoxy-d_3)-butyl (2*S*)-2-(4-isobutylphenyl)propanoate (**18b**)

^{1}H NMR (800 MHz, MeOD) δ 7.17 (d, *J* = 8.1 Hz, 2H), 7.08 (d, *J* = 8.0 Hz, 2H), 4.15 (dddd, *J* = 17.2, 13.7, 6.8, 4.4 Hz, 2H), 3.70 (q, *J* = 7.1 Hz, 1H), 2.44 (d, *J* = 7.1 Hz, 2H),

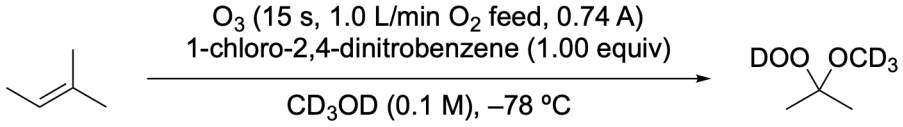
1.97 (t, *J* = 6.8 Hz, 2H), 1.87 – 1.77 (m, *J* = 6.6 Hz, 1H), 1.44 (d, *J* = 7.3 Hz, 3H), 1.14 (s, 3H), 0.89 (d, *J* = 6.6 Hz, 6H).

The signals were measured and deduced from the ^{1}H NMR of the crude reaction mixture.

Table 6.18 3-methylbut-3-en-1-yl (*S*)-2-(4-isobutylphenyl)propanoate (**18**) qNMR Data

Trial	**%18a**	**%18b**
1	2.4	97.3
2	2.4	97.2
3	2.3	96.3
average	2.4	96.9
st. dev.	0.077	0.512

6.8.4.4 *tri*-Substituted Alkenes



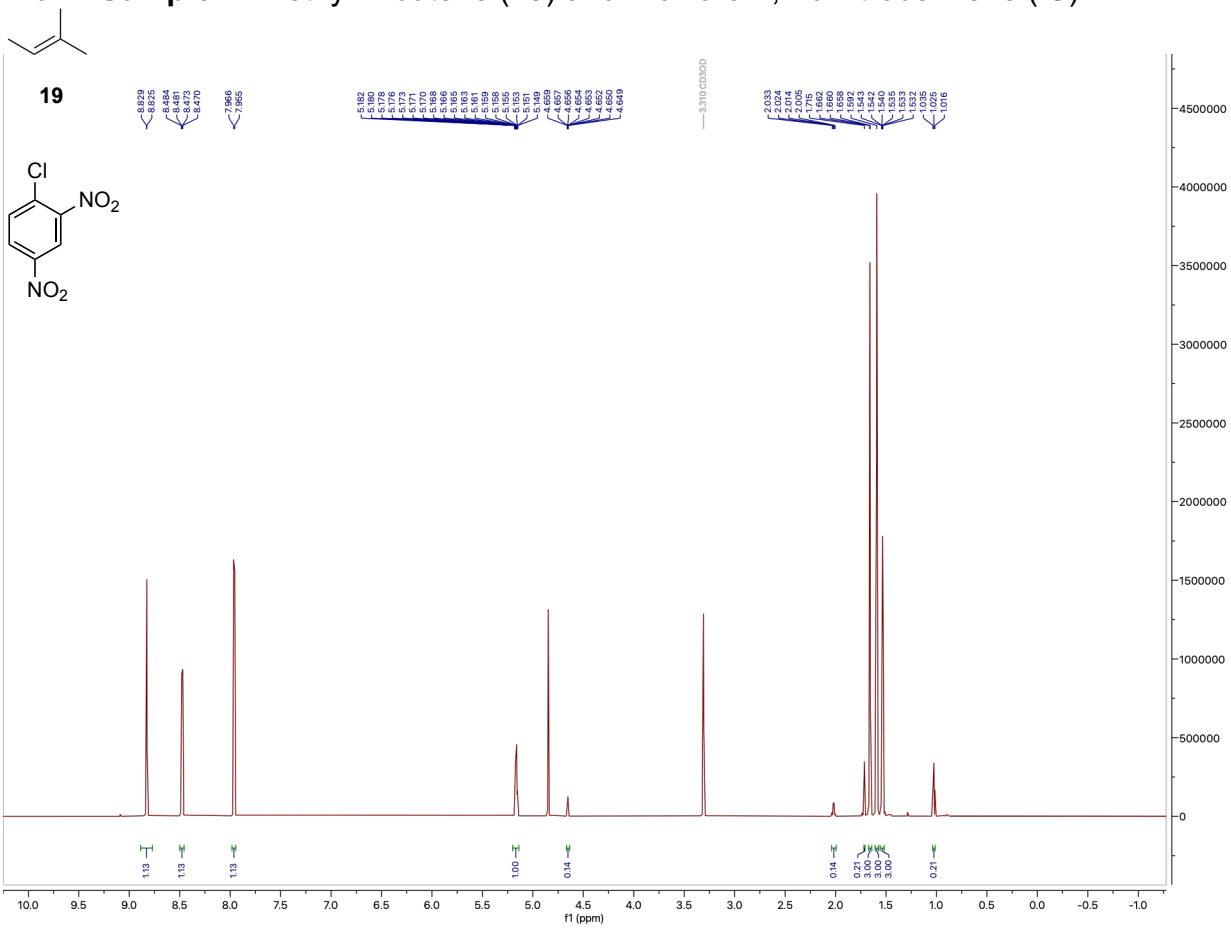
19 **19a**

2-methyl-2-butene (**19**)

Reaction Time: 15 seconds

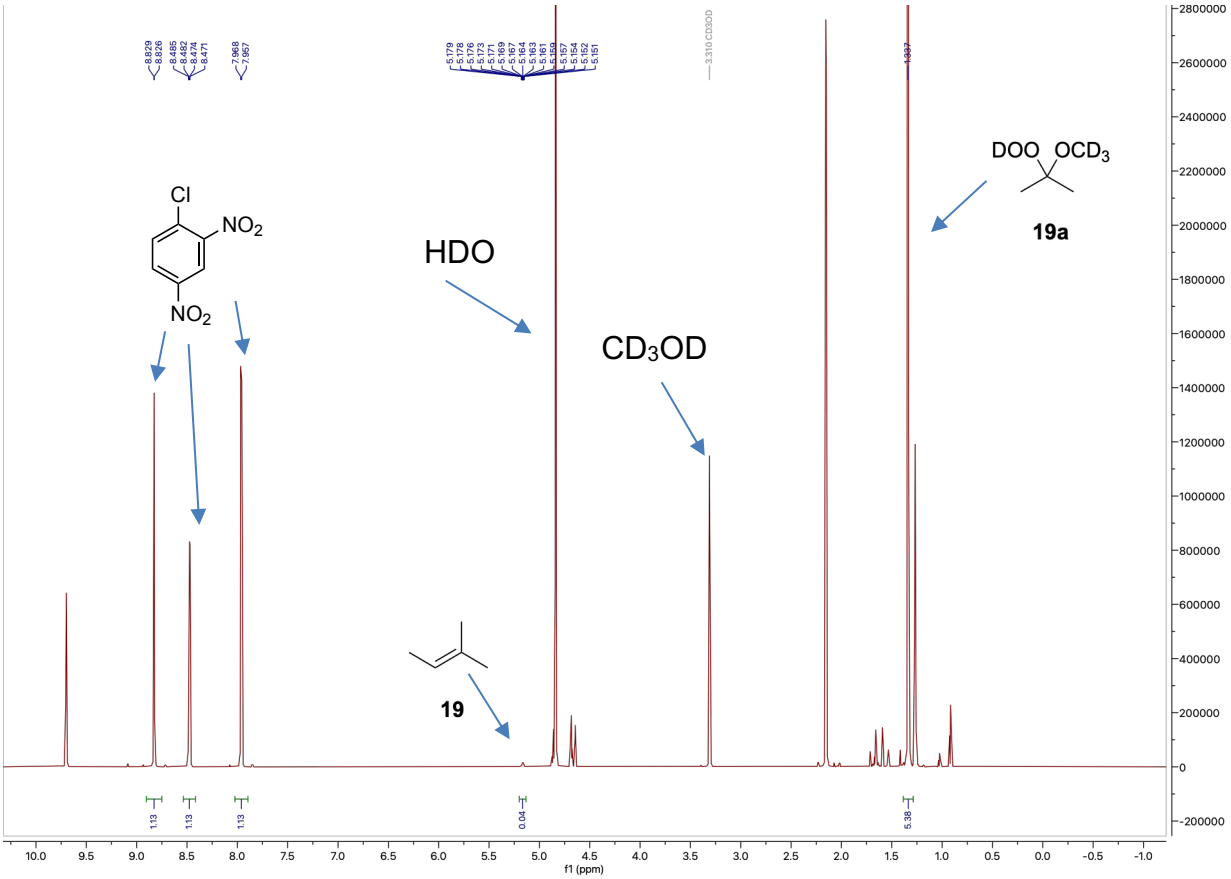
Alkene-to-IS Ratio: 1.00:1.13

Blank Sample: 2-methyl-2-butene (**19**) and 1-chloro-2,4-dinitrobenzene (**IS**)



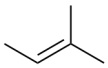
^{1}H NMR (800 MHz, CD_3OD), D1 = 10 s, 32 scans

Representative ^{1}H NMR: 2-methyl-2-butene (**19**) ozonolysis



^{1}H NMR (800 MHz, CD_3OD), D1 = 10 s, 32 scans

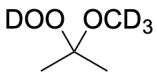
Characterization Data: 2-methyl-2-butene (**19**)



19

2-methyl-2-butene (**19**)

^{1}H NMR (800 MHz, MeOD) δ 5.20 – 5.14 (m, 1H), 1.69 – 1.62 (m, 3H), 1.59 (s, 3H), 1.54 (dt, *J* = 6.6, 1.3 Hz, 3H).



19a

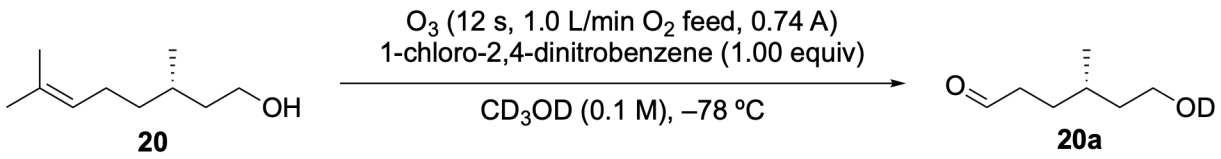
2-deuteroperoxy-2-(methoxy-d_3)propane (**19a**)

^{1}H NMR (800 MHz, MeOD) δ 1.34 (s, 6H).

The signals were measured from the ^{1}H NMR of the crude reaction mixture.

Table 6.19 2-methyl-2-butene (**19**) qNMR Data

Trial	% conversion	normalized %19a
1	96	93
2	94	94
3	92	94
average		94
st. dev.		0.47



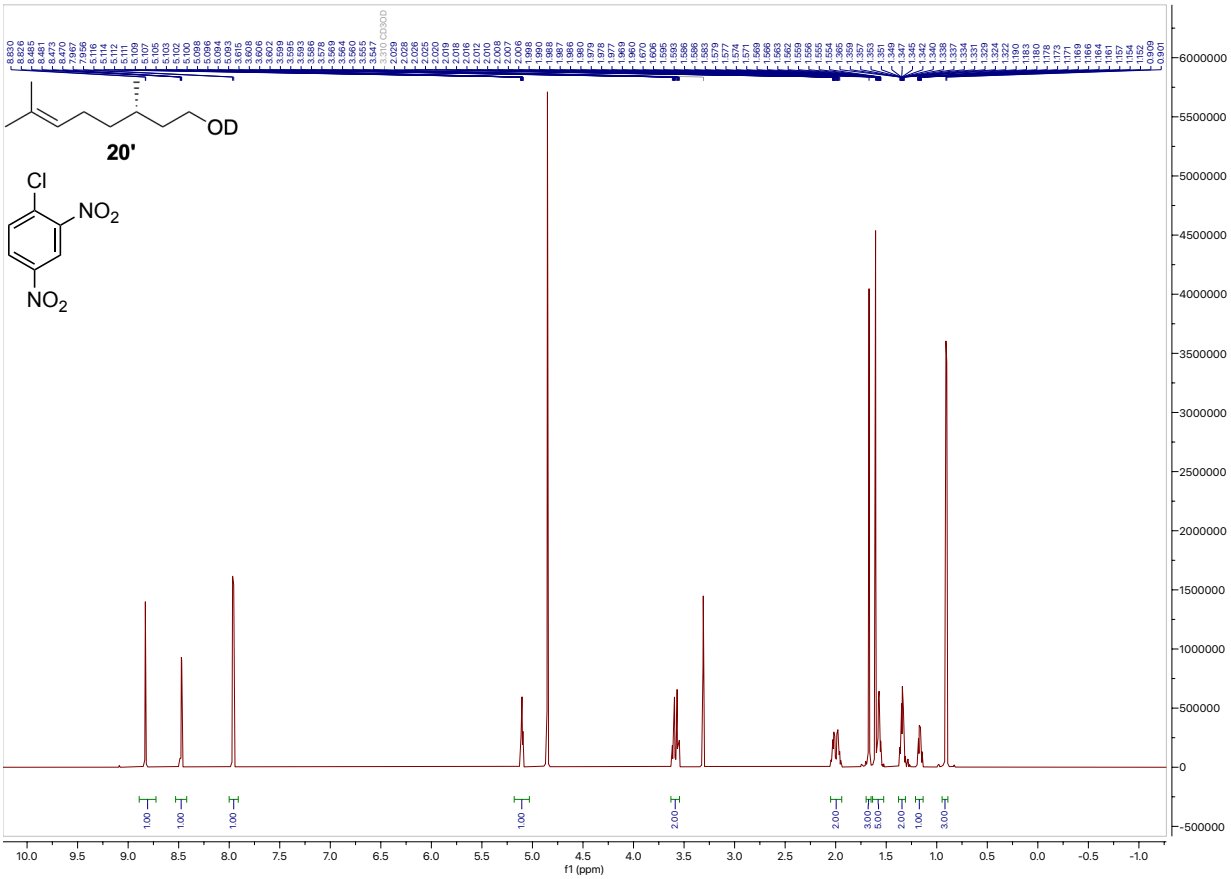
20 **20a**

(–)-β-citronellol (**20**)

Reaction Time: 12 seconds

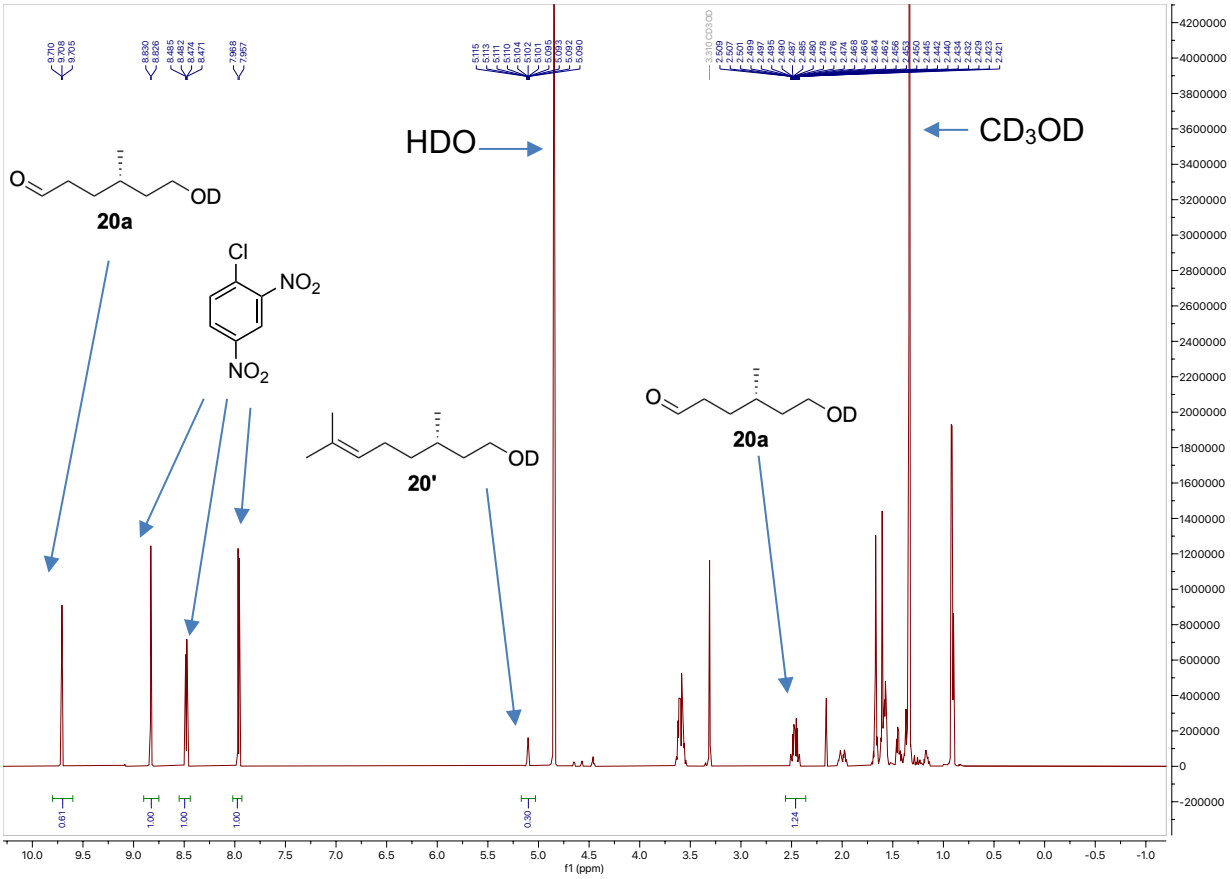
Alkene-to-IS Ratio: 1.00:1.13

Blank Sample: (–)-β-citronellol (**20**) and 1-chloro-2,4-dinitrobenzene (**IS**)



^{1}H NMR (800 MHz, CD_3OD), D1 = 10 s, 32 scans

Representative ^{1}H NMR: (–)-β-citronellol (**20**) ozonolysis



^{1}H NMR (800 MHz, CD_3OD), D1 = 10 s, 32 scans

Characterization Data: (–)-β-citronellol (**20**)

(–)-β-citronellol-*d* (**20'**)

^{1}H NMR (800 MHz, MeOD) δ 5.10 (tp, *J* = 7.1, 1.5 Hz, 1H), 3.63 – 3.54 (m, 2H), 2.05 – 1.94 (m, 2H), 1.67 (s, 3H), 1.61 (s, 3H), 1.60 – 1.54 (m, 2H), 1.38 – 1.31 (m, 2H), 1.17 (dddd, *J* = 13.4, 9.6, 7.6, 5.8 Hz, 1H), 0.90 (d, *J* = 6.6 Hz, 3H).

(*S*)-6-(hydroxy-*d*)-4-methylhexanal (**20a**)

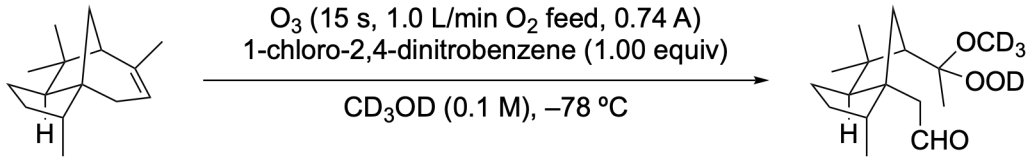
^{1}H NMR (800 MHz, MeOD) δ 9.71 (s, 1H), 3.83 – 3.48 (m, 2H), 2.68 – 2.28 (m, 2H), 1.67 (ddt, *J* = 13.9, 9.2, 6.0 Hz, 1H), 1.63 – 1.53 (m, 2H), 1.49 – 1.41 (m, 1H), 1.39 – 1.34 (m, 1H), 0.92 (d, *J* = 6.5 Hz, 3H).

1D Selective Gradient TOCSY was used to deduce the ^{1}H NMR signals from the crude ^{1}H NMR spectrum.

The signals were measured and deduced from the ^{1}H NMR of the crude reaction mixture.

Table 6.20 (–)-β-citronellol (**20**) qNMR Data

Trial	%conversion	Average %20a	normalized %20a
1	70	61.5	88
2	50	44	88
3	63	55	87
average			87.7
St. Dev.			0.47



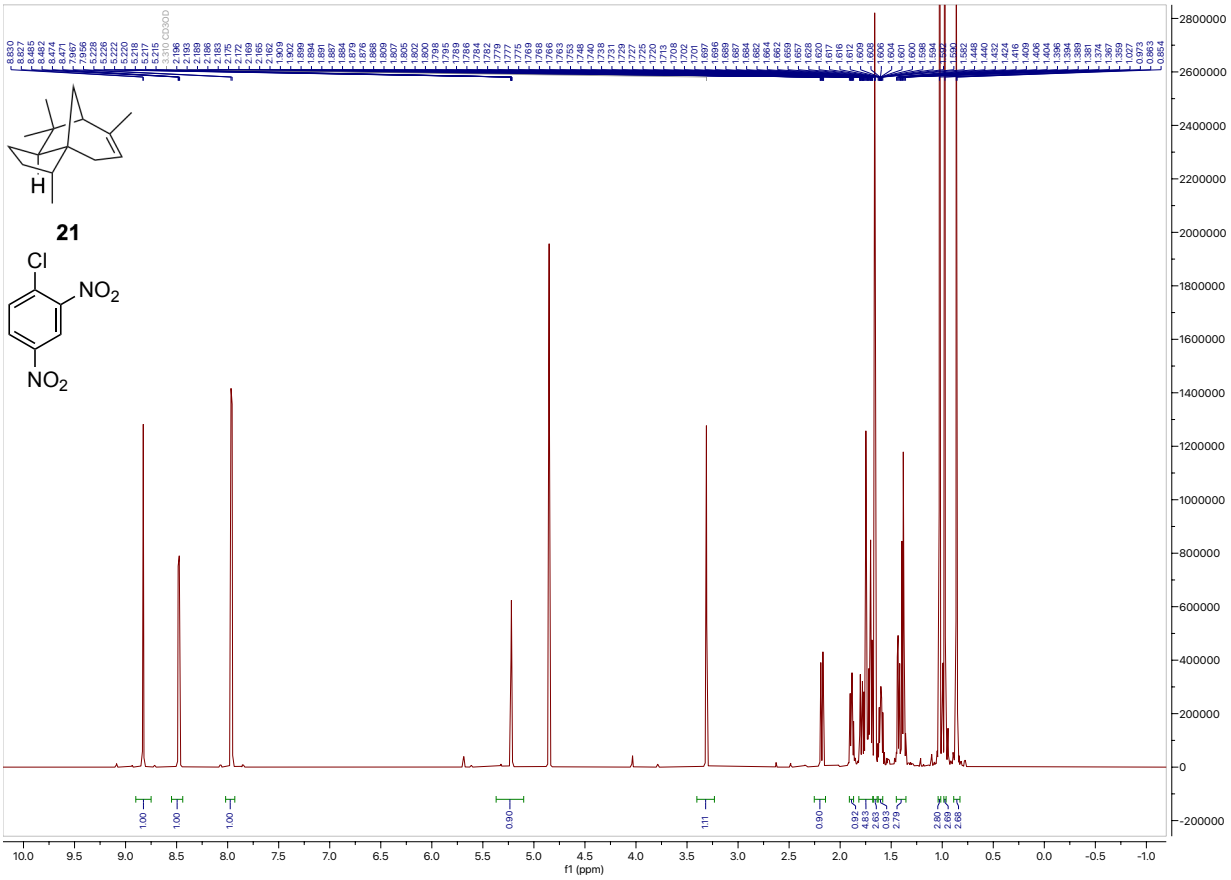
21 **21a**

(–)-α-cedrene (**21**)

Reaction Time: 15 seconds

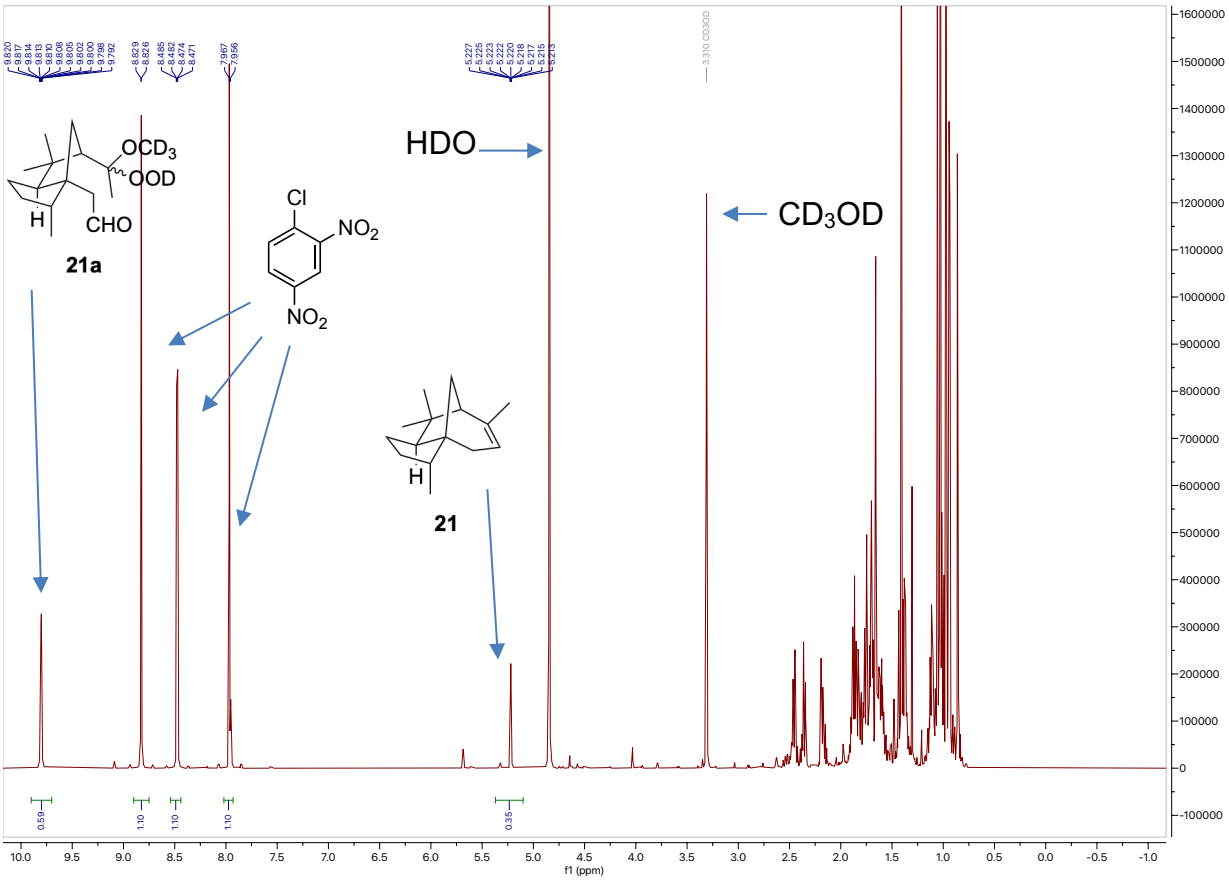
Alkene-to-IS Ratio: 0.90:1.00

Blank Sample: (–)-α-cedrene (**21**) and 1-chloro-2,4-dinitrobenzene (**IS**)



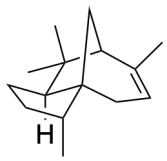
^{1}H NMR (800 MHz, CD_3OD)

Representative ^{1}H NMR: (–)-α-cedrene (**21**) ozonolysis



^{1}H NMR (800 MHz, CD_3OD), D1 = 10 s, 32 scans

Characterization Data: (–)-α-cedrene (**21**)

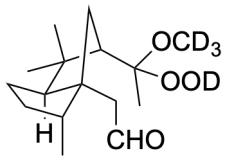


21

(–)-α-cedrene (**21**)

^{1}H NMR (800 MHz, MeOD) δ 5.22 (dh, *J* = 3.2, 1.7 Hz, 1H), 2.18 (dp, *J* = 16.7, 2.5 Hz, 1H), 1.89 (ddt, *J* = 12.3, 8.4, 6.2 Hz, 1H), 1.81 – 1.67 (m, 5H), 1.66 (q, *J* = 1.9 Hz, 3H),

1.60 (dddd, *J* = 12.7, 9.4, 8.2, 6.2 Hz, 1H), 1.43 (dq, *J* = 12.3, 6.0 Hz, 1H), 1.40 – 1.35 (m, 2H), 1.03 (s, 3H), 0.97 (s, 3H), 0.86 (d, *J* = 7.1 Hz, 3H).



21a

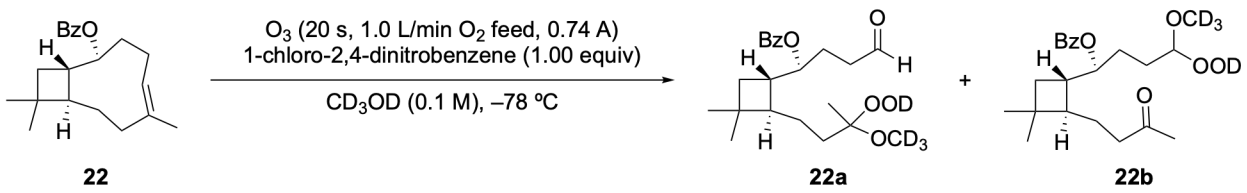
2-((2*R*,4*R*,6a*S*)-2-(1-deuteroperoxy-1-(methoxy-d_3)ethyl)-1,1,4-trimethylhexahydropentalen-3a(1*H*)-yl)acetaldehyde (**21a**)

^{1}H NMR (800 MHz, MeOD) δ 9.81 (dt, *J* = 6.0, 3.0 Hz, 1H), 2.52 – 0.65 (m, 23H).

Only the aldehyde CHO peak was clearly visible in the ^{1}H NMR of the crude reaction mixture. The remaining signals were measured and deduced from the ^{1}H NMR of the crude reaction mixture.

Table 6.21 (–)-α-cedrene (**21**) qNMR Data

Trial	**%conversion**	**%21a**	**normalized %21a**
1	75	69	92
2	65	59	92.3
3	90	84	93.3
average			92.5
St. Dev.			0.68

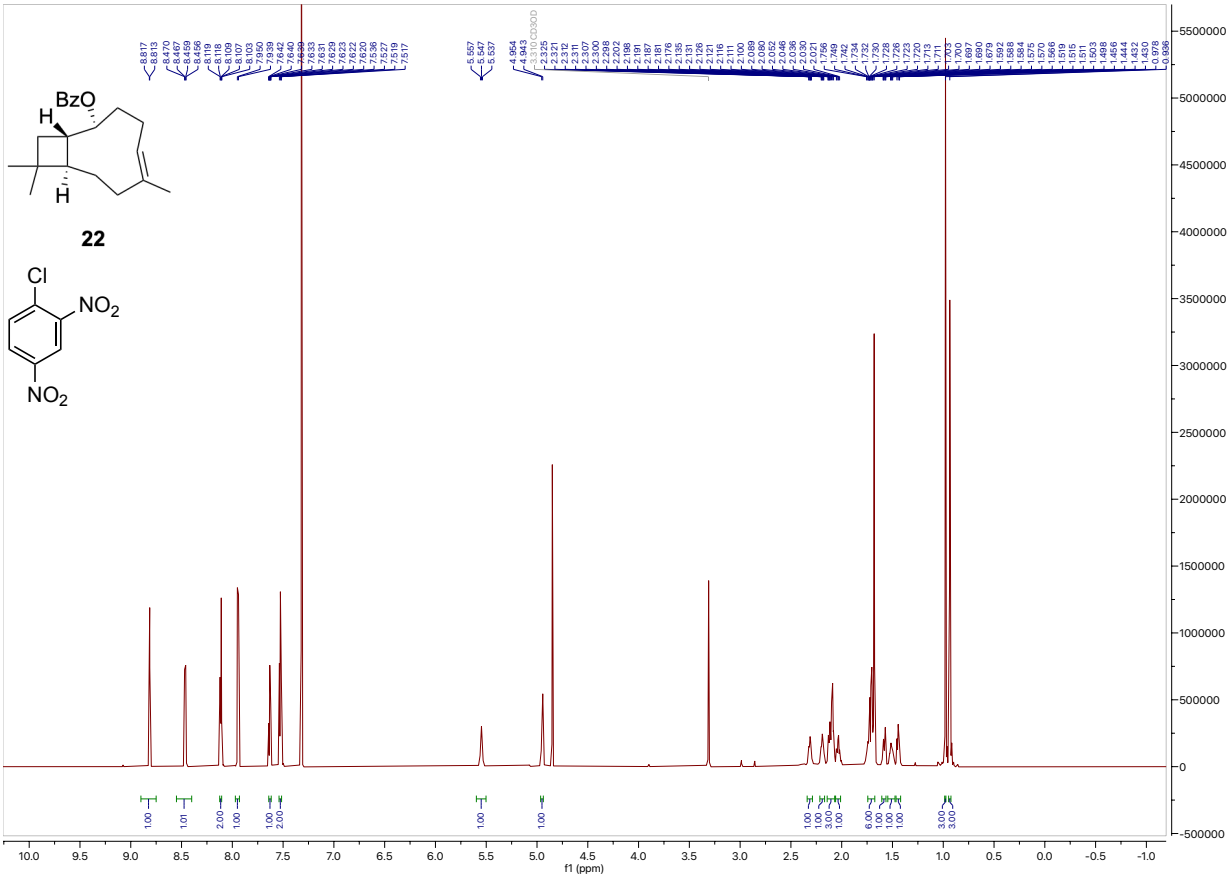


(1*S*,2*S*,9*R*,*E*)-6,10,10-trimethylbicyclo[7.2.0]undec-5-en-2-yl benzoate (**22**)

Reaction Time: 20 seconds

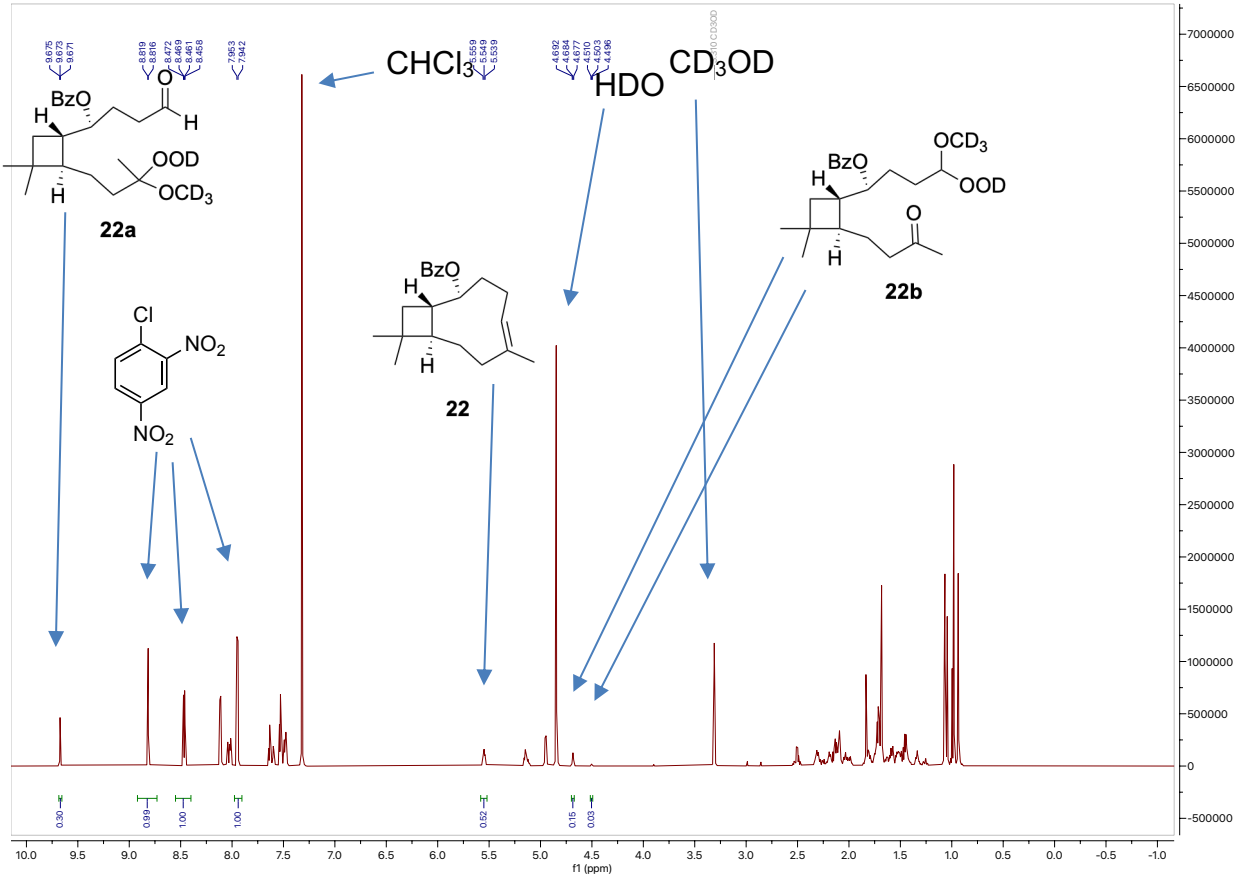
Alkene-to-IS Ratio: 1.00:1.00

Blank Sample: (1*S*,2*S*,9*R*,*E*)-6,10,10-trimethylbicyclo[7.2.0]undec-5-en-2-yl benzoate (**22**) and 1-chloro-2,4-dinitrobenzene (**IS**)



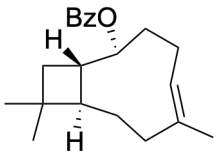
^{1}H NMR (800 MHz, CD_3OD), D1 = 10 s, 32 scans

Representative ^{1}H NMR: (1*S*,2*S*,9*R*,*E*)-6,10,10-trimethylbicyclo[7.2.0]undec-5-en-2-yl benzoate (**22**) ozonolysis



^{1}H NMR (800 MHz, CD_3OD), D1 = 10 s, 32 scans

Characterization Data: (1*S*,2*S*,9*R*,*E*)-6,10,10-trimethylbicyclo[7.2.0]undec-5-en-2-yl benzoate (**22**)

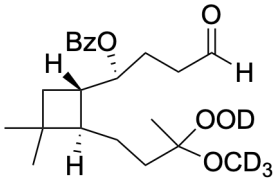


22

(1*S*,2*S*,9*R*,*E*)-6,10,10-trimethylbicyclo[7.2.0]undec-5-en-2-yl benzoate (**22**)

^{1}H NMR (800 MHz, MeOD) δ 8.11 (dd, *J* = 8.4, 1.4 Hz, 2H), 7.63 (tt, *J* = 7.3, 1.4 Hz, 1H), 7.53 (t, *J* = 7.8 Hz, 2H), 5.55 (t, *J* = 7.9 Hz, 1H), 4.95 (d, *J* = 8.5 Hz, 1H), 2.34 –

2.28 (m, 1H), 2.19 (td, *J* = 8.5, 3.3 Hz, 1H), 2.15 – 2.06 (m, 3H), 2.03 (tt, *J* = 10.7, 5.3 Hz, 1H), 1.80 – 1.64 (m, 3H), 1.68 (s, 3H), 1.58 (dt, *J* = 14.9, 3.8 Hz, 1H), 1.51 (tdd, *J* = 13.9, 10.0, 4.1 Hz, 1H), 1.47 – 1.42 (m, 1H), 0.98 (s, 3H), 0.94 (s, 3H).

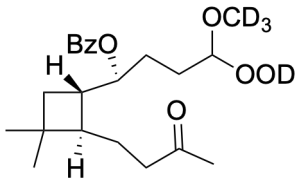


22a

(1*S*)-1-((1*S*,2*R*)-2-(3-deuteroperoxy-3-(methoxy-d_3)butyl)-3,3-dimethylcyclobutyl)-4-oxobutyl benzoate (**22a**)

^{1}H NMR (800 MHz, MeOD) δ 9.67 (t, *J* = 1.4 Hz, 1H), 8.08 – 8.01 (m, 2H), 7.68 – 7.59 (m, 1H), 7.53 – 7.45 (m, 2H), 5.17 (tt, *J* = 8.6, 3.3 Hz, 1H), 2.58 – 2.47 (m, 2H), 2.16 (td, *J* = 8.9, 7.1 Hz, 1H), 2.07 – 1.94 (m, 2H), 1.89 – 1.80 (m, 3H), 1.73 (ddd, *J* = 11.0, 8.5, 2.6 Hz, 2H), 1.48 (dd, *J* = 11.0, 9.5 Hz, 2H), 1.10 – 0.93 (m, 9H).

Most of the signals were visible and deduced from the 1D selective gradient TOCSY spectrum. The remaining signals were deduced from the ^{1}H NMR of the crude reaction mixture.



22b

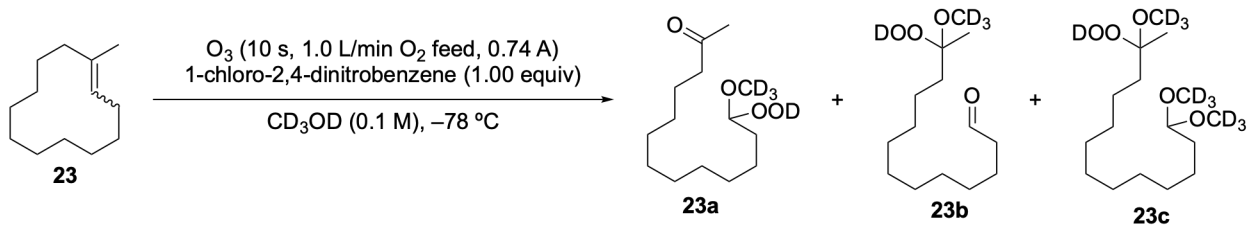
(1*S*)-1-((1*S*,2*R*)-3,3-dimethyl-2-(3-oxobutyl)cyclobutyl)-4-deuteroperoxy-4-(methoxy-d_3)butyl benzoate (**22b**)

^{1}H NMR (800 MHz, MeOD) δ 8.08 – 8.01 (m, 2H), 7.68 – 7.59 (m, 1H), 7.53 – 7.45 (m, 2H), 5.21 – 5.10 (m, 1H), 4.75 – 4.50 (m, 1H), 2.20 – 1.41 (m, 15H), 1.10 – 0.93 (m, 6H).

Most of the signals were visible and deduced from the 1D selective gradient TOCSY spectrum. The remaining signals were deduced from the ^{1}H NMR of the crude reaction mixture.

Table 6.22 (1*S*,2*S*,9*R*,*E*)-6,10,10-trimethylbicyclo[7.2.0]undec-5-en-2-yl benzoate (**22**) qNMR Data

Trial	**%conversion**	**%22a**	**normalized %22a**	**%22b**	**normalized %22b**
1	48	30	62.5	18	37.5
2	44	27	61.4	17	38.6
3	64	41	64.1	23	35.9
average			62.6		37.4
st. dev.			1.36		1.36

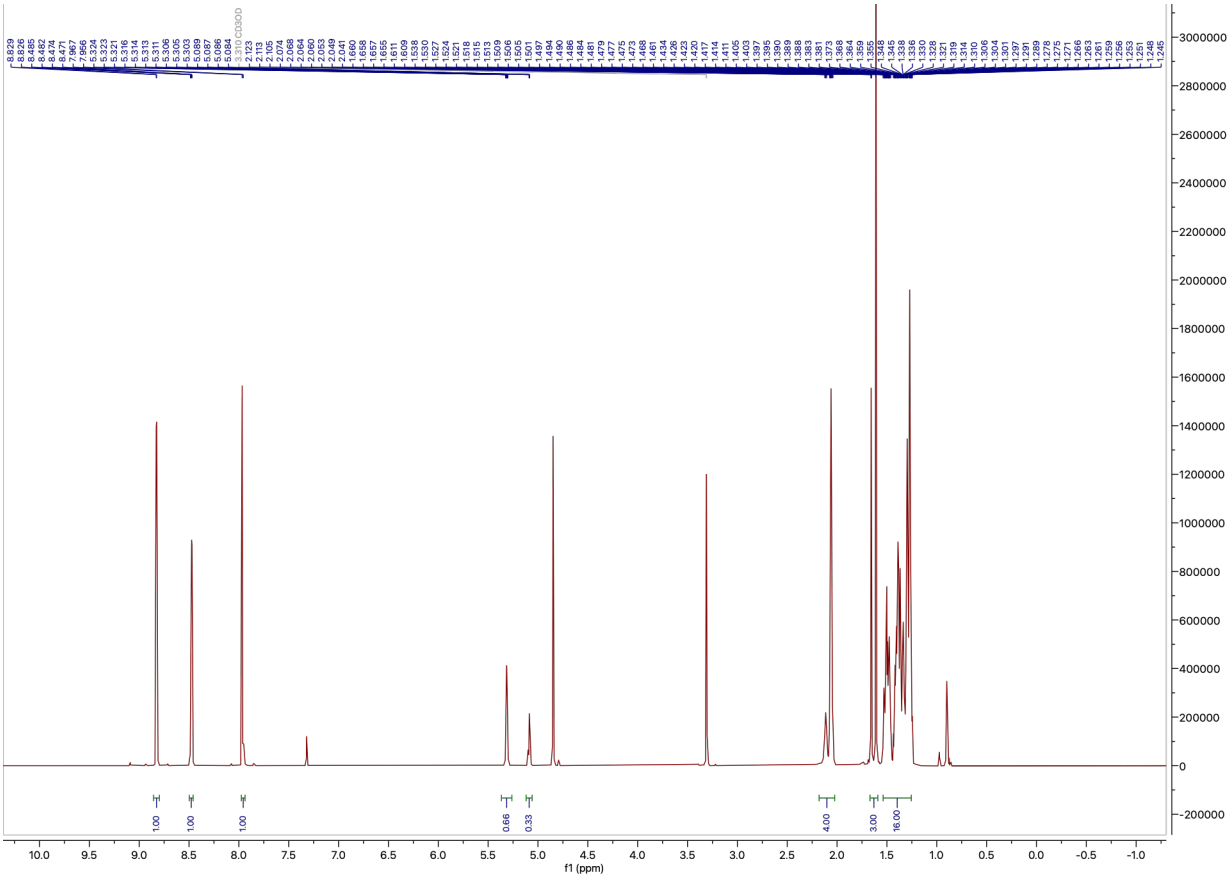


1-methylcyclododecene (**23**)

Reaction Time: 10 seconds

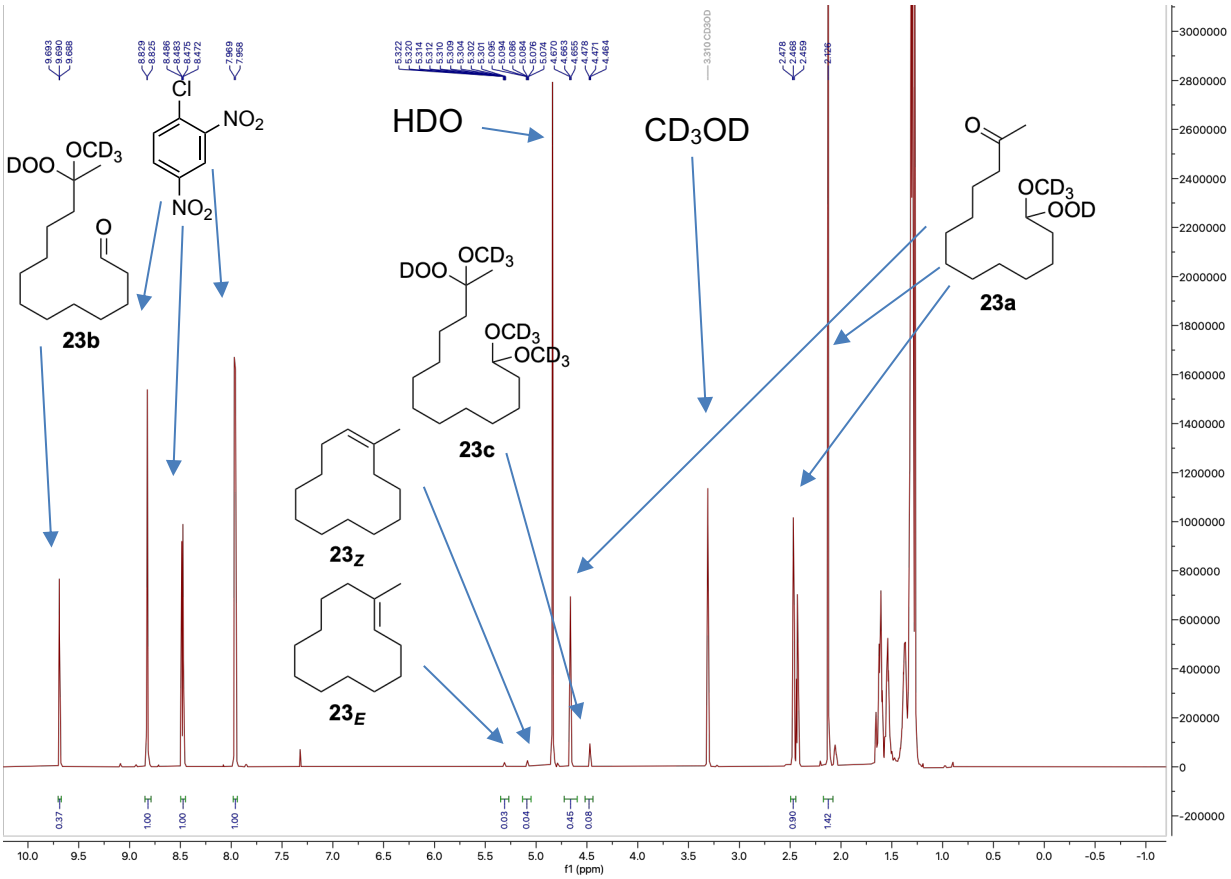
Alkene-to-IS Ratio: 1.00:1.00

Blank Sample: 1-methylcyclododecene (**23**) and 1-chloro-2,4-dinitrobenzene (**IS**)



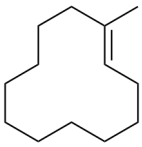
^{1}H NMR (800 MHz, CD_3OD)

Representative ^{1}H NMR: 1-methylcyclododecene (**23**) ozonolysis



^{1}H NMR (800 MHz, CD_3OD), D1 = 10 s, 32 scans

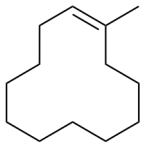
Characterization Data: 1-methylcyclododecene (**23**)



23*E*

(*E*)-1-methylcyclododecene (**23*E***)

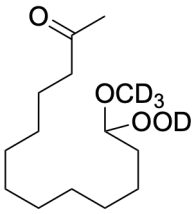
^{1}H NMR (800 MHz, MeOD) δ 5.31 (tq, *J* = 7.8, 1.4 Hz, 1H), 2.08 – 2.02 (m, 4H), 1.61 (d, *J* = 1.5 Hz, 3H), 1.56 – 1.21 (m, 16H).



23$_Z$

(*Z*)-1-methylcyclododecene (**23$_Z$**)

^{1}H NMR (800 MHz, MeOD) δ 5.09 (tq, *J* = 7.8, 1.4 Hz, 1H), 2.11 (t, *J* = 7.0 Hz, 4H), 1.66 (q, *J* = 1.3 Hz, 3H), 1.55 – 1.22 (m, 16H).

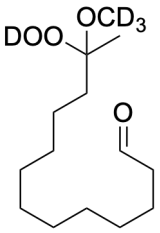


23a

13-deuteroperoxy-13-(methoxy-*d*$_3$)tridecan-2-one (**23a**)

^{1}H NMR (800 MHz, MeOD) δ 4.66 (t, *J* = 5.8 Hz, 1H), 2.47 (t, *J* = 7.4 Hz, 2H), 2.13 (s, 3H), 1.68 – 1.23 (m, 18H).

The signals were measured and deduced from the ^{1}H NMR of the crude reaction mixture.

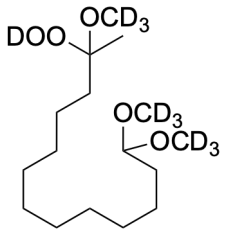


23b

12-deuteroperoxy-12-(methoxy-*d*$_3$)tridecanal (**23b**)

^{1}H NMR (800 MHz, MeOD) δ 9.69 (t, *J* = 1.8 Hz, 1H), 2.43 (td, *J* = 7.3, 1.8 Hz, 2H), 1.67 – 1.24 (m, 21H).

The signals were measured and deduced from the ^{1}H NMR of the crude reaction mixture.



23c

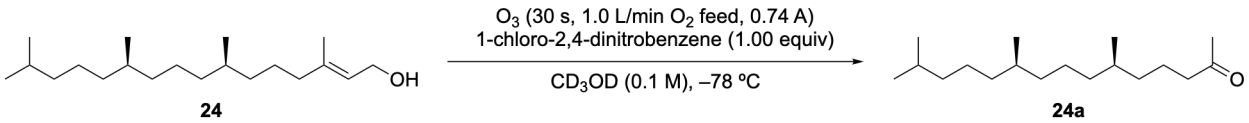
12-deuteroperoxy-1,1,12-tris(methoxy-*d*3)tridecane (**23c**)

^{1}H NMR (800 MHz, MeOD) δ 4.47 (t, *J* = 5.5 Hz, 1H), 1.70 – 1.20 (m, 23H).

The signals were measured and deduced from the ^{1}H NMR of the crude reaction mixture.

Table 6.23 1-methylcyclododecene (**23**) qNMR Data

Trial	**%conversion 23_E**	**%conversion 23_Z**	**%23a**	**%23b**	**%23c**	**normalized %23a**	**normalized %23b + %23c**
1	95	88	46	37	8	50	49
2	92	83	44	35	9	50	50
3	94	85	45	29	15	50	49
average						50	50
st. dev.						0.24	0.64



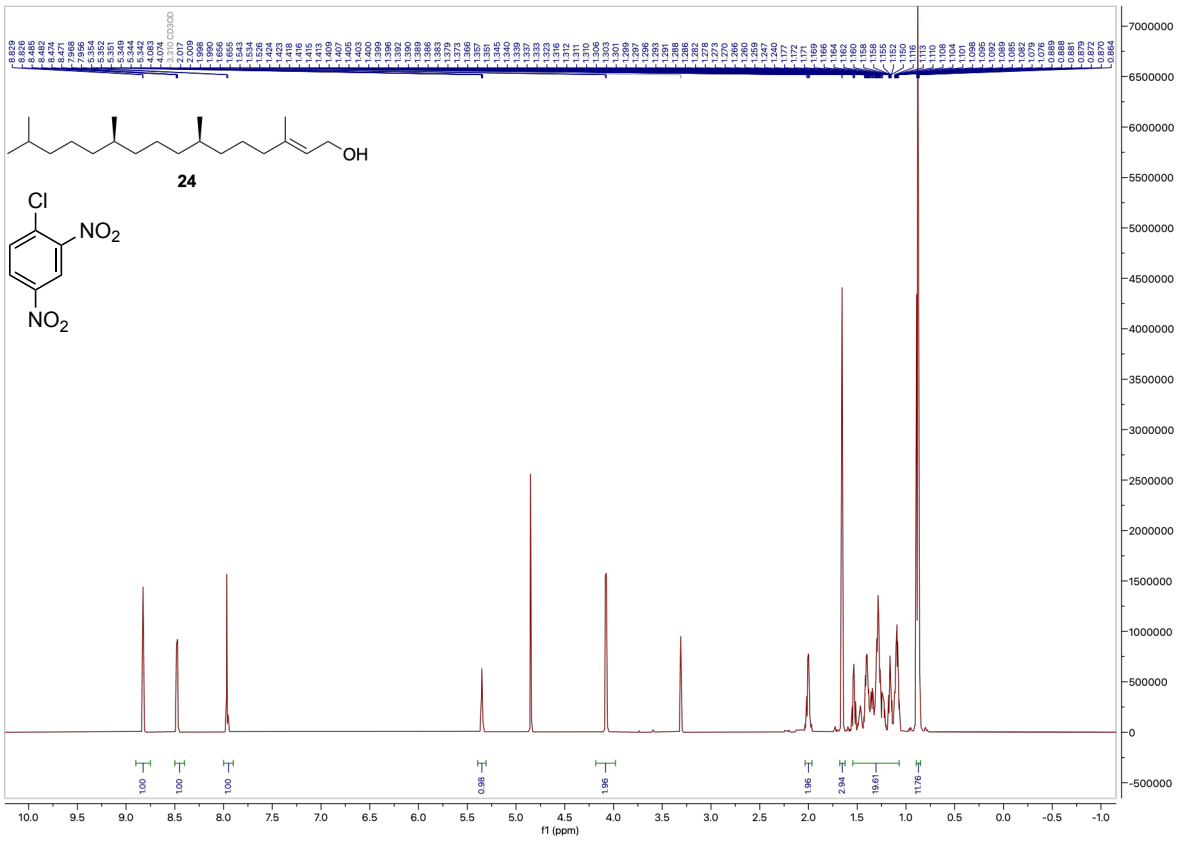
24 **24a**

(+)-phytol (**24**)

Reaction Time: 30 seconds

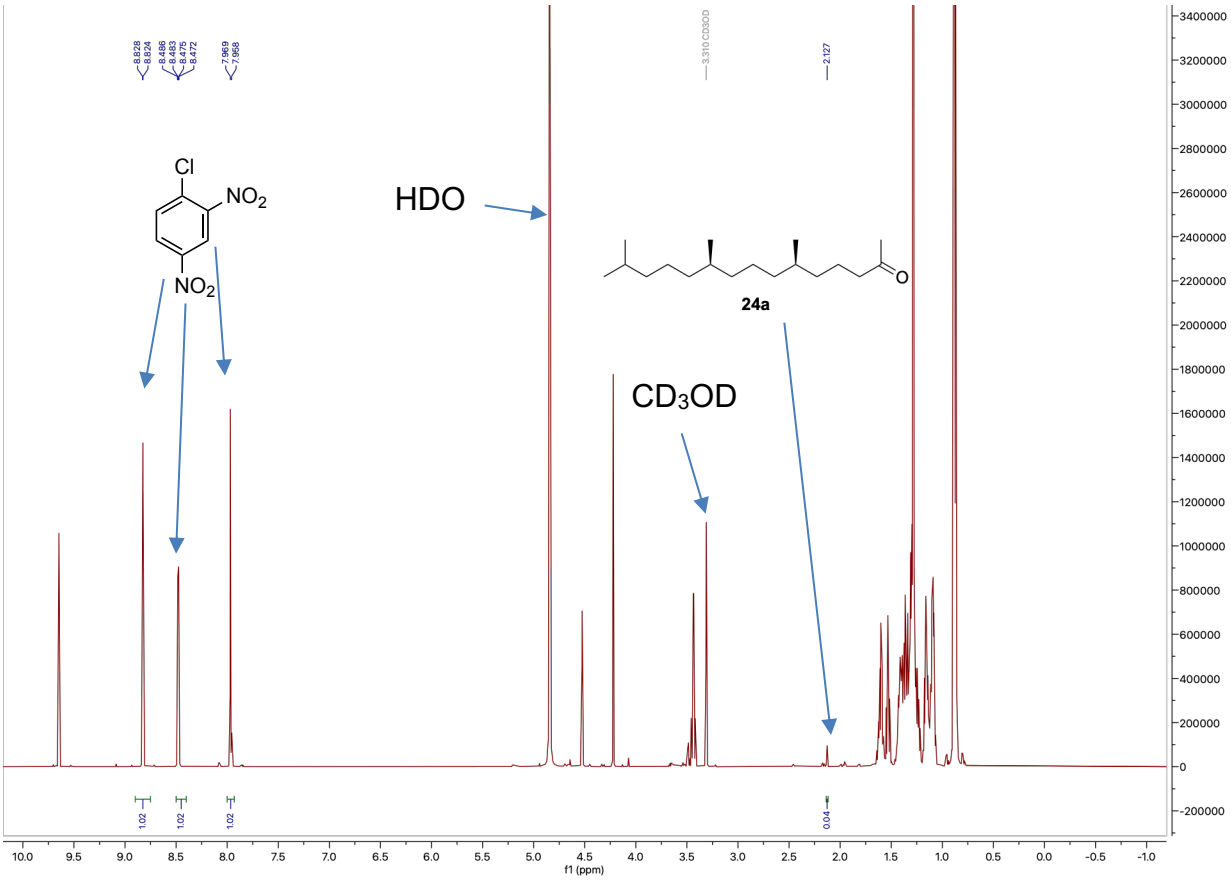
Alkene-to-IS Ratio: 0.98:1.00

Blank Sample: (+)-phytol (**24**) and 1-chloro-2,4-dinitrobenzene (**IS**)



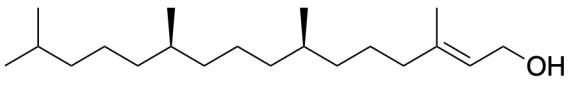
^{1}H NMR (800 MHz, CD_3OD), D1 = 10 s, 32 scans

Representative ^{1}H NMR: (+)-phytol (**24**) ozonolysis



^{1}H NMR (800 MHz, CD_3OD), D1 = 10 s, 32 scans

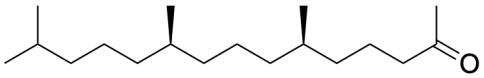
Characterization Data: (+)-phytol (**24**)



24

(+)-phytol (**24**)

^{1}H NMR (800 MHz, MeOD) δ 5.56 – 5.15 (m, 1H), 4.08 (d, *J* = 6.8 Hz, 2H), 2.00 (h, *J* = 8.0 Hz, 2H), 1.65 (s, 3H), 1.58 – 1.04 (m, 20H), 1.02 – 0.72 (m, 12H).



24a

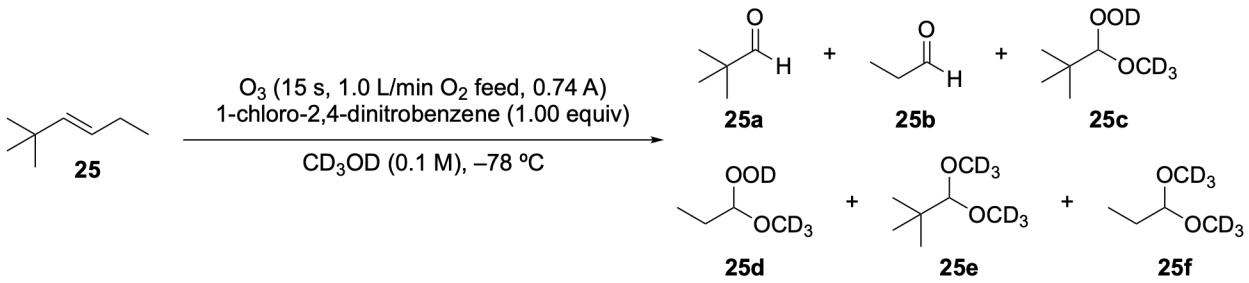
(6*R*,10*R*)-6,10,14-trimethylpentadecan-2-one (**24a**)

^{1}H NMR (800 MHz, MeOD) δ 2.45 (tt, *J* = 7.1, 3.6 Hz, 2H), 2.13 (s, 3H), 1.68 – 0.80 (m, 31H).

Table 6.24 (+)-phtyol (**24**) qNMR Data

Trial	**%24a**
1	1
2	1
3	1
average	1
St. Dev.	0

6.8.4.5 *trans*-1,2-Disubstituted Alkenes

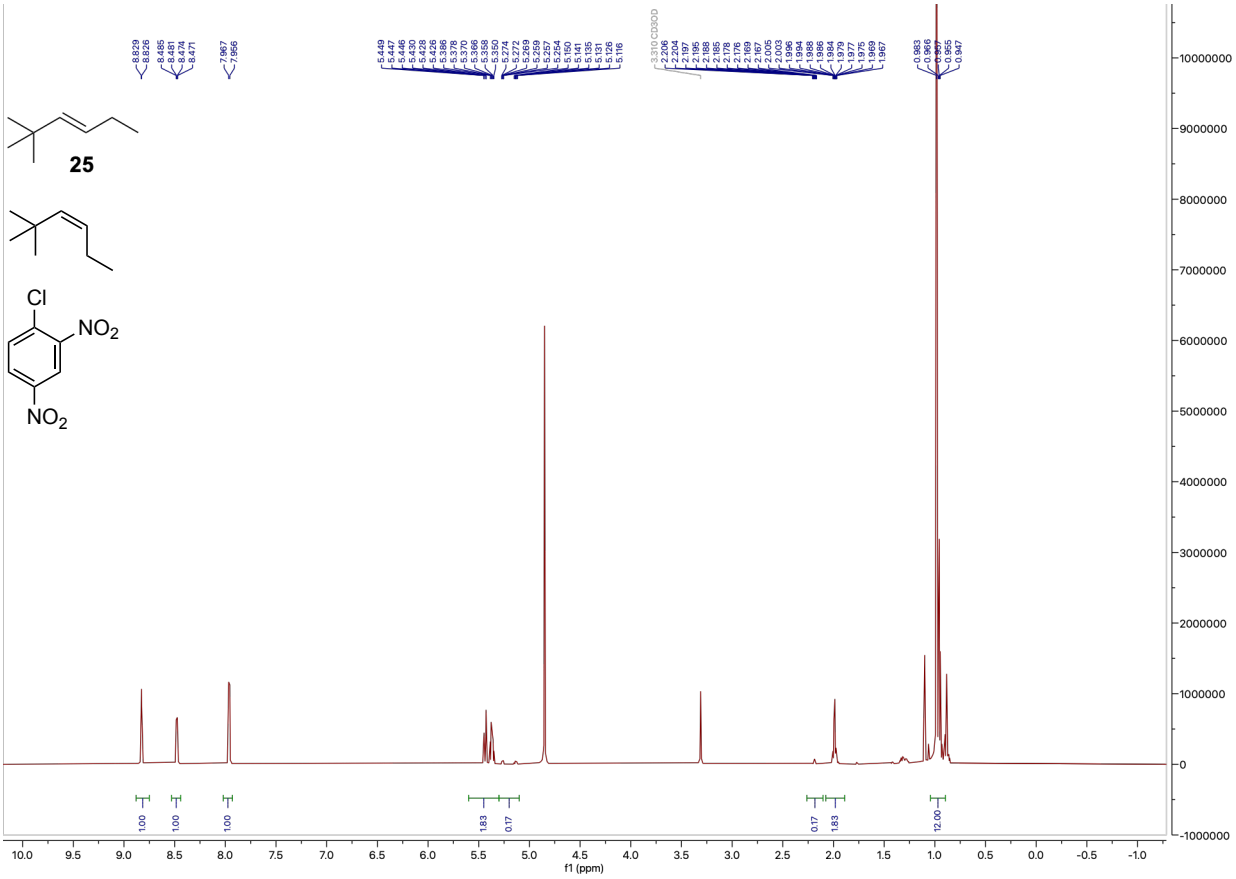


(*E*)-2,2-dimethylhex-3-ene (**25**)

Reaction Time: 15 seconds

Alkene-to-IS Ratio: 0.915:1.00

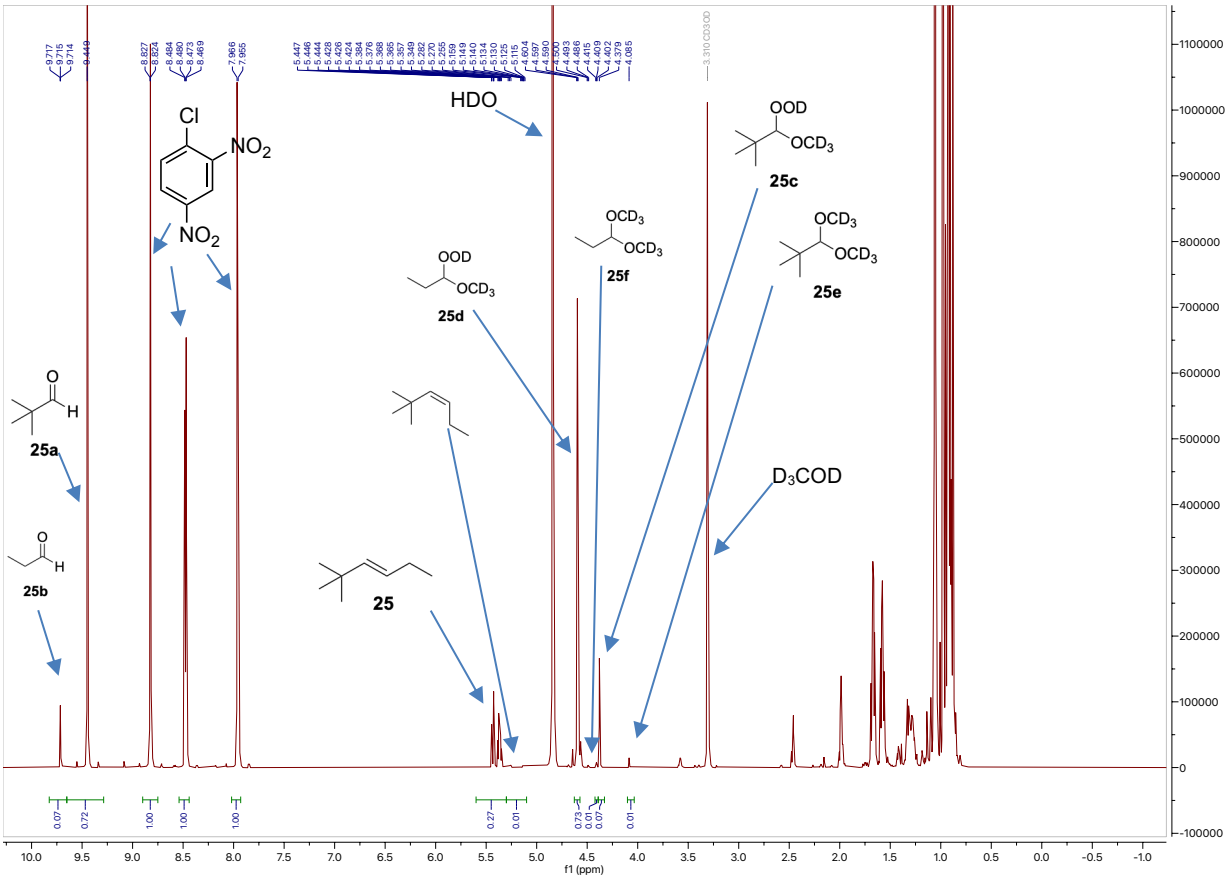
Blank Sample: (*E*)-2,2-dimethylhex-3-ene (**25**) and 1-chloro-2,4-dinitrobenzene (**IS**)



^{1}H NMR (800 MHz, CD_3OD), D1 = 10 s, 32 scans

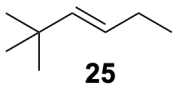
of (*E*)-2,2-dimethylhex-3-ene (**25**, 91.5%), (*Z*)-2,2-dimethylhex-3-ene (8.5%), and 1-chloro-2,4-dinitrobenzene

Representative ^{1}H NMR: (*E*)-2,2-dimethylhex-3-ene (**25**) ozonolysis



^{1}H NMR (800 MHz, MeOH-d_4), D1 = 10 s, 32 scans

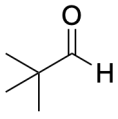
Characterization Data: (*E*)-2,2-dimethylhex-3-ene (**25**)



25

(*E*)-2,2-dimethylhex-3-ene (**25**)

^{1}H NMR (800 MHz, MeOD) δ 5.44 (dt, *J* = 15.6, 1.5 Hz, 1H), 5.37 (dt, *J* = 15.6, 6.3 Hz, 1H), 2.04 – 1.92 (m, 2H), 0.98 (s, 9H), 0.96 (t, *J* = 7.5 Hz, 3H).

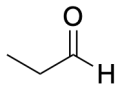


25a

pivalaldehyde (**25a**)

^{1}H NMR (800 MHz, MeOD) δ 9.45 (s, 1H), 1.06 (s, 9H).

The peaks were measured from the ^{1}H NMR of the crude reaction mixture.

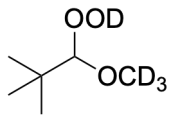


25b

propionaldehyde (**25b**)

^{1}H NMR (800 MHz, MeOD) δ 9.75 – 9.70 (m, 1H), 2.52–2.41 (m, 2H), 0.94 – 0.87 (m, 3H).

The peaks were measured from the ^{1}H NMR of the crude reaction mixture.

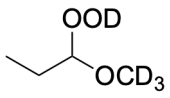


25c

1-deuteroperoxy-1-(methoxy-d_3)-2,2-dimethylpropane (**25c**)

^{1}H NMR (800 MHz, MeOD) δ 4.38 (s, 1H), 0.98 (s, 9H),

The peaks were measured from the ^{1}H NMR of the crude reaction mixture.

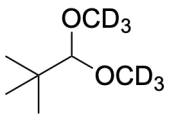


25d

1-deuteroperoxy-1-(methoxy-d_3)propane (**25d**)

^{1}H NMR (800 MHz, MeOD) δ 4.60 (t, *J* = 5.8 Hz, 1H), 1.97 – 1.63 (m, 1H), 1.63 – 1.52 (m, 1H), 0.93 (t, *J* = 7.6 Hz, 3H).

The peroxide α-CH peak was measured from the ^{1}H NMR of the crude reaction mixture. The other peaks were deduced from the 1D selective gradient TOCSY spectrum.

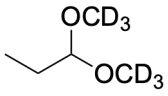


25e

1,1-bis(methoxy-d_3)-2,2-dimethylpropane (**25e**)

^{1}H NMR (800 MHz, MeOD) δ 4.09 (s, 1H), 0.95 (s, 9H).

The peaks were measured from the ^{1}H NMR of the crude reaction mixture.



25f

1,1-bis(methoxy-d_3)propane (**25f**)

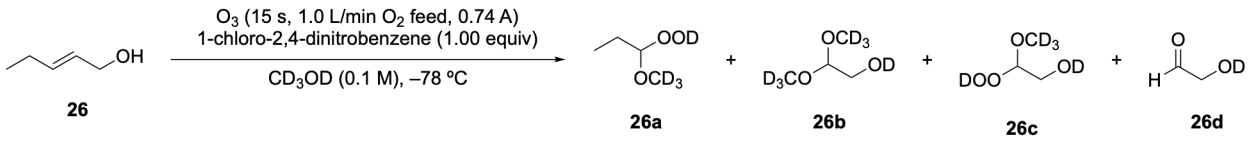
^{1}H NMR (800 MHz, MeOD) δ 4.41 (t, *J* = 5.4 Hz, 1H), 1.60–1.56 (m, 1H), 1.55–1.50 (m, 1H), 0.91 (t, J = 7.5 Hz, 3H).

The peroxide α-CH peak was measured from the ^{1}H NMR of the crude reaction mixture. The other peaks were deduced from the 1D selective gradient TOCSY spectrum.

Table 6.25 (*E*)-2,2-dimethylhex-3-ene (**25**) qNMR Data

Trial	%conversion	25a	25b	25c	25d	25e	25f
1	84	73	8	7	74	1	2
2	86	72	7	7	72	1	1
3	91	75	7	8	77	4	3
4	92	72	5	8	77	1	1

Trial	normalized 25a	normalized 25b	normalized 25c	normalized 25d	normalized 25e	normalized 25f
1	87	9.6	8.3	89	1.2	2.4
2	83	8.0	8.1	84	1.2	1.2
3	82	7.7	8.8	85	4.4	3.3
4	78	5.4	8.7	84	1.1	1.1
average	83	7.7	8.5	85	2.0	2.0
St. Dev.	3.6	1.7	0.32	2.2	1.6	1.1

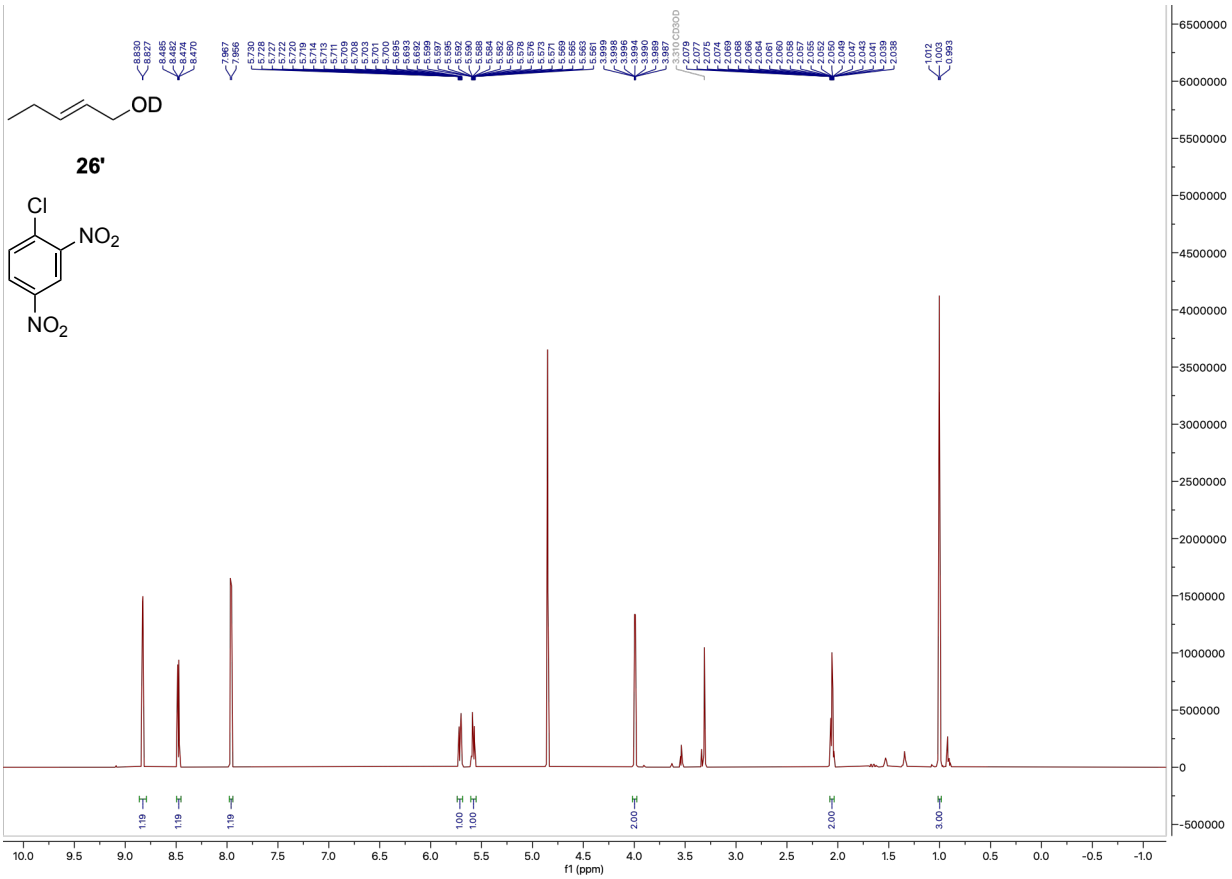


(*trans*)-pent-2-en-1-ol (**26**)

Reaction Time: 15 seconds

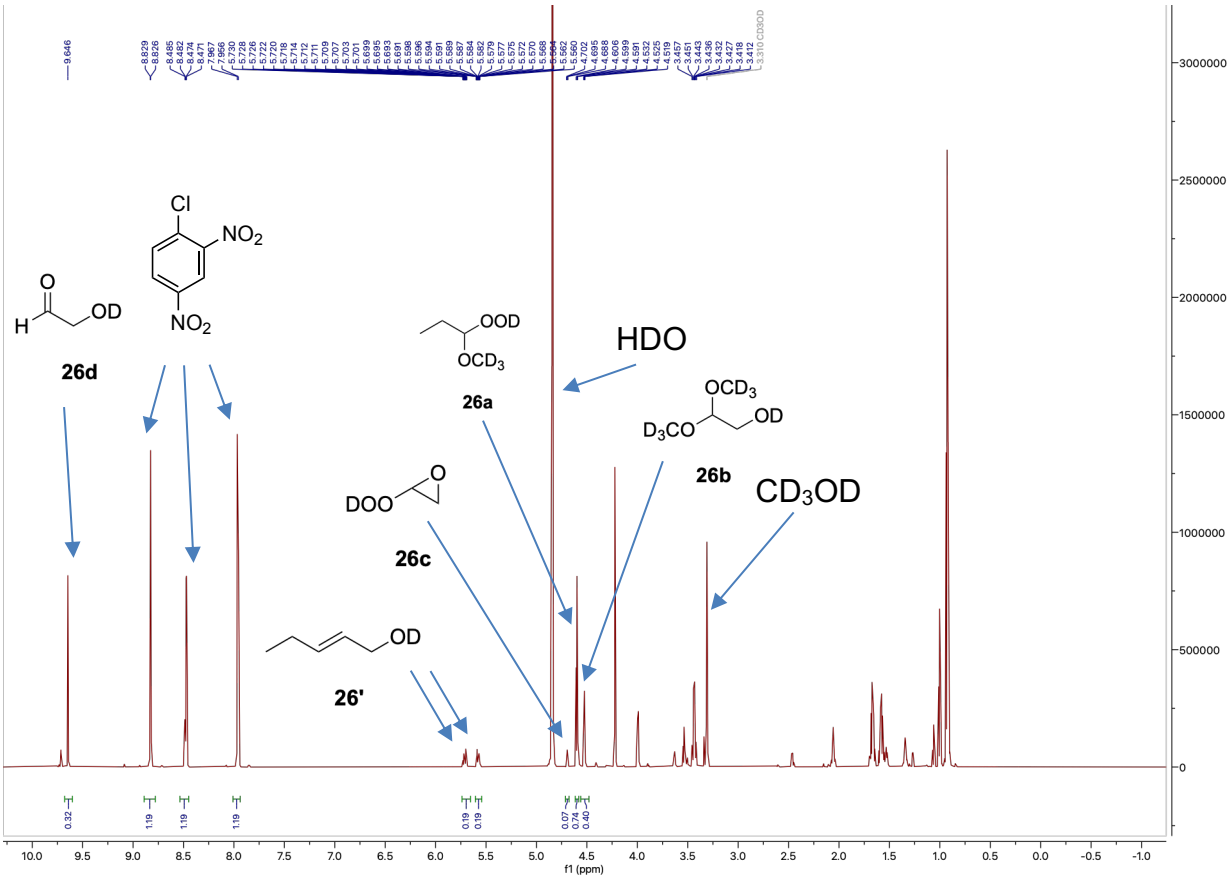
Alkene-to-IS Ratio: 0.81:1.00

Blank Sample: (*trans*)-pent-2-en-1-ol-*d* (**26'**) and 1-chloro-2,4-dinitrobenzene (**IS**)



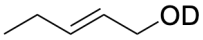
^{1}H NMR (800 MHz, CD_3OD), D1 = 10 s, 32 scans

Representative ^{1}H NMR: (*trans*)-pent-2-en-1-ol (**26**) ozonolysis



^{1}H NMR (800 MHz, CD_3OD), D1 = 10 s, 32 scans

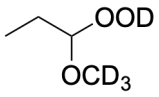
Characterization Data: (*trans*)-pent-2-en-1-ol (**26**)



26'

trans-pent-2-en-1-ol-*d* (**26'**)

^{1}H NMR (800 MHz, MeOD) δ 5.71 (dtt, *J* = 15.4, 6.3, 1.4 Hz, 1H), 5.58 (dtt, *J* = 15.1, 5.9, 1.6 Hz, 1H), 3.99 (dt, *J* = 5.9, 1.2 Hz, 2H), 2.06 (dtdd, *J* = 8.9, 7.5, 6.3, 1.4 Hz, 2H), 1.00 (t, *J* = 7.5 Hz, 3H).

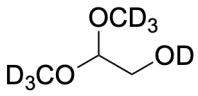


26a

1-deuteroperoxy-1-(methoxy-d_3)propane (**26a**)

^{1}H NMR (800 MHz, MeOD) δ 4.62 (t, *J* = 5.9 Hz, 1H), 1.69 (ddd, *J* = 13.8, 7.5, 6.0 Hz, 1H), 1.60 (ddd, *J* = 14.2, 7.6, 5.7 Hz, 1H), 0.95 (t, *J* = 7.5 Hz, 3H).

The peroxide α-CH peak was measured from the ^{1}H NMR of the crude reaction mixture. The other peaks were deduced from the 1D selective gradient TOCSY spectrum.

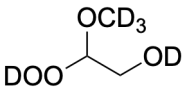


26b

2,2-bis(methoxy-d_3)ethan-1-ol-*d* (**26b**)

^{1}H NMR (800 MHz, MeOD) δ 4.54 (s, 1H), 3.61 – 3.20 (m, 2H).

The acetal α-CH peak was measured from the ^{1}H NMR of the crude reaction mixture. The other peaks were deduced from the 1D selective gradient TOCSY spectrum.



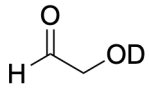
26c

2-deuteroperoxy-2-(methoxy-d_3)ethan-1-ol-*d* (**26c**)

^{1}H NMR (800 MHz, MeOD) δ 4.80 – 4.54 (m, 1H), 3.65 (dd, *J* = 11.8, 5.7 Hz, 1H), 3.53 (dd, *J* = 11.8, 5.2 Hz, 1H).

The peroxide α-CH peak was measured from the ^{1}H NMR of the crude reaction mixture.

The other peaks were deduced from the 1D selective gradient TOCSY spectrum.



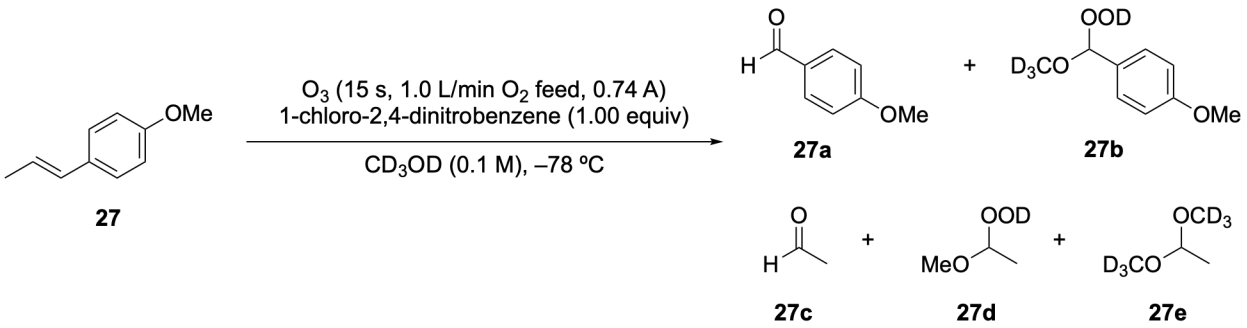
26d

2-(hydroxy-*d*)acetaldehyde (**26d**)

^{1}H NMR (800 MHz, MeOD) δ 9.65 (s, 1H), 3.46 – 3.40 (m, 2H).

Table 6.26 (*trans*)-pent-2-en-1-ol (**26**) qNMR Data

Trial	% conversion	%26a	%26b	%26c	%26d	normalized %26a	normalized %26b	normalized %26c	normalized %26d
1	81	74	40	7	32	91	49	8.6	40
2	100	91	46	9	43	91	46	9.0	43
3	84	76	31	8	43	90	37	10	51
average						91	44	9.1	45
st. dev.						0.44	6.5	0.44	6.0

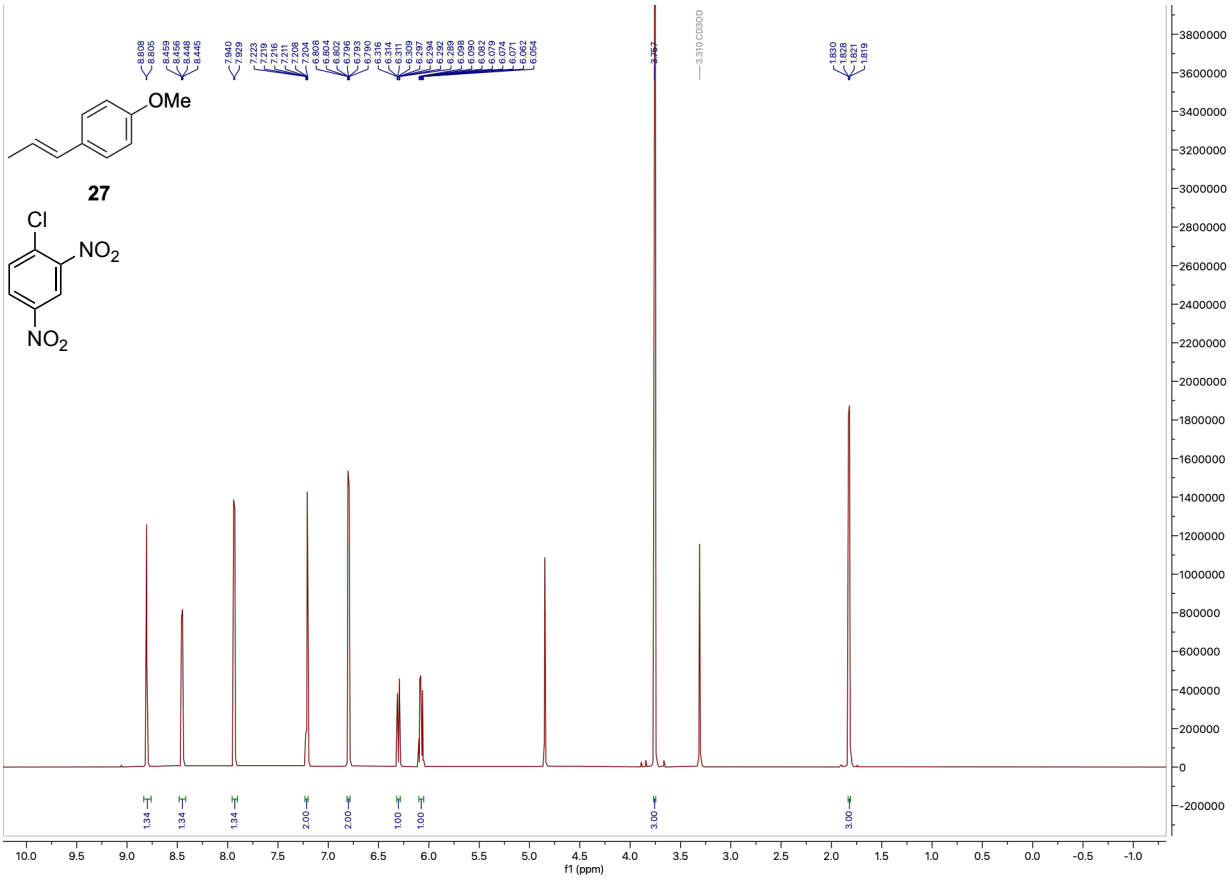


trans-anethole (**27**)

Reaction Time: 15 seconds

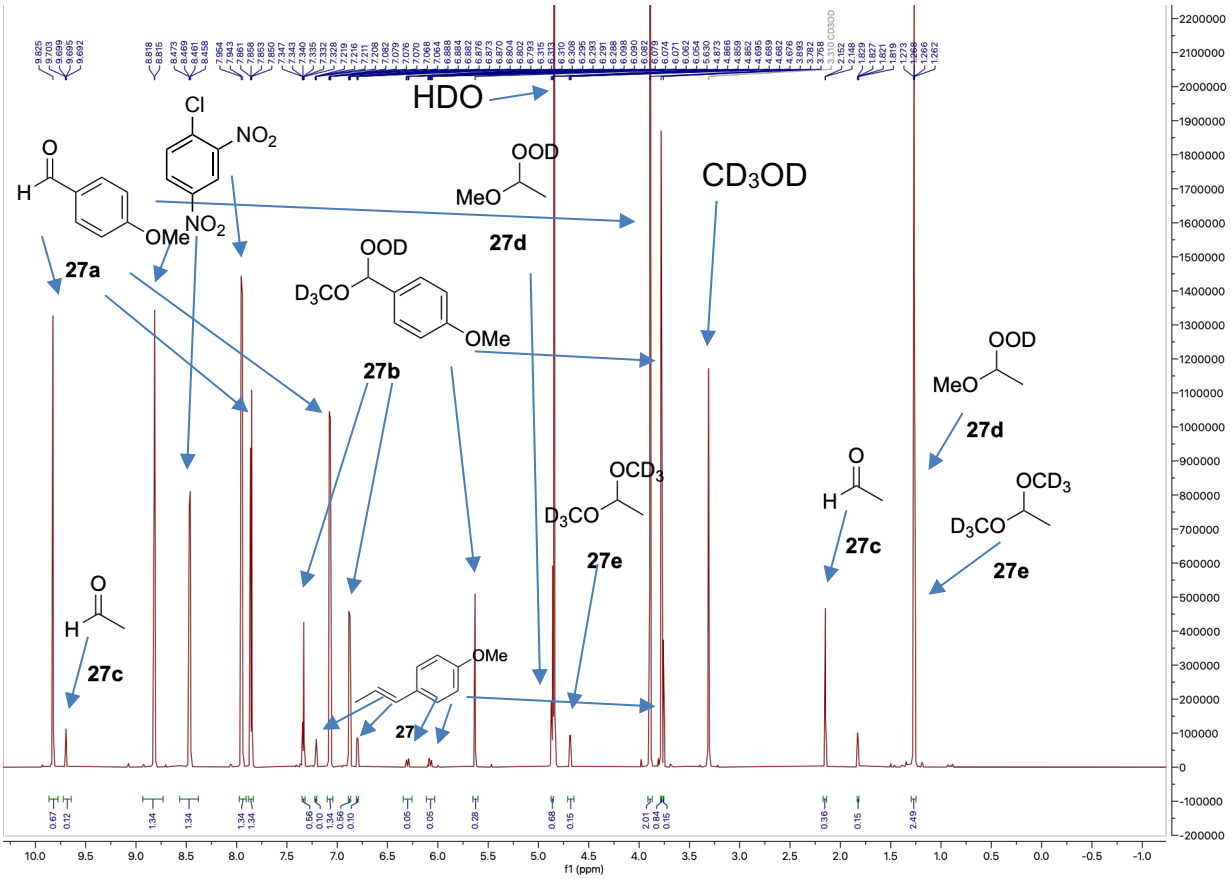
Alkene-to-IS Ratio: 0.66:1.00

Blank Sample: *trans*-anethole (**27**) and 1-chloro-2,4-dinitrobenzene (**IS**)



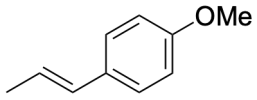
^{1}H NMR (800 MHz, CD_3OD), D1 = 10 s, 32 scans

Representative ^{1}H NMR: *trans*-anethole (**27**) ozonolysis



^{1}H NMR (800 MHz, CD_3OD), D1 = 10 s, 32 scans

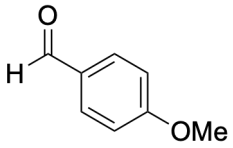
Characterization Data: *trans*-anethole (**27**)



27

trans-anethole (**27**)

^{1}H NMR (800 MHz, MeOD) δ 7.44 – 7.10 (m, 2H), 7.06 – 6.67 (m, 2H), 6.30 (dq, *J* = 15.8, 2.0 Hz, 1H), 6.08 (dq, *J* = 15.8, 6.6 Hz, 1H), 3.76 (s, 3H), 1.82 (dd, *J* = 6.6, 1.7 Hz, 3H).

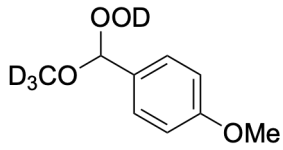


27a

4-methoxybenzaldehyde (**27a**)

^{1}H NMR (800 MHz, MeOD) δ 9.82 (s, 1H), 7.87 – 7.77 (m, 2H), 7.11 – 7.02 (m, 2H), 3.89 (s, 3H).

The signals were measured and deduced from the ^{1}H NMR of the crude reaction mixture.



27b

1-(deuteroperoxy(methoxy-d_3)methyl)-4-methoxybenzene (**27b**)

^{1}H NMR (800 MHz, MeOD) δ 7.41 – 7.30 (m, 2H), 6.96 – 6.86 (m, 2H), 5.63 (s, 1H), 3.78 (s, 3H).

The signals were measured and deduced from the ^{1}H NMR of the crude reaction mixture.

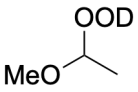


27c

acetaldehyde (**27c**)

^{1}H NMR (800 MHz, MeOD) δ 9.70 (q, *J* = 2.9 Hz, 1H), 2.15 (d, *J* = 2.8 Hz, 3H).

The signals were measured and deduced from the ^{1}H NMR of the crude reaction mixture.

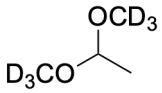


27d

1-deuteroperoxy-1-methoxyethane (**27d**)

^{1}H NMR (800 MHz, MeOD) δ 4.86 (q, *J* = 5.5 Hz, 1H), 1.28 – 1.25 (m, 3H).

The signals were measured and deduced from the ^{1}H NMR of the crude reaction mixture.



27e

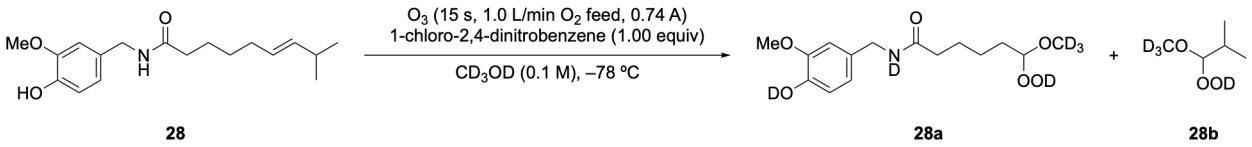
1,1-bis(methoxy-d_3)ethane (**27e**)

^{1}H NMR (800 MHz, MeOD) δ 4.69 (q, *J* = 5.2 Hz, 1H), 1.28 – 1.25 (m, 3H).

The signals were measured and deduced from the ^{1}H NMR of the crude reaction mixture.

Table 6.27 *trans*-anethole (**27**) qNMR Data

Trial	% conversion	%27a	%27b	%27c	%27d	%27e	normalized %27a	normalized %27b	normalized %27c	normalized %27d	normalized %27e
1	95	67	28	12	68	15	71	29	13	72	16
2	88	62	26	14	63	11	70	30	16	72	13
3	92	65	27	15	65	12	71	29	16	71	13
average							71	29	15	71	14
st. dev.							0.10	0.10	2.02	0.54	1.76



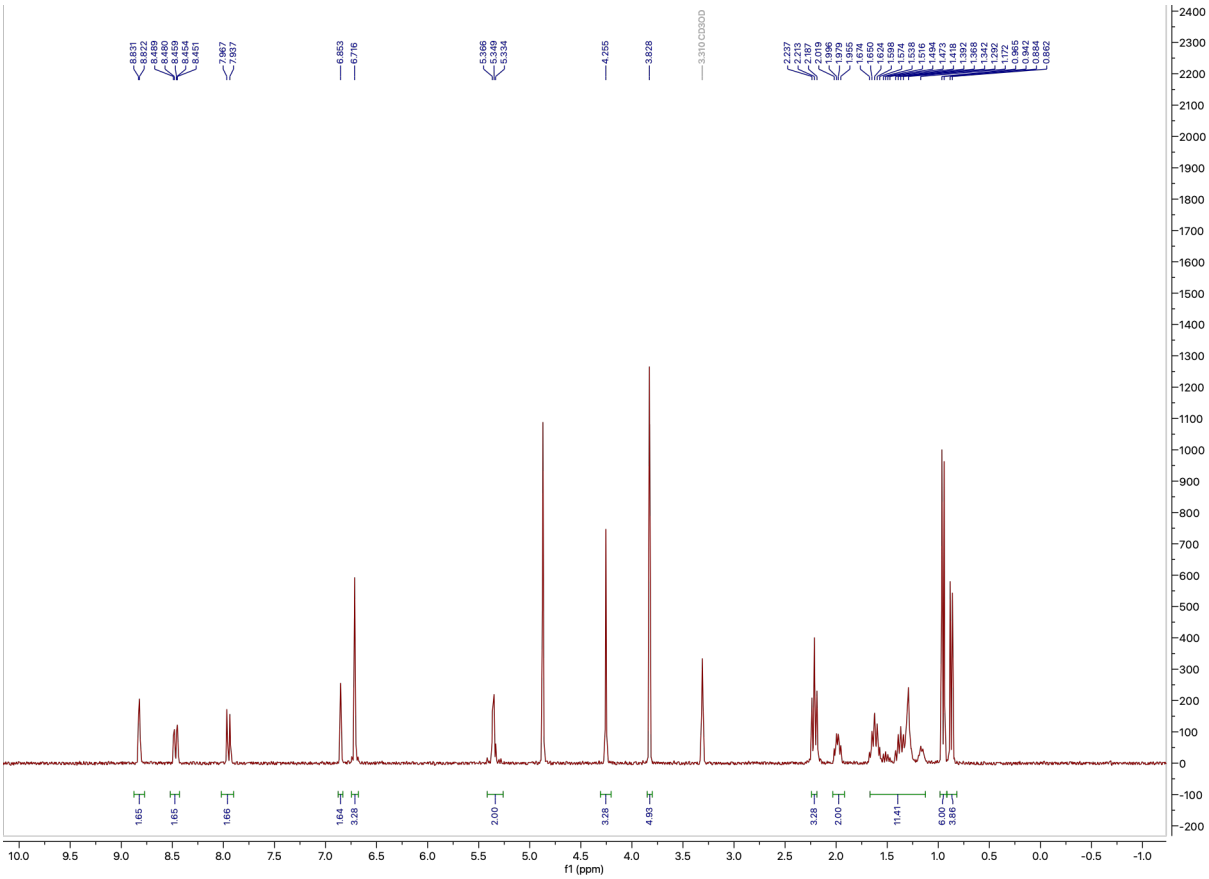
28 **28a** **28b**

capsaicin (**28**)

Reaction Time: 15 seconds

Alkene-to-IS Ratio: 0.675:1.00

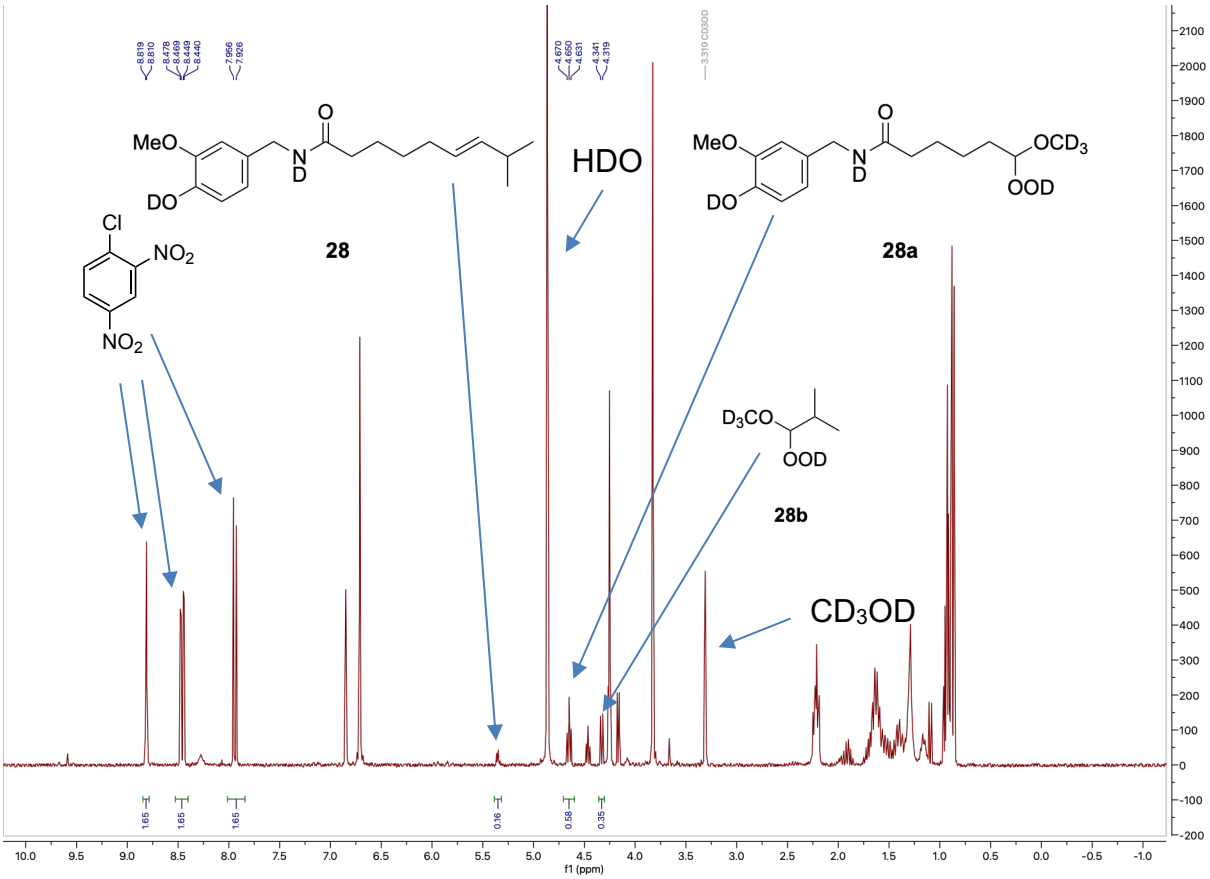
Blank Sample: capsaicin (**28**) and 1-chloro-2,4-dinitrobenzene (**IS**)



^{1}H NMR (300 MHz, CD_3OD), D1 = 10 s, 32 scans

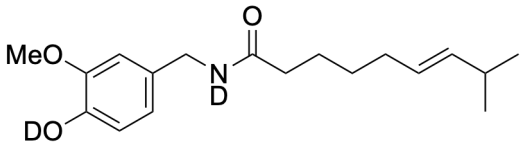
The impurity is dihydrocapsaicin (32.5%)

Representative ^{1}H NMR: capsaicin (**28**) ozonolysis



^{1}H NMR (300 MHz, CD_3OD), D1 = 10 s, 32 scans

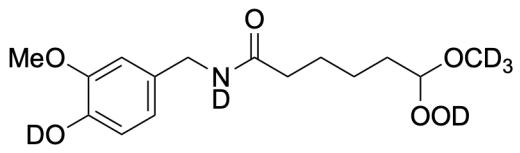
Characterization Data: capsaicin (**28**)



28'

Capsaicin-d_2 (**28'**)

^{1}H NMR (300 MHz, MeOD) δ 6.85 (s, 1H), 6.77 – 6.65 (m, 2H), 5.35 (t, *J* = 4.9 Hz, 2H), 4.26 (s, 2H), 3.83 (s, 3H), 2.21 (t, *J* = 7.5 Hz, 2H), 2.07 – 1.84 (m, 2H), 1.70 – 1.10 (m, 5H), 0.95 (d, *J* = 6.8 Hz, 6H).

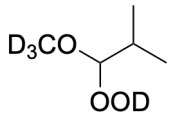


28a

6-deuteroperoxy-*N*-(4-(hydroxy-*d*)-3-methoxybenzyl)-6-(methoxy-d_3)hexanamide-*d* (**28a**)

^{1}H NMR (300 MHz, MeOD) δ 6.85 (s, 1H), 6.77 – 6.65 (m, 2H), 4.65 (t, *J* = 5.8 Hz, 1H), 4.25 (s, 2H), 3.83 (s, 3H), 2.31 – 2.16 (m, 2H), 2.01 – 1.07 (m, 6H).

The signals were measured and deduced from the ^{1}H NMR of the crude reaction mixture.



28b

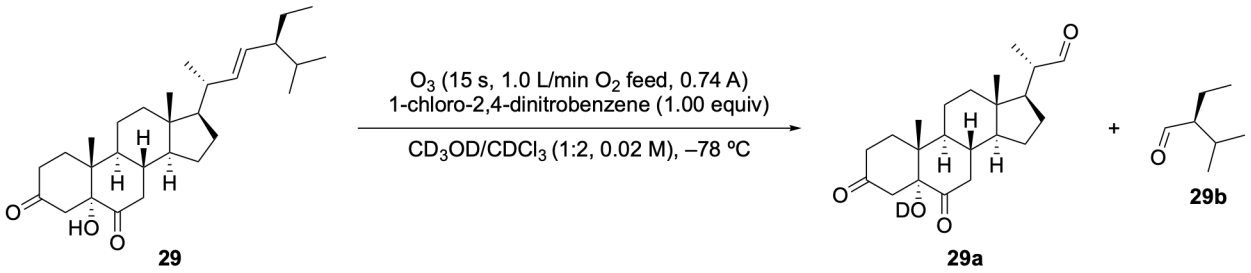
1-deuteroperoxy-1-(methoxy-d_3)-2-methylpropane (**28b**)

^{1}H NMR (300 MHz, MeOD) δ 4.33 (d, *J* = 6.8 Hz, 1H), 1.81 – 0.79 (m, 7H).

The signals were measured and deduced from the ^{1}H NMR of the crude reaction mixture.

Table 6.28 capsaicin (**28**) qNMR Data

Trial	%Conversion	%28a	normalized %28a	%28b	normalized %28b
1	92	58	63%	35	38%
2	93	57	61%	34	37%
3	95	58	61%	36	38%
average			62%		38%
st. dev.			0.011		0.0082



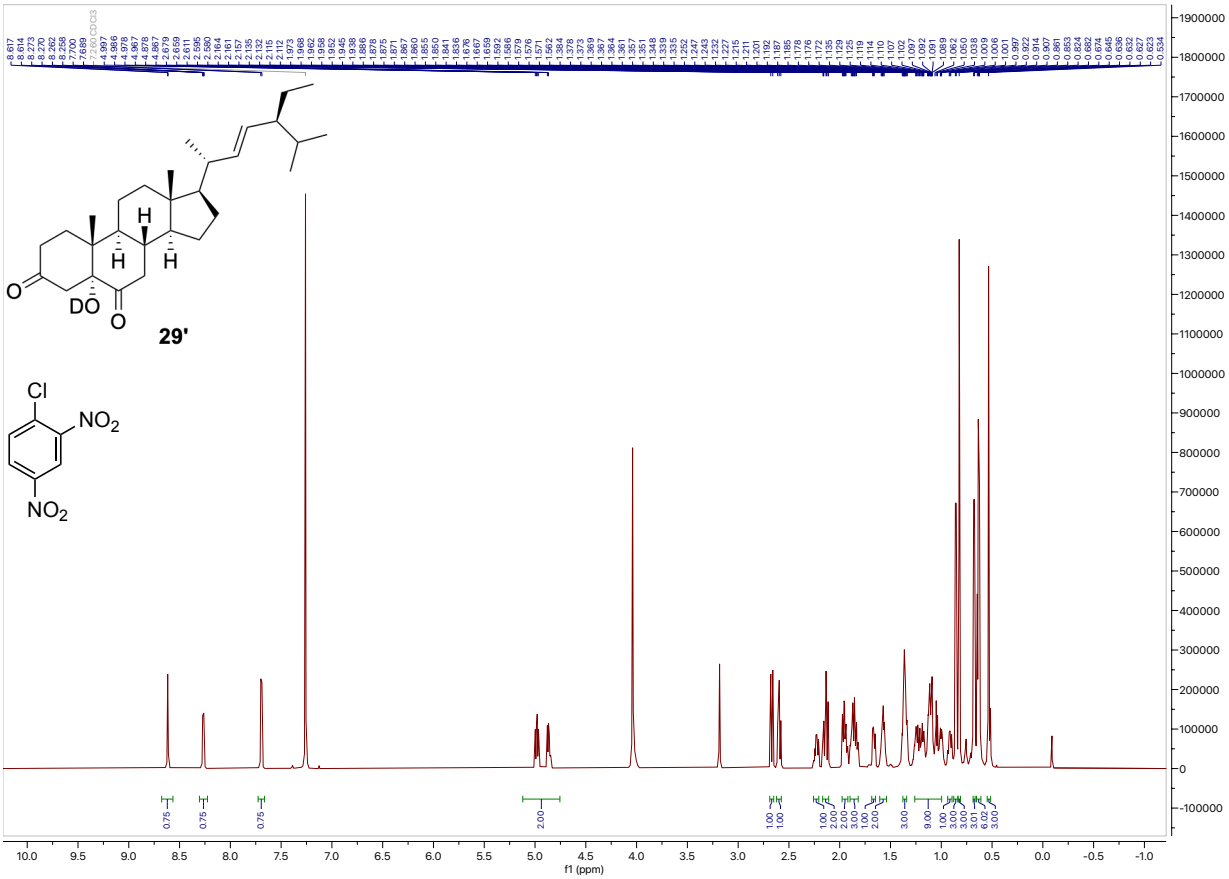
(22*R*,23*R*)-5α-hydroxy-22,23-stigmasten-3,6-dione (**29**)

Reaction Solvent: 1:2 $CD_3OD/CDCl_3$ (0.02 M) was used to homogenize the mixture

Reaction Time: 15 seconds

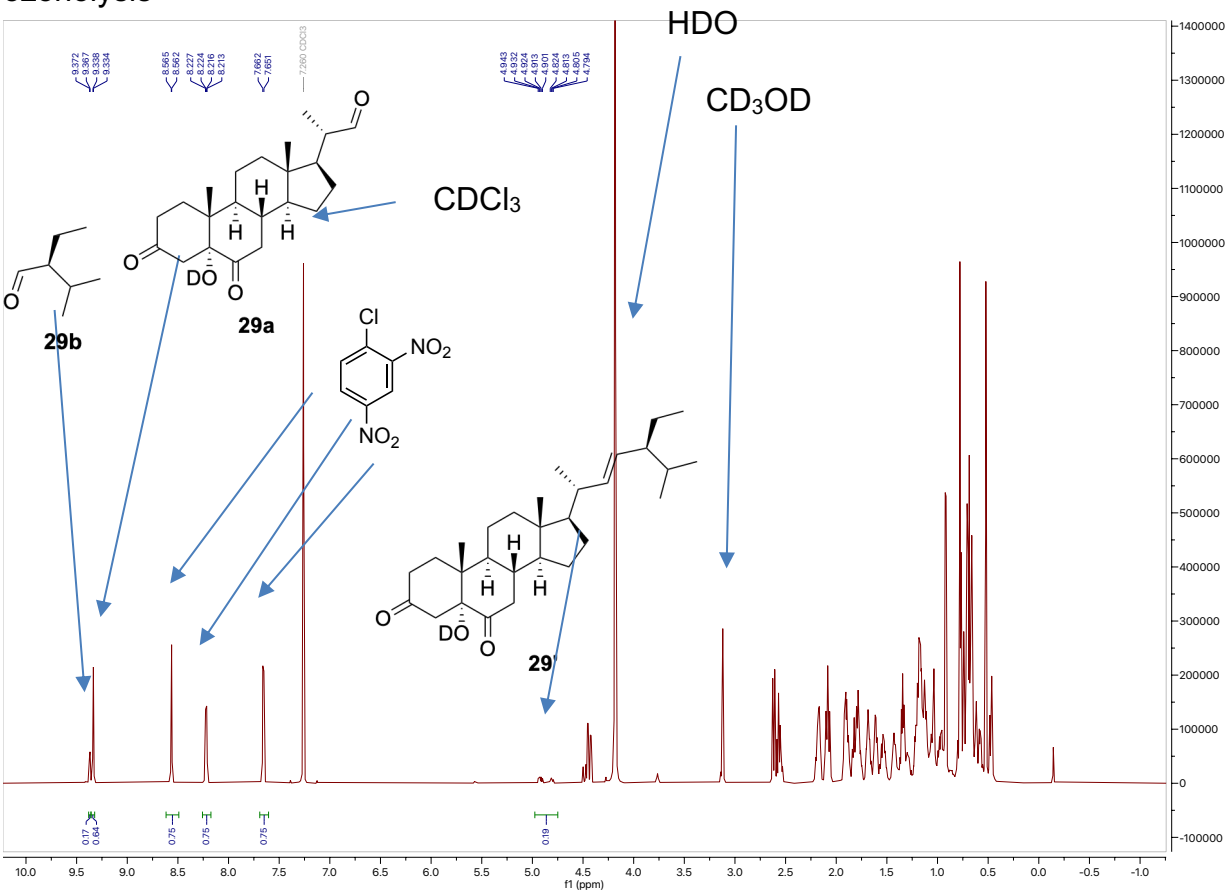
Alkene-to-IS Ratio: 1.00:0.75

Blank Sample: (22*R*,23*R*)-5α-hydroxy-22,23-stigmasten-3,6-dione (**29**) and 1-chloro-2,4-dinitrobenzene (**IS**)



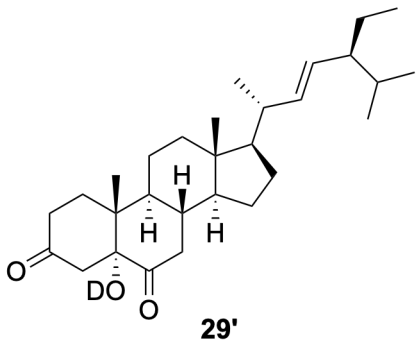
^{1}H NMR (800 MHz, 1:2 $CD_3OD/CDCl_3$)

Representative ^{1}H NMR: (22*R*,23*R*)-5α-hydroxy-22,23-stigmasten-3,6-dione (**29**) ozonolysis



^{1}H NMR (800 MHz, 1:2 $CD_3OD/CDCl_3$), D1 = 10 s, 32 scans

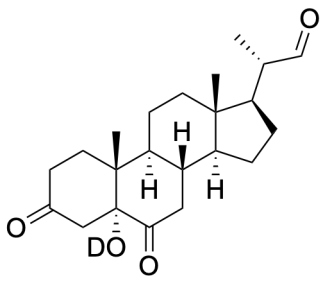
Characterization Data: (22*R*,23*R*)-5α-hydroxy-22,23-stigmasten-3,6-dione (**29**)



29'

(5a,22*E*)-5-hydroxy-*d*-stigmast-22-ene-3,6-dione (**29'**)

^{1}H NMR (800 MHz, MeOD) δ 4.98 (dd, *J* = 15.2, 8.8 Hz, 1H), 4.86 (dd, *J* = 15.2, 8.8 Hz, 1H), 2.67 (d, *J* = 15.6 Hz, 1H), 2.60 (t, *J* = 12.6 Hz, 1H), 2.23 (ddd, *J* = 15.8, 12.7, 7.2 Hz, 1H), 2.18 – 2.09 (m, 2H), 2.02 – 1.91 (m, 2H), 1.91 – 1.79 (m, 3H), 1.66 (dd, *J* = 13.2, 7.3 Hz, 1H), 1.62 – 1.51 (m, 2H), 1.44 – 1.31 (m, 3H), 1.29 – 0.95 (m, 9H), 0.91 (qd, *J* = 12.2, 6.3 Hz, 1H), 0.86 (d, *J* = 6.6 Hz, 3H), 0.82 (s, 3H), 0.68 (d, *J* = 6.4 Hz, 3H), 0.66 – 0.60 (m, 6H), 0.53 (s, 3H).

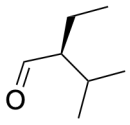


29a

3,6-dioxo-5a-hydroxy-*d*-cholan-24-al (**29a**)

^{1}H NMR (800 MHz, MeOD) δ 9.34 (d, *J* = 3.2 Hz, 1H), 2.67 – 0.38 (m, 30H).

1D selective gradient TOCSY of the aldehyde CHO peak revealed its aliphatic chain signasl. The remaining signals were deduced from the ^{1}H NMR of the crude reaction mixture.



29b

(*S*)-2-ethyl-3-methylbutanal (**29b**)

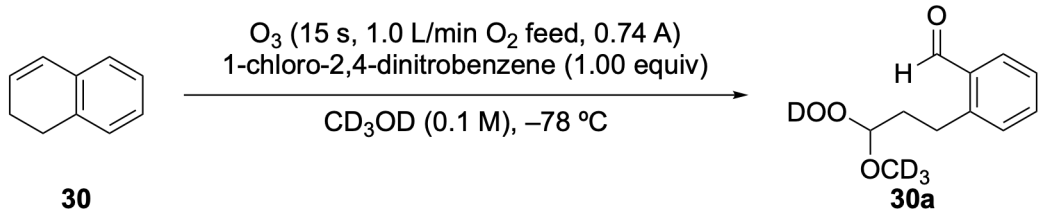
^{1}H NMR (800 MHz, 2:1 $CDCl_3$,MeOD) δ 9.37 (d, *J* = 3.6 Hz, 1H), 1.79 – 1.72 (m, 1H), 1.43 (dp, *J* = 15.8, 7.5 Hz, 2H), 1.36 – 1.31 (m, 1H), 0.77 – 0.72 (m, 6H), 0.67 (t, *J* = 7.5 Hz, 3H).

1D selective gradient TOCSY of the aldehyde CHO peak revealed its aliphatic chain signals. The signals were measured and deduced from the ^{1}H NMR of the crude reaction mixture.

Table 6.29 (22*R*,23*R*)-5α-hydroxy-22,23-stigmasten-3,6-dione (**29**) qNMR Data

Trial	%conversion	%29a	normalized %29a	%29b	normalized %29b
1	81	64	79	17	21
2	65	51	78	14	22
3	74	58	78	16	22
average			79		21
st. dev.			0.34		0.34

6.8.4.6 *cis*-1,2-Disubstituted Alkenes



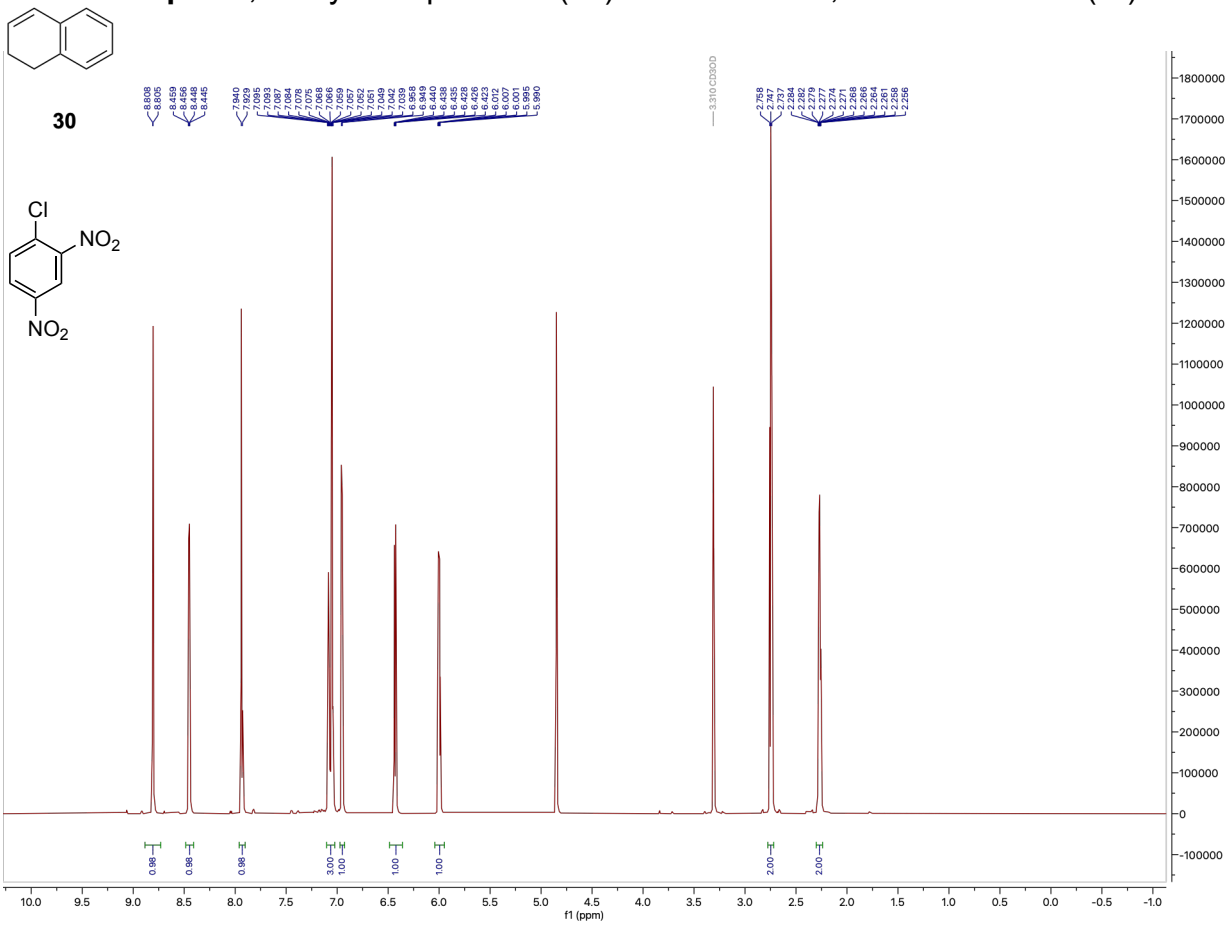
30 **30a**

1,2-dihydronapthalene (**30**)

Reaction Time: 15 seconds

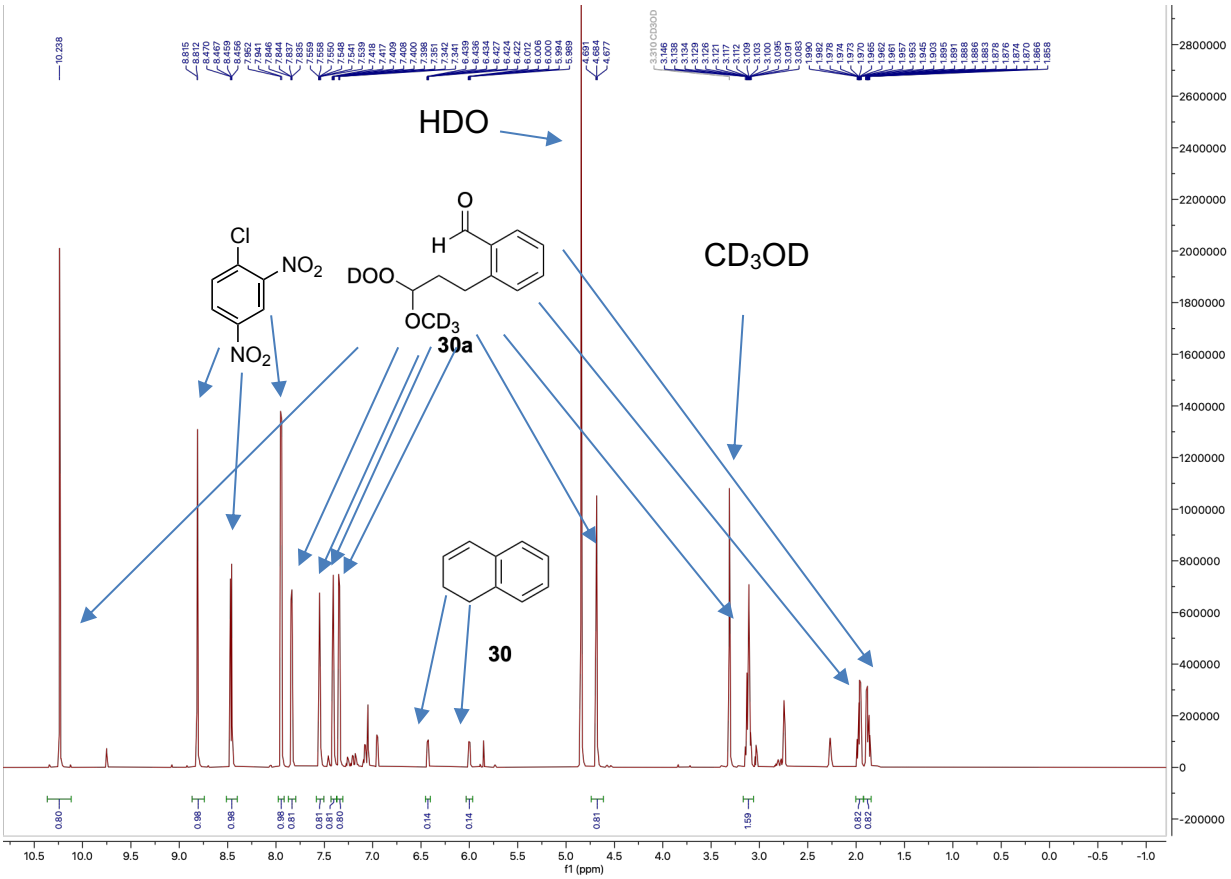
Alkene-to-IS Ratio: 1.00:0.98

Blank Sample: 1,2-dihydronapthalene (**30**) and 1-chloro-2,4-dinitrobenzene (**IS**)



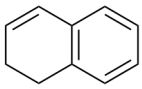
^{1}H NMR (800 MHz, CD_3OD), D1 = 10 s, 32 scans

Representative ^{1}H NMR: 1,2-dihydronapthalene (**30**) ozonolysis



^{1}H NMR (800 MHz, CD_3OD), D1 = 10 s, 32 scans

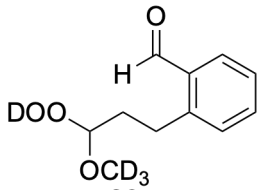
Characterization Data: 1,2-dihydronapthalene (**30**)



30

1,2-dihydronapthalene (**30**)

^{1}H NMR (800 MHz, MeOD) δ 7.14 – 7.00 (m, 3H), 6.95 (d, *J* = 7.0 Hz, 1H), 6.43 (dt, *J* = 9.6, 2.0 Hz, 1H), 6.00 (dt, *J* = 9.4, 4.3 Hz, 1H), 2.75 (t, *J* = 8.2 Hz, 2H), 2.27 (tdd, *J* = 8.0, 4.4, 1.9 Hz, 2H).



30a

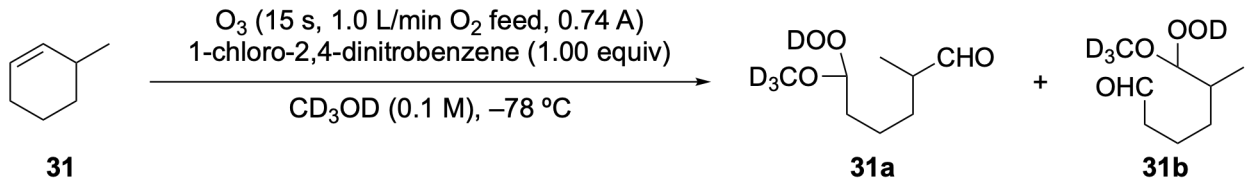
2-(3-deuteroperoxy-3-(methoxy-d_3)propyl)benzaldehyde (**30a**)

^{1}H NMR (800 MHz, MeOD) δ 10.24 (s, 1H), 7.84 (dd, *J* = 7.8, 1.6 Hz, 1H), 7.55 (td, *J* = 7.4, 1.5 Hz, 1H), 7.41 (td, *J* = 7.5, 1.2 Hz, 1H), 7.36 – 7.31 (m, 1H), 4.68 (t, *J* = 5.9 Hz, 1H), 3.17 – 3.06 (m, 2H), 1.97 (ddt, *J* = 13.9, 9.6, 6.3 Hz, 1H), 1.88 (ddt, *J* = 13.9, 9.5, 6.0 Hz, 1H).

The signals were measured and deduced from the ^{1}H NMR of the crude reaction mixture.

Table 6.30 1,2-dihydronapthalene (**30**) qNMR Data

Trial	% conversion	average %31a	normalized %31a
1	86	81	94
2	83	78	94
3	88	83	94
average			94
st. dev.			0.0017



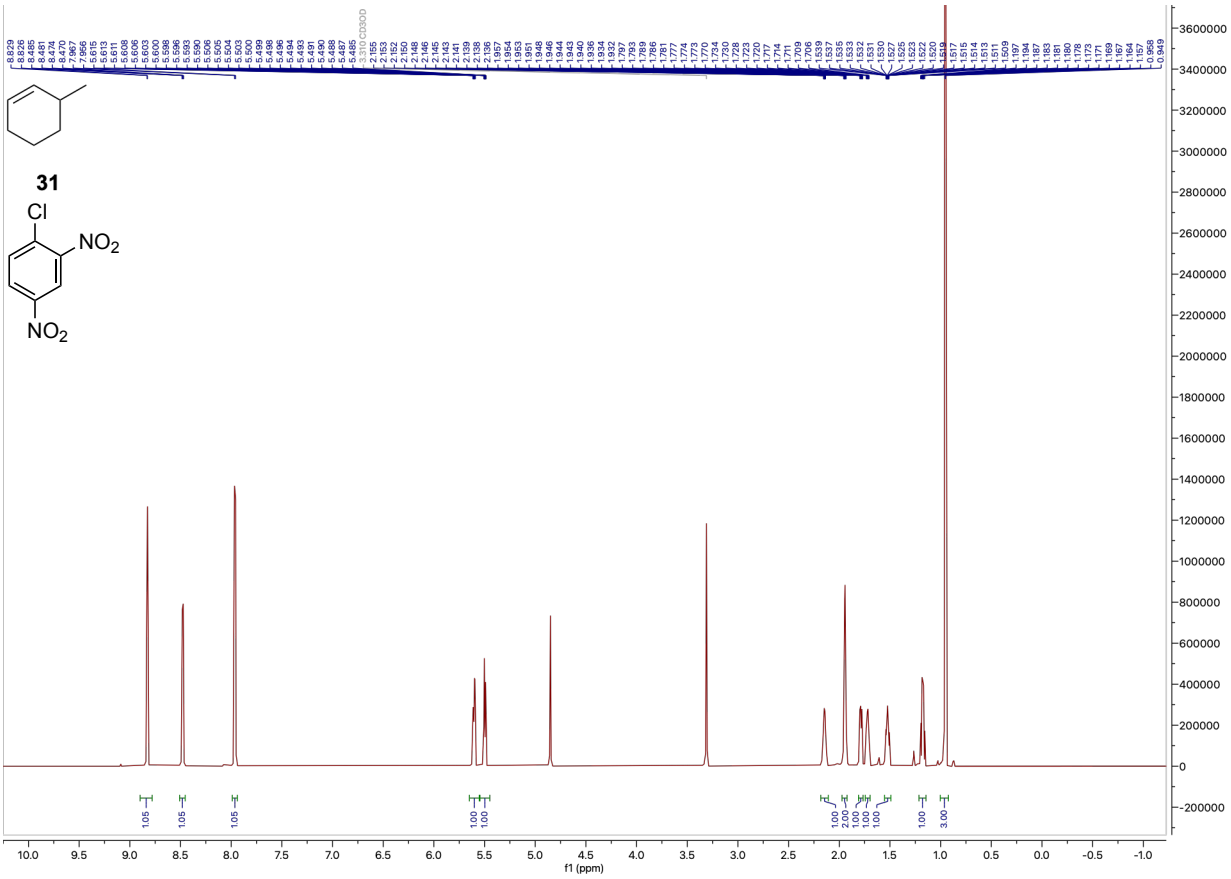
31 **31a** **31b**

3-methylcyclohexene (**31**)

Reaction Time: 15 seconds

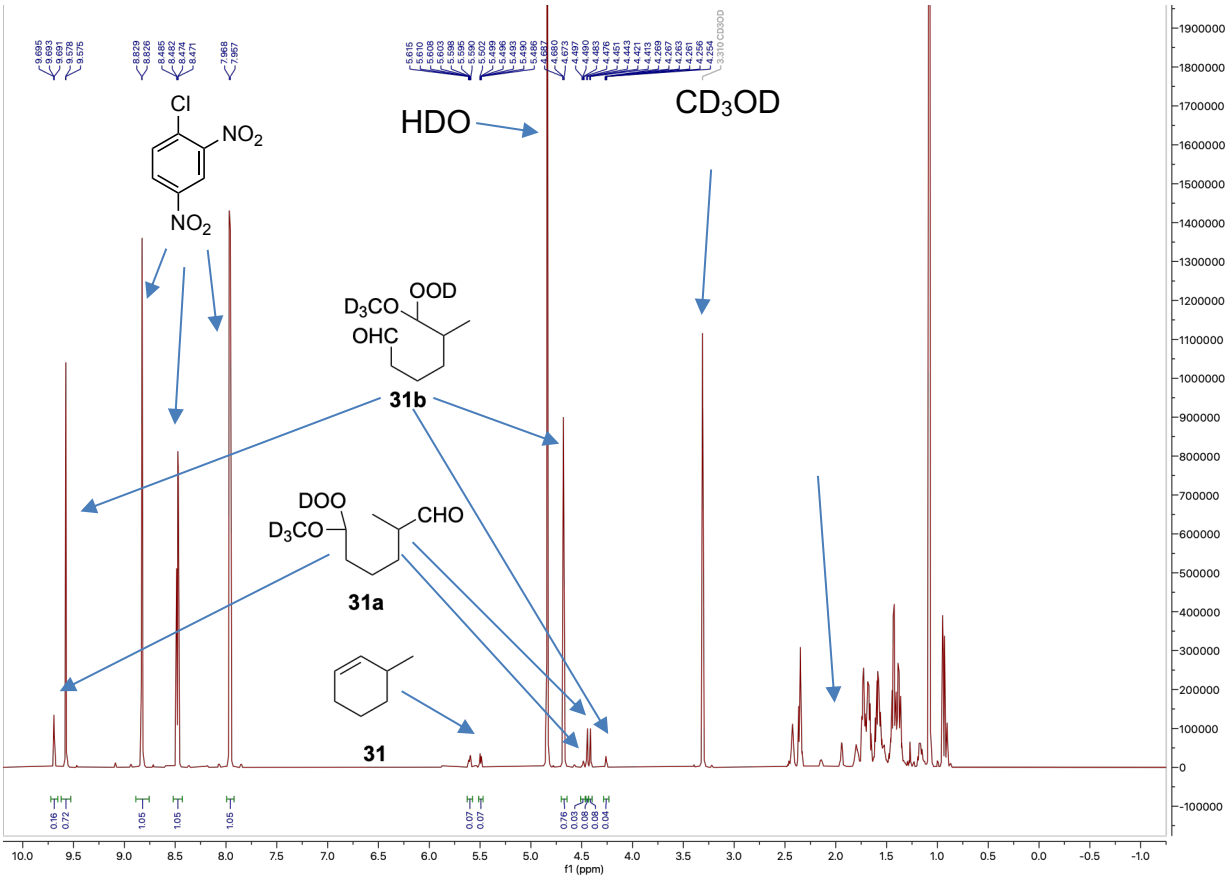
Alkene-to-IS Ratio: 0.95:1.00

Blank Sample: 3-methylcyclohexene (**31**) and 1-chloro-2,4-dinitrobenzene (**IS**)



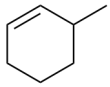
^{1}H NMR (800 MHz, CD_3OD), D1 – 10 s, 32 scans

Representative ^{1}H NMR: 3-methylcyclohexene (**31**) ozonolysis



^{1}H NMR (800 MHz, CD_3OD), D1 = 10 s, 32 scans

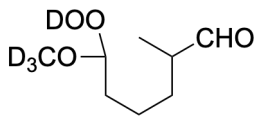
Characterization Data: 3-methylcyclohexene (**31**)



31

3-methylcyclohexene (**31**)

^{1}H NMR (800 MHz, MeOD) δ 5.78 – 5.54 (m, 1H), 5.50 (dqd, *J* = 10.1, 2.3, 1.0 Hz, 1H), 2.22 – 2.09 (m, 1H), 2.04 – 1.88 (m, 2H), 1.82 – 1.76 (m, 1H), 1.72 (dddd, *J* = 17.7, 8.4, 4.2, 1.9 Hz, 1H), 1.52 (ddddd, *J* = 13.0, 11.2, 10.1, 7.2, 2.8 Hz, 1H), 1.18 (dddd, *J* = 12.7, 11.2, 8.5, 2.8 Hz, 1H), 0.95 (d, *J* = 7.1 Hz, 3H).

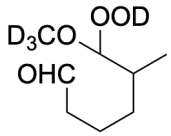


31a

6-deuteroperoxy-6-(methoxy-d_3)-2-methylhexanal (**31a**)

^{1}H NMR (800 MHz, MeOD) δ 9.58 (d, *J* = 2.1 Hz, 1H), 4.68 (t, *J* = 5.8 Hz, 1H), 2.35 (qd, *J* = 6.7, 1.9 Hz, 1H), 1.79 – 1.63 (m, 2H), 1.63 – 1.54 (m, 2H), 1.48 – 1.33 (m, 2H), 1.08 (d, *J* = 7.0 Hz, 3H).

The aldehyde CHO and peroxide α-CH peaks were determined from the ^{1}H NMR of the crude reaction mixture. The remaining peaks were deduced from the 1D TOCSY spectrum.



31b

6-deuteroperoxy-6-(methoxy-d_3)-5-methylhexanal (**31b**)

Diastereomer 1

^{1}H NMR (800 MHz, MeOD) δ 9.72 – 9.67 (m, 1H), 4.47 (d, *J* = 6.2 Hz, 1H), 2.50 – 2.34 (m, 2H), 1.91 – 1.76 (m, 1H), 1.76 – 1.66 (m, 1H), 1.63 – 1.54 (m, 1H), 1.23 – 1.14 (m, 2H), 0.95 (d, *J* = 6.9 Hz, 3H).

The aldehyde CHO and peroxide α-CH peaks were determined from the ^{1}H NMR of the crude reaction mixture. The remaining peaks were deduced from the 1D TOCSY spectrum.

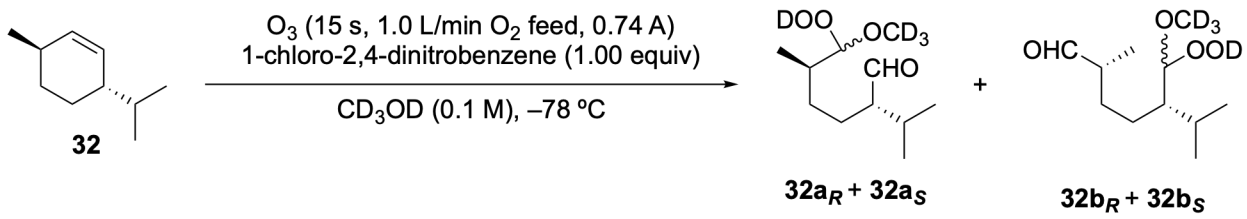
Diastereomer 2

^{1}H NMR (800 MHz, MeOD) δ 9.72 – 9.67 (m, 1H), 4.44 (d, *J* = 5.8 Hz, 1H), 2.47 – 2.41 (m, 2H), 1.89 – 1.76 (m, 1H), 1.74 – 1.67 (m, 1H), 1.60 – 1.51 (m, 1H), 1.24 – 1.13 (m, 2H), 0.97 (d, *J* = 6.9 Hz, 3H).

The aldehyde CHO and peroxide α-CH peaks were determined from the ^{1}H NMR of the crude reaction mixture. The remaining peaks were deduced from the 1D TOCSY spectrum.

Table 6.31 3-methylcyclohexene (**31**) qNMR Data

Trial	% conversion	average %31a	average %31b	normalized %31a	normalized %31b
1	91	74	17	81	19
2	93	76	18	82	19
3	92	75	17	81	18
average				81	19
st. dev.				0.50	0.17

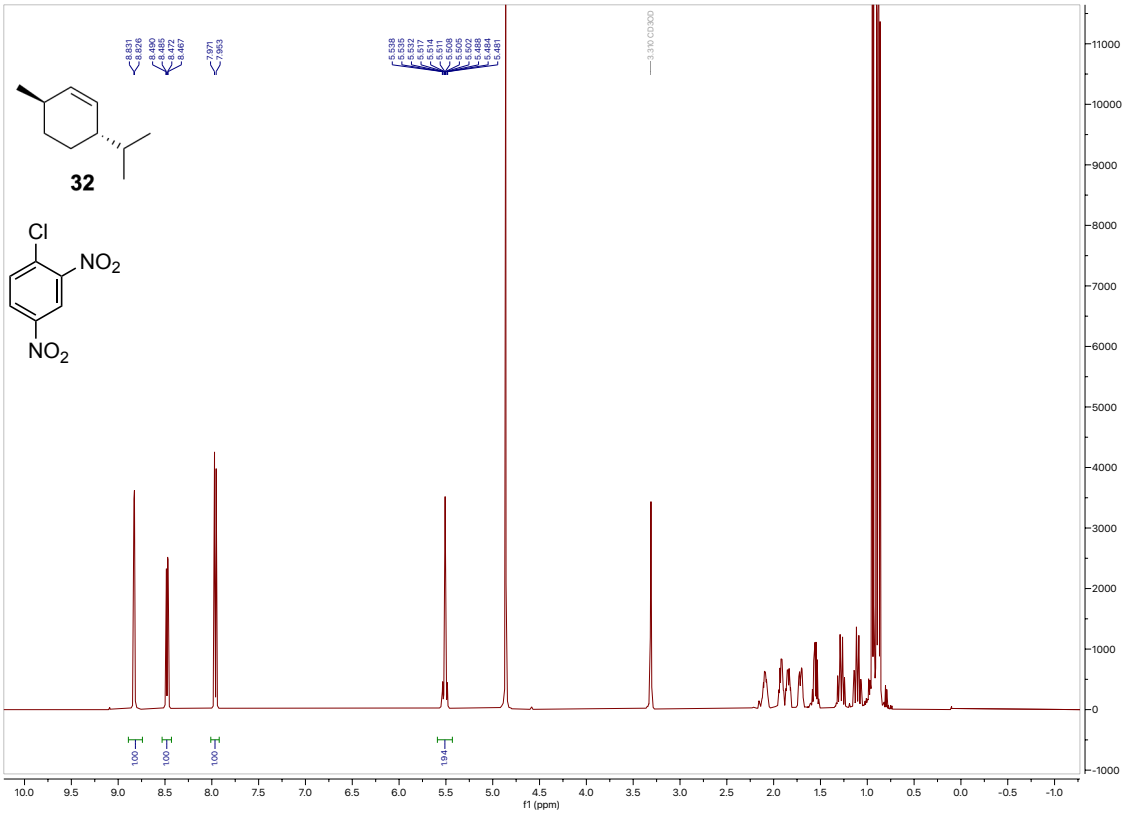


(+)-*trans*-p-menth-2-ene (**32**)

Reaction Time: 15 seconds

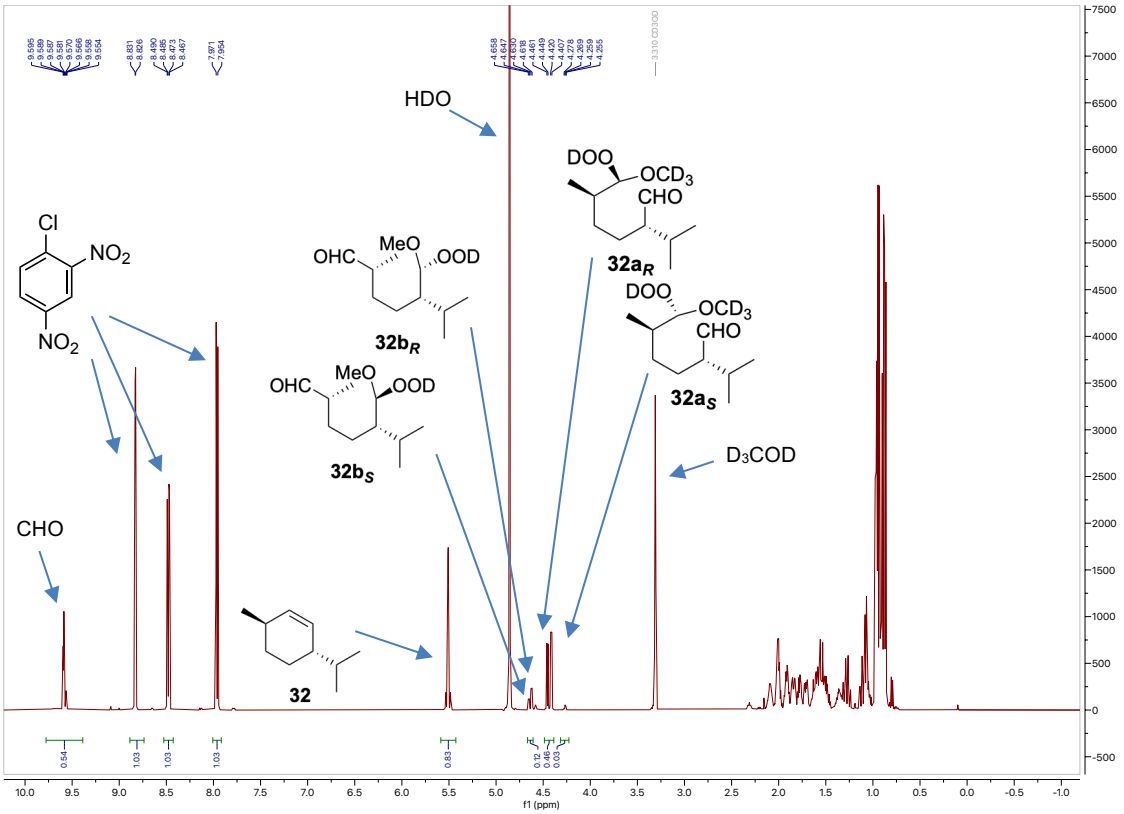
Alkene-to-IS Ratio: 1.00:1.00

Blank Sample: (+)-*trans*-p-menth-2-ene (**32**) and 1-chloro-2,4-dinitrobenzene (**IS**)



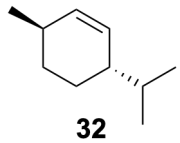
^{1}H NMR (500 MHz, MeOH-d_4), D1 = 10 s, 32 scans

Representative ^{1}H NMR: (+)-*trans*-p-menth-2-ene (**32**) ozonolysis



^{1}H NMR (500 MHz, CD_3OD), D1 = 10 s, 32 scans

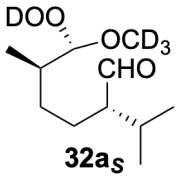
Characterization Data: (+)-*trans*-p-menth-2-ene (**32**)



32

(+)-*trans*-p-menth-2-ene (**32**)

^{1}H NMR (500 MHz, MeOD) δ 5.55 – 5.45 (m, 2H), 2.14 – 2.04 (m, 1H), 1.99 – 1.88 (m, 1H), 1.88 – 1.80 (m, 1H), 1.76 – 1.65 (m, 1H), 1.55 (pd, *J* = 6.9, 5.2 Hz, 1H), 1.28 (tdd, *J* = 13.1, 10.6, 2.7 Hz, 1H), 1.10 (tdd, *J* = 13.1, 10.5, 2.7 Hz, 1H), 0.94 (d, *J* = 7.2 Hz, 3H), 0.89 (d, *J* = 6.9 Hz, 3H), 0.87 (d, *J* = 6.7 Hz, 3H).



32a$_S$

(2*S*,5*R*,6*S*)-6-Deuteroperoxy-2-isopropyl-6-(methoxy-d_3)-5-methylhexanal (**32a$_S$**)

^{1}H NMR (800 MHz, 10:1 $CDCl_3$:CD_3OD) δ 9.60 (d, *J* = 3.1 Hz, 1H), 4.43 (d, *J* = 6.3 Hz, 1H), 2.06–1.95 (m, 1H), 1.81 (qtd, *J* = 9.5, 6.9, 4.6 Hz, 1H), 1.64–1.56 (m, 1H), 1.56–1.44 (m, 3H), 1.08–1.02 (m, 1H), 1.02 (d, *J* = 6.8 Hz, 3H), 0.94 (d, *J* = 6.9 Hz, 3H), 0.86 (d, *J* = 6.9 Hz, 3H).

1D Selective Gradient TOCSY at a frequency of 4.43 ppm revealed the spin-system for the peroxide α-CH and the splitting pattern (qtd) of the peroxide β-CH at 1.81 ppm. It also strongly showed the γ-methyl which indicates it is close in proximity to the peroxide α-CH. 1D Selective Gradient COSY at a frequency of 4.43 ppm confirmed the peroxide β-CH to be at 1.81 ppm. The *S*-configuration was assigned based on the Felkin–Ahn model (the A-value for R was assumed to be greater than the A-value for Me) for the capture of the Criegee intermediate by MeOH-d_4.

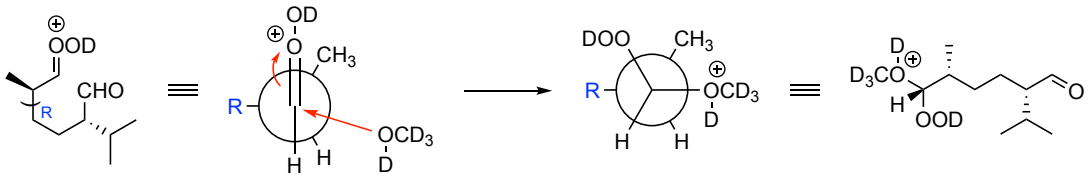


Figure 6.14 Felkin–Ahn Analysis for **32a*S***

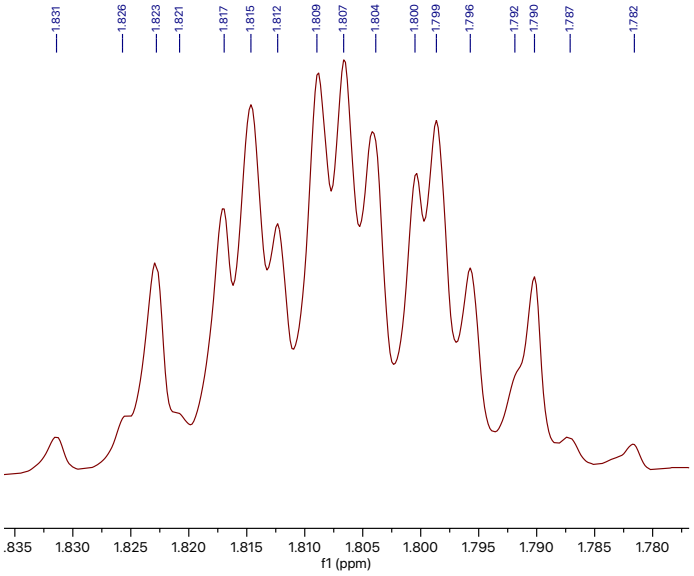
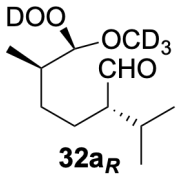


Figure 6.15 **1D Gradient Selective TOCSY** (800 MHz, 10:1 $CDCl_3$:CD_3OD) signal for the peroxide β-CH of (**32a*S***)



32a*R*

(2*S*,5*R*,6*R*)-6-Deuteroperoxy-2-isopropyl-6-(methoxy-d_3)-5-methylhexanal (**32a*R***)

^{1}H NMR (800 MHz, 10:1 $CDCl_3$:CD_3OD) δ 9.61 (d, *J* = 3.1 Hz, 1H), 4.47 (d, *J* = 6.3 Hz, 1H), 2.08–1.96 (m, 1H), 1.81 (qtd, *J* = 9.3, 6.7, 4.4 Hz, 1H), 1.67–1.58 (m, 1H), 1.58–1.48 (m, 3H), 1.12–1.03 (m, 1H), 1.02 (d, *J* = 6.9 Hz, 3H), 0.94 (d, *J* = 6.9 Hz, 3H), 0.86 (d, *J* = 6.6 Hz, 3H).

1D Selective Gradient TOCSY at a frequency of 4.47 ppm revealed the spin-system for the peroxide α-CH and the splitting pattern (qtd) of the peroxide β-CH at 1.81 ppm. It also strongly showed the γ-methyl which indicates it is close in proximity to the peroxide α-CH. 1D Selective Gradient COSY at a frequency of 4.47 ppm confirmed the peroxide β-CH to be at 1.81 ppm. The *R*-configuration was assigned based on the anti-Felkin–Ahn model (the A-value for R was assumed to be greater than the A-value for Me) for the capture of the Criegee intermediate by MeOH-d_4.

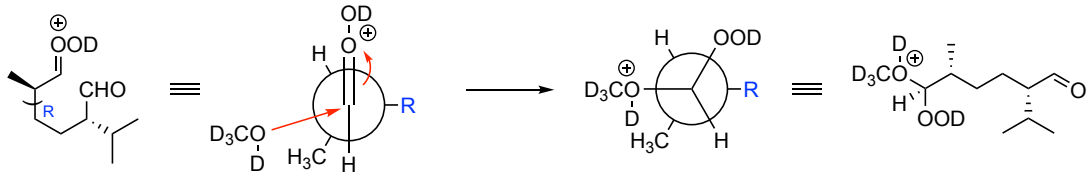


Figure 6.16 Felkin–Ahn Analysis for **32a*R***

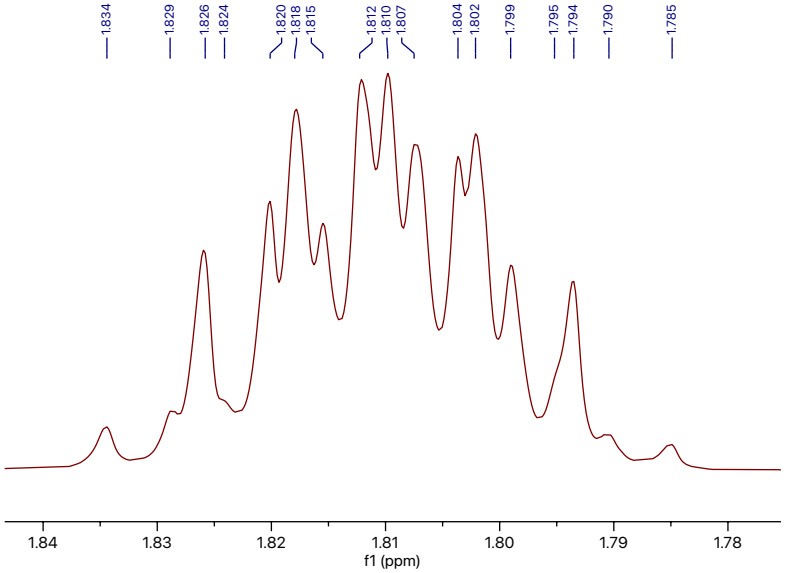
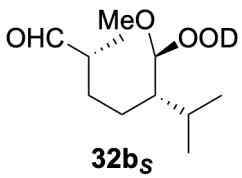


Figure 6.17 **1D Gradient Selective TOCSY** (800 MHz, 10:1 $CDCl_3$:CD_3OD) signal for the peroxide β-CH of Compound (**B*R***)



32b$_S$

(2*R*,5*S*)-5-((*S*)-Deuteroperoxy(methoxy-d_3)methyl)-2,6-dimethylheptanal (**32b$_S$**)

^{1}H NMR (800 MHz, 10:1 $CDCl_3$:CD_3OD) δ 9.58 (d, *J* = 2.0 Hz, 1H), 4.64 (d, *J* = 5.4 Hz, 1H), 2.35–2.18 (m, 1H), 1.97–1.70 (m, 2H), 1.52 (dtd, *J* = 6.1, 5.8, 4.4 Hz, 1H), 1.36–1.23 (m, 3H), 1.06 (d, *J* = 7.0 Hz, 3H), 0.88 (d, *J* = 6.9 Hz, 3H), 0.85 (d, *J* = 6.2 Hz, 3H).

1D Selective Gradient TOCSY at a frequency of 4.64 ppm revealed the spin-system for the peroxide α-CH and the splitting pattern (dtd) of the peroxide β-CH at 1.52 ppm. It also strongly showed the two γ-methyls of the *iso*-propyl group which indicates those signals are close to the peroxide α-CH. 1D Selective Gradient COSY at a frequency of 4.64 ppm confirmed the peroxide β-CH to be at 1.52 ppm. The *S*-configuration was assigned based on the anti-Felkin–Ahn model (the A-value for R was assumed to be smaller than the A-value for *i*Pr) for the capture of the Criegee intermediate by MeOH-d_4.

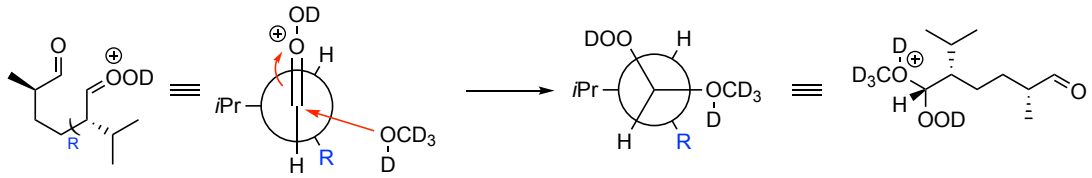


Figure 6.18 Felkin–Ahn Analysis for **32b*S***

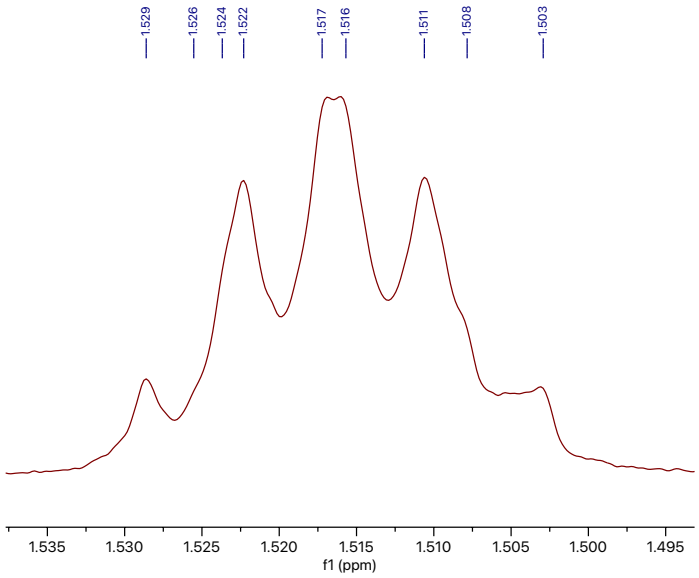
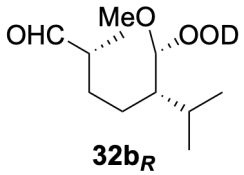


Figure 6.19 **1D Gradient Selective TOCSY** (800 MHz, 10:1 $CDCl_3$:CD_3OD) signal for the peroxide β-CH of Compound (**32b*S***)



32b$_R$

(2*R*,5*S*)-5-((*R*)-Deuteroperoxy(methoxy-d_3)methyl)-2,6-dimethylheptanal (**32b$_R$**)

^{1}H NMR (800 MHz, 10:1 $CDCl_3$:CD_3OD) δ 9.57 (d, *J* = 2.0 Hz, 1H), 4.67 (d, *J* = 6.8 Hz, 1H), 2.46–2.27 (m, 1H), 2.01–1.82 (m, 2H), 1.56 (dtd, *J* = 6.8, 5.4, 3.9 Hz, 1H), 1.46–1.30 (m, 3H), 1.14 (d, *J* = 7.0 Hz, 3H), 0.95 (d, *J* = 7.0 Hz, 3H), 0.90 (d, *J* = 6.9 Hz, 3H).

1D Selective Gradient TOCSY at a frequency of 4.67 ppm revealed the spin-system for the peroxide α-CH and the splitting pattern (dtd) of the peroxide β-CH at 1.56 ppm. It also strongly showed the two γ-methyls of the *iso*-propyl group which indicates those signals are close to the peroxide α-CH. 1D Selective Gradient COSY at a frequency of 4.67 ppm confirmed the peroxide β-CH to be at 1.56 ppm. The *R*-configuration was assigned based on the Felkin–Ahn model (the A-value for R was assumed to be smaller than the A-value for *i*Pr) for the capture of the Criegee intermediate by MeOH-d_4.

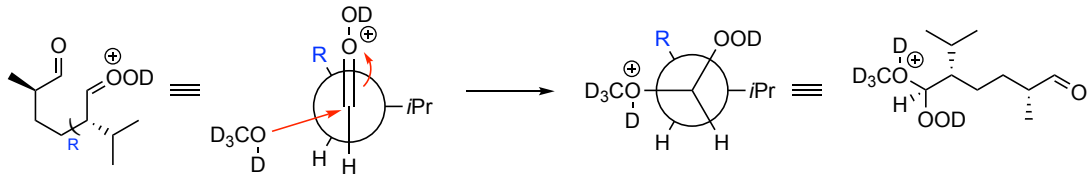


Figure 6.20 Felkin–Ahn Analysis for **32b*R***

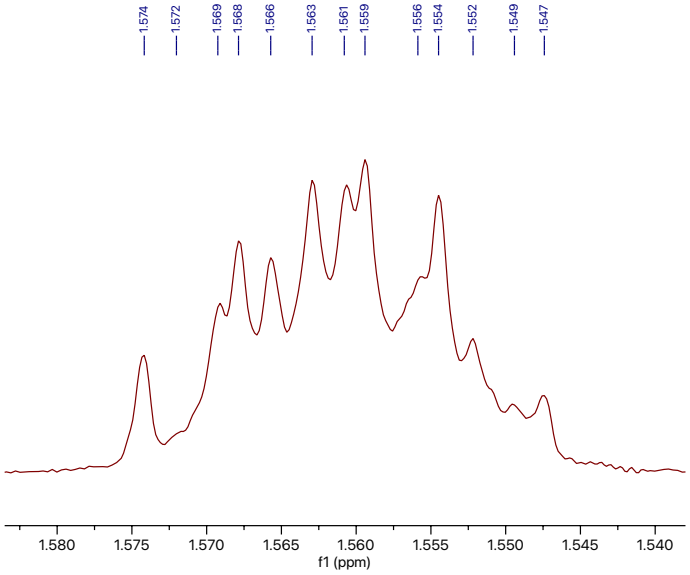


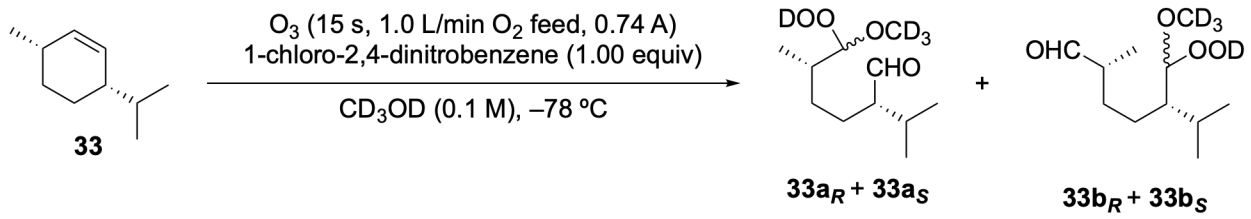
Figure 6.21 **1D Gradient Selective TOCSY** (800 MHz, 10:1 $CDCl_3$:CD_3OD) signal for the peroxide β-CH of Compound (**32b*R***)

Table 6.32 (+)-*trans*-p-menth-2-ene (**32**) qNMR Data

Trial	**%conversion**	**OOH a-CH %(32a$_R$+32a$_S$)**	**OOH a-CH %(32b$_R$+32b$_S$)**	**%CHO**
1	58.5	43	12	54
2	59.5	44	12	56
3	58.5	43	13	56
average	59	43	12	55
St. Dev.	0.58	0.58	0.58	1.2

Diastereomeric Ratios: (+)-*trans*-p-menth-2-ene (**32**)

Trial	**%32a$_R$**	**%32a$_S$**	**%32b$_S$**	**%32b$_R$**
1	21	22	4.0	8.0
2	22	22	4.0	8.0
3	21	22	4.0	9.0
average	21	22	4.0	8.3
St. Dev.	0.58	0.00	0.00	0.58

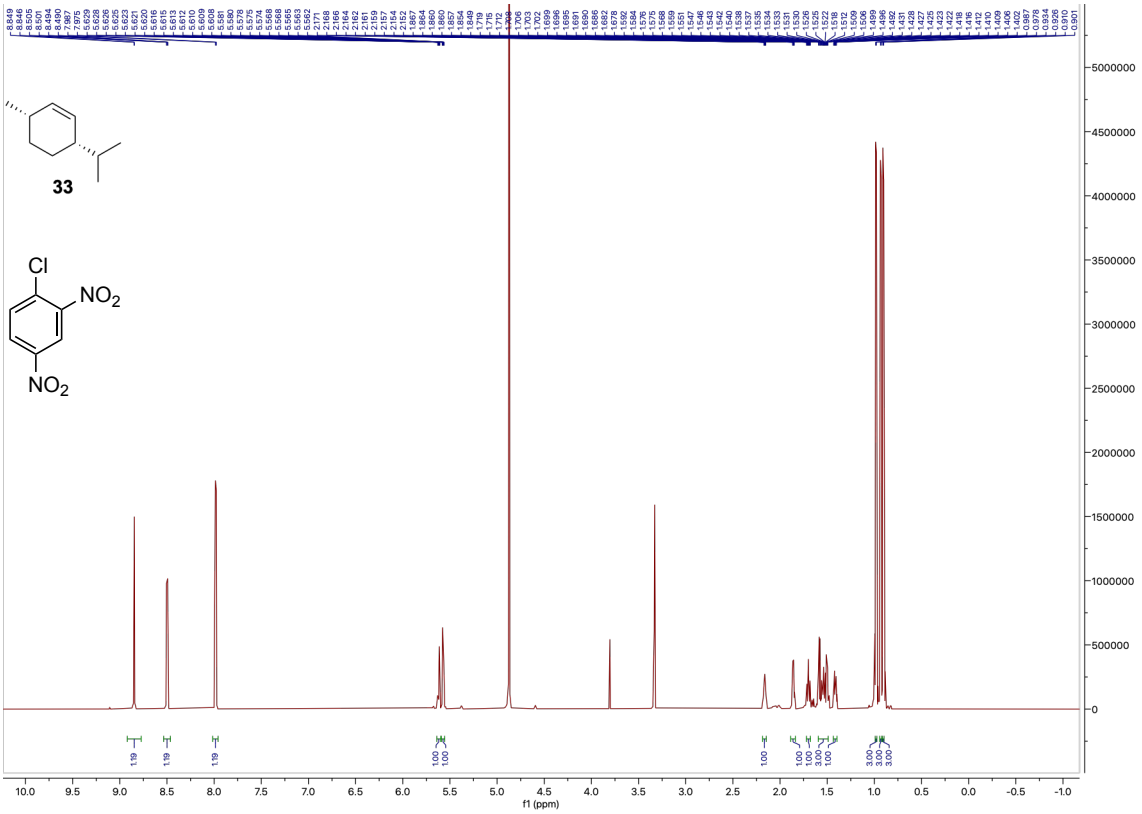


(–)-*cis*-p-menth-2-ene (**33**)

Reaction Time: 15 seconds

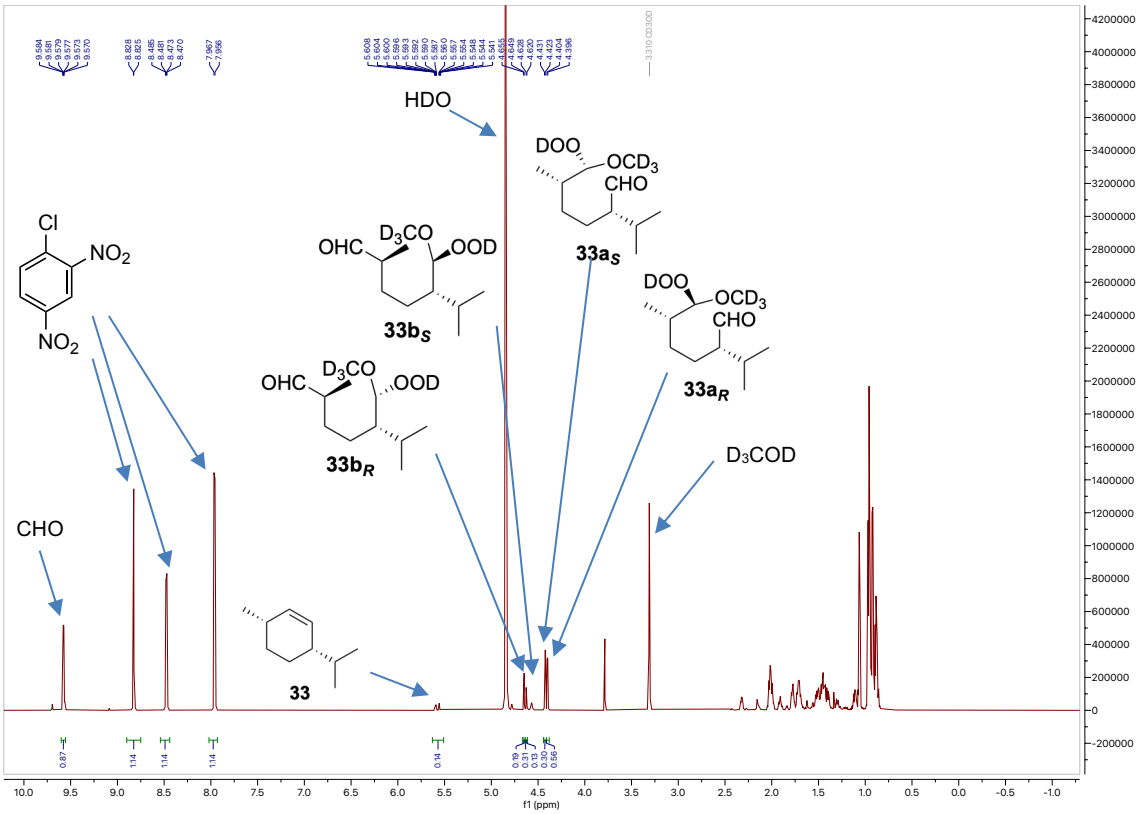
Alkene-to-IS Ratio: 1.00:1.19

Blank Sample: (+)-*trans*-p-menth-2-ene (**32**) and 1-chloro-2,4-dinitrobenzene (**IS**)



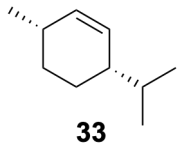
^{1}H NMR (800 MHz, CD_3OD), D1 = 10 s, 32 scans

Representative ^{1}H NMR: (–)-*cis*-p-menth-2-ene (**33**) ozonolysis



^{1}H NMR (800 MHz, CD_3OD), D1 = 10 s, 32 scans

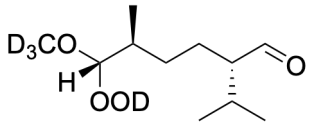
Characterization Data: (–)-*cis*-p-menth-2-ene (**33**)



33

(–)-*cis*-p-menth-2-ene (**33**)

^{1}H NMR (800 MHz, MeOD) δ 5.62 (dddd, *J* = 10.2, 3.6, 2.3, 0.8 Hz, 1H), 5.60 – 5.55 (m, 1H), 2.16 (ddtdd, *J* = 11.2, 7.3, 5.3, 3.4, 2.0 Hz, 1H), 1.86 (dtd, *J* = 8.2, 5.8, 2.5 Hz, 1H), 1.70 (dddd, *J* = 13.0, 10.6, 5.9, 3.4 Hz, 1H), 1.60 – 1.47 (m, 3H), 1.44 – 1.39 (m, 1H), 0.98 (d, *J* = 7.1 Hz, 3H), 0.93 (d, *J* = 6.8 Hz, 3H), 0.91 (d, *J* = 6.9 Hz, 3H).



33a$_S$

(2*S*,5*S*,6*S*)-6-Deuteroperoxy-2-isopropyl-6-(methoxy-d_3)-5-methylhexanal (**33a$_S$**)

^{1}H NMR (800 MHz, 10:1 $CDCl_3$:CD_3OD) δ 9.58 (d, *J* = 3.4 Hz, 1H), 4.40 (d, *J* = 6.5 Hz, 1H), 2.03 (ddt, *J* = 9.7, 6.6, 3.4 Hz, 1H), 1.81 (qtd, *J* = 9.0, 6.7, 3.8 Hz, 1H), 1.75–1.65 (m, 1H), 1.49–1.36 (m, 2H), 1.19–1.07 (m, 2H), 0.95 (d, *J* = 6.8 Hz, 3H), 0.92 (d, *J* = 6.9 Hz, 3H), 0.87 (d, *J* = 7.0 Hz, 3H).

1D Selective Gradient TOCSY at a frequency of 4.40 ppm revealed the spin-system for the peroxide α-CH and the splitting pattern (qtd) of the peroxide β-CH at 1.81 ppm. It also strongly showed the γ-methyl which indicates it is close in proximity to the peroxide α-CH. 1D Selective Gradient COSY at a frequency of 4.40 ppm confirmed the peroxide β-CH to be at 1.81 ppm. The *S*-configuration was assigned based on the Felkin–Ahn model (the A-value for R was assumed to be greater than the A-value for Me) for the capture of the Criegee intermediate by MeOH-d$_4$.

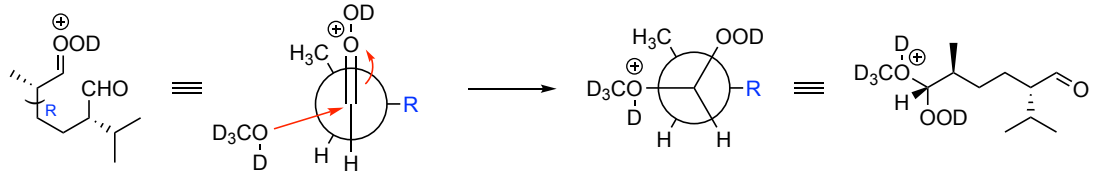


Figure 6.22 Felkin-Ahn Analysis of **33a$_S$**

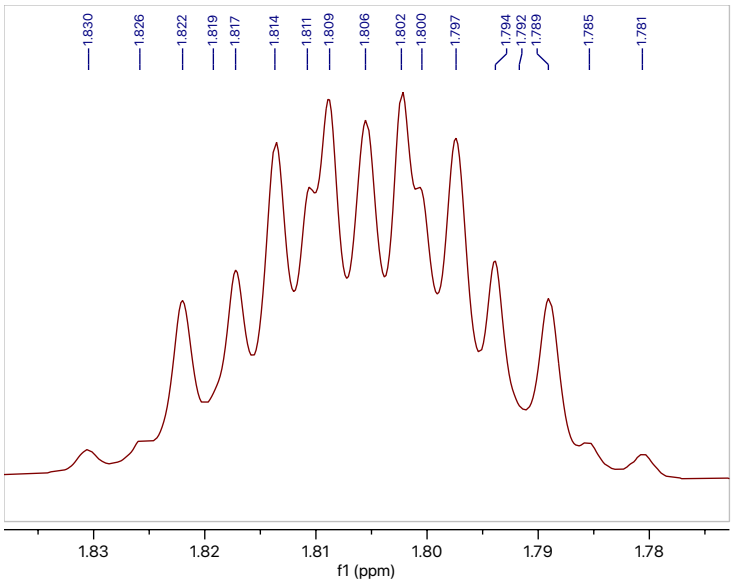
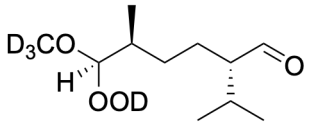


Figure 6.23 **1D Selective Gradient TOCSY** (800 MHz, 10:1 $CDCl_3$:CD_3OD) signal for the peroxide β-CH of Compound (**33a*S***)



33a$_R$

(2*S*,5*S*,6*R*)-6-Deuteroperoxy-2-isopropyl-6-(methoxy-d_3)-5-methylhexanal (**33a$_R$**)

^{1}H NMR (800 MHz, 10:1 $CDCl_3$:CD_3OD) δ 9.58 (d, *J* = 2.4 Hz, 1H), 4.43 (d, *J* = 4.4 Hz, 1H), 2.03 (ddd, *J* = 9.7, 6.6, 3.6 Hz, 1H), 1.79 (tqd, *J* = 7.5, 6.0, 4.1 Hz, 1H), 1.73–1.65 (m, 1H), 1.50–1.38 (m, 2H), 1.14–1.06 (m, 2H), 0.92 (dd, *J* = 6.9, 2.1 Hz, 3H), 0.90 (d, *J* = 3.0 Hz, 3H), 0.84 (d, *J* = 7.3 Hz, 3H).

1D Selective Gradient TOCSY at a frequency of 4.43 ppm revealed the spin-system for the peroxide α-CH and the splitting pattern (tqd) of the peroxide β-CH at 1.79 ppm. It also strongly showed the γ-methyl which indicates it is close in proximity to the peroxide α-CH. 1D Selective Gradient COSY at a frequency of 4.43 ppm confirmed the peroxide β-CH to be at 1.79 ppm. The *R*-configuration was assigned based on the anti-Felkin–Ahn model (the A-value for R was assumed to be greater than the A-value for Me) for the capture of the Criegee intermediate by MeOH-d_4.

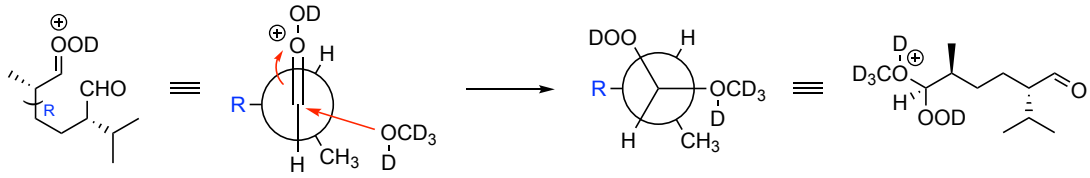


Figure 6.24 Felkin–Ahn Analysis of **33a$_R$**

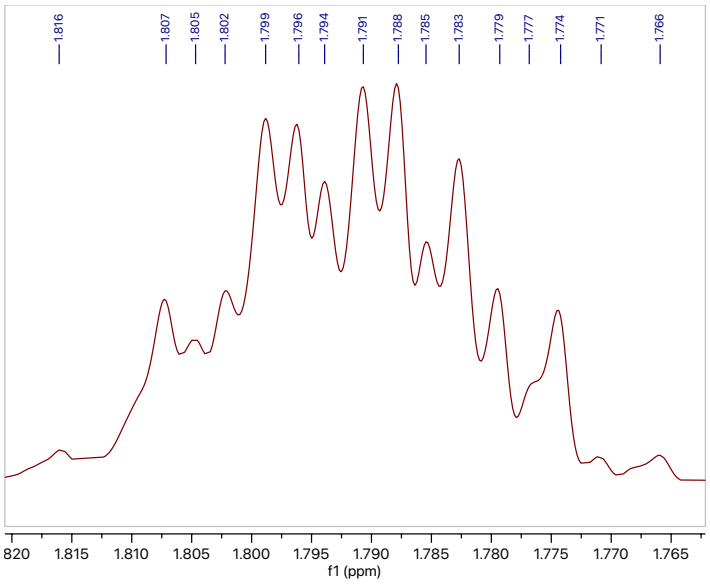
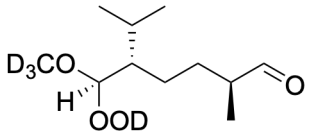


Figure 6.25 **1D Gradient Selective TOCSY** (800 MHz, 10:1 $CDCl_3$:CD_3OD) signal for the peroxide β-CH of Compound (**33a$_R$**)



33b$_S$

(2*S*,5*S*)-5-((*S*)-Deuteroperoxy(methoxy-d_3)methyl)-2,6-dimethylheptanal (**33b$_S$**)

^{1}H NMR (800 MHz, 10:1 $CDCl_3$:CD_3OD) δ 9.59 (d, *J* = 3.4 Hz, 1H), 4.62 (d, *J* = 6.8 Hz, 1H), 2.35 (qd, *J* = 6.8, 1.8 Hz, 1H), 1.93 (td, *J* = 6.9, 3.9 Hz, 1H), 1.79–1.65 (m, 1H), 1.61–1.49 (m, 2H), 1.48–1.34 (m, 1H), 1.35–1.25 (m, 1H), 1.10 (d, *J* = 6.9 Hz, 3H), 0.92 (d, *J* = 7.0 Hz, 3H), 0.87 (d, *J* = 6.9 Hz, 3H).

The β-CH to the peroxide α-CH was overlapped with another signal so 1D Selective Gradient COSY was used to identify the peroxide β-CH spin system instead of 1D Selective Gradient TOCSY. 1D Selective Gradient COSY was measured at a frequency of 4.62 ppm and revealed the peroxide β-CH to be at 1.53 ppm. It also indicated the spin-system to be a dtd (*J* = 7.2, 5.8, 4.6 Hz). 1D Selective Gradient TOCSY at a frequency of 4.62 ppm strongly showed the two γ-methyls of the *iso*-propyl group which indicates those signals are close to the peroxide α-CH. The *S*-configuration was assigned based on the anti-Felkin–Ahn model (the A-value for R was assumed to be smaller than the A-value for *i*Pr) for the capture of the Criegee intermediate by MeOH-d_4.

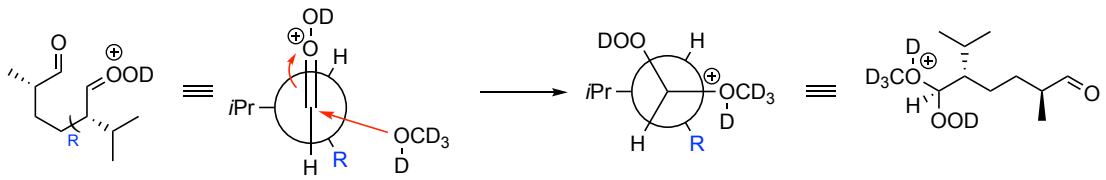


Figure 6.26 Felkin–Ahn Analysis of **33b$_S$**

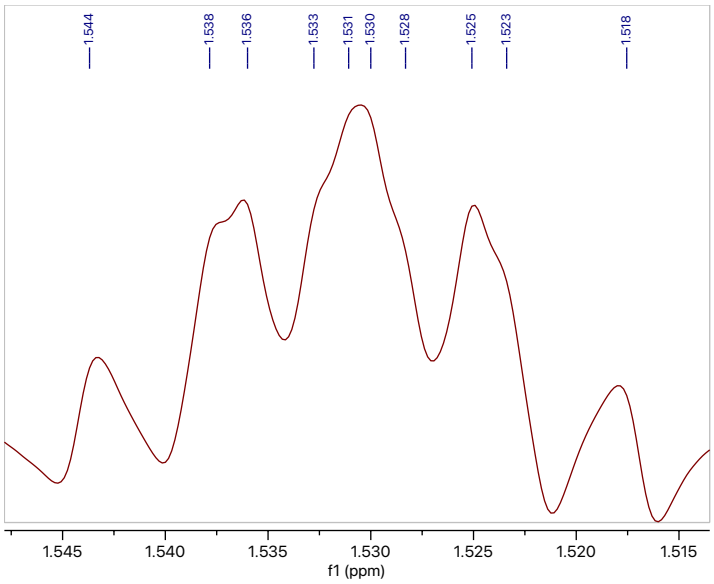
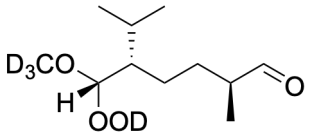


Figure 6.27 **1D Selective Gradient COSY** (800 MHz, 10:1 $CDCl_3$:CD_3OD) signal for the peroxide β-CH of Compound (**33b*s***)



33b$_R$

(2*S*,5*S*)-5-((*R*)-Deuteroperoxy(methoxy-d_3)methyl)-2,6-dimethylheptanal (**33b$_R$**)

^{1}H NMR (800 MHz, 10:1 $CDCl_3$:CD_3OD) δ 9.59 (d, *J* = 5.0 Hz, 1H), 4.65 (d, *J* = 5.4 Hz, 1H), 2.40–2.25 (m, 1H), 1.97–1.85 (m, 1H), 1.75–1.65 (m, 1H), 1.54 (ddt, *J* = 6.9, 5.6, 4.8 Hz, 1H), 1.52–1.47 (m, 1H), 1.39 (dddd, *J* = 13.9, 11.7, 6.8, 4.9 Hz, 1H), 1.33–1.19 (m, 1H), 1.07 (d, *J* = 7.0 Hz, 3H), 0.90 (d, *J* = 6.9 Hz, 3H), 0.87 (d, *J* = 7.0 Hz, 3H).

1D Selective Gradient TOCSY at a frequency of 4.65 ppm revealed the spin-system for the peroxide α-CH and the splitting pattern (ddt) of the peroxide β-CH at 1.54 ppm. It also strongly showed the two γ-methyls of the *iso*-propyl group which indicates those signals are close to the peroxide α-CH. 1D Selective Gradient COSY at a frequency of 4.65 ppm confirmed the peroxide β-CH to be at 1.54 ppm. The *R*-configuration was assigned based on the Felkin–Ahn model (the A-value for R was assumed to be greater than the A-value for *i*Pr) for the capture of the Criegee intermediate by MeOH-d_4.

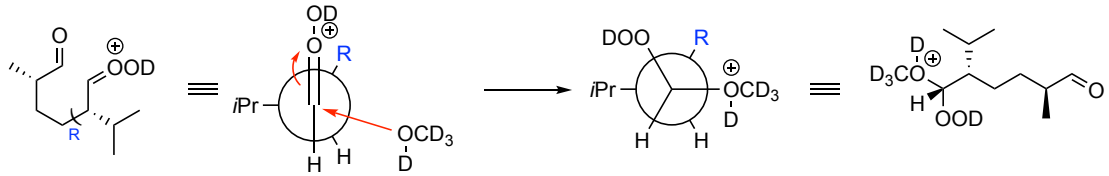


Figure 6.28 Felkin–Ahn Analysis of **33b$_R$**

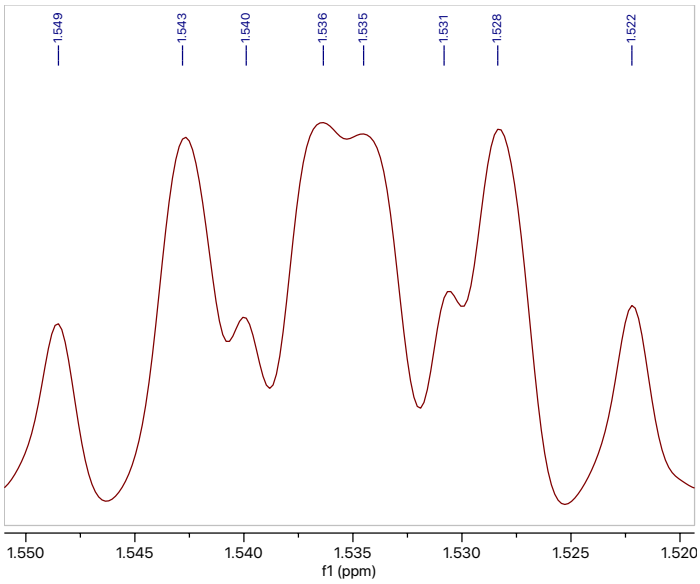


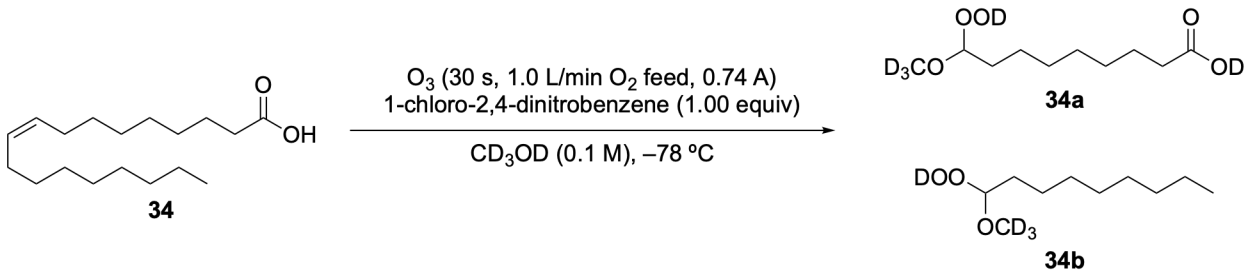
Figure 6.29 **1D Gradient Selective TOCSY** (800 MHz, 10:1 $CDCl_3$:CD_3OD) signal for the peroxide β-CH of Compound (**33b*R***)

Table 6.33 (–)-*cis*-p-menth-2-ene (**33**) qNMR Data

Trial	**%conversion**	**%(33a$_R$+33a$_S$)**	**%(33b$_R$+33b$_S$)**	**%CHO**
1	87	56	31	87
2	85	55	30	85
3	88	57	31	88
average	87	56	31	87
St. Dev.	1.5	1.0	0.57	1.5

Diastereomeric Ratios: (–)-*cis*-p-menth-2-ene (**33**)

Trial	**%33a$_R$**	**%33a$_S$**	**%33b$_S$**	**%33b$_R$**
1	26	30	12	19
2	25	30	12	18
3	26	31	12	19
average	26	30	12	19
St. Dev.	0.58	0.58	0.0	0.58

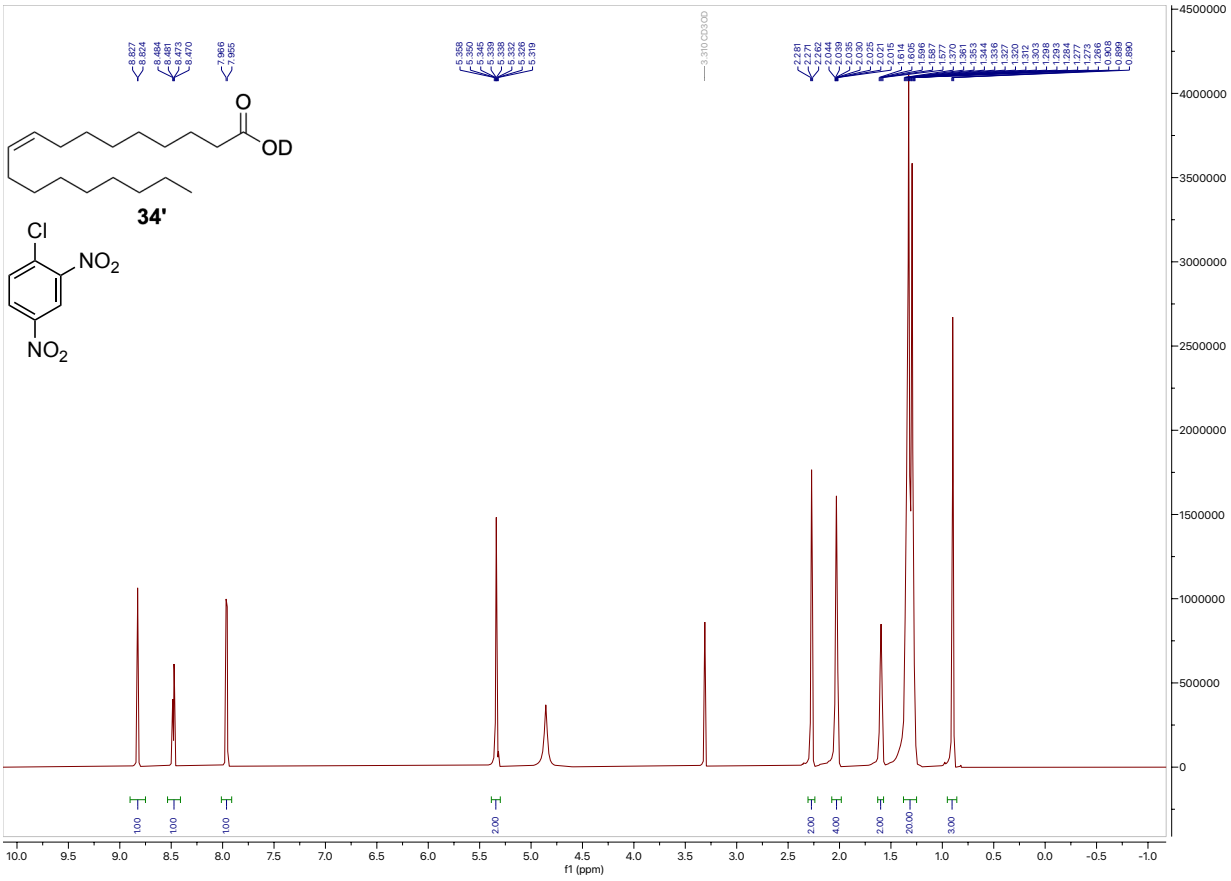


Oleic acid (**34**)

Reaction Time: 30 seconds

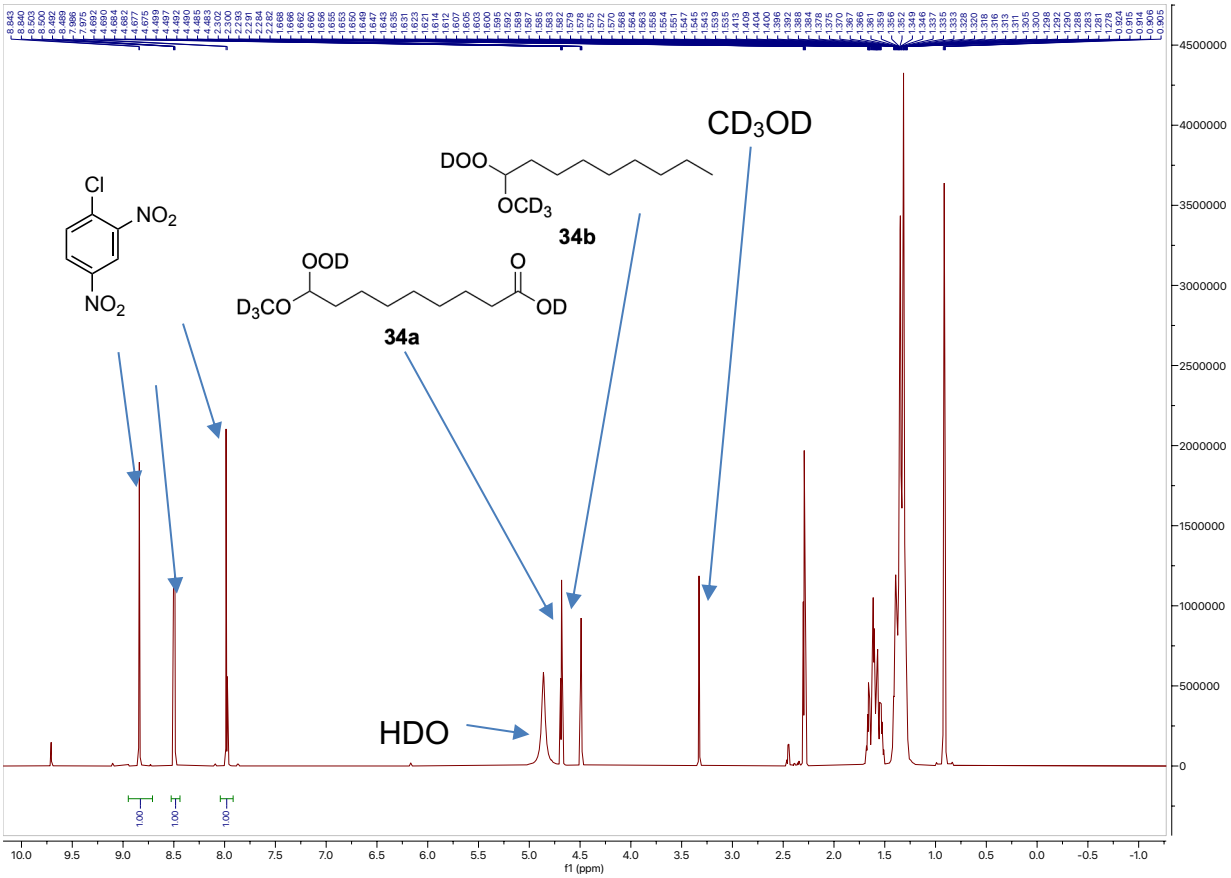
Alkene-to-IS Ratio: 1.00:1.00

Blank Sample: oleic acid-*d* (**34'**) and 1-chloro-2,4-dinitrobenzene (**IS**)



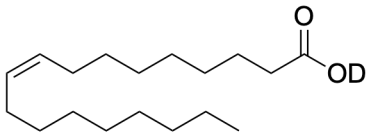
^{1}H NMR (800 MHz, CD_3OD), D1 = 10 s, 32 scans

Representative ^{1}H NMR: oleic acid (**34**) ozonolysis



^{1}H NMR (800 MHz, $CDCl_3$), D1 = 10 s, 32 scans

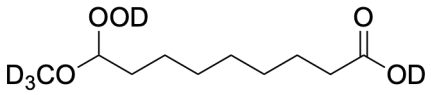
Characterization Data:



34'

Oleic acid-*d* (**34'**)

^{1}H NMR (800 MHz, MeOD) δ 5.57 – 5.13 (m, 2H), 2.27 (t, *J* = 7.5 Hz, 2H), 2.03 (dp, *J* = 7.8, 4.1 Hz, 4H), 1.60 (p, *J* = 7.4 Hz, 2H), 1.48 – 1.12 (m, 20H), 0.90 (t, *J* = 7.2 Hz, 3H).

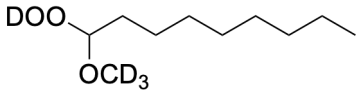


34a

9-deuteroperoxy-9-(methoxy-d_3)nonanoic acid-*d* (**34a**)

^{1}H NMR (800 MHz, MeOD) δ 4.68 (t, *J* = 5.8 Hz, 1H), 2.29 (t, *J* = 7.5 Hz, 2H), 1.73 – 1.48 (m, 4H), 1.45 – 1.22 (m, 8H).

The signals were measured and deduced from the ^{1}H NMR of the crude reaction mixture.



34b

1-deuteroperoxy-1-(methoxy-d_3)nonane (**34b**)

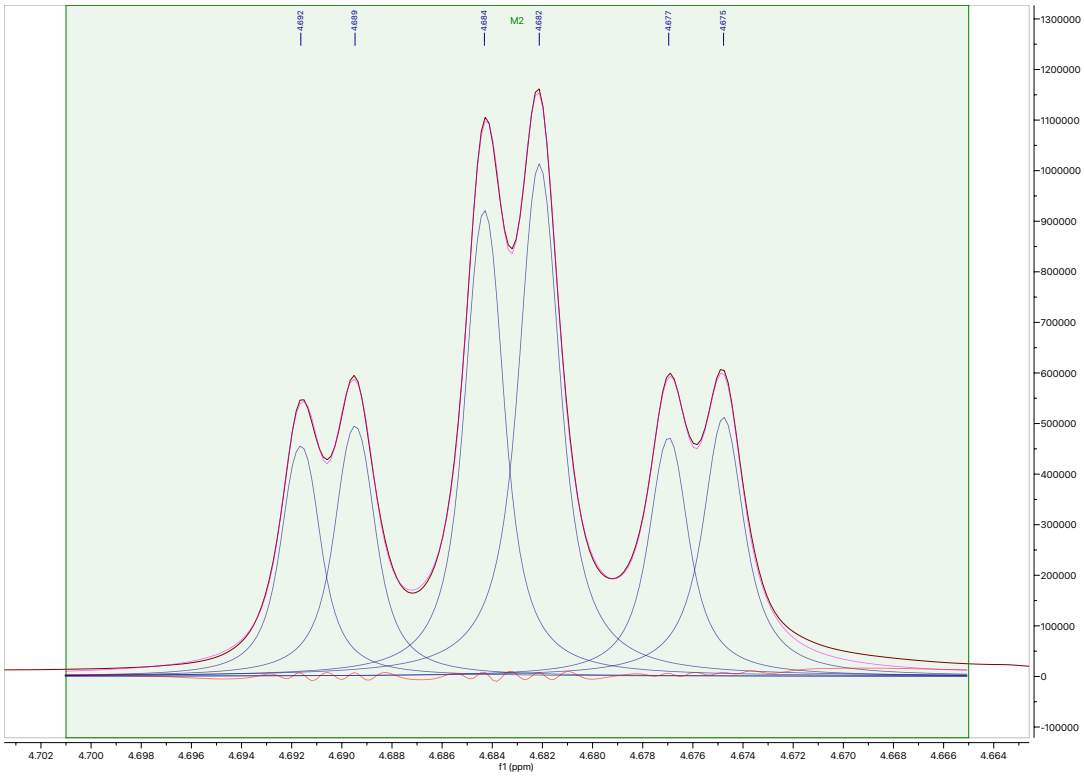
^{1}H NMR (800 MHz, MeOD) δ 4.68 (t, *J* = 5.8 Hz, 1H), 1.73 – 1.48 (m, 2H), 1.45 – 1.22 (m, 12H), 0.91 (t, *J* = 7.6 Hz, 3H).

The signals were measured and deduced from the ^{1}H NMR of the crude reaction mixture.

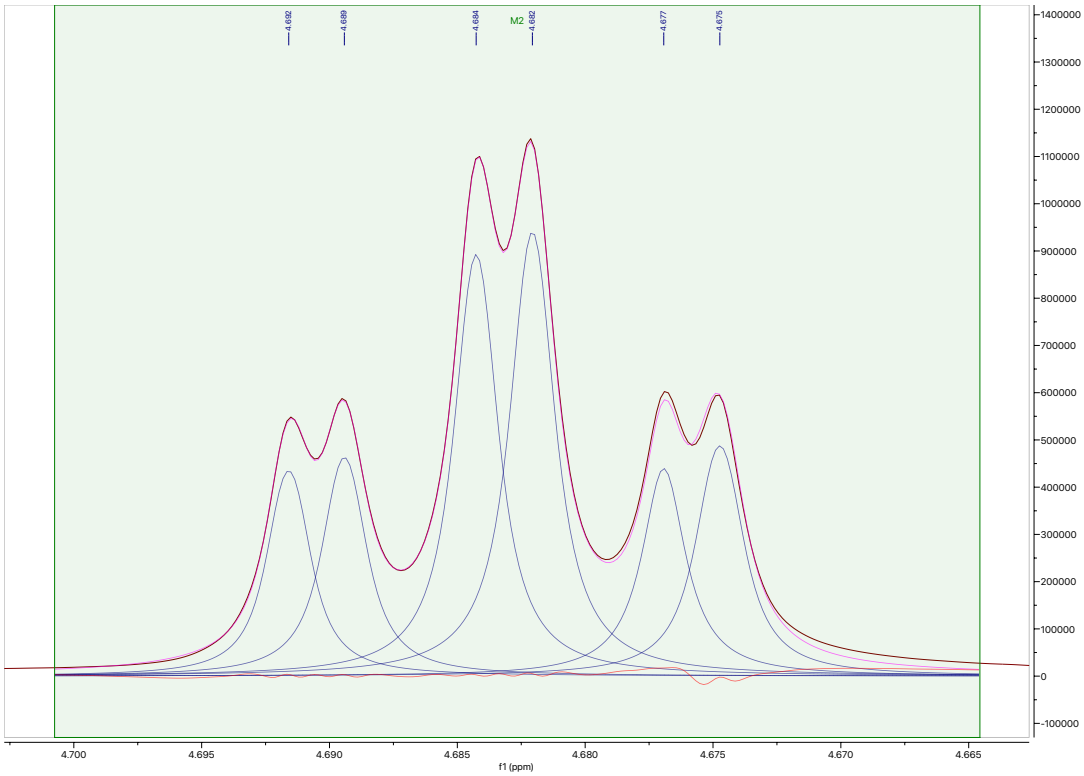
The overlapping region (4.665–4.701 ppm) was subjected to spectral deconvolution. Peak shapes were modeled using a generalized Lorentzian/Gaussian function, and the fit was iteratively optimized to minimize the residual error between the experimental spectrum and the calculated model. Spurious peaks were manually removed, and the final integration values were derived from the calculated peak areas. The chemical shift of **34a** was identified by Criegee ozonolysis of Ricinoleic acid (**35**) in methanol.

Table 6.34 oleic acid (**34**) qNMR Data

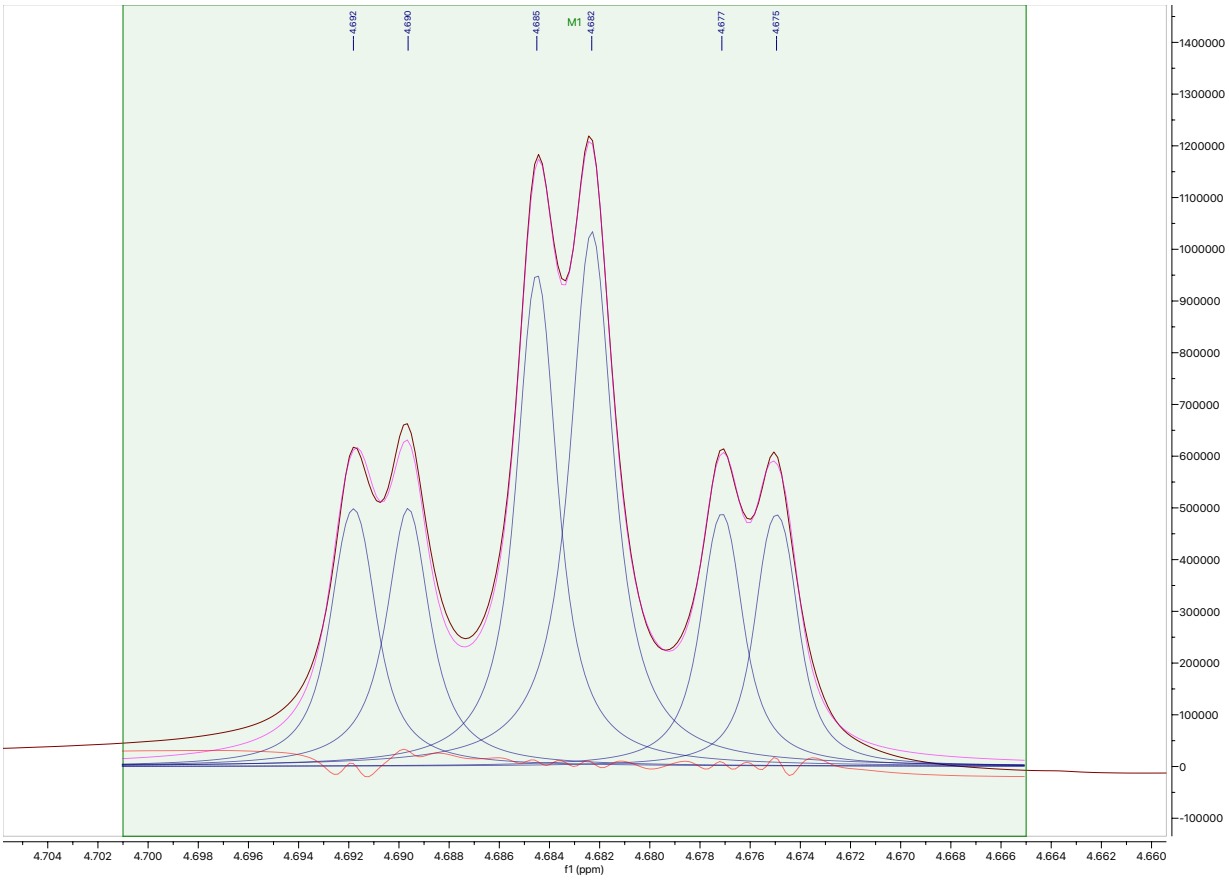
Trial	**34a**	**34b**	**residual error**
1	46.1	53.9	3.91×10^8
2	47.5	52.5	2.32×10^8
3	47.9	52.1	8.13×10^8
average	47.2	52.8	
st. dev.	0.944	0.944	



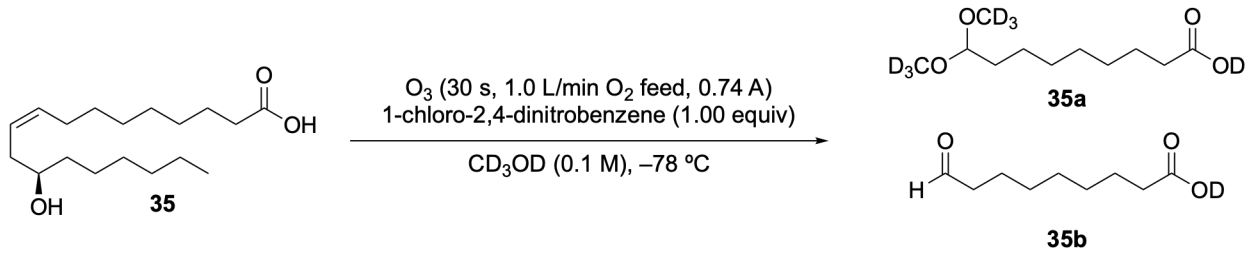
Trial 1 Line Fitting



Trial 2 Line Fitting



Trial 3 Line Fitting

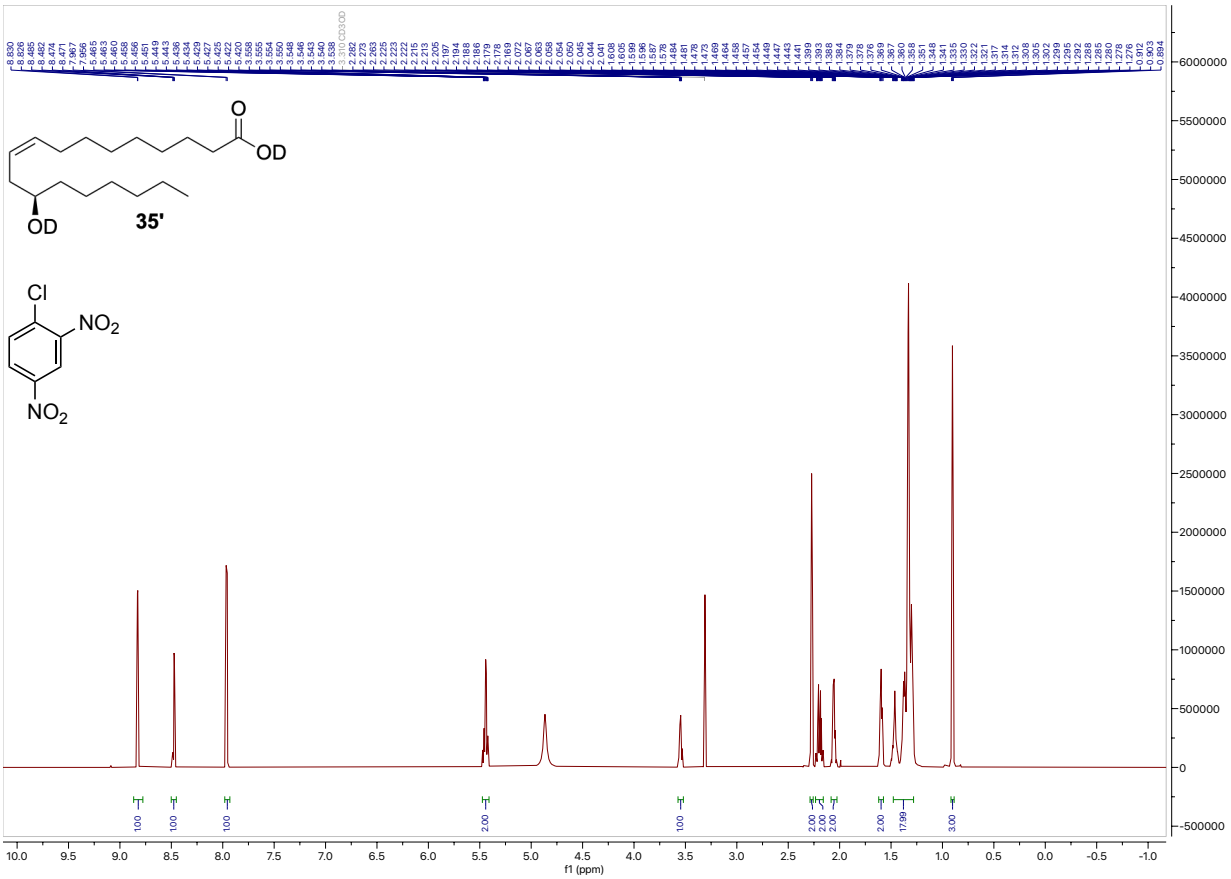


Ricinoleic acid (**35**)

Reaction Time: 30 seconds

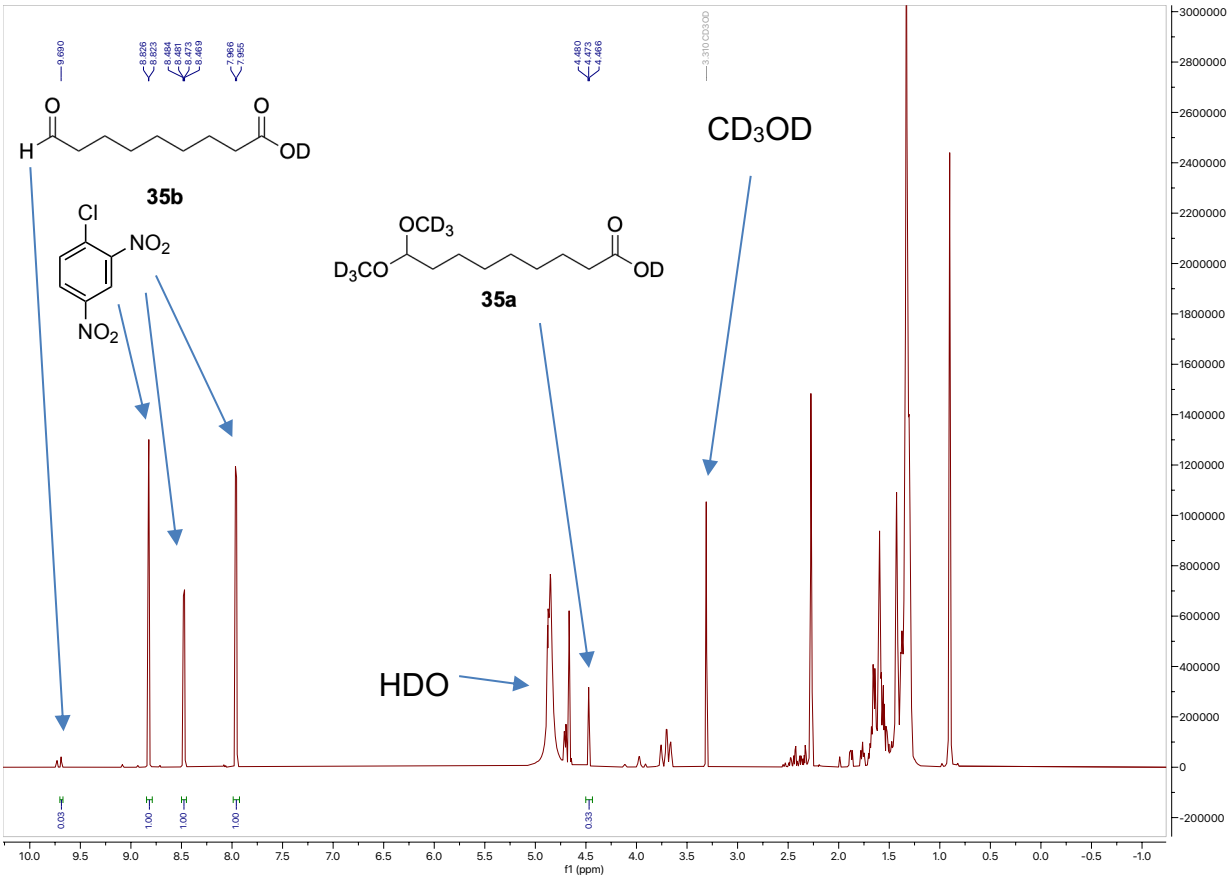
Alkene-to-IS Ratio: 1.00:1.00

Blank Sample: ricinoleic acid-d_2 (**34'**) and 1-chloro-2,4-dinitrobenzene (**IS**)



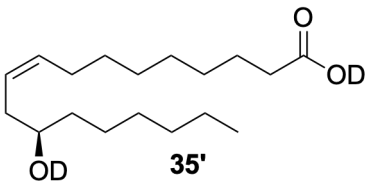
^{1}H NMR (800 MHz, CD_3OD)

Representative ^{1}H NMR: ricinoleic acid (**35**) ozonolysis



^{1}H NMR (800 MHz, $CDCl_3$), D1 = 10 s, 32 scans

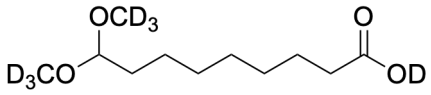
Characterization Data: ricinoleic acid (**35**)



35'

Ricinoleic acid-d_2 (**35'**)

^{1}H NMR (800 MHz, MeOD) δ 5.74 – 5.13 (m, 2H), 3.55 (dtd, *J* = 8.0, 6.2, 4.1 Hz, 1H), 2.27 (t, *J* = 7.5 Hz, 2H), 2.25 – 2.13 (m, 2H), 2.10 – 2.01 (m, 2H), 1.60 (dt, *J* = 9.5, 4.7 Hz, 2H), 1.52 – 1.24 (m, 18H), 0.90 (t, *J* = 7.2 Hz, 3H).

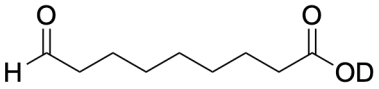


35a

9,9-bis(methoxy-d_3)nonanoic acid-*d* (**35a**)

^{1}H NMR (800 MHz, MeOD) δ 4.49 (t, *J* = 5.5 Hz, 1H), 2.29 (tt, *J* = 7.4, 1.8 Hz, 2H), 1.62 – 1.49 (m, 4H), 1.44 – 1.29 (m, 8H).

The signals were measured and deduced from the ^{1}H NMR of the crude reaction mixture.



35b

9-oxononanoic acid-*d* (**35b**)

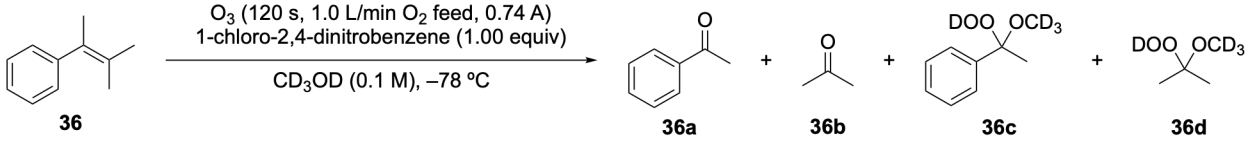
^{1}H NMR (800 MHz, MeOD) δ 9.71 (t, *J* = 1.8 Hz, 1H), 2.52 – 2.44 (m, 2H), 2.29 (tt, *J* = 7.4, 1.8 Hz, 2H), 1.74 – 1.22 (m, 10H).

The signals were measured and deduced from the ^{1}H NMR of the crude reaction mixture.

Table 6.35 ricinoleic acid (**35**) qNMR Data

Trial	**33a**	**33b**	**33a+33b**
1	39	4	43
2	33	3	36
3	33	3	36
average			38
st. dev.			4

6.8.4.7 *tetra*-Substituted Alkenes



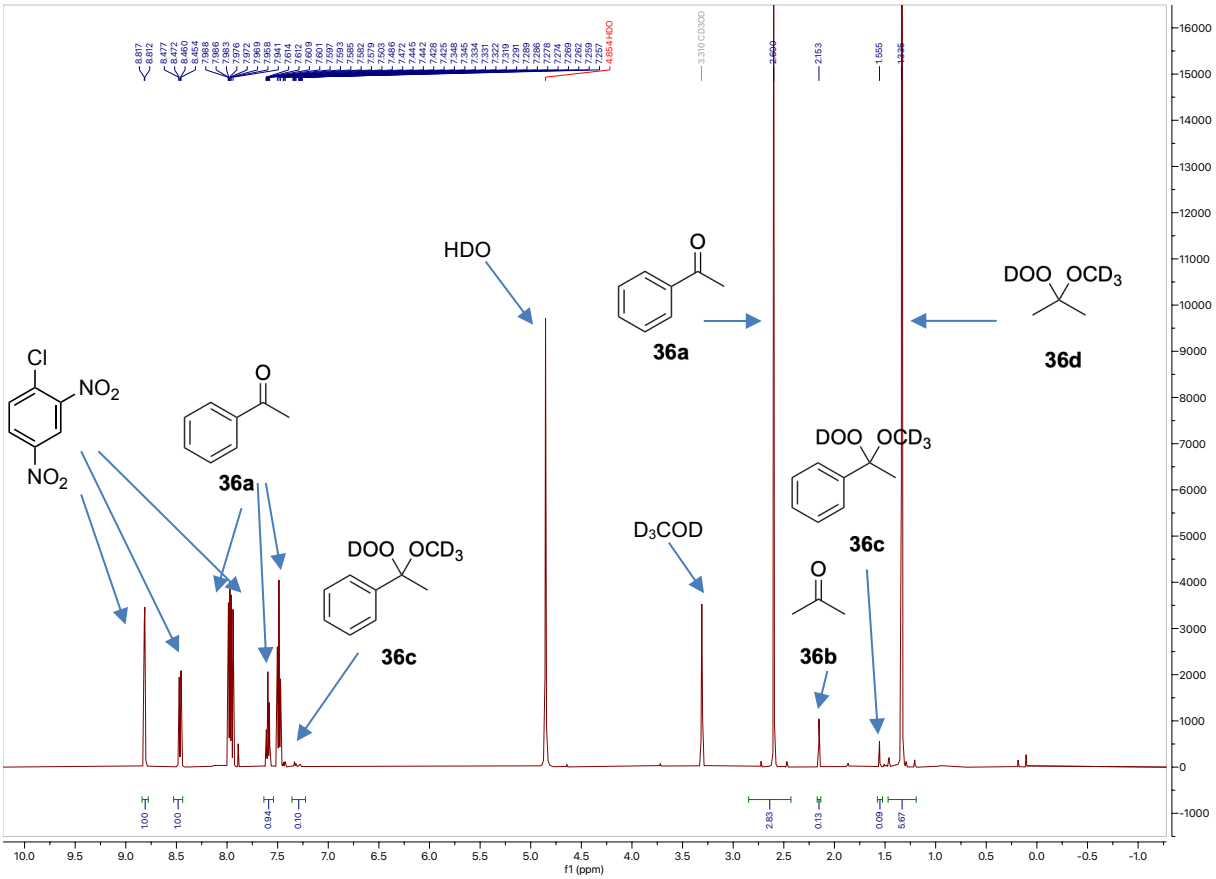
3-methyl-2-phenylbut-2-ene (**36**)

Reaction Time: 120 seconds

Three individual samples (0.333 mmol scale each) were prepared for 3-methyl-2-phenylbut-2-ene (**36**) using CD_3OD as the solvent.

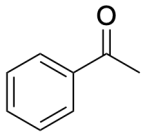
Alkene-to-IS Ratio: 1.00:1.00

Representative ^{1}H NMR: 3-methyl-2-phenylbut-2-ene (**36**) ozonolysis



^{1}H NMR (500 MHz, CD_3OD), D1 = 10 s, 32 scans

Characterization Data: 3-methyl-2-phenylbut-2-ene (**36**)



36a

acetophenone (**36a**)

^{1}H NMR (500 MHz, CD_3OD) δ 7.98 (dd, *J* = 8.5, 1.3 Hz, 2H), 7.60 (tt, *J* = 7.7, 1.3 Hz, 1H), 7.49 (t, *J* = 7.7 Hz, 2H), 2.60 (s, 3H) ppm.

The signals were measured and deduced from the ^{1}H NMR of the crude reaction mixture.

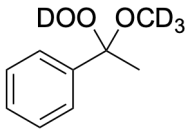


36b

acetone (**36b**)

^{1}H NMR (500 MHz, CD_3OD) δ 2.15 (s, 6H) ppm.

The signals were measured from the ^{1}H NMR of the crude reaction mixture.

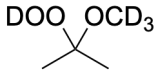


36c

(1-deuteroperoxy-1-(methoxy-d_3)ethyl)benzene (**36c**)

^{1}H NMR (500 MHz, CD_3OD) δ 7.44 (dd, *J* = 8.4, 1.4 Hz, 2H), 7.33 (td, *J* = 6.6, 1.6 Hz, 2H), 7.30 – 7.25 (tt, *J* = 7.5, 1.4 Hz, 1H), 1.55 (s, 3H).

The signals were measured and deduced from the ^{1}H NMR of the crude reaction mixture.



36d

2-deuteroperoxy-2-(methoxy-d_3)propane (**36d**)

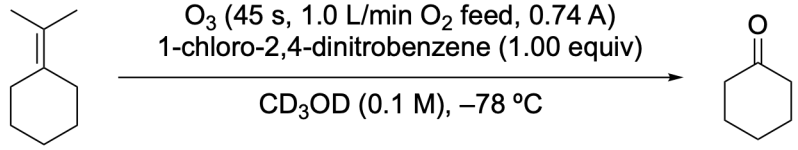
^{1}H NMR (500 MHz, CD_3OD) δ 1.34 (s, 6H) ppm.

The signals were measured from the ^{1}H NMR of the crude reaction mixture.

Table 6.36 3-methyl-2-phenylbut-2-ene (**36**) qNMR Data

Trial	%36a	%36b[1]	%36c	%36d
1	94.2	6.33	3.00	94.3
2	94.8	4.67	3.66	95.2
3	94.2	4.33	3.17	94.5
average	94.4	5.11	3.28	94.7
St. Dev.	0.346	1.07	0.343	0.473

[1]The acetone/dry ice bath may have contributed to the elevated acetone value.



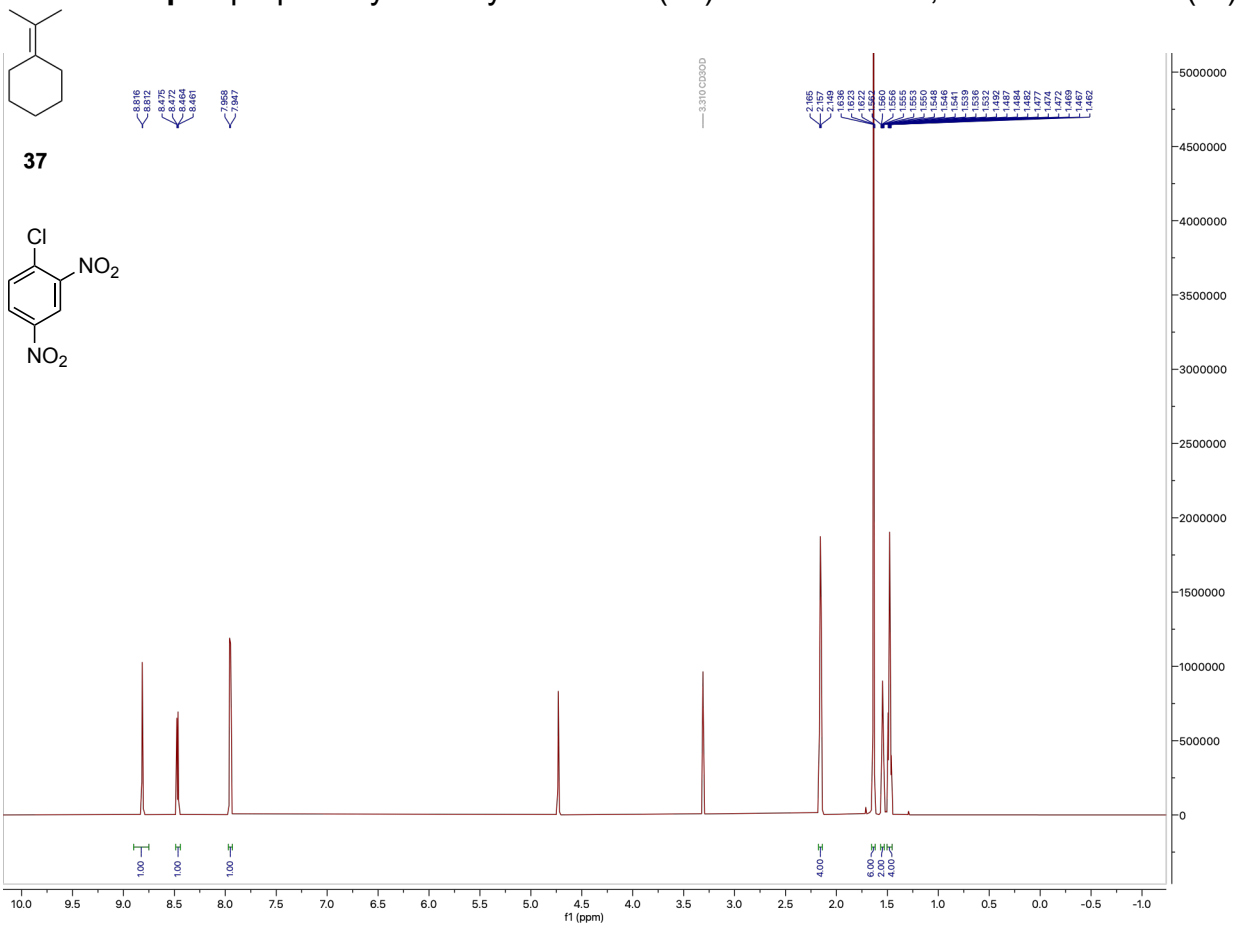
37 **37a**

propan-2-ylidenecyclohexane (**37**)

Reaction Time: 45 seconds

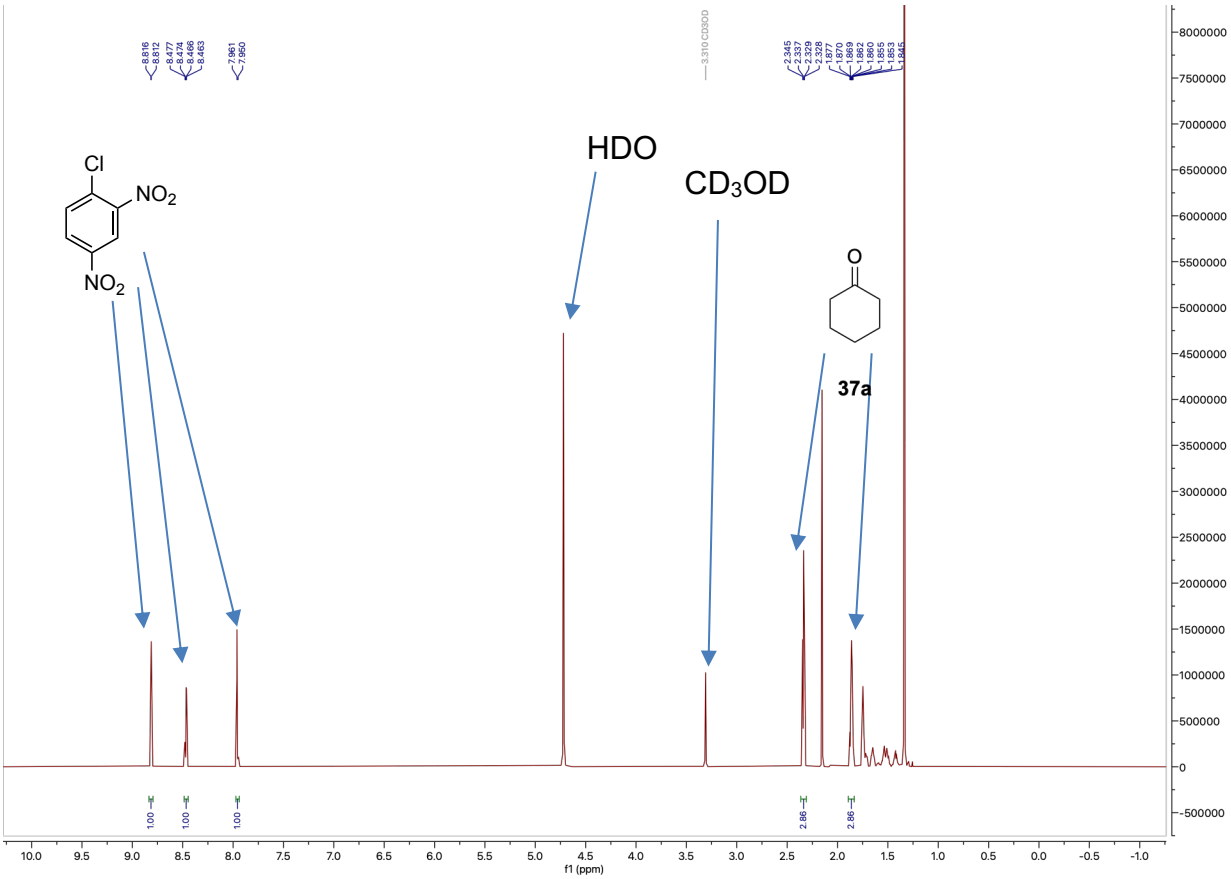
Alkene-to-IS Ratio: 1.00:1.00

Blank Sample: propan-2-ylidenecyclohexane (**37**) and 1-chloro-2,4-dinitrobenzene (**IS**)



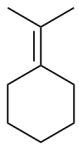
^{1}H NMR (800 MHz, CD_3OD)

Representative ^{1}H NMR: propan-2-ylidenecyclohexane (**37**) ozonolysis



^{1}H NMR (800 MHz, CD_3OD), D1 = 10 s, 32 scans

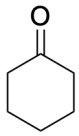
Characterization Data: propan-2-ylidenecyclohexane (**37**)



37

propan-2-ylidenecyclohexane (**37**)

^{1}H NMR (800 MHz, MeOD) δ 2.18 – 2.14 (m, 4H), 1.64 (s, 6H), 1.57 – 1.53 (m, 2H), 1.48 (tt, *J* = 8.1, 4.7 Hz, 4H).



37a

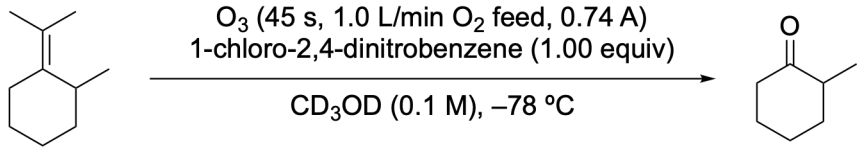
cyclohexanone (**37a**)

^{1}H NMR (800 MHz, MeOD) δ 2.45 – 2.21 (m, 4H), 1.97 – 1.84 (m, 4H), 1.81 – 1.72 (m, 2H).

The ketone α-CH_2 and β-CH_2 signals were measured from the ^{1}H NMR of the crude reaction mixture. The γ-CH_2 signal was deduced from the 1D selective gradient TOCSY spectrum.

Table 6.37 propan-2-ylidenecyclohexane (**37**) qNMR Data

Trial	**%37a**
1	72%
2	73%
3	72%
average	72%
st. dev.	0.58%



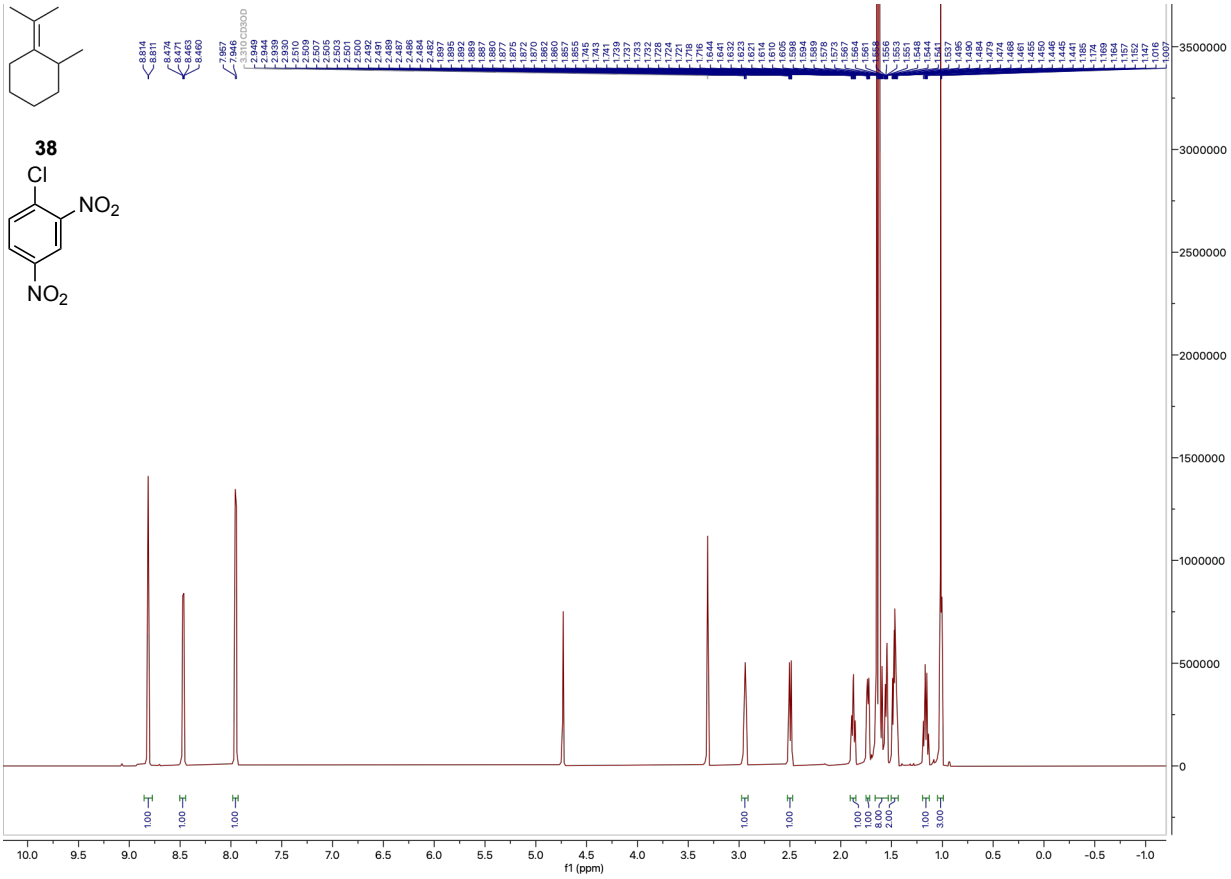
38 **38a**

1-methyl-2-(propan-2-ylidene)cyclohexane (**38**)

Reaction Time: 45 seconds

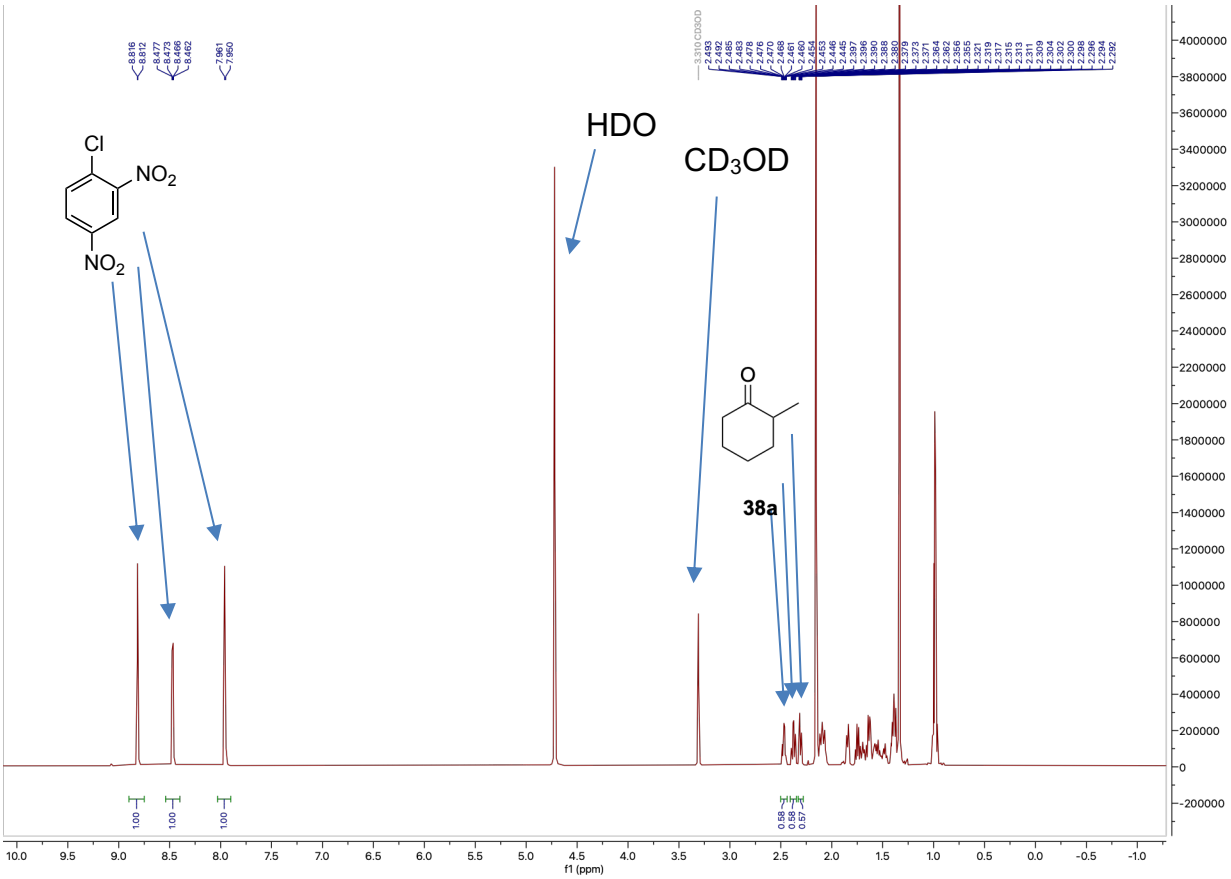
Alkene-to-IS Ratio: 1.00:1.00

Blank Sample: 1-methyl-2-(propan-2-ylidene)cyclohexane (**38**) and 1-chloro-2,4-dinitrobenzene (**IS**)



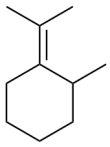
^{1}H NMR (800 MHz, CD_3OD), D1 = 10 s, 32 scans

Representative ^{1}H NMR: 1-methyl-2-(propan-2-ylidene)cyclohexane (**38**) ozonolysis



^{1}H NMR (800 MHz, CD_3OD), D1 = 10 s, 32 scans

Characterization Data: 1-methyl-2-(propan-2-ylidene)cyclohexane (**38**)

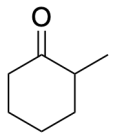


38

1-methyl-2-(propan-2-ylidene)cyclohexane (**38**)

^{1}H NMR (800 MHz, MeOD) δ 2.97 – 2.91 (m, 1H), 2.50 (dtt, *J* = 14.3, 3.1, 1.4 Hz, 1H), 1.87 (tdt, *J* = 13.9, 3.9, 1.8 Hz, 1H), 1.73 (dtd, *J* = 13.0, 3.8, 1.7 Hz, 1H), 1.64 (d, *J* = 2.2

Hz, 3H), 1.62 (d, *J* = 1.6 Hz, 3H), 1.67 – 1.53 (m, 2H), 1.50 – 1.43 (m, 2H), 1.16 (qt, *J* = 12.7, 3.9 Hz, 1H), 1.01 (d, *J* = 7.3 Hz, 3H).



38a

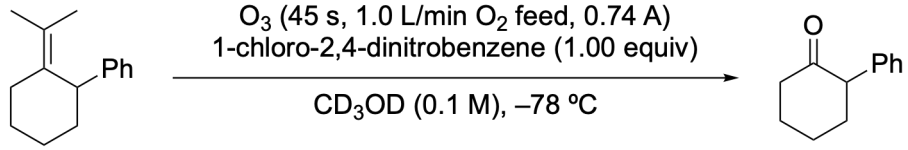
2-methylcyclohexanone (**38a**)

^{1}H NMR (800 MHz, MeOD) δ 2.47 (dddd, *J* = 12.2, 6.8, 5.5, 1.2 Hz, 1H), 2.38 (tdd, *J* = 13.0, 6.0, 1.4 Hz, 1H), 2.31 (ddq, *J* = 13.7, 4.5, 1.6 Hz, 1H), 2.16 – 2.05 (m, 2H), 1.86 (dtd, *J* = 13.5, 3.7, 1.7 Hz, 1H), 1.81 – 1.72 (m, 1H), 1.65 (qt, *J* = 13.3, 4.0 Hz, 1H), 1.47 – 1.30 (m, 1H), 1.00 (d, *J* = 6.6 Hz, 3H).

The ketone α-CH peaks were measured from the ^{1}H NMR of the crude reaction mixture. The remaining peaks were deduced from the 1D Selective Gradient TOCSY spectrum.

Table 6.38 1-methyl-2-(propan-2-ylidene)cyclohexane (**38**) qNMR Data

Trial	**38a**
1	58%
2	58%
3	57%
average	58%
st. dev.	5.8%



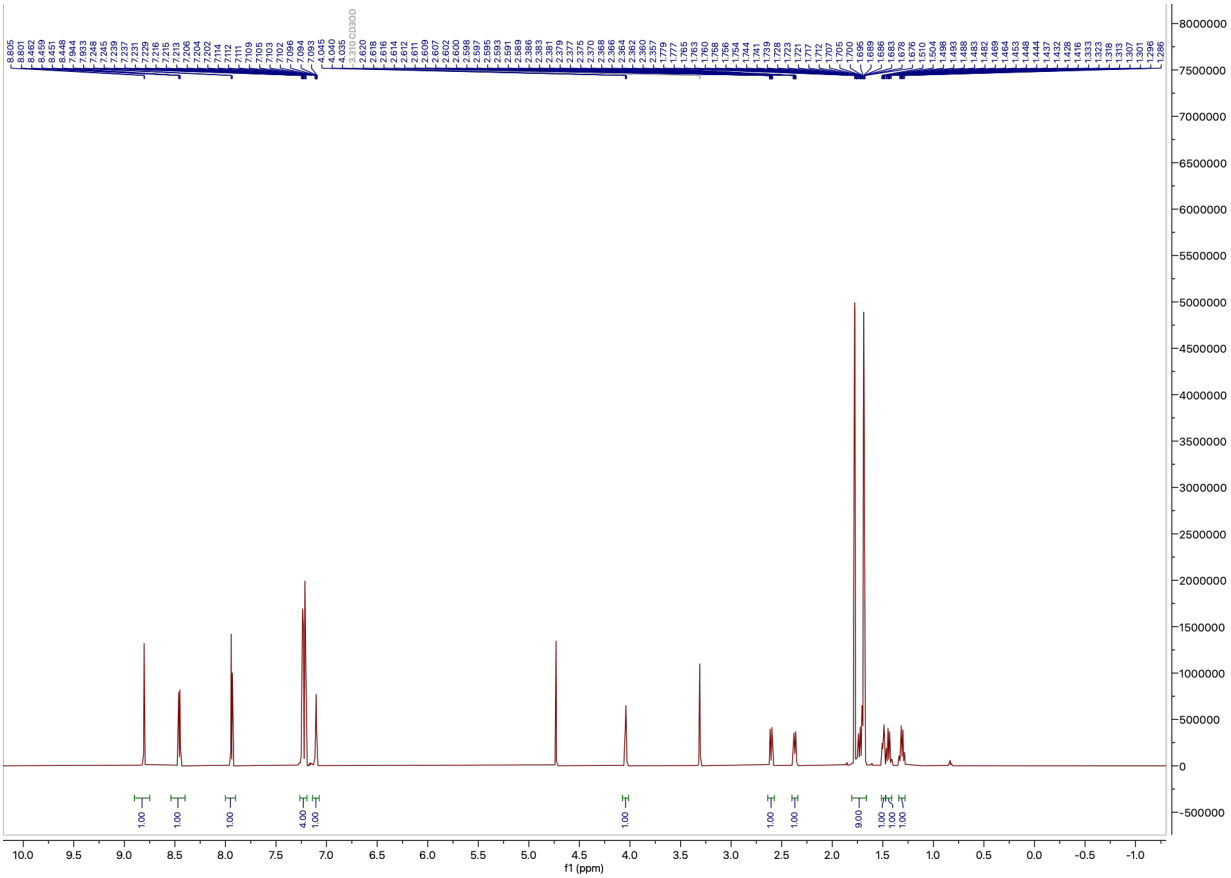
39 **39a**

(2-(propan-2-ylidene)cyclohexyl)benzene (**39**)

Reaction Time: 45 seconds

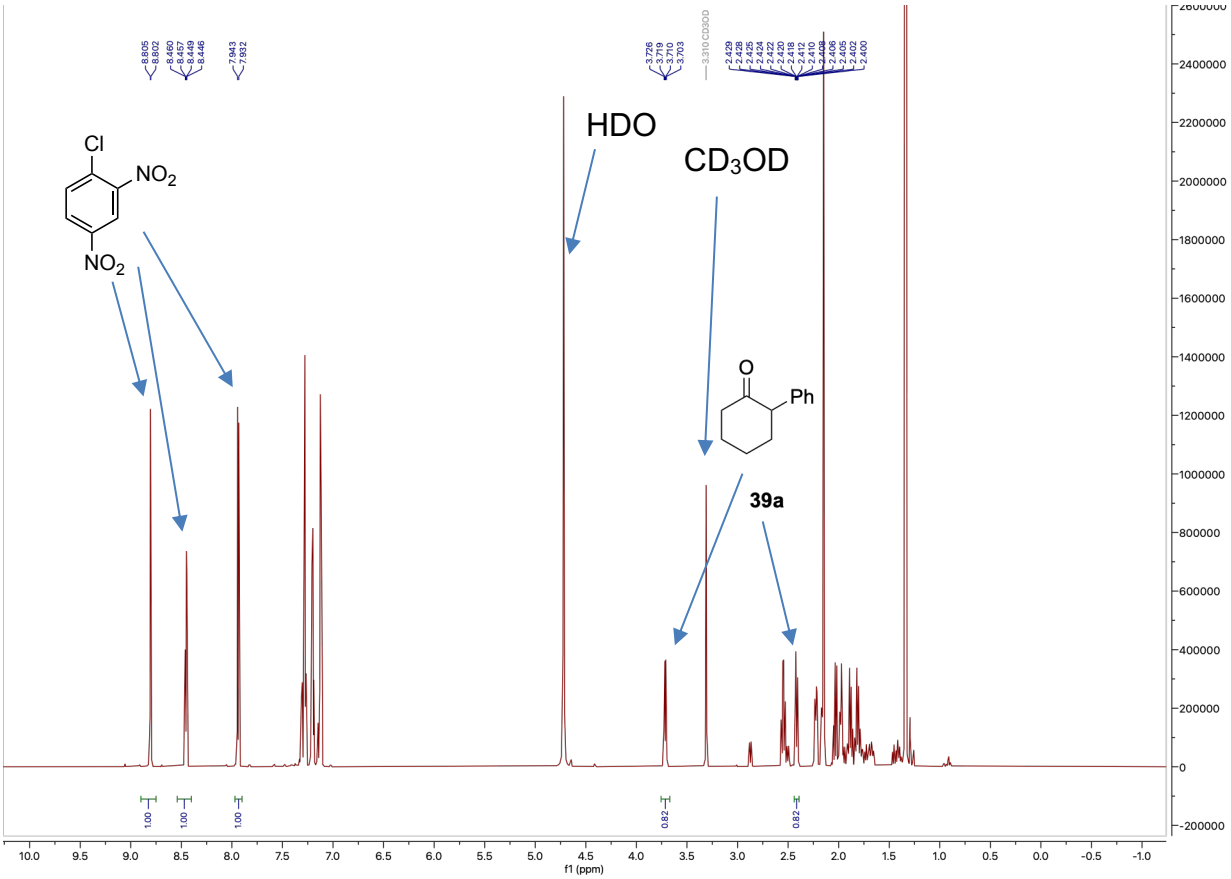
Alkene-to-IS Ratio: 1.00:1.00

Blank Sample: (2-(propan-2-ylidene)cyclohexyl)benzene (**39**) and 1-chloro-2,4-dinitrobenzene (**IS**)



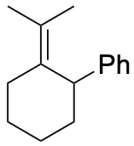
^{1}H NMR (800 MHz, CD_3OD), D1 = 10 s, 32 scans

Representative ^{1}H NMR: (2-(propan-2-ylidene)cyclohexyl)benzene (**39**) ozonolysis



^{1}H NMR (800 MHz, CD_3OD), D1 = 10 s, 32 scans

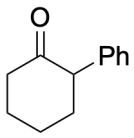
Characterization Data: (2-(propan-2-ylidene)cyclohexyl)benzene (**39**)



39

(2-(propan-2-ylidene)cyclohexyl)benzene (**39**)

^{1}H NMR (800 MHz, MeOD) δ 7.26 – 7.19 (m, 4H), 7.10 (tt, *J* = 7.3, 1.2 Hz, 1H), 4.07 – 4.01 (m, 1H), 2.60 (dtd, *J* = 14.0, 2.9, 1.5 Hz, 1H), 2.37 (ddt, *J* = 13.8, 3.3, 1.7 Hz, 1H), 1.81 – 1.66 (m, 9H), 1.51 – 1.47 (m, 1H), 1.44 (dddd, *J* = 16.9, 13.0, 8.5, 3.8 Hz, 1H), 1.31 (qt, *J* = 12.4, 4.2 Hz, 1H).



39a

2-phenylcyclohexanone (**39a**)

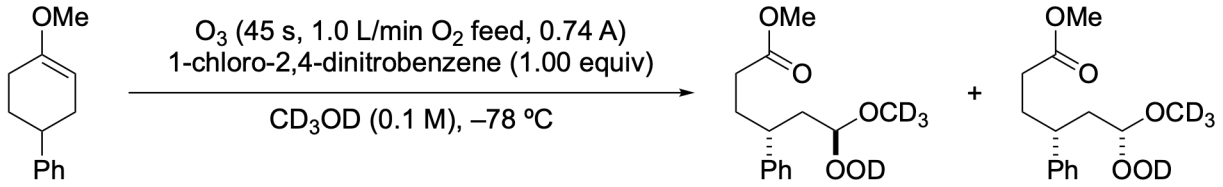
^{1}H NMR (800 MHz, MeOD) δ 7.28 (t, *J* = 7.7 Hz, 2H), 7.22 – 7.17 (m, 2H), 7.12 (dd, *J* = 8.2, 1.2 Hz, 1H), 3.73 (dd, *J* = 12.4, 5.6 Hz, 1H), 2.57 (td, *J* = 13.4, 6.0 Hz, 1H), 2.49 – 2.36 (m, 1H), 2.24 (ddt, *J* = 12.6, 6.3, 3.4 Hz, 1H), 2.18 (ddq, *J* = 13.0, 6.6, 3.3 Hz, 1H), 2.05 (qd, *J* = 12.6, 3.6 Hz, 1H), 2.02 – 1.97 (m, 1H), 1.90 (qt, *J* = 12.6, 3.7 Hz, 1H), 1.83 (qt, *J* = 12.9, 4.2 Hz, 1H).

The aromatic and benzylic CH peaks were measured from the ^{1}H NMR of the crude reaction mixture. The non-aromatic peaks were deduced from the 1D Selective Gradient TOCSY spectrum.

Table 6.39 (2-(propan-2-ylidene)cyclohexyl)benzene (**39**) qNMR Data

Trial	**39a**
1	82%
2	82%
3	82%
average	82%
st. dev.	0

6.8.4.8 Enol, Acyl, and Phosphoryl Ethers



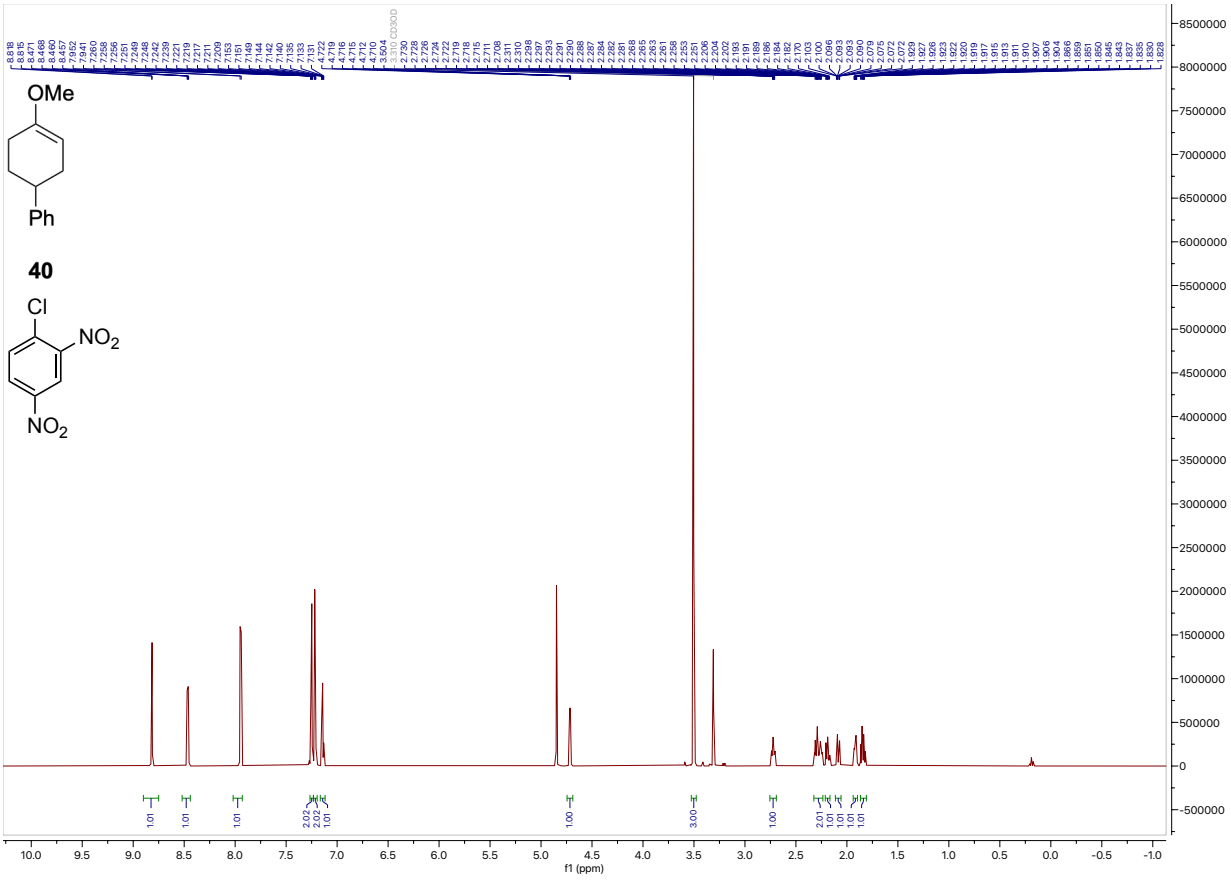
40 **40a$_{R*,S*}$** **40a$_{R*,R*}$**

4-methoxy-1,2,3,6-tetrahydro-1,1'-biphenyl (**40**)

Reaction Time: 45 seconds

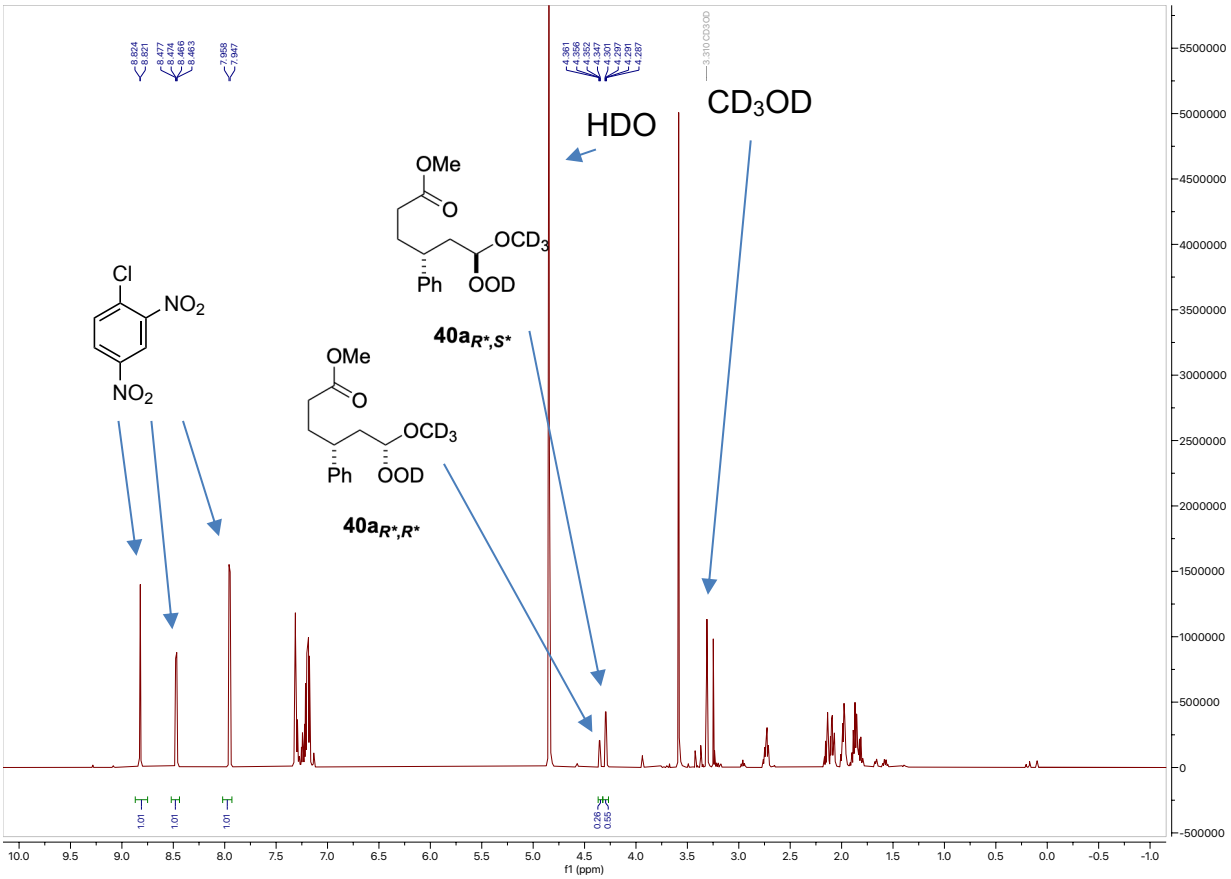
Alkene-to-IS Ratio: 0.99:1.00

Blank Sample: 4-methoxy-1,2,3,6-tetrahydro-1,1'-biphenyl (**40**) and 1-chloro-2,4-dinitrobenzene (**IS**)



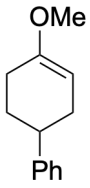
^{1}H NMR (800 MHz, CD_3OD)

Representative ^{1}H NMR: 4-methoxy-1,2,3,6-tetrahydro-1,1'-biphenyl (**40**) ozonolysis



^{1}H NMR (800 MHz, $CDCl_3$), D1 = 10 s, 32 scans

Characterization Data: 4-methoxy-1,2,3,6-tetrahydro-1,1'-biphenyl (**40**)

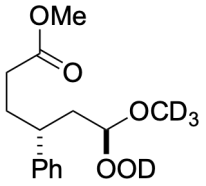


40

4-methoxy-1,2,3,6-tetrahydro-1,1'-biphenyl (**40**)

^{1}H NMR (800 MHz, MeOD) δ 7.28 – 7.23 (m, 2H), 7.22 (dd, *J* = 8.1, 1.6 Hz, 2H), 7.14 (tt, *J* = 6.8, 1.4 Hz, 1H), 4.71 (dt, *J* = 4.3, 2.2 Hz, 1H), 3.50 (s, 3H), 2.80 – 2.67 (m, 1H),

2.34 – 2.22 (m, 2H), 2.22 – 2.16 (m, 1H), 2.12 – 2.02 (m, 1H), 1.98 – 1.89 (m, 1H), 1.84 (dtd, *J* = 12.8, 11.5, 5.5 Hz, 1H).

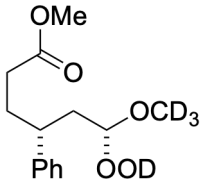


40a$_{R^*,S^*}$

methyl (4*R**,6*S**)-6-deuteroperoxy-6-(methoxy-d_3)-4-phenylhexanoate (**40a**$_{R^*,S^*}$)

^{1}H NMR (800 MHz, MeOD) δ 7.34 – 7.12 (m, 5H), 4.31 (dd, *J* = 8.2, 3.7 Hz, 1H), 3.58 (s, 3H), 2.74 (tt, *J* = 10.2, 5.1 Hz, 1H), 2.16 (ddd, *J* = 16.0, 8.8, 7.0 Hz, 1H), 2.11 (ddd, *J* = 16.0, 8.7, 5.7 Hz, 1H), 2.04 – 1.97 (m, 2H), 1.92 – 1.84 (m, 2H).

The peroxide α-CH peak, the aromatic region, and the ester methyl peak were measured from the ^{1}H NMR of the crude reaction mixture. The other peaks were deduced from the 1D selective gradient TOCSY spectrum.



40b$_{R^*,R^*}$

methyl (4*R**,6*R**)-6-deuteroperoxy-6-(methoxy-d_3)-4-phenylhexanoate (**40a**$_{R^*,R^*}$)

^{1}H NMR (800 MHz, MeOD) δ 7.34 – 7.12 (m, 5H), 4.37 (dd, *J* = 7.9, 4.1 Hz, 1H), 3.59 (s, 3H), 2.77 (tt, *J* = 10.2, 5.0 Hz, 1H), 2.20 – 2.07 (m, 3H), 2.00 (dddd, *J* = 13.9, 9.0, 7.0, 5.0 Hz, 1H), 1.90 – 1.80 (m, 2H).

The peroxide α-CH peak, the aromatic region, and the ester methyl peak were measured from the ^{1}H NMR of the crude reaction mixture. The other peaks were deduced from the 1D selective gradient TOCSY spectrum.

The configurations for the peroxides were assigned based on the modified Felkin–Ahn model (the A-value for R was assumed to be smaller than the A-value for Ph) for the capture of the Criegee intermediate by MeOH-d_4.

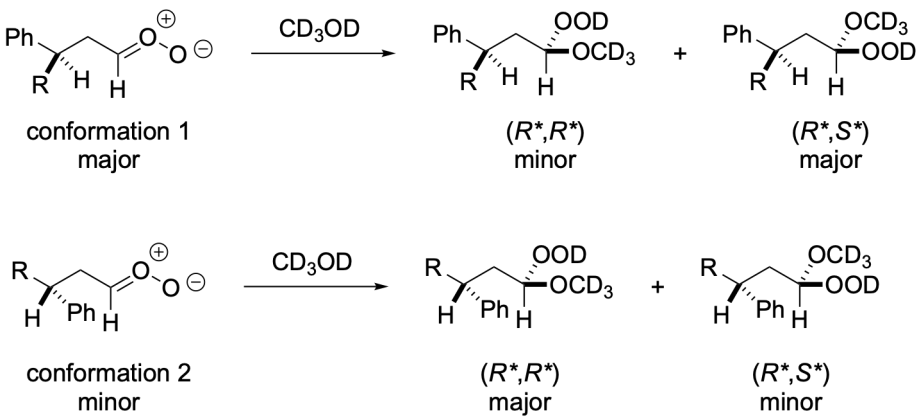
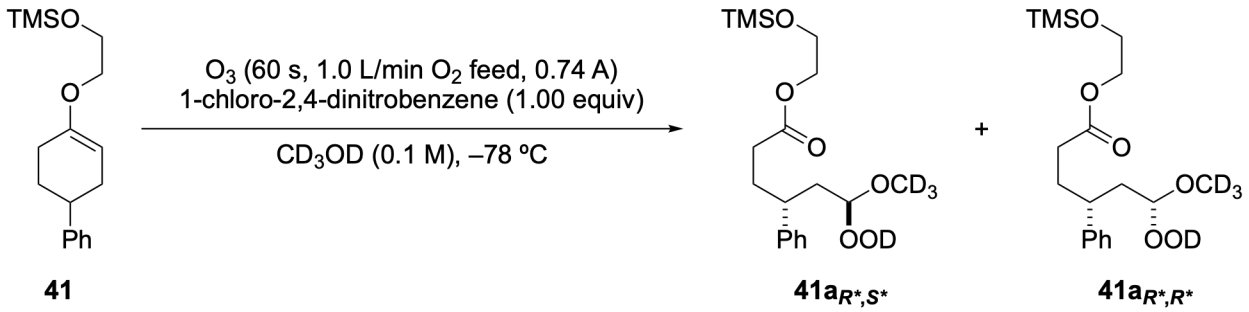


Figure 6.30 Felkin–Ahn Analysis for **40a**

Table 6.40 4-methoxy-1,2,3,6-tetrahydro-1,1'-biphenyl (**40**) qNMR Data

Trial	**40a**$_{R^*,R^*}$	**40a**$_{R^*,S^*}$	***d.r.***
1	27	56	1.0:2.1
2	26	55	1.0:2.1
3	29	53	1.0:1.8
average	27.3	54.7	1.0:2.0
st. dev.	1.53	1.53	

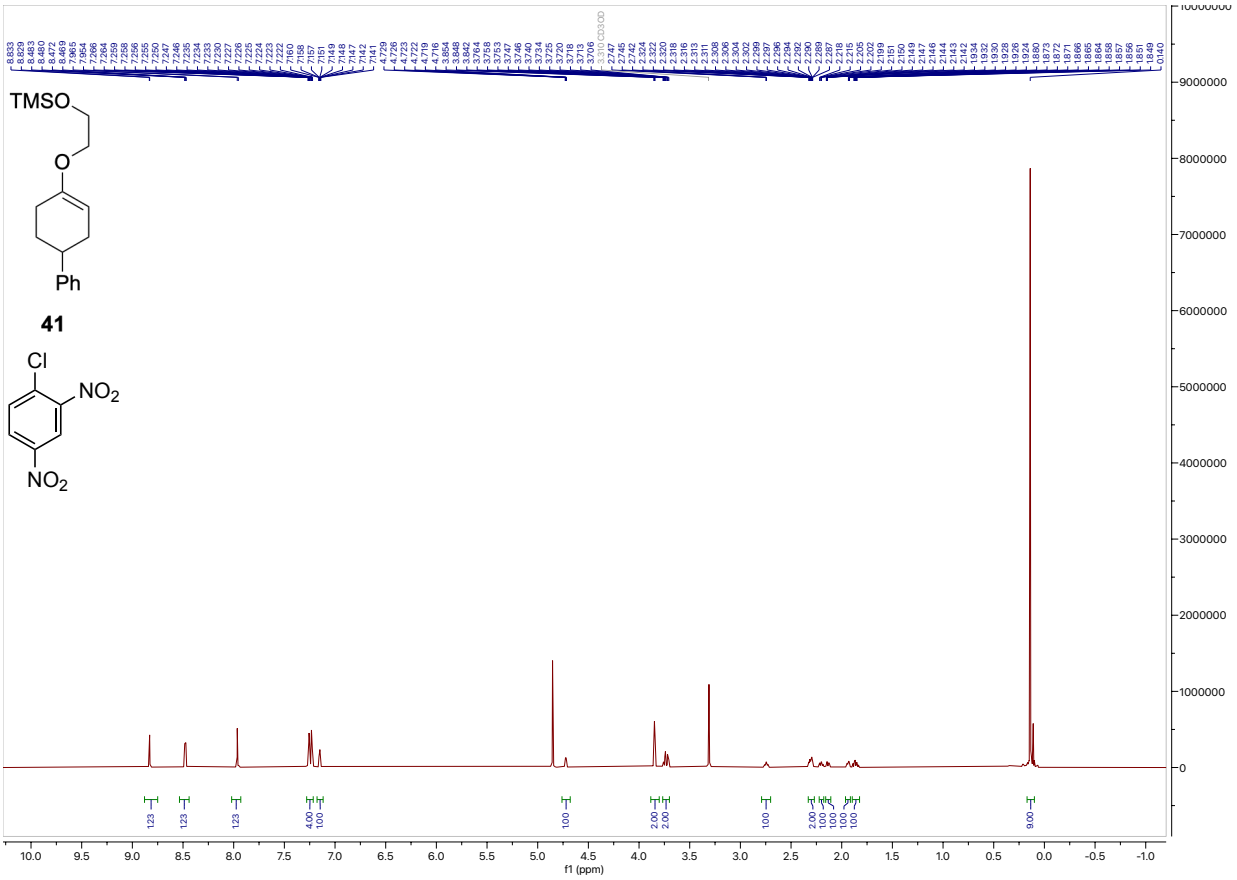


trimethyl(2-((1,2,3,6-tetrahydro-[1,1'-biphenyl]-4-yl)oxy)ethoxy)silane (**41**)

Reaction Time: 60 seconds

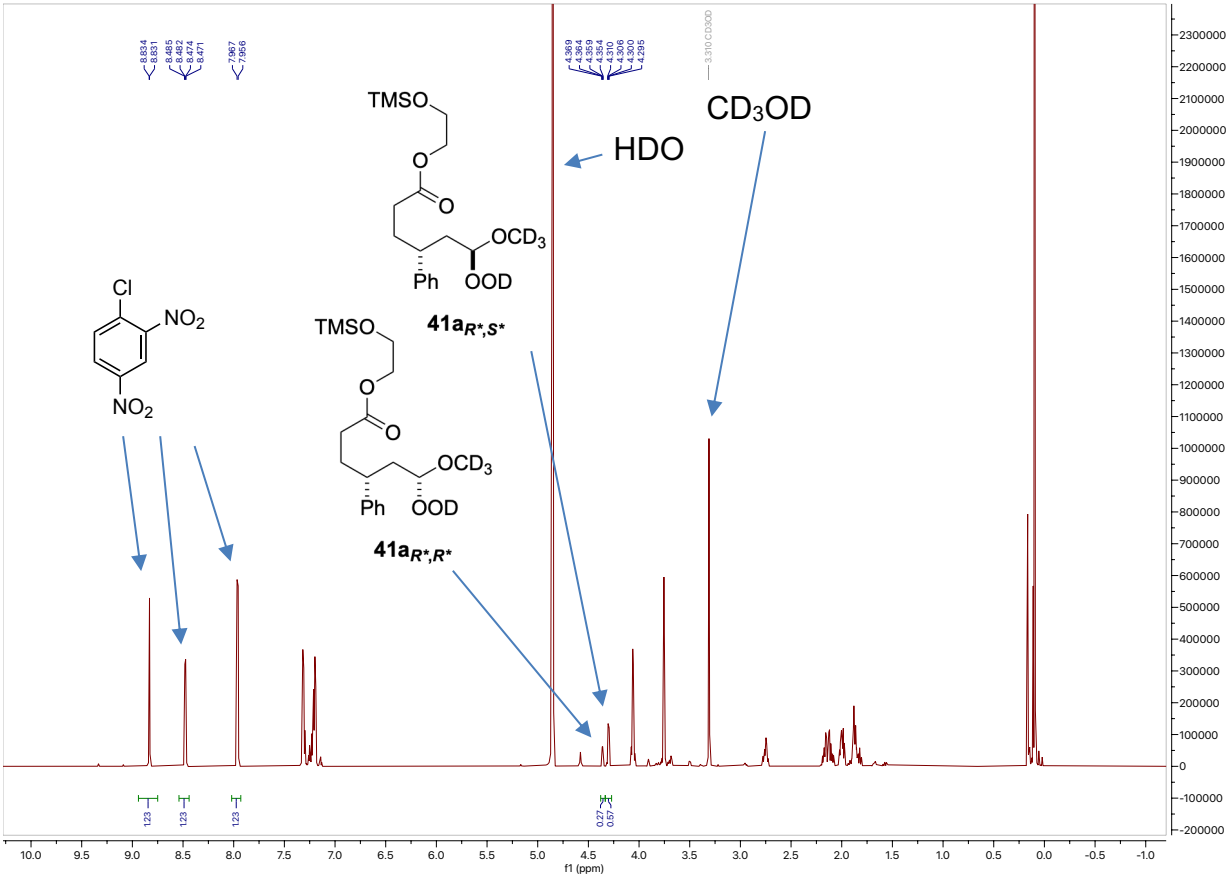
Alkene-to-IS Ratio: 0.99:1.00

Blank Sample: trimethyl(2-((1,2,3,6-tetrahydro-[1,1'-biphenyl]-4-yl)oxy)ethoxy)silane (**41**) and 1-chloro-2,4-dinitrobenzene (**IS**)



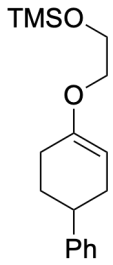
^{1}H NMR (800 MHz, CD_3OD), D1 = 10 s, 32 scans

Representative ^{1}H NMR: trimethyl(2-((1,2,3,6-tetrahydro-[1,1'-biphenyl]-4-yl)oxy)ethoxy)silane (**41**) ozonolysis



^{1}**H NMR** (800 MHz, $CDCl_3$), D1 = 10 s, 32 scans

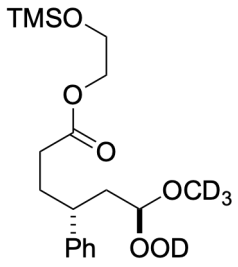
Characterization Data: trimethyl(2-((1,2,3,6-tetrahydro-[1,1'-biphenyl]-4-yl)oxy)ethoxy)silane (**41**)



41

trimethyl(2-((1,2,3,6-tetrahydro-[1,1'-biphenyl]-4-yl)oxy)ethoxy)silane (**41**)

^{1}H NMR (800 MHz, MeOD) δ 7.27 – 7.19 (m, 4H), 7.18 – 7.12 (m, 1H), 4.77 – 4.67 (m, 1H), 3.85 (t, *J* = 4.8 Hz, 2H), 3.78 – 3.65 (m, 2H), 2.77 – 2.71 (m, 1H), 2.36 – 2.25 (m, 2H), 2.25 – 2.17 (m, 1H), 2.17 – 2.09 (m, 1H), 1.98 – 1.91 (m, 1H), 1.91 – 1.79 (m, 1H), 0.14 (s, 9H).

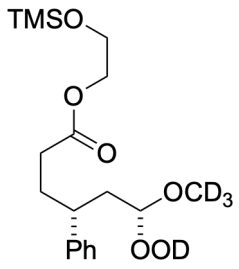


41a*R*,S**

2-((trimethylsilyl)oxy)ethyl (4*R**,6*S**)-6-deuteroperoxy-6-(methoxy-d_3)-4-phenylhexanoate (**41a*R*,S****)

^{1}H NMR (800 MHz, MeOD) δ 7.34 – 7.12 (m, 5H), 4.32 (dd, *J* = 8.3, 3.6 Hz, 1H), 4.10 – 4.04 (m, 2H), 3.75 (t, *J* = 4.9 Hz, 2H), 2.77 (tt, *J* = 10.2, 5.1 Hz, 1H), 2.22 – 2.10 (m, 2H), 2.07 – 1.97 (m, 2H), 1.94 – 1.84 (m, 2H), 0.10 (s, 9H).

The peroxide α-CH peak, the aromatic region, and the ester chain were measured from the ^{1}H NMR of the crude reaction mixture. The other peaks were deduced from the 1D selective gradient TOCSY spectrum.



41b$_{R^*,R^*}$

2-((trimethylsilyl)oxy)ethyl (4*R**,6*R**)-6-deuteroperoxy-6-(methoxy-d_3)-4-phenylhexanoate (**41a**$_{R^*,R^*}$)

^{1}H NMR (800 MHz, MeOD) δ 7.34 – 7.12 (m, 5H), 4.43 – 4.25 (m, 1H), 4.10 – 4.04 (m, 2H), 3.75 (t, *J* = 4.9 Hz, 2H), 2.79 (tt, *J* = 10.1, 5.2 Hz, 1H), 2.23 – 2.08 (m, 3H), 2.06 – 2.00 (m, 1H), 1.91 – 1.80 (m, 2H), 0.10 (s, 9H).

The peroxide α-CH peak, the aromatic region, and the ester chain were measured from the ^{1}H NMR of the crude reaction mixture. The other peaks were deduced from the 1D selective gradient TOCSY spectrum.

The configurations for the peroxides were assigned based on the modified Felkin–Ahn model (the A-value for R was assumed to be smaller than the A-value for Ph) for the capture of the Criegee intermediate by MeOH-d_4.

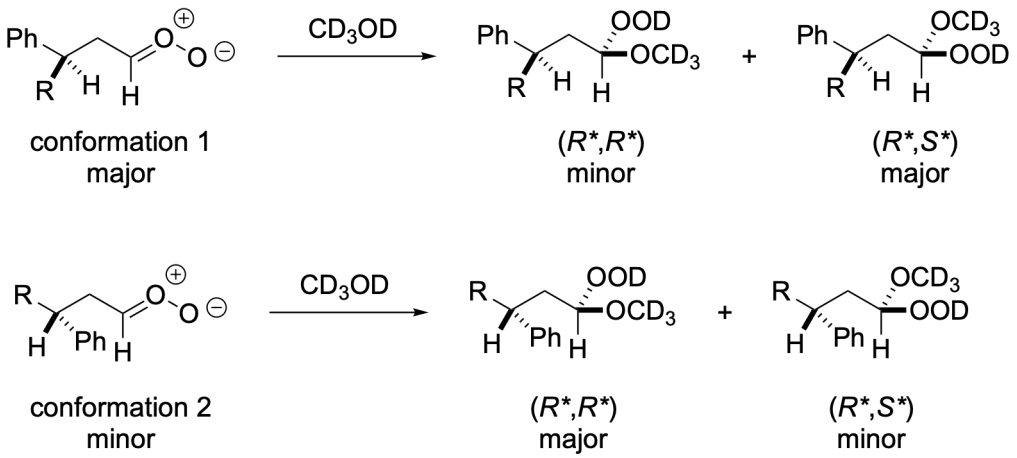
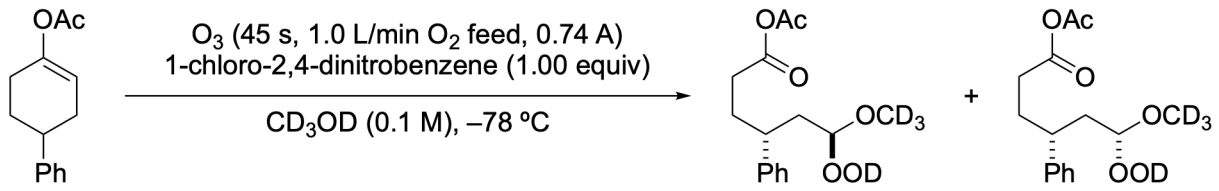


Figure 6.31 Felkin–Ahn analysis of **41a**

Table 6.41 trimethyl(2-((1,2,3,6-tetrahydro-[1,1'-biphenyl]-4-yl)oxy)ethoxy)silane (**41**) qNMR Data

Trial	**41a**$_{R^*,R^*}$	**41a**$_{R^*,S^*}$	*d.r.*
1	27	57	1.0:2.1
2	26	58	1.0:2.2
3	27	57	1.0:2.1
average	27	57	1.0:2.1
st. dev.	0.58	0.58	



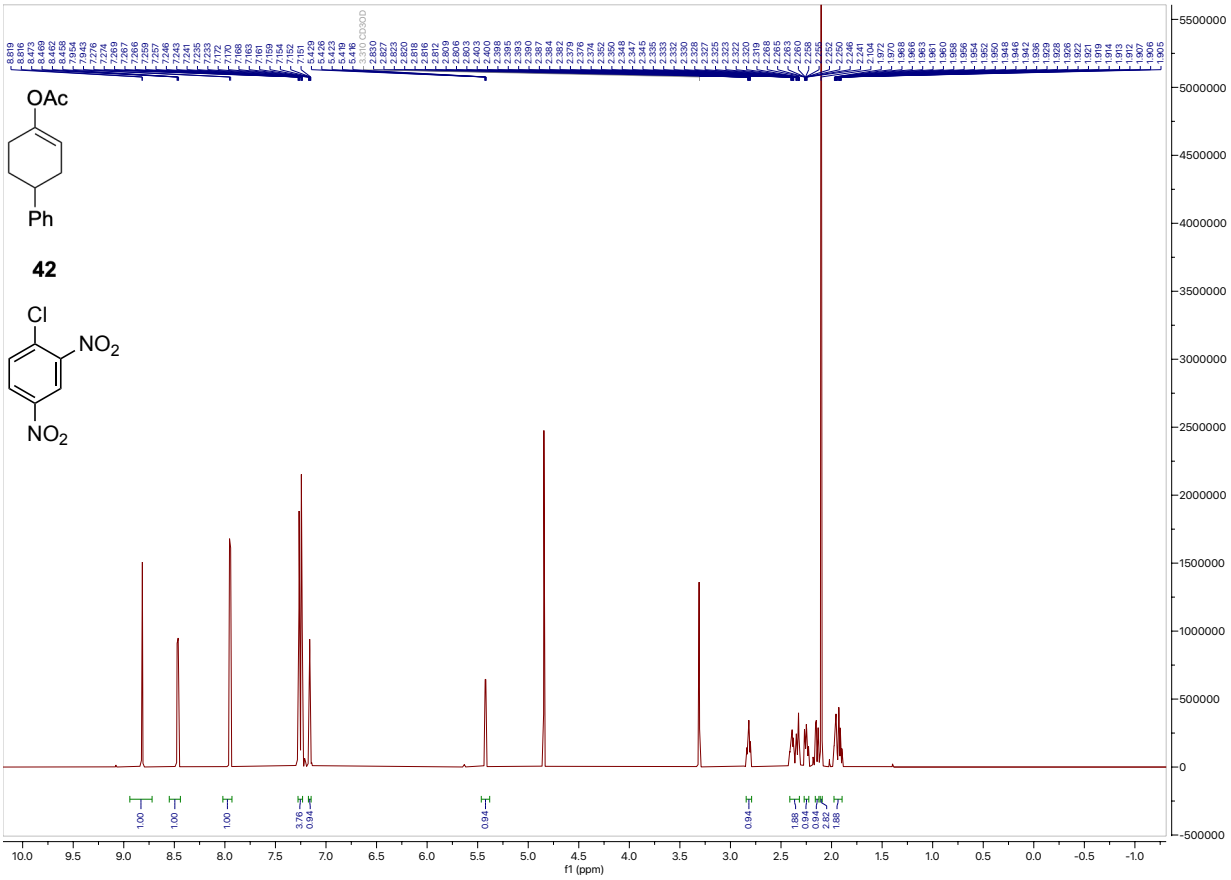
42 **42a$_{R^*,S^*}$** **42a$_{R^*,R^*}$**

1,2,3,6-tetrahydro-[1,1'-biphenyl]-4-yl acetate (**42**)

Reaction Time: 45 seconds

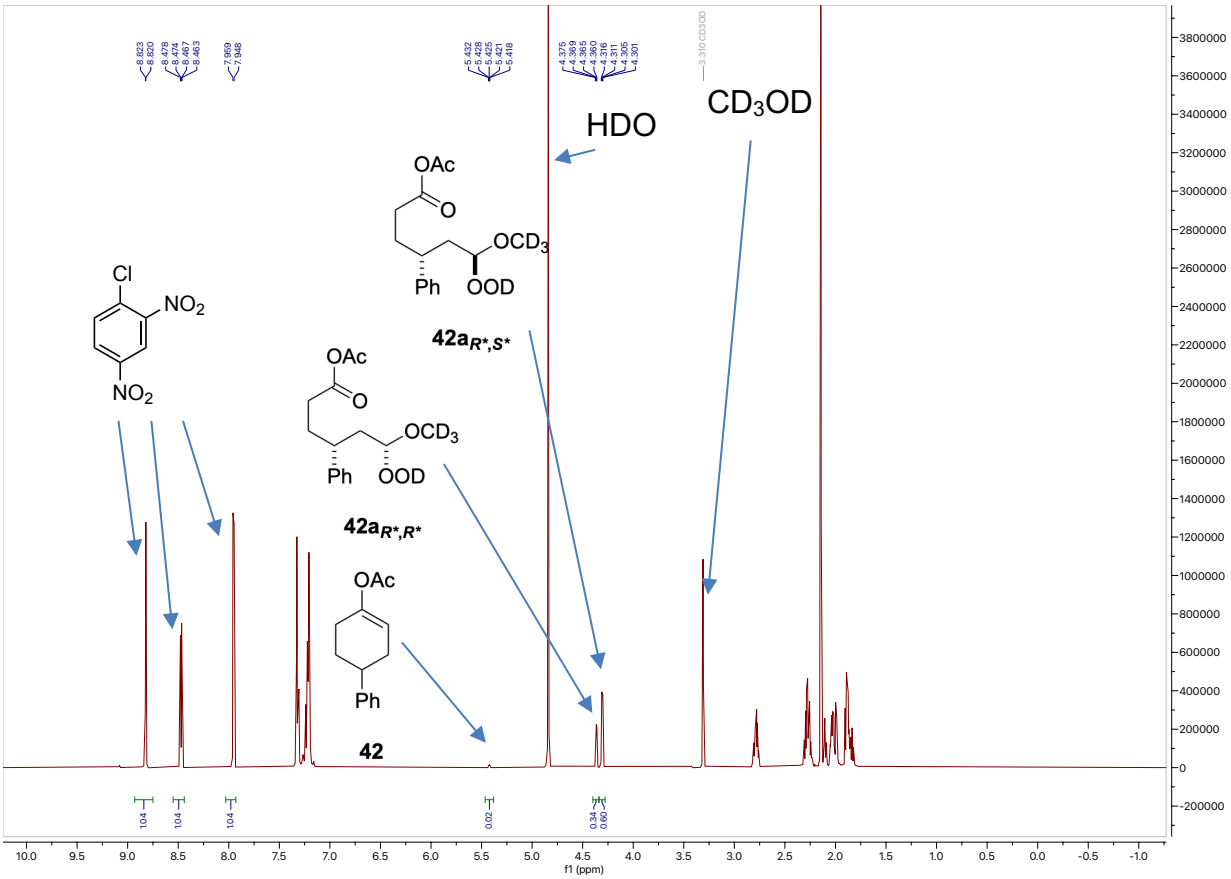
Alkene-to-IS Ratio: 0.94:1.00

Blank Sample: 1,2,3,6-tetrahydro-[1,1'-biphenyl]-4-yl acetate (**42**) and 1-chloro-2,4-dinitrobenzene (**IS**)



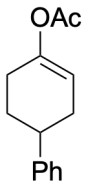
^{1}H NMR (800 MHz, CD_3OD), D1 = 10 s, 32 scans

Representative ^{1}H NMR: 1,2,3,6-tetrahydro-[1,1'-biphenyl]-4-yl acetate (**42**) ozonolysis



^{1}H NMR (800 MHz, $CDCl_3$), D1 = 10 s, 32 scans

Characterization Data: 1,2,3,6-tetrahydro-[1,1'-biphenyl]-4-yl acetate (**42**)

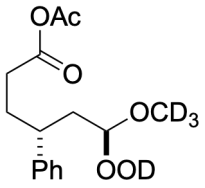


42

1,2,3,6-tetrahydro-[1,1'-biphenyl]-4-yl acetate (**42**)

^{1}H NMR (800 MHz, MeOD) δ 7.28 – 7.25 (m, 2H), 7.24 (dd, *J* = 8.2, 1.6 Hz, 2H), 7.16 (tt, *J* = 6.6, 1.5 Hz, 1H), 5.42 (dt, *J* = 5.4, 2.8 Hz, 1H), 2.82 (ddt, *J* = 13.7, 8.4, 3.1 Hz,

1H), 2.44 – 2.30 (m, 2H), 2.25 (dddt, *J* = 17.1, 10.3, 4.3, 2.5 Hz, 1H), 2.17 – 2.12 (m, 1H), 2.10 (s, 3H), 2.00 – 1.88 (m, 2H).

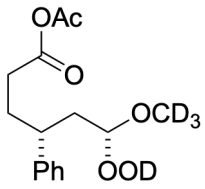


42a$_{R^*,S^*}$

acetic (4*R*,6*S*)-6-deuteroperoxy-6-(methoxy-d_3)-4-phenylhexanoic anhydride (**42a$_{R^*,S^*}$**)

^{1}H NMR (800 MHz, MeOD) δ 7.35 – 7.16 (m, 5H), 4.33 (dd, *J* = 8.3, 3.6 Hz, 1H), 2.80 (tt, *J* = 10.3, 5.2 Hz, 1H), 2.35 – 2.24 (m, 2H), 2.14 (s, 3H), 2.09 – 1.99 (m, 2H), 1.94 – 1.86 (m, 2H).

The peroxide α-CH peak, the aromatic region, and the anhydride methyl were measured from the ^{1}H NMR of the crude reaction mixture. The other peaks were deduced from the 1D selective gradient TOCSY spectrum.



42a$_{R^*,R^*}$

acetic (4*R*,6*R*)-6-deuteroperoxy-6-(methoxy-d_3)-4-phenylhexanoic anhydride (**42a$_{R^*,R^*}$**)

^{1}H NMR (800 MHz, MeOD) δ 7.35 – 7.16 (m, 5H), 4.39 (dd, *J* = 7.9, 4.1 Hz, 1H), 2.82 (tt, *J* = 10.2, 5.0 Hz, 1H), 2.35 – 2.24 (m, 2H), 2.15 (s, 3H), 2.12 (ddd, *J* = 14.3, 7.9, 5.2 Hz, 1H), 2.05 (dddd, *J* = 13.8, 8.7, 7.0, 5.1 Hz, 1H), 1.92 – 1.83 (m, 2H).

The peroxide α-CH peak, the aromatic region, and the anhydride methyl were measured from the ^{1}H NMR of the crude reaction mixture. The other peaks were deduced from the 1D selective gradient TOCSY spectrum.

The configurations for the peroxides were assigned based on the modified Felkin–Ahn model (the A-value for R was assumed to be smaller than the A-value for Ph) for the capture of the Criegee intermediate by MeOH-d_4.

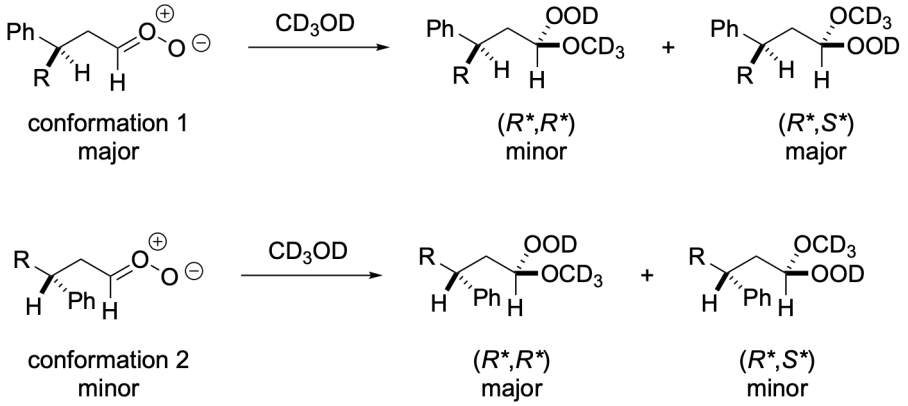
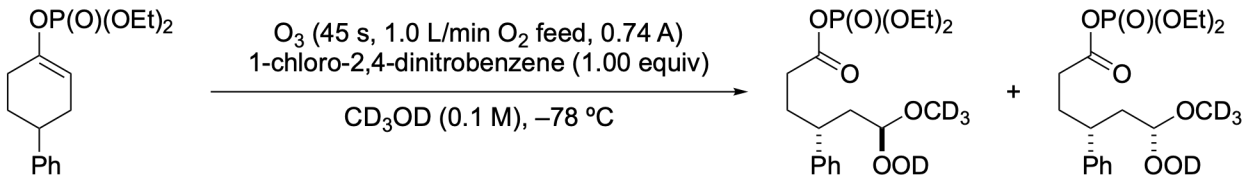


Figure 6.32 Felkin–Ahn analysis of **42a**

Table 6.42 1,2,3,6-tetrahydro-[1,1'-biphenyl]-4-yl acetate (**42**) qNMR Data

Trial	**%Conversion**	**42a**$_{R^*,R^*}$	**42b**$_{R^*,S^*}$	***d.r.***	**Normalized %B**
1	98	34	60	1.0:1.8	95.9
2	83	29	51	1.0:1.8	96.4
3	87	30	54	1.0:1.8	96.6
average	89.3	31	55	1.0:1.8	96.3
st. dev.	7.77	2.65	4.58		0.36



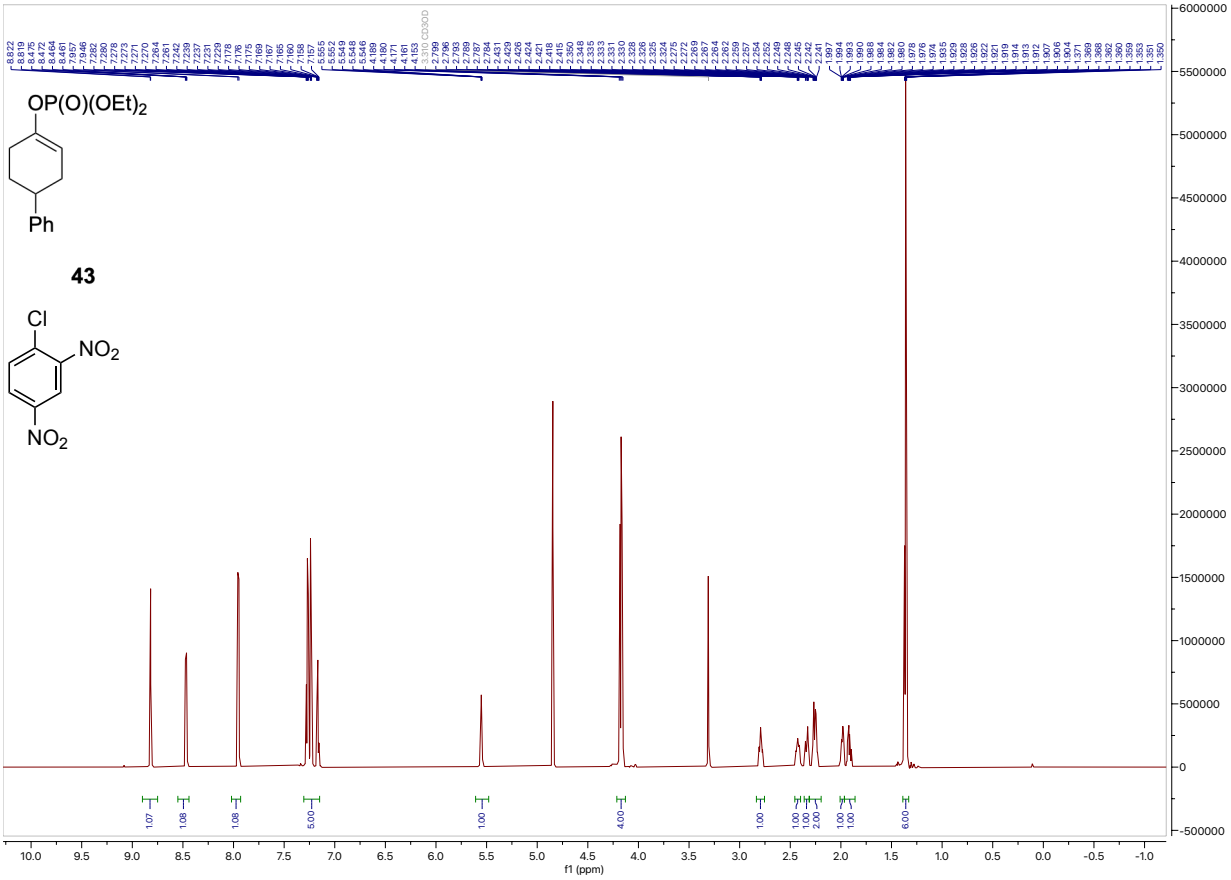
43 **43a$_{R^*,S^*}$** **43a$_{R^*,R^*}$**

diethyl (1,2,3,6-tetrahydro-[1,1'-biphenyl]-4-yl) phosphate (**43**)

Reaction Time: 45 seconds

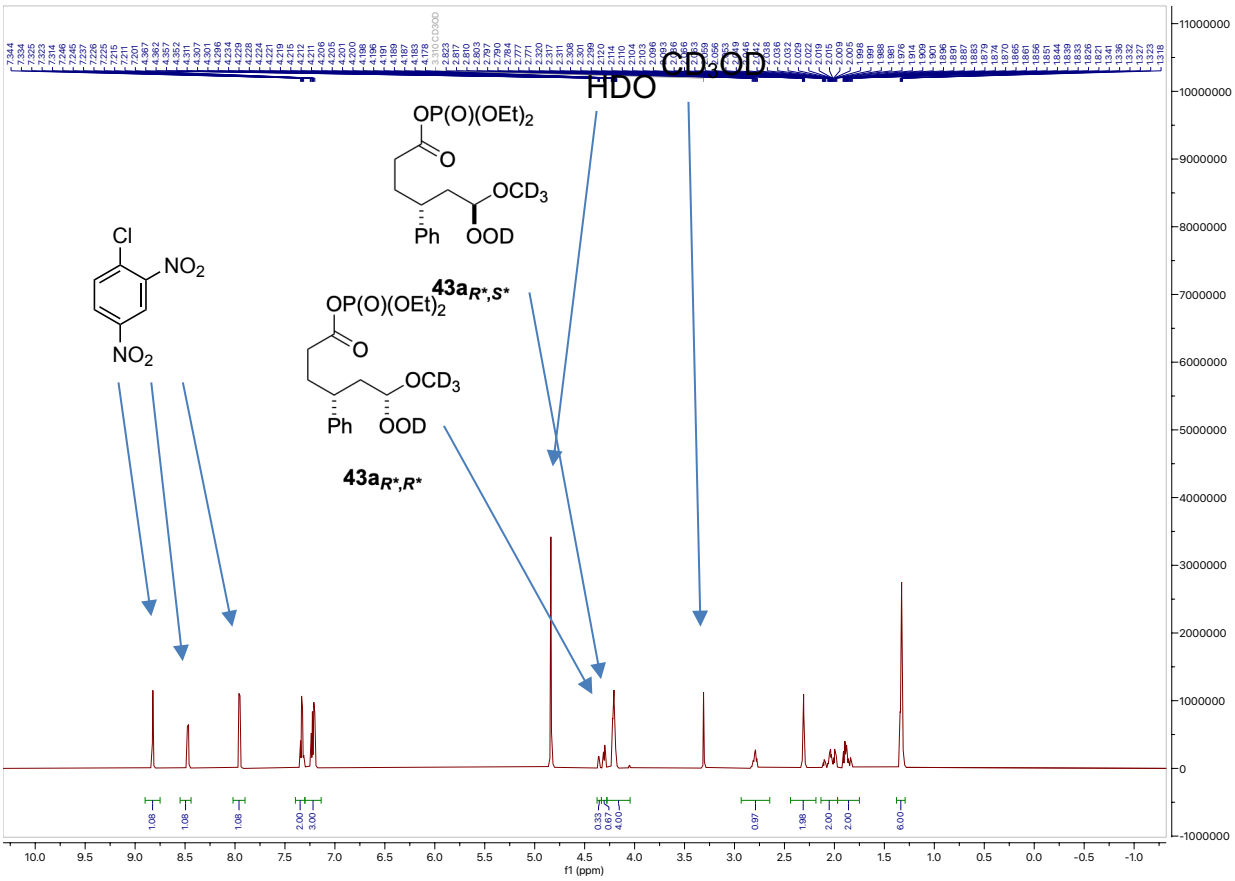
Alkene-to-IS Ratio: 0.92:1.00

Blank Sample: diethyl (1,2,3,6-tetrahydro-[1,1'-biphenyl]-4-yl) phosphate (**43**) and 1-chloro-2,4-dinitrobenzene (**IS**)



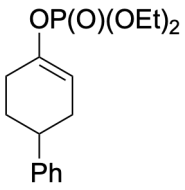
^{1}H NMR (800 MHz, CD_3OD)

Representative ^{1}H NMR: diethyl (1,2,3,6-tetrahydro-[1,1'-biphenyl]-4-yl) phosphate (**43**) ozonolysis



^{1}H NMR (800 MHz, $CDCl_3$), D1 = 10 s, 32 scans

Characterization Data: diethyl (1,2,3,6-tetrahydro-[1,1'-biphenyl]-4-yl) phosphate (**43**)

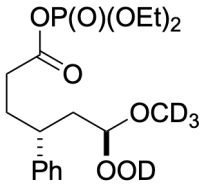


43

diethyl (1,2,3,6-tetrahydro-[1,1'-biphenyl]-4-yl) phosphate (**43**)

^{1}H NMR (800 MHz, MeOD) δ 7.30 – 7.25 (m, 2H), 7.25 – 7.22 (m, 2H), 7.17 (tt, *J* = 6.9, 1.4 Hz, 1H), 5.65 – 5.42 (m, 1H), 4.17 (p, *J* = 7.1 Hz, 4H), 2.79 (ddq, *J* = 15.1, 8.2, 3.0

Hz, 1H), 2.49 – 2.38 (m, 1H), 2.38 – 2.30 (m, 1H), 2.29 – 2.18 (m, 2H), 2.03 – 1.96 (m, 1H), 1.92 (dddd, *J* = 12.9, 11.7, 10.7, 5.6 Hz, 1H), 1.36 (tt, *J* = 7.0, 1.0 Hz, 6H).

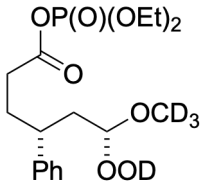


43a*R*,S**

(diethyl phosphoric) (4*R**,6*S**)-6-hydroperoxy-6-(methoxy-d_3)-4-phenylhexanoic anhydride (**43a*R*,S****)

^{1}H NMR (800 MHz, MeOD) δ 7.36 – 7.30 (m, 2H), 7.26 – 7.18 (m, 3H), 4.30 (dd, *J* = 8.3, 3.6 Hz, 1H), 4.21 (dddd, *J* = 12.1, 7.0, 5.6, 3.4 Hz, 4H), 2.80 (dtt, *J* = 15.5, 10.3, 5.1 Hz, 1H), 2.31 (td, *J* = 7.4, 2.3 Hz, 2H), 2.13 – 1.95 (m, 2H), 1.92 – 1.81 (m, 2H), 1.33 (td, *J* = 7.1, 3.8 Hz, 6H).

The peroxide α-CH peak, the aromatic, and the ethyl peaks were measured from the ^{1}H NMR of the crude reaction mixture. The other peaks were deduced from the 1D selective gradient TOCSY spectrum.



43a$_{R^*,R^*}$

(diethyl phosphoric) (4*R**,6*R**)-6-hydroperoxy-6-(methoxy-d_3)-4-phenylhexanoic anhydride (**43a$_{R^*,R^*}$**)

^{1}H NMR (800 MHz, MeOD) δ 7.36 – 7.30 (m, 2H), 7.26 – 7.18 (m, 3H), 4.36 (dd, *J* = 7.9, 4.1 Hz, 1H), 4.21 (dddd, *J* = 12.1, 7.0, 5.6, 3.4 Hz, 4H), 2.80 (dtt, *J* = 15.5, 10.3, 5.1 Hz, 1H), 2.31 (td, *J* = 7.4, 2.3 Hz, 2H), 2.13 – 1.95 (m, 2H), 1.92 – 1.81 (m, 2H), 1.33 (td, *J* = 7.1, 3.8 Hz, 6H).

The peroxide α-CH peak, the aromatic region, and the ethyl peaks were measured from the ^{1}H NMR of the crude reaction mixture. The other peaks were deduced from the 1D selective gradient TOCSY spectrum.

The configurations for the peroxides were assigned based on the modified Felkin–Ahn model (the A-value for R was assumed to be smaller than the A-value for Ph) for the capture of the Criegee intermediate by MeOH-d_4.

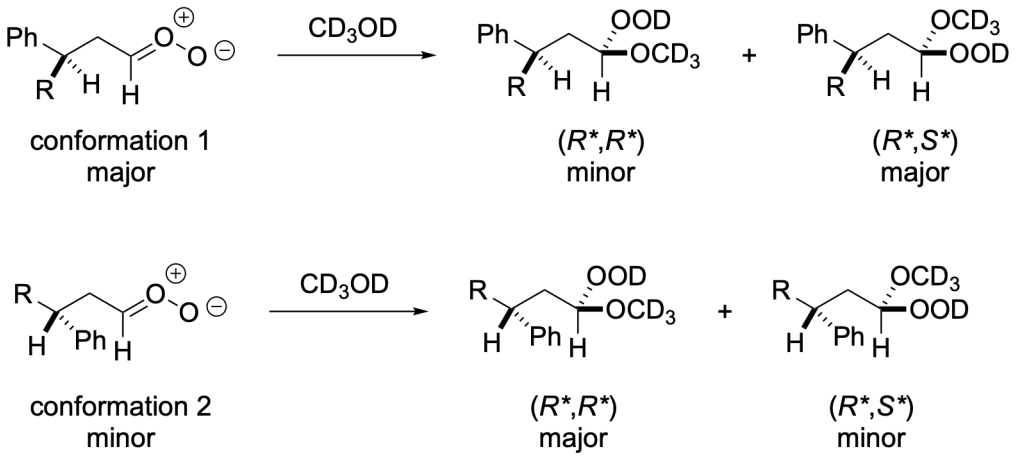
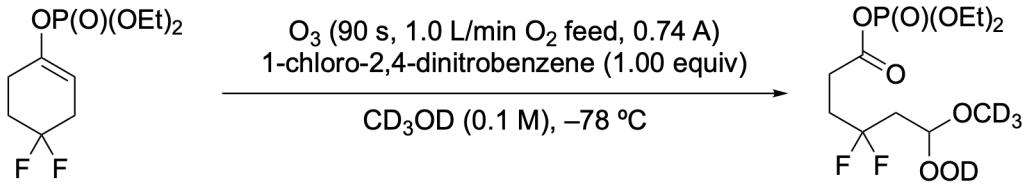


Figure 6.33 Felkin–Ahn Analysis of **43a**

Table 6.43 diethyl (1,2,3,6-tetrahydro-[1,1'-biphenyl]-4-yl) phosphate (**43**) qNMR Data

Trial	**43a**$_{R^*,R^*}$	**43a**$_{R^*,S^*}$	***d.r.***
1	33	67	1.0:2.0
2	37	63	1.0:1.7
3	38	62	1.0:1.6
average	36	64	1.0:1.8
st. dev.	2.65	2.65	



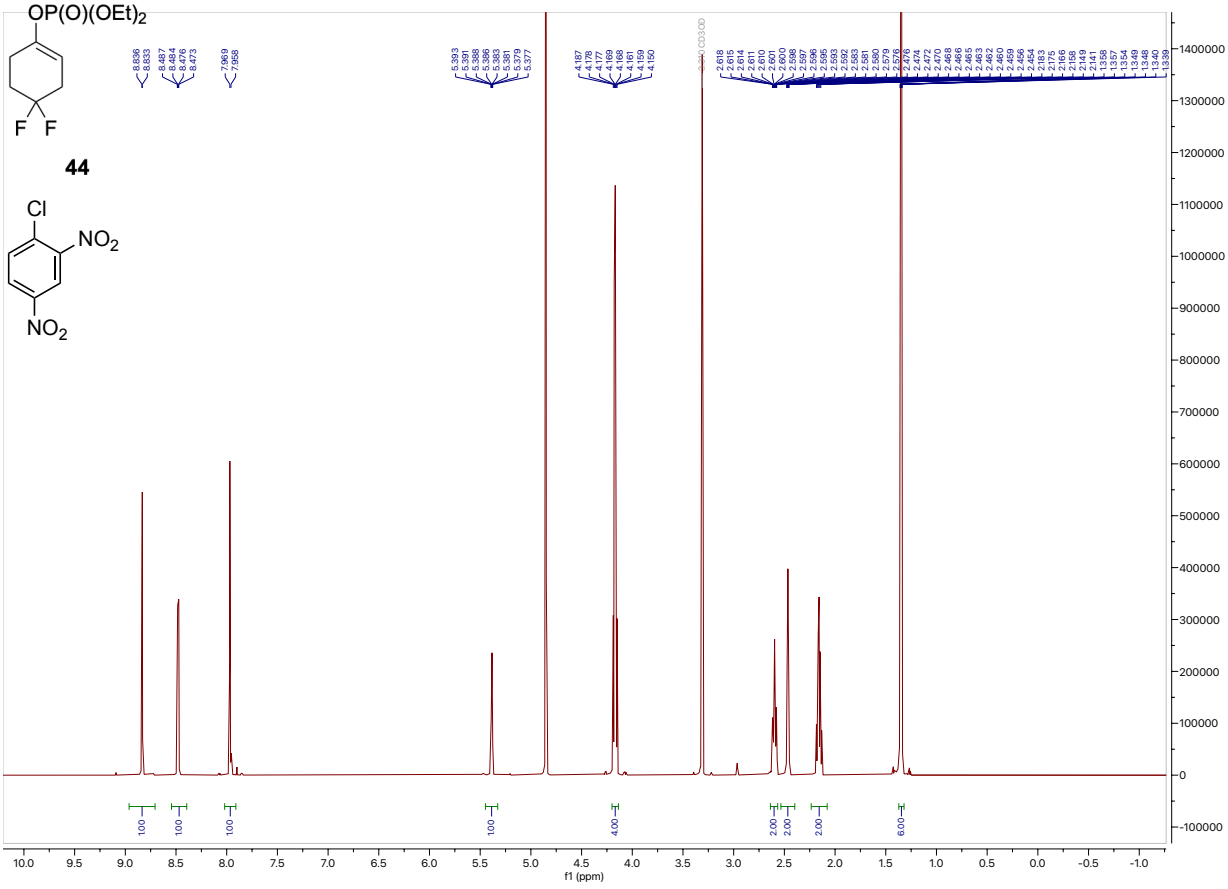
44 **44a**

4,4-difluorocyclohex-1-en-1-yl diethyl phosphate (**44**)

Reaction Time: 90 seconds

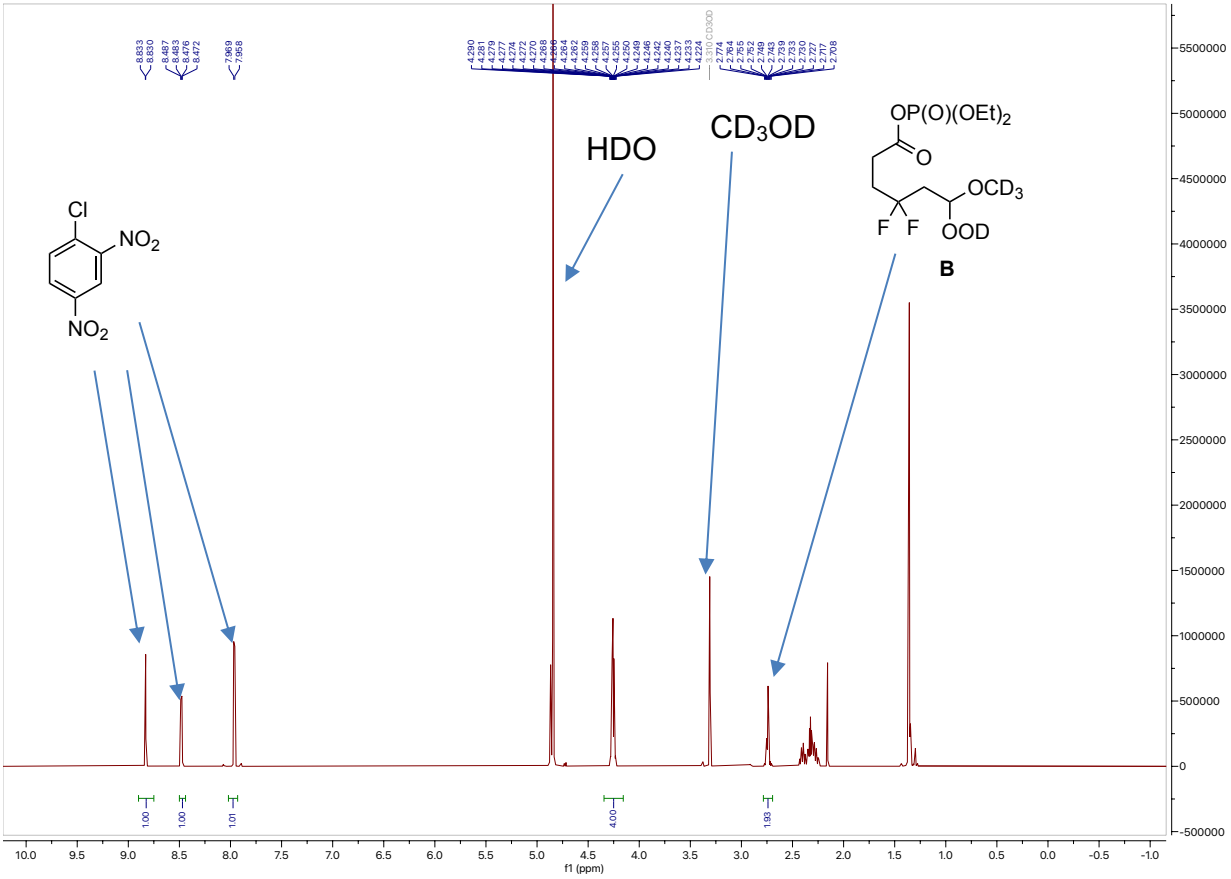
Alkene-to-IS Ratio: 1.00:1.00

Blank Sample: 4,4-difluorocyclohex-1-en-1-yl diethyl phosphate (**44**) and 1-chloro-2,4-dinitrobenzene (**IS**)



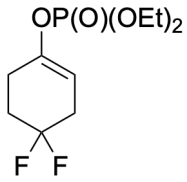
^{1}H NMR (800 MHz, CD_3OD), D1 = 10 s, 32 scans

Representative ^{1}H NMR: 4,4-difluorocyclohex-1-en-1-yl diethyl phosphate (**44**) ozonolysis



^{1}H NMR (800 MHz, $CDCl_3$), D1 = 10 s, 32 scans

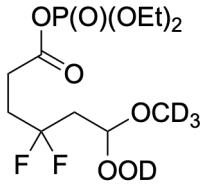
Characterization Data: 4,4-difluorocyclohex-1-en-1-yl diethyl phosphate (**44**)



44

4,4-difluorocyclohex-1-en-1-yl diethyl phosphate (**44**)

^{1}H NMR (800 MHz, MeOD) δ 5.38 (td, *J* = 3.9, 2.4 Hz, 1H), 4.17 (dq, *J* = 8.4, 7.1 Hz, 4H), 2.73 – 2.52 (m, 2H), 2.46 (dddd, *J* = 6.8, 4.6, 3.7, 1.8 Hz, 2H), 2.16 (tt, *J* = 13.7, 6.8 Hz, 2H), 1.35 (td, *J* = 7.1, 1.1 Hz, 6H).



44a

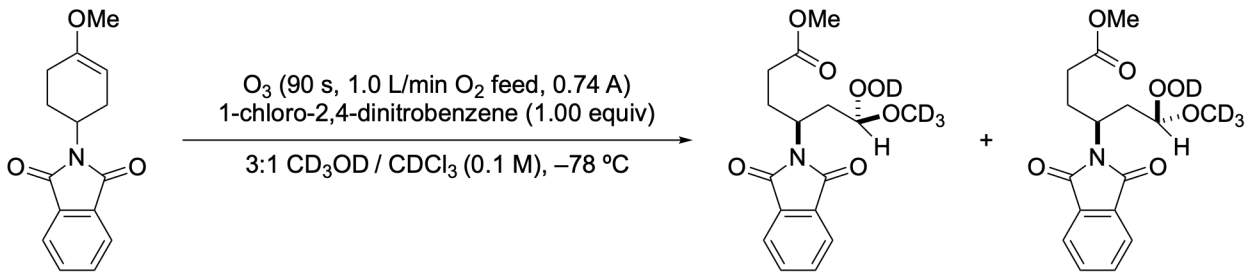
(diethyl phosphoric) 4,4-difluoro-6-deuteroperoxy-6-(methoxy-d_3)hexanoic anhydride (**44a**)

^{1}H NMR (800 MHz, MeOD) δ 4.87 (t, *J* = 5.3 Hz, 1H), 4.29 – 4.21 (m, 4H), 2.74 (td, *J* = 7.3, 2.5 Hz, 2H), 2.47 – 2.20 (m, 4H), 1.36 (td, *J* = 7.1, 1.2 Hz, 6H).

The peaks were measured and deduced from the ^{1}H NMR of the crude reaction mixture.

Table 6.44 4,4-difluorocyclohex-1-en-1-yl diethyl phosphate (**44**) qNMR Data

Trial	**%44a**
1	96.5
2	96.5
3	96.5
average	96.5
st. dev.	0



45 **45a**$_{S^*,R^*}$ **45a**$_{S^*,S^*}$

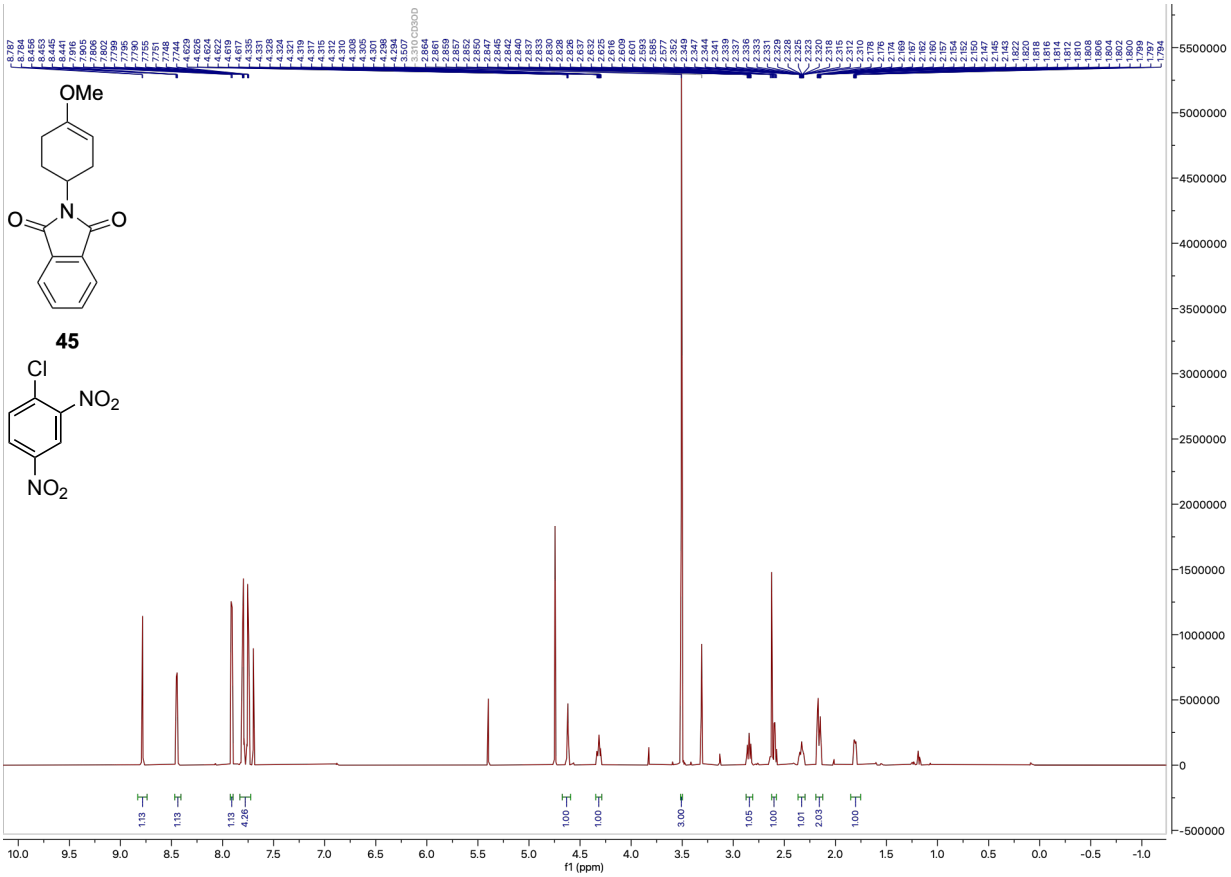
2-(4-methoxycyclohex-3-en-1-yl)isoindoline-1,3-dione (**45**)

Reaction Solvent: 3:1 $CD_3OD/CDCl_3$ (0.01 M) was used to homogenize the mixture

Reaction Time: 90 seconds

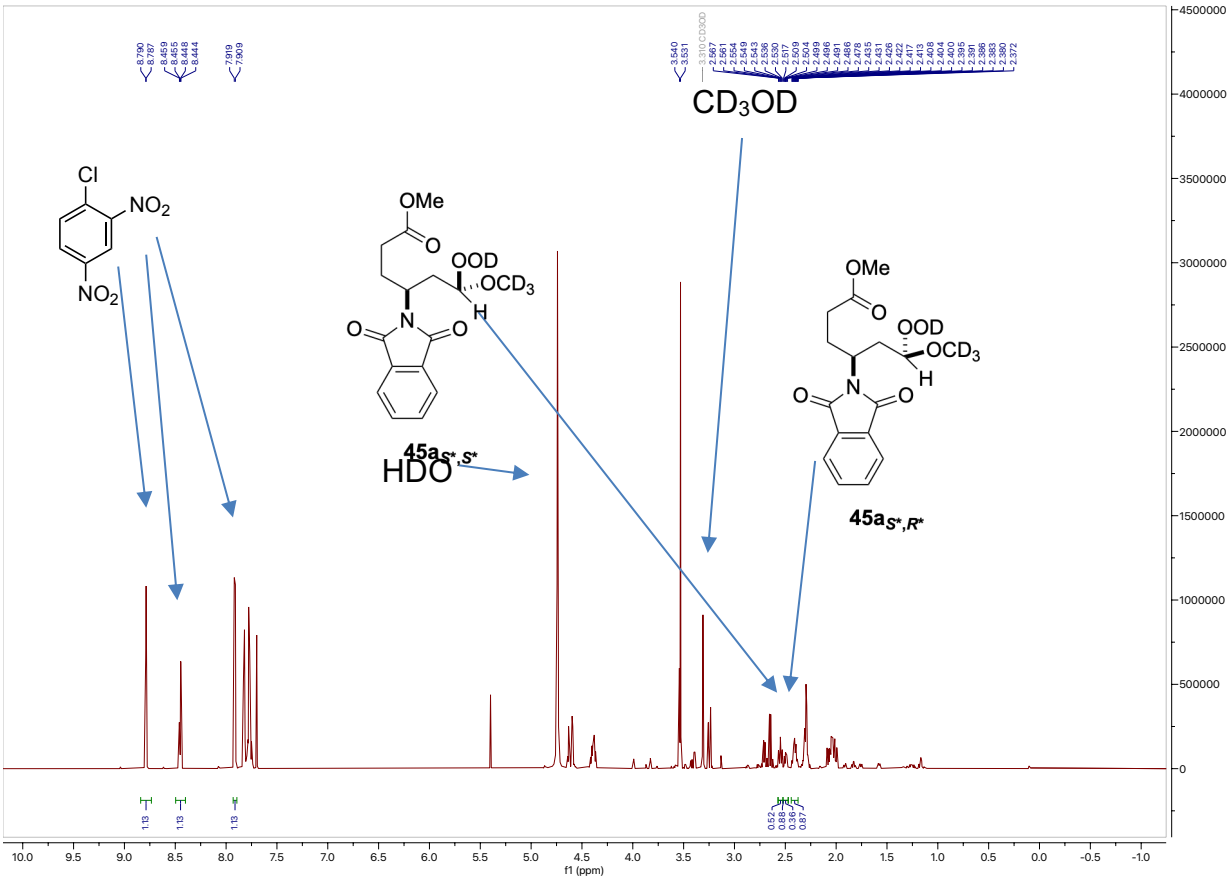
Alkene-to-IS Ratio: 0.87:1.00

Blank Sample: 2-(4-methoxycyclohex-3-en-1-yl)isoindoline-1,3-dione (**45**) and 1-chloro-2,4-dinitrobenzene (**IS**)



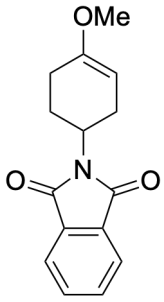
^{1}H NMR (800 MHz, 3:1 $CD_3OD/CDCl_3$), D1 = 10 s, 32 scans

Representative ^{1}H NMR: 2-(4-methoxycyclohex-3-en-1-yl)isoindoline-1,3-dione (**45**) ozonolysis



^{1}H NMR (800 MHz, 3:1 $CD_3OD/CDCl_3$), D1 = 10 s, 32 scans

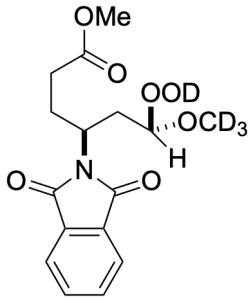
Characterization Data: 2-(4-methoxycyclohex-3-en-1-yl)isoindoline-1,3-dione (**45**)



45

2-(4-methoxycyclohex-3-en-1-yl)isoindoline-1,3-dione (**45**)

^{1}H NMR (800 MHz, 3:1 MeOD/$CDCl_3$) δ 7.80 (dd, *J* = 5.4, 3.1 Hz, 2H), 7.75 (dd, *J* = 5.5, 3.0 Hz, 2H), 4.62 (dt, *J* = 5.8, 2.0 Hz, 1H), 4.31 (dddd, *J* = 12.9, 11.2, 5.6, 3.2 Hz, 1H), 3.51 (s, 3H), 2.84 (dddt, *J* = 15.0, 11.2, 3.7, 1.8 Hz, 1H), 2.64 – 2.57 (m, 1H), 2.33 (dddt, *J* = 18.7, 11.7, 3.7, 1.8 Hz, 1H), 2.26 – 2.12 (m, 2H), 1.81 (dddd, *J* = 14.3, 6.3, 3.4, 1.7 Hz, 1H).

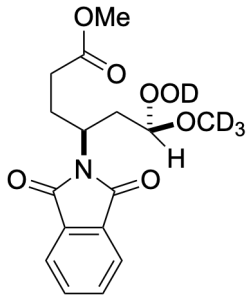


45a*S*,S**

methyl (4*S**,6*S**)-4-(1,3-dioxoisoindolin-2-yl)-6-deuteroperoxy-6-(methoxy-d_3)hexanoate (**45a*S*,S****)

^{1}H NMR (800 MHz, 3:1 MeOD/$CDCl_3$) δ 7.87 – 7.72 (m, 4H), 4.60 (dd, *J* = 7.1, 6.5 Hz, 1H), 4.38 (tt, *J* = 10.6, 4.4 Hz, 1H), 3.53 (s, 3H), 2.55 (ddd, *J* = 15.3, 10.3, 5.0 Hz, 2H), 2.41 (ddt, *J* = 14.0, 10.7, 6.9 Hz, 1H), 2.36 – 2.25 (m, 1H), 2.00 (ddd, *J* = 14.5, 6.6, 4.2 Hz, 2H).

The peroxide α-CH peak, the aromatic region, and the methyl ester peak were measured from the ^{1}H NMR of the crude reaction mixture. The other peaks were deduced from the 1D selective gradient TOCSY spectrum.



45a$_{S^*,R^*}$

methyl (4*S**,6*R**)-4-(1,3-dioxoisoindolin-2-yl)-6-deuteroperoxy-6-(methoxy-d_3)hexanoate (**45a**$_{S^*,R^*}$)

^{1}H NMR (800 MHz, 3:1 MeOD/$CDCl_3$) δ 7.87 – 7.72 (m, 4H), 4.63 (dd, *J* = 6.5, 6.1 Hz, 1H), 4.40 (tt, *J* = 10.5, 4.4 Hz, 1H), 3.54 (s, 3H), 2.50 (ddd, *J* = 14.6, 10.3, 6.2 Hz, 2H), 2.41 (ddt, *J* = 13.9, 10.6, 6.9 Hz, 1H), 2.30 (td, *J* = 7.2, 2.8 Hz, 1H), 2.08 (ddd, *J* = 14.5, 5.2, 4.2 Hz, 2H).

The peroxide α-CH peak, the aromatic region, and the methyl ester peak were measured from the ^{1}H NMR of the crude reaction mixture. The other peaks were deduced from the 1D selective gradient TOCSY spectrum.

The configurations for the peroxides were assigned based on the modified Felkin–Ahn model [the *N*-phthalimide (NPhth) group was placed perpendicular to the carbonyl oxide to minimize dipoles] for the capture of the Criegee intermediate by MeOH-d_4.

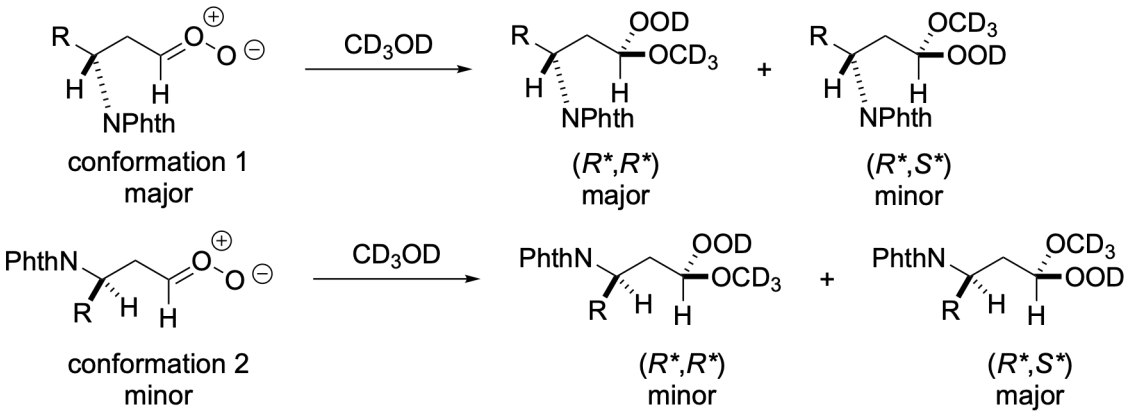
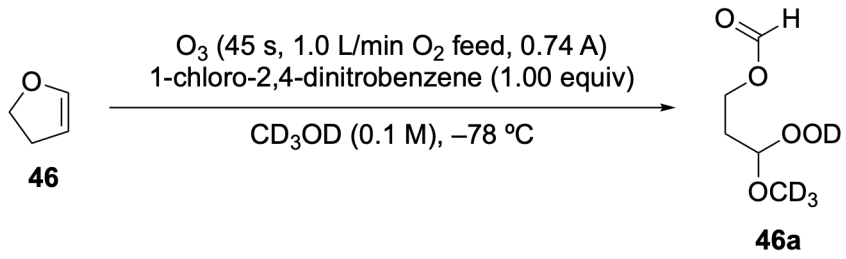


Figure 6.34 Felkin–Ahn Analysis of **45a**

Table 6.45 2-(4-methoxycyclohex-3-en-1-yl)isoindoline-1,3-dione (**45**) qNMR Data

Trial	**Average 45a**	**45a*S*,S****	**45a*S*,R****	***d.r.***
1	87.5	52	36	1.4:1
2	89.5	50	37	1.4:1
3	90	52	38	1.4:1
average	89	51.3	37	1.4:1
st. dev.	1.3	1.0	0.71	0



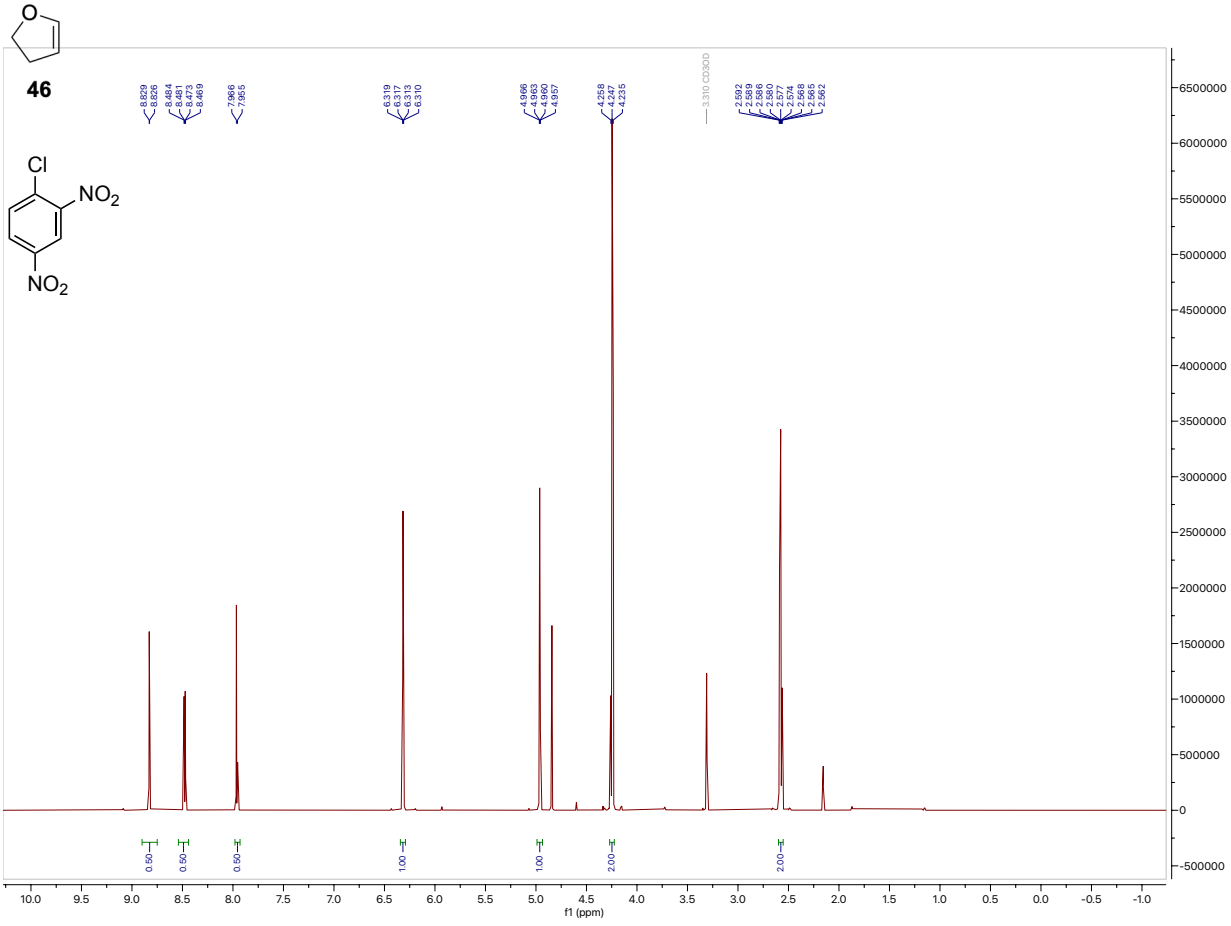
46 **46a**

3,4-dihydrofuran (**46**)

Reaction Time: 45 seconds

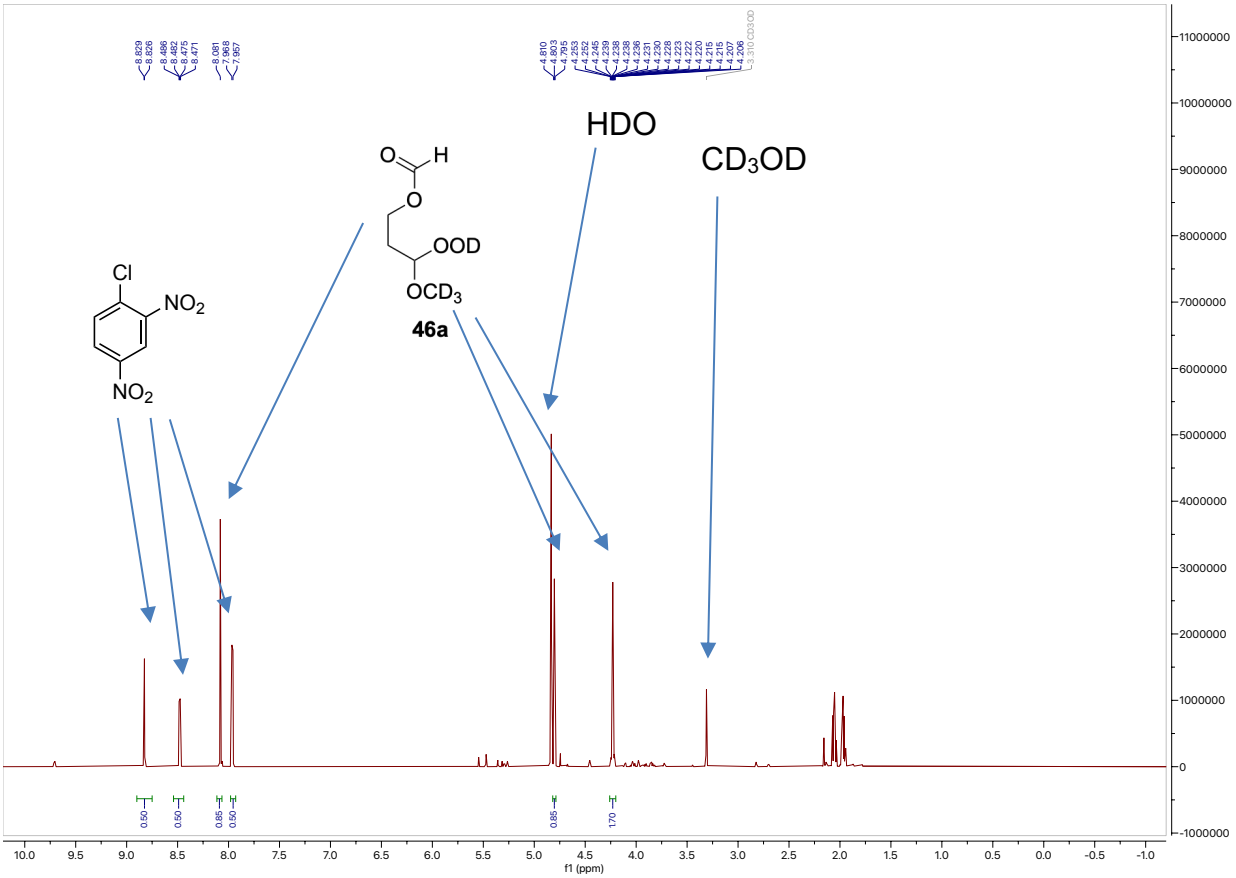
Alkene-to-IS Ratio: 0.97:1.00

Blank Sample: 3,4-dihydrofuran (**46**) and 1-chloro-2,4-dinitrobenzene (**IS**)



^{1}H NMR (800 MHz, CD_3OD), D1 = 10 s, 32 scans

Representative ^{1}H NMR: 3,4-dihydrofuran (**46**) ozonolysis



^{1}H NMR (800 MHz, CD_3OD), D1 = 10 s, 32 scans

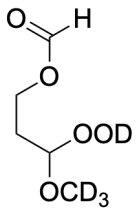
Characterization Data: 3,4-dihydrofuran (**46**)



46

3,4-dihydrofuran (**46**)

^{1}H NMR (800 MHz, MeOD) δ 6.31 (q, *J* = 2.3 Hz, 1H), 4.96 (q, *J* = 2.6 Hz, 1H), 4.25 (t, *J* = 9.5 Hz, 2H), 2.58 (tt, *J* = 9.6, 2.5 Hz, 2H).



46a

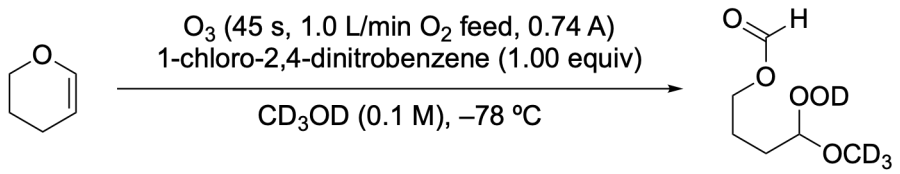
3-deuteroperoxy-3-(methoxy-d_3)propyl formate (**46a**)

^{1}H NMR (800 MHz, MeOD) δ 8.08 (s, 1H), 4.80 (t, *J* = 5.9 Hz, 1H), 4.23 (tt, *J* = 6.5, 0.9 Hz, 2H), 2.06 (dq, *J* = 14.6, 6.3 Hz, 1H), 1.96 (dq, *J* = 14.5, 6.3 Hz, 1H).

The signals were measured from the ^{1}H NMR of the crude reaction mixture.

Table 6.46 3,4-dihydrofuran (**46**) qNMR Data

Trial	**46a**
1	85
2	83.3
3	86
average	85
st. dev.	1.5



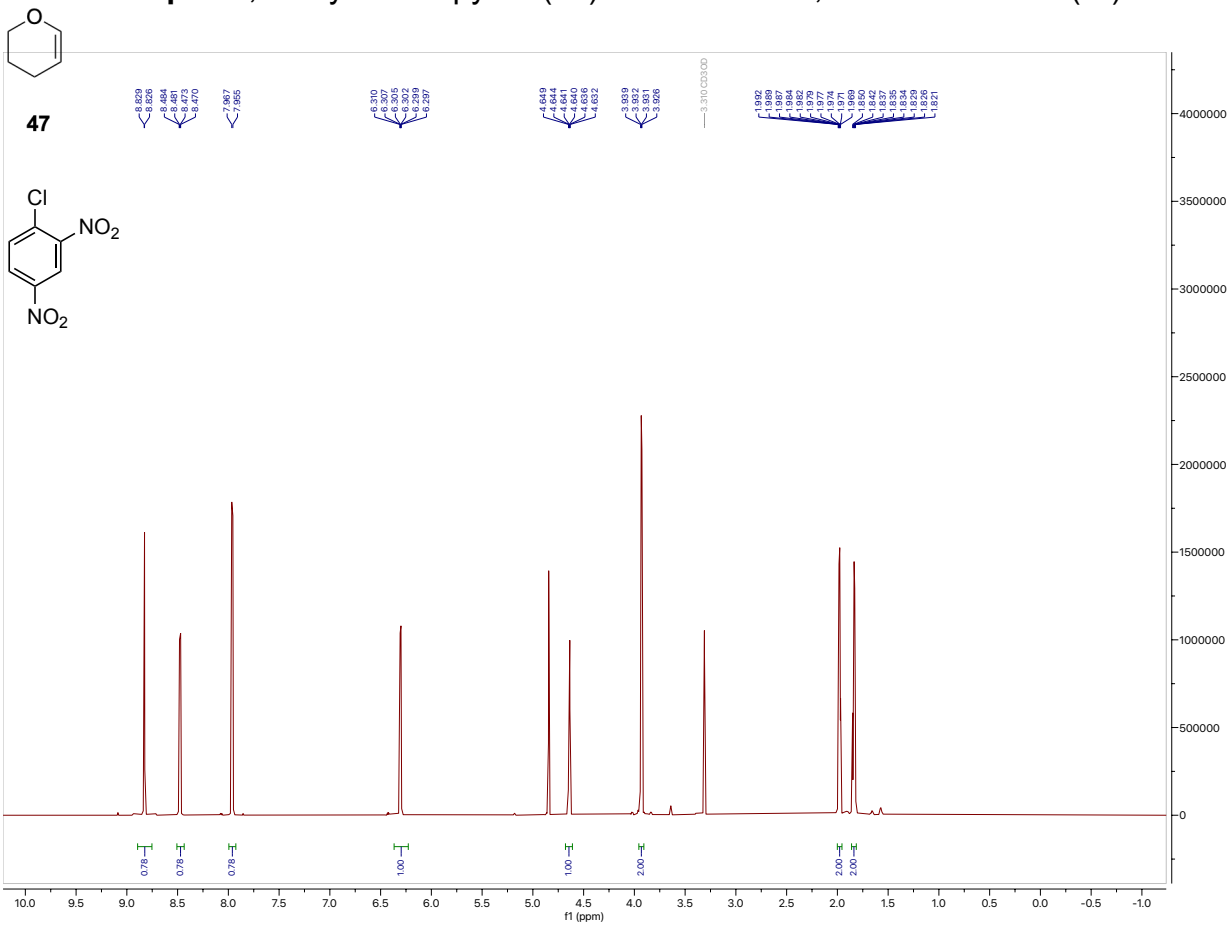
47 **47a**

3,4-dihydro-2*H*-pyran (**47**)

Reaction Time: 45 seconds

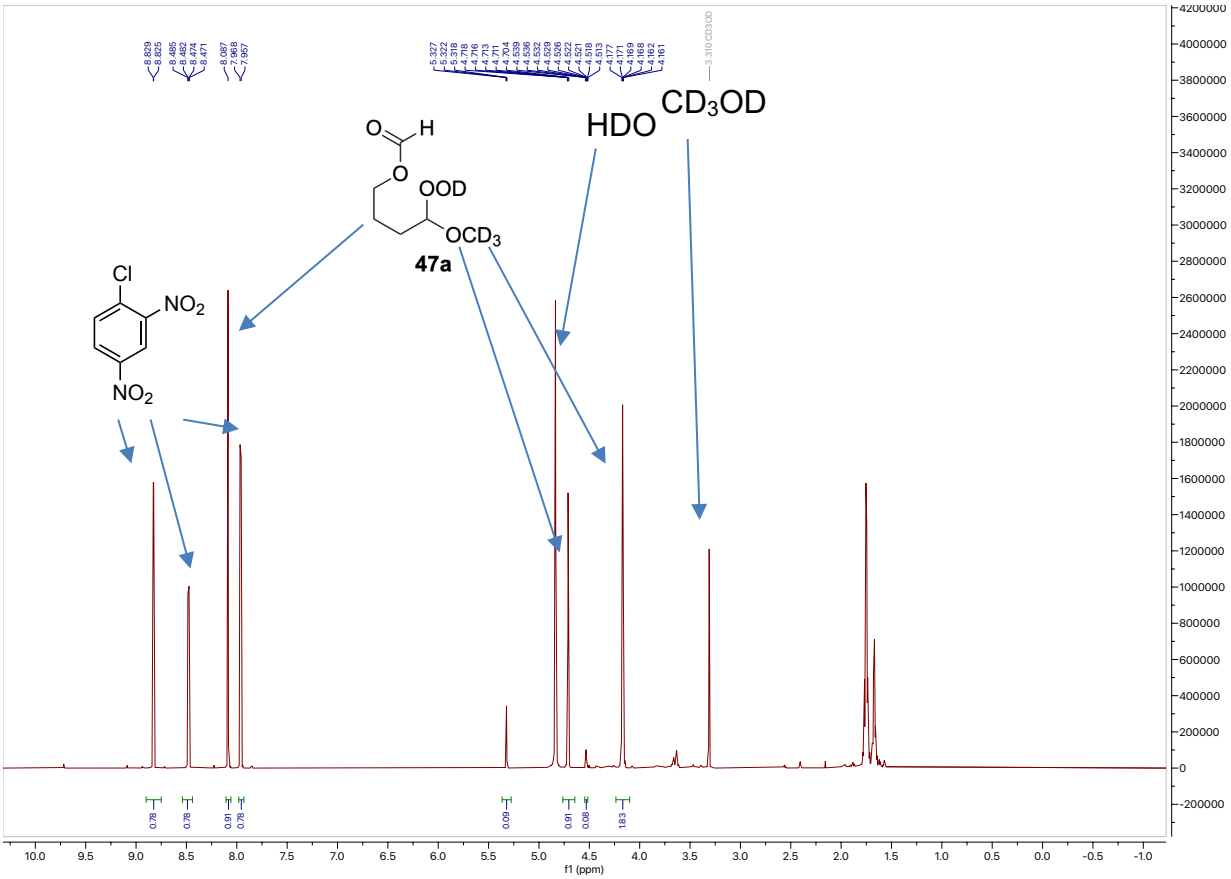
Alkene-to-IS Ratio: 0.78:1.00

Blank Sample: 3,4-dihydro-2*H*-pyran (**47**) and 1-chloro-2,4-dinitrobenzene (**IS**)



^{1}H NMR (800 MHz, CD_3OD), D1 = 10 s, 32 scans

Representative ^{1}H NMR: 3,4-dihydro-2*H*-pyran (**47**) ozonolysis



^{1}H NMR (800 MHz, CD_3OD), D1 = 10 s, 32 scans

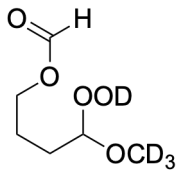
Characterization Data: 3,4-dihydro-2*H*-pyran (**47**)



47

3,4-dihydro-2*H*-pyran (**47**)

^{1}H NMR (800 MHz, MeOD) δ 6.30 (dt, *J* = 6.3, 2.0 Hz, 1H), 4.64 (dt, *J* = 6.5, 3.8 Hz, 1H), 3.93 (dd, *J* = 5.9, 4.6 Hz, 2H), 1.98 (tdd, *J* = 6.3, 3.8, 2.0 Hz, 2H), 1.90 – 1.75 (m, 2H).



47a

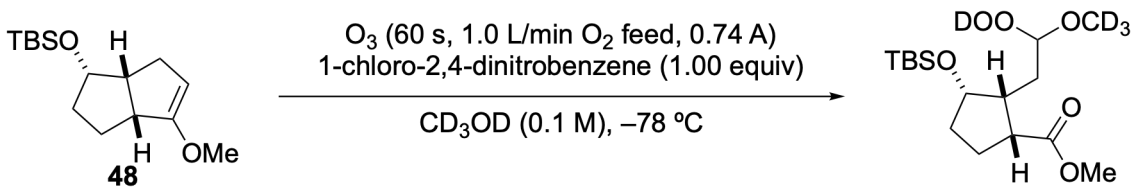
4-deuteroperoxy-4-(methoxy-d_3)butyl formate (**47a**)

^{1}H NMR (800 MHz, MeOD) δ 8.09 (s, 1H), 4.71 (t, *J* = 5.4 Hz, 1H), 4.17 (t, *J* = 6.2 Hz, 2H), 1.85 – 1.59 (m, 4H).

The signals were measured from the ^{1}H NMR of the crude reaction mixture.

Table 6.47 3,4-dihydro-2*H*-pyran (**47**) qNMR Data

Trial	**47a**
1	91
2	92
3	91.3
average	91
st. dev.	0.47

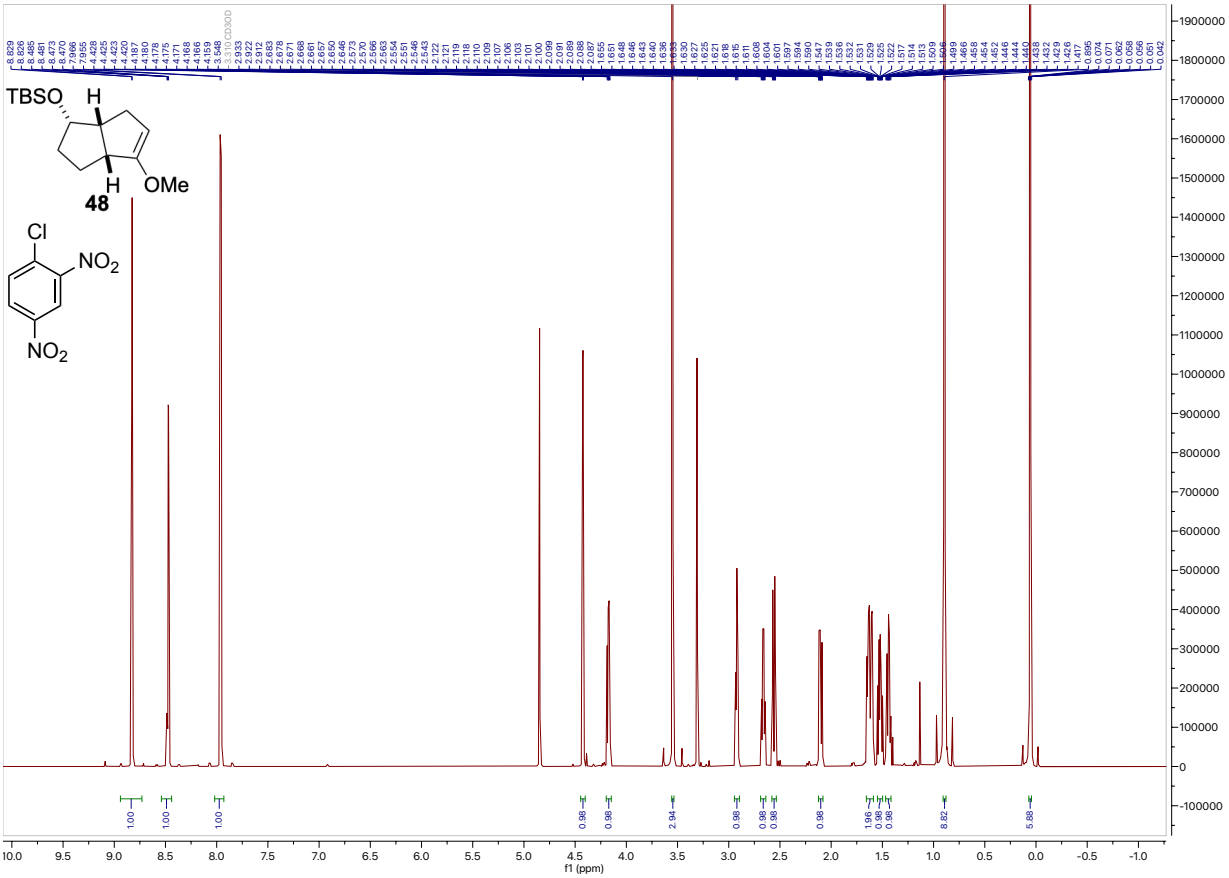


tert-butyl(((1S*,3aR*,6aR*)-4-methoxy-1,2,3,3a,6,6a-hexahydropentalen-1-yl)oxy)dimethylsilane (**48**)

Reaction Time: 60 seconds

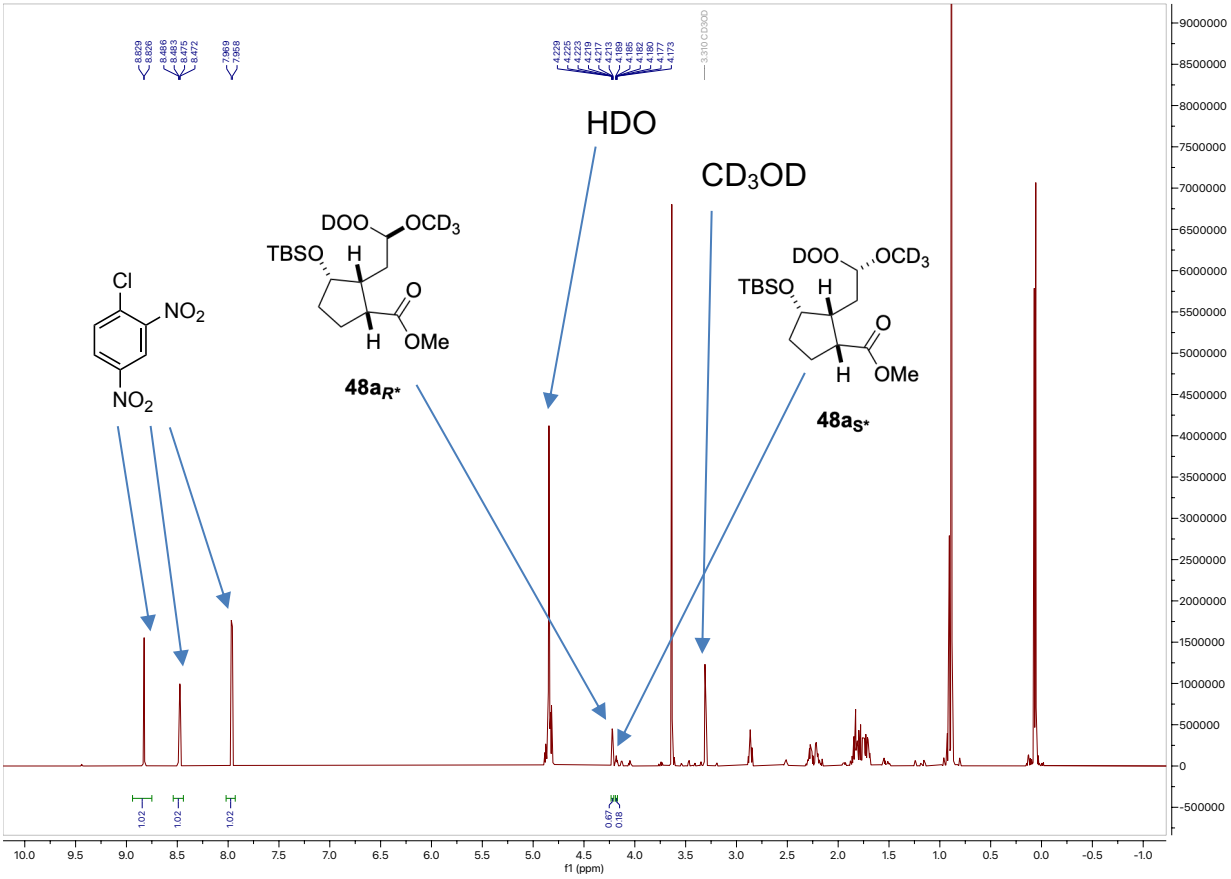
Alkene-to-IS Ratio: 0.98:1.00

Blank Sample: *tert*-butyl(((1S*,3aR*,6aR*)-4-methoxy-1,2,3,3a,6,6a-hexahydropentalen-1-yl)oxy)dimethylsilane (**48**) and 1-chloro-2,4-dinitrobenzene (**IS**)



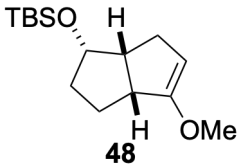
^{1}H NMR (800 MHz, CD_3OD), D1 = 10 s, 32 scans

Representative ^{1}H NMR: *tert*-butyl(((1S*,3aR*,6aR*)-4-methoxy-1,2,3,3a,6,6a-hexahydropentalen-1-yl)oxy)dimethylsilane (**48**) ozonolysis



^{1}H NMR (800 MHz, $CDCl_3$), D1 = 10 s, 32 scans

Characterization Data: *tert*-butyl(((1S*,3aR*,6aR*)-4-methoxy-1,2,3,3a,6,6a-hexahydropentalen-1-yl)oxy)dimethylsilane (**48**)

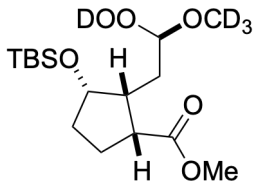


48

tert-butyl(((1S*,3aR*,6aR*)-4-methoxy-1,2,3,3a,6,6a-hexahydropentalen-1-yl)oxy)dimethylsilane (**48**)

^{1}H NMR (800 MHz, MeOD) δ 4.42 (q, *J* = 2.2 Hz, 1H), 4.17 (ddd, *J* = 9.5, 7.6, 5.4 Hz, 1H), 3.55 (s, 3H), 2.92 (t, *J* = 8.5 Hz, 1H), 2.66 (qd, *J* = 9.2, 3.6 Hz, 1H), 2.61 – 2.49 (m,

1H), 2.10 (dddd, *J* = 15.5, 9.7, 2.3, 0.9 Hz, 1H), 1.62 (dddt, *J* = 25.1, 11.4, 5.8, 2.6 Hz, 2H), 1.56 – 1.49 (m, 1H), 1.44 (tdd, *J* = 11.4, 9.4, 6.6 Hz, 1H), 0.90 (s, 9H), 0.06 (d, *J* = 2.1 Hz, 6H).

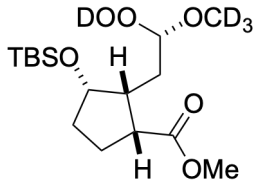


48a$_{R^*}$

methyl (1*R**,2*R**,3*S**)-3-((*tert*-butyldimethylsilyl)oxy)-2-((*R**)-2-deuteroperoxy-2-(methoxy-d_3)ethyl)cyclopentane-1-carboxylate (**48a$_{R^*}$**)

^{1}H NMR (800 MHz, MeOD) δ 4.84 (dd, *J* = 7.0, 5.4 Hz, 1H), 4.24 (td, *J* = 4.8, 2.7 Hz, 1H), 3.64 (s, 3H), 2.96 – 2.78 (m, 1H), 2.33 – 2.17 (m, 2H), 1.98 – 1.59 (m, 5H), 0.88 (d, *J* = 1.2 Hz, 9H), 0.06 (s, 6H).

The peroxide α-CH peak was measured from the ^{1}H NMR of the crude reaction mixture. The other peaks were deduced from the 1D selective gradient TOCSY spectrum.



48a$_{S^*}$

methyl (1*R**,2*R**,3*S**)-3-((*tert*-butyldimethylsilyl)oxy)-2-((*S**)-2-deuteroperoxy-2-(methoxy-d_3)ethyl)cyclopentane-1-carboxylate (**48a$_{S^*}$**)

^{1}H NMR (800 MHz, MeOD) δ 4.90 (t, *J* = 6.1 Hz, 1H), 4.23 – 4.16 (m, 1H), 3.63 (s, 3H), 2.90 (td, *J* = 8.0, 5.2 Hz, 1H), 2.43 – 2.26 (m, 1H), 2.26 – 2.15 (m, 1H), 1.94 – 1.80 (m, 2H), 1.81 – 1.66 (m, 3H), 0.91 (s, 9H), 0.07 (s, 6H).

The peroxide α-CH peak was measured from the ^{1}H NMR of the crude reaction mixture. The other peaks were deduced from the 1D selective gradient TOCSY spectrum.

The configurations for the peroxides were assigned based on the modified Felkin–Ahn model (the A-value for OTBS is larger than the A-value for CO_2Me) for the capture of the Criegee intermediate by MeOH-d_4.

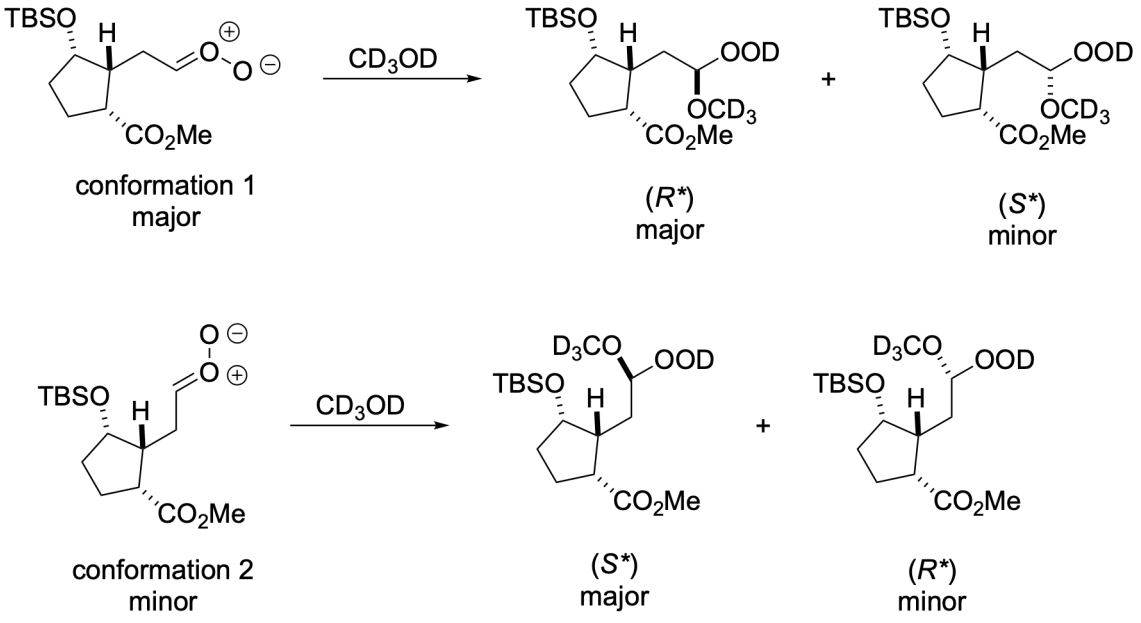
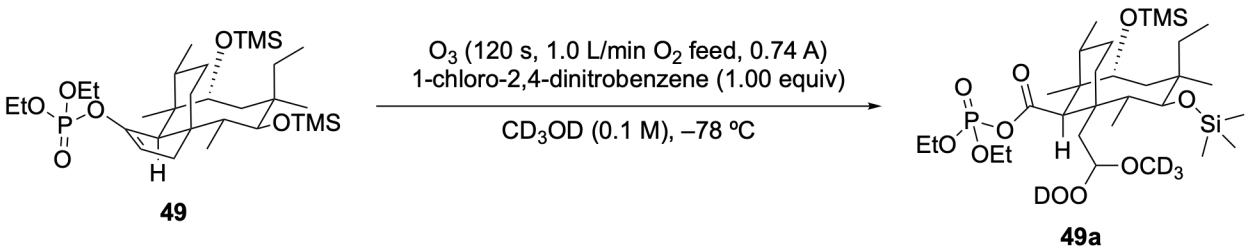


Figure 6.35 Felkin–Ahn Analysis of **48**

Table 6.48 *tert*-butyl(((1S*,3aR*,6aR*)-4-methoxy-1,2,3,3a,6,6a-hexahydropentalen-1-yl)oxy)dimethylsilane (**48**) qNMR Data

Trial	**48a**$_{R^*}$	**48a**$_{S^*}$	***d.r.***

1	67	18	3.7:1.0
2	67	18	3.7:1.0
3	67	17	3.9:1.0
average	67	18	3.7:1.0
st. dev.	0	0.58	0.12

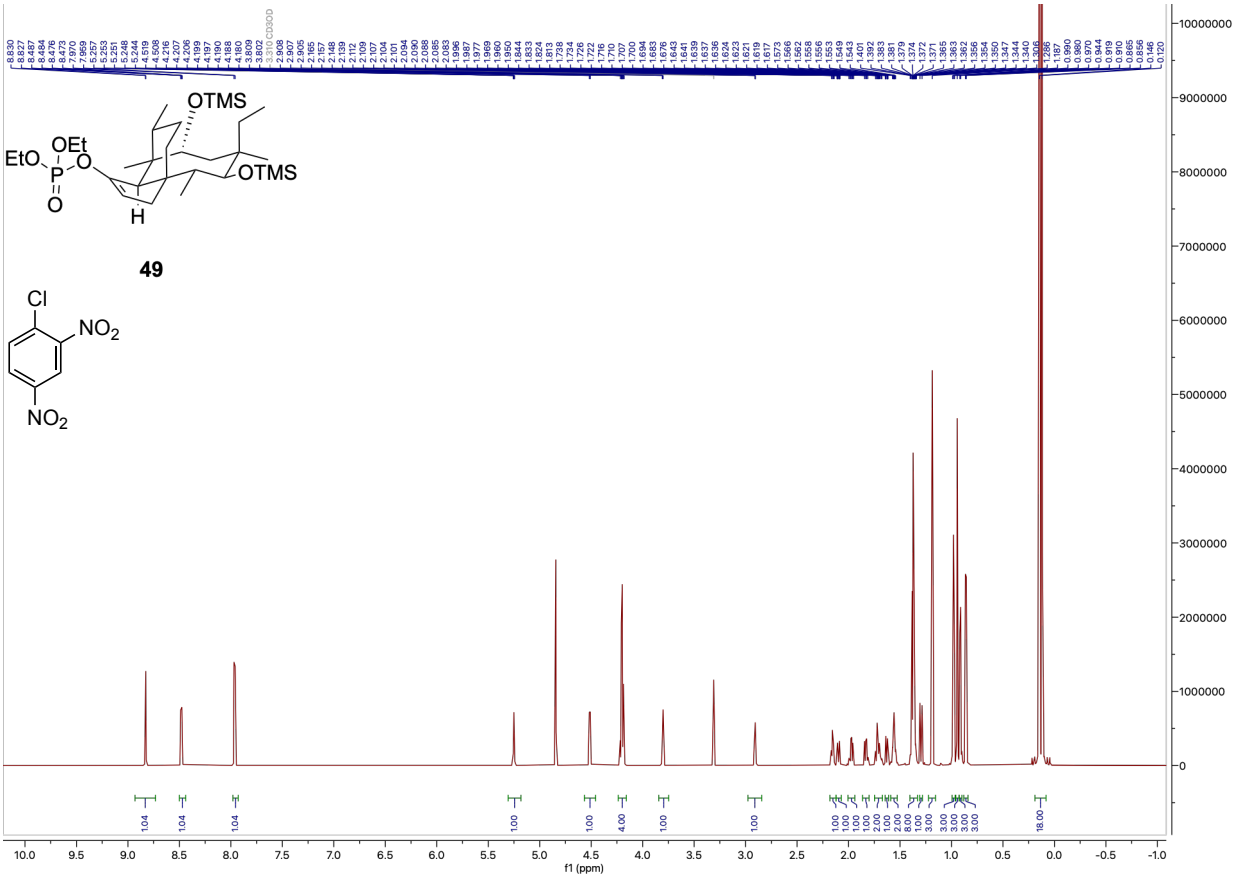


(+)-bis(trimethylsilyl)hydromutilin enol diethylphosphate (**49**)

Reaction Time: 120 seconds

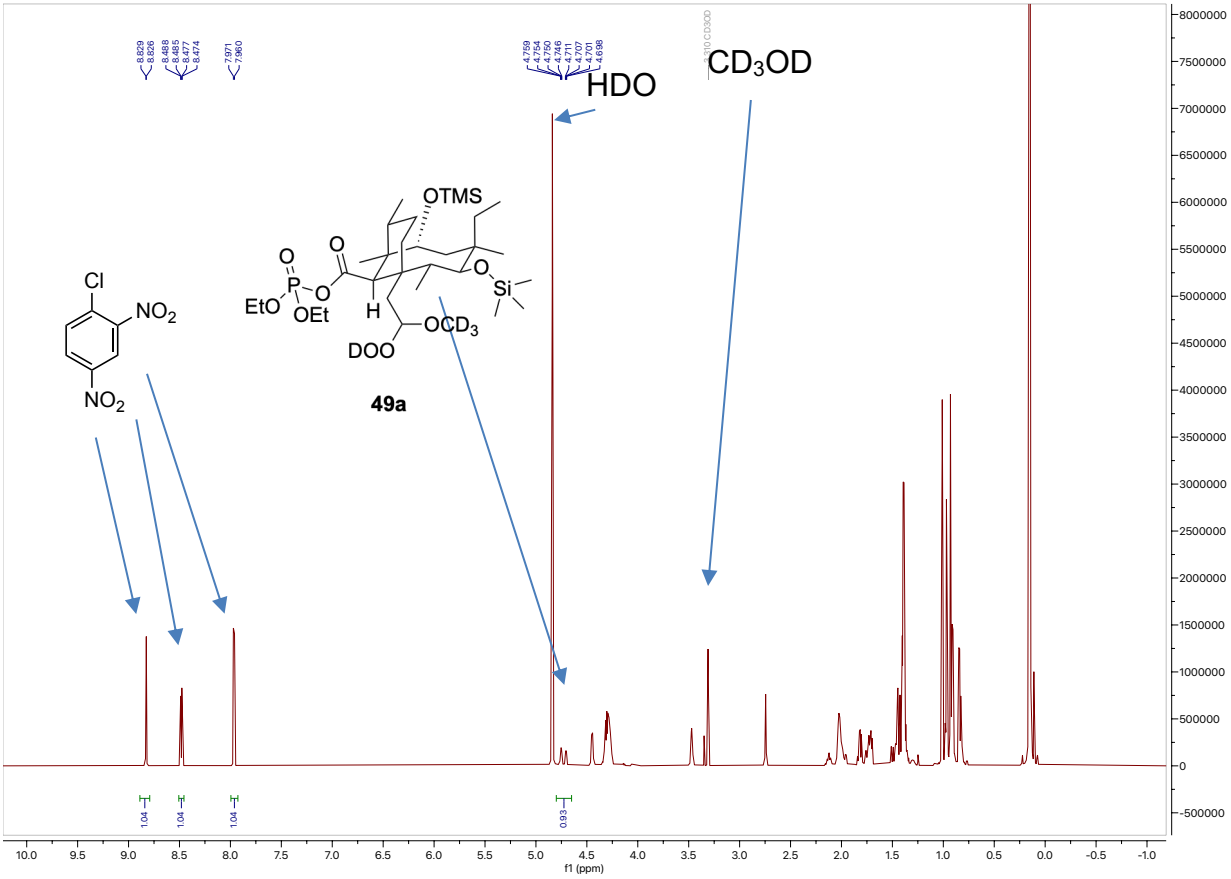
Alkene-to-IS Ratio: 0.96:1.00

Blank Sample: (+)-bis(trimethylsilyl)hydromutilin enol diethylphosphate (**49**) and 1-chloro-2,4-dinitrobenzene (**IS**)



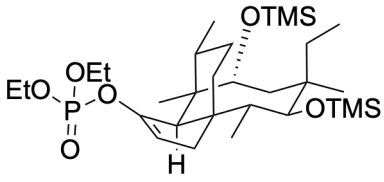
^{1}H NMR (800 MHz, CD_3OD), D1 = 10 s, 32 scans

Representative ^{1}H NMR: (+)-bis(trimethylsilyl)hydromutilin enol diethylphosphate (**49**) ozonolysis



^{1}H NMR (800 MHz, CD_3OD), D1 = 10 s, 32 scans

Characterization Data: (+)-bis(trimethylsilyl)hydromutilin enol diethylphosphate (**49**)

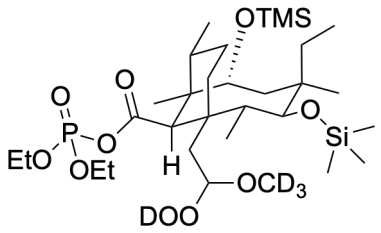


49

(+)-bis(trimethylsilyl)hydromutilin enol diethylphosphate (**49**)

^{1}H NMR (800 MHz, MeOD) δ 5.25 (q, *J* = 2.5 Hz, 1H), 4.51 (d, *J* = 8.5 Hz, 1H), 4.20 (dq, *J* = 8.2, 7.1 Hz, 4H), 3.81 (d, *J* = 6.3 Hz, 1H), 2.98 – 2.84 (m, 1H), 2.16 (p, *J* = 7.1 Hz, 1H), 2.10 (ddt, *J* = 14.9, 4.6, 2.4 Hz, 1H), 1.97 (dq, *J* = 15.4, 7.6 Hz, 1H), 1.83 (dd, *J* = 928

16.1, 8.4 Hz, 1H), 1.75 – 1.67 (m, 2H), 1.63 (ddt, *J* = 14.9, 3.1, 1.3 Hz, 1H), 1.59 – 1.53 (m, 2H), 1.37 (tt, *J* = 7.0, 1.4 Hz, 8H), 1.30 (d, *J* = 16.2 Hz, 1H), 1.19 (s, 3H), 0.98 (t, *J* = 7.6 Hz, 3H), 0.94 (s, 3H), 0.91 (d, *J* = 6.8 Hz, 3H), 0.86 (d, *J* = 7.1 Hz, 3H), 0.13 (d, *J* = 21.0 Hz, 18H).



49a

(diethyl phosphoric) (1*S*,2*R*,3*S*,4*R*,6*S*,7*R*,8*R*,11*S*)-4-ethyl-1-(2-deuteroperoxy-2-(methoxy-d_3)ethyl)-2,4,8-trimethyl-3,6-bis((trimethylsilyl)oxy)bicyclo[5.3.1]undecane-11-carboxylic anhydride (**49a**)

^{1}H NMR (800 MHz, MeOD) δ [4.83 – 4.72 (m, 0.58H) and 4.72 (dd, *J* = 7.4, 2.8 Hz, 0.42H)], 4.53 – 4.40 (m, 1H), 4.37 – 4.23 (m, 4H), 3.47 (dd, *J* = 7.3, 3.9 Hz, 1H), 2.74 (s, 1H), 2.18 – 1.67 (m, 6H), 1.58 – 1.24 (m, 10H), 1.07 – 0.75 (m, 15H), 0.18 – 0.14 (m, 18H).

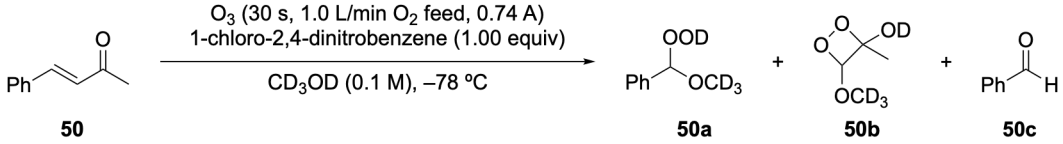
The peroxide α-CH peak was measured from the ^{1}H NMR of the crude reaction mixture. The peroxide chain signals were deduced from the 1D selective gradient TOCSY spectrum. The remaining peaks were deduced from the ^{1}H NMR of the crude reaction mixture.

Table 6.49 (+)-bis(trimethylsilyl)hydromutilin enol diethylphosphate (**49**) qNMR Data

Trial	**49a**	***d.r.***

1	87	1.0:1.7
2	88	1.0:1.4
3	93	1.0:1.4
average	89.3	1.0:1.5
st. dev.	3.06	

6.8.4.9 α,β-Unsaturated Carbonyls

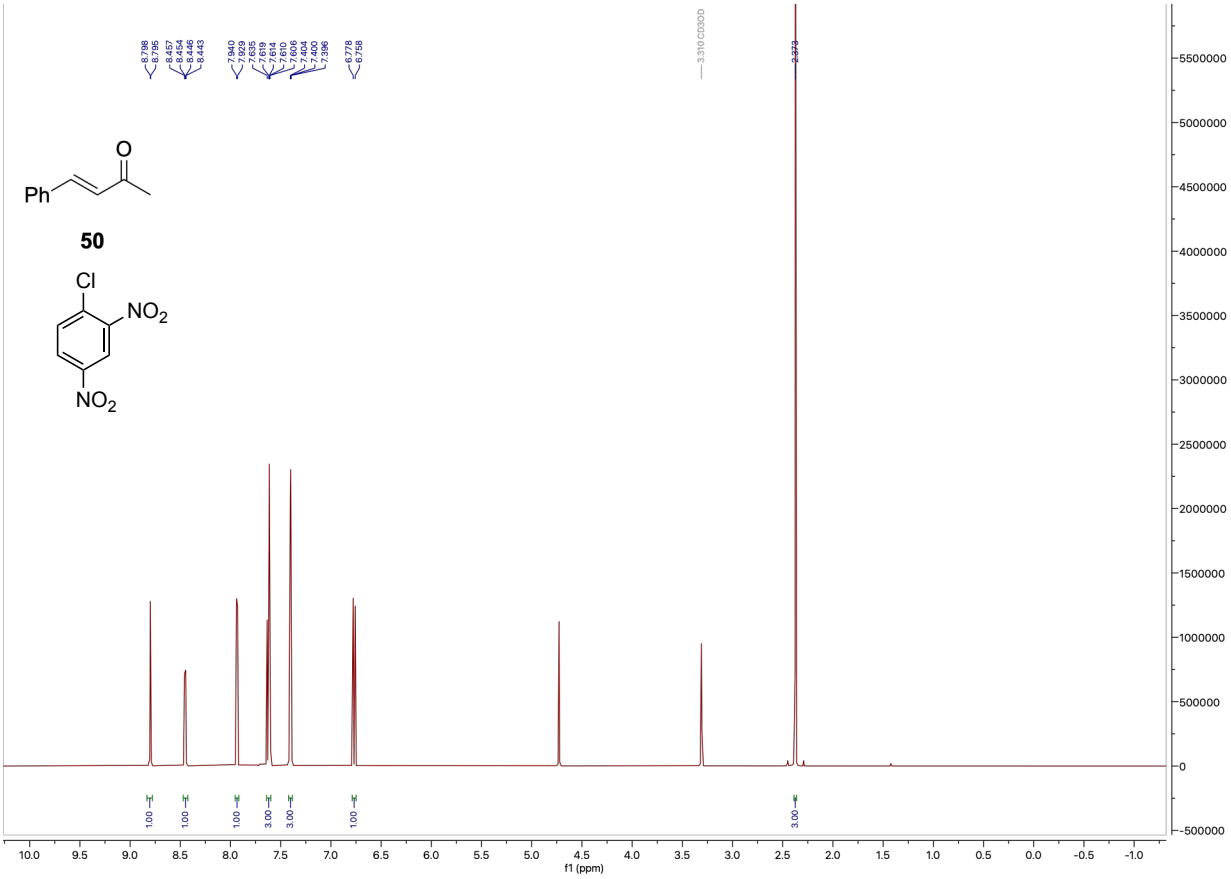


methyl styryl ketone (**50**)

Reaction Time: 30 seconds

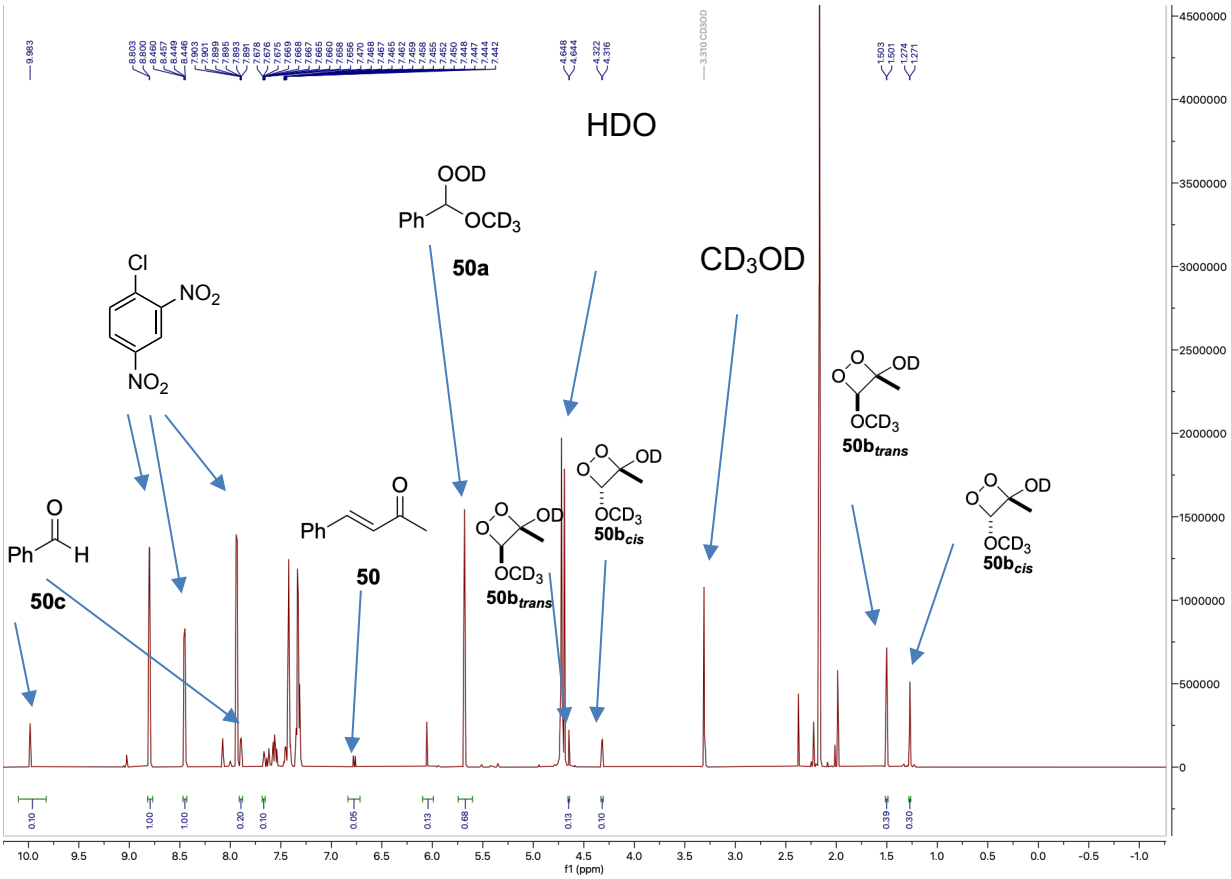
Alkene-to-IS Ratio: 1.00:1.00

Blank Sample: methyl styryl ketone (**50**) and 1-chloro-2,4-dinitrobenzene (**IS**)



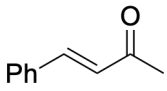
^{1}H NMR (800 MHz, CD_3OD), D1 = 10 s, 32 scans

Representative ^{1}H NMR: methyl styryl ketone (**50**) ozonolysis



^{1}H NMR (800 MHz, CD_3OD), D1 = 10 s, 32 scans

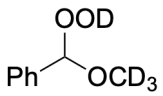
Characterization Data: methyl styryl ketone (**50**)



50

methyl styryl ketone (**50**)

^{1}H NMR (800 MHz, MeOD) δ 7.67 (d, *J* = 16.0 Hz, 1H), 7.57 (ddt, *J* = 4.7, 3.0, 1.7 Hz, 2H), 7.39 (td, *J* = 4.5, 2.5 Hz, 3H), 6.50 (dd, *J* = 16.0, 1.7 Hz, 1H), 2.37 (s, 3H).

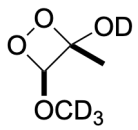


50a

(deuteroperoxy(methoxy-d_3)methyl)benzene (**50a**)

^{1}H NMR (800 MHz, MeOD) δ 7.47 – 7.28 (m, 5H), 5.68 (s, 1H).

The peroxide α-CH peak was measured from the ^{1}H NMR of the crude reaction mixture. The other peaks were in assigned in accordance with the literature [40].

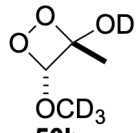


50b*trans*

(3*S**,4*S**)-4-(methoxy-d_3)-3-methyl-1,2-dioxetan-3-ol-*d*

^{1}H NMR (800 MHz, MeOD) δ 4.65 (d, *J* = 3.0 Hz, 1H), 1.50 (d, *J* = 1.7 Hz, 3H).

The signals were measured and deduced from the ^{1}H NMR of the crude reaction mixture.

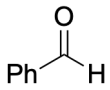


50b*cis*

(3*S**,4*R**)-4-(methoxy-d_3)-3-methyl-1,2-dioxetan-3-ol-*d*

^{1}H NMR (800 MHz, MeOD) δ 4.32 (d, *J* = 4.3 Hz, 1H), 1.27 (d, *J* = 2.5 Hz, 3H).

The signals were measured and deduced from the ^{1}H NMR of the crude reaction mixture.



50c

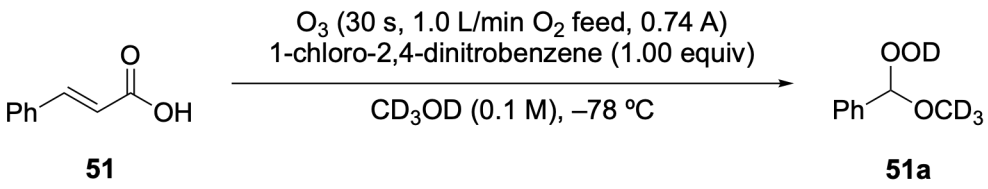
benzaldehyde (**50c**)

^{1}H NMR (800 MHz, MeOD) δ 9.98 (s, 1H), 7.91 – 7.87 (m, 2H), 7.68 – 7.65 (m, 1H), 7.47 – 7.44 (m, 2H).

The signals were measured and deduced from the ^{1}H NMR of the crude reaction mixture.

Table 6.50 methyl styryl ketone (**50**) qNMR Data

Trial	% conversion	%50a	%50b$_{trans}$	%50b$_{cis}$	%50c	normalized %50a	normalized %50b$_{trans}$	normalized %50b$_{cis}$	normalized %50c
1	95	68	13	10	10	80	14	11	11
2	100	71	15	10	10	79	15	10	10
3	92	66	13	10	10	80	14	11	11
average						80	14	11	11
st. dev.						0.58	0.47	0.47	0.47



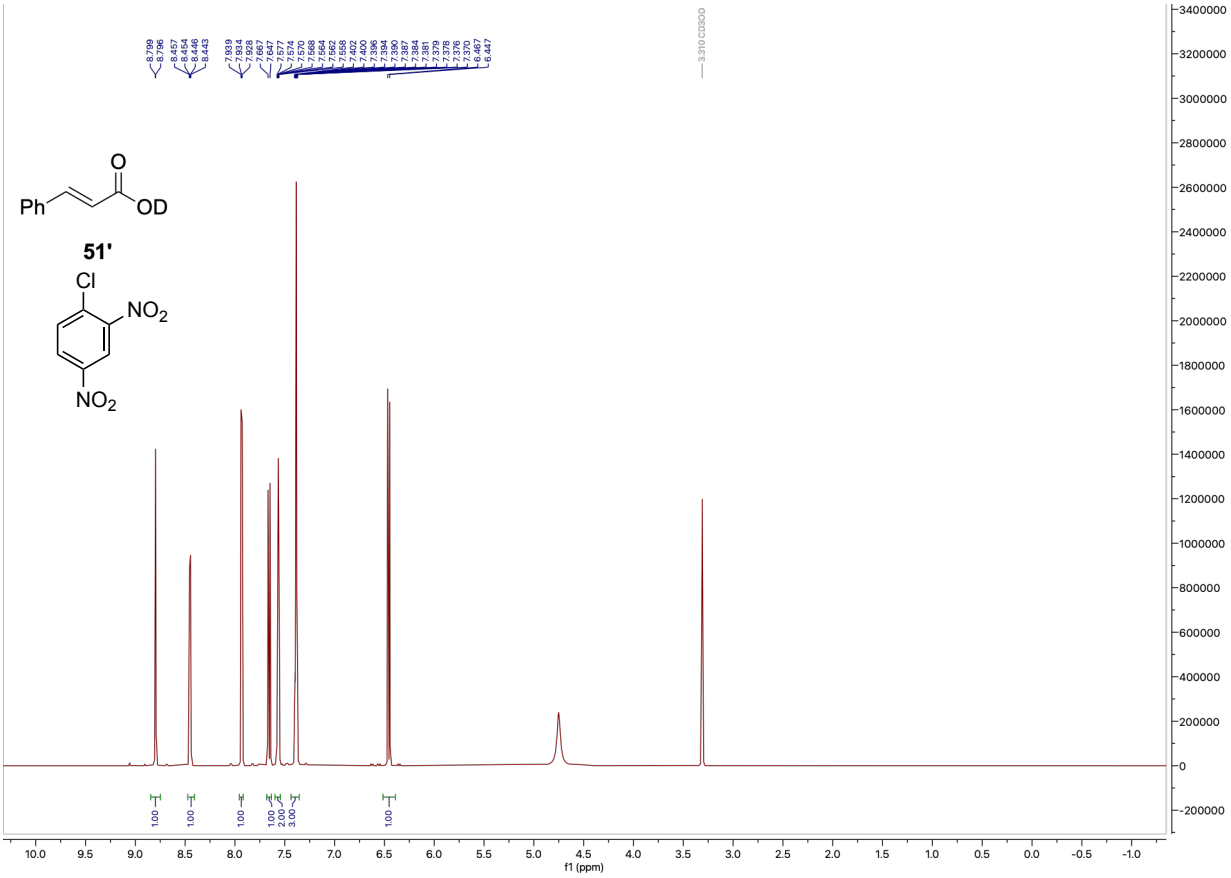
51 **51a**

cinnamic acid (**51**)

Reaction Time: 30 seconds

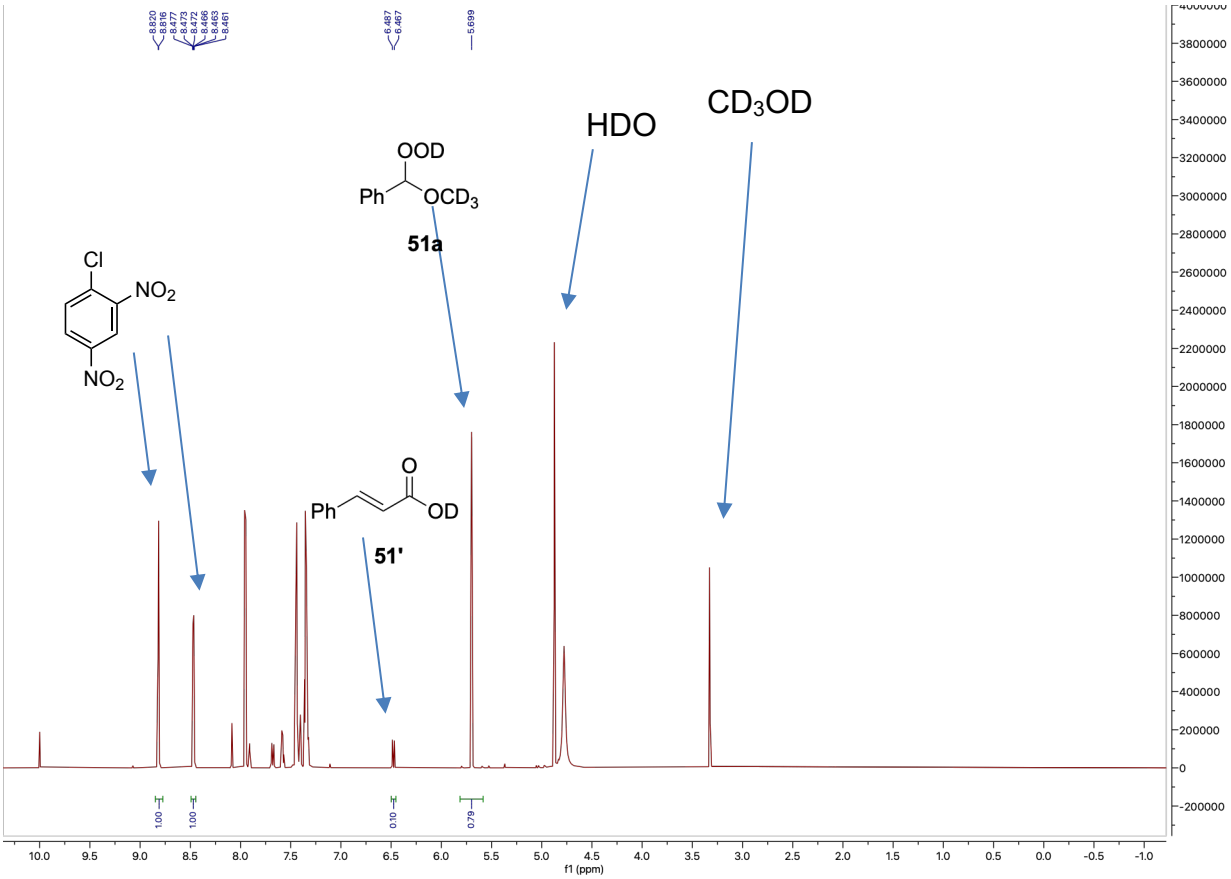
Alkene-to-IS Ratio: 1.00:1.00

Blank Sample: cinnamic acid-*d* (**51'**) and 1-chloro-2,4-dinitrobenzene (**IS**)



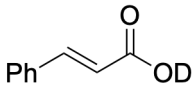
^{1}H NMR (800 MHz, CD_3OD), D1 = 10 s, 32 scans

Representative ^{1}H NMR: cinnamic acid (**51**) ozonolysis



^{1}H NMR (800 MHz, CD_3OD), D1 = 10 s, 32 scans

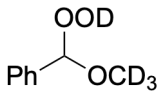
Characterization Data: cinnamic acid (**51**)



51'

cinnamic acid-*d* (**51'**)

^{1}H NMR (800 MHz, MeOD) δ 7.66 (d, *J* = 16.0 Hz, 1H), 7.57 (dt, *J* = 7.0, 2.3 Hz, 2H), 7.42 – 7.33 (m, 3H), 6.46 (d, *J* = 16.0 Hz, 1H).



51a

(deuteroperoxy(methoxy-d_3)methyl)benzene (**51a**)

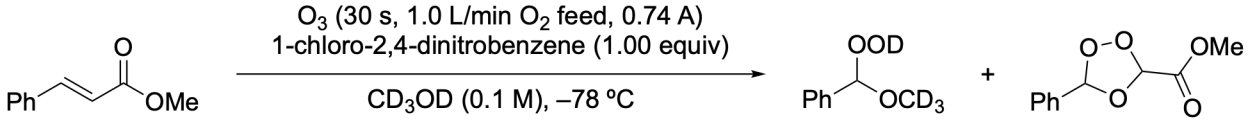
^{1}H NMR (800 MHz, MeOD) δ 7.47 – 7.28 (m, 5H), 5.68 (s, 1H).

The peroxide α-CH peak was measured from the ^{1}H NMR of the crude reaction mixture.

The other peaks were in assigned in accordance with the literature [40].

Table 6.51 cinnamic acid (**51**) qNMR Data

Trial	**% conversion**	**%51a**	**normalized %51a**
1	100	89	89
2	90	79	88
3	93	83	89
average			89
st. dev.			0.58



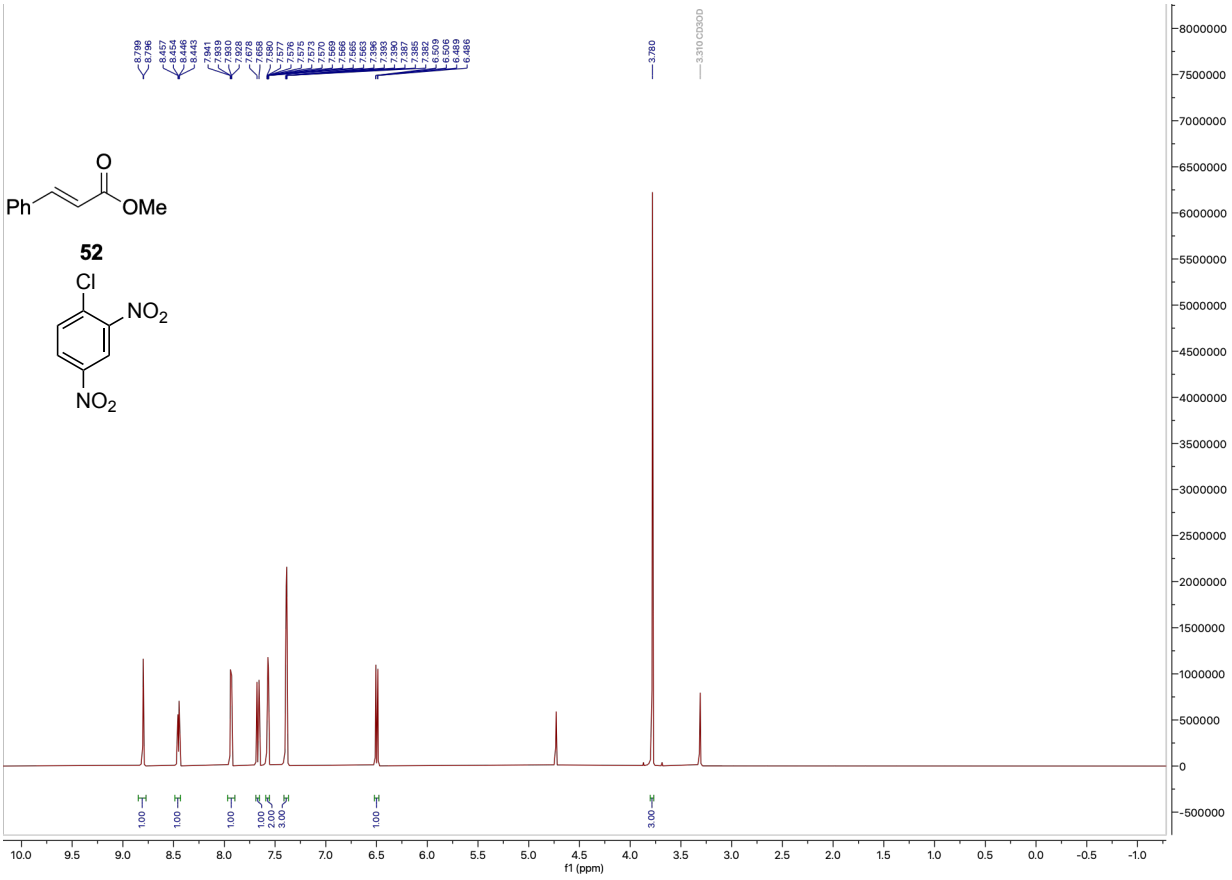
52 **52a** **52b**

methyl cinnamate (**52**)

Reaction Time: 30 seconds

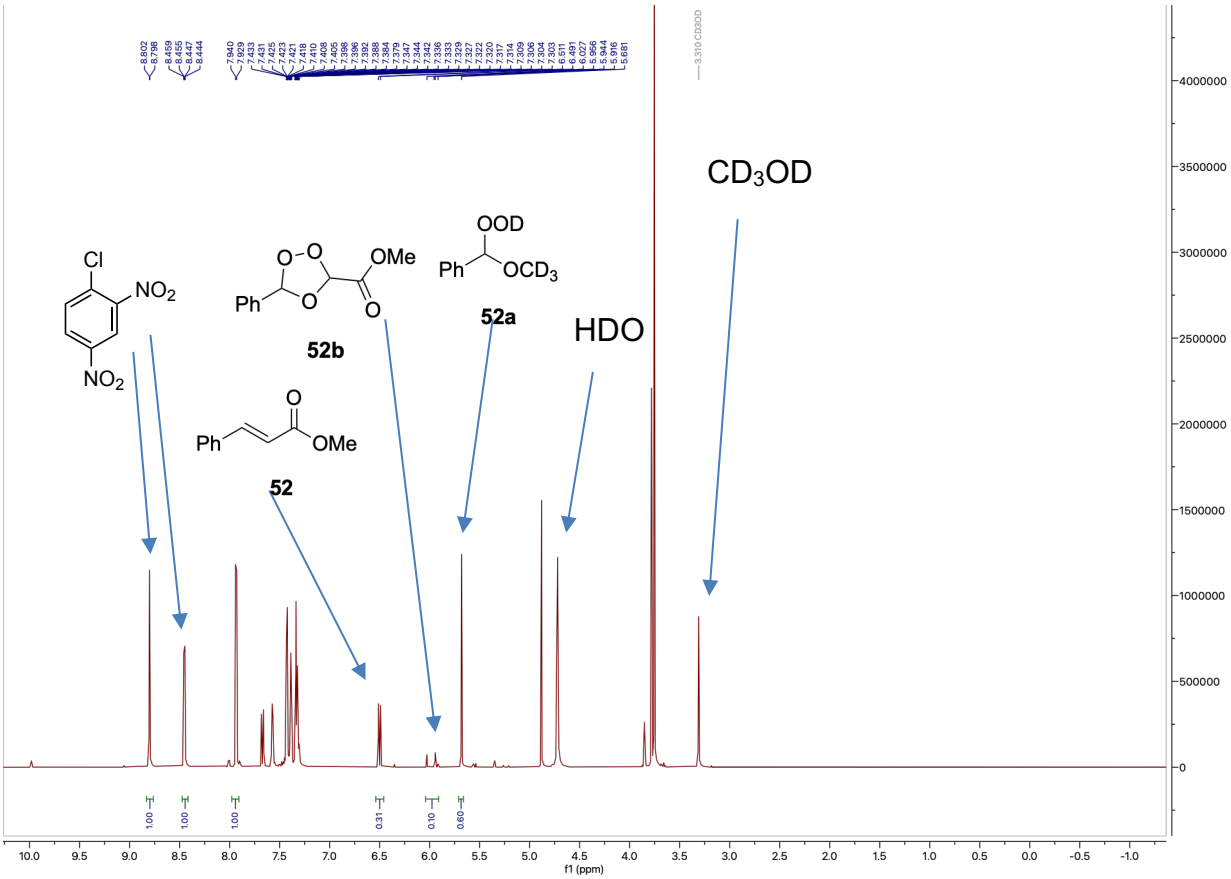
Alkene-to-IS Ratio: 1.00:1.00

Blank Sample: methyl cinnamate (**52**) and 1-chloro-2,4-dinitrobenzene (**IS**)



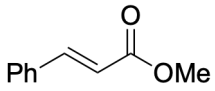
^{1}H NMR (800 MHz, CD_3OD), D1 = 10 s, 32 scans

Representative ^{1}H NMR: methyl cinnamate (**52**) ozonolysis



^{1}H NMR (800 MHz, $CDCl_3$), D1 = 10 s, 32 scans

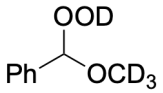
Characterization Data: methyl cinnamate (**52**)



52

methyl cinnamate (**52**)

^{1}H NMR (800 MHz, MeOD) δ 7.67 (d, *J* = 16.0 Hz, 1H), 7.64 – 7.54 (m, 2H), 7.39 (td, *J* = 4.5, 2.5 Hz, 3H), 6.50 (dd, *J* = 16.0, 1.7 Hz, 1H), 3.78 (s, 3H).

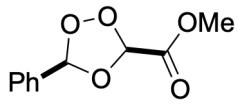


52a

(deuteroperoxy(methoxy-d_3)methyl)benzene (**52a**)

^{1}H NMR (800 MHz, MeOD) δ 7.47 – 7.28 (m, 5H), 5.68 (s, 1H).

The peroxide a-CH peak was measured from the ^{1}H NMR of the crude reaction mixture. The other peaks were in assigned in accordance with the literature [40].

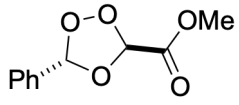


52b*cis*

methyl (*cis*)-5-phenyl-1,2,4-trioxolane-3-carboxylate (**52b*cis***)

^{1}H NMR (800 MHz, MeOD) δ 7.49 – 7.22 (m, 5H), 6.03 (s, 1H), 5.94 (s, 1H), 3.85 (s, 3H).

The aliphatic CH signals were measured from the ^{1}H NMR of the crude reaction mixture. The aromatic signals were deduced from the ^{1}H NMR of the crude reaction mixture.



52b*trans*

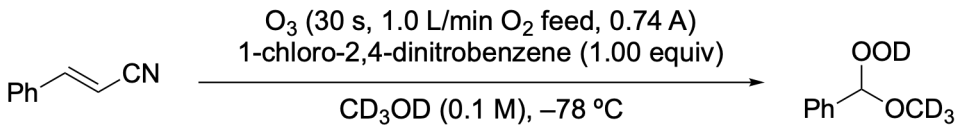
methyl (*trans*)-5-phenyl-1,2,4-trioxolane-3-carboxylate (**52b*trans***)

^{1}H NMR (800 MHz, MeOD) δ 7.49 – 7.22 (m, 5H), 5.96 (s, 1H), 5.92 (s, 1H), 3.85 (s, 3H).

The aliphatic CH signals were measured from the ^{1}H NMR of the crude reaction mixture. The aromatic signals were deduced from the ^{1}H NMR of the crude reaction mixture.

Table 6.52 methyl cinnamate (**52**) qNMR Data

Trial	**% conversion**	**%52a**	**%52b**	**normalized %52a**	**normalized %52b**
1	69	61	5	88	7.2
2	70	61	5	87	7.1
3	69	60	5	88	7.2
average				88	7.2
st. dev.				0.58	0.067



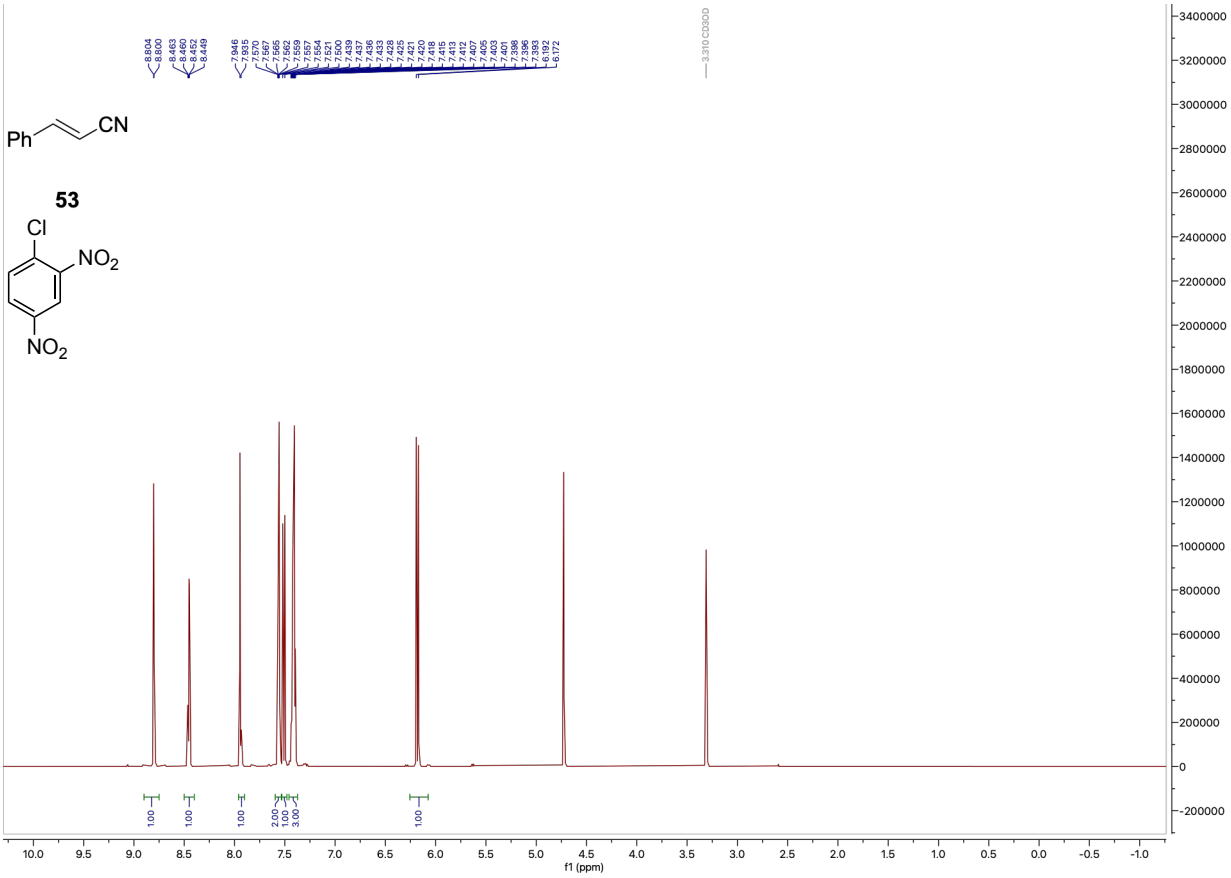
53 **53a**

cinnamonitrile (**53**)

Reaction Time: 30 seconds

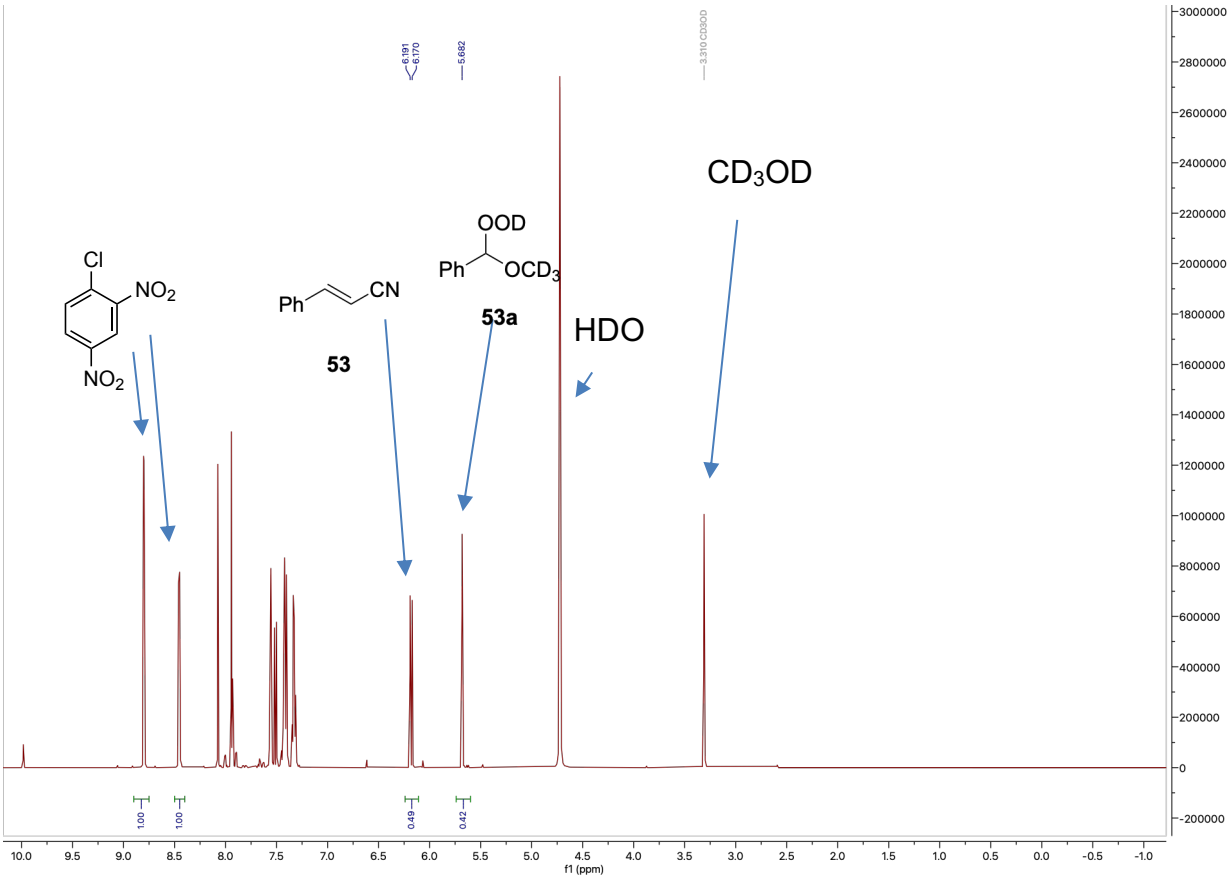
Alkene-to-IS Ratio: 1.00:1.00

Blank Sample: cinnamonitrile (**53**) and 1-chloro-2,4-dinitrobenzene (**IS**)



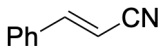
^{1}H NMR (800 MHz, CD_3OD), D1 = 10 s, 32 scans

Representative ^{1}H NMR: cinnamonitrile (**53**) ozonolysis



^{1}H NMR (800 MHz, CD_3OD), D1 = 10 s, 32 scans

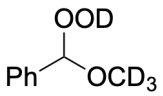
Characterization Data: cinnamonitrile (**53**)



53

cinnamonitrile (**53**)

^{1}H NMR (800 MHz, MeOD) δ 7.56 (dt, *J* = 6.6, 1.8 Hz, 2H), 7.51 (d, *J* = 16.7 Hz, 1H), 7.46 – 7.35 (m, 3H), 6.18 (d, *J* = 16.6 Hz, 1H).



53a

(deuteroperoxy(methoxy-d_3)methyl)benzene (**53a**)

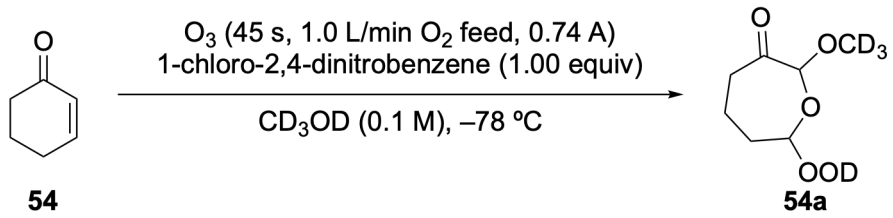
^{1}H NMR (800 MHz, MeOD) δ 7.47 – 7.28 (m, 5H), 5.68 (s, 1H).

The peroxide a-CH peak was measured from the ^{1}H NMR of the crude reaction mixture.

The other peaks were in assigned in accordance with literature [40].

Table 6.53 cinnamonitrile (**53**) qNMR Data

Trial	**% conversion**	**%53a**	**normalized %53a**
1	57	48	84
2	60	50	83
3	51	42	82
average			83
st. dev.			1.0



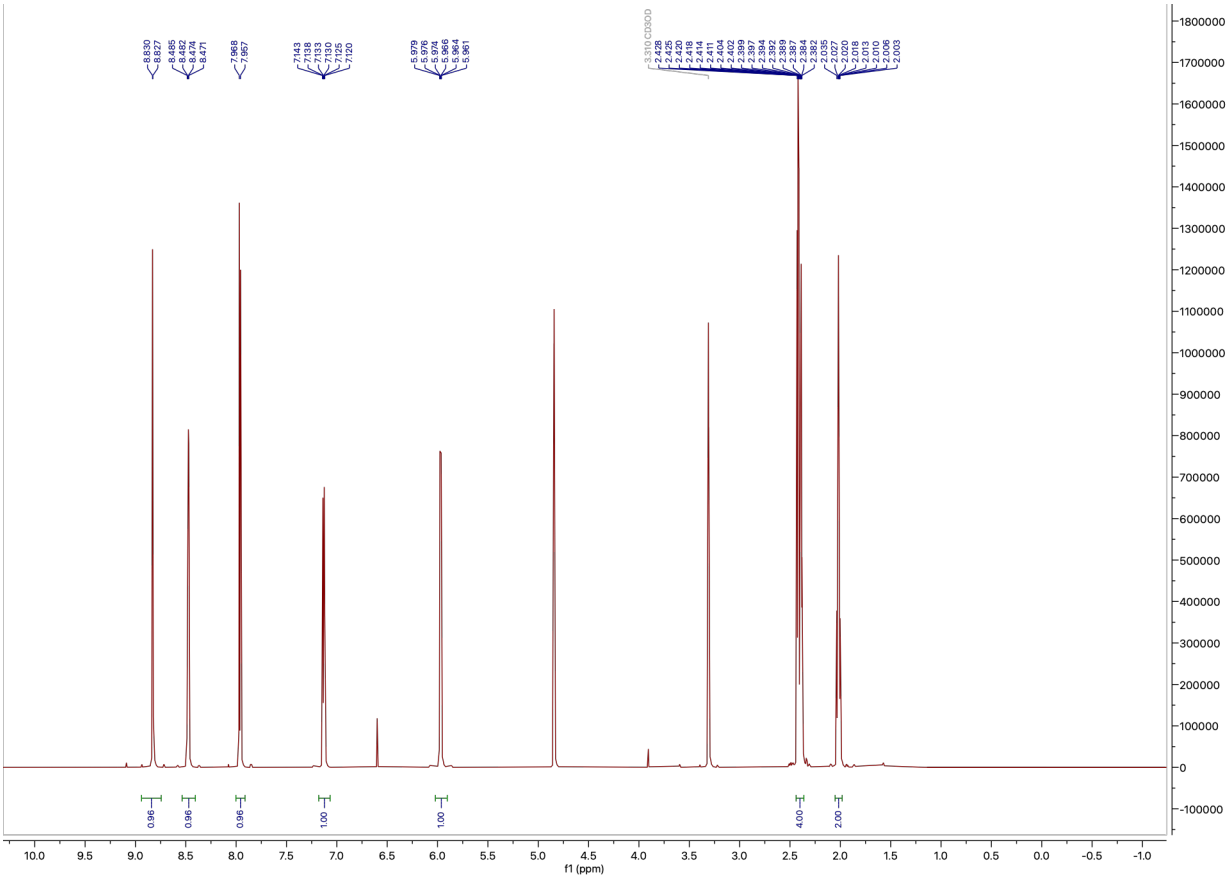
54 **54a**

cyclohexenone (**54**)

Reaction Time: 45 seconds

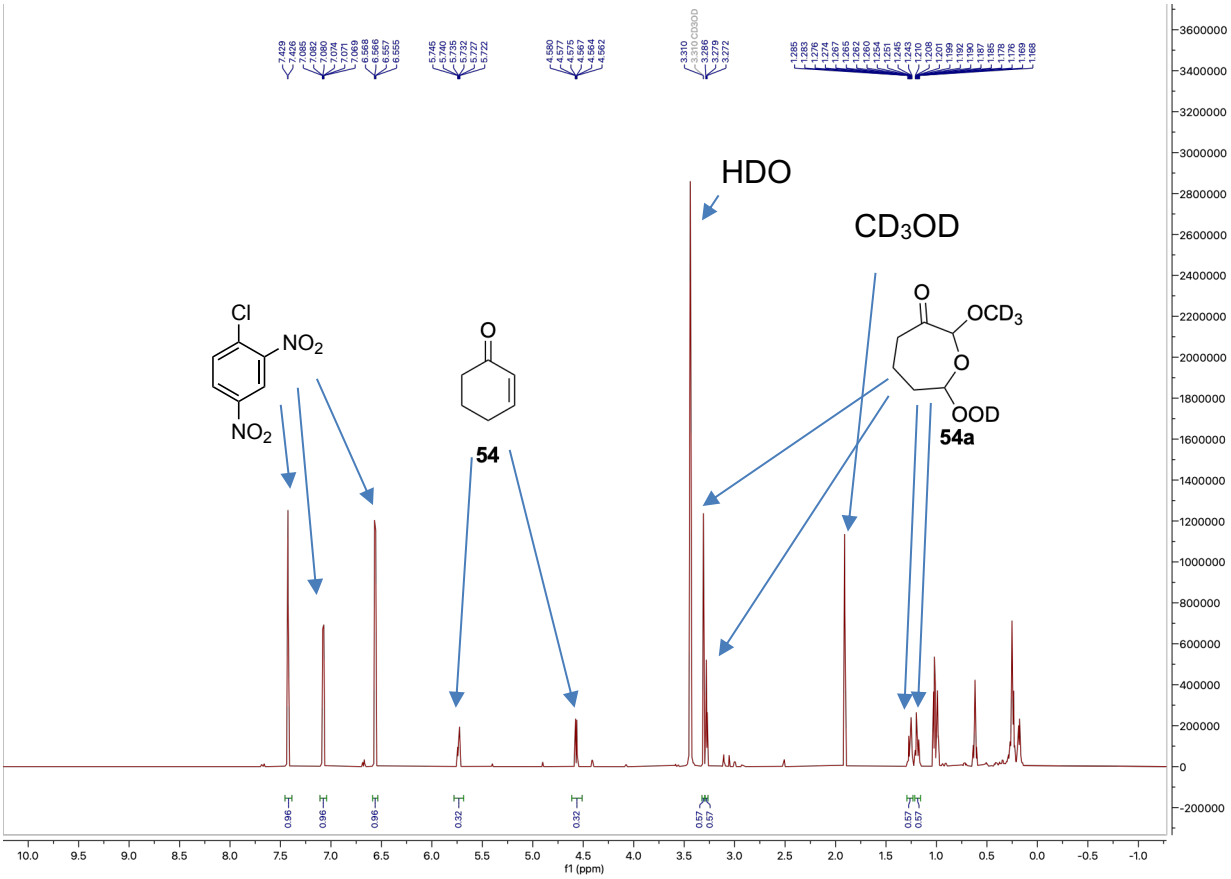
Alkene-to-IS Ratio: 1.04:1.00

Blank Sample: cyclohexenone (**54**) and 1-chloro-2,4-dinitrobenzene (**IS**)



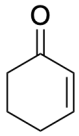
^{1}H NMR (800 MHz, CD_3OD), D1 = 10 s, 32 scans

Representative ^{1}H NMR: cyclohexenone (**54**) ozonolysis



^{1}H NMR (800 MHz, CD_3OD), D1 = 10 s, 32 scans

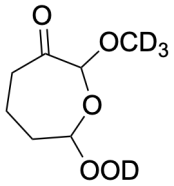
Characterization Data: cyclohexenone (**54**)



54

cyclohexenone (**54**)

^{1}H NMR (800 MHz, MeOD) δ 7.13 (dt, *J* = 10.2, 4.1 Hz, 1H), 5.97 (dt, *J* = 10.1, 2.1 Hz, 1H), 2.83 – 2.29 (m, 4H), 2.28 – 1.72 (m, 2H).

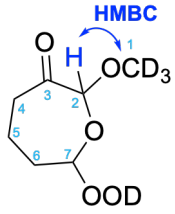


54a

7-deuteroperoxy-2-(methoxy-d_3)oxepan-3-one (**54a**)

^{1}H NMR (800 MHz, MeOD) δ 4.73 – 4.69 (m, 1H), 4.69 – 4.65 (m, 1H), 2.71 – 2.62 (m, 1H), 2.62 – 2.53 (m, 1H), 1.69 – 1.61 (m, 3H), 1.61 – 1.54 (m, 1H).

The acetal and carbonyl α-CH peaks were measured from the ^{1}H NMR of the crude reaction mixture. The other ^{1}H signals were deduced from the 1D selective gradient TOCSY spectrum. HMBC was used to assign configuration.



54a

Table 6.54 cyclohexenone (**54**) qNMR Data

Trial	% conversion	%54a	normalized %54a
1	55	47	85
2	68	57	84
3	69	59	84
average			84
st. dev.			0.47

6.8.5 Computational Section

Jia-Qi Li developed the computational model under the supervision of Professor Xin Hong. The model used may be found at https://github.com/jackie-illiilli/Alkene_Ozone_Predict.

6.8.6 Data Analysis

6.8.6.1 Performance per Category

The model performance per category per alkene was generated by plotting the experimental values on the x-axis and the computational prediction on the y-axis for each substrate. The datasets were then colored per alkene type. The line of ideality (y = x) was plotted over the graph.

6.8.6.2 Accuracy

Accuracy was calculated by taking the absolute value of the difference computational value from the experimental value. The difference was divided by the computational value. The quotient was then subtracted from 1.

$$accuracy = 1 - \frac{|experimental - computational|}{computational}$$

6.8.6.3 Error

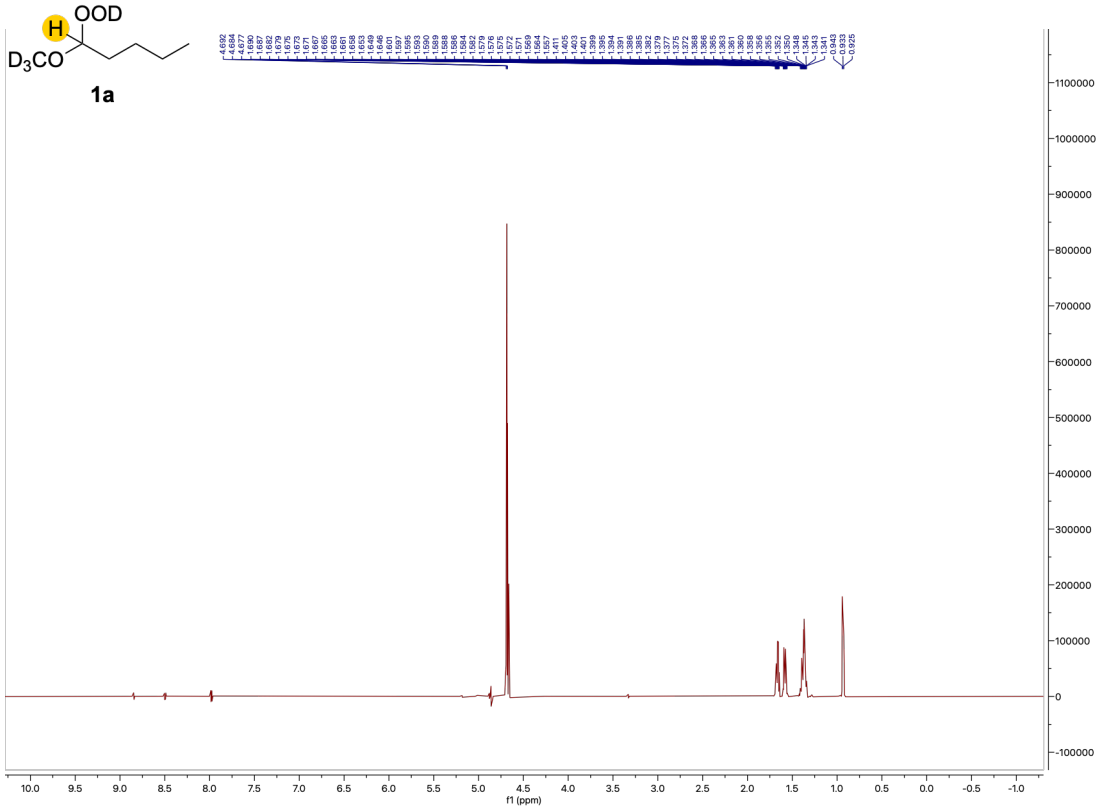
Absolute error was calculated by subtracting the predicted value from the experimental value and dividing by 100.

$$error = \frac{experimental - computational}{100}$$

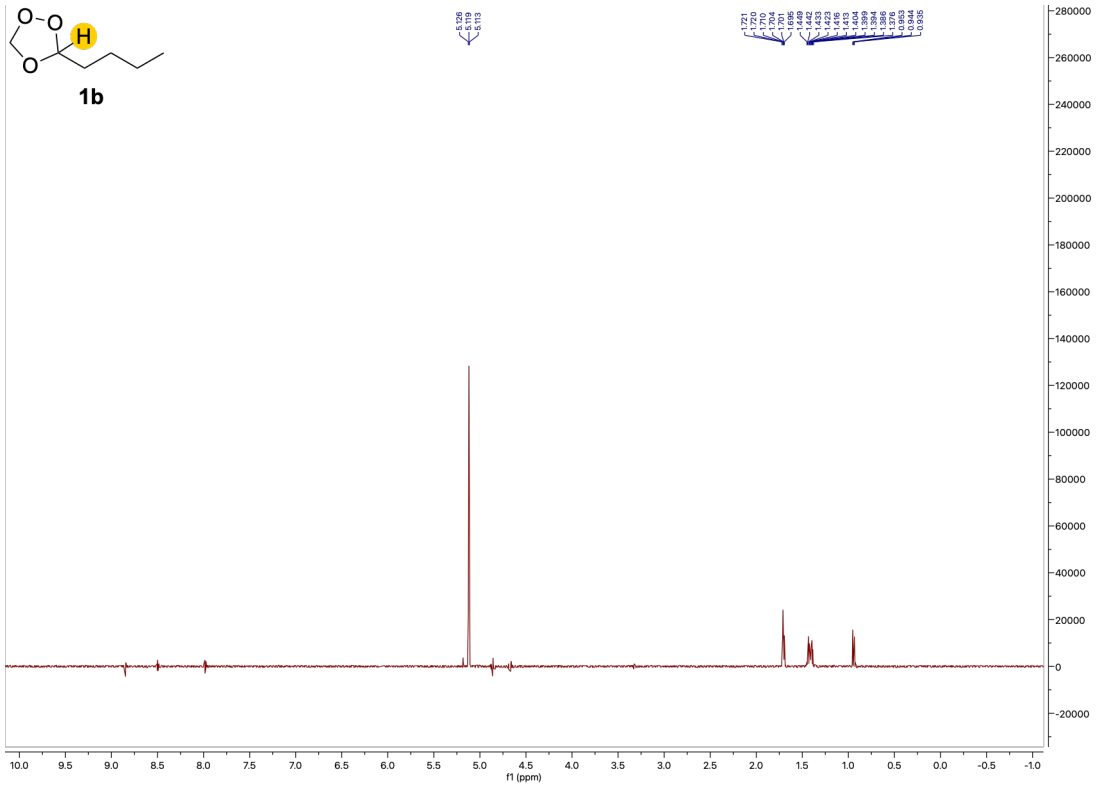
A histogram was generated by plotting the number of substrates matching each x-axis value. Values falling on the edge were matched to the left-edge.

A Gaussian model was traced over the histogram using the NORM.DIST function in Microsoft Excel, using average error and the standard deviation of the error. The values were multiplied by a 5% of the data count.

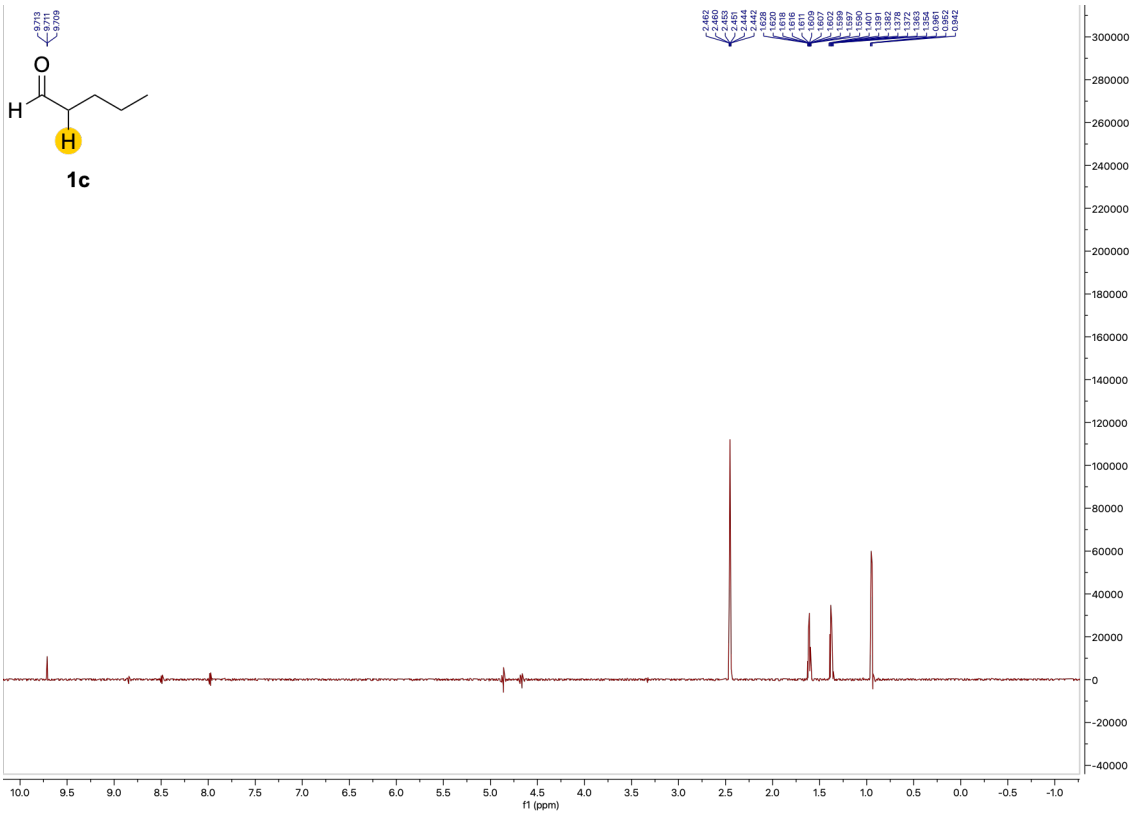
6.8.7 Copies of NMR Spectra



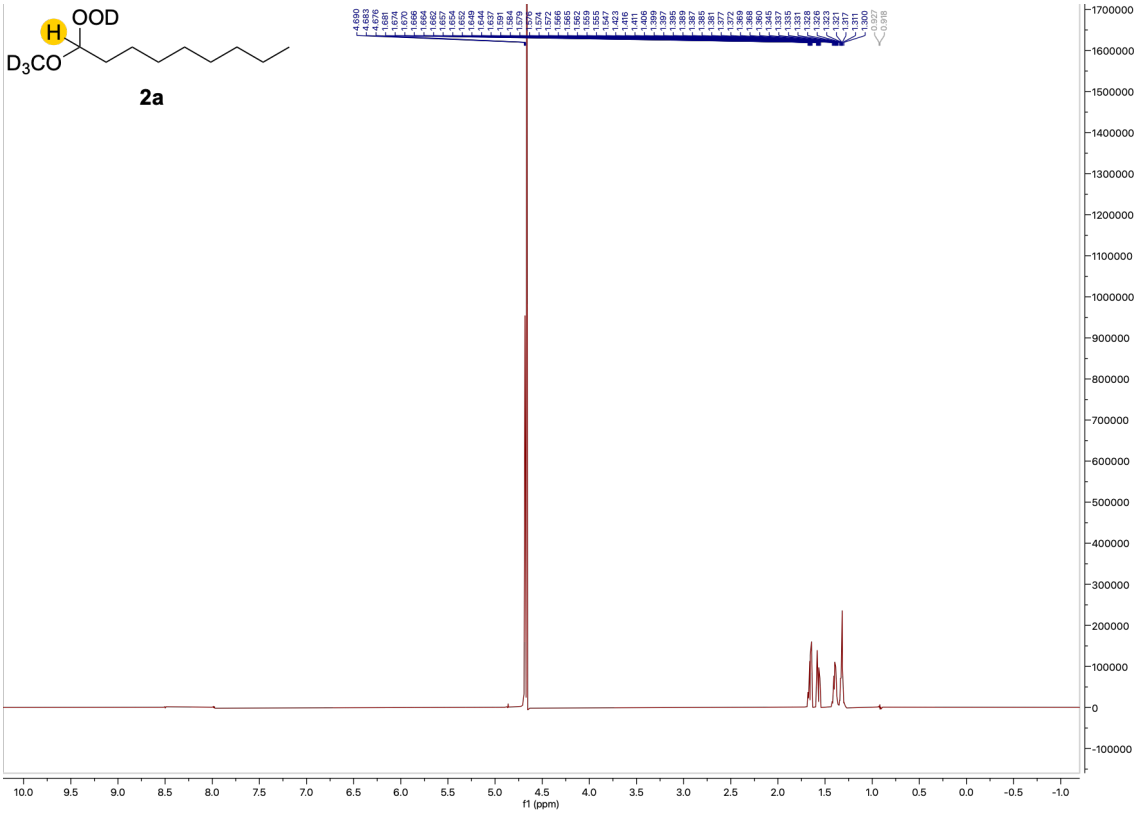
1D Selective Gradient TOCSY (800 MHz, CD_3OD) at 4.690 ppm of **1a**



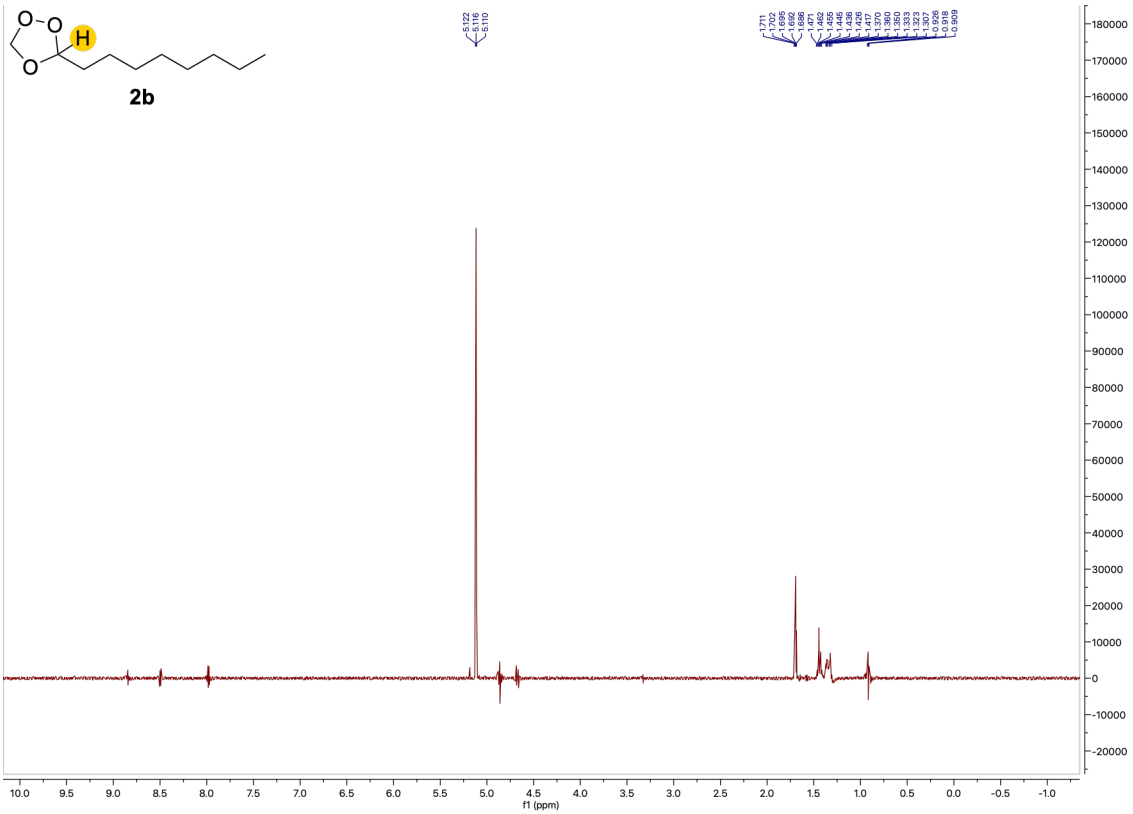
1D Selective Gradient TOCSY (800 MHz, CD_3OD) at 5.119 ppm of **1b**



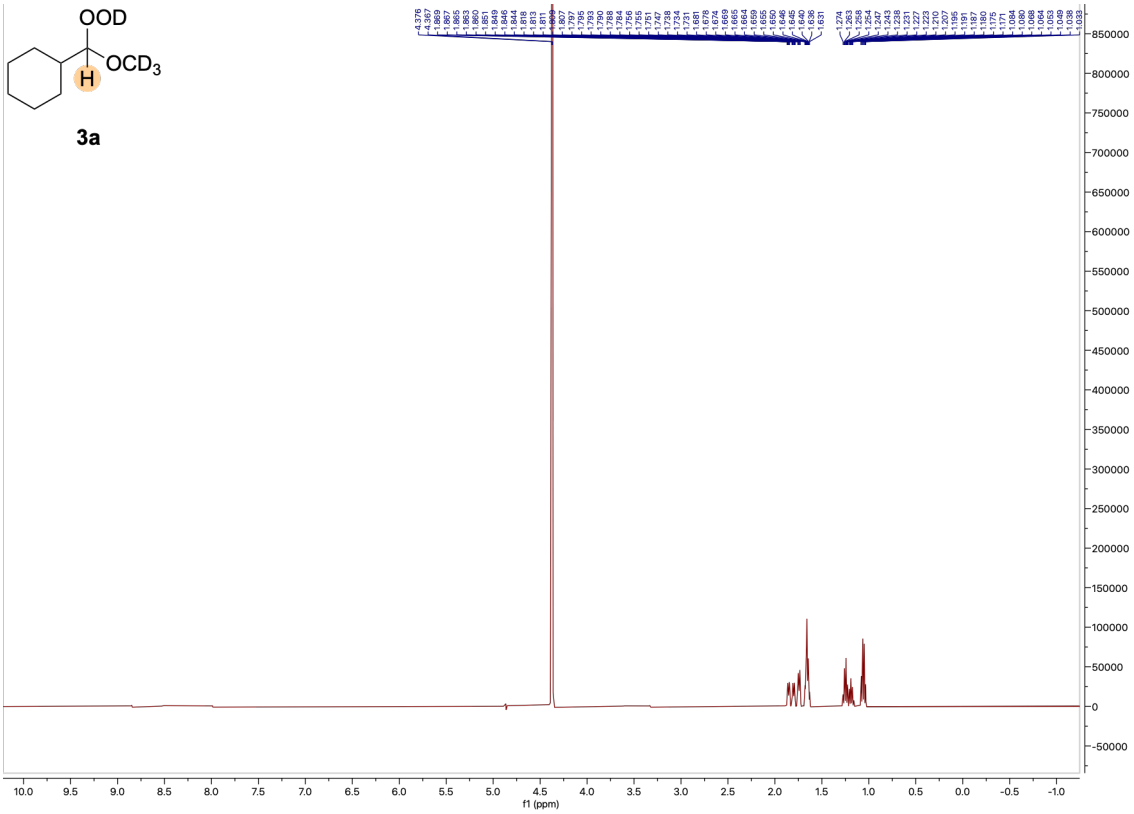
1D Selective Gradient TOCSY (800 MHz, CD_3OD) at 2.451 ppm of **1c**



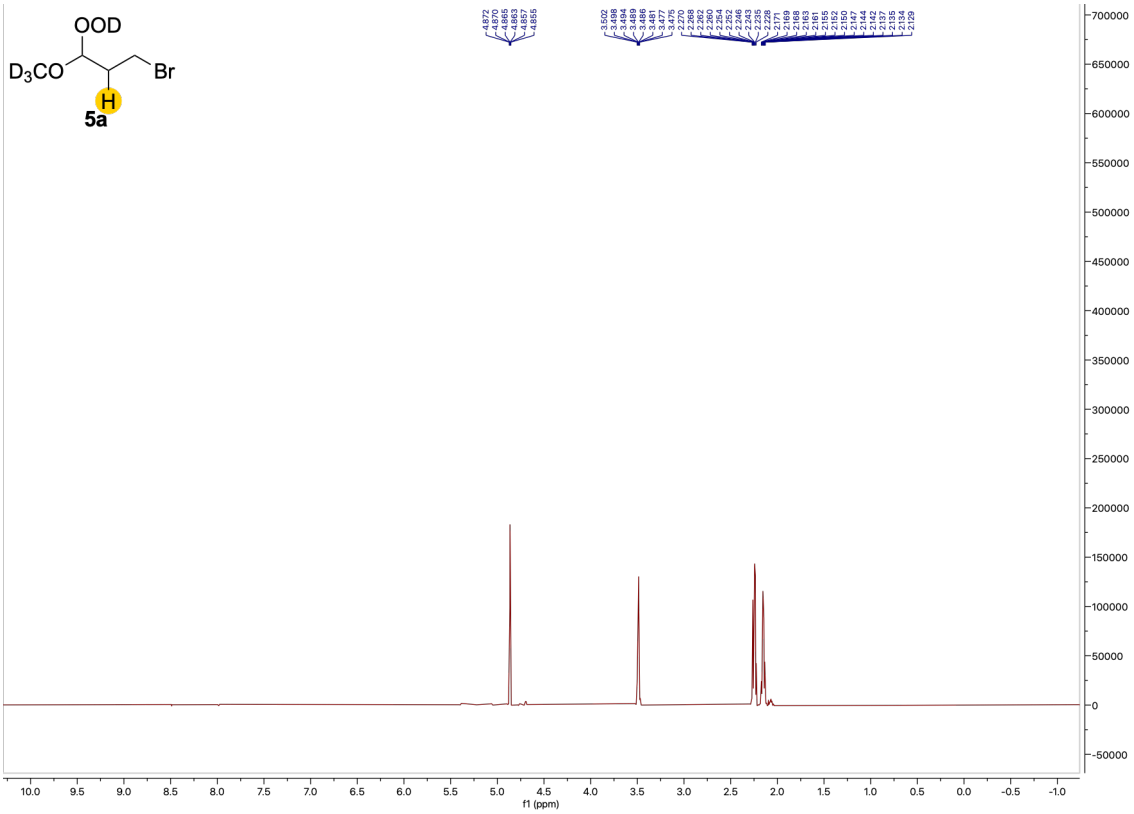
1D Selective Gradient TOCSY (800 MHz, CD_3OD) at 4.684 ppm of **2a**



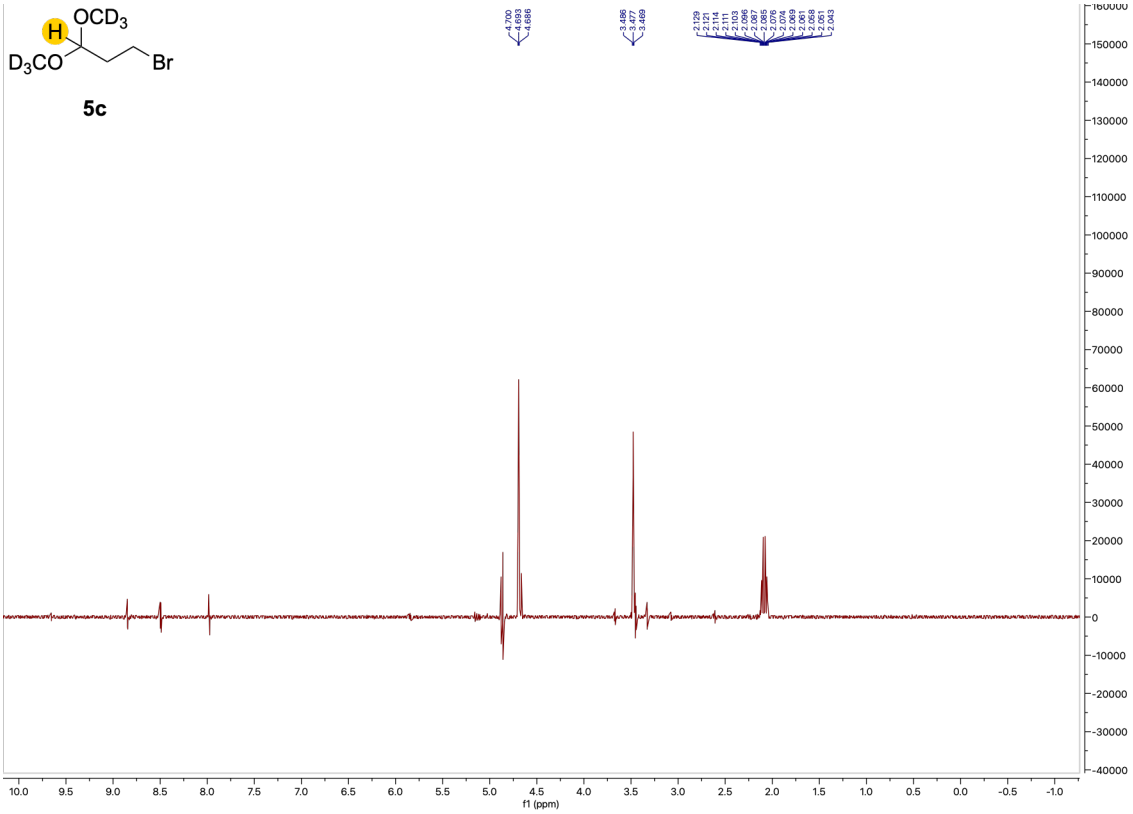
1D Selective Gradient TOCSY (800 MHz, CD_3OD) at 5.116 ppm of **2b**



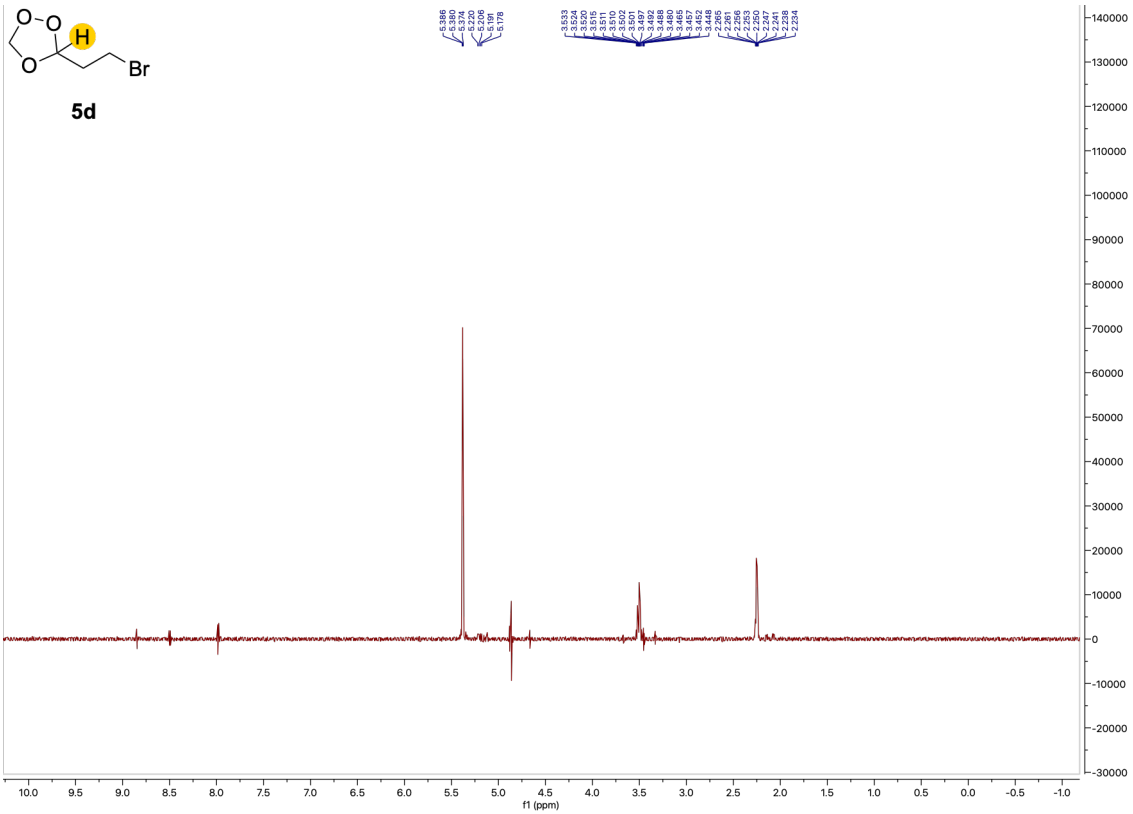
1D Selective Gradient TOCSY (800 MHz, CD_3OD) at 4.370 ppm of **3a**



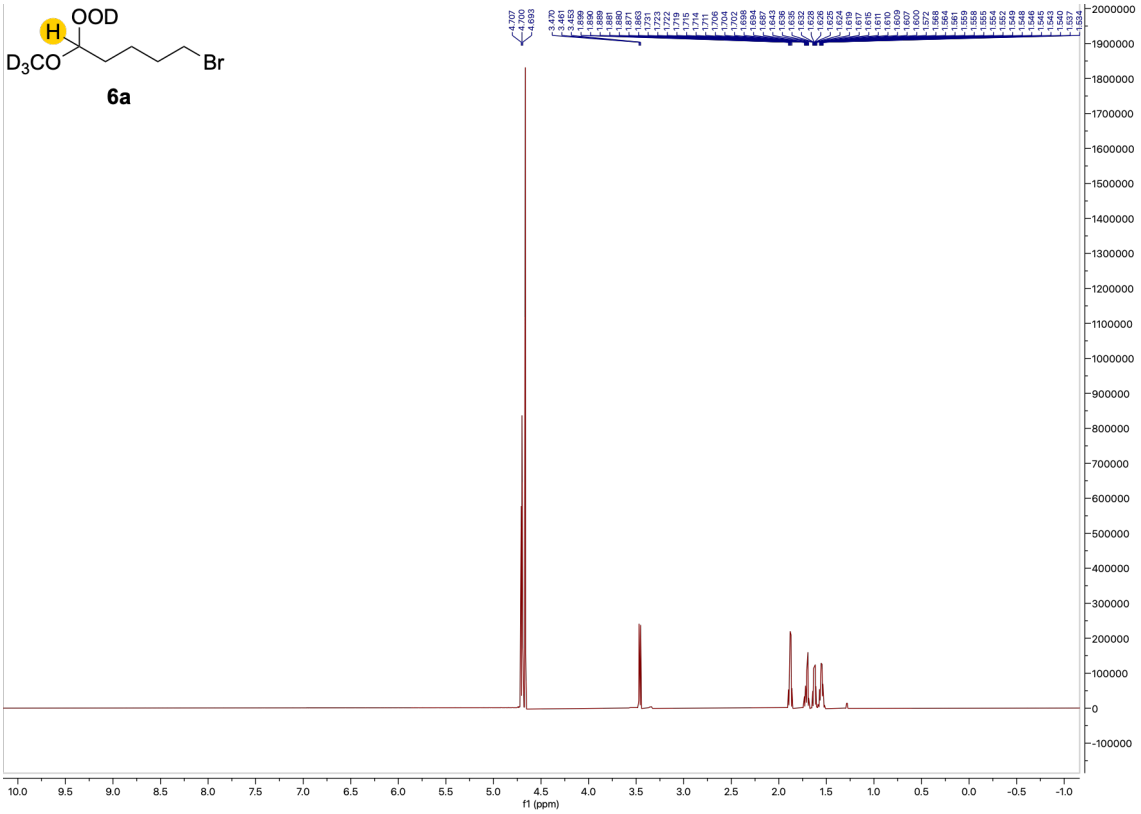
1D Selective Gradient TOCSY (800 MHz, CD_3OD) at 2.160 ppm of **5a**



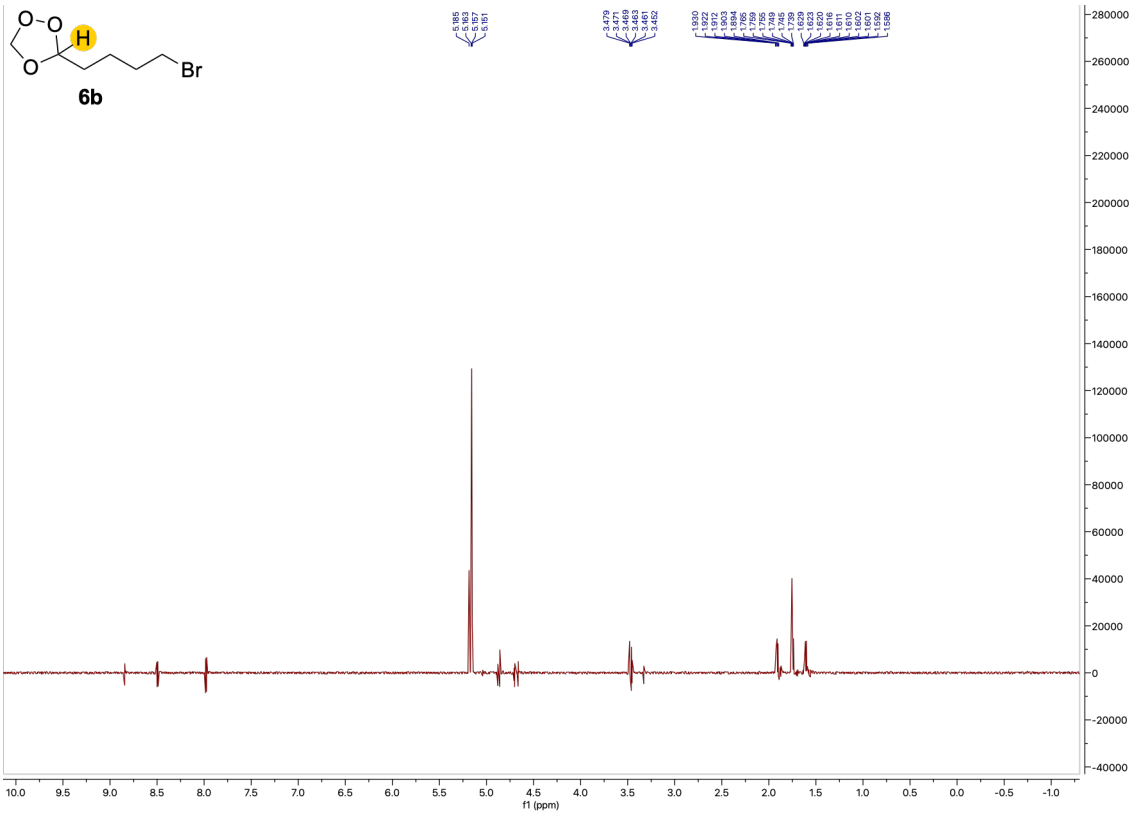
1D Selective Gradient TOCSY (800 MHz, CD_3OD) at 4.697 ppm of **5c**



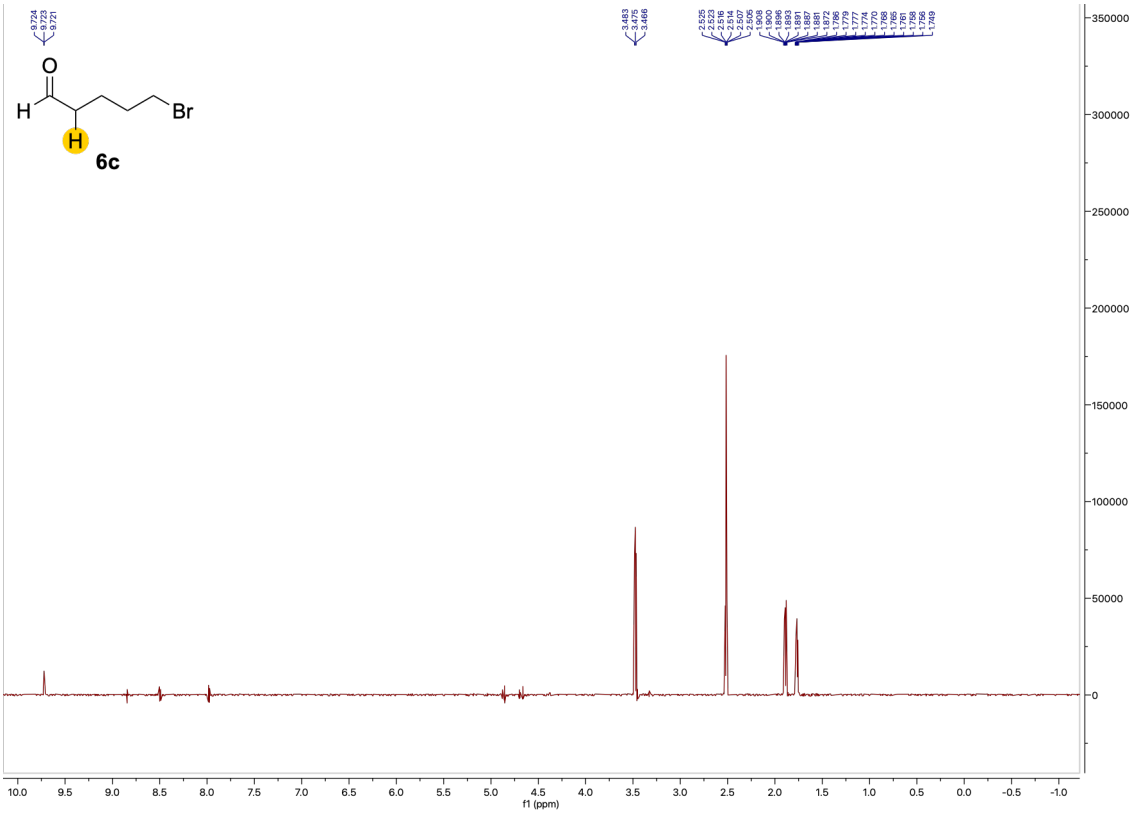
1D Selective Gradient TOCSY (800 MHz, CD_3OD) at 5.380 ppm of **5d**



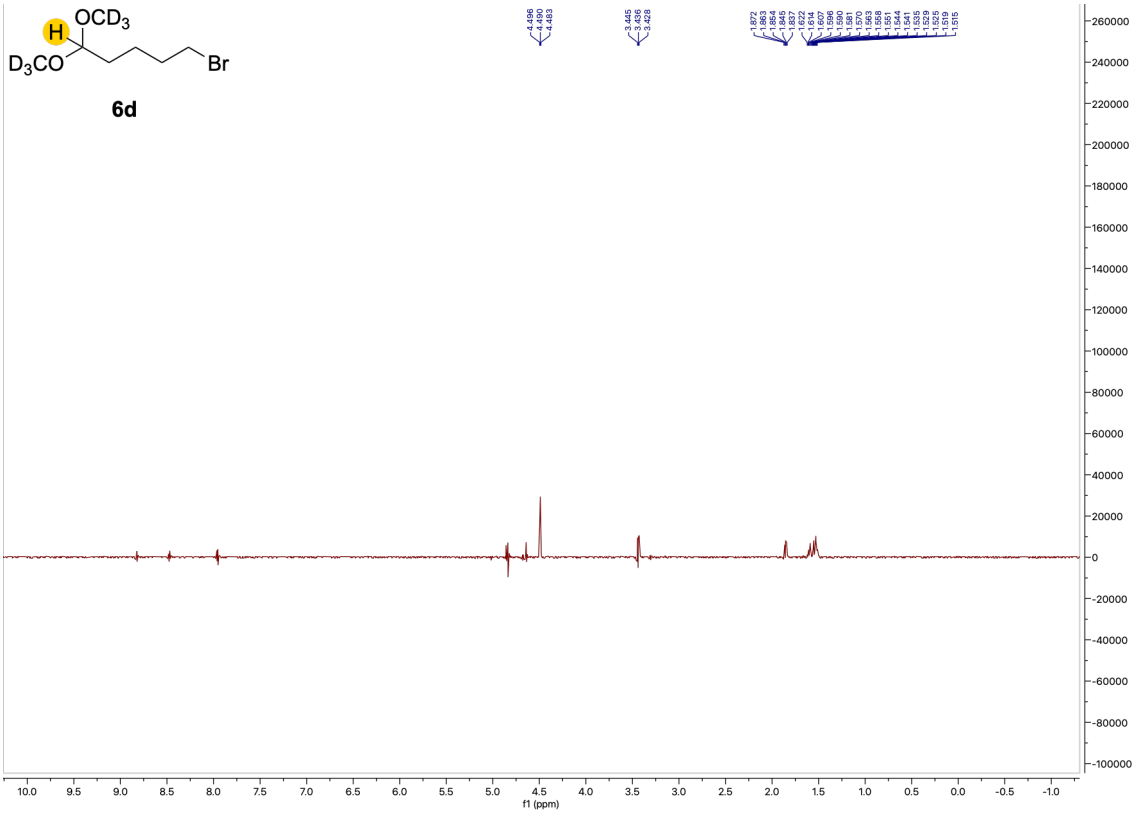
1D Selective Gradient TOCSY (800 MHz, CD_3OD) at 4.680 ppm of **6a**



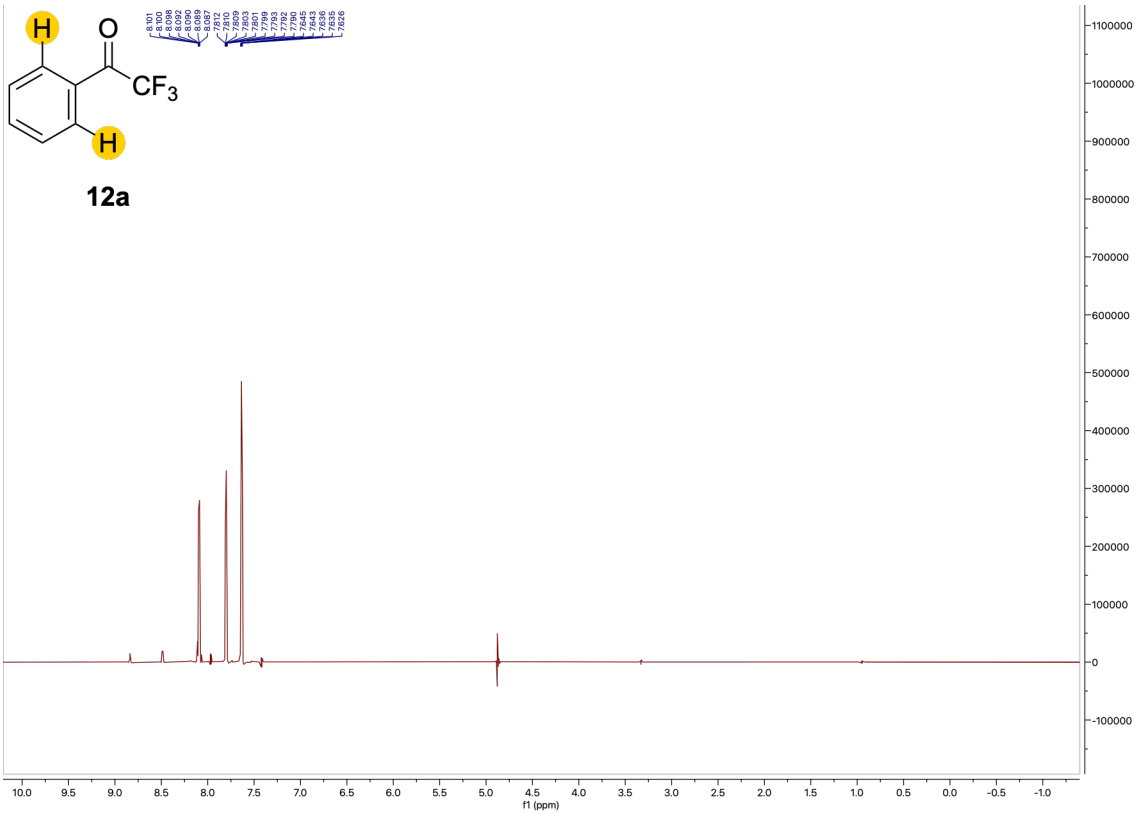
1D Selective Gradient TOCSY (800 MHz, CD_3OD) at 5.157 ppm of **6b**



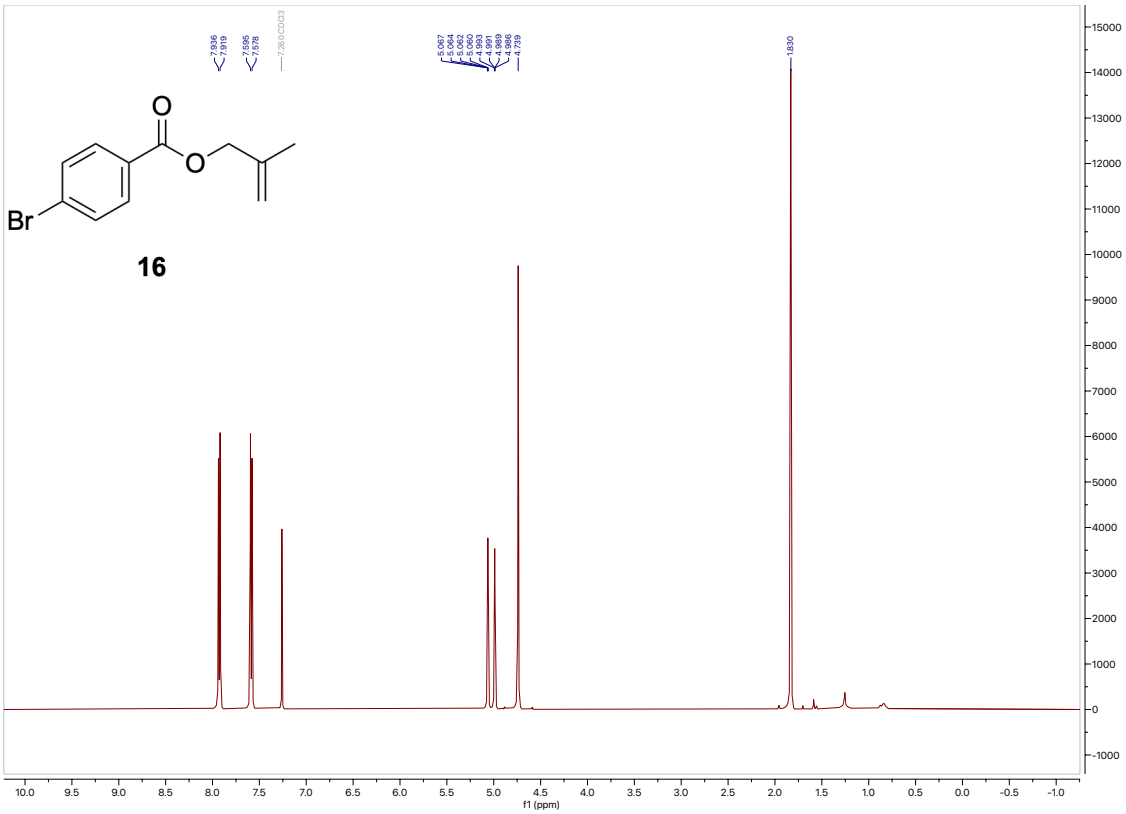
1D Selective Gradient TOCSY (800 MHz, CD_3OD) at 2.498 ppm of **6c**

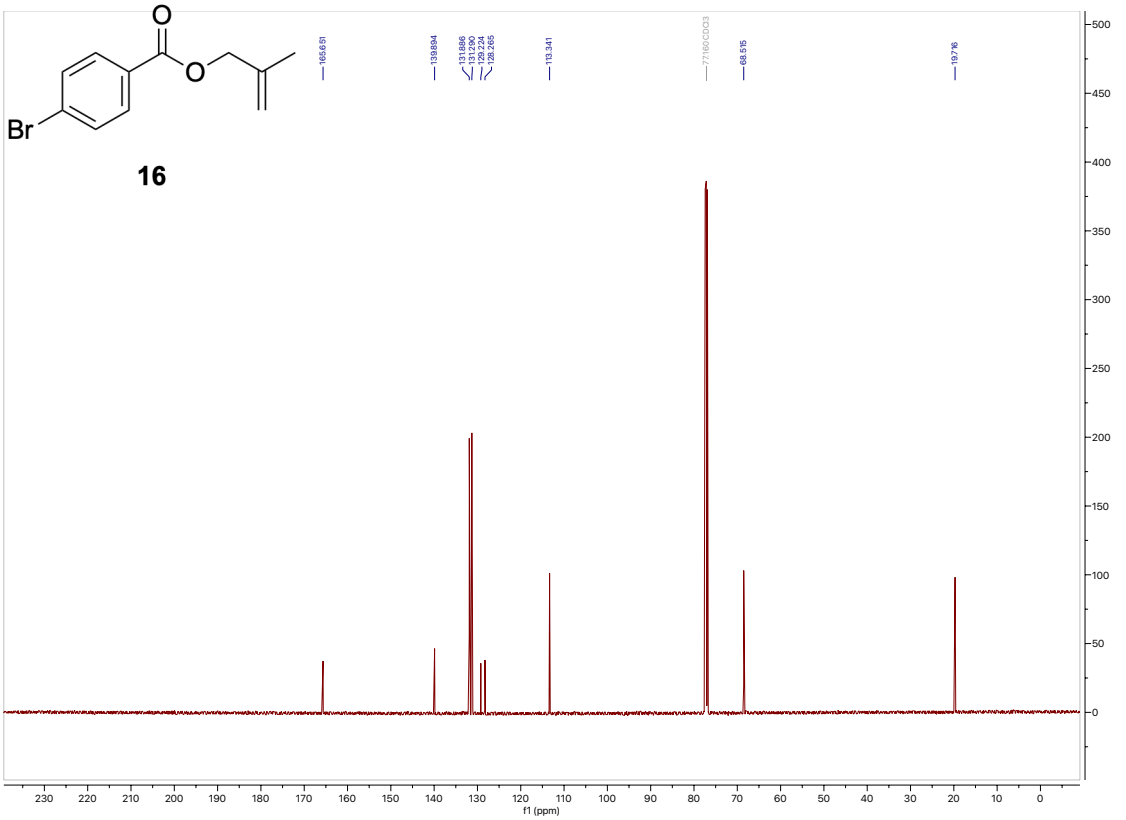


1D Selective Gradient TOCSY (800 MHz, CD_3OD) at 4.490 ppm of **6d**

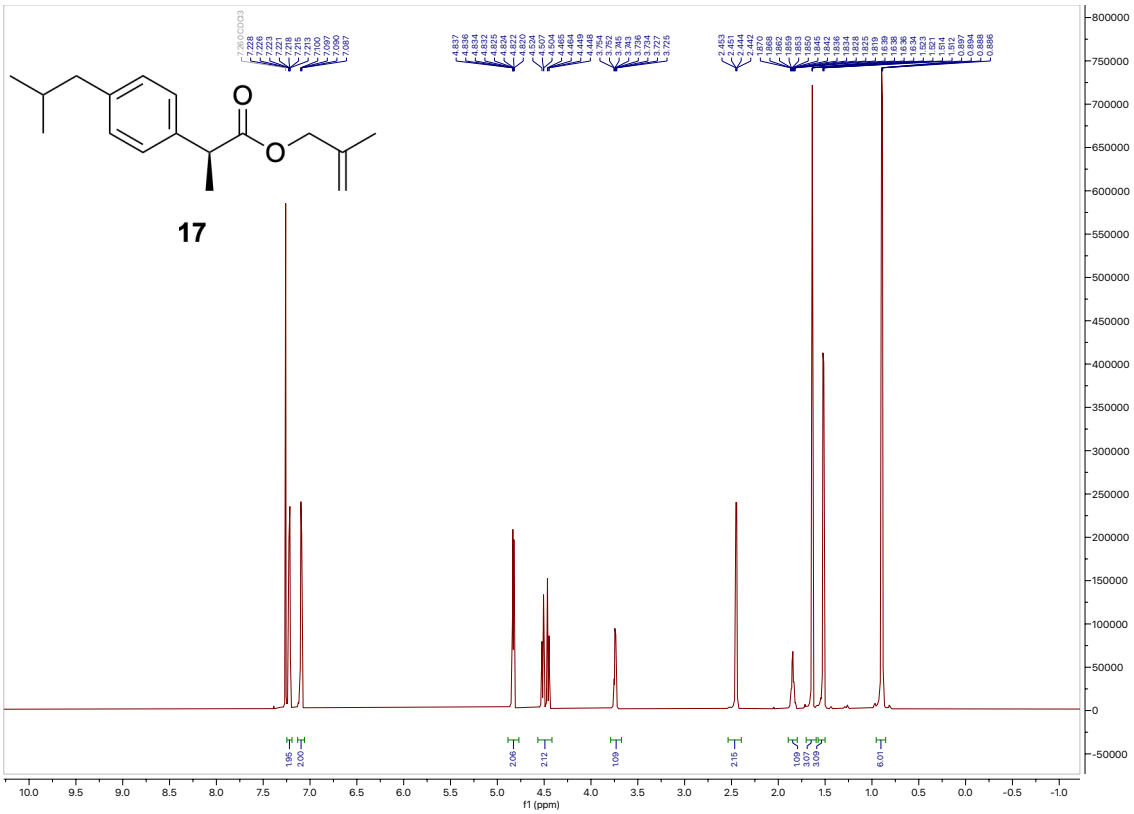


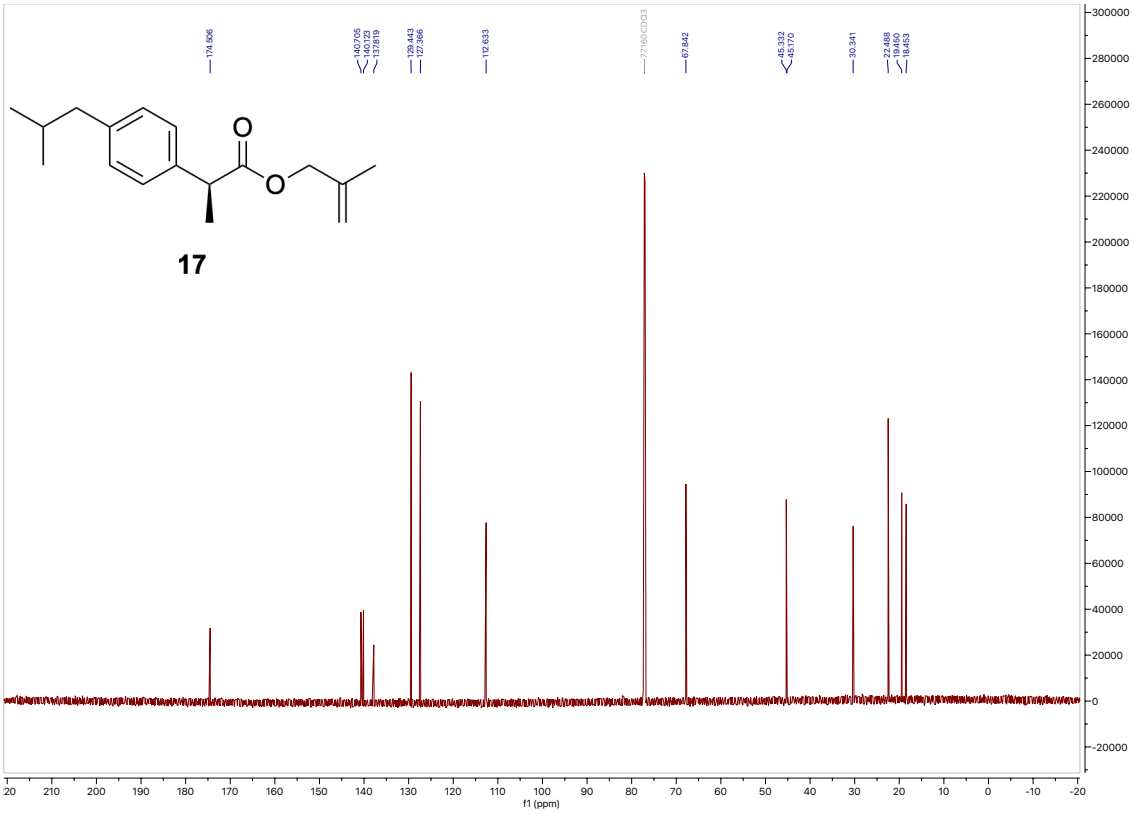
1D Selective Gradient TOCSY (800 MHz , CD_3OD) at 8.095 ppm of **12a**



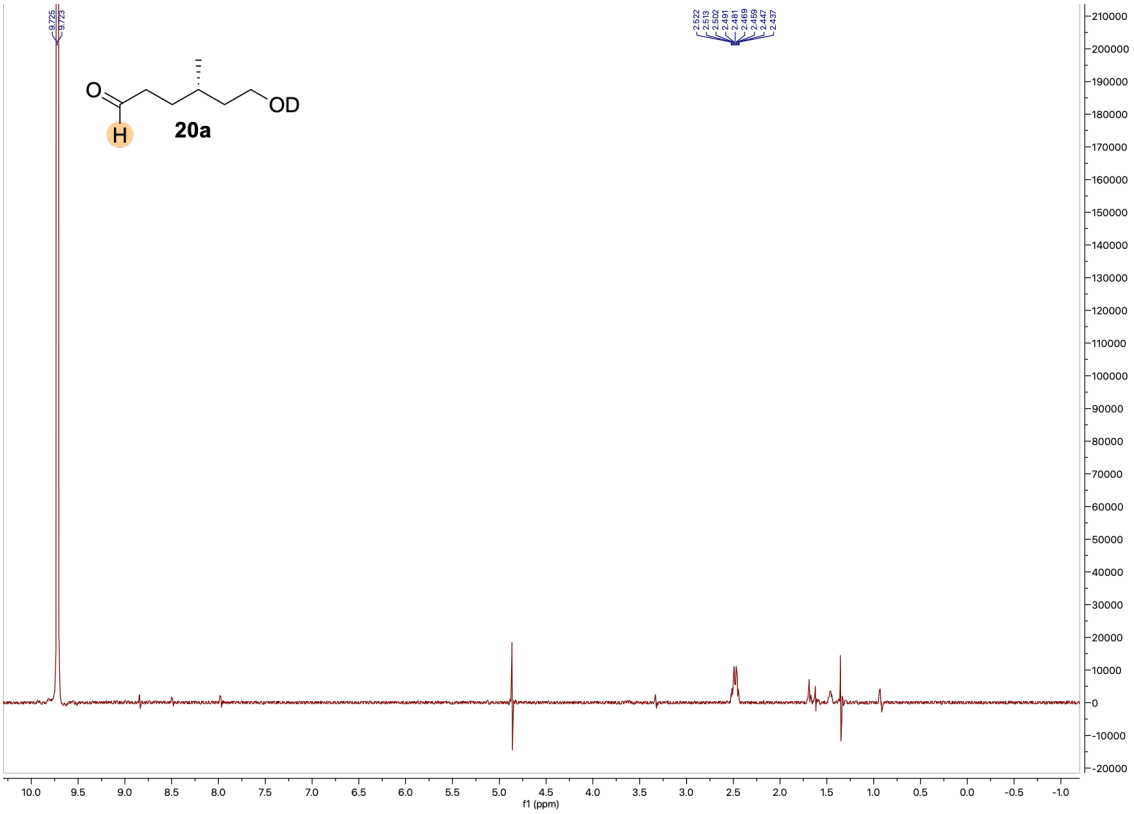


^{1}H NMR (500 MHz, $CDCl_3$) and **^{13}C NMR** (126 MHz, $CDCl_3$) of **16**

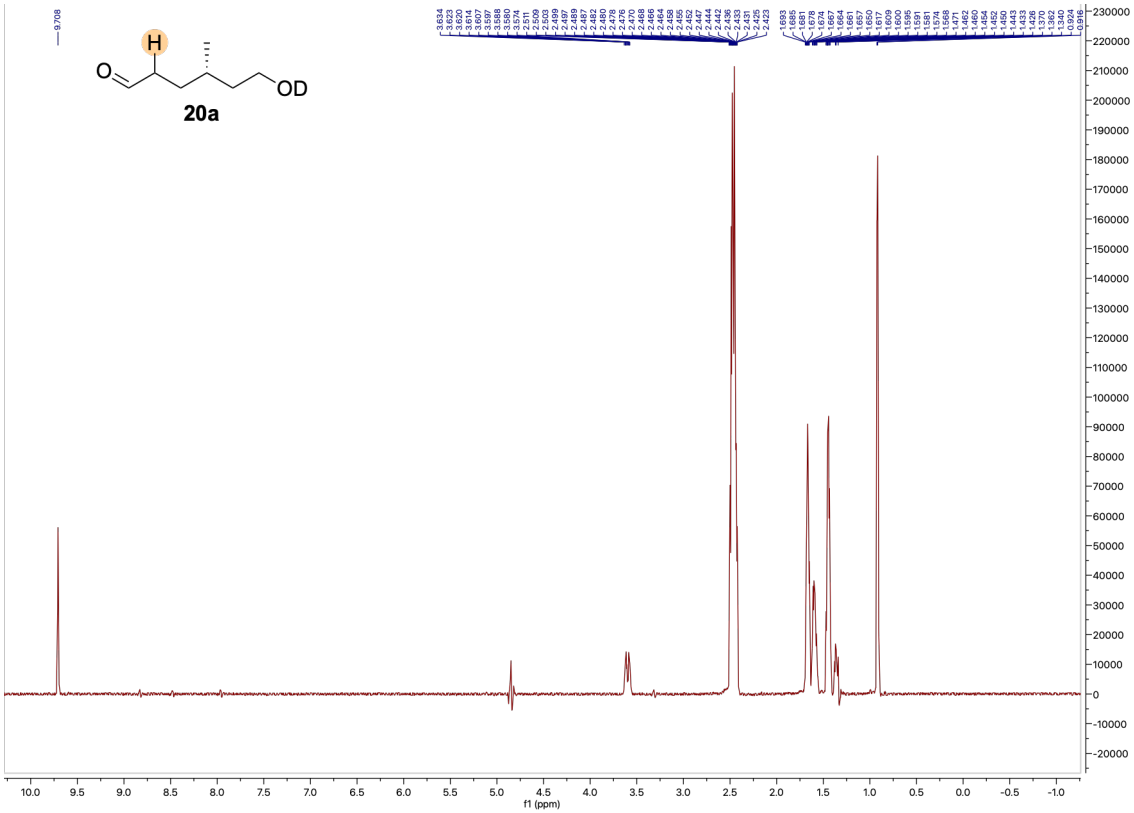




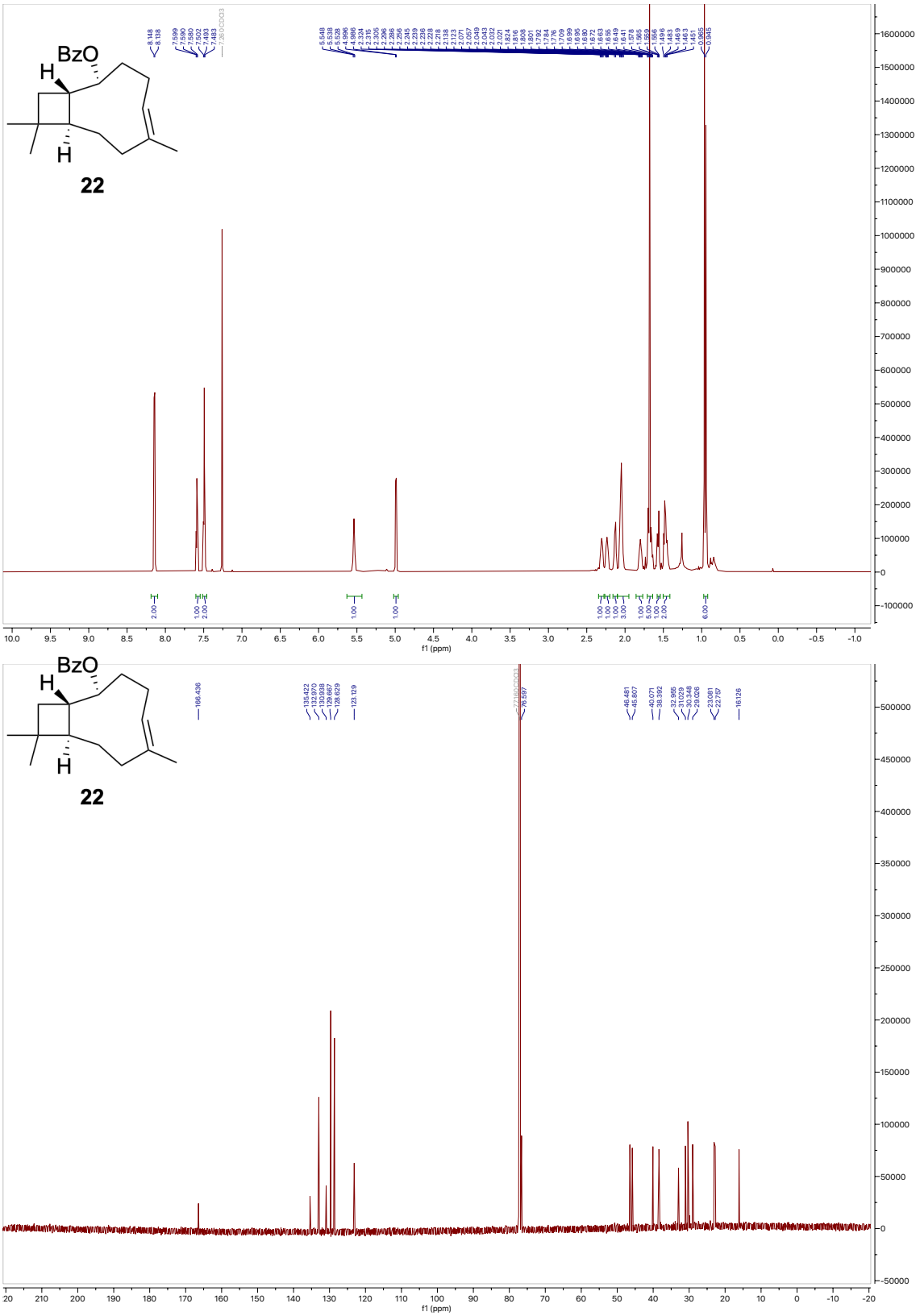
^{1}H NMR (800 MHz, $CDCl_3$) and **^{13}C NMR** (201 MHz, $CDCl_3$) of **17**



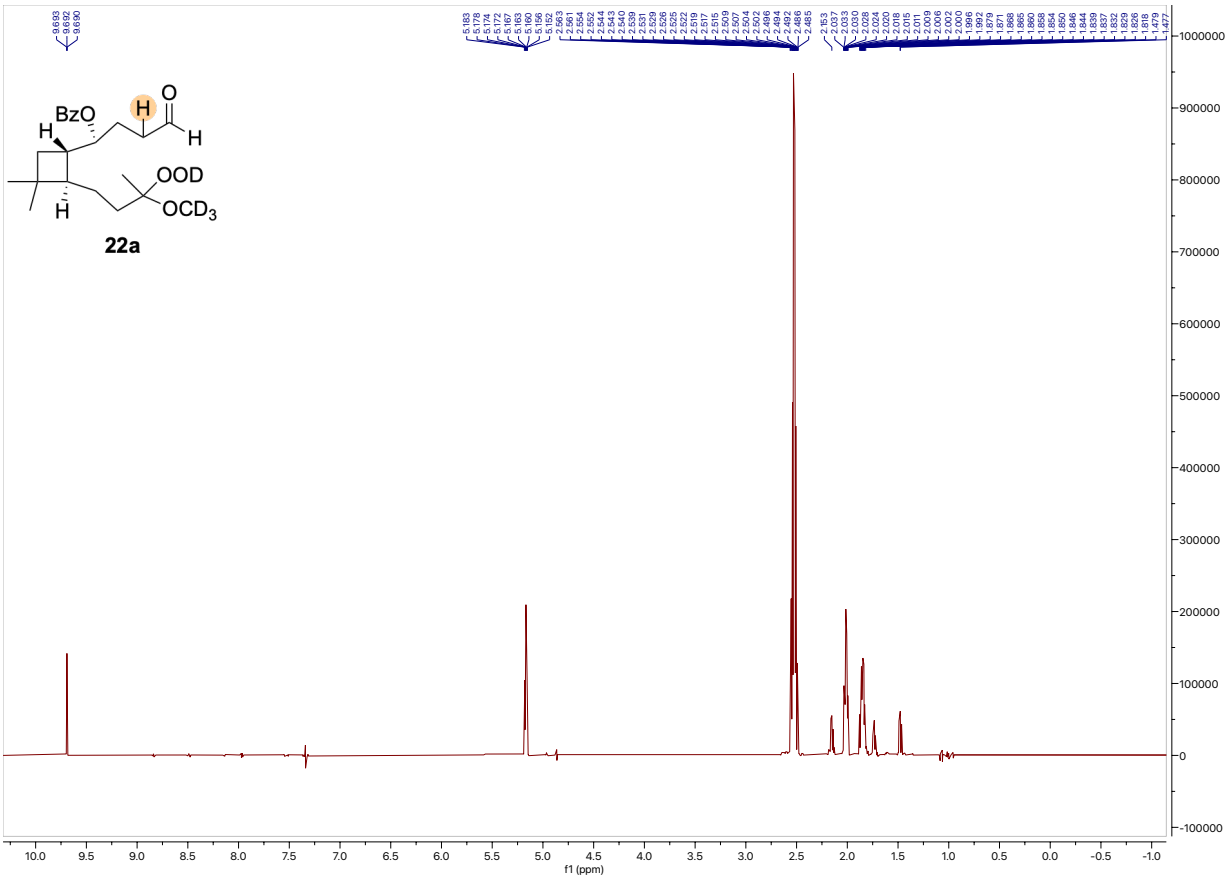
1D Selective Gradient TOCSY (800 MHz, CD_3OD) at 9.724 ppm of **20a**



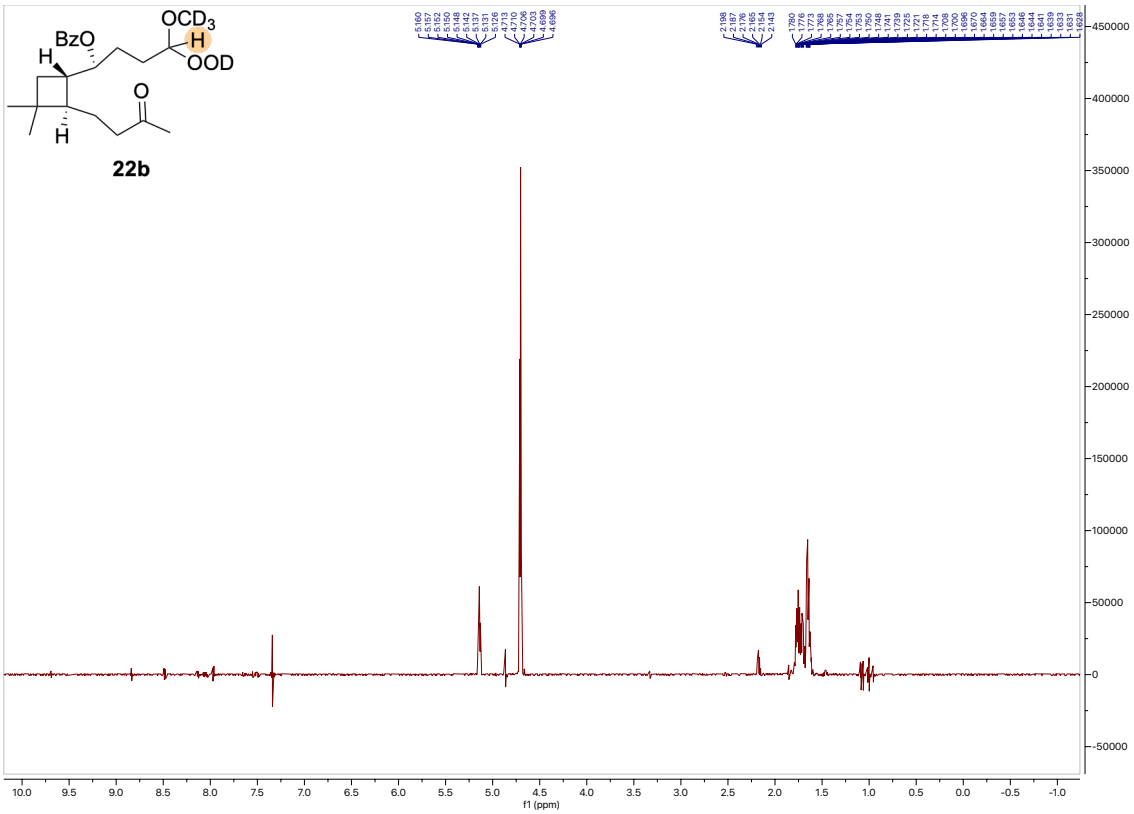
1D Selective Gradient TOCSY (800 MHz, CD_3OD) at 2.480 ppm of **20a**



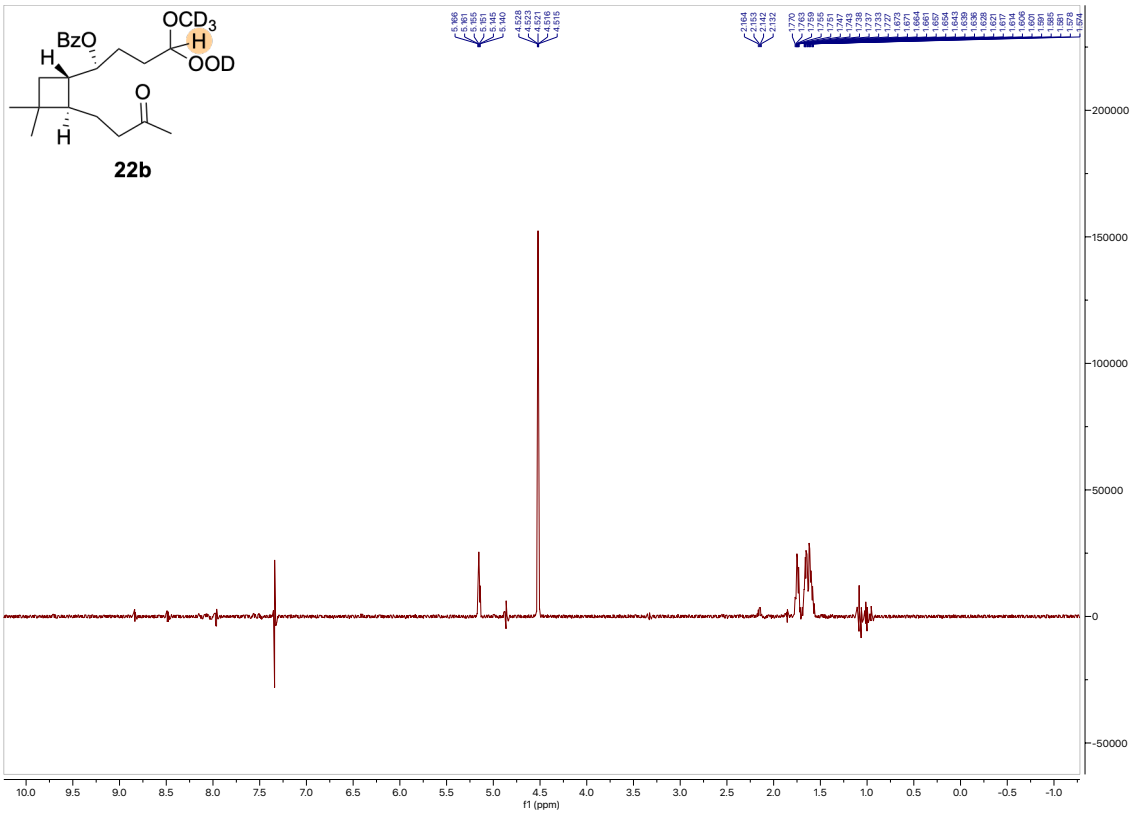
^{1}H NMR (800 MHz, $CDCl_3$) and **^{13}C NMR** (201 MHz, $CDCl_3$) of **22**



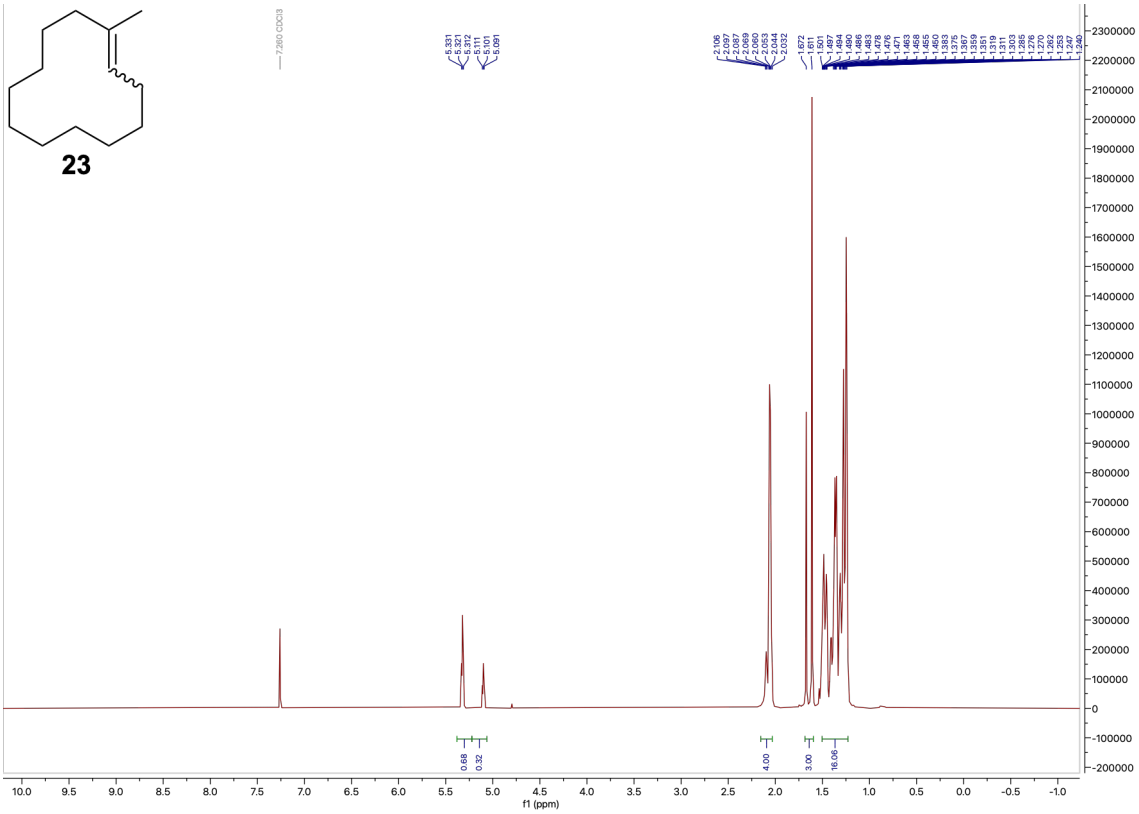
1D Selective Gradient TOCSY (800 MHz, MeOD) at 2.523 ppm of **22a**

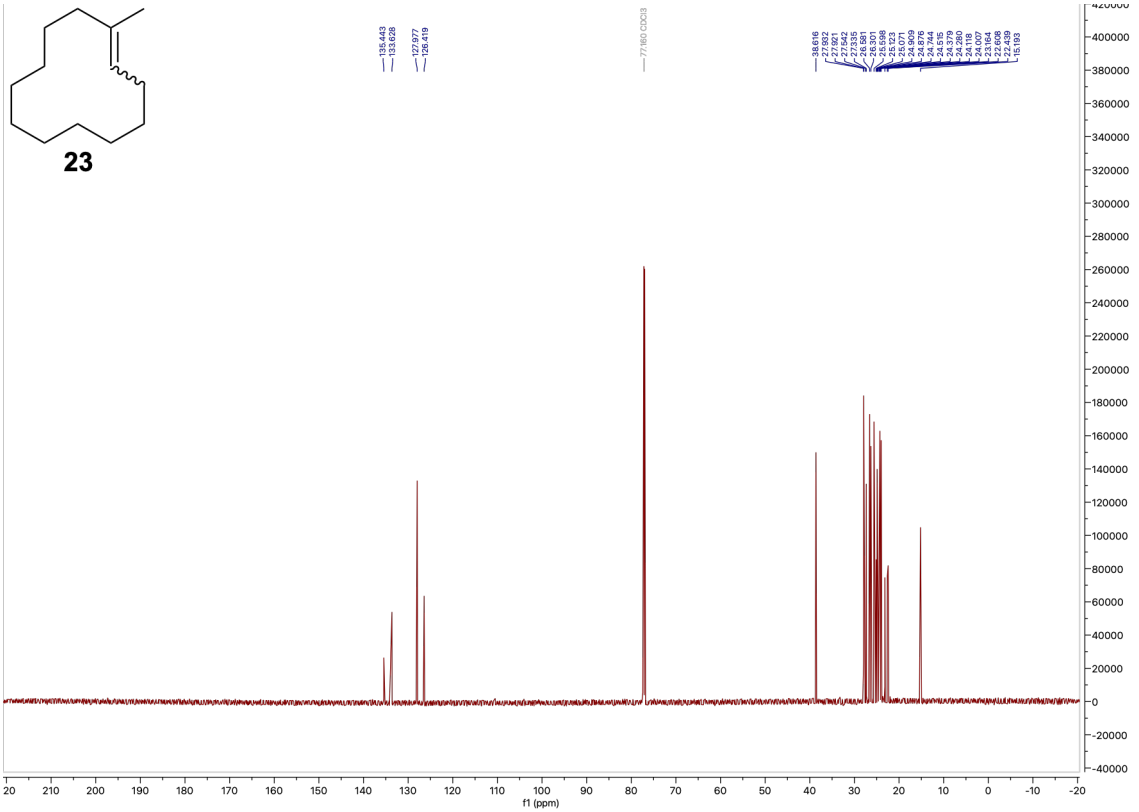


1D Selective Gradient TOCSY (800 MHz, MeOD) at 4.701 ppm of **22b**

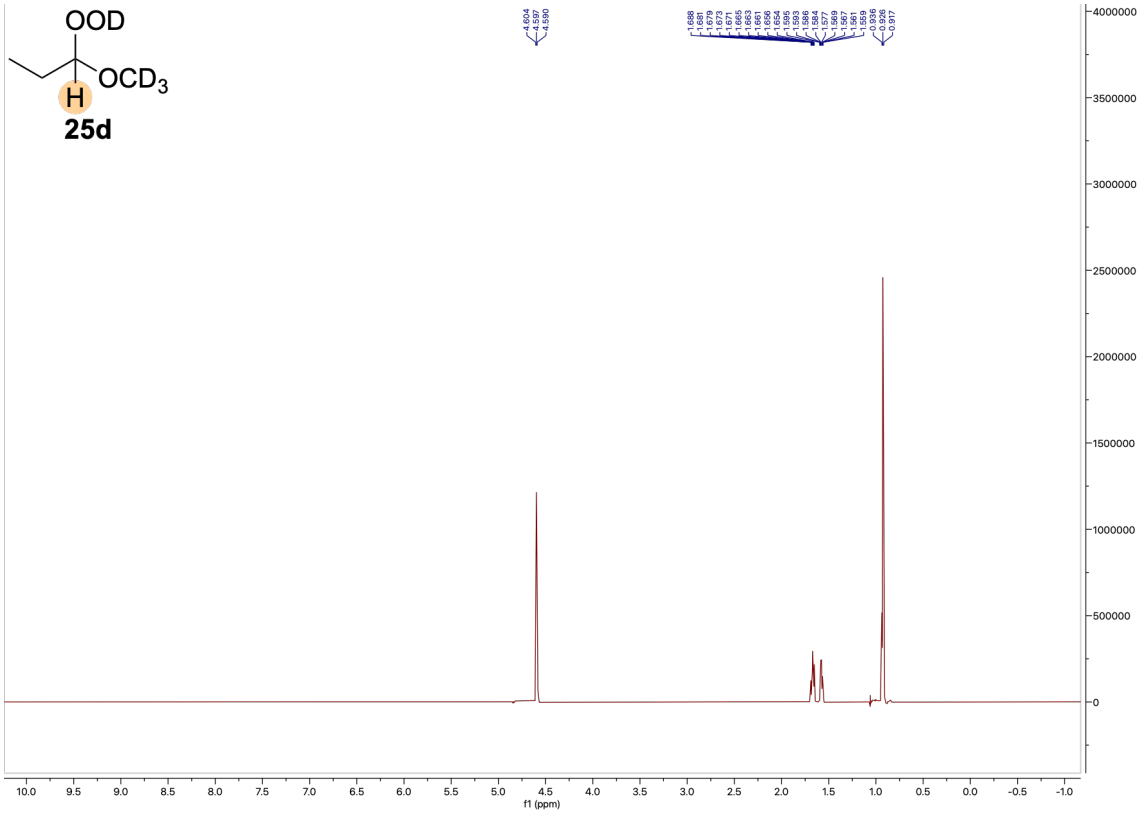


1D Selective Gradient TOCSY (800 MHz, MeOD) at 4.524 ppm of **22b**

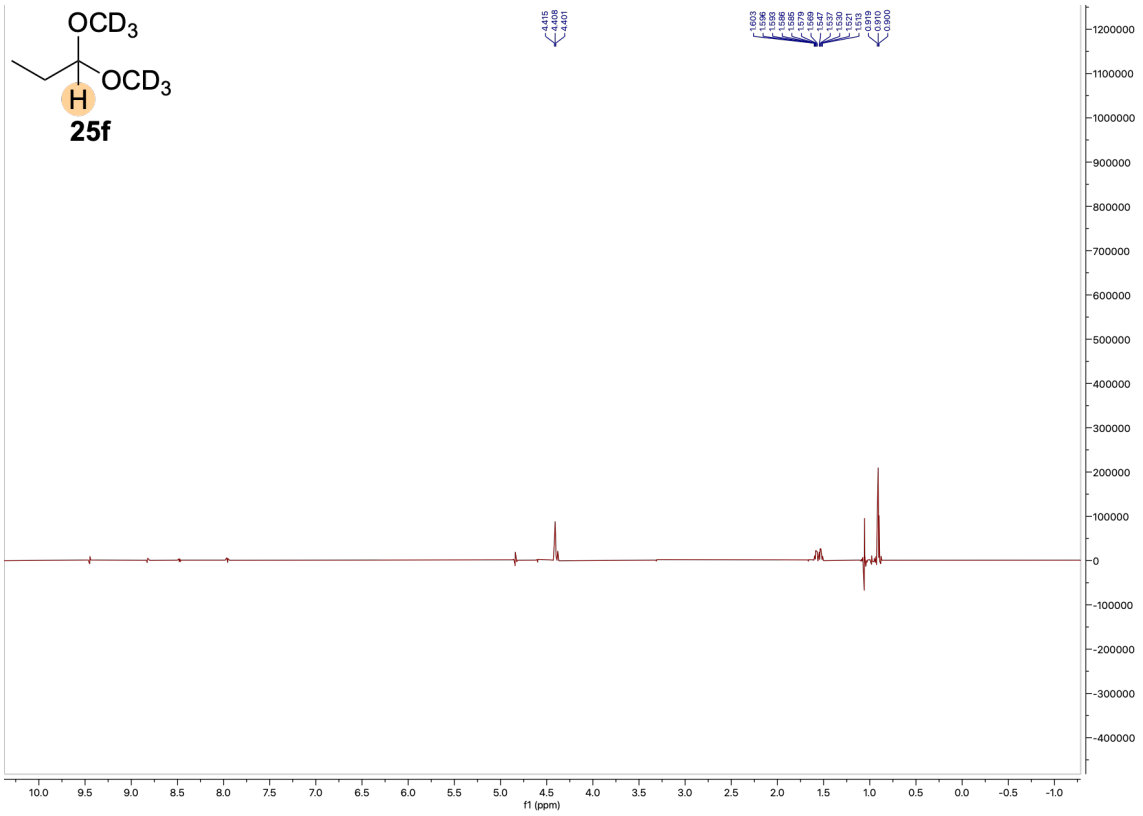




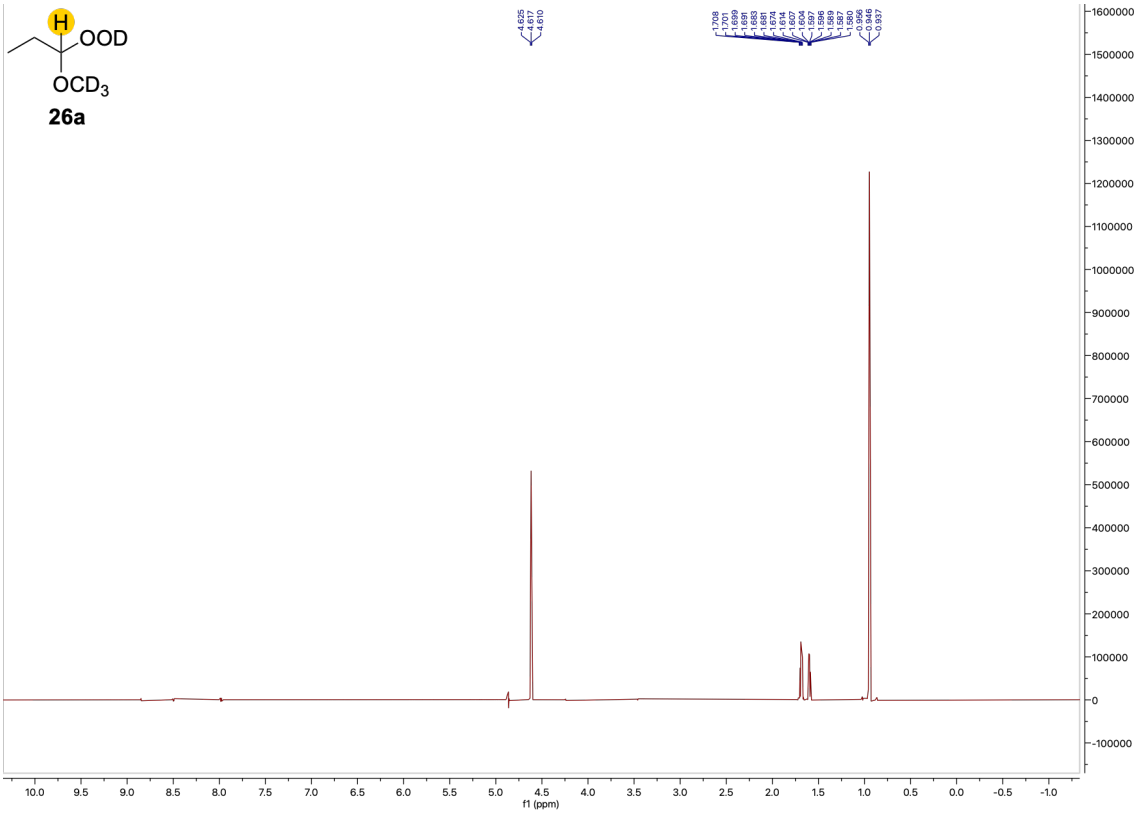
^{1}H NMR (800 MHz, $CDCl_3$) and **^{13}C NMR** (201 MHz, $CDCl_3$)



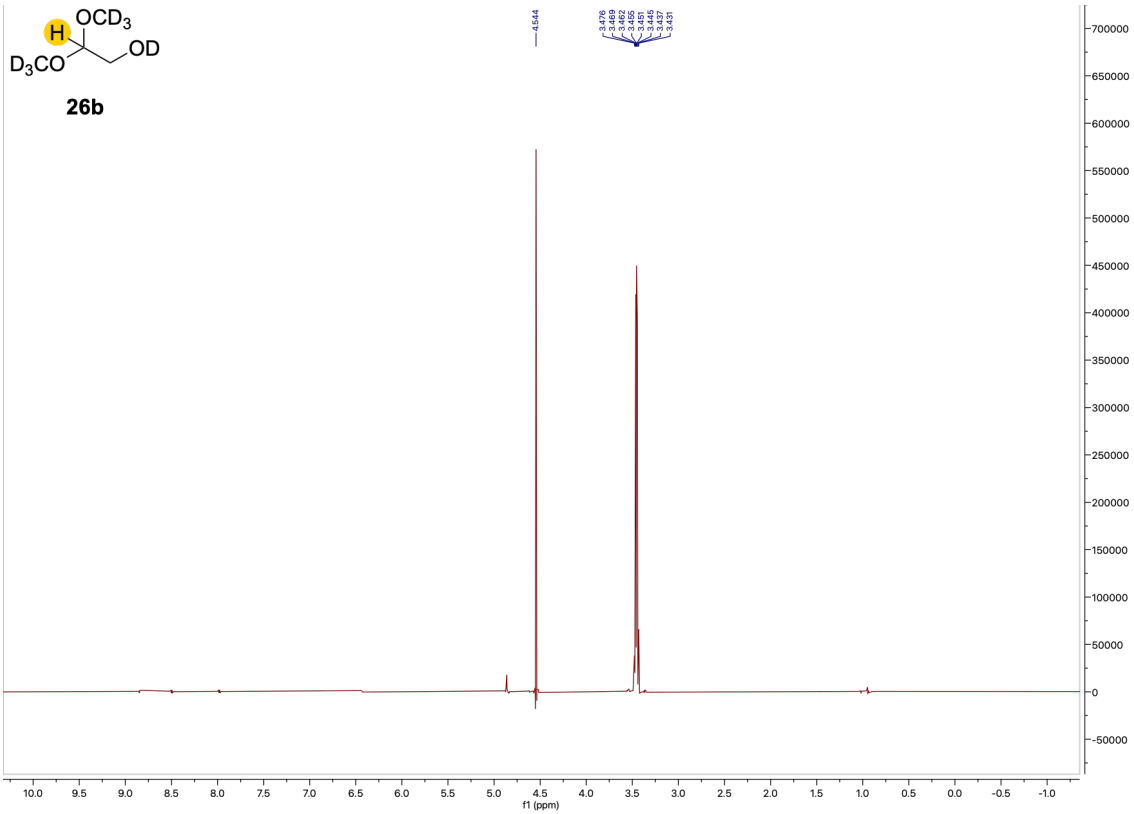
1D Selective Gradient TOCSY (800 MHz, CD_3OD) at 4.616 ppm of **25d**



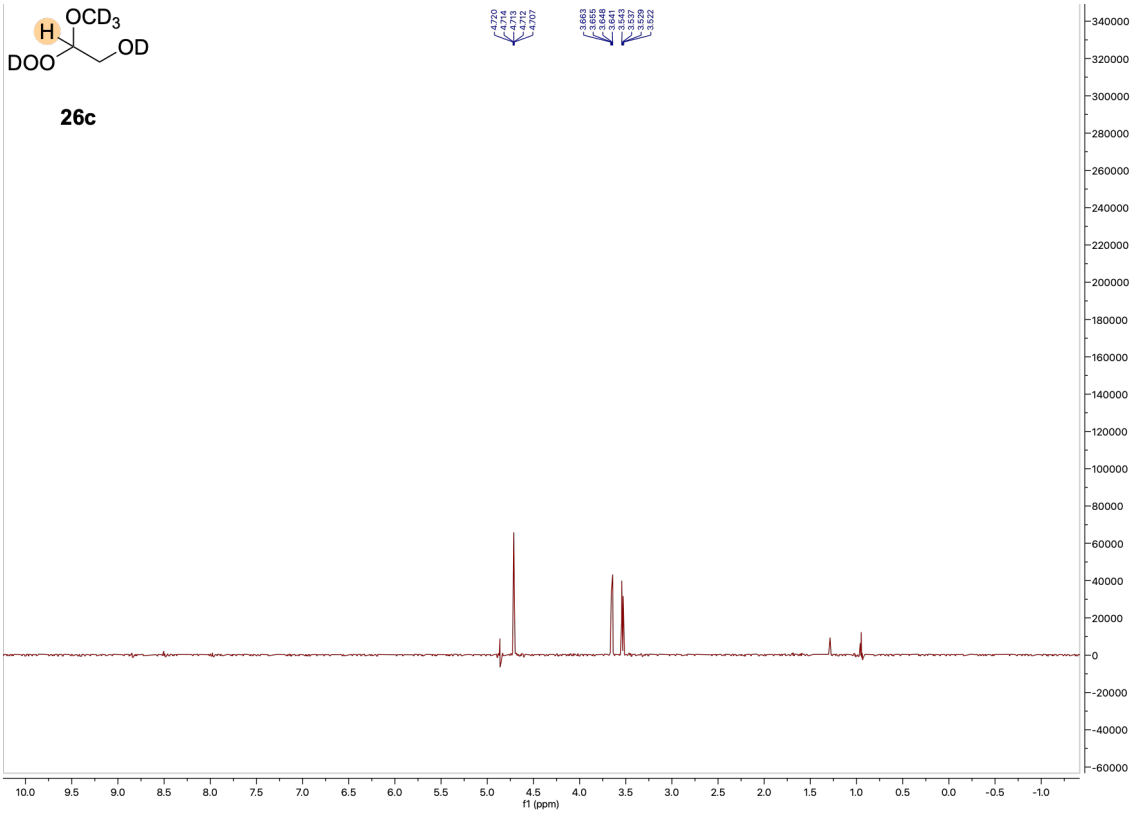
1D Selective Gradient TOCSY (800 MHz, CD_3OD) at 4.427 ppm of **25f**



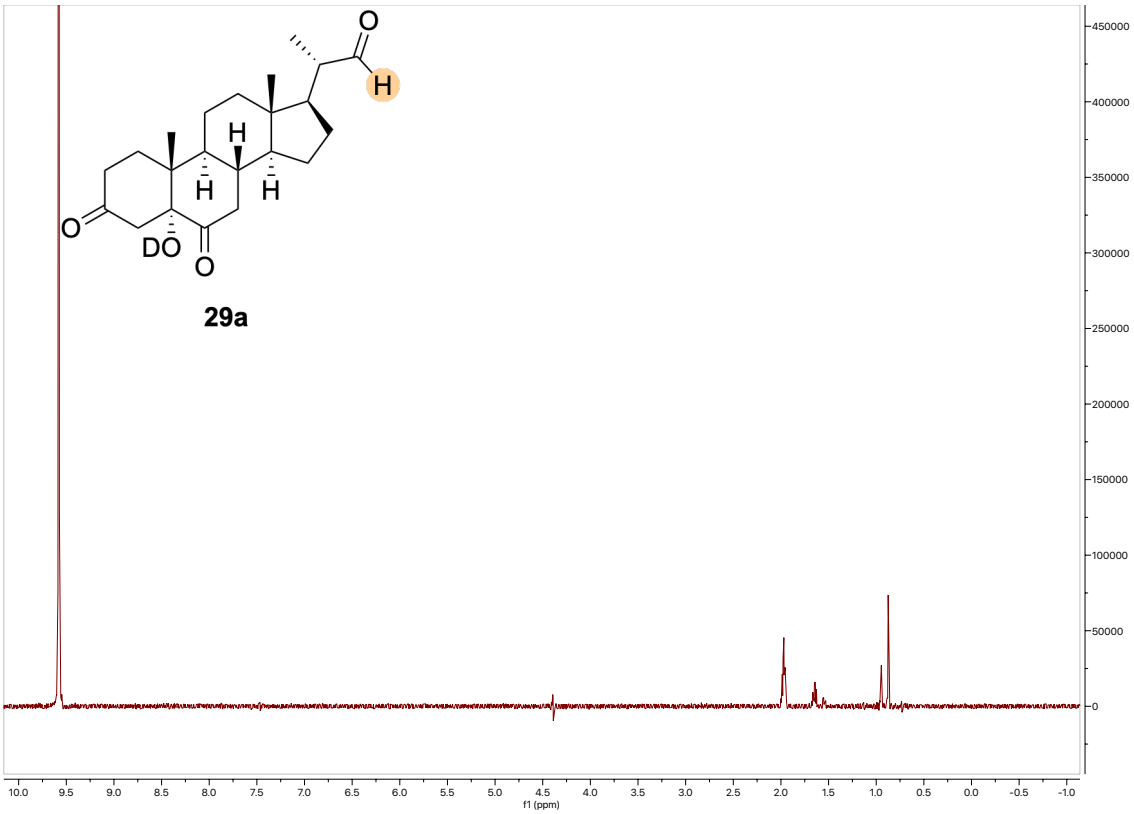
1D Selective Gradient TOCSY (800 MHz, CD_3OD) at 4.617 ppm of **26a**



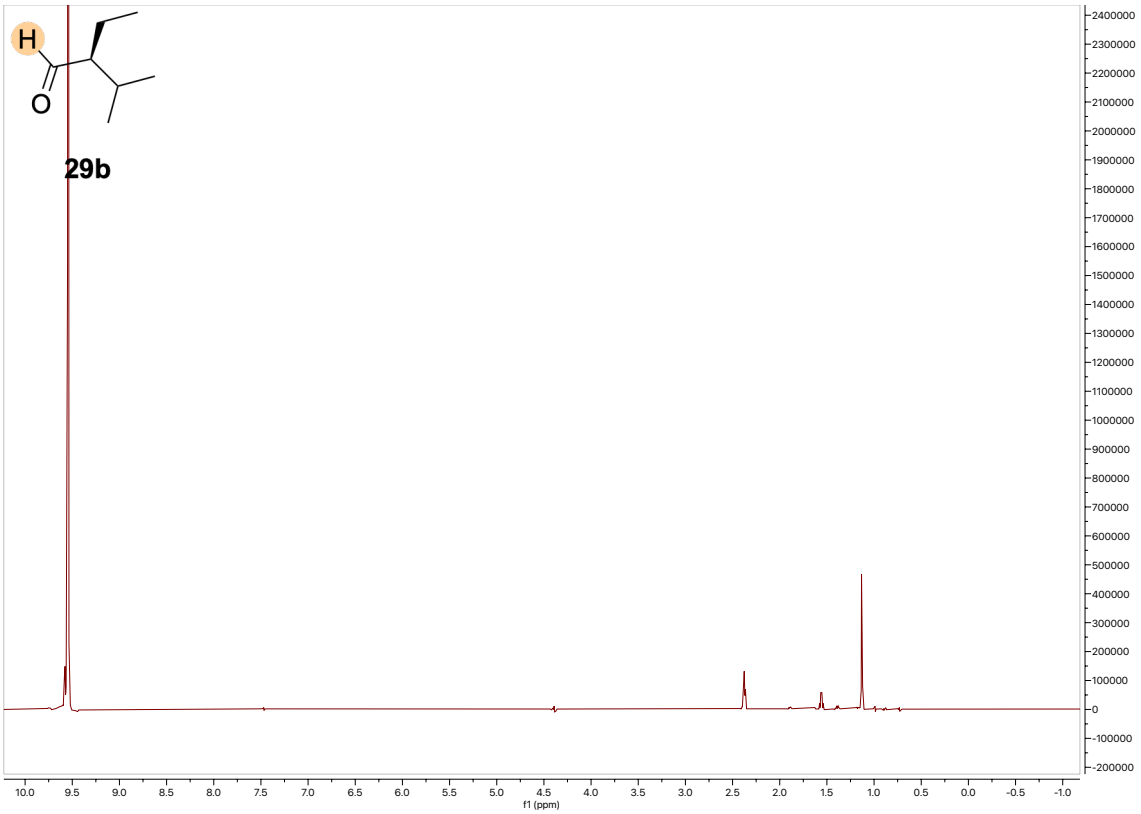
1D Selective Gradient TOCSY (800 MHz, CD_3OD) at 4.554 ppm of **26b**



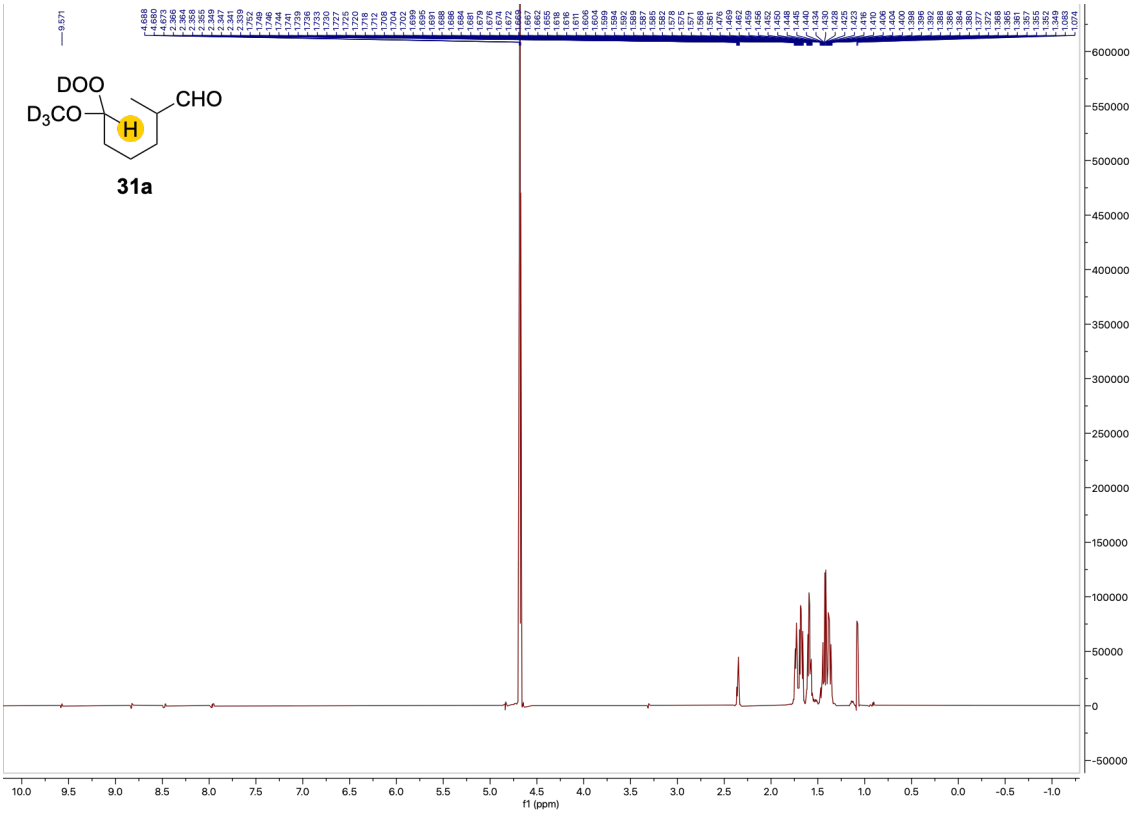
1D Selective Gradient TOCSY (800 MHz, CD_3OD) at 4.713 ppm of **26c**



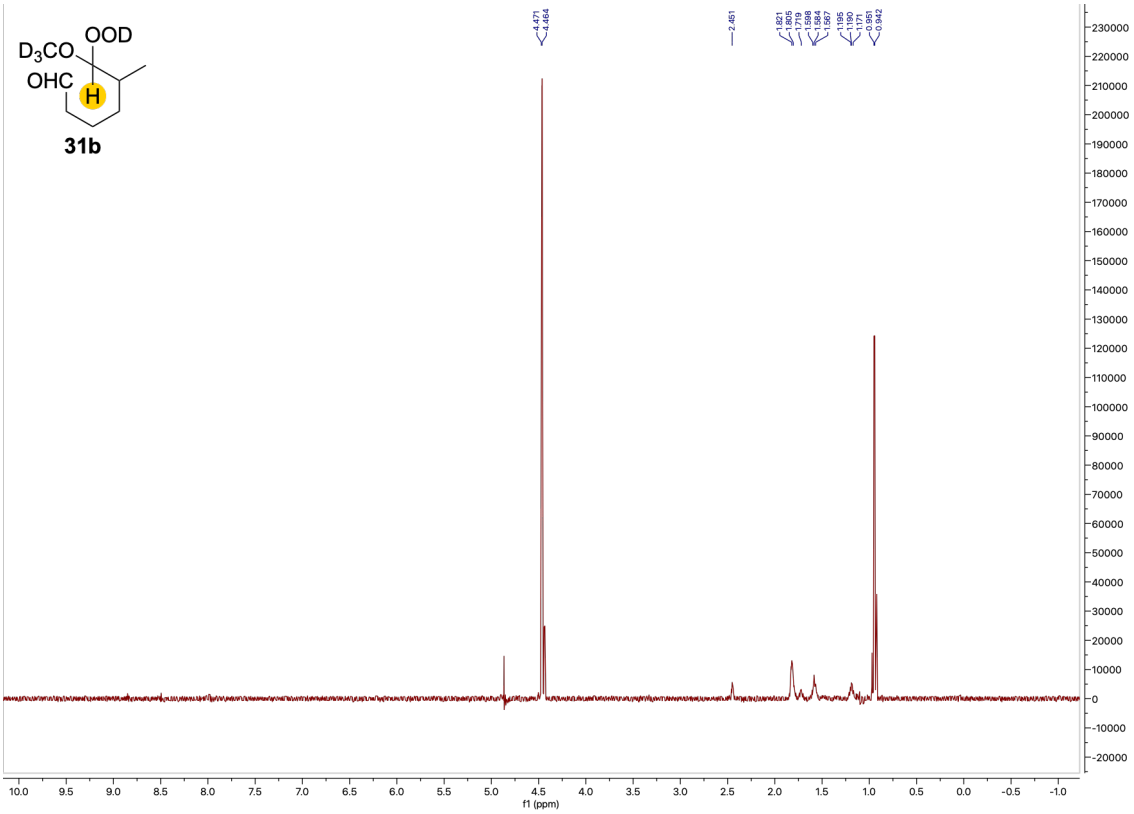
1D Selective Gradient TOCSY (800 MHz, CD_3OD) at 9.34 ppm of **29a**



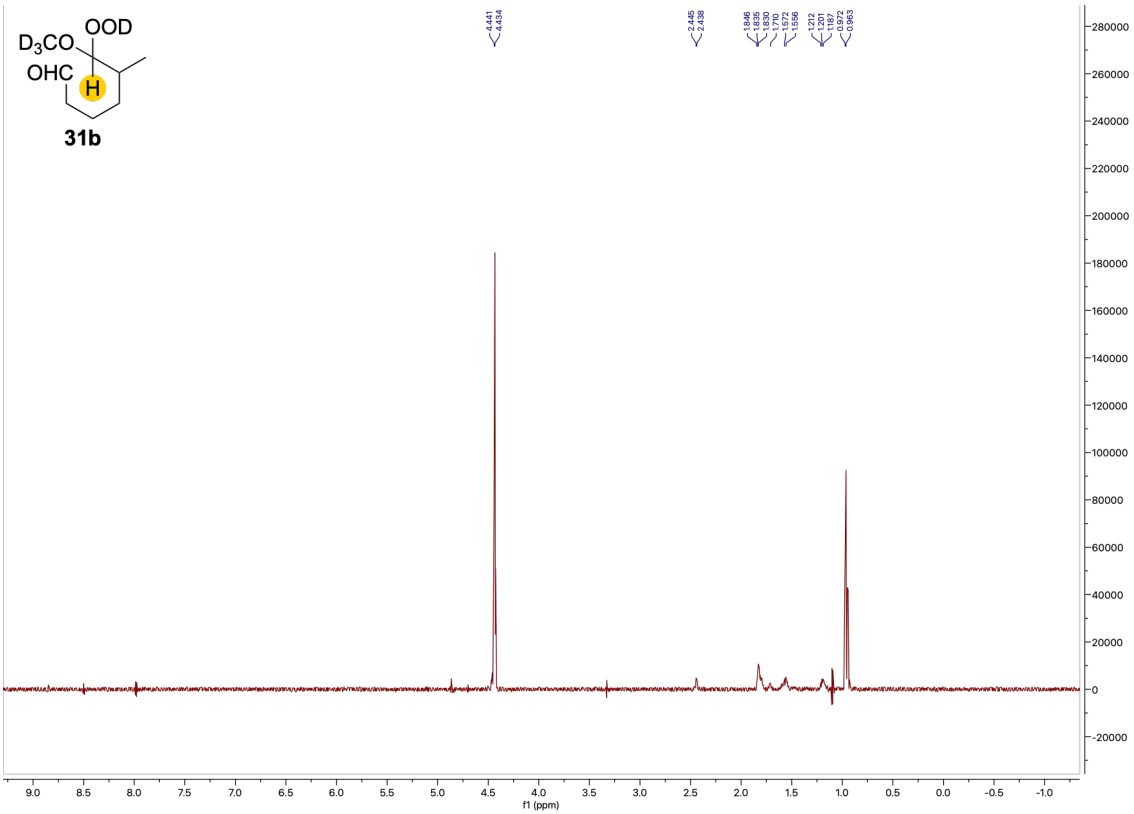
1D Selective Gradient TOCSY (800 MHz, CD_3OD) at 9.37 ppm of **29b**



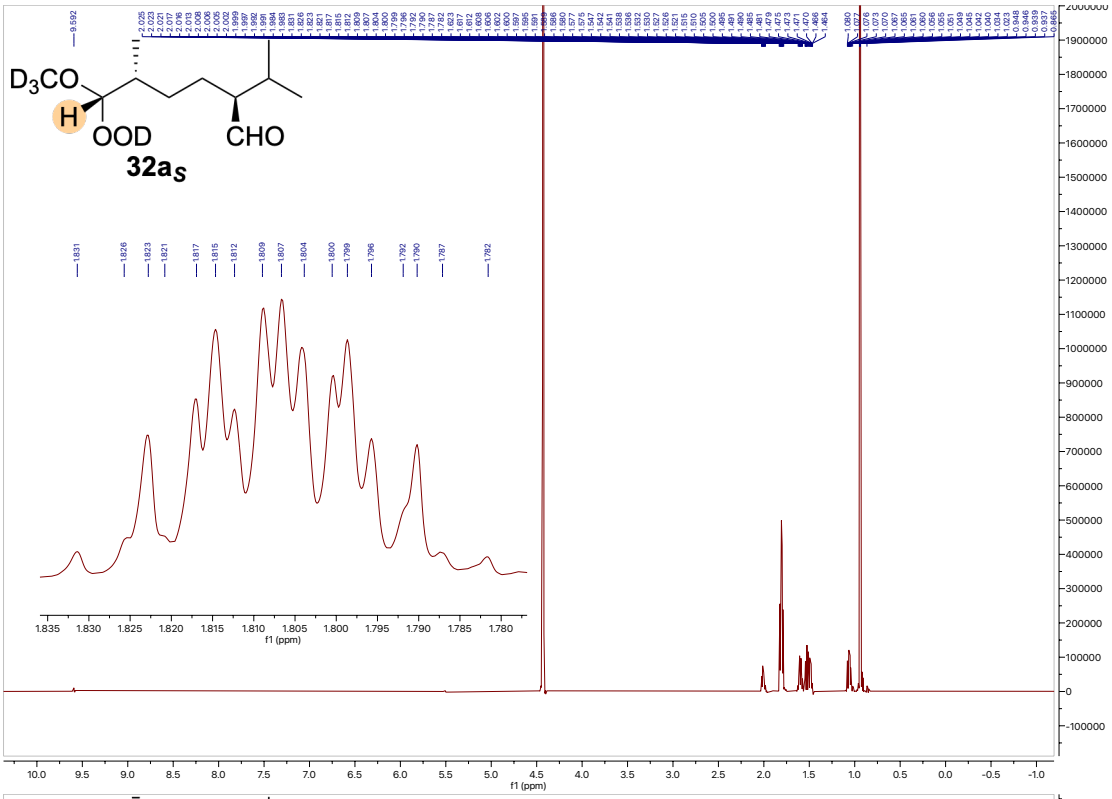
1D Selective Gradient TOCSY (800 MHz, CD_3OD) at 4.680 ppm of **31a**

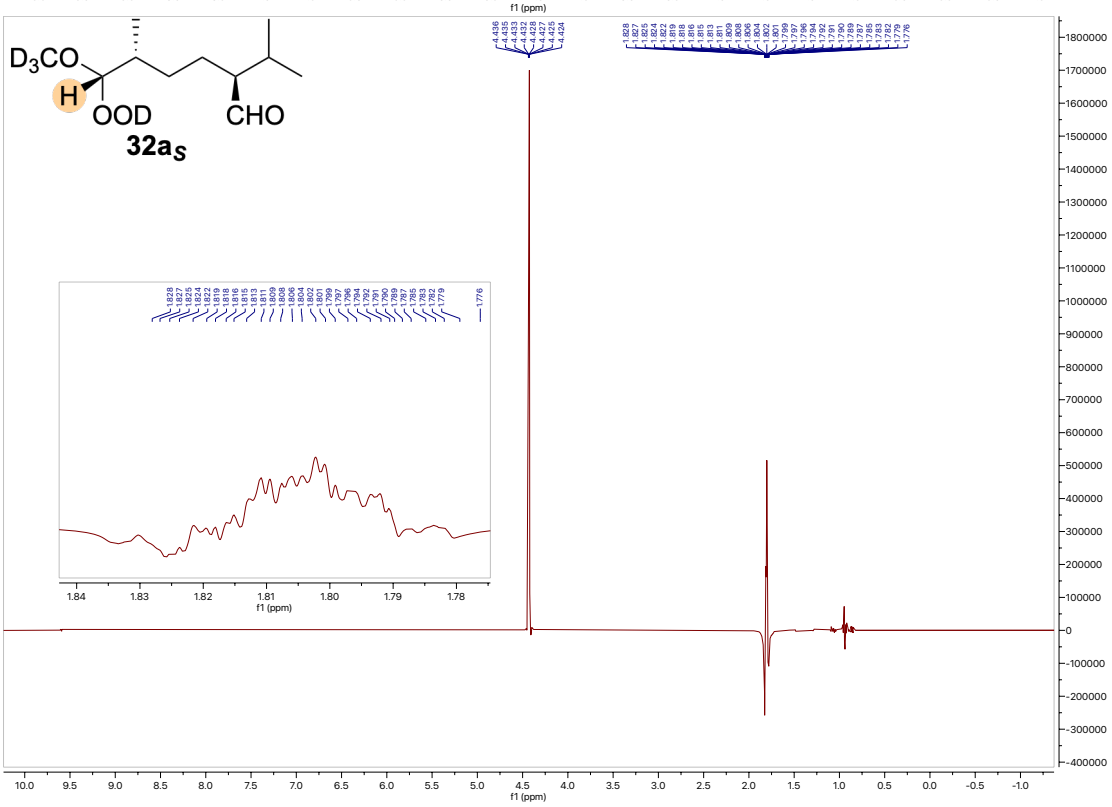


1D Selective Gradient TOCSY (800 MHz, CD_3OD) at 4.471 ppm of **31b**

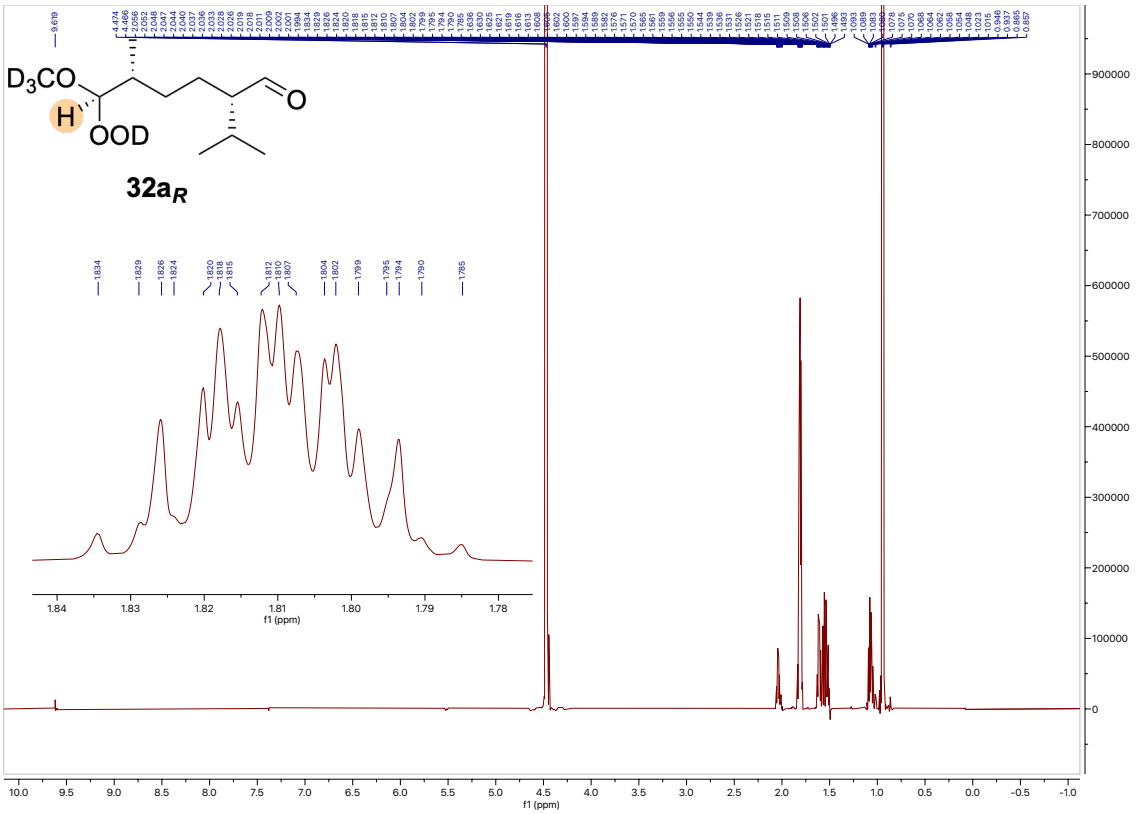


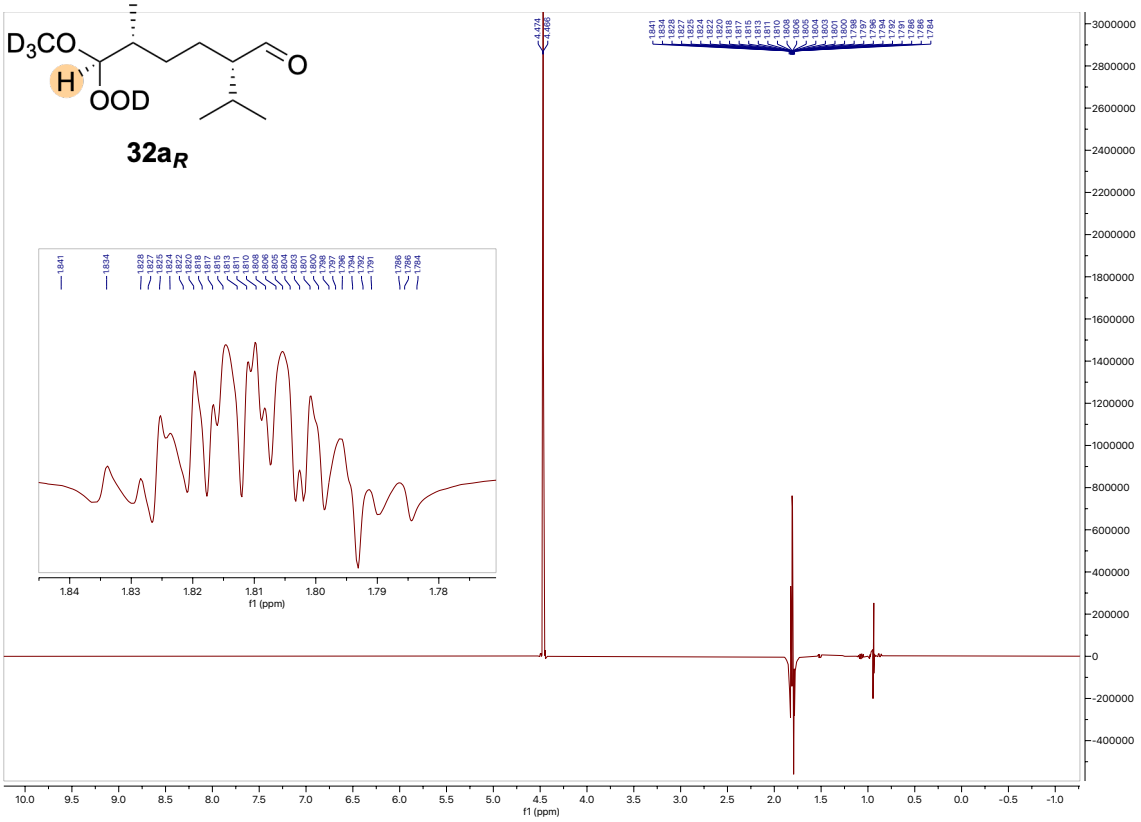
1D Selective Gradient TOCSY (800 MHz, CD_3OD) at 4.441 ppm of **31b**



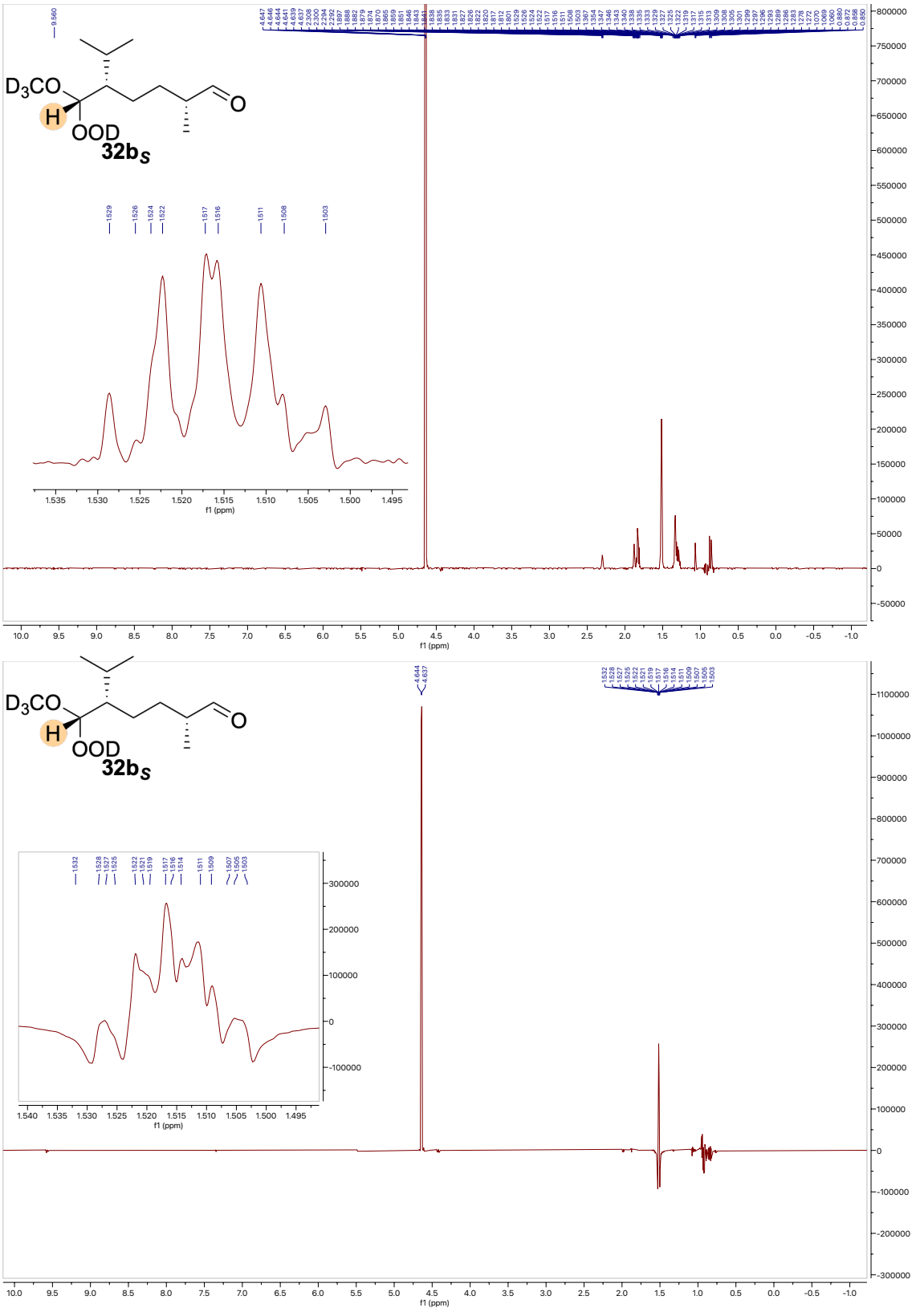


1D Selective Gradient TOCSY and **1D Selective Gradient COSY** at 4.64 ppm of **32b*s***

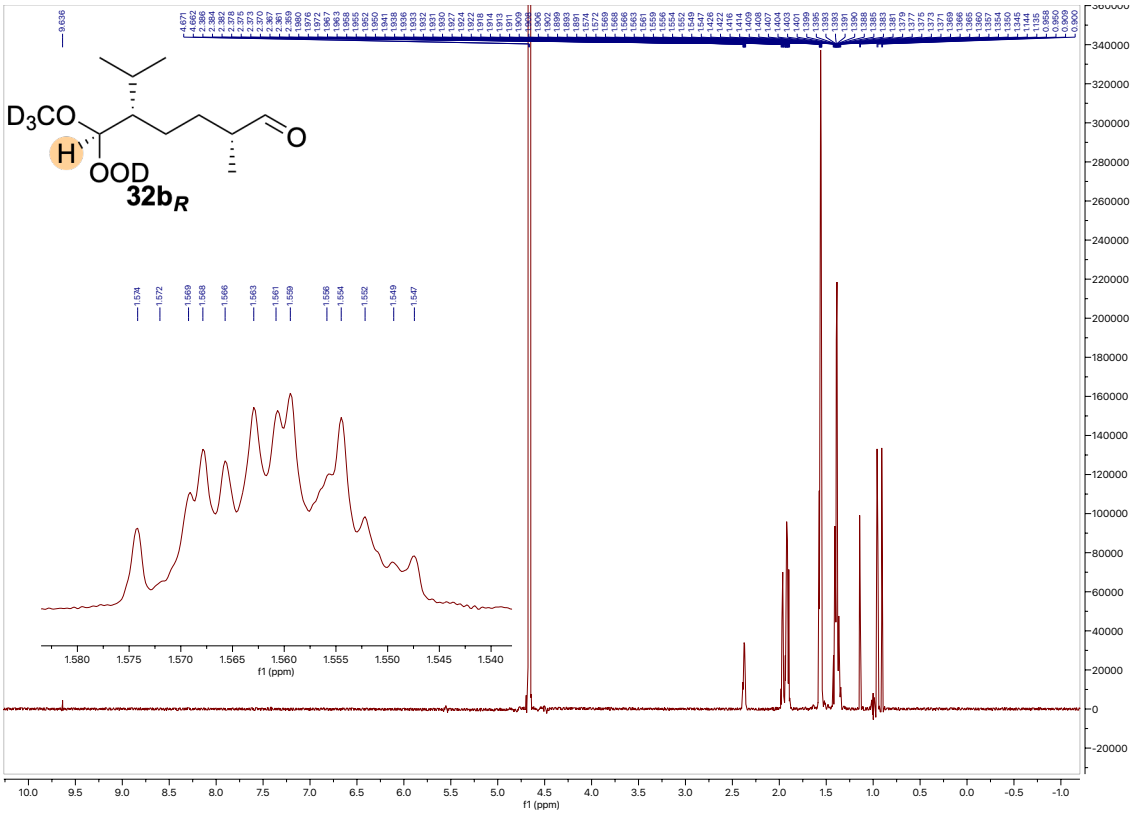


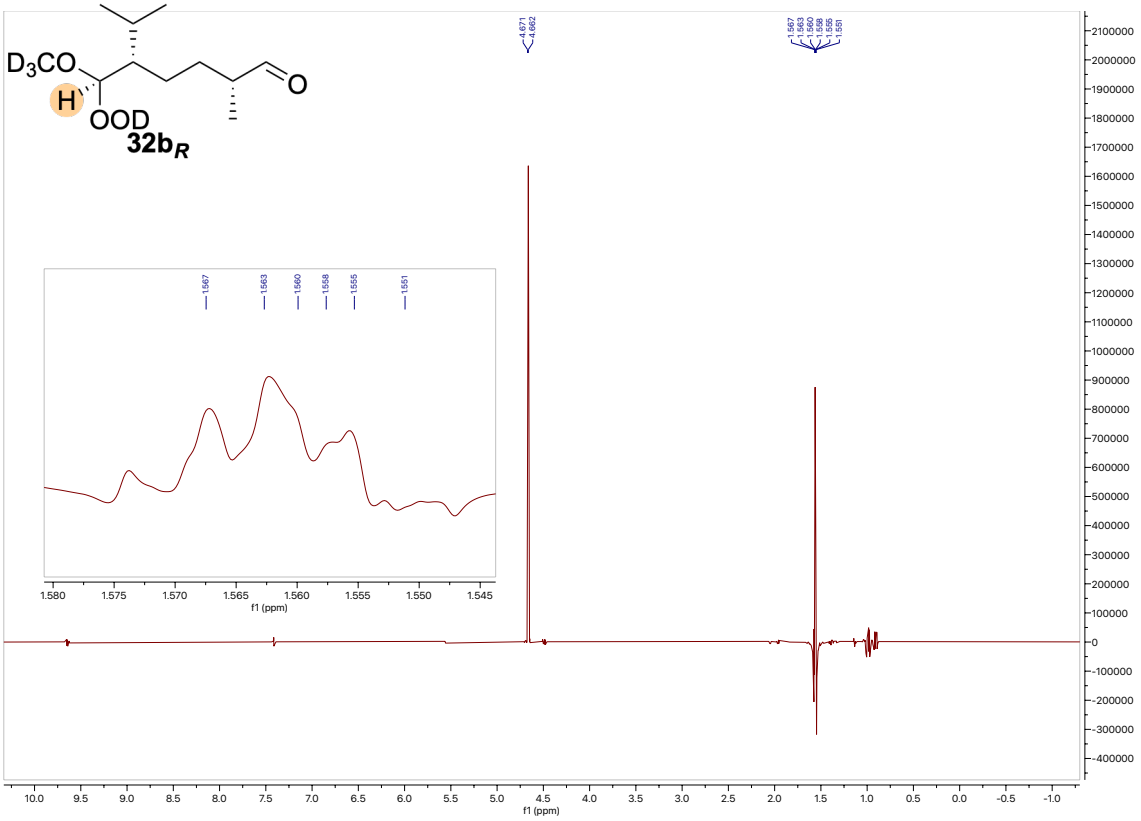


1D Selective Gradient TOCSY and **1D Selective Gradient COSY** at 4.64 ppm of **32a*R***

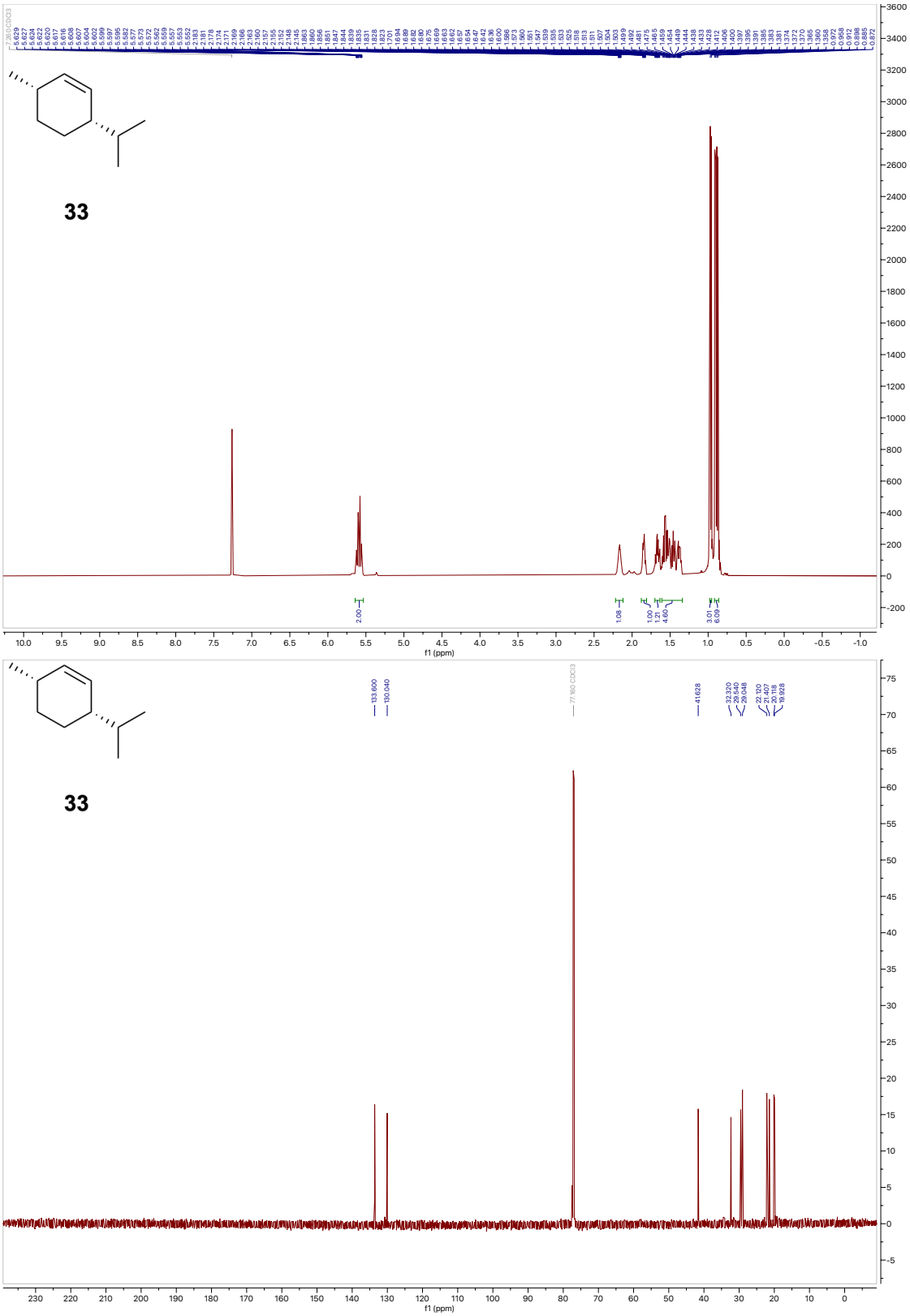


1D Selective Gradient TOCSY and **1D Selective Gradient COSY** at 4.64 ppm of **32b*S***

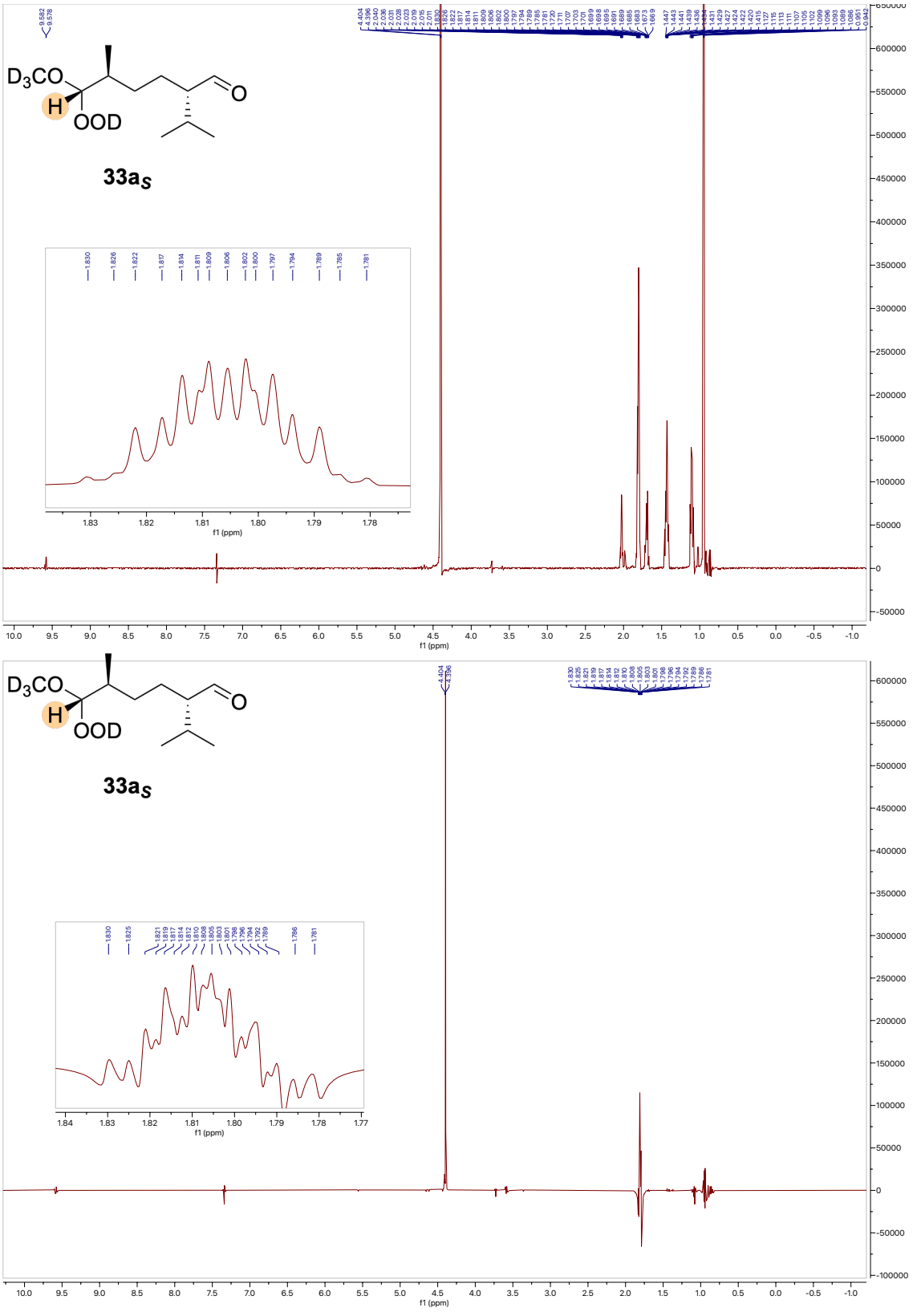




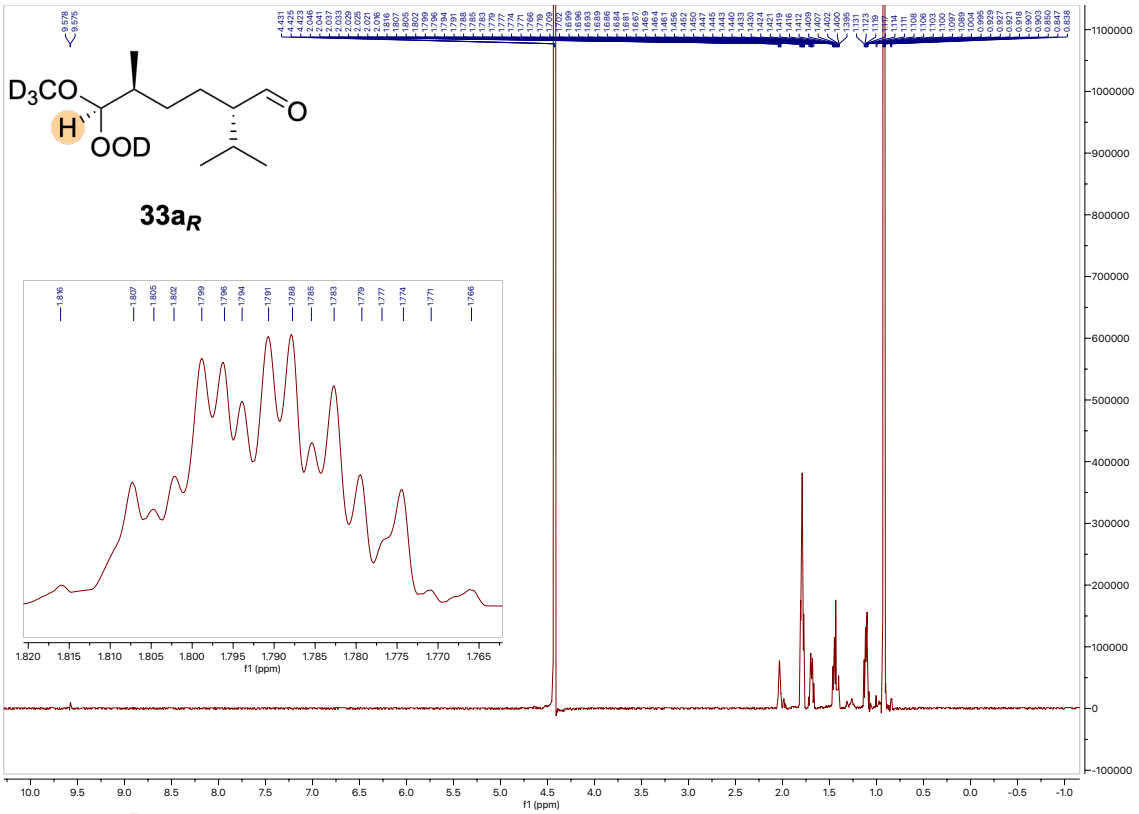
1D Selective Gradient TOCSY and **1D Selective Gradient COSY** at 4.67 ppm of **32b*R***

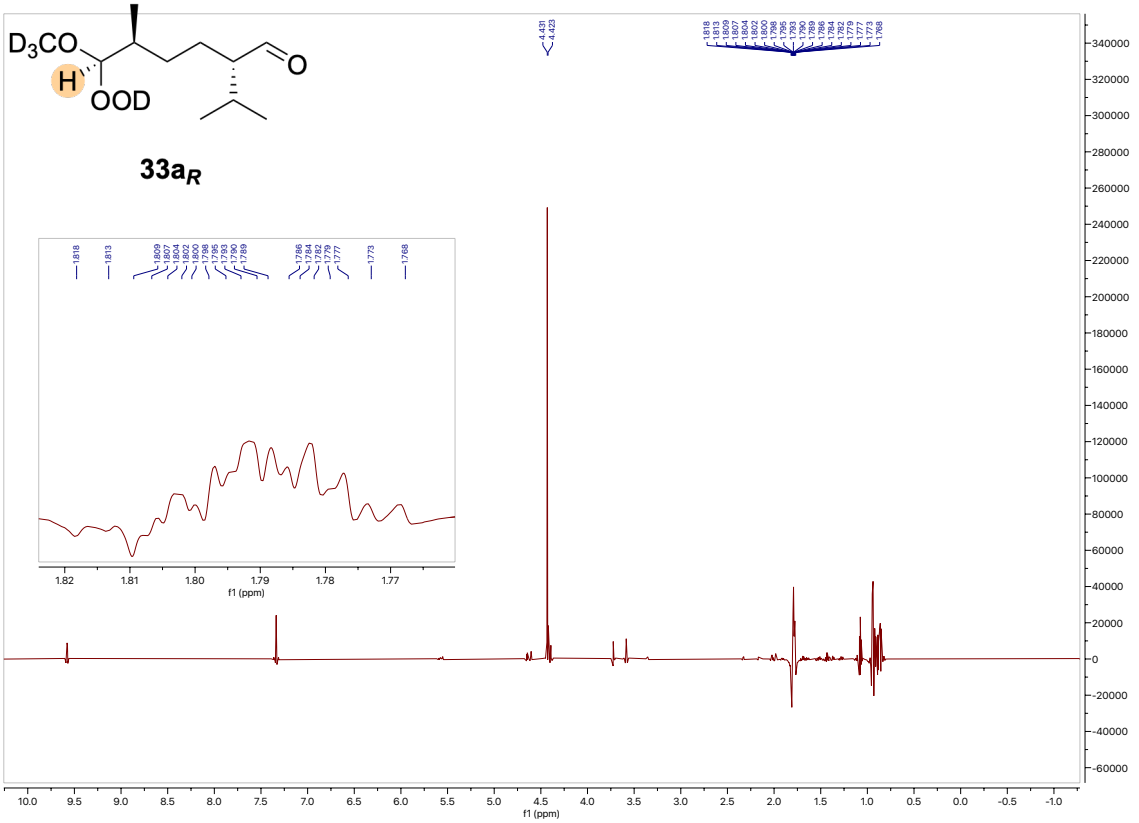


^{1}H NMR (500 MHz, $CDCl_3$) and **^{13}C NMR** (126 MHz, $CDCl_3$) of **33**

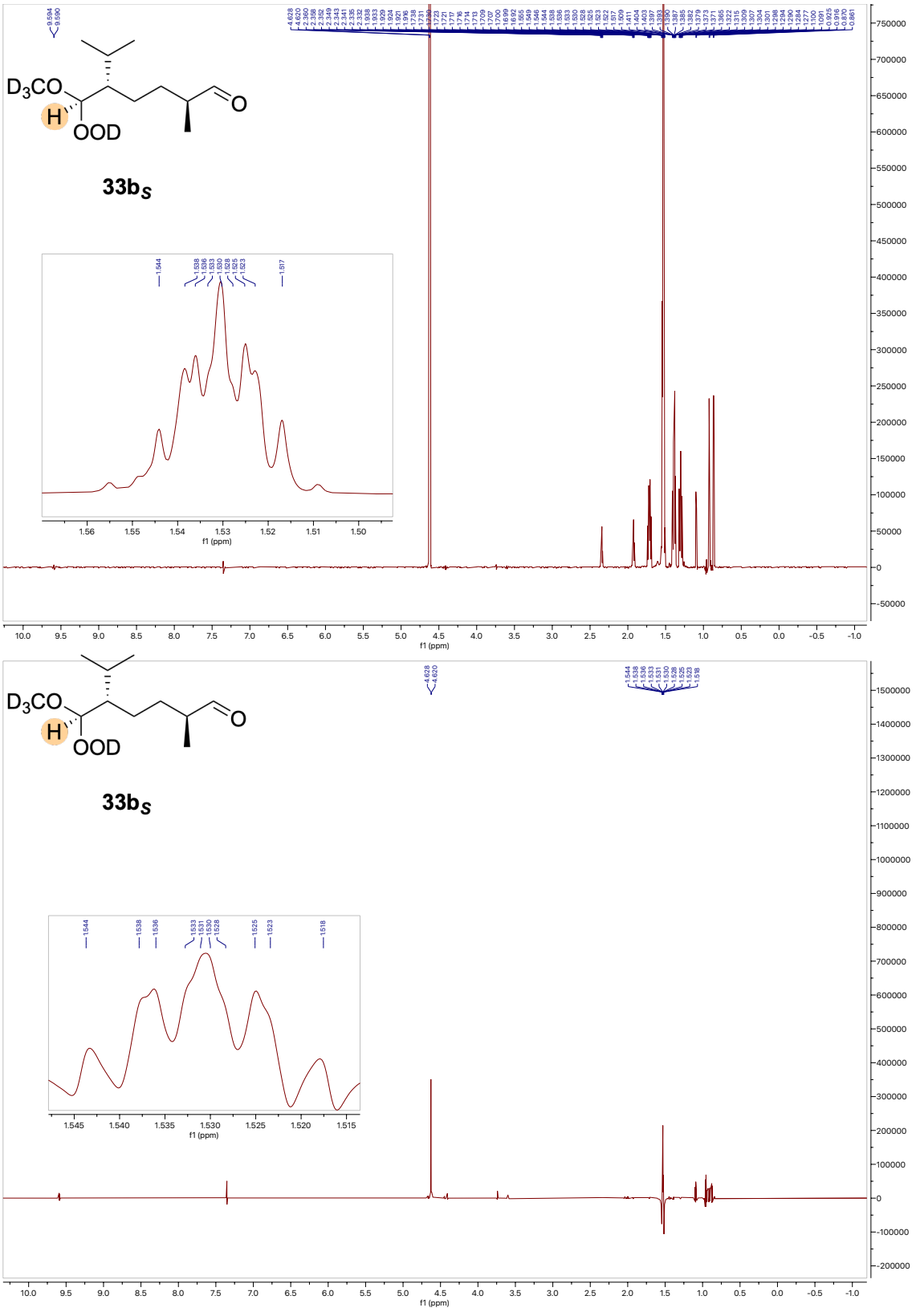


1D Selective Gradient TOCSY and **1D Selective Gradient COSY** at 4.64 ppm of **33a*s***

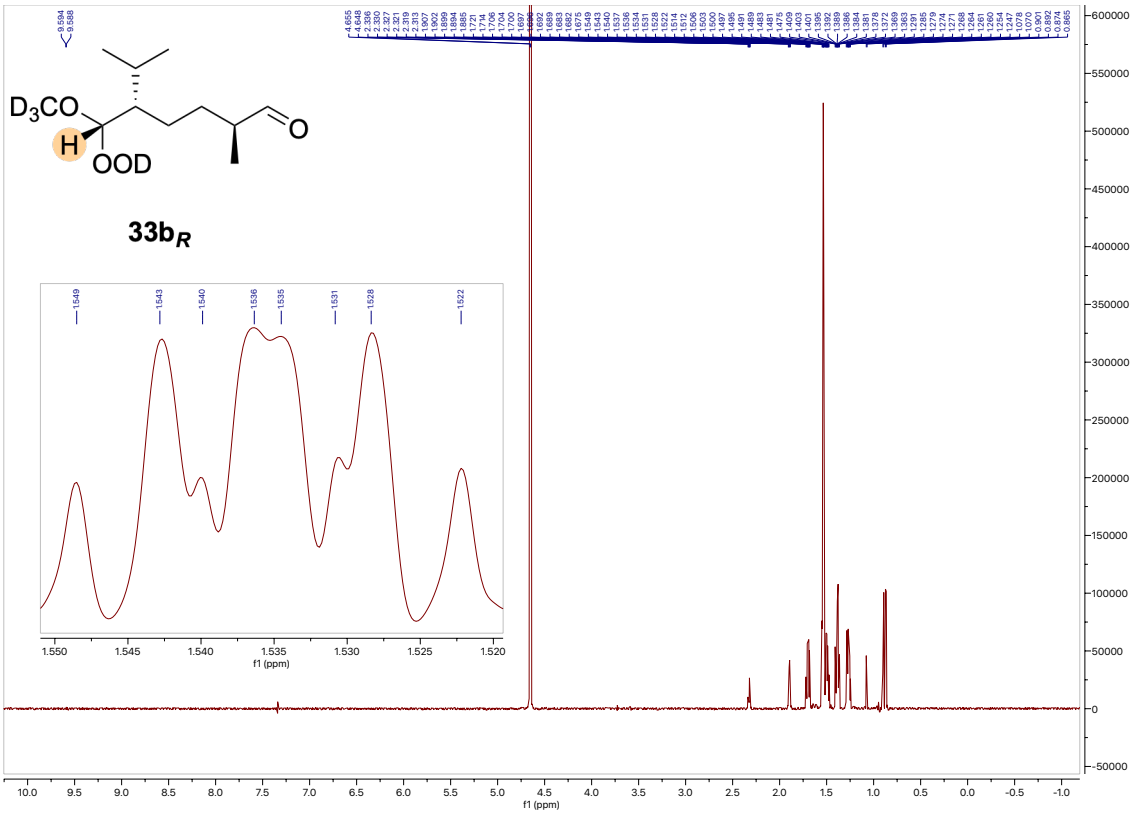


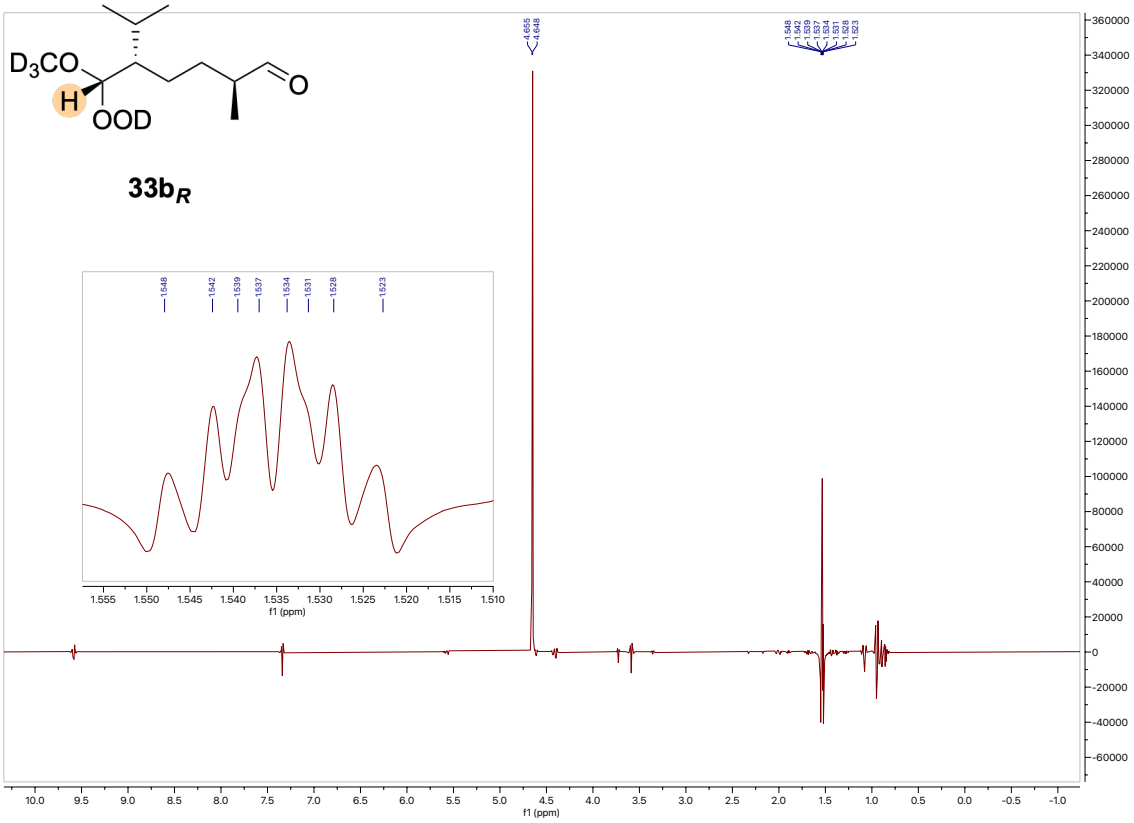


1D Selective Gradient TOCSY and **1D Selective Gradient COSY** at 4.64 ppm of **33a*R***

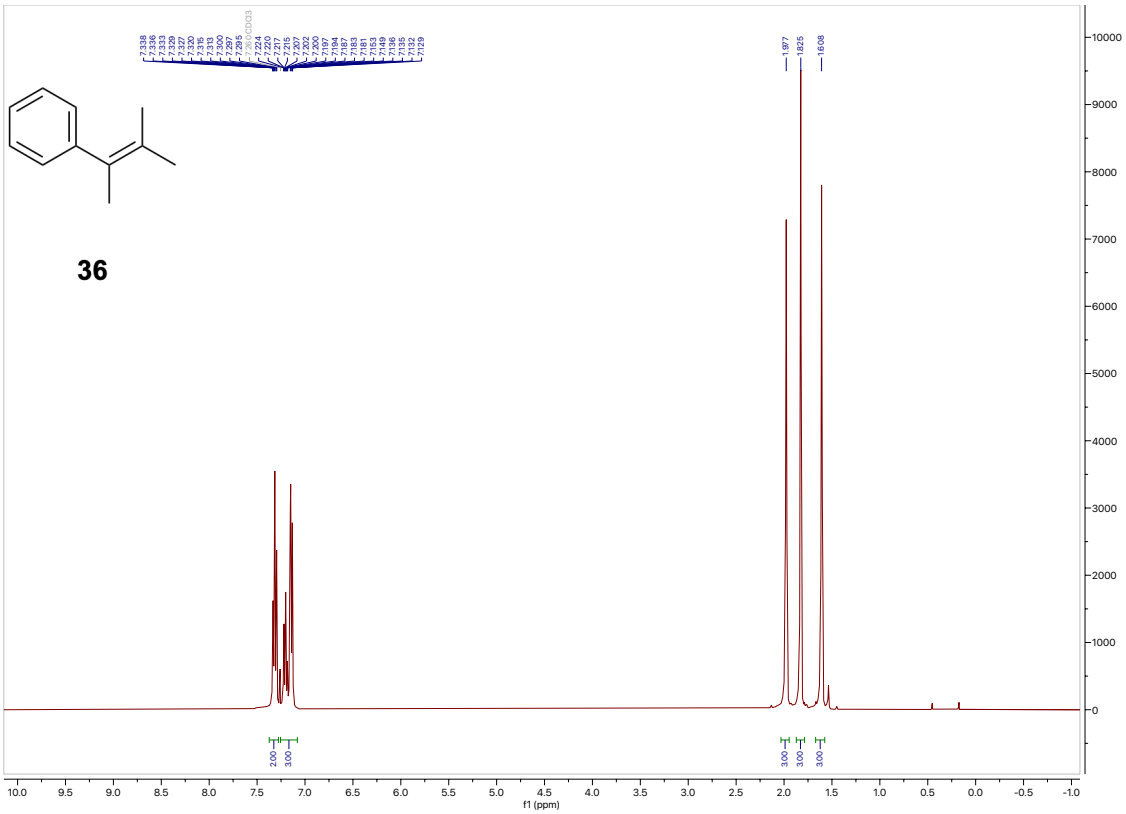


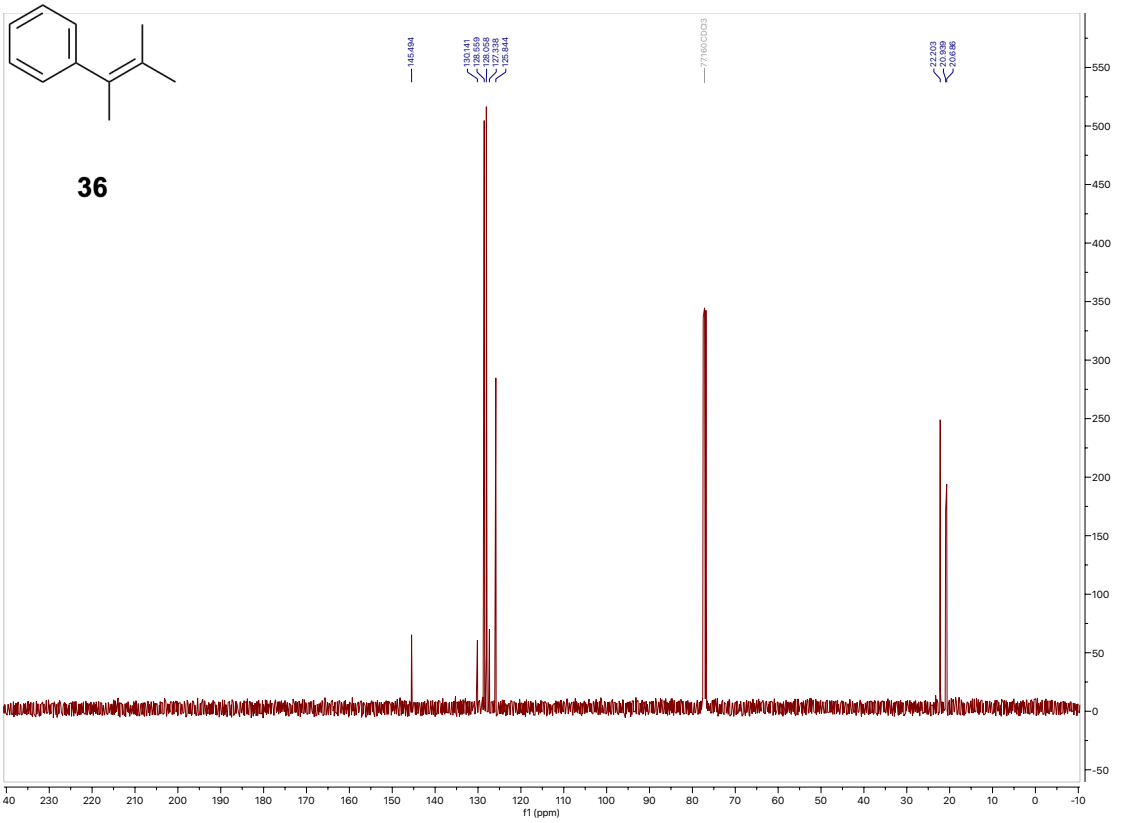
1D Selective Gradient TOCSY and **1D Selective Gradient COSY** at 4.67 ppm of **33b*S***



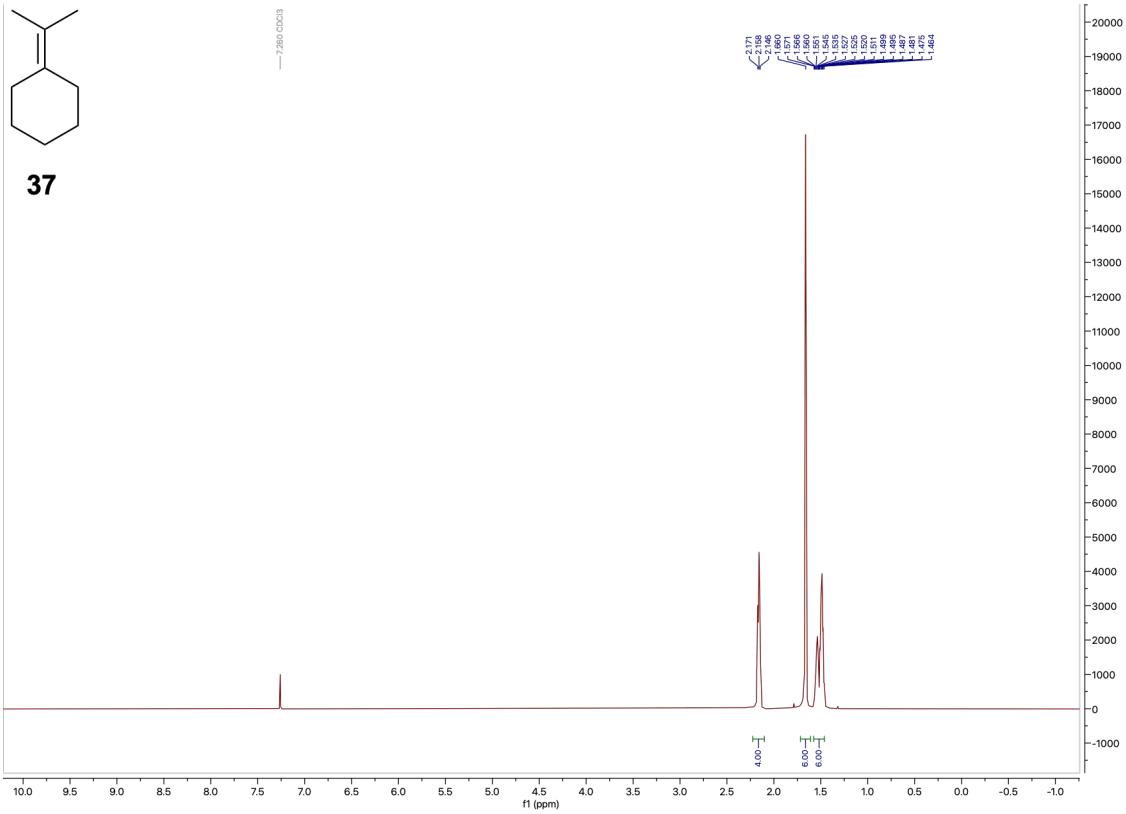


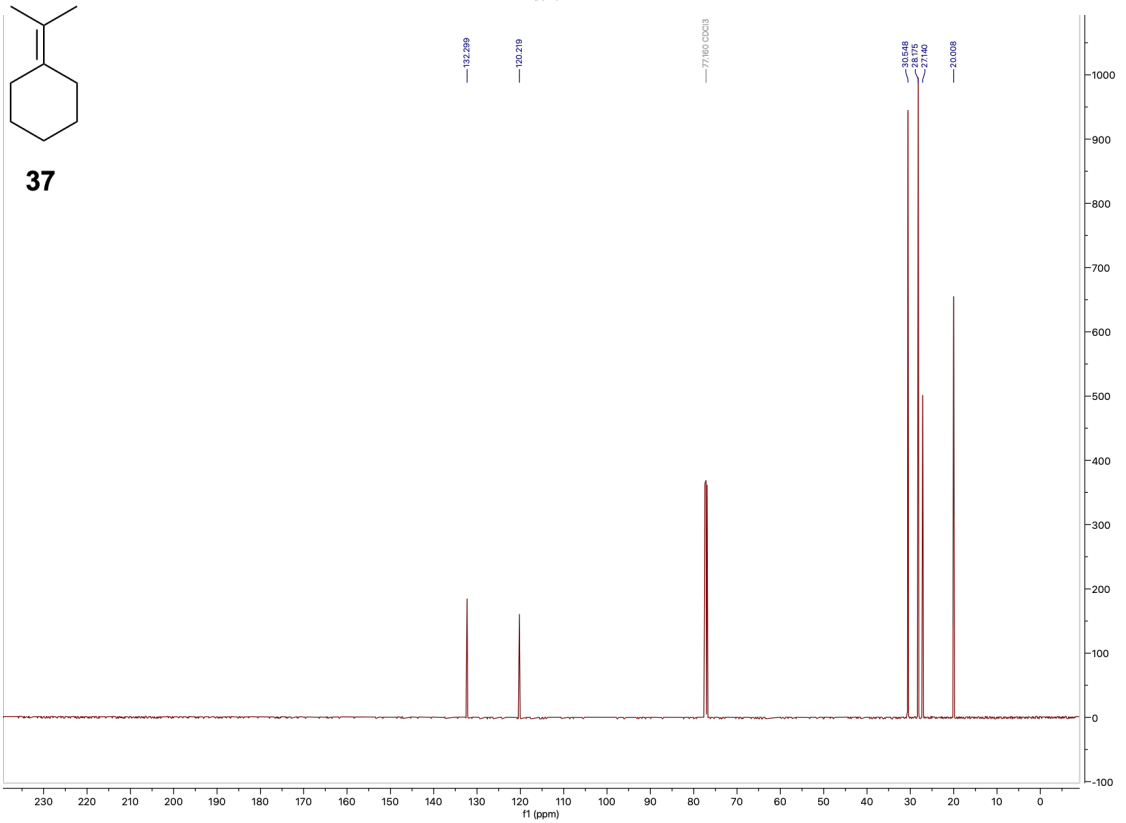
1D Selective Gradient TOCSY and **1D Selective Gradient COSY** at 4.64 ppm of **33b*R***



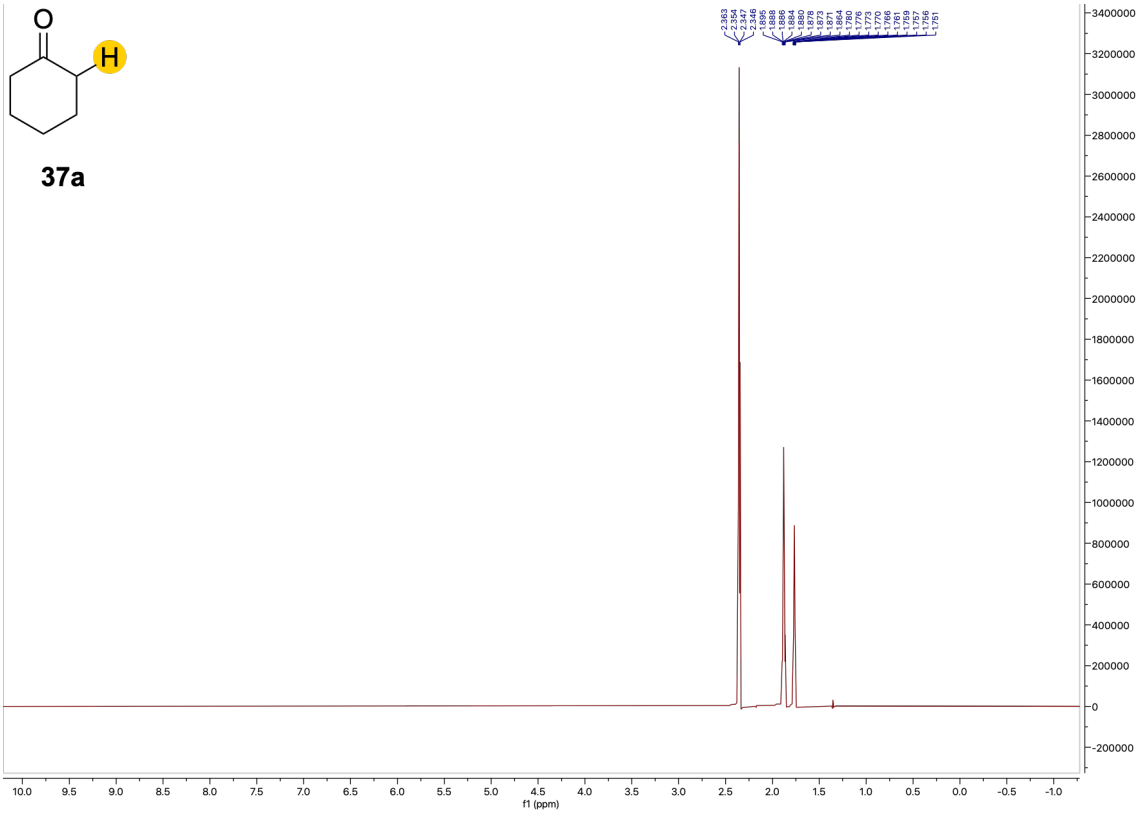


^{1}H NMR (400 MHz, $CDCl_3$) and **^{13}C NMR** (101 MHz, $CDCl_3$) of **36**

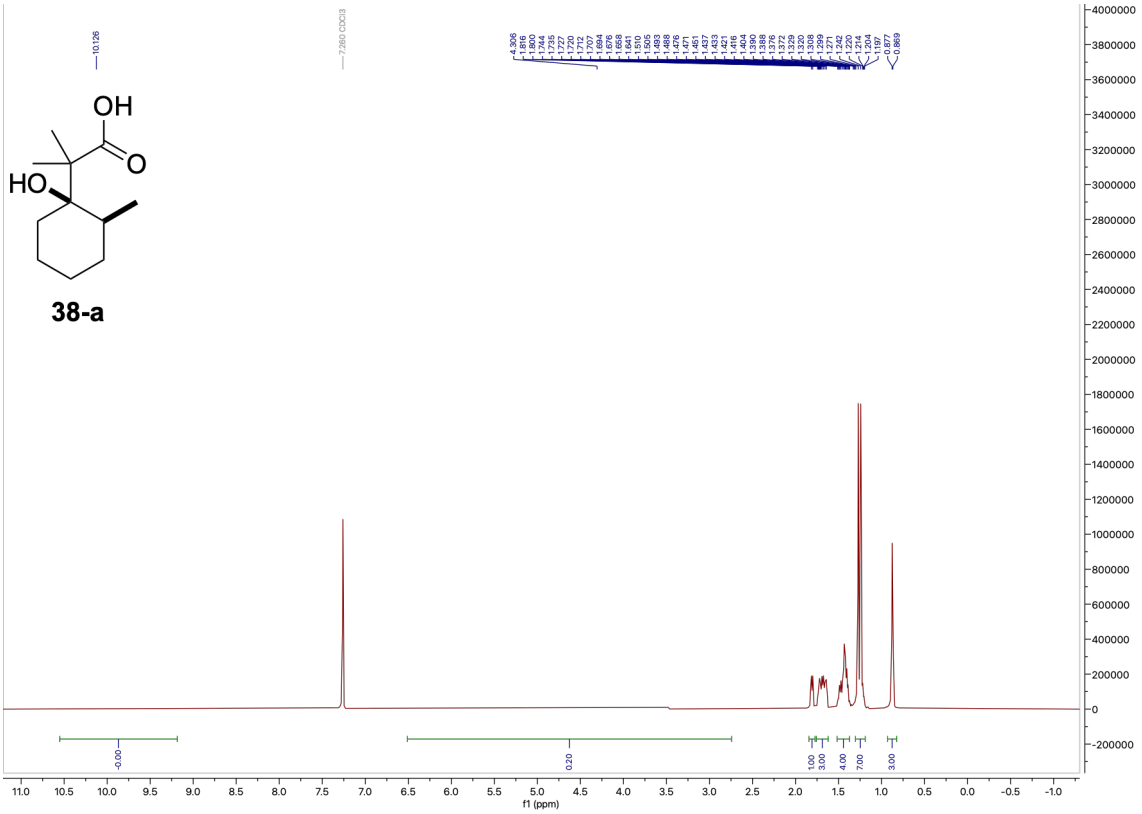


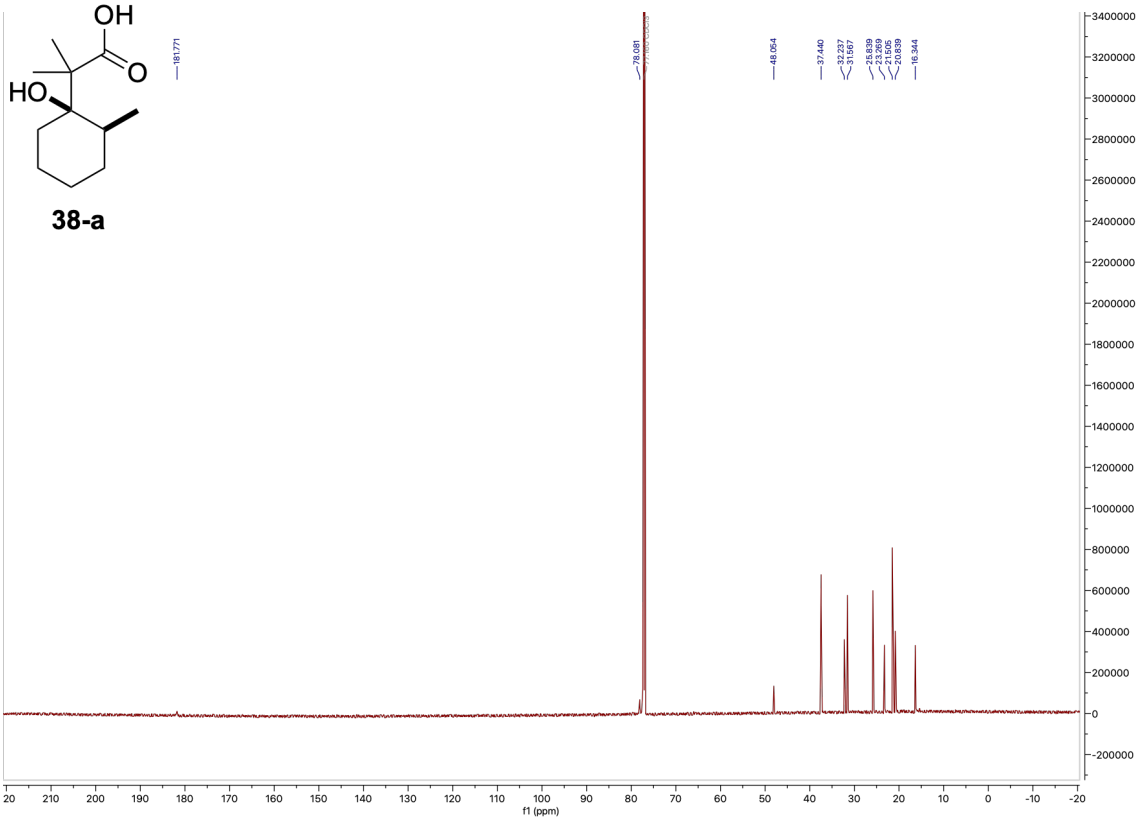


^{1}H NMR (500 MHz, $CDCl_3$) and **^{13}C NMR** (126 MHz, $CDCl_3$) of **37**

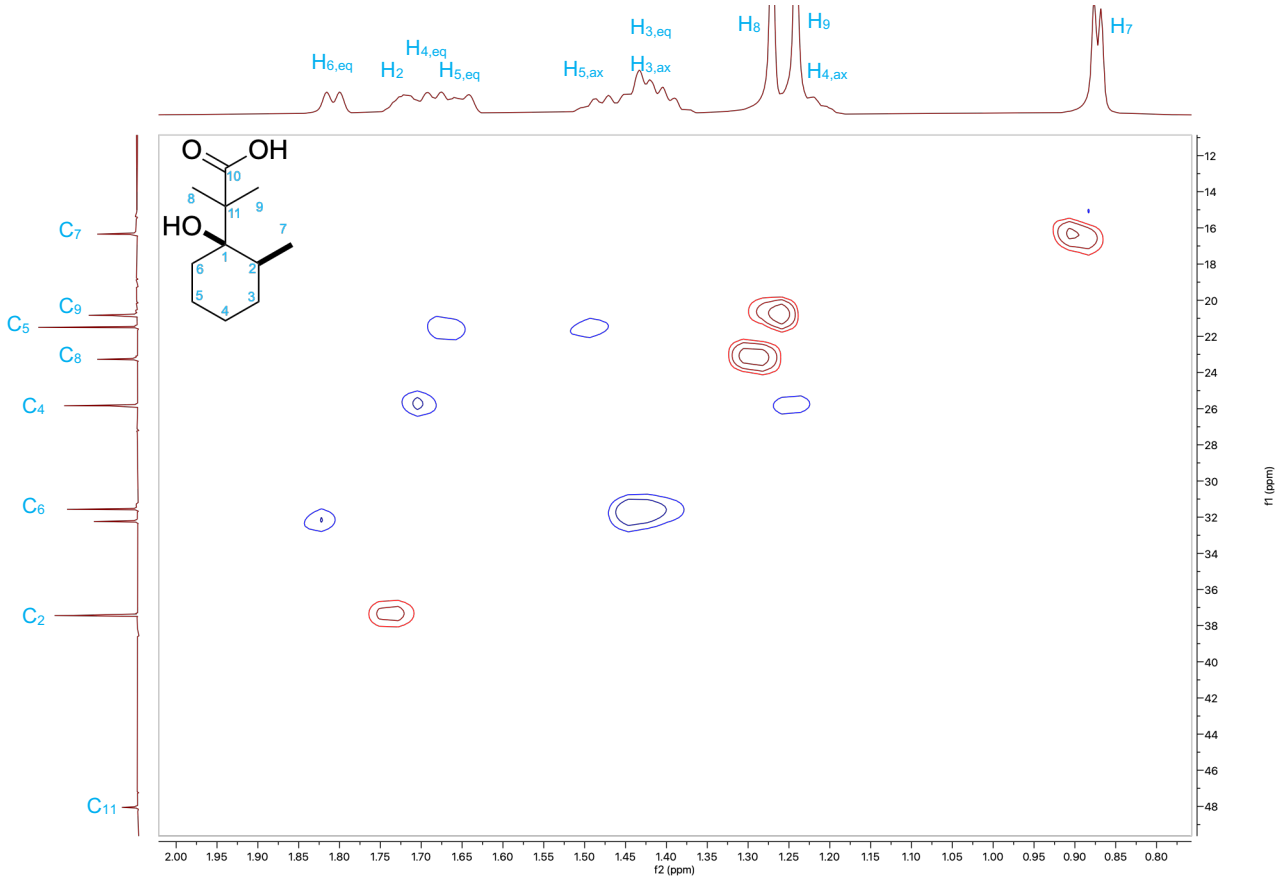


1D Selective Gradient TOCSY (800 MHz, CD_3OD) at 2.353 ppm of **37a**

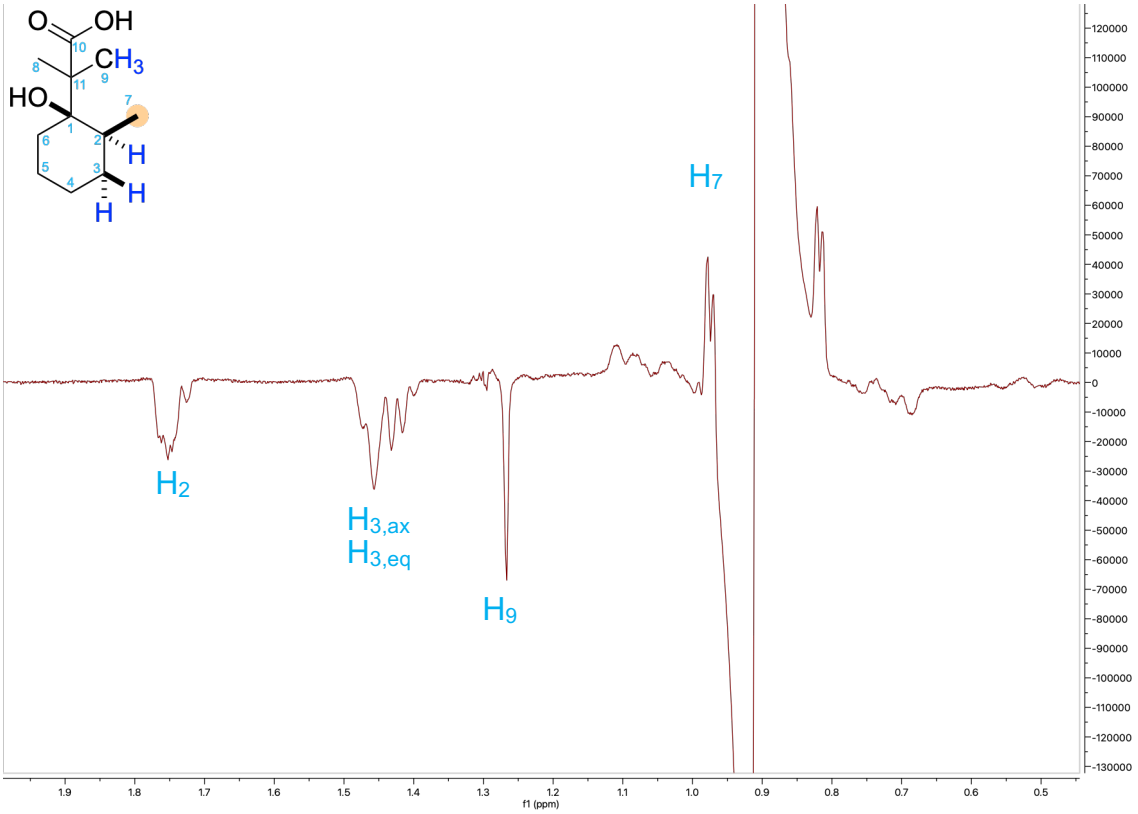




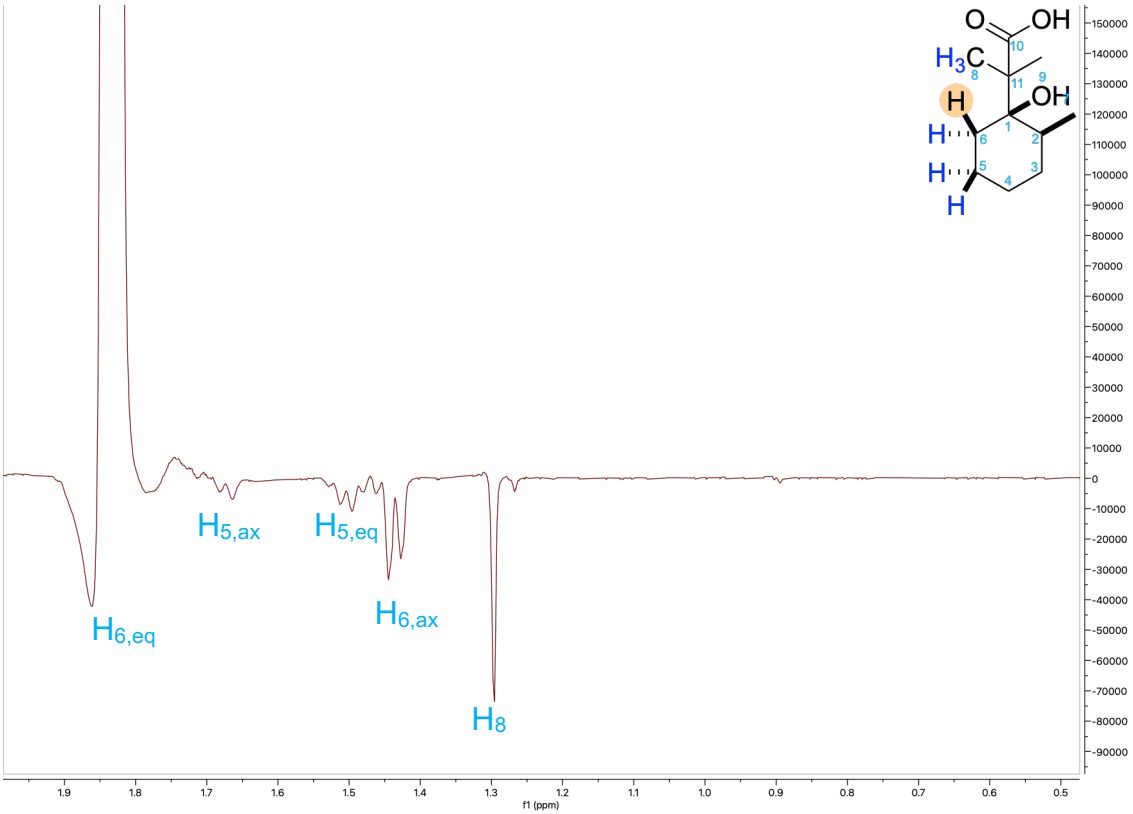
^{1}H NMR (800 MHz, $CDCl_3$) and **^{13}C NMR** (201 MHz, $CDCl_3$) of **38-a**



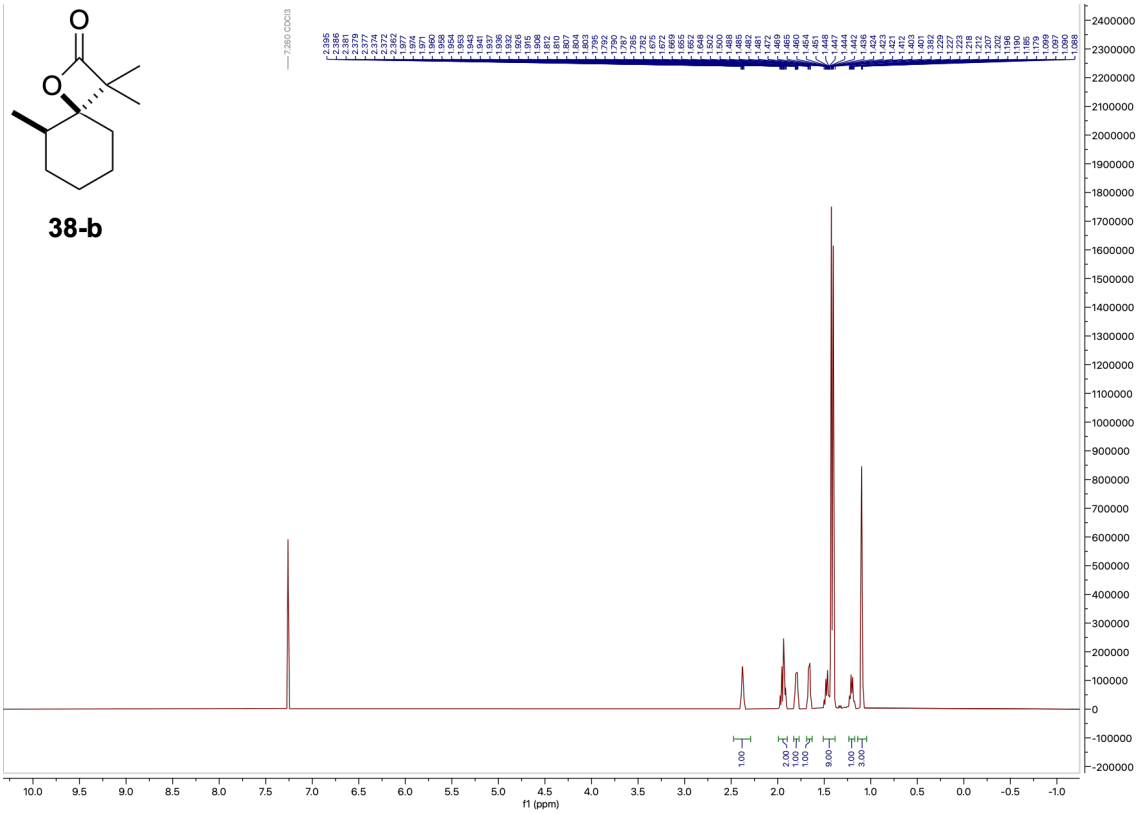
HSQC ($CDCl_3$) of **38-a**

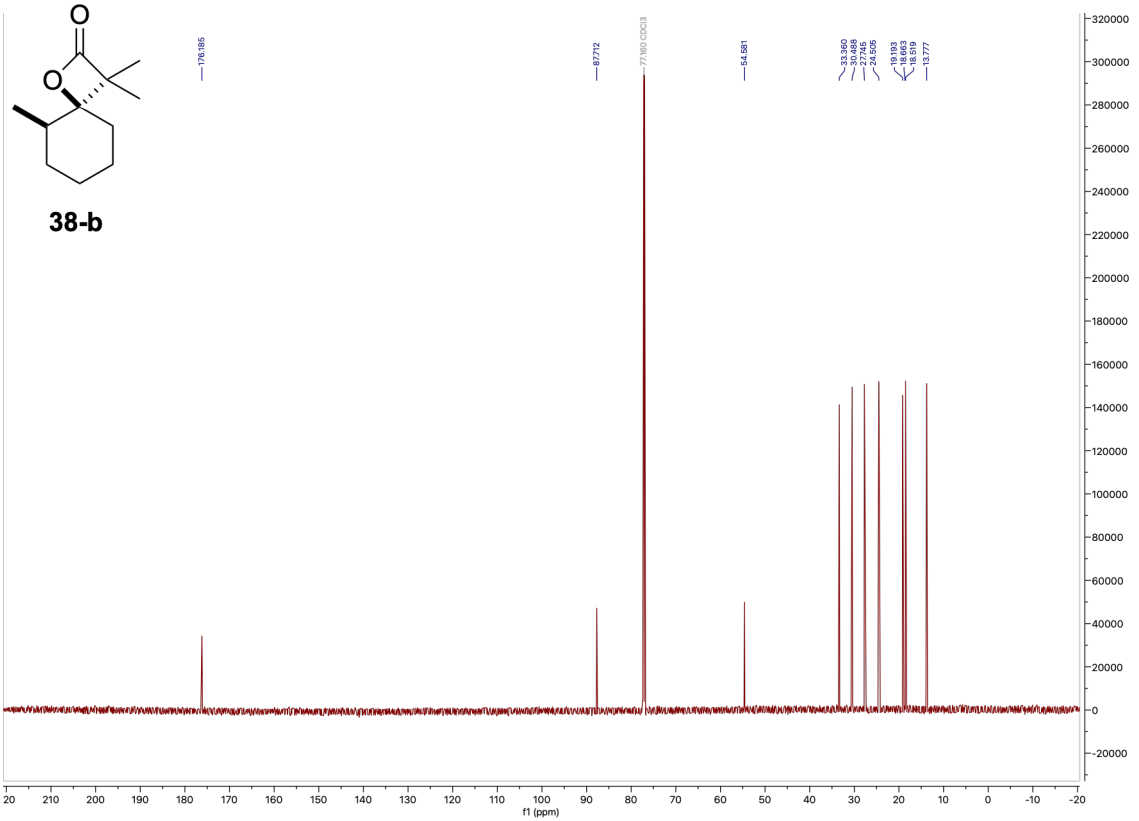


1D Selective Gradient NOESY (800 MHz, $CDCl_3$) at 0.904 ppm of **38-a**

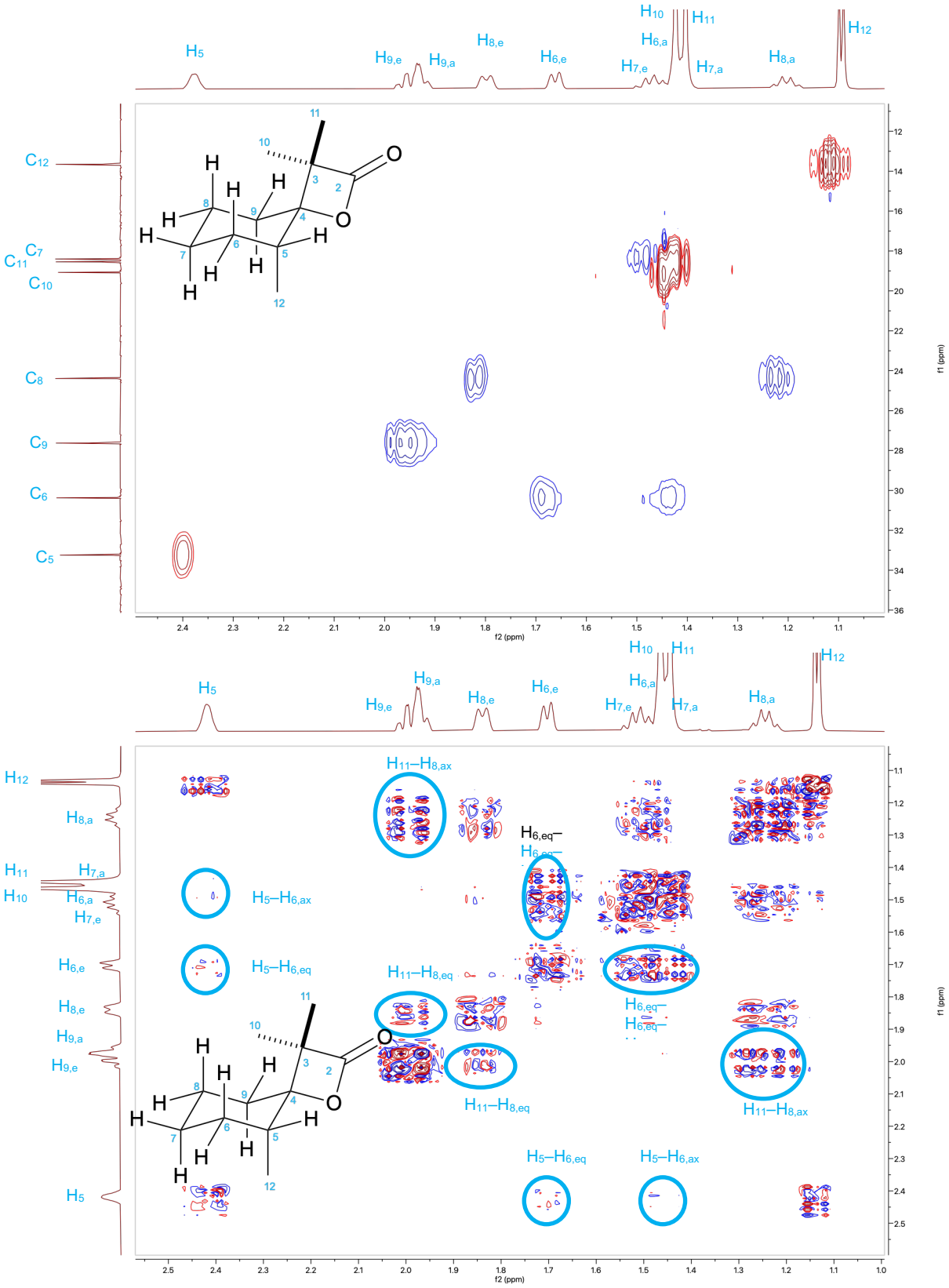


1D Selective Gradient NOESY (800 MHz, $CDCl_3$) at 1.856 ppm of **38-a**

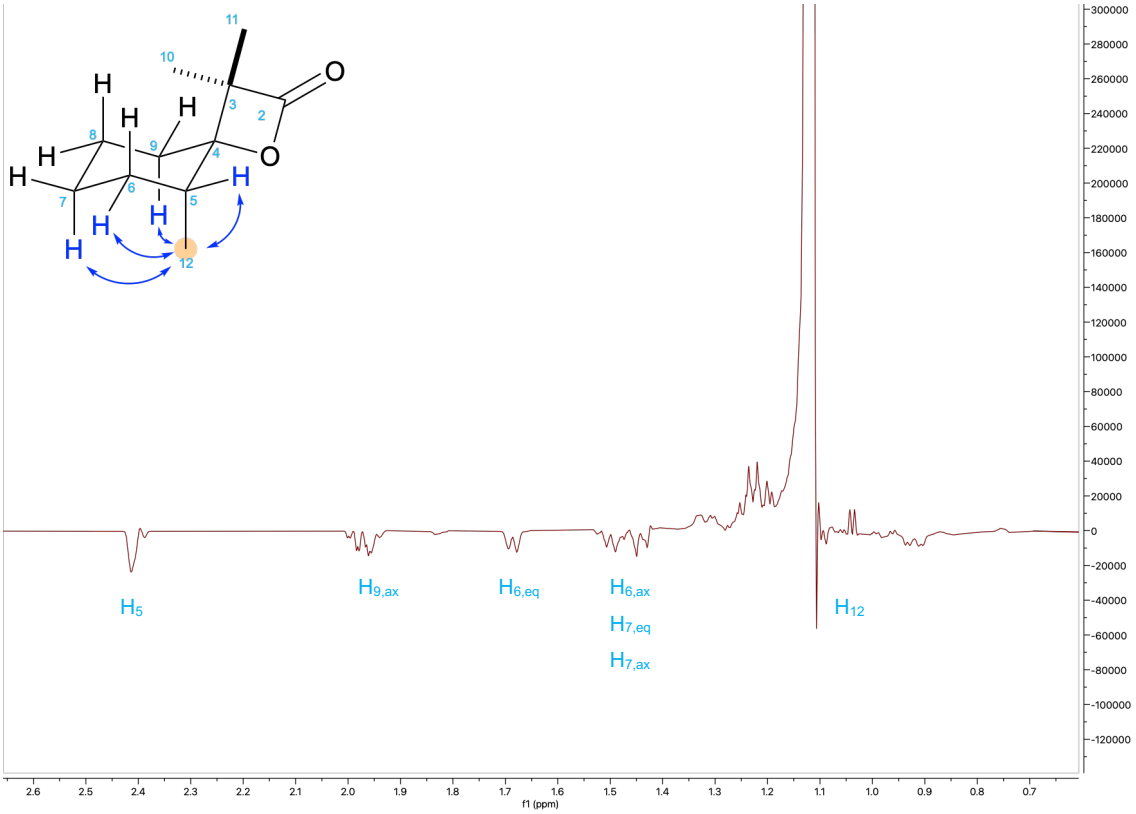




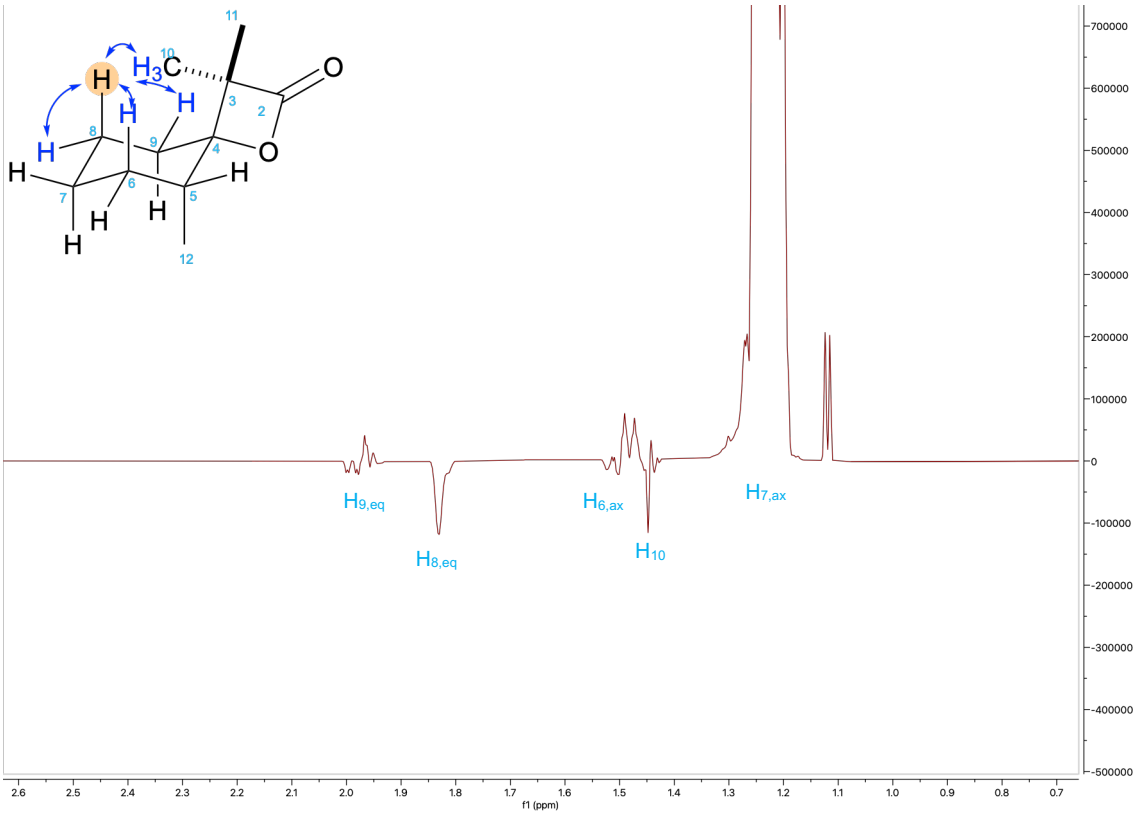
^{1}H NMR (800 MHz, $CDCl_3$) and **^{13}C NMR** (201 MHz, $CDCl_3$) of **38-b**



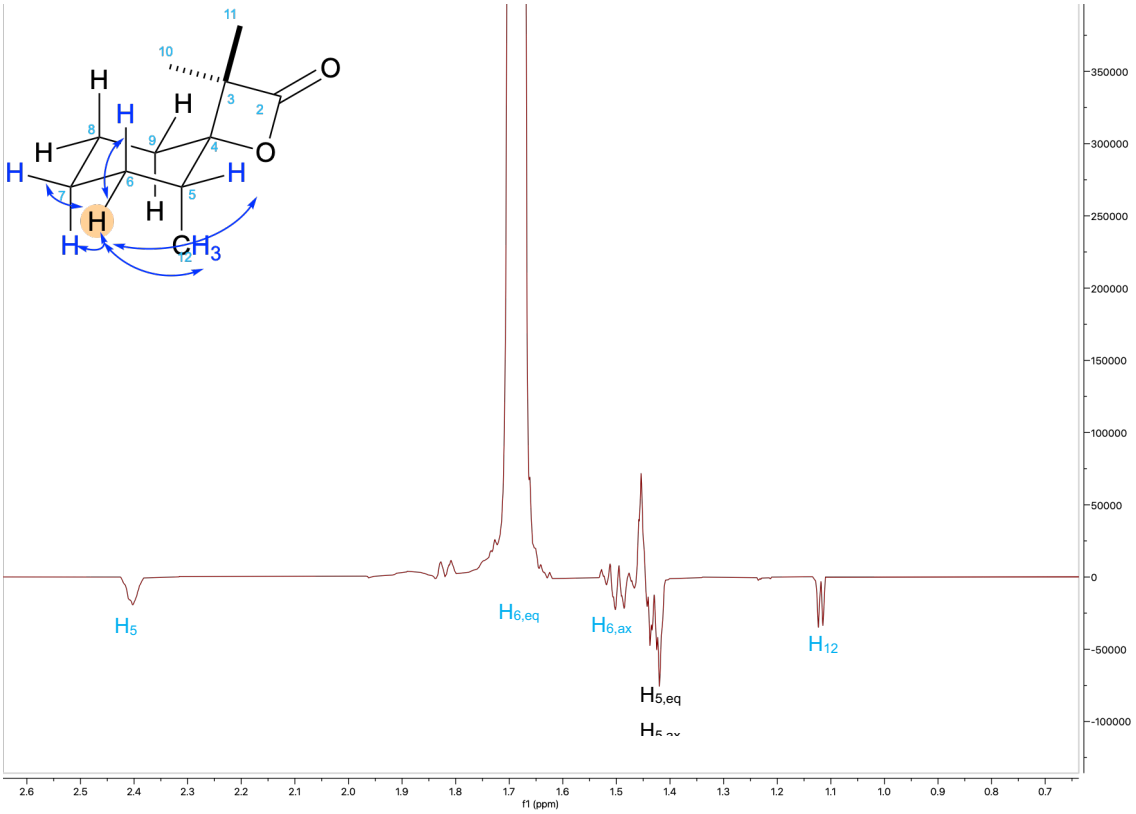
HSQC ($CDCl_3$) and **COSY** ($CDCl_3$) of **38-b**



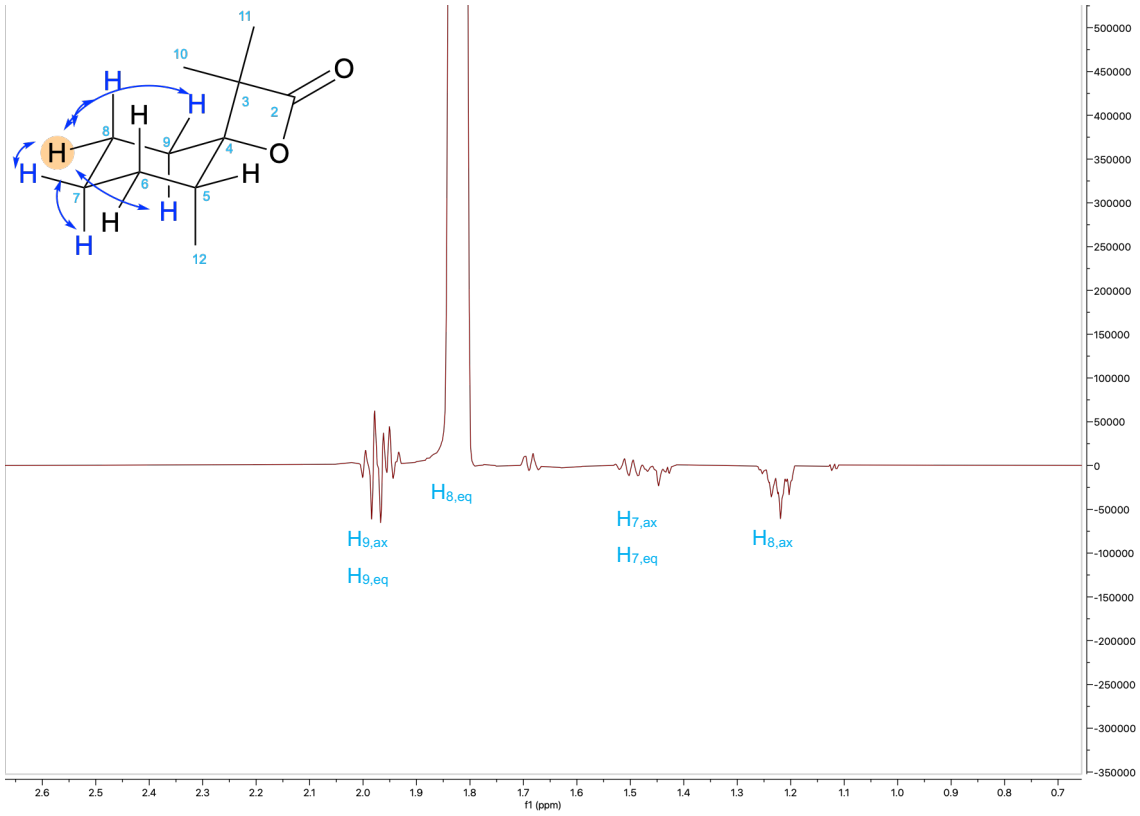
1D Selective Gradient NOESY (800 MHz, $CDCl_3$) at 1.115 ppm of **38-b**



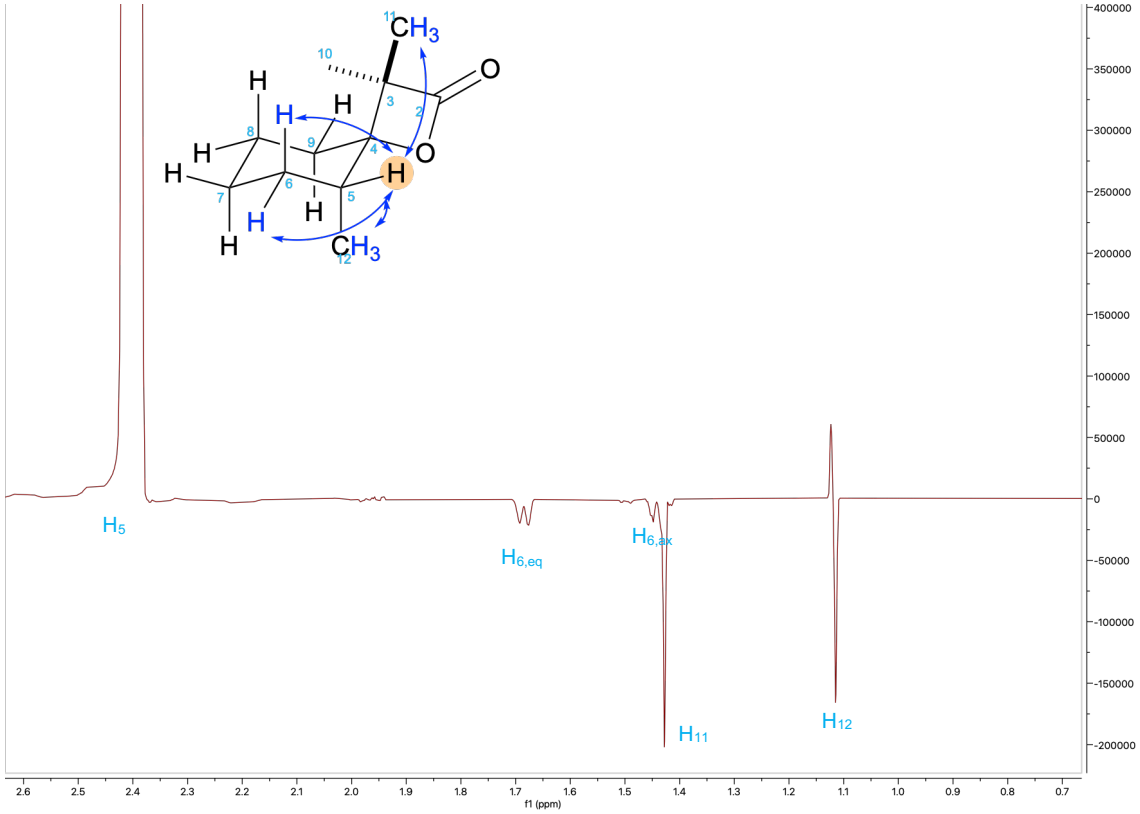
1D Selective Gradient NOESY (800 MHz, $CDCl_3$) at 1.228 ppm of **38-b**



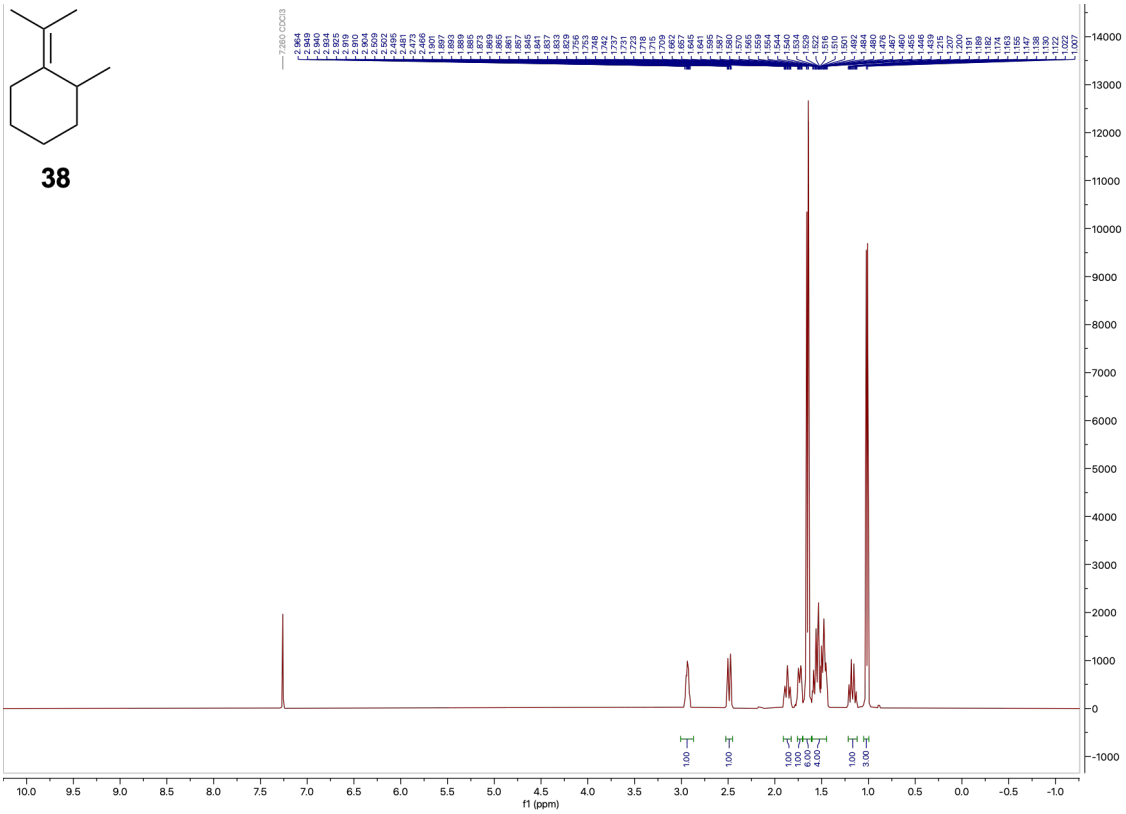
1D Selective Gradient NOESY (800 MHz, $CDCl_3$) at 1.688 ppm of **38-b**

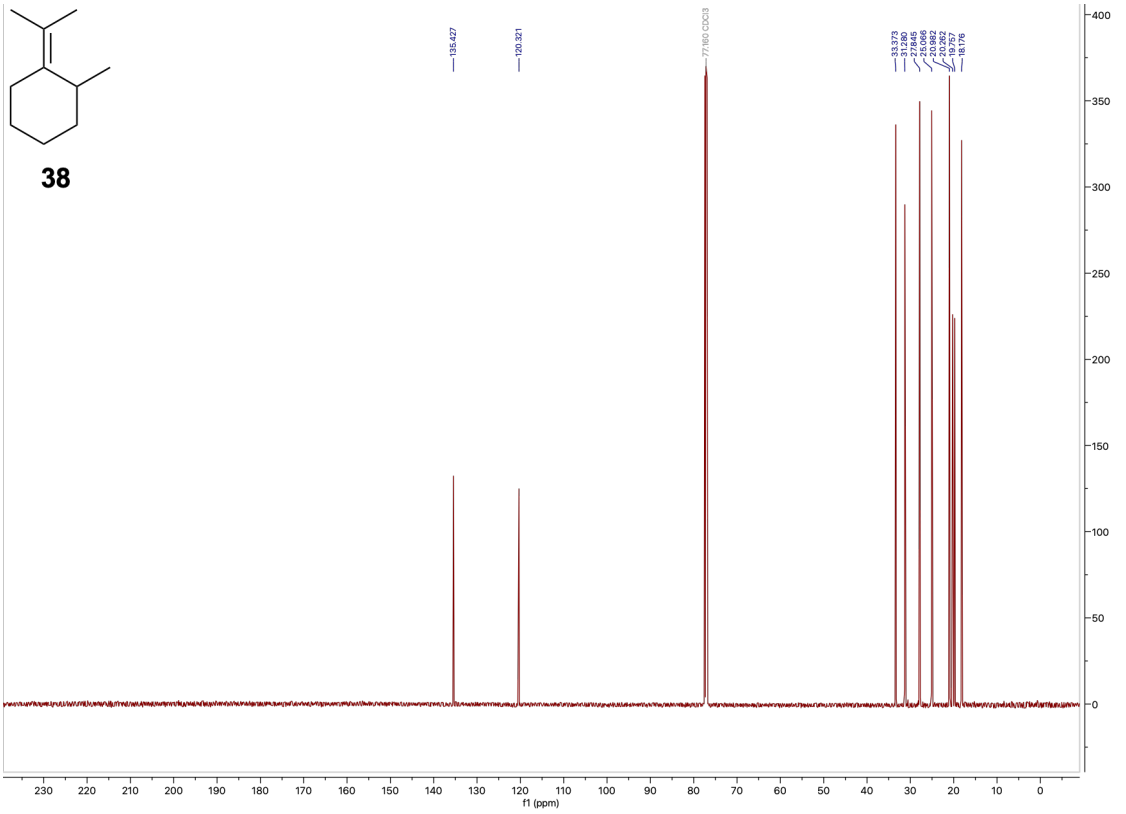


1D Selective Gradient NOESY (800 MHz, $CDCl_3$) at 1.818 ppm of **38-b**

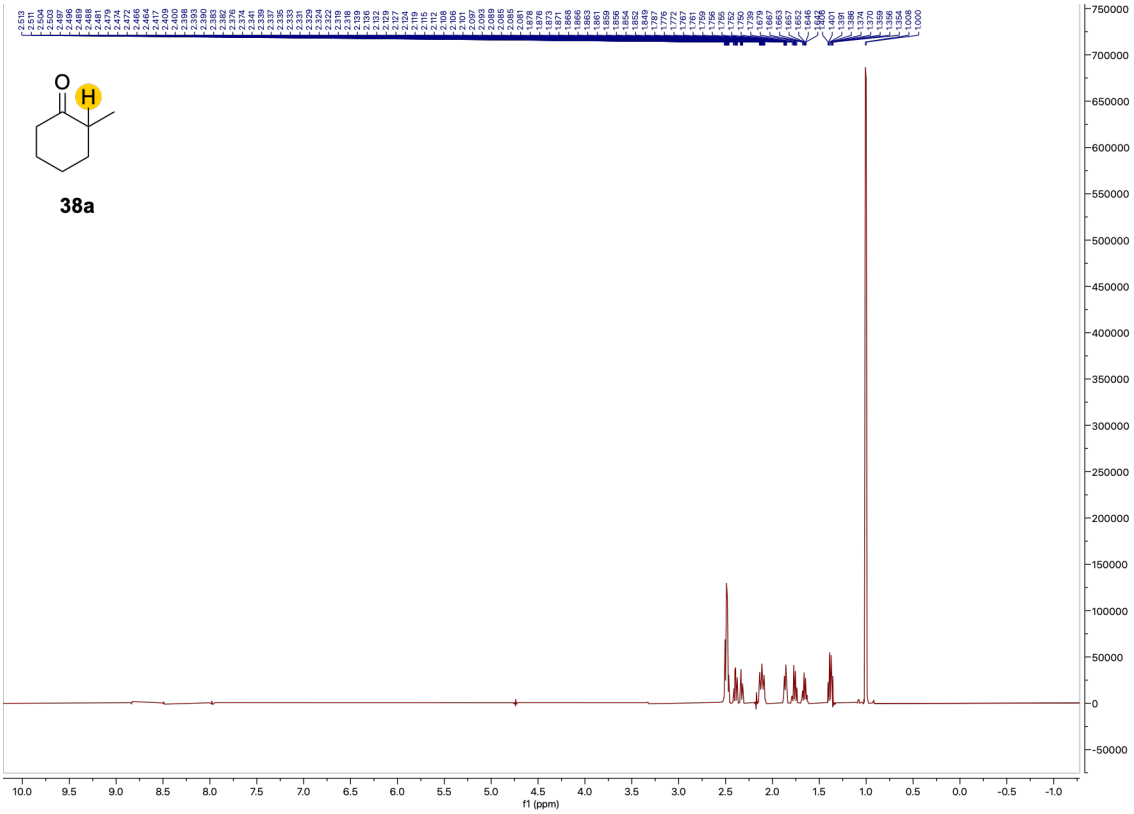


1D Selective Gradient NOESY (800 MHz, $CDCl_3$) at 2.405 ppm of **38-b**

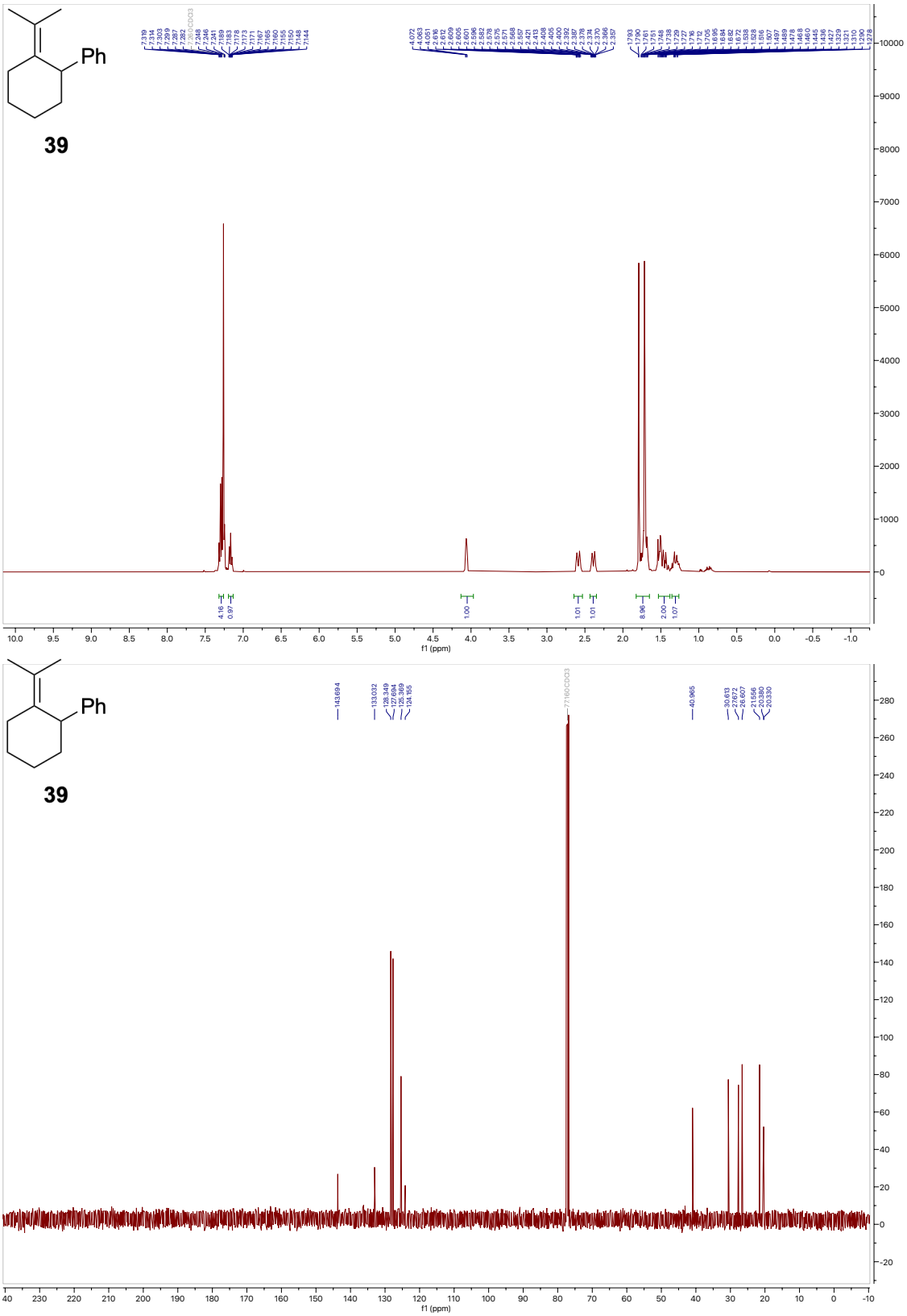




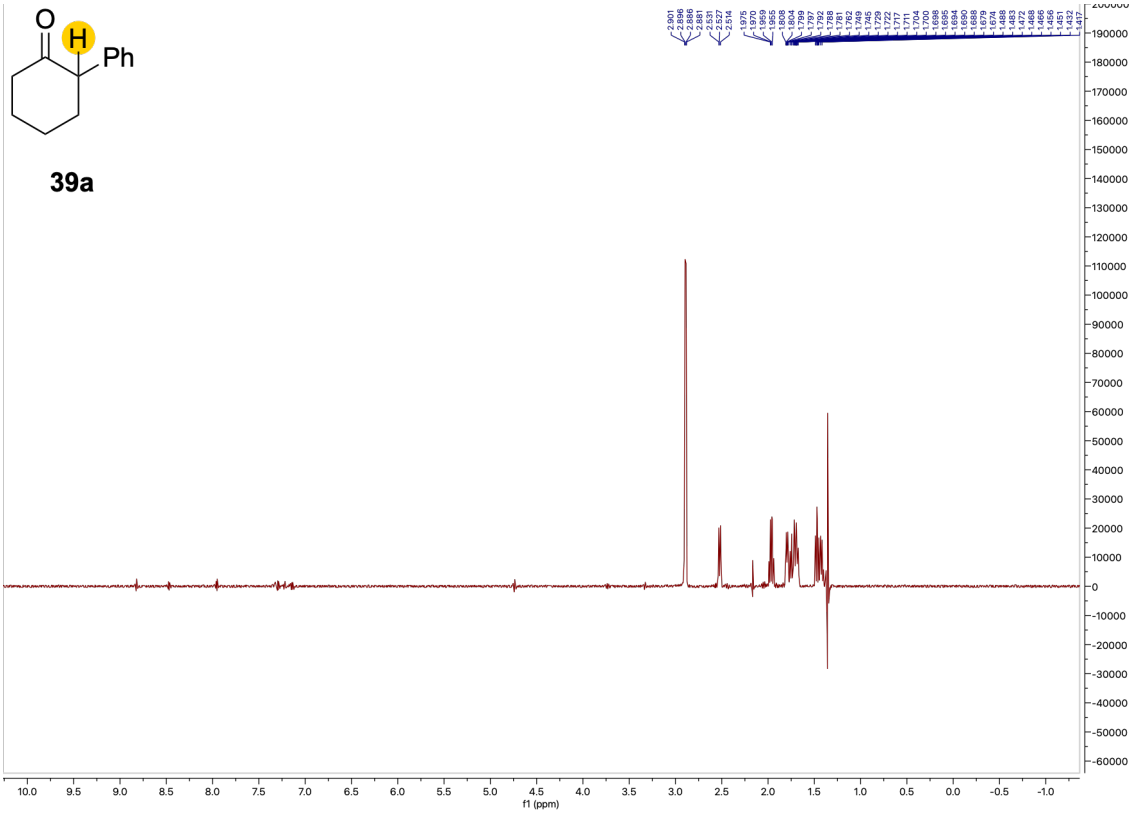
^{1}H NMR (500 MHz, $CDCl_3$) and **^{13}C NMR** (126 MHz, CDC_3) of **38**



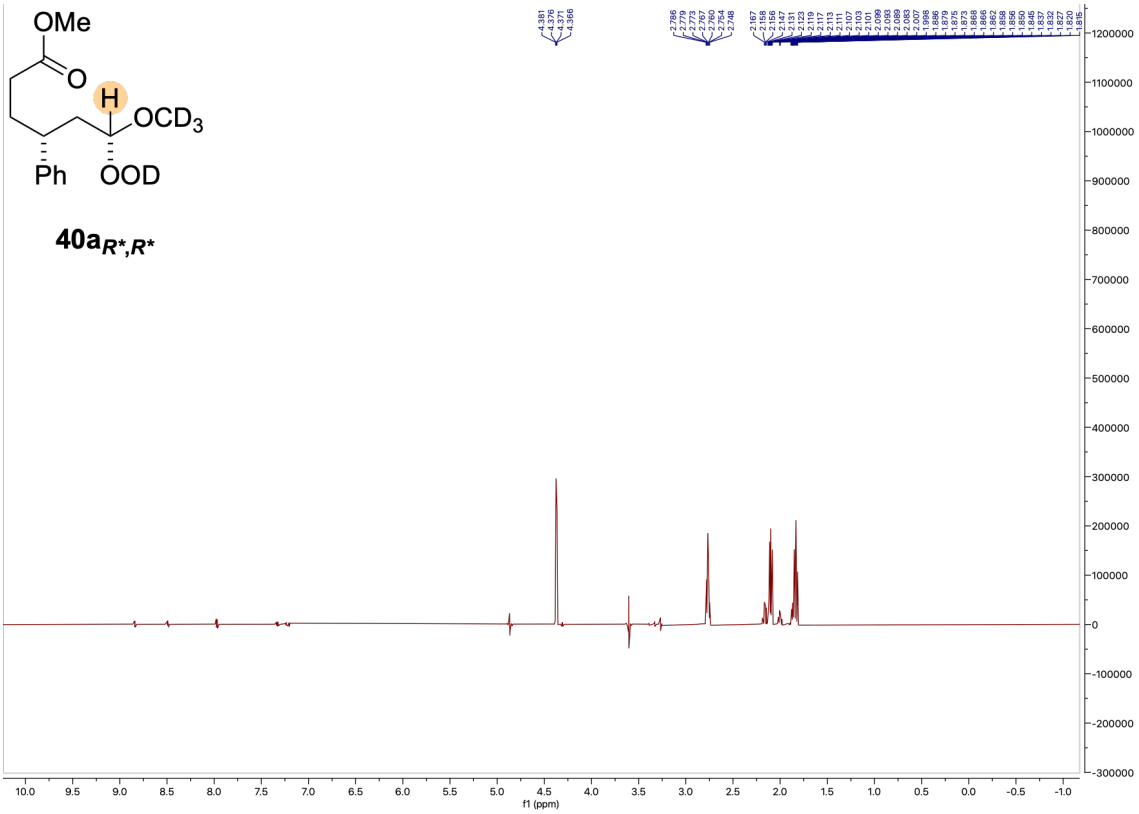
1D Selective Gradient TOCSY (800 MHz, CD_3OD) at 2.470 ppm of **38a**



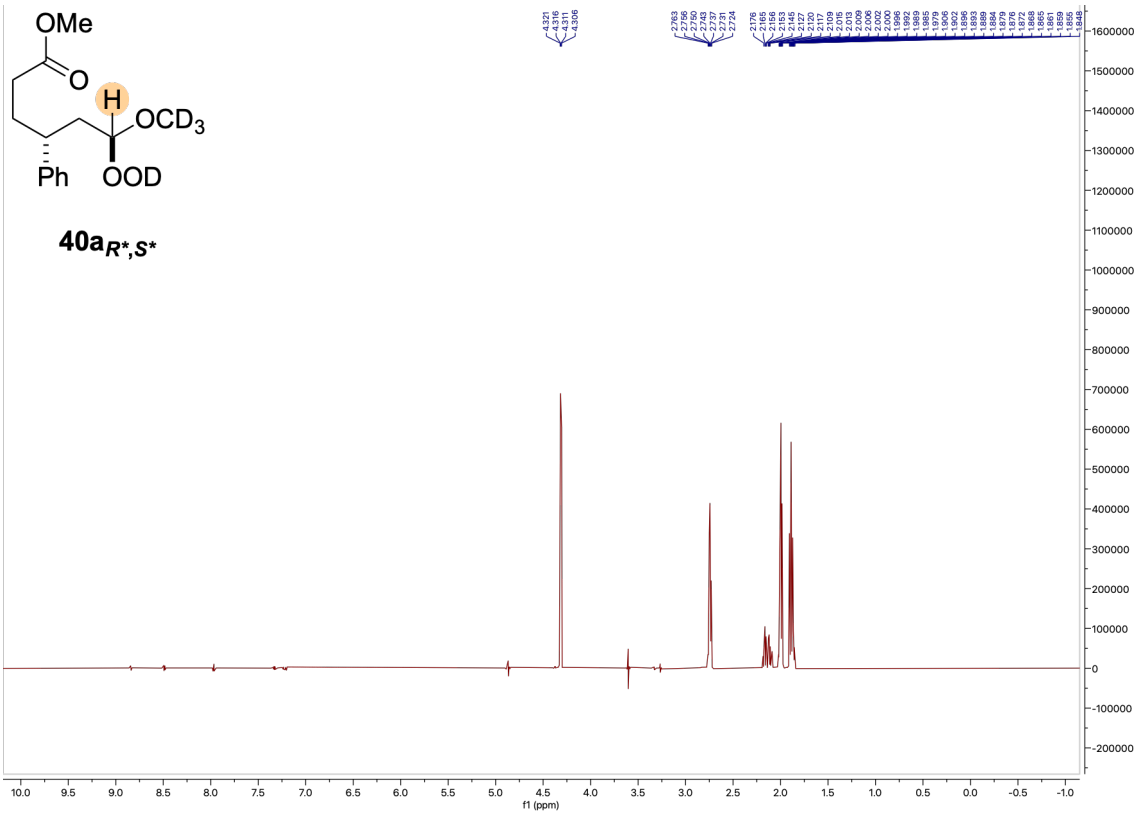
^{1}H NMR (400 MHz, $CDCl_3$) and **^{13}C NMR** (101 MHz, $CDCl_3$) of **39**



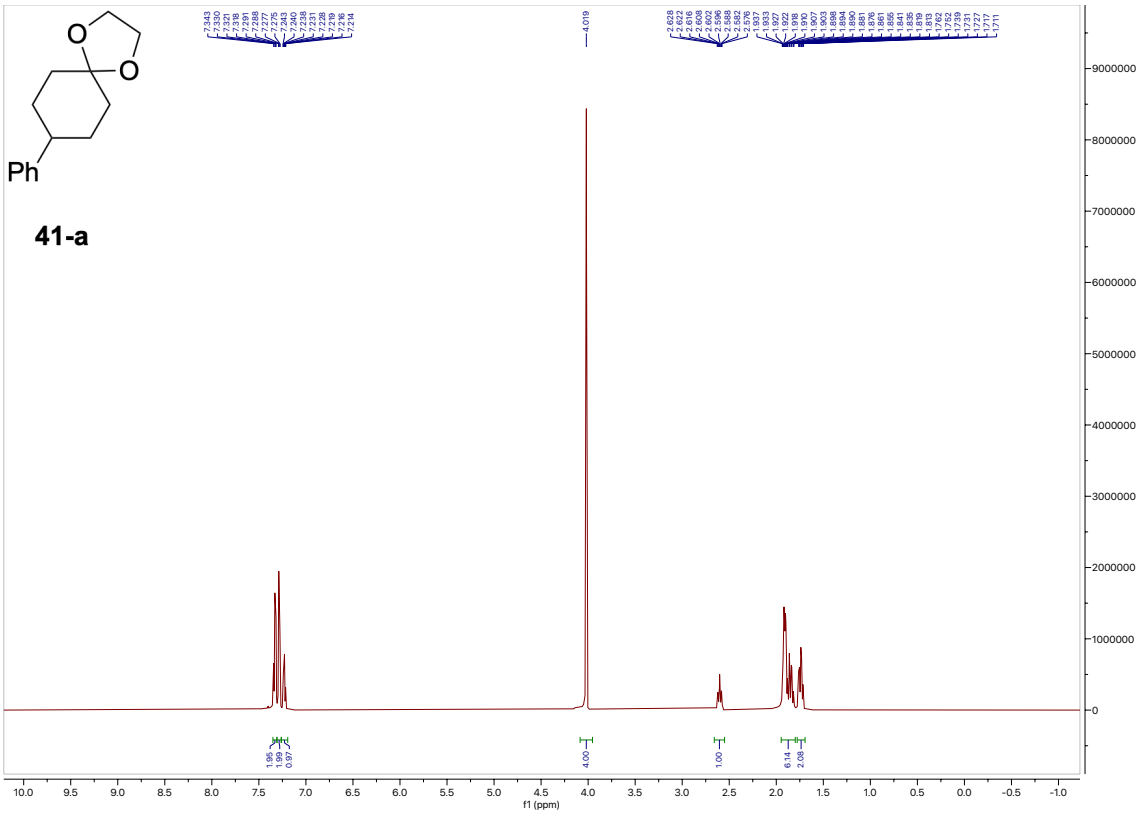
1D Selective Gradient TOCSY (800 MHz, CD_3OD) at 2.89 ppm of **39a**

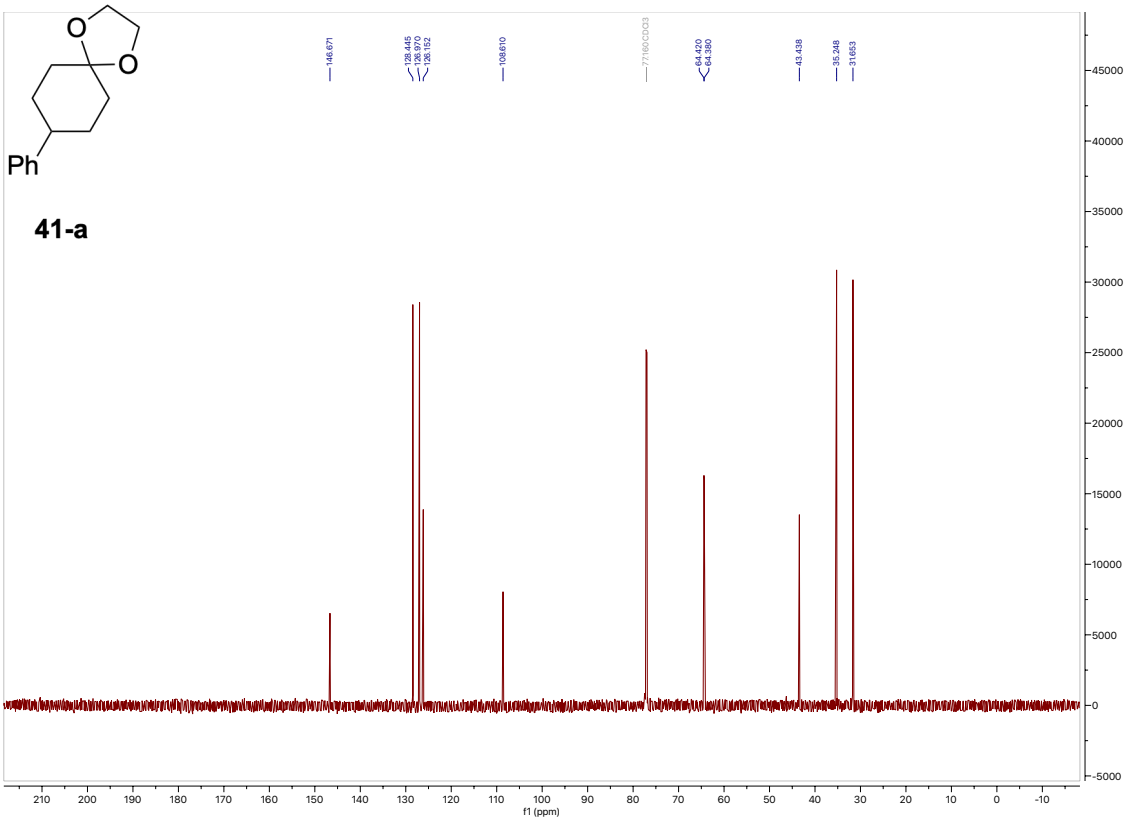


1D Selective Gradient TOCSY (800 MHz, CD_3OD) at 4.376 ppm of **40a*R*,R****

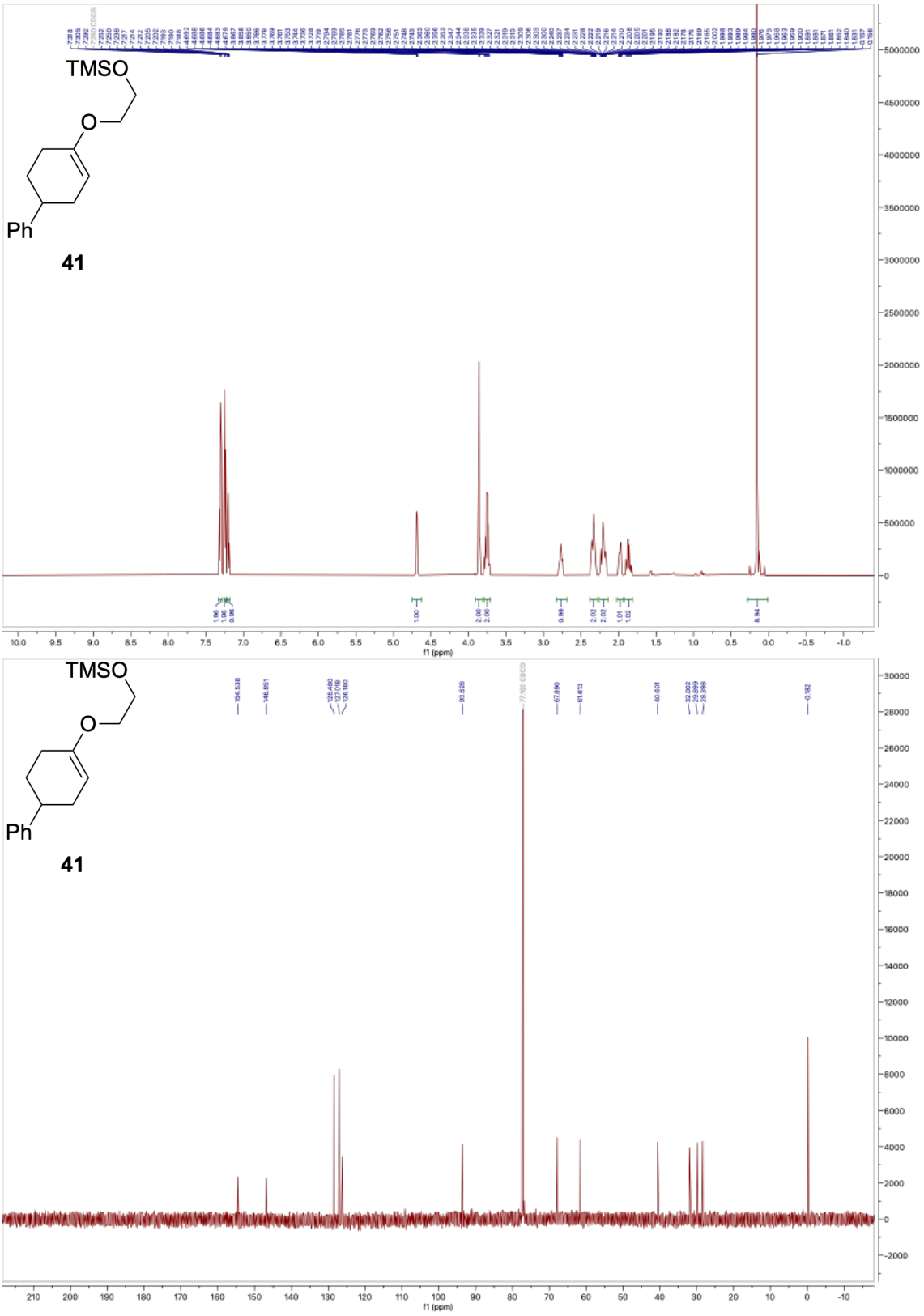


and **1D Selective Gradient TOCSY** (800 MHz, CD_3OD) at 4.313 ppm of **40a*R*,S****

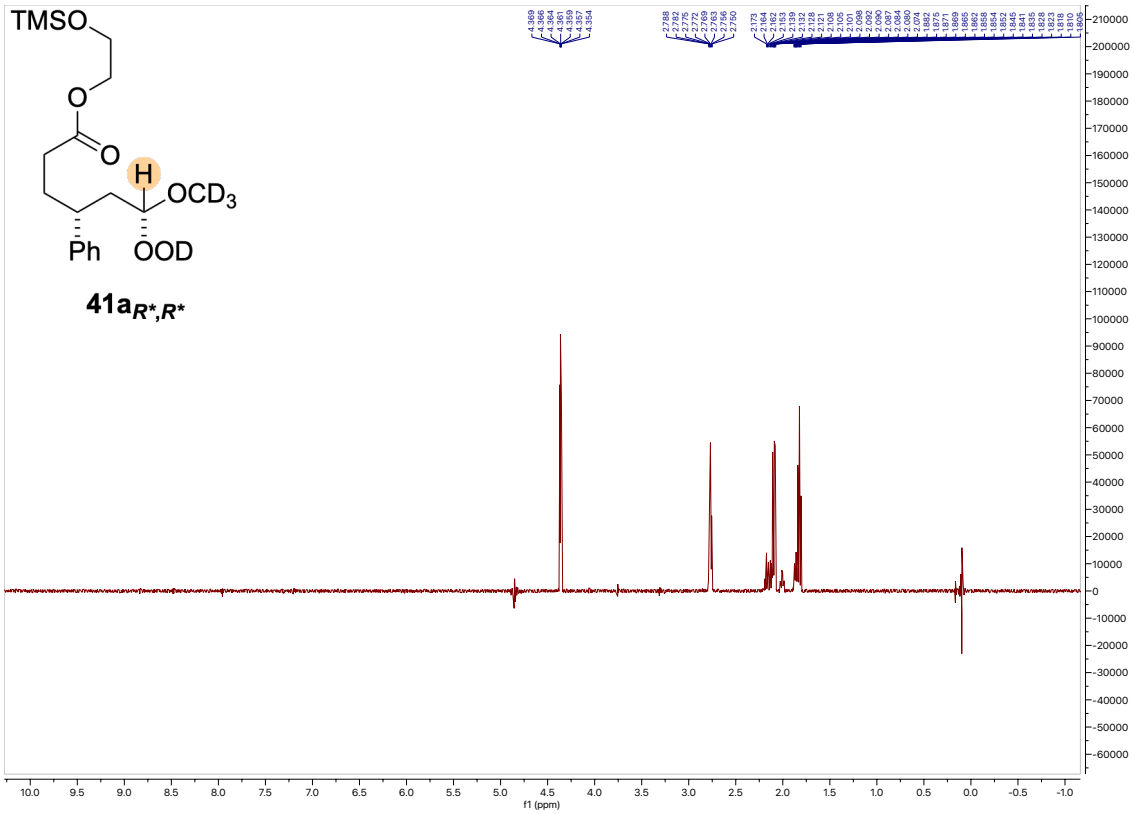




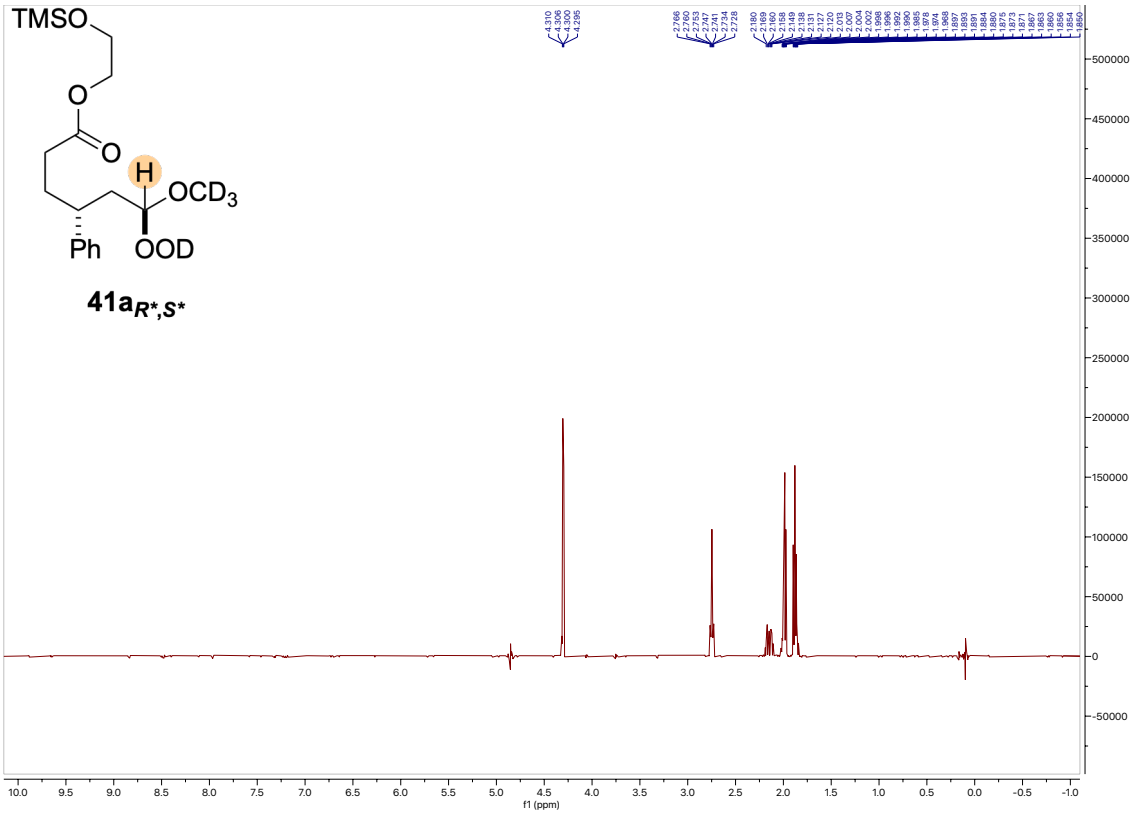
^{1}H NMR (400 MHz, $CDCl_3$) and **^{13}C NMR** (151 MHz, $CDCl_3$) of **41-a**



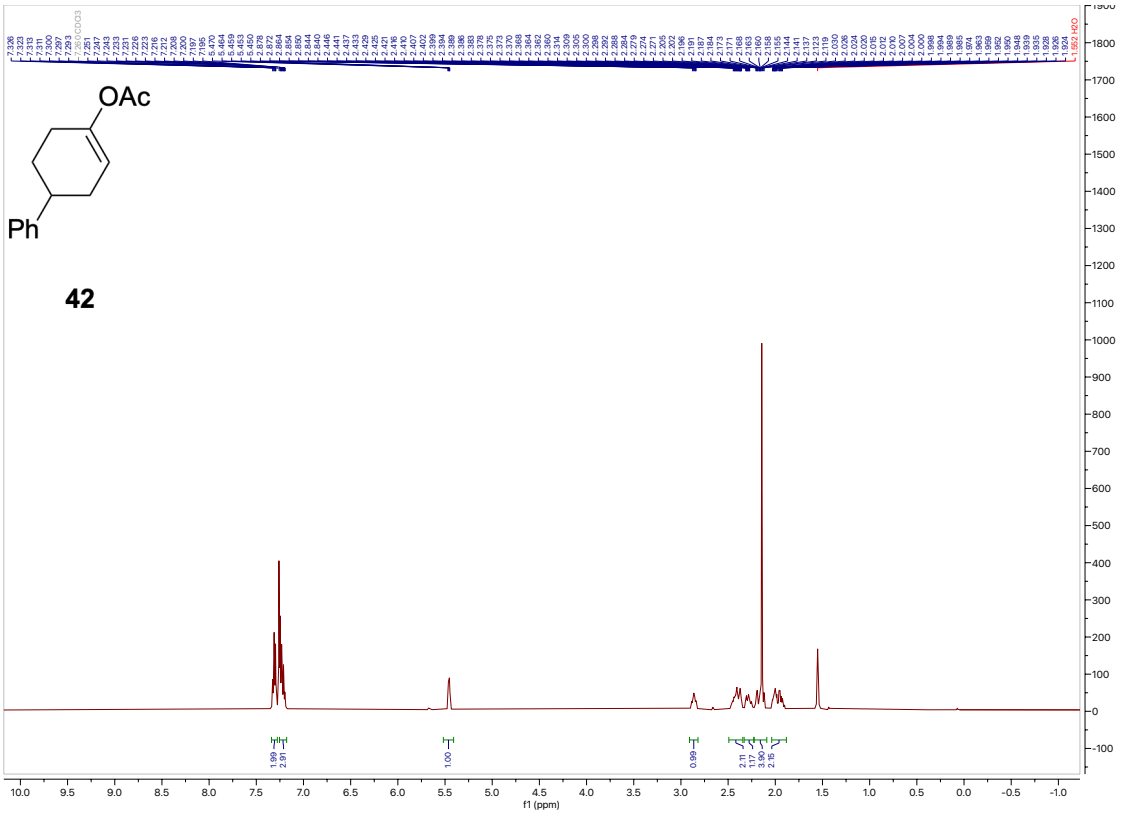
^{1}H NMR (600 MHz, $CDCl_3$) and **^{13}C NMR** (101 MHz, $CDCl_3$) of **41**

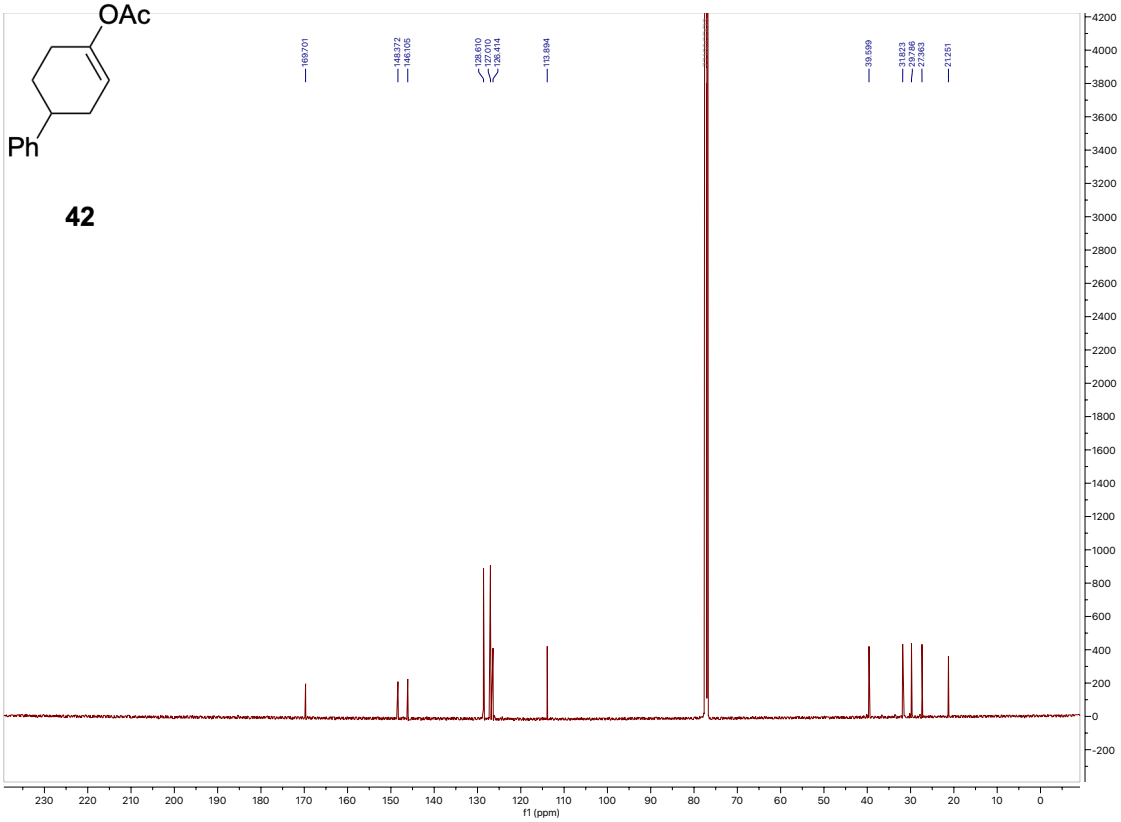


1D Selective Gradient TOCSY (800 MHz, CD_3OD) at 4.36 ppm of **41a*R*,R****

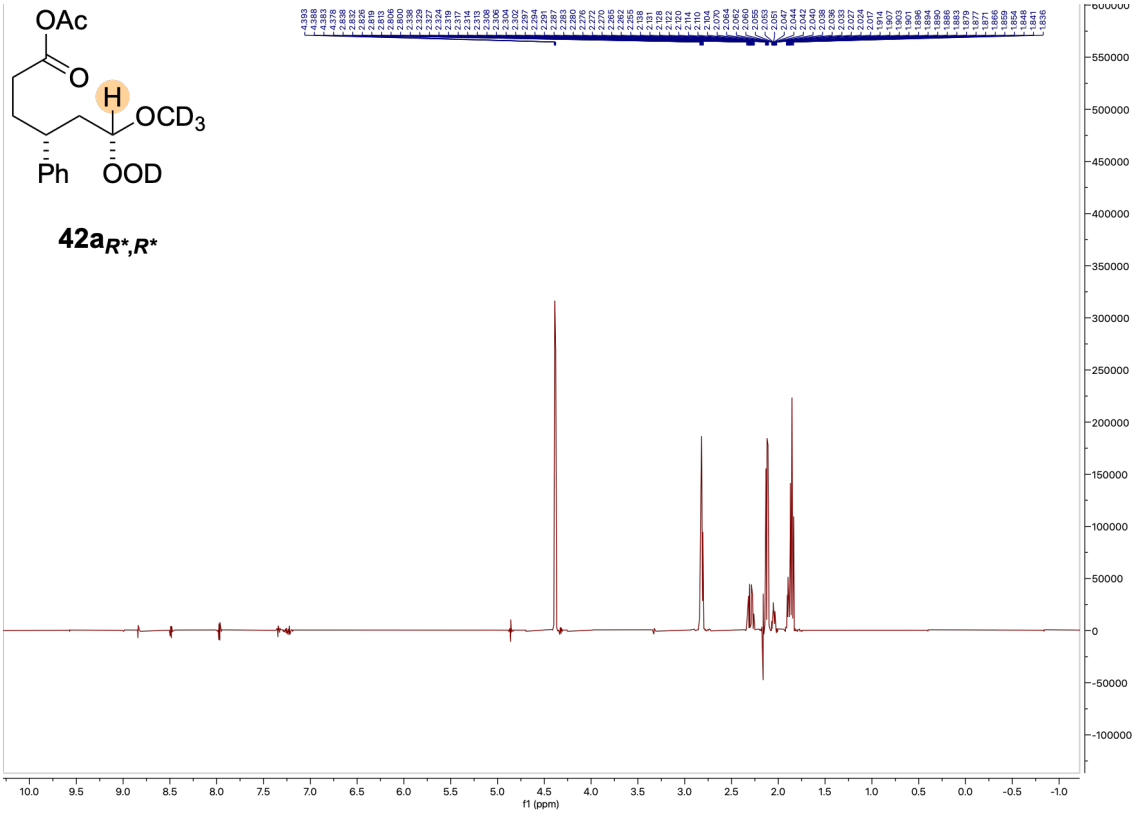


1D Selective Gradient TOCSY (800 MHz, CD_3OD) at 4.30 ppm of **41a*R*,S****

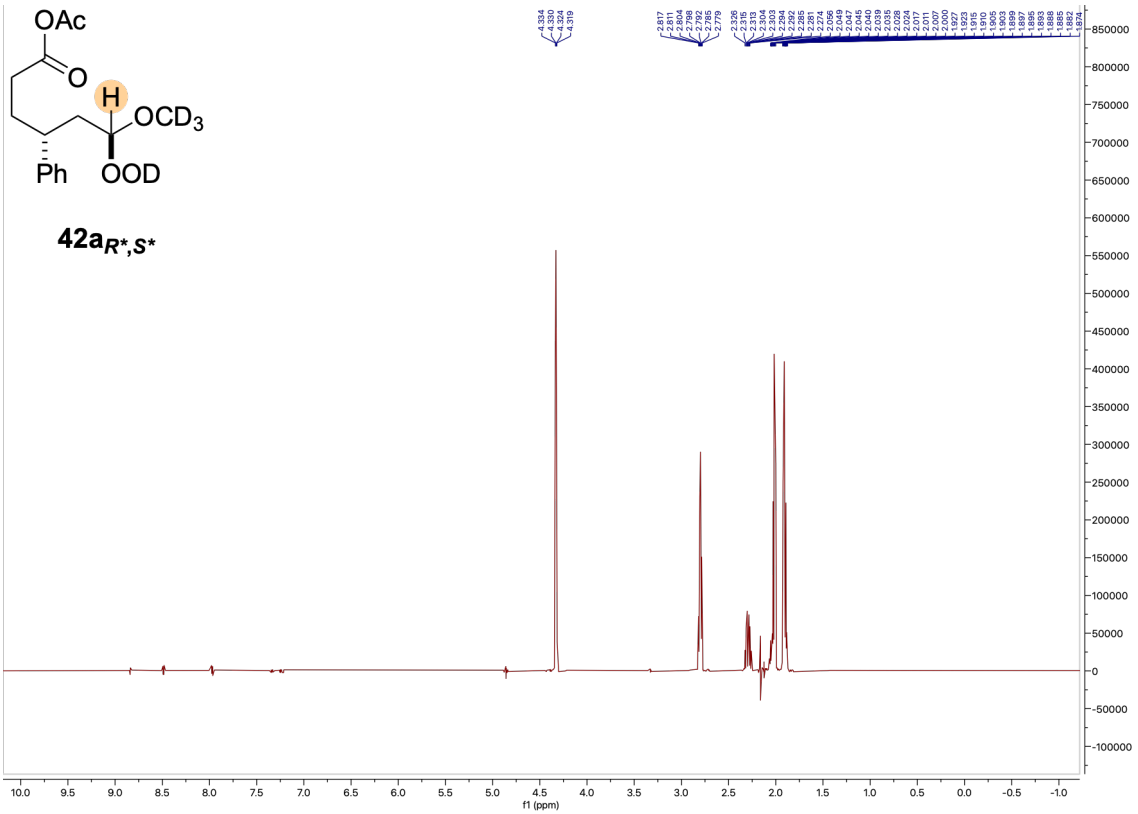




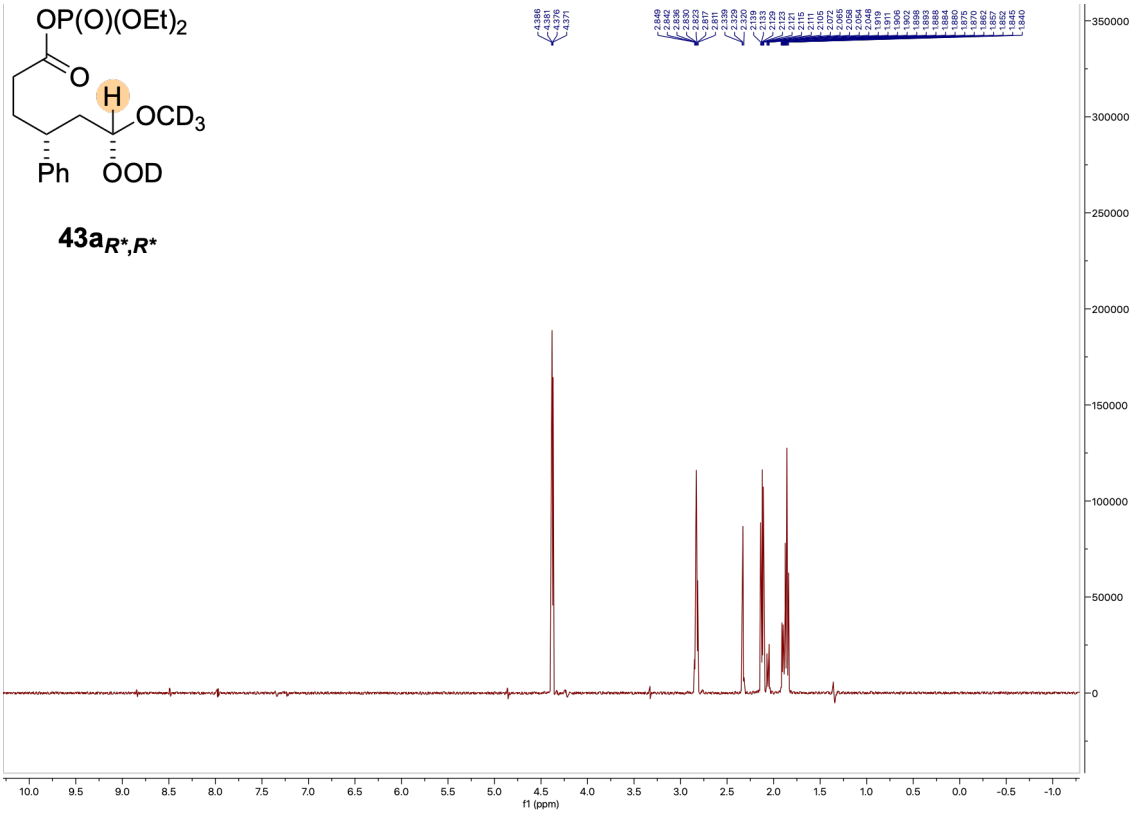
^{1}H NMR (500 MHz, $CDCl_3$) and **^{13}C NMR** (126 MHz, $CDCl_3$) of **42**



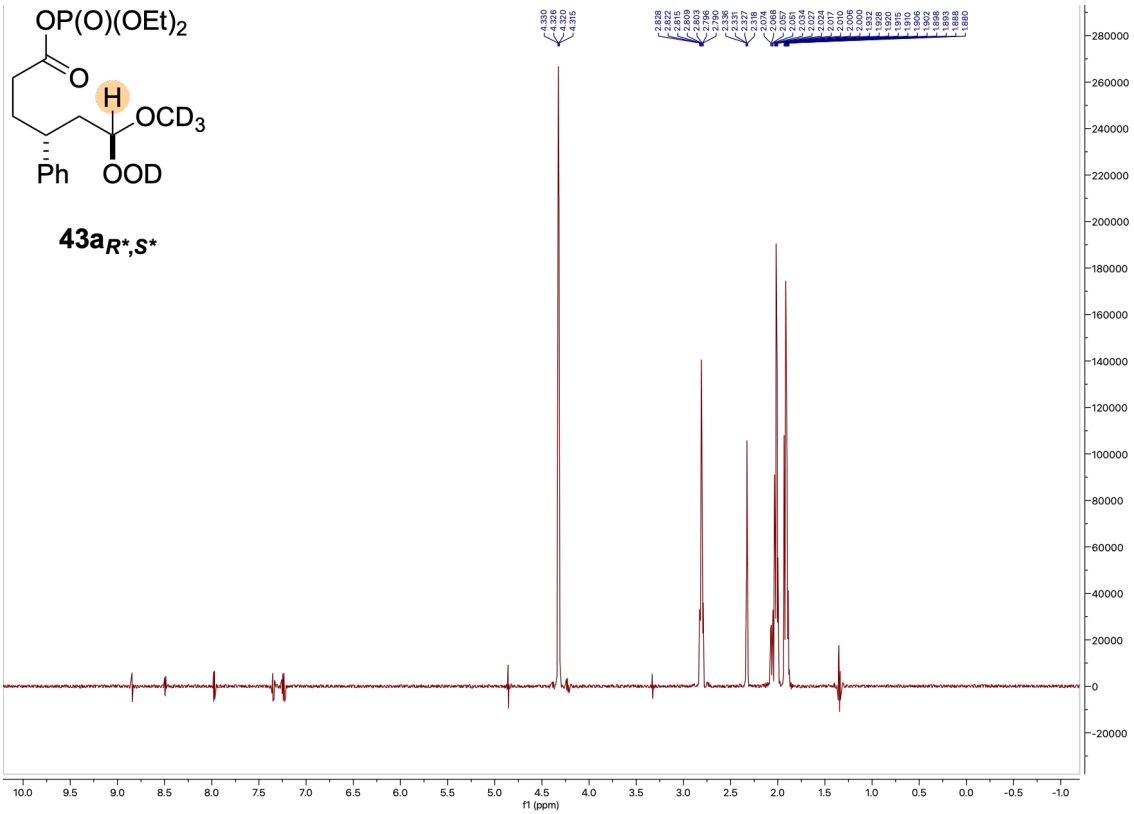
1D Selective Gradient TOCSY (800 MHz, CD_3OD) at 4.391 ppm of **42a*R*,R****



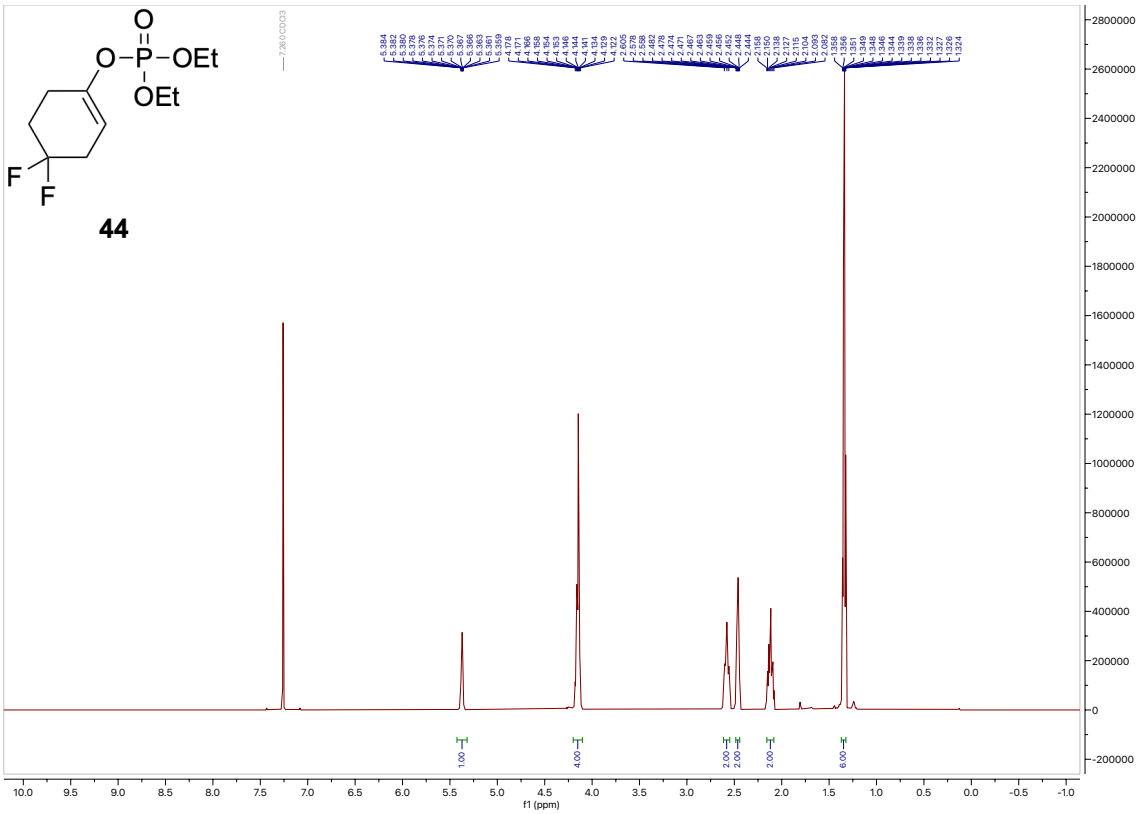
1D Selective Gradient TOCSY (800 MHz, CD_3OD) at 4.327 ppm of **42a**$_{R^*,S^*}$

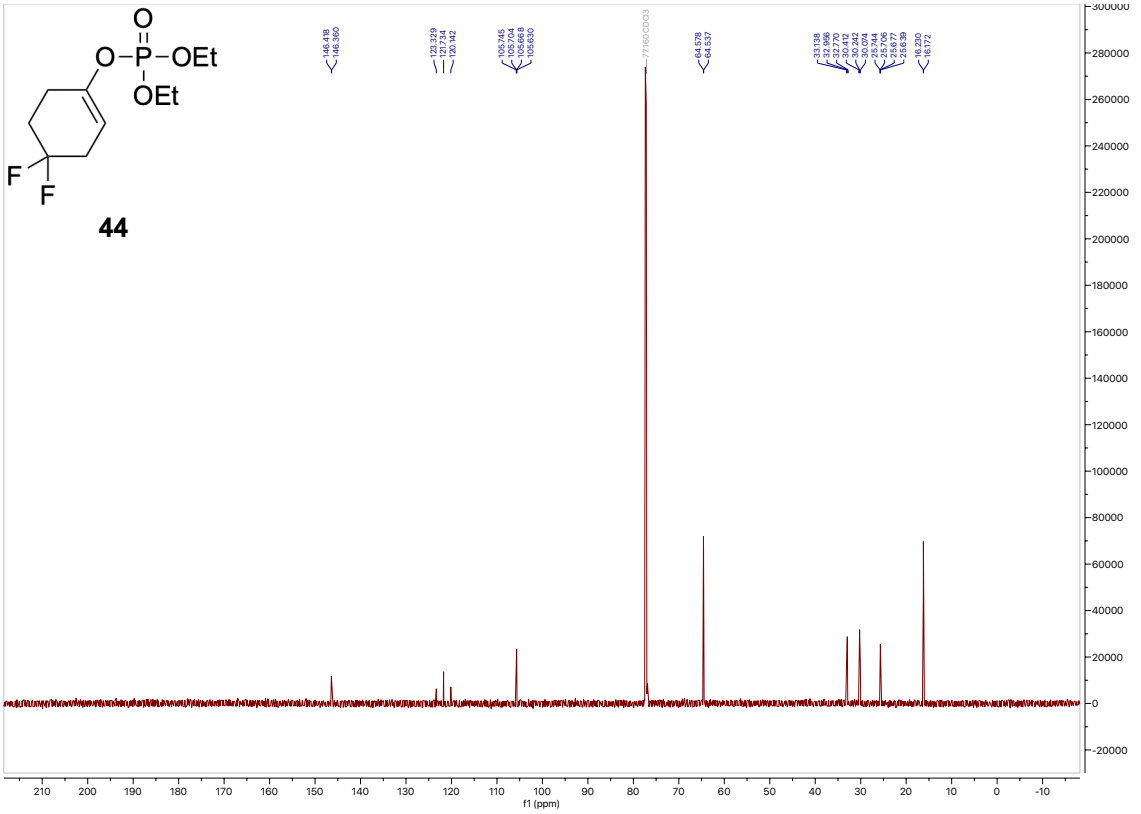


1D Selective Gradient TOCSY (800 MHz, CD_3OD) at 4.382 ppm of **43a*R*,R****

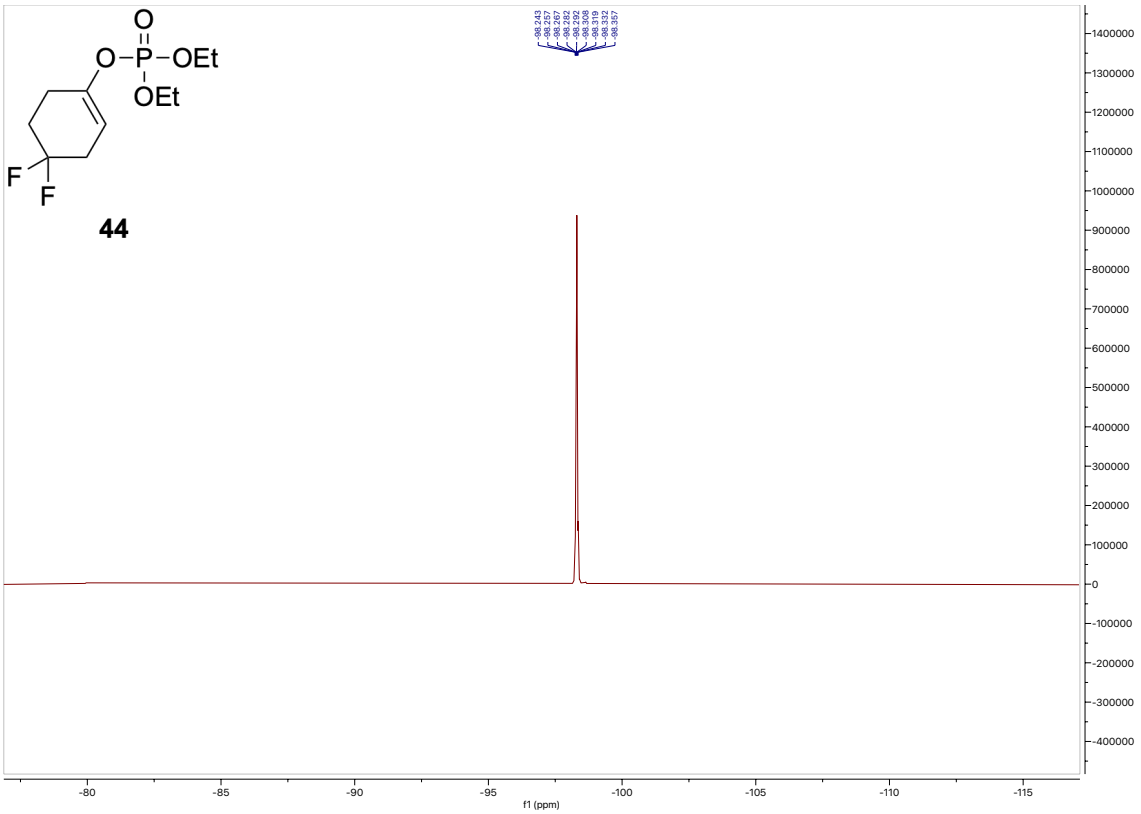


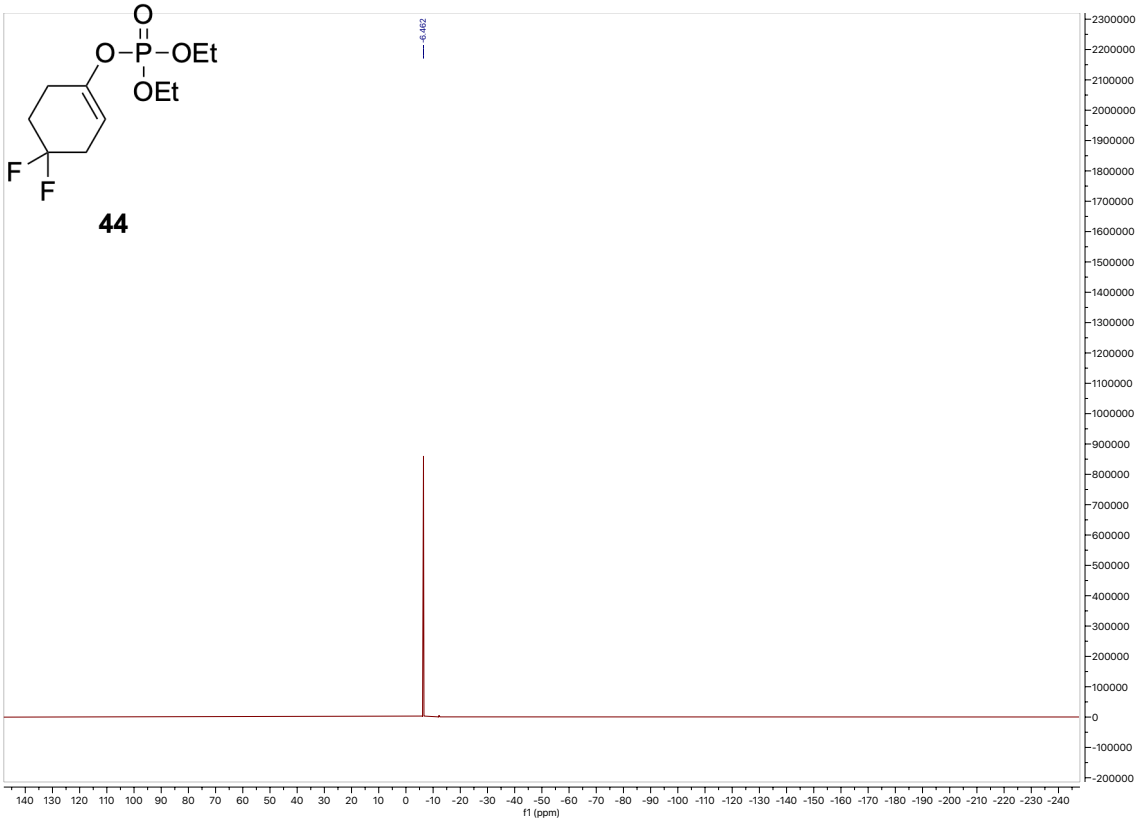
1D Selective Gradient TOCSY (800 MHz, CD_3OD) at 4.323 ppm of **43a*R*,S**



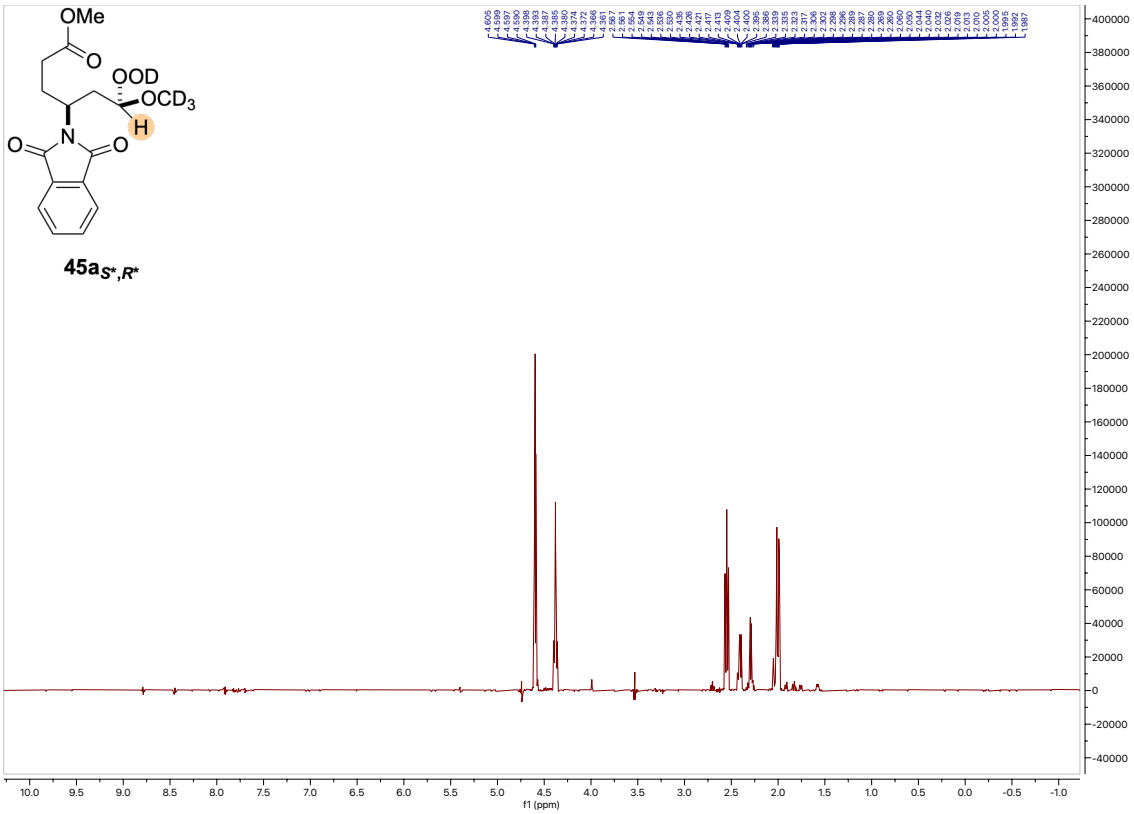


^{1}H NMR (600 MHz, $CDCl_3$) and **^{13}C NMR** (151 MHz, $CDCl_3$) of **44**

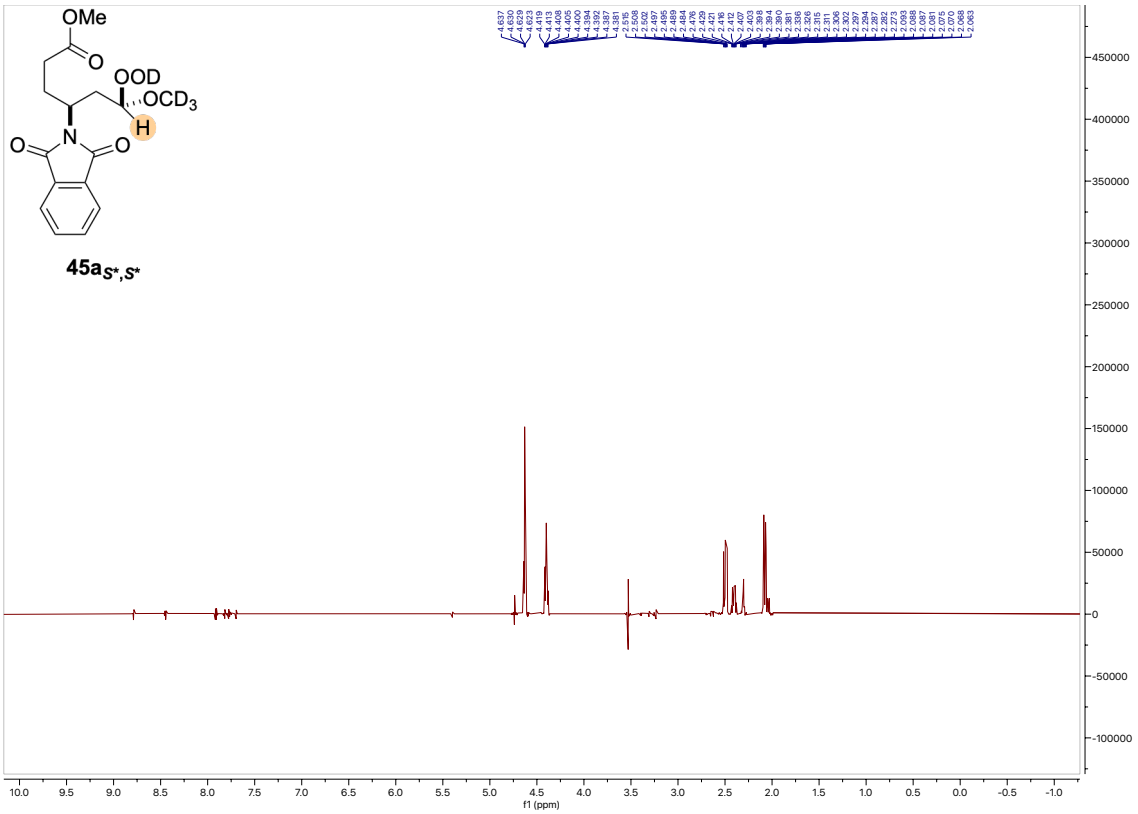




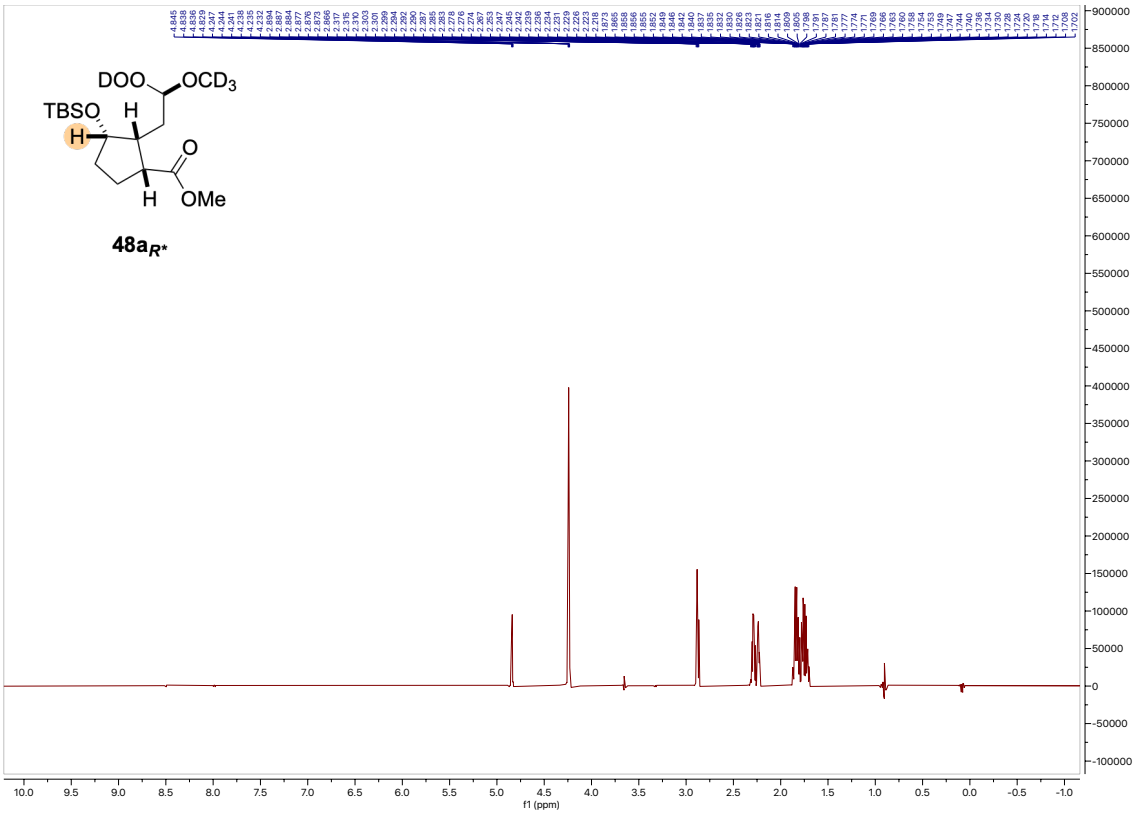
^{19}F NMR (565 MHz, $CDCl_3$) and **^{31}P NMR** (243 MHz, $CDCl_3$) of **44**



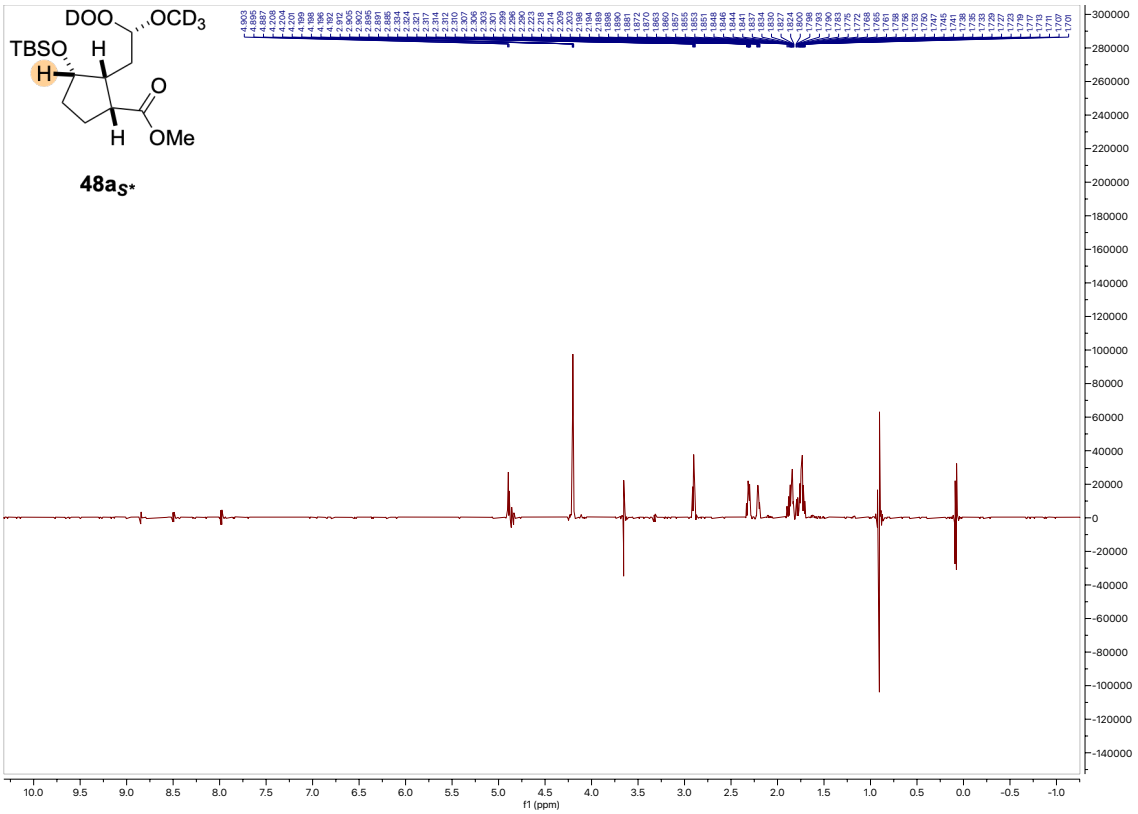
1D Selective TOCSY (800 MHz, CD_3OD) at 4.59 ppm of **45a*S*,R**



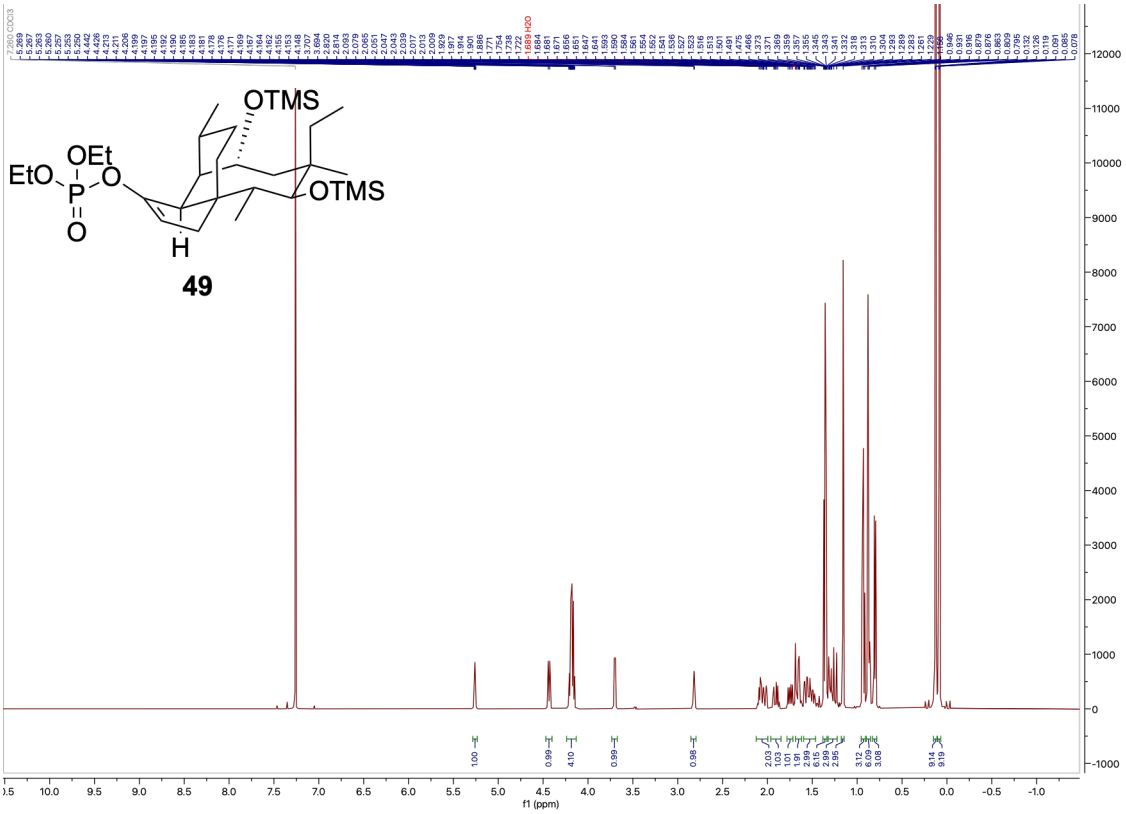
1D Selective TOCSY (800 MHz, CD_3OD) at 4.63 ppm of **45a**$_{S^*,S^*}$

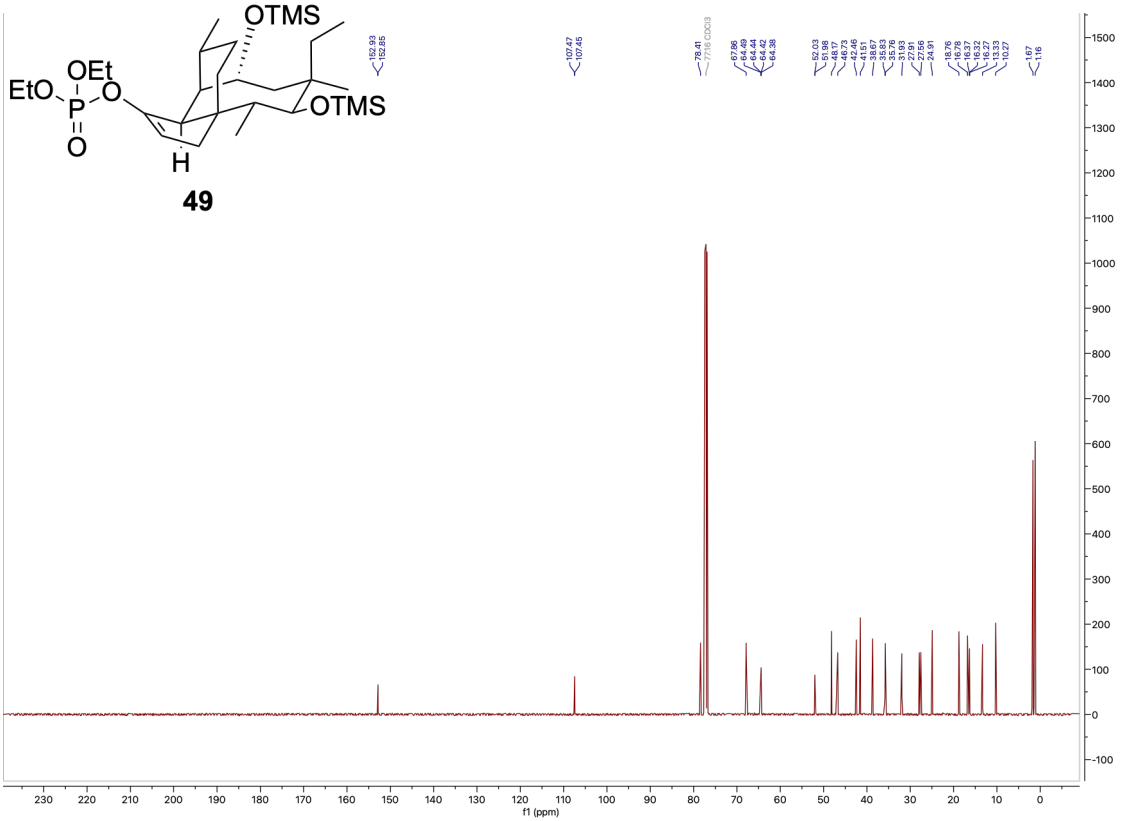


1D Selective Gradient TOCSY (800 MHz, CD_3OD) at 4.24 ppm of **48a*R*****

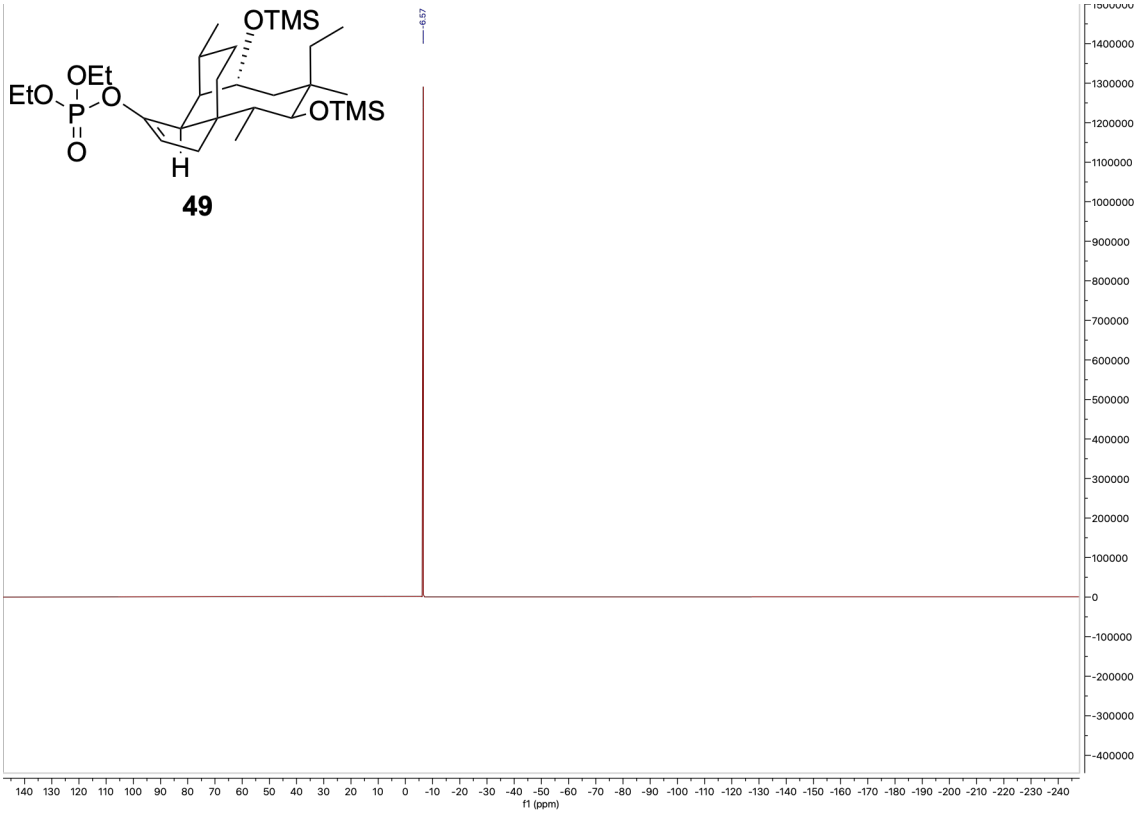


and **1D Selective Gradient TOCSY** (800 MHz, CD_3OD) at 4.20 ppm of **48a$_{S*}$**

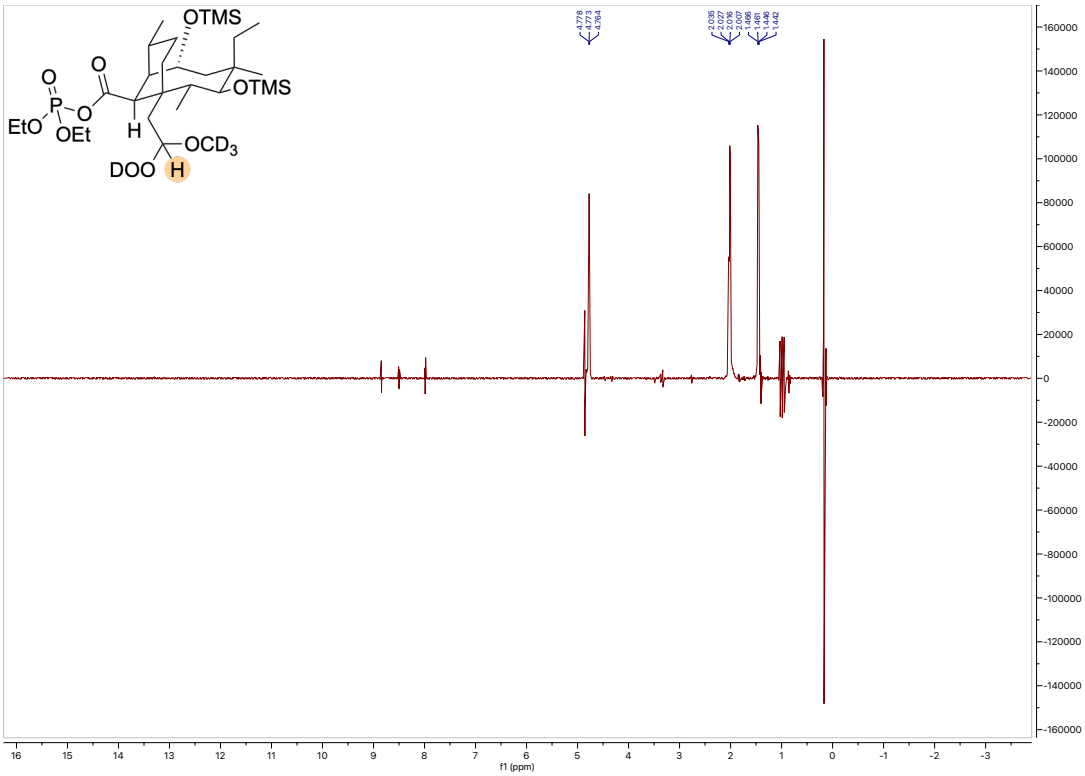




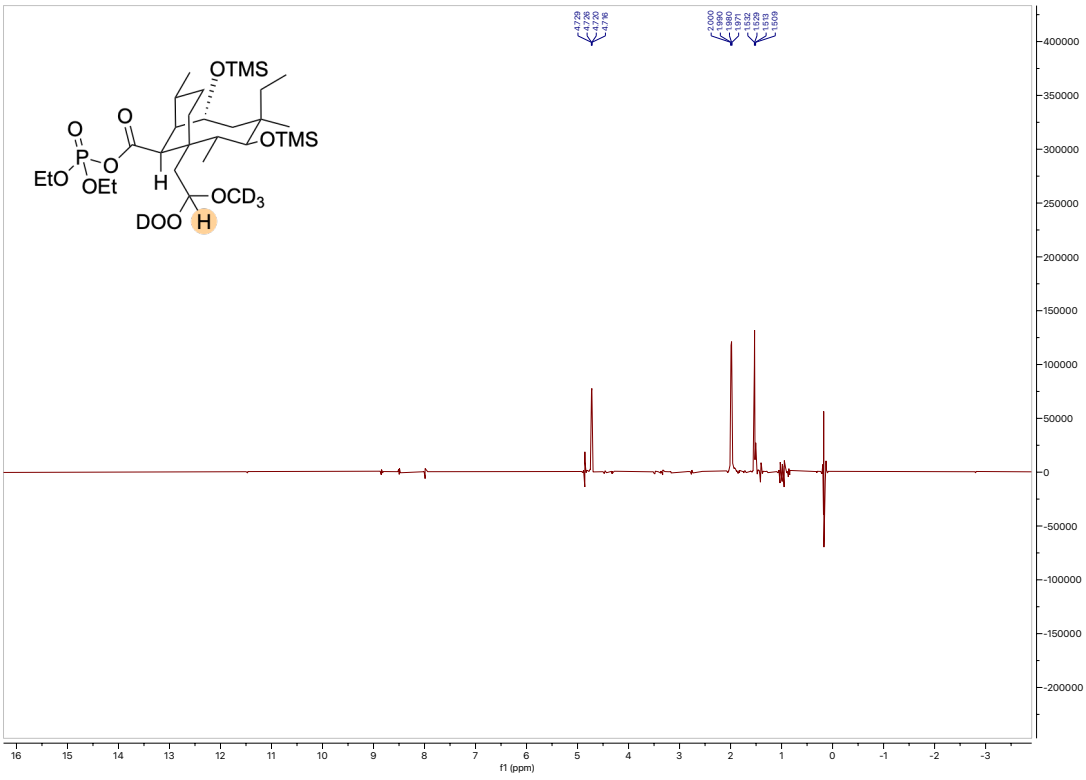
^{1}H NMR (500 MHz, $CDCl_3$) and **^{13}C NMR** (126 MHz, $CDCl_3$) of **49**



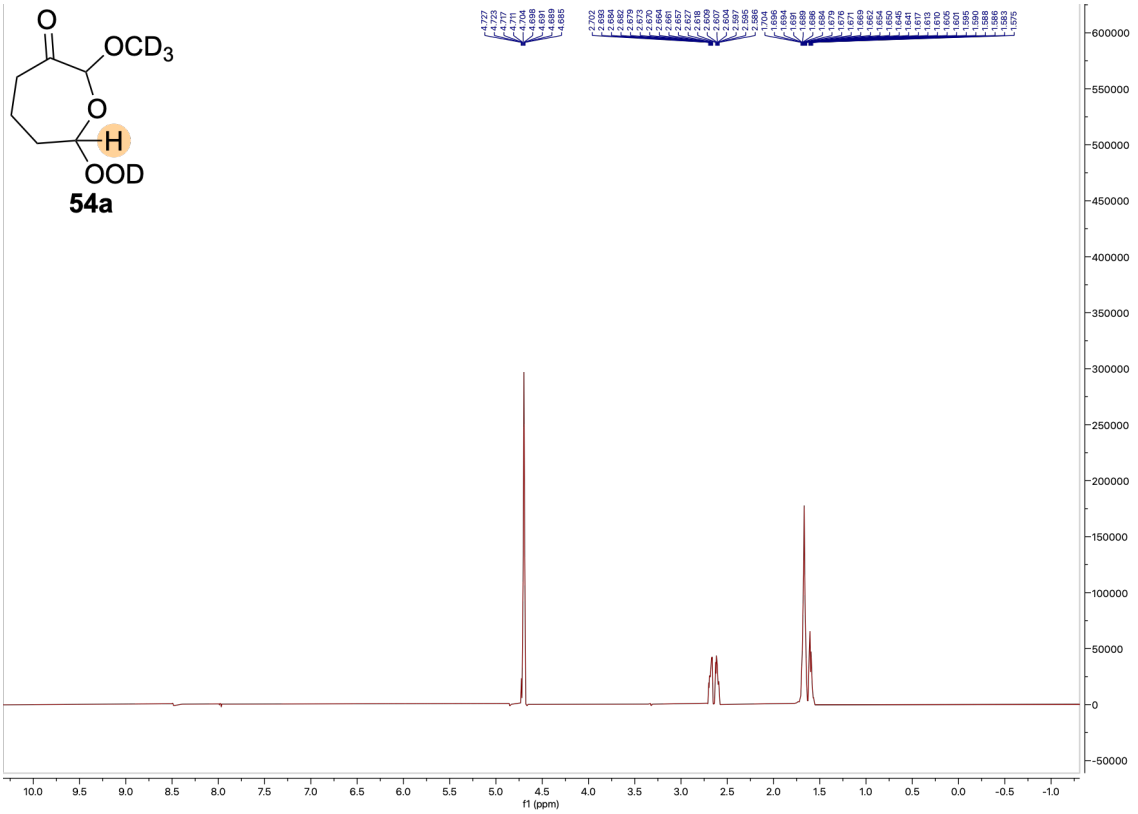
^{31}P NMR (243 MHz, $CDCl_3$) of **49**



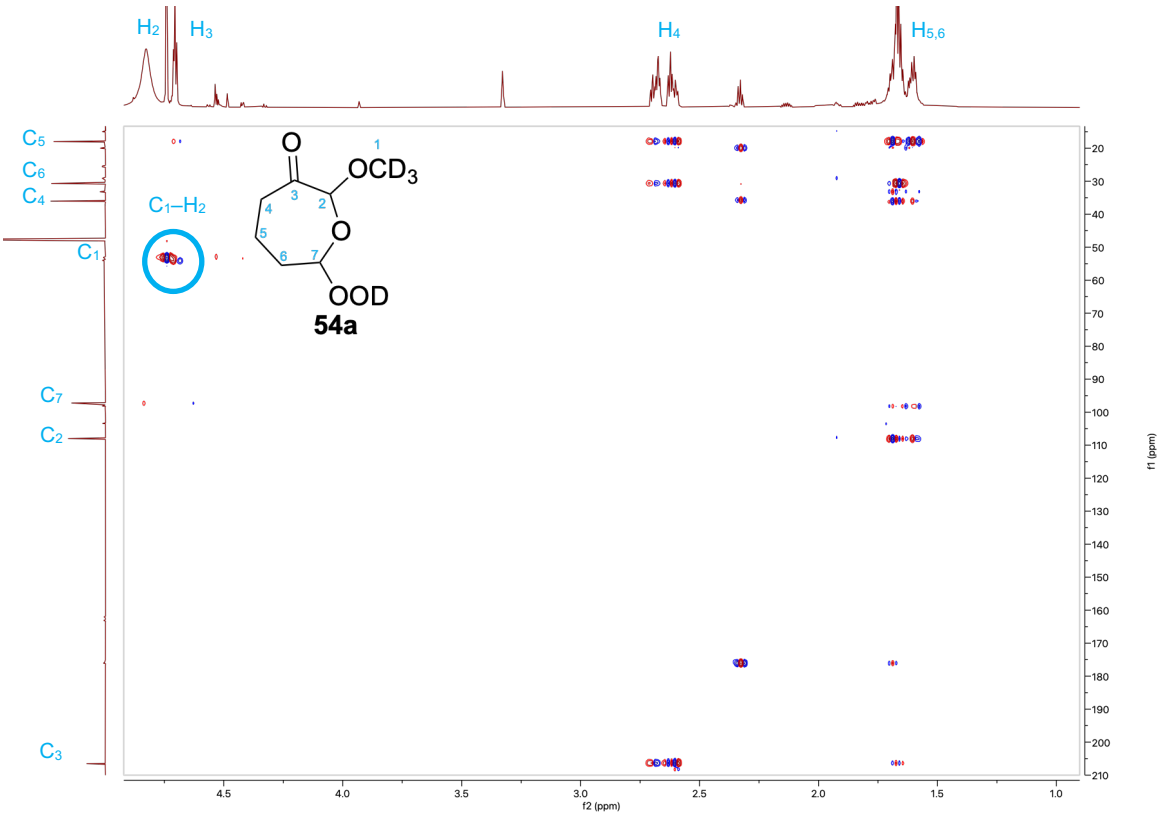
1D Selective Gradient TOCSY (800 MHz, MeOD) at 4.775 ppm of **49a *diastereomer 1***



1D Selective Gradient TOCSY (800 MHz, MeOD) at 4.719 ppm of **49a *diastereomer 2***



1D Selective Gradient TOCSY (800 MHz, CD_3OD) at 4.693 ppm of **54a**



HMBC (CD_3OD) of **54a**

6.9 References

[1] Levin, M. D.; Sarpong, R. S.; Wendlandt, A. E. What is Editing? *Acc. Chem. Res.* **2025**, *58* (12), 1725–1726.

[2] (a) Jurczyk, J.; Woo, J.; Kim, S. F.; Dherange, B. D.; Sarpong, R.; Levin, M. D. Single-Atom Logic for Heterocycle Editing. *Nat. Synth.* **2022**, *1* (5), 352–364. (b) Notman, N. Editing the Structure of Molecules. *Chemistry World* [Online], March 27, 2023. https://www.chemistryworld.com/features/editing-the-structure-of-molecules/4017084.article (accessed Jan 15, 2026). (c) Peplow, M. 'Almost magical': Chemists Can Now Move Single Atoms in and Out of a Molecule's Core. *Nature* **2023**, *618* (7963), 21–24. (d) Miles, N. C. 'Endless possibilities': The Chemists Changing Molecules Atom by Atom. *The Guardian* [Online], August 5, 2023. https://www.theguardian.com/science/2023/aug/05/skeletal-editing-chemistry-molecule-atom-medicine-drug-development-sustainable (accessed Jan 15, 2026). (e) Rustad, N. Skeletal Editing: Chemistry's Next Frontier. *Berkeley Scientific Journal* [Online], March 24, 2024. https://www.bsj.studentorg.berkeley.edu/skeletal-editing-chemistry-next-frontier (accessed Jan 15, 2026). (f) Atkinson, V. Skeletal Editing Provides Quick Access to Pharmaceutical 'Matching Pairs'. *Chemistry World* [Online], May 9, 2025. https://www.chemistryworld.com/news/skeletal-editing-provides-quick-access-to-pharmaceutical-matching-pairs/4021471.article (accessed Jan 15, 2026). (g) Barbu, B. Skeletal Editing: How Close Are We to True Cut-and-Paste Chemistry? *Chem. Eng. News* [Online], **2025**, *103* (23), July 15. https://www.cen.acs.org/synthesis/Skeletal-editing-cutpaste-chemistry/103/web/2025/07 (accessed Jan 15, 2026).

[3] (a) Dworkin, J. H.; Dehnert, B. W.; Kwon, O. When All C–C Breaks LO–Ose. *Trends Chem.* **2023**, *5* (3), 174–200. (b) Dehnert, B. W.; Dworkin, J. H.; Kwon, O. Dealkenylative Functionalization: Conversion of Alkene $C(sp^3)$–$C(sp^2)$ Bonds to $C(sp^3)$–X Bonds Using Redox-Based Radical Processes. *Synthesis* **2024**, *56* (1), 71–86. (c) Šimek, M.; Dworkin, J. H.; Kwon, O. Synthesis Through $C(sp^3)$–$C(sp^2)$ Bond Scission in Alkenes and Ketones. *Acc. Chem. Res.* **2025**, *58* (10), 1547–1561.

[4] Criegee, R. Mechanism of Ozonolysis. *Angew. Chem. Int. Ed.* **1975**, *14* (11), 745–752.

[5] Fliszár, S.; Granger, M. A Quantitative Investigation of the Ozonolysis Reaction. VIII. On the Direction of Cleavage of Primary Ozonides of Selected Unymmetrical Olefins. *J. Am. Chem. Soc.* **1969**, *91* (12), 3330–3337.

[6] Fliszár, S.; Granger, M. A Quantitative Investigation of the Ozonolysis Reaction. XI. On the Effects of Substituents in Directing Ozone Cleavage of trans-1,2-Disubstituted Ethylenes. *J. Am. Chem. Soc.* **1970**, *92* (11), 3361–3369.

[7] Fliszár, S.; Renard, J. Quantitative Investigation of the Ozonolysis Reaction. XIV. A Simple Carbonium Ion Stabilization Approach to the Ozone Cleavage of Unsymmetrical Olefins. *Can. J. Chem.* **1970**, *48* (19), 3002–3018.

[8] Wagner, J. P.; Schreiner, P. R. London Dispersion in Molecular Chemistry—Reconsidering Steric Effects. *Angew. Chem. Int. Ed.* **2015**, *54* (42), 12274–12296.

[9] Bunnelle, W. H. Substituent and Structural Effects in the Ozonolysis of Cyclic Vinylogous Esters. *Adv. Cycloaddit.* **1993**, *3*, 67–98.

[10] Nóvoa, L.; Trulli, L.; Parra, A.; Tortosa, M. Stereoselective Diboration of Spirocyclobutenes: A Platform for the Synthesis of Spirocycles with Orthogonal Exit Vectors. *Angew. Chem. Int. Ed.* **2021**, *60* (21), 11763–11768.

[11] Zhang, Z.; Sun, Z.; Song, J.; Guo, H.; Wang, Y.; Hu, X. Construction of the A-B-C Ring of Simplicissin through an Oxidative Dearomatization/Iodination/[3+2] Annulation Cascade. *Org. Lett.* **2023**, *25* (45), 8645–8649.

[12] Liang, Q.-J.; Yang, C.; Meng, F.-F.; Jiang, B.; Xu, Y.-H.; Loh, T.-P. Chelation versus Non-Chelation Control in the Stereoselective Alkenyl sp^2 C–H Bond Functionalization Reaction. *Angew. Chem. Int. Ed.* **2017**, *56* (18), 5091–5095.

[13] Aelterman, M.; Biremond, T.; Jubault, P.; Poisson, T. Electrochemical Synthesis of gem-Difluoro- and γ-Fluoro-Allyl Boronates and Silanes. *Chem. Eur. J.* **2022**, *28* (54), e202202194.

[14] Jiang, Y.-M.; Yu, Y.; Wu, S.-F.; Yan, H.; Yuan, Y.; Ye, K.-Y. Electrochemical Fluorosulfonylation of Styrenes. *Chem. Commun.* **2021**, *57* (89), 11481–11484.

[15] Walker, J. C. L.; Oestreich, M. Regioselective Transfer Hydrodeuteration of Alkenes with a Hydrogen Deuteride Surrogate Using $B(C_6F_5)_3$ Catalysis. *Org. Lett.* **2018**, *20* (20), 6411–6414.

[16] McCourt, R. O.; Scanlan, E. M. Atmospheric Oxygen Mediated Radical Hydrothiolation of Alkenes. *Chem. Eur. J.* **2020**, *26* (68), 15804–15810.

[17] Xu, J.; Liu, B. Metal Free Functionalization of Saturated Heterocycles with Vinylarenes and Pyridine Enabled by Photocatalytic Hydrogen Atom Transfer. *Chem. Eur. J.* **2024**, *30* (31), e202400612.

[18] Xian, N.; Li, Z.; Ji, X.; Xiao, L.; Yin, J.; Huang, H. Tetralone Formation through Visible-Light-Driven Photocyclization of Aryl Sulfoxonium Ylides with Unactivated Alkenes. *Org. Lett.* **2025**, *27* (20), 9310–9315.

[19] Syntrivanis, L.-D.; Némethová, I.; Schmid, D.; Levi, S.; Prescimone, A.; Bissegger, F.; Major, D. T.; Tiefenbacher, K. Four-Step Access to the Sesquiterpene Natural Product Presilphiperfolan-1-ol and Unnatural Derivatives via Supramolecular Catalysis. *J. Am. Chem. Soc.* **2020**, *142* (13), 5894–5900.

[20] Ma, S.-J.; Yu, J.; Zhang, Q.; Yan, D.-W.; Wang, D.-C.; Gao, J.-M. Meroterpene-like compounds derived from β-caryophyllene as potent α-glucosidase inhibitors. *Org. Biomol. Chem.* **2018**, *16* (44), 9454–9460.

[21] Crossley, S. W. M.; Barabé, Francis; Shenvi, R. A. Simple, Chemoselective, Catalytic Olefin Isomerization. *J. Am. Chem. Soc.* **2014**, *136* (48), 16788–16791.

[22] Lou, S.-J.; Wang, P.; Wen, X.; Mishra, A.; Cong, X.; Zhuo, Q.; An, K.; Nishiura, M.; Luo, Y.; Hou, Z. (Z)-Selective Isomerization of 1,1-Disubstituted Alkenes by Scandium-Catalyzed Allylic C−H Activation. *J. Am. Chem. Soc.* **2024**, *146* (39), 26766–26776.

[23] Lin, L.-H. C. Base-Catalyzed Rearrangements of Epoxides. Ph.D. Dissertation, Indiana University, Bloomington, IN, 1967.

[24] Rummens, F. H. A.; de Haan, J. W. Spectroscopic Studies on Olefins-III: NMR of Cis- and Trans-Disubstituted Olefins. *Org. Magn. Reson.* **1970**, *2* (4), 351–355.

[25] Carvalho, J. F. S.; Cruz Silva, M. M.; Sá e Melo, M. L. Highly efficient epoxidation of unsaturated steroids using magnesium bis(monoperoxyphthalate) hexahydrate. *Tetrahedron* **2009**, *65* (14), 2773–2781.

[26] Bernardo-Otero, Y.; Alonso-Becerra, E.; Guerra-Martínez, F.; Martínez-Massanet, G.; Pérez-Martínez, C.; Coll-Manchado, F. Synthesis and biological activity of epoxy analogues of 3-dehydroteasterone. *J. Chem. Res.* **2007**, *2007* (5), 268–271.

[27] Roszkowski, P.; Maurin, J. K.; Czarnocki, Z. New N,N-diamine ligands derived from (-)-menthol and their application in the asymmetric transfer hydrogenation. *Tetrahedron: Asymmetry* **2017**, *28* (4), 532–538.

[28] Villa, G.; Povie, G.; Renaud, P. Radical Chain Reduction of Alkylboron Compounds with Catechols. *J. Am. Chem. Soc.* **2011**, *133* (15), 5913–5920.

[29] Hass, H. B.; Bender, M. L. A Proposed Mechanism of the Alkylation of Benzyl Halides with Nitro Paraffin Salts. *J. Am. Chem. Soc.* **1949**, *71* (10), 3482–3485.

[30] Adam, W.; Arnold, M. A.; Grune, M.; Nau, W. M.; Pischel, U.; Saha-Möller, C. R. Spiroiminodihydantoin Is a Major Product in the Photooxidation of 2'-Deoxyguanosine by the Triplet States and Oxyl Radicals Generated from Hydroxyacetophenone Photolysis and Dioxetane Thermolysis. *Org. Lett.* **2002**, *4* (4), 537–540.

[31] Adam, W.; Baeza, J.; Liu, J.-C. Stereospecific Introduction of Double Bonds via Thermolysis of β-Lactones. *J. Am. Chem. Soc.* **1972**, *94* (6), 2000–2006.

[32] Dworkin, J. H.; Chen, Z. M.; Cheasty, K. C.; Rubio, A. V.; Kwon, O. Hydrodealkenylated C(sp^3)–C(sp^2) Bond Fragmentation Using Isayama-Mukaiyama Peroxidation. *J. Am. Chem. Soc.* **2025**, *147* (23), 13531–13544.

[33] Schlosser, M.; Schaub, B. Instant-Ylid: ein lagerfähiges und gebrauchsfertiges Wittig-Reagenz. *Chimia* **1982**, *36* (10), 396–400.

[34] Munnuri, S.; Falck, J. R. Directed, Remote Dirhodium C(sp3)–H Functionalization, Desaturative Annulation, and Desaturation. *J. Am. Chem. Soc.* **2022**, *144* (39), 17989–17998.

[35] Gassman, P. G.; Burns, S. J.; Pfister, K. B. Synthesis of Cyclic and Acyclic Enol Ethers (Vinyl Ethers). *J. Org. Chem.* **1993**, *58* (6), 1449–1457.

[36] Prout, E. S.; Kwon, O.; Silva, T. G. Regioselective Synthesis of Methyl Enol Ethers from Cycloalkanones via O-Methylation of Kinetic Enolates. *Synthesis* **2026**, *58* (10), SS-2026-01-0027-OP.

[37] Bedoukian, P. Z. Synthesis of α-Bromoketones. *J. Am. Chem. Soc.* **1945**, *67* (9), 1430–1431.

[38] Kerkovius, J. K.; Wong, R. A.; Mak, V. W.; Reisman, S. E. A Convergent Fragment Coupling Strategy to Access Quaternary Stereogenic Centers. *Chem. Sci.* **2023**, *14* (17), 4397–4400.

[39] Mizuta, S.; Galicia-López, O.; Engle, K. M.; Verhoog, S.; Wheelhouse, K.; Rassias, G.; Gouverneur, V. Trifluoromethylation of Allylsilanes under Copper Catalysis. *Chem. Eur. J.* **2012**, *18* (28), 8583–8587.

[40] Žmitek, K.; Zupan, M.; Stavber, S.; Iskra, J. The Effect of Iodine on the Peroxidation of Carbonyl Compounds. *J. Org. Chem.* **2007**, *72* (17), 6534–6540.

CHAPTER SEVEN

Extraction of Cycloalkanone α-C(sp^3) atoms with ozone and Samarium

Unpublished proof-of-concept results requiring further research.

Contributing authors: Dworkin, J. H.; Chen, Z. M.; Bioteau, J. A.; Wang, J. M.; and Kwon, O.

The dissertation author originated the idea for the project and conducted the initial experiments to prove the efficacy of the idea.

7.1 Abstract

Progress towards the extraction of cycloalkanone α-C(sp^3) atoms with ozone and Samarium is reported within this chapter. There are three mechanistic ideas within this work: ozonolysis of enol ethers, single electron reduction of peroxides with SmI_2, and a proof-of-concept of the ring-contraction idea. The Criegee ozonolysis of enol ethers was optimized using 10:1 hexanes/methanol as the ideal solvent. The single electron reduction of peroxides with Sm(II) was demonstrated to be possible with MeOH and H_2O the solvent. The reaction is proposed to proceed through a solvent mediated chair-like transition state. The ring-contraction was demonstrated to be possible using polar-aprotic amide solvents in low yields. Further optimization is required to turn this idea into a robust methodology.

7.2 Proposal and Background

Ring contractions belong to one of the most fundamental transformations in organic synthesis [1]. They can be divided by the reaction mechanism into cationic, anionic, and carbenoid categories [2]. Although widely applied, known contractions of cycloalkanones usually follow a rearrangement mechanism reorganizing the carbon skeleton but not deleting any of the present carbon atoms. The result is the expulsion of one carbon atom from the contracted cycle, thus changing the overall architecture. Furthermore, the rearrangement tendency is usually predetermined by the nature of attached substituents and the geometry of the substrate.

The ozonolysis of vinyl compounds CR_2=CR–X has been shown to cleave the double bond and place the Creigee intermediate on the α-carbon of the former carbonyl group [3,4]. In the case of endocyclic enol ethers, ozonolysis leads to hydroperoxides carbon-chain tethered with a carboxylic acid function. The fact that the C=O or C–O bonds of carboxylic acid derivatives can be inserted by metal complexes brings the opportunity to exploit them as acyl surrogates in subsequent acylation reactions [5]. In this sense, numerous applications utilizing chromium-, nickel-, or palladium-catalyzed activation of methyl esters [6] acyl chlorides [7], or carbonates [8,9] have been developed. This reactivity, together with a simultaneously orchestrated catalytic hydroperoxide reduction/fragmentation, can be used in net ring contraction reactions by deleting one carbon atom from cycloalkanones or anisoles.

We propose to develop a radical ring contraction sequence for the selective deletion a carbon atom from the α-position of endocyclic enol ethers to reaction to furnish contracted ring systems without changing the connectivity in the carbon skeleton. In the

case of cyclopentenone synthesis, a pericyclic approach, such as the Pauson-Khand reaction and Nazarov cyclization, dominate synthetic options, but our method will provide a unique radical approach to the synthesis of compounds from this class. The methodology will allow the skeletal editing of complex ring-containing scaffolds with the application in the preparation of complex molecules and natural product synthesis. Our synthetic strategy hinges on a samarium-Barbier reaction to form our cycloalkanones.

In our reaction design (Figure 7.1), the model substrate, (+)-dihydrocarvone hydrate (prepared in 1 step from (+)-dihydrocarvone hydrate $0.37/g), is transformed into the ring contracted 3-(2-hydroxypropan-2-yl)cyclopentanone (commercially available as a racemate, $1232/g), as a single (*R*)-enantiomer. First, the corresponding thermodynamic methyl enol ether **I** (kinetic enolization/*O*-alkylation is also possible)[10] is generated, thus choosing the position of the deleted carbon atom. Formed methyl enol ether **I** is then submitted in a one-pot fashion to Criegee ozonolysis conditions in methanol creating the α-alkoxy hydroperoxide **II**. A solvent swap to THF followed by subsequent single electron transfer by SmI_2 (–1.33 V vs $Ag/AgNO_3$ reference in THF; –0.89 V vs SCE) [11–13] forms the reduced alkoxy radical (**III**). Fragmentation ($k > 10^8\ M^{-1}s^{-1}$) [14] removes a carbon equivalent as methyl acetate and delivers a new alkyl radical that is captured by a Sm(II) species forming complex **IV**. Through a samarium-Barbier reaction, the alkyl-samarium complex adds across the methyl ester C=O bond furnishing tetrahedral intermediate **V** which delivers the enantiopure ring-contracted product upon acidic work-up [15]. Although additives are not required for classical Sm-Barbier coupling reactions, the addition of HMPA boosts the reductive capability of SmI_2 via complexation to accelerate the rate for the initial electron transfer. With four equivalents of HMPA,

$[Sm(THF)_2(HMPA)_4]I_2$ (confirmed by x-ray crystallography) is generated, and its reduction potential is extremely low (–1.79 V vs SCE) [13,16]. By comparison, the standard reduction potentials of alkyl radicals are also quite low, (–0.92 V, –1.10 V, –1.44 V, –1.45 V, and –1.55 V (vs SCE) for methyl, ethyl, 2-propyl, benzyl, and *tert*-butyl radicals, respectively) [17] enabling a formal radical-polar crossover event with the use of Sm-HMPA as a mechanistic possibility.

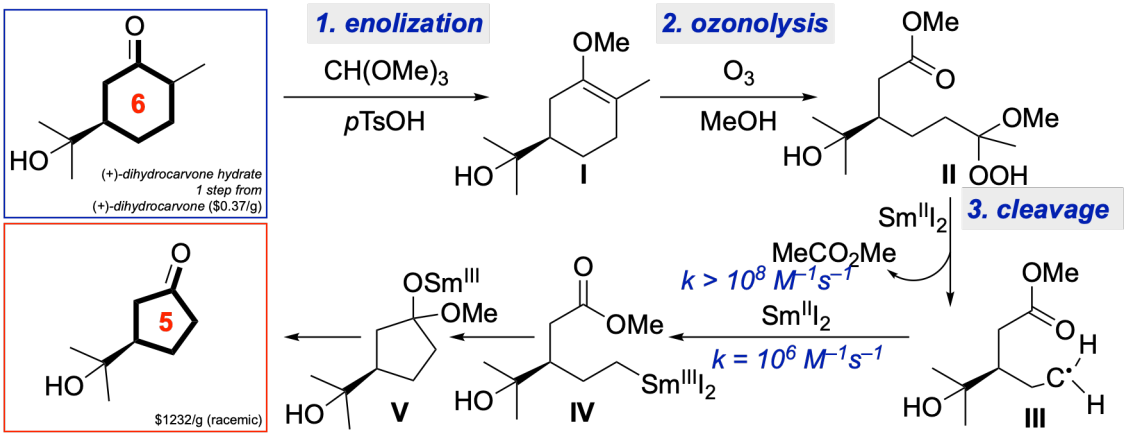


Figure 7.1 Initial Plan

We believe several factors will contribute to the successful development of this methodology. First, lanthanides are known to reduce hydrogen peroxide to yield a metal-hydroxide and a hydroxyl radical [18]. In 1989 the first instances of organic peroxide reductions were reported, where SmI_2 was used to reduce alkyl endoperoxides, yielding the corresponding diols in >60% yields [19]. Another application of SmI_2 for endoperoxides was conducted in 1992 with artemisinin, yielding a reduced product in 61% yield [20]. These organic applications demonstrate that SmI_2 is capable of reducing even the most hindered of organic peroxides. Second, for a couple of reasons, we expect the reduction of our α-alkoxy hydroperoxides to be faster than the reduction of the ozone-

generated methyl ester. While the reduction of aldehydes by SmI_2 is rapid, the reduction of ketones is slow (k = 7 x10^{-4} $M^{-1}s^{-1}$ for 2-butanone), and carboxylic acids and esters are not reduced by SmI_2 alone [21,22]. Even with a stronger reductant, [$Sm(HMPA)_6I_2$], the reduction of 2-butanone is slow (k = 8 x10^{-3} $M^{-1}s^{-1}$). However, with the addition of water, SmI_2–H_2O (–1.0 to –1.3 V vs SCE) is capable of reducing esters [12]. In general, the reduction of carbonyl substrates occurs through an inner sphere process, which gives rise the decreased rates of reduction for ketones and esters as compared to aldehydes [13,23]. Third, both the coupling to the alkyl radical by SmI_2 (k = 10^6 $M^{-1}s^{-1}$) [24] and the rate of β-scission of α-alkoxy hydroperoxides (k > 10^8 $M^{-1}s^{-1}$) [14] are fast, therefore, at high dilution of the reaction and low concentration of radical species, side-radical reactions, such as dimerization (k = 1.7 x10^8 $M^{-1}s^{-1}$) and disproportionation (1.8 x10^8 $M^{-1}s^{-1}$) should be mitigated [14]. These rates also indicate a kinetic window for our proposed mechanism because the second SET from SmI_2 is slower than β-scission by a factor of 10^2. Fourth, the tetrahedral intermediate **V** will also be relatively stable until acidic work-up, further preventing the formation of a potentially reactive ketone towards cross-coupling side-products [15]. Fifth, the intramolecular nature of the reaction will overall increase the rate for our desired pathway because slower side-reactions such as the coupling to the excised methyl ester by-product will be prevented.

If our Sm-Barbier reaction design proves unsuccessful, we have envisioned an alternative set of conditions to achieve this transformation (Figure 7.2). Our proposed mechanism begins with a similar preparation of the hydroperoxide **II** from the starting ketone, (+)-dihydrocarvone hydrate. Then, a slow addition of the peroxide into a Ni(II)/Sm(III) dual-catalytic cycle using Mn(0) as a sacrificial reductant will yield the

product. Theoretically, Ni(I) may be exchanged for Cu(I) or Co(II), and Mn^0 may be substituted for Mg^0 to achieve the same result. A prepared mixture of $SmCl_3$, $NiCl_2$, and Mn^0 will initiate SET from Mn^0 to Ni(II) generating Ni(0) and Ni(I) [25]. Addition of the peroxide to this slurry will induce a second SET from Ni(I) to the peroxide forming Ni(II), hydroxide, and an α-methoxy alkoxy radical **III**. Rapid β-scission ($k > 10^8$ $M^{-1}s^{-1}$) [14] ejects methyl acetate and forms an alkyl radical which is coupled with Ni(II) ($k = 10^7$–10^6 $M^{-1}s^{-1}$). A third SET from Mn^0 or $Mn^{I}X$ to alkyl-Ni(III) species **IV-I** will form the alkyl-Ni(II) complex **IV-II**. Transmetallation to Sm(III) to will create the alkyl–Sm(III) species **IV-III** and turn over Ni(II). A Sm-Barbier coupling will convert **IV-III** to **V**. A final ligand exchange will regenerate Sm(III) and provides the ring contracted product. Overall, this process can be conducted with catalytic Sm and Ni, two toxic and precious metals (7.05 ppm and 84 ppm in the Earth's crust, respectively), shifting the environmental impact to a more abundant metal, Mn (950 ppm) or Mg (2.33×10^4 ppm) [26]. The amount of Mn^0 or Mg^0 required will only need to be half an equivalent, where two of its electrons are inevitably shuttled into the starting material to convert it into the product.

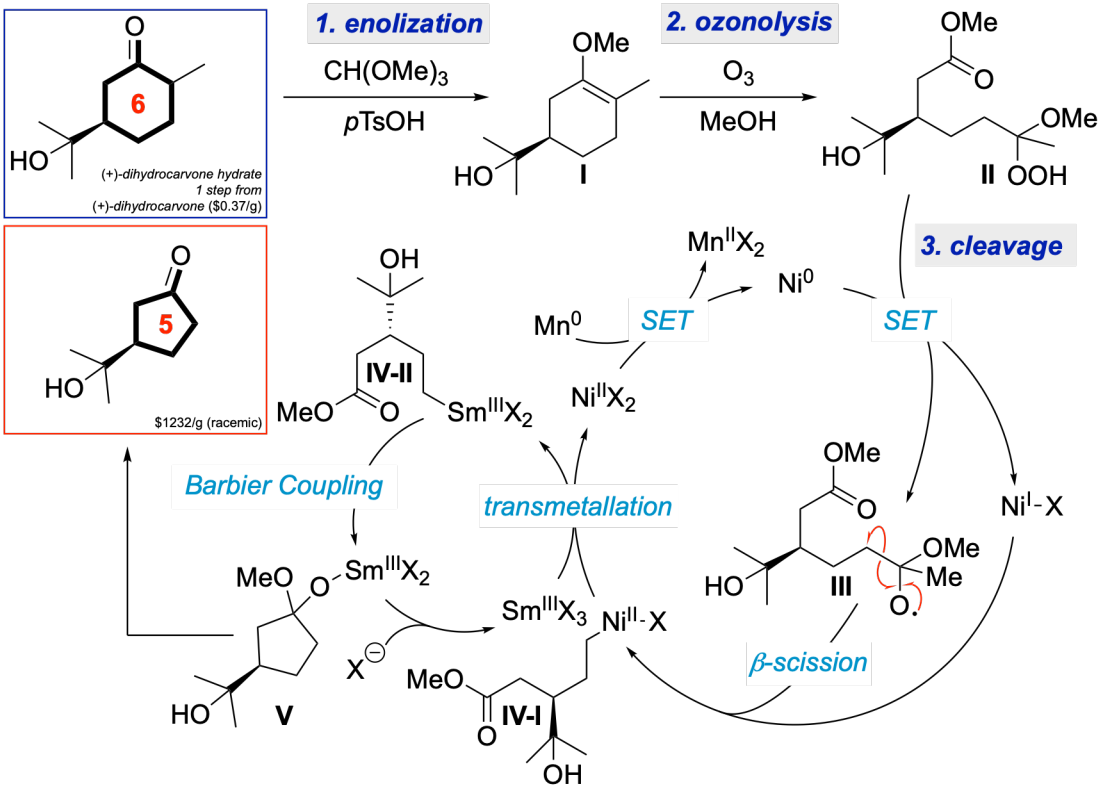


Figure 7.2 Backup Plan

The anticipated success in developing this alternative option hinges on the interplay of several contributing factors. First, in the classical Sm-Barbier reaction, formation of an alkyl-Sm(III) species is the essential mechanistic step for the addition to carbonyls [27]. In our catalytic reaction design, the choice of metal for SET is limited to metals which can form alkyl-metal radical-caged pairs. Base metals such as Cu, Ni, and Co are known to form alkyl-metal radical pairs [28–30], and salts from these metals are suitable for both the Sm-Barbier reaction [15d] and the reduction of alkyl hydroperoxides [28,31]. Second, we foresee β-hydride elimination as a confounding pathway for our proposed alkyl-Nickel complexes (**IV-I** and **IV-II**). Use of a ligand may be required to both increase the d-electron count and saturate the coordination sites of our metal to suppress formation of the alkene. Based upon the work of Guo and Maruoka in the Ni-catalysed Suzuki coupling

from alkyl trimethylsilylperoxides, we intend to use di-*tert*-butyl bipyridine (dtbpy) or 2-pyridone as preliminary ligands [31]. Third, ligand exchange to remove the product alkoxide from the Sm(III) center may be slow. Increasing the concentration of X-type ligands will shift this equilibrium towards the product. Fourth, high dilution will likely be necessary to achieve the desired intramolecular coupling because the formed ketone will provide a better electrophilic coupling partner, and dimerization of the material or re-addition into the excised methyl acetate will result in non-productive products. Fifth, the transmetallation from Ni(II) to Sm(III) must be faster than the coupling of Ni(II)-alkyl with another alkyl radical ($k = 10^7 – 10^6$ $M^{-1}s^{-1}$) [32] followed by a slower reductive elimination step. Ideally, high dilution and a lower quantity of nickel relative to samarium should disfavor this confounding pathway. Despite these perceived pitfalls, we are confident our mechanism will predominate to provide our desired product.

Should our first two mechanistic ideas fail, a third option involves insertion into the acyl C–O bond (Figure 7.3). First, it has been shown that oxidative addition to methyl esters can be successfully with nickel complexes in synergy with Lewis acids [33]. Therefore, intermediate **II** could be engaged in an identical transformation applying $Ni(cod)_2$/SIPr complex and $Al(O\textit{t}Bu)_3$ as an ester-activating Lewis acid. Second, the Criegee ozonolysis of silyl enol ethers analogously leads to the formation of α-alkoxy hydroperoxides tethered with silyl esters that rapidly desilylate, giving free carboxylic acids **VI**. The carboxylic acid function can be, for our purposes, *in situ* activated by Boc_2O or DMDC (dimethyl dicarbonate), forming acyl carbonates that effectively undergo oxidative addition by nickel complexes in a similar catalytic cycle [8,34]. The extra activation step can, most likely, be performed in a one-pot fashion, thus not decreasing

the overall efficiency of the reaction sequence. The simultaneous activation of the hydroperoxide moiety cannot be excluded, but it is inconsequential at this stage. Third, the ozonolysis of preformed vinyl carbonates has been shown to deliver acyl carbonates [4], that could be engaged by nickel complexes as previously described. Such ozonolysis can be performed in the sense of Griesbaum coozonolysis with an external aldehyde (*e.g.,* benzaldehyde) [35]. The carbonyl oxide intermediate undergoes a cycloaddition with the aldehyde forming a fragmentable 1,2,4-trioxanes **VII** under conditions avoiding nucleophilic methanol incompatibility with acylcarbonates used above. Identically to α-alkoxy hydroperoxide **II,** trioxolane **VII** will be reduced and cleaved by a nickel complex, simultaneously coupling to the alkyl radical and inserting into the C–O bond of acylcarbonates following the desired reaction pathway. We plan to explore cyclization aptitudes of cycloalkanones with varying ring-sizes to potentially synthesize four to seven-membered ring systems.

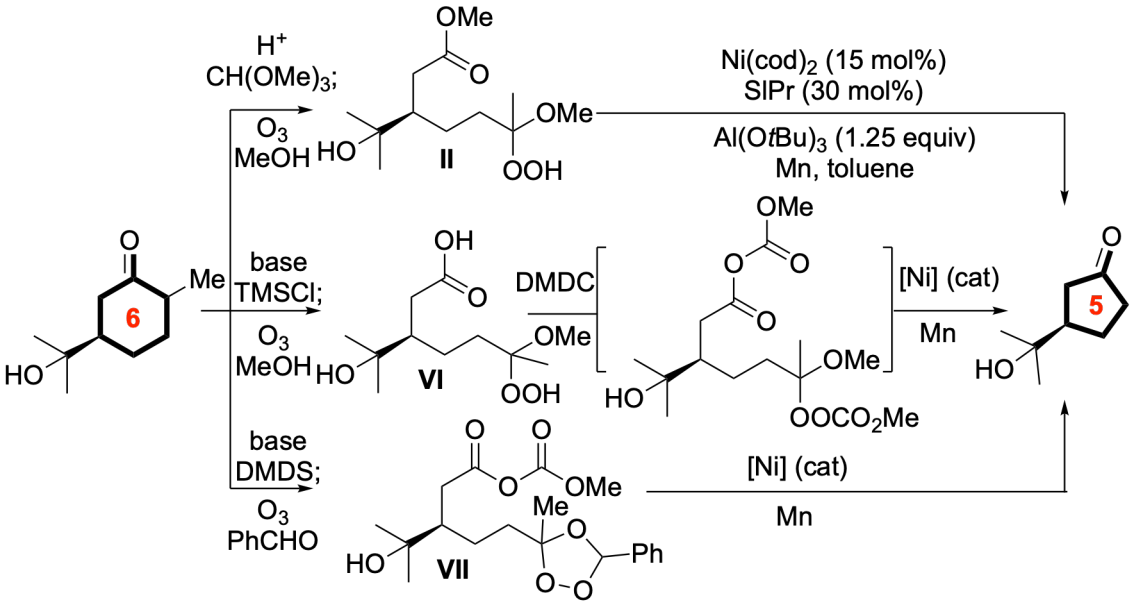


Figure 7.3 Alternative Plans

7.3 Enol Ether Synthesis

At the beginning of this project, in 2023, the efficient generation of the enol ethers required for this research was difficult. One-pot procedures involving deprotonation to generate the enolate followed by *O*-alkylation initially led to mixtures of *C*-alkylation and *O*-alkylation. These reactions were further complicated by the difficult purification required to not hydrolyze the formed enol ethers. As a result, we initially opted for the formalized 2-step procedure, first accessing the ketal then conducting Lewis-acid mediated enolization with TMSI or TMSOTf in the presence of an amine base [36,37]. Further research led by Prout, E. S. in the Kwon group resulted in the development of a robust method to generate methyl enol ethers [38]. Below are a list of the ketals and enol ethers synthesized for this project (Figure 7.4).

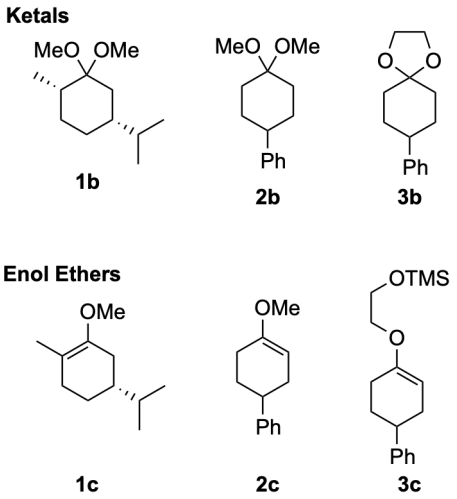


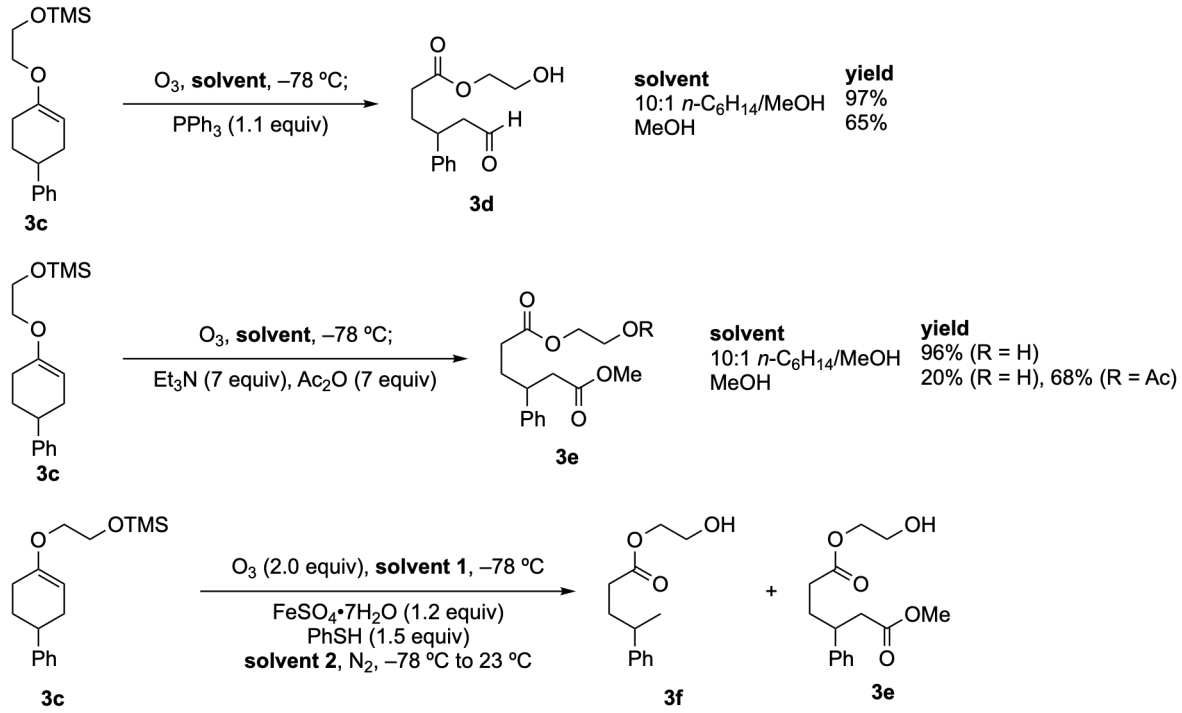
Figure 7.4 Ketals and Enol Ethers

7.4 Ozonolysis Optimization

The first proposed step after enolization was Criegee ozonolysis in methanol. To evaluate the efficiency of the ozonolysis reaction, a short solvent screen was conducted. The reaction outcome was evaluated by 2-electron reduction, 2-electron oxidation, and 1 electron reduction using hydrodealkenylation [39]. With methanol as the solvent, reduction with triphenylphoshine resulted in the corresponding aldehyde **3d** in 65% (Figure 7.5). Oxidation with triethylamine and acetic anhydride, on the other hand, led to the methyl ester **3e** in 88% combined yield. Swapping the solvent for a 10:1 hexanes/methanol mixture improved the yield in both cases to 97% and 96% respectively.

Next, we tested the enol ethers versus standard hydrodealkenylation. Ozonolysis of **3c** in methanol followed by addition of iron(II) sulfate heptahydrate and benzenethiol provided the expected product **3f** in 69% yield, and the ester **3e** in 13% yield. For the reaction with samarium, we anticipated the requirement of a solvent swap, so after ozonolysis, the methanol was evaporated, then the peroxide was re-dissolved in a new solvent and added to a solution of iron(II) sulfate heptahydrate and benzenethiol in methanol. The addition of the peroxide to the iron(II) is the inverse of the standard hydrodealkenylation condition and improved the yield in all cases. Using methanol to re-dissolve the peroxide provided the desired product **3f** in 74% yield, with 14% of the ester side-product **3e**. Moving to the optimal 10:1 hexanes/methanol solvent system for ozonolysis, then adding the peroxide solution directly into the methanolic solution of iron(II) sulfate heptahydrate and benzenethiol resulted in 78% yield of the desired product **3f** and 17% yield of the ester **3e**. There was almost no difference when the peroxide was dried after ozonolysis in 10:1 hexanes/methanol dissolution in methanol and inverse

addition. These results indicated that the ozonolysis reaction should be done in 10:1 hexanes/methanol for enol ethers, inverse addition results in better conversion to the desired product, and evaporation of the peroxide prior to reduction does not impact the overall yield.

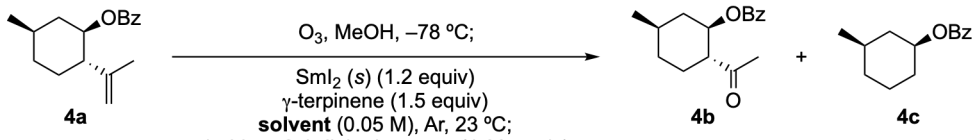


solvent 1	solvent 2	method	3f%	3e%
MeOH	MeOH	standard hydrodealkenylation	69%	13%
MeOH	MeOH	evaporate to dry, inv. add.	74%	14%
10:1 hexane/MeOH	MeOH	evaporate to dry, inv. add.	78%	18%
10:1 hexane/MeOH	1:1 hexane/MeOH	direct inv. add.	78%	17%

Figure 7.5 Ozonolysis of Enol Ether Optimization

7.5 Hydrodealkenylation with Samarium(II)

Historical precedent revealed Sm(II) reacts with organic peroxides to reduce them to the corresponding alkoxides [19,20]. Therefore, we needed to validate that Sm(II) could reduce the Criegee ozonolysis peroxides to the corresponding alkoxyl radicals required for our transformation. We chose to use *O*-benzoyl isopulegol as the model substrate for this transformation and to track the products formed with qNMR. We pursued a solvent screen using solid SmI_2 as the reductant and γ-terpinene as the hydrogen atom donor (Figure 7.6). The SmI_2 was not very soluble in benzene, and almost none of the desired product was observed. MeCN provided a slight increase in solubility but none of the desired product. MeOH and H_2O were excellent solvents to dissolve SmI_2 and we observed similar quantities of the desired product at 24% and 23%, respectively. Other H-bond donors such as *t*BuOH, HFIP, EtOH, and *i*PrOH were tested, but the SmI_2 solution was added to the peroxide as in "normal addition". In every case, the product was either minimally (<5%) or not observed. From this initial screen, we concluded that MeOH and H_2O were promising solvents, and a larger quantity of SmI_2 was likely required to improve the conversion.



solvent	scale (mmol)	4b%	4c%	Notes
benzene	0.120	98%	1%	inverse addition
MeCN	0.200	100%	0%	inverse addition
MeOH	0.103	66%	24%	inverse addition
H_2O	0.077	65%	23%	inverse addition
*t*BuOH	0.206	97%	3%	normal addition
HFIP	0.105	100%	0%	normal addition
EtOH	0.176	92%	5%	normal addition
*i*PrOH	0.135	100%	0%	normal addition

Figure 7.6 SmI_2 Hydrodealkenylation: Solvent Screen

A literature search revealed that SmI_2 reacts with proton sources through a chair-like transition state to reduce carbonyls [40]. We invoked a similar idea to rationalize the results we found with MeOH and H_2O (Figure 7.7).

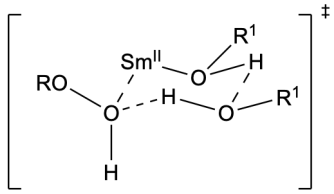
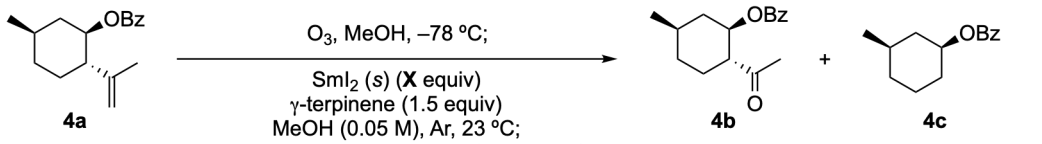


Figure 7.7 Proposed TS‡ for SmI_2 reduction of peroxides with a proton source

Increasing the quantity of SmI_2 improved the yield of the hydrodealkenylation product (Figure 7.8). With 1.8 equivalents, instead of 1.2, we saw 46% (NMR yield) of the desired product. Increasing to 2.4 equivalents resulted in 64% (NMR yield) of the hydrodealkenylation product.

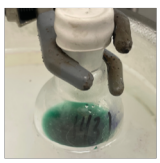


X	scale (mmol)	4b%	4c%
1.8	0.132	40%	46%
2.4	0.141	21%	64%

Figure 7.8 SmI_2 Hydrodealkenylation: Equivalent Screen

Decreasing the temperature also had a positive effect on the reaction. We noticed that the reaction color would change as the peroxide was added. Initial dissolution of SmI_2 in MeOH was a green/turquoise color (Figure 7.9). Upon stirring at room temperature, the color would slowly dissipate into a grey solution, indicating reduction of MeOH. For previous examples with less equivalents of SmI_2, the reaction would become a red/yellow color prior to complete addition of the peroxide, indicating the formation of triiodide (I_3^-).

When the reaction was cooled, the reduction of MeOH became slower which enabled a larger quantity of the SmI_2 to be available to reduce the peroxide. As such, –10 ºC and –78 ºC provided only 5% and 4%, respectively, of the ketone side-product. The reaction also remained green throughout addition of the peroxide. We interpreted this result to indicate that 95% and 96%, respectively, of the peroxide was going through a β-scission pathway.



SmI_2 (s) in MeOH at –78 ºC
initial dissolution



SmI_2 (s) in MeOH at 23 ºC
after some time

Figure 7.9 Colors of SmI_2 (s) in MeOH

Due to the fact that SmI_2 would reduce MeOH, we were interested in determining if there was a minimum quantity of MeOH we could add to the reaction to enable the desired transformation. We used the thermodynamic methyl enol ether **1b** derived from dihydrocarvone **1a** and high throughput experimentation (HTE) to test our hypothesis. A screen from 0–2400 equivalents of MeOH relative to SmI_2 was conducted. A solution of the ozonolysis peroxide was prepared, evaporated and re-dissolved to create a stock solution. SmI_2 as a solution in THF was transferred into a 4-dram vials and cooled to –10 ºC. Next, the desired quantity of MeOH was added to a single vial, followed by the peroxide. The sequence was then continued for the remaining vials. After completion, each vial was quenched with 1 M HCl, then a small quantity of a stock solution of an internal standard (1-chloro-2,4-dinitrobenzene) in ethyl acetate was added. GCMS was then measured and the peak area ratios were normalized and graphed (Figure 7.10).

Analysis revealed about 100 equivalents of MeOH was required per SmI_2 equivalent to enable the ring-contraction. We attribute the simultaneous increase in hydrodealkenylation product as indicative of the generation of an alkyl samarium(III) species that protodemetalates prior to Barbier cyclization. We attributed the persistence of the dimerization product with the increase in MeOH equivalents to a saturated Sm(II) center that prevented the alkyl radical from accessing the metal. In turn this would promote dimerization. Overall, these results indicate the initial SET and β-scission events do occur, even with minimal MeOH. But, the capture of the alkyl radical for the desired cyclization pathway is limited because of the possibility for protodemetalation and the likely saturation of MeOH around the metal.

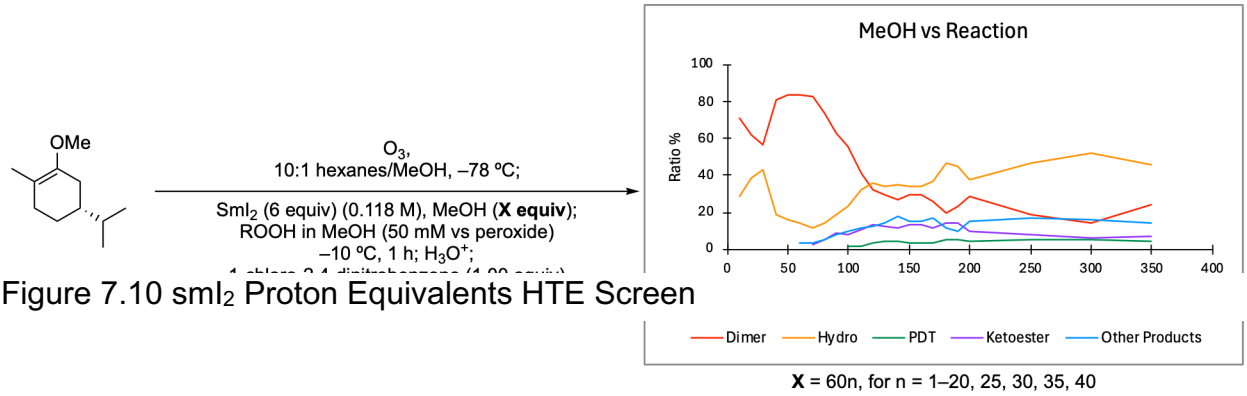


Figure 7.10 smI_2 Proton Equivalents HTE Screen

7.6 Cycloalkanone α-C(sp^3) Extraction Efforts

4-Phenyl cyclohexanone **2a** was chosen to be the model substrate for the Samarium-Barbier reaction. The phenyl ring enabled ultraviolet detection, and the boiling points of the respective products were low enough to analyze crude reaction mixtures using GCMS. Reference standards for all possible products were synthesized (Figure 7.11). The aldehyde **2c** was made in 99% yield by ozonolysis of the methyl enol ether **2b** in 10:1 hexanes/methanol then reduction with triphenylphosphine. Using both acetic anhydride and triethylamine in ethyl acetate instead of triphenylphsophine provided the corresponding methyl ester **2d** in 99% yield. The styrene **2e** was synthesized in 49% yield treating the ozonolysis peroxide with iron(II) sulfate heptahydrate with copper(II) acetate. The hydrodealkenylation product **2f** was accessed in 53% yield using standard conditions [39]. The dimer **2g** was synthesized in 72% yield by treating the ozonolysis peroxide with iron(II) sulfate heptahydrate. Finally, the alcohol **2h** was formed in 95% yield by treatment of the ozonolysis peroxide with sodium borohydride. With all of these products in hand, the GCMS traces for each optimization reaction became much easier to interpret.

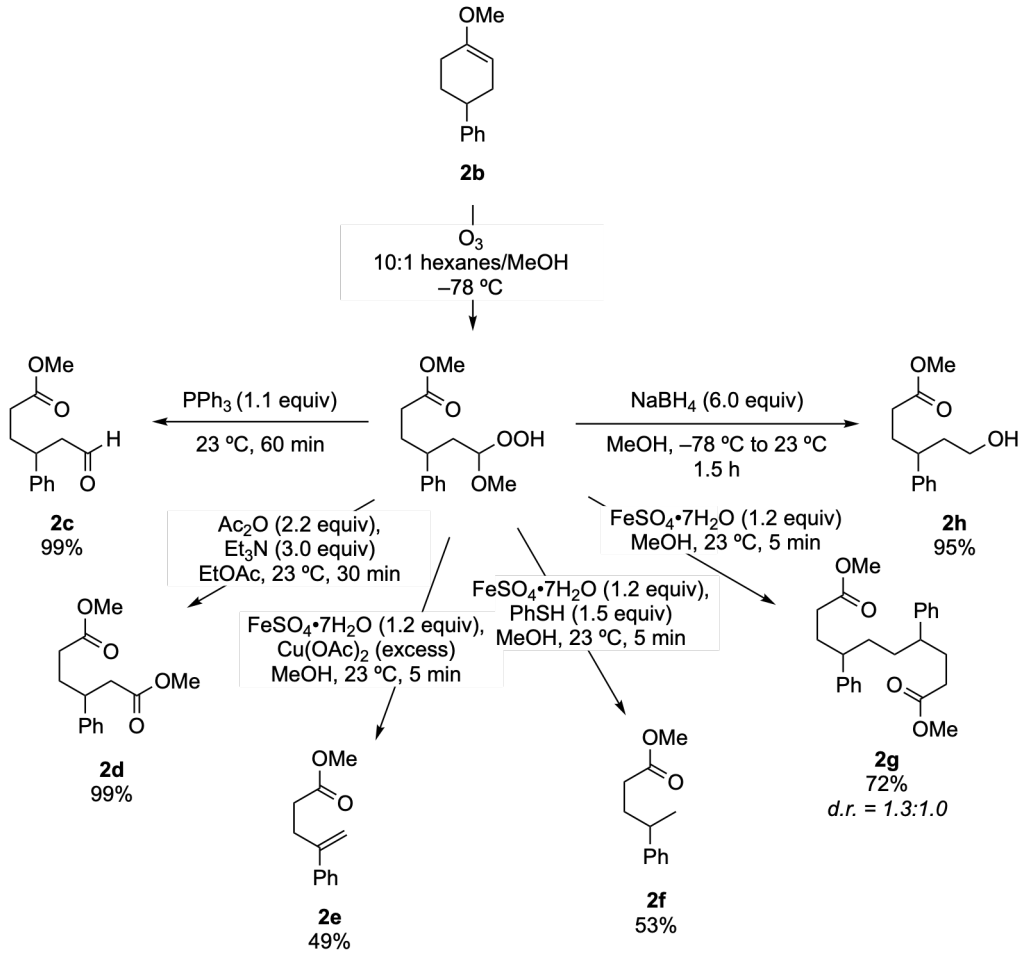
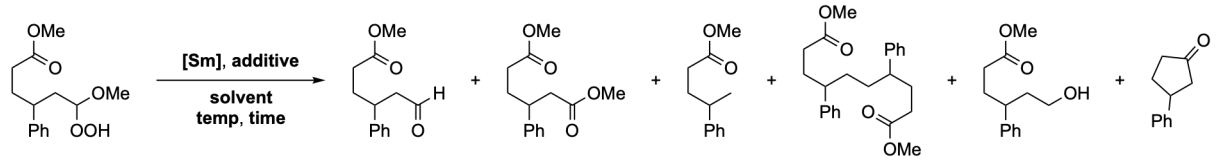


Figure 7.10 4-Phenylcyclohexanone Potential Reaction Products

Reaction screening commenced with H_2O and alcoholic solvents: MeOH, EtOH, and *i*PrOH (Table 7.1). Water and methanol performed the best for enabling β-scission, but none of the protic solvents tested resulted in formation of the desired product. We then moved to polar aprotic media. Dissolving the peroxide in DMF and adding it to a solution of SmI_2 in 5:6 THF/DMF at –10 ºC provided an initial hit of product **2i** formation (13%). The product was confirmed by HRMS as well as ^1H and ^{13}C NMR versus known values. However, there was still a significant quantity of hydrodealkenylation product **2f** (17%) and dimerization **2g** (10%). We hypothesized there was not enough samarium(II) in

solution to efficiently capture the formed radicals, so we doubled the equivalents of SmI_2. We observed a 10% decrease in hydrodealkenylation **2f** but no change in dimerization **2g**. Furthermore, there was less overall β-scission because more of the over-reduction aldehyde **2c** and alcohol **2h** products were detected. Decreasing the Sm(II) equivalents to 6 while also decreasing the DMF activator solvent shut down the reaction. The Sm(II) catalyst was not very soluble in THF and additional DMF was required for dissolution. Stronger stirring with a slower addition of the peroxide may rescue reactivity but was not tested. Different nickel(II) additives were tested. While these additives suppressed the formation of the hydrodealkenylation **2f** and dimerization **2g** products, there was also about half as much overall β-scission based products. Other amide (DMA, NMP) and urea (DMPU) activators were tested, but none of them provided significantly better results than DMF. Finally, –78 ºC was tested. The colder temperature decreased solubility of the Sm(II) catalyst and also promoted the formation of the ester **2d**. Overall, polar aprotic activators appear to promote the reaction and Ni(II) additives suppressed alternative radical pathways. A combination of a weaker amide activator in combination with a Ni(II) additive appears to be a promising direction for future testing. Alternatively, DMPU and HMPA are both strong activators of Sm(II) and can efficiently reduce the alkyl radical. Designing a method to promote β-scission with these activators may also be promising. Finally, it could be proposed that the product **2i** forms during the initial addition of the peroxide, then hydroxide generated in solution may shut down reaction.

Table 7.1 Ring Contraction Optimization

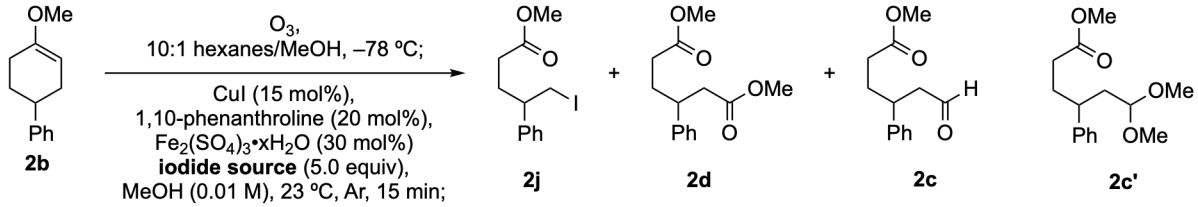


peroxide (µmol)	[Sm]	additive	solv.	ºC	min	2c	2d	2f	2g	2h	2i
172	s, 4.0		H_2O	0 to 23	100	19%*	41%*	31%*	36%*	–	–
122	s, 4.0		MeOH	– 78 to 23	55	24%*	30%*	24%*	22%*	–	–
118	s, 4.0		EtOH	– 78 to 23	210	2%	67%	11%	4%	17%	–
140	s, 4.0		*i*PrOH	– 78 to 23	210	10%	45%	–	–	45%	–
141	s, 4.0		5:6 THF/DMF	– 10	20	14%	31%	17%	13%	12%	13%
108	8.0		5:6 THF/DMF	23	180	5%	22%	6%	10%	28%	13%
108	6.1		10:1 THF/DMF	23	15	87%	3%	1%	2%	5%	1%
108	8.0	$NiBr_2$(dme) 10 mol%	1:1 THF/DMF	23	30	57%	14%	2%	2%	14%	11%
155	8.0	NiI_2 10 mol%	1:1 THF/DMF	23	30	15%	22%	4%	1%	39%	12%
155	8.0	NiI_2 5 mol%	1:1 THF/DMA	23	60	33%	13%	3%	3%	30%	15%
155	8.0	NiI_2 5 mol%	1:1 THF/DMPU	23	120	30%	4%	5%	–	60%	1%
155	8.0		1:1 THF/NMP	23	60	6%	25%	12%	3%	23%	11%
155	8.0		2:1 to 5:1 THF/DMF	– 78 to 23	120	7%	51%	20%	9%	4%	8%

7.7 Iododealkenylation

Due to stalled efforts to achieve a direct reduction of the alkyl radical and Barbier-cyclization we pursued the formation of an initial alkyl iodide intermediate. Capture of alkyl radicals from peroxides to form alkyl iodides is well precedented in the literature [41,42].

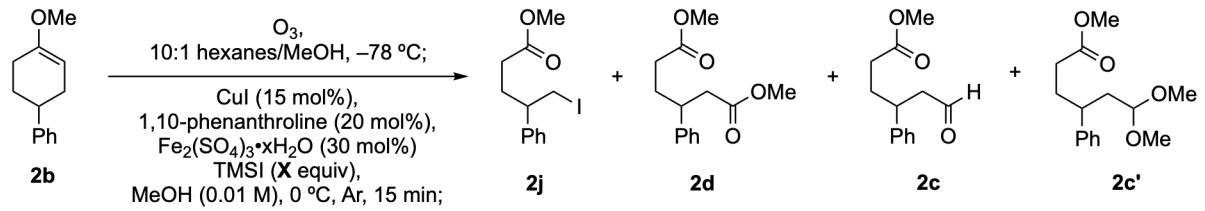
We began our optimization by screening iodide sources. Of all tested, TMSI resulted in a significantly higher yield of the iodide **2j** (~20%) than any other source (Figure 7.12).



iodide source	2j	2d	2c	2c'
LiI	29%	18%	36%	–
NaI	43%	20%	24%	–
KI	22%	23%	43%	–
CsI	20%	20%	38%	–
ZnI_2	39%	26%	28%	–
$BaI_2•2H_2O$	12%	11%	29%	–
TBAI	19%	18%	52%	–
TMSI	62%	18%	–	19%

Figure 7.11 Iododealkenylation: Iodide Source

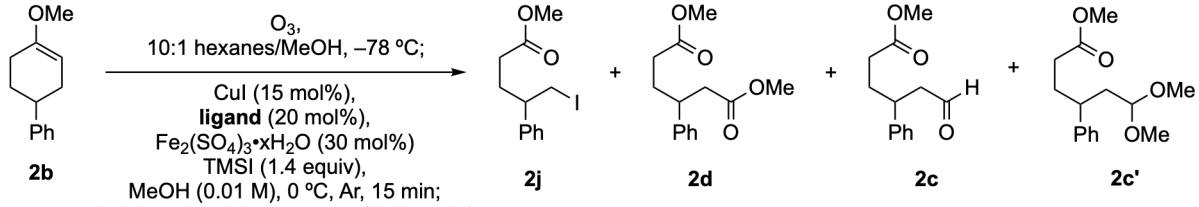
Next, we screened TMSI quantities (Figure 7.13). At least 1.3 equivalents were necessary to deliver the desired iodide product **2j** Additional equivalents did not significantly improve the yield of the product. We observed similar quantities of the ester **2d** side product in these reactions as we did for the Sm(II) cyclization screening. It may be the amount of ester **2d** that forms is independent of the metal used.



X equiv	2j	2d	2c	2c'
0.0	0%	6%	–	–
1.2	54%	22%	14%	3%
1.3	62%	21%	13%	1%
1.4	64%	20%	15%	–
2.0	63%	19%	–	14%
3.0	60%	19%	10%	10%
4.0	62%	19%	2%	16%
5.0	64%	18%	–	18%

Figure 7.12 Iododealkenylation: TMSI Quantities

We next screened ligands (Figure 7.14). The extreme acidity of the TMSI appeared to destroy any complexation to the metals because the no ligand control experiment provided similar results to all ligands tested.



ligand	2d	2d	2c	2c'
1,10-phenanthroline	64%	20%	15%	–
none	65%	19%	4%	4%
4,4'-di-*t*Bu-bpy	65%	20%	3%	6%
PyBox	61%	20%	4%	7%
4,4',4''-tri-*t*Bu-tpy	66%	21%	1%	6%

Figure 7.13 Iododealkenylation: Ligand Screen

The next steps in this optimization should be to investigate the metal quantities. The reaction may be more efficient with larger quantities.

7.8 Conclusion and Future Directions

The enolization and ozonolysis step for this transformation have been optimized. Significant efforts have been made to enable the reductive cyclization step. Alkyl peroxides are now able to be reduced with 1-electron by SmI_2 using MeOH or H_2O as a co-solvent in the reaction. The polar protic solvents are proposed to activate the Sm(II) center through a chair-like transition state with the peroxide to promote reduction. Two equivalents of the activator are required in the transition state, so the ratio of activator to samarium was investigated. Approximately 10 equivalents of activator relative to Sm(II) was required to promote the reaction, with at least 100 equivalents per Sm(II) required to enable the desired reductive cyclization pathway. Polar aprotic solvents were shown to promote the reductive cyclization more efficiently than polar protic solvents. A minimum quantity was necessary to promote dissolution of the activated Sm(II) complex in THF, and stronger activators reduced the quantity of β-scission products observed. The role Ni(II) of additives is still unknown, but they appear to suppress off-target radical pathways. Regardless of the current optimization of the reaction, a proof-of-concept for the transformation was found.

The use of the 4-phenylcyclohexanone model system is recommended for future optimization because the retention times for all reaction products have been characterized by GCMS. An activator must be identified which will promote SET and capture of the alkyl radical while also providing a kinetic window for β-scission to occur. Weaker, non-reducible Lewis bases should be screened first, and phosphine ligands may be a good option to pursue. The application of Ni(II) additives may help promote capture of the generated alkyl radicals should the Sm(II) become too deactivated. Should all future

attempts at the direct reduction of the alkyl radical and Barbier-cyclization fail, a two-step procedure through the alkyl iodide may be viable. Current iododealkenylation optimization caps the yield at 65% (by NMR). These iodination products still need to be tested for the Barbier cyclization, which may no longer require samarium but could use magnesium or lithium.

Overall, the progress in this project is promising. I wish the next chemist who picks it up good luck with the synthesis of SmI_2 and their optimization efforts.

7.9 Supporting Information and Experimental Details

7.9.1 Materials and Methods

Glassware

Unless otherwise stated, all reactions were conducted in glassware that had been washed sequentially with 12 M HCl and Alconox, oven-dried, and fitted with rubber septa; the reaction mixtures were stirred with Teflon-coated magnetic stir bars.

Solvents and Reagents

For dry or air-free reactions, standard Schlenk techniques were used to transfer liquid reagents and solvents. Argon was used as the gas for inert atmosphere reactions. Methanol (MeOH) was distilled over magnesium under an argon atmosphere. Dichloromethane (DCM), acetonitrile (MeCN), and triethylamine (Et_3N) were distilled over calcium hydride under an argon atmosphere. Tetrahydrofuran (THF), diethyl ether (Et_2O), benzene, and toluene were distilled over sodium/benzophenone ketyl under an argon atmosphere. All other solvents and reagents were used as received from commercial sources, unless otherwise noted.

Reaction Temperatures

Reaction temperatures above room temperature (23 ºC) and below 50 ºC refer to water bath temperatures, unless otherwise stated. Reaction temperatures above 50 ºC refer to silicone oil bath temperatures.

SiO_2 Chromatography

Thin layer chromatography (TLC) was performed using SiliCycle silica gel 60 F-254 precoated plates (0.25 mm) with visualization under UV irradiation and with a bromocresol green, cerium ammonium molybdate (CAM), potassium permanganate ($KMnO_4$), or vanillin stain. SiliCycle Silica-P silica gel (particle size: 40–63 μm) was used for flash column chromatography (FCC).

Melting Point

Melting points are uncorrected and were recorded using an Electrothermal® capillary melting point apparatus.

Infrared (IR) Spectroscopy

IR spectra were recorded using a Jasco FTIR-4100 spectrometer with a Zirconium–Selenium crystal ATR attachment or an Agilent Cary 630 FTIR with a diamond ATR attachment.

High Resolution Mass Spectrometry (HRMS)

HRMS was performed using a Thermo Fisher Scientific Exactive Plus spectrometer equipped with an IonSense ID-CUBE DART source or an Agilent 6545 Q-TOF LC/MS with 1260 Infinity LC.

Gas Chromatography Mass Spectrometry (GCMS)

GCMS was performed with an Agilent 7250 Q-TOF GC/MS with low energy EI or an Agilent Intuvo 9000 GC with a 5977B GC/MSD.

Liquid Chromatography Mass Spectrometry (LCMS)

LCMS was performed with an Agilent 1260 Infinity II LC using a poroshell 120 EC-C18 (2.7 μm, 4.6x100 mm) column coupled to a low resolution 6120 Quadrupole MSD. The mobile phase consisted of H_2O/MeCN mixtures spiked with 0.1% formic acid.

Nuclear Magnetic Resonance Spectroscopy

Samples were prepared in $CDCl_3$ saturated with K_2CO_3 as a desiccant or MeOD-*d*$_4$ which was used as received. ^1H, ^{13}C, and 2D NMR spectra were recorded using AV-800, NEO-600, AV-500, AV-400, or AV-300 MHz spectrometers, with ^{13}C NMR spectroscopic operating frequencies of 201, 151, 126, 101, or 75 MHz, respectively. NMR spectra were analyzed using the MestReNova software application (v.14.2.3-29241). Standard auto-baseline and auto-phase corrections were applied to all spectra prior to manual integration and manual peak picking. Chemical shifts (δ) are reported in parts per million (ppm) relative to the (residual protonated) signal of the solvent $CDCl_3$ (choloroform-*d*, δ = 7.26 for ^1H NMR; δ = 77.2 for ^{13}C NMR) or CD_3OD (MeOD-d_4, δ = 3.31 for ^1H NMR; δ = 49.0 for ^{13}C NMR). Data for ^1H NMR spectra are reported as follows: chemical shift, multiplicity, coupling constants (Hz), and number of hydrogen atoms. Data for ^{13}C NMR spectra are reported in terms of chemical shift. The following abbreviations are used to

describe the multiplicities: s = singlet; d = doublet; t = triplet; q = quartet; m = multiplet; br = broad.

Glovebox

A Vacuum Atmospheres Company (VAC) Nexus Glovebox was used to set up some reactions and store inert materials. See specific details for each section. Argon was used to create the inert atmosphere.

7.9.2 Safety

Caution: Organic peroxides are typically high-risk shock-sensitive compounds prone to explosion. Although we have not encountered any peroxide-related safety issues in our lab, the peroxides generated using the reported methods should be handled only by properly trained individuals and the isolated compounds should be stored at cryogenic temperatures. The use of a blast-shield is also recommended, especially for reactions performed on larger scales.

7.9.3 Preparation of Starting Materials

7.9.3.1 Samarium(II) Synthesis

Samarium(II) iodide was prepared from Sm(0) and diiodomethane according to a literature procedure [43,44].

We found that the addition of a second portion of Sm(0) (0.5–2.0 additional equivalents) after 12–24 hours of initial stirring of the reaction improved the conversion of remaining diiodoethane into SmI_2.

7.9.3.2 Samarium(II) Iodide in THF Titration

Prepared solutions of SmI_2 in THF were titrated weekly by adapting a GCMS volumetric method described in the literature [45]. The THF, H_2O, and Et_3N required for the titration were degassed by sparging with argon prior to use.

Procedure: A GCMS calibration curve was generated for 2-heptanone using 1,4-dimethoxybenzene as an internal standard. An example of the calibration curve preparation is presented below.

1. To a 50 mL volumetric flask was added 120 mg of 1,4-dimethoxybenzene. The flask was filled to the mark with chloroform and inverted a 10 times to mix forming a 2.4 mg/mL stock solution of internal standard (IS).

2. To a 10 mL volumetric flask was added 30.0 mg of 2-heptanone. The flask was filled to the mark with the stock solution of IS. This formed a 3.000 mg/mL solution of 2-heptanone with 2.4 mg/mL of IS.

3. To a 10 mL volumetric flask was added 5.000 mL of the 3.000 mg/mL solution of 2-heptanone using a volumetric pipette. The flask was filled to the mark with the IS stock solution. This formed a 1.500 mg/mL solution of 2-heptanone with 2.4 mg/mL of IS.

4. To a 10 mL volumetric flask was added 2.000 mL of the 3.000 mg/mL solution of 2-heptanone using a volumetric pipette. The flask was filled to the mark with the IS stock solution. This formed a 0.6000 mg/mL solution of 2-heptanone with 2.4 mg/mL of IS.

5. GCMS samples were prepared from each dilution as well as a blank of chloroform.

6. Each sample was measured in triplicate, running the blank sample on the instrument between each change in concentration to ensure consistency. The average of the normalized peak areas for each sample were plotted versus their known concentrations. Linear regression was performed to provide the $y = mx + b$ formula and an $R^2 > 0.99$ fit value. Samples of unknown concentration within the calibration window could then be calculated by substituting their average normalized peak area for y and solving for x, the concentration.

7. Sample preparation. A 15 mL round bottom flask equipped with a Teflon-coated magnetic stir bar was flame dried under vacuum. To the sealed flask was added 2-heptanone (approximately 100 μmol) and the exact mass was noted down. Dry THF distilled from sodium/benzophenone was degassed. For quantities of THF larger than 50 mL, the freeze-pump-thaw method was used. For quantities of THF less than 50 mL, sparging with argon for 15 minutes was sufficient to degass. Of the degassed, dry THF, approximately 2 mL (0.6 mM relative to 2-heptanone) was added. From the degassed Et_3N and H_2O was added 3.0 equiv and 4.0 equiv respectively and sequentially. The sealed flask was taped shut and transferred to the glovebox containing the SmI_2 in THF

solution. Without opening the flask, the solution of SmI_2 in THF (1.0 mL) was added dropwise to the 2-heptanone reaction flask while stirring. The reaction vessel was then removed from the glovebox and transferred to a 5.000 mL volumetric flask containing 1,4-dimethoxybenzene (11.7 mg). The reaction flask was rinsed with $CHCl_3$ until the 5.000 mL mark was met. A GCMS sample was then prepared from the volumetric flask. Three runs on the instrument were performed and the residual 2-heptanone was quantified versus the internal standard using the generated calibration curve.

8. The unknown concentration of SmI_2 was calculated from the measured quantity of 2-heptanone remaining after the reaction. Figure 7.15 depicts the overall reaction where 2.0 equiv of SmI_2 is required to achieve full conversion of 2-heptanone to 2-heptanol. Therefore, subtracting double the percent conversion from the theoretical value of 200% nets the equivalents of SmI_2 added. From there, the mmol of SmI_2 is known and the concentration can be calculated by dividing by the volume of SmI_2 in THF added to the reaction.

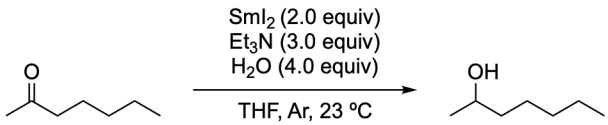
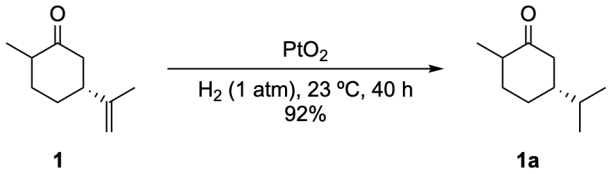


Figure 7.14 SmI_2 Titration

7.9.3.2 Ketones



1 **1a**

(+)-Carvomenthone (**1a**) was prepared from (+)-dihydrocarvone (**1**).

To a 25 mL round bottom flask equipped with a Teflon-coated magnetic stirrer bar was added (+)-dihydrocarvone (81:19 *trans*/*cis,* 2.04 g, 13.4 mmol, 1.00 equiv) and platinum oxide (24.3 mg, 0.107 mmol, 0.8 mol%). The flask was sealed and purged by evacuating and backfilling with hydrogen (3x). A hydrogen balloon was affixed to the vessel and the reaction was stirred for 40 hours. After complete conversion (as monitored by ^{1}H NMR) the material was diluted with diethyl ether and filtered through SiO_2. The ether was removed by rotatory evaporation to afford a 81:19 mixture of (2*S*,5*S*)-(+)carvomenthone and (2*R*,5*S*)-(+)-carvomenthone as a clear colorless oil (1.90 g, 12.3 mmol) in 92% yield. Characterization agreed with the literature [46].

Scale: 13.4 mmol

Yield: 92% (1.90 g)

R_f = 0.36 (5% *v/v* EtOAc/hexanes + vanillin stain) [incidental R_f]

Purification: SiO_2 (Et_2O)

Physical State: clear colorless oil

IR (ATR, neat) $\tilde{\nu}_{max}$: 2961, 2955, 2941, 2929, 2890, 2870, 2853, 1711, 1261, 1101, 1094, 1068, 1042, 1031, 1019, 798 cm^{-1}

HRMS–DART (*m/z*): $[M + H]^+$ calc'd for $C_{10}H_{19}O$ 155.1430, found 155.1430

Specific Rotation: $[\alpha]_D^{24\ ^oC}$ = +20 (*c* = 2.6, $CHCl_3$)

trans-(+)-carvomenthone

^{1}H NMR (500 MHz, $CDCl_3$) δ 2.39 (dt, *J* = 12.8, 3.4 Hz, 1H), 2.32 (tq, *J* = 12.5, 6.2 Hz, 1H), 2.10 (ddd, *J* = 13.4, 6.2, 2.9 Hz, 1H), 2.03 (d, *J* = 12.7 Hz, 1H), 1.85 (dt, *J* = 13.0, 3.2 Hz, 1H), 1.60 – 1.50 (m, 1H), 1.48 – 1.37 (m, 2H), 1.35 – 1.23 (m, 1H), 1.00 (d, *J* = 6.3 Hz, 3H), 0.91 – 0.86 (m, 6H).

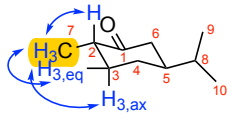
^{13}C NMR (126 MHz, $CDCl_3$) δ 213.9, 46.7, 45.5, 45.1, 35.2, 32.9, 29.0, 19.8, 19.5, 14.5.

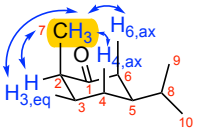
cis-(+)-carvomenthone

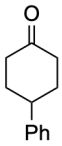
^{1}H NMR (500 MHz, $CDCl_3$) δ 2.55 – 2.38 (m, 1H), 2.38 – 2.26 (m, 1H), 2.16 (s, 1H), 1.99 – 1.80 (m, 1H), 1.79 – 1.58 (m, 3H), 1.48 (d, *J* = 7.9 Hz, 1H), 1.36 (s, 1H), 1.09 (d, *J* = 7.0 Hz, 3H), 0.91 – 0.86 (m, 6H).

^{13}C NMR (126 MHz, $CDCl_3$) δ 215.5, 44.9, 44.4, 43.1, 31.5, 30.8, 25.0, 20.2, 20.1, 16.1.

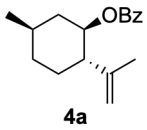
1D Selective Gradient TOCSY and NOESY spectra are provided to support configurational assignment. NOE correlations are presented below. See section 7.9.9 for more details.





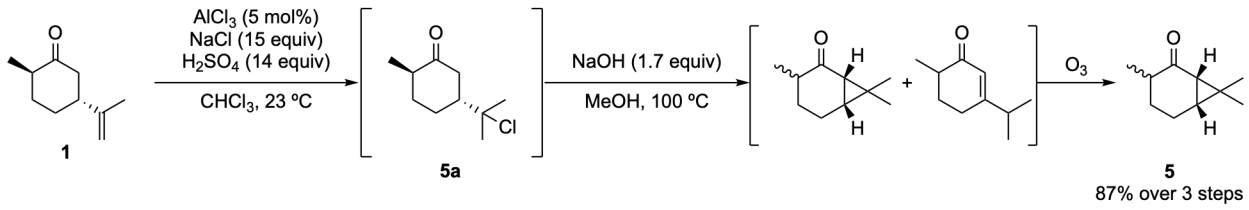


4-phenylclyclohexanone (**2a**) was purchased from Oakwood Chemical and purified by vacuum kugelrohr distillation prior to use [47].



4a

O-benzoyl isoulegol was prepared according to a literature procedure [48].



The preparation of 2-Caranone (**5**) from (+)-dihydrocarvone (**1**) was adapted from a literature procedure [49,50], then ozonolysis was conducted to remove alkene impurities.

Step 1: Hydrochlorination

A 250 mL Dreschel bottle was equipped with a Teflon-coated magnetic stirrer bar and charged with *trans*-(+)-dihydrocarvone (21.0 g, 1.00 equiv, 138 mmol) then $CHCl_3$ (130 mL) was added, followed by $AlCl_3$ (920 mg, 5.0 mol%, 6.90 mmol). The outlet valve was connected to an aqueous NaOH (2.5 M) solution via a Nalgene PVC tube affixed with a glass pipette at one end for bubbling. Using Nalgene PVC tubing, the inlet valve was connected to the outlet of a 25 mL bubbler containing H_2SO_4 (5 mL), which was used to dry the HCl gas before it entered the Dreschel bottle. A 500 mL Schlenk flask was charged with a Teflon-coated magnetic stirrer bar and NaCl (121 g, 2.07 mol, 15.0 equiv), and an addition funnel, greasing all joints to prevent gas leakages. The flask was connected to the Schlenk line at the top of the addition funnel with a glass adapter, and the outlet gas-port was sealed. The flask and the NaCl were then flame-dried under vacuum. After cooling to room temperature, the gas-port outlet from the Schlenk flask was connected to the H_2SO_4 bubbler inlet with Nalgene PVC tubing. The addition funnel was charged with H_2SO_4 (193 g, 105 mL, 14.3 equiv, 1.97 mol). The entire system was purged with argon for 5 minutes. During the purge, the lines and connections were inspected for leakages. After purging, the gas flow was decreased to a low, constant flow, and dropwise addition

of the H_2SO_4 was initiated at a rate of approximately 0.4 mL/min. HCl gas bubbles were observed to form as the H_2SO_4 reacted with the NaCl. After complete addition of the H_2SO_4 (4 h), the Schlenk flask was a slurry. The reaction was then left under the same constant flow of argon overnight as the H_2SO_4 reacted with the NaCl. After the slurry had solidified, and the reaction was as judged complete by lack of alkene peaks in the crude ^{1}H NMR, the reaction solution was filtered through basic alumina, eluting with diethyl ether (1 L). The filtrate was cooled to 4 ºC and concentrated under reduced pressure to afford the product, (2*R*,5*R*)-5-(2-chloropropan-2-yl)-2-methylcyclohexan-1-one (**5a**), as a yellow oil (26.0 g, 138 mmol, >99% yield). The Schlenk flask was quenched placing it into an ice bath, followed addition of ice chips. Once the ice had melted the aqueous solution was decanted and the process repeated until all salts had melted. The combined aqueous solutions were basified with an aq. NaOH solution (2.5 M) at 0 ºC until pH = 7.

Scale: 21.0 g

Yield: >99%

R_f = 0.75 (20% *v/v* EtOAc/hexane + Vanillin stain)

Purification: Al_2O_3 (diethyl ether)

Physical State: yellow oil

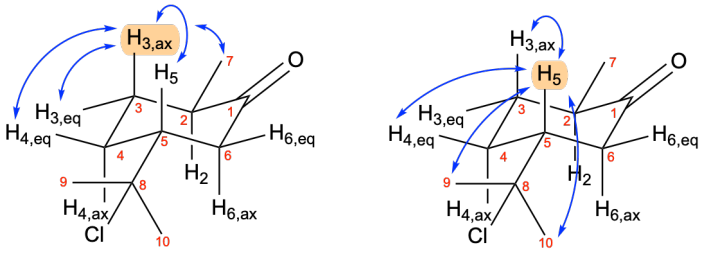
crude IR (ATR, neat) $\tilde{\nu}_{max}$: 2977, 2962, 2930, 1715, 1456, 1387, 1260, 1123, 1109, 1087, 1052, 1027, 1019, 805, 798 cm^{-1}

crude HRMS–DART (*m/z*): $[M + H]^+$ calc'd for $C_{10}H_{18}OCl$ 189.1041, found 189.1042.

crude ^{1}H NMR (500 MHz, $CDCl_3$) δ 2.62 (ddd, *J* = 13.3, 4.0, 2.4 Hz, 1H), 2.41 – 2.25 (m, 2H), 2.12 (dddt, *J* = 19.1, 16.5, 6.3, 3.4 Hz, 2H), 1.99 – 1.84 (m, 1H), 1.73 – 1.62 (m, 1H), 1.59 (s, 4H), 1.55 (s, 4H), 1.31 (qd, *J* = 12.5, 2.7 Hz, 1H), 1.03 (d, *J* = 6.6 Hz, 3H).

crude ^{13}C NMR (126 MHz, $CDCl_3$) δ 212.4, 72.8, 51.5, 44.6, 43.7, 33.9, 30.9, 30.6, 26.9, 14.2.

HSQC and **1D Selective Gradient NOESY** were measured from the crude reaction mixture to determine the stereochemistry of the major product. The NOESY correlations are pictured below.

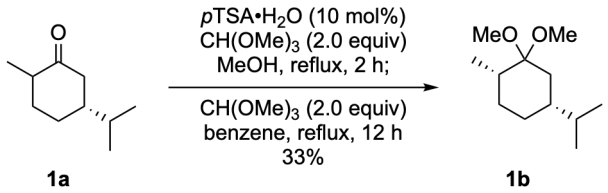


Step 2 & 3: **SN1 Cyclization and Ozonolysis**

To the oil of (2*R*,5*R*)-5-(2-chloropropan-2-yl)-2-methylcyclohexan-1-one (**5a**, 26.0 g, 1.00 equiv, 138 mmol) from the previous step was added NaOH (9.6 g, 1.7 equiv, 0.24 mol) in dry MeOH (44 mL) and a Teflon-coated magnetic stirrer bar. The cloudy mixture was heated at 100 ºC for 2.5 hours. The mixture was allowed to cool to room temperature then filtered through celite and diluted with diethyl ether. The ethereal solution was washed with brine, dried over magnesium sulfate, filtered through cotton, and concentrated. The crude oil was vacuum distilled (boiling point: 67–68 ºC, 1 mmHg) to afford a mixture of 2-carone and carvenone. The neat distillate was ozonolyzed at room temperature for 2 hours to completely oxidize the 2-carvenone. The 2-carone (**5**) was isolated after column

chromatography (SiO_2, 20% *v/v* Et_2O/pentane) as a clear colorless oil in 87% yield (18.3 g, 120 mmol). Characterization matched with literature values [51].

7.9.3.4 Ketals



(2*S*,5*R*)-5-isopropyl-1,1-dimethoxy-2-methylcyclohexane (**1b**) was prepared from (+)-carvomenthone (**1a**)

Procedure: To a 25 mL RBF equipped with a Teflon-coated magnetic stir bar was added (R)-carvomenthone (2.00 g, 13.0 mmol, 1.00 equiv) and *p*TSA•H_2O (247 mg, 1.30 mmol, 0.100 equiv). The contents were dissolved in dry methanol (15.6 mL) and then trimethyl orthoformate (2.75 g, 2.84 mL, 25.9 mmol, 2.00 equiv) was added. A water condenser was affixed to the flask then the mixture was heated to reflux (solution became red/pink). After 2 hours of reflux (solution became red/purple) benzene (5 mL) was added and the mixture was concentrated by distillation. After distillation the benzene and methanol fractions were added back to the flask and additional trimethyl orthoformate (2.75 g, 2.84 mL, 25.9 mmol, 2.00 equiv) was also added. The solution was heated to reflux overnight but did not reach completion. The reaction was quenched with 5% *m/m* aq. KOH (15 mL) and transferred to a separatory funnel. The aqueous layer was extracted with three times with pentane (5 mL) then the combined organic layers were washed with brine (15 mL), dried over sodium sulfate, and concentrated at 0 ºC and 75 mbar. The crude material was purified through FCC (0–2.5% Et_2O/pentane) to afford (2*S*,5*R*)-5-isopropyl-1,1-dimethoxy-2-methylcyclohexane as a pale-yellow liquid in 33% yield (848 mg, 4.23 mmol).

Scale: 13.0 mmol

Yield: 33% (848 mg, 4.23 mmol)

R_f = 0.20 (5% *v/v* EtOAc/hexanes + vanillin stain)

Purification: SiO_2 (0–2.5% *v/v* Et_2O/pentane)

Physical State: pale-yellow oil

IR (ATR, neat) $\tilde{\nu}_{max}$: 2940, 2871, 2826, 1466, 1382, 1368, 1180, 1155, 1114, 1105, 1083, 1053, 1006, 986, 945, 912, 844, 830 cm^{-1}

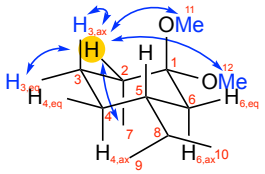
HRMS–DART (*m/z*): $[M–OMe]^+$ calc'd for $C_{11}H_{21}O$ 169.1587, found 169.1582

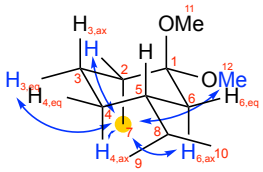
Specific Rotation: $[\alpha]_D^{25}$= +10 (*c* = 1.0, $CHCl_3$)

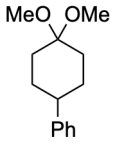
^{1}H NMR (500 MHz, $CDCl_3$) δ 3.15 (s, 3H), 3.14 (s, 3H), 2.10 – 2.01 (m, 1H), 1.80 – 1.66 (m, 2H), 1.54 – 1.36 (m, 3H), 1.27 – 1.09 (m, 3H), 0.91 (d, *J* = 7.2 Hz, 3H), 0.88 (d, *J* = 6.7 Hz, 3H), 0.87 (d, *J* = 6.7 Hz, 3H).

^{13}C NMR (126 MHz, $CDCl_3$) δ 103.3, 47.4, 47.1, 40.5, 33.2, 32.6, 30.3, 29.1, 23.2, 20.0, 19.7, 14.2.

2D NMR HSQC and NOESY and **1D Selective Gradient NOESY** spectra are provided to support configurational assignment. NOE correlations are presented below. See section 7.9.9 for more details.

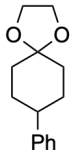






2b

(4,4-dimethoxycyclohexyl)benzene (**2b**) was prepared from 4-phenylcyclohexanone (**2a**) according to a literature procedure [52].



3b

8-Phenyl-1,4-dioxaspiro[4.5]decane (**3b**) was prepared through an adapted literature procedure [53]. Full characterization was missing from the literature, so we have provided it herein.

Procedure: To a 100 mL round bottom flask equipped with a Teflon-coated magnetic stirrer bar was added 4-phenylcyclohexanone (3.93 g, 22.6 mmol, 1.00 equiv) and *p*-toluenesulfonic acid monohydrate (21.5 mg, 0.113 mmol, 0.500 mol%). Next, dry benzene was added (45 mL) and the mixture was stirred until it was homogeneous. Ethylene glycol (1.68 g, 1.51 mL, 27.1 mmol, 1.20 equiv) was added via syringe. A Dean–Stark apparatus was affixed, and the mixture was refluxed for 4 hours. The reaction mixture was cooled to room temperature, and then half of the volume was removed by rotatory evaporation. The remaining solution was directly loaded to a column packed with SiO_2/hexanes and eluted with 5% *v/v* EtOAc/hexanes. The pure fractions were collected and evaporated to provide 8-phenyl-1,4-dioxaspiro[4.5]decane as a white amorphous solid (4.71 g) in 96% yield.

Scale: 22.6 mmol (3.93 g)

Yield: 96% (4.71 g)

R_f = 0.45 (15% *v/v* EtOAc/hexane + UV/vanillin stain)

Purification: SiO_2 (0–5% *v/v* EtOAc/hexanes)

Physical State: white amorphous solid

Melting Point: 54–56 ºC

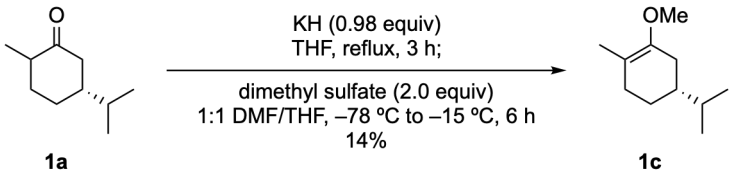
IR (ATR, neat) $\tilde{\nu}_{max}$: 2930, 2872, 1493, 1445, 1373, 1363, 1282, 1239, 1171, 1128, 1096, 1034, 964, 943, 924, 904, 867, 799, 755, 698, 664 cm^{-1}

HRMS–DART (*m/z*): $[M + H]^+$ calc'd for $C_{14}H_{19}O_2$ 219.1380, found 219.1377

^{1}H NMR (600 MHz, $CDCl_3$) δ 7.33 (t, *J* = 7.6 Hz, 2H), 7.31–7.26 (m, 2H), 7.26–7.19 (m, 1H), 4.02 (s, 4H), 2.60 (tt, *J* = 11.8, 3.6 Hz, 1H), 1.95–1.80 (m, 6H), 1.74 (td, *J* = 12.9, 4.9 Hz, 2H).

13C NMR (151 MHz, $CDCl_3$) δ 146.7, 128.4, 127.0, 126.2, 108.6, 64.4, 64.4, 43.4, 35.2, 31.7.

7.9.3.5 Enol Ethers



(*R*)-4-isopropyl-2-methoxy-1-methylcyclohex-1-ene (**1c**) was prepared from (+)-carvomenthone (**1a**).

Procedure: To an oven-dried 100 mL 2-neck round bottom flask equipped with an oven-dried Teflon-coated magnetic stirrer bar was added potassium hydride (276 mg, 6.88 mmol, 0.98 equiv) in the glovebox. The flask was removed from the glovebox, then anhydrous THF (17.5 mL) was added. To the suspension was dropwise added a solution of (*R*)-carvomenthone (1.08 g, 7.00 mmol, 1.00 equiv) in THF (23 mL + 3 x 4 mL) prepared in an oven dried 50 mL round bottom flask. The solution was stirred at reflux (oil bath temp 85 ºC) for 3 hours, then cooled to –78 ºC in an acetone/dry ice bath. Anhydrous DMF (17.5 mL) was added, and the solution was stirred for 15 minutes at –78 ºC before dimethyl sulfate (1.77 g, 1.34 mL, 14.0 mmol, 2.0 equiv) was added dropwise. The reaction was left to stir until the –78 ºC bath had warmed to –15 ºC (approx. 6 hours) then 14 mL sat. aq. $NaHCO_3$ was added. The mixture was transferred to a separatory funnel and 80 mL DI H_2O was added to homogenize the aqueous layer. The aqueous layer was extracted with 1:1 Ether/pentane (3 x 20 mL) and the combined organic layers were washed with brine (2 x 10 mL), dried over sodium sulfate, filtered through cotton, and evaporated at 0 ºC. The residue was purified through FCC (pentane + 1% *v/v* Et_2NH) using SiO_2 packed with Et_2NH to afford (*R*)-4-isopropyl-2-methoxy-1-methylcyclohex-1-ene as a pale-yellow oil in 14% yield (159 mg).

Scale: 7.00 mmol

Yield: 14% (159 mg)

R_f = 0.48 (5% *v/v* EtOAc/hexanes + vanillin stain)

Purification: SiO_2 (pentane + 1% *v/v* Et_2NH)

Physical State: pale yellow oil

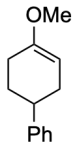
IR (ATR, neat) $\tilde{\nu}_{max}$: 2956, 2914, 2871, 2831, 1692, 1459, 1437, 1385, 1367, 1331, 1297, 1282, 1225, 1200, 1141, 1108, 1075, 1046, 1019, 999, 853, 708 cm^{-1}

HRMS–DART (*m/z*): $[M + H]^+$ calc'd for $C_{11}H_{21}O$ 169.1587, found 169.1582

Specific Rotation: $[\alpha]_D^{27}$ = +92 (*c* = 1.0, $CHCl_3$)

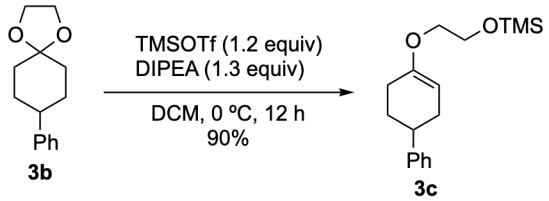
^{1}H NMR (600 MHz, $CDCl_3$) δ 3.49 (s, 3H), 2.10 – 2.05 (m, 1H), 2.05 – 1.97 (m, 1H), 1.96 – 1.89 (m, 1H), 1.85 (dddt, *J* = 16.5, 12.9, 4.0, 2.1 Hz, 1H), 1.74 – 1.65 (m, 1H), 1.62 – 1.58 (m, 3H), 1.50 (h, *J* = 6.7 Hz, 1H), 1.41 – 1.32 (m, 1H), 1.20 – 1.09 (m, 1H), 0.91 (d, *J* = 3.6 Hz, 3H), 0.89 (d, *J* = 3.6 Hz, 3H).

^{13}C NMR (151 MHz, $CDCl_3$) δ 147.9, 114.0, 56.3, 41.5, 32.4, 30.5, 28.6, 26.4, 20.1, 19.8, 15.5.



2c

4-methoxy-1,2,3,6-tetrahydro-1,1'-biphenyl (**2c**) was prepared from 4-phenylcyclohexanone (**2a**) according to a literature procedure [38].



Trimethyl(2-((1,2,3,6-tetrahydro-[1,1'-biphenyl]-4-yl)oxy)ethoxy)silane (**3c**) was prepared from 8-Phenyl-1,4-dioxaspiro[4.5]decane (**3b**) according to a modified literature procedure [37].

Procedure: To a flame-dried round bottom flask equipped with a Teflon-coated magnetic stirrer bar was added 8-phenyl-1,4-dioxaspiro[4.5]decane (0.990 g, 4.54 mmol, 1.00 equiv) followed by dry DCM (7.4 mL) and stirred until homogeneous. The mixture was cooled to 0 ºC in an ice-water bath and DIPEA (0.762 g, 1.03 mL, 5.90 mmol, 1.30 equiv), was added. TMSOTf (1.21 g, 1.00 mL, 5.4 mmol, 1.2 equiv) was added via syringe to the stirred solution dropwise over a period of approximately 5 min. The solution was allowed to warm to, and was subsequently stirred at, ambient temperature for 12 hours. After completion, approximately 70% of the solvent was removed by distillation at atmospheric pressure and replaced with a roughly equal volume of pentane, added dropwise with vigorous stirring. The resulting slurry was sealed and cooled to –20 ºC overnight for 2 hours to assist in precipitating the N,N-diisopropylethylammonium triflate salt. After the supernatant solution was removed, the residual salt was rinsed with three 100-mL portions of pentane. The filtrate was directly loaded onto an SiO_2 column and purified by FCC (1% *v/v* EtOAc/hexanes) to afford a clear colorless oil (1.18 g, 4.06 mmol) in 90% yield.

Scale: 4.54 mmol

Yield: 90%

Physical State: clear colorless liquid

Purification: FCC (1% *v/v* EtOAc/hexanes)

R_f = 0.34 (5% *v/v* / + UV/vanillin stain)

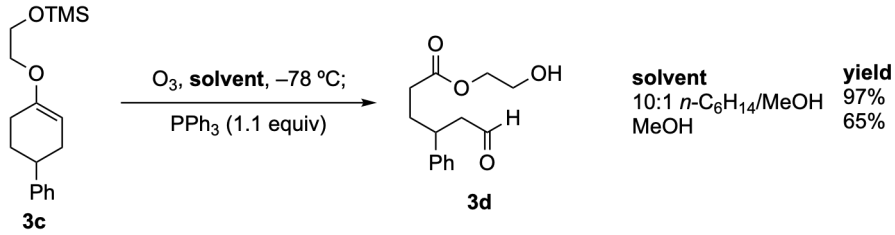
IR (ATR, neat) $\tilde{\nu}_{max}$: 3061, 3027, 2953, 2927, 2872, 2842, 1249, 1217, 1185, 1134, 1107, 874, 840, 754, 699 cm^{-1}

HRMS–DART (*m/z*): $[M + H]^+$ calc'd for $C_{17}H_{27}O_2Si$ 291.1775, found 291.1771

^{1}H NMR (600 MHz, $CDCl_3$) δ 7.31 (t, *J* = 7.5 Hz, 2H), 7.26 – 7.23 (m, 2H), 7.20 (td, *J* = 7.0, 1.4 Hz, 1H), 4.75 – 4.62 (m, 1H), 3.86 (t, *J* = 5.2 Hz, 2H), 3.75 (qt, *J* = 10.2, 5.1 Hz, 2H), 2.77 (tdd, *J* = 11.2, 5.1, 3.0 Hz, 1H), 2.38 – 2.28 (m, 2H), 2.26 – 2.14 (m, 2H), 1.98 (ddt, *J* = 15.3, 5.5, 2.5 Hz, 1H), 1.87 (qd, *J* = 12.2, 5.6 Hz, 1H), 0.16 (d, *J* = 0.9 Hz, 9H).

^{13}C NMR (151 MHz, $CDCl_3$) δ 154.5, 146.9, 128.5, 127.0, 126.2, 93.6, 67.9, 61.6, 40.6, 32.0, 29.9, 28.4.

7.9.4 Ozonolysis Optimization



2-hydroxyethyl 6-oxo-4-phenylhexanoate (**3d**)

Procedure: To a 25 mL round bottom flask equipped with a Teflon-coated magnetic stirrer bar was added trimethyl(2-((1,2,3,6-tetrahydro-[1,1'-biphenyl]-4-yl)oxy)ethoxy)silane (96.7 mg, 0.333 mmol, 1.00 equiv) and hexanes (3.03 mL). The mixture was stirred until homogeneous then cooled to –78 ºC in an acetone/dry ice bath. The flask was open to air and no cap was used to seal the system. Oxygen was bubbled through a 16G x 4" needle at 1.0 L/min into the solution. Methanol (0.303 mL) was added then the Globalozone GO-D3G ozone generator was turned on at 0.74 amps. After 120 seconds (full conversion) the ozone generator was switched off and the excess ozone was removed using oxygen. Triphenylphosphine (96.1 mg, 0.366 mmol, 1.10 equiv) was added. The solution was warmed to room temperature and stirred until full consumption of the peroxide (R_f = 0.11, 15% *v/v* EtOAc/hexanes + UV/vanillin stain). The methanol was evaporated, and the product was isolated after FCC (0–50% *v/v* EtOAc/hexanes) as a clear colorless liquid (81.0 mg, 0.324 mmol) in 97% yield.

When methanol (3.3 mL) was used instead of the hexanes/methanol mixture, the isolated yield was 65%.

Physical State: clear colorless oil

Purification: SiO_2 (0–50% *v/v* EtOAc/hexanes)

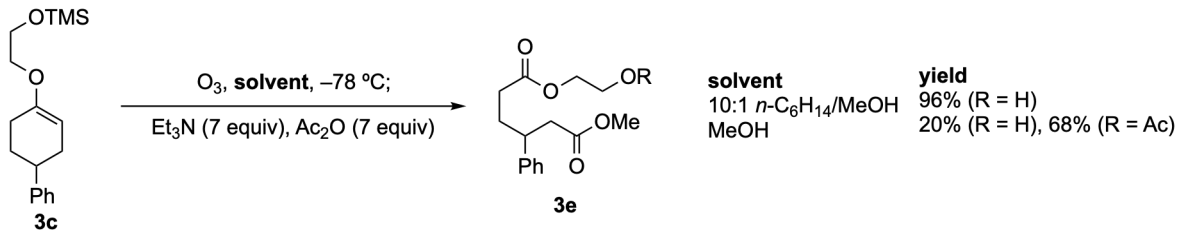
R_f = 0.18 (50% *v/v* EtOAc/hexanes + UV/vanillin stain)

IR (ATR, neat) $\tilde{\nu}_{max}$: 3445, 3084, 3062, 3028, 2944, 2730, 1719, 1495, 1453, 1176, 1159, 1076, 1027, 764, 703 cm^{-1}

HRMS–DART (*m/z*): $[M - H]^+$ calc'd for $C_{14}H_{17}O_4$ 249.1132, found 249.1143

^{1}H NMR (600 MHz, $CDCl_3$) δ 9.68 (t, *J* = 1.8 Hz, 1H), 7.35 – 7.26 (m, 2H), 7.25 – 7.21 (m, 1H), 7.20 – 7.15 (m, 2H), 4.23 – 4.08 (m, 2H), 3.79 (t, *J* = 4.6 Hz, 2H), 3.23 (dtd, *J* = 10.4, 7.3, 4.6 Hz, 1H), 2.82 – 2.71 (m, 2H), 2.26 – 2.17 (m, 2H), 2.12 – 1.83 (br, 1H), 2.12 – 2.01 (m, 1H), 1.90 (dddd, *J* = 14.0, 10.4, 8.0, 6.3 Hz, 1H).

^{13}C NMR (151 MHz, $CDCl_3$) δ 201.5, 173.5, 142.6, 129.0, 127.7, 127.2, 66.2, 61.3, 50.6, 39.2, 32.1, 31.4.



2-hydroxyethyl 6-oxo-4-phenylhexanoate (**3e**)

Procedure: To a 25 mL round bottom flask equipped with a Teflon-coated magnetic stirrer bar was added trimethyl(2-((1,2,3,6-tetrahydro-[1,1'-biphenyl]-4-yl)oxy)ethoxy)silane (96.7 mg, 0.333 mmol, 1.00 equiv) and hexanes (3.03 mL). The mixture was stirred until homogeneous then cooled to –78 ºC in an acetone/dry ice bath. The flask was open to air and no cap was used to seal the system. Oxygen was bubbled through a 16G x 4" needle at 1.0 L/min into the solution. Methanol (0.303 mL) was added then the Globalozone GO-D3G ozone generator was turned on at 0.74 amps. After 120 seconds (full conversion) the ozone generator was switched off and the excess ozone was removed using oxygen. Triphenylphosphine (96.1 mg, 0.366 mmol, 1.10 equiv) was added. The solution was warmed to room temperature and stirred until full consumption of the peroxide (R_f = 0.11, 15% *v/v* EtOAc/hexanes + UV/vanillin stain). The methanol was evaporated, and the product was isolated after FCC (0–50% *v/v* EtOAc/hexanes) as a clear colorless liquid (81.0 mg, 0.324 mmol) in 97% yield.

When methanol (3.33 mL) was used instead of 10:1 hexanes/MeOH, the yield of **3e** was 20%. The remaining mass was the conversion of **3e** to its acetate derivative, 6-(2-acetoxyethyl) 1-methyl 3-phenylhexanedioate (68%).

Physical State: clear colorless oil

Purification: SiO_2 (0–50% *v/v* EtOAc/hexanes)

R_f = 0.18 (50% *v/v* EtOAc/hexanes + UV/vanillin stain)

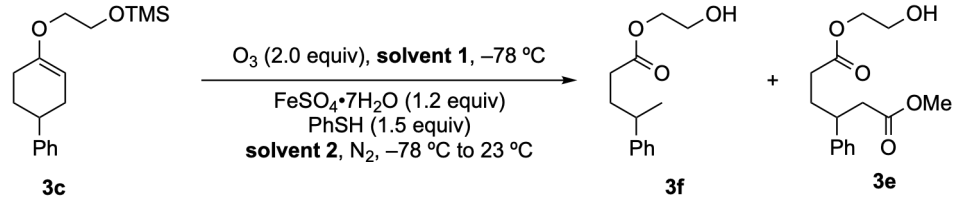
IR (ATR, neat) $\tilde{\nu}_{max}$: 3445, 3084, 3062, 3028, 2944, 2730, 1719, 1495, 1453, 1176, 1159, 1076, 1027, 764, 703 cm^{-1}

HRMS–DART (*m/z*): $[M - H]^+$ calc'd for $C_{14}H_{17}O_4$ 249.1132, found 249.1143

^{1}H NMR (600 MHz, $CDCl_3$) δ 9.68 (t, *J* = 1.8 Hz, 1H), 7.35 – 7.26 (m, 2H), 7.25 – 7.21 (m, 1H), 7.20 – 7.15 (m, 2H), 4.23 – 4.08 (m, 2H), 3.79 (t, *J* = 4.6 Hz, 2H), 3.23 (dtd, *J* = 10.4, 7.3, 4.6 Hz, 1H), 2.82 – 2.71 (m, 2H), 2.26 – 2.17 (m, 2H), 2.12 – 1.83 (br, 1H), 2.12 – 2.01 (m, 1H), 1.90 (dddd, *J* = 14.0, 10.4, 8.0, 6.3 Hz, 1H).

^{13}C NMR (151 MHz, $CDCl_3$) δ 201.5, 173.5, 142.6, 129.0, 127.7, 127.2, 66.2, 61.3, 50.6, 39.2, 32.1, 31.4.

Table 7.2 Enol Ether Hydrodealkenylation Optimization

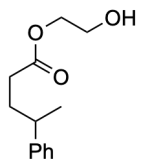


solvent 1	solvent 2	method	3f%	3e%
MeOH	MeOH	standard hydrodealkenylation	69%	13%
MeOH	MeOH	evaporate to dry, then inverse addition	74%	14%
10:1 hexanes/MeOH	MeOH	evaporate to dry, then inverse addition	78%	18%
10:1 hexanes/MeOH	10:1 hexanes/MeOH	direct inverse addition	78%	17%

Procedure: To a 25 mL round bottom flask equipped with a Teflon-coated magnetic stirrer bar was added trimethyl(2-((1,2,3,6-tetrahydro-[1,1'-biphenyl]-4-yl)oxy)ethoxy)silane (96.7 mg, 0.333 mmol, 1.00 equiv) and dissolved in **solvent 1**. The solution was cooled to –78 ºC in an acetone/dry ice bath. The flask was open to air and no cap was used to seal the system. Oxygen was bubbled through a 16G x 4" needle at 1.0 L/min into the solution. If **solvent 1** contained hexanes, then methanol (0.303 mL) was added at this point. The Globalozone GO-D3G ozone generator was turned on at 0.74 amps. After 120 seconds (full conversion) the ozone generator was switched off and

the excess ozone was removed using oxygen. For standard hydrodealkenylation and direct inverse addition, the reaction was sealed with a rubber septum and sparged with argon for 5 minutes. Otherwise, the solvent was then evaporated, and the atmosphere of the flask was evacuated and backfilled 3x with argon. The ozonolysis peroxide was dissolved in dry MeOH (0.500 mL).

To a separate 25 mL round bottom flask equipped with a Teflon-coated magnetic stirrer bar was added iron sulfate heptahydrate (0.111 g, 0.399 mmol, 1.20 equiv) and the atmosphere was evacuated and backfilled 3x with argon. To the round bottom flask containing the iron sulfate heptahydrate was added methanol and stirred until homogenous before benzenethiol (0.055 g, 0.499 mmol, 1.50 equiv) was then added. The ozonolysis peroxide was dropwise cannulated into the solution of iron sulfate heptahydrate and benzenethiol and the peroxide flask was rinsed with methanol (0.25 mL) twice. After reaction completion, the mixture was transferred to a separatory funnel and diluted with water (10 mL). Extracted 3x with ethyl acetate then washed with brine (10 mL), dried over sodium sulfate, filtered, and evaporated. The crude material was purified through FCC (0–80% *v/v* EtOAc/hexanes) to provide the products. The results are provided in Table 7.2.



2-hydroxyethyl 4-phenylpentanoate (**3f**)

Scale: 0.333 mmol (96.7 mg)

Yield: 78% (57.8 mg)

Physical State: clear colorless liquid

Purification: SiO_2 (0–50% *v/v* EtOAc/hexanes)

R_f = 0.56 (50% *v/v* EtOAc/hexanes + UV/vanillin stain)

IR (ATR, neat) $\tilde{\nu}_{max}$: 3441, 3083, 3061, 3026, 2958, 2928, 2872, 1730, 1494, 1452, 1419, 1379, 1349, 1324, 1308, 1279, 1254, 1206, 1161, 1075, 1047, 1024, 948, 909, 884, 763, 700 cm^{-1}

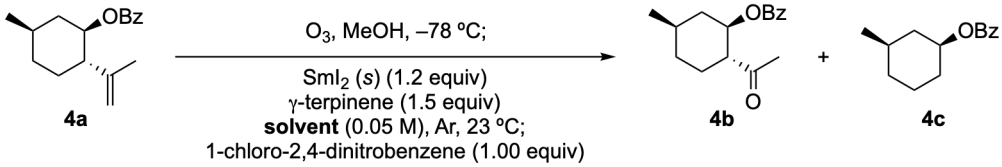
HRMS–DART (*m/z*): $[M + K]^+$ calc'd for $C_{13}H_{18}O_2K$ 261.0888, found 261.0894

^{1}H NMR (400 MHz, $CDCl_3$) δ 7.33 – 7.26 (m, 2H), 7.22 – 7.15 (m, 3H), 4.14 (ddd, *J* = 6.0, 3.5, 1.1 Hz, 2H), 3.81 – 3.68 (m, 2H), 2.72 (dp, *J* = 8.9, 6.8 Hz, 1H), 2.38 – 2.26 (br, 1H), 2.23 (ddd, *J* = 8.8, 7.3, 6.0 Hz, 2H), 2.01 – 1.84 (m, 2H), 1.28 (d, *J* = 7.0 Hz, 3H).

^{13}C NMR (101 MHz, $CDCl_3$) δ 174.1, 146.2, 128.6, 127.1, 126.3, 66.0, 61.1, 39.5, 33.1, 32.5, 22.3.

7.9.5 Hydrodealkenylation with Sm(II)

Table 7.3 Hydrodealkenylation with SmI_2 Solvent Screen



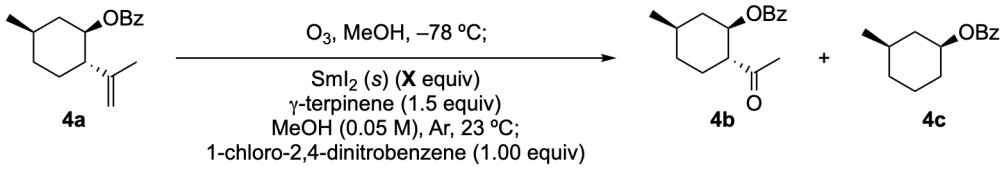
solvent	**scale (mmol)**	**4b%**	**4c%**	**Notes**
benzene	0.120	98%	1%	inverse addition
MeCN	0.200	100%	0%	inverse addition
MeOH	0.103	66%	24%	inverse addition
H_2O	0.077	65%	23%	inverse addition
*t*BuOH	0.206	97%	3%	normal addition
HFIP	0.105	100%	0%	normal addition
EtOH	0.176	92%	5%	normal addition
*i*PrOH	0.135	100%	0%	normal addition

Procedure: A 25 mL round bottom flask with Teflon-coated magnetic stirring bar was flame dried and put under vacuum. It was transferred to the glove box (Ar) and loaded with SmI_2 (s, 1.2 equiv). It was then attached to the Schlenck line with a purged argon line.

A 25 mL round bottom flask was loaded with the alkene (1.0 equiv) and dissolved in MeOH (0.1 M). It. was cooled to –78 ºC and ozone was bubbled until the alkene was consumed (by TLC), about 1 – 2 min. The MeOH was evaporated at 30 ºC and 60 mmHg then flask was evaporated and backfilled 3x with argon. The solvent (0.05 M) was added followed by γ-terpinene (1.5 equiv). The solvent was added to the SmI_2 to make a 0.1 M solution. For benzene, MeCN, H_2O, and MeOH the peroxide solution was cannulated into the SmI_2 flask. For *t*BuOH, EtOH, and HFIP the SmI_2 solution was cannulated into the peroxide solution.

After 15 minutes, the internal standard was added and the solvent was removed. The residue was taken into ethyl acetate and washed with sodium thiosulfate then brine, dried over sodium sulfate, filtered, and evaporated. NMR was measured to determine the yield versus the benzoate α-C–H [48]. The results are indicated in Table 7.3.

Table 7.4 Hydrodealkenylation with SmI_2 Equivalents Screen



X	**scale (mmol)**	**4b%**	**4c%**
1.8	0.132	40%	46%
2.4	0.141	21%	64%

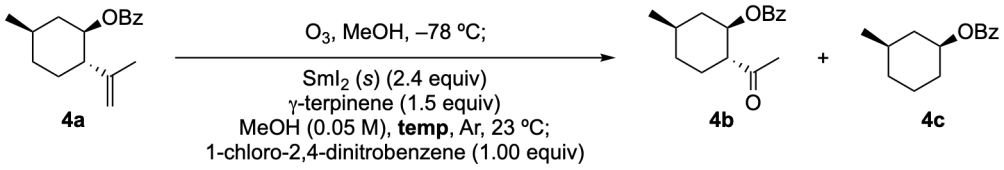
Procedure: A 25 mL round bottom flask with Teflon-coated magnetic stirring bar was flame dried and put under vacuum. It was transferred to the glove box (Ar) and loaded with SmI_2 (s, **X** equiv). It was then attached to the Schlenck line with a purged argon line.

A 25 mL round bottom flask was loaded with the alkene (1.0 equiv) and dissolved in MeOH (0.1 M). It. was cooled to –78 ºC and ozone was bubbled until the alkene was consumed (by TLC), about 1 – 2 min. The MeOH was evaporated at 30 ºC and ~60 mmHg then flask was evaporated and backfilled 3x with argon. Then degassed MeOH (0.1 M) was added and the peroxide was dissolved.

Then MeOH was added to the SmI_2 to make a 0.1 M solution and stirred for 1 minute. Next, γ-terpinene (1.5 equiv) was added and was immediately followed by the peroxide solution.

After 15 minutes, the internal standard was added and the solvent was removed. The residue was taken into ethyl acetate and washed with sodium thiosulfate then brine, dried over sodium sulfate, filtered, and evaporated. NMR was measured to determine the yield versus the benzoate α-C–H [48]. The results are indicated in Table 7.4.

Table 7.5 Hydrodealkenylation with SmI_2 Temperature Screen



temp	scale (mmol)	4b%	4c%
–10 ºC	0.133	40%	46%
–78 ºC	0.147	21%	64%

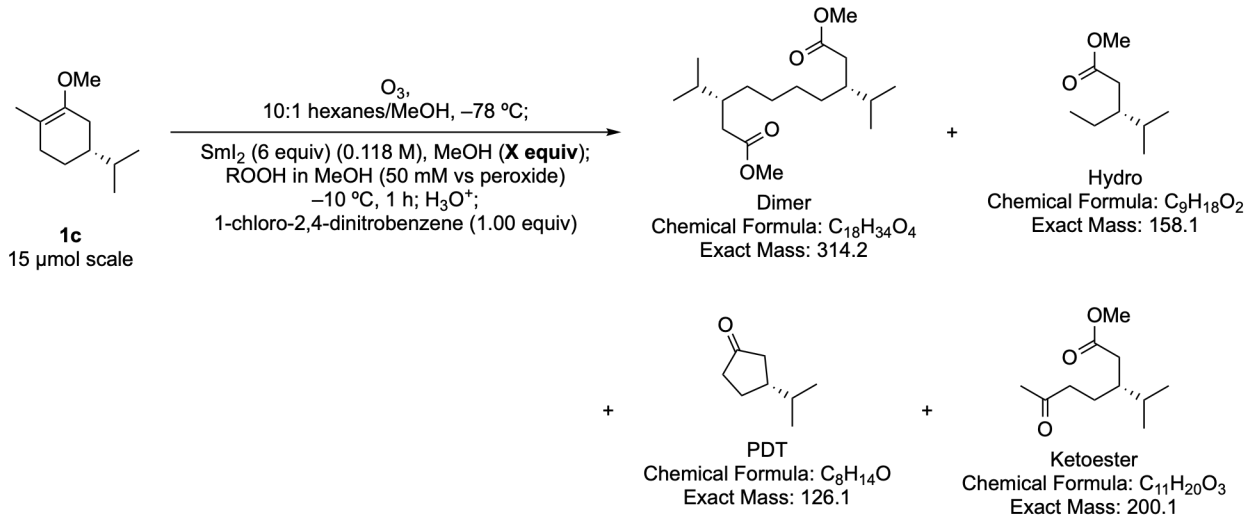
Procedure: A 25 mL round bottom flask with Teflon-coated magnetic stirring bar was flame dried and put under vacuum. It was transferred to the glove box (Ar) and loaded with SmI_2 (s, 2.4 equiv). It was then attached to the Schlenck line with a purged argon line.

A 25 mL round bottom flask was loaded with the alkene (1.0 equiv) and dissolved in MeOH (0.1 M). It. was cooled to –78 ºC and ozone was bubbled until the alkene was consumed (by TLC), about 1 – 2 min. The MeOH was evaporated at 30 ºC and ~60 mmHg then flask was evaporated and backfilled 3x with argon. Then degassed MeOH (0.1 M) was added and the peroxide was dissolved then cooled to **temp** (–10 ºC or –78 ºC).

Then degassed MeOH was cooled to **temp** (–10 ºC or –78 ºC) added via cannulation to the SmI_2 flask, which was also in the cold bath) to make a 0.1 M solution and stirred for 1 minute. Next, γ-terpinene (1.5 equiv) was added, immediately followed by the pre-cooled peroxide solution.

After de-coloration to grey, the internal standard was added and the solvent was removed. The residue was taken into ethyl acetate and washed with sodium thiosulfate then brine, dried over sodium sulfate, filtered, and evaporated. NMR was measured to determine the yield versus the benzoate α-C–H [48]. The results are indicated in Table 7.5.

7.9.6 High Throughput Experimentation (HTE)



Procedure: A 25 mL round bottom flask equipped with a Teflon-coated magnetic stirrer bar was charged with (*R*)-4-isopropyl-2-methoxy-1-methylcyclohex-1-ene (**1c**, 73.1 mg, 0.434 mmol) and dissolved in hexanes (4 mL). The solution was cooled to –78 ºC in an acetone/dry ice bath. The flask was open to air and no cap was used to seal the system. Oxygen was bubbled through a 16G x 4" needle at 1.0 L/min into the solution. Then methanol (0.4 mL) was added at this point. The Globalozone GO-D3G ozone generator was turned on at 0.74 amps. After 4 min (full conversion) the ozone generator was switched off and the excess ozone was removed using oxygen. The solvent was removed, then the flask was evaporated and backfilled with argon (3x).The formed peroxide was then dissolved in MeOH (10 mL) that was degassed by the freeze-pump-thaw method. The stock solution was sealed then pumped into an Unchained Junior Automated Chemical Experimentation device. Within the device, a 24 well plate was stocked with 4 mL vials, each equipped with a magnetic stir bar. The plate was cooled to –10 ºC. The robot then dispensed SmI_2 in THF (0.078 M, 1.01 mL, 0.12 mmol, 6.0 equiv) was into each vial. The needle was rinsed with MeOH (3x) after the SmI_2 dispensing was

complete. Then, to a single vial was added the desired quantity of MeOH (60–1200 equivalents in steps of 60, 1500, 1800, 2100, and 2400). The MeOH was pre-cooled to –10 ºC before dispensing and the volume was calculated by accounting for the density at –10 ºC, 0.819 g/mL. The peroxide as a solution in MeOH was then added to the vial (0.05 M, 0.4 mL, 2.52 mg, 0.2 mmol, 1.0 equiv). The needle was rinsed with MeOH (3x) then the robot moved onto the next vial and repeated the protocol with a higher level of MeOH. After completion, the vials were removed from the machine and quenched with 1 M HCl (0.15 mL). A stock solution of 1-chloro-2,4-dinitrobenzene (91.2 mg in 3.00 mL EtOAc) was prepared and 100 µL was added to each vial. Brine (1 mL) was added to separate phases. A GCMS sample was prepared from the organic layer. GCMS was then measured and the peak area ratios were normalized and graphed (Figures 7.16–7.21). A moving average with a period of 2 was fit over each dataset to create a trendline.

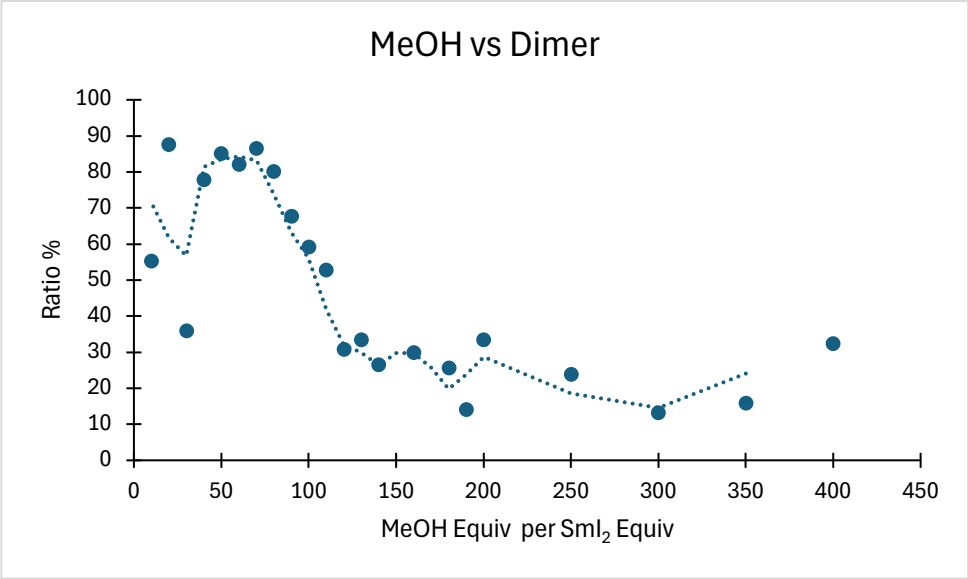


Figure 7.15 HTE Results: MeOH vs Dimer

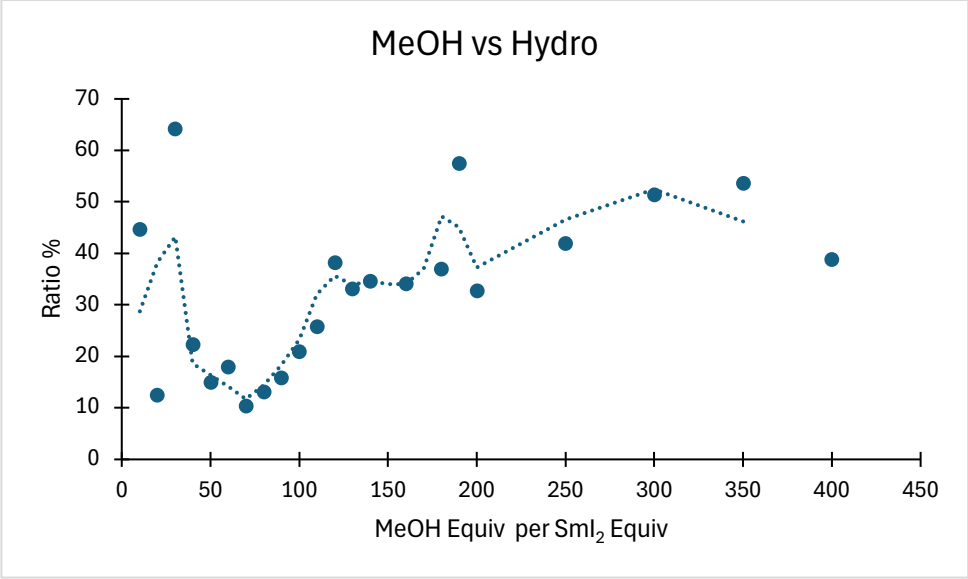


Figure 7.16 HTE Results: MeOH vs Hydro

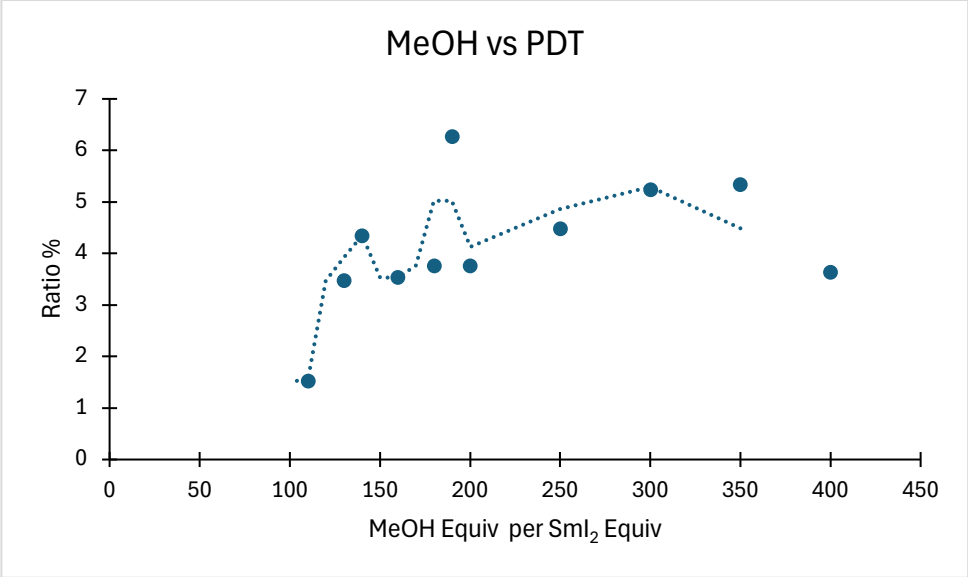


Figure 7.17 HTE Results: MeOH vs PDT

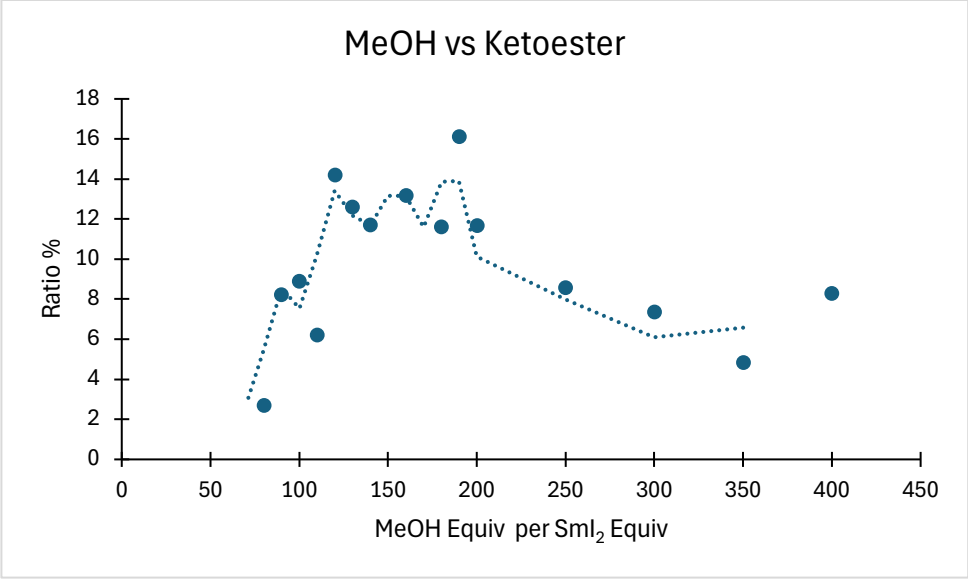


Figure 7.18 HTE Results: MeOH vs Ketoester

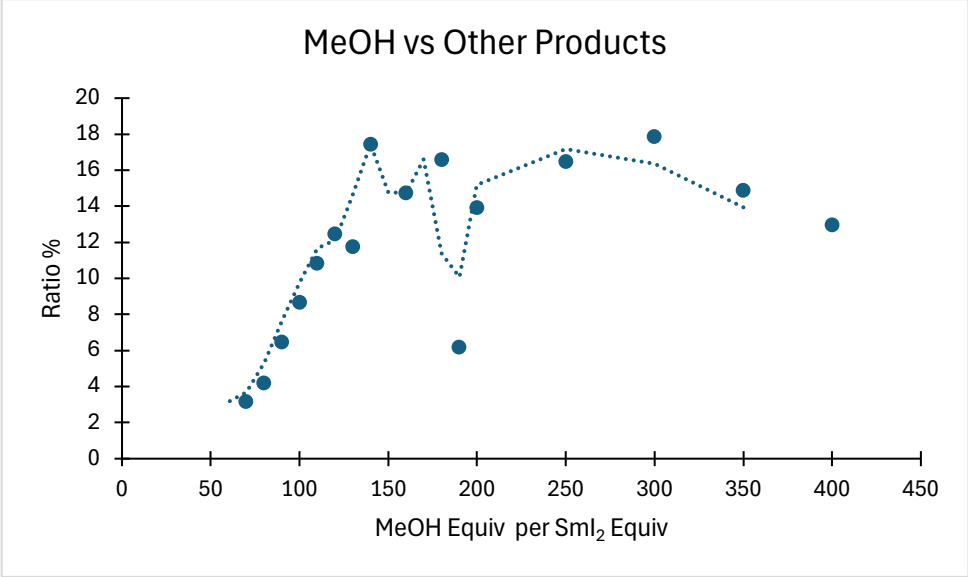


Figure 7.19 HTE Results: MeOH vs Other Products

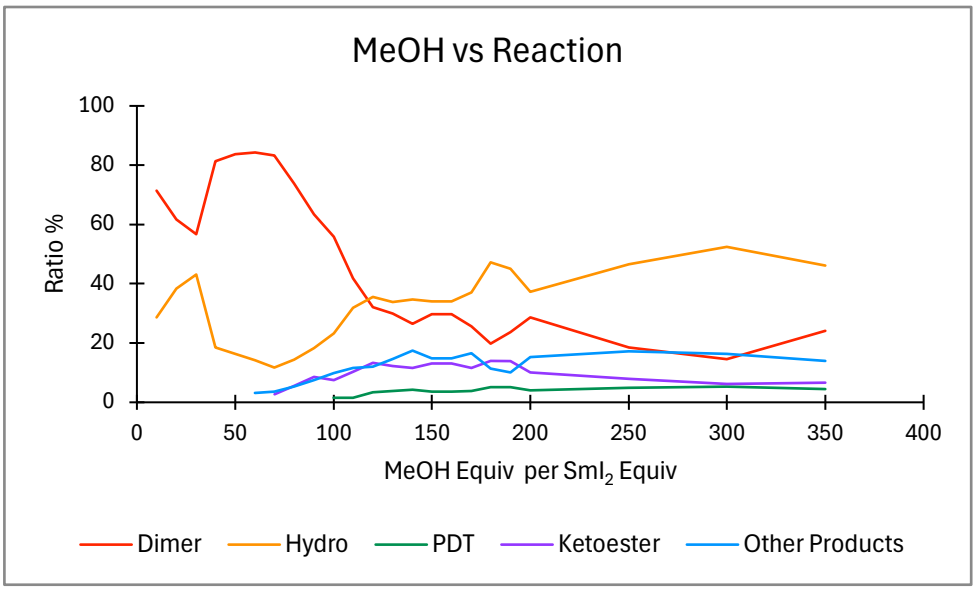
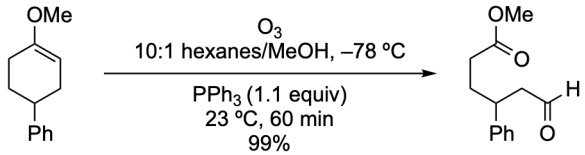


Figure 7.20 HTE Results MeOH vs Reaction

7.9.7 Cycloalkanone α-C(sp^3) Extraction Efforts

7.9.7.1 Preparation of Analytes



Methyl 6-oxo-4-phenylhexanoate (**2c**) was prepared from 4-methoxy-1,2,3,6-tetrahydro-1,1'-biphenyl (**2b**).

Procedure: To a 25 mL round bottom flask equipped with a Teflon-coated magnetic stirrer bar was added 4-methoxy-1,2,3,6-tetrahydro-1,1'-biphenyl (94.1 mg, 0.500 mmol, 1.00 equiv) and hexanes (4.45 mL). The mixture was stirred until homogeneous then cooled to –78 ºC in an ethyl acetate/dry ice bath. The flask was open to air and no cap was used to seal the system. Oxygen was bubbled through a 16G x 4" needle at 1.0 L/min into the solution. Methanol (0.455 mL) was added then the Globalozone GO-D3G ozone generator was turned on at 0.74 amps. After 150 seconds (full conversion) the ozone generator was switched off and the excess ozone was removed using air. Triphenylphosphine (144 mg, 0.550 mmol, 1.10 equiv) was added and the mixture was stirred at room temperature for 60 minutes. The volatiles were evaporated, then the crude material was isolated after FCC (0–30% *v/v* EtOAc/hexanes) as a clear colorless liquid (110 mg, 0.500 mmol) in 99% yield.

Scale: 0.500 mmol

Yield: 99% (110 mg)

R_f = 0.42 (30% *v/v* EtOAc/hexanes + UV/CAM stain)

Purification: SiO_2 (0–30% *v/v* EtOAc/hexanes)

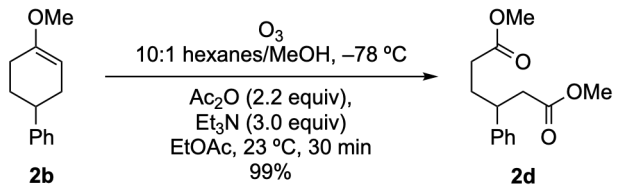
Physical State: clear colorless liquid

IR (ATR, neat) $\tilde{\nu}_{max}$: 3028, 2950, 2827, 2723, 1724, 1495, 1454, 1437, 1374, 1251, 1214, 1198, 1161, 1023, 764, 702 cm^{-1}

HRMS–DART (*m/z*): $[M + H]^+$ calc'd for $C_{13}H_{17}O_3$ 221.1172, found 221.1169

^{1}H NMR (500 MHz, $CDCl_3$) δ 9.66 (dd, *J* = 3.8, 1.8 Hz, 1H), 7.31 (t, *J* = 7.5 Hz, 2H), 7.24 – 7.20 (m, 1H), 7.18 (d, *J* = 7.9 Hz, 2H), 3.61 (s, 3H), 3.25 – 3.16 (m, 1H), 2.83 – 2.66 (m, 2H), 2.24 – 2.12 (m, 2H), 2.09 – 2.00 (m, 1H), 1.95 – 1.85 (m, 1H).

^{13}C NMR (126 MHz, $CDCl_3$) δ 201.4, 173.7, 142.6, 129.0, 127.7, 127.1, 51.7, 50.6, 39.4, 31.9, 31.5.



Dimethyl 3-phenylhexanedioate (**2d**) was prepared from 4-methoxy-1,2,3,6-tetrahydro-1,1'-biphenyl (**2b**).

Procedure: To a 25 mL round bottom flask equipped with a Teflon-coated magnetic stirrer bar was added 4-methoxy-1,2,3,6-tetrahydro-1,1'-biphenyl (94.1 mg, 0.500 mmol, 1.00 equiv) and hexanes (4.45 mL). The mixture was stirred until homogeneous then cooled to –78 ºC in an ethyl acetate/dry ice bath. The flask was open to air and no cap was used to seal the system. Oxygen was bubbled through a 16G x 4" needle at 1.0 L/min into the solution. Methanol (0.455 mL) was added then the Globalozone GO-D3G ozone generator was turned on at 0.74 amps. After 150 seconds (full conversion) the ozone generator was switched off and the excess ozone was removed using air. The solvent was removed by rotatory evaporation and replaced with ethyl acetate (2.50 mL). Acetic anhydride (112 mg, 0.104 mL, 1.10 mmol, 2.20 equiv) was added followed by triethylamine (152 mg, 0.210 mL, 1.50 mmol, 3.00 equiv) and the reaction was stirred at room temperature for 30 minutes (full consumption of the peroxide R_f = 0.14, 20% *v/v* EtOAc/hexanes + UV/vanillin stain). The volatiles were evaporated, then the crude material was isolated after FCC (0–20% *v/v* EtOAc/hexanes) as a clear colorless liquid (125 mg, 0.500 mmol) in 99% yield.

Scale: 0.500 mmol

Yield: 99% (125 mg)

R_f = 0.43 (20% *v/v* EtOAc/hexanes + UV/CAM stain)

Purification: SiO_2 (0–20% *v/v* EtOAc/hexanes)

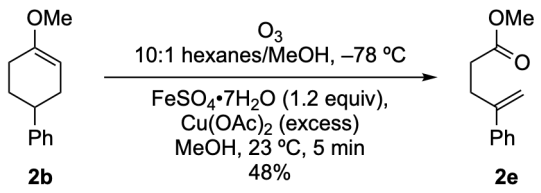
Physical State: clear colorless liquid

IR (ATR, neat) $\tilde{\nu}_{max}$: 3028, 3001, 2952, 1734, 1495, 1454, 1436, 1372, 1258, 1194, 1168, 1149, 1084, 1015, 764, 702 cm^{-1}

HRMS–DART (*m/z*): $[M + H]^+$ calc'd for $C_{14}H_{19}O_4$ 251.1278, found 251.1273

^{1}H NMR (500 MHz, $CDCl_3$) δ 7.29 (t, *J* = 7.7 Hz, 2H), 7.23 – 7.19 (m, 1H), 7.19 – 7.14 (m, 2H), 3.60 (s, 3H), 3.58 (s, 3H), 3.11 (dtd, *J* = 10.4, 7.5, 4.6 Hz, 1H), 2.69 – 2.57 (m, 2H), 2.22 – 2.01 (m, 3H), 1.95 – 1.85 (m, 1H).

^{13}C NMR (126 MHz, $CDCl_3$) δ 173.8, 172.6, 142.8, 128.8, 127.6, 127.0, 51.7, 51.7, 41.7, 41.6, 32.1, 31.1.



Methyl 4-phenylpent-4-enoate (**2e**) was prepared from 4-methoxy-1,2,3,6-tetrahydro-1,1'-biphenyl (**2b**).

Procedure: To a 25 mL round bottom flask equipped with a Teflon-coated magnetic stirrer bar was added 4-methoxy-1,2,3,6-tetrahydro-1,1'-biphenyl (94.1 mg, 0.500 mmol, 1.00 equiv) and hexanes (4.45 mL). The mixture was stirred until homogeneous then cooled to –78 ºC in an ethyl acetate/dry ice bath. The flask was open to air and no cap was used to seal the system. Oxygen was bubbled through a 16G x 4" needle at 1.0 L/min into the solution. Methanol (0.455 mL) was added then the Globalozone GO-D3G ozone generator was turned on at 0.74 amps. After 150 seconds (full conversion) the ozone generator was switched off and the excess ozone was removed using air. The solvent was removed by rotatory evaporation. A saturated solution of $Cu(OAc)_2$ was prepared in MeOH and 5.0 mL was added to the neat peroxide. Iron(II) sulfate heptahydrate (167 mg, 0.600 mmol, 1.20 equiv) was dissolved into MeOH and added dropwise. The blue solution reaction became green then red/brown. After stirring for 5 minutes at room temperature, the reaction was diluted with in ethyl acetate (5 mL) and diluted with water (10 mL). The mixture was transferred to a separatory funnel, and the aqueous layer was extracted twice more with ethyl acetate (5 mL each time). The combined organics were washed with brine, dried over sodium sulfate, filtered through cotton, and evaporated. The product was isolated after FCC (0–14% *v/v* EtOAc/hexanes) as a clear colorless liquid (46.2 mg, 0.243 mmol) in 49% yield.

Scale: 0.500 mmol

Yield: 49% (46.2 mg)

R_f = 0.42 (10% *v/v* EtOAc/hexanes + UV/vanillin stain)

Purification: SiO_2 (0–14% *v/v* EtOAc/hexanes)

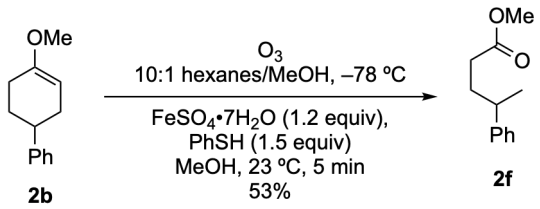
Physical State: clear colorless liquid

IR (ATR, neat) $\tilde{\nu}_{max}$: 3083, 3055, 3023, 2989, 2950, 1735, 1629, 1600, 1575, 1495, 1436, 1361, 1323, 1254, 1196, 1157, 1029, 988, 899, 778, 703 cm^{-1}

HRMS–DART (*m/z*): $[M + H]^+$ calc'd for $C_{12}H_{15}O_2$ 191.1067, found 191.1065

^{1}H NMR (500 MHz, $CDCl_3$) δ 7.41 (dd, *J* = 7.2, 1.1 Hz, 2H), 7.34 (t, *J* = 7.8 Hz, 2H), 7.29 – 7.25 (m, 1H), 5.31 (s, 1H), 5.10 (d, *J* = 1.1 Hz, 1H), 3.66 (s, 3H), 3.00 – 2.74 (m, 2H), 2.49 (dd, *J* = 9.3, 6.4 Hz, 2H).

^{13}C NMR (126 MHz, $CDCl_3$) δ 173.6, 146.9, 140.6, 128.5, 127.7, 126.2, 112.9, 51.7, 33.1, 30.5.



methyl 4-phenylpentanoate (**2f**) was prepared from 4-methoxy-1,2,3,6-tetrahydro-1,1'-biphenyl (**2b**).

Procedure: To a 25 mL round bottom flask equipped with a Teflon-coated magnetic stirrer bar was added 4-methoxy-1,2,3,6-tetrahydro-1,1'-biphenyl (94.1 mg, 0.500 mmol, 1.00 equiv) and hexanes (4.45 mL). The mixture was stirred until homogeneous then cooled to –78 ºC in an ethyl acetate/dry ice bath. The flask was open to air and no cap was used to seal the system. Oxygen was bubbled through a 16G x 4" needle at 1.0 L/min into the solution. Methanol (0.455 mL) was added then the Globalozone GO-D3G ozone generator was turned on at 0.74 amps. After 150 seconds (full conversion) the ozone generator was switched off and the excess ozone was removed using air. The solvent was removed by rotatory evaporation. The peroxide was redissolved in MeOH (5.00 mL) and cooled to –78 ºC in an ethyl acetate/dry ice bath. Benzenethiol (82.6 mg, 0.077 mL, 0.750 mmol, 1.50 equiv) was added immediately followed by iron(II) sulfate heptahydrate (167 mg, 0.600 mmol, 1.20 equiv). The stirring bath was removed and the solution was slowly warmed to room temperature. The reaction red/brown. After stirring for 5 minutes at room temperature, the reaction was diluted with in ethyl acetate (5 mL) and diluted with water (10 mL). The mixture was transferred to a separatory funnel, and the aqueous layer was extracted twice more with ethyl acetate (5 mL each time). The combined organics were washed with brine, dried over sodium sulfate, filtered through cotton, and

evaporated. The product was isolated after FCC (0–14% *v/v* EtOAc/hexanes) as a clear colorless liquid (50.8 mg, 0.264 mmol) in 53% yield.

Scale: 0.500 mmol

Yield: 53% (50.8 mg)

R_f = 0.42 (10% *v/v* EtOAc/hexanes + UV/vanillin stain)

Purification: SiO_2 (0–14% *v/v* EtOAc/hexanes)

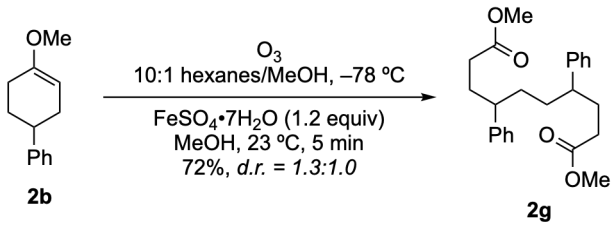
Physical State: clear colorless liquid

IR (ATR, neat) $\tilde{\nu}_{max}$: 3026, 2956, 2929, 2871, 1734, 1494, 1452, 1436, 1377, 1354, 1325, 1308, 1254, 1207, 1161, 1105, 1071, 1057, 1020, 985, 910, 762, 699 cm^{-1}

HRMS–DART (*m/z*): $[M + H]^+$ calc'd for $C_{12}H_{17}O_2$ 193.1223, found 193.1223.

^{1}H NMR (500 MHz, $CDCl_3$) δ 7.44 – 7.27 (m, 2H), 7.25 – 7.06 (m, 3H), 3.63 (s, 3H), 2.73 (dt, *J* = 8.9, 6.6 Hz, 1H), 2.32 – 2.13 (m, 2H), 2.03 – 1.85 (m, 2H), 1.29 (d, *J* = 6.9 Hz, 3H).

13C NMR (126 MHz, $CDCl_3$) δ 174.1, 146.3, 128.5, 127.1, 126.3, 51.5, 39.5, 33.3, 32.4, 22.2.



Dimethyl 4,7-diphenyldecanedioate (**2g**) was prepared from 4-methoxy-1,2,3,6-tetrahydro-1,1'-biphenyl (**2b**).

Procedure: To a 25 mL round bottom flask equipped with a Teflon-coated magnetic stirrer bar was added 4-methoxy-1,2,3,6-tetrahydro-1,1'-biphenyl (94.1 mg, 0.500 mmol, 1.00 equiv) and hexanes (4.45 mL). The mixture was stirred until homogeneous then cooled to –78 ºC in an ethyl acetate/dry ice bath. The flask was open to air and no cap was used to seal the system. Oxygen was bubbled through a 16G x 4" needle at 1.0 L/min into the solution. Methanol (0.455 mL) was added then the Globalozone GO-D3G ozone generator was turned on at 0.74 amps. After 150 seconds (full conversion) the ozone generator was switched off and the excess ozone was removed using air. The solvent was removed by rotatory evaporation and replaced with methanol (5.00 mL). Iron(II) sulfate heptahydrate (167 mg, 0.600 mmol, 1.20 equiv) was added as a crushed powder. The reaction became orange then red/brown. After stirring for 5 minutes at room temperature, the solvent was removed by rotatory evaporation. The crude material was dissolved in ethyl acetate (5 mL) and diluted with water (5 mL). The mixture was transferred to a separatory funnel, and the aqueous layer was extracted twice more with ethyl acetate (5 mL each time). The combined organics were washed with brine, dried over sodium sulfate, filtered through cotton, and evaporated. The products were isolated as an inseparable mixture of diastereomers after FCC (0–23% *v/v* EtOAc/hexanes) as a clear colorless liquid (69.0 mg, 0.180 mmol) in 72% yield.

Scale: 0.500 mmol

Yield: 72% (69.0 mg), *d.r.* = 1.3:1

R_f = 0.31 (10% *v/v* EtOAc/hexanes + UV)

Purification: SiO_2 (0–23% *v/v* EtOAc/hexanes)

Physical State: clear colorless liquid

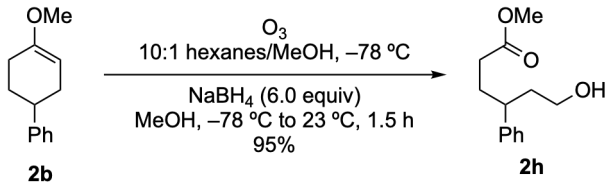
IR (ATR, neat) $\tilde{\nu}_{max}$: 3026, 2927, 2858, 1731, 1601, 1493, 1452, 1436, 1358, 1328, 1285, 1245, 1207, 1192, 1153, 1092, 1075, 1026, 882, 858, 762, 699 cm^{-1}

HRMS–DART (*m/z*): $[M + H]^+$ calc'd for $C_{24}H_{31}O_4$ 383.2217, found 383.2203.

^{1}H NMR (400 MHz, $CDCl_3$) δ 7.31 – 7.23 (m, 4H), 7.22 – 7.14 (m, 2H), 7.13 – 6.95 (m, 4H), 3.59 (s, 3H), 3.57 (s, 3H), 2.56 – 2.33 (m, 2H), 2.14 – 1.99 (m, 4H), 1.98 – 1.84 (m, 2H), 1.81 – 1.67 (m, 2H), 1.60 – 1.33 (m, 4H).

^{13}C NMR (101 MHz, $CDCl_3$) δ 174.18, 174.16, 144.5, 144.3, 128.6, 128.5, 127.8, 127.7, 126.41, 126.39, 51.52, 51.51, 45.8, 45.4, 34.9, 34.2, 32.24, 32.23, 32.1, 31.7.

The relative configuration of the diastereomers was unable to be ascertained.



methyl 6-hydroxy-4-phenylhexanoate (**2h**) was prepared from 4-methoxy-1,2,3,6-tetrahydro-1,1'-biphenyl (**2b**).

Procedure: To a 25 mL round bottom flask equipped with a Teflon-coated magnetic stirrer bar was added 4-methoxy-1,2,3,6-tetrahydro-1,1'-biphenyl (42.8 mg, 0.227 mmol, 1.00 equiv) and hexanes (2.07 mL). The mixture was stirred until homogeneous then cooled to –78 ºC in an acetone/dry ice bath. The flask was open to air and no cap was used to seal the system. Oxygen was bubbled through a 16G x 4" needle at 1.0 L/min into the solution. Methanol (0.207 mL) was added then the Globalozone GO-D3G ozone generator was turned on at 0.74 amps. After 90 seconds (full conversion) the ozone generator was switched off and the excess ozone was removed using air. The solvent was removed by rotatory evaporation and replaced with methanol (2.27 mL). Sodium borohydride (51.6 mg, 1.36 mmol, 6.00 equiv) was added in three portions over a period of 1.5 hours. After complete conversion, the reaction was diluted with ethyl acetate (5 mL) and quenched with water (5 mL). The mixture was transferred to a separatory funnel and the aqueous layer was extracted twice more with ethyl acetate (5 mL). The combined organics were washed with brine (5 mL), dried over sodium sulfate, filtered through cotton, and evaporated. The crude material was purified through FCC (5–30% V/V EtOAc/hexanes) to afford the product as a clear colorless oil (48.0 mg, 0.216 mmol) in 95% yield.

Scale: 0.227 mmol

Yield: 95% (48.0 mg)

R_f = 0.11 (20% *v/v* EtOAc/hexanes + UV/vanillin stain)

Purification: SiO_2 (5–30% *v/v* EtOAc/hexanes)

Physical State: clear colorless oil

IR (ATR, neat) $\tilde{\nu}_{max}$: 3441, 3027, 2930, 2878, 1734, 1494, 1452, 1437, 1374, 1208, 1154, 1045, 1027, 990, 762, 701 cm^{-1}

HRMS–DART (*m/z*): $[M + H]^+$ calc'd for $C_{13}H_{19}O_3$ 223.1329, found 223.1326

^{1}H NMR (500 MHz, $CDCl_3$) δ 7.28 (t, *J* = 7.6 Hz, 2H), 7.22 – 7.16 (m, 1H), 7.13 (d, *J* = 7.8 Hz, 2H), 3.59 (s, 3H), 3.52 (dt, *J* = 12.4, 6.2 Hz, 1H), 3.43 (dt, *J* = 10.5, 6.9 Hz, 1H), 2.70 (dp, *J* = 9.9, 5.0 Hz, 1H), 2.21 – 2.07 (m, 2H), 2.06 – 1.97 (m, 1H), 1.96 – 1.73 (m, 4H).

^{13}C NMR (126 MHz, $CDCl_3$) δ 174.2, 143.8, 128.7, 127.7, 126.6, 60.8, 51.6, 41.8, 39.5, 32.1, 31.6.

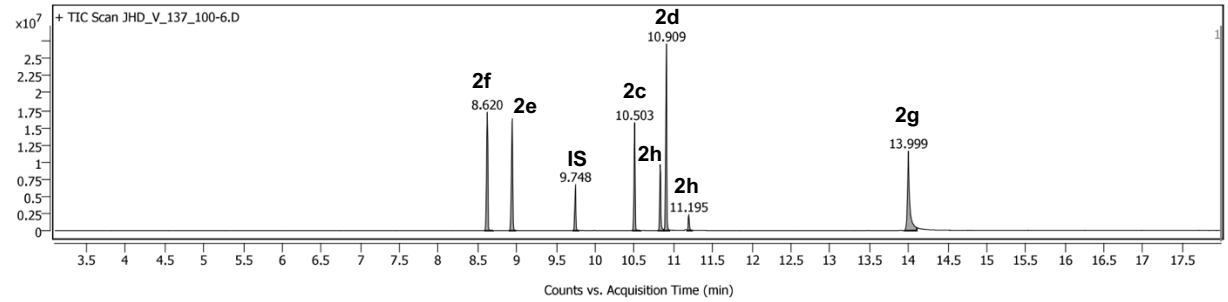
7.9.7.2 4-Phenylcyclohexanone α-C(sp^3) Analyte GCMS Analysis

To a 4.0000 mL volumetric flask was added 13.6 mg of **2f**, 13.4 mg of **2c**, 11.7 mg of **2h**, 15.0 mg of **2d**, 12.4 mg of **2e**, and 7.3 mg of **2g**. The flask was filled to the mark with a 3.15 mg/mL solution of 1-chloro-2,4-dinitrobenzene (**IS**, prepared by dissolving 315 mg of it into 100.0000 mL of CHCl3 in a volumetric flask). This solution was named "100%". From "100%" was removed 0.75 mL with a volumetric pipette and diluted to 1.0000 mL with the 3.15 mg/mL solution to create "75%". From "100%" was removed 0.50 mL with a volumetric pipette and diluted to 1.0000 mL with the 3.15 mg/mL solution to create "50%". From "100%" was removed 0.25 mL with a volumetric pipette and diluted to 1.0000 mL with the 3.15 mg/mL solution to create "25%". From "100%" was removed 1.00 mL with a volumetric pipette and diluted to 10.0000 mL with the 3.15 mg/mL solution to create "10%". From "100%" was removed 0.50 mL with a volumetric pipette and diluted to 5.0000 mL with the 3.15 mg/mL solution to create "01%".

These solutions were each measured 5x on an Agilent Intuvo 9000 GC system with a 50:1 split into an Agilent 5977B GC/MSD, measuring a blank CHCl3 sample in between each new dilution. The method used was 60 ºC for 1 min, then ramp 15 ºC / min until 180 ºC, then ramp 30 ºC / min until 300 ºC at a gas flow rate of 2.5000 mL/min at 17.484 psi.

Figure 7.21 4-Phenylcyclohexanone α-C(sp^3) Analyte GCMS Traces

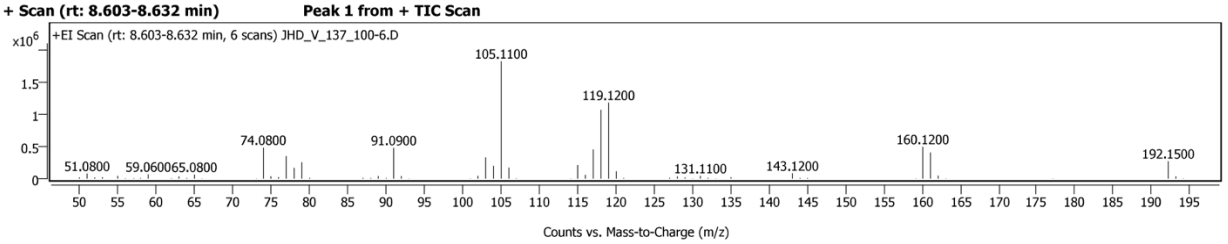
Sample Chromatograms



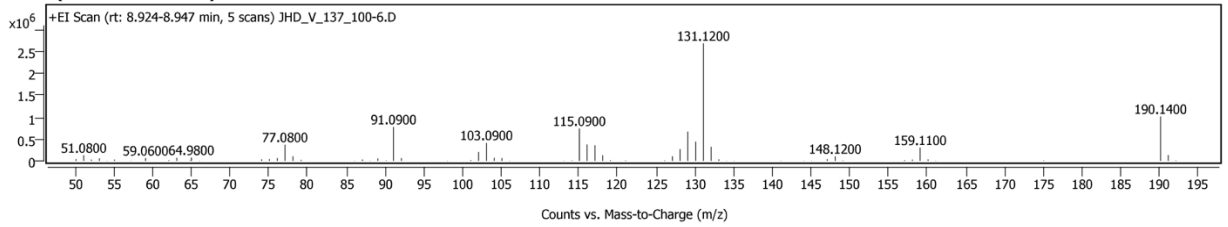
Chromatogram Peaks

Peak	Start	RT	End	Height	Area	Area %	SNR
1	8.581	8.620	8.695	17222444	20436538	78.31	
2	8.895	8.941	8.981	16287163	20120161	77.09	
3	9.708	9.748	9.788	6698060	7090775	27.17	
4	10.469	10.503	10.577	15697195	15482220	59.32	
5	10.795	10.829	10.875	9604076	9992493	38.29	
6	10.875	10.909	10.949	27120591	26098386	100.00	
7	11.172	11.195	11.235	2324599	2344098	8.98	
8	13.953	13.999	14.108	11558031	23662363	90.67	

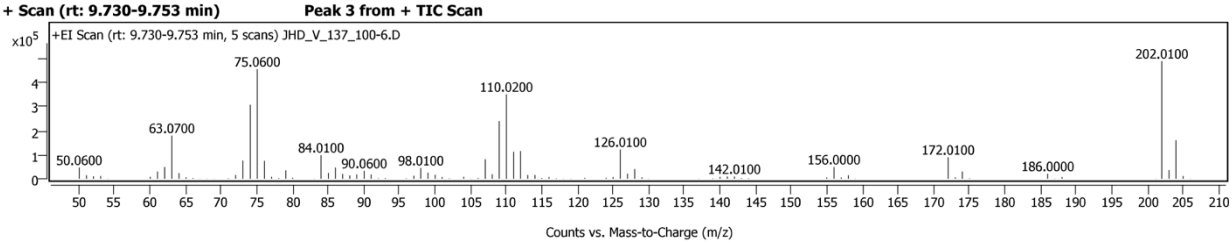
+ Scan (rt: 8.603-8.632 min) **Peak 1 from + TIC Scan**



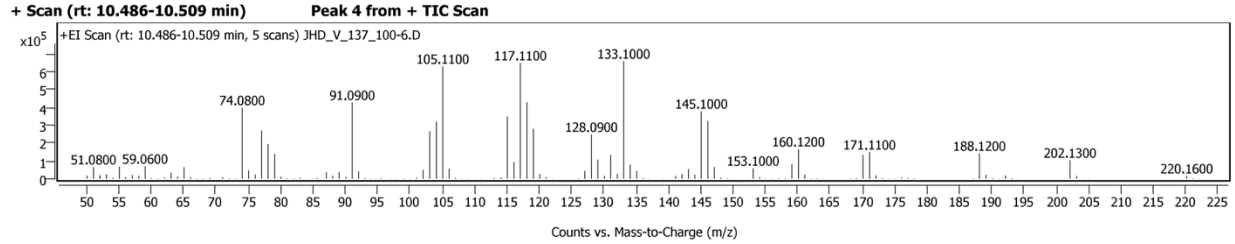
+ Scan (rt: 8.924-8.947 min) **Peak 2 from + TIC Scan**



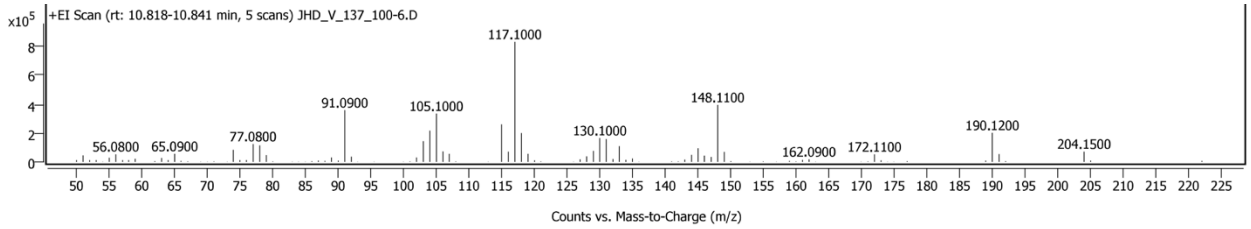
+ Scan (rt: 9.730-9.753 min) **Peak 3 from + TIC Scan**



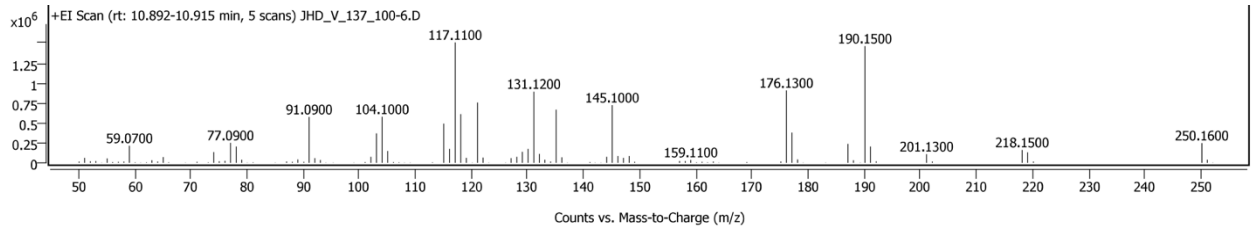
+ Scan (rt: 10.486-10.509 min) **Peak 4 from + TIC Scan**



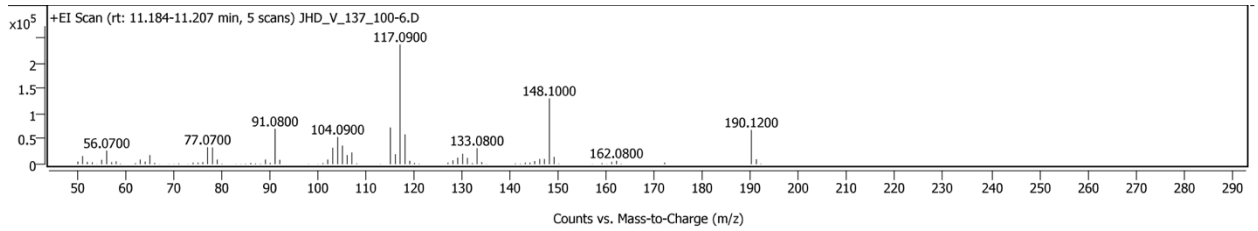
+ Scan (rt: 10.818-10.841 min) **Peak 5 from + TIC Scan**



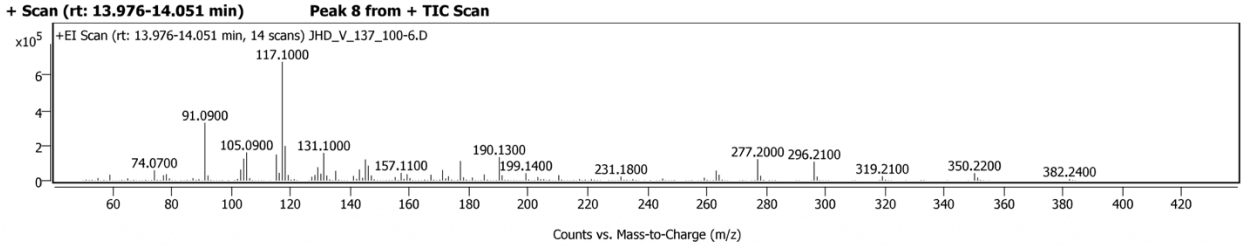
+ Scan (rt: 10.892-10.915 min) **Peak 6 from + TIC Scan**



+ Scan (rt: 11.184-11.207 min) **Peak 7 from + TIC Scan**



+ Scan (rt: 13.976-14.051 min) **Peak 8 from + TIC Scan**



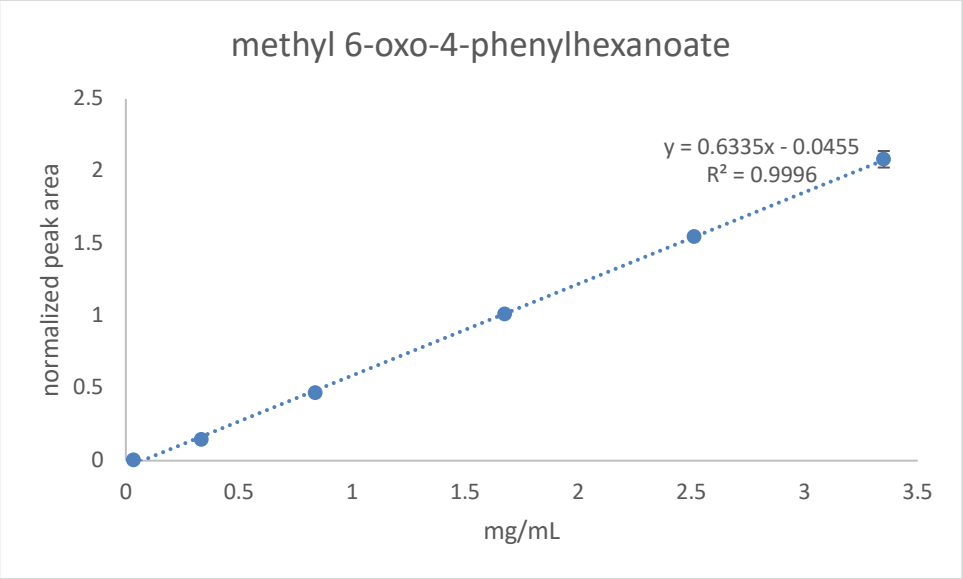


Figure 7.22 Calibraiton Curve for **2c**

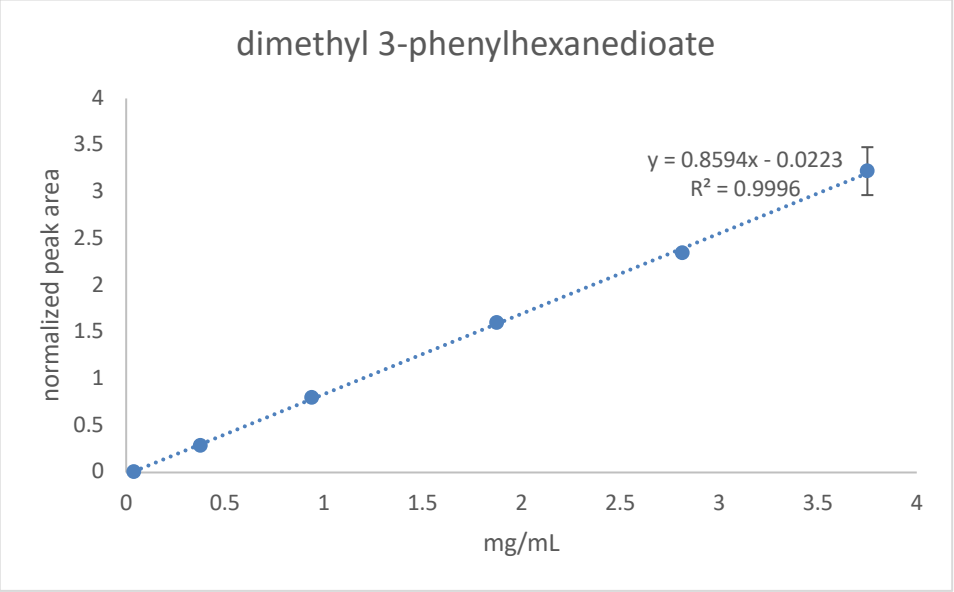


Figure 7.23 Calibration Curve for **2d**

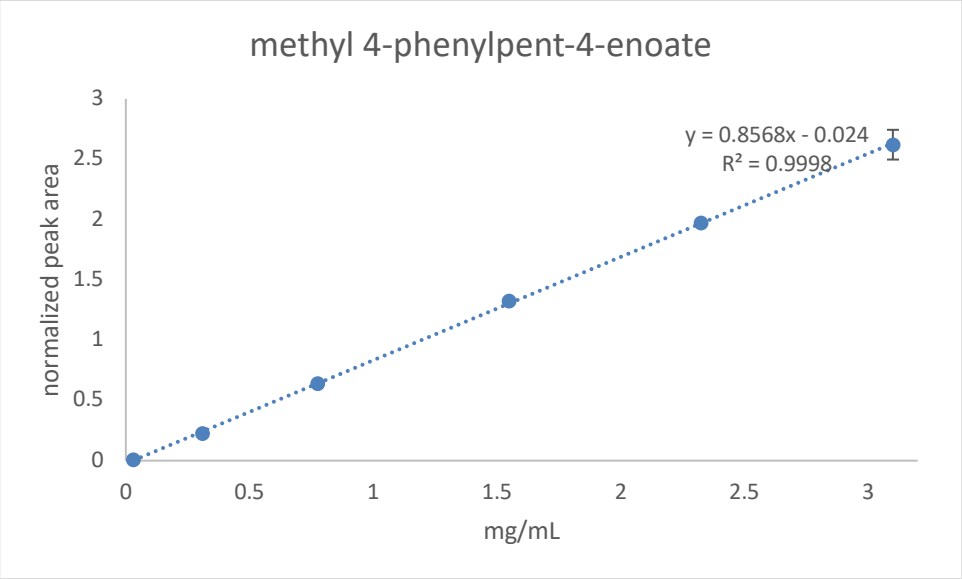


Figure 7.24 Calibration Curve for **2e**

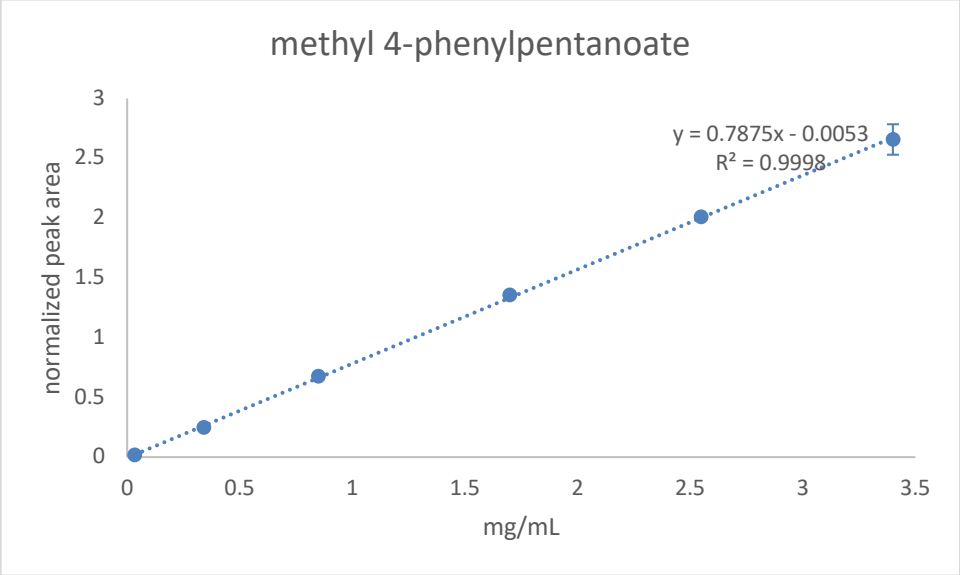


Figure 7.25 Calibration Curve for **2f**

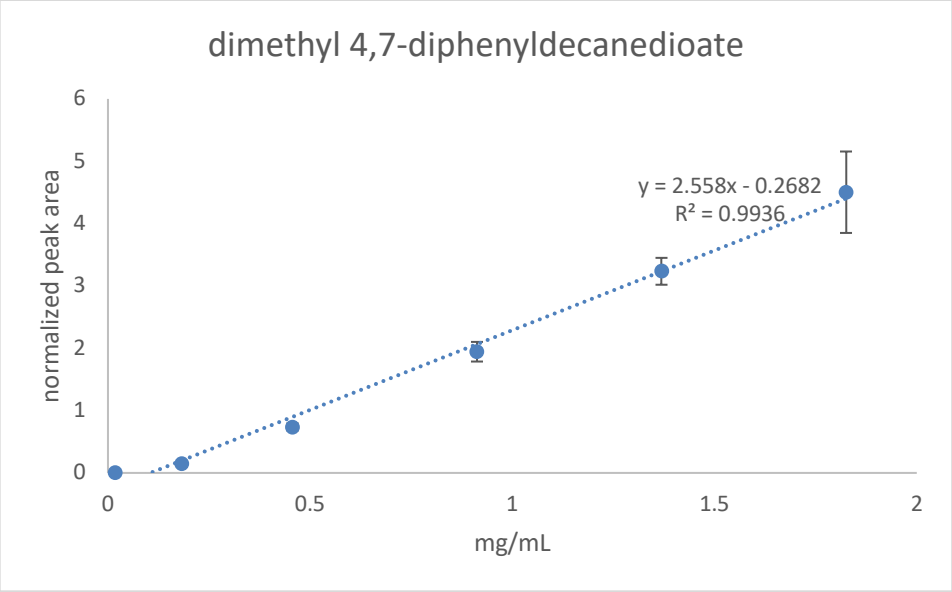


Figure 7.26 Calibration Curve for **2g**

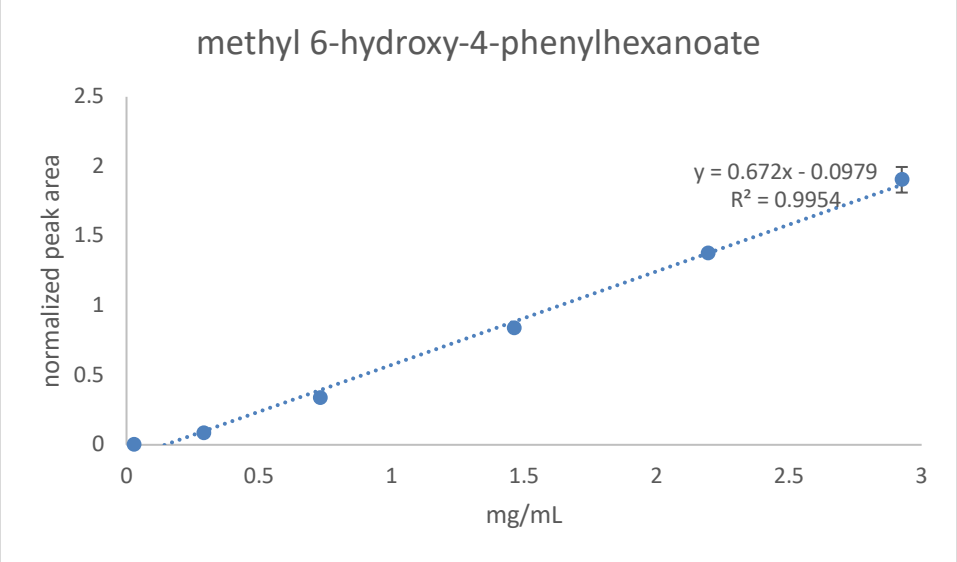
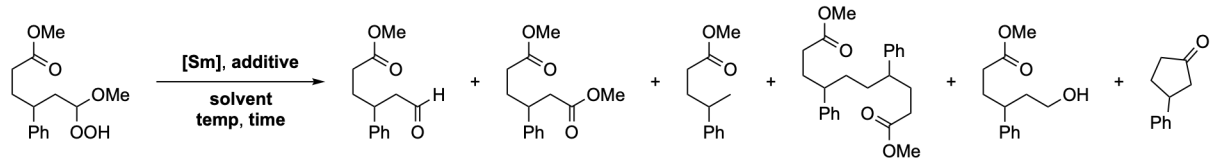


Figure 7.27 Calibration Curve for **2h**

7.9.7.3 Reaction Screening

Table 7.6 Ring Contraction Reaction Screening



#	peroxide (μmol)	[Sm]	additive	solv.	ºC	min	2c	2d	2f	2g	2h	2i
1	172	s, 4.0		H_2O	0 to 23	100	19%*	41%*	31%*	36%*	–	–
2	122	s, 4.0		MeOH	–78 to 23	55	24%*	30%*	24%*	22%*	–	–
3	118	s, 4.0		EtOH	–78 to 23	210	2%	67%	11%	4%	17%	–
4	140	s, 4.0		*i*PrOH	–78 to 23	210	10%	45%	–	–	45%	–
5	141	s, 4.0		5:6 THF/DMF	–10	20	14%	31%	17%	13%	12%	13%
6	108	8.0		5:6 THF/DMF	23	180	5%	22%	6%	10%	28%	13%
7	108	6.1		10:1 THF/DMF	23	15	87%	3%	1%	2%	5%	1%
8	108	8.0	$NiBr_2$(dme) 10 mol%	1:1 THF/DMF	23	30	57%	14%	2%	2%	14%	11%
9	155	8.0	NiI_2 10 mol%	1:1 THF/DMF	23	30	15%	22%	4%	1%	39%	12%
10	155	8.0	NiI_2 5 mol%	1:1 THF/DMA	23	60	33%	13%	3%	3%	30%	15%
11	155	8.0	NiI_2 5 mol%	1:1 THF/DMPU	23	120	30%	4%	5%	–	60%	1%
12	155	8.0		1:1 THF/NMP	23	60	6%	25%	12%	3%	23%	11%
13	155	8.0		2:1 to 5:1 THF/DMF	–78 to 23	120	7%	51%	20%	9%	4%	8%

General Procedure

Ozonolysis

A 25 mL round bottom flask was loaded with the alkene (1.0 equiv) and dissolved in hexanes (0.1 M). It. was cooled to –78 ºC then MeOH (0.01 M) was added. The mixture was stirred until homogeneous then cooled to –78 ºC in an acetone/dry ice bath. The flask was open to air and no cap was used to seal the system. Oxygen was bubbled through a 16G x 4" needle at 1.0 L/min into the solution. Methanol (0.01 M) was added then the Globalozone GO-D3G ozone generator was turned on at 0.74 amps. After full conversion (as indicated by TLC, approx. 2 min) the ozone generator was switched off and the excess ozone was removed using air. The solvent was removed by rotatory evaporation at 25 ºC. The flask was then sealed with a rubber septum the evacuated and backfilled with argon (3x). Degassed THF (0.1 M) was added to dissolve the peroxide, then the entire solution was cooled to ***temp***.

Reduction

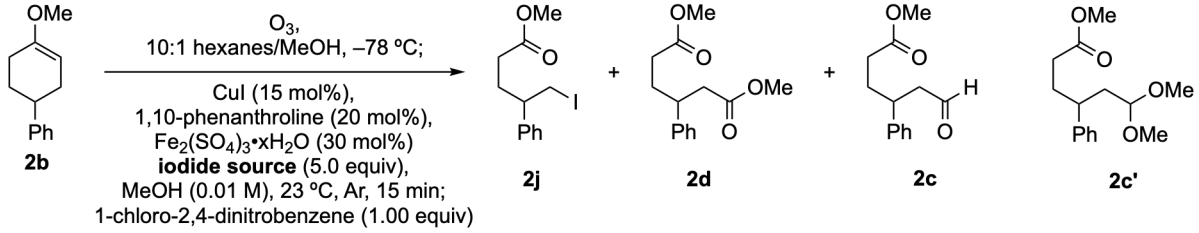
A 25 mL round bottom flask with Teflon-coated magnetic stirring bar was flame dried and put under vacuum. It was transferred to the glove box (Ar) and loaded with SmI_2 (s, 4.0 equiv) or SmI_2 as a solution in THF (**equiv**). The SmI_2 solution was always titrated within 3 days of use. The ***additive*** was also measured in the glove box and added at this time. The flask containing the SmI_2 was then removed from the glove box and attached to the Schlenck line with a purged argon line.

Degassed ***solvent*** (0.1 M in the case of solid SmI_2 or ***ratio*** if in THF solution) was added to the SmI_2 and stirred for 2 min. The solid SmI_2 dissolved to become a solution of color red/purple for H_2O, green for MeOH, purple for EtOH and *i*PrOH. The THF solution of

SmI_2 was blue and became green upon addition of DMF, DMA, or NMP and purple upon addition of DMPU. During this time, a cannulation needle was set up to transfer the peroxide into the SmI_2 flask dropwise. The SmI_2 flask was cooled to ***temp***. After dropwise addition, the peroxide flask was rinsed 3x0.5 mL degassed THF. The reaction was then stirred from ***time*** hours at ***temp***. The ***solvent*** was removed by rotatory evaporation then the residue was dissolved in EtOAc and washed with $Na_2S_2O_3$ (10 mL), 1 M HCl (10 mL), and brine (10 mL). The organics were dried over sodium sulfate and filtered. The internal standard, 1-chloro-2,4-dinitrobenzene (1.00 equiv) was added, then the organic solvents were removed. The crude mixture was dissolved in chloroform and diluted to 10 mL in a volumetric flask. A GCMS sample was then prepared and measured. The data were compared with the synthesized potential analytes (**2c**–**2h**) GCMS retention factors. Percentages are reported as normalized ratios versus the internal standard peak area.

7.9.8 Iododealkenylation

Table 7.7 Iododealkenylation: Iodide Source



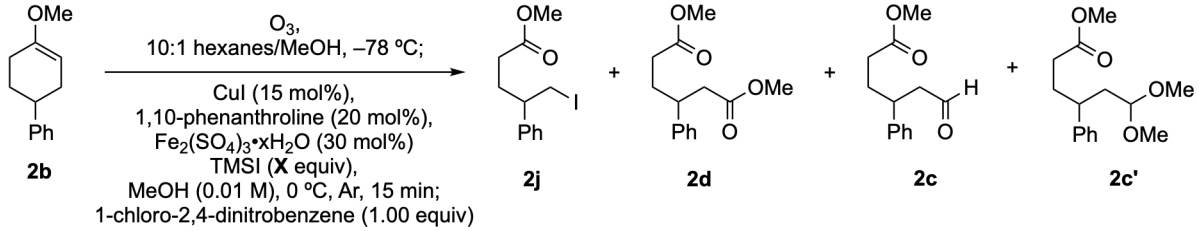
iodide source	2j	2d	2c	2c'
LiI	29%	18%	36%	–
NaI	43%	20%	24%	–
KI	22%	23%	43%	–
CsI	20%	20%	38%	–
ZnI_2	39%	26%	28%	–
$BaI_2•2H_2O$	12%	11%	29%	–
TBAI	19%	18%	52%	–
TMSI	62%	18%	–	19%

To a flame-dried 100 mL round bottom flask, added iron(III) sulfate hydrate (25.1 mg, 0.600 mmol, 30 mol%), copper(I) iodide (5.7 mg, 0.30 mmol, 15 mol%), 1,10-phenanthrolione (7.2 mg, 0.40 mmol, 20 mol%), and iodide source (5.0 equiv), excluding TMSI. The flask was evacuated and backfilled 3x with argon then dry MeOH (10 mL) was added. The mixture was stirred for 10 minutes and a red color was observed, (except ZnI_2 which became yellow). For TMSI, it was added dropwise after stirring the initial solution for 10 min, then the mixture was stirred for an additional 10 min after addition.

A 25 mL round bottom flask was loaded with the enol ether (**2b**, 37.7 mg, 0.200 mmol, 1.0 equiv) and dissolved in hexanes (1.8 mL). It was cooled to –78 ºC in an acetone/dry ice bth. The flask was open to air and no cap was used to seal the system. Oxygen was

bubbled through a 16G x 4” needle at 1.0 L/min into the solution. Methanol (0.20 mL) was added then the Globalozone GO-D3G ozone generator was turned on at 0.74 amps. After full conversion (as indicated by TLC, approx. 2 min) the ozone generator was switched off and the excess ozone was removed using air. The solvent was removed by rotatory evaporation at 25 ºC. The flask was then sealed with a rubber septum the evacuated and backfilled with argon (3x). Degassed MeOH (5 mL) was added to dissolve the peroxide, then the entire solution was cannulated into the reaction flask and rinsed 2x with 2.5 mL MeOH. The reaction was stirred for 15 min then added 1-chloro-2,4-dinitrobenzene (40.5 mg, 0.200 mmol, 1.00 equiv) and concentrated. Diluted with ethyl acetate and water then extracted 3x with ethyl acetate. Washed the organics with sodium thiosulfate, brine, and dried over sodium sulfate, filtered and evaporated. Measured NMR yield (D1 = 10 s, ns = 16).

Table 7.8 Iododealkenylation: TMSI Quantities



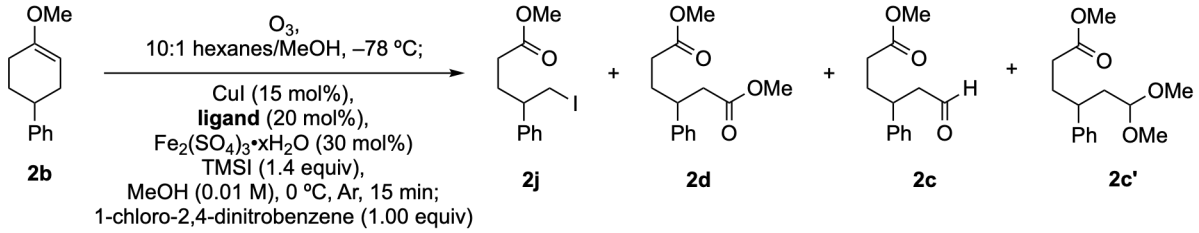
X equiv	2j	2d	2c	2c'
0.0	0%	6%	–	–
1.2	54%	22%	14%	3%
1.3	62%	21%	13%	1%
1.4	64%	20%	15%	–
2.0	63%	19%	–	14%
3.0	60%	19%	10%	10%
4.0	62%	19%	2%	16%
5.0	64%	18%	–	18%

To a flame-dried 100 mL round bottom flask, added iron(III) sulfate hydrate (25.1 mg, 0.600 mmol, 30 mol%), copper(I) iodide (5.7 mg, 0.30 mmol, 15 mol%), and 1,10-phenanthrolione (7.2 mg, 0.40 mmol, 20 mol%). The flask was evacuated and backfilled 3x with argon then dry MeOH (10 mL) was added. The mixture was stirred for 10 minutes then TMSI (***equiv***) was added dropwise, then the mixture was stirred for an additional 10 min after addition.

A 25 mL round bottom flask was loaded with the enol ether (**2b**, 37.7 mg, 0.200 mmol, 1.0 equiv) and dissolved in hexanes (1.8 mL). It was cooled to –78 ºC in an acetone/dry ice bth. The flask was open to air and no cap was used to seal the system. Oxygen was bubbled through a 16G x 4” needle at 1.0 L/min into the solution. Methanol (0.20 mL) was

added then the Globalozone GO-D3G ozone generator was turned on at 0.74 amps. After full conversion (as indicated by TLC, approx. 2 min) the ozone generator was switched off and the excess ozone was removed using air. The solvent was removed by rotatory evaporation at 25 ºC. The flask was then sealed with a rubber septum the evacuated and backfilled with argon (3x). Degassed MeOH (5 mL) was added to dissolve the peroxide, then the entire solution was cannulated into the reaction flask and rinsed 2x with 2.5 mL MeOH. The reaction was stirred for 15 min then added 1-chloro-2,4-dinitrobenzene (40.5 mg, 0.200 mmol, 1.00 equiv) and concentrated. Diluted with ethyl acetate and water then extracted 3x with ethyl acetate. Washed the organics with sodium thiosulfate, brine, and dried over sodium sulfate, filtered and evaporated. Measured NMR yield (D1 = 10 s, ns = 16).

Table 7.9 Iododealkenylation: Ligand Screen

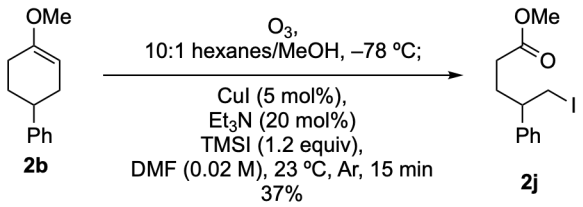


Ligand	2j	2d	2c	2c'
1,10-phenanthroline	64%	20%	15%	–
none	65%	19%	4%	4%
4,4'-di-*t*Bu-bpy	65%	20%	3%	6%
PyBox	61%	20%	4%	7%
4,4',4"-tri-*t*Bu-tpy	66%	21%	1%	6%

To a flame-dried 100 mL round bottom flask, added iron(III) sulfate hydrate (25.1 mg, 0.600 mmol, 30 mol%), copper(I) iodide (5.7 mg, 0.30 mmol, 15 mol%), and ***ligand*** (20 mol%). The flask was evacuated and backfilled 3x with argon then dry MeOH (10 mL) was added. The mixture was stirred for 10 minutes then TMSI (56.0 mg, 39.8 µL, 0.280 mmol, 1.4 equiv) was added dropwise, then the mixture was stirred for an additional 10 min after addition.

A 25 mL round bottom flask was loaded with the enol ether (**2b**, 37.7 mg, 0.200 mmol, 1.0 equiv) and dissolved in hexanes (1.8 mL). It was cooled to –78 ºC in an acetone/dry ice bth. The flask was open to air and no cap was used to seal the system. Oxygen was bubbled through a 16G x 4" needle at 1.0 L/min into the solution. Methanol (0.20 mL) was added then the Globalozone GO-D3G ozone generator was turned on at 0.74 amps. After full conversion (as indicated by TLC, approx. 2 min) the ozone generator was switched

off and the excess ozone was removed using air. The solvent was removed by rotatory evaporation at 25 ºC. The flask was then sealed with a rubber septum the evacuated and backfilled with argon (3x). Degassed MeOH (5 mL) was added to dissolve the peroxide, then the entire solution was cannulated into the reaction flask and rinsed 2x with 2.5 mL MeOH. The reaction was stirred for 15 min then added 1-chloro-2,4-dinitrobenzene (40.5 mg, 0.200 mmol, 1.00 equiv) and concentrated. Diluted with ethyl acetate and water then extracted 3x with ethyl acetate. Washed the organics with sodium thiosulfate, brine, and dried over sodium sulfate, filtered and evaporated. Measured NMR yield (D1 = 10 s, ns = 16).



methyl 5-iodo-4-phenylpentanoate (**2j**)

Procedure: The procedure was adapted from the literature [54]. A 25 mL round bottom flask was flame dried and CuI (19.0 mg, 0.100 mmol, 5 mol%) was added. The flask was evacuated and backfilled 3x with Ar. Dry DMF (10 mL) then dry Et_3N (40.5 mg, 55.8 µL, 0.400 mmol, 20 mol%) was added followed by TMSI (480 mg, 339 µL, 2.40 mmol,1.2 equiv). The alkene **2b** (377 mg, 2.00 mmol, 1.00 equiv) was dissolved in 10:1 hexanes/MeOH (20 mL/2 mL) and ozonized for 4.5 min. The peroxide was evaporated and azeotroped twice with benzene before being evacuated and backfilled 3x with Ar. Alkyl hydroperoxide evacuated and backfilled with argon (3 x) then was dissolved in DMF (3 mL). The peroxide solution was cannulated to the copper iodide solution. The flask was rinsed twice with DMF (1 mL each) and the mixture was stirred at room temperature for 15 min. The color changed from yellow/orange to red. The reaction mixture was diluted with the mixture of EtOAc/hexane = 1:3 and washed with H_2O (3 x). The organic layer was dried over Na_2SO_4, filtrated and concentrated under reduced pressure. The crude product was purified by flash column chromatography on silica gel (eluted with 0–10% EtOAc/hexanes then 70% EtOAc/hexanes) to give the methyl 5-iodo-4-phenylpentanoate (**2j**) as a clear liquid (234 mg, 0.736 mmol) in 37% yield.

Scale: 2.00 mmol

Yield: 37%

Physical State: clear liquid

Purification: SiO_2 (0–5% *v/v* EtOAc/hexanes)

$\boldsymbol{R_f}$ = 0.77 (40% *v/v* EtOAc/hexanes + UV/vanillin stain)

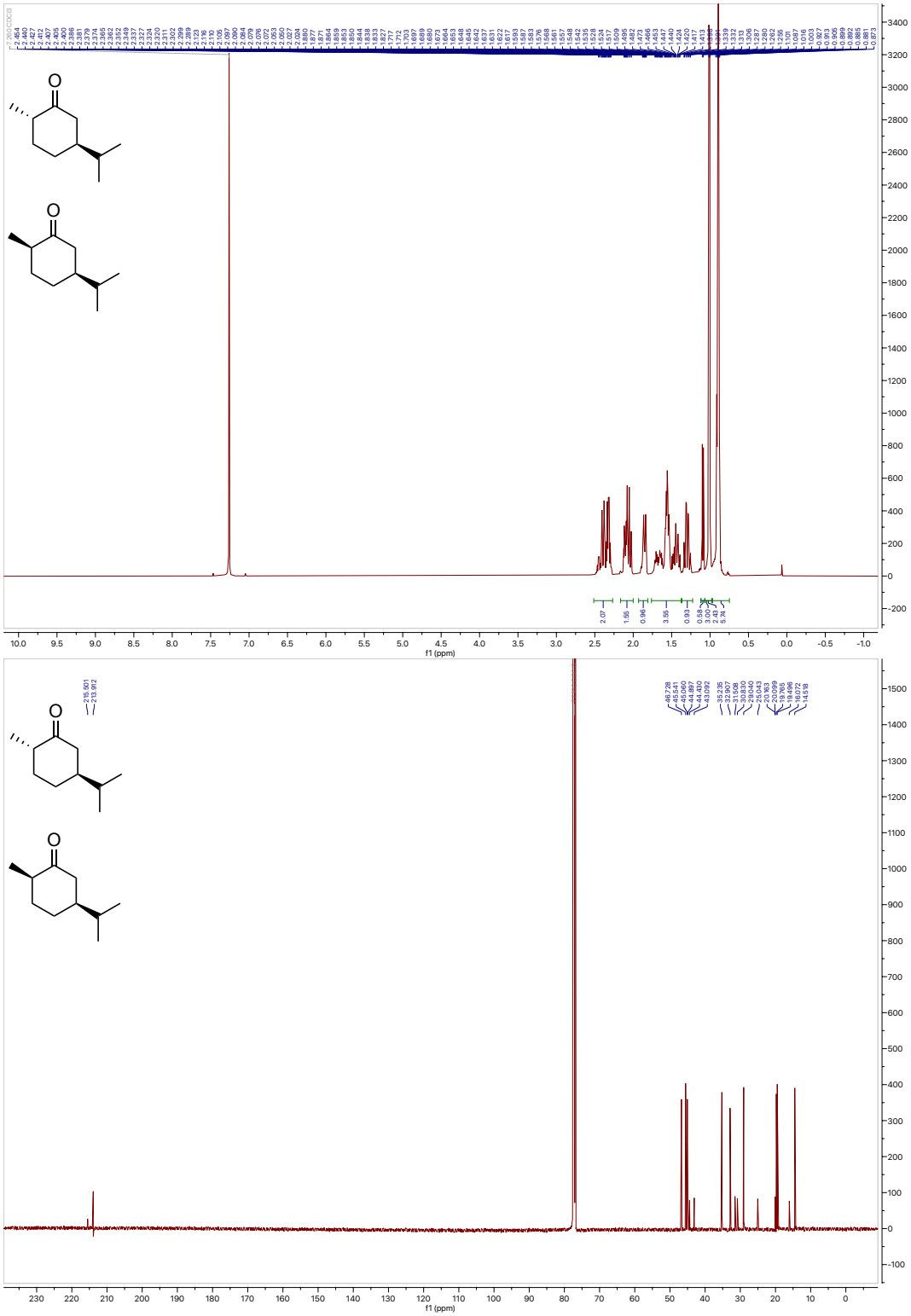
IR (ATR, neat) $\tilde{\nu}_{max}$: 3026, 3001, 2948, 1730, 1494, 1452, 1434, 1370, 1322, 1278, 1254, 1208, 1165, 1073, 1025, 990, 885, 850, 755, 698 cm^{-1}

HRMS–DART (*m/z*): $[M + H]^+$ calc'd for $C_{12}H_{16}O_2$ 319.0190, found 319.0190

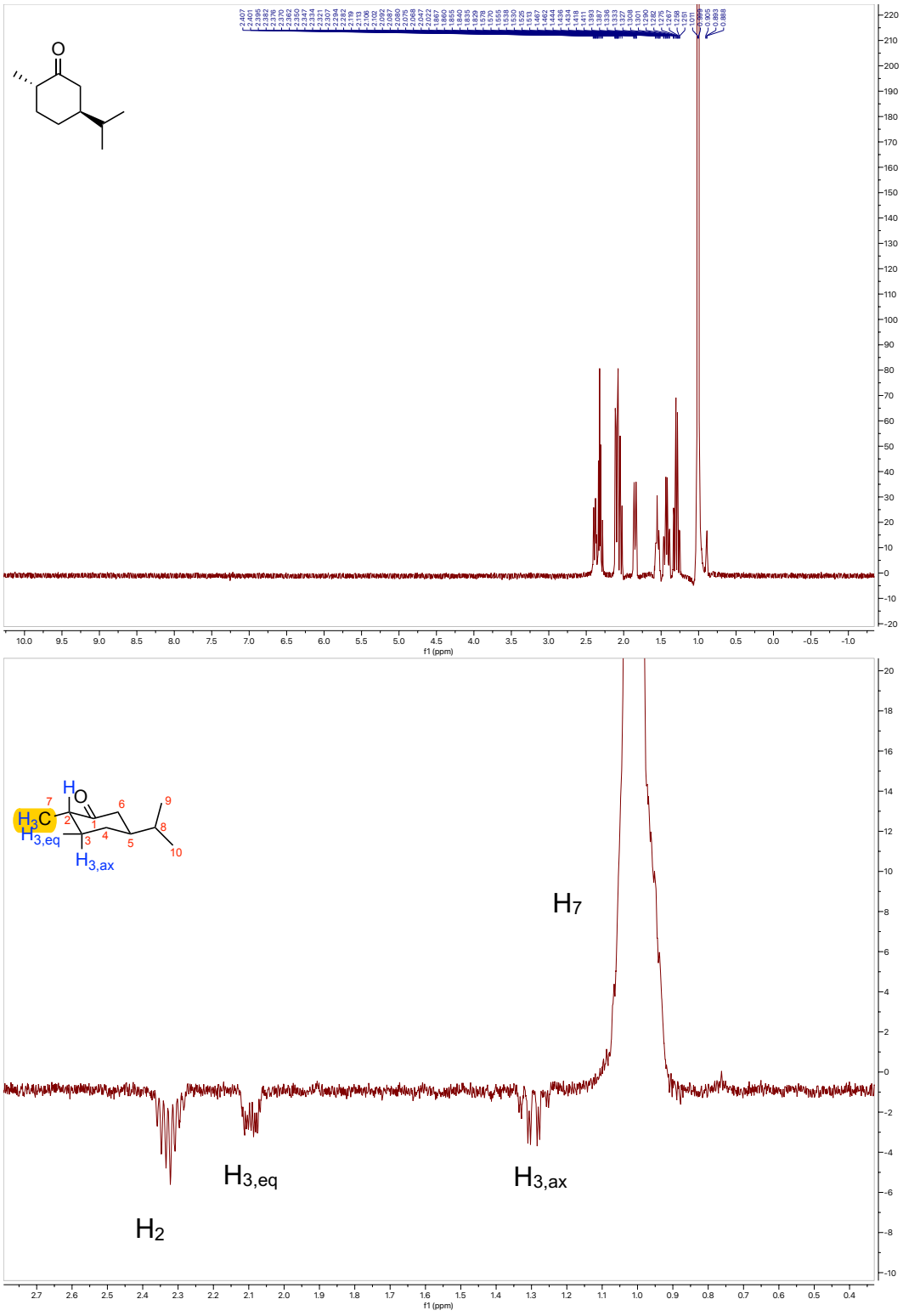
^{1}H NMR (600 MHz, $CDCl_3$) δ 7.35 – 7.29 (m, 2H), 7.29 – 7.23 (m, 1H), 7.18 – 7.11 (m, 2H), 3.68 – 3.55 (m, 3H), 3.44 – 3.31 (m, 2H), 2.88 (dtd, *J* = 11.2, 7.2, 4.1 Hz, 1H), 2.36 – 2.24 (m, 1H), 2.17 (td, *J* = 7.2, 2.8 Hz, 2H), 2.01 – 1.83 (m, 1H).

^{13}C NMR (151 MHz, $CDCl_3$) δ 173.5, 141.9, 128.8, 127.4, 127.4, 51.7, 47.7, 32.1, 30.9, 12.7.

7.9.9 Copies of NMR Spectra

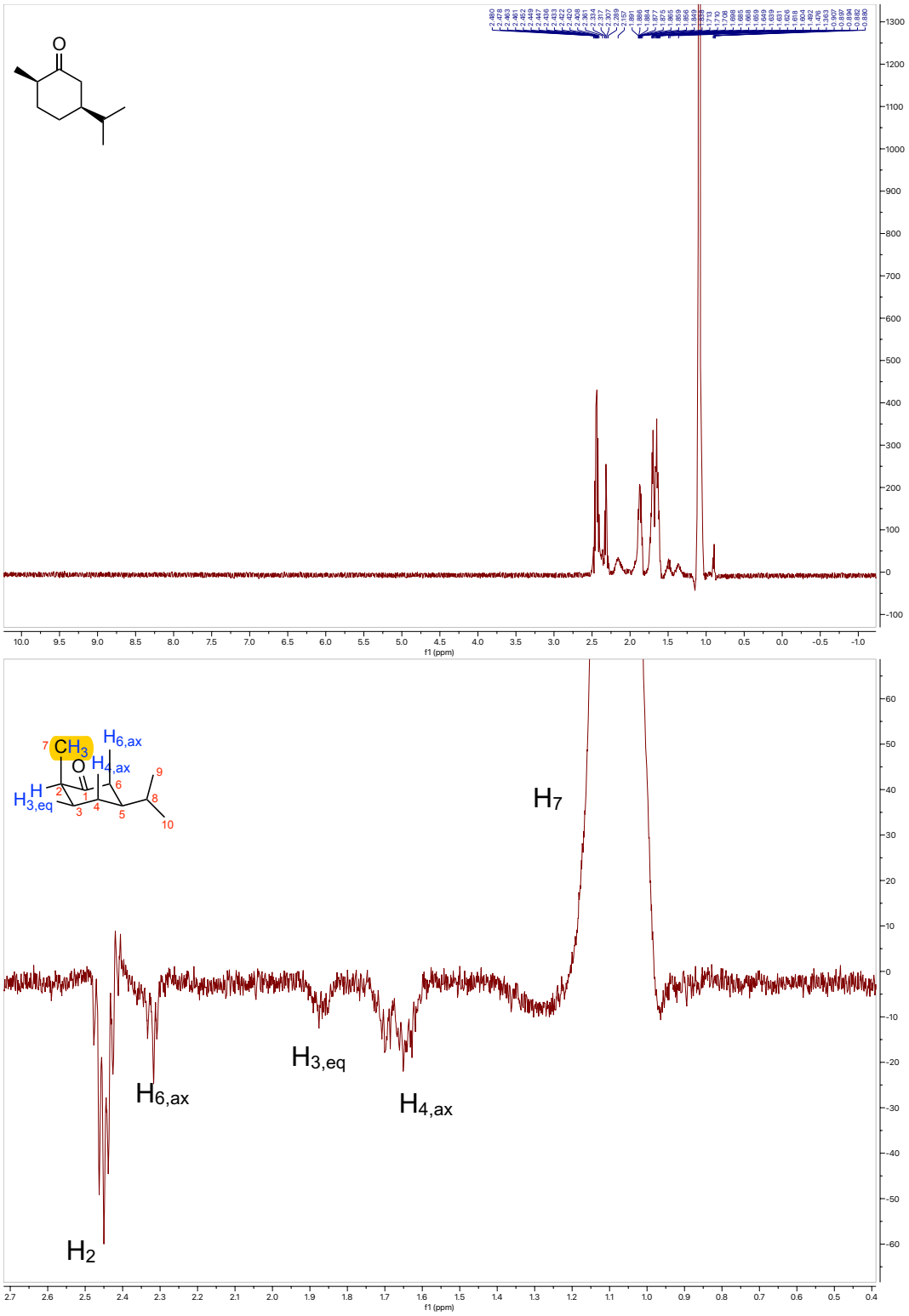


^{1}H NMR (500 MHz, $CDCl_3$) and **^{13}C NMR** (126 MHz, $CDCl_3$) of **1a**

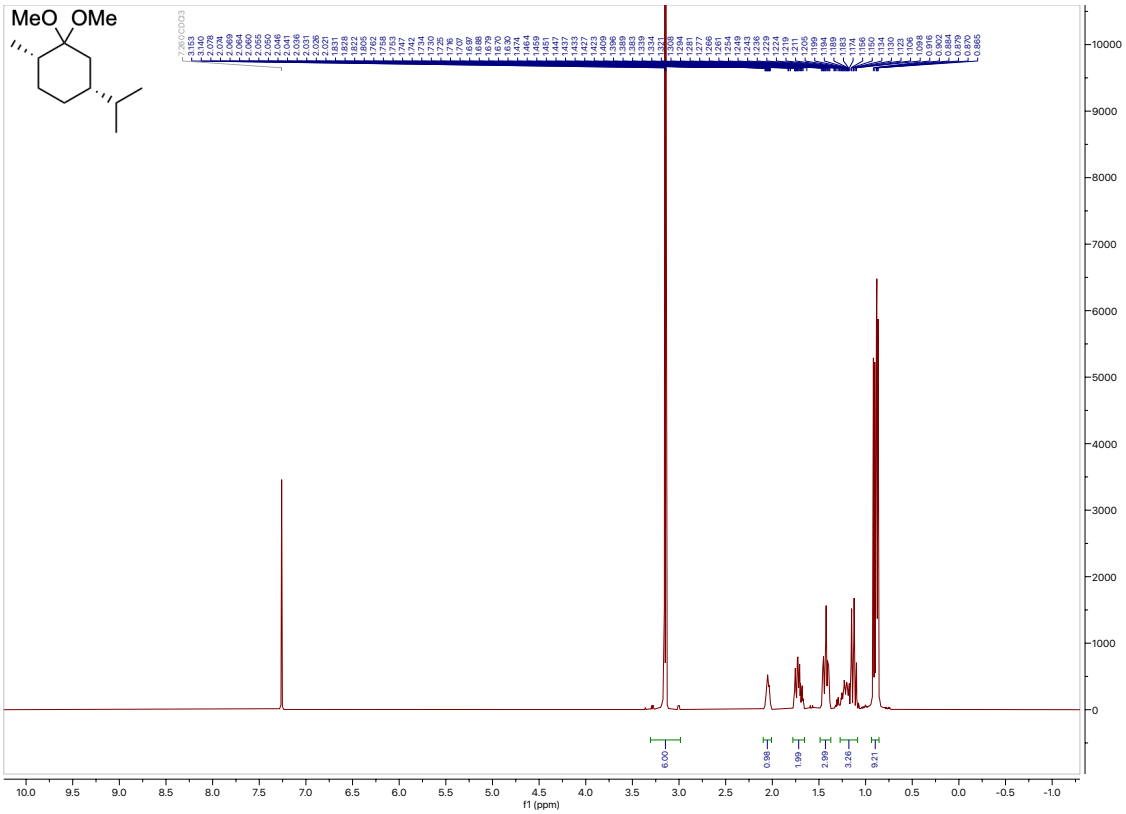


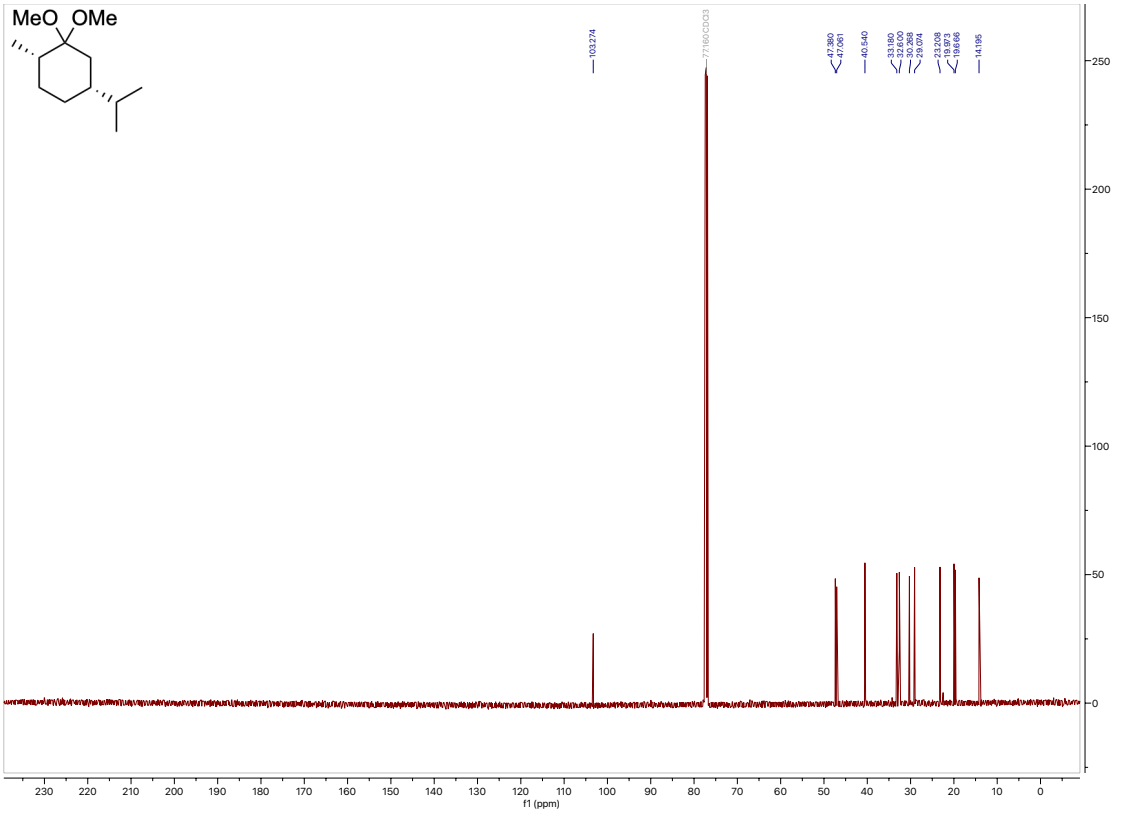
1D Selective TOCSY at 1.035 ppm (500 MHz, $CDCl_3$) of **1a**

and **1D Selective NOESY** at 1.035 ppm (500 MHz, $CDCl_3$) of **1a**

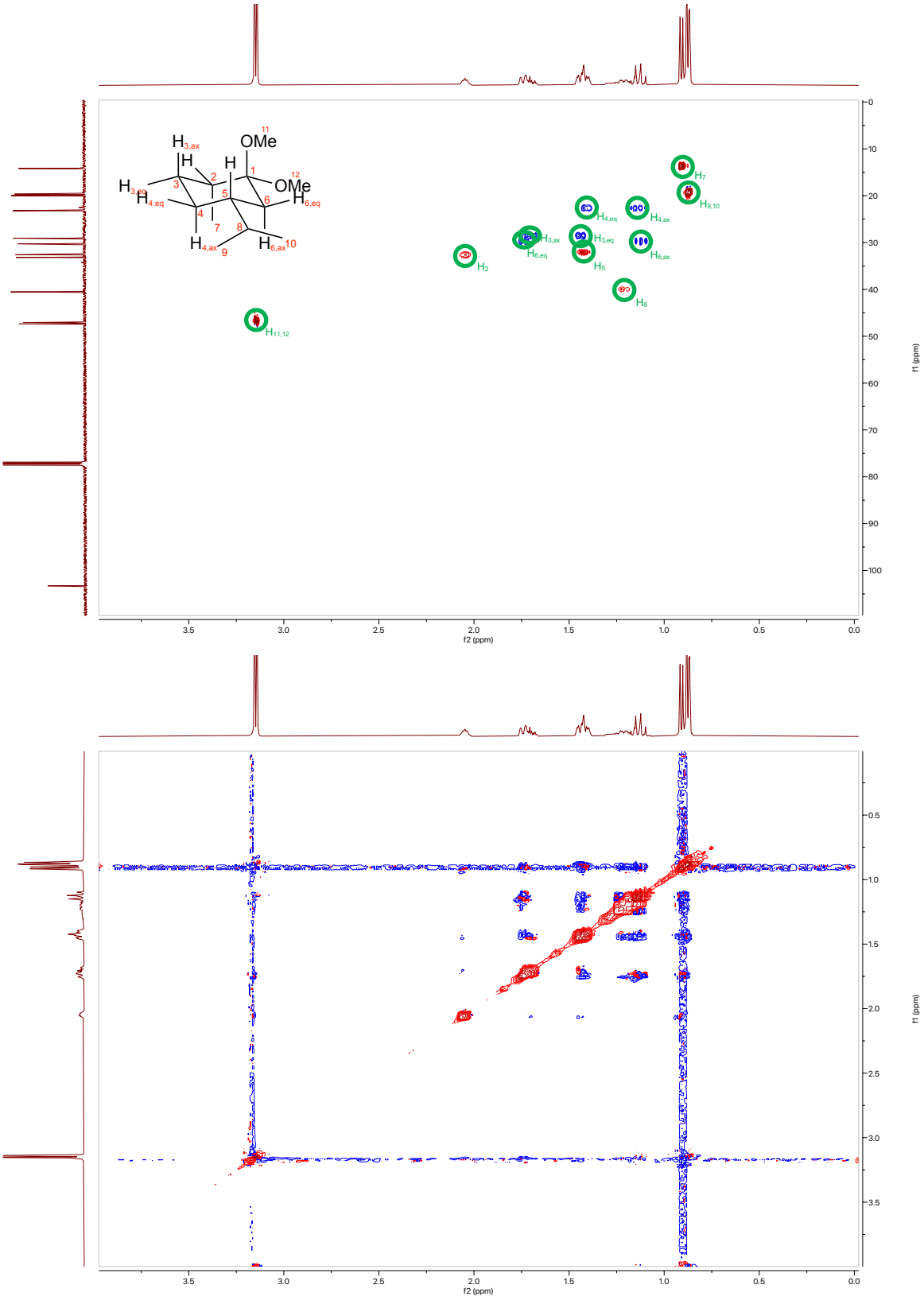


1D Selective TOCSY at 1.118 ppm (500 MHz, $CDCl_3$) of **1a**
and **1D Selective NOESY** at 1.118 ppm (500 MHz, $CDCl_3$) of **1a**

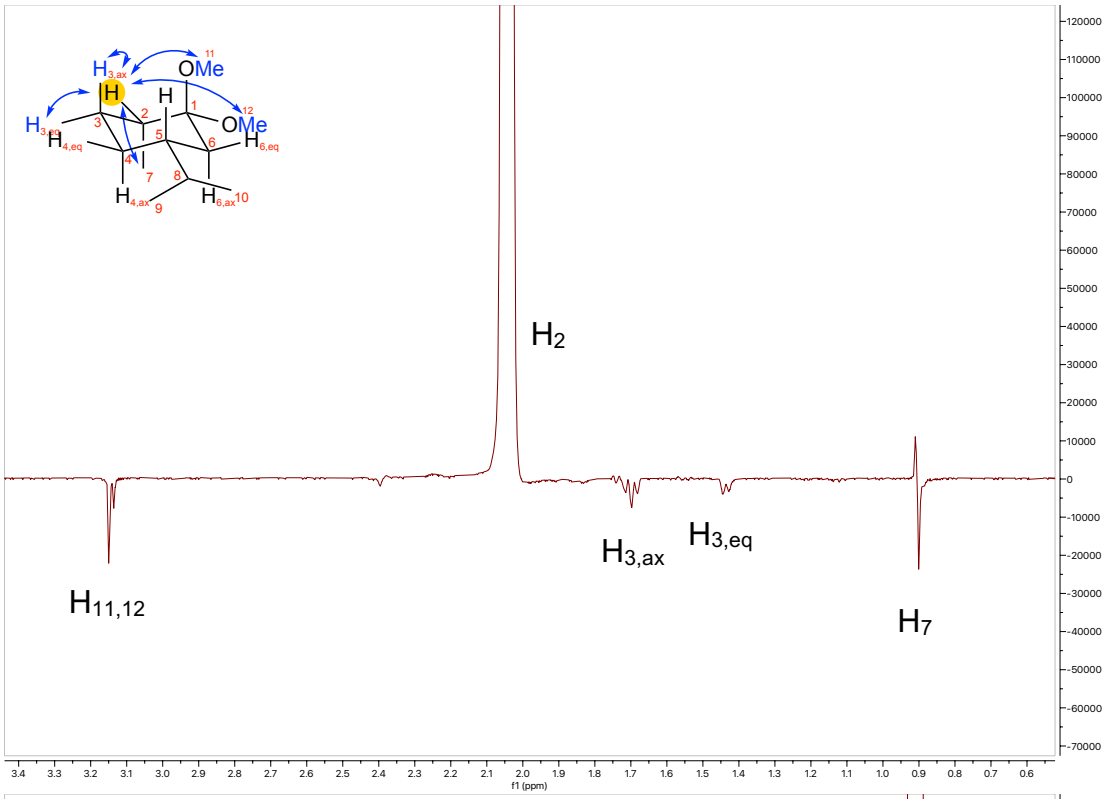


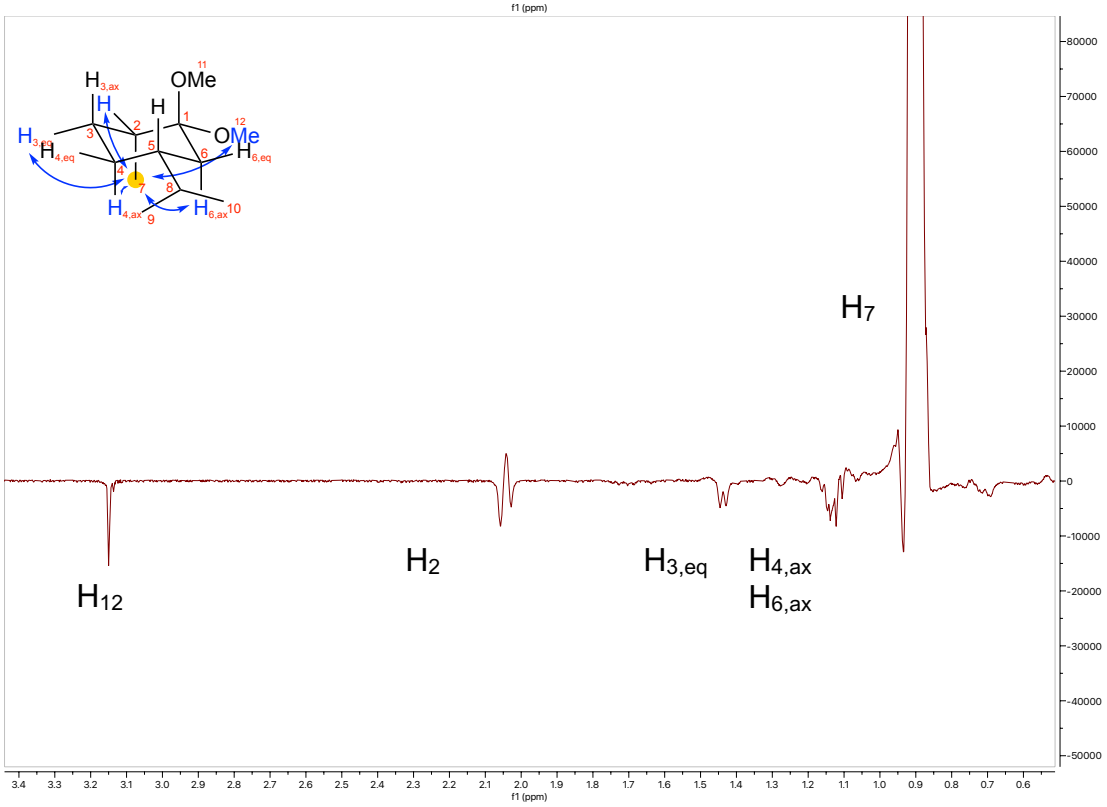


^{1}H NMR (500 MHz, $CDCl_3$) and **^{13}C NMR** (126 MHz, $CDCl_3$) of **1b**



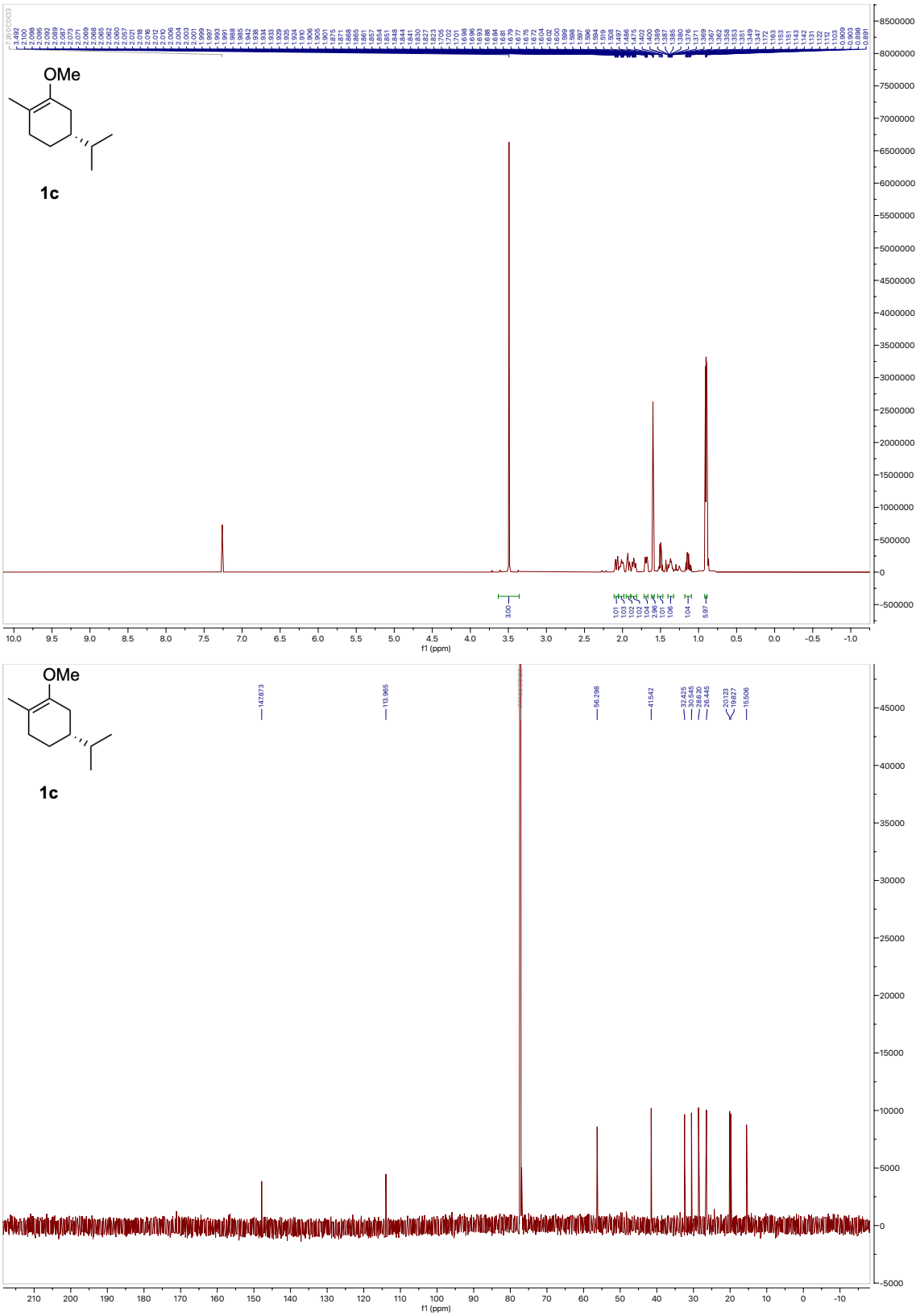
HSQC ($CDCl_3$) and **NOESY** ($CDCl_3$) of **1b**



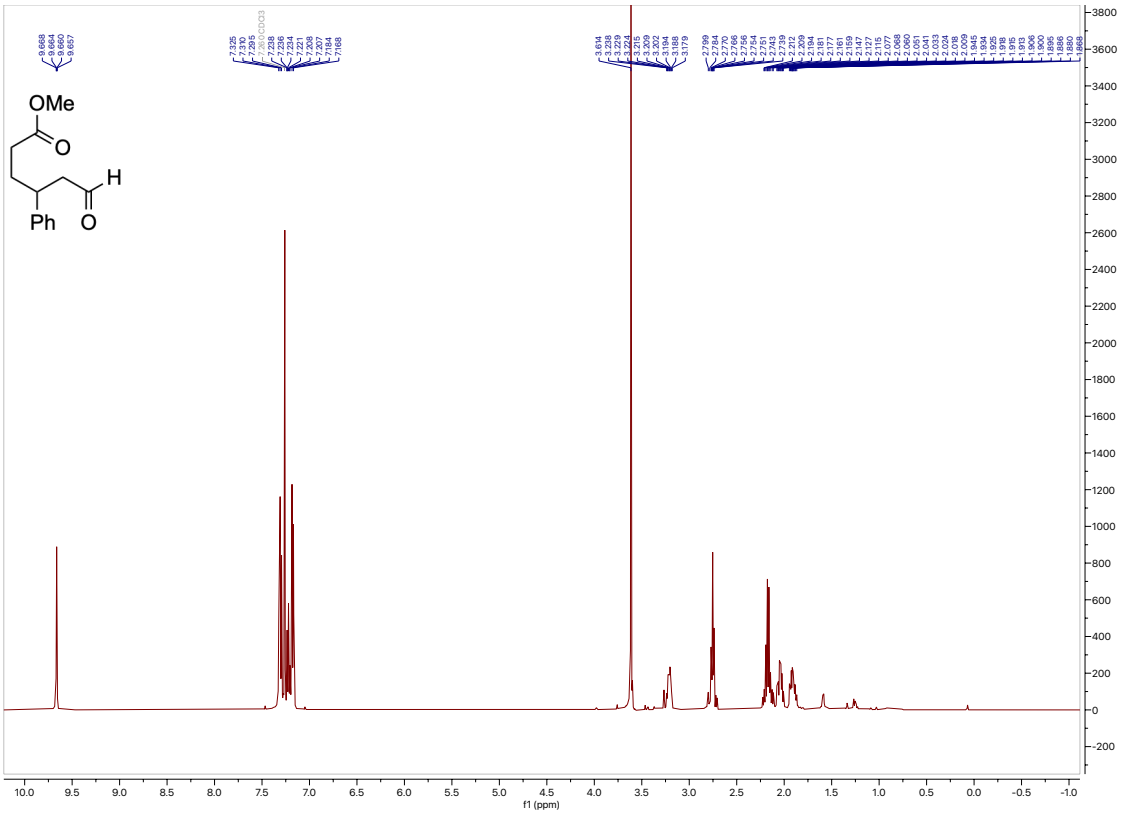


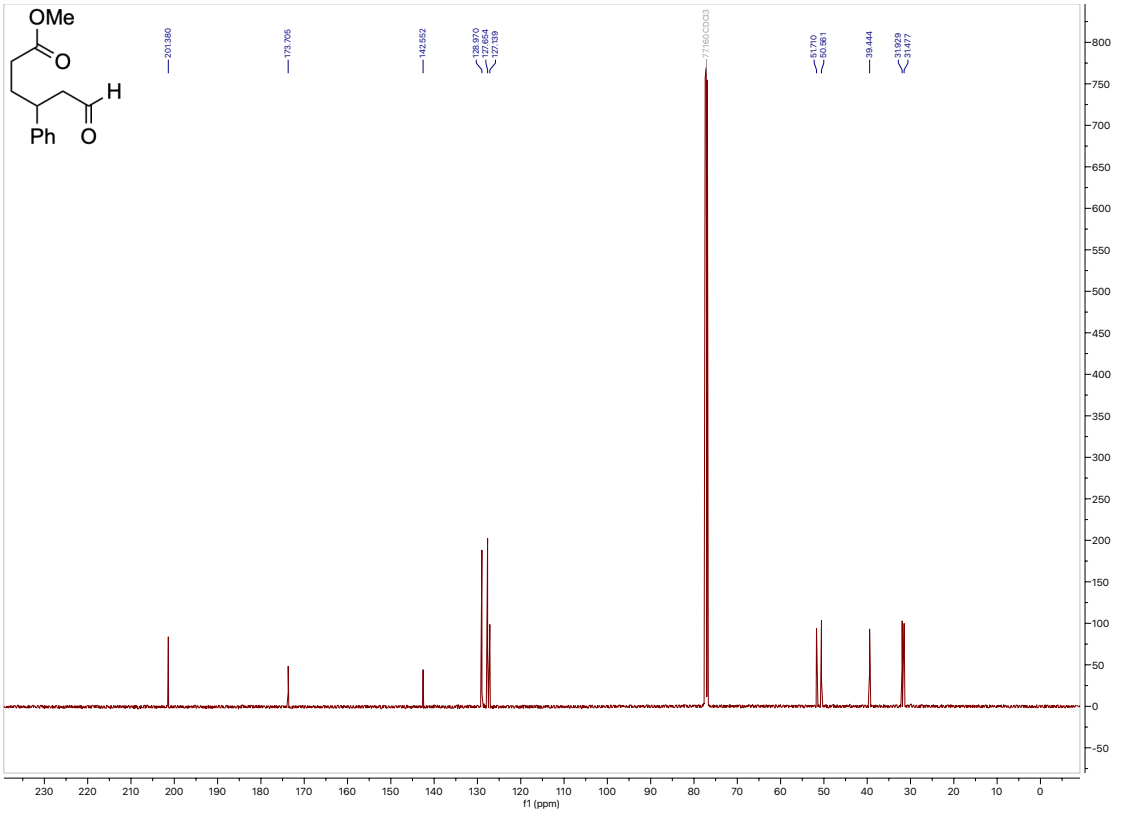
1D Selective Gradient NOESY at 2.05 ppm ($CDCl_3$) of **1b**

And **1D Selective Gradient NOESY** at 0.91 ppm ($CDCl_3$) of **1b**

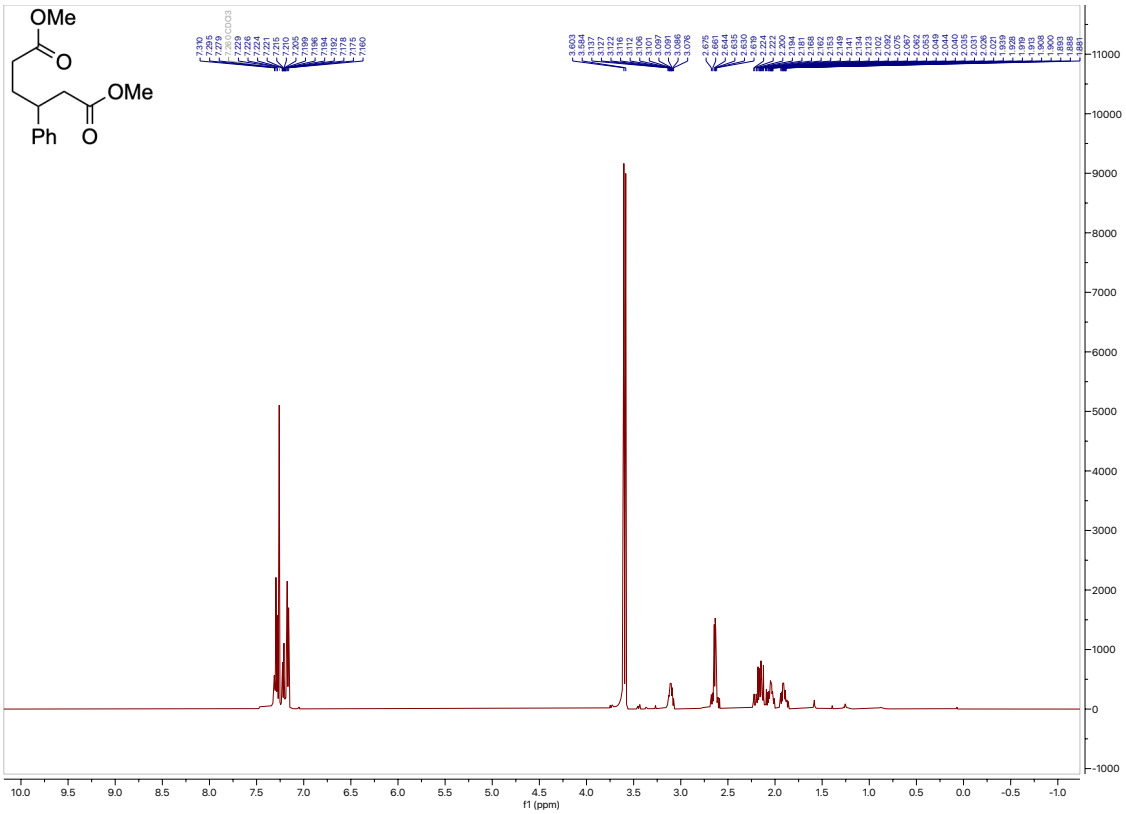


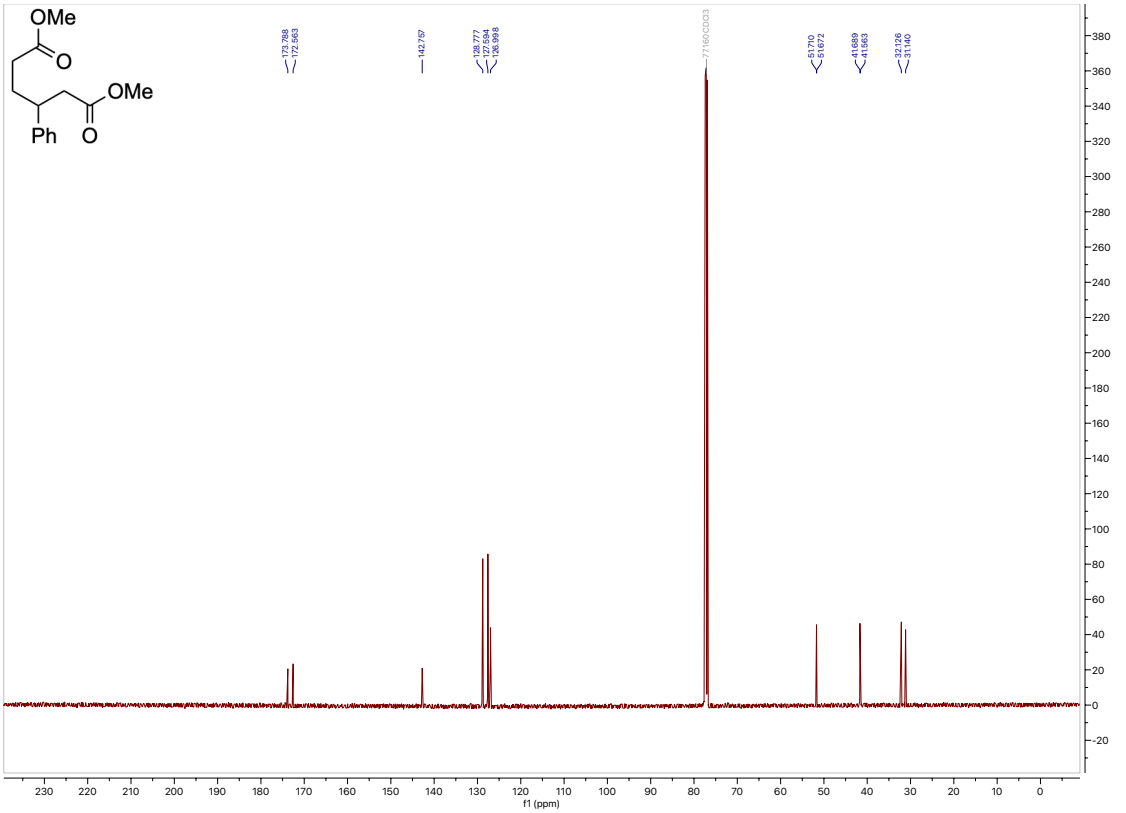
^{1}H NMR (600 MHz, $CDCl_3$) and **^{13}C NMR** (151 MHz, $CDCl_3$) of **1c**



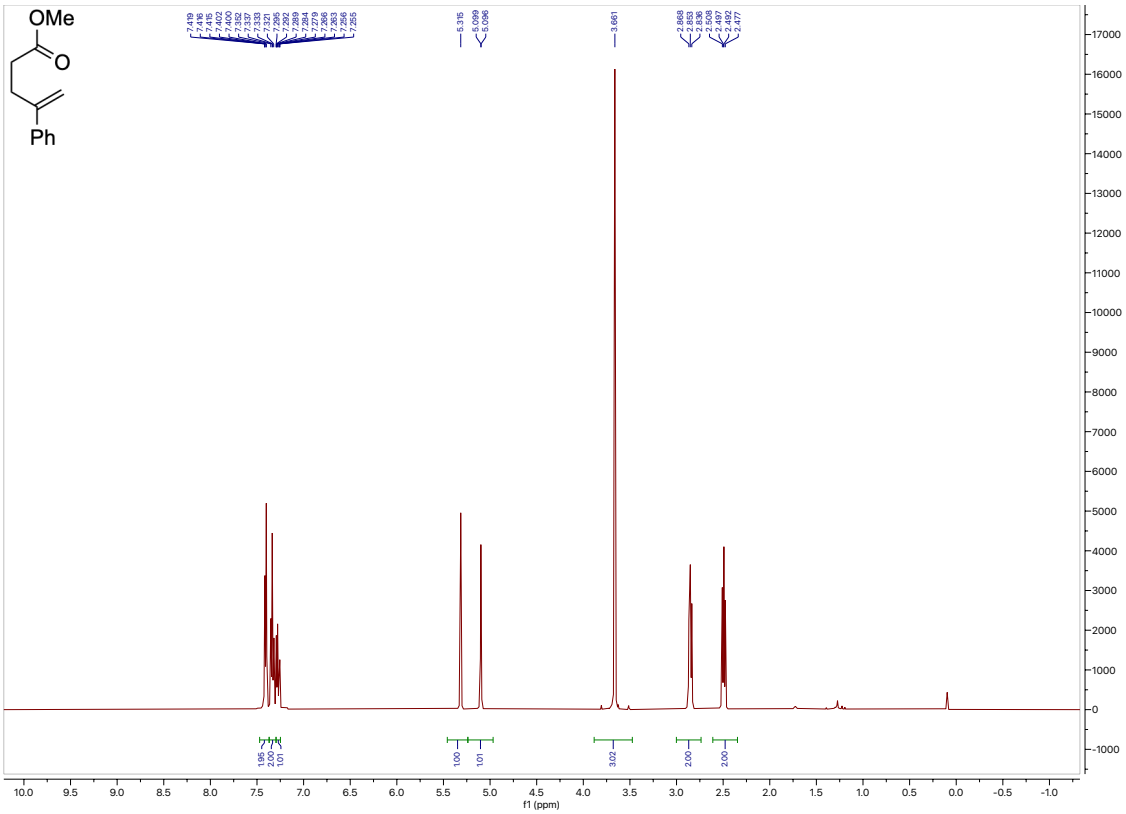


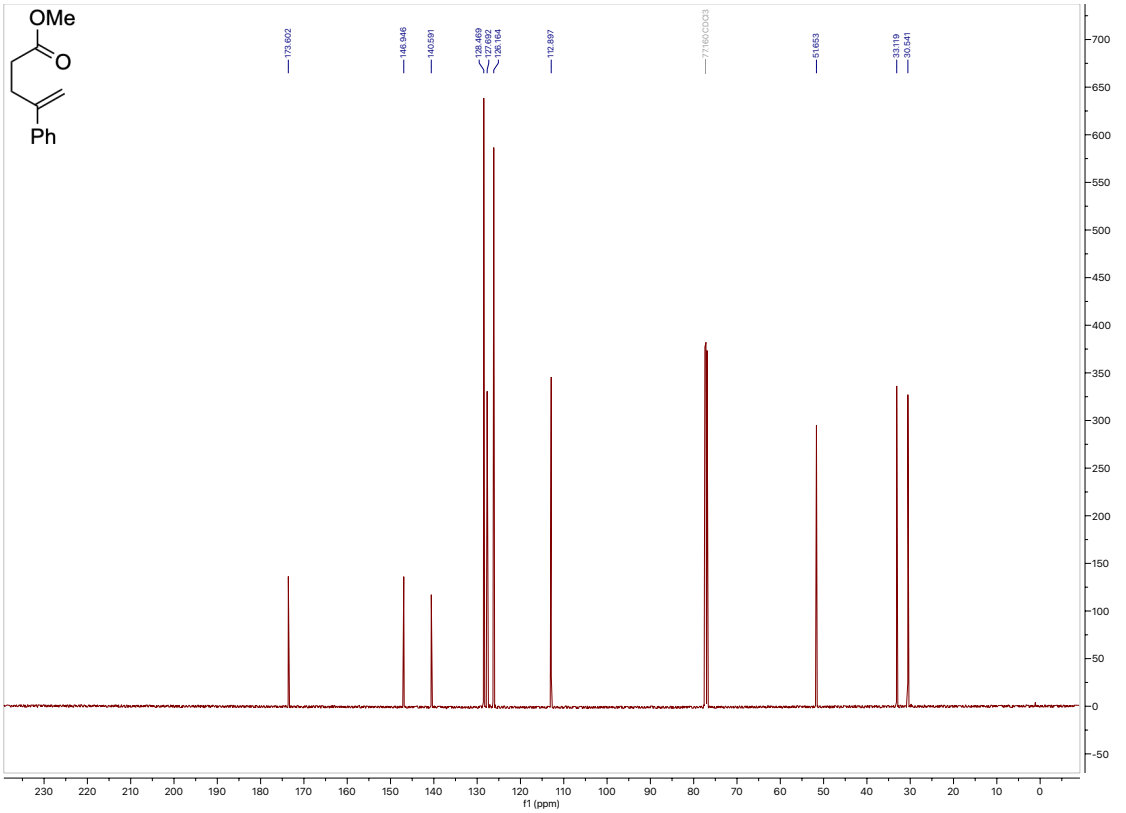
^{1}H NMR (500 MHz, $CDCl_3$) and **^{13}C NMR** (126 MHz, $CDCl_3$) of **2c**



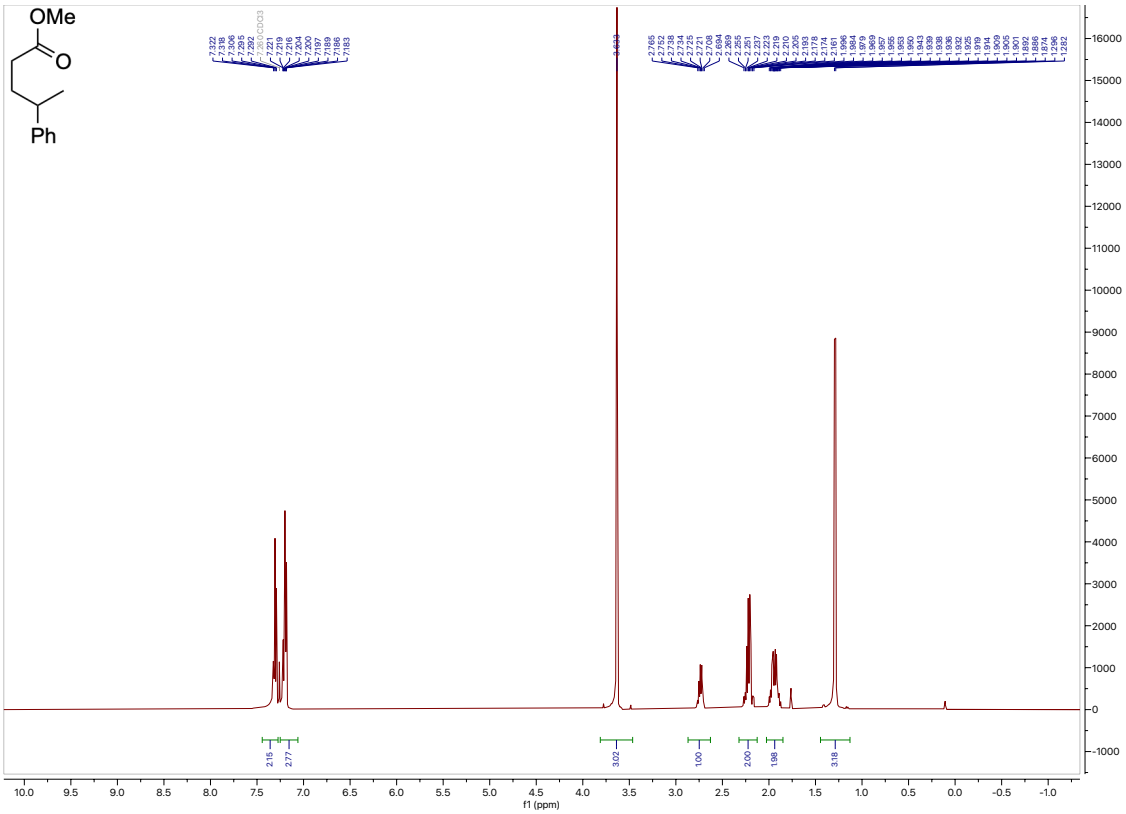


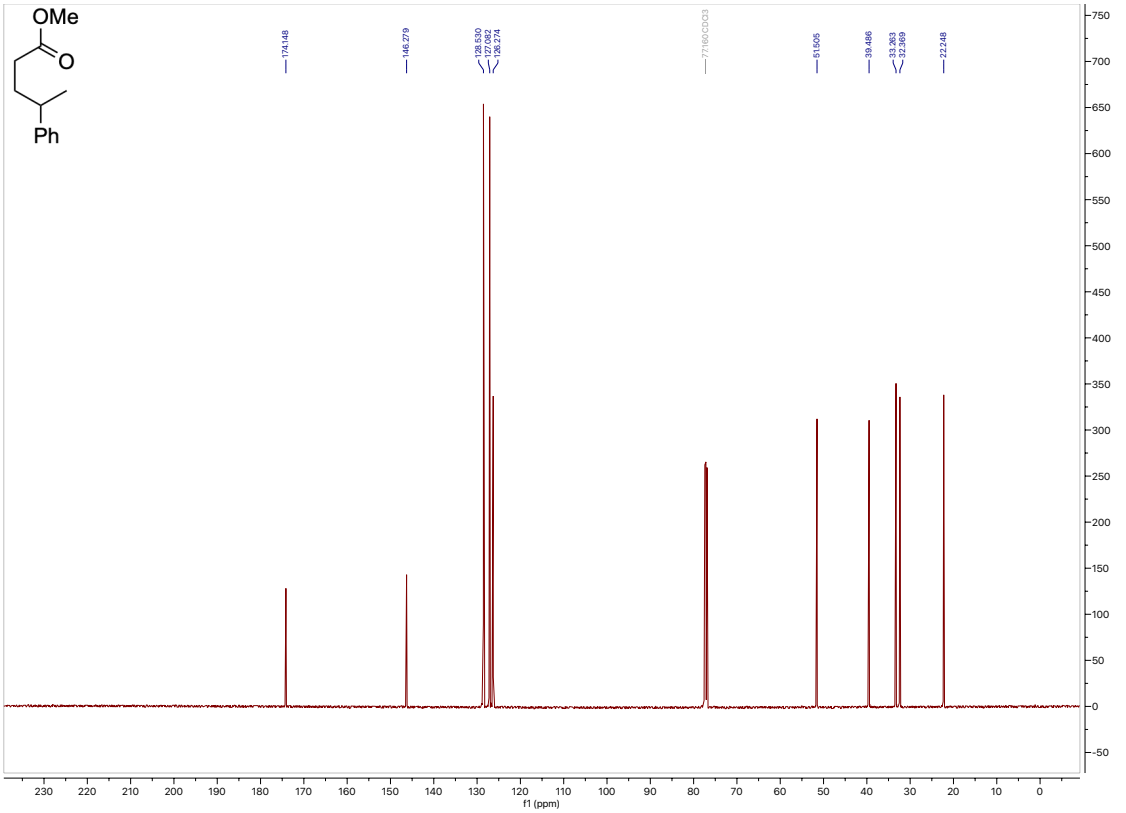
^{1}H NMR (500 MHz, $CDCl_3$) and **^{13}C NMR** (126 MHz, $CDCl_3$) of **2d**



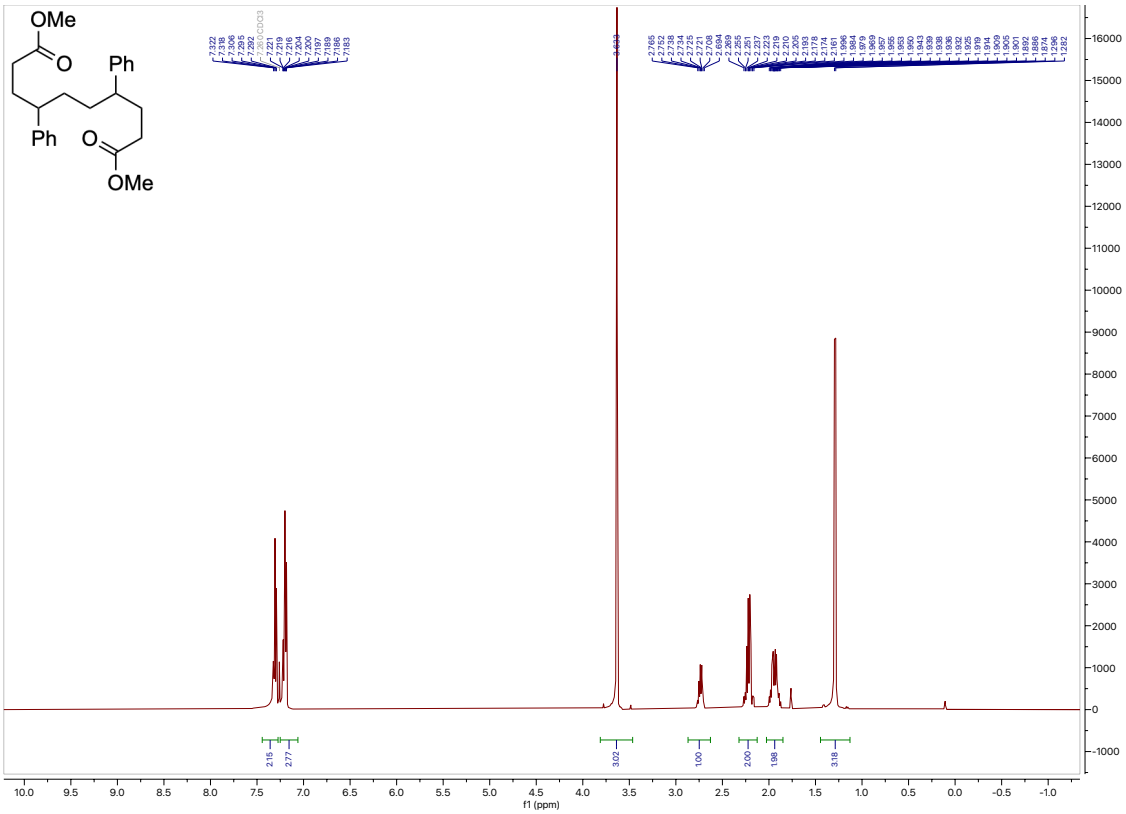


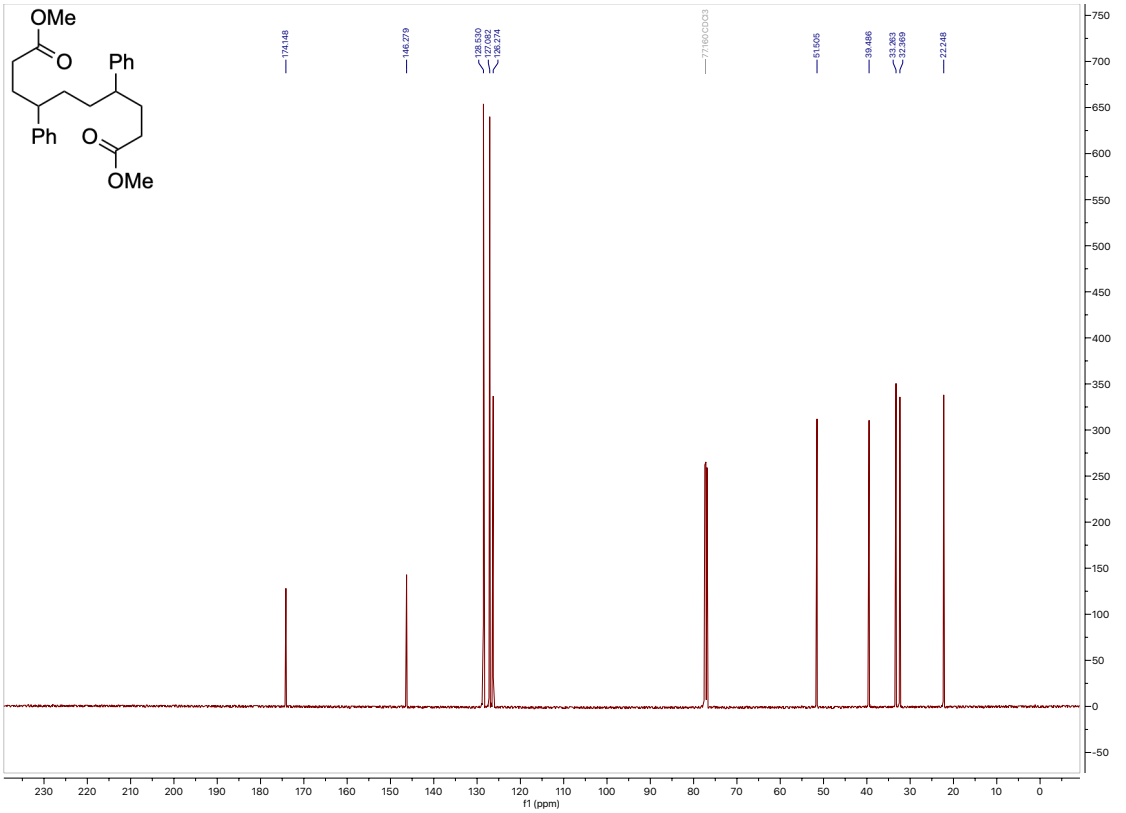
^{1}H NMB (500 MHz, $CDCl_3$) and **^{13}C NMR** (126 MHz, $CDCl_3$) of **2e**



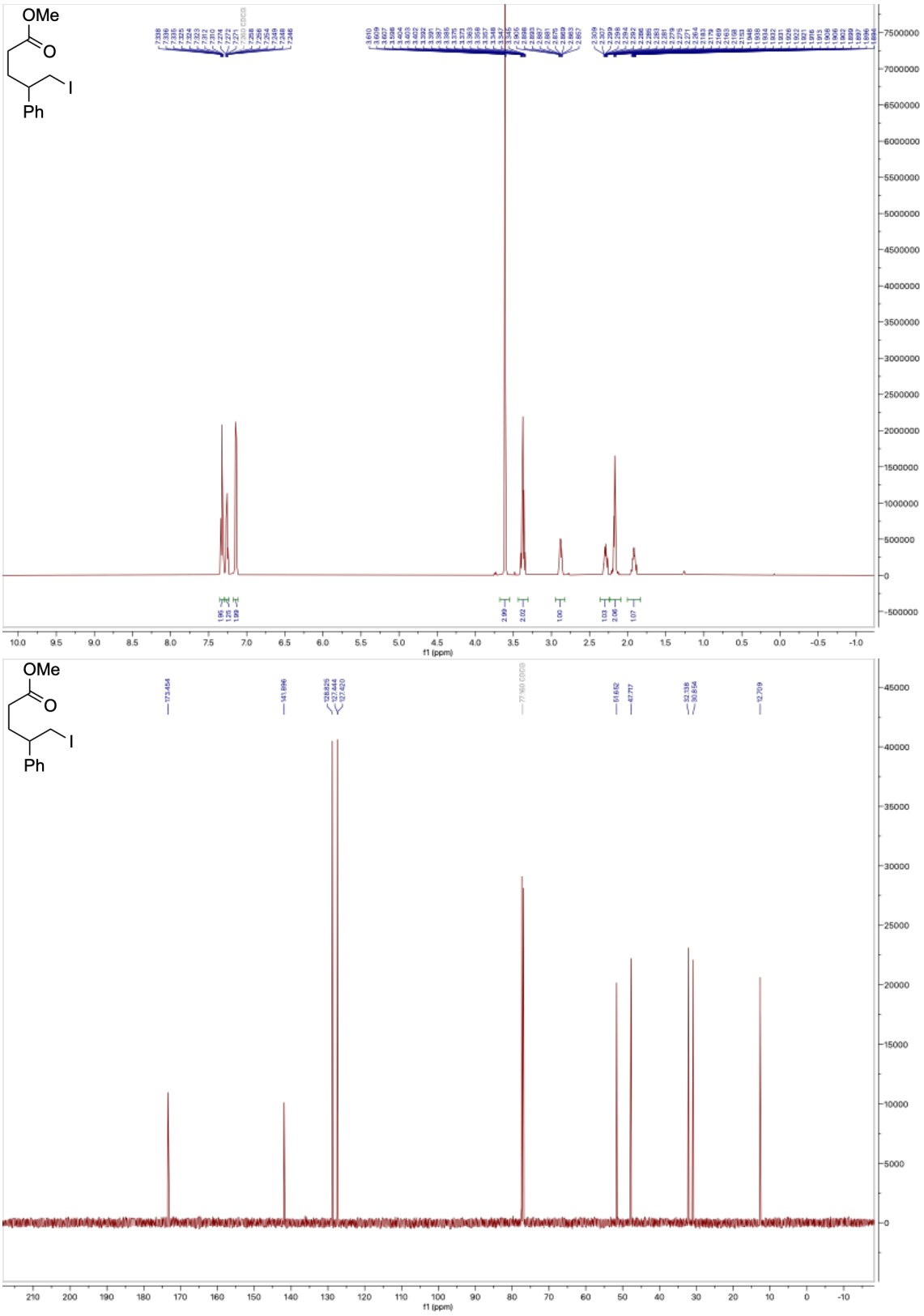


^{1}H NMB (500 MHz, $CDCl_3$) and **^{13}C NMR** (126 MHz, $CDCl_3$) of **2f**

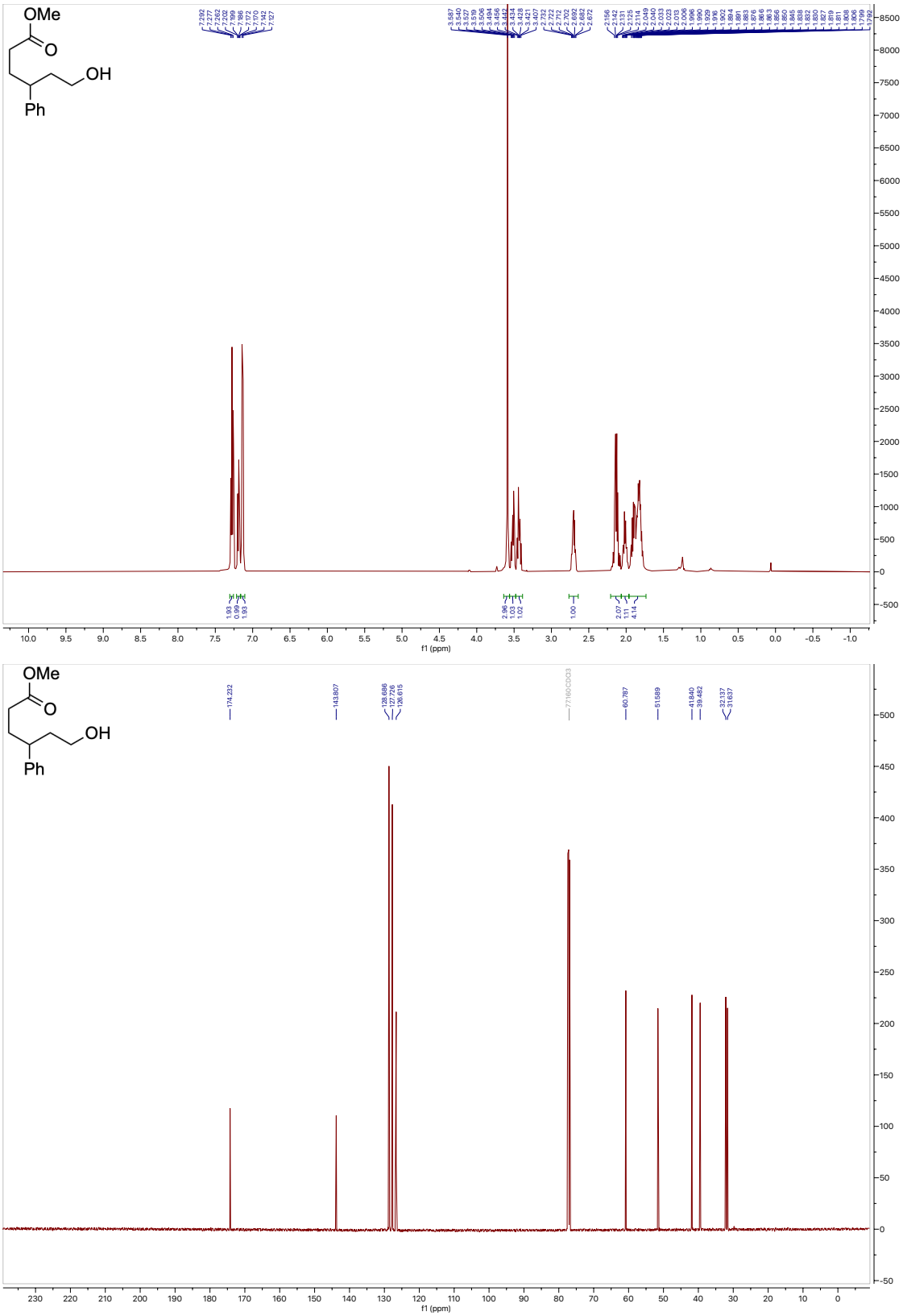




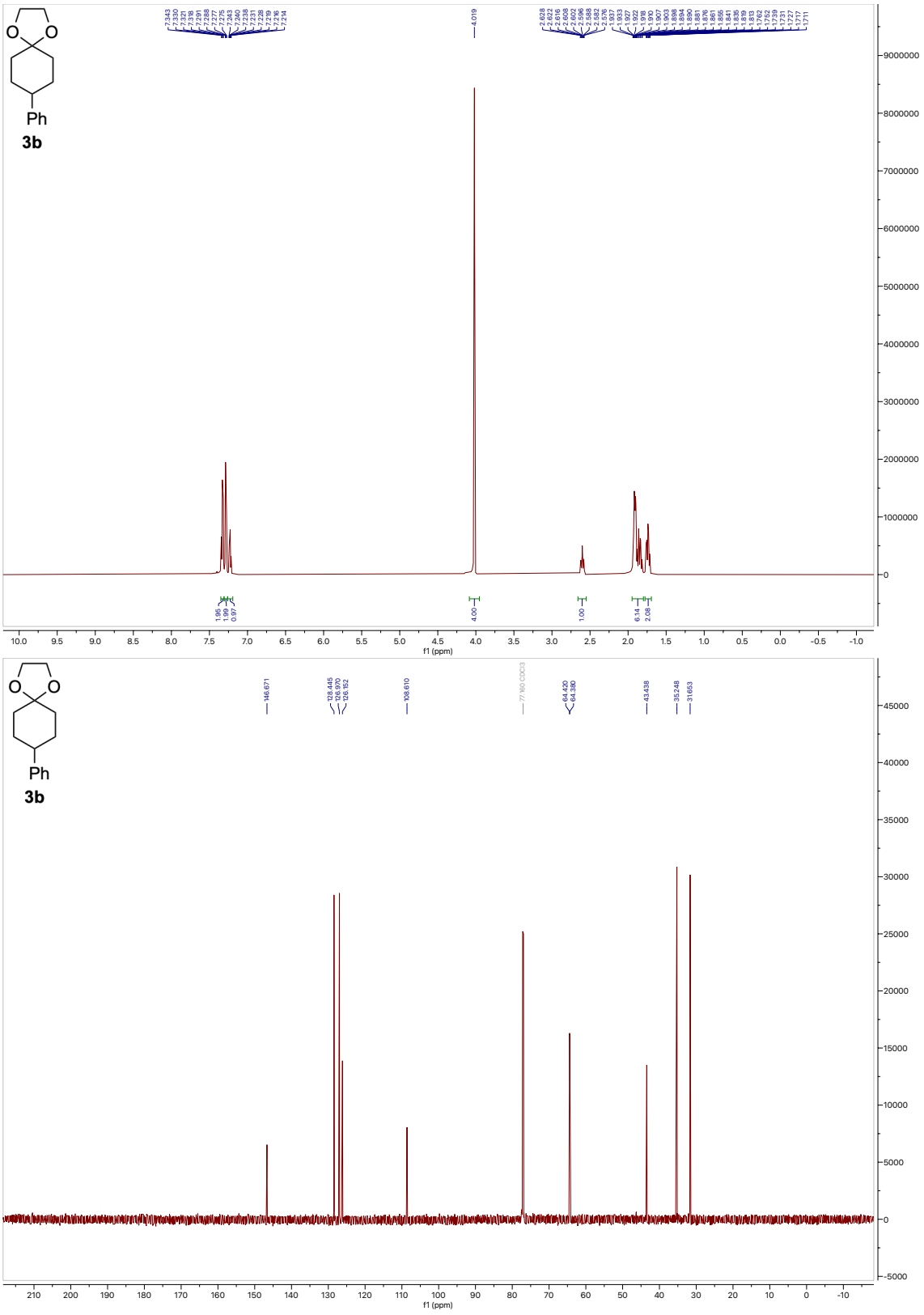
^{1}H NMB (500 MHz, $CDCl_3$) and **^{13}C NMR** (126 MHz, $CDCl_3$) of **2g**



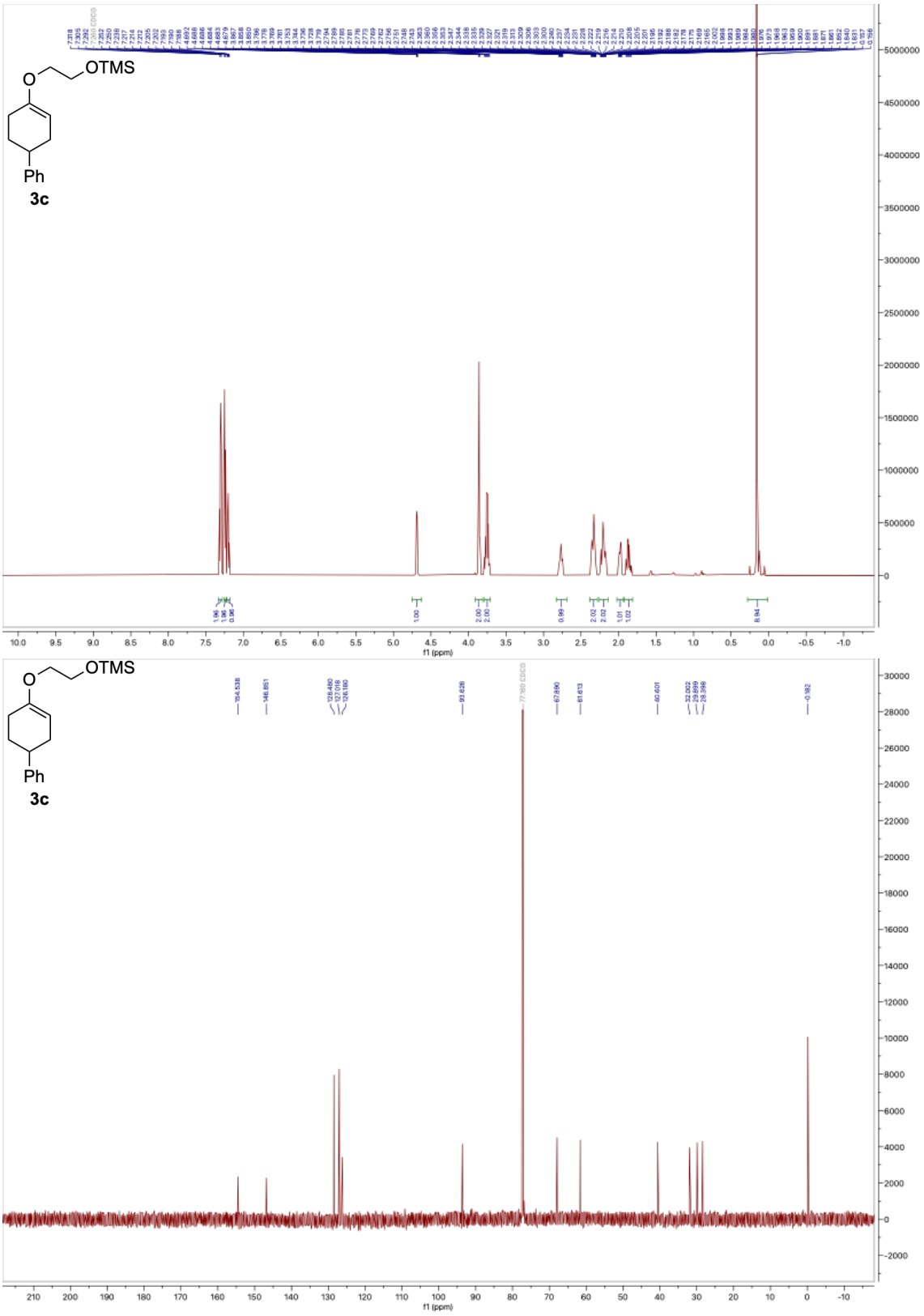
^{1}H NMR (600 MHz, $CDCl_3$) and **^{13}C NMR** (151 MHz, $CDCl_3$) of **2j**



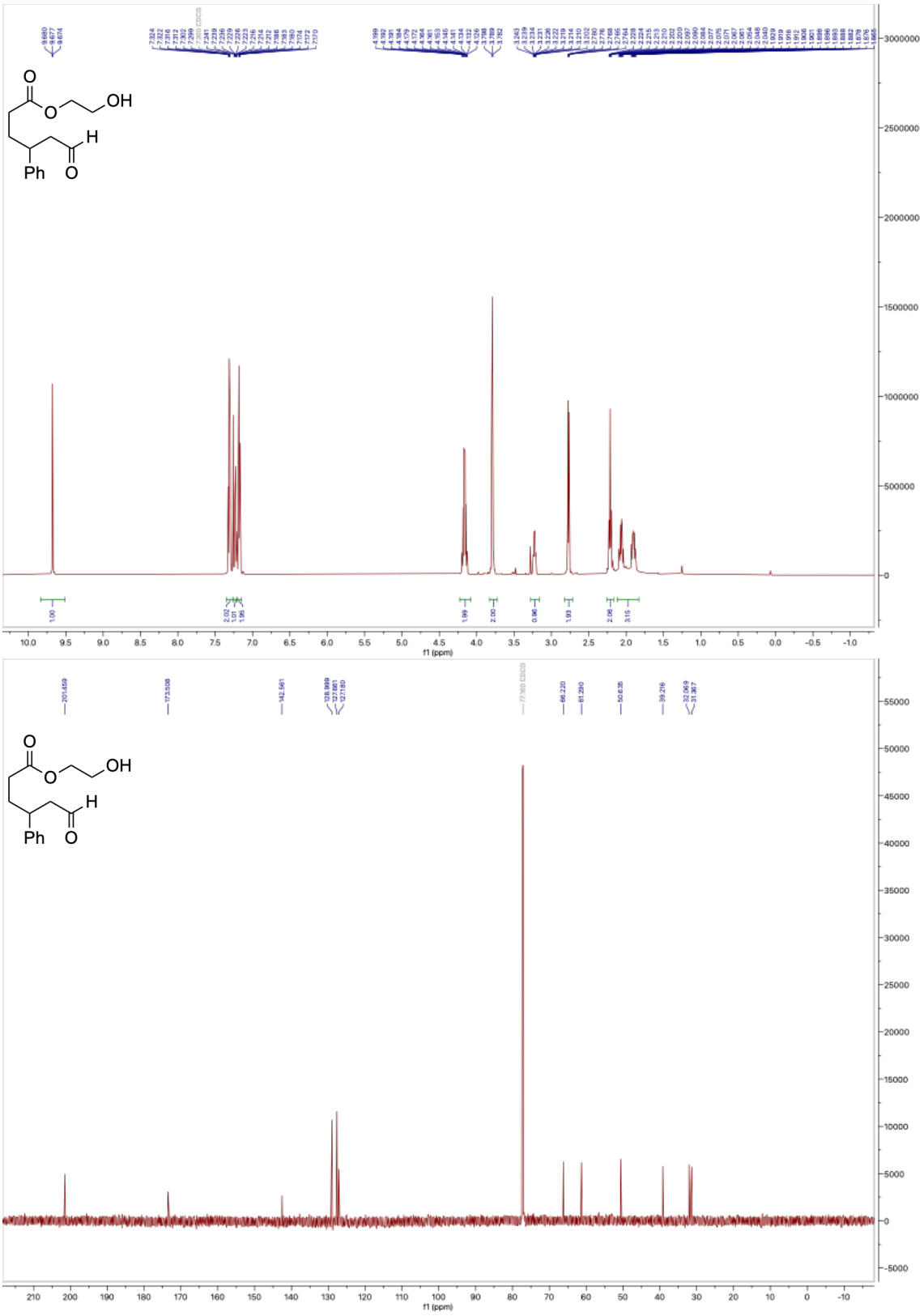
^{1}H NMR (500 MHz, $CDCl_3$) and **^{13}C NMR** (126 MHz, $CDCl_3$) of **2h**



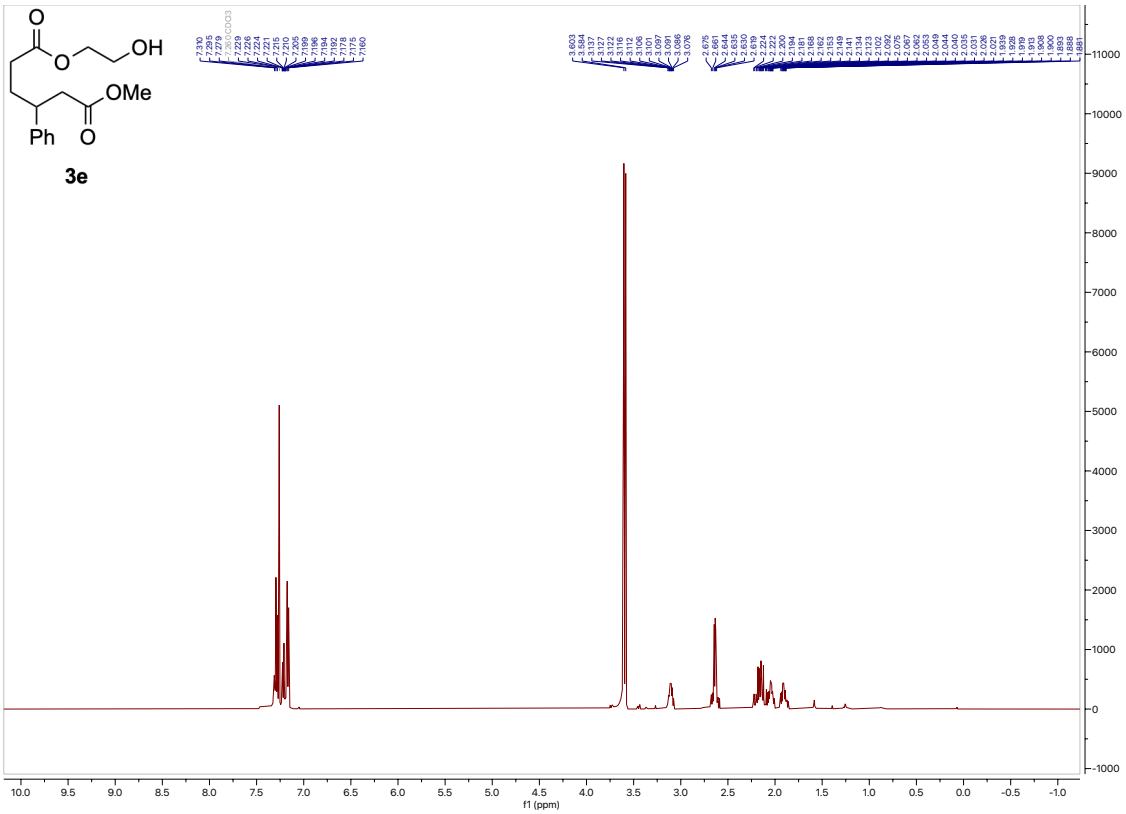
^{1}H NMR (400 MHz, $CDCl_3$) and **^{13}C NMR** (151 MHz, $CDCl_3$) of **3b**

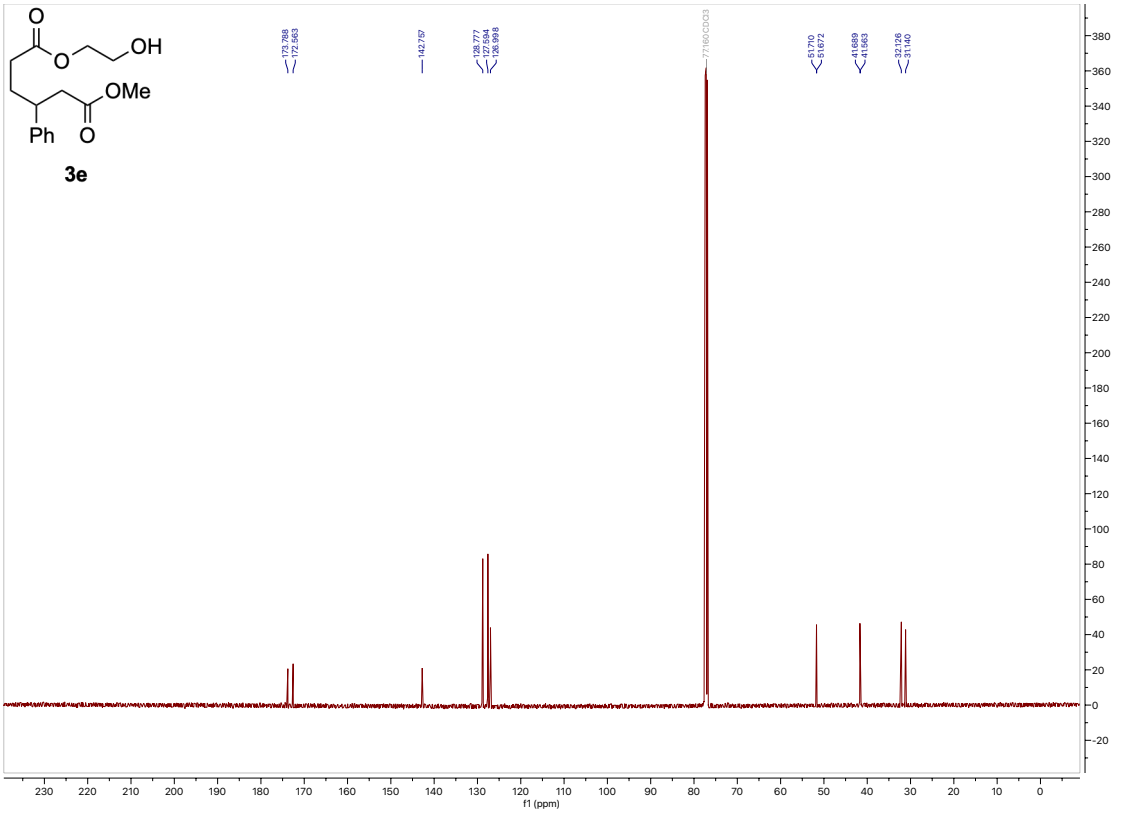


^{1}H NMR (600 MHz, $CDCl_3$) and **^{13}C NMR** (101 MHz, $CDCl_3$) of **3c**

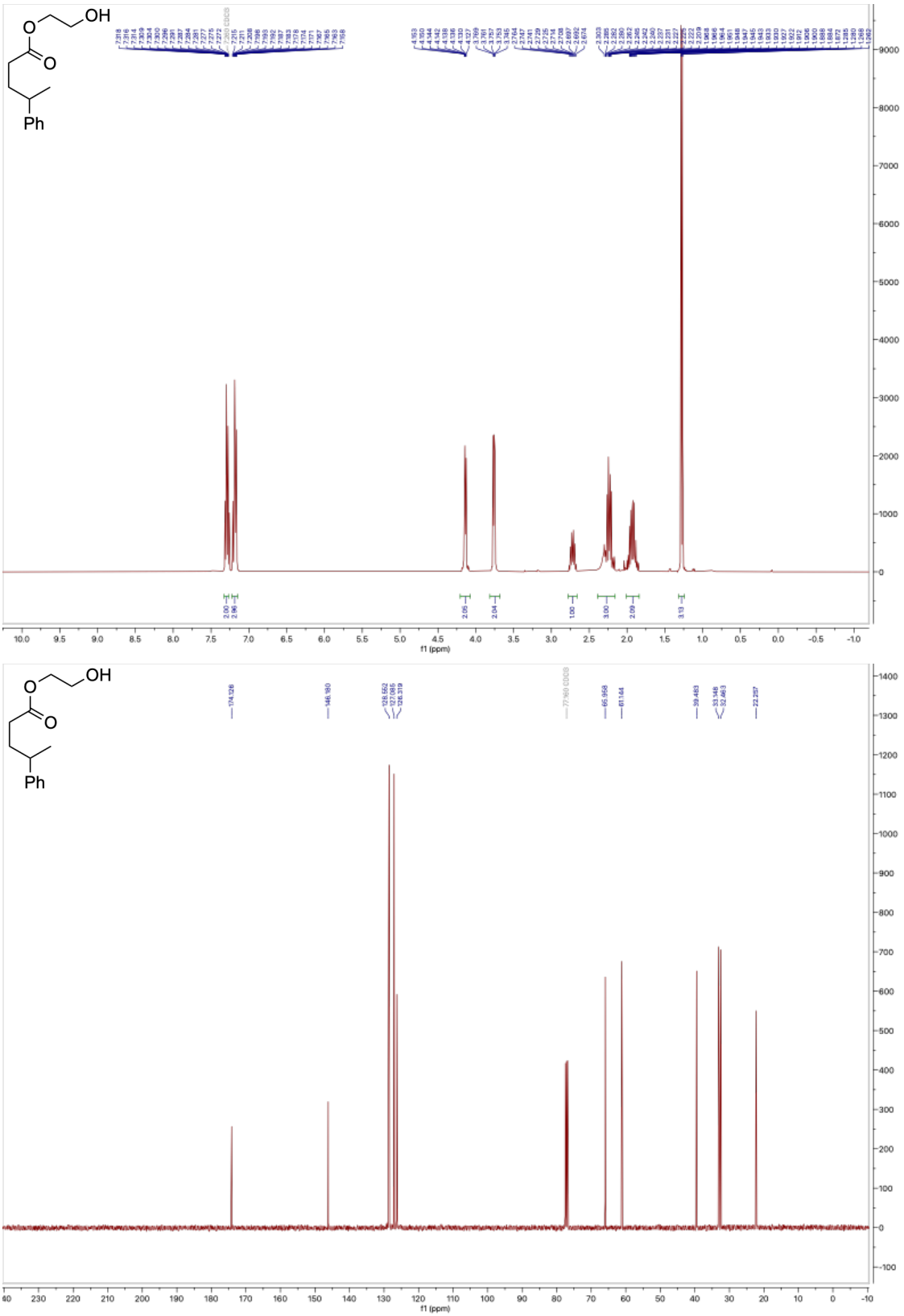


^{1}H NMR (600 MHz, $CDCl_3$) and **^{13}C NMR** (151 MHz, $CDCl_3$) of **3d**

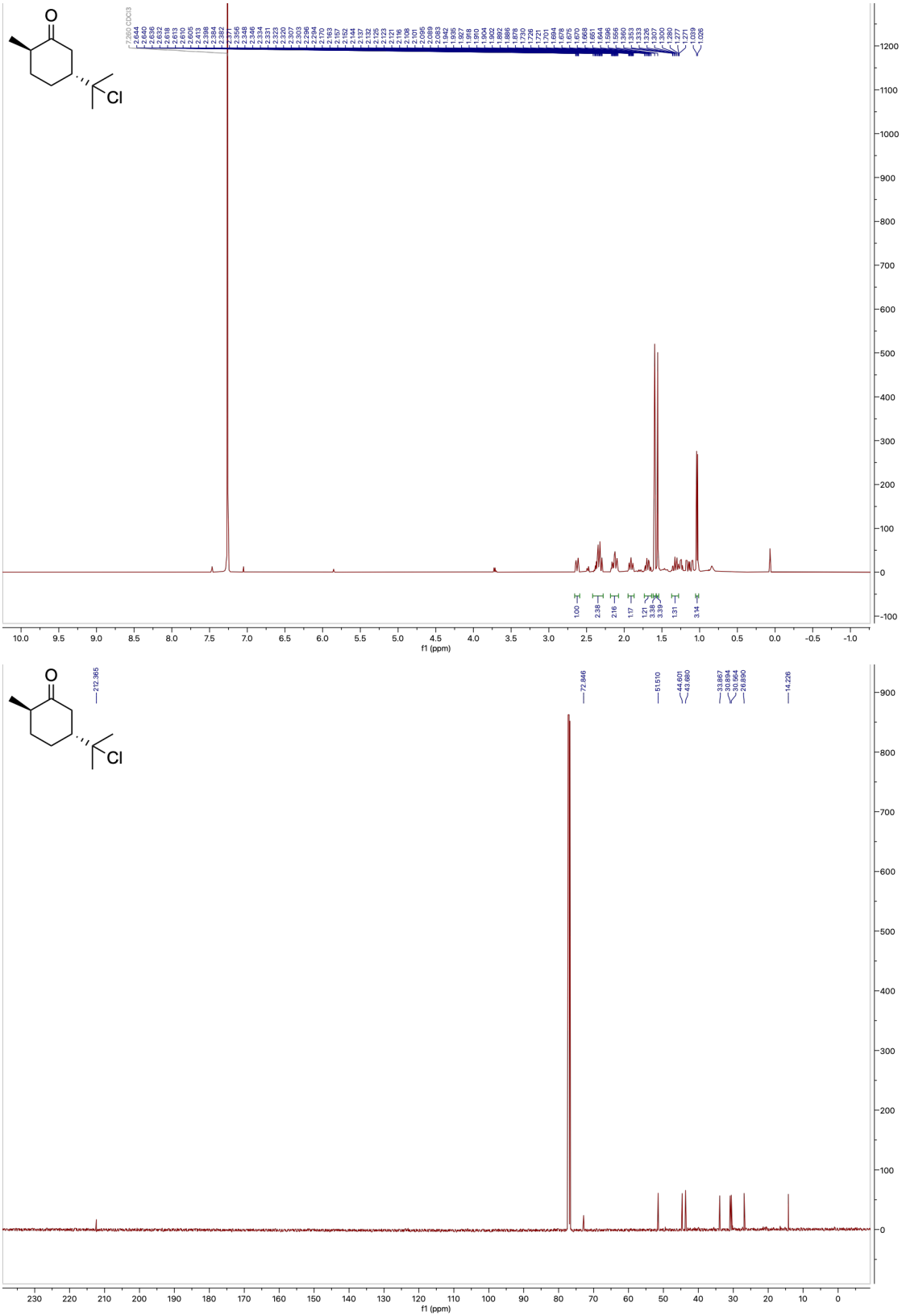




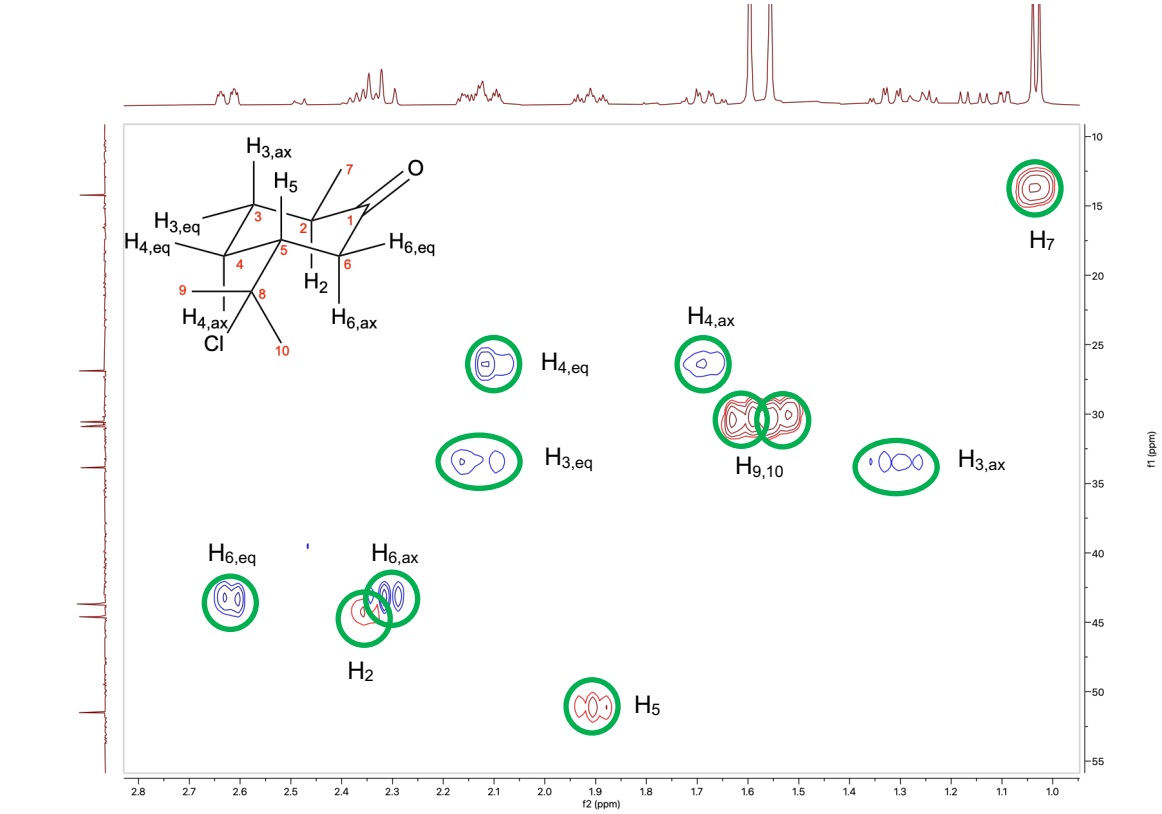
^{1}H NMR (500 MHz, $CDCl_3$) and **^{13}C NMR** (126 MHz, $CDCl_3$) of **3e**

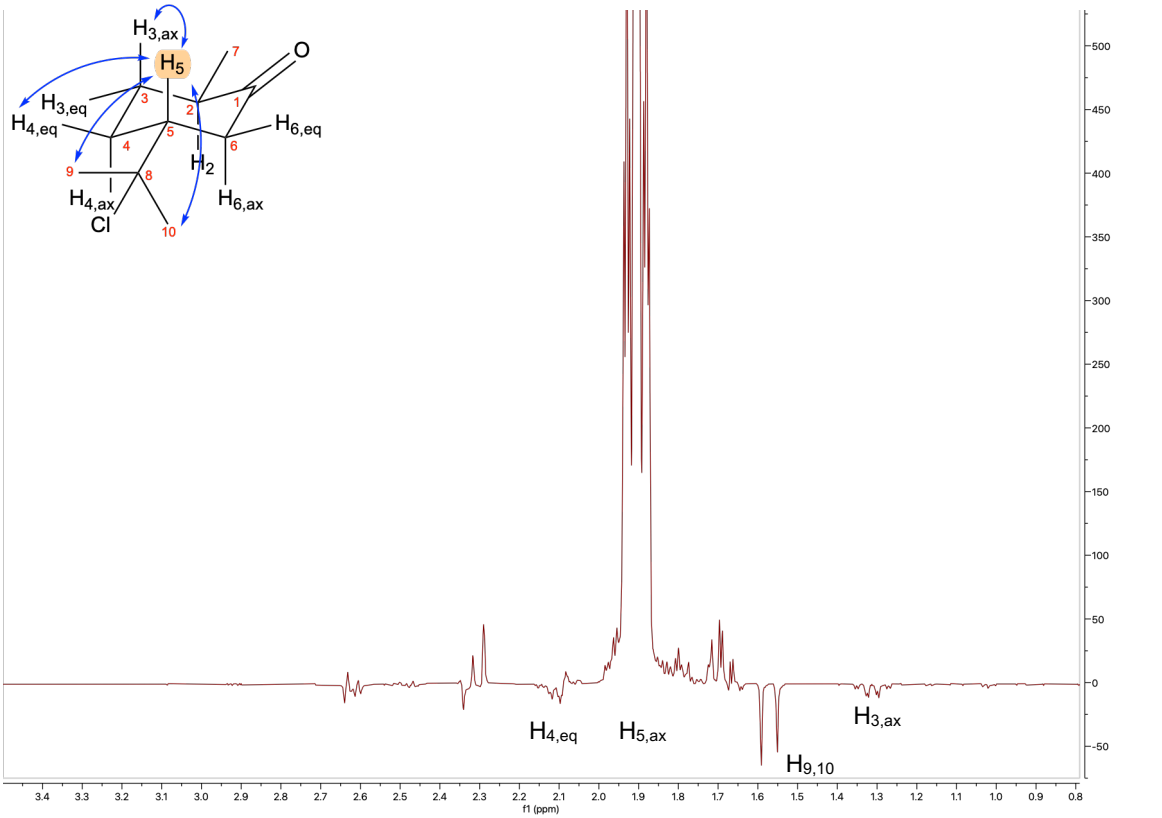


^{1}H NMR (400 MHz, $CDCl_3$) and **^{13}C NMR** (101 MHz, $CDCl_3$) of **3f**

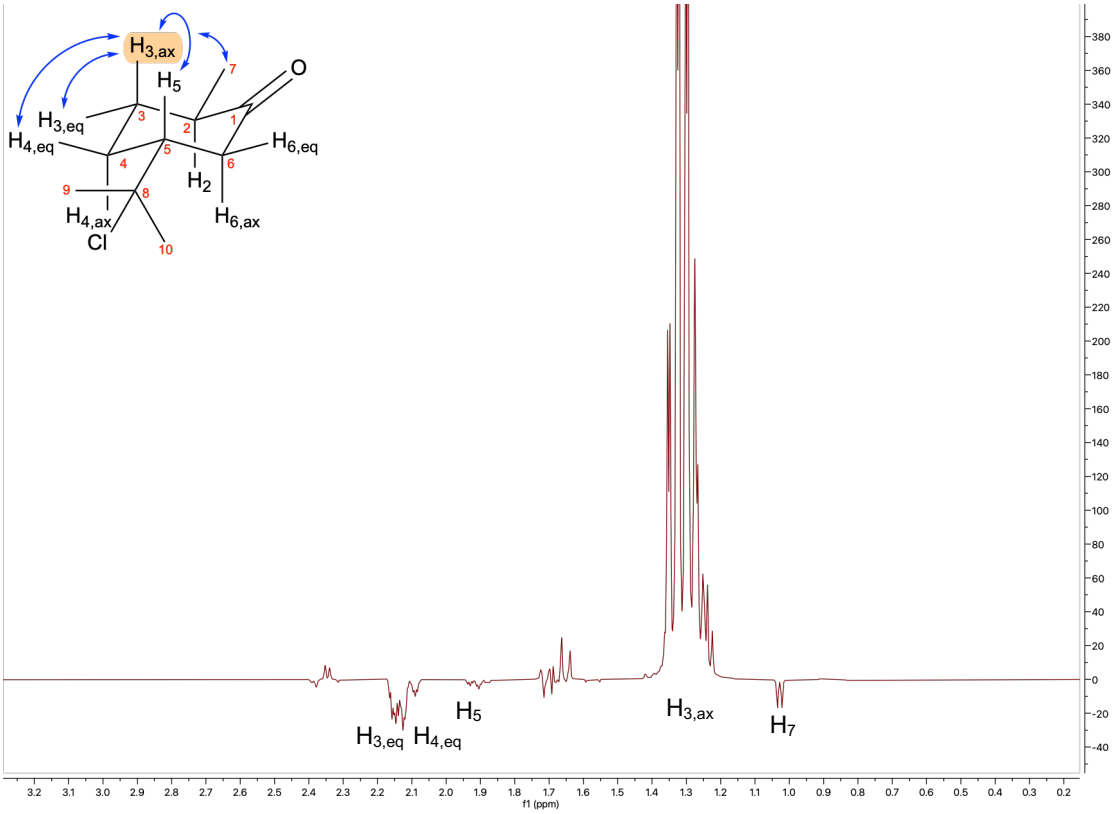


crude ^{1}H NMR (500 MHz, $CDCl_3$) and **crude ^{13}C NMR** (126 MHz, $CDCl_3$) of **5a**





crude HSQC ($CDCl_3$), **crude 1D Selective Gradient NOESY** ($CDCl_3$) at 1.935 ppm **5a**



crude 1D Selective Gradient NOESY ($CDCl_3$) at 1.350 ppm of **5a**

7.10 References

[1] Hui, C.; Craggs, L.; Antonchick, A. P. Ring Contraction in the Synthesis of Functionalized Carbocycles. *Chem. Soc. Rev.* **2022**, *51* (22), 8652–8675.

[2] Silva, L. F. Construction of Cyclopentyl Units by Ring Contraction Reactions. *Tetrahedron* **2002**, *58* (45), 9137–9161.

[3] Clark, R. D.; Heathcock, C. H. Ozonization of Silyloxyalkenes. *Tetrahedron Lett.* **1974**, *15* (23), 2027–2030.

[4] Leitzke, A.; Flyunt, R.; Theruvathu, J. A.; von Sonntag, C. Ozonolysis of Vinyl Compounds, CH2=CH–X, in Aqueous Solution—The Chemistries of the Ensuing Formyl Compounds and Hydroperoxides. *Org. Biomol. Chem.* **2003**, *1* (6), 1012–1019.

[5] (a) Daneshfar, O.; Newman, S. G. Esters as Viable Acyl Cross-Coupling Electrophiles. In *Amide Bond Activation*; Szostak, M., Ed.; CRC Press: Boca Raton, FL, 2022; pp 403–451. (b) Boit, T. B.; Bulger, A. S.; Dander, J. E.; Garg, N. K. Activation of C–O and C–N Bonds Using Non-Precious-Metal Catalysis. *ACS Catal.* **2020**, *10* (20), 12109–12126.

[6] Ling, L.; Chen, C.; Luo, M.; Zeng, X. Chromium-Catalyzed Activation of Acyl C–O Bonds with Magnesium for Amidation of Esters with Nitroarenes. *Org. Lett.* **2019**, *21* (6), 1912–1916.

[7] Blangetti, M.; Rosso, H.; Prandi, C.; Deagostino, A.; Venturello, P. Suzuki-Miyaura Cross-Coupling in Acylation Reactions, Scope and Recent Developments. *Molecules* **2013**, *18* (1), 1188–1213.

[8] Zhao, C.; Jia, X.; Wang, X.; Gong, H. Ni-Catalyzed Reductive Coupling of Alkyl Acids with Unactivated Tertiary Alkyl and Glycosyl Halides. *J. Am. Chem. Soc.* **2014**, *136* (51), 17645–17651.

[9] Jiang, X.; Sheng, F.-T.; Zhang, Y.; Deng, G.; Zhu, S. Ligand Relay Catalysis Enables Asymmetric Migratory Reductive Acylation of Olefins or Alkyl Halides. *J. Am. Chem. Soc.* **2022**, *144* (47), 21448–21456.

[10] Ahmad, S. A. Z.; Jena, T. K.; Khan, F. A. Alkyl Enol Ethers: Development in Intermolecular Organic Transformation. *Chem. Asian J.* **2021**, *16* (13), 1685–1702.

[11] Flowers, R. A., II. Mechanistic Studies on the Roles of Cosolvents and Additives in Samarium(II)-Based Reductions. *Synlett* **2008**, *2008* (10), 1427–1439.

[12] Szostak, M.; Spain, M.; Procter, D. J. Determination of the Effective Redox Potentials of SmI2, SmBr2, SmCl2, and Their Complexes with Water by Reduction of Aromatic Hydrocarbons. Reduction of Anthracene and Stilbene by Samarium(II) Iodide–Water Complex. *J. Org. Chem.* **2014**, *79* (6), 2522–2537.

[13] Miller, R. S.; Sealy, J. M.; Shabangi, M.; Kuhlman, M. L.; Fuchs, J. R.; Flowers, R. A., II. Reactions of SmI2 with Alkyl Halides and Ketones: Inner-Sphere vs Outer-Sphere Electron Transfer in Reactions of Sm(II) Reductants. *J. Am. Chem. Soc.* **2000**, *122* (32), 7718–7722.

[14] Swain, M.; Bulger, T. B.; Kim, J.; Kwon, O. Dealkenylative Alkynylation Using Catalytic FeII and Vitamin C. *J. Am. Chem. Soc.* **2022**, *144* (32), 14828–14837.

[15] (a) Molander, G. A.; McKie, J. A. Samarium(II) Iodide Induced Sequential Intramolecular Nucleophilic Acyl Substitution and Stereospecific Intramolecular

Meerwein-Ponndorf-Verley Reduction/Oppenauer Oxidation. *J. Org. Chem.* **1993**, *58* (25), 7216–7227. (b) Molander, G. A.; McKie, J. A. Intramolecular Nucleophilic Acyl Substitution Reactions of Halo-Substituted Esters and Lactones. New Applications of Organosamarium Reagents. *J. Am. Chem. Soc.* **1993**, *115* (13), 5821–5822. (c) Molander, G. A.; Harris, C. R. Sequenced Reactions with Samarium(II) Iodide. Tandem Nucleophilic Acyl Substitution/Ketyl-Olefin Coupling Reactions. *J. Am. Chem. Soc.* **1996**, *118* (17), 4059–4071. (d) Machrouhi, F.; Hamann, B.; Namy, J.-L.; Kagan, H. B. Improved Reactivity of Diiodosamarium by Catalysis with Transition Metal Salts. *Synlett* **1996**, *1996* (07), 633–634. (e) Machrouhi, F.; Namy, J.-L.; Kagan, H. B. Nucleophilic Acylation of Esters by Acid Chlorides Mediated by Samarium Diiodide: Formation and Use of Samarium Enediolates. *Tetrahedron Lett.* **1997**, *38* (41), 7183–7186. (f) Molander, G. A.; Sono, M. Sequenced Reactions with Samarium(II) Iodide. Intermolecular Ketyl-Olefin Coupling / Intramolecular Nucleophilic Acyl Substitution for the Preparation of Six-, Seven-, and Eight-Membered Carbocycles. *Tetrahedron* **1998**, *54* (32), 9289–9302. (g) Molander, G. A.; Alonso-Alija, C. Sequenced Reactions with Samarium(II) Iodide. Sequential Intermolecular Carbonyl Addition/Intramolecular Nucleophilic Acyl Substitution for the Preparation of Seven-, Eight-, and Nine-Membered Carbocycles. *J. Org. Chem.* **1998**, *63* (13), 4366–4373. (h) Molander, G. A.; Machrouhi, F. Sequenced Reactions with Samarium(II) Iodide. A Complementary Annulation Process Providing Access to Seven-, Eight-, and Nine-Membered Carbocycles. *J. Org. Chem.* **1999**, *64* (11), 4119–4123. (i) Machrouhi, F.; Namy, J.-L. Samarium Diiodide/Nickel Diiodide an Efficient System for Homo and Heterocoupling Reactions of Imines. *Tetrahedron Lett.* **1999**, *40* (7), 1315–1318. (j) Kawamura, K.; Hinou, H.; Matsuo, G.; Nakata, T. Efficient Strategy for

Convergent Synthesis of *trans*-Fused Polycyclic Ethers Based on an Intramolecular SmI2-Promoted Cyclization of Iodo Ester. *Tetrahedron Lett.* **2003**, *44* (28), 5259–5261.

[16] Cabrera, A.; Salmón, M.; Rosas, N.; Pérez-Flores, J.; Velasco, L.; Espinosa-Pérez, G.; Arias, J. L. Characterization of a Novel [Sm(HMPA)4I2]I Complex by Positive Ion Fast Atom Bombardment and High Resolution Mass Spectrometry. *Polyhedron* **1998**, *17* (2–3), 193–197.

[17] Wayner, D. D. M.; Houmam, A. Redox Potentials of Free Radicals. *Acta Chem. Scand.* **1998**, *52* (4), 377–384.

[18] Wang, X.; Andrews, L.; Fang, Z.; Thanthiriwatte, K. S.; Chen, M.; Dixon, D. A. Properties of Lanthanide Hydroxide Molecules Produced in Reactions of Lanthanide Atoms with H2O2 and H2 + O2 Mixtures: Roles of the +I, +II, +III, and +IV Oxidation States. *J. Phys. Chem. A* **2017**, *121* (8), 1779–1796.

[19] (a) Johnson, C. R.; Senanayake, C. H. Polyhydroxylated Seven-Membered Chiral Building Blocks. Asymmetric Synthesis of Compactin Analogues. *J. Org. Chem.* **1989**, *54* (3), 735–736. (b) Feldman, K. S.; Simpson, R. E. Stereochemical Studies on the Preparation and Subsequent Reductive Cleavage of 1,2-Dioxolanes. Application to the Synthesis of (±)-Yashabushitrol. *Tetrahedron Lett.* **1989**, *30* (50), 6985–6988.

[20] Posner, G. H.; Oh, C. H. A Regiospecifically Oxygen-18 Labeled 1,2,4-Trioxane: A Simple Chemical Model System to Probe the Mechanism(s) for the Antimalarial Activity of Artemisinin (Qinghaosu). *J. Am. Chem. Soc.* **1992**, *114* (21), 8328–8330.

[21] Flowers, R. A., II; Prasad, E. Samarium(II) Based Reductants. In *Handbook on the Physics and Chemistry of Rare Earths*; Gschneidner, K. A., Jr., Bünzli, J.-C. G., Pecharsky, V. K., Eds.; Elsevier: Amsterdam, 2006; Vol. 36, Chapter 230, pp 393–473.

[22] Prasad, E.; Flowers, R. A., II. Reduction of Ketones and Alkyl Iodides by SmI2 and Sm(II)-HMPA Complexes. Rate and Mechanistic Studies. *J. Am. Chem. Soc.* **2002**, *124* (24), 6895–6899.

[23] Enemaerke, R. J.; Daasbjerg, K.; Skrydstrup, T. Is Samarium an Inner or Outer Sphere Electron Donating Reagent? *Chem. Commun.* **1999**, *1999* (4), 343–344.

[24] Curran, D. P.; Fevig, T. L.; Jasperse, C. P.; Totleben, M. J. New Mechanistic Insights into Reductions of Halides and Radicals with Samarium(II) Iodide. *Synlett* **1992**, *1992* (12), 943–961.

[25] Vanysek, P. Electrochemical Series. In *CRC Handbook of Chemistry and Physics*, 92nd ed.; Haynes, W. M., Ed.; CRC Press: Boca Raton, FL, 2011; pp 80–89.

[26] Haynes, W. M. Abundance of Elements in the Earth's Crust and in the Sea. In *CRC Handbook of Chemistry and Physics*, 97th ed.; Haynes, W. M., Ed.; CRC Press: Boca Raton, FL, 2016; pp 14–17.

[27] (a) Flowers, R. A., II. Mechanistic Studies on the Roles of Cosolvents and Additives in Samarium(II)-Based Reductions. *Synlett* **2008**, *2008* (10), 1427–1439. (b) Choquette, K. A.; Sadasivam, D. V.; Flowers, R. A., II. Catalytic Ni(II) in Reactions of SmI2: Sm(II)- or Ni(0)-Based Chemistry? *J. Am. Chem. Soc.* **2011**, *133* (28), 10655–10661. (c) Chciuk, T. V.; Anderson, W. R.; Flowers, R. A., II. Preparation and Use of Samarium Diiodide (SmI_2) in Organic Synthesis: The Mechanistic Role of HMPA and Ni(II) Salts in the Samarium Barbier Reaction. *J. Vis. Exp.* **2013**, *2013* (72), e4323.

[28] Crossley, S. W. M.; Obradors, C.; Martinez, R. M.; Shenvi, R. A. Mn-, Fe-, and Co-Catalyzed Radical Hydrofunctionalizations of Olefins. *Chem. Rev.* **2016**, *116* (15), 8912–9000.

[29] (a) Lo, J. C.; Kim, D.; Pan, C.-M.; Edwards, J. T.; Yabe, Y.; Gui, J.; Qin, T.; Gutiérrez, O.; Giacoboni, J.; Smith, M. W.; Holland, P. L.; Shackeldeer, M. N.; Radical, N. D.; Olefin, F. Iron–Nickel Dual Catalysis: A New Engine for Olefin Functionalization and the Formation of Quaternary Centers. *J. Am. Chem. Soc.* **2018**, *140* (36), 11317–11324. (b) Shevick, S. L.; Obradors, C.; Shenvi, R. A. Mechanistic Interrogation of Co/Ni-Dual Catalyzed Hydroarylation. *J. Am. Chem. Soc.* **2018**, *140* (38), 12056–12068.

[30] He, Z.; Moreno, J. A.; Swain, M.; Wu, J.; Kwon, O. Aminodealkenylation: Ozonolysis and Copper Catalysis Convert C(sp3)–C(sp2) Bonds to C(sp3)–N Bonds. *J. Am. Chem. Soc.* **2023**, *145* (16), 8761–8767.

[31] (a) Chen, L.; Yang, J.-C.; Xu, P.; Zhang, J.-J.; Duan, X.-H.; Guo, L.-N. Nickel-Catalyzed Suzuki Coupling of Cycloalkyl Silyl Peroxides with Boronic Acids. *J. Org. Chem.* **2020**, *85* (11), 7515–7525. (b) Tsuzuki, S.; Sakurai, S.; Matsumoto, A.; Kano, T.; Maruoka, K. Ni-Catalyzed C(sp2)–H Alkylation of *N*-Quinolylbenzamides Using Alkylsilyl Peroxides as Structurally Diverse Alkyl Sources. *Chem. Commun.* **2021**, *57* (64), 7942–7945. (c) Kharasch, M. S.; Pauson, P.; Nudenberg, W. The Chemistry of Hydroperoxides. XII. The Generation and Properties of Free RO_2• Radicals. *J. Org. Chem.* **1953**, *18* (3), 322–327. (d) Kharasch, M. S.; Fono, A. New Metal Salt-Induced Homolytic Reactions. I. A New Method of Introducing Peroxy Groups into Organic Molecules. *J. Org. Chem.* **1959**, *24* (1), 72–78. (e) Kharasch, M. S.; Fono, A. New Metal Salt-Induced Homolytic Reactions. II. Modification of Free Radical Reactions by Copper Salts. *J. Org. Chem.* **1959**, *24* (5), 606–1614.

[32] Dawson, G. A.; Spielvogel, E. H.; Diao, T. Nickel-Catalyzed Radical Mechanisms: Informing Cross-Coupling for Synthesizing Non-Canonical Biomolecules. *Acc. Chem. Res.* **2023**, *56* (24), 3640–3653.

[33] Hie, L.; Fine Nathel, N. F.; Hong, X.; Yang, Y.-F.; Houk, K. N.; Garg, N. K. Nickel-Catalyzed Activation of Acyl C−O Bonds of Methyl Esters. *Angew. Chem. Int. Ed.* **2016**, *55* (8), 2810–2814.

[34] (a) Amani, J.; Molander, G. A. Direct Conversion of Carboxylic Acids to Alkyl Ketones. *Org. Lett.* **2017**, *19* (13), 3612–3615. (b) Whyte, A.; Yoon, T. P. Selective Cross-Ketonization of Carboxylic Acids Enabled by Metallaphotoredox Catalysis. *Angew. Chem. Int. Ed.* **2022**, *61* (50), e202213739.

[35] Bunnelle, W. H. Preparation, Properties, and Reactions of Carbonyl Oxides. *Chem. Rev.* **1991**, *91* (3), 335–362.

[36] Miller, R. D.; McKean, D. R. A Facile Preparation of Methyl Enol Ethers from Acetals and Ketals Using Trimethylsilyl Iodide. *Tetrahedron Lett.* **1982**, *23* (3), 323–326.

[37] Gassman, P. G.; Burns, S. J.; Pfister, K. B. Synthesis of Cyclic and Acyclic Enol Ethers (Vinyl Ethers). *J. Org. Chem.* **1993**, *58* (6), 1449–1457.

[38] Prout, E. S.; Kwon, O.; Silva, T. G. Regioselective Synthesis of Methyl Enol Ethers from Cycloalkanones via *O*-Methylation of Kinetic Enolates. *Synthesis* **2026**, *58* (10), 1527–1538.

[39] Smaligo, A. J.; Swain, M.; Quintana, J. C.; Tan, M. F.; Kim, D. A.; Kwon, O. Hydrodealkenylative C(sp^3)–C(sp^2) Bond Fragmentation. *Science* **2019**, *364*, 681–685.

[40] Chciuk, T. V.; Anderson, W. R., Jr.; Flowers, R. A., II. Proton-Coupled Electron Transfer in the Reduction of Carbonyls by Samarium Diiodide–Water Complexes. *J. Am. Chem. Soc.* **2016**, *138* (28), 8738–8741.

[41] Dworkin, J. H.; Dehnert, B. W.; Kwon, O. When All C–C Breaks LO–Ose. *Trends Chem.* **2023**, *5* (3), 174–200.

[42] Dehnert, B. W.; Yin, Y.; Kwon, O. Halodealkenylation: Ozonolysis and Catalytic Fe[II] with Vitamin C Convert C(sp^3)–C(sp^2) Bonds to C(sp^3)–Halide Bonds. *Org. Lett.* **2024**, *26* (50), 10921–10927.

[43] Szostak, M.; Spain, M.; Procter, D. J. Selective Synthesis of 3-Hydroxy Acids from Meldrum's Acids Using SmI2-H2O. *Nat. Protoc.* **2012**, *7* (5), 970–977.

[44] Szostak, M.; Spain, M.; Procter, D. J. Preparation of Samarium(II) Iodide: Quantitative Evaluation of the Effect of Water, Oxygen, and Peroxide Content, Preparative Methods, and the Activation of Samarium Metal. *J. Org. Chem.* **2012**, *77* (7), 3049–3059.

[45] Dahlén, A.; Hilmersson, G. Microwave-Assisted Generation of Lanthanide(II) Halides in THF and Simple Quantitative Determination. *Eur. J. Inorg. Chem.* **2004**, *2004* (15), 3020–3024.

[46] Schneider, D. F.; Viljoen, M. S. Stereoselective Synthesis of (*6R*)- and (*6S*)-Diosphenol and Ψ-Diosphenol. *Tetrahedron* **2002**, *58* (26), 5307–5315.

[47] Colonge, J. Addition of Aromatic Compounds to Ethylenic Ketones. I. α-Ethylenic Ketones and Benzene, Toluene, and Anisole. *Bull. Soc. Chim. Fr.* **1949**, 177–185.

[48] Dworkin, J. H.; Chen, Z. M.; Cheasty, K. C.; Rubio, A. V.; Kwon, O. Hydrodealkenylated C(sp^3)–C(sp^2) Bond Fragmentation Using Isayama-Mukaiyama Peroxidation. *J. Am. Chem. Soc.* **2025**, *147* (23), 13531–13544.

[49] Dauben, W. G.; Shaffer, G. W.; Deviny, E. J. Photoisomerization of Conjugated Cyclopropyl Ketones. *J. Am. Chem. Soc.* **1970**, *92* (21), 6273–6281.

[50] Aoyama, Y.; Araki, Y.; Konoike, T. Stereoselective Total Synthesis of (–)-α-Eudesmol, a P/Q-Type Calcium Channel Blocker. *Synthesis* **2001**, *2001* (10), 1452–1456.

[51] Fürstner, A.; Hannen, P. Platinum- and Gold-Catalyzed Rearrangement Reactions of Propargyl Acetates: Total Syntheses of (–)-α-Cubebene, (–)-Cubebol, Sesquicarene and Related Terpenes. *Chem. Eur. J.* **2006**, *12* (11), 3006–3019.

[52] Matsumoto, A.; Shiozaki, Y.; Sakurai, S.; Maruoka, K. Synthesis of Functionalized Aliphatic Acid Esters via the Generation of Alkyl Radicals from Silylperoxyacetals. *Chem. Asian J.* **2021**, *16* (17), 2431–2434.

[53] Kurihara, M.; Hakamata, W. Convenient Preparation of Cyclic Acetals, Using Diols, TMS-Source, and a Catalytic Amount of TMSOTf. *J. Org. Chem.* **2002**, *68*, 3213–3415.

[54] Xu, W.; Zhong, W.; Yang, Q.; Kato, T.; Liu, Y.; Maruoka, K. *In-Situ*-generation of alkyl hydroperoxides and their subsequent copper-catalyzed functionalization with organosilicon compounds. *Tetrahedron Lett.* **2021**, *75*, 153144.

CHAPTER EIGHT

Ozonolysis of a C–C σ-Bond

Unpublished results to be submitted in collaboration with the K. N. Houk group as Dworkin, J. H.; Maertens, A. J.; Houk, K. N.; Kwon, O. The dissertation author originated the idea for the project, was the primary researcher of this manuscript, and conducted all experiments.

8.1 Abstract

Ozone is widely recognized for its ability to oxidatively cleave C=C double bonds. In contrast, C–C single bonds are conventionally viewed as unreactive towards ozone. In this study, we show that bicyclo[1.1.0]butane and bicyclo[2.1.0]pentane architectures diverge from this paradigm and undergo C–C single bond ozonolysis to yield 1,3- and 1,4-dicarbonyl products. These reactions were observed to occur with similar rates of ozonolysis to C=C double bonds. Instead of a classical pericyclic trajectory, DFT and multireference diradical calculations show that the reaction proceeds via a radical S_H2 mechanistic pathway to form an initial trioxidanyl diradical. The open-shell coordinate predicts two major pathways from this juncture, either the synthesis of a transient 1,2,3-trioxane intermediate that fragments via a formal [2+2+2] *retro*-cycloaddition, or the direct ejection of oxygen followed by β-scission. Overall, this transformation adds a new mode of reactivity to a two-century-old ozonolysis process.

8.2 Introduction

Ozone has been intensively studied since its discovery by Shöenbein in 1839 because the ozonolysis reaction is one of the most powerful and atom-economical oxidation methods [*1*]. It has been applied in countless syntheses to generate new carbonyls from alkene C=C double bonds, and within the last decade it has emerged as a cornerstone of the dealkenylation methodology [*2*].

The synthetic power of ozone is driven by its unique electronic structure that opens wide array of competing reaction pathways (Figure 8.1A). The most prevalent ozone reaction is the Creigee ozonolysis of alkenes which follows a triple pericyclic sequence of (3+2) cycloadditions to generate trioxolanes [*3*, *4*]. Not only does ozone possess a 4π-electron system that enables cycloadditions, but also the diradical character to promote potent one-electron oxidations. In the absence of alkenes, it acts as a radical oxidant by abstracting hydrogen atoms from alkanes to initiate oxidation to alcohols and carbonyls, whereas with alkynes, a stepwise radical addition leads to 1,2,3-trioxolenes [*5*–*9*]. Ozone also has a low energy LUMO that enables electrophilic reactivity. Soft nucleophiles, such as nitrogen, phosphorus, and sulfur are quickly oxidized by ozone through either one or two electron processes. With sterically hindered alkenes, dioxygen is extruded from ozone to form an epoxide through, what has been described to be a concerted “butterfly,” cheletropic transition state [*10*]. Similarly, with electron-rich aromatics, such as phenol, an electrophilic aromatic substitution pathway becomes operative, generating catechols, muconic acid, and quinones [*11*]. Finally, the presence of strong electrophiles generated from FSO_3H•SbF_6 ‘magic acid’ enable a rare nucleophilic addition of ozone to carbocations [*12*]. Each of these non-classical cases showcase the versatility of ozone to

engage in a variety of reaction mechanisms. Notably missing from this list is the direct insertion of ozone into C–C single bonds.

Highly strained bicyclo[*n*.1.0]alkane frameworks present a compelling frontier for ozone reactivity. The central linkages of these systems are formally σ-bonds, yet their immense geometric strain forces rehybridization to higher s-character, creating a pseudo-π-system with partial diradical character [*13*–*15*]. As a result, the strained C–C bonds in bicycloalkanes are increasingly leveraged for their distinct reactivity in organic synthesis [*14,16*]. Despite the thermodynamic driving force of strain release, literature precedents indicate that these bicyclic cores emerge unscathed after ozonation (Figure 8.1B). For example, when bicyclo[4.1.0]heptane (strain energy = 29.6 kcal/mol) is exposed to ozone the core remains unreactive [*13*]. Instead, ozone oxidizes peripheral C–H bonds to yield alcohols and ketones [*17*]. The same is true for bicyclo[3.1.0]hexanes (BCH, strain energy = 33.5 kcal/mol) [*13*]. In (+)-β-thujone, a naturally occurring BCH, the peripheral isopropyl group is oxidized to yield 7-hydroxy-β-thujone [*6*]. Even as ring size further contracts and strain energy massively increases [56.1 kcal/mol in the bicyclo[2.1.0]pentane (BCP) and 65.9 kcal/mol in the bicyclo[1.1.0]butane (BCB)], the core has been reported to remain intact after ozonation [*13,18*–*22*]. A boundary therefore emerges, where oxidizes C=C π-bonds or accessible C–H bonds but does not touch C–C single bonds. To challenge this paradigm, the insertion of aryl and carbonyl bridgehead substituents were envisioned to increase the diradical character of bicylco[*n*.1.0]alkanes to enable reactions with ozone (Figure 8.1C). Under this structural design, a transient bicyclic 1,2,3-trioxane intermediate would become accessible, adding to the 1,2,3-trioxolane and 1,2,3-trioxepane analogues

that have been previously realized in a flask [*23,24*]. Accessing this elusive six-membered heterocycle would expand the boundaries of classical ozone reactivity.

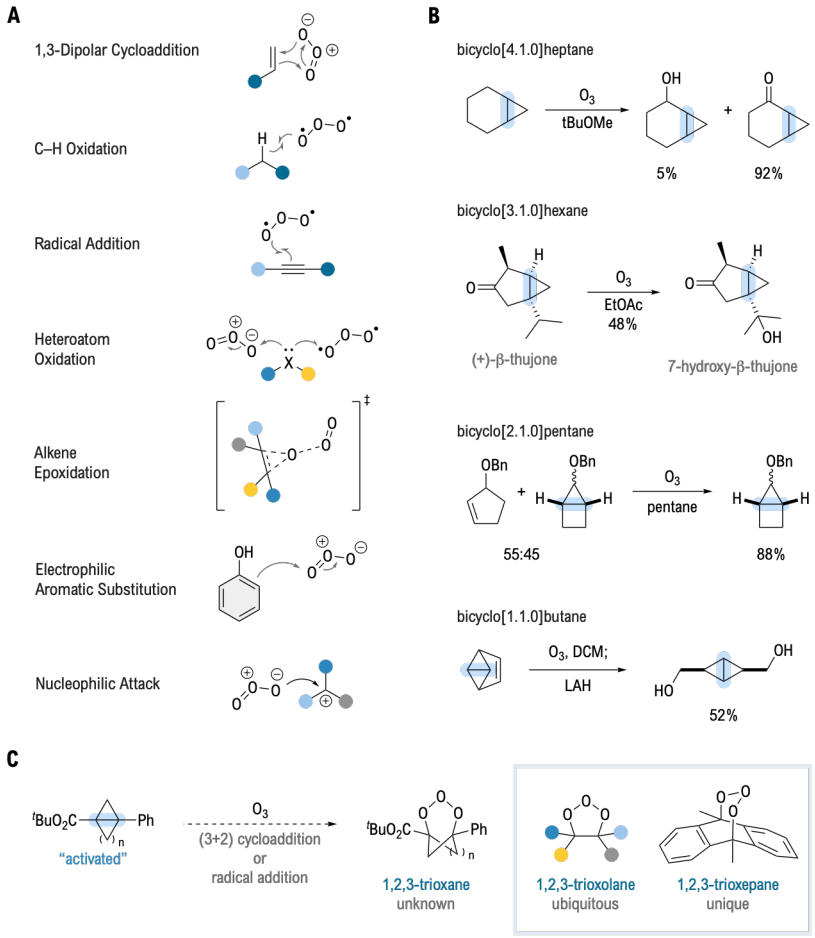


Figure 8.1 Introduction to Ozone

A. Mechanistic Paradigms of Ozone
B. Literature Examples of Bicyclo[*n*.1.0]alkanes Surviving Ozonolysis
C. This Work: 1,2,3-trioxanes by σ-bond ozonolysis

8.3 Experimental Results

To evaluate the synthetic profile and explore the structural boundaries of this novel transformation, we prepared a structurally unified series of bicyclo[*n*.1.0]alkanes (BCB **1**, BCP **2**, BCH **3**) possessing identical activating 1,3-disubstitution at the bridgehead positions: a *tert*-butyl ester and a phenyl ring (Figure 8.2A). Criegee ozonolysis of BCB **1** in methanol at –78 ºC followed by reductive work-up with triphenylphosphine (PPh_3) smoothly delivered a 1,3-dicarbonyl **4** in 83% isolated yield with the surprising loss of a carbon atom. Despite a decrease in strain energy, the reactivity was extendable to the BCP **2** and a 1,4-dicarbonyl **5** was accessed in 69% isolated yield, again with the loss of a carbon atom. Ozonation of BCH **3** resulted in no reaction, even when an extreme excess of ozone was delivered. To contextualize this non-classical reaction of ozone with σ-bonds against traditional π-bonds, we sought to establish the relative reaction rates of BCB **1** and BCP **2** with α-methylstyrene (AMS) and *tert*-butylacrylate (*t*BuA) by quantitative NMR(qNMR) analysis (Figure 8.2B, see the Supplementary Materials for more details). Amazingly, the rate of ozonolysis of the single bond of BCB **1** competed kinetically with C=C double bonds. We found that BCB **1** reacted slower than AMS but faster than *t*BuA, each by a factor of 3. BCP **2**, however, was significantly slower to react than either AMS (60-fold) or *t*BuA (20-fold). The lack of a reaction between ozone and BCH **3** as well as the decrease in rate for BCP **2** ozonolysis suggests the strain energy of the system is a requirement to promote the reaction.

To excise a carbon and yield the final dicarbonyl architectures we envisioned a two-part pathway (Figure 8.2C). First the generated 1,2,3-trioxane could undergo a formal $[\sigma 2_s+\sigma 2_s+\sigma 2_s]$ *retro*-cycloaddition, of which the only known $[\sigma 2_s+\sigma 2_s+\sigma 2_s]$ *retro*-

cycloadditions are restricted to tris-σ-homobenzenes—such as diademane, *cis*-benzene trioxide, and *cis*-triaza-tris-σ-homobenzene—and the thermal decomposition of Meldrum's acid [*25*–*28*]. This fragmentation would break apart the cyclobutene core to produce singlet dioxygen and an alkene **6** tethered to the first of the two carbonyls in the product. Then, standard Criegee ozonolysis and reduction of the newly formed alkene **6** would lead to the second observed carbonyl in the final product **4**.

To gather experimental support for our hypothesized cascade, we sought to characterize the reaction intermediates and products. Partial ozonolysis of BCB **1** (31% conversion) in deuterated methanol followed by quantitative NMR analysis revealed formation of the 1,3-dicarbonyl **4-*d*** (5%), an alkene **6** (6%), and a 1,2-dioxolane **7** (20%) (Figure 8.2D). Repeating the experiment with full conversion of BCB **1** indicated formation of the 1,3-dicarbonyl **4-*d*** (10%), the 1,2-dioxolane **7** (75%), and the open-chain deuteroperoxide **8** (13%). These findings support the formation of an intermediate alkene leading to the 1,3-dicarbonyl **4**, but experimental evidence for the presence of the 1,2,3-trioxane and the reality of a [$_{\sigma}2_s+_{\sigma}2_s+_{\sigma}2_s$] *retro*-cycloaddition remained elusive. Postulating the 1,2,3-trioxane may be stable at low temperatures, we attempted to reduce it to the corresponding 1,3-diol with isopropyl magnesium chloride at –130 ºC and –116 ºC [*29*]. However, even at these cryogenic temperatures, any transient intermediate of BCB **1** ozonolysis had completely fragmented prior to addition of the Grignard reagent. We then turned to density functional theory (DFT) calculations to investigate our mechanistic hypothesis and the possibility of the [$_{\sigma}2_s+_{\sigma}2_s+_{\sigma}2_s$] *retro*-cycloaddition.

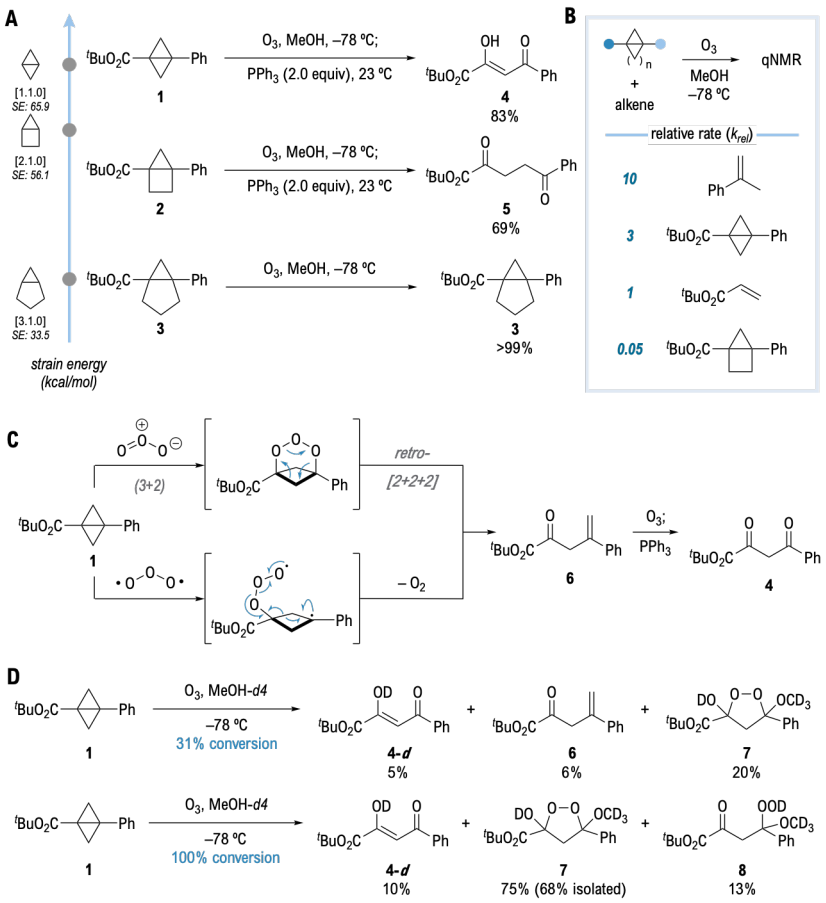


Figure 8.2 Experimental Results

(**A**) Bicyclo[*n*.1.0]alkane reactions with ozone. (**B**) Kinetic competition study. (**C**) Mechanistic options to explain the loss of a carbon. (**D**) Observations consistent with the intermediate alkene.

8.4 Computational Results

DFT calculations and multireference quantum chemical calculations were performed to interrogate the C–C single bond ozonolysis reaction mechanism and rationalize the observed reactivity trends (Figure 8.3). Computation revealed an entirely radical mechanism. The ozonolysis reaction of BCB **1** begins with an S_H2-like addition of ozone into the bridging σ-bond of **1**, rather than initiating with a synchronous, concerted (3+2) cycloaddition due to the sterically hindered convex face of **1**. This electrophilic radical mechanism, typically invoked for alkyne ozonolysis, is an underexplored mode of reactivity for ozone (*9*). Attack may occur at either the *tert*-butyl ester α-carbon (C_1) or the benzylic carbon (C_3) (**TS1** $\Delta G^{\ddagger}$ = 9.2 kcal/mol or **TS1'** $\Delta G^{\ddagger}$ = 11.7 kcal/mol) to form trioxidanyl diradical intermediates **1a** or **1a'**, respectively. The calculated low activation barrier is consistent with a rapid reaction of BCB **1** and ozone under the experimental conditions.

To unveil the fundamental electronic origins of this reactivity, we calculated the diradical character (y_0) of each reactant and the key transition states (**TS1**) via complete active space self-consistent field (CASSCF) calculations. The active space utilized for the CASSCF calculation for ozone was (8,5), for BCB 1 was (2,2) and for TS1 was (6,6). Diradical character is computed from the occupation number of the lowest unoccupied natural orbital (n_{LUNO}). Both BCB **1** and ozone show significant diradical character in the ground state at 4% and 36% respectively [*30,31*]. The diradical character of BCB **1** originates from the highly strained central σ-bond (~64 kcal/mol) which dramatically narrows the HOMO-LUMO gap, while the near degenerate π–π* gap in ozone **2** leads to its high diradical character [*30,31*]. Upon progression to the transition state (**TS1**) where

ozone reacts with the σ-bond, the diradical character climbs to 51%. Visualization of the spin density difference plot in the transition state highlights the evolution of the trioxidanyl radical along the reaction coordinate (Figure 8.3B, top). Ozone attack at C_1 is predicted to be more favorable ($\Delta\Delta G^{\ddagger}$ = 2.5 kcal/mol) due to the formation of the more stabilized tertiary benzylic radical in **1a**. From these diradical states, a barrierless radical recombination occurs to form the common 1,2,3-trioxane intermediate **1b**, the net transformation of which is a formal (3+2) cycloaddition.

For the final stage of ozonolysis, we considered the plausibility of a [$_{\sigma}2_s$+$_{\sigma}2_s$+$_{\sigma}2_s$] *retro*-cycloaddition from the 1,2,3-trioxane **1b**. The 1,2,3-trioxane fragmentation is predicted to occur through a stepwise, homolytic bond-cleavage cascade to achieve a formal *retro*-cycloaddition rather than a concerted pericyclic mechanism. The formal [$_{\sigma}2_s$+$_{\sigma}2_s$+$_{\sigma}2_s$] *retro*-cycloaddition is initiated by homolysis of a trioxane O–O σ-bond (**TS1b** $\Delta G^{\ddagger}$ = 15.0 kcal/mol or **TS1b'** $\Delta G^{\ddagger}$ = 15.6 kcal/mol) to form an alkoxyl-peroxyl diradical intermediate **1c** or **1c'**. From here, a cascade of low-barrier steps rapidly unfolds. First, β-scission of the alkoxyl radical (**TS1c** $\Delta G^{\ddagger}$ = 1.7 kcal/mol or **TS1c'** $\Delta G^{\ddagger}$ = 0.0 kcal/mol) cleaves a cyclobutane C–C bond to afford a carbon centered diradical **1d** or **1d'**. A second β-scission event from the alkyl radical (**TS1d** $\Delta G^{\ddagger}$ = 2.6 kcal/mol or **TS1d'** $\Delta G^{\ddagger}$ = 2.6 kcal/mol) then releases singlet molecular oxygen to afford the β,γ unsaturated ketone **6** or **6'**, respectively. Spin density difference plots of the three transition states along this formal [2+2+2] *retro*-cycloaddition show the sequential accumulation of radical character as each bond breaks in succession (Figure 8.3B, bottom). The result of this formal [$_{\sigma}2_s$+$_{\sigma}2_s$+$_{\sigma}2_s$] *retro*-cycloaddition is the spontaneous rearrangement of an *in situ*

generated 1,2,3-trioxane to realize the ozonolysis of a C–C σ-bond from a strained bicyclo[*n*.1.0]alkane.

To rule out a pericyclic mechanism, we probed whether the 1,2,3-trioxane **1b** could undergo a concerted, pericyclic [$_{\sigma}2_s+_{\sigma}2_s+_{\sigma}2_s$] *retro*-cycloaddition. While the transition states **TS1b′** and **TS1c′** were computationally located, both featuring simultaneous bond cleavage of all three σ-bonds through a chair-like geometry, they revealed a highly asynchronous trajectory (Figure 8.3C). In these geometries the C–C σ-bond is significantly distorted (2.16 Å or 2.17 Å), the O–O σ-bond is slightly elongated (2.01 Å or 1.96 Å), and the C–O σ-bond is minimally perturbed (1.55 Å or 1.52 Å). However, this concerted [$_{\sigma}2_s+_{\sigma}2_s+_{\sigma}2_s$] *retro*-cycloaddition mechanism was found to be kinetically infeasible under the reaction conditions with activation barriers reaching 43.2 kcal/mol and 48.0 kcal/mol, respectively.

Crucially, exploration of the potential energy landscape revealed a competitive, alternative mechanistic pathway that could preclude the formation of the 1,2,3-trioxane entirely. Diradicals **1a** or **1a'** could undergo direct O–O σ-bond homolysis (**TS1a'** $\Delta G^{\ddagger}$ = 0.5 kcal/mol or **TS1a"** $\Delta G^{\ddagger}$ = 0.9 kcal/mol) to eject molecular oxygen. The ensuing alkyl-alkoxyl diradical species rapidly rearranges to yield β,γ unsaturated ketones **6** or **6a**. Both mechanisms are predicted to be rapid at –78 ºC and afford the same products. However, recombination to form the 1,2,3-trioxane **1b** is favored kinetically and is thus proposed to be the major pathway. The low difference in activation barriers between the competing mechanisms indicates that, dynamically, the non-trioxane homolysis route may operate as an active, parallel contributor to the overall ozonolysis of BCB **1**.

Globally, both of these kinetically fast and highly exergonic mechanistic pathways are driven thermodynamically by strain release of the BCB and formation of C=C, C=O and O=O π-bonds. From the transient β,γ unsaturated ketone intermediates, a second equivalent of ozone initiates another ozonolysis reaction at the newly formed alkene via the classical Criegee mechanism (see Supplementary Materials for more details) and results in the experimentally observed diketone. The distinct kinetic and thermodynamic profile of this reaction highlights exactly why our system reacts selectively at the C–C σ-bond where historical literature precedents do not (Figure 8.1B). The 1,3-bridgehead di-substitution acts as a structural linchpin to stabilize radical nature of the transition states and intermediates at each junction of the cascade to cleanly enforce a productive σ-bond cleavage.

Finally, to confirm the generality of this mechanism, the ozonolysis of the less-strained BCP **2** was also explored computationally (Figure 8.3D). Mirroring the BCB system, ozonolysis begins with the S_H2 radical addition of ozone at C_1 or the benzylic carbon C_3 (**TS2** $\Delta G^{\ddagger}$ = 10.6 kcal/mol or **TS2'** $\Delta G^{\ddagger}$ = 16.1 kcal/mol) to form trioxidanyl diradical intermediates **2a** or **2a'** respectively. While both pathways are kinetically feasible, the formation of the benzylic tertiary radical remains favored. A subsequent barrierless radical recombination occurs to form the 1,2,3-trioxepane intermediate **2b** which is proposed to undergo an analogous formal [$_{\sigma}2_s+_{\sigma}2_s+_{\sigma}2_s$] *retro*-cycloaddition and subsequent ozonolysis as the 1,2,3-trioxane **1b** from BCB **1**.

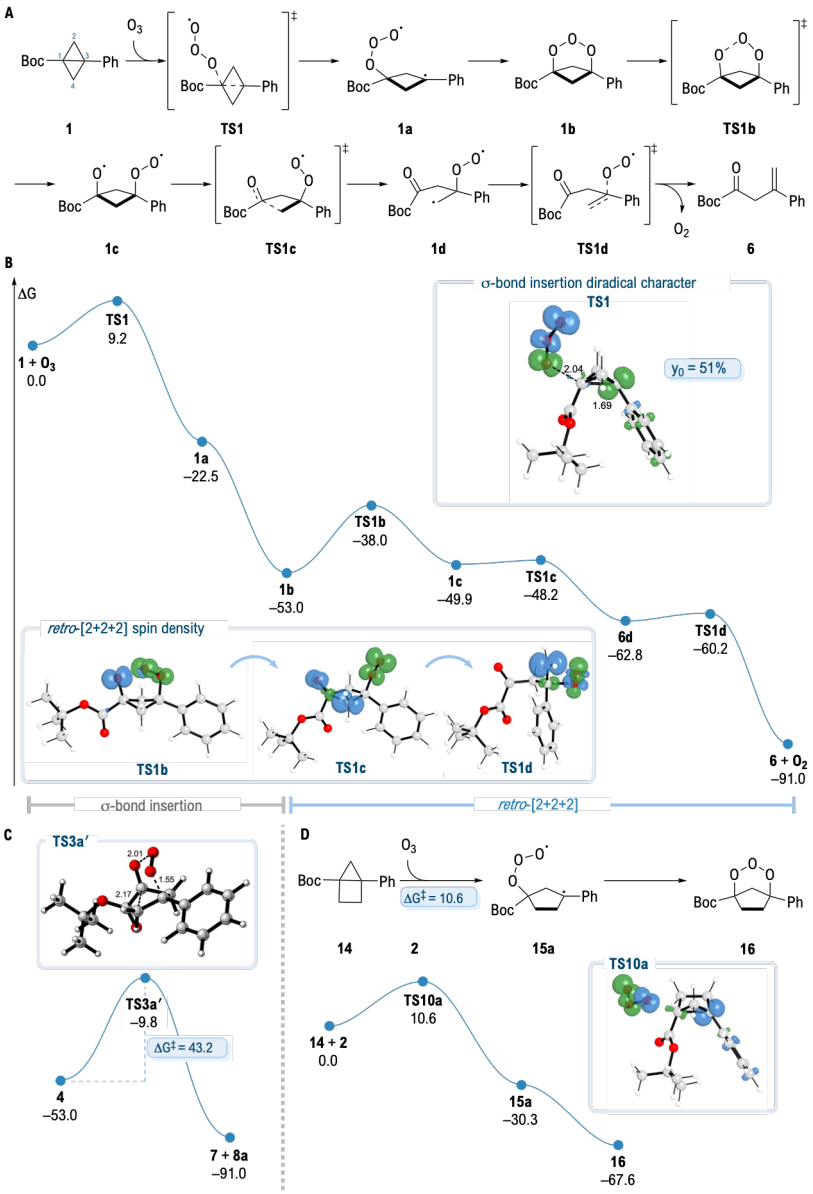


Figure 8.3 Computational Mechanistic Investigations

A) Calculated mechanism for ozonolysis of a BCB C–C σ-bond. (**B**) Reaction coordinate diagram of the lowest energy pathway, diradical character of **TS1** and spin density difference plot of [2+2+2] *retro*-cycloaddition. (**C**) Concerted [2+2+2] *retro*-cycloaddition mechanism. (**D**) Calculated mechanism for ozonolysis of a BCP C–C σ-bond. All Gibbs free energies were calculated using (U)ωB97X-D/def2-TZVPP/SMD(MeOH)//(U)ωB97X-D/def2-SVP at 195.15 K and 1M. Diradical character calculations were performed at SC-NEVPT2/CASSCF(6,6)/def2-TZVPP//(U)ωB97X-D/def2-SVP. Molecular orbitals and spin density difference plots are visualized using isosurfaces rendered in PyMOL. Frontier molecular orbitals are drawn at an isovalue of ±0.02 a.u. and spin-density surfaces at ±0.01 a.u. Transition state structures are rendered using CylView20.

8.5 Conclusion

We have achieved the ozonolysis of C–C single bonds. By adding stabilizing substituents across strained BCB and BCP frameworks, we successfully activated the central bridging bond and enabled a radical S_H2 mechanistic pathway for ozone, leveraging the diradical character of ozone and strained alkanes. Our proposed mechanism led to the synthesis of a transient 1,2,3-trioxane, which fragmented via a formal [$_\sigma2_s$+$_\sigma2_s$+$_\sigma2_s$] *retro*-cycloaddition. Our mechanistic hypothesis is supported by DFT and multireference diradical calculations and backed with experimental identification of downstream reaction intermediates.

We also established a clear relationship between strain energy and delocalization for this reactivity. Both BCB and BCP reacted with ozone, but BCH did not. From both BCB and BCP we accessed 1,3- and 1,4-dicarbonyl compounds, respectively, defined by the loss of the single bridging methylene carbon atom from the original bicycle. Furthermore, we showed that the BCB σ-bond, typical for radical reactions, reacts competitively with alkenes, trailing AMS by a mere 3-fold rate difference but reacting 3-fold faster than *t*BuA. Overall, our ozonolysis of C–C single bonds opens a new frontier of reactivity for a nearly two-century-old reaction.

8.6 Supporting Information and Experimental Details

8.6.1 Materials and Methods

Glassware

Unless otherwise stated, all reactions were conducted in glassware that had been washed sequentially with 12 M HCl and Alconox, oven-dried, and fitted with rubber septa; the reaction mixtures were stirred with Teflon-coated magnetic stir bars.

Solvents and Reagents

For dry or air-free reactions, standard Schlenk techniques were used to transfer liquid reagents and solvents. Argon was used as the gas for inert atmosphere reactions. Methanol (MeOH) was distilled over magnesium under an argon atmosphere. Dichloromethane (DCM) and acetonitrile (MeCN) were distilled over calcium hydride under an argon atmosphere. Tetrahydrofuran (THF) and diethyl ether (Et_2O) were distilled over sodium/benzophenone ketyl under an argon atmosphere. All other solvents and reagents were used as received from commercial sources, unless otherwise noted.

Reaction Temperatures

Reaction temperatures above room temperature (23 ºC) and below 50 ºC refer to water bath temperatures, unless otherwise stated. Reaction temperatures above 50 ºC refer to silicone oil bath temperatures. Reaction temperatures of 0 ºC refer to an ice-water bath. Reaction temperatures of –78 ºC refer to an acetone-dry ice bath. Reaction temperatures

of –116 ºC refer to a diethyl ether-liquid N_2 slurry bath. Reaction temperatures of –130 ºC refer to a pentane-liquid N_2 slurry bath.

SiO_2 Chromatography

Thin layer chromatography (TLC) was performed using SiliCycle silica gel 60 F-254 precoated plates (0.25 mm) with visualization under UV irradiation and with a bromocresol green, ceric ammonium molybdate (CAM), potassium permanganate ($KMnO_4$), or vanillin stain. SiliCycle Silica-P silica gel (particle size: 40–63 μm) was used for flash column chromatography (FCC).

Melting Point

Melting points are uncorrected and were recorded using an Electrothermal® capillary melting point apparatus.

Infrared (IR) Spectroscopy

IR spectra were recorded using a Jasco FTIR-4100 spectrometer with a Zirconium–Selenium crystal ATR attachment or an Agilent Cary 630 FTIR with a diamond ATR attachment.

High Resolution Mass Spectrometry (HRMS)

HRMS was performed using a Thermo Fisher Scientific Exactive Plus spectrometer equipped with an IonSense ID-CUBE DART source or an Agilent 6545 Q-TOF LC/MS with 1260 Infinity LC.

Gas Chromatography Mass Spectrometry (GCMS)

GCMS was performed with an Agilent 7250 Q-TOF GC/MS with low energy EI or an Agilent Intuvo 9000 GC with a 5977B GC/MSD.

Liquid Chromatography Mass Spectrometry (LCMS)

LCMS was performed with an Agilent 1260 Infinity II LC using a poroshell 120 EC-C18 (2.7 μm, 4.6x100 mm) column coupled to a low resolution 6120 Quadrupole MSD. The mobile phase consisted of H_2O/MeCN mixtures spiked with 0.1% formic acid.

Nuclear Magnetic Resonance Spectroscopy

Samples were prepared in $CDCl_3$ saturated with K_2CO_3 as a desiccant or MeOD-d_4 which was used as received. ^{1}H, ^{13}C, and 2D NMR spectra were recorded using AV-800, NEO-600, AV-500, AV-400, or AV-300 MHz spectrometers, with ^{13}C NMR spectroscopic operating frequencies of 201, 151, 126, 101, or 75 MHz, respectively. NMR spectra were analyzed using the MestReNova software application (v.14.2.3-29241). Standard auto-baseline and auto-phase corrections were applied to all spectra prior to manual integration and manual peak picking. Chemical shifts (δ) are reported in parts per million

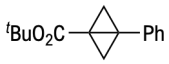
(ppm) relative to the (residual protonated) signal of the solvent $CDCl_3$ (choloroform-*d*, δ = 7.26 for ^1H NMR; = δ = 77.2 for ^{13}C NMR) or CD_3OD (MeOD-d_4, δ = 3.31 for ^1H NMR; δ = 49.0 for ^{13}C NMR). Data for ^1H NMR spectra are reported as follows: chemical shift, multiplicity, coupling constants (Hz), and number of hydrogen atoms. Data for ^{13}C NMR spectra are reported in terms of chemical shift. The following abbreviations are used to describe the multiplicities: s = singlet; d = doublet; t = triplet; q = quartet; m = multiplet; br = broad.

8.6.2 Safety

Caution: Organic peroxides are typically high-risk shock-sensitive compounds prone to explosion. Although we have not encountered any peroxide-related safety issues in our lab, the peroxides generated using the reported methods should be handled only by properly trained individuals and the isolated compounds should be stored at cryogenic temperatures. The use of a blast-shield is also recommended, especially for reactions performed on larger scales.

8.6.3 Substrate Preparation

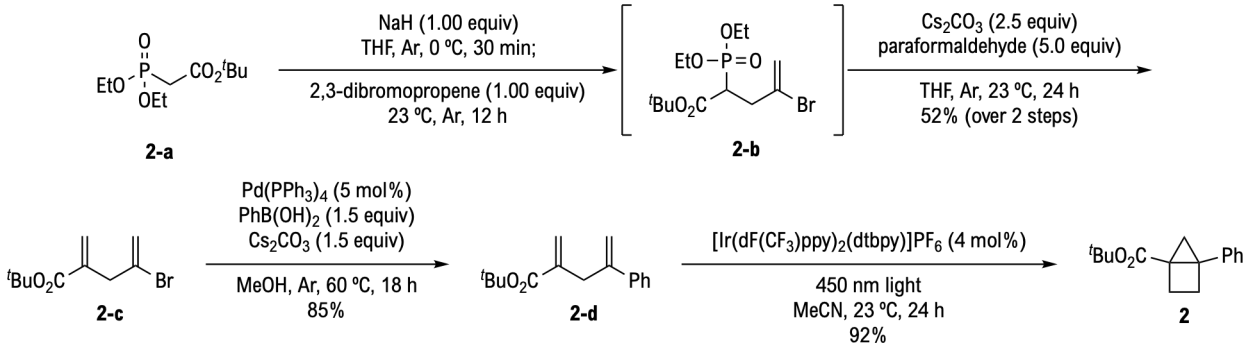
8.6.3.1 *tert*-Butyl 3-phenylbicyclo[1.1.0]butane-1-carboxylate



1

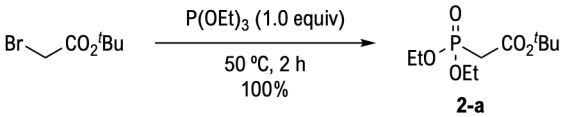
Compound **1** was synthesized according to a literature procedure [*32*].

8.6.3.2 *tert*-Butyl 4-phenylbicyclo[2.1.0]pentane-1-carboxylate



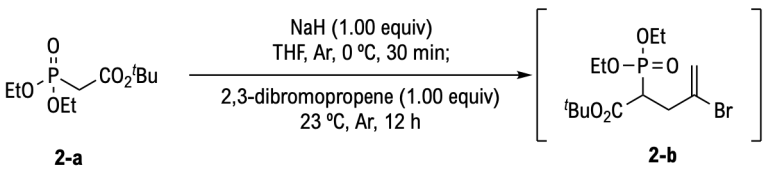
The synthesis of compound **2** was adapted from a literature procedure [*33*].

Step 1: Arbuzov Reaction



The *tert*-butyl 2-(diethoxyphosphoryl)acetate (**2-a**) was prepared from *tert*-butyl 2-bromoacetate and triethylphosphite according to a literature procedure [34].

Step 2: Alkylation



The 2,3-dibromopropene was vacuum distilled (bp: 40.5 °C, 18 mmHg) immediately prior to use [35].

A 50 mL round bottom flask equipped with a Teflon-coated magnetic stir bar and two 25 mL round bottom flasks were flame-dried under vacuum. The flasks were evacuated and backfilled with argon (3x) while hot. After cooling, sodium hydride (60% *w*/*w*, 242 mg, 6.05 mmol, 1.00 equiv) was added to the 50 mL round bottom flask, and the flask was evacuated and backfilled with argon (3x). Dry THF (6 mL) was added, and the stirred suspension was cooled to 0 ºC in an ice-water bath.

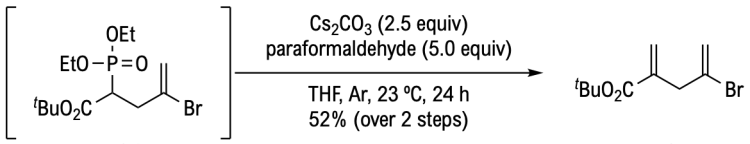
The prepared *tert*-butyl 2-(diethoxyphosphoryl)acetate (**1-a**, 1.53 g, 6.05 mmol, 1.00 equiv) was added to one of the 25 mL flasks using a syringe. Dry THF (6 mL) was added, and the solution was cannulated dropwise into the sodium hydride suspension. The mixture was stirred for 30 minutes at 0 ºC to form the stabilized ylide.

2,3-Dibromopropene (2.10 g, 10.5 mmol, 1.00 equiv) was added to the remaining empty 25 mL round bottom flask using a syringe. Dry THF (6 mL) was added, and the solution was cannulated dropwise into the ylide solution. The reaction was allowed to warm to room temperature and stirred overnight.

Water (10 mL) was added to quench the reaction, and the biphasic mixture was transferred to a separatory funnel. The aqueous layer was extracted with ethyl acetate (3 x 10 mL). The combined organics were washed with brine (10 mL), dried over magnesium sulfate, filtered through cotton, and evaporated to afford *tert*-butyl 3-bromo-2-

(diethoxyphosphoryl)but-3-enoate (**1-b**, 2.18 g, 5.87 mmol) as a yellow oil with a 97% crude yield.

Step 3: Horner–Wadsworth–Emmons Olefination



2-b **2-c**

The paraformaldehyde was ground with a mortar and pestle then dried in a vacuum desiccator over P_2O_5 for 24 hours prior to use.

A 100 mL round bottom flask equipped with a Teflon-coated magnetic stir bar was flame-dried under vacuum. Cesium carbonate (4.78 g, 14.7 mmol, 2.5 equiv) and paraformaldehyde (882 mg, 29.4 mmol, 5.00 equiv) were added, then the flask was evacuated and backfilled with argon (3x). Dry THF (12 mL) was added, and the suspension was stirred for 15 minutes at room temperature. The *tert*-butyl 3-bromo-2-(diethoxyphosphoryl)but-3-enoate (**1-b**, 2.18 g, 5.87 mmol, 1.00 equiv) from the previous step was dissolved in dry THF (12 mL) and cannulated into the 100 mL flask. The reaction was stirred at room temperature for 24 hours, then quenched with water (50 mL). The biphasic mixture was transferred to a separatory funnel. The aqueous layer was extracted with ethyl acetate (3 x 10 mL). The combined organics were washed with brine (10 mL), dried over magnesium sulfate, filtered through cotton, and evaporated. The crude material was purified through SiO_2 (1% *v/v* EtOAc/hexanes) to afford *tert*-butyl 4-bromo-2-methylenepent-4-enoate (**1-c**, 789 mg, 3.19 mmol) as a pale-yellow oil in 54% yield.

Scale: 6.05 mmol

Yield: 52% over 2 steps (789 mg, 3.19 mmol)

R_f = 0.48 (10% *v/v* EtOAc/hexanes + $KMnO_4$ stain)

Purification: SiO_2 (1% *v/v* EtOAc/hexanes)

Physical State: Pale-yellow oil

IR (ATR, neat) $\tilde{\nu}_{max}$: 3006, 2979, 2932, 1715, 1631, 1477, 1458, 1423, 1394, 1368, 1339, 1308, 1286, 1256, 1228, 1149, 951, 892, 851, 816 cm–1

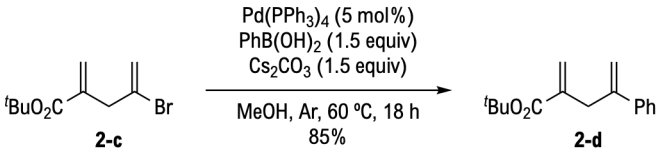
HRMS–DART (m/z): $[M–C_4H_9O]^+$ calc'd for $C_6H_6O^{79}Br$ 172.9597, found 172.9598

$[M–C_4H_9O]^+$ calc'd for $C_6H_6O^{81}Br$ 174.9576, found 174.9576

^{1}H NMR (800 MHz, $CDCl_3$) δ 6.26 (d, J = 1.5 Hz, 1H), 5.66 – 5.64 (m, 1H), 5.64 – 5.63 (m, 1H), 5.51 (d, J = 1.8 Hz, 1H), 3.40 (s, 2H), 1.49 (s, 9H).

^{13}C NMR (201 MHz, CDCl3) δ 165.4, 137.8, 130.6, 127.0, 118.6, 81.1, 43.7, 28.0.

Step 4: Suzuki–Miyaura Coupling



2-c **2-d**

A 100 mL Schlenk flask equipped with a Teflon-coated magnetic stir bar was charged with *tert*-butyl 4-bromo-2-methylenepent-4-enoate (**2-c**, 789 mg, 3.19 mmol, 1.00 equiv), phenylboronic acid (584 mg, 4.79 mmol, 1.50 equiv), tetrakis(triphenylphosphine)palladium(0) (184 mg, 0.160 mmol, 5 mol%), and cesium carbonate (1.56 g, 4.79 mmol, 1.50 equiv). The flask was sealed with a rubber septum

then evacuated and backfilled with argon (3x). Dry, degassed methanol (6.4 mL) was added. The reaction was heated to 60 ºC under positive pressure of argon for 18 hours. After completion, the reaction was cooled to room temperature and transferred to a separatory funnel containing water (10 mL). The aqueous layer was extracted with ethyl acetate (3 x 10 mL). The combined organics were washed with brine (10 mL), dried over sodium sulfate, filtered through cotton, and evaporated. The crude material was purified through FCC (1% *v/v* EtOAc/hexanes) to provide *tert*-butyl 2-methylene-4-phenylpent-4-enoate as a pale-yellow oil (**2-d**, 663 mg, 3.19 mmol) in 85% yield.

Scale: 3.19 mmol

Yield: 85% (663 mg)

R_f = 0.58 (10% *v/v* EtOAc/hexanes + UV/vanillin stain)

Purification: SiO_2 (1% *v/v* EtOAc/hexanes)

Physical State: Pale-yellow oil

IR (ATR, neat) $\tilde{\nu}_{max}$: 3085, 3058, 2979, 2931, 1714, 1631, 1495, 1477, 1447, 1392, 1368, 1314, 1278, 1255, 1222, 1145, 948, 904, 851 cm^{-1}

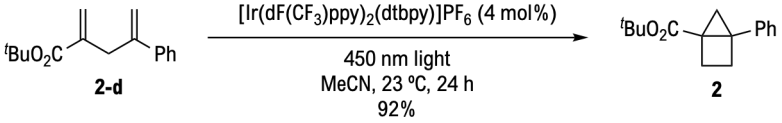
HRMS–DART (*m/z*): $[M + H]^+$ calc'd for $C_{15}H_{21}O_2$ 245.1536, found 245.1540

$[M – C_4H_9O]^+$ calc'd for $C_{12}H_{11}O$ 171.0804, found 171.0798

^{1}H NMR (800 MHz, $CDCl_3$) δ 7.42 (d, *J* = 8.0 Hz, 2H), 7.38 – 7.30 (m, 2H), 7.27 (s, 1H), 6.14 (s, 1H), 5.47 (d, *J* = 1.2 Hz, 1H), 5.45 (s, 1H), 5.09 (d, *J* = 1.0 Hz, 1H), 3.47 (s, 2H), 1.48 (s, 9H).

^{13}C NMR (201 MHz, $CDCl_3$) δ 166.5, 145.7, 140.9, 140.1, 128.4, 127.6, 126.2, 125.8, 114.5, 80.8, 37.4, 28.2.

Step 5: [2 + 2] Cycloaddition



Two 20-mL vials equipped each with a Teflon-coated magnetic stir bar were charged with *tert*-butyl 2-methylene-4-phenylpent-4-enoate (**2-d**, 244 mg, 0.500 mmol, 1.00 equiv). A solution of $[Ir(dF(CF_3)ppy)_2(dtbpy)]PF_6$ (44.9 mg, 40.0 μmol, 4 mol%) in dry MeCN (0.50 mL) was prepared and divided equally into each vial. Additional dry MeCN (9.75 mL) was added to each vial and the vials were sealed. The vials were degassed using the freeze-pump-thaw (3x) method. After degassing, the vials were irradiated for 24 hours in an Acceled photoreactor m2 with 450 nm light at 100% power, 6800 rpm fan speed, and 2000 rpm stirring. The vials were combined in a 100 mL round bottom flask, rinsing each vial with ethyl acetate (3 x 1 mL). The volatiles were evaporated and the crude material was purified through SiO_2 (1% *v/v* EtOAc/hexanes) to afford the *tert*-butyl 4-phenylbicyclo[2.1.0]pentane-1-carboxylate as a colorless oil **2**, 447 mg, 1.83 mmol) in 92% yield.

Scale: 2 x 1.00 mmol

Yield: 92% (447 mg, 1.83 mmol)

R_f = 0.59 (10% *v/v* EtOAc/hexanes + UV/vanillin stain)

Purification: SiO_2 (1% *v/v* EtOAc/hexanes)

Physical State: Clear colorless oil

IR (ATR, neat) $\tilde{\nu}_{max}$: 3061, 2976, 2928, 2856, 1704, 1603, 1503, 1449, 1367, 1345, 1245, 1143, 911, 853 cm^{-1}

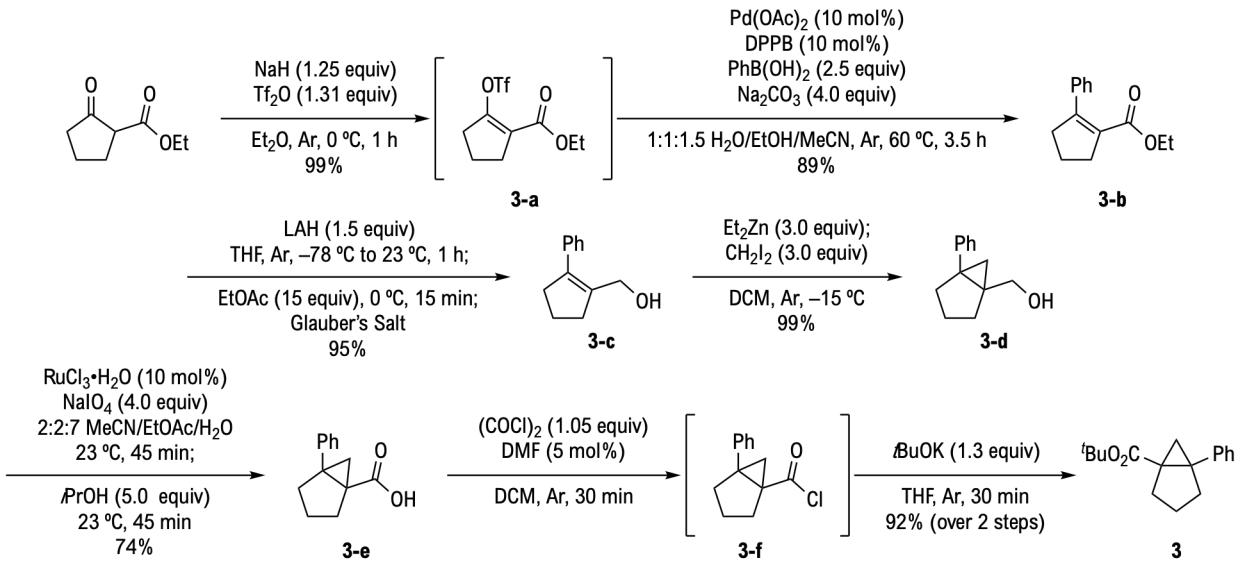
HRMS–DART (*m/z*): $[M + H]^+$ calc'd for $C_{16}H_{21}O_2$ 245.1536, found 245.1537

$[M – C_4H_9O]^+$ calc'd for $C_{12}H_{11}O$ 171.0804, found 171.0804

^{1}H NMR (600 MHz, $CDCl_3$) δ 7.36 – 7.32 (m, 2H), 7.29 (td, *J* = 6.8, 2.0 Hz, 2H), 7.19 (tt, *J* = 7.1, 1.5 Hz, 1H), 2.70 – 2.47 (m, 2H), 2.28 (dt, *J* = 4.0, 1.9 Hz, 1H), 1.83 – 1.76 (m, 1H), 1.70 – 1.61 (m, 1H), 1.58 (d, *J* = 4.6 Hz, 1H), 1.22 (s, 9H).

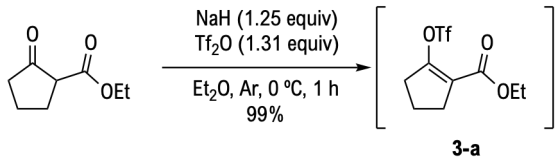
^{13}C NMR (151 MHz, $CDCl_3$) δ 170.5, 138.4, 128.1, 127.8, 126.6, 80.1, 42.2, 35.8, 28.2, 28.2, 25.2, 21.3.

8.6.3.3 *tert*-Butyl 5-phenylbicyclo[3.1.0]hexane-1-carboxylate



Compound **3** was prepared in 7 steps from ethyl 2-oxocyclopentane-1-carboxylate.

Step 1: Enol Triflate Preparation

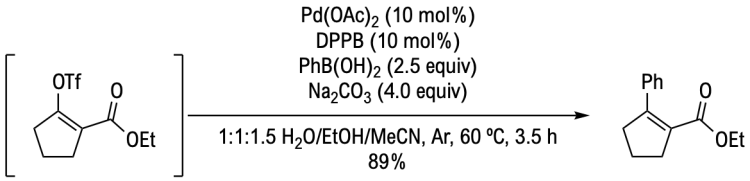


The synthesis of **3-a** was adapted from a literature procedure [*36,37*].

To a cold (0 °C), stirred suspension of sodium hydride (960 mg, 60% *w/w*, 24.0 mmol, 1.25 equiv) in dry Et_2O (80.0 mL) was added slowly a solution of ethyl 2-oxocyclopentane-1-carboxylate (3.00 g, 1 Eq, 19.2 mmol) in dry Et_2O (16 mL). After the mixture had been stirred at 0 °C for 10 min, trifluoromethanesulfonic anhydride (7.10 g, 4.22 mL, 25.2 mmol, 1.31 equiv) was added slowly. Stirring was continued at 0 °C for 1 hour. The reaction mixture was diluted with Et_2O (60 mL) and then was filtered through a short column of Florisil (elution with Et_2O). The combined eluate was evaporated to afford ethyl 2-(((trifluoromethyl)sulfonyl)oxy)cyclopent-1-ene-1-carboxylate (**3-a**, 5.49 g, 19.0 mmol,

99% yield) as pale-yellow oil, which was immediately used in the next step without further purification.

Step 2: Suzuki–Miyaura Coupling



3-a **3-b**

The synthesis of compound **3-b** was adapted from a literature procedure [38].

To a flame-dried 250 mL Schlenk flask equipped with a Teflon-coated magnetic stir bar was added sodium carbonate (8.08 g, 76.2 mmol, 4.0 equiv), 4-diphenylphosphanylbutyl(diphenyl)phosphane (DPPB, 812 mg, 1.90 mmol, 10 mol%), phenylboronic acid (5.81 g, 47.6 mmol, 2.5 equiv), and palladium(II) acetate (428 mg, 1.90 mmol, 10 mol%). The flask was sealed then evacuated and backfilled with argon (3x).

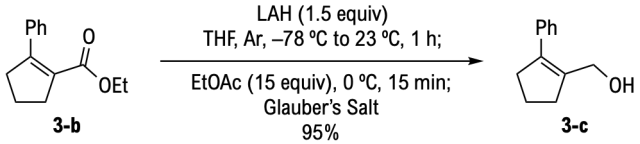
The MeCN (46 mL), EtOH (38 mL) and H_2O (38 mL) were mixed in a sealed round bottom flask and sparged with argon for 15 minutes to degas it.

The 50 mL pear shaped flask containing the crude ethyl 2-(((trifluoromethyl)sulfonyl)oxy)cyclopent-1-ene-1-carboxylate (**3-a**, 5.49 g, 19.0 mmol, 1.0 equiv) from the previous step was dissolved in degassed MeCN (15 mL).

The degassed MeCN, EtOH, H_2O solution was cannulated into the Schlenk flask followed by the substrate solution and rinsing the flask with MeCN (3 mL).

The reaction was heated to 70 ºC for 3.5 hours as confirmed by LCMS. The solution was then diluted with water (200 mL) and extracted with ethyl acetate (3 x 100 mL). The combined organics were washed with brine (100 mL), dried over sodium sulfate, vacuum filtered through celite to remove black solids, then evaporated. Benzene (20 mL) was added, and the solution was evaporated again. The crude material was purified through SiO_2 0–5% *v/v* EtOAc/hexanes to afford ethyl 2-phenylcyclopent-1-ene-1-carboxylate (**3-b**, 3.66 g, 16.9 mmol, 89% yield) as a clear colorless oil. Characterization matched with literature values [*38*].

Step 3: LAH Reduction



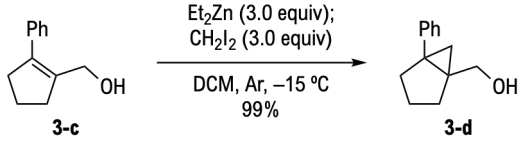
3-b **3-c**

The synthesis of compound **3-c** was adapted from a literature procedure [*39*].

To a flame-dried 250 mL round bottom flask equipped with a Teflon-coated magnetic stir bar was added lithium aluminum hydride (LAH, 848 mg, 22.3 mmol, 1.5 equiv). The flask was evacuated and backfilled with argon (3x) then THF (112 mL) was added. The suspension was then cooled to –78 °C in an acetone-dry ice bath.

A 50 mL round bottom flask was charged with ethyl 2-phenylcyclopent-1-ene-1-carboxylate (**3-b**, 3.22 g, 14.9 mmol, 1.0 equiv) and evacuated and backfilled with argon (3x). THF (37 mL) was added, and the flask was manipulated until the solution became homogeneous. The solution was then cannulated dropwise into the Schlenk flask containing the LAH suspension. The reaction was stirred at –78 °C for 1 hour then warmed to 23 °C and stirred for 1 hour. After completion the reaction was cooled to 0 °C and EtOAc (20 g, 22 mL, 0.23 mol, 15 equiv) was slowly added to quench the reaction. After stirring at 0 ºC for 30 min, crushed sodium sulfafe decahydrate (Glauber's salt, 3.4 g, 11 mmol, 0.71 equiv) was added in two portions and the reaction was stirred for an additional 30 min at 0 °C. The reaction was then filtered through celite, washing with EtOAc (3 x 75mL) to afford (2-phenylcyclopent-1-en-1-yl)methanol (**3-c**, 2.46 g, 14.1 mmol, 95%) as a white solid. Characterization matched with literature values [*39*].

Step 4: Simmons–Smith–Furukawa Cyclopropanation



To a flame-dried 500 mL round bottom flask equipped with a Teflon-coated magnetic stir bar was added (**3-c**, 2-phenylcyclopent-1-en-1-yl)methanol (1.93 g, 11.1 mmol, 1.00 equiv). The flask was evacuated and backfilled with argon (3x) then dry DCM (111 mL) was added. The flask was placed in acetone-ice bath (–15 °C) and cooled for 15 min. Next, a 1 M solution of diethylzinc in hexanes (33.2 mL, 33.2 mmol, 3.00 equiv) was slowly added and the solution was stirred at –15 °C for 15 min. Finally, diiodomethane (8.90 g, 2.68 mL, 33.2 mmol, 3.00 equiv.) was added and the cooling bath was removed. The

reaction was allowed to warm to 23 °C and stirred for 2 hours. The solution became cloudy with a fine white precipitate. After consumption of the starting material (TLC: 30% *v/v* EtOAc/hexanes+UV/KMnO4 stain indicated the absence of a yellow spot staining at room temperature; or LCMS monitoring) the reaction was cooled to 0 °C in an ice-water bath and quenched with sat. aq. NH_4Cl (20 mL) then stirred for 15 min. The biphasic solution was warmed to room temperature and diluted with water (20 mL) then filtered through celite, washing with ethyl acetate. The mixture was concentrated before being transferred to a separatory funnel. The aqueous phase was extracted with ethyl acetate (3 x 50 mL) and the combined organics were washed with brine, dried over sodium sulfate, filtered through cotton, and evaporated. The crude material was purified through SiO_2 (0–50% *v/v* EtOAc/hexanes) to afford 5-phenylbicyclo[3.1.0]hexan-1-yl)methanol (**3-d**, 2.07 g, 11.0 mmol) as an amorphous white solid in 99% yield.

Scale: 11.1 mmol

Yield: 99% (2.07 g)

$\boldsymbol{R_f}$ = 0.59 (40% *v/v* EtOAc/hexanes + UV/vanillin stain)

Purification: SiO_2 (0–50% *v/v* EtOAc/hexanes)

Physical State: Amorphous white solid

Melting Point: 70–71 ºC

IR (ATR, neat) $\tilde{\nu}_{max}$: 3362, 3059, 3025, 2995, 2934, 2860, 1603, 1498, 1447, 1031 cm^{-1}

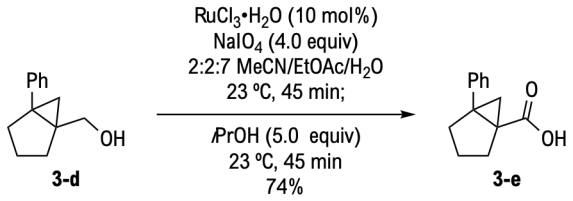
HRMS–DART (*m/z*): $[M + H]^+$ calc'd for $C_{13}H_{17}O$ 189.1274, found 189.1274

$[M – OH]^+$ calc'd for $C_{13}H_{15}$ 171.1168, found 171.1164

^{1}H NMR (400 MHz, $CDCl_3$) δ 7.33 – 7.28 (m, 4H), 7.20 (dddd, *J* = 6.2, 5.3, 2.8, 1.5 Hz, 1H), 3.40 (d, *J* = 4.2 Hz, 2H), 2.17 – 1.94 (m, 4H), 1.80 – 1.73 (m, 1H), 1.37 – 1.26 (m, 1H), 1.10 (s, 1H), 0.94 (d, *J* = 1.3 Hz, 2H).

^{13}C NMR (101 MHz, $CDCl_3$) δ 142.4, 129.1, 128.5, 126.4, 66.4, 37.7, 36.8, 36.5, 30.6, 20.9, 14.9.

Step 5: Lemieux–Johnson Oxidation



A 250 mL round bottom flask was charged with (5-phenylbicyclo[3.1.0]hexan-1-yl)methanol (**3-d**, 2.07 g, 11.0 mmol, 1.00 equiv), a Teflon-coated magnetic stir bar, and EtOAc (40.0 mL). The mixture was sonicated until it became homogeneous, then MeCN (40.0 mL) was added. A 250 mL Erlenmyer flask was charged with ruthenium(III)chloride hydrate (248 mg, 1.10 mmol, 10 mol%) and water (100 mL). The aqueous solution was poured into the reaction flask, and the Erlenmeyer was rinsed with water (2 x 20 mL). Next, the sodium periodate (9.41 g, 44.0 mmol, 4.0 equiv) was added in one portion. The reaction was stirred at 23 °C for 45 min when TLC (40% v/v EtOAc/hexanes + UV/vanillin and UV/bromocresol green; starting material stains with vanillin, product stains with bromocresol green) and LCMS indicated the reaction was complete. The reaction was quenched with the addition of isopropyl alcohol (3.30 g, 4.21 mL, 55.0 mmol, 5.0 equiv) at 23 °C for another 45 min. The solution was transferred to a separatory funnel and diluted with ethyl acetate (200 mL). The organic phase was washed with aq. NaOH (1 M,

3 x 100 mL) and the combined organics were acidified to pH = 3 at 0 ºC by dropwise addition of HCl (12 M, 25 mL). The aqueous layer was then extracted with ethyl acetate (5 x 50 mL). The organic extracts were washed with sat. aq. sodium thiosulfate (2 x 50 mL) and brine (2 x 50 mL), then dried over sodium sulfate, filtered through cotton, and evaporated. The crude product was initially purified through SiO_2 (0–10% *v/v* EtOAc/hexanes+1% AcOH) then recrystallized from DCM at 0 ºC to afford 5-phenylbicyclo[3.1.0]hexane-1-carboxylic acid (**3-e**, 1.64 g, 8.11 mmol, 74 %) as white, reticular bladed crystals.

Scale: 11.0 mmol

Yield: 74% (1.64 g)

R_f = 0.53 (30% *v/v* EtOAc/hexanes + UV/Bromocresol Green stain)

Purification: SiO_2 (0–10% *v/v* EtOAc/hexanes + 1% *v/v* AcOH)

Physical State: White, reticular bladed crystals

Melting Point: 149–151 ºC

IR (ATR, neat) $\tilde{\nu}_{max}$: 3081, 3024, 2968, 2952, 2904, 2874, 2834, 2671, 2618, 1679, 1603, 1496, 1473, 1450, 1431, 1362, 1337, 1295, 1233, 1173, 1039, 951, 913 cm^{-1}

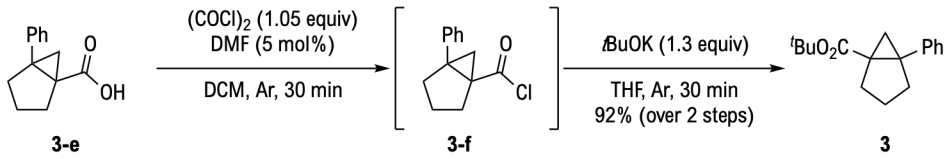
HRMS–DART (*m/z*): $[M + H]^+$ calc'd for $C_{13}H_{15}O_2$ 203.1067, found 203.1065

$[M – H]^–$ calc'd for $C_{13}H_{13}O_2$ 201.0921, found. 201.0924

^{1}H NMR (500 MHz, $CDCl_3$) δ 10.41 (br, 1H), 7.28 – 7.17 (m, 5H), 2.46 (td, *J* = 12.4, 8.2 Hz, 1H), 2.13 – 2.03 (m, 2H), 1.96 (dd, *J* = 12.9, 7.9 Hz, 1H), 1.85 (d, *J* = 5.0 Hz, 1H), 1.78 (dt, *J* = 15.3, 7.7 Hz, 1H), 1.35 – 1.22 (m, 2H).

^{13}C NMR (126 MHz, $CDCl_3$) δ 178.5, 140.5, 129.0, 128.3, 126.8, 77.4, 45.9, 37.2, 36.9, 28.9, 23.0, 21.1, 18.7, 12.6.

Steps 6 & 7: Acid to Acyl Chloride Transmutation & Esterification



3-e **3-f** **3**

The synthesis of compounds **3-f** and **3** was adapted from a literature procedure [40].

To a 50 mL pear shaped flask equipped with a Teflon-coated magnetic stir bar was added 5-phenylbicyclo[3.1.0]hexane-1-carboxylic acid (621 mg, 3.07 mmol, 1.00 equiv). The flask was sealed with a rubber septum then evacuated and backfilled with argon (3x). Dry DCM (6.21 mL) was added, and the solution was stirred until homogeneous. Next, oxalyl chloride (409 mg, 282 µL, 3.22 mmol, 1.05 equiv) was added in one portion, followed by DMF (11 mg, 12 µL, 0.15 mmol, 5 mol%). The solution changed from colorless to yellow, and bubbles were observed. After 30 min at 23 °C the outgassing had ceased and then the volatiles were removed by rotatory evaporation. The crude acyl chloride **3-f** was placed on high vacuum for 15 minutes, then backfilled with argon and dissolved in dry THF (6.21 mL).

A flame-dried 25 mL round bottom flask was charged with potassium *tert*-butoxide (448 mg, 3.99 mmol, 1.30 equiv) in a glovebox. The flask was sealed and removed from the glovebox, then dry THF (3.99 mL) was added to make a 1 M solution. The solution was

transferred to the dissolved acyl chloride **3-f**, and the ensuing reaction was stirred at 23 °C for 30 min. After 30 minutes, ethyl acetate (50 mL) was added, followed by water (25 mL). The aqueous layer was separated then extracted with ethyl acetate (3 x 50 mL). The combined organics were washed with brine (50 mL), dried over sodium sulfate, filtered through cotton, and evaporated. The crude material was purified through FCC (0–2% *v/v* EtOAc/hexanes) to afford *tert*-butyl 5-phenylbicyclo[3.1.0]hexane-1-carboxylate (**3**, 732 mg, 2.83 mmol, 92%) as a clear colorless oil.

Scale: 3.07 mmol

Yield: 92% (732 mg)

R_f = 0.70 (15% *v/v* EtOAC/hexanes + UV/CAM stain)

Purification: SiO_2 (0–2% *v/v* EtOAc/hexanes)

Physical State: Clear colorless oil

IR (ATR, neat) $\tilde{\nu}_{max}$: 3085, 3060, 3026, 2005, 2974, 2931, 2871, 1706, 1602, 1498, 1477, 1453, 1390, 1366, 1280, 1250, 1145, 1112, 1047, 949, 914, 852 cm^{-1}

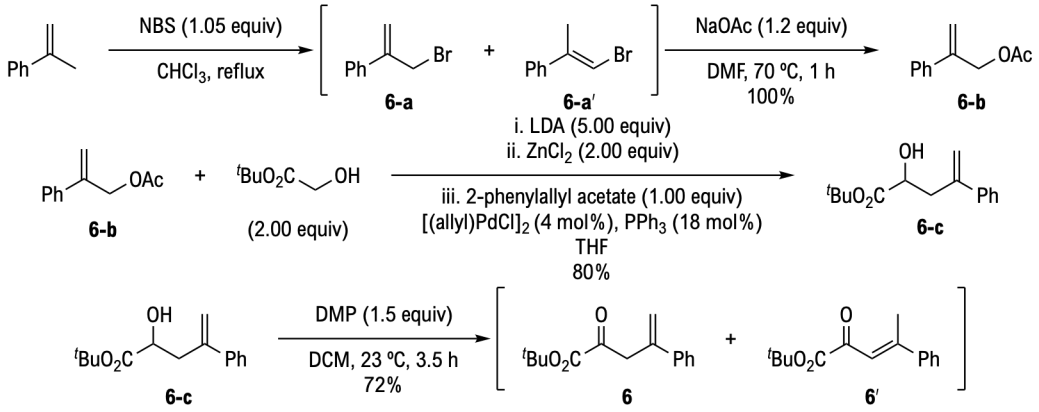
HRMS–DART (*m/z*): $[M + H]^+$ calc'd for $C_{17}H_{23}O_2$ 259.1693, found 259.1693

$[M – C_4H_9O]^+$ calc'd for $C_{13}H_{13}O$ 185.0961, found 185.0957

^{1}H NMR (400 MHz, $CDCl_3$) δ 7.38 – 7.26 (m, 4H), 7.26 – 7.19 (m, 1H), 2.64 – 2.41 (m, 1H), 2.20 (dddt, *J* = 13.8, 11.5, 7.7, 1.8 Hz, 1H), 2.09 (ddt, *J* = 13.0, 7.7, 1.3 Hz, 1H), 2.04 – 1.94 (m, 1H), 1.95 – 1.88 (m, 1H), 1.89 – 1.77 (m, 1H), 1.40 – 1.28 (m, 1H), 1.23 (dd, *J* = 5.0, 2.3 Hz, 1H), 1.10 (s, 9H).

^{13}C NMR (101 MHz, $CDCl_3$) δ 171.7, 141.3, 129.3, 128.0, 126.5, 79.6, 43.9, 38.2, 36.8, 29.1, 27.7, 21.1, 17.3.

8.6.3.4 *tert*-Butyl 2-oxo-4-phenylpent-4-enoate

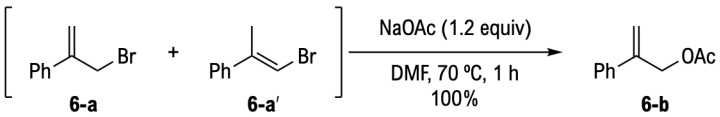


Compound **6** was prepared in 4 steps from α-methylstyrene.

Step 1: Radical Bromination

Compound **6-a** was prepared according to a literature procedure [*41*]. Despite multiple attempts, the isomerization of **6-a** to **6-a'** occurred under the reported reaction conditions. Compound **6-a'** is difficult to separate from **6-a** through either chromatography or distillation. Nonetheless, the presence of **6-a'** did not affect the formation of **6-b,** and the purity of **6-a** was considered in calculating the yield of **6-b**.

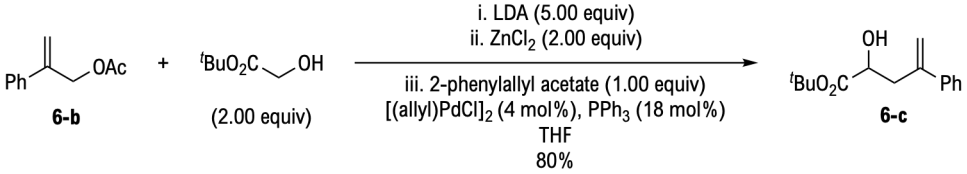
Step 2: Substitution



A 50 mL round bottom flask equipped with a Teflon-coated magnetic stir bar was charged with a 92:8 mixture of (3-bromoprop-1-en-2-yl)benzene (**6-a**, 4.79 g, 24.3 mmol, 1.00 equiv) and ((*E*)-1-bromoprop-1-en-2-yl)benzene (**6-a'**, 417 mg, 2.11 mmol). The alkenes were dissolved in DMF (15 mL) then sodium acetate (2.39 g, 29.2 mmol, 1.20 equiv) was

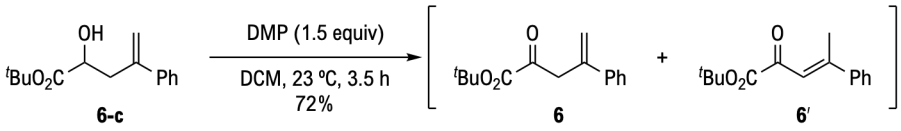
added in a single portion. The reaction was heated to 70 ºC for 1 hour, then cooled to room temperature and diluted with pentane (50 mL). The mixture was transferred to a separatory funnel containing 10% *w/w* aq. LiCl (100 mL). The organic phase was separated and extracted twice more with pentane (50 mL each). The combined organics were washed with half saturated brine (50 mL), dried over sodium sulfate, filtered, and evaporated. The crude material was purified through SiO_2 (0–5% *v/v* EtOAc/hexanes) to afford 2-phenylallyl acetate (**6-b**, 4.29 g, 24.3 mmol, 100% yield) as a clear colorless oil. Characterization matched with literature values [*42*].

Step 3: Palladium-Catalyzed Allylic Alkylation



Compound **6-c** was prepared according to a literature procedure [*43*].

Step 4: Dess–Martin Periodinane Oxidation



A 100 mL round bottom flask equipped with a Teflon-coated magnetic stir bar was charged with *tert*-butyl 2-hydroxy-4-phenylpent-4-enoate (**6-c**, 338 mg, 1.36 mmol, 1.00 equiv) and DCM (13.6 mL). Once the solution was homogeneous, DMP (866 mg, 1.5 Eq, 2.04 mmol) was added in one portion. The reaction was then stirred at 23 °C for 3.5 hour. After completion, the reaction was quenched with a 1:1 mixture of sat. aq. $NaHCO_3$ and sat. aq. $Na_2S_2O_3$. The organic layer was separated, then the aqueous layer was extracted

with DCM (3 x 10 mL). The combined organics were dried over magnesium sulfate, filtered, and evaporated. The crude material was purified through SiO_2 (5% *v/v* EtOAc/hexanes) to afford an inseparable mixture (1:2.4) of *tert*-butyl 2-oxo-4-phenylpent-4-enoate and *tert*-butyl (*E*)-2-oxo-4-phenylpent-3-enoate (241 mg, 978 µmol, 72%) as a yellow oil. Compound **6** isomerizes to **6'** at room temperature in $CDCl_3$ and MeOD-*d4*.

Scale: 1.36 mmol

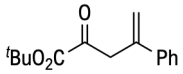
Purification: SiO_2 (5% *v/v* EtOAc/hexanes)

Physical State: Yellow oil

IR (ATR, neat) $\tilde{\nu}_{max}$: 3058, 2979, 2933, 1718, 1685, 1590, 1571, 1446, 1368, 1301, 1254, 1158, 1088, 967, 836, 818, 751, 693 cm^{-1}

HRMS–DART (*m/z*): $[M + H]^+$ calc'd for $C_{15}H_{19}O_3$ 247.1329, found 247.1329

$[M - C_4H_9]^+$ calc'd for $C_{11}H_9O_3$ 189.0546, found 189.0546



6

tert-butyl 2-oxo-4-phenylpent-4-enoate (**6**)

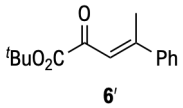
Yield: 21% (ca. 70.1 mg)

***R*f** = 0.38 (15% *v/v* EtOAc/hexanes + UV/vanillin stain)

^{1}H NMR (400 MHz, $CDCl_3$) δ 7.44 – 7.22 (m, 5H), 5.77 – 5.42 (m, 1H), 5.18 (p, *J* = 1.0 Hz, 1H), 3.92 (dd, *J* = 2.0, 1.0 Hz, 2H), 1.47 (s, 9H).

^{1}H NMR (300 MHz, MeOD) δ 7.50 – 7.20 (m, 5H), 5.59 (d, *J* = 1.5 Hz, 1H), 5.31 – 5.09 (m, 1H), 3.96 (d, *J* = 1.4 Hz, 2H), 1.47 (s, 9H).

^{13}C NMR (101 MHz, $CDCl_3$) δ 192.8, 160.6, 139.7, 139.7, 128.4, 127.9, 125.9, 117.2, 84.1, 45.3, 27.7.



6'

tert-butyl (*E*)-2-oxo-4-phenylpent-3-enoate (**6'**)

Yield: 51% (ca. 170.9 mg)

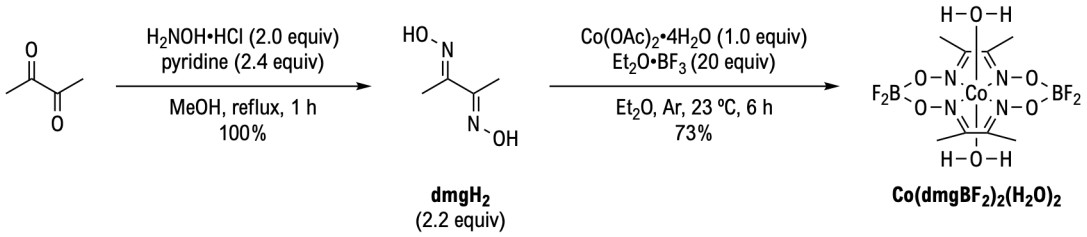
***R*$_f$** = 0.33 (15% *v/v* EtOAc/hexanes + UV/vanillin stain)

^{1}H NMR (400 MHz, $CDCl_3$) δ 7.58 – 7.50 (m, 2H), 7.41 – 7.35 (m, 3H), 7.18 (p, *J* = 1.0 Hz, 1H), 2.61 (t, *J* = 1.1 Hz, 3H), 1.56 (d, *J* = 2.1 Hz, 9H).

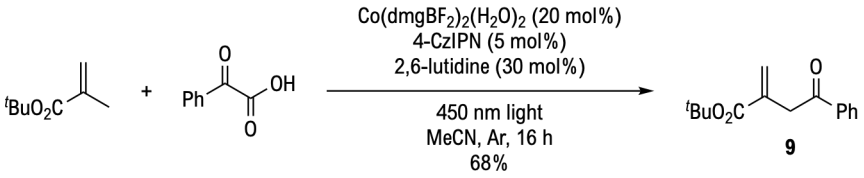
^{1}H NMR (300 MHz, MeOD) δ 7.60 (dtt, *J* = 6.1, 3.7, 0.9 Hz, 2H), 7.43 (dddd, *J* = 4.1, 2.8, 2.1, 1.0 Hz, 3H), 7.17 – 7.02 (m, 1H), 2.60 (dt, *J* = 2.6, 1.2 Hz, 3H), 1.56 (s, 9H).

^{13}C NMR (101 MHz, $CDCl_3$) δ 183.6, 161.9, 160.8, 141.8, 130.0, 128.6, 126.7, 119.0, 83.4, 27.8, 19.0.

8.6.3.5 *tert*-Butyl 2-methylene-4-oxo-4-phenylbutanoate



The dimethylglyoxime ligand (**dmgH₂**) was prepared according to a literature procedure (*43*). **Co(dmgBF₂)₂(H₂O)₂** was prepared according to a literature procedure [*44*].



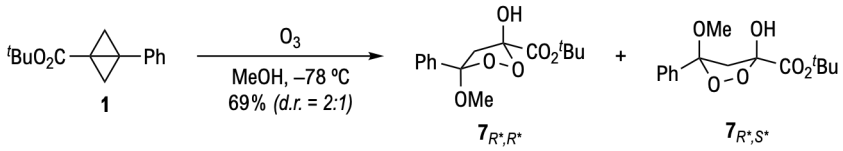
Compound **9** was prepared from *tert*-butyl methylacrylate and 2-oxo-2-phenylacetic acid using the prepared **Co(dmgBF₂)₂(H₂O)₂** according to a literature procedure and characterization matched with literature values [*45*]. Additional ^{1}H and ^{13}C NMR measurements in MeOD-d_4 were conducted and the values are provided below.

^{1}H NMR (800 MHz, MeOD) δ 8.01 (dd, *J* = 8.4, 1.4 Hz, 2H), 7.61 (tt, *J* = 7.1, 1.3 Hz, 1H), 7.57 – 7.45 (m, H), 6.25 (d, *J* = 1.6 Hz, 1H), 5.66 (d, *J* = 1.4 Hz, 1H), 4.03 (s, 2H), 1.40 (s, 9H).

^{13}C NMR (201 MHz, MeOD) δ 199.4, 167.2, 138.3, 138.0, 134.4, 129.8, 129.3, 128.1, 82.1, 43.0, 28.2.

8.6.4 Ozonolysis Products

8.6.4.1 *tert*-Butyl 3-phenylbicyclo[1.1.0]butane-1-carboxylate Ozonolysis



Compound **7** was prepared from BCB **1**.

To a 10 mL round-bottom flask was added *tert*-butyl 3-phenylbicyclo[1.1.0]butane-1-carboxylate (**1**, 50.0 mg, 0.217 mmol, 1.00 equiv) and a Teflon-coated magnetic stir bar. Methanol (2.17 mL) was added, and the mixture was stirred until it became homogeneous. The flask was cooled to –78 ºC in an acetone/dry ice bath. The flask was opened to air with no cap used to seal the system. Oxygen was bubbled through a 16G x 4" needle at 1.0 L/min into that solution. Then the Globalozone GO-D3G ozone generator was turned on at 0.74 amps. After 180 seconds the ozone generator was switched off, and the excess ozone was removed using air. The solvent was evaporated then the sample was purified by SiO_2 column chromatography (5% *v/v* EtOAc/hexanes) to afford *tert*-butyl 3-hydroxy-5-methoxy-5-phenyl-1,2-dioxolane-3-carboxylate (**7**) as an amorphous white solid (44.2 mg) in 69% yield as an inseparable mixture of diastereomers (***7*****$_{R^*,R^*}$**/***7*****$_{R^*,S^*}$** = *2:1*).

Scale: 0.217 mmol

Yield: 69%, ***7*****$_{R^*,R^*}$**/***7*****$_{R^*,S^*}$** = *2:1* (44.2 mg)

R**$_f$** = 0.20 (10% *v/v* EtOAc/hexanes + vanillin stain) [incidental R_f]

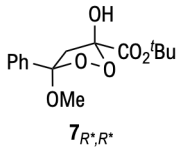
Purification: SiO_2 (5% *v/v* EtOAc/hexanes)

Physical State: Amorphous white solid

Melting Point: 80–81 ºC

IR (ATR, neat) $\tilde{\nu}_{max}$: 3481, 2980, 2939, 1739, 1371, 1310, 1256, 1221, 1155, 1045, 936, 839, 766, 701 cm^{-1}

HRMS–DART (*m/z*): $[M+H]^+$ calc'd for $C_{15}H_{21}O_6$ 297.1333, found 297.1319



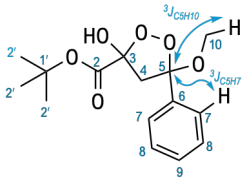
7$_{R^*,R^*}$

tert-butyl (3*R**,5*R**)-3-hydroxy-5-methoxy-5-phenyl-1,2-dioxolane-3-carboxylate (**7**$_{R^*,R^*}$)

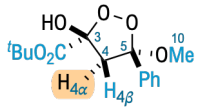
^{1}H NMR (500 MHz, $CDCl_3$) δ 7.54 (dd, *J* = 8.2, 1.5 Hz, 2H), 7.46 – 7.30 (m, 3H), 4.35 (br, 1H), 3.61 (d, *J* = 13.6 Hz, 1H), 3.27 (s, 3H), 2.84 (d, *J* = 13.4 Hz, 1H), 1.56 (s, 9H).

^{13}C NMR (126 MHz, $CDCl_3$) δ 165.7, 135.9, 128.9, 128.8, 126.5, 110.3, 104.3, 85.0, 58.4, 51.0, 27.9 [incidental].

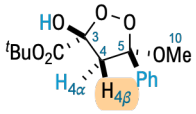
2D NMR (HMBC, **HSQC**, and **NOESY)** spectra are provided to support configurational assignment. HMBC and NOE correlations are presented below. See section 8.6.9 for more details.



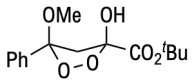
HMBC Correlations



1D Selective NOESY Correlations



1D Selective NOESY Correlations



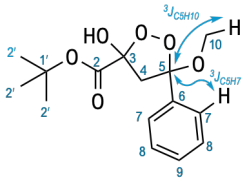
7$_{R^*,S^*}$

tert-butyl (3*R**,5*S**)-3-hydroxy-5-methoxy-5-phenyl-1,2-dioxolane-3-carboxylate (**7**$_{R^*,S^*}$)

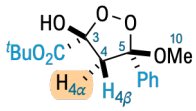
^{1}H NMR (500 MHz, $CDCl_3$) δ 7.49 (dd, *J* = 7.8, 1.8 Hz, 2H), 7.45 – 7.31 (m, 3H), 5.02 (br, 1H), 3.30 (s, 3H), 3.22 (d, *J* = 13.3 Hz, 1H), 3.00 (d, *J* = 13.1 Hz, 1H), 1.53 (s, 9H).

^{13}C NMR (126 MHz, $CDCl_3$) δ 166.3, 134.5, 129.2, 128.9, 126.6, 109.4, 103.7, 84.5, 56.4, 50.9, 27.9 [incidental].

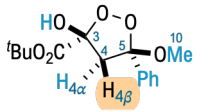
2D NMR (HMBC, **HSQC**, and **NOESY)** spectra are provided to support configurational assignment. HMBC and NOE correlations are presented below. See section 8.6.9 for more details.



HMBC Correlations

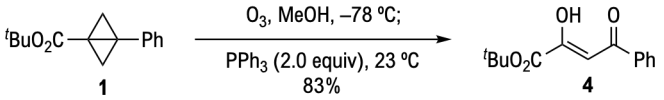


1D Selective NOESY Correlations



1D Selective NOESY Correlations

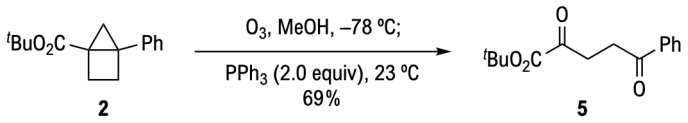
8.6.4.2 *tert*-Butyl 3-phenylbicyclo[1.1.0]butane-1-carboxylate Reductive Ozonolysis



(*Z*)-5-(*tert*-butoxy)-3-hydroxy-1-phenylpent-2-en-4-yn-1-one (**4**) was synthesized from BCB **1**.

A 10 mL round bottom flask equipped with a Teflon-coated magnetic stir bar was charged with *tert*-butyl 3-phenylbicyclo[1.1.0]butane-1-carboxylate (51.0 mg, 0.221 mmol, 1.00 equiv). Methanol (2.21 mL) was added, and the flask was cooled to –78 ºC in an acetone/dry ice bath for 10 minutes. The flask was open to air and no cap was used to seal the system. Oxygen was bubbled through a 16G x 4" needle at 1.0 L/min into the solution. Then the Globalozone GO-D3G ozone generator was turned on at 0.74 amps. After 180 seconds the ozone generator was switched off, and the excess ozone was removed using oxygen. The reaction was judged to be complete by full conversion on TLC. The starting material appeared at R_f = 0.26 in 50% *v/v* DCM/hexanes, visualized with UV/vanillin as a blue spot. The peroxide product appeared at R_f = 0.17, 50% *v/v* DCM/hexanes visualized with UV/vanillin as a red spot. Triphenylphosphine (116 mg, 0.443 mmol, 2.00 equiv) and a rubber septum were added, and the solution was stirred at room temperature for 18 hours. After the reduction had finished, as judged by TLC, the solvent was evaporated. The crude material was purified through SiO_2, eluting the excess triphenylphosphine with 50% *v/v* benzene/hexanes before eluting the product with 5% *v/v* EtOAc/hexanes spiked with 0.5% EtOH to minimize streaking. (*Z*)-5-(*tert*-butoxy)-3-hydroxy-1-phenylpent-2-en-4-yn-1-one (**4**) was isolated as a yellow oil (45.7 mg) in 83% yield. Characterization matched with literature values [*46*].

8.6.4.3 *tert*-Butyl 4-phenylbicyclo[2.1.0]pentane-1-carboxylate Ozonolysis



2 5

Compound **5** was prepared from BCP **2**.

A 25 mL round bottom flask equipped with a Teflon-coated magnetic stir bar was charged with *tert*-butyl 4-phenylbicyclo[2.1.0]pentane-1-carboxylate (129 mg, 95% purity, 0.500 mmol, 1.00 equiv) and MeOH (5.0 mL). The solution was cooled to –78 ºC in an acetone/dry-ice bath for 10 minutes. The flask was open to air with no cap used to seal the system. Oxygen was bubbled through a 16G x 4” needle at 1.0 L/min into that solution. Then the Globalozone GO-D3G ozone generator was turned on at 0.74 amps. The reaction became blue after 8.5 minutes. At 10 minutes the ozone generator was switched off, and the excess ozone was removed using air. Triphenylphosphine (262 mg, 1.00 mmol, 2.00 equiv) was added and the reaction was stirred at room temperature for 36 hours. After complete reduction of the peroxide, the stir bar was removed and the reaction was evaporated. The crude material was purified through SiO_2 (0–15% *v/v* EtOAc/hexanes) to afford *tert*-butyl 2,5-dioxo-5-phenylpentanoate (**5**, 90.6 mg, 0.346 mmol) as a pale-yellow oil in 69% yield.

Scale: 0.500 mmol

Yield: 69% (90.6 mg, 0.346 mmol)

R_f = 0.24 (10% *v/v* EtOAc/hexanes + UV/vanillin stain)

Purification: SiO_2 (0–15% *v/v* EtOAc/hexanes)

Physical State: Pale-yellow oil

IR (ATR, neat) $\tilde{\nu}_{max}$: 2979, 2932, 1741, 1718, 1685, 1597, 1581, 1478, 1448, 1394, 1368, 1294, 1277, 1256, 1236, 1209, 1155, 1082, 1073, 1042, 1024, 1001, 984, 954, 852, 835, 763, 751, 738, 689 cm^{-1}

HRMS–DART (*m/z*): $[M + H]^+$ calc'd for $C_{15}H_{19}O_4$ 263.1278, found 263.1279

$[M – C_4H_9O]$ calc'd for $C_{11}H_9O_3$, 189.0546, found 189.0547

^{1}H NMR (300 MHz, $CDCl_3$) δ 7.99 – 7.90 (m, 2H), 7.56 – 7.49 (m, 1H), 7.46 – 7.38 (m, 2H), 3.32 (td, *J* = 6.1, 1.0 Hz, 2H), 3.26 – 3.14 (m, 2H), 1.54 (s, 9H).

^{13}C NMR (75 MHz, $CDCl_3$) δ 197.6, 194.2, 160.1, 136.3, 133.3, 128.6, 128.1, 84.0, 33.0, 32.4, 27.8.

8.6.5 Kinetic Competition Experiments

8.6.5.1 Derivation from the First Order Rate Law

To determine the relative rate of consumption BCB **1** and BCP **2** versus an unactivated alkene, α-methylstyrene (**AMS**), and a deactivated alkene, *tert*-butyl acrylate (***t*BuA**) a competitive rate study was conducted. The bicyclo[*n*.1.0]alkane was paired with an alkene in a flask and ozonized. The remaining material was measured with quantitative NMR (qNMR) and used to calculate the relative rate. Experiments were conducted in triplicate and the values averaged then rounded to 1 significant figure.

The relative rates were derived from using a first-order rate law for each material where A and B are both reactants, O_3 is the common reagent, and k_A and k_B are the absolute rate constants.

(1) First Order Rate Laws

$$-\frac{d[A]}{dt} = k_A[A][O_3]^x$$

$$-\frac{d[B]}{dt} = k_B[B][O_3]^x$$

(2) Divide to remove the shared $[O_3]^x$ term and the dt term because, ignoring mass transport, A and B experience the same concentration of ozone for the same period of time

$$\frac{d[A]}{d[B]} = \frac{k_A[A]}{k_B[B]}$$

(3) Rearrange to separate A and B on either side of the equal sign

$$\frac{1}{[A]}d[A] = \frac{k_A}{k_B} \cdot \frac{1}{[B]}d[B]$$

(4) Integrate from $t = 0$ to $t = t$.

$$\int_{[A]_0}^{[A]_t} \frac{1}{[A]} d[A] = \frac{k_A}{k_B} \cdot \int_{[B]_0}^{[B]_t} \frac{1}{[B]} d[B]$$

(5) Solve the integral

$$\ln[A]_t - \ln[A]_0 = \frac{k_A}{k_B} \cdot (\ln[B]_t - \ln[B]_0)$$

(6) Simplify

$$\ln(\frac{[A]_t}{[A]_0}) = \frac{k_A}{k_B} \cdot \ln(\frac{[B]_t}{[B]_0})$$

(7) Rearrange

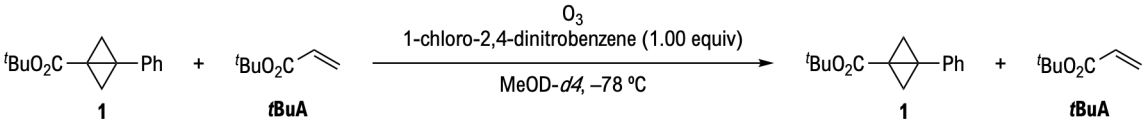
$$k_{rel} = \frac{k_A}{k_B} = \frac{\ln(\frac{[A]_t}{[A]_0})}{\ln(\frac{[B]_t}{[B]_0})}$$

(8) Since both $[A]_0$= $[B]_0$ = 1.00 at $t = 0$, the equation simplifies again

$$k_{rel} = \frac{\ln([A]_t)}{\ln([B]_t)}$$

The relative rate (k_{rel}) between A and B is therefore a direct readout of the remaining A and B after the reaction is complete.

8.6.5.2 *tert*-Butyl 3-phenylbicyclo[1.1.0]butane-1-carboxylate vs *tert*-Butyl Acrylate



To a 10 mL test tube was added *tert*-butyl 3-phenylbicyclo[1.1.0]butane-1-carboxylate (**1**, 69.1 mg, 0.300 mmol, 1.00 equiv), *tert*-butyl acrylate (***t*BuA**, 38.5 mg, 1.00 equiv), and 1-chloro-2,4-dinitrobenzene (60.8 mg, 0.300 mmol, 1.00 equiv). CD_3OD (3.00 mL) was added and the mixture was swirled until it became homogeneous. A 0.35 mL aliquot was removed, loaded into an NMR tube, and set aside as a blank. The remaining mixture was divided into three 0.750 mL portions and transferred into separate 10 mL test tubes and capped with rubber septum. All of the tubes were cooled to –78 ºC in an acetone/dry ice bath. One flask was opened to air with no cap used to seal the system. Oxygen was bubbled through a 16G x 4" needle at 1.0 L/min into that solution. Then the Globalozone GO-D3G ozone generator was turned on at 0.74 amps. After 25 seconds the ozone generator was switched off, and the excess ozone was removed using air. The sample was warmed to room temperature and transferred to an NMR tube to be measured. ^{1}H NMR was measured with a delay (D1) of 10 seconds with 32 scans per sample. The reaction was repeated for each of the remaining two test tubes and the data are recorded in the table below.

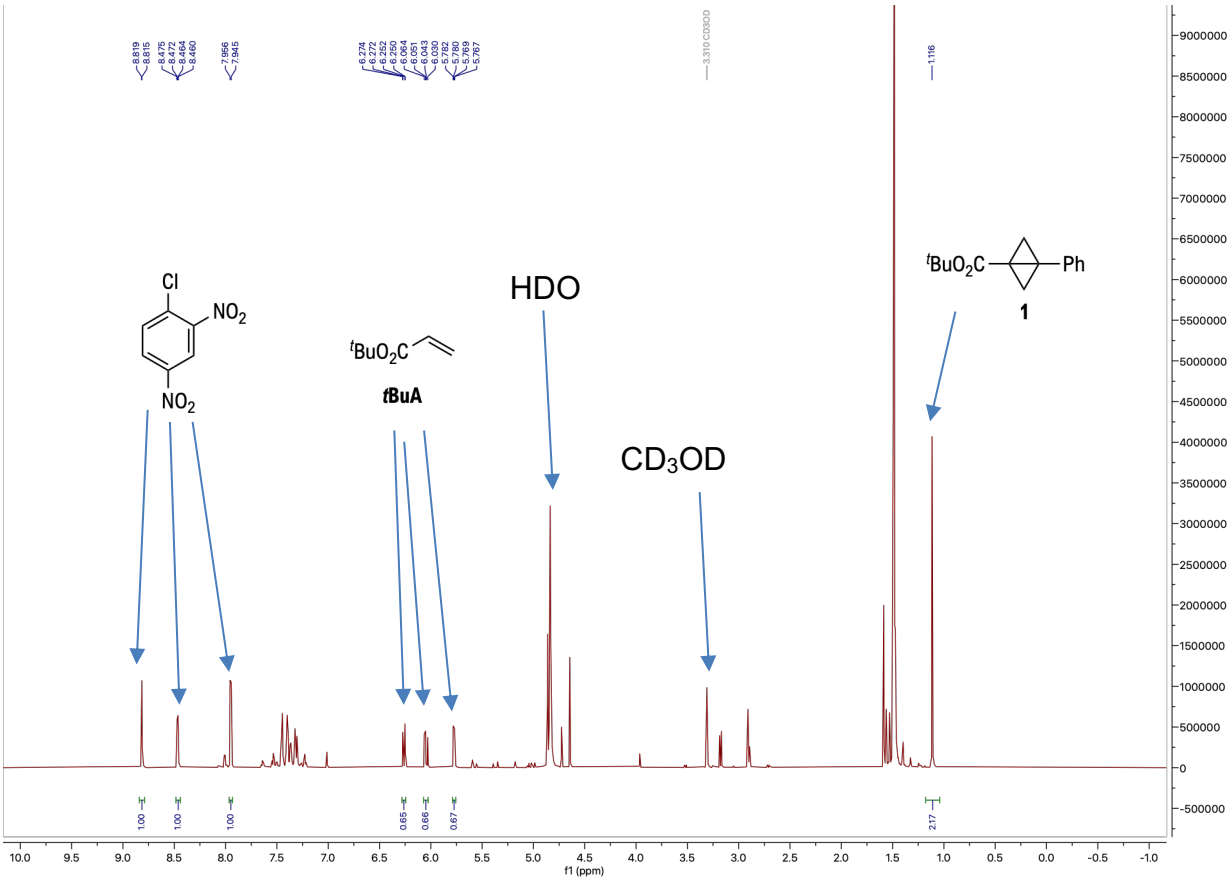
Each NMR spectrum was processed in MestReNova by first applying a standard baseline and phase correction. The residual solvent peak (CD_3OD) was set to 3.310 ppm. The non-overlapping internal standard (1-chloro-2,4-dinitrobenzene) peaks were integrated. The 3-CH peak (1H) was integrated from 8.840–8.790 ppm. The 4-CH peak (1H) was

integrated from 8.484–8.449 ppm. The 5-CH peak (1H) was integrated from 7.965–7.932 ppm. The blank sample was used to determine the measured ratio between the internal standard and each analyte. The internal standard peaks were set to a value of 1.00 for each sample. The BCB **1** corresponded a 0.9:1 to the internal standard. The ***t*BuA** corresponded to a 1:1 ratio to the internal standard. The remaining BCB **1** was quantified by integration of the *tert*-butyl signal (9H) from 1.178–1.04 ppm. The remaining ***t*BuA** was quantified by integration of the vinyl hydrogens (1H each) from 6.281–6.245 ppm, 6.071–6.026 ppm, and 5.789–5.757 ppm. A representative NMR spectrum of the crude reaction is annotated below.

Table 8.1 qNMR data from partial competitive Criegee ozonolysis of BCB **1** and ***t*BuA**.

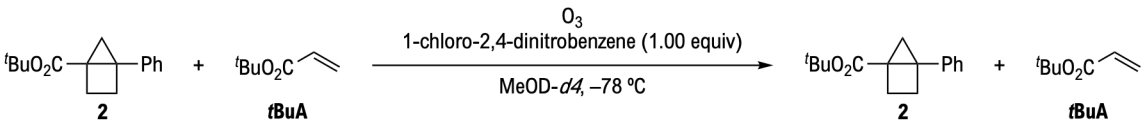
	average remaining ***t*BuA**	average remaining **1**	$\frac{\ln(\mathbf{1})}{\ln(\boldsymbol{t}\mathbf{BuA})}$	
trial 1	66.0	26.8	3.17	
trial 2	67.7	29.5	3.125	
trial 3	62.	24.9	2.97	
			3.09	average
			0.104	st. dev.

Crude qNMR from partial competitive Criegee ozonolysis of BCB **1** and ***t*BuA**.



^{1}H NMR (800 MHz, CD_3OD), D1 = 10, 32 scans

8.6.5.3 *tert*-Butyl 4-phenylbicyclo[2.1.0]pentane-1-carboxylate vs *tert*-Butyl Acrylate



To a 10 mL test tube was added *tert*-butyl 4-phenylbicyclo[2.1.0]pentane-1-carboxylate (**2**, 73.3 mg, 0.300 mmol, 1.00 equiv), *tert*-butyl acrylate (***t*BuA**, 38.5 mg, 1.00 equiv), and 1-chloro-2,4-dinitrobenzene (60.8 mg, 0.300 mmol, 1.00 equiv). CD_3OD (3.00 mL) was added and the mixture was swirled until it became homogeneous. A 0.35 mL aliquot was removed, loaded into an NMR tube, and set aside as a blank. The remaining mixture was divided into three 0.750 mL portions and transferred into separate 10 mL test tubes and capped with rubber septum. All of the tubes were cooled to –78 ºC in an acetone/dry ice bath. One flask was opened to air with no cap used to seal the system. Oxygen was bubbled through a 16G x 4" needle at 1.0 L/min into that solution. Then the Globalozone GO-D3G ozone generator was turned on at 0.74 amps. After 30 seconds the ozone generator was switched off, and the excess ozone was removed using air. The sample was warmed to room temperature and transferred to an NMR tube to be measured. ^{1}H NMR was measured with a delay (D1) of 10 seconds with 32 scans per sample. The reaction was repeated for each of the remaining two test tubes and the data are recorded in the table below.

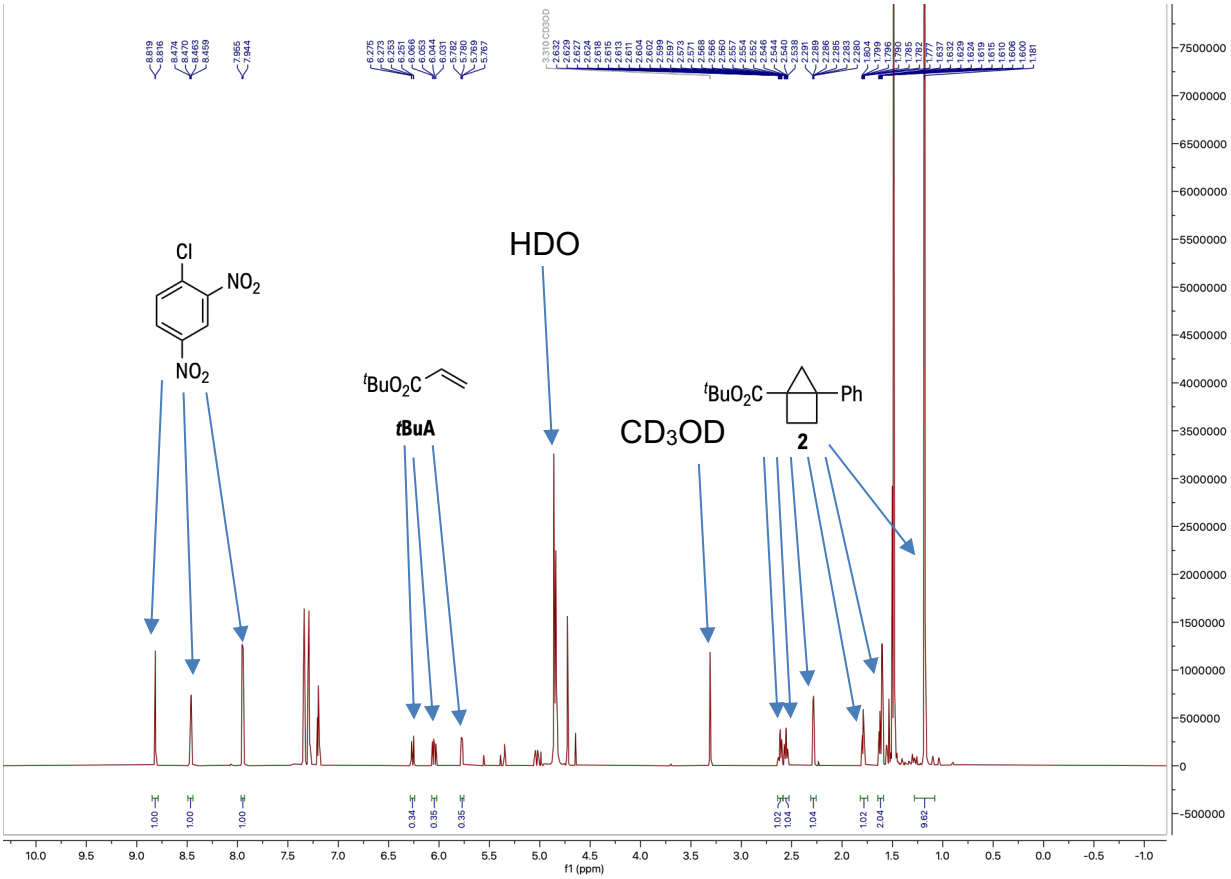
Each NMR spectrum was processed in MestReNova by first applying a standard baseline and phase correction. The residual solvent peak (CD_3OD) was set to 3.310 ppm. The non-overlapping internal standard (1-chloro-2,4-dinitrobenzene) peaks were integrated. The 3-CH peak (1H) was integrated from 8.840–8.790 ppm. The 4-CH peak (1H) was

integrated from 8.484–8.449 ppm. The 5-CH peak (1H) was integrated from 7.965–7.932 ppm. The blank sample was used to determine the measured ratio between the internal standard and each analyte. The internal standard peaks were set to a value of 1.00 for each sample. The BCP **2** corresponded a 1.10:1 to the internal standard. The ***t*BuA** corresponded to a 1.12:1 ratio to the internal standard. The remaining BCP **1** was quantified by integration of the following signals: 2.693–2.587 ppm (1H), 2.586–2.527 ppm (1H), 2.311–2.257 ppm (1H), 1.816–1.765 ppm (2H), 1281–1.08 ppm (9H). The remaining ***t*BuA** was quantified by integration of the vinyl hydrogens (1H each) from 6.284–6.242 ppm, 6.072–6.022 ppm, and 5.788–5.753 ppm. Trial 3 appeared to be an outlier and was not considered for the calculation of the average or standard deviation. A representative NMR spectrum of the crude reaction is annotated below.

Table 8.2 qNMR data from partial competitive Criegee ozonolysis of BCP **2** and ***t*BuA**

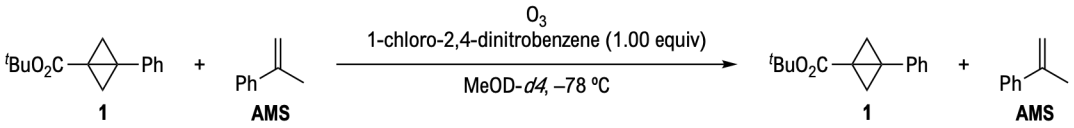
	average remaining ***t*BuA**	average remaining **2**	$\frac{\ln(\boldsymbol{t}\mathbf{BuA})}{\ln(\mathbf{2})}$	
trial 1	31.0	94.1	19.2	
trial 2	28.6	93.1	17.5	
trial 3	9.8	92.9	31.5	
			18.4	average
			1.17	st. dev.

Crude qNMR from partial competitive Criegee ozonolysis of BCB **2** and ***t*BuA**.



^{1}H NMR (800 MHz, CD_3OD), D1 = 10, 32 scans

8.6.5.4 *tert*-Butyl 3-phenylbicyclo[1.1.0]butane-1-carboxylate vs α-Methyl Styrene



α-Methyl styrene (**AMS**) was vacuum distilled immediately prior to use [*47*].

To a 10 mL test tube was added *tert*-butyl 3-phenylbicyclo[1.1.0]butane-1-carboxylate (**1**, 69.1 mg, 0.300 mmol, 1.00 equiv), α-methyl styrene (**AMS**, 38.5 mg, 1.00 equiv), and 1-chloro-2,4-dinitrobenzene (60.8 mg, 0.300 mmol, 1.00 equiv). CD_3OD (3.00 mL) was added and the mixture was swirled until it became homogeneous. A 0.35 mL aliquot was removed, loaded into an NMR tube, and set aside as a blank. The remaining mixture was divided into three 0.750 mL portions and transferred into separate 10 mL test tubes and capped with rubber septum. All of the tubes were cooled to –78 ºC in an acetone/dry ice bath. One flask was opened to air with no cap used to seal the system. Oxygen was bubbled through a 16G x 4" needle at 1.0 L/min into that solution. Then the Globalozone GO-D3G ozone generator was turned on at 0.74 amps. After 15 seconds the ozone generator was switched off, and the excess ozone was removed using air. The sample was warmed to room temperature and transferred to an NMR tube to be measured. ^{1}H NMR was measured with a delay (D1) of 10 seconds with 32 scans per sample. The reaction was repeated for each of the remaining two test tubes and the data are recorded in the table below.

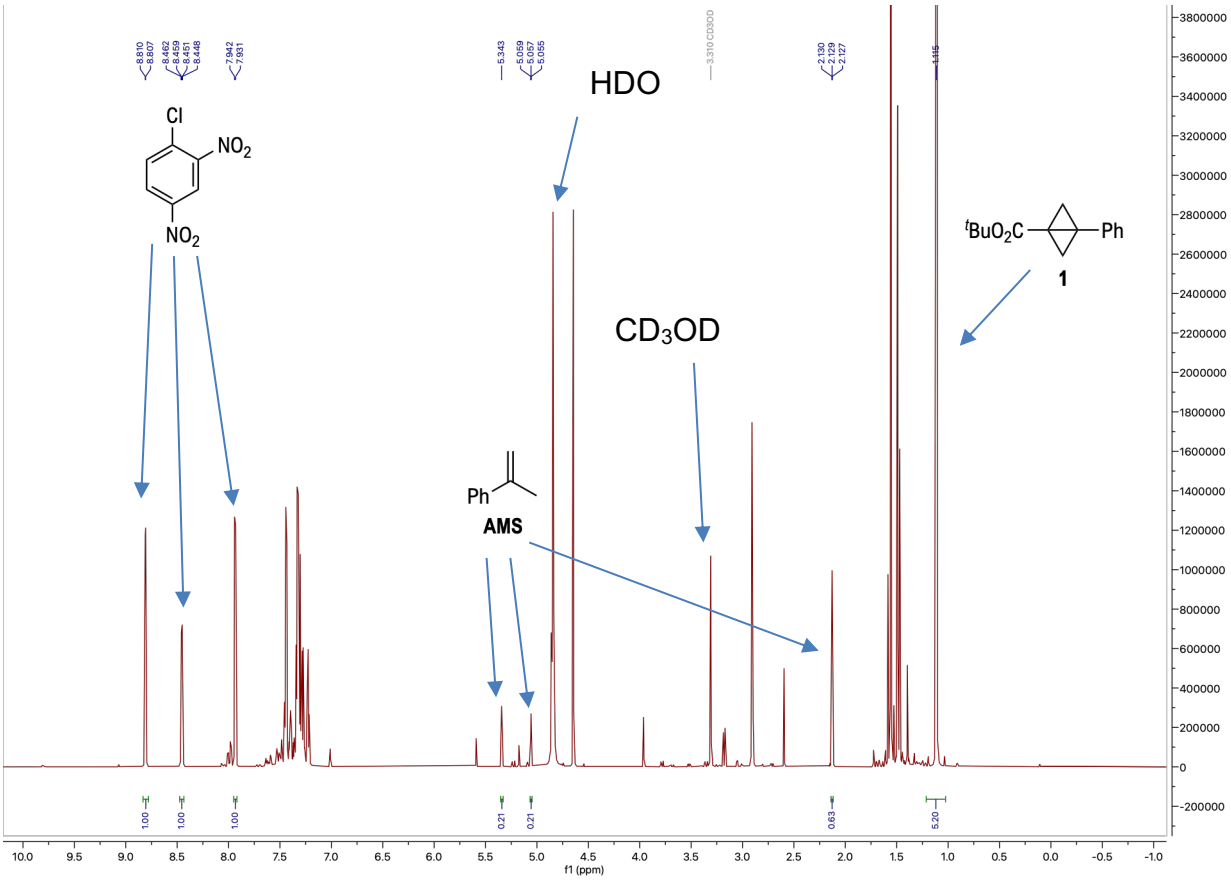
Each NMR spectrum was processed in MestReNova by first applying a standard baseline and phase correction. The residual solvent peak (CD_3OD) was set to 3.310 ppm. The

non-overlapping internal standard (1-chloro-2,4-dinitrobenzene) peaks were integrated. The 3-CH peak (1H) was integrated from 8.828–8.769 ppm. The 4-CH peak (1H) was integrated from 8.465–8.423 ppm. The 5-CH peak (1H) was integrated from 7.944–7.908 ppm. The blank sample was used to determine the measured ratio between the internal standard and each analyte. The internal standard peaks were set to a value of 1.00 for each sample. The BCB **1** corresponded a 0.9:1 to the internal standard. The **AMS** corresponded to a 1:1 ratio to the internal standard. The remaining BCB **1** was quantified by integration of the *tert*-butyl signal (9H) from 1.213–1.025 ppm. The remaining **AMS** was quantified by integration of the methyl (3H) peak from 2.142–2.115 ppm and the vinyl hydrogens (1H each) from 5.357–5.334 ppm and 5.068–5.045 ppm. A representative NMR spectrum of the crude reaction is annotated below.

Table 8.3 qNMR data from partial competitive Criegee ozonolysis of BCB **1** and **AMS**

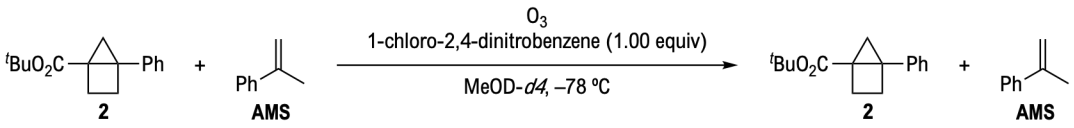
	average remaining **AMS**	average remaining **1**	$\frac{\ln(\mathbf{AMS})}{\ln(\mathbf{1})}$	
trial 1	21.0	64.2	3.54	
trial 2	16.0	59.5	3.53	
trial 3	7.00	40.9	2.97	
			3.34	average
			0.320	st. dev.

Crude qNMR from partial competitive Criegee ozonolysis of BCB **1** and **AMS**.



^{1}H NMR (800 MHz, CD_3OD), D1 = 10, 32 scans

8.6.5.5 *tert*-Butyl 4-phenylbicyclo[2.1.0]pentane-1-carboxylate vs α-Methyl Styrene



α-Methyl styrene (**AMS**) was vacuum distilled immediately prior to use [*47*].

To a 10 mL test tube was added *tert*-butyl 4-phenylbicyclo[2.1.0]pentane-1-carboxylate (**2**, 73.3 mg, 0.300 mmol, 1.00 equiv), α-methyl styrene (**AMS**, 38.5 mg, 1.00 equiv), and 1-chloro-2,4-dinitrobenzene (60.8 mg, 0.300 mmol, 1.00 equiv). CD_3OD (3.00 mL) was added and the mixture was swirled until it became homogeneous. A 0.35 mL aliquot was removed, loaded into an NMR tube, and set aside as a blank. The remaining mixture was divided into three 0.750 mL portions and transferred into separate 10 mL test tubes and capped with rubber septum. All of the tubes were cooled to –78 ºC in an acetone/dry ice bath. One flask was opened to air with no cap used to seal the system. Oxygen was bubbled through a 16G x 4" needle at 1.0 L/min into that solution. Then the Globalozone GO-D3G ozone generator was turned on at 0.74 amps. After 20 seconds the ozone generator was switched off, and the excess ozone was removed using air. The sample was warmed to room temperature and transferred to an NMR tube to be measured. ^{1}H NMR was measured with a delay (D1) of 10 seconds with 32 scans per sample. The reaction was repeated for each of the remaining two test tubes and the data are recorded in the table below.

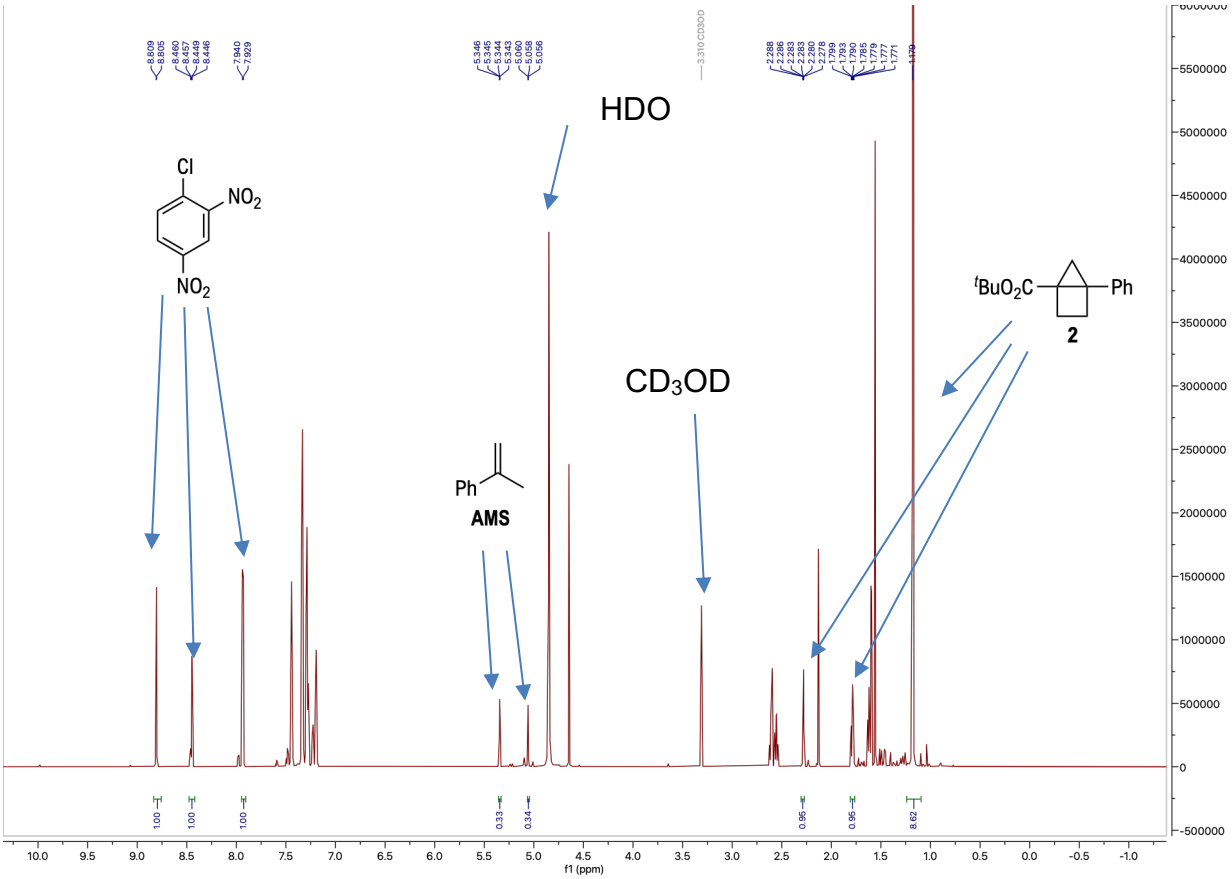
Each NMR spectrum was processed in MestReNova by first applying a standard baseline and phase correction. The residual solvent peak (CD_3OD) was set to 3.310 ppm. The

non-overlapping internal standard (1-chloro-2,4-dinitrobenzene) peaks were integrated. The 3-CH peak (1H) was integrated from 8.833–8.747 ppm. The 4-CH peak (1H) was integrated from 8.466–8.419 ppm. The 5-CH peak (1H) was integrated from 7.947–7.906 ppm. The blank sample was used to determine the measured ratio between the internal standard and each analyte. The internal standard peaks were set to a value of 1.00 for each sample. The BCP **2** corresponded a 0.97:1 to the internal standard. The **AMS** corresponded to a 1:1 ratio to the internal standard. The remaining BCP **2** was quantified by integration of the following signals: 2.305–2.559 ppm (1H), 1.818–1.749 ppm (2H), and 1.241–1.095 ppm (9H). The remaining **AMS** was quantified by integration of the vinyl hydrogens (1H each) from 5.356–5.330 ppm and 5.065–5.044 ppm. A representative NMR spectrum of the crude reaction is annotated below.

Table 8.4 qNMR data from partial competitive Criegee ozonolysis of BCP **2** and **AMS**

	average remaining **AMS**	average remaining **2**	$\frac{\ln(\mathbf{AMS})}{\ln(\mathbf{2})}$	
trial 1	34.0	98.1	57.1	
trial 2	29.0	97.9	58.3	
trial 3	33.5	98.2	60.4	
			58.6	average
			1.66	st. dev.

Crude qNMR from partial competitive Criegee ozonolysis of BCP **2** and **AMS**.



^{1}H NMR (800 MHz, CD_3OD), D1 = 10, 32 scans

8.6.5.6 Relative Rate Calculation

Due to the extremely low conversion of BCP **2** relative to **AMS**, these data points were omitted from the calculation of the relative rates for the series **AMS**, **1**, ***t*BuA**, and **2**. Error propogation analysis indicated that a minor variation of ±1% in the qNMR integration values would result in an order-of-magnitude shift in the calculated relative rate. Consequently, ***t*BuA** was selected as an internal anchor to normalize the data set from which the relative comparison between **AMS** and **2** was calculated.

Given its relative rate as slower than BCB **1** but faster than BCP2**3**, ***t*BuA** was referenced to the benchmark value of 1. Every other relative rate was calculated relative to this benchmark.

(1) Calculate BCB **1** relative to ***t*BuA**

$$\frac{k_{\boldsymbol{t}\mathbf{BuA}}}{k_{\mathbf{BCB}}} = 0.324;\ k_{\mathbf{BCB}} = \frac{k_{\boldsymbol{t}\mathbf{BuA}}}{0.324} = \frac{1}{0.324} = 3.09$$

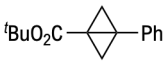
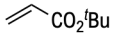
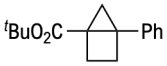
(2) Calculate BCB **1** relative to **AMS**

$$\frac{k_{\mathbf{AMS}}}{k_{\mathbf{BCB}}} = 0.341;\ k_{\mathbf{AMS}} = k_{\mathbf{BCB}} \cdot 3.341;\ k_{\mathbf{AMS}} = 3.086 \cdot 3.341 = 10.3$$

(3) Calculate BCP **2** relative to ***t*BuA**

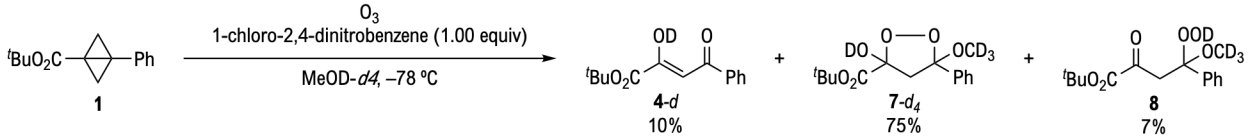
$$\frac{k_{\boldsymbol{t}\mathbf{BuA}}}{k_{\mathbf{BCP}}} = 18.4;\ k_{\mathbf{BCP}} = \frac{k_{\boldsymbol{t}\mathbf{BuA}}}{18.4} = \frac{1}{18.4} = 0.0544$$

Simplifying to 1 significant figure provides the following relative rates

				
	AMS	**1**	**tBuA**	**2**
k_{rel}	10	3	1	0.05

8.6.6 Ozonolysis of *tert*-Butyl 3-phenylbicyclo[1.1.0]butane-1-carboxylate in MeOD-*d4*

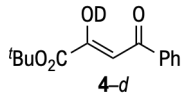
8.6.6.1 One-Minute Ozonolysis of *tert*-Butyl 3-phenylbicyclo[1.1.0]butane-1-carboxylate



Compounds **2**, **7** and **8** were observed in the ^{1}H NMR of the crude reaction mixture from the ozonolysis of BCB **1**.

To a 10 mL test tube was added *tert*-butyl 3-phenylbicyclo[1.1.0]butane-1-carboxylate (**1**, 69.1 mg, 0.300 mmol, 1.00 equiv) and 1-chloro-2,4-dinitrobenzene (60.8 mg, 0.300 mmol, 1.00 equiv). CD_3OD (3.00 mL) was added and the mixture was swirled until it became homogeneous. A 0.35 mL aliquot was removed, loaded into an NMR tube, and set aside as a blank. The remaining mixture was divided into three 0.750 mL portions and transferred into separate 10 mL test tubes and capped with rubber septum. All of the tubes were cooled to –78 ºC in an acetone/dry ice bath. One flask was opened to air with no cap used to seal the system. Oxygen was bubbled through a 16G x 4” needle at 1.0 L/min into that solution. Then the Globalozone GO-D3G ozone generator was turned on at 0.74 amps. After 60 seconds the ozone generator was switched off, and the excess ozone was removed using air. The sample was warmed to room temperature and transferred to an NMR tube to be measured. ^{1}H NMR was measured with a delay (D1) of 10 seconds with 32 scans per sample. The reaction was repeated for each of the remaining two test tubes and the data are recorded in the table below.

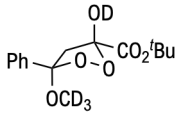
Each NMR spectrum was processed in MestReNova by first applying a standard baseline and phase correction. The residual solvent peak (CD_3OD) was set to 3.310 ppm. The non-overlapping internal standard (1-chloro-2,4-dinitrobenzene) peaks were integrated. The 3-CH peak (1H) was integrated from 8.933–8.713 ppm. The 4-CH peak (1H) was integrated from 8.499–8.445 ppm. The 5-CH peak (1H) was integrated from 7.964–7.922 ppm. The blank sample was used to determine the measured ratio between the internal standard and the analyte. The internal standard peaks were set to a value of 1.14 for each sample to normalize the analyte values to whole integer values. Compound **2**-*d* was quantified by integration of the singlet peak (1H) at 7.01 ppm. The peroxide $\mathbf{7}_{R^*,R^*}$-*d4* was quantified by integration of the CH_2 peak (1H each) from 3.556–3.498 ppm and 2.721–2.699 ppm. The peroxide $\mathbf{7}_{S^*,R^*}$-*d4* was quantified by integration of the CH_2 peak (1H each) from 3.202–3.144 ppm and 2.927–2.882 ppm. The peroxide **8** was quantified by integration of the pair of doublets (1H each) from 3.562–3.502 ppm. Deduced ^{1}H NMR signals for compound **4**-*d*, **7**-*d4*, and **8** are listed below. A representative NMR spectrum of the crude reaction is annotated below.



4–*d*

tert-butyl (*Z*)-2-(hydroxy-*d*)-4-oxo-4-phenylbut-2-enoate (**2**-*d*)

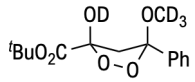
crude ^{1}H NMR (800 MHz, MeOD) δ 8.02 – 8.00 (m, 2H), 7.64 (tt, *J* = 7.1, 1.3 Hz, 1H), 7.55 – 7.52 (m, 2H), 7.01 (s, 1H), 1.59 (s, 9H).



$\mathbf{7}_{R^*,R^*}$–d_4

tert-butyl (3*R**,5*R**)-3-(hydroxy-*d*)-5-(methoxy-d_3)-5-phenyl-1,2-dioxolane-3-carboxylate (**7**$_{R^*,R^*}$-*d4*)

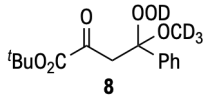
crude ^{1}H NMR (800 MHz, MeOD) δ 7.46 – 7.33 (m, 5H), 3.52 (d, *J* = 13.5 Hz, 1H), 2.71 (d, *J* = 13.4 Hz, 1H), 1.53 (s, 9H).



$\mathbf{7}_{R^*,S^*}$–d_4

tert-butyl (3*R**,5*S**)-3-(hydroxy-d)-5-(methoxy-d_3)-5-phenyl-1,2-dioxolane-3-carboxylate (**7**$_{R^*,S^*}$-*d4*)

crude ^{1}H NMR (800 MHz, MeOD) δ 7.47 – 7.31 (m, 5H), 3.18 (d, *J* = 13.3 Hz, 1H), 2.90 (d, *J* = 13.4 Hz, 1H), 1.49 (s, 9H).

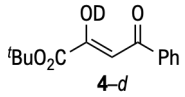


8

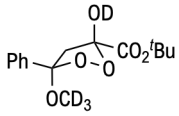
tert-butyl 4-deuteroperoxy-4-(methoxy-d_3)-2-oxo-4-phenylbutanoate (**8**)

crude ^{1}H NMR (800 MHz, MeOD) δ 7.47 – 7.34 (m, 5H), 3.54 (d, *J* = 19.2 Hz, 1H), 3.51 (d, *J* = 15.8 Hz, 1H), 1.53 (s, 9H).

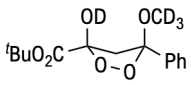
Compound **8** was assigned based on the expected chemical shift of the methylene hydrogens and their appearance as a pair of diastereotopic doublets.



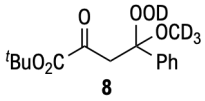
4–*d*



7$_{R^*,R^*}$–d_4



7$_{R^*,S^*}$–d_4

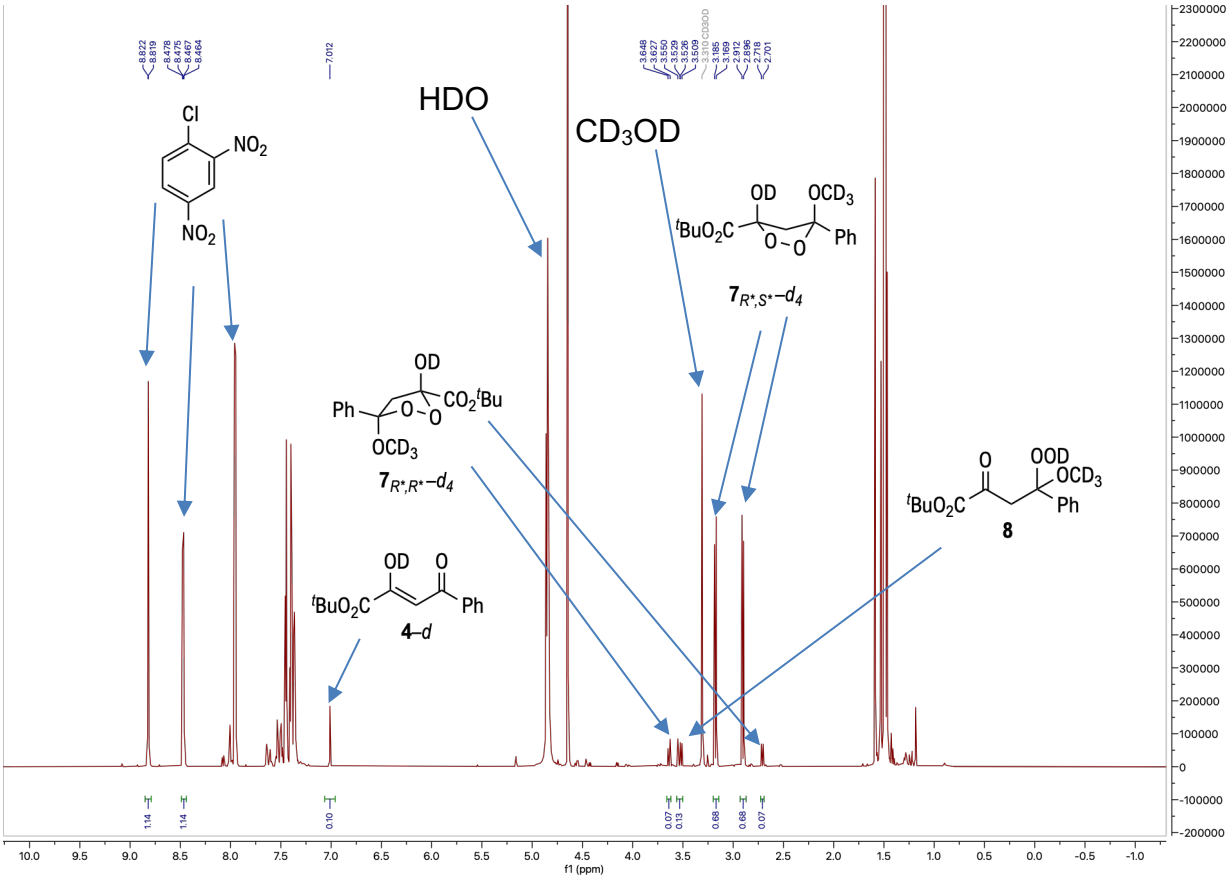


8

Table 8.5 qNMR data from Criegee ozonolysis of BCB **1**

Trial	**%4d**	**%7**$_{R^*,R^*}$	**%7**$_{R^*,S^*}$	**%8**
1	10	7	68	7
2	10	7	68	7
3	10	7	68	7

Crude qNMR from Criegee ozonolysis of BCB **1**.



^{1}H NMR (800 MHz, CD_3OD), D1 = 10, 32 scans

The after measurement of the crude ^{1}H NMR from the ozonolysis of BCB **1**, the three samples were combined, evaporated, and purified through FCC (5% *v/v* EtOAc/hexanes) to afford an off-white amorphous solid (43 mg) in 64% yield.

Scale: 0.225 mmol

Yield: 64%, $\mathbf{7}_{R^*,R^*}/\mathbf{7}_{S^*,R^*}$ = *5.5:1,* (43 mg)

$\boldsymbol{R}_\mathbf{f}$ = 0.20 (10% *v/v* EtOAc/hexanes + vanillin stain) [incidental R_f]

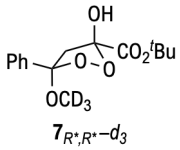
Purification: SiO_2 (5% *v/v* EtOAc/hexanes)

Physical State: Off-white amorphous solid

Melting Point: 81–82 ºC

IR (ATR, neat) $\tilde{\nu}_{max}$: 3464, 2930, 2850, 1735, 1449, 1370, 1307, 1253, 1219, 1148, 1100, 1073, 1044, 1021, 933, 837, 759, 747, 699, 671 cm^{-1}

HRMS–DART (*m/z*): $[M - OH]^+$ calc'd for $C_{15}H_{17}D_3O_5$ 283.1494, found 283.1501



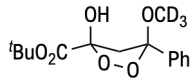
$\mathbf{7}_{R^*,R^*}$–d_3

tert-butyl (3*R**,5*R**)-3-hydroxy-5-(methoxy-d_3)-5-phenyl-1,2-dioxolane-3-carboxylate ($\mathbf{7}_{R^*,R^*}$-*d3*)

^{1}H NMR (800 MHz, $CDCl_3$) δ 7.51 (d, *J* = 7.8 Hz, 2H), 7.45 – 7.34 (m, 3H), 4.42 (br, 1H), 3.64 (d, *J* = 13.7 Hz, 1H), 2.87 (d, *J* = 13.7 Hz, 1H), 1.58 (s, 9H).

^{13}C NMR (201 MHz, $CDCl_3$) δ 165.6, 135.8, 128.8, 128.6, 126.4, 110.2, 104.2, 84.9, 58.3, 50.1 (septet), 27.8.

See characterization of $\mathbf{7}_{R^*,R^*}$ for stereochemical assignments.



$\mathbf{7}_{R^*,S^*}$-d_3

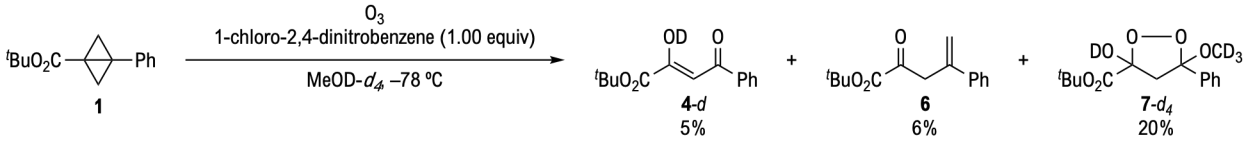
tert-butyl (3*R**,5*S**)-3-hydroxy-5-(methoxy-d_3)-5-phenyl-1,2-dioxolane-3-carboxylate ($\mathbf{7}_{R^*,S^*}$-*d3*)

^{1}H NMR (800 MHz, $CDCl_3$) δ 7.51 (d, *J* = 7.8 Hz, 2H), 7.45 – 7.34 (m, 3H), 5.07 (br, 1H), 3.25 (d, *J* = 13.3 Hz, 1H), 3.02 (d, *J* = 13.2 Hz, 1H), 1.55 (s, 9H).

^{13}C NMR (201 MHz, $CDCl_3$) δ 166.2, 134.4, 129.1, 128.8, 126.5, 109.3, 103.6, 84.4, 56.3, 50.1 (septet), 29.7.

See characterization of $\mathbf{7}_{S^*,R^*}$ for stereochemical assignments.

8.6.6.2 Fifteen-Second Ozonolysis of *tert*-Butyl 3-phenylbicyclo[1.1.0]butane-1-carboxylate

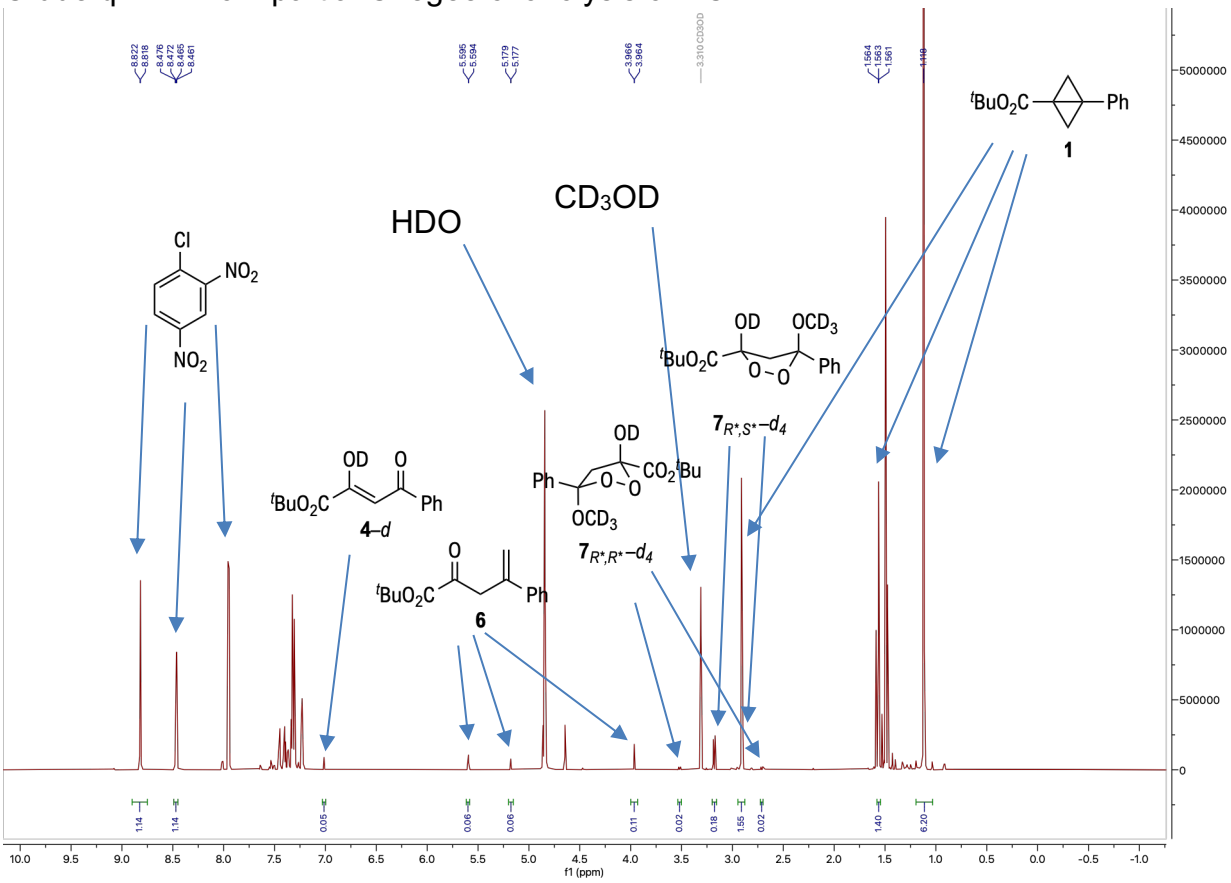


The blank sample was poured back into a 10 mL test tube and capped with a rubber septum. The tube was cooled to 78 ºC in an acetone/dry ice bath for 5 minutes. The flask was opened to air and oxygen was bubbled through a 16G x 4” needle at 1.0 L/min into that solution. Then the Globalozone GO-D3G ozone generator was turned on at 0.74 amps. After 15 seconds the ozone generator was switched off, and the excess ozone was removed using air. The sample was warmed to room temperature and transferred to an NMR tube to be measured. ^{1}H NMR was measured with a delay (D1) of 10 seconds with 32 scans.

The NMR spectrum was processed in MestReNova by first applying a standard baseline and phase correction. The residual solvent peak (CD_3OD) was set to 3.310 ppm. The non-overlapping internal standard (1-chloro-2,4-dinitrobenzene) peaks were integrated to the 1.14 value, as previously determined, to normalize the analyte values to whole integer values. Remaining BCB **1** was quantified by integration of a methylene triplet (2H) from 1.579–1.544 ppm and the *tert*-butyl group (9H) from 1.196–1.032 ppm. Compound **4**-*d* was quantified by integration of the singlet peak (1H) at 7.01 ppm. Compound **6** was quantified by integration of the double vinyl peaks (1H each) from 5.616–5.583 ppm and 5.200–5.154 ppm as well as the methylene (2H) doublet from 3.999–3.932 ppm. The peroxide $\mathbf{7}_{R^*,R^*}$-*d4* was quantified by integration of the CH_2 peak (1H each) from 3.556–3.498 ppm and 2.721–2.699 ppm. The peroxide $\mathbf{7}_{S^*,R^*}$-*d4* was quantified by integration of

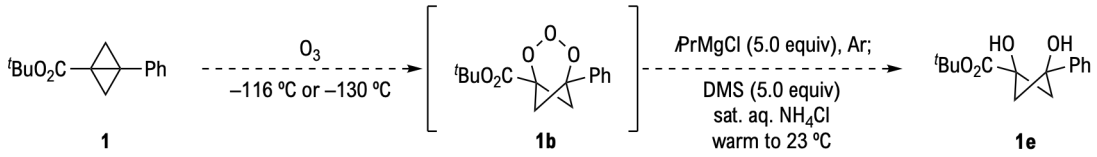
the CH_2 peak (1H each) from 3.202–3.144 ppm and 2.927–2.882 ppm. The peroxide **8** was not detected in the reaction mixture. Alkene **9** was also not detected in the reaction mixture, providing supporting evidence for an initial ozone attack and subsequent fragmentation leading alkene **6** as the major pathway. The ^{1}H NMR spectrum of the crude reaction is annotated below.

Crude qNMR from partial Criegee ozonolysis of BCB **1**.



^{1}H NMR (800 MHz, CD_3OD), D1 = 10, 32 scans

8.6.7 Attempts to Capture a 1,2,3-Trioxane



In an attempt to capture the 1,2,3-trioxane **1b** as the diol **1e**, the low temperature ozonolysis then reduction of BCB **1** was performed [*29*].

8.6.7.1 –116 ºC Ozonolysis of *tert*-Butyl 3-phenylbicyclo[1.1.0]butane-1-carboxylate

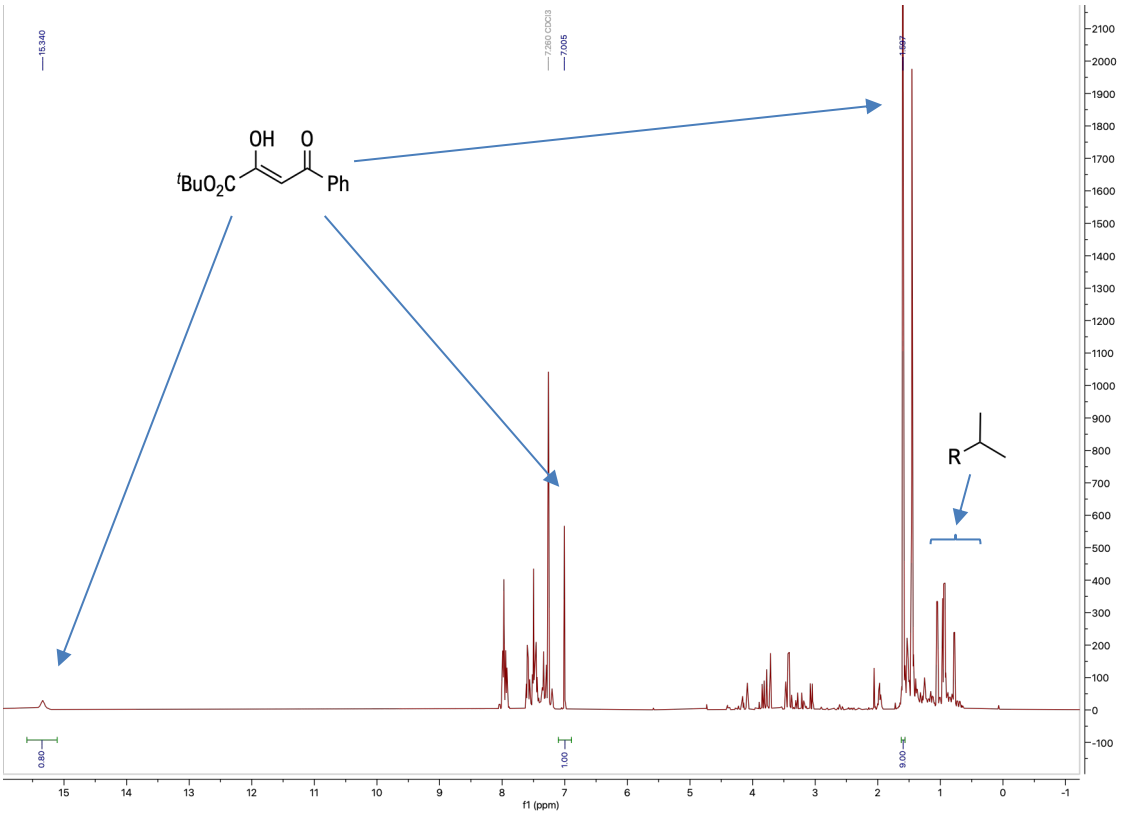
A –116 ºC bath was prepared by rapidly stirring diethyl ether in a dewar and slowly and constantly adding liquid nitrogen until the ether became a slurry. Rapid stirring was essential to prevent the surface of the diethyl ether from freezing. In the event the surface of the bath froze, a metal spatula was used to crush the frozen diethyl ether then liquid nitrogen addition was continued.

An oven-dried 25 mL round bottom flask was charged with *tert*-butyl 3-phenylbicyclo[1.1.0]butane-1-carboxylate (**1**, 0.50 mmol, 1.0 equiv.), a large magnetic stir bar and freshly distilled (Na/Benzophenone) diethyl ether (5 mL). The flask was sealed with a septum and a balloon of argon and chilled to an external temperature of −116 °C. Ozone was passed over the solution at a flow rate of 1 L/min until the solution turned blue (1.5 min). The vessel was purged with argon gas for 10 min at an external temperature of −116 °C. Warning: failure to remove all oxygen and ozone may result in a fire or an explosion upon addition of the Grignard reagent. A solution of isopropyl magnesium bromide (2.5 mmol, 5.0 equiv., 1.0 M) in diethyl ether was added and the reaction was

allowed to stir for 20 minutes. A saturated ammonium chloride solution (5 mL) was added followed by dimethyl sulfide (0.18 mL, 2.5 mmol, 5.0 equiv.). The flask was removed from the bath and allowed to warm to room temperature. Saturated brine solution (20 mL) was added, and the mixture was extracted with ethyl acetate (3 x 10 mL). The combined organic layers were dried with sodium sulfate, filtered through silica and evaporated.

The crude ^{1}H NMR spectrum revealed compound **4** was the major product. The presence of multiple doublet methyl signals from 0.5–1.1 ppm also indicates the addition of multiple equivalents of the *iso*-propyl magnesium chloride either ketone of **4** or the *tert*-butyl ester. Separation of the *iso*-propyl adducts from compound **4** was not possible by SiO_2 column chromatography.

Crude NMR after extraction and filtration through SiO_2 from the –116 ºC ozonolysis of BCB **1**.



^{1}H NMR (500 MHz, $CDCl_3$)

8.6.7.2 –130 ºC Ozonolysis of *tert*-Butyl 3-phenylbicyclo[1.1.0]butane-1-carboxylate

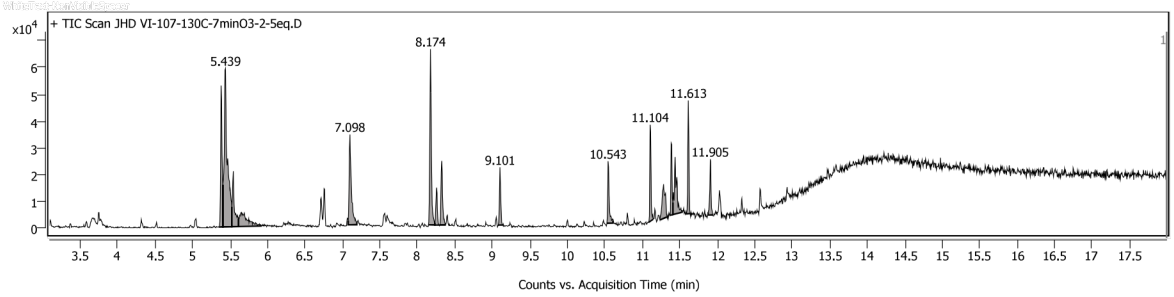
A –130 ºC bath was prepared by rapidly stirring pentane in a dewar and slowly and constantly adding liquid nitrogen until the pentane became a slurry. Rapid stirring was essential to prevent the surface of the pentane from freezing. In the event the surface of the bath froze, a metal spatula was used to crush the frozen pentane then liquid nitrogen addition was continued.

An oven-dried 25 mL round bottom flask was charged with *tert*-butyl 3-phenylbicyclo[1.1.0]butane-1-carboxylate (**1**, 0.50 mmol, 1.0 equiv.), a large magnetic stir bar and cyclopentyl methyl ether (CpME, 5 mL). The flask was sealed with a septum and a balloon of argon and chilled to an external temperature of −130 °C. Ozone was passed over the solution at a flow rate of 1 L/min until the solution turned blue (7 min). The vessel was purged with argon gas for 10 min at an external temperature of −130 °C. Warning: failure to remove all oxygen and ozone may result in a fire or an explosion upon addition of the Grignard reagent. A solution of isopropyl magnesium bromide (1.25 mmol, 2.5 equiv., 1.0 M) in diethyl ether was added and the reaction was allowed to stir for 20 minutes. A saturated ammonium chloride solution (5 mL) was added followed by dimethyl sulfide (0.18 mL, 2.5 mmol, 5.0 equiv.). The flask was removed from the bath and allowed to warm to room temperature. Saturated brine solution (20 mL) was added, and the mixture was extracted with ethyl acetate (3 x 10 mL). The combined organic layers were dried with sodium sulfate, filtered through cotton, evaporated. GCMS was then measured.

The crude GCMS spectrum exhibited many peaks, each displaying a characteristic fragment ion at *m/z* = 105, which corresponds to the benzylideneoxonium species. The observed mass-to-charge ratios correlate with fragmentation pathways arising from the

progressive oxygenation of compound **4** or alkene **6**. This fragmentation pattern suggests that compound **4** or compound **6** may have formed *in situ* during the reaction and undergone further ozonolysis. Given the extended reaction time required for the complete consumption of BCB **1** at –130 ºC, this sequential transformation may be plausible.

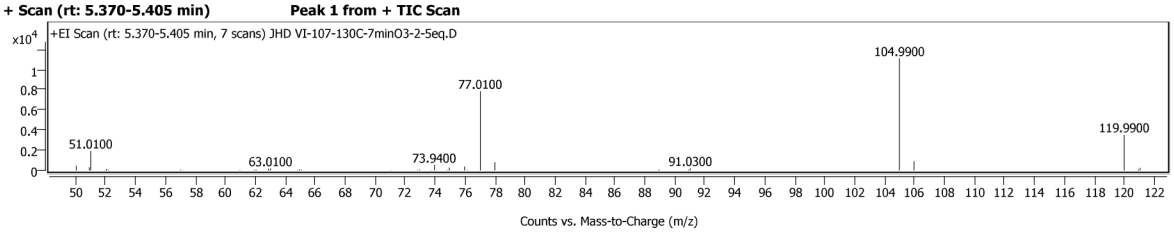
Sample Chromatograms



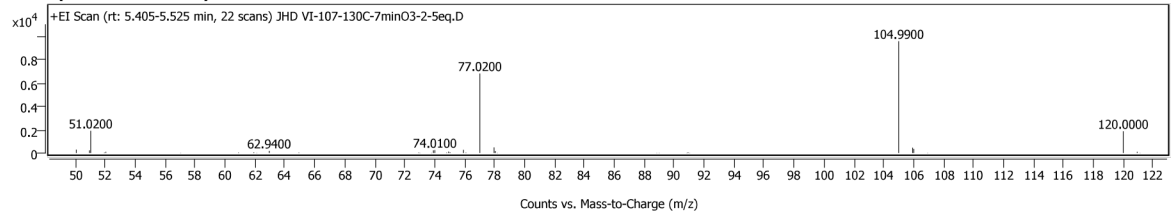
Chromatogram Peaks

Peak	Start	RT	End	Height	Area	Area %	SNR
1	5.359	5.382	5.405	52958	69655		
2	5.405	5.439	5.525	59316	178204		
3	5.525	5.542	5.611	20735	40121		
4	5.611	5.651	5.914	5325	40650		
5	7.075	7.098	7.190	33813	67980		
6	8.147	8.174	8.231	65794	91988		
7	8.231	8.254	8.291	13986	18496		
8	8.298	8.323	8.369	23926	35350		
9	9.079	9.101	9.137	21583	25004		
10	10.526	10.543	10.606	23185	31190		
11	11.081	11.104	11.144	36160	39140		
12	11.235	11.281	11.327	12900	36826		
13	11.367	11.384	11.407	26892	29387		
14	11.407	11.436	11.522	21394	48152		
15	11.590	11.613	11.637	42384	39686		
16	11.876	11.905	11.938	20852	25167		

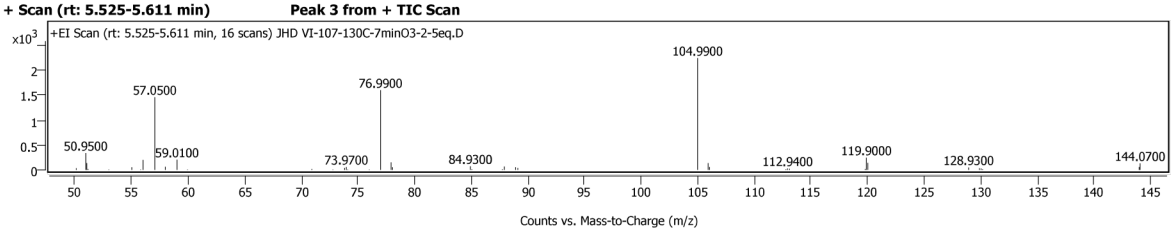
+ Scan (rt: 5.370-5.405 min) **Peak 1 from + TIC Scan**



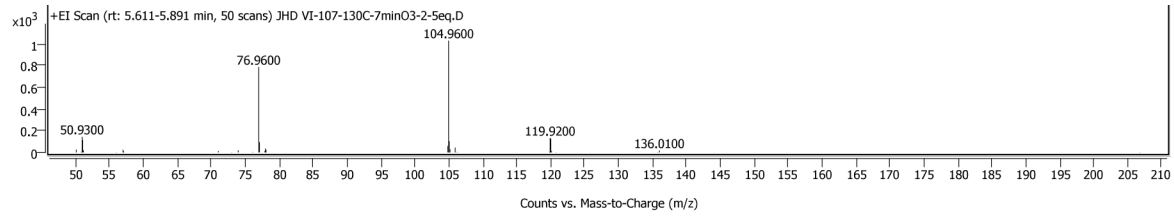
+ Scan (rt: 5.405-5.525 min) **Peak 2 from + TIC Scan**



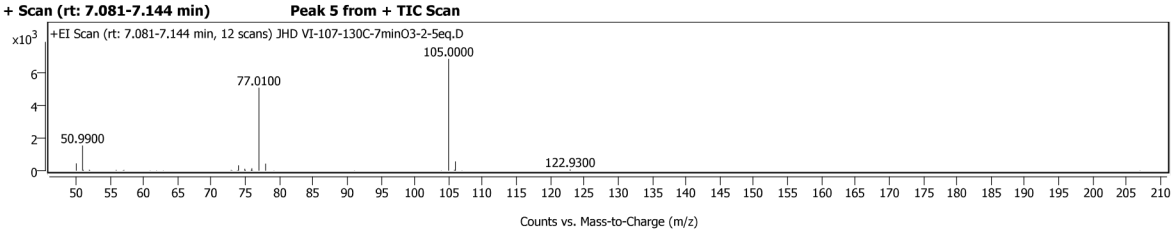
+ Scan (rt: 5.525-5.611 min) **Peak 3 from + TIC Scan**



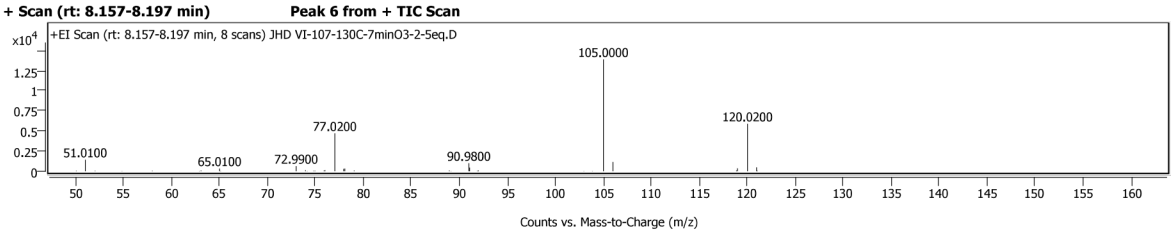
+ Scan (rt: 5.611-5.891 min) **Peak 4 from + TIC Scan**



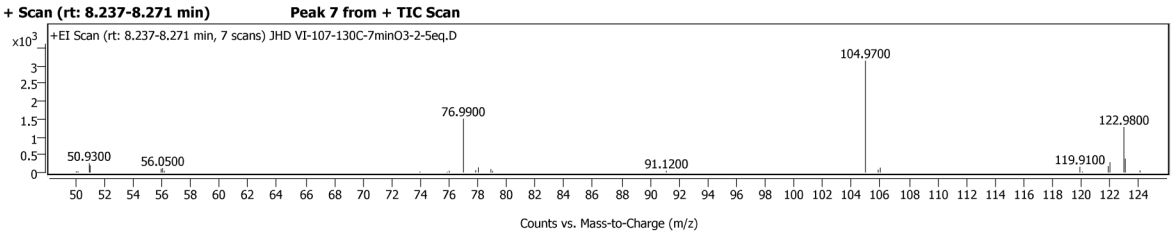
+ Scan (rt: 7.081-7.144 min) **Peak 5 from + TIC Scan**



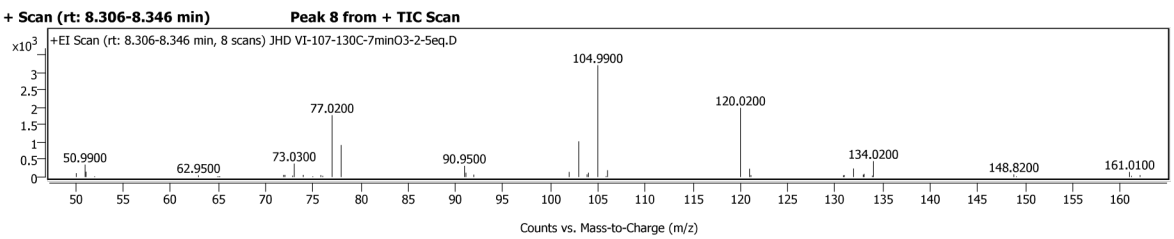
+ Scan (rt: 8.157-8.197 min) **Peak 6 from + TIC Scan**



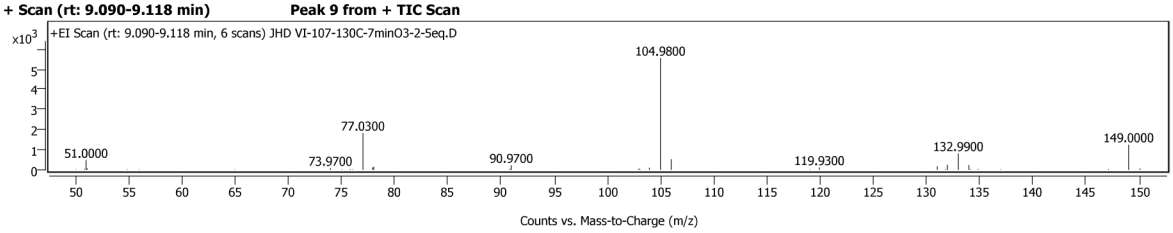
+ Scan (rt: 8.237-8.271 min) **Peak 7 from + TIC Scan**



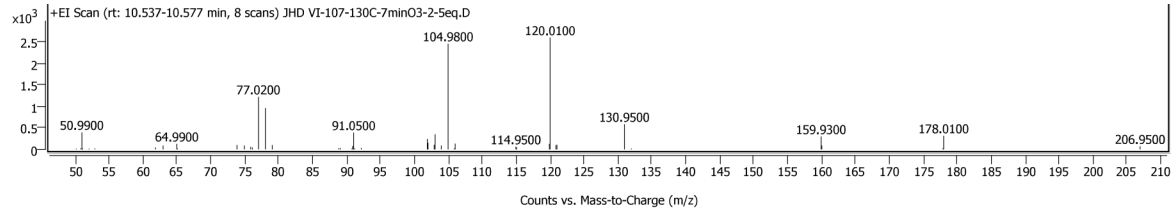
+ Scan (rt: 8.306-8.346 min) **Peak 8 from + TIC Scan**



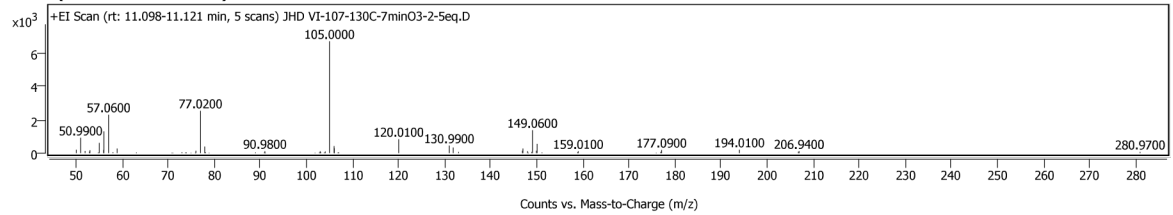
+ Scan (rt: 9.090-9.118 min) **Peak 9 from + TIC Scan**



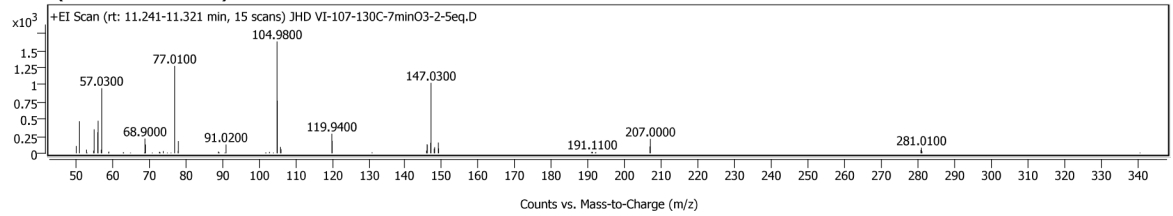
+ Scan (rt: 10.537-10.577 min) **Peak 10 from + TIC Scan**



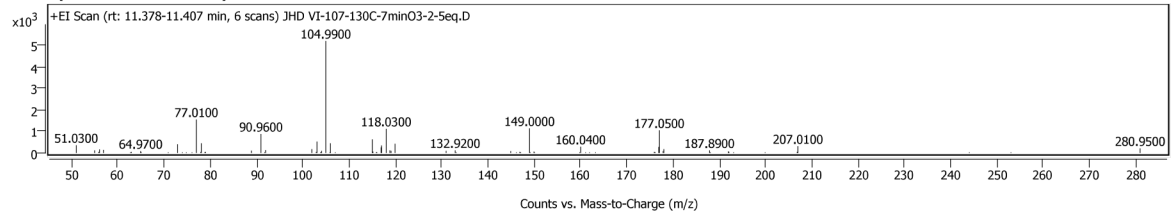
+ Scan (rt: 11.098-11.121 min) **Peak 11 from + TIC Scan**



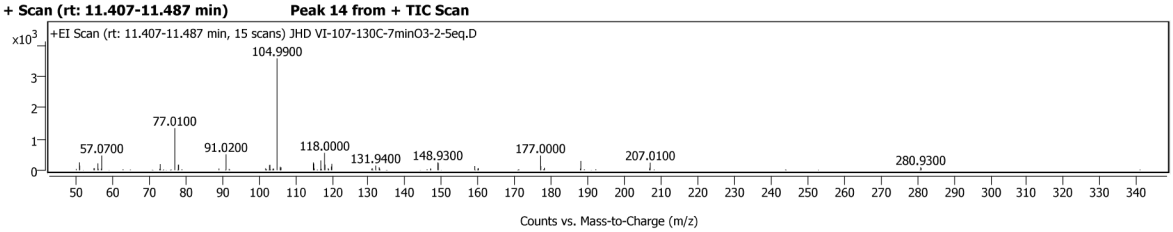
+ Scan (rt: 11.241-11.321 min) **Peak 12 from + TIC Scan**

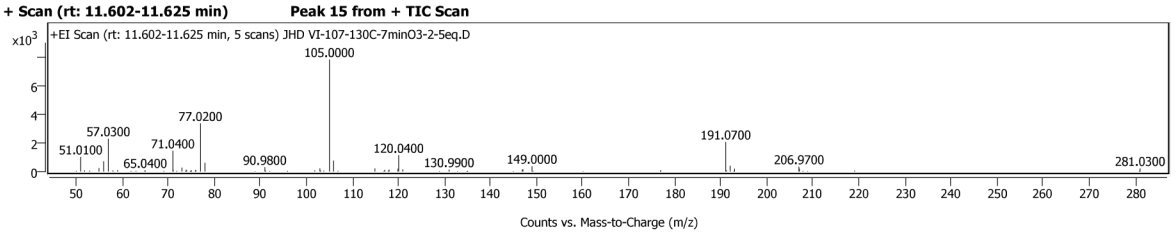


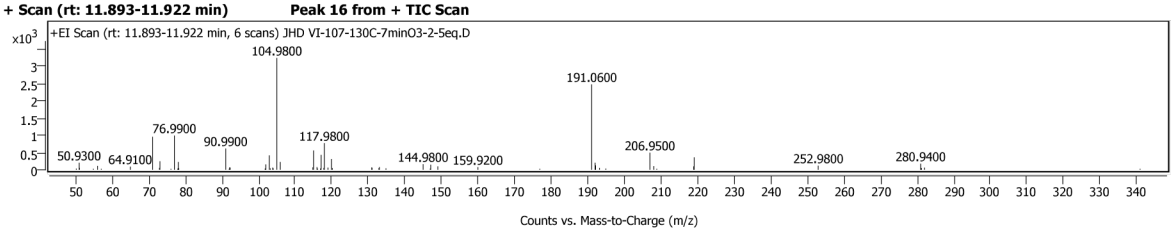
+ Scan (rt: 11.378-11.407 min) **Peak 13 from + TIC Scan**



+ Scan (rt: 11.407-11.487 min) **Peak 14 from + TIC Scan**







Both the –116 ºC and –130 ºC experiments did not enable the capture of the 1,2,3-trioxane **1b** , should it have formed. We rationalize these results as follows. It is known that the POZ from *cis*-alkenes have shorter lifetimes than POZs from the corresponding *trans*-alkene isomers [*48*]. The inherent difference in POZ stability led to the development of the –130 ºC condition by Arriaga, D. K. & Thomas, A. A. (*29*). In this case, the 1,2,3-trioxane **1b** is expected to be less stable than a primary ozonide from a *cis*-alkene because due to the fact that it is a bicycle. Therefore, it should have a short lifetime even at –130 ºC. Furthermore, solvent may change the reaction. Our calculations, using methanol as a solvent at –78 ºC, indicated only a small difference in energy (+0.5 kcal/mol) between formation or the 1,2,3-trioxane **1b** or immediate loss of O_2 after formation of the trioxidanyl radical, see section 7. Such a small energy difference could be significantly different depending on the reaction solvent.

8.6.8 Computational Section

Computational Energies calculated by Alexander J. Maertens

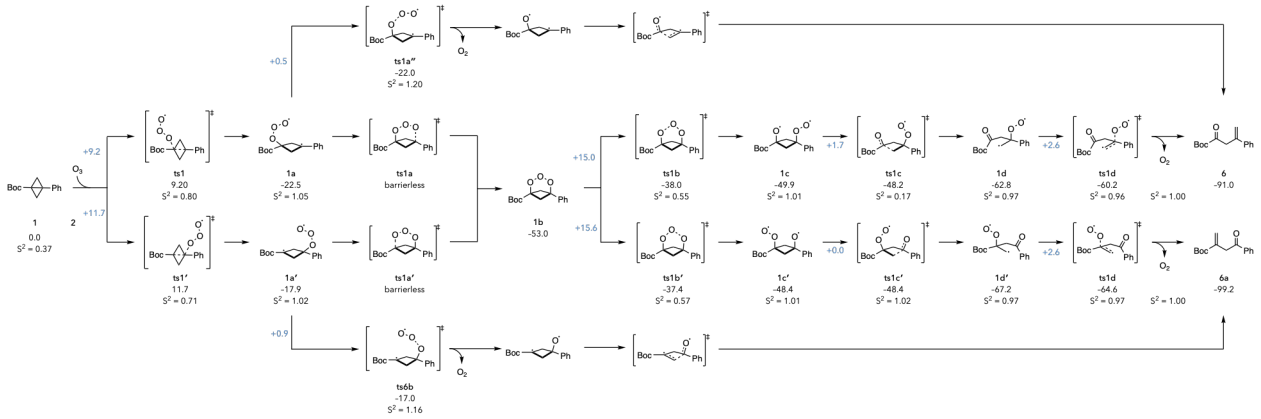


Figure 8.4 Potential Energy Surface for Ozonolysis of BCB σ-Bond

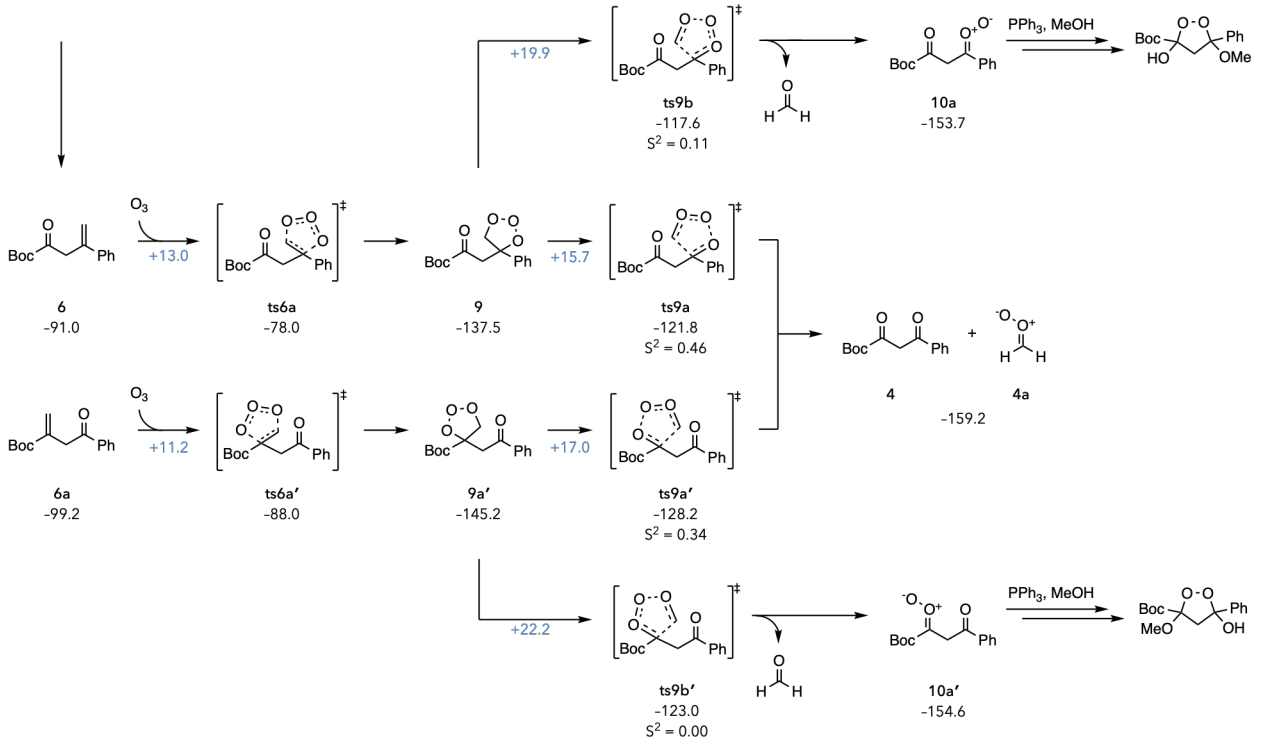
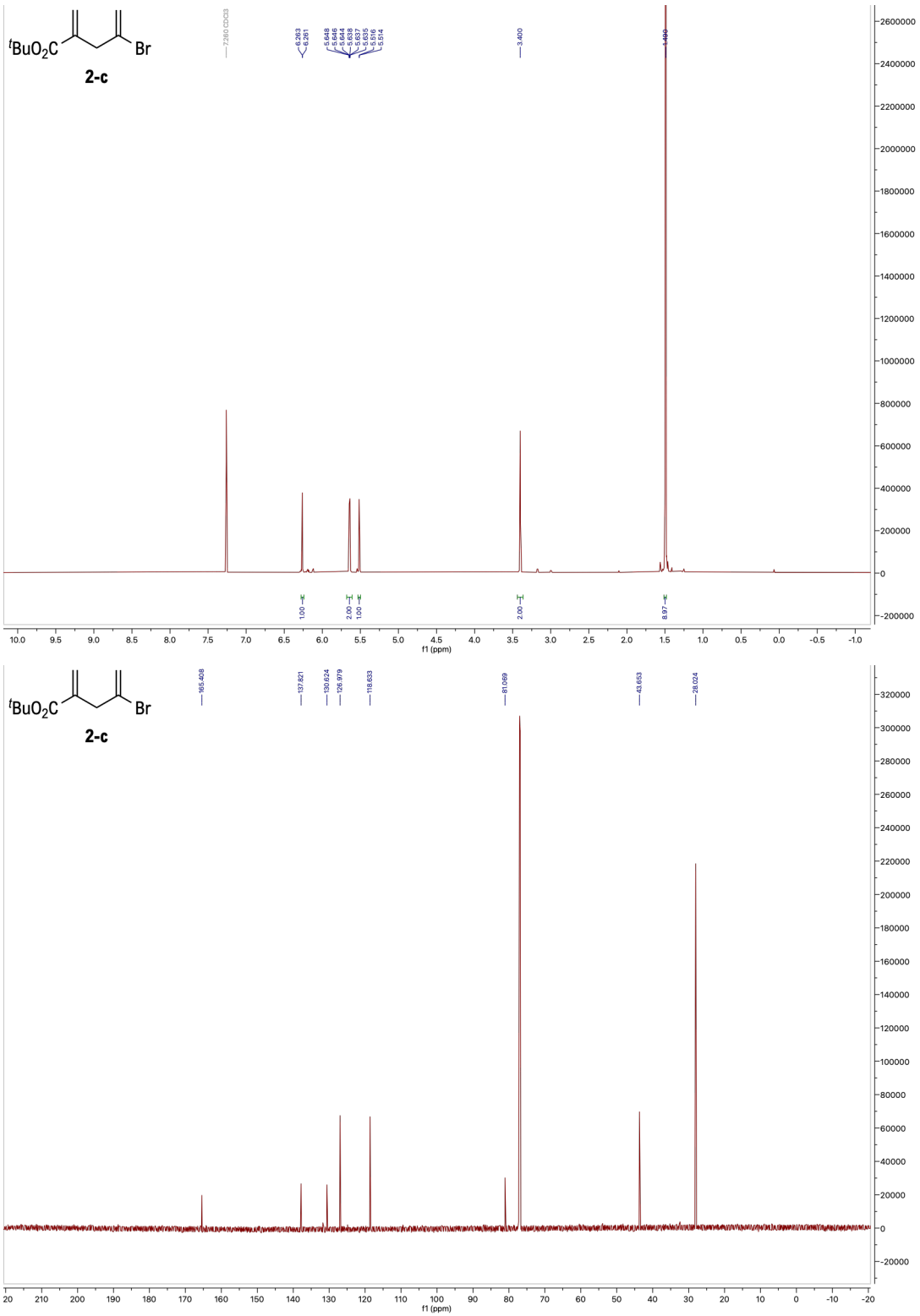
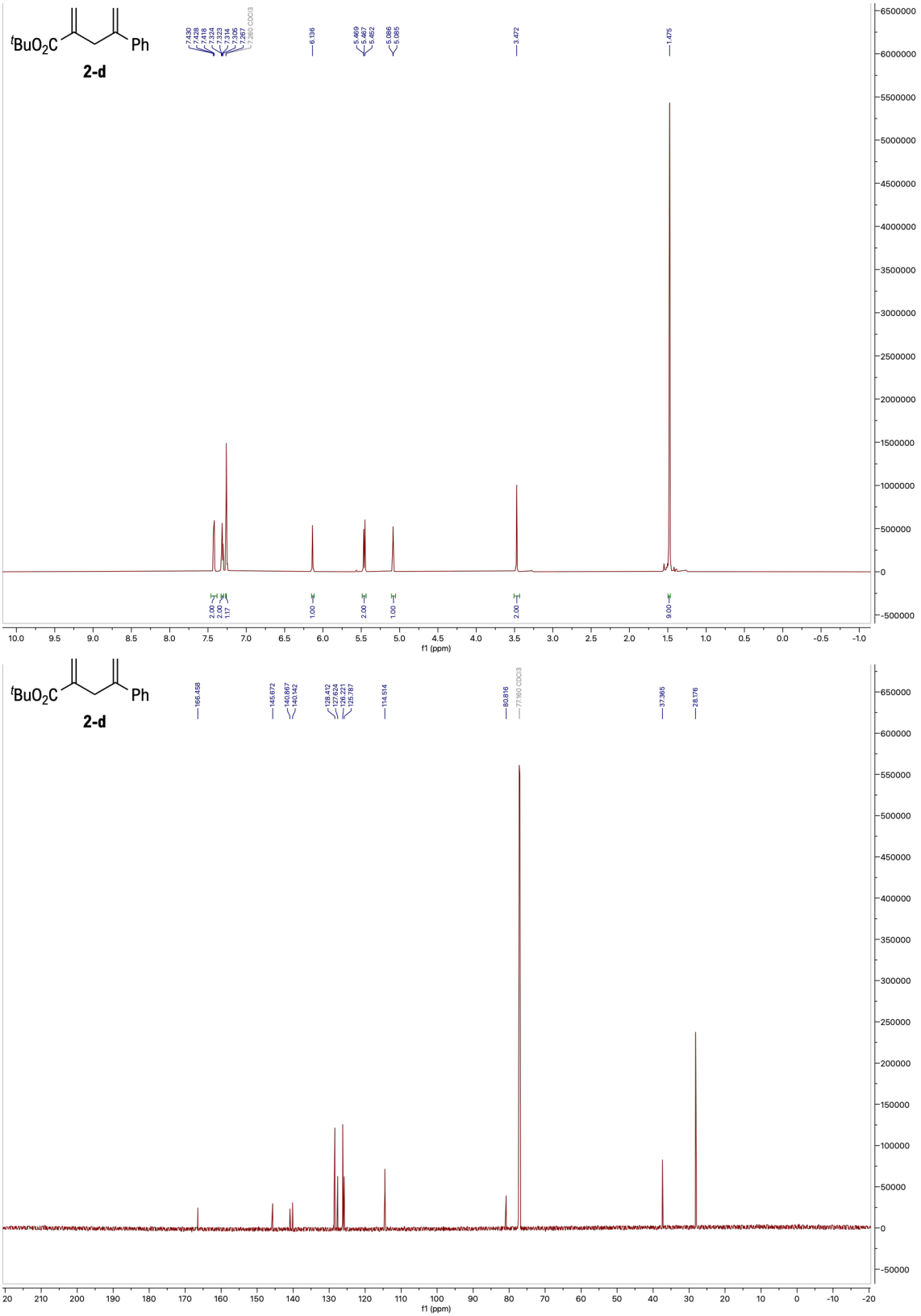


Figure 8.5 Potential Energy Surface for BCB Second Ozone Addition

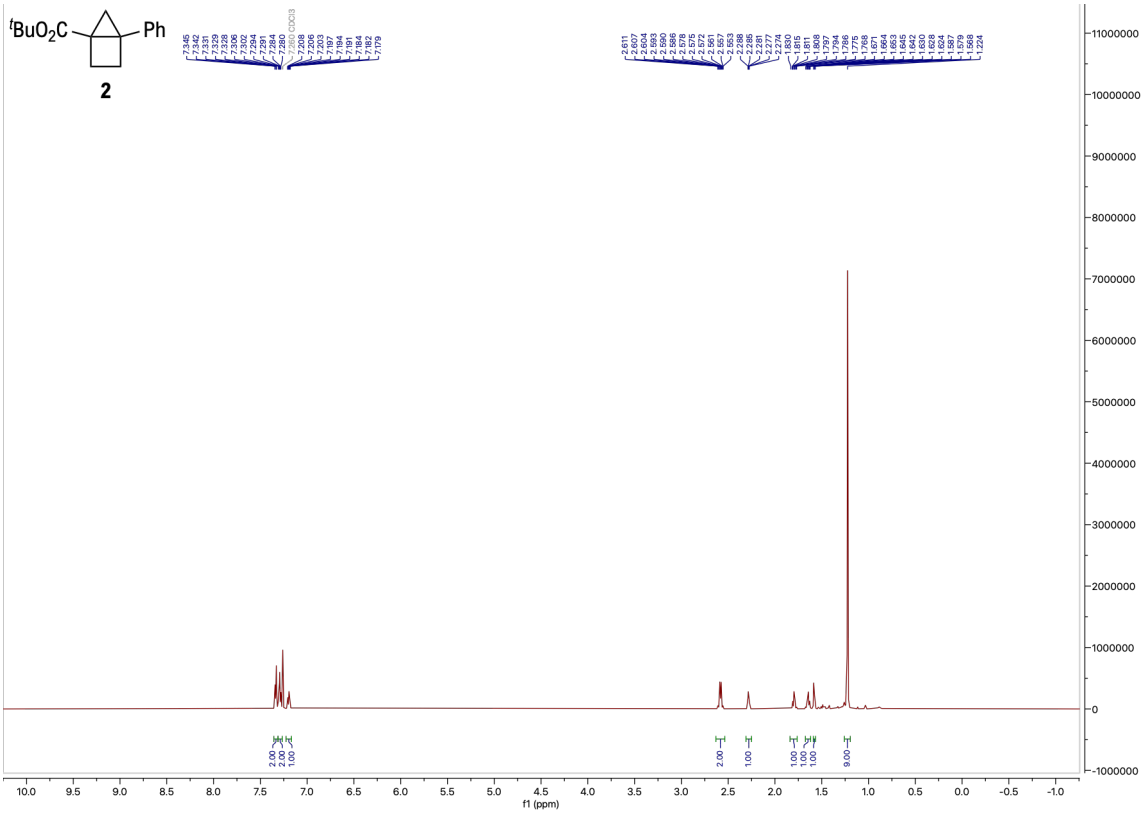
8.6.9 Copies of NMR Spectra

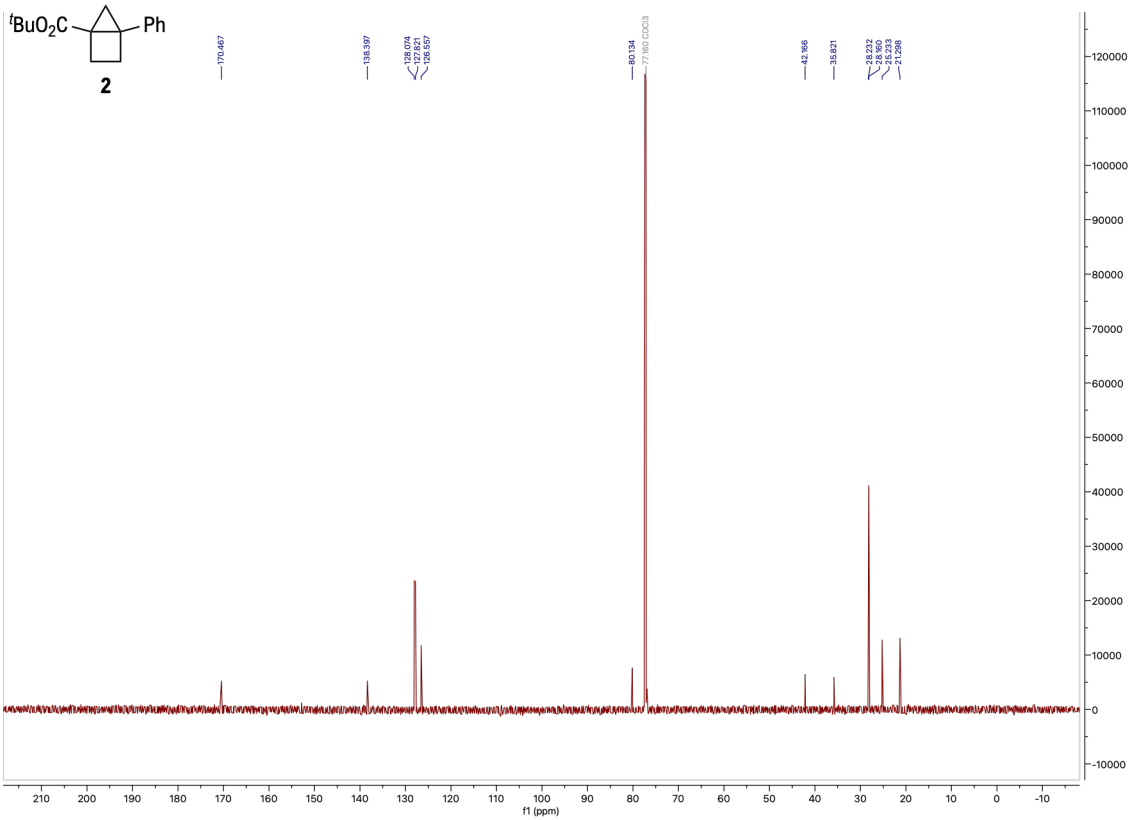


^{1}H NMR (800 MHz, $CDCl_3$) and **^{13}C NMR** (201 MHz, $CDCl_3$) of **2-c**

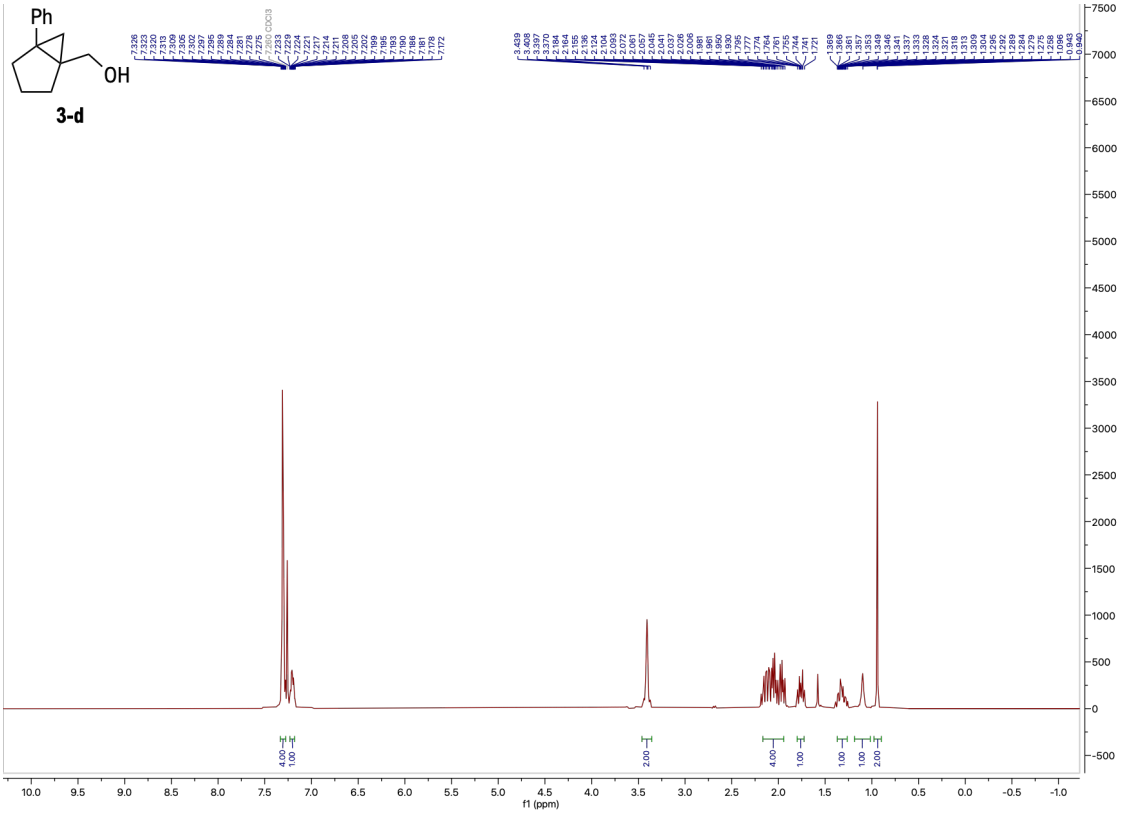


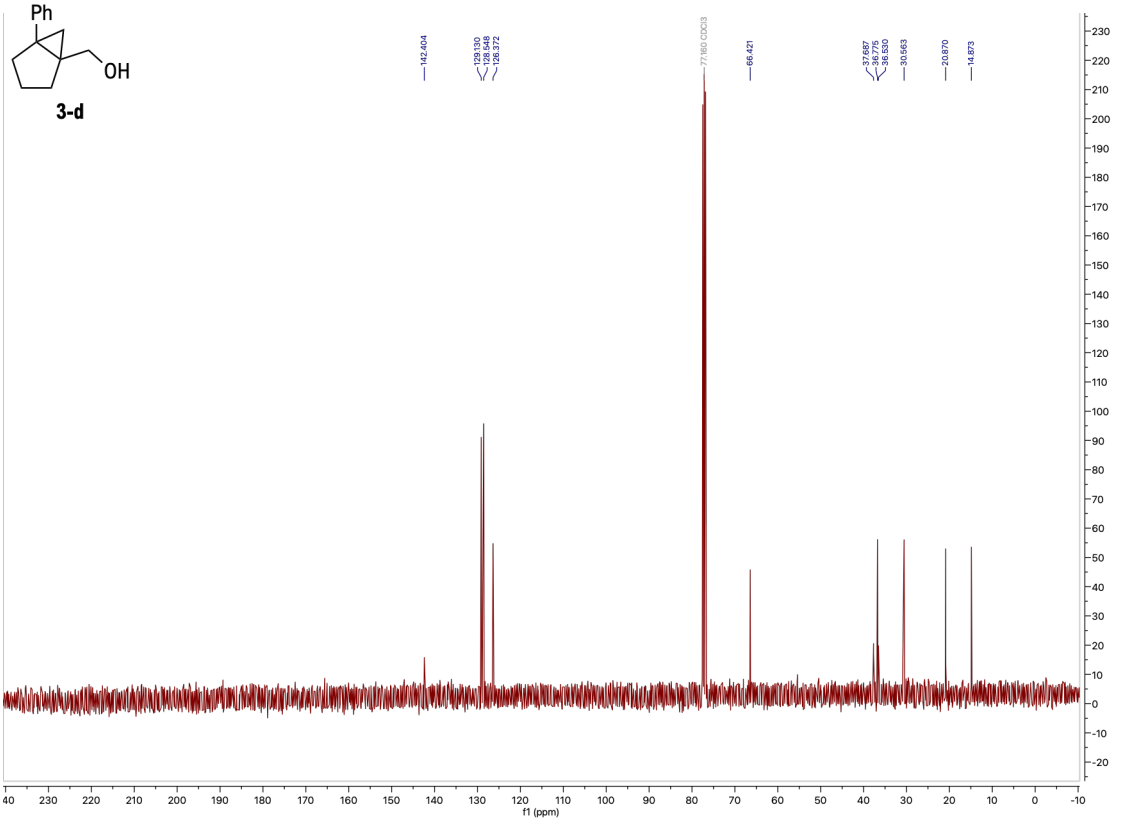
^{1}H NMR (800 MHz, $CDCl_3$) and **^{13}C NMR** (201 MHz, $CDCl_3$) of **2-d**



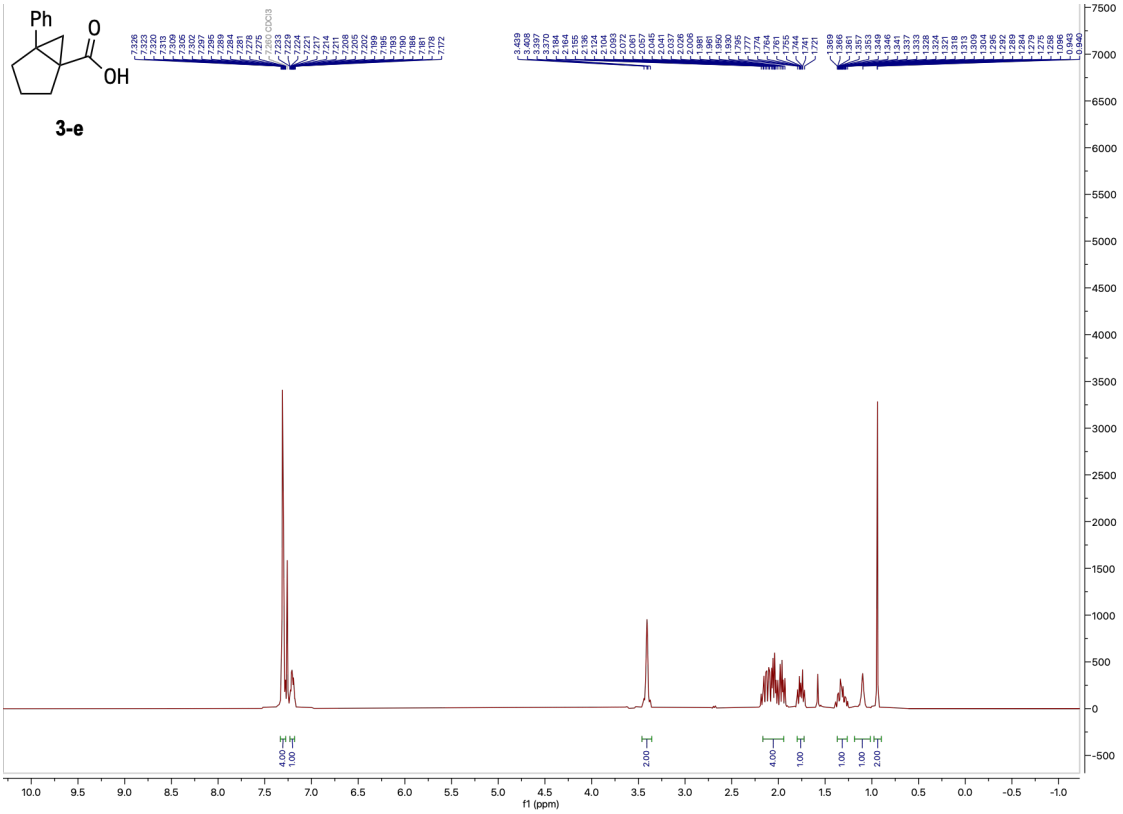


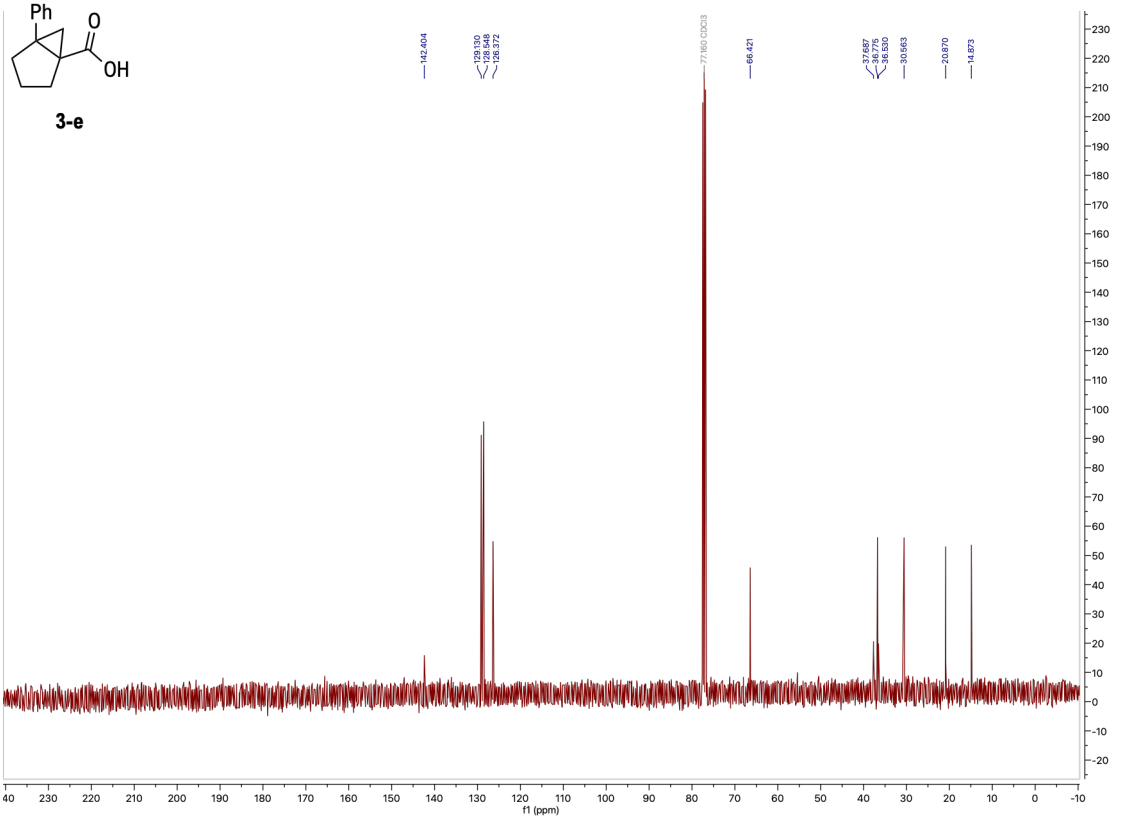
^{1}H NMR (600 MHz, $CDCl_3$) and **^{13}C NMR** (151 MHz, $CDCl_3$) of **2**



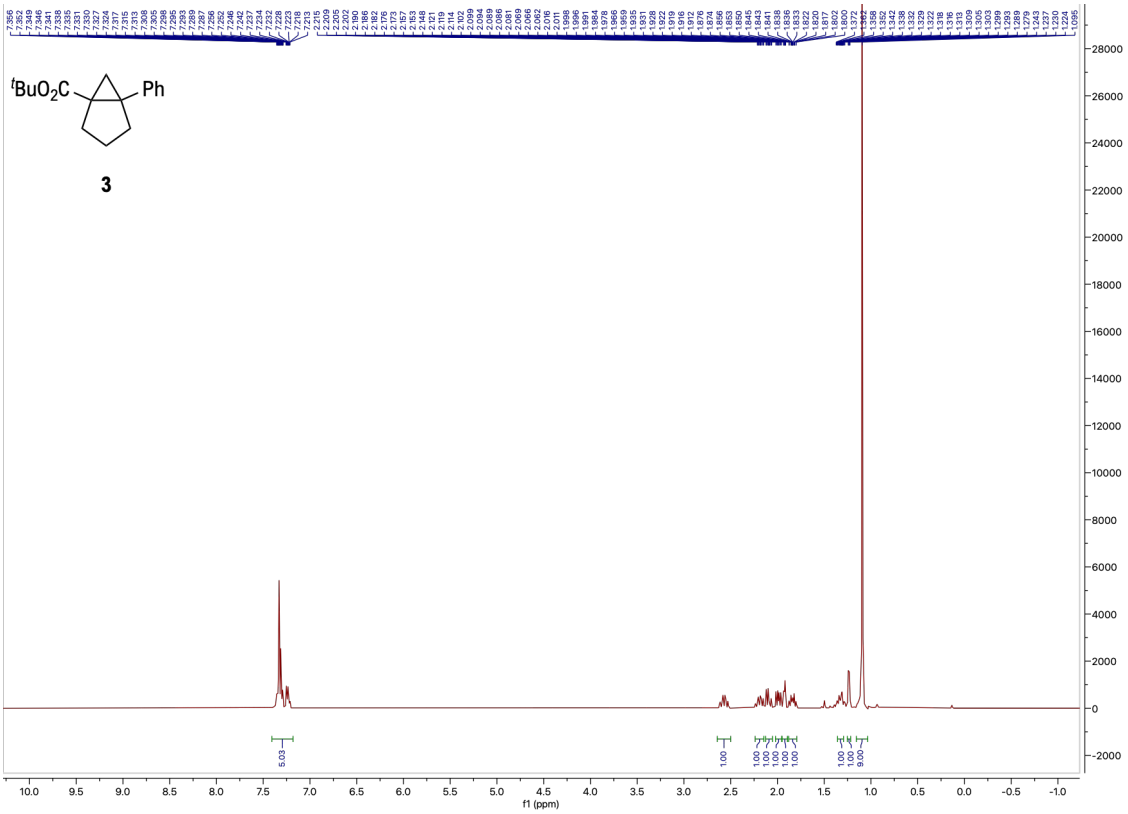


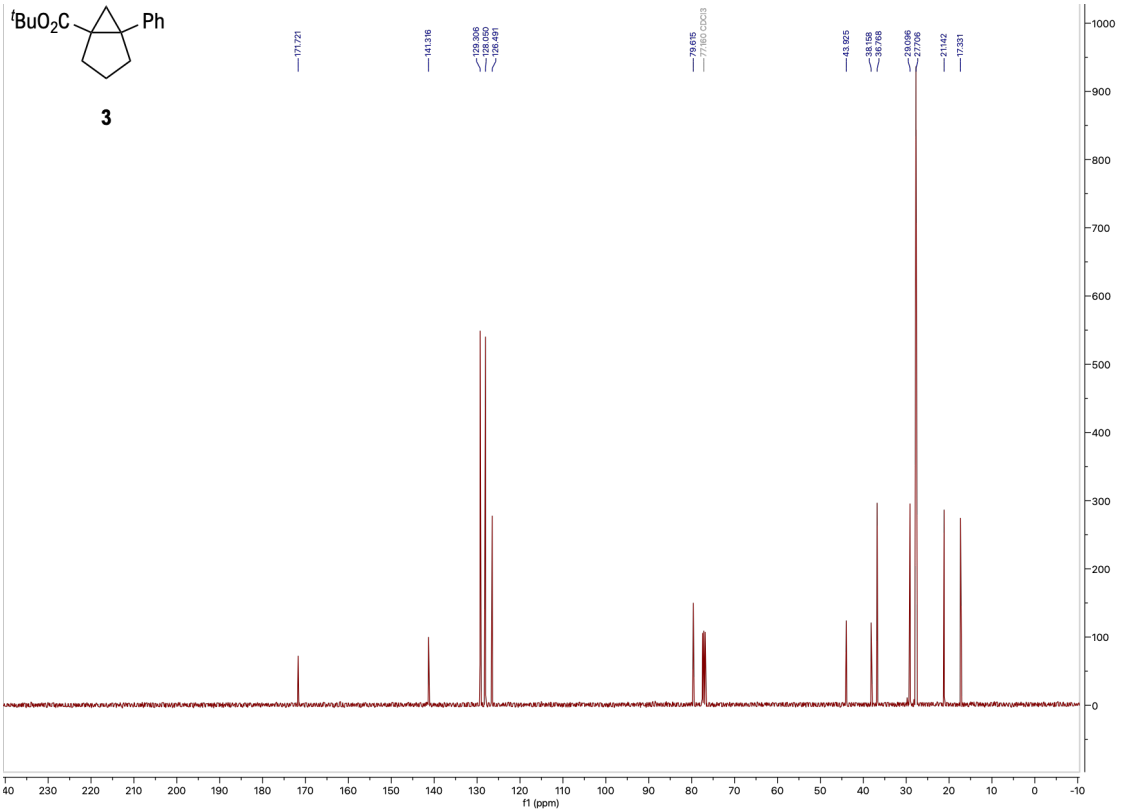
^{1}H NMR (400 MHz, $CDCl_3$) and **^{13}C NMR** (101 MHz, $CDCl_3$) of **3-d**



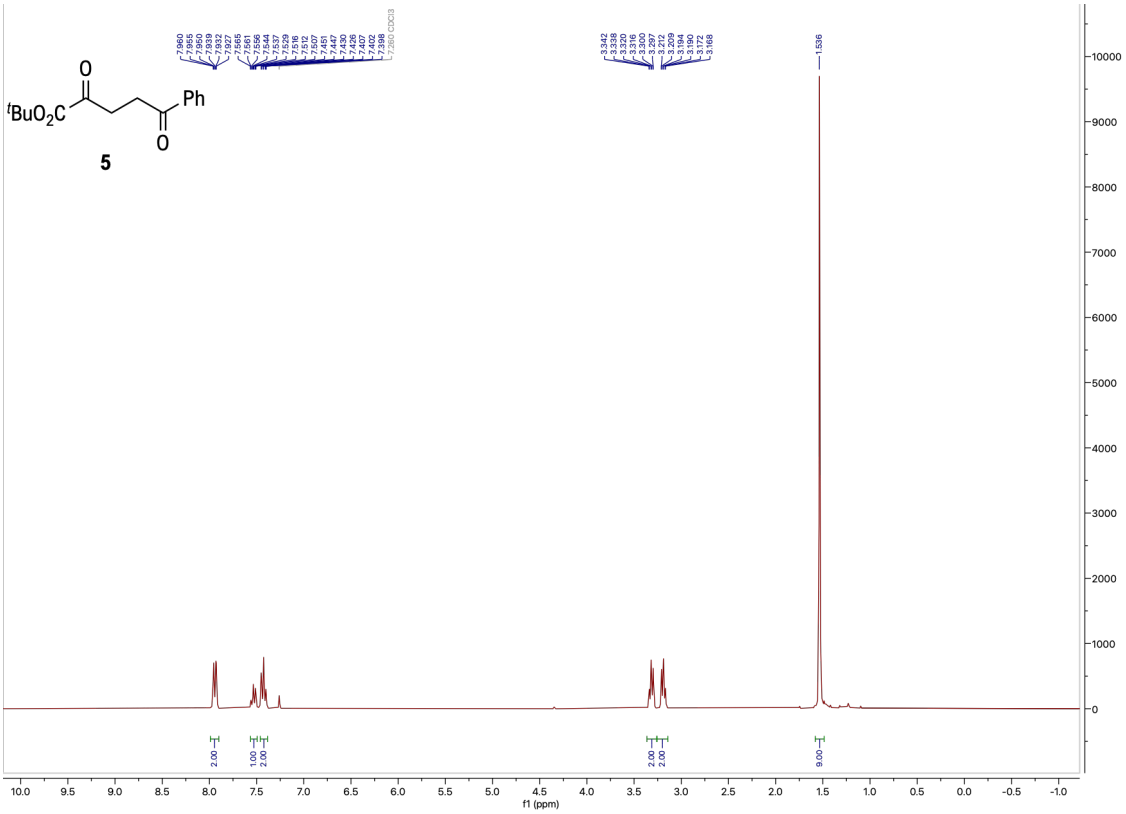


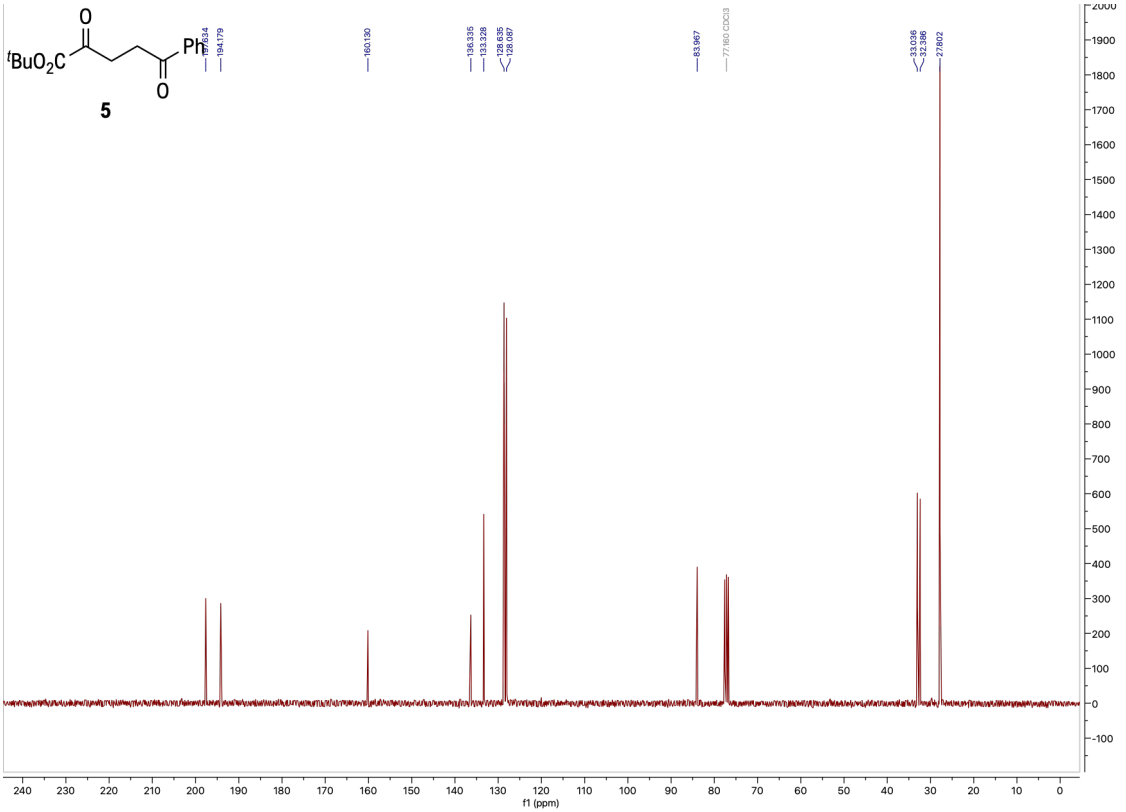
^{1}H NMR (400 MHz, $CDCl_3$) and **^{13}C NMR** (101 MHz, $CDCl_3$) of **3-e**



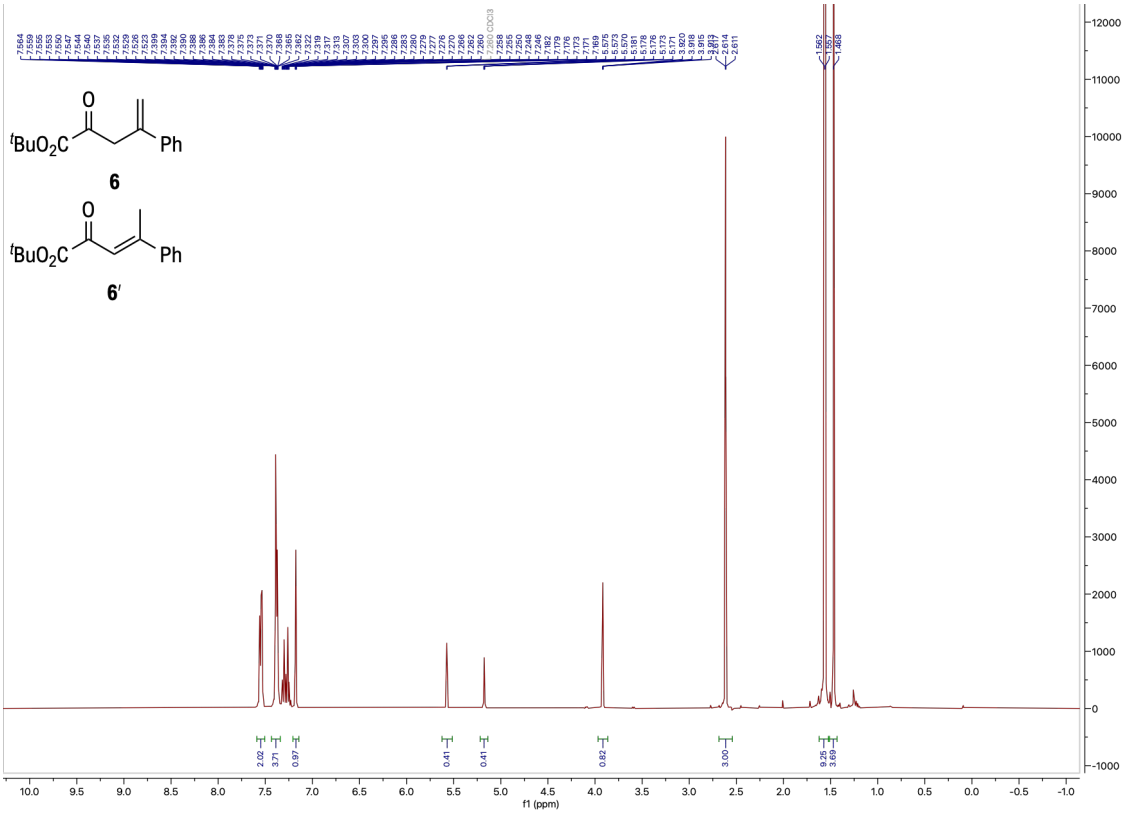


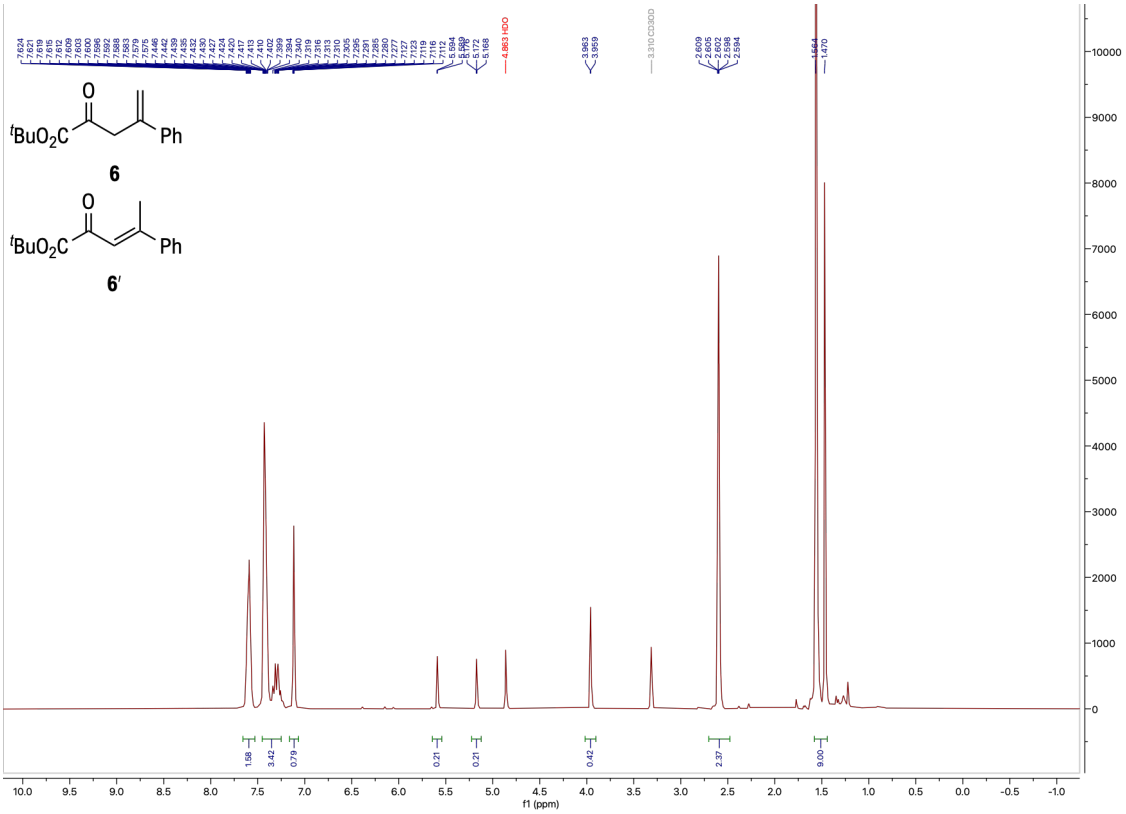
^{1}H NMR (400 MHz, $CDCl_3$) and **^{13}C NMR** (101 MHz, $CDCl_3$) of **3**



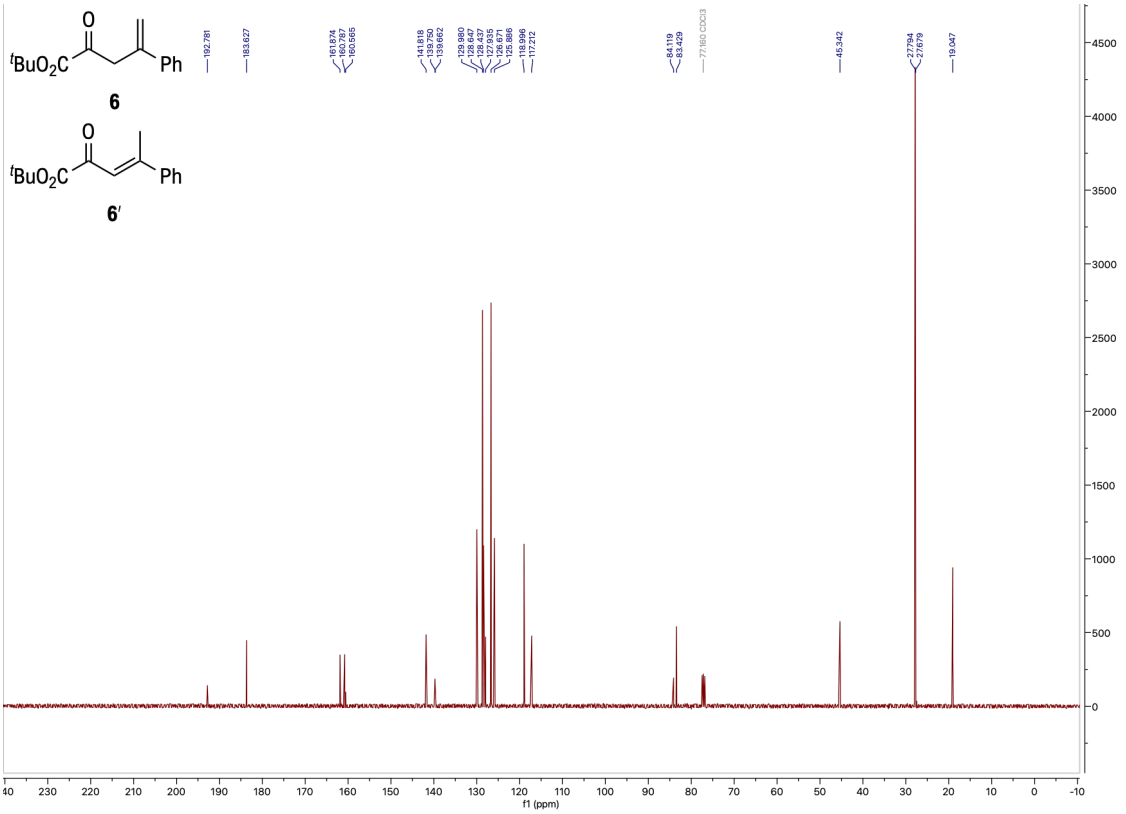


^{1}H NMR (300 MHz, $CDCl_3$) and **^{13}C NMR** (75 MHz, $CDCl_3$) of **5**

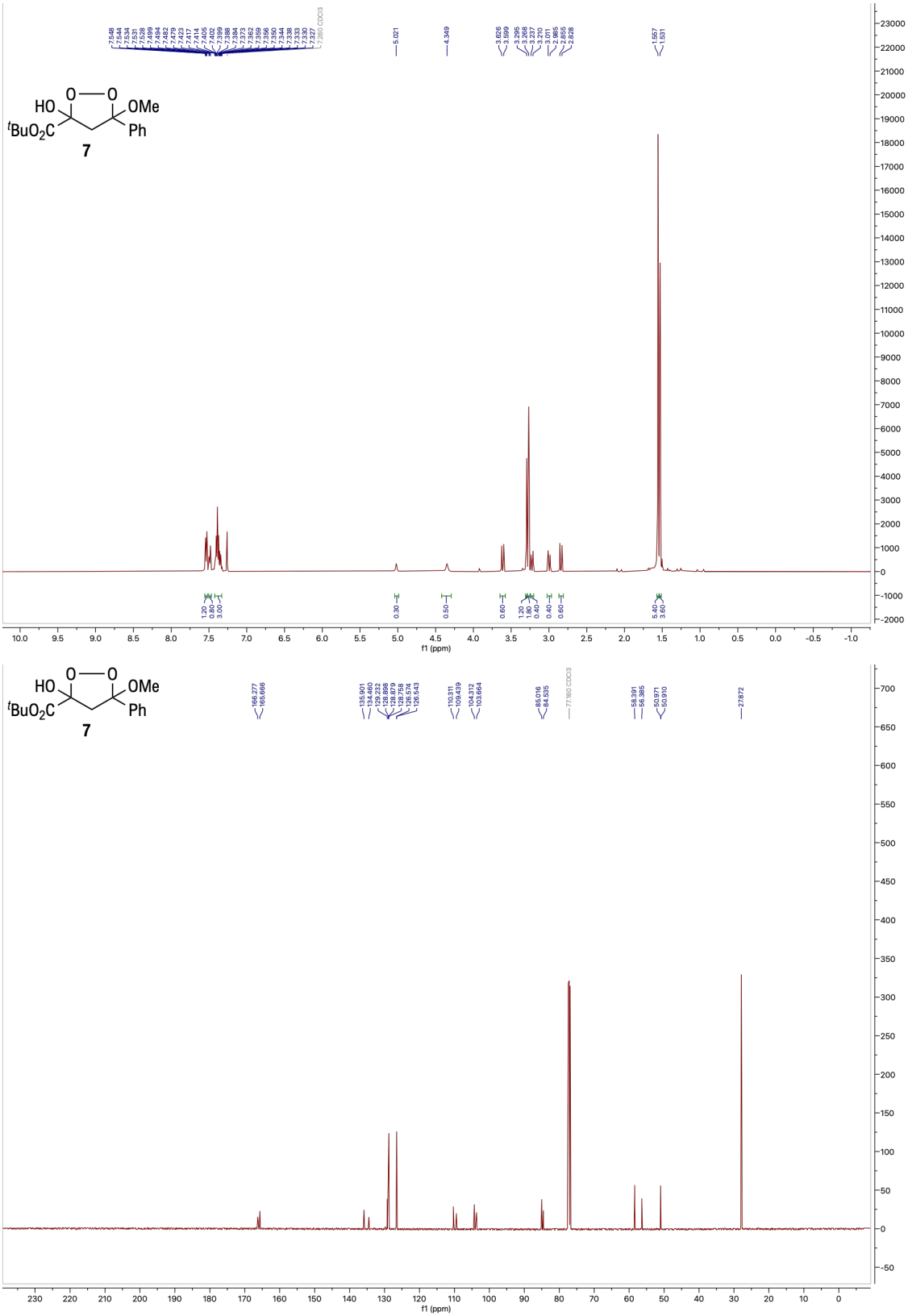




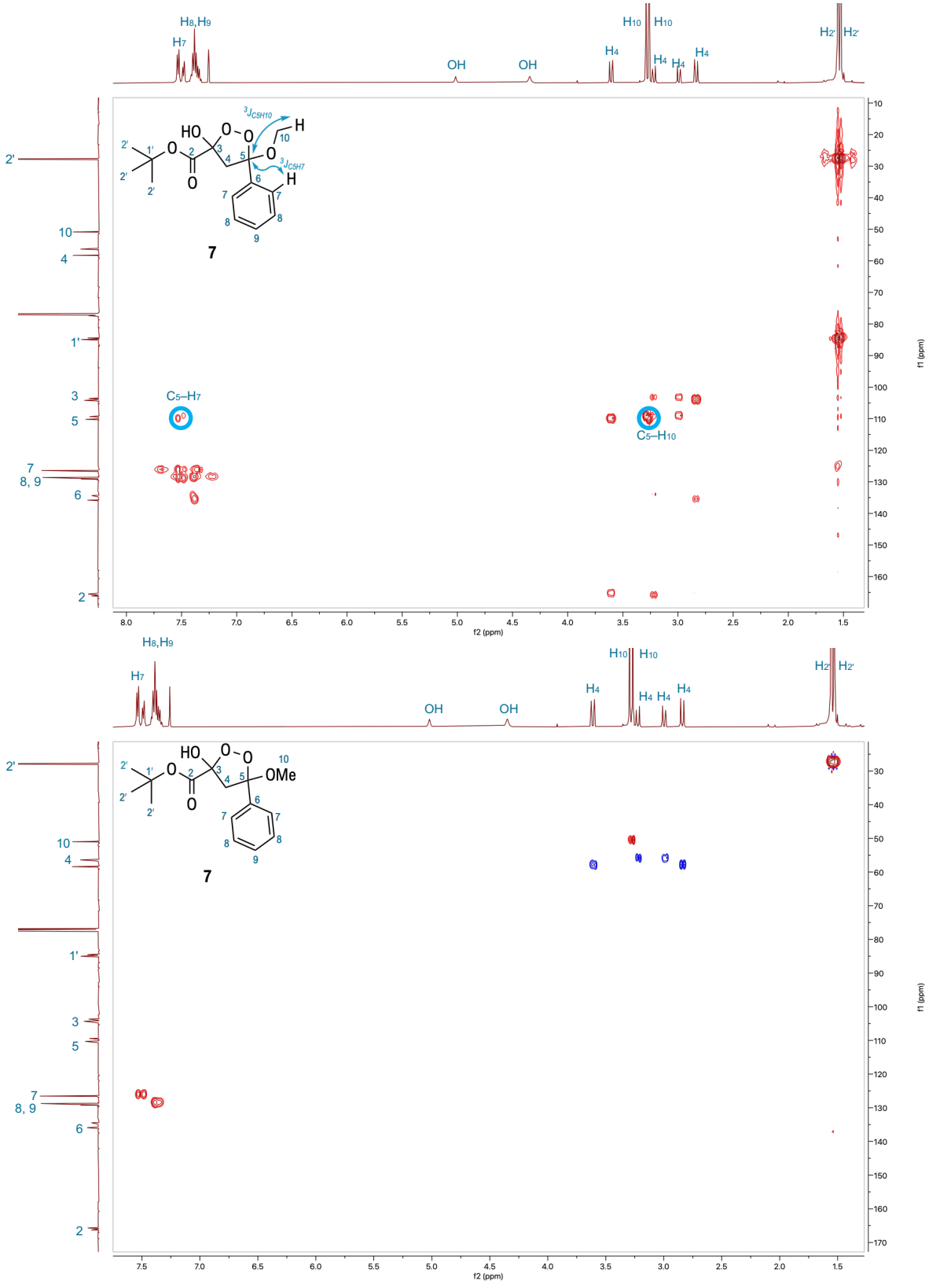
^{1}H NMR (400 MHz, $CDCl_3$) and **^{1}H NMR** (300 MHz, MeOD-d_4) of **6** and **6'**



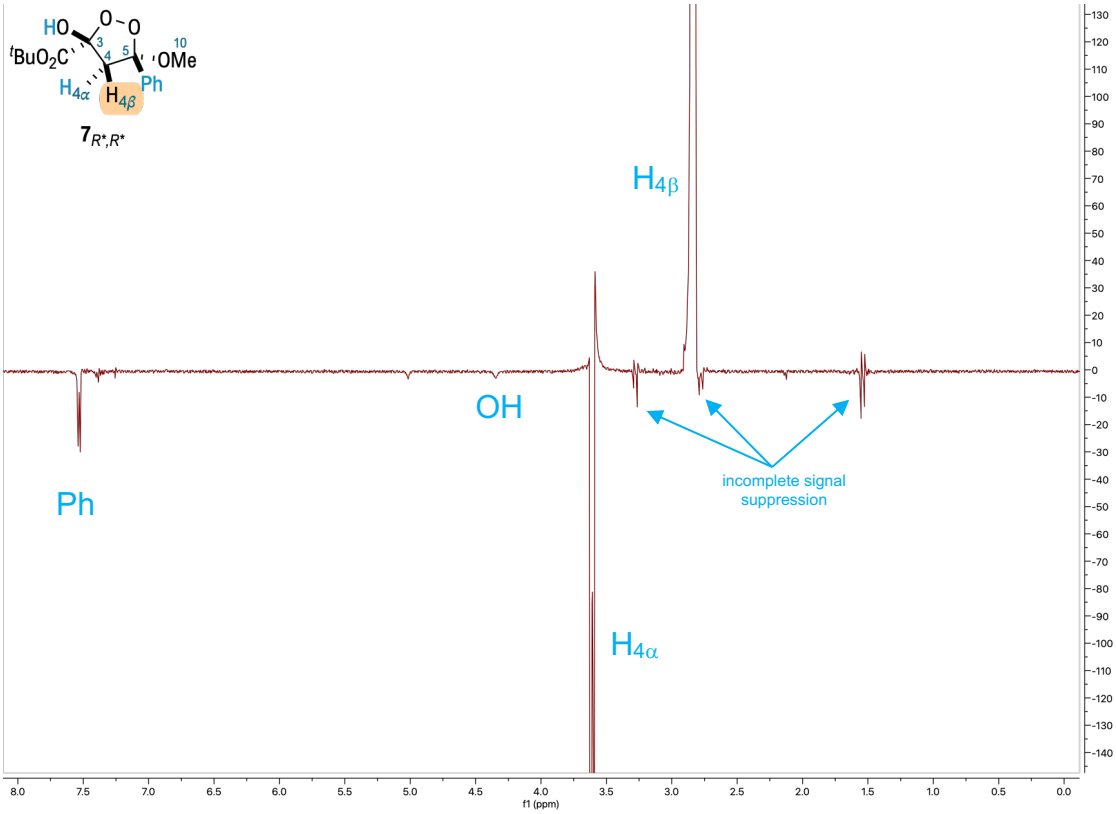
^{13}C NMR (101 MHz, $CDCl_3$) of **6** and **6'**



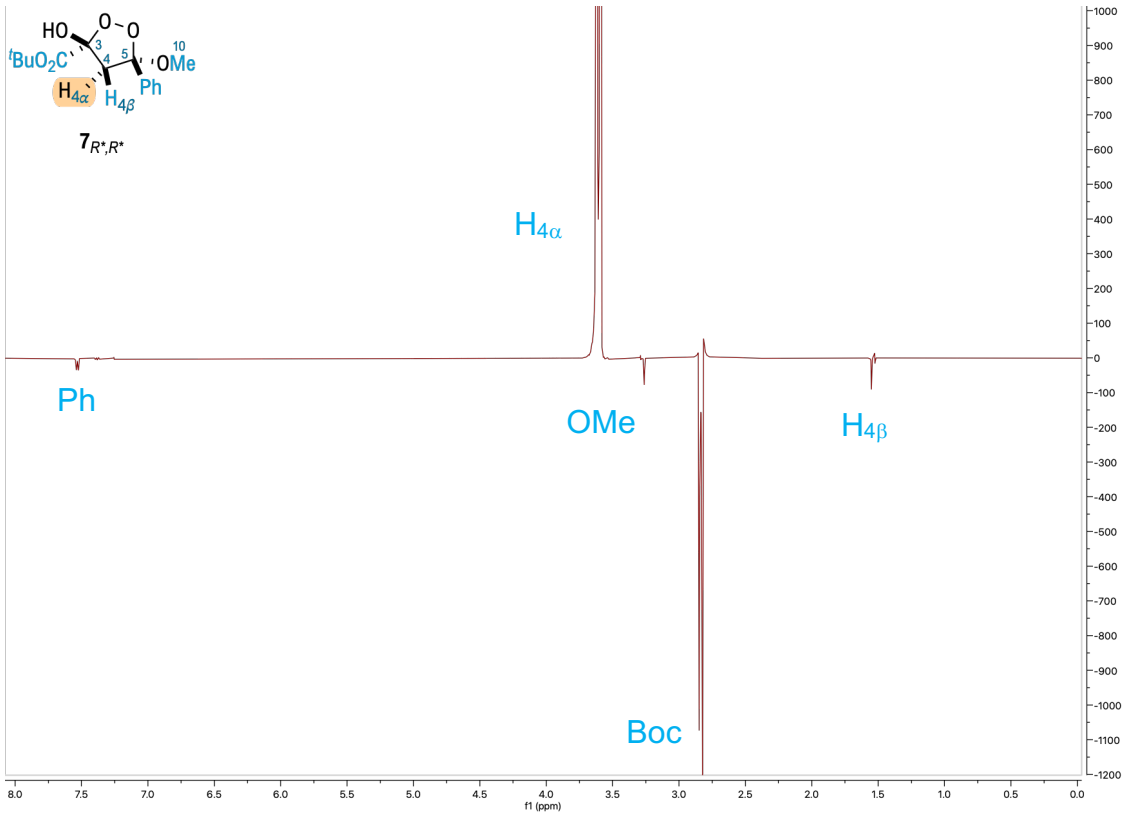
^{1}H NMR (500 MHz, $CDCl_3$) and **^{13}C NMR** (126 MHz, $CDCl_3$) of **7**



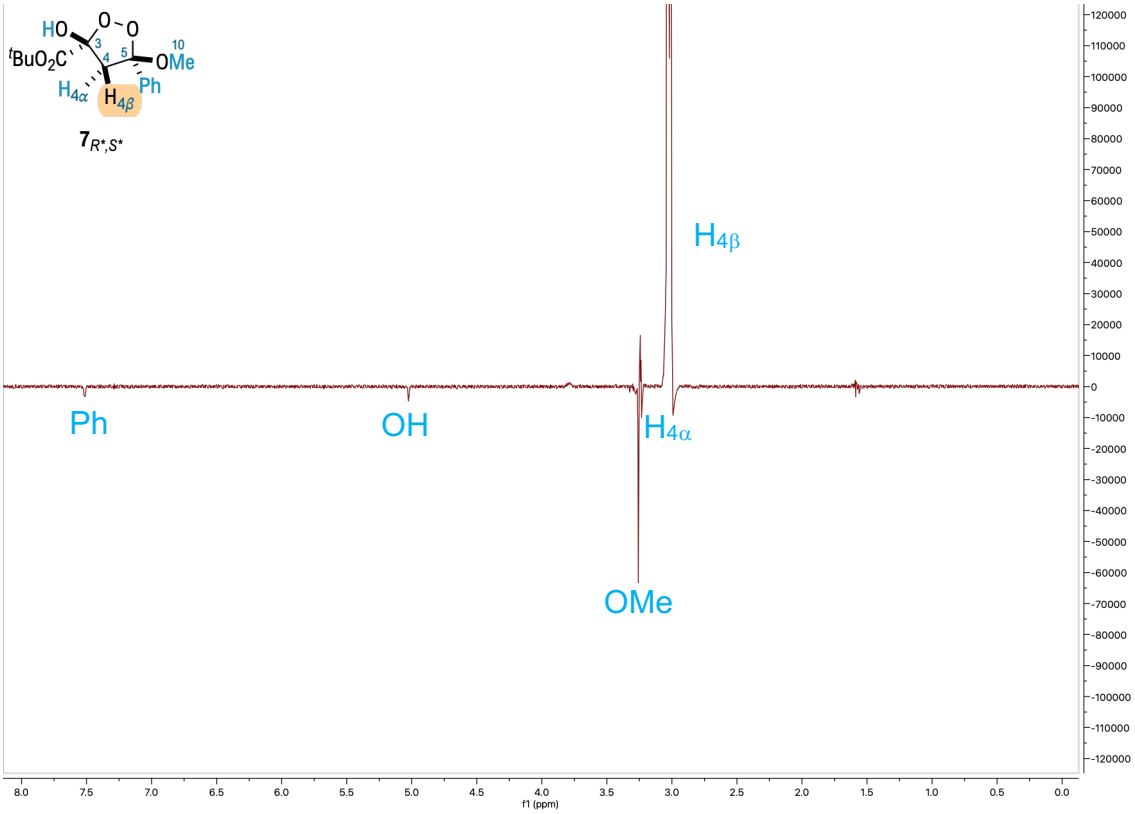
HMBC ($CDCl_3$) and **HSQC** ($CDCl_3$) of **7**



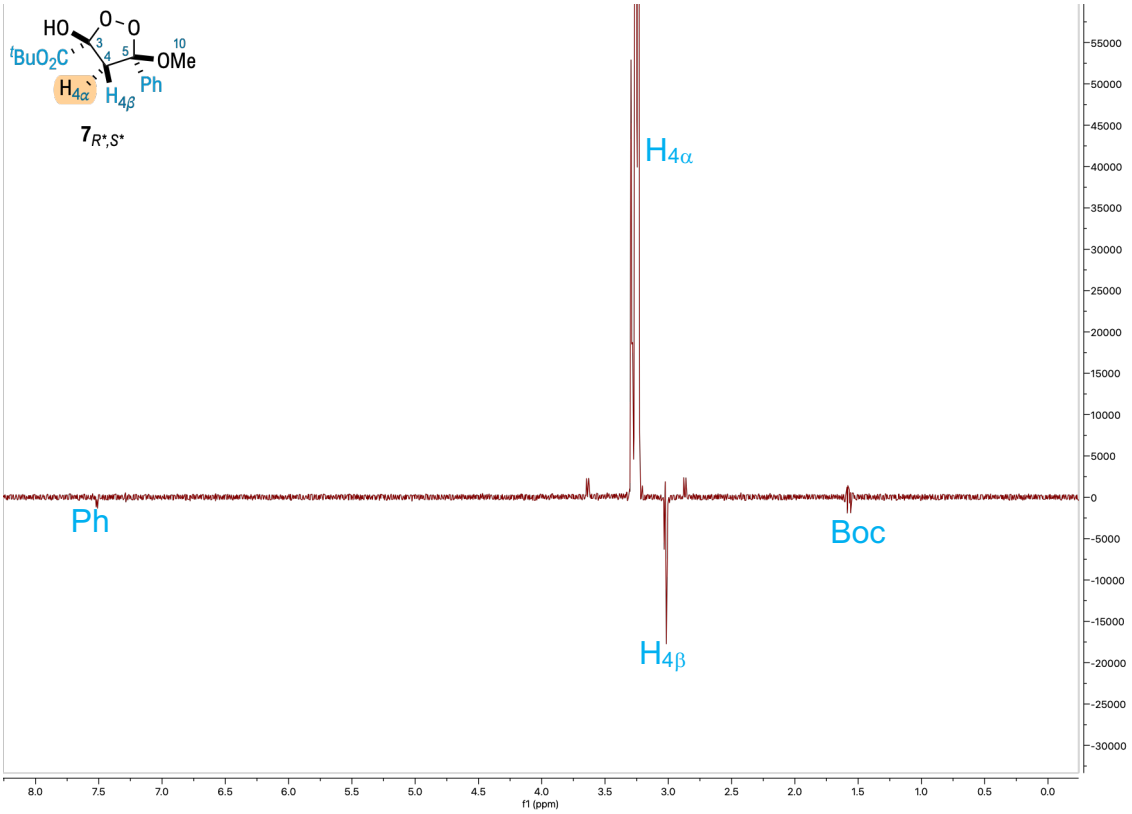
1D Selective Gradient NOESY (500 MHz, $CDCl_3$) at 2.862 ppm



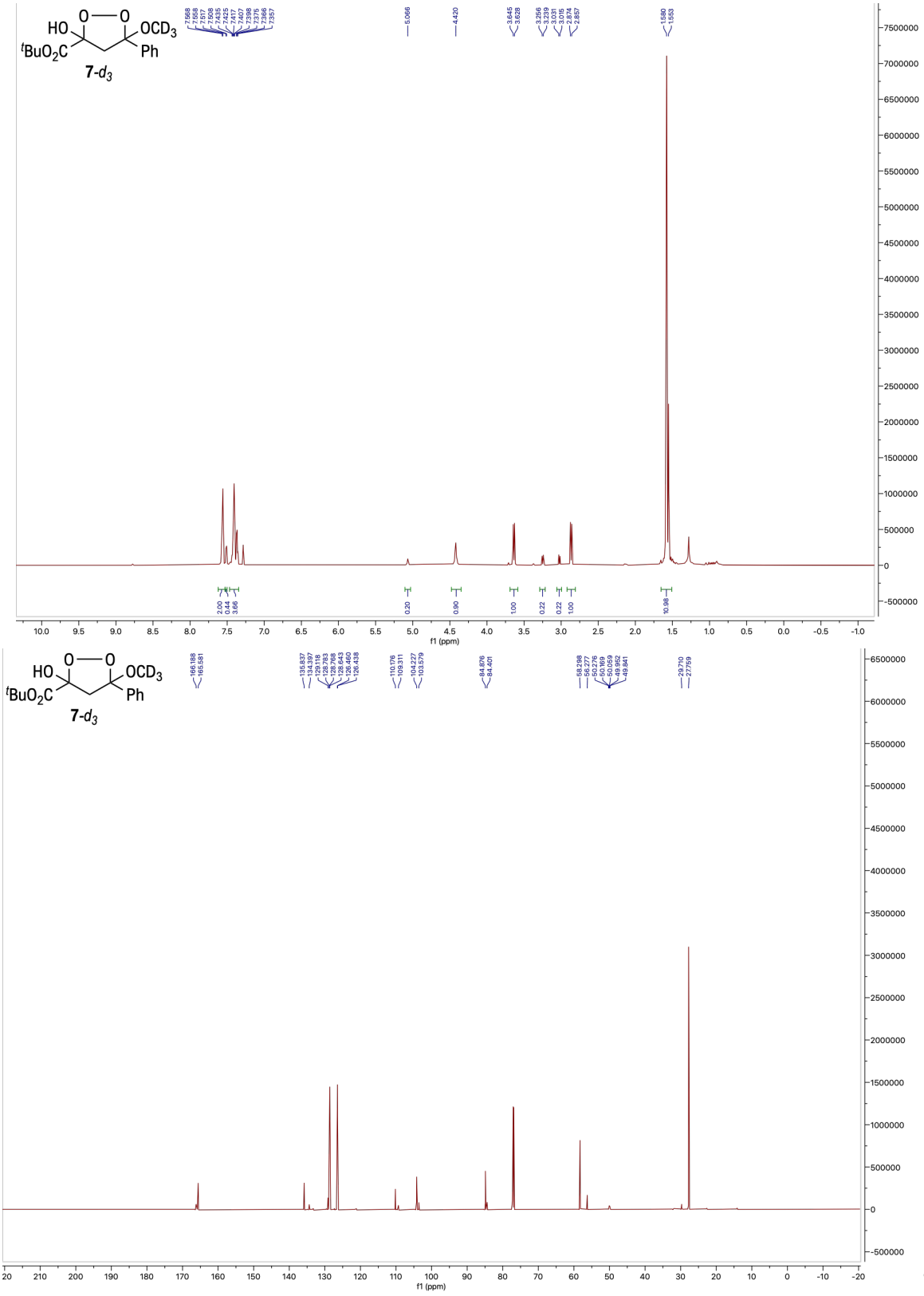
1D Selective Gradient NOESY (500 MHz, $CDCl_3$) at 3.636 ppm of **7**$_{R^*,R^*}$



1D Selective Gradient NOESY (800 MHz, $CDCl_3$) at 3.022 ppm



1D Selective Gradient NOESY (800 MHz, $CDCl_3$) at 3.246 ppm of **7**$_{R^*,S^*}$



^{1}H NMR (800 MHz, $CDCl_3$) and **^{13}C NMR** (201 MHz, $CDCl_3$) of **7**-d_3

8.7 References

[1] Bailey, P. S. Ozonation in Organic Chemistry. Volume 1: Olefinic Compounds; Academic Press: New York, 1978.

[2] Šimek, M.; Dworkin, J. H.; Kwon, O. Synthesis Through C(sp^3)–C(sp^2) Bond Scission in Alkenes and Ketones. Acc. Chem. Res. **2025**, 58 (10), 1547–1561.

[3] Criegee, R.; Wenner, G. Die Ozonisierung des 9,10-Oktalins. Justus Liebigs Ann. Chem. **1949**, 564 (1), 9–15.

[4] Criegee, R. Mechanism of Ozonolysis. Angew. Chem. Int. Ed. Engl. **1975**, 14 (11), 745–752.

[5] Whiting, M. C.; Bolt, A. J. N.; Parish, J. H. The Reaction Between Ozone and Saturated Compounds. In Oxidation of Organic Compounds, Volume III. Ozone Chemistry, Photo and Singlet Oxygen and Biochemical Oxidations; Advances in Chemistry, Vol. 77; American Chemical Society: Washington, DC, 1968; pp 4–14.

[6] Sirisoma, N. S.; Höld, K. M.; Casida, J. E. α- and β-Thujones (Herbal Medicines and Food Additives): Synthesis and Analysis of Hydroxy and Dehydro Metabolites. J. Agric. Food Chem. **2001**, 49 (4), 1915–1921.

[7] Khalitova, L. R.; Grabovskiy, S. A.; Antipin, A. V.; Spirikhin, L. V.; Kabal'nova, N. N. Products of Ozone Oxidation of Some Saturated Cyclic Hydrocarbons. Russ. J. Org. Chem. **2015**, 51 (12), 1710–1716.

[8] Foley, P.; Kendall, A. The Oxidation of Carbon-Hydrogen Bonds Using Ozone. WO 2022/192578 A1, September 15, 2022.

[9] DeMore, W. B. Rates and Mechanism of Alkyne Ozonation. Int. J. Chem. Kinet. **1971**, 3 (2), 161–173.

[10] Bailey, P. S.; Hwang, H. H.; Chiang, C.-Y. Mechanisms of Epoxidation During Ozonation of Carbon–Carbon Double Bonds. J. Org. Chem. **1985**, 50 (2), 231–234.

[11] Mvula, E.; von Sonntag, C. Ozonolysis of Phenols in Aqueous Solution. Org. Biomol. Chem. **2003**, 1 (10), 1749–1756.

[12] Olah, G. A.; Yoneda, N.; Parker, D. G. Oxyfunctionalization of Hydrocarbons. 3. Superacid Catalyzed Oxygenation of Alkanes with Ozone Involving Protonated Ozone, O3H+. J. Am. Chem. Soc. **1976**, 98 (17), 5261–5268.

[13] Kelly, C. B.; Milligan, J. A.; Tilley, L. J.; Sodano, T. M. Bicyclobutanes: From Curiosities to Versatile Reagents and Covalent Warheads. Chem. Sci. **2022**, 13 (40), 11721–11737.

[14] Sterling, A. J.; Smith, R. C.; Anderson, E. A.; Duarte, F. Beyond Strain Release: Delocalization-Enabled Organic Reactivity. J. Org. Chem. **2024**, 89 (14), 9979–9989.

[15] Chang, S.-J.; McNally, D.; Shary-Tehrany, S.; Hickey, M. J.; Boyd, R H. The Heats of Combustion and Strain Energies of Bicyclo[n.m.0]alkanes. J. Am. Chem. Soc. **1970**, 92 (10), 3109–3118.

[16] Eržen, E.; Cerkovnik, J.; Plesničar, B. endo/exo Isomerism in Norcarane and 2-Norcaranol Hydrotrioxides (ROOOH). J. Org. Chem. **2003**, 68 (24), 9129–9131.

[17] Tufariello, J. J.; Bayer, A. C.; Spadaro, J. J., Jr. Synthesis and Reactivity of exo- and endo-Bicyclo[2.1.0]pentan-5-ol and Their Derivatives. J. Am. Chem. Soc. **1979**, 101 (12), 3309–3315.

[18] Leininger, H.; Lazendörfer, F.; Christl, M. Über die Reduktion des Benzvalenozonids zum cis-1,3-Cyclobutandimethanol mit LiAlH4. Chem. Ber. **1983**, 116 (2), 669–680.

[19] Hogeveen, H.; Zwart, L. Synthesis and Properties of Functionalized 2,4-Ethano-Bridged Bicyclobutanes. Isr. J. Chem. **1981**, 21 (2–3), 221–228.

[20] Heldeweg, R. F.; Hogeveen, H.; Schudde, E. P. Oxidation of a Bicyclobutane-Bridged Diene with 1O2 and O3. Wittig Reactions of the Corresponding Enone and Dione. J. Org. Chem. **1978**, 43 (10), 1912–1916.

[21] Snyder, G. J.; Dougherty, D. A. 2,4-Dimethylene-1,3-cyclobutanediyl, the Non-Kekulé Isomer of Benzene. Synthesis, EPR, and Electronic Spectroscopy. J. Am. Chem. Soc. **1989**, 111 (11), 3927–3942.

[22] Lay, T. H.; Yamada, T.; Tsai, P.-L.; Bozzelli, J. W. Thermodynamic Parameters and Group Additivity Ring Corrections for Three- to Six-Membered Oxygen Heterocyclic Hydrocarbons. J. Phys. Chem. A **1997**, 101 (13), 2471–2477.

[23] Erickson, R. E.; Bailey, P. S.; Davis, J. C., Jr. Structure of the Monoözonide of 9,10-Dimethylanthracene. Tetrahedron **1962**, 18 (4), 388–395.

[24] Spanget-Larsen, J.; Gleiter, R. Rearrangement of Tris-σ-homobenzenes to 1,4,7-Cyclononatrienes. Angew. Chem. Int. Ed. Engl. **1978**, 17 (6), 441–442.

[25] Schwesinger, R.; Breuninger, M.; Gallenkamp, B.; Müller, K.-H.; Hunkler, D.; Prinzbach, H. „cis-Triaza-tris-σ-homobenzole“ („cis-Benzoltriimine“) Synthesen und [σ2s + σ2s + σ2s]-Cycloreversionen zu 4,7-Dihydro-1H-1,4,7-triazoninen. Chem. Ber. **1980**, 113 (10), 3127–3160.

[26] Ciganek, E. The Intramolecular Diels–Alder Reaction. Org. React. **1984**, 32, 1–374.

[27] Borzilleri, R. M. Product Class 6: Eight- and Nine-Membered Hetarenes and Heteroannulenes with One or More Heteroatoms. In Science of Synthesis; Vol. 17; Thieme: Stuttgart, 2004; pp 979–1024.

[28] McNab, H. Meldrum's Acid. Chem. Soc. Rev. **1978**, 7 (3), 345–358.

[29] Arriaga, D. K.; Thomas, A. A. Capturing Primary Ozonides for a syn-Dihydroxylation of Olefins. Nat. Chem. **2023**, 15 (9), 1262–1267.

[30] Hay, P. J.; Dunning, T. H., Jr.; Goddard, W. A., III. Configuration Interaction Studies of O3 and O3+ Ground and Excited States. J. Chem. Phys. **1975**, 62 (10), 3912–3924.

[31] Hayes, E. F.; Siu, A. K. Q. Electronic Structure of the Open Forms of Three-Membered Rings. J. Am. Chem. Soc. **1971**, 93 (9), 2090–2091.

[32] Bychek, R.; Mykhailiuk, P. K. A Practical and Scalable Approach to Fluoro-Substituted Bicyclo[1.1.1]pentanes. *Angew. Chem. Int. Ed.* **2022**, *61* (29), e202205103.

[33] Zhang, F.; Domack, J.; Hölter, N.; Daniliuc, C. G.; Glorius, F. Divergent Housane Synthesis via Intramolecular [2 + 2] Cycloaddition of 1,4-Dienes. *Nat. Synth.* **2026**, *5* (6), 897–906.

[34] Davies, S. G.; Fletcher, A. M.; Roberts, P. M.; Smith, A. D. Asymmetric Synthesis of Sedum Alkaloids via Lithium Amide Conjugate Addition. *Tetrahedron* **2009**, *65* (50), 10192–10213.

[35] Hatch, L. F.; Alexander, H. E.; Randolph, J. D. Dehydrohalogenation of Several Vinyl Halides. *J. Org. Chem.* **1950**, *15* (3), 654–656.

[36] Birck, M. R.; Clinch, K.; Gainsford, G. J.; Schramm, V. L.; Tyler, P. C. Syntheses of 5-Chlorouracils/Thymines with 1-[Phosphono(Methyl/Difluoromethyl)]-1,2-Unsaturated-Moiety-Substituted Methyl Groups at N(1) and Human Thymidine Phosphorylase Inhibitory Activity. *Helv. Chim. Acta* **2009**, *92* (5), 823–834.

[37] Piers, E.; Tse, H. L. A. A New Annulation Method. Total Syntheses of the Sesquiterpenoids (±)-Chiloscyphone and (±)-6-*epi*-Chiloscyphone. *Can. J. Chem.* **1993**, *71* (7), 983–994.

[38] Calvin, J. R.; Frederick, M. O.; Laird, D. L. T.; Remacle, J. R.; May, Scott A. Rhodium-Catalyzed and Zinc(II)-Triflate-Promoted Asymmetric Hydrogenation of Tetrasubstituted α,β-Unsaturated Ketones. *Org. Lett.* **2012**, *14* (4), 1038–1041.

[39] Logan, A. W. J.; Parker, J. S.; Hallside, M. S.; Burton, J. W. Manganese(III) Acetate Mediated Oxidative Radical Cyclizations. Toward Vicinal All-Carbon Quaternary Stereocenters. *Org. Lett.* **2012**, *14* (12), 2940–2943.

[40] Armstrong, A.; Ferguson, A. Synthesis and Ring Openings of Cinnamate-Derived *N*-Unfunctionalised Aziridines. *Beilstein J. Org. Chem.* **2012**, *8*, 1747–1752.

[41] Rigotti, T.; Bach, T. Bicyclo[2.1.1]hexanes by Visible Light-Driven Intramolecular Crossed [2 + 2] Photocycloadditions. *Org. Lett.* **2022**, *24* (48), 8821–8825.

[42] Ruan, J.; Li, X.; Saidi, O.; Xiao, J. Oxygen and Base-Free Oxidative Heck Reactions of Arylboronic Acids with Olefins. *J. Am. Chem. Soc.* **2008**, *130* (8), 2424–2425.

[43] Huang, X.-Y.; Ding, R.; Mo, Z.-Y.; Xu, Y.-L.; Tang, H.-T.; Wang, H.-S.; Chen, Y.-Y.; Pan, Y.-M. Photocatalytic Construction of S–S and C–S Bonds Promoted by Acridinium Salt: An Unexpected Pathway To Synthesize 1,2,4-Dithiazoles. *Org. Lett.* **2018**, *20* (16), 4819–4823.

[44] Xu, Y.; Yang, H.; Wang, J.; Zhang, Q.; Zhuang, X.; Sun, B.; Jin, C. Synergistic Cobalt and Cerium LMCT Photocatalysis for Decarboxylative Heck Type Reaction Facilitated by Efficient Acceptorless Dehydrogenation. *Chin. J. Chem.* **2025**, *43* (23), 3453–3460.

[45] Zhong, J.-J.; Ni, H. Selective Photoredox Decarboxylation of α-Ketoacids to Allylic Ketones and 1,4-Dicarbonyl Compounds Dependent on Cobaloxime Catalysis. *Chem. Commun.* **2020**, *56* (84), 12530–12533.

[46] Baughman, B. M.; Slavish, P. J.; DuBois, R. M.; Boyd, V. A.; White, S. W.; Webb, T. R. Identification of Influenza Endonuclease Inhibitors Using a Novel Fluorescence Polarization Assay. *ACS Chem. Biol.* **2012**, *7* (3), 526–534.

[47] Cope, A. C.; Foster, T. T.; Towle, P. H. Thermal Decomposition of Amine Oxides. *J. Am. Chem. Soc.* **1949**, *71* (12), 3929–3935.

[48] Greenwood, F. L. Ozonolysis of Planar Alkenes. *J. Org. Chem.* **1964**, *29* (10), 3108–3109.

CHAPTER NINE

Closing Remarks

Enclosed in this dissertation are eight research projects related to ozonolysis and dealkenylation. The research began with two review articles (Chapters 1 and 2). Discovering the vast knowledge and work that has been done in this space prepared the dissertation author for the research to come. The momentum continued into the first (Chapter 3) and second (Chapter 5) projects which both investigated methods to either avoid the use of ozone for dealkenylation, or to engineer conditions to make the reaction work. A third review was then completed at this point (Chapter 4), centered entirely on the C–C scission chemistry developed in the Kwon lab. The research then evolved to investigate more deeply the ozonolysis reaction with the goal of decoupling the efficiency of the first ozonolysis step from second reductive functionalization techniques (Chapter 6). A quantitative predictive computational model was developed for the ozonolysis reaction. With such a model, the efficiency of the reductive functionalization step could then be inferred and would provide a more complete picture of the overall dealkenylation process. The next project (Chapter 7) of this dissertation took the research in a new direction. The earlier projects focused on the ozonolysis reaction, but the dissertation author originated the idea for a ring contraction methodology using Samarium(II) iodide. Proof-of-concept was demonstrated, which not only validates the idea but also paves the way for future work to develop the idea into a robust methodology. The final research project (Chapter 8) returns to the ozonolysis reaction and resulted in the ozonolysis of σ-bonds, expanding the scope of the nearly two-century old reaction.

I am thankful to my co-workers for their teamwork and support. Overall, I am proud of the ideas I developed and the problems I have solved. For the works I leave unfinished, I wish the researchers who may continue these projects good luck.